Tire-Pavement Interaction Noise (TPIN) Modeling Using Artificial Neural Network (ANN)

Tan Li

Dissertation submitted to the faculty of the Virginia Polytechnic Institute and State University in partial fulfillment of the requirements for the degree of

Doctor of Philosophy
In
Mechanical Engineering

Ricardo A. Burdisso (Co-Chair)
Corina Sandu (Co-Chair)
Saied Taheri
Ronald H. Kennedy
Scott L. Hendricks

July 19, 2017
Blacksburg, VA, USA

Keywords: tire-pavement interaction noise, noise separation, artificial neural network, tread pattern, tire size, rubber hardness, speed exponent

Copyright © 2017 Tan Li

Tire-Pavement Interaction Noise (TPIN)
Modeling Using Artificial Neural Network (ANN)

Tan Li

Abstract

Tire-pavement interaction is a dominant noise source for passenger cars and trucks above 25 mph (40 km/h) and 43 mph (70 km/h), respectively. For the same pavement, tires with different tread pattern and construction generate noise of different levels and frequencies. In the present study, forty-two different tires were tested over a range of speeds (45-65 mph, i.e., 72-105 km/h) on a non-porous asphalt pavement (a section of U.S. Route 460, both eastbound and westbound). An On-Board Sound Intensity (OBSI) system was instrumented on the test vehicle to collect the tire noise data at both the leading and trailing edge of the tire contact patch. An optical sensor recording the once-per-revolution signal of the wheel was also installed to monitor the vehicle speed and, more importantly, to provide the data needed to perform the order tracking analysis in order to break down the tire noise into two components. These two components are: the tread pattern and the non-tread pattern noise. Based on the experimental noise data collected, two artificial neural networks (ANN) were developed to predict the tread pattern (ANN_1) and the non-tread pattern noise (ANN_2) components, separately. The inputs of ANN_1 are the coherent tread profile spectrum and the air volume velocity spectrum calculated from the digitized 3D tread pattern. The inputs of ANN_2 are the tire size and tread rubber hardness. The vehicle speed is also included as input for the two ANN's. The optimized ANN's are able to predict the tire-pavement interaction noise well for different tires on the pavement tested. Another outcome of this work is the complete literature review on Tire-Pavement Interaction Noise (TPIN), as an appendix of this dissertation and covering ~1000 references, which might be the most comprehensive compilation of this topic.

Tire-Pavement Interaction Noise (TPIN)
Modeling Using Artificial Neural Network (ANN)

Tan Li

General Audience Abstract

A lot of people think the car noise is mostly from the engine, exhaust, or wind. However, this is not true. The noise in the exterior mainly comes from tires at over 25 mph. At normal highway speed, e.g., 60 mph, tire noise contributes over 70% of total noise. A quiet tire is desired for driving comfort. A number of attempts to reduce tire noise have been made in tire industries, including the tread pattern optimization and the tire structure design. In this work, a model was developed to predict the tire noise based on the tread pattern, tire size, tread rubber hardness, and vehicle speed. The model is called Artificial Neural Network Model of Tire-Pavement Interaction Noise (ANN Model of TPIN, or AMOT). This model is able to predict the noise contributions from the tread pattern and the pavement separately. Tire companies can use the model to design quite tires while customers can have an insight on choosing quite tires based on the tread patterns and/or tire structure.

Dedication

This dissertation is dedicated to world peace, that makes us so relaxed to care about things like tire noise.

Acknowledgements

This should be the most difficult part of my dissertation. I am not a person who is very good at expressing gratitude, which makes it even more difficult. I really tried to recall all the people who helped me along the way. However, if you are not mentioned or emphasized here, it doesn't mean you are not important, but I really appreciate all the help from you.

To begin with, I would like to thank my two advisors. Arranging the order of them burns my brain. It's like a child was asked a question "who is your favorite, mom or dad?". Luckily, alphabetical order saves me in the end.

Dr. Burdisso (dad) serves as my co-advisor just for two years, but this never diminishes the importance of him. I thought I was the most stubborn person in the world until I met him. He might be the most academically strict professor in the department. If you ask me whether I regret inviting him as my co-advisor two years ago, I would say, yes, I wish I could have done it earlier. He is always the leading person in my dissertation project and guides me through all the difficulties. He earns most of the credits for the success of the project and the completion of my dissertation.

Dr. Sandu (mom) serves as my co-advisor for four years, the full duration when I have been at Virginia Tech. I still remember the day when we first talked on Skype when I was still in China and then I got the offer on March 1, 2013, after which my adventures here started. She is always considerate, encourages me to do everything that helps enrich my knowledge, and provides valuable guidance through my PhD studies and career path. It is also because of her that I still stick with tire research that might become my lifework.

I also wish to have Dr. Taheri as my co-advisor if triple-advisor is allowed. His knowledge on tire, both in academia and industry, always enlightens me; this also applies to Dr. Kennedy. Dr. Taheri and Dr. Kennedy took part in nearly all the academic meetings/conferences I attended during my PhD; sometimes even my actual co-advisors were not with me then. As a past member of my advisory committee, Dr.

Furukawa also provides important insights in the topic of tire noise. Dr. Hendricks is the first lecturer of my PhD courses, and the best and my favorite. His course (Intermediate Dynamics, ME students know how difficult it is) was the only one I attended in the morning; I usually do not get up until the afternoon, which all my friends know (yes, I am an owl).

Speaking of friends, also as my labmates, Jianxiong Feng and Sterling McBride offered great help with my dissertation project. Dr. Patricio Ravetta (AVEC) provided important support with the experimental equipment.

As the project sponsor, the Center for Tire Research (CenTiRe) must be mentioned, I really appreciate this opportunity to work and communicate with tire industries. I would like to thank Dr. Lin Kung (Nexen), Mr. Brian Baddorf (Hankook), Mr. Bart Kimble (Goodyear), Dr. Hamid Aboutorabi and Dr. Anudeep Bhoopalam (Giti) for providing special support for my project. I would also like to extend thanks to Dr. Yousof Azizi (Bridgestone), Dr. Jun Han (Cooper), Dr. Toshio Tada (Sumitomo), Dr. Smruti Panigrahi (Ford), Dr. Abhishek Verma (MRF), Dr. Jinman Jang (Kumho), Dr. Yonghun Kim (Hankook), Mr. Bharatkumar Makwana and Mr. P. Sankarganesh (Apollo) for their kind support and guidance as industry mentors. Last but not least, special thanks to Dr. Bin Chung and Maxxis for offering me the Senior NVH Engineer position after my graduation, so that I have the chance to apply what I studied at VT to real products in tire industries.

As a past-GTA, I would like to thank my supervisors: Dr. Brian Lattimer, Dr. John Kennedy, Dr. Mehdi Ahmadian, Dr. Javid Bayandor, Dr. Kevin Kochersberger, Dr. Jan Helge Bøhn, Dr. Rolf Müller, Dr. David Poling, and Dr. Richard Clark. I would also like to thank Ms. Cathy Hill for taking care of the graduate affairs.

In the end, I want to say I am so happy to meet all of you here, to all my friends and colleagues that I haven't mentioned: Rui He, Emilio Jimenez, Aamir Khan, Sebastien Corner, Hoda Moosavi, Yitao Zhu, Zhi Chai, Mark Hurtado, Daniel Wu, Yang Chen, Yunbo Hou, Zebo Zhu… I wish all of you the best in your journey!

Table of Contents

Abstract ..... **ii**
General Audience Abstract ..... **iii**
Dedication ..... **iv**
Acknowledgements ..... **v**
Table of Contents ..... **vii**
List of Figures ..... **xi**
List of Tables ..... **xvii**
List of Abbreviations ..... **xx**
Nomenclature ..... **xxix**
1 Introduction **1**
1.1 Motivation *1*
1.2 Objectives *3*
1.3 Contributions *3*
1.4 Organization *3*
2 Literature Review on TPIN **6**
2.1 Measurement Techniques *7*
2.1.1 Roadside Measurement 8
2.1.2 On-board Measurement 11
2.1.3 Lab Measurement 14
2.1.4 Summary 17
2.2 Physical Mechanisms *18*
2.2.1 Generation Mechanisms 19
2.2.2 Amplification Mechanisms 19
2.2.3 Attenuation Mechanisms 20
2.2.4 Summary 21
2.3 Influencing Parameters *23*
2.3.1 Driver Influence Parameters 24
2.3.2 Tire Related Parameters 25
2.3.3 Tread Pattern Parameters 26
2.3.4 Pavement Related Parameters 28
2.3.5 Environmental Parameters 30
2.3.6 Summary 30

2.4 Existing Models *30*
2.4.1 Deterministic Models 31
2.4.2 Statistical Models 38
2.4.3 Hybrid Models 45
2.4.4 Summary 51
2.5 Review and the Present Study *52*
3 Experiments and Data Analysis 54
3.1 Experiments *54*
3.1.1 Test Tires 54
3.1.2 Test Pavement 57
3.1.3 Test Equipment 57
3.1.4 Test Condition 60
3.2 Tread Pattern Characterization *61*
3.2.1 Tread Profile Spectrum 62
3.2.2 Air Volume Velocity Spectrum 65
3.3 Tire Noise Analysis *67*
3.3.1 Tire Noise Components 67
3.3.2 Order Tracking Analysis 70
3.3.3 Tire Noise Separation 72
3.3.4 Order Spectrum 77
3.4 Correlation between Tread Pattern and Tire Noise *78*
3.5 Summary *81*
4 Artificial Neural Network (ANN) 82
4.1 Introduction *82*
4.1.1 Structure 82
4.1.2 Development 84
4.2 Existing ANN Models Related to TPIN *84*
4.2.1 Che et al. Model 85
4.2.2 Li et al. Model 86
4.2.3 Fry et al. Model 86
4.2.4 Other ANN Models 88
4.3 Proposed ANN for TPIN *89*
4.4 Summary *92*
5 ANN Model for Tread Pattern Noise (ANN_1) 93

5.1 Input and Output *93*
5.1.1 Input Parameters 93
5.1.2 Output Parameters 95
5.2 Speed as an Input Parameter *97*
5.2.1 Two Approaches to Handling Speed 97
5.2.2 Speed Exponent Optimization 98
5.3 ANN_1 at 60 mph *102*
5.4 ANN_1 at Different Speed *109*
5.5 Other ANN_1 Configurations *119*
5.5.1 ANN_1 at 60 mph 119
5.5.2 ANN_1 at Different Speed 123
5.5.3 Other Input and Output Data Set 126
5.5.4 Summer/All-Season Tires Only 131
5.6 Conversion from Order Spectrum to Frequency Spectrum *132*
5.7 Summary *134*
6 ANN Model for Non-Tread Pattern Noise (ANN_2) 135
6.1 Effect of Rubber Hardness *135*
6.1.1 Literature Survey 135
6.1.2 Regression Analysis 137
6.1.3 ANN Model 139
6.1.4 Other ANN_2 Configurations 142
6.2 Effect of Tire Size *145*
6.2.1 Literature Survey 145
6.2.2 Tire Size Effect on Spectral Distribution 147
6.2.3 Nonlinear Correlation 152
6.2.4 Tire Size Scaling 153
6.3 Summary *154*
7 ANN Model of TPIN (AMOT) 156
7.1 Structure of AMOT *156*
7.2 Development of AMOT *158*
7.3 Results of AMOT (Test Set) *159*
7.3.1 Individual Tires 160
7.3.2 All Tires 175
7.4 Summary *176*

8 Conclusions and Future Work **178**
References **181**
Appendix A: Tread Pattern Analysis **210**
Appendix B: Results of AMOT (Train and Validation Set) **229**
Appendix C: Effect of Speed **242**
Appendix D: Effect of Tire Inflation Pressure **267**
Appendix E: Tones due to Pavement Distress **277**
Appendix F: Rough and Smooth Pavement **288**
Appendix G: Characteristics of TPIN from Slick Tire **300**
Appendix H: A Literature Review of Tire-Pavement Interaction Noise **306**

List of Figures

Figure 2.1: Literature records count (generated via Engineering Village on Aug 12, 2016, search query for "tire" & "noise" in subject/title/abstract from databases of Compendex, Inspec & NTIS) 7

Figure 2.2: Experimental setup of roadside measurement techniques..... 11

Figure 2.3: Experimental setup of on-board measurement techniques..... 14

Figure 2.4: Experimental setup of roadside measurement techniques..... 17

Figure 2.5: Illustration of generation mechanisms 19

Figure 2.6: Illustration of amplification mechanisms 20

Figure 2.7: Illustration of attenuation mechanisms..... 21

Figure 3.1: Tread patterns of the test tires (arrow indicates rotation direction)..... 56

Figure 3.2: Test pavement (source from Google Map)..... 57

Figure 3.3: Test vehicles (left: Chevy Impala; right: Chevy Tahoe)..... 58

Figure 3.4: On-board sound intensity (OBSI) with optical sensor installed on the test vehicle 59

Figure 3.5: Issues in testing tires of different sizes (left: larger tires on Impala; right: smaller tires on Tahoe) 60

Figure 3.6: Wheel adapter..... 60

Figure 3.7: Illustration of 3D tread profile of Tire 12..... 62

Figure 3.8: (a) Tread profile power spectra for all circumferential sections; (b) incoherent tread profile spectrum; (c) coherent tread profile spectrum at 60 mph for Tire 12 (12.5 Hz resolution) 63

Figure 3.9: Incoherent and coherent tread profile spectra at 60 mph for all tires (legend includes tire number and pitch passing frequency)..... 65

Figure 3.10: Illustration of calculation of air volume velocity spectrum (Tire 12) 66

Figure 3.11: Air volume velocity spectrum at 60 mph for all tires (legend includes tire number and pitch passing frequency) 67

Figure 3.12: Spectrogram of microphone 1 (leading inboard) for Tire 12 accelerating from 45 mph to 65 mph 68

Figure 3.13: Spectrogram of microphone 1 (leading inboard) for Tire 15 accelerating from 45 mph to 65 mph 69

Figure 3.14: Illustration of two excitation sources and tire noise components 70

Figure 3.15: Illustration of separation of tread-pattern noise and non-tread-pattern noise (60 mph test) 72

Figure 3.16: Total, tread-pattern, and non-tread pattern noise components at 60 mph

(A-weighted, 5 Hz resolution) 73

Figure 3.17: Total, tread-pattern, and non-tread pattern noise components at 60 mph (A-weighted, 5 Hz resolution) 76

Figure 3.18: Frequency spectrum (resolution = 5 Hz) and order spectrum (resolution = 1) for tread pattern noise of Tire 12 at 60 mph (~13 Hz) 78

Figure 3.19: Comparison between the tread pattern spectra in red and the tire noise spectra in black for Tire 12 at 60 mph (number of pitches = 77)..... 79

Figure 3.20: Comparison between the tread pattern spectra in red and the tire noise spectra in black for Tire 19 at 60 mph (number of pitches = 60)..... 80

Figure 4.1: Schematic of a typical artificial neural network (ANN) 82

Figure 4.2: Two-stage ANN models for pass-by noise (Source from Fry and Jennings, 2003 [381], Figure 3) 87

Figure 4.3: Single ANN to predict TPIN 90

Figure 4.4: Two sub-ANN's to predict TPIN..... 90

Figure 4.5: Total, tread pattern, and non-tread pattern noise data at 60 mph for developing ANN models 91

Figure 5.1: Gaussian curve fitting of the tread pattern spectra at different number of terms (Tire 12) 94

Figure 5.2: Tread pattern noise spectrum in frequency narrowband (5 Hz resolution), 1/3 octave band, 1/12 octave band, and order narrowband (1 resolution) for Tire 12 at 60 mph 96

Figure 5.3: Input and output parameters for ANN_1..... 96

Figure 5.4: Two approaches to handling speed..... 97

Figure 5.5: Scaled tread pattern noise spectra using different speed exponents (Tire 01) 100

Figure 5.6: Standard deviation versus speed exponent for all test tires..... 101

Figure 5.7: Optimized speed exponent for all test tires 101

Figure 5.8: Comparison between measured (red) and predicted (green) tread pattern noise spectrums [ANN_1 at 60 mph]..... 104

Figure 5.9: Comparison between measured and predicted SPL at different order [ANN_1 at 60 mph] 107

Figure 5.10: Average dB error at different order (the number in the legend is the average value across all the orders for the specific sample set) [ANN_1 at 60 mph] 107

Figure 5.11: Comparison between measured and predicted overall SPL [ANN_1 at 60 mph] 108

Figure 5.12: Post-processing for ANN_1 output (Tire 09 at 60 mph)..... 109

Figure 5.13: Comparison between measured (red) and predicted (green) tread pattern

noise spectrums [ANN_1 at different speed]..... 113

Figure 5.14: Comparison between measured and predicted SPL at different order [ANN_1 at different speed]..... 116

Figure 5.15: Average dB error at different order (the number in the legend is the average value across all the orders for the specific sample set) [ANN_1 at different speed]. 117

Figure 5.16: Comparison between measured and predicted overall SPL [ANN_1 at different speed] 118

Figure 5.17: Comparison between measured and predicted overall SPL sorted by tires [ANN_1 at different speed] 118

Figure 5.18: Speed exponent scaling and conversion from order domain to frequency domain..... 133

Figure 6.1: Surface fitting for rubber hardness effect..... 138

Figure 6.2: Schematic of preliminary ANN_2 (215/60R16) 139

Figure 6.3: Spectral results for preliminary ANN_2 (215/60R16) (red denotes measured, green denotes predicted) 141

Figure 6.4: OASPL results for preliminary ANN_2 (215/60R16) 141

Figure 6.5: Post-processing for ANN_2 output (Tire 09 at 60 mph)..... 142

Figure 6.6: Results for different ANN_2 configurations..... 144

Figure 6.7: Tire size parameters..... 145

Figure 6.8: Tires of different sizes 147

Figure 6.9: Non-tread pattern noise spectra for tires of different sizes (narrowband, 5 Hz resolution) 148

Figure 6.10: Correlation between central frequency and tire size parameters (blue circle denotes original data; red line denotes fitted curve) (the text above each subplot includes: R^2, coefficient of determination; *rms*, root mean squared value; [a, b], coefficients in regression equation $y = ax+b$) 150

Figure 6.11: Correlation between amplitude and tire size parameters (blue circle denotes original data; red line denotes fitted curve) (the text above each subplot includes: R^2, coefficient of determination; *rms*, root mean squared value; [a, b], coefficients in regression equation $y = ax+b$)..... 151

Figure 6.12: Correlation between spread and tire size parameters (blue circle denotes original data; red line denotes fitted curve) (the text above each subplot includes: R^2, coefficient of determination; *rms*, root mean squared value; [a, b], coefficients in regression equation $y = ax+b$)..... 152

Figure 6.13: Different types of correlations between the central frequency of non-tread pattern noise and the carcass width..... 153

Figure 6.14: Non-tread pattern noise spectra for tires of different sizes after tire size scaling 154

Figure 7.1: Structure of ANN Model of TPIN (AMOT) (the solid circle at the intersection of two lines denotes there is connection while hollow circle denotes no connection) 157

Figure 7.2: Results of AMOT for Tire 09 (in a-f, red denotes measured, green denotes predicted; in g-i, the value above the plot is the average dB error) 161

Figure 7.3: Results of AMOT for Tire 15 (in a-f, red denotes measured, green denotes predicted; in g-i, the value above the plot is the average dB error) 163

Figure 7.4: Results of AMOT for Tire 18 (in a-f, red denotes measured, green denotes predicted; in g-i, the value above the plot is the average dB error) 165

Figure 7.5: Results of AMOT for Tire 22 (in a-f, red denotes measured, green denotes predicted; in g-i, the value above the plot is the average dB error) 167

Figure 7.6: Results of AMOT for Tire 23 (in a-f, red denotes measured, green denotes predicted; in g-i, the value above the plot is the average dB error) 169

Figure 7.7: Results of AMOT for Tire 45 (in a-f, red denotes measured, green denotes predicted; in g-i, the value above the plot is the average dB error) 171

Figure 7.8: Results of AMOT for Tire 49 (in a-f, red denotes measured, green denotes predicted; in g-i, the value above the plot is the average dB error) 173

Figure 7.9: Results of AMOT for Tire 55 (in a-f, red denotes measured, green denotes predicted; in g-i, the value above the plot is the average dB error) 175

Figure 7.10: Results of AMOT in overall A-weighted sound pressure level (OASPL) (the value above each subplot denotes the average dB error between measurement and prediction) 176

Figure A.1: Tread profile power spectra for all circumferential sections at 60 mph 213

Figure B.1: Total noise in narrowband linear scale (red denotes measured, green denotes predicted) 229

Figure B.2: Tread pattern noise in narrowband linear scale (red denotes measured, green denotes predicted) 230

Figure B.3: Non-tread pattern noise in narrowband linear scale (red denotes measured, green denotes predicted) 231

Figure B.4: Total noise in narrowband dB scale (red denotes measured, green denotes predicted) 232

Figure B.5: Tread pattern noise in narrowband dB scale (red denotes measured, green denotes predicted) 233

Figure B.6: Non-tread pattern noise in narrowband dB scale (red denotes measured, green denotes predicted) 234

Figure B.7: Total noise in 1/3 octave band linear scale (red denotes measured, green denotes predicted) 235

Figure B.8: Tread pattern noise in 1/3 octave band linear scale (red denotes measured, green denotes predicted) 236

Figure B.9: Non-tread pattern noise in 1/3 octave band linear scale (red denotes measured, green denotes predicted) 237

Figure B.10: Total noise in 1/3 octave band dB scale (red denotes measured, green denotes predicted) 238

Figure B.11: Tread pattern noise in 1/3 octave band dB scale (red denotes measured, green denotes predicted) 239

Figure B.12: Non-tread pattern noise in 1/3 octave band dB scale (red denotes measured, green denotes predicted) 240

Figure B.13: Overall A-weighted Sound Pressure Level (OASPL) (the value above each subplot denotes the average dB error between measurement and prediction) 241

Figure C.1: Tread patterns of the test tires (arrow indicates rotation direction) 245

Figure C.2: Test pavement (source from Google Map) 246

Figure C.3: On-board sound intensity (OBSI) with optical sensor installed on the test vehicle 247

Figure C.4: Spectrogram of microphone 1 (leading inboard) for Tire 12 accelerating from 45 mph to 65 mph 248

Figure C.5: Total, tread-pattern, and non-tread pattern noise components at 60 mph (5 Hz resolution) 250

Figure C.6: Total noise spectrums for different speeds 252

Figure C.7: Tread-pattern-noise spectrums for different speeds 253

Figure C.8: Non-tread-pattern-noise spectrums for different speeds 254

Figure C.9: Effect of speed on the overall A-weighted sound pressure level (OASPL) 256

Figure C.10: Standard deviation versus scaling law for the total noise 258

Figure C.11: Scaled total noise spectrums for different speeds 259

Figure C.12: Standard deviation versus scaling law for the tread pattern noise 260

Figure C.13: Scaled tread pattern noise spectrums for different speeds 263

Figure C.14: Standard deviation versus scaling law for the non-tread pattern noise 263

Figure C.15: Scaled non-tread pattern noise spectrums for different speeds 265

Figure C.16: Scaling laws for the leading edge versus trailing edge 266

Figure D.1: Effect of inflation pressure on total noise level (OASPL) 270

Figure D.2: Effect of inflation pressure on tread pattern noise level (OASPL) 270

Figure D.3: Effect of inflation pressure on non-tread pattern noise level (OASPL) 271

Figure D.4: Effect of inflation pressure on total noise spectrum 272

Figure D.5: Effect of inflation pressure on tread pattern noise spectrum 273

Figure D.6: Effect of inflation pressure on non-tread pattern noise spectrum 273

Figure D.7: Effect of inflation pressure on total noise level speed exponent 274

Figure D.8: Effect of inflation pressure on tread pattern noise level speed exponent 275

Figure D.9: Effect of inflation pressure on non-tread pattern noise level speed exponent 275

Figure E.1: Two test sections (normal section and corrugation section) 279

Figure E.2: Tread patterns of the test tires (arrow indicates rotation direction) 280

Figure E.3: On-board sound intensity (OBSI) with optical sensor installed on the test vehicle 281

Figure E.4: Total noise spectrums at 60 mph (5 Hz resolution). 282

Figure E.5: Total, tread-pattern, and non-tread pattern noise components at 60 mph (5 Hz resolution) 284

Figure E.6: Tread pattern noise spectrums at 60 mph (5 Hz resolution) 285

Figure E.7: Non-tread pattern noise spectrums at 60 mph (5 Hz resolution) 286

Figure E.8: Non-tread pattern noise spectrums at different speeds for Tire 12 on the corrugation section (1 Hz resolution) 286

Figure F.1: Two east sections (rough section and smooth section) (Source from Google Street View)..... 290

Figure F.2: Tread patterns of the test tires (arrow indicates rotation direction)..... 291

Figure F.3: On-board sound intensity (OBSI) with optical sensor installed on the test vehicle 292

Figure F.4:Total noise spectrums at 60 mph (5 Hz resolution)..... 293

Figure F.5: Total, tread-pattern, and non-tread pattern noise components at 60 mph (5 Hz resolution) 295

Figure F.6: Tread pattern noise spectrums at 60 mph (5 Hz resolution)..... 296

Figure F.7: Non-tread pattern noise spectrums at 60 mph (5 Hz resolution)..... 297

Figure G.1: Noise separation analysis (60 mph, 32 psi, eastbound, leading inboard mic) 302

Figure G.2: Total noise spectral comparisons (red: slick tire; green: patterned tire) (60 mph, 32 psi, eastbound, leading inboard mic) 303

Figure G.3: Tread pattern noise spectral comparisons (red: slick tire; green: patterned tire) (60 mph, 32 psi, eastbound, leading inboard mic)..... 304

Figure G.4: Non-tread pattern noise spectral comparisons (red: slick tire; green: patterned tire) (60 mph, 32 psi, eastbound, leading inboard mic) 305

List of Tables

Table 2.1: Category of TPIN measurement techniques 8
Table 2.2: Summary of roadside measurement techniques..... 10
Table 2.3: Summary of on-board measurement techniques..... 13
Table 2.4: Summary of lab measurement techniques 16
Table 2.5: Dominant frequencies for different TPIN components..... 18
Table 2.6: Tire-Pavement Interaction Noise (TPIN) Mechanisms..... 22
Table 2.7: Overview of parameters affecting TPIN (source from Sandberg and Ejsmont, 2002 [24])..... 24
Table 2.8: Summary of driver influence parameters affecting TPIN..... 25
Table 2.9: Summary of tire-related parameters affecting TPIN..... 26
Table 2.10: Summary of tread pattern parameters affecting TPIN 27
Table 2.11: Summary of pavement-related parameters affecting TPIN..... 29
Table 2.12: Summary of environmental parameters affecting TPIN 30
Table 2.13: Summary of conventional physics models on TPIN..... 33
Table 2.14: Summary of finite element and boundary element models on TPIN..... 35
Table 2.15: Summary of computational fluid dynamics models on TPIN..... 37
Table 2.16: Summary of traditional regression models on TPIN 40
Table 2.17: Summary of principal component analysis models on TPIN 42
Table 2.18: Summary of fuzzy curve fitting models on TPIN..... 44
Table 2.19: Summary of tire-pavement interface models on TPIN 46
Table 2.20: Summary of mechanism separation models on TPIN..... 48
Table 2.21: Summary of noise propagation models on TPIN..... 50
Table 3.1: Specifications of the test tires 55
Table 3.2: Different tire sizes tested..... 58
Table 3.3: Noise data collection field tests 61
Table 3.4: Overall A-weighted sound pressure level of noise components (red indicates snow tire) 74
Table 4.1: Input and output parameters of ANN (Che et al., 2012 [266]) 85
Table 4.2: Metrics for two-stage ANN models for pass-by noise (Fry and Jennings, 2003 [381])..... 88
Table 5.1: Identification of optimized speed exponent *n* for Tire 01 (red indicates optimized *n* where the standard deviation is minimum)..... 99

Table 5.2: Subsets of samples for developing ANN_1 at 60 mph (red indicates winter tire) 102

Table 5.3: Input/output configurations for ANN_1 at 60 mph 119

Table 5.4: Results for different input/output configurations of ANN_1 at 60 mph..... 120

Table 5.5: Overall SPL error for different input/output configurations of ANN_1 at 60 mph (red indicates optimized)..... 123

Table 5.6: Results for different speed exponents of ANN_1 at all speeds 123

Table 5.7: Overall SPL error for different speed exponents of ANN_1 at all speeds (red indicates optimized) 125

Table 5.8: Other input data sets for ANN_1 at 60 mph 126

Table 5.9: Results for other input data sets of ANN1 at 60 mph 127

Table 5.10: Overall SPL error for other input data sets of ANN_1 at 60 mph (red indicates optimized) 128

Table 5.11: Other output data sets for ANN_1 at 60 mph 128

Table 5.12: Results for other output data sets of ANN_1 at all speeds 129

Table 5.13: Overall SPL error for other output data sets of ANN_1 at all speeds (red indicates optimized) 131

Table 5.14: Comparison between the ANN_1 for all tires and ANN_1 for summer/all-season tires only..... 132

Table 6.1: Effect of rubber hardness on TPIN level..... 136

Table 6.2: Subsets of samples for developing the preliminary ANN_2 model (215/60R16) 140

Table 6.3: Configurations for preliminary ANN_2 (215/60R16) 142

Table 7.1: Sub-models of ANN Model of TPIN (AMOT)..... 158

Table 7.2: Subsets of samples for developing ANN_1 and ANN_2 159

Table A.1: 2D tread patterns of test tires..... 210

Table A.2: Comparison between coherent tread profile spectrum in red and TPIN spectra in black 213

Table A.3: Comparison between air volume velocity spectrum in red and TPIN spectra in black 218

Table A.4: Incoherent tread profile spectrum, coherent tread profile spectrum, and volume velocity spectrum (blue: original; red: Gaussian) 222

Table C.1: Speed exponents for different TPIN mechanisms 242

Table C.2: Specifications of the test tires..... 244

Table C.3: Identification of optimized scaling law n for total noise of Tire 01 at leading inboard edge (red indicates optimized n)..... 257

Table C.4: Scaling law for total tire noise 258
Table C.5: Scaling law for tread pattern noise 261
Table C.6: Scaling law for non-tread pattern noise 264
Table E.1: Specifications of the test tires 280
Table F.1: OASPL of total noise on rough and smooth sections 293
Table F.2: OASPL of tread pattern noise on rough and smooth sections 296
Table F.3: OASPL of non-tread pattern noise on rough and smooth sections 298
Table F.4: Percent contribution from tread pattern noise component 299
Table G.1: Testing of slick tires (red arrow indicates rotation direction) 300

List of Abbreviations

Abbreviation	Stands For
2W	Two-Wheeler
AASHTO	American Association of State Highway and Transportation Officials
AC	Asphalt Concrete
Accel.	Acceleration
ACEA	European Automobile Manufacturers' Association
ALE	Arbitrary Lagrange-Eulerian Formulation/Method
AML	Auto Extruding Perfectly Matched Layer
AMOT	ANN Model of TPIN
AMPT	Asphalt Mixture Performance Tester
ANC	Active Noise Control
ANN	Artificial Neural Network
ANN Model of TPIN	Artificial Neural Network Model of Tire-Pavement Interaction Noise
ANSI	American National Standards Institute
AR	Auto-Rickshaw
ARC	Asphalt Rubber Concrete
ARD	Automatic Relevance Determination
ARFC	Asphalt Rubber Friction Course
ASA	Acoustical Society of America
ASTM	American Society for Testing and Materials
ATC	American Test Center
AVEC, Inc.	Acoustical and Vibrations Engineering Consultants
BASt	Federal Highway Research Institute of Germany
BEM	Boundary Element Method/Model
BP	Back-Propagation
BPF	Block Passing/Passage Frequency
BPN	British Pendulum Number
BSS	Blind Source Separation

Abbreviation	Stands For
BTT	Behind The Tire
C-GTRA	China Green Tyre Rating Assessment
CadnaA	Computer Aided Noise Abatement
CAE	Computer-Aided Engineering
CB	Coast-By
CBSWL	Coast-By Sound Power Level
CC	Cement Concrete
CDG	Conventional Diamond Grind
CDOT	Colorado Department of Transportation
CenTiRe	Center for Tire Research
CFD	Computational Fluid Dynamics
CLD	Constraint Layer Damping
CPB	Controlled Pass-By
CPCB	Central Pollution Control Board
CPI	Close-Proximity Sound Intensity
CPX	Close-Proximity Trailer
CRTN	Calculation of Road Traffic Noise
CTC	Cross-Talk Cancellation
CTIM	Continuous-Flow Traffic Time-Integrated Method
CTM	Circular Track Meter
CTWIST	Circumferential Tread Wear Imaging System
DAC	Dense Asphalt Concrete
DAQ	Data Acquisition System
DC	Direct Current (Steady-State)
DFT	Dynamic Friction Tester
DFT	Discrete Fourier Transform
DGA	Dense Graded Asphalt
DGAC	Dense-Graded Asphalt Concrete
DoT	Department of Transportation
DR	Laboratory Drum

Abbreviation	Stands For
e.g.	exempli gratia (for example)
E/H Vehicles	Electric and Hybrid Motor Vehicles
EBEA	Energy Boundary Element Analysis
EC	European Commission
ECE	Economic Commission for Europe
EEC	European Economic Community
EFEA	Energy Finite Element Analysis
END	Environmental Noise Directive
EPA	Environmental Protection Agency
EPA	United States Environmental Protection Agency
EPC	Enhanced Porosity Concrete
ESAL	Equivalent Single Axle Load
ESC	Electronic Stability Control
ESPI	Electronic Speckle Pattern Interferometry
ETRMA	European Tyre & Rubber Manufacturers' Association
ETRTO	European Tyre and Rim Technical Organisation
EU	European Union
F-GA	Fuzzy Genetic Arithmetic
FAAT	Far-field Acoustic Array Technology
FDOT	Florida Department of Transportation
FE	Finite Element
FEA	Finite Element Analysis
FEHRL	Forum of European National Highway Research Laboratories
FEM	Finite Element Method/Model
FFT	Fast Fourier Transform
FHWA	Federal Highway Administration
FM	Fineness Modulus
FMAC	Fiber-Modified Asphalt Concrete
FMBEM	Fast Multipole Boundary Element Method
FRF	Frequency Response Function

Abbreviation	Stands For
FSI	Fluid-Structure Interaction
FT	Fourier Transform
FW-H	Ffowcs-Williams and Hawkings Approach
FWD	Falling Weight Deflectometer
GA	Genetic Algorithms
GB	Guobiao (Chinese National Standards)
GM	General Motors Corporation
GTA	Graduate Teaching Assistant
GVW	Gross Vehicle Weight
HCV	Heavy Commercial Vehicle
HGV	Heavy Goods Vehicle
HMA	Hot Mix Asphalt
HPM	Highway Prediction Model
HyRoNE	Hybrid Rolling Noise Estimation
I-INCE	International Institute of Noise Control Engineering
i.e.	that is
I/UCRC	Industry/University Cooperative Research Centers
IAB	Industrial Advisory Board
IEC	International Electrotechnical Commission
IFEM	Infinite/Finite Element Method
IFRF	Inverse Frequency Response Function
IFSTTAR	French institute of science and technology for transport, spatial planning, development and networks
IRI	International Roughness Index
ISO	International Organization for Standardization
ISQDH	Institute for Safe, Quiet, and Durable Highways
IV	In Vehicle
JASO	Japanese Automotive Standards Organization
KTH	Royal Institute of Technology
LCCA	Life Cycle Cost Analysis

Abbreviation	Stands For
LCV	Light Commercial Vehicle
LD	Laboratory Drum
LDV	Laser-Doppler Vibrometer
LES	Large Eddy Simulation
LS	Least-Squares Analysis
LT	Light Truck
M-ALE	Modal-Arbitrary Lagrangian Eulerian
MATV	Modal Acoustic Transfer Vector
MCF	Multiple Coherence Filtering
MCMC	Monte Carlo Markov Chain
MEJ	Modular Expansion Joint
MFAH	Moving Frame Acoustic Holography
MI	Multiple Imputation
Mic	Microphone
MLE	Mixed Lagrangian-Eulerian Method
MLP	Multi-Layer Perceptron
MOE	Ministry of the Environment
MOGA	Multi-Objective Genetic Arithmetic
MPD	Mean Profile Depth
MPE	Mean Percentage Error
MTD	Mean Texture Depth
N&V	Noise and Vibration
NAAT	Near-field Acoustic Array Technology
NAH	Near-field Acoustic Holography
NCAT	National Center for Asphalt Technology
NCHRP	United States National Cooperative Highway Research Program
NF	Norme Française (French Standard)
NGCS	Next Generation Concrete Surface
NHTSA	National Highway Traffic Safety Administration
NPB with	Novel Pass-By with Novel Close Proximity

Abbreviation	Stands For
NCPX	
NPL	National Physical Laboratory
NSF	National Science Foundation
NTIS	National Technical Information Service
NTPN	Non-Tread Pattern Noise
NVH	Noise, Vibration, and Harshness
NZ	New Zealand
OASIL	Overall A-weighted Sound Intensity Level
OASPL	Overall A-weighted Sound Pressure Level
OBSI	On-Board Sound Intensity
OBSP	On-Board Sound Pressure
OGAC	Open-Graded Asphalt Concrete
OGPA	Open Graded Porous Asphalt
OLS	Ordinary Least-Squares
OPA	Operational Path Analysis
ORTF	On-resonance Force Transmissibility Factors
OSPL	Overall Sound Pressure Level
OTPA	Operational Transfer Path Analysis
PAH	Pass-by Acoustic Holography
PBN	Pass-By Noise
PCA	Principal Component Analysis
PCC	Portland Cement Concretes
PCI	Pavement Condition Index
PCL	Percentage Contact Length
PCR	Principal component regression
PERS	Poroelastic Road Surface
PI	Pressure Intensity Index
PIARC	Permanent International Association of Road Congresses
PMAC	Polymer-Modified Asphalt Concrete
PNB	Pass-by Noise Beamforming

Abbreviation	Stands For
PNCS	Pirelli Noise Cancelling System
PSD	Power Spectral Density
PWL	Sound Power Level
RAC	Rubberized Asphalt Concrete
RAC-G	Gap-graded Rubberized Asphalt Concrete
RAC-O	Open-graded Rubberized Asphalt Concrete
Re.	Reference
Ref.	Reference
REMELS	Reference Energy Mean Emission Levels
Resp.	Respectively
RMS	Root Mean Square
RODAS	ROad Design Acoustic Simulation
RPROP	Resilient Back-Propagation
RPS	Revolution Per Second
SAE	Society of Automotive Engineers
SEA	Statistical Energy Analysis
SI	Sound Intensity
SIF	Sound Intensity Field
SIL	Sound Intensity Level
SIP	Statistical Isolated Pass-by
SMA	Stone Mastic Asphalt
SN	Skid Number
SNR	Signal to Noise Ratio
SP	Sound Pressure
SPB	Statistical Pass-By
SPB/TA	Statistical Pass-By and Time-Averaged Wayside
SPBI	Statistical Pass-By Index
SPL	Sound Pressure Level
SR	Surface Rating
SRTT	Standard Reference Test Tire

Abbreviation	Stands For
ST	Silence Tuned
STFT	Short Term Fourier Transform
STSF	Spatial Transformation of Sound Fields
SWL	Sound Power Level
TA	Temporal Array
TCB	Trailer Coast-By
TCM	Tire Cavity Microphone
TCSMM	Tire Cavity Sound Measurement Method
TD	Texture Depth
TI	Texture Index
TIM	Two-scale Iterative Method
TNA	Traffic Noise Auralization
TNM	Traffic Noise Model
TNS	Traffic Noise Synthesizer
TPIN	Tire-Pavement Interaction Noise
TPMS	Tire Pressure Monitoring System
TPN	Tread Pattern Noise
TPTA	Tire-Pavement Test Apparatus
TRIAS	Tyre Road Interaction Acoustic Simulation
TRN	Tire/Road Noise
TTN	Total Tire Noise
TVM	Tire Vibration Measurements
TXDOT	Texas Department of Transportation
TYDAS	TYre Design Acoustic Simulation
UK	United Kingdom
UN	United Nations
US	United States
USA	United States of America
UTQG	Uniform Tire Quality Grading standard
VMA	Voids in the Mineral Aggregate

Abbreviation	Stands For
VT	Virginia Tech (Virginia Polytechnic Institute and State University)
VTI	Swedish National Road and Transport Research Institute
WBG	World Bank Group
WFE	Wave Finite Element
WFEM	Waveguide Finite Element Method
WHO	World Health Organization
WP-NERV	Working Party on Noise Emissions of Road Vehicles
WSDOT	Washington State Department of Transportation
WT	Wavelet Transform

Nomenclature

Some nomenclature is described in List of Abbreviations.

1 Introduction

This chapter introduces the motivation of the present study, the objectives and contributions of the project, and the organization of this dissertation.

1.1 Motivation

"Environmental pollution" might suggest, to many people, air pollution, water pollution, or similar concepts. But another pollution, which is not quite visible but encountered by more and more cities, is noise pollution. According to many opinion polls traffic noise is considered to be the number one noise nuisance affecting millions of people. Among the different sources of traffic noise (road vehicles, railways and airplanes) the sound generated by cars is most important because there are millions of them and because they are almost ubiquitous (Heckl, 1986 [1]).

Noise barriers that are up to 6 meters tall have to be built to shield the neighborhoods from road noise for hundreds of meters along busy highways (Wayson, 2014 [2]). However, noise barriers have many disadvantages: (1) noise barriers have a very high initial cost ($1.3-3 million per mile [3], two or three times as expensive as the 2-lane pavement); (2) locations such as hillsides and intersections are not suitable for building noise barriers; (3) most noise barriers block the view, which does not look beautiful; (4) barrier on one side will increase reflection to the other side (Kohler, 2010 [4]). Therefore, reducing the noise at the source is more of a viable solution. For the noise control, it's usually better to treat the source (vehicle noise) than the path (noise barrier).

It is generally accepted that there are five major sources of noise for a running vehicle: engine (power train), intake system, exhaust system, aerodynamic turbulence (wind) and tire-pavement interaction (Braun et al., 2013 [5]). These noise sources contribute differently for different speed (Rasmussen et al., 2007 [6]). Sandberg (2001) [7] indicated that tire-pavement interaction noise (TPIN) dominates for passenger vehicles above 40 km/h and 70 km/h for trucks. That is to say, at normal highway speed, tire-pavement interaction noise is the most important noise contributor (up to 80-90% at speed of over 70-80 km/h for

passenger cars [8]).

The motivation for reducing tire-pavement interaction noise is multiple and different across different countries. One is to pass the legal approval for exterior noise level, especially in Europe (Sandberg, 2001 [9]); one is to reduce the annoyance level in car interior space and increase passenger comfort (Harrison, 2004 [10]); one is to boycott foreign tire imports (Chen, 2014 [11]). As electric and hybrid motor vehicles (E/H vehicles) gained increasing interest, there might be a significant reduction (3~4 dB) of traffic noise emissions (Jabben et al., 2012 [12]), making TPIN more dominant. On the other hand, concerns arise that E/H vehicles with quiet pavements might pose a severe threat to the safety of vulnerable road users due to poor vehicle detection ability (Mendonça, 2013 [13]). Some regulations start to focus on limiting the minimum sound of electric vehicles, e.g., NHTSA requires all hybrid and electric light vehicles with four wheels and a gross vehicle weight rating of 10,000 pounds or less make audible noise when traveling in reverse or forward at speeds up to 30 km/h until 2019 (NHTSA, 2016 [14]–[16]). However, Sandberg (2013) [17] pointed out that it is currently far more justified to work towards reducing the noise emission of the noisiest vehicles than adding noise to the quiet ones. In addition, the electric and hybrid vehicles are very quiet only at low speed and still noisy at higher speed when tire noise is dominant. Without the masking of engine noise, tire noise can be more easily perceived (high frequencies) inside the vehicle.

In tire/automotive industry, NVH (noise, vibration & harshness) is considered at the very first phase of design, because it will be much higher cost at later phase, e.g., after prototype. Therefore, a model is needed to predict the tire noise based on the tread pattern and tire structure before prototype. However, no such validated model providing sufficient accuracy can be found from literature. In addition, in order to reduce the TPIN or limit it within a certain level range, its physical mechanisms and influencing parameters need to be investigated. However, due to the complexity of TPIN, none of the current models are able to either fully explain the mechanisms, or accurately predict TPIN based on the influencing parameters.

1.2 Objectives

The main objectives of the present study are:

(1) To develop an artificial neural network (ANN) model to predict the tire-pavement interaction noise (TPIN);

(2) To validate the model using real data from field testing;

(3) To use the model to provide insight in the noise generation mechanisms.

1.3 Contributions

The main contributions of the present study are:

(1) An extensive literature review was conducted. Over 2000 references related to TPIN were exhaustively collected; around 1000 selected references were reviewed. The existing models, noise generation mechanisms, influencing parameters, measurement techniques were documented.

(2) A large number of different tires (forty-two) with different tread patterns and of different sizes were tested on a non-porous asphalt pavement at different speeds. Some tires were also tested on a different pavement. Noise data at different tire inflation pressure were also collected for some tires. This database is one of the most extensive and complete in the open literature.

(3) An ANN Model of TPIN (AMOT) was developed and validated for tires of different sizes with typical tread patterns at normal highway speed on a non-porous asphalt pavement. The novelty of this model includes: (a) it is the first model to predict tread pattern-related noise and non-tread pattern-related noise, separately; (b) it accounts for tire size; (c) it is able to predict tire noise in narrowband.

1.4 Organization

This dissertation is organized in seven chapters with a number of appendices.

In Chapter 1, an introduction of the present study is provided.

In Chapter 2, a comprehensive literature survey is presented on four major topics related to TPIN: measurement techniques, physical mechanisms, influencing parameters, and existing models.

In Chapter 3, the experiments for collecting tire noise data are firstly discussed. Secondly, the digitization and parameterization of tread pattern are demonstrated. Thirdly, the tire noise data are analyzed, including breaking down the total noise into two noise components (tread pattern-related and non-tread pattern-related). Lastly, the correlation between the tread pattern parameters and tire noise are conducted.

In Chapter 4, the fundamentals of artificial neural network (ANN) are briefly introduced. The existing ANN models related to tire noise are then presented. In the end, the proposed ANN model for TPIN in the present study is described.

In Chapter 5, the development and validation of the first part of ANN model for TPIN, i.e., ANN_1 on tread pattern noise, is investigated. The ANN_1 with optimized configurations are presented, including the definition of input and output, the ANN structure, and the evaluation of the model accuracy. Some other ANN configurations are also investigated.

In Chapter 6, the development and validation of the second part of ANN model for TPIN, i.e., ANN_2 on non-tread pattern noise, is investigated. The effects of tire size, tread rubber hardness, and vehicle speed on the non-tread pattern noise are discussed.

In Chapter 7, the complete tire-pavement interaction noise (TPIN) model using artificial neural network (ANN) is presented. The complete model is named as ANN Model of TPIN (AMOT), including the ANN_1 sub-model for tread pattern noise, ANN_2 sub-model for non-tread pattern noise, and some other necessary sub-models.

In Chapter 8, the conclusions from this study and recommendations for future work are presented.

In Appendices, the relevant results of the present work are presented, including the Tread Pattern Analysis, Results of AMOT (Train and Validation Set), Effect of Speed, Effect of Tire Inflation Pressure, Tones due to Pavement Distress, Rough and Smooth Pavement,

Characteristics of TPIN from Slick Tire, and A Literature Review of Tire-Pavement Interaction Noise. It should be noted that Appendices D, E, F, and G are presented only for the purpose of completeness. However, not all data were used in the AMOT modeling.

2 Literature Review on TPIN

The term “Tire-Pavement Interaction Noise” was first found as early as in 1976 (Thrasher et al., 1976 [18] and Miller and Thrasher, 1976 [19]), also later in 1986 (Pottinger et al., 1986 [20]) and 1998 (Donavan et al., 1998 [21]). The acronym TPIN was first found in 2008 (Khazanovich and Izevbekhai, 2008 [22]), later also in 2013 (Syamkumar et al., 2013 [23]). Tire-Pavement Interaction Noise (TPIN) is also known as tire-road interaction noise, tire-pavement noise, tire road noise, or tire noise. Tire-pavement interaction noise is defined as the noise emitted from a rolling tire as a result of the interaction between the tire and road surface (Sandberg and Ejsmont, 2002 [24]).

Modern TPIN research started around mid-1970’s as engine became less noisy and aerodynamic design of vehicle body were optimized. Sandberg and Ejsmont (1995) [25] have collected a computerized bibliography termed "TRN BIBLIOGRAPHY" totaling 1280 documents as of August 1994. However, most of these references were from special conference proceedings, industrial/government reports rather than archival journals. The author of this dissertation also collected over 2000 relevant references and reviewed over half of them. A large number of literatures have advanced the modeling of tire-pavement interaction noise, as displayed in Figure 2.1. However, up to date TPIN is still in mystery and difficult to describe or predict accurately, and the findings still seem fragmented probably due to the many complex generation mechanisms. Although a tire seems to be a simple structure at first glance, the combination of its geometrical properties and multi-layer composite structure leads to highly complex vibrational behavior (Sabiniarz and Kropp, 2010 [26]).

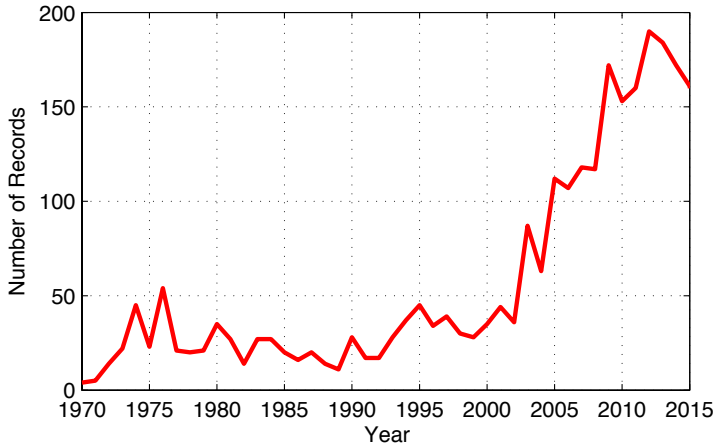

Figure 2.1: Literature records count (generated via Engineering Village on Aug 12, 2016, search query for "tire" & "noise" in subject/title/abstract from databases of Compendex, Inspec & NTIS)

In this chapter, a brief literature survey is presented on four major topics related to TPIN: measurement techniques, physical mechanisms, influencing parameters, and existing models. The comprehensive and complete literature review is attached in Appendix H: A Literature Review of Tire-Pavement Interaction Noise.

2.1 Measurement Techniques

There are a number of different techniques to measure tire-pavement interaction noise (TPIN). Each method has advantages and disadvantages, and is applied differently under different situations. These methods can be divided into different categories according to different criterion, as listed in Table 2.1.

Sound pressure is the quantity utilized by most measurement techniques, but it is dependent of some other external factors for a given tire-pavement combinations, such as measurement position. Sound power is able to deal with this problem perfectly. Sound intensity has been more and more widely used, especially in USA. However, some researchers claimed that they require a noise source emitting stationary noise, which is not the case of the tire pavement interaction noise (Campillo-Davo et al., 2013 [27]).

Far-field noise is also called Pass-by Noise (PBN) that corresponds to several measurement techniques, such as Statistical Pass-By (SPB), Controlled Pass-By (CPB),

Coast-By (CB) and such.

Table 2.1: Category of TPIN measurement techniques

Criterion	Measured Parameter	Sound Field	Acoustic Equipment (Instrumentation)	Test Environment	Measured Noise Source	Standard
Category	Sound pressure, sound intensity, sound power	Near-field, far-field	Microphone, intensity probe, microphone array	Roadside, on-board, lab	TPIN, vehicle, traffic	Standardized, non-standardized

The instrumentation for vehicle noise and vibration measurements includes microphones, accelerometers, Laser scanning vibrometry, force gauges, or load cells. However, when it comes to acoustical noise, it basically refers to only one sensor: microphone. It should be noted that most of the data analysis in the current literature are focused on overall sound levels, octave band levels or 1/3 octave band levels while few of them are in narrowband.

Although the measurement techniques vary, the digital processing methods are almost the same. The first step is to acquire a certain period of sound level data. The second step is transforming the time domain data to frequency domain data using Fast Fourier Transform (FFT) or Short Term Fourier Transform (STFT). Conventional Fourier Transform (FT) is good at analyzing frequency domain signal but loses time information. Short Term Fourier Transform (STFT) is able to analyze the frequency domain in local time range (Zakelj, 2000 [28]), but is not able to analyze variety of time-varying signals [29] (He et al., 2011). Another transform is Wavelet Transform (WT), which does a better job in handling non-stationary random signal and becomes popular recently (He et al., 2011 [30]; He et al., 2011 [29]; SungWook et al., 2012 [31]; Chen et al., 2013 [32]).

In this section, the measurement techniques on TPIN were reviewed and divided into three categories based on the test environment: roadside, on-board and lab.

2.1.1 Roadside Measurement

The roadside measurement technique measures the far-field noise of the moving vehicle at

the roadside with the measurement equipment stationary.

The roadside measurement techniques reviewed are summarized in Table 2.2 with examples of experimental setup displayed in Figure 2.2. Most of the techniques have corresponding standards where typically the maximum sound pressure level ($L_{p\max}$) is measured as the vehicle passes by. The advantage is the measurement equipment is usually just one microphone, which is very simple. However, the TPIN usually cannot be isolated from the total vehicle noise or traffic noise.

Table 2.2: Summary of roadside measurement techniques

No.	Method	Acronym	Current Standard[2]	First Version[1,2]	Equipment	Measured Parameter	Main Noise Source[3]	Category	Advantage[4]	Disadvantage[4]	References
1	Statistical Pass-By	SPB	ISO 11819-1 [33], ISO 11819-4 [34]	ISO (1997) [33], ISO (2013) [34]	1 Mic	$L_{p\max}$	Traffic	Roadside Far-field	Minimal equipment No traffic control Good to evaluate pavements at receiver	Time-consuming Weather sensitive Noise source isolation not possible	[35]–[38]
2	Controlled Pass-By	CPB	NF S S1 119-2 [39], ISO 362 [40], [41]	NF (1999) [39], ISO (1981) [42], ISO (1985) [43]	1 Mic	$L_{p\max}$	Vehicle	Roadside Far-field	Flexible and repeatable Less time needed	Traffic control required TPIN not isolated	[44], [45]
3	Coast-By	CB	ISO 13325 [46]	ISO (2003) [46]	1 Mic	$L_{p\max}$	All tires	Roadside Far-field	TPIN isolated	Speed not constant	[24], [47]
4	Statistical Pass-By and Time-Averaged Wayside	SPB/TA	N/A	Hanson and James (2004) [48]	1-3 Mic's	L_{peq}	Traffic	Roadside Far-field	Similar to CTIM Not standardized	Similar to SPB TPIN not isolated	[37], [48], [49]
5	Statistical Isolated Pass-by	SIP	AASHTO TP-98 [50]	AASHTO (2012) [51]	1 Mic or 2	$L_{p\max}$	Vehicle	Roadside Far-field	Similar to SPB One vehicle isolated	Similar to SPB TPIN not isolated	[52]
6	Continuous-Flow Traffic Time-Integrated Method	CTIM	AASHTO TP-99 [53]	AASHTO (2012) [54]	1 Mic	L_{peq}	Traffic	Roadside Far-field	Similar to SPB	Similar to SPB/TA	[55]
7	Coast-By Sound Power Level	CBSWL	N/A	Campillo-Davo et al. (2013) [27]	10 Mic's	L_W	All tires	Roadside Far-field	Similar to NCPX Easy procedure	Not capable of isolating TPIN from one tire	[27]

[1]"First Version" refers to the first standard if the method has been standardized; otherwise it refers to the first measurement attempt.
[2]Some of the references in "First Version" are the same as in "Current Standard", except the published year.
[3]"Main Noise Source" refers to where the measured noise mainly comes from.
"One tire" means from the specific tested tire on which the testing equipment is mounted;
"All tires" means from all the tires (usually four) of the tested vehicle or trailer;
"Vehicle" means from the tested vehicle (TPIN, powertrain, air intake and outlet, and aerodynamics noise);
"Traffic" means from all the vehicles on the road.
[4]The advantage and disadvantage are in terms of TPIN investigation.
*The notes above also apply to Table 2.3 and Table 2.4.

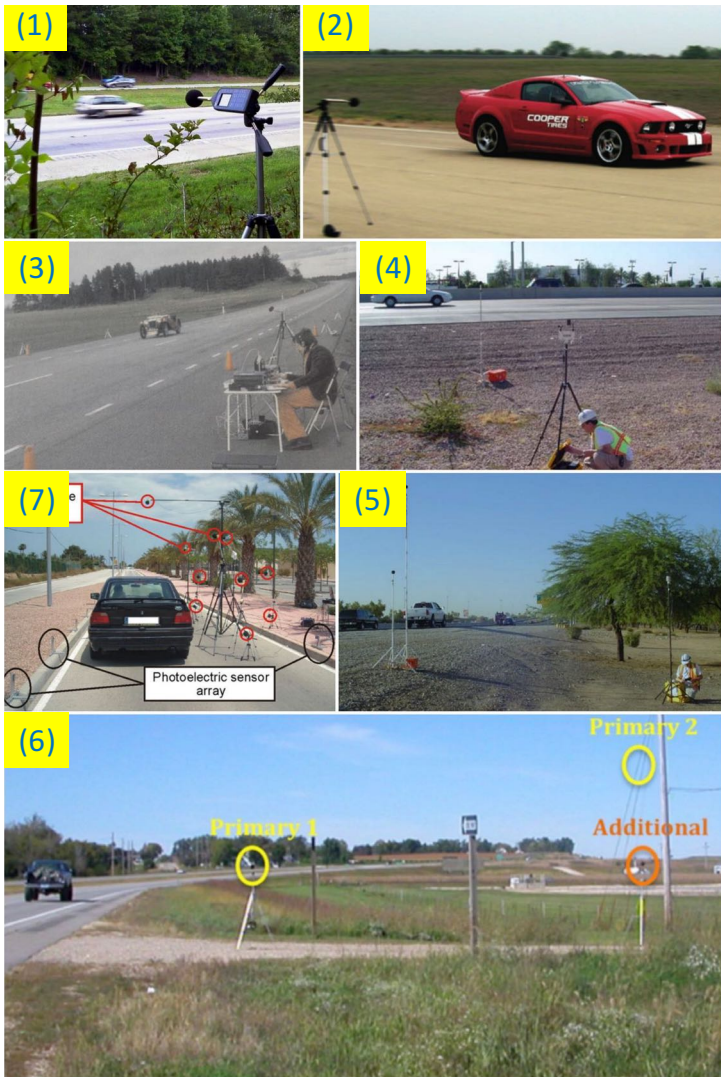

Figure 2.2: Experimental setup of roadside measurement techniques

(1) Statistical Pass-by (SPB) (Source from Wang et al., 2011 [36], Figure 2.1)
(2) Controlled Pass-By (CPB) (Source from Copeland and Wilhoit, 2012 [44], Figure 1)
(3) Coast-By (CB) (Source from Sandberg and Ejsmont, 2002 [24], Fig. 14.3)
(4) Statistical Pass-By and Time-Averaged Wayside (SPB/TA) (Source from Bernhard and Wayson, 2005 [49], Figure 6.4)
(5) Statistical Isolated Pass-by (SIP) (Source from Lodico et al., 2012 [52], Figure 1)
(6) Continuous-Flow Traffic Time-Integrated Method (CTIM) (Source from Rochat et al., 2012 [55], Figure 2)
(7) Coast-By Sound Power Level (CBSWL) (Source from Campillo-Davo et al., 2013 [27], Figure 13)

2.1.2 On-board Measurement

The on-board technique measures the near-field tire noise with the measurement equipment fixed on the running vehicle.

The on-board measurement techniques reviewed are summarized in Table 2.3 with examples of experimental setup displayed in Figure 2.3. This type of measurement techniques has emerged since 1972, but few of them have been standardized, probably because the equipment used is complex and difficult to standardize, especially when trailer is needed. The advantage is, the noise components except the tire noise are basically excluded or can be ignored.

Table 2.3: Summary of on-board measurement techniques

No.	Method	Acronym	Current Standard	First Version	Equipment	Measured Parameter	Main Noise Source	Category	Advantage	Disadvantage	References
1	Behind The Tire	BTT	N/A	Siddon (1972) [56]	1 Mic	L_p	One tire	On-board Near-field	First on-board approach Easy	Bad correlation with CPB Inaccurate	[56]–[64]
2	Trailer Coast-By	TCB	SAE J57 [65], ISO 13325 [46]	SAE (1977) [66], ISO (2003) [46]	1 Mic	$L_{p\max}$	All tires on trailer	Trailer Far-field	Similar to CB	Expensive Towing vehicle noise	[67], [68]
3	On-Board Sound Pressure	OBSP	N/A	Osman and May (1980) [69]	1-4 Mic's	L_p	One tire	On-board Near-field	TPIN isolated	Similar to BTT	[69]–[80]
4	Close Proximity Sound Intensity	CPI	N/A	Donavan and Oswald (1980) [81]	1 Probe	L_I	One tire	On-board Near-field	Same as CPX Trailer not necessary	Real vehicle but not account for all types	[49], [82], [83]
5	Sound Intensity Field	SIF	N/A	Donavan and Oswald (1981) [84]	>=1 Probes	L_I	One tire	On-board Sound field	Capable of locating sound source	Time-consuming Asynchronous tests	[81], [84]–[86]
6	Tire Cavity Microphone	TCM	N/A	Bschorr et al. (1981) [87]	1 Mic	L_p	One tire	Inside tire Near-field	Not sensitive to background noise	Bad/complex correlation with external TPIN	[88]–[90]
7	Close-Proximity Trailer	CPX	ISO 11819-2 [91]	ISO (2000) [92]	>=2 Mic's 1 Trailer	$L_{p\mathrm{avg}}$	One tire	Trailer Near-field	Less sensitive to weather/traffic	Trailer cost/space Not typical/real vehicle	[24], [49], [70], [93], [94]
8	In Vehicle	IV	GB/T 18697 [95]	GB (2002) [95]	1-4 Mic's	$L_{p\mathrm{avg}}$	Vehicle	Interior Near-field	Easiest way	Worst correlation with TPIN	[6], [96]
9	On-Board Sound Intensity	OBSI	AASHTO TP-76 [97], ASTM WK26025 [98]	AASHTO (2008) [99], ASTM (2009) [98]	1 or 2 Probes	L_I	One tire	On-board Near-field	Same as CPI More accurate	Device protrusion out of vehicle subject to law	[4], [22], [36], [100]–[112]

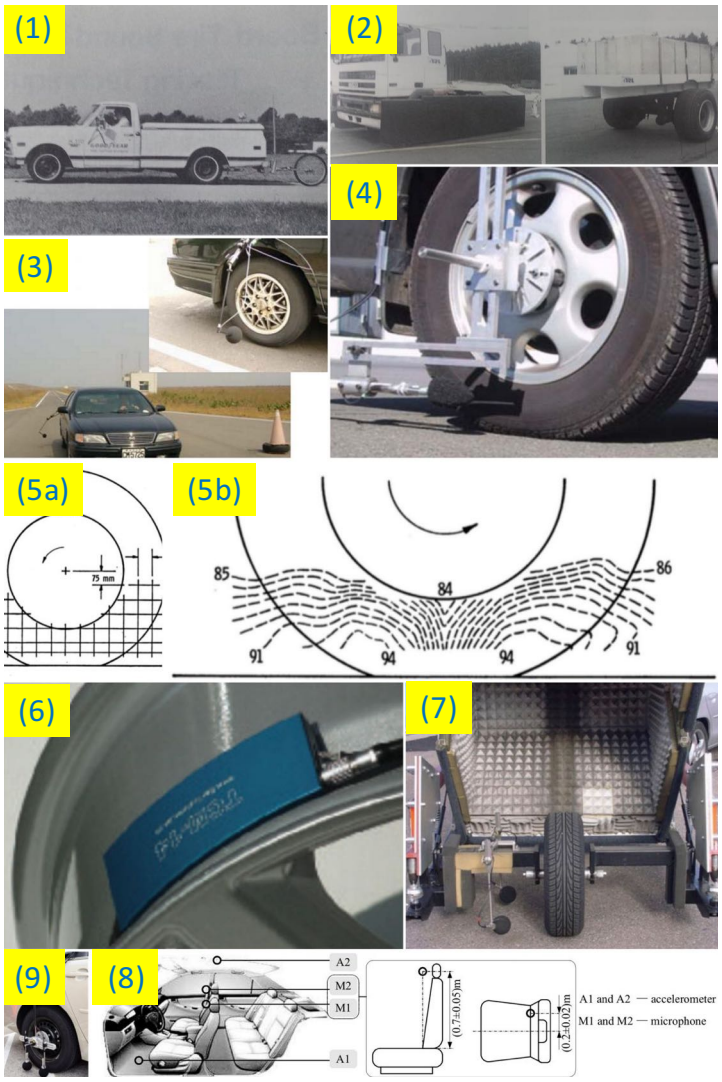

Figure 2.3: Experimental setup of on-board measurement techniques

(1) Behind The Tire (BTT) (Source from Landers et al., 1977 [60], Figure 1)
(2) Trailer Coast-By (TCB) (Source from Sandberg and Ejsmont, 2002 [24], Fig. 16.30)
(3) On-Board Sound Pressure (OBSP) (Source from Chuang et al., 2005 [80], Figure 4)
(4) Close-Proximity Sound Intensity (CPI) (Source from Bernhard and Wayson, 2005 [49], Figure 6.6)
(5) Sound Intensity Field (SIF) (Source from Donavan and Oswald, 1981 [84], Figure 11 and Figure 12)
(6) Tire Cavity Microphone (TCM) (Source from Bennetts and Crookes, 2013 [89], Figure 1)
(7) Close-Proximity Trailer (CPX) (Source from Wang et al., 2011 [36], Figure 2.2)
(8) In Vehicle (IV) (Source from He et al., 2011 [29], Figure 3)
(9) On-Board Sound Intensity (OBSI) (Source from Mogrovejo et al., 2014 [113], Figure 1)

2.1.3 Lab Measurement

The roadside and on-board measurement techniques are intended for field test or road test. As far as the more sophisticated and accurate measurement, lab environment is usually

necessary, or the outdoor test environment needs to be carefully controlled.

The lab measurement techniques reviewed are summarized in Table 2.4 with examples of experimental setup displayed in Figure 2.4. The measurement equipment is various and flexible, such that no standards have been found except for laboratory drum method. However, multiple sound parameters are possible to be measured, including the sound field. In addition, the effect of environmental parameters, such as air temperature and wind speed, can be greatly reduced if the test is conducted in the lab.

Table 2.4: Summary of lab measurement techniques

No.	Method	Acronym	Current Standard	First Version	Equipment	Measured Parameter	Main Noise Source	Category	Advantage	Disadvantage	References
1	Tire Vibration Measurements	TVM	N/A	Reiter and Eberhardt (1974) [114]	LDV or accelerometer	Vibration velocity	One tire	N/A	Analysis of TPIN mechanisms	Interpretation of structure-borne TPIN only	[115]
2	Laboratory Drum	DR	JASO C606-81 [116]	JASO (1981) [116]	Various	Various	One tire	Lab Near/Far-field	Precise control of parameters	Not real pavements	[6], [115], [117]–[124]
3	Near-field Acoustic Array Technology	NAAT	N/A	Ginn (1990) [125]	Mic array	Typically, $L_{p\mathrm{avg}}$	One tire	Lab/Trailer Near-field	Capable of detecting TPIN source	Expensive No correlation to CPB reported	[125]–[132]
4	Novel Pass-By with Novel Close Proximity	NPB with NCPX	N/A	Cho and Mun (2008) [133]	5 Mic's 1 Surface mic	$L_{p\mathrm{max}}$, $L_{p\mathrm{avg}}$, L_W	One tire	On-board/roadside Near/far-field	Sound power is independent of environment	Complex procedure Correction factor	[133], [134]
5	Far-field Acoustic Array Technology	FAAT	N/A	Fonseca and Gerges (2010) [135]	Mic array	$L_{p\mathrm{max}}$	Vehicle	Roadside Far/sound field	Capable of distinguishing vehicle noise sources	Doppler effect limitation	[135]–[139]
6	Traffic Noise Auralization	TNA	N/A	Maillard and Jagla (2012) [140]	Auralization equipment	L_p	Traffic	Virtual sound	Capable of non-stationary traffic evaluation	TPIN not isolated	[140]

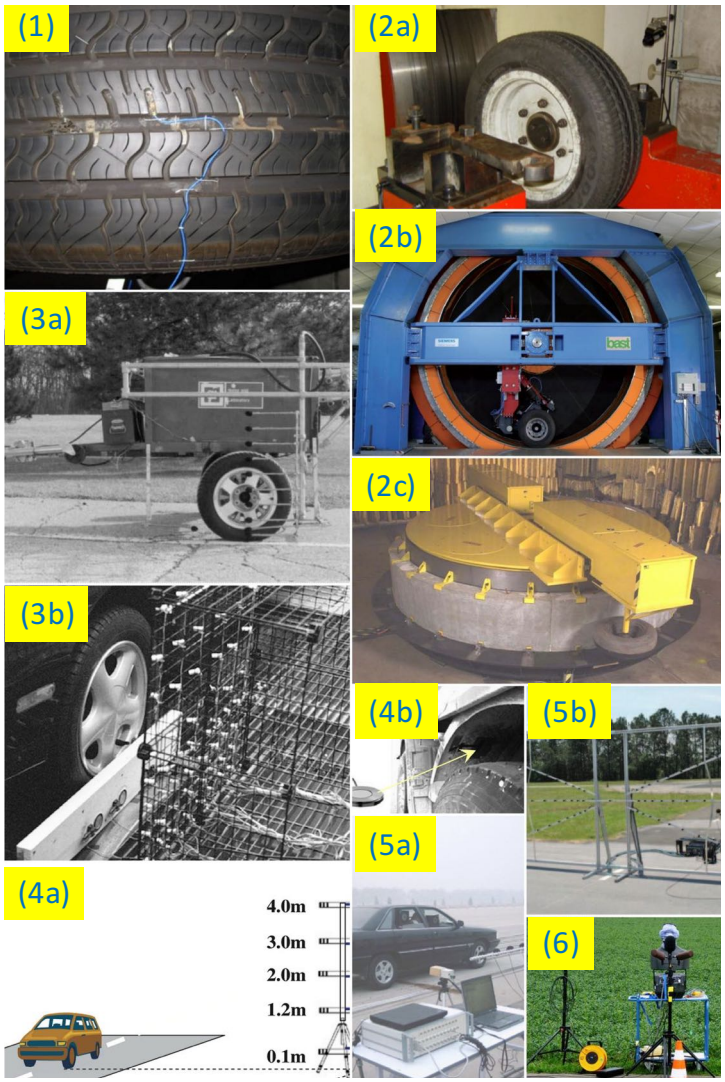

Figure 2.4: Experimental setup of roadside measurement techniques

(1) Tire Vibration Measurements (TVM) (Source from Dare, 2012 [115], Figure 3.11)
(2a) Laboratory Drum (DR) Outer Rotating Drum (Source from Tong et al., 2014 [141], Figure 5)
(2b) Laboratory Drum (DR) Inner Rotating Drum (Source from BASt website, [142])
(2c) Laboratory Drum (DR) Outer Stationary Drum (Source from Bernhard and Wayson, 2005 [49], Figure 6.9)
(3a) Near-field Acoustic Array Technology (NAAT) Trailer (Source from Ruhala and Burroughs, 1999 [126], Figure 1)
(3b) Near-field Acoustic Array Technology (NAAT) Lab Drum (Source from Dumbacher et al., 1995 [127], Figure 9)
(4) Novel Pass-By (NPB) with Novel Close Proximity (NCPX) (Source from Cho and Mun, 2008 [133], Figure 1 and Figure 3)
(5a) Far-field Acoustic Array Technology (FAAT) Pass-by Acoustic Holography (PAH) (Source from Yang et al., 2011 [136], Figure 5)
(5b) Far-field Acoustic Array Technology (FAAT) Pass-by Noise Beamforming (PNB) (Source from Zavala et al., 2013 [137], Figure 9)
(6) Traffic Noise Auralization (TNA) (Source from Maillard and Jagla, 2012 [140], Figure 2)

2.1.4 Summary

The measurement techniques on TPIN have evolved from simple overall sound pressure

level test, to the more accurate on-board sound intensity test, then to the sound field holography in the lab. Each technique has advantages and disadvantages. The roadside measurement is very easy, but not accurate or informative; the lab measurement is very flexible and inspiring, but usually unaffordable in equipment and sometimes fails to represent the actual driving conditions on the road; the on-board measurement is intermediate between the above two. In summary, the selection of the measurement technique should be based on the equipment available, measurement goals, and test environment. The measurement technique selected in the project for this dissertation is on-board sound intensity (OBSI).

2.2 Physical Mechanisms

Tire-pavement interaction occurs under fairly harsh and complex conditions, inherently making noise mechanisms very difficult to identify. Numerous mechanisms take place simultaneously, to varying degrees, depending on specific tire-pavement combination (Rasmussen et al., 2007 [1]). In this section, these physical mechanisms are divided into three categories: generation mechanisms, amplification mechanisms and attenuation mechanisms.

Different mechanisms take place at different tire components, all as noise sources contributing to the total tire-pavement interaction noise (TPIN). A summary of dominant frequencies for different TPIN components is listed in Table 2.5.

Table 2.5: Dominant frequencies for different TPIN components

	Dominant Frequency [Hz]	References
Leading Edge of Contact Patch	500-2000	[131], [143]
Trailing Edge of Contact Patch	500-2000	[143]–[145]
Tire Side Wall	500-1000	[132], [146]
Rim	200-400	[147]
Tire/Rim Assembly	220-280	[148]
Wheel Housing	500-600	[149]
Interior	250	[150], [151]

It should be noted that even though a large body of literature has attempted to uncover and distinguish these mechanisms since mid 1970's (Reiter and Eberhardt, 1974 [152]; Bergmann, 1980 [153]; Plotkin et al., 1980 [154]), they are by no means clear-cut. Too many speculations

still exist and never reach an agreement. In addition, the mechanisms themselves may have changed over time due to changes in tire and pavement technology (Dare, 2012 [115]). However, all the possible mechanisms are presented below to the best knowledge of the present author. A summary table could be found in Table 2.6 at the end.

2.2.1 Generation Mechanisms

Generation mechanisms are fundamental mechanisms that make sound and explain where sound begins. Sound pressure maps (a damped progressive wave field) indicate that TPIN mainly generates in the vicinity of the applied force on the contact patch (Lee et al., 2000 [151]).

The noise generated includes two types: structure-borne noise and airborne noise [155]. The former corresponds to impact mechanism and adhesion mechanism; the latter corresponds to air displacement mechanism. The structure-borne mechanism includes impact mechanism (tread impact, pavement texture impact), and adhesion mechanism (stick/slip, stick/snap); the airborne mechanism includes air pumping, and air turbulence. The illustrations of the generation mechanisms are shown in Figure 2.5.

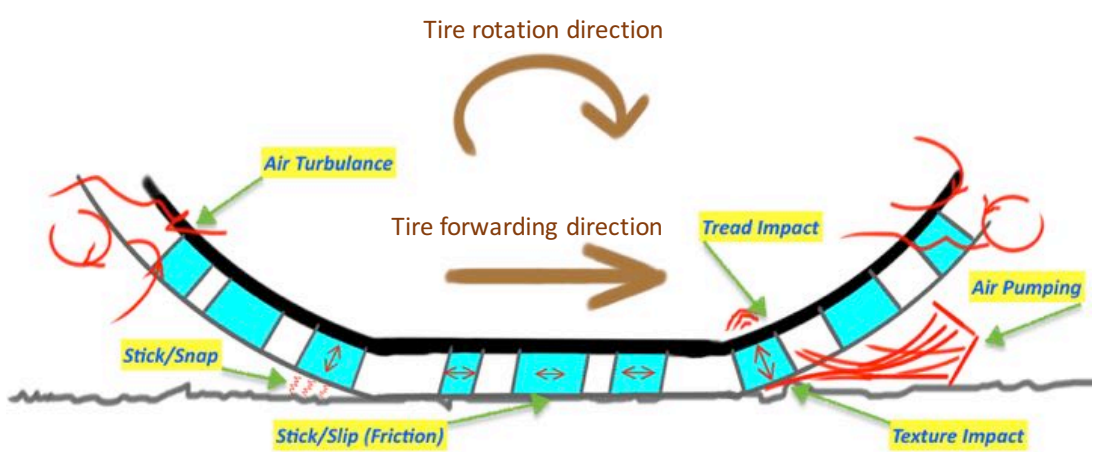

Figure 2.5: Illustration of generation mechanisms

2.2.2 Amplification Mechanisms

The mechanisms in this subsection amplify the sound produced by the above generation

mechanisms, making TPIN even louder. The amplification mechanisms are mostly based on resonance (like many musical instruments [6]), so different mechanisms will play different roles at different frequencies, as shown in Table 2.6.

The amplification mechanisms are no less simple than generation mechanisms and are influenced by different parameters to various degrees. As a result, to reduce the TPIN that is heard, not only should the generation be restrained, but also the amplification should be avoided, especially at those frequencies sound is amplified the most (Rasmussen et al., 2007 [1]). Amplification mechanisms include tire resonances, air resonances and horn effect mechanisms. The illustrations of the amplification mechanisms are shown in Figure 2.6.

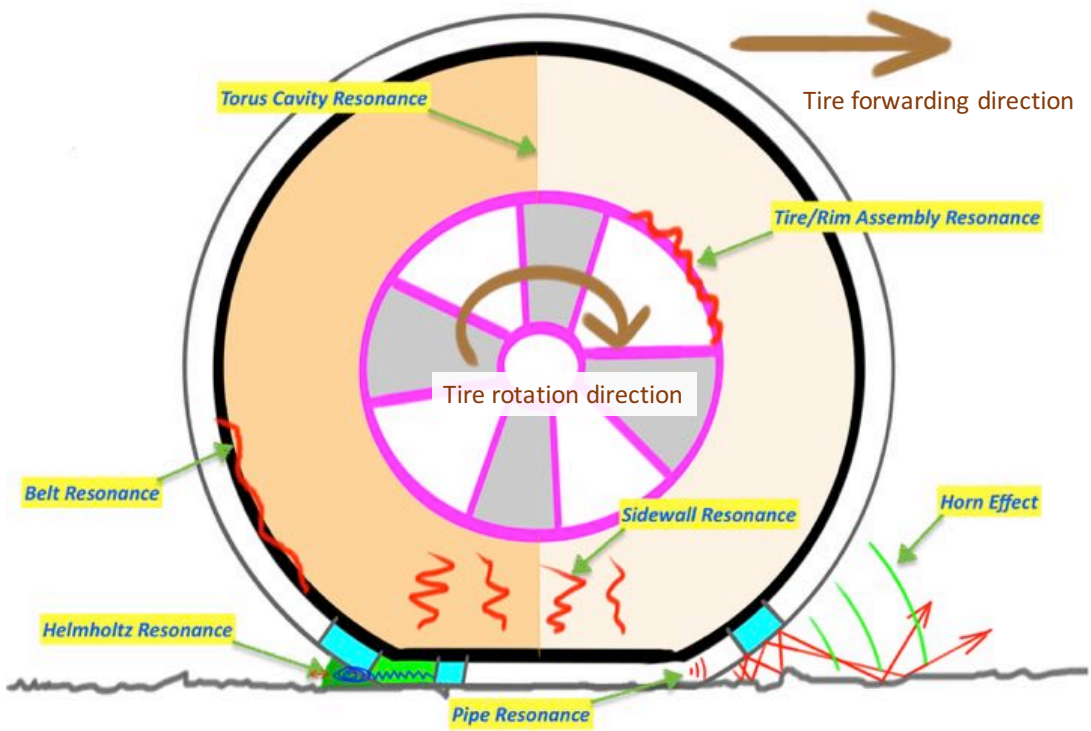

Figure 2.6: Illustration of amplification mechanisms

2.2.3 Attenuation Mechanisms

The sound must travel from the tire to the receiver or measurement device after it has been generated and amplified. During the propagation, attenuation or reduction mechanisms occur

[115], such as car body interferences (Sakamoto et al., 1999 [156]; Anfosso-Lédée, 2004 [157]), propagation over pavement (Klein and Hamet, 2007 [158]), and atmospheric conditions (wind [159] and temperature [160], [161]).

Most of those mechanisms are much more important for far field measurements such as pass-by tests than near field measurements such as CPX or OBSI. However, there are two major attenuation mechanisms that are also very important for near field sound, i.e., pavement absorption (acoustical impedance) and vibration transfer (mechanical impedance). The illustrations of the attenuation mechanisms are shown in Figure 2.7.

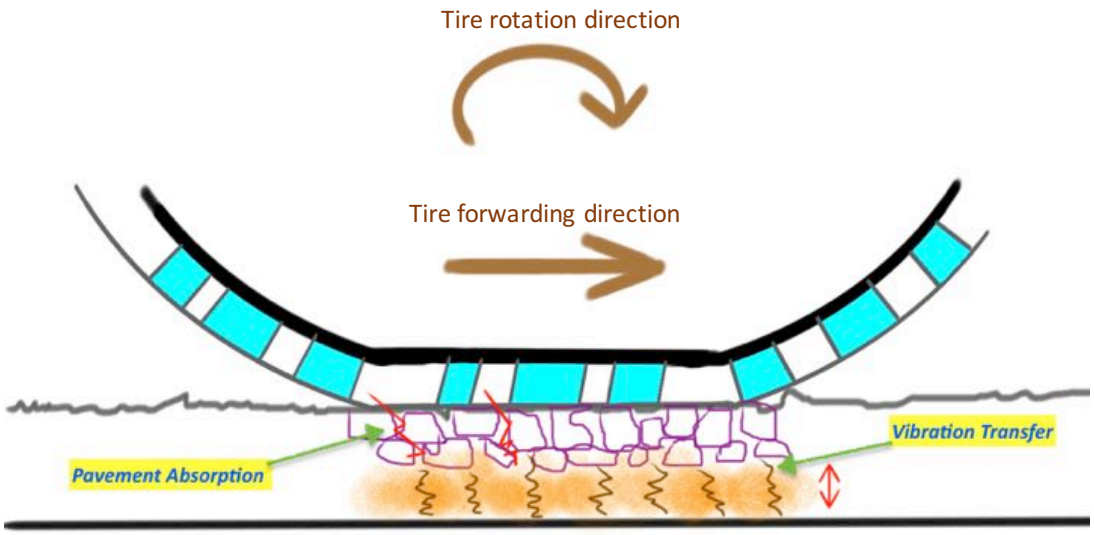

Figure 2.7: Illustration of attenuation mechanisms

2.2.4 Summary

A summary of TPIN mechanisms of generation, amplification and attenuation is listed in Table 2.6. The earliest reference found for the investigation of each mechanism is included. The dominant frequency and potential noise influence are generally for near field TPIN from lightweight passenger cars in the exterior at normal highway speed. Each mechanism also includes the parameters that have influence, and an analogous example that has similar physics.

Table 2.6: Tire-Pavement Interaction Noise (TPIN) Mechanisms

				Earliest Investigation	Dominant Frequency [Hz]	Potential Influence [dB]	Major Influencing Parameters (red ↑ or green ↓)	Physical Analogy	References
Generation Mechanisms	Structure-borne	Impact (Shock)	Tread Impact	Archibald (1974) [162]	800-1000	7	Tread depth, groove width, rubber hardness	Rubber hammer	[29], [149], [163], [164]
			Texture Impact	Thrasher et al. (1976) [18]	800-1200	5	Mechanical impedance, macrotexture		[123], [165], [166]
		Adhesion	Stick/Slip (Friction)	Timmons (1976) [167]	1000-3000	2	Normal tire force, temperature, pavement texture at all wavelengths and whether it is positive	Sneaker	[168]–[170]
			Stick/Snap	Nilsson (1979) [171]	2500-4000	2	Pavement wetness, microtexture	Suction cup	[131], [172], [173]
	Airborne	Air Displacement	Air Pumping	Hayden (1971) [174]	1000-2500	10	Porosity, macrotexture	Clapping	[145], [154], [175]–[177]
			Air Turbulence	Chanaud (1969) [178]	~300 & >3000	2	Speed, tread pattern	Spinning disk	[126], [179], [180]
Amplification Mechanisms	Tire Resonance		Belt Resonance	Richards (1974) [181]	600-1300	4	Tread bending stiffness	Circular belt	[182]–[184]
			Torus Cavity Resonance	Bschorr (1985) [185]	200-250	3	Cavity geometry, tire load, vehicle speed, inflated gas	Balloon	[147], [186]–[193]
			Sidewall Resonance	Reiter et al. (1974) [59]	500-1000	2	Tire construction	Speaker membrane	[84], [131], [146], [179], [183]
			Tire/Rim Assembly Resonance	Ni et al. (1997) [194]	250-300	Unknown	Tire mass, rim mass	Sanding disk	[147], [194], [195]
	Air Resonance		Pipe Resonance	Pope and Reynolds (1976) [196]	1000-3000	6	Porosity, macrotexture, tread pattern	Organ pipe	[197]–[200]
			Helmholtz Resonance	Nilsson et al. (1979) [201]	1000-2500	Unknown	Porosity, macrotexture, tread pattern	Pop bottle	[7], [149], [202], [203]
	Horn Effect		Horn Effect	Nilsson (1979) [204]	1500-3000	10	Porosity, sound absorption, tire width	Megaphone	[205]–[211]
Attenuation Mechanisms	Acoustical Impedance		Pavement Absorption	Underwood and Nelson (1984) [62]	300-2000	7	Porosity	Foam	[212]–[215]
	Mechanical Impedance		Vibration Transfer	Sandberg (1987) [216]	500-1000	2	Pavement stiffness	Cushion	[217], [218]

Most frequency spectra of exterior tire-pavement interaction noise have prominent peak in the range of 700-1300 Hz (sometimes might be shifted within the range 630-2000 Hz), especially for car tires after A-weighting (Sandberg, 2003 [219]). A-weighting is the most commonly used procedure when considering human hearing perception (loudness and annoyance) defined in the International standard IEC 61672 (IEC, 2003 [220]). A-weighting gives the most weight to frequency range of 1000-5000 Hz. It somewhat explains the TPIN spectrum peak around 1000 Hz, but not completely.

It is believed that the peak is mostly due to the fact that dominant frequencies for many mechanisms fall under this range (Bernhard, 2005 [221]), as shown in Table 2.6. Therefore, scattering or decentralization of these dominant frequencies will be a promising approach to effectively reduce tire-pavement interaction noise. For truck tires, the peak is usually at about two third-octave bands lower frequency than for car tires due to larger tire tread pitch, which is within 500-1000 Hz (Sandberg, 2003 [203]).

In summary, impact and air pumping are the most important generation mechanisms, which have been extensively investigated and included in most of the existing TPIN models as well as the artificial neural network model in the present study. As an amplification mechanism, the cavity resonance has also drawn particular attention and interest. However, the dominant frequencies of the cavity resonance are so low that it might only has considerable effect on the vehicle interior noise rather than the exterior TPIN. The attenuation mechanisms are significantly related with the pavement characteristics, which might be the key to reducing TPIN. It should be pointed out that, a lot of the physical mechanisms are based on reasonable engineering guess but have not been conclusively proven with solid evidence.

2.3 Influencing Parameters

Generally, the types of vehicles play major roles in the tire-pavement interaction noise (TPIN), such as heavy commercial vehicle (HCV), bus, light commercial vehicle (LCV), car, auto-rickshaw (AR), and two-wheeler (2W). Overall noise level increases with increase in size of the vehicles. That is, the noise produced by heavy commercial vehicle and bus is 10 dB higher than that produced by a two-wheeler when all these vehicles were driven at 70 km/h (Syamkumar et al., 2013 [23]). There are also some vehicle construction related parameters

that might influence TPIN (Sandberg and Ejsmont, 2002 [24]), such as vehicle geometry, rim effect, wheel housing and underbody screening, but these vehicular parameters are not of interest in this section. Instead, it is assumed that the tested vehicle is of the same type or at least similar.

Different parameters affect TPIN to different degrees, as shown in Table 2.7 (Sandberg and Ejsmont, 2002 [24]).

Table 2.7: Overview of parameters affecting TPIN (source from Sandberg and Ejsmont, 2002 [24])

Parameters	Potential Noise Variation [dB]	
Speed	25	
Pavement	10	
Tire	10	
Studs in Tire	8	
Load & Inflation	5	
Road Condition	5	
Temperature	4	
Wheel Torque	3	
	Cars	Trucks
Due to Vehicles	7	12
Due to Pavements	9	6

In this section, the influencing parameters are divided into five categories: driver influence parameters, tire related parameters, tread pattern parameters, pavement related parameters, and environmental parameters. The pertinent frequency, relation with tire noise, potential noise contribution, measurement equipment and relevant mechanism of each parameter are listed in the table as a summary at the end of each corresponding section.

2.3.1 Driver Influence Parameters

Driver influence parameters are those that can be changed by drivers after tire/pavement combination has been determined. A lot of parameters of this type are difficult to quantify, such as steering speed. A few most important factors are discussed below.

The driver influence parameters affecting TPIN are summarized in Table 2.8. It can be seen

that vehicle speed is the most important single parameter influencing TPIN over all frequencies. Accelerating, braking or cornering also largely increases TPIN due to the increase of stick/slip mechanism, especially at higher frequencies. The effects of tire load and inflation pressure are insignificant. Positive camber angle is favorable for TPIN reduction at higher frequencies.

Table 2.8: Summary of driver influence parameters affecting TPIN

No.	Parameter	Pertinent Frequency [Hz]	Relation (↑↓)	Potential Noise Variation [dB]	Measurement Equipment	Relevant Mechanism	References
1	Speed	250-8000	↑	25	Speedometer, wheel/axle-mounted encoder, GPS	Various: impact, air pumping	[7], [23], [222]
2	Longitudinal Force/Slip	800-1600	↑	10	Accelerometer	Stick/slip	[40], [163], [223], [224]
3	Lateral Force/Slip	1000-8000	↑	7	Accelerometer, gyroscope	Stick/slip	[24], [225], [226]
4	Tire Load	800-1600	↑	2	Dynamometer	Impact, air pumping	[227]–[235]
5	Inflation Pressure	1600-3200	Complex	1	Tire pressure gauge/sensor	Impact, air pumping	[229], [236]
6	Tire Camber Angle	1000-3000	↓	5	Protractor	Impact, stick/slip	[237]

2.3.2 Tire Related Parameters

Tire properties have major influence on TPIN emission, especially for truck tires (Reinink et al., 2005 [238]). The spread between the noisiest and the quietest tire might be 10 dB, irrespective of pavement type (Sandberg and Ejsmont, 2000 [94]).

The tire-related parameters affecting TPIN are summarized in Table 2.9. The tire type (radial/biased) and size can influence TPIN, however, the most important tire parameters are those affecting the contact characteristics between the tire tread band and the pavement, such as tread porosity, embedded stud, wear/aging, and rubber hardness. The parameters that affect the mechanical characteristics of the tire, such as belt stiffness, damping loss factor, non-uniformity, tire cavity content, and rolling resistance, are less influential. The tire width has a greater influence on TPIN than tire diameter.

Table 2.9: Summary of tire-related parameters affecting TPIN

No.	Parameter	Pertinent Frequency [Hz]	Relation (↑↓)	Potential Noise Variation [dB]	Measurement Equipment	Relevant Mechanism	References
1	Tire Type/Construction	N/A	Complex	3	N/A	Various	[146], [239]–[242]
2	Tire Width	500-1000	↑	3	Measure tape	Various	[205], [243]
3	Tire Diameter	N/A	↓	1	Measure tape	Impact, horn	[205], [244], [245]
4	Belt Stiffness	500-8000	↓	2	Loading test rig with bar	Tire resonance	[120], [182], [246]
5	Damping (Loss Factor)	250-500	↓	1	N/A	Tire resonance	[247]
6	Non-uniformity	20-200	↑	1	Wheel balancing machines	Tire resonance	[120], [248]
7	Rubber Hardness	1000-3000	↑	3	Durometer	Stick/slip	[249], [250]
8	Wear/Aging	1000-3000	↑ (then ↓)	5	N/A	Various	[141], [251]–[253]
9	Retreaded	500 & 2000-3000	Complex	2	N/A	Impact	[254]–[256]
10	Studded	400-3000 & above 5000	↑	6	N/A	Impact, stick/slip	[257], [258]
11	Tread Porosity	N/A	↓	7	N/A	Air pumping, horn effect	[123], [259]
12	Tire Cavity Content	400-1100	Complex (↓)	2	N/A	Cavity resonance	[20], [148], [260]
13	Rolling Resistance	N/A	↑ (Weak correlation)	0	Dynamometer drum: ISO 18164 [261]	N/A	[94], [262]–[264]

2.3.3 Tread Pattern Parameters

Tread pattern used to be considered as the most important tire parameter influencing TPIN, and it is also the one that is easiest to modify.

There are approximately 16,000 different tire tread patterns used on tires (Hanson et al., 2004 [265]). It is not an easy task to parameterize the tread pattern. A lot of parameters are just qualitative, making the results questionable in some sense. A alternative and smart method to parameterize 2D tread pattern is through image processing (Che et al., 2012 [266]). The drawback of 2D tread pattern is the loss of tread/groove depth information. Ge et al. (2004) [267] found that sound pressure level increased by 10 dBA as the groove depth increased from 0 to 12 mm for a single groove tire. As such, 3D tread profile is an alternative and often applied with 3D laser scanner (CTWIST). The tread patterns under investigation were usually hand-cut from slick tires, so it might not represent the industrious tires on the market, for example unwanted reduction of dynamic stiffness of the tread might occur (Iwao and Yamazaki , 1996 [163]).

It is believed among general public that TPIN comes mainly from the effect of tread pattern impact on the pavement (Cao et al., 2008 [268]) and the non-patterned tire is the quietest tire. However, this is not the case. In fact, non-patterned tire might be the noisiest tire if tested on the rough pavement (VTI, 2001 [255]). Fong (1998) [269] found that the sound levels from smooth tires (P175/70R13) were slightly greater than the patterned tire over all the chipseal pavements. Generally, for the same tire construction and rolling speed, the lowest TPIN is produced by a rib tread design (VTI, 2001 [255]). Having said that, tread pattern is an important factor that is easy to modify for TPIN reduction. It affects nearly all mechanisms, especially on smooth pavement (Sandberg and Ejsmont, 2002 [24]). In addition, it was found that the noise spectra from slick tire and standard patterned tire were different, especially around 1000 Hz (Alt et al., 2006, [270]).

The tread pattern parameters affecting TPIN are summarized in Table 2.10. It is shown that appropriate tread pattern optimization is able to reduce TPIN, such as increasing the offset between the tread blocks, and increasing the tread groove ventilation. However, the effects of many other tread pattern design techniques are marginal, such as normal randomization, addition of small sipes. It should be noted that, very few literatures have conclusively and quantitatively reported the effect of tread pattern on TPIN, even though the general public considered the tread pattern as an important factor influencing TPIN.

Table 2.10: Summary of tread pattern parameters affecting TPIN

No.	Parameter	Pertinent Frequency [Hz]	Relation (↑↓)	Potential Noise Variation [dB]	Measurement Equipment	Relevant Mechanism	References
1	Randomization	600-1000	↓	0 or marginal	N/A	Tread impact	[24], [164]
	Elimination of Groove Footprint Coinciding	800-1000	↓	N/A	N/A	Tread impact	[24], [164]
	Offset between Left and Right Side	N/A	↓	5	Caliper	Tread impact	[24], [164], [271]
2	Rotation Direction / Side Asymmetry	N/A	↑	3	N/A	Various	[24], [164]
3	Ventilation	800-1000 & 1600-4000	↓	2	N/A	Air pumping, air resonance	[24], [164], [255]
4	Addition of Mirror Image Grooves	Above 4000	↓	0	N/A	Air pumping, air resonance	[24], [164]
	Addition of Lamellae	800-1000	↓	N/A	N/A	Air pumping, air resonance	[24], [164]
	Groove Width	800-2000	↑ 9 mm ↓	N/A	Caliper	Air pumping	[24], [164], [255]
	Groove Angle (Relative to Lateral)	800-2000	↓	N/A	Protractor	Tread impact	[24], [164], [255]

2.3.4 Pavement Related Parameters

Pavement parameters might be more important than tire parameters (Sandberg and Ejsmont, 2002 [24]) in terms of tire noise. As a matter of fact, two thirds of literature focus on the pavement effects while only one third focus on the tire effects (Sandberg and Ejsmont, 2002 [24]). Fong (1998) [269] demonstrated that the pavement texture dominated in noise generation for chipseal surfaces.

Generally, pavement can be categorized into two major types: cement concrete pavement and asphalt concrete pavement. Different types of pavements have different acoustic performance (Donavan, 2005 [272]). It was found TPIN levels on cement concrete pavements are 2 dB higher than TPIN levels on asphalt pavements (Syamkumar et al., 2013 [23]). The high frequency noise (over 1 kHz) and low frequency noise (below 250 Hz) was found to be much higher on the cement concrete pavements than on the asphalt pavements (Sandberg et al., 1990 [273]). Characteristics of asphalt pavements are affected largely by the mixture design whereas for concrete pavements, the texturing pattern is the key contributor (Rasmussen, 2009 [274]).

Different pavement parameters affect different generation and propagation mechanisms. The pavement related parameters could be categorized into primary parameters, secondary parameters and tertiary parameters. The primary parameters are those for pavement design or mixture properties, such as grading size distribution, content of binder and thickness; the secondary parameters are characteristics that show up and remain relatively constant after the pavement is built, such as porosity, texture and impedance (Li et al., 2009 [275]); the tertiary parameters are those that might change with time, such as wetness, wear/age, and surface rating.

The pavement-related parameters affecting TPIN are summarized in Table 2.11. It can be seen that the most important factor is the pavement texture, especially the macro- and mega-texture; so are the related or derivative parameters, such as mean profile depth, IRI, positive or transverse or anisotropic texture, joints, wear/age, and surface rating. Some parameters have an effect on the air pumping mechanism, such as porosity, sound absorption, and airflow resistance; some parameters have an effect on the impact mechanism, such as

thickness of the pavement layer, and stiffness. However, the normal adhesion or tangential friction of the pavement is shown to be of little influence. In addition, it is widely known that wet pavement is noisier than dry pavement.

Table 2.11: Summary of pavement-related parameters affecting TPIN

No.	Parameter	Pertinent Frequency [Hz]	Relation (↑↓)	Potential Noise Variation [dB]	Measurement Equipment	Relevant Mechanism	References
1	Micro-texture (below 0.5 mm)	2000-4000	↓	N/A but Marginal	Laser profiler: ISO 13473 [276]; Circular Track Meter (CTM): ASTM E2157 [277] for macro-texture only	Stick/slip, stick/snap	[278], [279]
	Macro-texture (0.5-50 mm)	100-1000 & 2000-4000	↓ & (10 mm) ↑	N/A but Significant		Texture impact, air pumping	[35], [280], [281]
	Mega-texture (50-500 mm)	100-1000	↑	N/A but Significant		Texture impact	[281], [282]
	Unevenness (500-800 mm)	N/A	↑	4		N/A	[8]
	Unevenness (10-50 m)	200-1500	↓	1			
2	MPD/MTD/ Texture	N/A	Complex	10	Sand patch method: ASTM E965 [283], ASTM E1845 [284] and ISO 13473-1 [285]	Same as macro-texture	[286]
3	International Roughness Index (IRI)	Same as unevenness	Same as unevenness	Same as unevenness	Profilometer: ASTM E1926 [287] and ASTM E1364 [288]	Same as unevenness	[4]
4	Positive versus Negative Texture	N/A	↑	N/A	Laser profiler	Texture impact, air pumping	[289]
5	Transverse Texture	N/A	↑	N/A	Laser profiler	Texture impact	[290]
6	Anisotropic Texture	N/A	↑	N/A	Laser profiler	Texture impact, air pumping	[291]
7	Joints	800-1000	↑	3	Laser profiler	Texture impact, air pumping	[222], [292]–[296]
8	Porosity	500-1600 & 3000	↓	7	Pavement core sample: ASTM D7063/D7063M [297]	Various	[218], [298]–[300]
9	Sound Absorption	Similar to Porosity	Similar to Porosity	Similar to Porosity	Impedance tube: ISO 10534-1 [301] and ISO 13472-1 [302]	Pavement absorption	[213], [215], [235]
10	Airflow Resistance	N/A	↑	N/A	Impedance tube: ISO 9053 [303] and ANSI/ASA S1.18 [304]	Air pumping, air resonance	[305]–[307]
11	Thickness of Layer	500-1600	↓	5	Measure tape	Acoustic and mechanical impedance	[24]
12	Stiffness (Mechanical Impedance)	800-1250	↑	1	Impact hammer device: AASHTO T 342 [308]	Vibration Transfer	[165], [202], [309]–[311]
13	Normal Adhesion	2000-4000	↑	1	N/A	Stick/snap	[24]
14	Tangential Friction	2500-6300	↑	0	Dynamic Friction Tester (DFT): ASTM E1911 [312]	Stick/slip	[94]
15	Wear/Age	1000-4000	↑	2	N/A	Impact, absorption	[113], [313]–[315]
16	Surface Rating (SR)	N/A	↓	N/A	N/A	Impact	[316], [317]
17	Wetness	Above 1000 Hz	↑	3	N/A	Water splash effect	[23], [318], [319]
18	Mixture Parameters/Materials	N/A	Complex	Significant	N/A	Various	[83], [320]

2.3.5 Environmental Parameters

Environmental or atmospheric parameters can influence tire-pavement properties and the characteristics of the transmission path. Therefore, sometimes they cannot be neglected and have been included in many TPIN models.

The environmental parameters affecting TPIN are summarized in Table 2.12. The environmental parameters have an influence on the sound propagation and thus on the noise level measured in the far field. However, if these parameters are within the normal range when at least the field tests can be successfully conducted, they can be ignored.

Table 2.12: Summary of environmental parameters affecting TPIN

No.	Parameter	Pertinent Frequency [Hz]	Relation (↑↓)	Potential Noise Variation [dB]	Measurement Equipment	Relevant Mechanism	References
1	Temperature	1000-4000	↓	3	Thermometer	Impact	[321], [322]
2	Air Humidity	N/A	↓	1	Air humidity meter	Sound propagation	[323]
3	Wind	300 & 2000	↑	N/A	Wind meter	Air turbulence	[23], [324]

2.3.6 Summary

In general, on the same pavement and under the same environmental conditions, the most important parameters are speed, longitudinal force/slip (acceleration), wear/aging, and tread pattern. The tread pattern might not be the most important influencing factor, but it is considered to be the most easily modified property of a tire. The pavement parameters, such as pavement texture, are usually more important than tread pattern and other tire parameters.

2.4 Existing Models

A lot of relevant models have been developed to describe and predict tire vibrations and tire-pavement interaction noise (TPIN). However, all of these models are restricted in some sense (Dare, 2012 [115]). For example, some models only describe one or two particular generation mechanisms; some assume two-dimensional tire and pavement; some only include limited tire/pavement combinations, such as slick tire on rough road; some only calculate noise level at the source without considering sound propagation; some are only concerned on tire structural dynamics, and neglect the effect of the nonlinear aerodynamics surrounding the tire.

Generally speaking, it is difficult to evaluate the accuracy of specific models due to different model objectives and the lack of validation (Kuijpers and van Blokland, 2001 [172]). In addition, most of current models only focus on passenger car tires. Very few literatures reported noise models for truck tires that might have more influence on traffic noise. As the increased popularity of porous asphalt pavement, more and more models include pavement absorption and mechanical impedance as parameters of interest.

The current models can also be divided into three categories based on the characteristics of the approach used: deterministic model, statistical model and hybrid model. The deterministic models are usually focused on low frequencies (below 500 Hz). However, the main spectral content of real tire noise is located from 600-1200 Hz. Therefore, these models tend to have considerable errors. The statistical and hybrid model usually cover the entire dominant frequency of tire noise, resulting in better accuracy. However, most of the models only investigate pavement parameters.

In this section, 36 deterministic models, 18 statistical models, and 16 hybrid models were reviewed.

2.4.1 Deterministic Models

Deterministic models are also called analytical or numerical models. Recent methods, such as finite element method (FEM) (Lou, 2007 [325]) and boundary element method (BEM) (Wang et al., 2011 [326]; Nakajima et al., 1993 [327]), require large computational effort. A large number of parameters are also required, including tire geometry, deformation of the tire, material parameters, boundary conditions and so on (Yang et al., 2013 [243]). On the other hand, generally, the influence of single parameters on TPIN is possible to be investigated only by deterministic models (Biermann et al., 2007 [328]).

In this subsection, 36 deterministic models were reviewed, including 16 conventional physics models, 16 finite element and boundary element models, and 4 computational fluid dynamics models. The model name, method, output noise parameter with noise measurement technique, investigated noise generation mechanisms, and investigated input parameters of each model are listed in tables as a summary.

2.4.1.1 Conventional Physics Models

The conventional physics models typically utilize traditional analytical methods and classic mathematics, such as modal analysis, to present and investigate the dynamical behavior of the tire that is usually modeled as a ring or shell. Traditional acoustic equations are sometimes applied to analyze the structural wave propagation mode in the tire tread and wall, as well as the acoustical mode in the tire cavity.

The conventional physics models are summarized in Table 2.13. It can be seen that this type of modeling has been steadily improved since 1971. However, most models only focused on structure-borne noise, especially that due to the impact between the tire and pavement. Therefore, the tire vibration was usually the output parameter rather than sound pressure level. The frequency range was typical below 500 Hz; some models claimed to be able to predict higher frequencies, but still limited to structure-borne noise. In addition, a large part of the models only considered stationary tire, which is quite different from the normal driving conditions. Only one specific tire or one specific pavement was investigated in some of the models.

Table 2.13: Summary of conventional physics models on TPIN

No.	Author	Model Name	Year	Ref.	Method	Output	Frequency Range [Hz]	Mechanism	Driver Parameter	Tire Parameter	Pavement Parameter	Environment Parameter
1	Hayden	Monopole	1971	[174]	Monopole	L_p	N/A	Air pumping	Speed	Groove geometry	N/A	N/A
2	Plotkin and Stusnick	Unified	1981	[329]	Thin shell	Near field, normalized radiation	0-8000	Impact, air pumping	Speed, tire load	Various	Texture	N/A
3	Keltie	Truck Tire	1982	[247]	Thin shell	1/3 octave sound power level	100-2000	Structure-borne	Inflation	Damping, bending stiffness	N/A	N/A
4	Kung et al.	2D Ring	1986	[330]	Modal expansion	Near field, SPL	0-400	Structure-borne	Tire load	Various	Texture	N/A
5	Heckl	Various Mechanisms	1986	[1]	Various	LDV, vibration, SPL	0-2000 Hz	Various	Rotating, loaded	Tread pattern	Roughness	N/A
6	Bremner et al.	Tire Vibration	1997	[331]	SEA, wavenumber decomposition	Far field (7.5 m), 1/3 octave SPL	100-4000	Impact	Speed, 40 psi	Tread pattern, materials	Texture	N/A
7	Bérengier et al.	Porous Pavement	1997	[332]	Image source	Impedance, absorption	100-5000	Pavement absorption	N/A	N/A	Airflow resistivity, porosity, tortuosity	N/A
8	Bolton et al.	Wavenumber Decomposition	1998	[260]	Wavenumber decomposition	Point mobility, wavenumber	0-1000	Structure-borne	Stationary, inflation, gas type	215/70R14	N/A	N/A
9	Kropp	Orthotropic Plate	1999	[333]	Multipole synthesis	DR, TVM, LDV, acc., 1/3 octave SPL	125-2500	Structure-borne	Unloaded	Slick	Rough, 1× 30 mm step	N/A
10	Kim and Bolton	Shell	2002	[334]	Wave number decomposition	Vibration	0-4000	Point impact	Speed	N/A	N/A	N/A
11	Molisani et al.	Coupled Cavity	2003	[335]	Donnell-Mushtari theory, structural acoustic	Modal amplitude, force at spindle	0-1250	Cavity resonance	Stationary without rotating	100/50R12	N/A	N/A
12	Kim et al.	Waveguide	2007	[336]	Spring-mass, elastically supported beam, cylindrical shell	Vibration, flexural wave, eigen-frequency	0-2000	Structure-borne	Stationary	Geometry, structure	N/A	N/A
13	Feng et al.	Cavity	2009	[337]	Coordinate transform	Cavity SPL, narrowband	100-300	Cavity resonance	Speed, tire load	N/A	N/A	Temperature
14	O'Boy and Dowling	3D Multilayer	2009	[338]	Bessel equation	Vibration	0-2000	Structure-borne	Tire load, break/acc.	225/45ZR17	N/A	20 ° C
15	Arteaga	Green's Function	2011	[339]	Modal-ALE	Vibration	0-300	Impact	Tire load, speed	185/70SR14	N/A	N/A
16	Bolton and Cao	Coupled Mode	2013	[340]	Structural-acoustic coupling	LDV, vibration	0-6000	Structure-borne	Stationary & 50 m/s, 3 bar	225/55R17	N/A	N/A

2.4.1.2 Finite Element and Boundary Element Models

The finite element method (FEM), also known as finite element analysis (FEA) or finite element (FE) for short, is a numerical technique for solving problems in partial differential form. FEM subdivides the entire body, including the surrounding boundary, into smaller/simpler parts called finite elements. A system of linear equations that model these finite elements are then integrated to generate the solution equations of the entire body. Unlike the FEM, boundary element method (BEM) only subdivides the boundary of the body into finite elements, which is generally more computationally efficient.

With the advancement of computers, BEM and FEM have become the two dominant numerical techniques in computer-aided engineering (CAE). BEM and FEM are often coupled with other methods and have several derivations, such as waveguide finite element method (WFEM), infinite/finite element method (IFEM), wave finite element (WFE), energy boundary element analysis (EBEA), and energy finite element analysis (EFEA), which will be discussed in the following. It is often used to calculate the vibrations of the tire, and then together with fluid-structure interaction (FSI) method to analyze the sound generation and propagation into the air. Sixteen models were reviewed in this section.

The finite element and boundary element models are summarized in Table 2.14. The finite element method has been applied to TPIN modeling since 1986. Similar to the conventional physics model, the finite element and boundary element model also generally focused on structure-borne noise. However, the near field or far field sound pressure level could be easily predicted with the structure-fluid coupling technique. The frequency range was almost exclusively below 500 Hz or even lower, such as 150 Hz, due to the inherent drawback of the finite element method. Vehicle speed was typically included in the modeling as an input. Tire parameters were heavily investigated, but the pavement parameters seemed not to be of much interest.

Table 2.14: Summary of finite element and boundary element models on TPIN

No.	Author	Model Name	Year	Ref.	Method	Output	Frequency Range [Hz]	Mechanism	Driver Parameter	Tire Parameter	Pavement Parameter	Environment Parameter
1	Saigal et al.	Toroidal Membrane	1986	[341]	Membrane FE	Vibration	Low	Structure-borne	Inflation, nonrotating, unloaded	Geometry, structure	N/A	N/A
2	Wright and Koopmann	Acoustic Radiation	1986	[342]	FE, Helmholtz integral	Near field, sound pressure, intensity	80-200	Vibration, radiation	Stationary, point-excited	N/A	N/A	N/A
3	Richards	FEA Coupling	1991	[343]	Weighted residual approximation	Vibration	0-400	Cavity resonance	N/A	185/70R14	N/A	N/A
4	Larsson and Kropp	3D 2 Plate	1992	[344]	FE	Pass-by, SPL	0-2000	Structure-borne	Tire load	Various, slick 205/60R15	Texture	N/A
5	De Roo and Gerretsen	TRIAS	2000	[345]	FEA, BEM	Near field, 1/3 octave SPL Pass-by, SPL	N/A	Impact, air pumping	N/A	Various, TYDAS	Various, RODAS	N/A
6	Nilsson	WFEM	2004	[346]	WFEM	Point mobility, wavenumber	0-1500	Structure-borne	Stationary	Geometry, structure	N/A	N/A
7	Biermann et al.	IFEM	2007	[328]	IFEM, Astley-Leis elements	Far field (1 m), 1/3 octave SPL	0-1400	Impact	Speed	Slick	Texture	N/A
8	Brinkmeier et al.	FEM & BEM	2008	[347]	FEA, BEM, ALE	Pass-by, 1/3 octave SPL	100-850	Structure-borne	40-120 km/h	N/A	Texture spectrum	N/A
9	Waki et al.	WFE	2011	[348]	FE, modal decomposition	Vibration	0-1500	Impact	Inflation: 220/180 kPa	225/45R17 265/70R17	N/A	N/A
10	Kido et al.	Road Input	2011	[349]	FE	Axle vibration	0-150	Texture impact	Speed, tire load	Patch area	Texture	N/A
11	Yang et al.	FSI	2013	[243]	FEA	Near field, 1/3 octave SPL	500-2500	TPIN	70-90 km/h	PIARC	N/A	N/A
12	Tong et al.	Wear	2013	[350]	Acoustic FE	Near field, SPL	0-500	Impact	Tire load, speed, inflation	Wear	N/A	N/A
13	Vlahopoulos et al.	EFEA/EBEA	2013	[351]	EFEA, EBEA, panel contribution analysis	Interior noise	200-8000	Airborne	N/A	N/A	N/A	N/A
14	Mohamed and Wang	Cavity	2015	[245]	FEM, Bessel root method	Tire cavity SPL	150-500	Torus cavity resonance	N/A	Tire size	N/A	N/A
15	Wei et al.	MLE	2016	[352]	Mixed Lagrangian-Eulerian, FE, BEM	Near field, 1/3 octave SPL	Time domain, 0-1250	Vibration	70 km/h	Truck/bus, 315/60R22.5 385/65R22.5	N/A	N/A
16	Banz et al.	Time Domain BEM	2016	[353]	BEM	L_p, 1/3 octave	200-2000	Radiation	Steady-state moving	Pass./truck, slick	N/A	N/A

2.4.1.3 Computational Fluid Dynamics Models

Computational fluid dynamics (CFD) uses numerical algorithms to solve and analyze fluid flow problems in computer-aided engineering (CAE). It can be applied to the modeling of airborne TPIN.

The computational fluid dynamics models are summarized in Table 2.15. The CFD models started in 1999, somewhat later than the previous two categories. With the help of CFD, the TPIN modeling was extended from structure-borne noise only to airborne noise (air pumping mechanism). Near field sound pressure level was widely accepted as the output parameter of the model. The tire tread pattern was the most important input parameter investigated. However, none of the current models have included pavement parameters that the author believe are also important, because the air voids within the contact patch are formed between the tread pattern and the pavement texture.

Table 2.15: Summary of computational fluid dynamics models on TPIN

No.	Author	Model Name	Year	Ref.	Method	Output	Frequency Range [Hz]	Mechanism	Driver Parameter	Tire Parameter	Pavement Parameter	Environment Parameter
1	Gagen	Shock Wave	1999	[354]	CFD	Near field, sound pressure/energy	N/A, time domain	Air pumping	Speed	Groove angle, geometry	N/A	N/A
2	Kim et al.	Hybrid CFD	2006	[175]	CFD, Kirchhoff integral	Far field, 1/3 octave SPL	250-8000	Air pumping, pipe resonance	100 km/h	Ventilation groove, 165/70SR13	N/A	N/A
3	Chen et al.	CFD	2014	[11]	CFD	Near field, 1/3 octave SPL	0-2000	Airborne	N/A	Tread pattern	N/A	N/A
4	Gautam and Chandy	Air Pumping CFD	2016	[355]	CFD	Near/far field, drum, narrowband SPL	1000-10000	Airborne, air pumping	40 km/h	215/60R16, transverse slots	N/A	N/A

2.4.2 Statistical Models

Due to the fact that much of the physics of tire-pavement interaction noise (TPIN) generation is uncovered, statistical models are more common, especially in industry. Statistical or semi-empirical models are based on correlating measured noise data to tire-pavement parameters. For example, measured TPIN can be correlated with pavement texture, including texture levels at different wavelengths in the longitudinal direction (Rasmussen et al., 2006 [280]; Rasmussen et al., 2006 [356]; Dare and Bernhard, 2009 [278]) and overall texture mean profile depth (MPD) (Fujikawa et al., 2004 [78]; Fujikawa et al., 2009 [357]; Fujikawa et al., 2007 [358]; Storeheier, 2004 [359]).

The statistical models have better accuracy than deterministic ones since the model parameter values are obtained by actual measured data. However, empirical measurements can never account for all potential conditions, so statistical confidence level and confidence interval are usually analyzed in the meantime. In addition, some of the parameters in these models are not real physical parameters but derived parameters such as a texture spectrum [172], which means they are not adjustable directly. In order to change these parameters, the parameters have to be translated back to original physical parameters, which is not always explicit or even impossible for nonlinear relationships.

A couple of different statistical analysis algorithms can be used. In this subsection, 18 statistical models were reviewed, including 10 traditional regression models, 3 principal component analysis models, and 5 fuzzy curve-fitting models.

2.4.2.1 Traditional Regression Models

The traditional regression models include linear regression models and non-linear regression models. The linear regression is easier to model while the non-linear regression is more flexible.

The traditional regression models are summarized in Table 2.16. The regression analysis was most early applied to statistical TPIN modeling. It has been widely used for traffic noise prediction by government transportation agencies. Non-linear regression was dominant before the early 2000's, while linear regression has prevailed thereafter, likely because linear

regression has easy forms and needs less data to improve the accuracy. Besides pass-by noise measurement, more advanced and professional noise measurement techniques, such as on-board sound intensity (OBSI), have been frequently used, where the 1/3 octave band noise spectrum was typically the output with large frequency range of 500-5000 Hz. The vehicle speed was usually included in the modeling. Unlike most deterministic models, however, tire load or other tire parameters were not of much interest. Various types of pavement parameters were included, such as pavement type, slope, texture, friction, age, and wetness. Environmental parameters were also of more interest, such as temperature and wind. However, the traditional regression model was unlikely to give insight into noise generation mechanism or separate them.

Table 2.16: Summary of traditional regression models on TPIN

No.	Author	Model Name	Year	Ref.	Method	Output	Frequency Range [Hz]	Mechanism	Driver Parameter	Tire Parameter	Pavement Parameter	Environment Parameter
1	BMVI	RLS (Germany)	1990	[360]	Non-linear Regression	Pass-by, L_{eq}	N/A	Traffic	Speed, vehicle type	N/A	Slope	Propagation attenuation
2	CNR	CNR (Italia)	1991	[361]	Non-linear Regression	Pass-by, L_{eq}	N/A	Traffic	Speed, vehicle type	N/A	Slope	Propagation attenuation
3	FHWA	TNM (US)	1998	[362]	Non-linear regression	Pass-by, 1/3 octave	500-5000	Vehicle and traffic	Speed, vehicle type, acceleration	N/A	Type	N/A
4	Hanson and James	Dense Graded	2004	[48], [265]	Non-linear Regression	CPX, CPI, OASPL	N/A	TPIN	72 km/h	N/A	FM, voids, age	N/A
5	Rasmussen	Concrete Texture	2009	[274]	Linear regression, bridging filter	OBSI, 1/3 octave	500-5000 630-1000	Texture impact	Buick Century, 97 km/h	SRTT	Texture, skewness	N/A
6	Fujikawa et al.	Asperity	2009	[357]	Linear regression	BTT, OASPL, octave	500-4000	TPIN	80 km/h, 3.2 kN, 170 kPa	185/65R15, rib pattern	Asperity spacing, asperity height unevenness, MPD	N/A
7	Reyes and Harvey	Pavement Core	2011	[305]	Linear regression	OBSI, 1/3 octave, OASIL	500-5000	TPIN	N/A	SRTT	Airflow resistance, MPD	N/A
8	N/A	CNOSSOS (EU)	2012	[363]	Non-linear Regression	Pass-by, L_W, octave	125-4000	TPIN, vehicle and traffic	Speed, vehicle type, acceleration	Studded	Type, age	Air temperature
9	Syamkumar et al.	Mode-wise	2013	[23]	Linear regression, sensitivity analysis	CPB, OASPL	N/A	TPIN	Speed, tire load, vehicle type	N/A	Type, wetness	Pavement temperature, wind direction
10	Wayson et al.	FDOT	2014	[102]	Linear regression	OBSI, OASIL, pass-by, OASPL	500-4000	TPIN	88 km/h 97 km/h	SRTT	FN, MPD, AG4	Wind < 4 km/h

2.4.2.2 Principal Component Analysis Models

Principal component analysis (PCA) uses an orthogonal transformation to identify a smaller number of uncorrelated variables, called "principal components", from a larger number of possibly correlated variables. Principal component regression (PCR) is a regression analysis technique based on principal component analysis (PCA). The advantage of the PCA models is that least number of variables (principal components) can be used to explain the maximum amount of variance.

The principal component analysis models are summarized in Table 2.17. The input and output parameters of the model are similar to those of the traditional regression model. The principal component regression is more advanced than linear or non-linear regression, and may include more input parameters in one model.

Table 2.17: Summary of principal component analysis models on TPIN

No.	Author	Model Name	Year	Ref.	Method	Output	Frequency Range [Hz]	Mechanism	Driver Parameter	Tire Parameter	Pavement Parameter	Environment Parameter
1	Ongel et al.	Asphalt Pavement	2008	[364]	OLS, PCR	OBSI, OASIL	N/A	TPIN	97 km/h	SRTT	Various	Pavement temperature
2	Zhang et al.	MTD	2014	[57], [365]	PCA Energy	BTT, energy	0-2000	TPIN	Speed	Same tire	MTD	N/A
3	Li et al.	Thin Surfacing	2015	[366]	Principal Component Regression	CPX, 1/3 octave, OASPL	315-3150	TPIN	80 km/h	N/A	Texture, MPD, absorption	N/A

2.4.2.3 Fuzzy Curve Fitting Models

A fuzzy curve fitting model is used to solve a nonlinear complex system by a few simple "If...Then" fuzzy rules (Roychowdhury, 1998 [367]). The increase of such rules gives a better modeling capability, especially with the advancement of computer technology. The advantage is that no specific form of equations is needed to fit the parameters. The fuzzy logic imitates the human learning process, and has a couple of derivative applications, such as artificial neural network (ANN), neuro-fuzzy system, and fuzzy genetic arithmetic (F-GA), which will be discussed in the following.

The fuzzy curve fitting models are summarized in Table 2.18. Fuzzy logic technique, such as artificial neural network, has been widely applied to various engineering problems, including TPIN modeling, since the late 1990's. The input and output parameters are similar to those of the regression models. The tire parameters, however, such as tread pattern, are more commonly included as input parameters.

Table 2.18: Summary of fuzzy curve fitting models on TPIN

No.	Author	Model Name	Year	Ref.	Method	Output	Frequency Range [Hz]	Mechanism	Driver Parameter	Tire Parameter	Pavement Parameter	Environment Parameter
1	Fry et al.	CPB ANN	1999	[368]	Resilient BP	CPB, OASPL	N/A	Vehicle	50 km/h (accel.), gear	Material, geometry, slick incl.	ISO 10844	N/A
2	Khazanovich and Izevbekhai	Pavement Aging	2008	[22]	Levenberg-Marquardt	OBSI, OASIL	N/A	TPIN	97 km/h	SRTT	Type, ESAL, Age, IRI, SR	30 ° C
3	Li et al.	F-GA	2009	[369]	F-GA	L_p, octave	125-4000	TPIN	N/A	Tread pattern	N/A	N/A
4	Che et al.	ANN	2012	[266]	GA-BP	DR, L_p, octave	125-4000	TPIN	Speed, tire load, inflation	Size, tread pattern	Standard surface	N/A
5	Yu and Lu	Bayesian	2013	[370]	Bayesian, MCMC, MI	OBSI, 1/3 octave, OASIL	500-5000	TPIN	Traffic volume	N/A	Age, voids, MPD, thickness	Precipitation

2.4.3 Hybrid Models

Hybrid model can generally be divided into deterministic sub-models and statistical sub-models. In the deterministic sub-models, physical preprocessing and conditioning of input quantities are conducted to acquire intermediate parameters as inputs to the following statistical sub-models. In most cases, the relations in the statistical sub-models can be significantly improved by including the preprocessing part of data. The purpose of hybrid models is to find a compromise between the level of physical detail and statistical accuracy. During recent years, the hybrid model seems to be more and more popular because it keeps the accuracy of statistical models and meantime gains insight like physical models.

In this subsection, 16 hybrid models were reviewed, including 8 tire-pavement interface models, 4 mechanism separation models, and 4 noise propagation models.

2.4.3.1 Tire-Pavement Interface Models

These models calculate the excitation characteristics of the interface between the tire and pavement within the contact patch. For example, the pavement texture is converted to what the tire actually sees with envelope technique. The contact force/pressure spectrum is then obtained for further analysis of the tire vibrations. TPIN is finally correlated with the contact force/pressure spectrum (intermediate parameters) using experimental data.

The summary of tire-pavement interface models is shown in Table 2.19. Since the late 1990's, more efforts were put on the contact force/pressure distribution for TPIN modeling. The pavement texture was also converted to intermediate parameters that were potentially more correlated with TPIN. For either near field or far field noise, all the models were able to predict the noise spectrum usually of broad frequency range, not just the overall noise level. Vehicle speed was typically included as an input parameter. However, the contact force/pressure spectrum was generally calculated based on pavement texture while assuming a slick tire tread, which might not be accurate for normal patterned tires.

Table 2.19: Summary of tire-pavement interface models on TPIN

No.	Author	Model Name	Year	Ref.	Method	Output	Frequency Range [Hz]	Mechanism	Driver Parameter	Tire Parameter	Pavement Parameter	Environment Parameter
1	Fong	Truck Contact	1998	[269]	Transfer function	OBSP, 1/3 octave	10-4000	TPIN	45 km/h	Passenger and truck	Texture, contact pressure spectrum	N/A
2	Domenichini et al.	DGAC Texture	1999	[8]	Cross-correlation, regression	OBSP, pass-by, OASPL	22-5500	TPIN	Speed	Slick & normal	Texture index	N/A
3	Beckenbauer and Kuijpers	SPERoN	2001	[289]	Multivariate regression analysis	CB, $L_{pA,max}$, 1/3 octave SPL	125-5000	TPIN	50-120 km/h	Slick, tire width	Shape factor, contact pressure spectrum	N/A
4	Kuijpers and Blokland	Enhanced SPERoN	2003	[371]	Multivariate regression analysis	CB, $L_{pA,max}$, 1/3 octave SPL	125-5000	TPIN	50-120 km/h	Tread pattern, tire width, rubber hardness	Shape factor, contact pressure spectrum, mechanical impedance	20 ° C
5	Klein and Hamet	HyRoNE	2007	[158]	Envelopment, regression	CPB, $L_{pA,max}$, 1/3 octave SPL	100-5000	TPIN	70, 90, 110 km/h	Michelin Energy XH1/E3A	Enveloped texture, absorption, airflow resistance	20 ° C
6	Rustighi et al.	Road Excitation	2008	[372]	FEM, BEM, 2D Gaussian	Vibration, SPL	10-400	Texture impact, radiation, interior	20-100 km/h	Smooth	Texture excitation	N/A
7	Dubois et al.	Viscoelastic Contact	2011	[373]	Macro-scale, multi-asperity	Near field, 1/3 octave SPL	315-1000	Texture impact	90 km/h	Slick 186/57R15	Texture, contact force spectrum	N/A
8	Dubois et al.	Contact Distribution	2013	[374]	Weighted linear regression	CPX, 1/3 octave	315-1250	Impact	50-110 km/h	Slick and Patterned	Texture, contact force spectrum	N/A

2.4.3.2 Mechanism Separation Models

In these models, an equation form for each noise generation mechanism is assumed based on its physics. Then, the total TPIN is obtained by summing up all the generation mechanisms. Finally, the parameters in the assumed equations are statistically determined via experimental data.

The summary of mechanism separation models is shown in Table 2.20. This type of modeling is able to analyze each noise generation mechanism individually and identify each noise source, which has become popular since the late 2000's. Both structure-borne and airborne noise was generally investigated. The output of the models was the noise spectrum in 1/3 octave band or in narrowband. It is seen that pavement texture was more frequently included than tire parameters, such as tread pattern.

Table 2.20: Summary of mechanism separation models on TPIN

No.	Author	Model Name	Year	Ref.	Method	Output	Frequency Range [Hz]	Mechanism	Driver Parameter	Tire Parameter	Pavement Parameter	Environment Parameter
1	Cao et al.	Tire/Road Coupling	2008	[268]	N/A	SPL, narrowband	0-5000	Various	N/A	Tread pattern	Texture, absorption	N/A
2	Dare	Mechanism Decomposition	2012	[115]	Nonlinear least squares	OBSI, 1/3 octave	500-5000	Sidewall, treadband, tangential vibration	Speed	SRTT	Texture levels, skewness, absorption, friction	N/A
3	Winroth et al.	Air Pumping Separation	2013	[375]	Curve fitting	CPB, 1/3 octave SPL	125-4000	Tire vibration, air pumping	50-120 km/h	Slick	Texture	N/A
4	Mohamed and Wang	Deterministic SEA	2016	[376]	ICMM, SEA	SPL, energy, narrowband	0-500	Cavity resonance	Stationary, shaker	205/65R15	N/A	N/A

2.4.3.3 Noise Propagation Models

In these models, the sound power of TPIN is typically statistically acquired. Sound propagation theory is then applied to obtain the sound pressure level (SPL) at a given location.

The summary of noise propagation models is shown in Table 2.21. These models were generally used to predict the far-field noise level at a specific distance from the traffic. The input parameters typically included the vehicle speed, vehicle type, and some pavement parameters. The environmental parameters influencing sound propagation were more important than in the other type of models and were usually included.

Table 2.21: Summary of noise propagation models on TPIN

No.	Author	Model Name	Year	Ref.	Method	Output	Frequency Range [Hz]	Mechanism	Driver Parameter	Tire Parameter	Pavement Parameter	Environment Parameter
1	DOT	CRTN (UK)	1988	[377]	Line source	Far field, L_{10}	N/A	Traffic	Speed, vehicle type	N/A	Type, MPD, slope	N/A
2	N/A	NMPB (France)	1996	[378]	Segmentation of line source	Far field, octave, power, L_{den}	125-4000	Traffic	Speed, vehicle type, acceleration	N/A	Slope	Atmospheric absorption
3	Dai and Lee	Highway	2010	[379]	Ray acoustics	Pass-by, L_p, octave	N/A	Traffic	Speed, vehicle type, traffic volume	N/A	Type, porosity, permeability	Temperature, pressure
4	Wei et al.	Air Pumping	2016	[380]	Transfer function	Drum, SPL, narrowband	0-3500	Air pumping, radiation	461 kg, 180 kPa, 80 km/h	205/55R16, hand cut pattern	ISO 10844	N/A

2.4.4 Summary

In this section, the models on the tire-pavement interaction noise (TPIN) were divided into three categories: deterministic models, statistical models, and hybrid models.

The deterministic TPIN models include conventional physics models, finite element and boundary element models, and computational fluid dynamics models. They generally give insight into the noise generation and propagation mechanisms. The influence of each specific parameter on TPIN can be numerically analyzed. The conventional physics models typically use dynamic laws to calculate the tire vibration modes; the finite element and boundary element models are capable of obtaining the structure-borne tire noise under arbitrary excitations; the computational fluid dynamics models are intended for the airborne noise analysis. However, a large number of tire parameters are unavoidably needed for deterministic modeling, which is usually very difficult in practice. In addition, most of the models were limited to the frequency range of below 500 Hz, and few models went through the experimental validation. Therefore, the accuracy of these models is in question.

The statistical TPIN models include traditional regression models, principal component analysis models, and fuzzy curve fitting models. They generally correlate the noise levels with the influencing parameters using only experimental data without the knowledge of underlying mechanisms. It typically has better accuracy than the deterministic model. The traditional regression, including linear and non-linear regression, is widely used for models with easy form of equations and not too many variables; the principal component analysis can be used to reduce the number of variables; fuzzy logic has the advantage that no specific form of equations is needed for modeling. However, large amounts of data are needed for the statistical modeling, especially when the number of variables is large, which usually requires expensive labor cost. In addition, most of the current models only included variables related to the pavement; few models investigated the influence of tire parameters except for some fuzzy curve fitting models. It was also unlikely or impossible to gain insight into the noise generation mechanisms or separate these mechanisms.

The hybrid TPIN models include tire-pavement interface models, mechanism separation models, and noise propagation models. They combine the advantage of deterministic model

and statistical model. It sheds light on the noise generation mechanism as deterministic model, and meanwhile has good accuracy as statistical model. The tire-pavement interface model gives insight into the interaction and excitation between the tire and pavement; the mechanism separation model investigates the noise source individually; the noise propagation model is capable of predicting the TPIN at arbitrary locations. However, the hybrid model tends to be more complex than deterministic or statistical model. The careful selection of intermediate parameters is often the key to the success of the later statistical correlation procedure.

2.5 Review and the Present Study

In the present study, the measurement technique used is the on-board sound intensity (OBSI) and the physical mechanism considered is impact and air pumping. The influencing parameters include the tread pattern, tire size, and pavement texture and the modeling approach taken is artificial neural network (ANN). Thus, it is relevant to review previous attempts to use ANN for tire noise research.

There are few ANN models related to TPIN. Che et al. (2012) [266] correlated tire parameters with tire noise using ANN. Li et al. (2009) [271], [369] used Fuzzy Genetic Arithmetic (F-GA) to statistically correlate tread pattern parameters with noise levels. Fry et al. developed an ANN model to predict vehicle controlled pass-by (CPB) noise based on vehicle design parameters (Fry et al., 1999 [368]; Fry and Jennings, 2003 [381]). Additional details on these models are provided in Section 4.2.

Strictly speaking, Che et al. (2012) [266] is the only work relevant to the present study. There are several differences between the work in [266] and the present study. They are as follows:

(1) tire noise data were collected in a laboratory (drum method) in [266] while realistic data are collected on roads in the present study;

(2) tread pattern was quantified by direct and very simple parameters, such as groove length and groove width (i.e., statistical model) in [266] while the tread pattern is quantified by intermediate spectral parameters characterizing noise generation mechanisms in the

present study (i.e., hybrid model);

(3) the output of the ANN was the total tire noise in [266], while in the present study the output includes not only the total tire noise, but also the tread pattern-related tire noise and the non-tread pattern-related tire noise separately;

and (4) the noise predicted in [266] was in octave band while it is in narrowband in the present study.

3 Experiments and Data Analysis

In this chapter, the experiments for collecting tire noise data are firstly discussed. Secondly, the digitization and parameterization of tread pattern are demonstrated. Thirdly, the tire noise data are analyzed, including breaking down the total noise into two noise components (tread pattern-related and non-tread pattern-related). Lastly, the correlation between the tread pattern parameters and tire noise are conducted.

3.1 Experiments

In this section, the experimental setup for tire noise data collection is introduced, including test tires, test pavement, test equipment, and test condition [382], [383].

3.1.1 Test Tires

The forty-two tires tested are listed in Table 3.1. Pictures of their tread patterns are displayed in Figure 3.1. The red arrow in Figure 3.1 indicates the rotation direction for directional tires in the test. The full-circle tread pattern for each tire is illustrated in Table A.1 in Appendix A.1. The first nineteen tires have different tread patterns but with the same size and aspect ratio (215/60R16). Tire 20 is the Standard Reference Test Tire (SRTT). All the tires are radial tubeless tires. Most of the tires are passenger car tires, including all-season tires, winter/snow tires, one competition slick tire, and some tires just for lab purpose but not for sale. Some tires are for light truck (Tires 41 and 42), Tire 53 is for trailer only, and Tire 56 is a spare tire.

The number of pitches (or blocks), as shown in Table 3.1, is the total number of tread elements around the full tire circumference. The values range from 56 to 81, excluding the slick tire (Tire 21) of which the number of pitches is obviously zero. The number of plies in the tread band and the sidewall is different for different tires, indicating that the structure of the tires is different. However, the number of plies is shown to be not very different for the tires tested, thus it is not of interest in this study. The tread rubber hardness was the average of several measurements; it is generally accepted that the tolerance for rubber hardness measurements is ± 2 Shore A. Most of the tires are pretty new and well stored in the lab, and

the rubber hardness is generally in the range between 60 and 70 Shore A, while some tires, especially the bigger tires, are very old (over 10 years) and the rubber hardness is usually over 70 Shore A due to the age hardening effect. It is also noted that the tread of Tires 35 and 41 is intentionally shaved off, and the tread of Tires 46 and 57 is heavily worn down.

Table 3.1: Specifications of the test tires

No.	Size	Condition	Number of Pitches	Number of Plies (Tread/ Sidewall)	Rubber Hardness [Shore A]
01	215/60R16	All season	70	5/2	66.0
02	215/60R16	All season	64	4/1	63.3
03	215/60R16	All season	72	4/2	67.5
04	215/60R16	All season	64	4/1	66.5
05	215/60R16	All season	76	4/1	68.5
06	215/60R16	All season	70	4/1	64.5
07	215/60R16	All season	76	4/1	70.3
08	215/60R16	All season	56	4/2	63.7
09	215/60R16	Winter/Snow	62	3/1	59.0
10	215/60R16	All season	72	4/1	63.7
11	215/60R16	All season	72	4/1	61.7
12	215/60R16	Winter/Snow	77	4/1	57.5
13	215/60R16	All season	66	4/1	64.3
14	215/60R16	All season	68	4/1	64.0
15	215/60R16	All season	72	4/1	56.5
16	215/60R16	All season	72	4/1	67.0
17	215/60R16	All season	72	4/1	59.3
18	215/60R16	All season	65	5/2	65.8
19	215/60R16	Winter/Snow	60	5/2	66.0
20	225/60R16	All season	81	3/1	66.0
21	225/50R16	Competition	0	6/3	56.0
22	225/60R16	All season	60	5/2	65.0
23	225/60R16	All season	60	5/2	65.0
24	215/60R16	Winter/Snow	77	4/1	61.3
25	215/60R16	Winter/Snow	60	5/2	67.3
26	215/60R16	Winter/Snow	77	4/1	59.0
27	215/60R16	Winter/Snow	60	5/2	68.0

No.	Size	Condition	Number of Pitches	Number of Plies (Tread/ Sidewall)	Rubber Hardness [Shore A]
29	215/60R16	Winter/Snow	60	5/2	66.8
35	265/70R17	Bald	50	5/2	77.0
37	265/70R17	All season	50	5/2	71.5
39	255/55R18	Not for sale	85	5/2	76.5
41	235/85R16	Bald (LT)	66	5/2	72.0
42	235/85R16	All season (LT)	66	5/2	72.0
43	215/60R16	All season	28	5/2	70.0
45	235/55R19	All season	80	6/2	71.0
46	225/60R16	Worn	81	3/1	76.0
49	205/70R15	Not for sale	65	4/2	74.0
53	235/80R16	Trailer	67	5/2	79.0
54	245/40R18	All season	64	5/2	68.5
55	235/70R16	All season	72	4/2	61.5
56	125/70D16	Spare	40	3/2	75.0
57	225/60R16	Worn	66	5/2	76.5

- Tires 19, 25, 27, and 29 are the same tire for repeatability evaluation.
- Tires 12, 24, and 26 are the same tire but in different rotation direction (Tire 12 in the wrong direction; Tires 24 and 26 in the correct direction).
- Tires 35 and 37 are identical but one normal tread one bald tread. Tires 41 and 42 are identical but one normal one bald. Tire 46 is SRTT but with tread heavily worn down.
- Tire 43 has long tread blocks instead of square blocks commonly seen in other tires.
- Tire 57 has the same tread pattern as Tire 13 but different tire size and tread depth.

Figure 3.1: Tread patterns of the test tires (arrow indicates rotation direction)

It should be noted that, the noise data collected for Tire 21 (slick tire) is not valid, because small stones were picked up and stuck in the tread due to its soft rubber, making the tread not slick. Therefore, the results for Tire 21 will be presented only for completeness.

3.1.2 Test Pavement

The test pavement is U.S. Route 460 near Virginia Tech (between Toms Creek Rd. and North Main St. with one way distance of around 1.3 mile), as shown in Figure 3.2. It is a non-porous asphalt pavement, dense graded hot mix asphalt (HMA). Both eastbound section and westbound section were tested, but only results on eastbound section will be discussed; the results on westbound section show the same trends.

Figure 3.2: Test pavement (source from Google Map)

3.1.3 Test Equipment

The vehicle used for testing depends on the tire size, to be more specific, the tire outer diameter. The different sizes tested are shown in Table 3.2. For smaller tires with outer diameter smaller than 700 mm, a 2012 Chevrolet Impala LT (front-wheel drive) was used, as shown in Figure 3.3 (left). For larger tires, a 2017 Chevrolet Tahoe LT was used (all-wheel drive), as shown in Figure 3.3 (right).

Table 3.2: Different tire sizes tested

Tire Size	Section Width [mm]	Aspect Ratio [%]	Rim Diameter [inch]	Section Height [mm]	Inner Diameter [mm]	Outer Diameter [mm]
125/70D16	125	70	16	87.50	406.40	581.40
205/70R15	205	70	15	143.50	381.00	668.00
215/60R16	215	60	16	129.00	406.40	664.40
225/60R16	225	60	16	135.00	406.40	676.40
235/55R19	235	55	19	129.25	482.60	741.10
235/70R16	235	70	16	164.50	406.40	735.40
235/80R16	235	80	16	188.00	406.40	782.40
235/85R16	235	85	16	199.75	406.40	805.90
245/40R18	245	40	18	98.00	457.20	653.20
255/55R18	255	55	18	140.25	457.20	737.70
265/70R17	265	70	17	185.50	431.80	802.80

Figure 3.3: Test vehicles (left: Chevy Impala; right: Chevy Tahoe)

The equipment used for collecting noise data was an on-board sound intensity (OBSI) system based on standard AASHTO TP-76 [97]. The setup of the OBSI system is shown in Figure 3.4. The system was installed at the rear right tire with a camber angle close to zero. The conventional OBSI system has two sound intensity probes, one at the leading edge of the tire-road contact patch, the other at the trailing edge. The distance between the two probes is 8.25 inches; the distance between the probes and the tire side wall is 4.5 inches; the distance between the probes and the ground is 3.5 inches. Each probe consists of two microphones to

record the sound pressure. The sound intensity along the direction of the two microphones (away from the tire) is then calculated. Therefore, a typical OBSI has four microphones: leading inboard (Mic 1), leading outboard (Mic 2), trailing inboard (Mic 3), trailing outboard (Mic 4). The present OBSI system also has an optical sensor installed, as shown in Figure 3.4. The optical sensor radiates a beam onto the side face of the black disk rotating with the tire, and once the beam encounters the retroreflective tape and gets reflected to the optical sensor, the optical sensor generates a pulse. Therefore, a pulse signal is recorded at the exact time the tire completes one revolution. The optical signal (once-per-revolution signal) can be used to accurately calculate vehicle speed, acceleration, as well as used for the order tracking analysis, which will be discussed later. The microphone and optical signals were recorded simultaneously at 25.6 kHz.

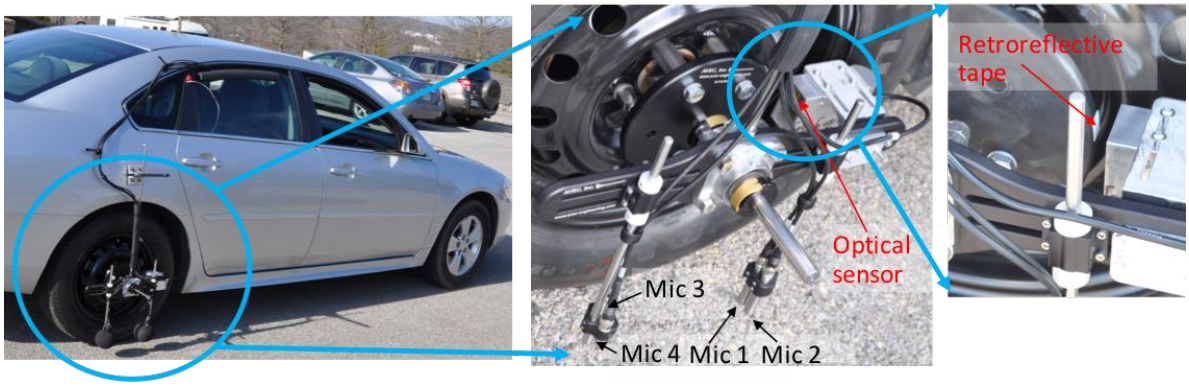

Figure 3.4: On-board sound intensity (OBSI) with optical sensor installed on the test vehicle

It should be noted that, larger tires can only be tested on Chevy Tahoe because they don't fit into the wheel cavity of Chevy Impala, as shown in Figure 3.5 (left). Smaller tires can only be tested on Impala, because once they are installed on Chevy Tahoe, the ABS/ESC keeps braking the smaller tire automatically because its rotational speed is much faster than the other tires; this issue was still not solved even after the fuses of ABS and stability control were unplugged, as shown in Figure 3.5 (right). That is, there is no tire available to us that can be tested on both Chevy Impala and Chevy Tahoe. Therefore, the repeatability evaluation for Chevy Impala and Chevy Tahoe is not available. However, it is supposed that the only difference that influences TPIN between Chevy Impala and Chevy Tahoe is the tire vertical load. Generally, for passenger car radial tires TPIN increased by 1 to 2 dBA per doubling of

wheel load when inflation pressure was adjusted to the load; by 0.7 to 1.5 dBA if inflation pressure was not adjusted (Taryma, 1982 [384]). The load difference between Impala and Tahoe should be less than doubling, so the TPIN error should be less than ~1 dBA, which is considered as insignificant in acoustics. As such, the data collected on Impala and Tahoe are deemed as comparable.

Figure 3.5: Issues in testing tires of different sizes (left: larger tires on Impala; right: smaller tires on Tahoe)

Another issue met in testing on Chevy Tahoe is that, the wheel bolt pattern is 6x5.5 in. while the rim bolt pattern of tested tires is 5x4.5. Therefore, a wheel adapter converting from 6x5.5 to 5x4.5 was used, as shown in Figure 3.6.

Figure 3.6: Wheel adapter

3.1.4 Test Condition

The noise data collection tests were conducted from early 2016 to early 2017, as shown in Table 3.3. For each tire, the noise data were collected under five different vehicle speeds, i.e., 45, 50, 55, 60, and 65 mph (72, 80, 89, 97, and 105 km/h). In addition, an acceleration test was

also conducted where the vehicle accelerated from 45 to 65 mph (from 72 to 105 km/h) within 10 seconds. The inflation pressure was set to 32 psi (221 kPa) for tires on Impala, and to 40 psi (276 kPa) for tires on Tahoe. For some tires, 26, 32, and 40 psi (179, 221, and 276 kPa) were all tested, but will not be discussed here. The inflation pressure does not have much influence on TPIN, as shown in Appendix D: Effect of Tire Inflation Pressure. The ambient temperature range during the test days was 37-86 °F (3-30 °C). For repeatability evaluation, Tire 19 was tested in multiple test sets as indicated by Tires 25, 27, and 29; very good repeatability was shown (error < 1 dB), indicating temperature does not have much influence.

Table 3.3: Noise data collection field tests

Test Set	Tire No.	Test Date	Temperature [°F]
1	12 15 18 19 20 21	Mar 8-11, 2016	55-74
2	02 07 08 09 10 11 13 17 24 25	Jun 13-16, 2016	62-82
3	01 03 04 05 06 14 16 22 23 26 27	Sep 6-8, 2016	72-86
4	29 43 46 49	Nov 22, 2016	37-47
5	54 56 57	Feb 17, 2017	55-62
6	35 37 39 41 42 45 53 55	Apr 5-8, 2017	45-67

3.2 Tread Pattern Characterization

Tread pattern contributes to tire pavement interaction noise through two major mechanisms: (1) tread impact due to the interaction between the tread blocks and the pavement texture, and (2) air pumping due to the air compression/expansion in the tread grooves. In this section, two tread pattern spectra, i.e., tread profile spectrum and air volume velocity spectrum, are calculated from the three-dimensional tread profile to characterize the two mechanisms, respectively.

The 3D tread pattern/profile was obtained using a CTWIST laser scanning machine. An example of the digitized 3D profile is illustrated in Figure 3.7. The measurement resolution is ~0.5 mm in the length/width direction and <0.01 mm in the height direction. It is noted that the CTWIST data are not available for all the tires; most of the bigger tires were not scanned. Therefore, the results in this section only include smaller tires, but the analysis procedure is valid for all the tires of different sizes.

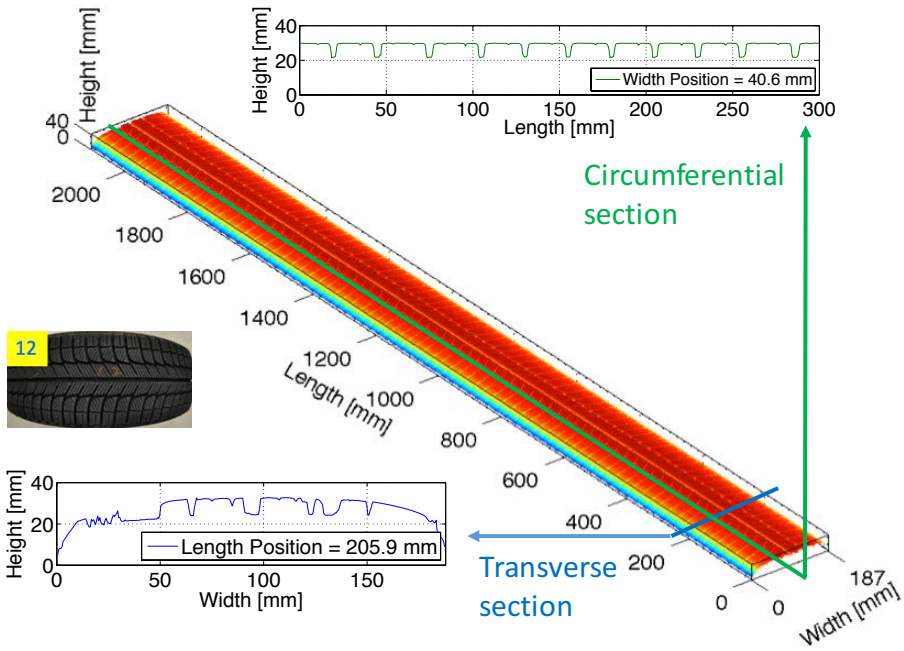

Figure 3.7: Illustration of 3D tread profile of Tire 12

3.2.1 Tread Profile Spectrum

The tread impact mechanism of tire noise generation is the sudden impulse contact between tire tread blocks and pavement. The resulting sound can be considered as the contribution of hundreds of small hammer strokes each second [6]. At the leading edge, the impact mechanism occurs as the tread block is pushed in toward the tire center; at the trailing edge, the release of the tread block can be considered as an inverse impact [149]. This mechanism is caused by the nonhomogeneities of the tire tread assuming the pavement surface is smooth and homogeneous. The parameter used to quantify the nonhomogeneities of the tire tread is the tread profile spectrum characterizing the height variations of the tire tread. The tread profile height for each circumferential section is converted from the spatial domain (height versus length) to the time domain (height versus time) assuming a vehicle speed, e.g., 60 mph. The time domain signal is then Fourier transformed, complex data that contain both amplitude and phase, and then the spectrum is computed. Figure 3.8a illustrates the resulting profile spectra for all circumferential sections (width of tire) as a 2D color plot for tire. In this plot, the tread pattern pitch passing frequency is easily observed at around 1000 Hz. The pitch passing frequency is computed as the number of pitches times the tire angular velocity in Hz

(e.g., ~13 Hz at 60 mph). The spectral colormap for other tires is demonstrated in Figure A.1 in Appendix A.2.

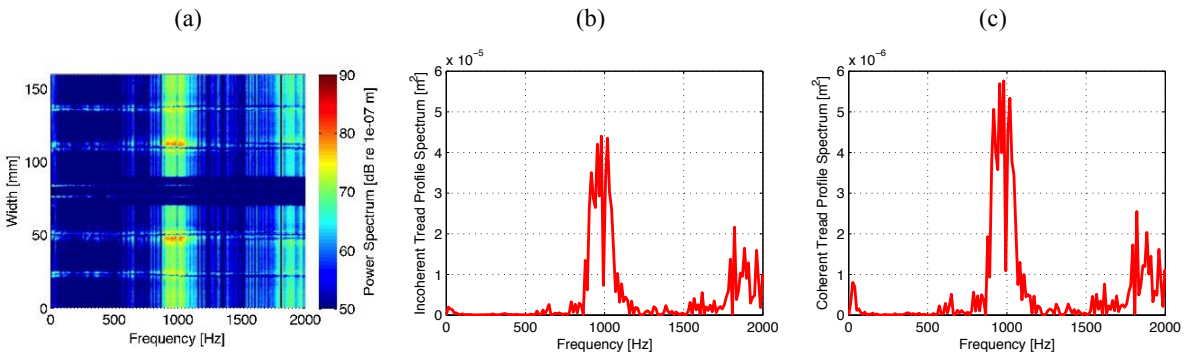

Figure 3.8: (a) Tread profile power spectra for all circumferential sections; (b) incoherent tread profile spectrum; (c) coherent tread profile spectrum at 60 mph for Tire 12 (12.5 Hz resolution)

There are two options to reduce the 2D spectral information in Figure 3.8a to a single representative spectrum. The simplest approach is to compute the average spectrum across the tire width, i.e., incoherent addition, as illustrated in Figure 3.8b. This approach ignores the phase information (i.e., offsets between different rows of tread elements) and it doesn't correlate well with the tire noise. Therefore, this approach is not considered further. If the tread block offset information is to be accounted for, the averaging process across the tire width must be performed using the Fourier transform complex data and then the spectrum computed from the average Fourier Transform. This average power spectrum is called coherent tread profile spectrum since it accounts for the relative phase between tread profile along the tire width. As an illustration, the coherent tread profile spectra for test tire 12 is displayed in Figure 3.8c. It can be observed that peaks occur around the pitch passing frequency (77×12.7≈980 Hz) indicating that the number of pitches has the greatest influence on the tread profile spectrum.

The incoherent and coherent tread profile spectra are displayed in Figure 3.9 for all test tires. It is shown that, the coherent tread profile spectrum is nearly an order of magnitude smaller than that of incoherent tread profile, indicating that the process of tread element randomization and offset plays a great role in making the tread pattern less aggressive, especially for Tire 02, where the incoherent tread profile spectrum is among the largest while

its coherent tread profile spectrum is much smaller.

Based on the coherent tread profile spectrum, the most "aggressive" tread patterns are Tires 09, 12, and 19, which are winter tires. Their tread patterns tend to be symmetric with respect to the central line of the tire tread band and the length of each block is nearly the same. There are marginal cancellation effects (destructive interference) between rows in the tread pattern. On the contrary, the noise produced by these rows adds constructively since they produce nearly phased noise, i.e., influence of tread element randomization and offset is not significant. They are called directional tires that tend to have symmetric tread pattern style leading to large coherent tread profile spectra.

(a) Incoherent tread profile spectrum

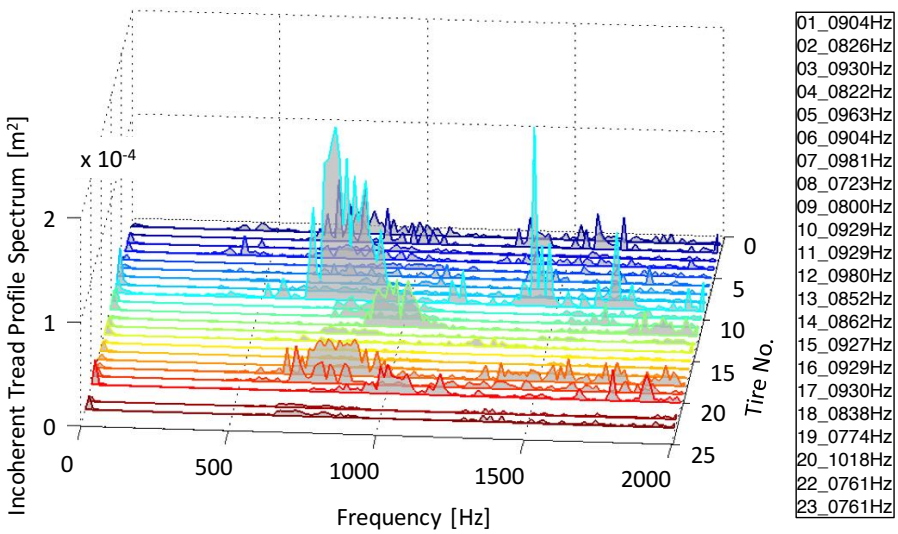

(b) Coherent tread profile spectrum

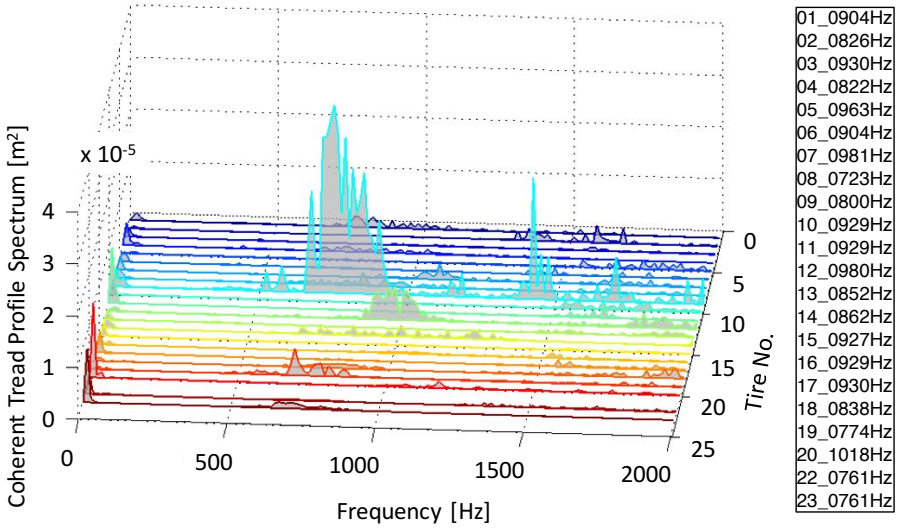

Figure 3.9: Incoherent and coherent tread profile spectra at 60 mph for all tires (legend includes tire number and pitch passing frequency)

It is found that the coherent tread profile spectrum is better correlated with tire noise generation than the incoherent tread profile spectrum. Therefore, the coherent tread profile spectrum is used as the tread pattern parameter to characterize the tread impact mechanism. In the following, the tread profile spectrum refers to the coherent one unless otherwise specified.

3.2.2 Air Volume Velocity Spectrum

The air pumping mechanism is caused by the variation of the air volume enclosed between the tread and the road surface in the contact patch. As the tire rotates, the air volume in the contact patch changes with time becoming a noise source. This noise generation mechanism is known as air pumping [6],[35]. In terms of acoustics [385], noise is produced by the rate of change of air volume (volume velocity). Likewise, Figure 3.10 illustrates the approach implemented to estimate the volume velocity time history and spectrum for the tires tested. Firstly, a simple rectangular-shaped contact patch geometry is assumed, as seen in Figure 3.10a. In the future, this contact patch shape can be improved to better represent the actual contact patch. Secondly, the tire is assumed to rotate at 60 mph, so the contact patch also moves along the tire circumference at 60 mph, e.g., to the right in Figure 3.10a. Next, utilizing the 3D digitized tread profile, the air volume in the tread grooves within the contact patch at

each moment of time is calculated and illustrated as air volume versus time in Figure 3.10b. Then, the air volume signal is differentiated with respect to time to yield the volume velocity trace in Figure 3.10c. Finally, the air volume velocity spectrum is obtained by taking the Fourier transform shown in Figure 3.10d. It should be noted that this process doesn't account for the deformation of rubber due to loading that might change the air volume. However, it should not have much influence on the spectral shape in Figure 3.10d.

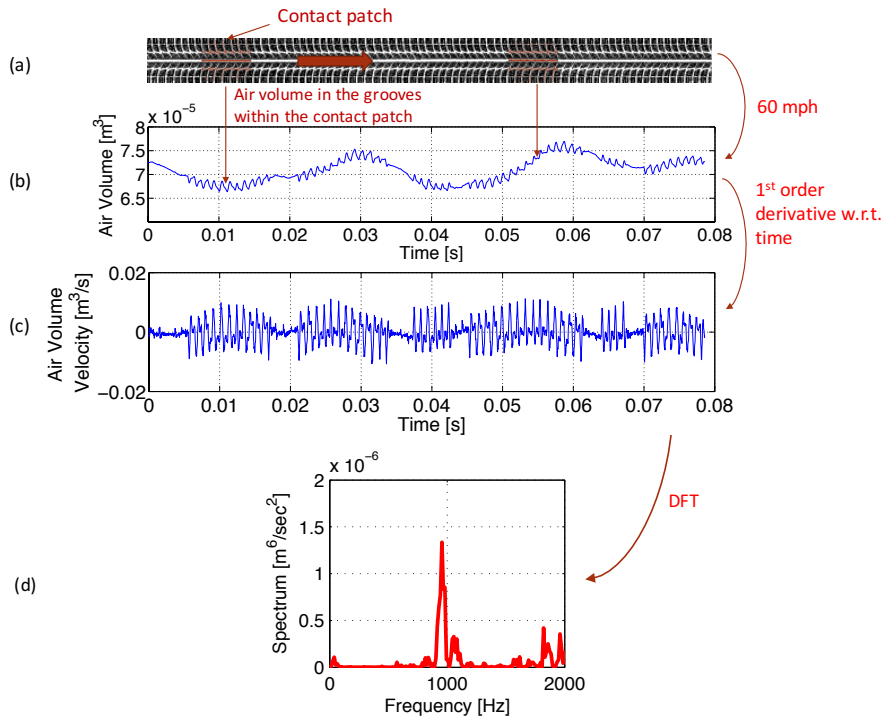

Figure 3.10: Illustration of calculation of air volume velocity spectrum (Tire 12)

The air volume velocity spectra for the test tires are shown in Figure 3.11. Similar to the coherent tread profile spectra, the dominant part of the volume velocity spectrum also occurs around the pitch passing frequency. However, there is no significant spreading of the energy around the pitch passing frequency, i.e., usually a single dominant peak at the pitch passing frequency. The spectral content agreement between the coherent tread profile and air volume velocity spectra indicates the tread impact and air pumping mechanisms have the same dominant frequency ranges (around pitch passing frequency). This is expected since they are both produced by the same periodic tread pattern). This observation is different than the results reported from most literature where it was argued that the tread impact is dominant in

the low frequency below 1000 Hz while the air pumping is dominant in the high frequency over 1000 Hz [24].

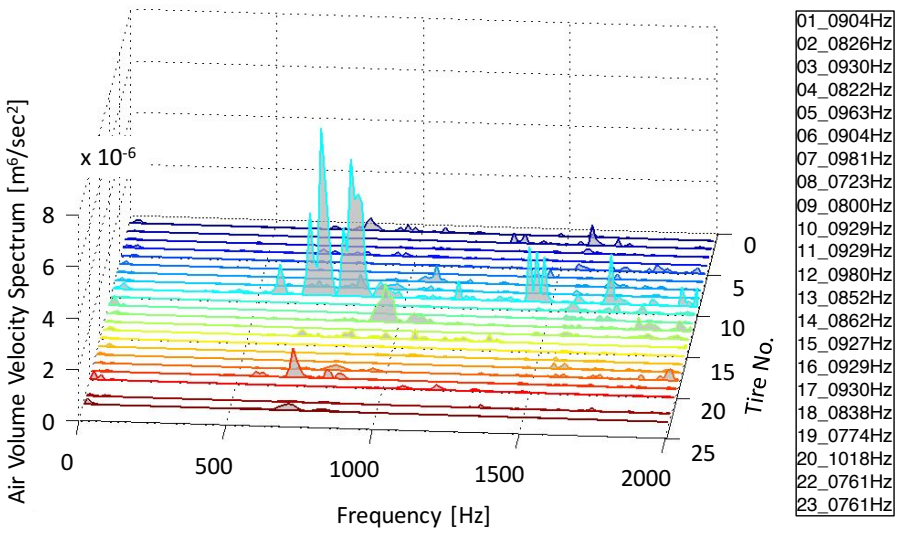

Figure 3.11: Air volume velocity spectrum at 60 mph for all tires (legend includes tire number and pitch passing frequency)

3.3 Tire Noise Analysis

In each test run, the total time duration of data collected was 73-106 seconds depending on the vehicle speed. A high-pass filter at 20 Hz was applied to the sound pressure time signals to eliminate contamination from wind noise. In this section, only the signal from the leading inboard microphone (Mic 1) will be used for the illustration unless otherwise specified. However, the same results were observed and conclusions drawn from the other microphones.

As indicated in 3.2, the tread pattern data are basically available for smaller tires for the moment. As such, correspondingly, the results for the tire noise analysis are presented only for the smaller tires in this section. However, the analysis procedure is valid for all the tires of different sizes; the results are later shown in Figure 4.5. It should be pointed out that all the results presented in this section are only valid for the pavement tested.

3.3.1 Tire Noise Components

The un-weighted sound pressure level spectrogram (dB) for Tire 12 during the acceleration

test (from 45 mph to 65 mph within 10 seconds) is shown in Figure 3.12. This figure is used to illustrate that there exist two main noise components in the dominant part of the spectrum, i.e., 600 to 1200 Hz. The first component is clearly associated to the vehicle speed or tire speed with the center band frequency going from 700 to 1000 Hz as the vehicle speed increases from 45 mph to 65 mph. The second component is independent of the vehicle speed (or tire rotation) with the spectral content encompassed always within the fixed frequency range between 600-1200 Hz.

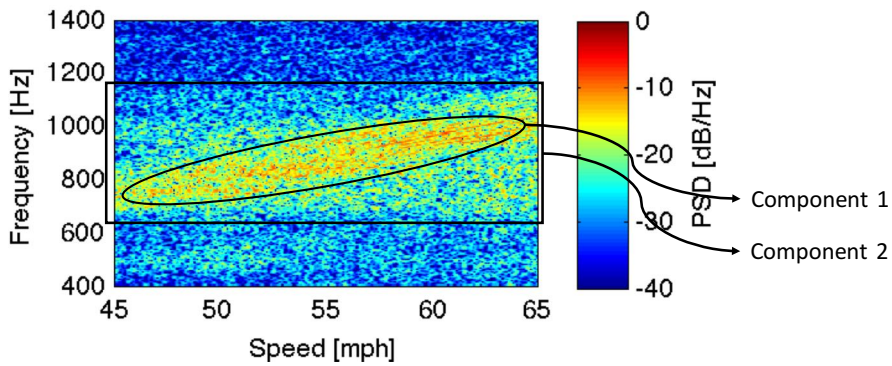

Figure 3.12: Spectrogram of microphone 1 (leading inboard) for Tire 12 accelerating from 45 mph to 65 mph

Both, the tread impact and the air pumping, are periodic with the rotation of the tire. It is reasonable to infer that the first component of noise is related to the tread pattern. This noise component is, thus, referred to as tread pattern noise (TPN). The second component is clearly not related to the periodic tread pattern and it is most likely due to tire structural vibration excited by the roughness of the pavement. However, for the sake of generality, this second noise component is referred here as non-tread pattern noise (NTPN). It should be noted that, the tread pattern noise and non-tread pattern noise are categorized by the excitation source (periodic tread pattern or non-periodic pavement) rather than the vibration response position (tire tread or carcass). Both tire tread noise and tire carcass noise consist of both tread pattern noise and non-tread pattern noise. To be more specific, the tire tread noise includes two parts: (1) tread pattern noise that is periodic and related to the geometry/layout of the tread elements, and (2) vibration noise of tread elements that is randomly excited by the pavement and more related to the stiffness of the tread elements, which is not considered as tread-pattern related, thus belongs to the non-tread pattern noise. Likewise, the tire carcass noise also consists of

tread pattern noise and non-tread pattern noise.

For the results of another tire (Tire 15) shown in Figure 3.13, there is no obvious oblique component, which means the tread pattern noise is insignificant.

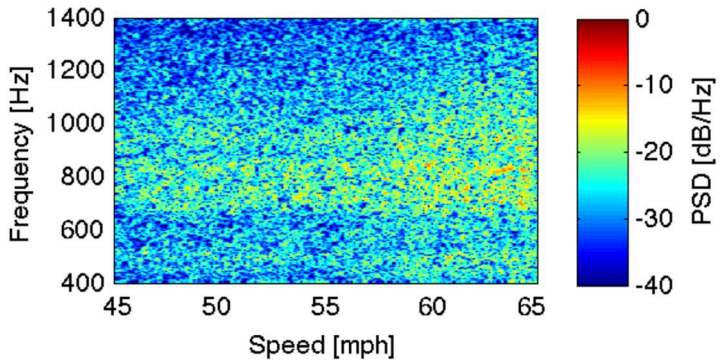

Figure 3.13: Spectrogram of microphone 1 (leading inboard) for Tire 15 accelerating from 45 mph to 65 mph

Perhaps another way to define the two tire noise components can be illustrated in Figure 3.14. Assuming a tire with no tread pattern (e.g., slick tire) on a purely smooth pavement (e.g., steel drum), as shown in Figure 3.14a, there will be negligible tire noise generated due to no excitation source. Assuming a tire with tread pattern on a purely smooth pavement, as shown in Figure 3.14b, the tire noise generated is basically due to tread pattern excitation, i.e., tread pattern noise. Assuming a tire with no tread pattern on a rough pavement, as shown in Figure 3.14c, the tire noise generated is basically due to pavement texture excitation, i.e., pavement texture noise. Under normal conditions, i.e., a tire with tread pattern on a rough pavement, as shown in Figure 3.14d, the tire noise generated is basically due to two excitation sources: (1) tread pattern excitation that is periodic (self-repeated per tire revolution); (2) pavement texture excitation that is random. The characteristics of response (noise generated) are supposed to be the same as the excitation source. Therefore, the tread pattern noise is periodic while the pavement texture noise (or non-tread pattern noise for generality) is random, based on which the two noise components can be separated.

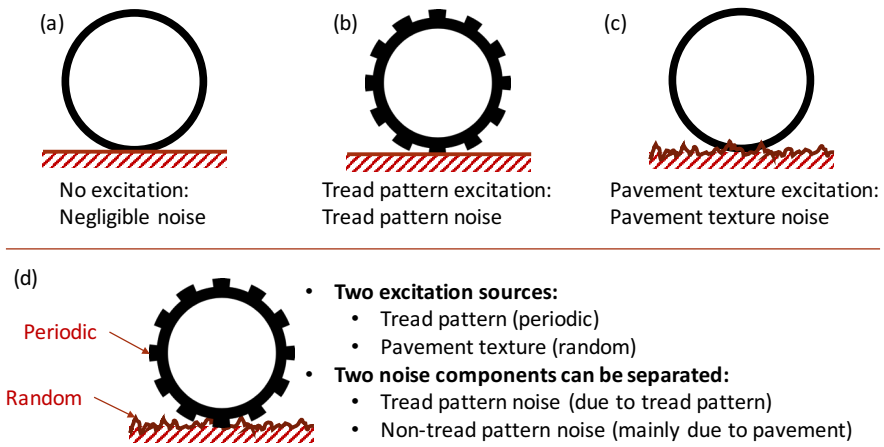

Figure 3.14: Illustration of two excitation sources and tire noise components

For a proper correlation analysis between the tire noise and the tread pattern, these two noise components must be separated. The pipe resonance due to longitudinal tread grooves is considered as a noise amplification mechanism rather than a noise generation mechanism, i.e., the pipe resonance is able to amplify both tread pattern noise and non-tread pattern noise. For some cement concrete pavement tined with evenly spaced lateral slots, a tonal noise whose frequency scale with speed can be generated due to the periodic pavement texture, as shown in Appendix E: Tones due to Pavement Distress. However, as long as the pavement texture is not exactly periodic (some errors of slot intervals may inevitably occur), this tonal noise will be separated into the non-tread pattern noise using order tracking analysis, which indicates the separation technique discussed in the present paper is still valid (results not shown here). It should be noted that the results and conclusions on the speed effect in the present paper is only valid for the tested pavement which is isotropic.

3.3.2 Order Tracking Analysis

The technique used for the separation of the tread-pattern and non-tread-pattern noise components using the optical sensor signal is a conventional approach called order tracking analysis. This separation technique is briefly described here. Figure 3.15a shows a typical trace from the optical sensor. The time elapsed between successive pulses represents a full revolution of the tire been tested. Since the optical signal was simultaneously recorded with the microphone sound pressure signals, these pulses were then used to identify the

microphone signal windows corresponding to each tire revolution as shown in Figure 3.15b. Each individual microphone windowed signal was resampled to have the same number of data points (1800 points here), independent of their actual time length. The resampled microphone windowed signals were then Fourier Transformed and coherently averaged, thus, rejecting the noise signal not related to the tire rotation (i.e., tread pattern). The averaged complex value Fourier Transform is then converted back to the time domain by taking the inverse Fourier Transform as illustrated in Figure 3.15c. The non-tread pattern noise component, as shown in Figure 3.15d, is computed by subtracting (window by window) the tread-pattern noise time traced from the total (or original) resampled signal, i.e., difference between Figure 3.15b and Figure 3.15c.

(a) Optical sensor signal example

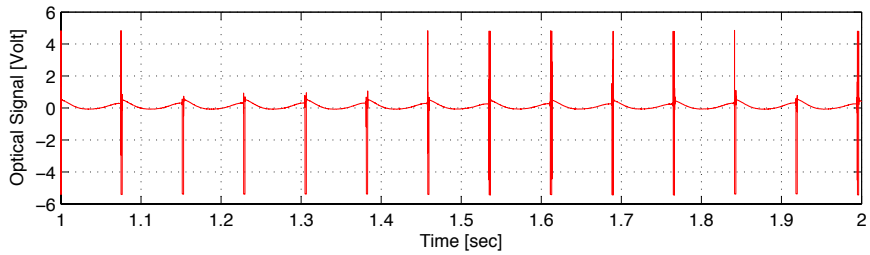

(b) Total microphone signal (each window representing one tire revolution)

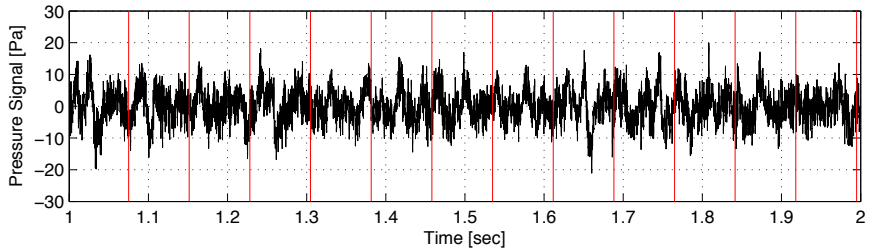

(c) Tread-pattern noise signal

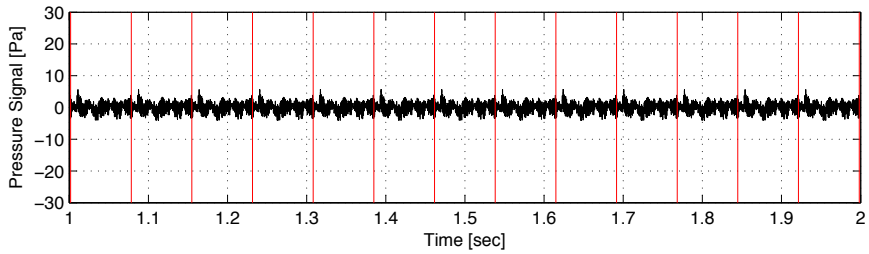

(d) Non-tread-pattern noise signal

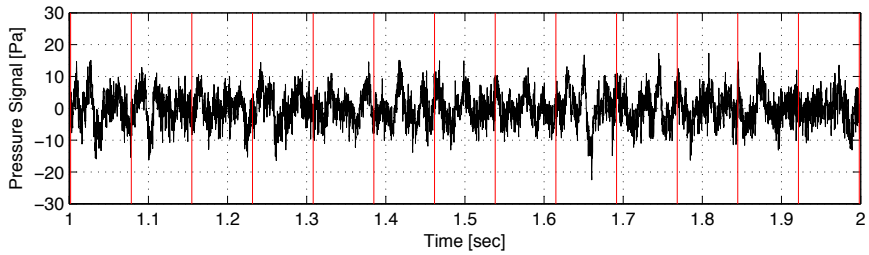

Figure 3.15: Illustration of separation of tread-pattern noise and non-tread-pattern noise (60 mph test)

3.3.3 Tire Noise Separation

In this section, order tracking analysis utilizing the optical signal is performed to separate the two components of noise signals. The total tire noise (TTN), tread pattern noise (TPN) and non-tread pattern noise (NTPN) spectra for each tire are displayed in Figure 3.16. It can be observed that the tread pattern noise component is significant (10~50% of total noise) for Tires 01, 09, 12, 16, and 19. For the other tires, the tread pattern noise is significantly lower than the non-tread pattern noise. It also explains why the total noise spectrum coincides to a large degree with the non-tread pattern noise spectrum for those tires, as shown in Figure 3.16. The tread pattern noise contribution is displayed in Table 3.4. It can be seen that for most of tires, the tread pattern noise on the non-porous asphalt pavement tested contributes marginally to the total noise (below 5%). Only five tires (Tires 01, 09, 12, 16, and 19) have tread pattern noise contribution of over 10%. For Tire 09, about half of the energy comes from tread pattern noise. It is also implied that winter tires (Tires 09, 12, and 19) tend to have large tread pattern noise.

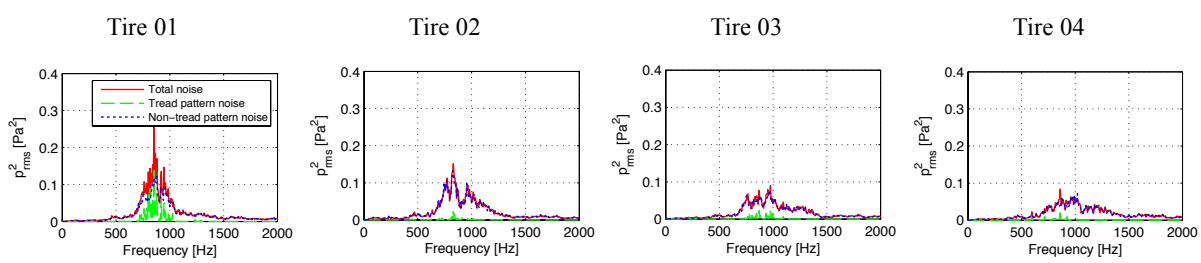

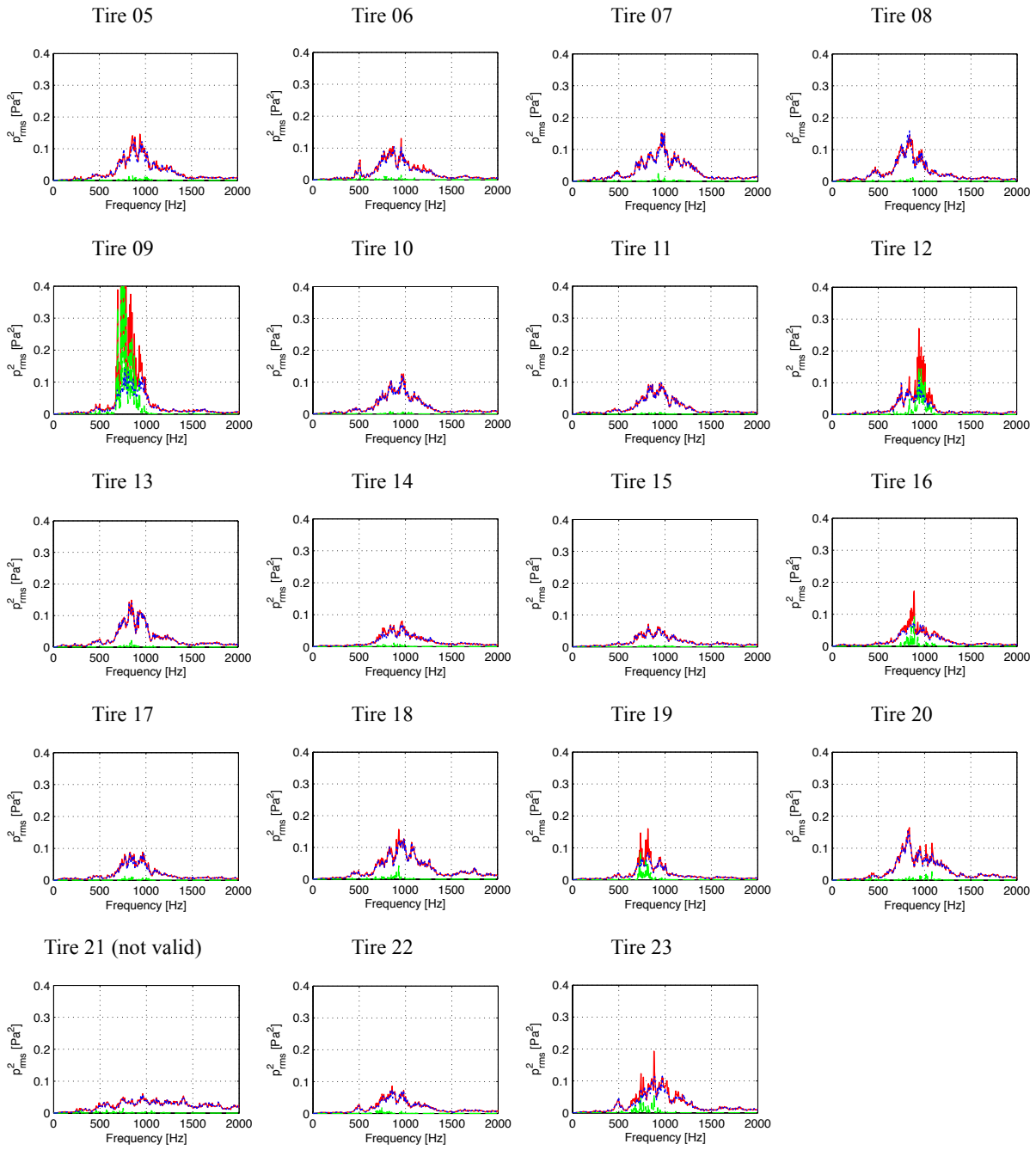

Figure 3.16: Total, tread-pattern, and non-tread pattern noise components at 60 mph (A-weighted, 5 Hz resolution)

Table 3.4: Overall A-weighted sound pressure level of noise components (red indicates snow tire)

Tire No.	Total Noise Level [dBA]	Tread Pattern Noise Level [dBA]	Non-Tread Pattern Noise Level [dBA]	Tread Pattern Noise Contribution [%]
01	**104.1**	**95.8**	**103.3**	**15.1**
02	103.7	88.1	103.6	2.7
03	102.8	90.2	102.6	5.4
04	102.9	87.4	102.7	2.9
05	104.5	89.2	104.3	3.0
06	103.8	88.7	103.6	3.1
07	105.1	87.6	105.0	1.8
08	104.4	86.7	104.3	1.7
09	**106.3**	**102.7**	**103.5**	**45.4**
10	103.8	86.8	103.8	2.0
11	103.3	85.5	103.2	1.7
12	**103.4**	**97.1**	**102.3**	**23.4**
13	104.4	88.4	104.3	2.5
14	102.4	87.4	102.2	3.2
15	102.1	86.6	102.0	2.8
16	**102.8**	**92.9**	**102.3**	**10.3**
17	102.8	88.0	102.7	3.3
18	105.2	90.6	105.1	3.5
19	**102.4**	**93.1**	**101.8**	**12.0**
20	105.0	90.7	104.8	3.8
21	104.4	89.5	104.3	3.2
22	102.6	88.2	102.5	3.6
23	104.6	92.6	104.2	6.5

It is important to mention that the relative contribution of tread-pattern and non-tread pattern noise components is a function of the pavement, as shown in Appendix F: Rough and Smooth Pavement. Thus, the results presented here are only valid for the pavement tested. Preliminary data from testing on a newer and smoother asphalt pavement show that the tread pattern noise contribution increases, e.g., to 50% of the total tire noise for Tire 12, and to ~70% of the total tire noise for Tire 09.

The total, tread pattern, and non-tread pattern noise spectra for all test tires are shown in Figure 3.17. Figure 3.17a shows that the total noise has a dominant frequency range between 400 and 1400 Hz for all the tires, but the location and amplitude of spectral peaks differ. Figure 3.17b shows that the tread pattern noise varies a lot for different tires, which is expected because the tread pattern noise is dependent on the tread pattern. Figure 3.17c shows that, after the tread pattern noise is removed from the total noise, all the non-tread pattern noise spectra of the test tires are similar, which makes sense because non-tread pattern noise is supposed to be independent on the tread pattern, but dependent on the pavement and tire structure, and all the tires have similar structure and were tested on the same pavement. Table 3.4 also shows that the non-tread pattern noise level ranges from 101.8 to 105.1 dBA (3.3 dBA difference), not as large a range as tread pattern noise from 85.5 to 102.7 dBA (17.2 dBA difference). However, even though typically not dominant, the tread pattern noise is usually tonal noise with frequencies around pitch passing frequency, which sounds annoying to human ears. The non-tread pattern noise is more like broadband noise, which sounds more pleasant even though it is generally larger than the tread pattern noise.

(a) Total noise spectra

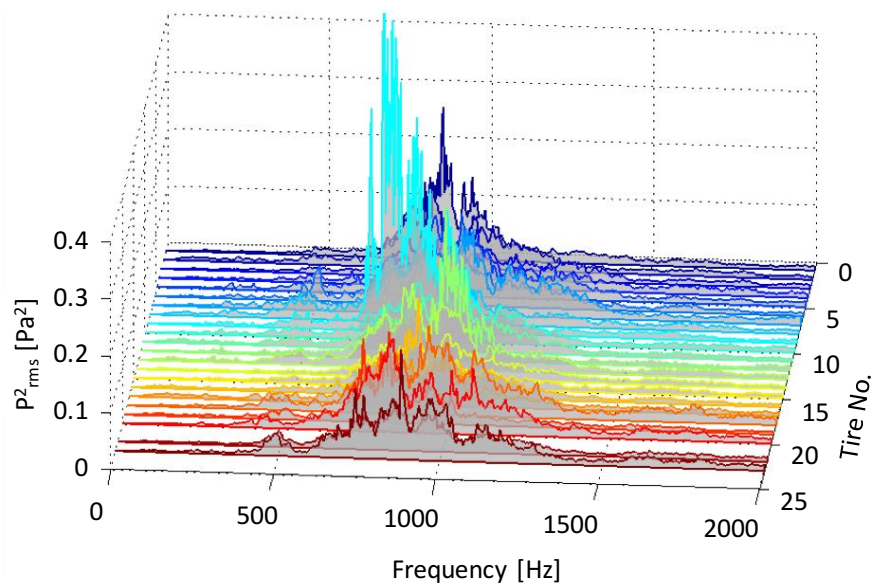

(b) Tread pattern noise spectra

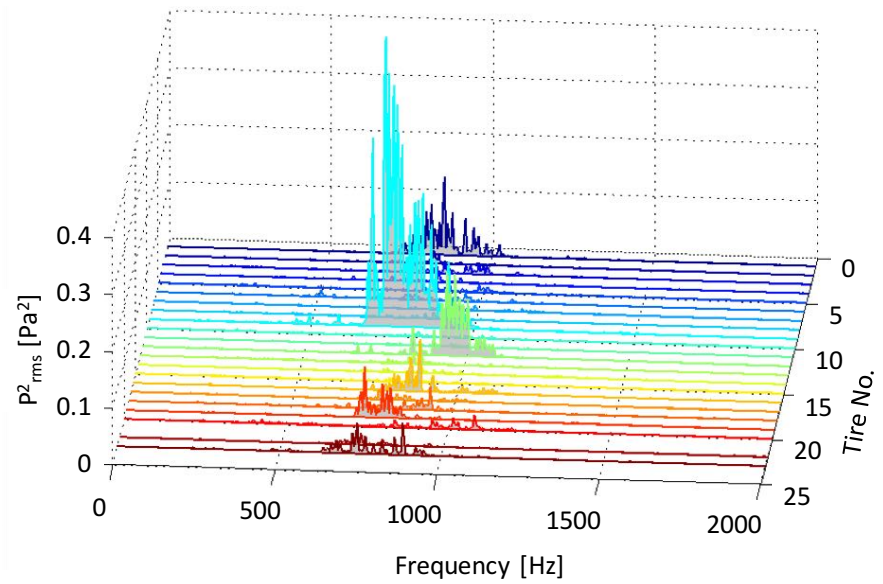

(c) Non-tread pattern noise spectra

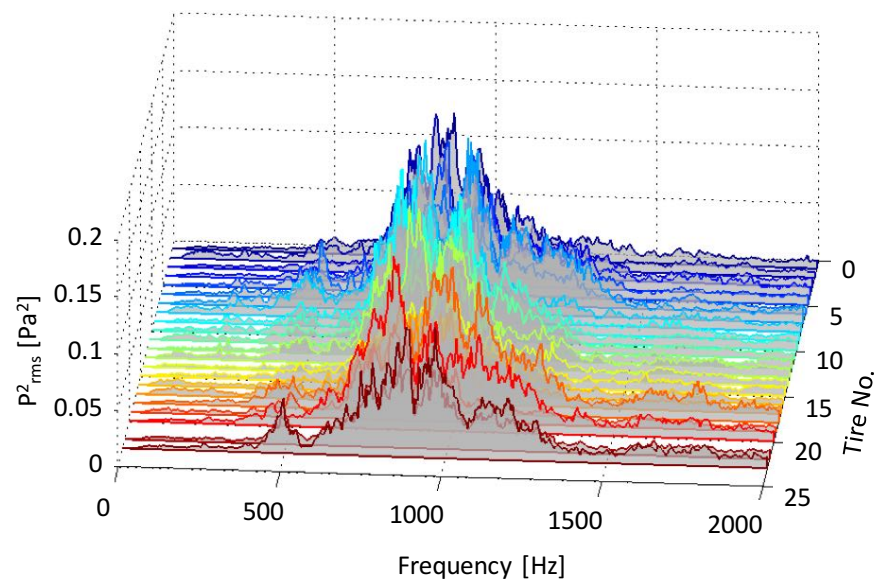

Figure 3.17: Total, tread-pattern, and non-tread pattern noise components at 60 mph (A-weighted, 5 Hz resolution)

For the tires that have a large component of tread pattern noise, more oblique spectral contents will occur in the spectrogram of acceleration test, as shown in Figure 3.12. For the

tires that have a small component of tread pattern noise, the spectral contents in the spectrogram of acceleration test will remain nearly level, as shown in Figure 3.13. This explains why the results contradicted each other in some of the literature [270], [386]. Alt [270] showed that the dominant frequencies of TPIN do not change with speed while Schumacher [386] indicated that they do. The present study suggests that both circumstances exist. The reasons no previous literature have reported this finding might be: (1) most studies used pass-by noise measurement technique, which is not suitable for acceleration test that requires relatively long duration of noise collection; (2) the studies using lab drum to collect acceleration noise data might be subjected to contamination from drum noise.

The non-tread pattern noise can be potentially considered as the minimum tire noise for a specific tire when the tread pattern is perfectly randomized and the tread pattern noise is reduced to zero. A perfectly randomized tread pattern is similar to a slick tread pattern in perspective of tire pavement interaction noise generation. That is also to say, usually for the tires for which the tread patterns are already well randomized, further optimization of tread patterns will not result in too much noise reduction. An important conclusion of this study is that the easier way to reduce tire noise is to reduce the non-tread pattern noise which is shown by the data to be the major component, at least for the pavement used in this field tests. This also explains why sometimes the slick tire is among the noisiest [255], as it is the non-tread pattern noise rather than the tread pattern noise that predominantly determines the acoustic performance of a tire for a specific pavement. This is further investigated in Appendix G: Characteristics of TPIN from Slick Tire.

3.3.4 Order Spectrum

When analyzing periodic sound and vibration signals from rotating or reciprocating machinery, order power spectrum is often used instead of frequency power spectrum. Order can be considered to be a normalized frequency defined as frequency in Hz divided by rotational speed also in Hz, giving a non-dimensional unit. An example for converting frequency spectrum to order spectrum is illustrated in Figure 3.18. It should be noted that, the actual definition and calculation of order spectrum is more complicated than this, and the Fourier Transform (FT) should be performed in the angle domain converted from the time domain. However, for the quasi-steady-state condition (rotational speed varies just a little bit

with time) in this case, it can be considered as valid. The shape of frequency spectrum and order spectrum in Figure 3.18 seems a little bit different, and this is because the frequency resolution is 5 Hz (< 13 Hz) for the former while the order resolution for the latter is 1. Therefore, Figure 3.18a looks denser (13/5 = 2.6 times denser or precise) than Figure 3.18b. Physically speaking, order can only be at integers.

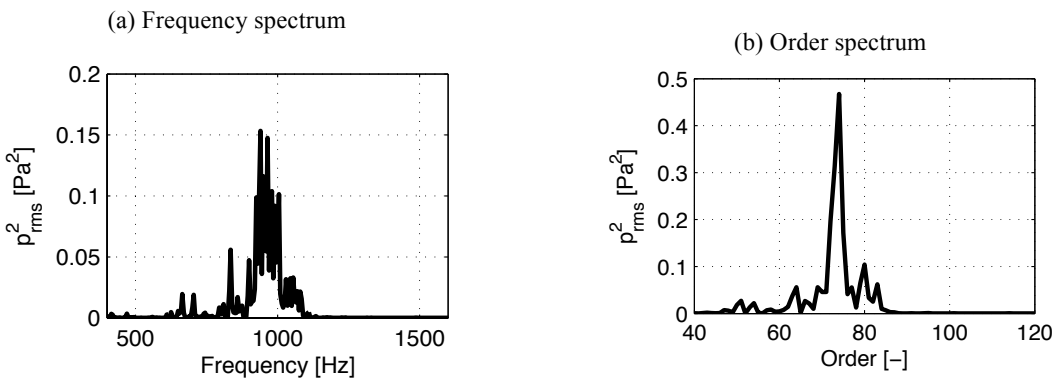

Figure 3.18: Frequency spectrum (resolution = 5 Hz) and order spectrum (resolution = 1) for tread pattern noise of Tire 12 at 60 mph (~13 Hz)

There are some advantages to present tread pattern noise in order spectrum compared to frequency spectrum: (1) the spectral position doesn't shift with speed (independent of speed, only amplitude changes); (2) order is correlated with number of pitches, e.g., as shown in Figure 3.18, order spectrum shows peak at 77 which is exactly the number of pitches for this tire; (3) for constant speed cases, order spectrum (order resolution = 1) can be easily converted to frequency spectrum if rotational speed is given (frequency resolution = rotational speed in Hz).

In the following, the tread pattern spectra and tread pattern noise spectrum will be analyzed in order spectrum.

3.4 Correlation between Tread Pattern and Tire Noise

To correlate the tread pattern to the tire noise, the spectral content of the tire tread pattern and the tire noise are compared. If there is agreement in the shape and frequency content of the spectrums, they are believed to be related and one can be used to estimate the other. To

achieve this, the coherent tread profile and the air volume velocity spectral shapes are compared with the tire noise spectral shape, including the total noise, tread pattern noise component, and non-tread pattern noise component. The results for Tires 12 and 19 are shown in Figure 3.19 and Figure 3.20, respectively. The coherent tread profile and the air volume velocity spectra are first calculated in the frequency domain assuming the tire rotates at 60 mph, then converted to order domain (divide frequency by the tire rotational speed in Hz). The noise spectra are calculated directly in the order domain. It is noted that the order resolution for all the spectra is 1.

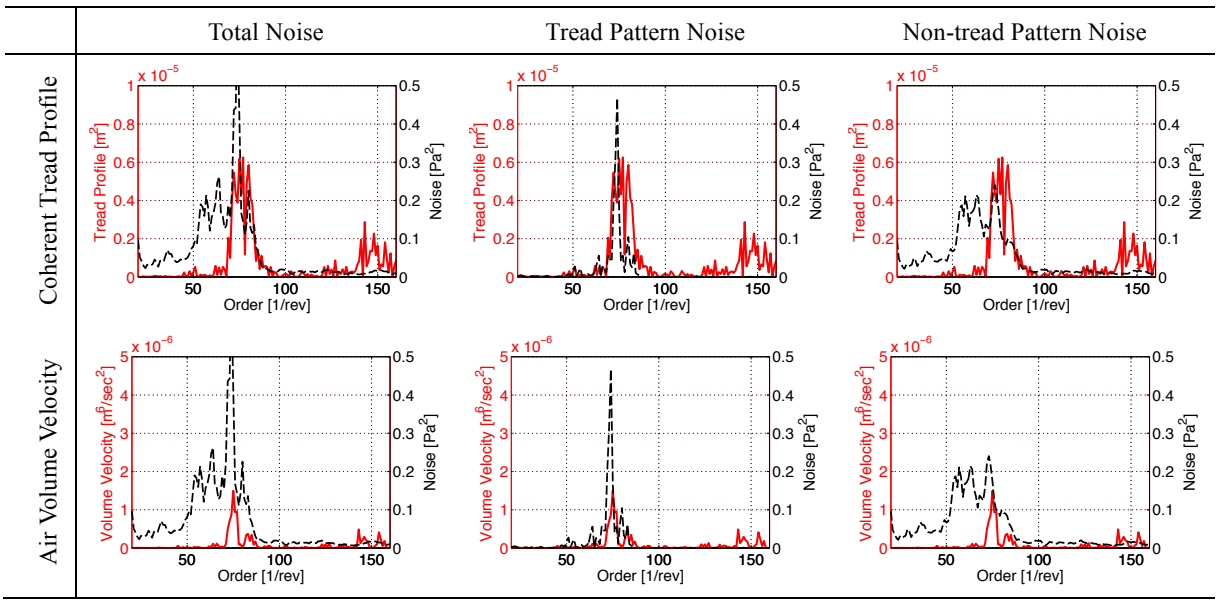

Figure 3.19: Comparison between the tread pattern spectra in red and the tire noise spectra in black for Tire 12 at 60 mph (number of pitches = 77)

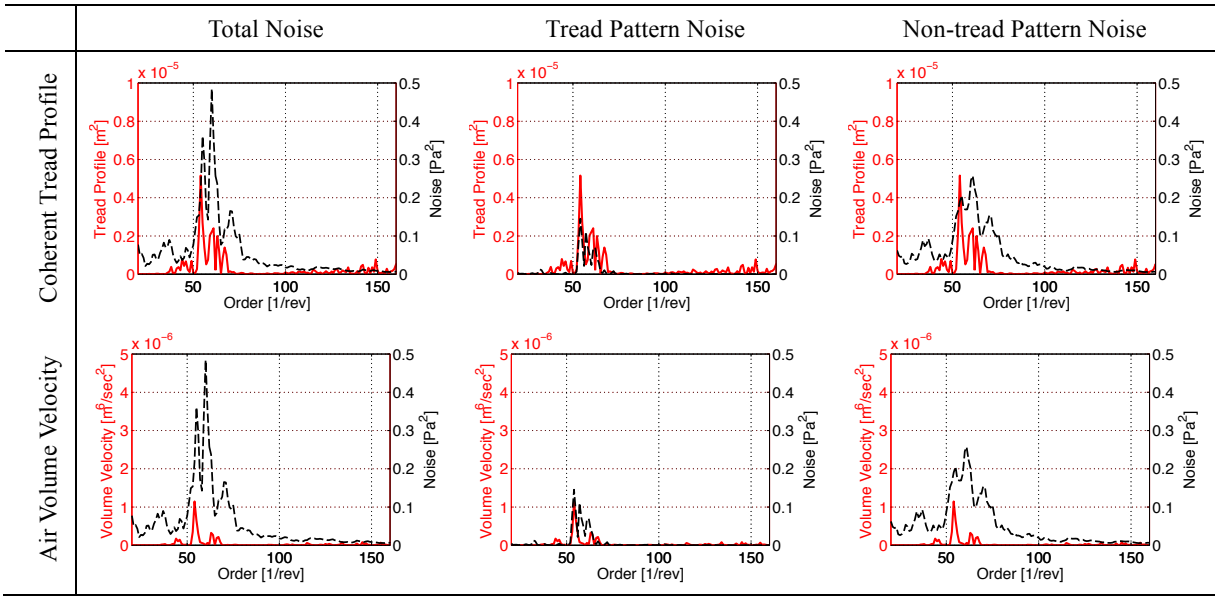

Figure 3.20: Comparison between the tread pattern spectra in red and the tire noise spectra in black for Tire 19 at 60 mph (number of pitches = 60)

The plots for all the test tires are demonstrated in Table A.2 and Table A.3 in Appendix A.3. From general inspection of these figures, it is clear that the tread pattern spectra (profile and air volume velocity) do not completely match the total noise spectrum of the tire (left side plots), or the non-tread pattern noise spectrum (right side plots). However, it can be observed that a good match is observed between the tread pattern spectra when compared to only the tread pattern noise component (middle plots), especially around pitch passing frequency (number of pitches in order spectrum). This agreement is also found for the other driving speeds, as shown in Appendix C: Effect of Speed. For example, Figure 3.19 (top left) shows that the tread pattern profile spectrum doesn't match the total tire noise spectrum in the order range of 20 to 70. However, when the non-tread pattern noise component is removed, there is a good agreement in the spectral content in the order range of 40 to 120, as shown in Figure 3.19 (top middle). The spectral agreement is also good when the same comparison is performed for the air volume velocity spectrum in Figure 3.19 (bottom middle). It is supposed that both tread impact and air pumping contribute to tread pattern noise. The separation of the two mechanisms can be investigated in the future.

It is also important to note that the tread profile spectral content at high frequencies over

the order of 140 (around twice the pitch passing frequency) do not generate corresponding tread pattern noise.

3.5 Summary

Through the separation of the total tire-pavement interaction noise (TPIN) into two components, tread pattern noise and non-tread pattern noise component, it is demonstrated that the tread pattern noise varies a lot (17.2 dBA difference) for different tread patterns. It is generally accepted that the most important TPIN generation mechanisms related to tread pattern are tread impact and air pumping. To characterize the two mechanisms, the 3D tread pattern is parameterized using two spectra: coherent tread profile spectrum and contact patch air volume velocity spectrum. These two spectra correlate very well with the tread pattern noise spectrum, supporting the conclusion that the tread pattern leads to the tread pattern noise. In the next chapters, an artificial neural network (ANN) model is developed to predict the tread pattern noise from the tread pattern spectra.

Another notable result is that for the non-porous asphalt pavement tested (not very smooth), the tread pattern noise from the commonly used tires (summer or all-season pattern design) is usually not the dominant noise source (~5% of total noise). Considerable tread pattern noise (10-50% of total noise) only exists for some specific tires, especially snow tires or directional tires whose tread patterns look aggressive due to traction requirement and are not perfectly randomized. However, for a smoother pavement (limited data collected), the tread pattern noise for the same tire is shown to be more significant but its spectral shape doesn't change.

4 Artificial Neural Network (ANN)

In this chapter, the fundamentals of artificial neural network (ANN) are briefly introduced. The existing ANN models related to tire noise are then presented. In the end, the proposed ANN model for TPIN in the present study is described.

4.1 Introduction

Artificial neural network (ANN) is a powerful tool to solve complex and highly nonlinear problems, such as TPIN. It is widely used to develop statistical relations between two sets of parameters (input parameters and output parameters) with experimental data.

4.1.1 Structure

Without getting into a detailed technical description, the ANN consists of multiple layers of neurons as shown in Figure 4.1. A neuron can be mathematically interpreted as a non-linear transfer function controlled by weights. The ANN receives the input data (such as tire and pavement parameters) in the "input layer". In the same way, the layer that outputs the results (such as noise spectrum in narrowband, 1/1 octave or 1/3 octave) is called "output layer". The layers between the input layer and output layer are commonly called "hidden layers". The simplest neural network is composed of an input and an output layer, i.e., no hidden layers. The hidden layers usually improve the capacity of the network to solve complex problems.

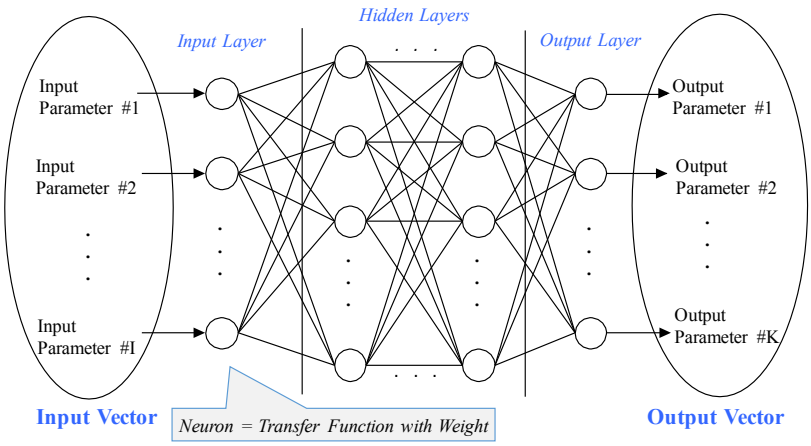

Figure 4.1: Schematic of a typical artificial neural network (ANN)

The structure of the ANN has no best answer and cannot be generally quantified for a particular case. For example, the number of neurons in the hidden layers does not follow any special rule and it is chosen by the user based on experience. If the number is too small, it will be difficult for the ANN model to capture all the relations. If the number is too large, the time for training will increase and "over-match" problem might occur. The suggested number of hidden neurons for an I-J-K ANN with I inputs, J hidden neurons (one layer) and K output neurons is given by (3.1) [387].

$$J = \sqrt{IK} \tag{3.1}$$

The following empirical equation is also sometimes used [266],

$$J = \sqrt{I + K} + \alpha \tag{3.2}$$

where α is a constant from 1 to 10.

The number of samples (examples or cases) N should not be too small in order to capture the trend of the data, but also not too large in order to avoid over-training or over-fitting where the ANN tries to fit the random noise. The rule of thumb is

$$\begin{aligned} W &= (I+1)J + (J+1)K \\ N &= (3 \sim 30)W \end{aligned} \tag{3.3}$$

where W is the number of free variables including weights and biases. As such, the lower limit of number of samples is below.

$$N_{lower} = 3\sqrt{IK}\left(I + K + \sqrt{\frac{K}{I}} + 1 \right) \tag{3.4}$$

Usually, I is much larger than K, the equation becomes

$$N_{lower} \approx 3I^{1.5}K^{0.5} \tag{3.5}$$

where it is indicated that I is more important than K when $I \gg K$.

If I is much smaller than K, the equation becomes

$$N_{lower} \approx 3I^{1.5}K^{1.5} + 3K \tag{3.6}$$

where it is indicated that both I and K are important when $I \ll K$.

4.1.2 Development

Real experimental data are needed to train the ANN to develop correlations between the input parameters and the output parameters. The available data are generally divided into three subsets [388], which is also embedded in MATLAB® [389]. The first subset is the training set, used for adjusting the network weights and biases. Given a specific input the network produces a specific output (predicted data). Then, the output is compared to the target (real data). This process is repeated, computing the gradient and adjusting the weights, until the difference between output and target reaches a desired error tolerance. The second subset is the validation set for preventing overfitting or overtraining. The error on the validation set normally decreases during the initial phase of training, as does the training set error. However, when the network begins to overfit the data, i.e., to capture the random noise more than the general trend, the error on the validation set typically begins to rise, which triggers an "early stopping" of the training process. The third subset is the test set, which is not used during training but is used for demonstrating the accuracy of the model. In a good division of the data set, the error in the test set typically reaches a minimum at the same iteration number as the validation set error.

The main advantages of the ANN over non-linear regression analysis used by current hybrid methods are two-fold. Firstly, no knowledge of the functional relationship between the input parameters and the output parameters (noise spectrum) is needed. Secondly, the amount of data needed for training is less in the ANN than the non-linear regression.

4.2 Existing ANN Models Related to TPIN

From literature, the current ANN models related to tire noise were reviewed and presented here.

4.2.1 Che et al. Model

Che et al. (2012) [266] utilized an artificial neural network (ANN) model to correlate tire parameters with tire noise. The input and output parameters are shown in Table 4.1. It is noted that the tests were conducted using laboratory drum (DR) method (Yong et al., 2009 [390]), and the surface was considered constant, so there are no inputs of pavement parameters. The ANN statistical equation can be given as

$$L_p(f) = g\left(T_w, T_p, T_R, P_A, P_C, P_N, P_T, P_R, P_L, P_S, P_D, V, L, F\right) \tag{3.7}$$

where f is the center frequency of corresponding octave band.

Table 4.1: Input and output parameters of ANN (Che et al., 2012 [266])

	Parameter	Symbol	Description
Input	Tire Structure (Size)	T_w	Tire width
		T_p	Aspect ratio
		T_R	Tire radius
	Tread Pattern	P_A	Area of single-pitch tread pattern block
		P_C	Area of single-pitch tread pattern groove
		P_N	Number of tread blocks per pitch
		P_T	Total number of pattern pitch
		P_R	Arrangement rule of pitch
		P_L	Displacement (offset) between the pattern strips
		P_S	Symmetrical characteristics of tread patterns
		P_D	Groove depth
	Operation	V	Vehicle speed
		L	Tire load
		F	Inflation pressure
Output	Sound Pressure Level	$L_{p,125}$	Sound pressure level at the octave band of 125 Hz
		$L_{p,250}$	Sound pressure level at the octave band of 250 Hz
		$L_{p,500}$	Sound pressure level at the octave band of 500 Hz
		$L_{p,1000}$	Sound pressure level at the octave band of 1000 Hz
		$L_{p,2000}$	Sound pressure level at the octave band of 2000 Hz
		$L_{p,4000}$	Sound pressure level at the octave band of 4000 Hz

The study employed back-propagation (BP) network training based on genetic algorithms (GA) utilizing crossover and mutation operation to determine the number of hidden neurons (6), number of training epochs (6000), and the initial weights (global optimization). This ANN model has a structure of 14-6-6.

In this study, the training data obtained from the tests were divided into two parts including training samples (50 groups) and test samples (10 groups). It is reported that the average error was 1.4%.

4.2.2 Li et al. Model

Similar to Che et al. Model, Li et al. (2009) [271], [369] used Fuzzy Genetic Arithmetic (F-GA) to statistically correlate tread pattern parameters with noise levels. The input tread pattern parameters include the width and length of tread block, the width and length of groove, the number of pattern strip, the basic number of pattern pitch, the pitch array and the pattern displacement. The output noise levels are the spectral area that excess a noise standard line (curve M) provided by American Test Center (ATC), as given below.

$$\delta = \sum_{i=1}^{k} \left(L_{p,i} - L_{p,i,M} \right) \tag{3.8}$$

where i is index for each frequency band (125-4000 Hz), $L_{p,i}$ is the sound pressure level corresponding to specific tread pattern input, $L_{p,i,M}$ is the standard sound pressure level in curve M, and δ is the model output. It was claimed that the model successfully optimized the parameters of tread pattern for low noise tires utilizing fitness function iteration. Unfortunately, further details on the optimized parameters and the accuracy of the model were not reported.

It should be noted that both Che et al. Model and Li et al. Model assumed tread pattern noise is independent of tread block shape (only size matters).

4.2.3 Fry et al. Model

Fry et al. developed an artificial neural network (ANN) model to correlate vehicle design parameters with vehicle controlled pass-by (CPB) noise (Fry et al., 1999 [368]; Fry and

Jennings, 2003 [381]).

According to ISO 362 [40], [41], the vehicle enters the test track (ISO 10844 [391]) with an initial speed of 50 km/h, then drives through at 100% acceleration. The measurements are conducted in both directions, in 2nd and 3rd gear, while the maximum sound pressure level (Max_{2nd} and Max_{3rd}) is recorded for each test run. The final average drive-by noise level *DBN* is given by (3.9).

$$DBN = \frac{Max_{2nd} + Max_{3rd}}{2} - 1 \text{ dBA} \tag{3.9}$$

The input parameters of the ANN model cover seven functional categories: powertrain, intake, exhaust, tire, test conditions, engine bay and vehicle performance. The binary and categorical inputs were encoded to numeric values. 75 were on the short list refined from over 200 parameters by five vehicle noise experts. Unfortunately, the details on these parameters were not published. The relevant tire parameters included material, geometry, and tread pattern. The only one output of the ANN model is the pass-by noise level.

At least 2000 test runs were needed, which was barely enough in the beginning (2064 samples) before more data was collected (Fry et al., 1999 [368]). In order to reduce the number of parameters, the ANN was divided into two sub-models, as shown in Figure 4.2.

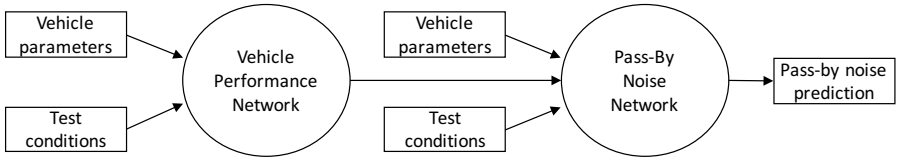

Figure 4.2: Two-stage ANN models for pass-by noise (Source from Fry and Jennings, 2003 [381], Figure 3)

The vehicle acceleration was firstly used as the output of vehicle performance network (20-5-1) with a mean percentage error (MPE) of ±7% (R^2 = 0.9) (Fry et al., 1999 [368]). Then the output was changed to engine speed at the exit of the test track, based on the fact that the pass-by noise has a strong correlation with the engine speed (9 dBA per 1000 rpm). The error was found to decrease to ±4.8%.

The type of neural network used is multi-layer perceptron (MLP), which is the most widely

used. The training algorithm is error back-propagation, or back-propagation. 85% of published neural network applications were created using some variant of back-propagation (Wasserman, 1993, [392]). The corresponding algorithm in MATLAB is RPROP (Resilient Back-Propagation) where the inputs were transformed to zero mean and unit variance to avoid "stuck units" (Tarassenko, 1998 [387]). Both the logsig (logistic sigmoid) and tansig (hyperbolic tangent sigmoid) transfer functions in MATLAB® were tried for the hidden neurons. The best network found for vehicle performance network and pass-by noise network is displayed in Table 4.2.

Table 4.2: Metrics for two-stage ANN models for pass-by noise (Fry and Jennings, 2003 [381])

Sub-ANN	Structure	Set for Training and Validation	Set for Test	Accuracy
Vehicle Performance Network	25-15-1	2503 samples from 24 vehicles	997 samples from 13 vehicles	±4.8%
Pass-By Noise Network	58-19-1	4282 samples from 21 vehicles	1424 samples from 7 vehicles	±1.4%

This model provides insight into the vehicle acoustic performance in the early design stage before a prototype has been built, which saves a lot of costs and engineering efforts. The prediction error of the model is within ±1.4% (i.e., ±1.1 dBA for the noise limit of 74 dBA), which is better than the guess from experienced engineer (±3 dBA).

The model also works for diesel and turbo-charged vehicles but is not valid for automatic transmission since its gear ratio will not be constant during the test. The author also suggest a technique combining neural networks with Bayesian statistics, called Automatic Relevance Determination (ARD) to refine input selection [393] to potentially obtain better prediction accuracy.

4.2.4 Other ANN Models

Kumar et al. (2013) [394] utilized Multi-Objective Genetic Arithmetic (MOGA) to optimize tire tread pitch sequence accounting for several performance parameters (noise, handling and wear). The other study (Kostial et al., 2013 [395]) correlated the tire radial frequencies (output) with the tire structural parameters (input), such as the nominal width, profile number, rim diameter, load index and speed index. Further input parameters were also

included, such as radial static stiffness, circumferential static stiffness, lateral static stiffness, static torsional stiffness. It was reported that the ANN results were qualitatively comparable with FEM simulations with a root mean square error of 4.314 Hz. Another study (Kongrattanaprasert et al., 2009 [396]; Kongrattanaprasert et al., 2010 [397]) correlated the road surface states (output), such as snowy, slushy, wet, and dry states, with the measured tire noise of passing vehicles (input). An accuracy of approximately 90% was reported. A similar study (Kandpal et al., 2013 [398]) correlated the vehicle categories (output) with the measured noise (input).

The ANN approach can be applied to various research areas. For the interest, ANN was also applied for the tire contact optimization to improve the handling and wearing performance (Nakajima, 1999 [399]). The input is the sidewall and tread band contour; the output is the uniformness of contact pressure distribution. El-Gindy et al. (1999 [400], 2001 [401]) developed a tire/pavement contact-stress model based on an artificial neural network for truck tires. The input parameters included were vertical load and inflation pressure. No tire parameters were included; however, ANN models were developed for one radial-ply tire, and one bias-ply tire separately.

4.3 Proposed ANN for TPIN

In this study, an artificial neural network (ANN) model is proposed to predict TPIN including tire parameters (and pavement parameters, not in this dissertation but for future work), as illustrated in Figure 4.3. The input of ANN is tire/pavement parameters, as well as some other parameters such as speed; the output is TPIN in narrowband, 1/3 octave band, or overall A-weighted sound pressure level (OASPL). In this dissertation, the pavement parameters are not investigated, but left for future work.

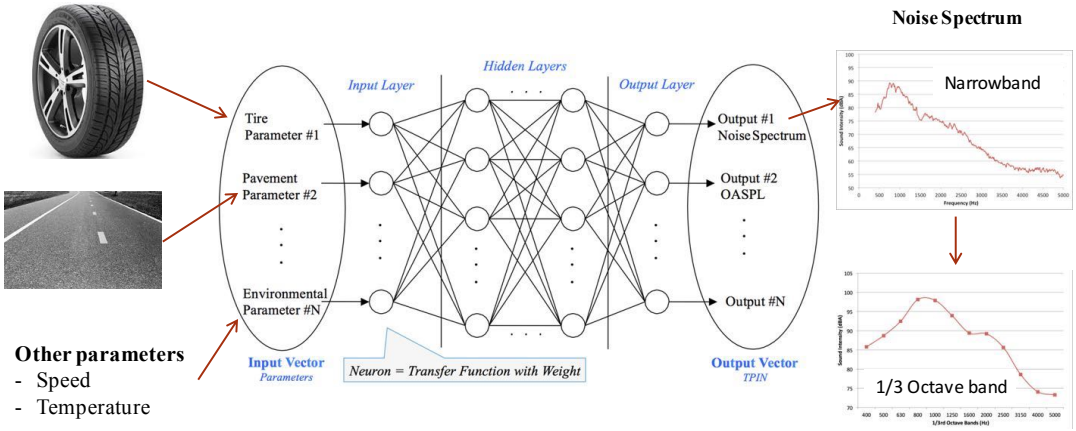

Figure 4.3: Single ANN to predict TPIN

As discussed above, the total TPIN can be broken down into two noise components: tread pattern noise and non-tread pattern noise. Therefore, the ANN model is separated into two sub-models correspondingly, as illustrated in Figure 4.4. One sub-ANN (ANN_1) is focused on the tread pattern to predict the tread pattern noise; the other sub-ANN (ANN_2) is mainly focused on the pavement to predict the non-tread pattern noise. This is a new approach, which is not found in any open literature.

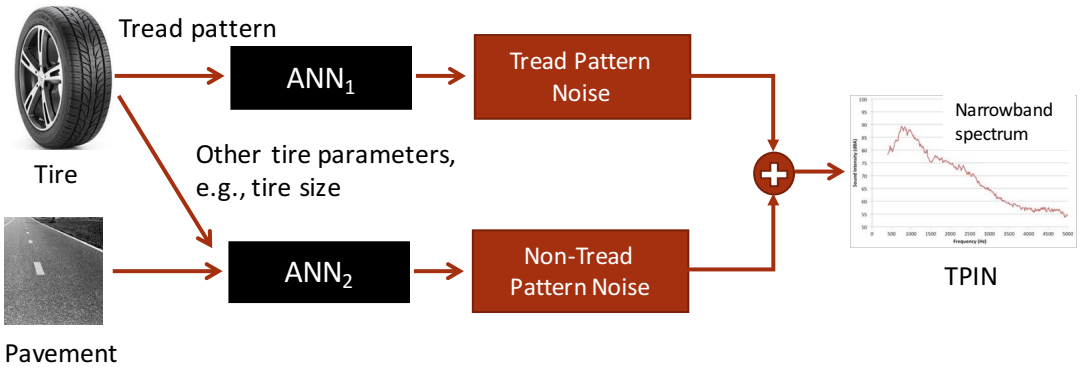

Figure 4.4: Two sub-ANN's to predict TPIN

The complete noise data for the development of the ANN's are shown in Figure 4.5 (60 mph only). The spectral peaks for some tires seem to be cropped, because the amplitude is too large (> 0.4).

(a) Total noise spectra

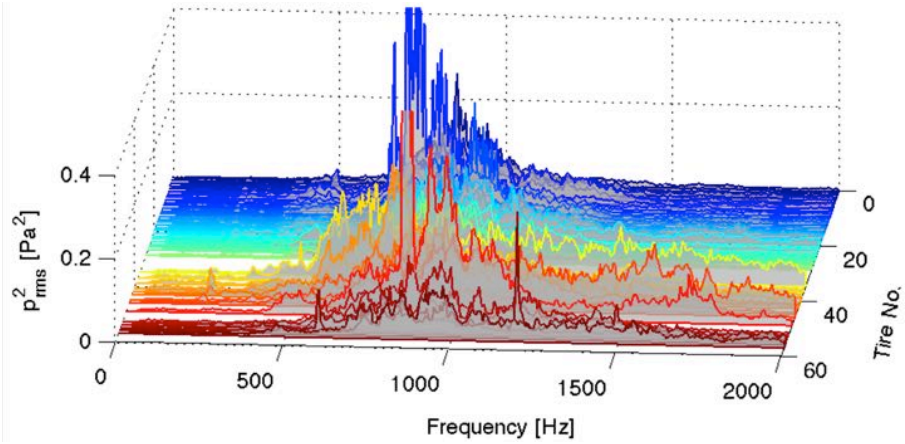

(b) Tread pattern noise spectra

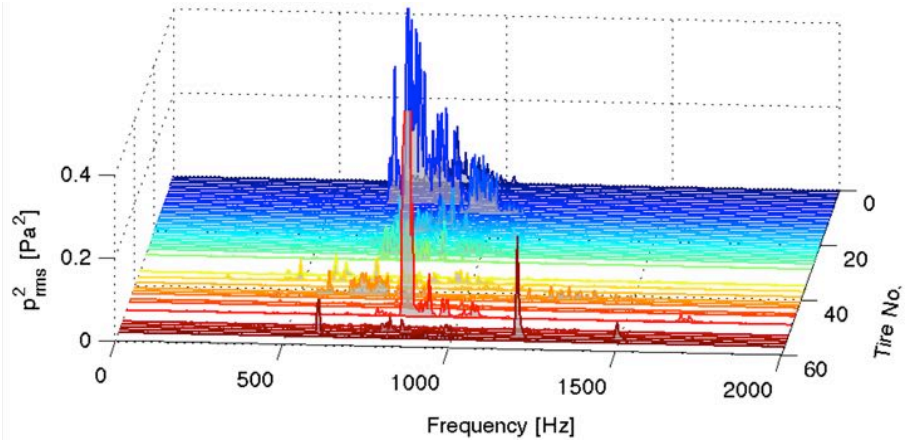

(c) Non-tread pattern noise spectra

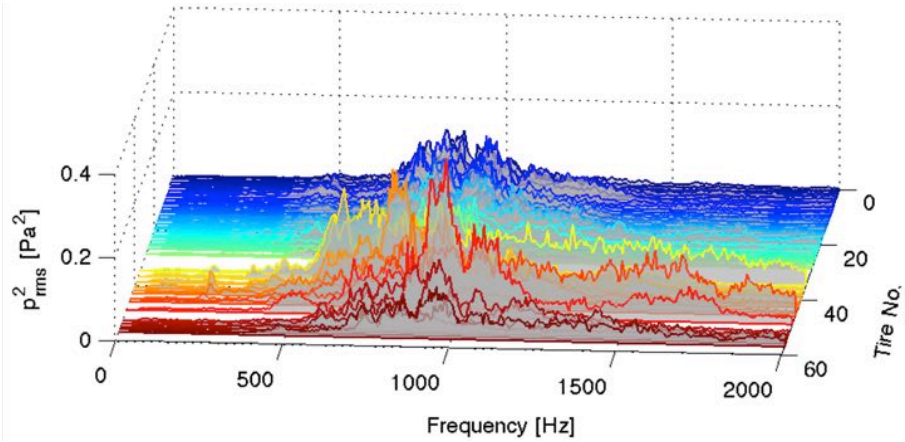

Figure 4.5: Total, tread pattern, and non-tread pattern noise data at 60 mph for developing ANN models

4.4 Summary

Artificial neural network is a promising approach to correlate tire/pavement parameters with TPIN. A couple of ANN models have been attempted according to literature, especially for the tread pattern design. However, the tread pattern parameters included were not defined in a universal way. No current ANN models include pavement parameters, and TPIN cannot be predicted in narrowband. In the following, the development of ANN model to predict TPIN in narrowband is investigated, including two sub-ANN's, ANN_1 for tread patter noise and ANN_2 for non-tread patter noise.

5 ANN Model for Tread Pattern Noise (ANN_1)

The development and validation of the first part of ANN model for TPIN, i.e., ANN_1 on tread pattern noise, is investigated in this chapter. The ANN_1 with optimized configurations are presented, including the definition of input and output, the ANN structure, and the evaluation of the model accuracy. Some other ANN configurations are also investigated.

5.1 Input and Output

The input to the ANN_1 is the tread pattern-related parameters, and the output of ANN_1 is the tread pattern noise in the order domain. As is already known, the two tread pattern spectra (coherent tread profile spectrum and air volume velocity spectrum) look correlated with the tread pattern noise spectrum. Therefore, it is reasonable to define the two tread pattern spectra as the input, and the tread pattern noise spectrum as the output of ANN_1. However, if all the spectral points (81 points for each order narrowband spectrum) are to be included into the ANN model, the number of input and output parameters turn out to be too large for the ANN model to be successfully trained. Therefore, the number of parameters needs to be reduced. In this section, the ANN_1 is firstly designed at 60 mph, and the speed effect is investigated in Section 5.2. The final approach for the tread pattern noise modeling is: the tread pattern noise at 60 mph can be predicted from ANN_1, and the tread pattern noise at other speeds is based on speed exponent scaling.

5.1.1 Input Parameters

The input tread pattern spectra are reduced via Gaussian curve fitting. The equation is given by

$$y = \sum_{i=1}^{n} a_i e^{-\left(\frac{x-b_i}{c_i}\right)^2} \tag{4.1}$$

where x, y is the coordinates of the fitted curve, a is the amplitude, b is the centroid (central location), c is related to the peak width (spread), n is the number of peaks to fit (number of terms). The total number of parameters is $3n$ for each Gaussian model. The total number of

parameters for the two tread pattern spectra is then $6n$.

The results of the Gaussian curve fitting at different number of terms for Tire 12 are shown in Figure 5.1. The abscissa is order, as mentioned before, considered as the normalized frequency. The order range of the original data is from 40 to 120 with a resolution of 1. It can be seen that, the dominant spectral contents are around the number of blocks (77 for Tire 12), the same value as that of order. In addition, as shown in Figure 5.1, the tread pattern spectral contents at very low and high frequencies do not contribute to corresponding tread pattern noise. Therefore, in the Gaussian curve fitting, the data points around the number of blocks are given larger weight, while the data points far away from the number of blocks are given smaller weight, so only the peaks around the number of blocks are captured.

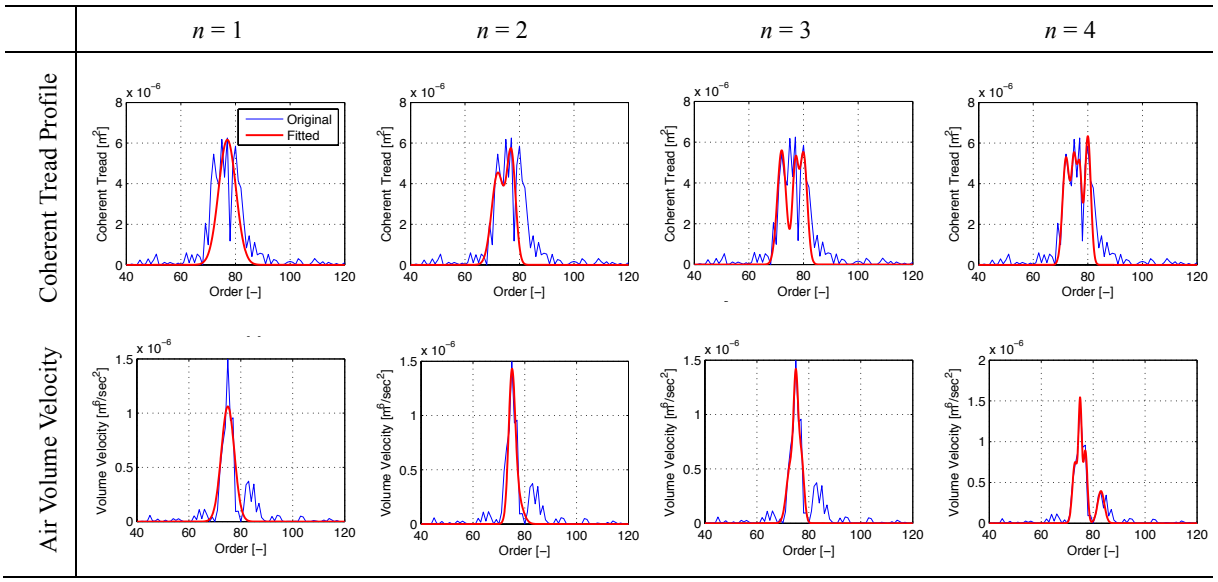

Figure 5.1: Gaussian curve fitting of the tread pattern spectra at different number of terms (Tire 12)

In Figure 5.1, it is also demonstrated that, as the number of terms increases, more spectral peaks are captured, and the fitted Gaussian curve is better matched with the original spectral curve. Therefore, a compromise between parameter reduction and information richness is needed. It has been shown that two-term Gaussian generates the best results for ANN_1, which will be discussed below. The number of input parameters will be reduced from the initial 162 to 12. The two-term Gaussian curve fittings for the tread pattern spectra of all test tires are exhibited in Table A.4 in Appendix A.4.

5.1.2 Output Parameters

For the reduction of output parameters, if in frequency spectrum, the narrowband tread pattern noise spectrum can be simply converted to a less precise band, such as 1/3 octave band, 1/12 octave band, as shown in Figure 5.2. The frequencies of interest in narrowband are from 400 to 1600 Hz with a resolution of 5 Hz (other resolution can also be used based on the noise data processed); the number of parameters is 241. In 1/3 octave band, the number of parameters is reduced to 7. In 1/12 octave band, the number of parameters is reduced to 24. If in order spectrum, which is preferred, with a resolution of 1 and range from 40 to 120, the number of parameters is 81. It can be easily seen that, the more number of parameters, the more precise the spectrum. All the spectra are A-weighted except for order narrowband that is not applicable, because A-weighting is based exclusively on frequency. However, for the order spectrum, when converted to the frequency spectrum, which is needed later, the A-weighting is applied.

In this ANN_1 model, the output parameters selected is the order narrowband (81 parameters), which will be discussed below. It is noted that the order spectrum (measurement) used for training ANN_1 is directly calculated from the original noise data collected in the time domain rather than converted from the frequency domain. However, after ANN_1 is well trained, the output (prediction) in the order domain will be converted to the frequency domain, because frequency spectrum is more acceptable to the general public. The conversion procedure is described in Section 5.6.

(a) Frequency narrowband (241 parameters)

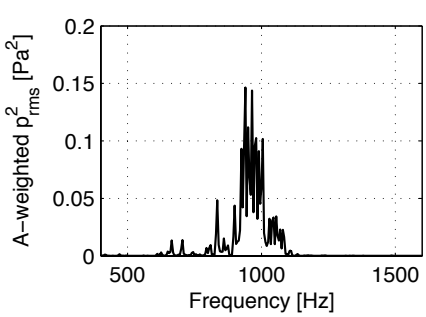

(b) 1/3 octave band (7 parameters)

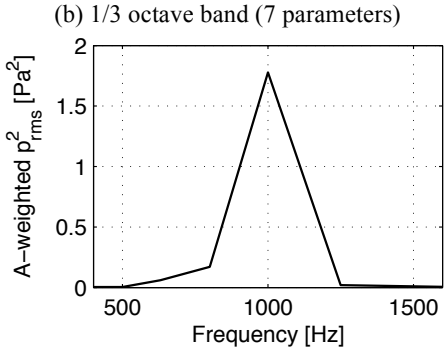

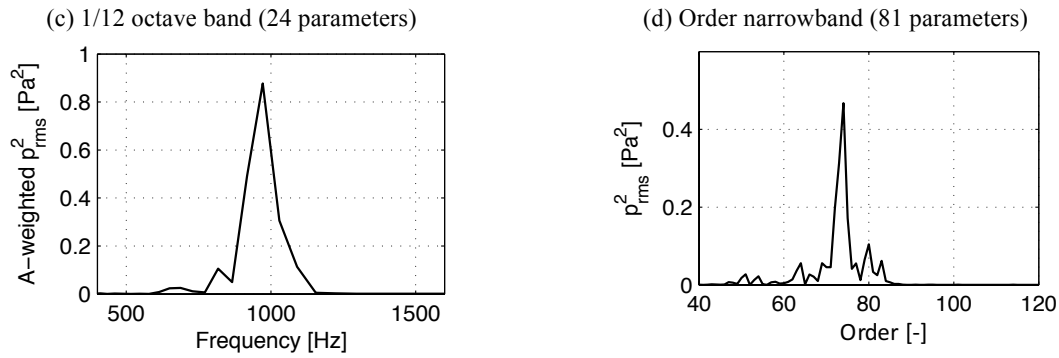

Figure 5.2: Tread pattern noise spectrum in frequency narrowband (5 Hz resolution), 1/3 octave band, 1/12 octave band, and order narrowband (1 resolution) for Tire 12 at 60 mph

In summary, the input and the output parameters for ANN_1 are illustrated in Figure 5.3. The input consists of two-term Gaussian parameters for coherent tread profile in order spectrum and air volume velocity spectrum in order spectrum while the output is tread pattern noise in order spectrum.

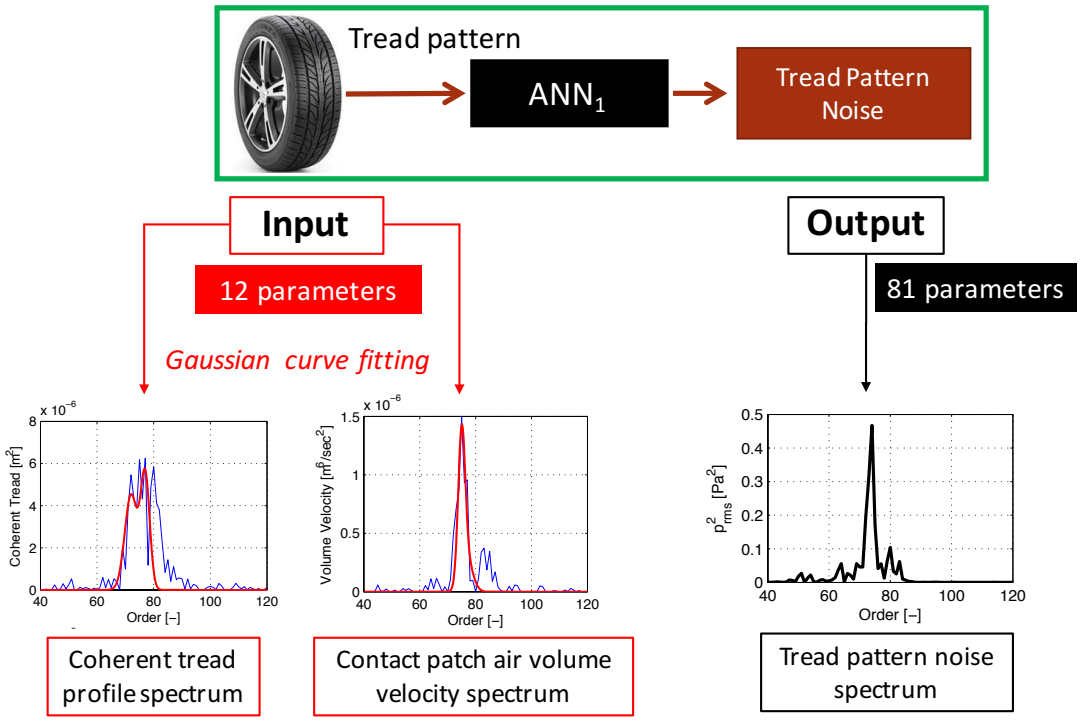

Figure 5.3: Input and output parameters for ANN_1

5.2 Speed as an Input Parameter

To predict tread pattern noise at different speed, the speed (vehicle speed or tire rotational speed) also needs to be an input to ANN_1.

5.2.1 Two Approaches to Handling Speed

There are two approaches considered as illustrated in Figure 5.4.

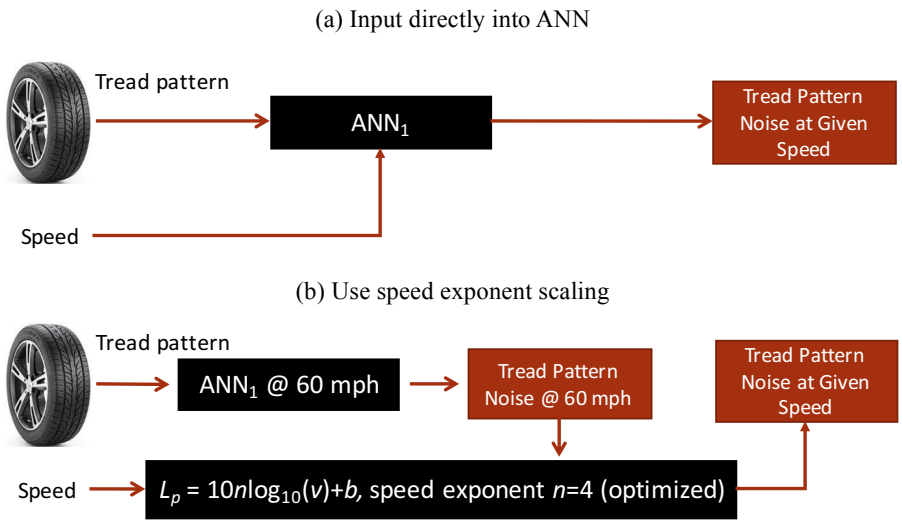

Figure 5.4: Two approaches to handling speed

The first approach is to include speed into ANN_1 as an input parameter, i.e., to develop ANN_1 using all the data at different speeds, as shown in Figure 5.4a. Unfortunately, it didn't work quite well, likely because the ANN model is not able to capture the trend for speed due to the existence of numerous tread pattern parameters. As shown in Figure 5.4b, the second approach is to firstly develop ANN_1 only using data at 60 mph, then scale the noise at 60 mph to other specific speeds using the noise scaling equation given below

$$L_p = 10n\log_{10}(v) + b \tag{4.2}$$

where L_p is sound pressure level (SPL) in narrowband or overall level, n is speed exponent or called scaling law, v is vehicle speed, b is a coefficient. The speed exponent n indicates how tire noise changes with speed. If n is positive, tire noise increases with speed; if n is negative, tire noise decreases with speed. The larger the magnitude of n, the greater influence speed has

on tire noise level.

5.2.2 Speed Exponent Optimization

The optimized speed exponent n for each tire is identified through an iteration process, as shown in Table 5.1. The first row (n = 0) shows the overall sound pressure level at different speed; the standard deviation in the right column is computed from the five numbers. It should be noted that, standard deviation for dB is mathematically wrong, but here is only for the purpose of identifying the optimized speed exponent. From the second to last row, SPL at the five speeds are all scaled to 60 mph using the equation below with different speed exponent n.

$$L_p(60\text{mph}) = L_p(v) + n \cdot 10\log_{10}(60\text{mph}/v) \tag{4.3}$$

where L_p(60mph) is the scaled OASPL, $L_p(v)$ is the original OASPL at the speed of v before scaling. To be more precise, the tire rotational speed in rev/sec or Hz is used instead of vehicle speed in mph. Therefore, all speeds are actually scaled to 13.1 Hz (~60 mph, but varies slightly for different tires). The column of 60 mph in Table 5.1 displays the values of OASPL scaled from 60 mph to 13.1 Hz. The vehicle speed of 60 mph is a nominal speed, and the real tire rotational speed that might be different from 13.1 Hz is calculated from the optical signal. It can be seen that, as speed exponent n increases, the standard deviation decreases at first then increases. The optimized speed exponent for this tire (Tire 01) is 3.3 when standard deviation is minimum. In addition, the optimized speed exponent can also be obtained through nonlinear regression. The results are almost the same for the two algorithms.

Table 5.1: Identification of optimized speed exponent *n* for Tire 01 (red indicates optimized *n* where the standard deviation is minimum)

Speed Exponent [-]	45 mph [dBA]	50 mph [dBA]	55 mph [dBA]	60 mph [dBA]	65 mph [dBA]	Standard Deviation [dBA]
0.0	90.8	93.1	94.9	96.0	95.7	2.1
1.0	92.1	93.9	95.2	96.0	95.3	1.6
2.0	93.3	94.6	95.6	96.0	95.0	1.0
3.0	94.5	95.4	95.9	96.0	94.6	0.7
3.3	**94.8**	**95.6**	**96.0**	**96.0**	**94.5**	**0.7**
4.0	95.7	96.1	96.3	96.0	94.2	0.8
5.0	96.9	96.9	96.7	96.0	93.9	1.3
6.0	98.2	97.6	97.0	95.9	93.5	1.8
7.0	99.4	98.4	97.4	95.9	93.2	2.4
8.0	100.6	99.1	97.7	95.9	92.8	3.0
9.0	101.8	99.9	98.1	95.9	92.4	3.6
10.0	103.0	100.6	98.5	95.9	92.1	4.3

The scaled tread pattern noise spectra using different speed exponents are demonstrated in Figure 5.5. For each sub-figure, the tread pattern noise spectra at different speeds are scaled to 60 mph using a specific speed exponent n. It can be seen that, when $n = 0$ in Figure 5.5a, there is large difference (~20 dB) between the five curves at dominant order from 60 to 70. When $n = 3.3$ (optimized speed exponent) in Figure 5.5b, the error is much smaller (less than 10 dB). When $n = 4$ in Figure 5.5c, the five curves still collapse well, and the standard deviation in Table 5.1 just goes up from 0.7 to 0.8, indicating the speed exponent around the optimized value is not sensitive, and 4 is also a good value for speed exponent scaling. However, as n reaches 10 in Figure 5.5d, the curves do not collapse any more, especially at the order range of 70 to 100. It is noted that the original order spectra at different speeds were calculated from the raw noise data rather than converted from the frequency domain.

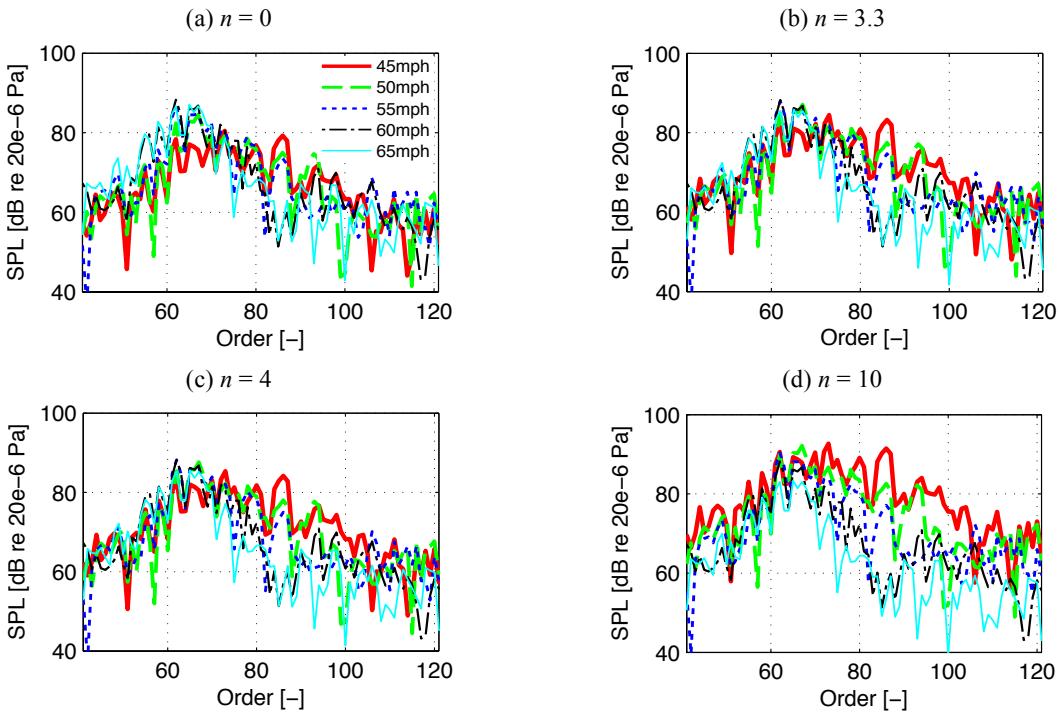

Figure 5.5: Scaled tread pattern noise spectra using different speed exponents (Tire 01)

Figure 5.6 displays the plot of standard deviation versus speed exponent for all test tires. It can be seen that a speed exponent of 4 is generally good for all the tires with the standard deviation of typically less than 2 dB.

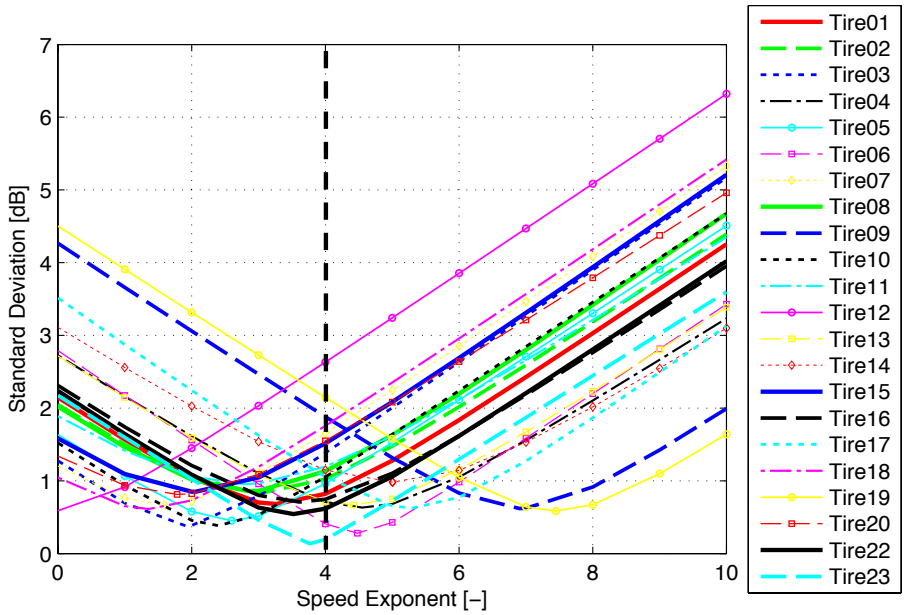

Figure 5.6: Standard deviation versus speed exponent for all test tires

The optimized speed exponent for all test tires is plotted in Figure 5.7. It is shown that the optimized speed exponent varies for different tread patterns. The average of the optimized speed exponent is around 4 (a larger weight is given to tires that have large tread pattern noise, e.g., Tires 09 and 19 that have a speed exponent of ~7). Therefore, a speed exponent of 4 is used for scaling the ANN_1 at 60 mph to other speeds. This will lead to a consequence that the ANN_1 will work well for tires where the speed exponent is around 4. If n is significantly different than 4 (e.g., n = 8 for Tire 19), the model will not work very well.

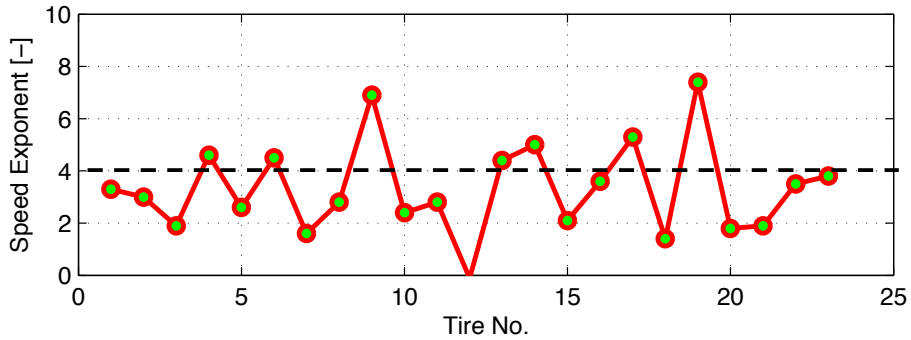

Figure 5.7: Optimized speed exponent for all test tires

5.3 ANN_1 at 60 mph

As discussed in Section 5.1, the optimized ANN_1 at 60 mph has 12 input parameters in the input layer and 81 output parameters in the output layer. A one-hidden-layer ANN structure is used, because the input and output are well correlated by visual inspection and no more intermediate processing stages are needed. If using Eq. (3.1), the suggested number of neurons in the hidden layer is given by $J = \sqrt{IK} = \sqrt{12 \times 81} \approx 31$. If using Eq. (3.2), the suggested number of neurons in the hidden layer (α is set to 10) is given by $J = \sqrt{I+K} + \alpha = \sqrt{12+81} + 10 \approx 20$. The average of the two suggested numbers gives 25, which is used here. In summary, the ANN_1 at 60 mph has a 12-25-81 structure.

The suggested number of training samples is given by Eq. (3.4) $N_{lower} = 3\sqrt{IK}\left(I + K + \sqrt{K/I} + 1\right) = 3\sqrt{12 \times 81}\left(12 + 81 + \sqrt{81/12} + 1\right) \approx 6023$, which is much larger than the number of samples available. However, as the input and output have very good correlations, the ANN is capable to capture their relations using a much less amount of data.

To develop the ANN_1 at 60 mph, the total samples (22 tires) are divided into the three subsets, as shown in Table 5.2. The assignment of tires into the three subsets is basically by random choice, but it is guaranteed that each subset has both all-season and winter tires in order to cover the two categories that have different tread pattern noise characteristics. It is also noted that all the samples are for 60 mph at inflation pressure of 32 psi tested on the eastbound section.

Table 5.2: Subsets of samples for developing ANN_1 at 60 mph (red indicates winter tire)

Subset	Train Set	Validation Set	Test Set
Purpose	Train ANN	Stop training ANN and avoid over-training	Examine/validate the accuracy of the trained model
Number of Tires	13	4	5
Tires	01 02 03 04 05 06 07 08 10 11 13 17 **19**	**12** 14 16 20	**09** 15 18 22 23

The measured and predicted tread pattern noise spectrums for each sample are compared

and shown in Figure 5.8. It can be seen that the predicted spectrum matches very well with the measured spectrum. The agreement for the train set indicates the ANN obtained successfully processes the training data and captures the trend. The agreement for the validation set is not as good as for the train set but still acceptable, likely because this subset is indented for preventing over-training. The agreement for the test set, most importantly, is also good, indicating that the developed ANN is able to predict new samples, i.e., tread pattern noise from new tread patterns.

(a) Train Set

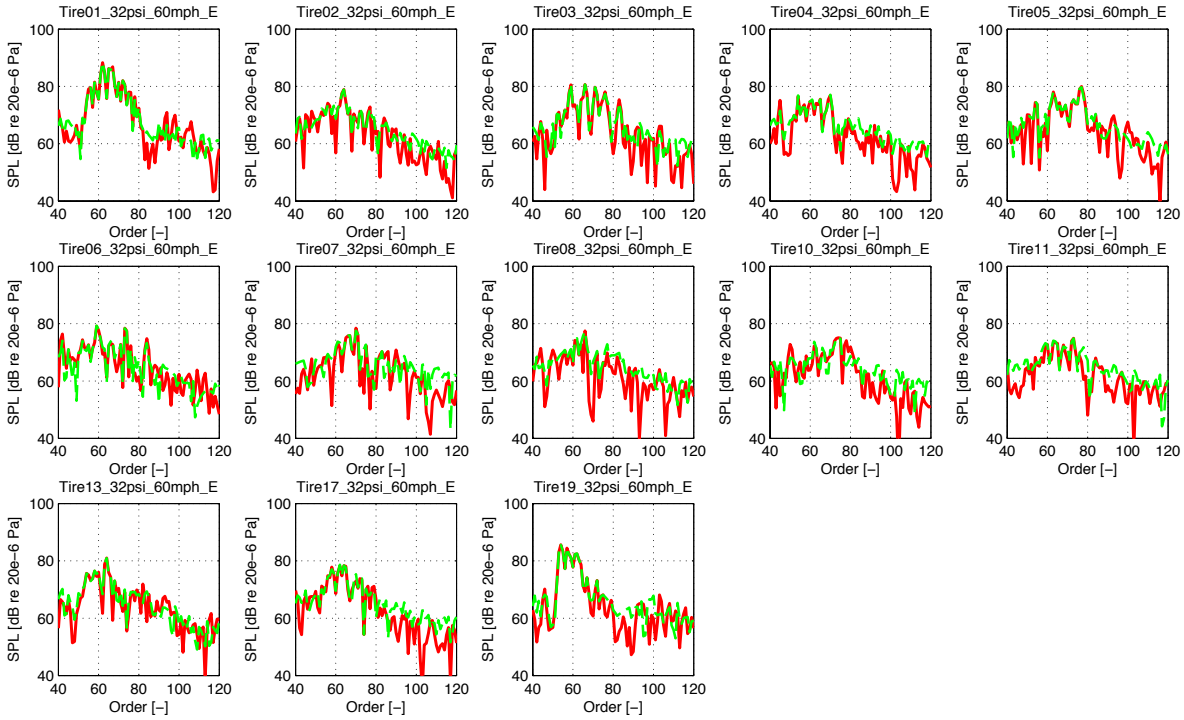

(b) Validation Set

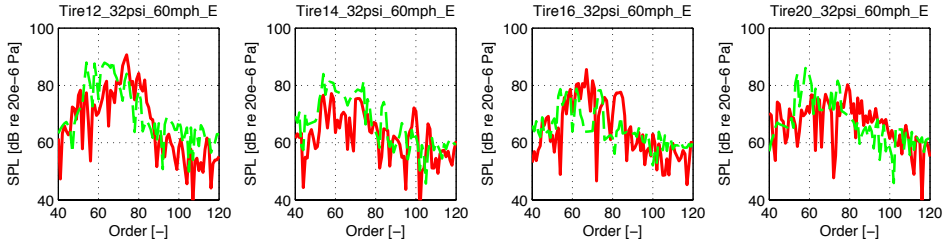

(c) Test Set

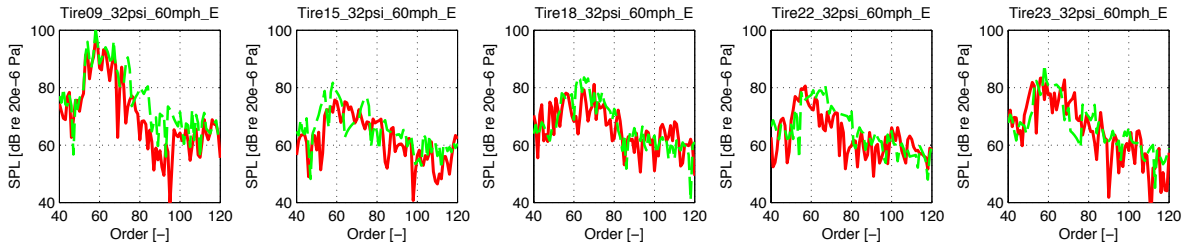

Figure 5.8: Comparison between measured (red) and predicted (green) tread pattern noise spectrums [ANN_1 at 60 mph]

The measured and predicted sound pressure levels (SPL) at different order are compared and demonstrated in Figure 5.9. It can be seen that for each order, most of the points align well around the diagonal reference line, indicating a good agreement between the measured and predicted data.

Order Range	Measured and Predicted SPL				
40~44	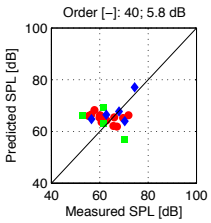 Order [−]: 40; 5.8 dB	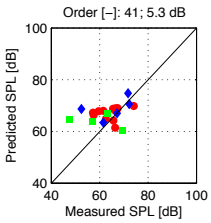 Order [−]: 41; 5.3 dB	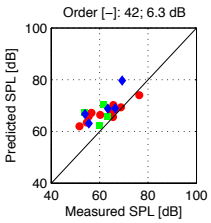 Order [−]: 42; 6.3 dB	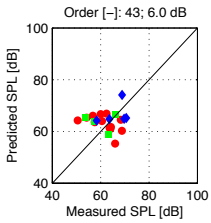 Order [−]: 43; 6.0 dB	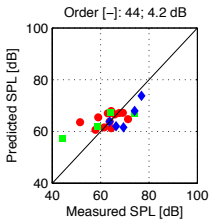 Order [−]: 44; 4.2 dB
45~59	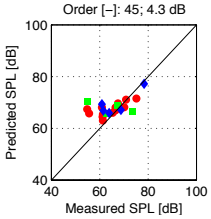 Order [−]: 45; 4.3 dB	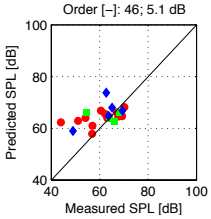 Order [−]: 46; 5.1 dB	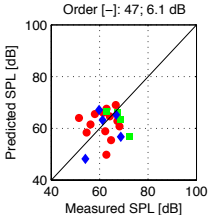 Order [−]: 47; 6.1 dB	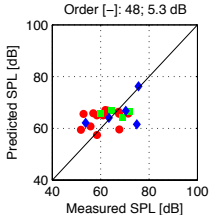 Order [−]: 48; 5.3 dB	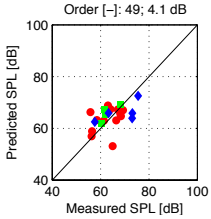 Order [−]: 49; 4.1 dB
50~54	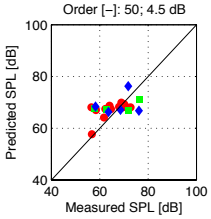 Order [−]: 50; 4.5 dB	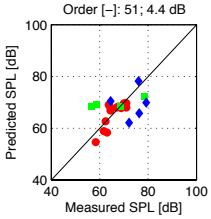 Order [−]: 51; 4.4 dB	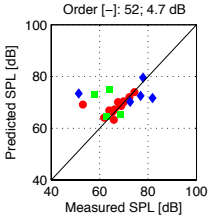 Order [−]: 52; 4.7 dB	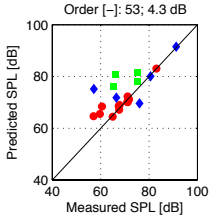 Order [−]: 53; 4.3 dB	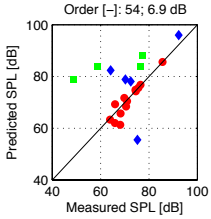 Order [−]: 54; 6.9 dB

Order Range	Measured and Predicted SPL
55~59	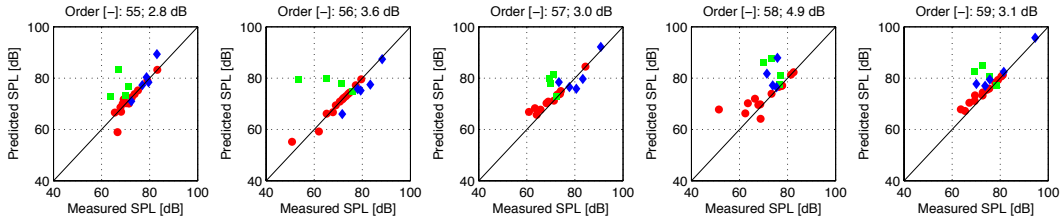
60~64	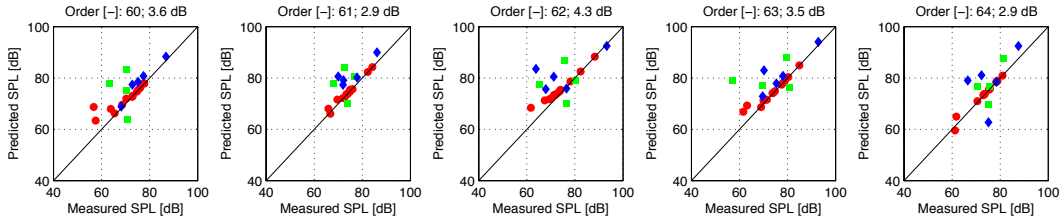
65~69	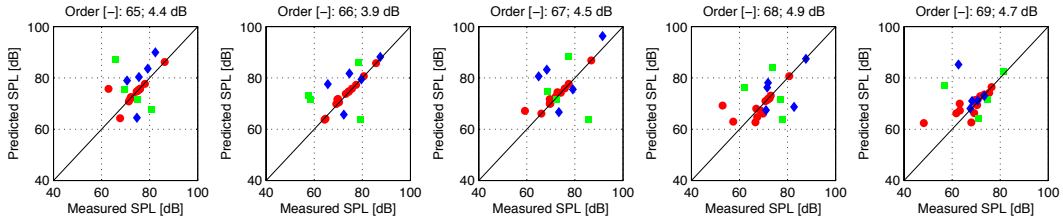
70~74	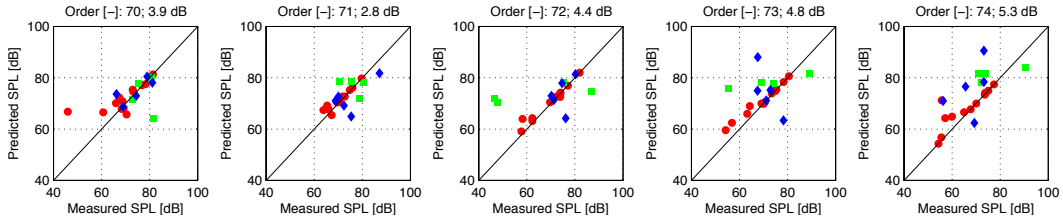
75~79	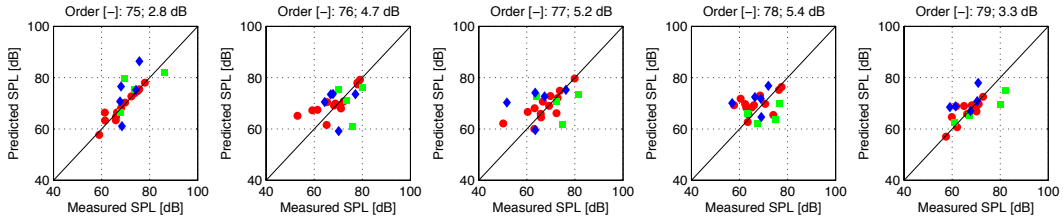
80~84	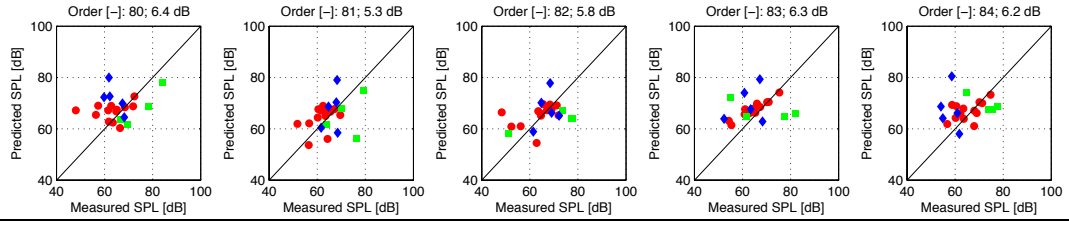

Order Range	Measured and Predicted SPL
85~89	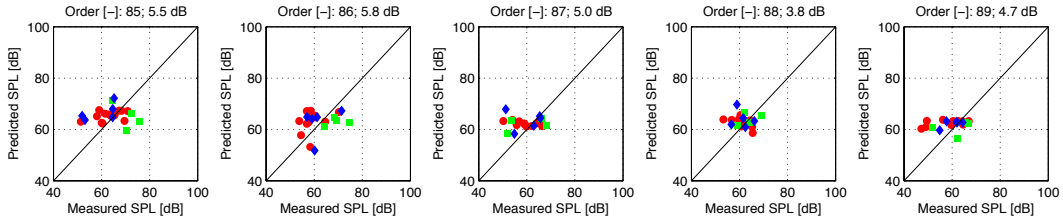
90~94	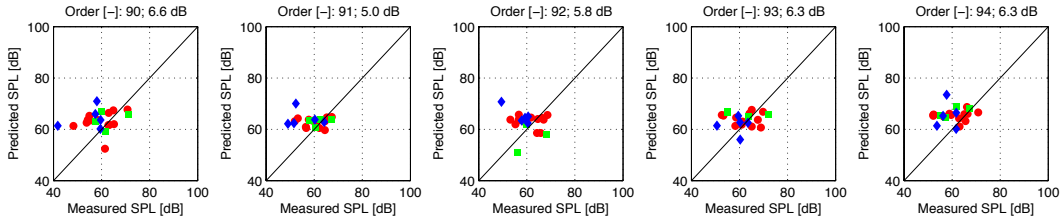
95~99	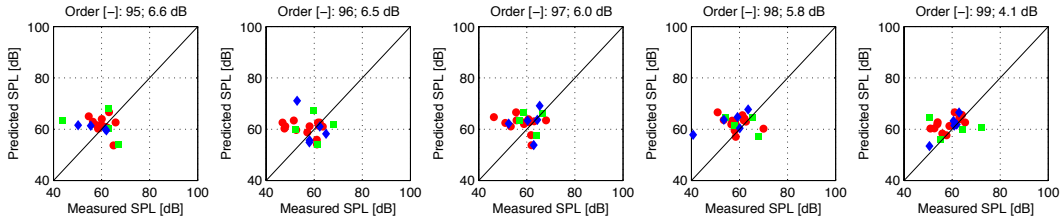
100~104	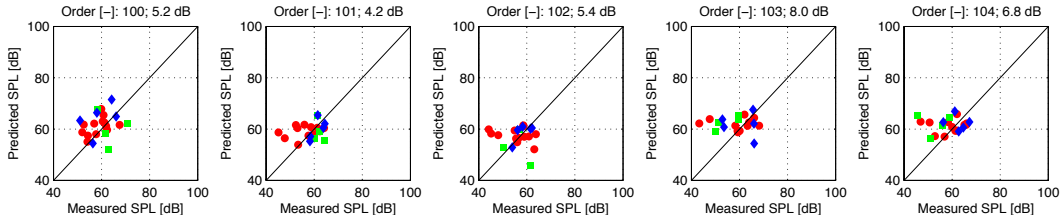
105~109	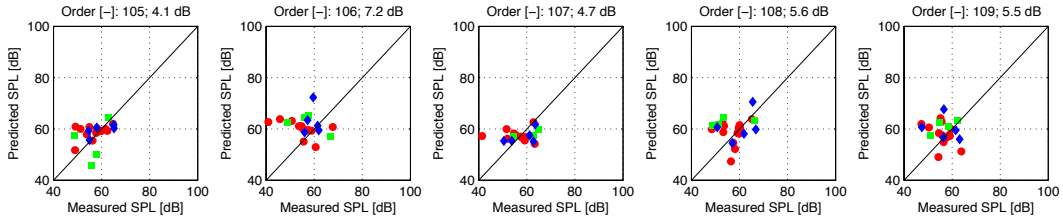
110~114	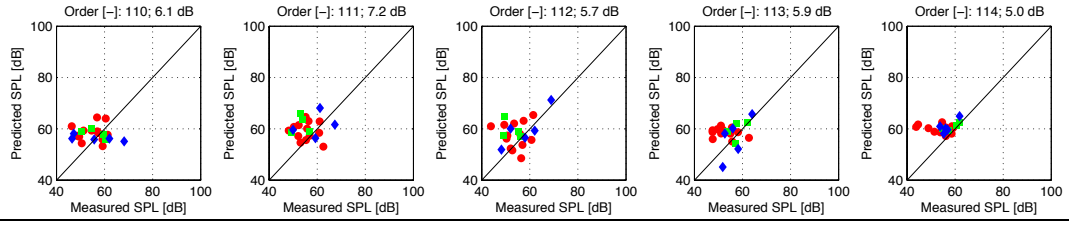

Order Range	Measured and Predicted SPL
115~119	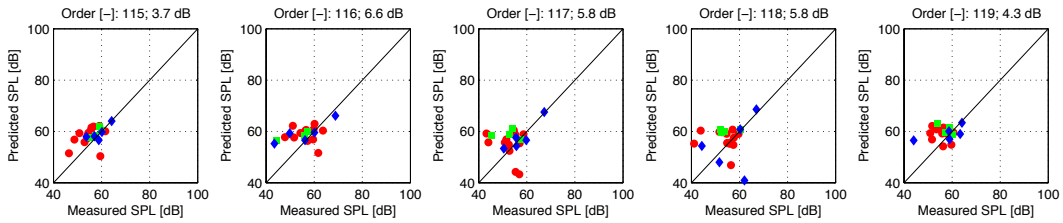
120	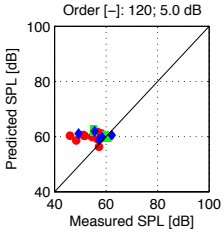

*Red points are samples from train set, green from validation set, and blue from test set. The numbers after the order value in the title of each subplot is the average dB error for the SPL at the specific order.

Figure 5.9: Comparison between measured and predicted SPL at different order [ANN_1 at 60 mph]

The average absolute dB error for all samples at different order is plotted and displayed in Figure 5.10. It is shown that, the train set has the smallest dB error, especially in the range from 50 to 80 (< 2 dB for the dominant spectral range), while the validation set has the largest.

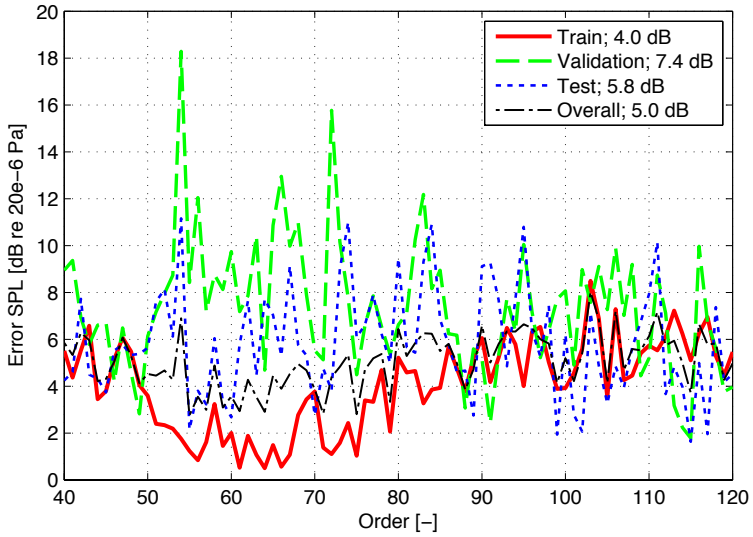

Figure 5.10: Average dB error at different order (the number in the legend is the average value across all the orders for the specific sample set) [ANN_1 at 60 mph]

The overall sound pressure levels for the measured and predicted tread pattern noise in the predicted order range of 40 to 120 are compared in Figure 5.11. The average dB error for train, validation, and test set is 0.5, 3.6, and 2.3 dB, respectively. The average dB error for all the samples at 60 mph is 1.5 dB, which is very good in terms of prediction accuracy. It should be noted that for the test set, a bit of over-prediction occurs. This might be due to the data set selected for the train/validation/test, and a different configuration of the data set might solve this issue. The author tried some different configurations, but failed. However, some other configurations that have not been tried might work.

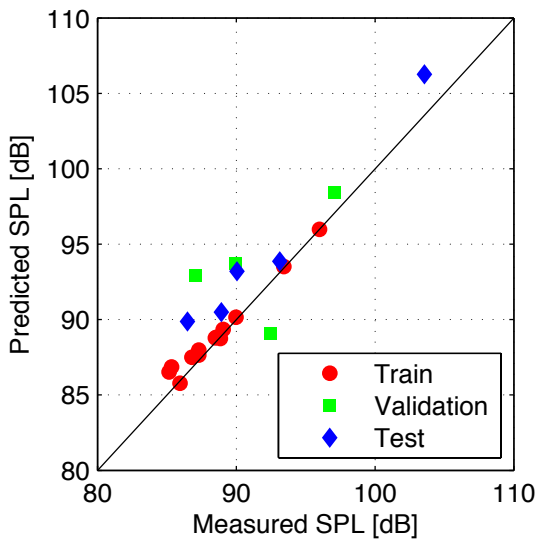

Figure 5.11: Comparison between measured and predicted overall SPL [ANN_1 at 60 mph]

It should be noted that, sometimes the direct ANN_1 output values in linear scale at specific frequencies are negative, which is physically wrong. Therefore, the negative values are set to a reference value, i.e., p^2_{ref} = (20e-6)^2, in post-processing as illustrated in Figure 5.12. In addition, talking about frequency or order is the same here, because only a single speed (60 mph) is considered.

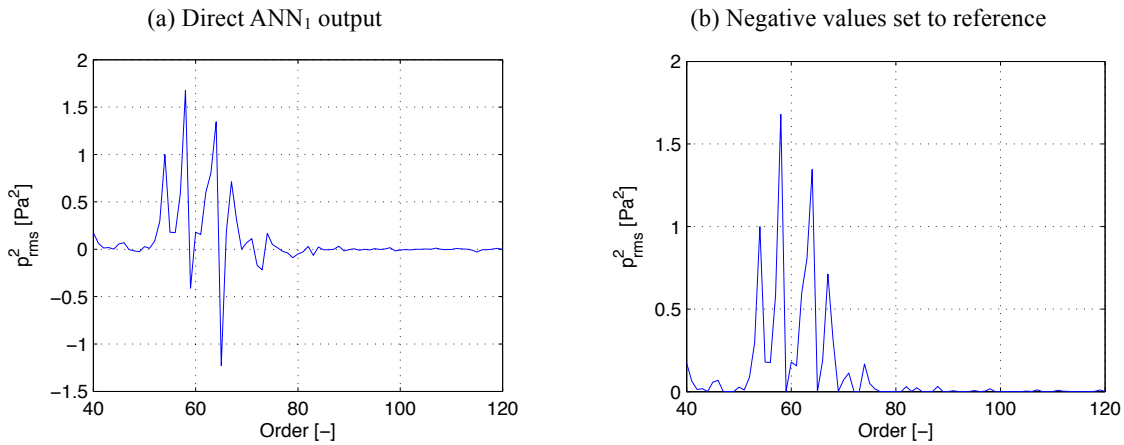

Figure 5.12: Post-processing for ANN_1 output (Tire 09 at 60 mph)

5.4 ANN_1 at Different Speed

As illustrated in Figure 5.4b, the predicted tread pattern noise at speed v is obtained from the noise at 60 mph by the following equation.

$$L_p(v) = L_p(60\text{mph}) + n \cdot 10\log_{10}(v/60\text{mph}) \tag{4.4}$$

The measured and predicted tread pattern noise spectrums for each sample are compared and shown in Figure 5.13. It can be seen that the predicted spectrum matches very well with the measured spectrum at all speeds except for a few cases, in particular at the lowest speeds of 50 and 45 mph. It is because the $n = 4$ used is not the correct value for particular tires, e.g., Tires 09 and 19 where n should be around 7 or 8. Also it is expected that when moving further away from 60 mph, predictions get worse. This scaling process is not perfect, but this has nothing to do with the accuracy of the ANN.

Tire No.	45 mph	50 mph	55 mph	60 mph	65 mph
	(a) Train Set				
01	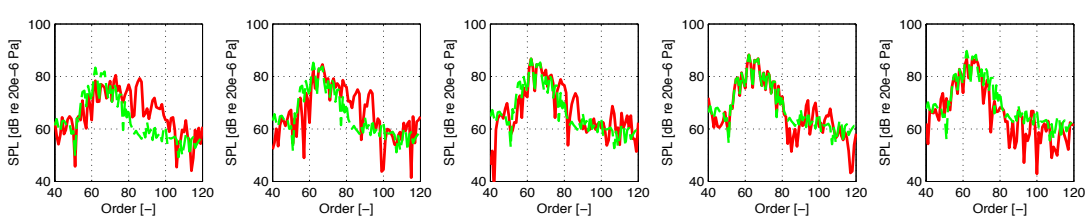				

Tire No.	45 mph	50 mph	55 mph	60 mph	65 mph
02	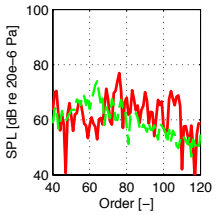	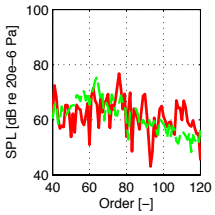	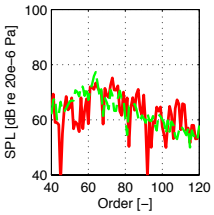	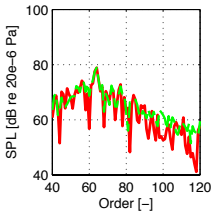	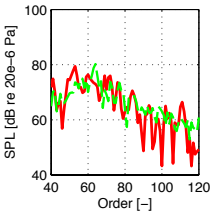
03	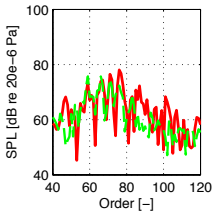	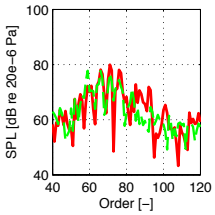	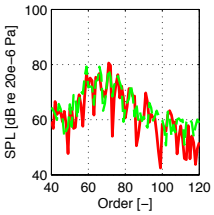	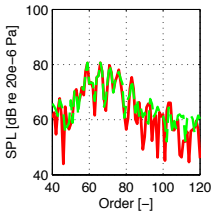	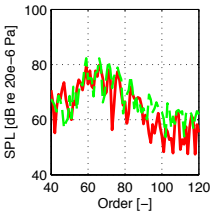
04	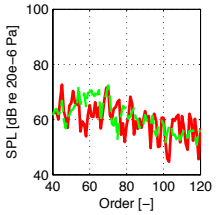	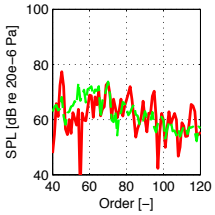	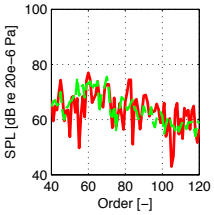	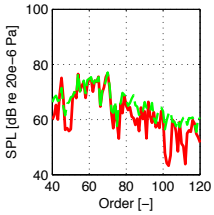	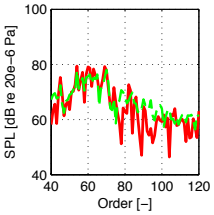
05	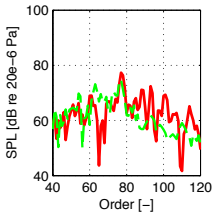	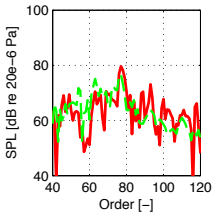	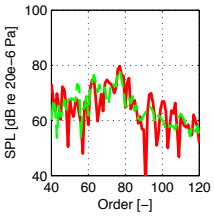	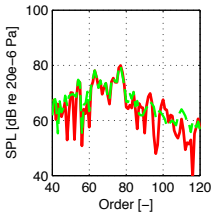	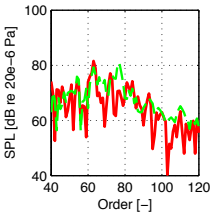
06	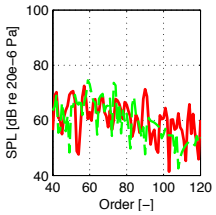	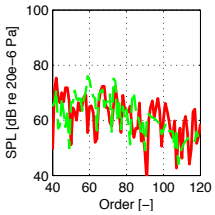	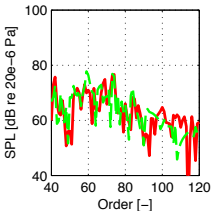	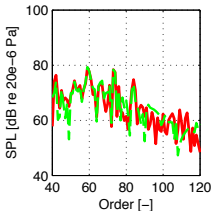	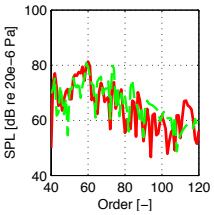
07	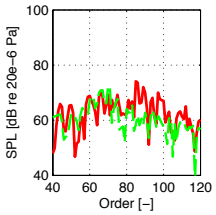	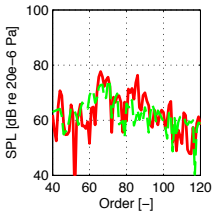	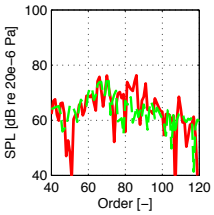	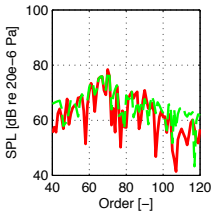	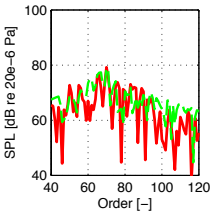

Tire No.	45 mph	50 mph	55 mph	60 mph	65 mph
08	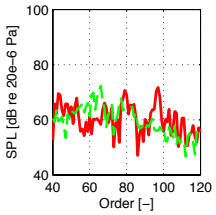	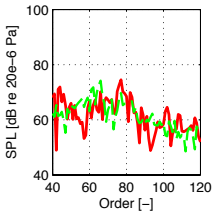	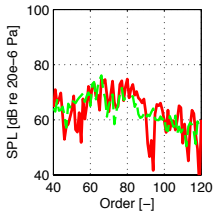	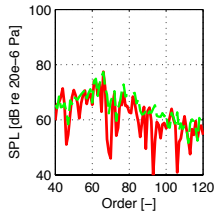	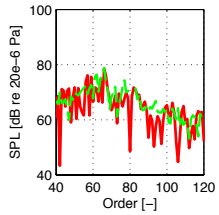
10	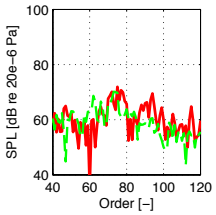	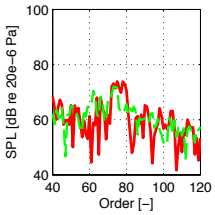	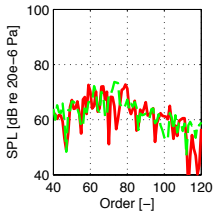	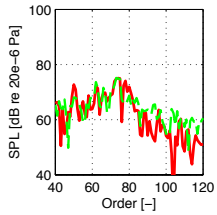	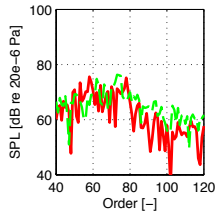
11	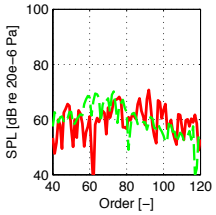	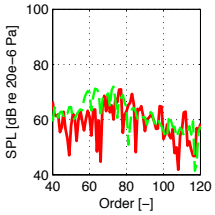	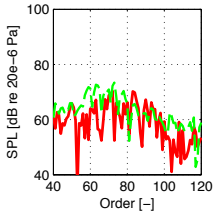	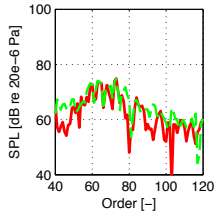	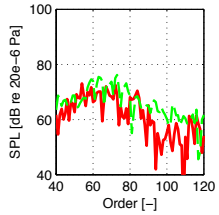
13	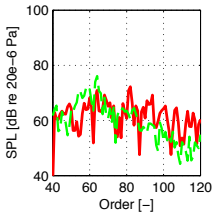	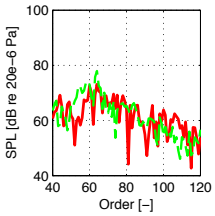	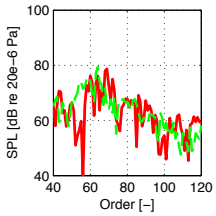	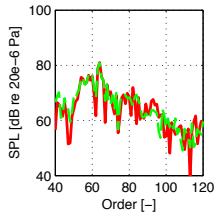	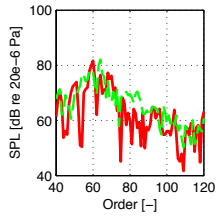
17	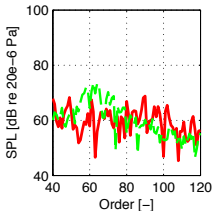	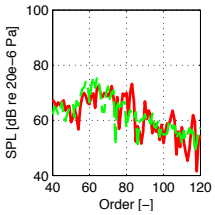	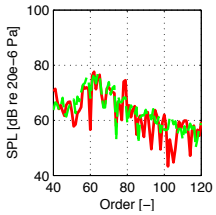	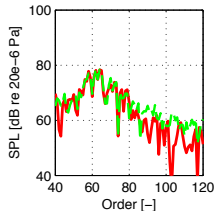	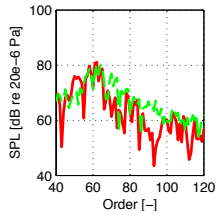
19	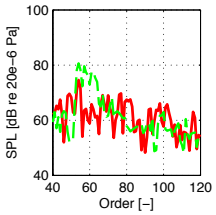	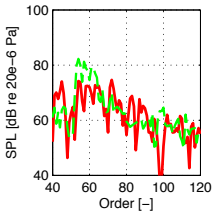	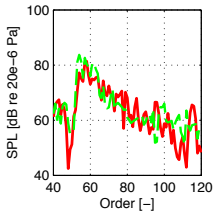	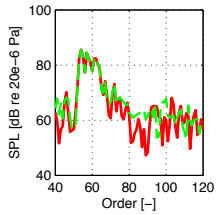	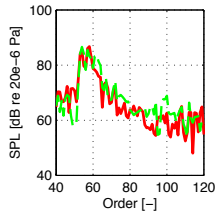

(b) Validation Set

Tire No.	45 mph	50 mph	55 mph	60 mph	65 mph
12	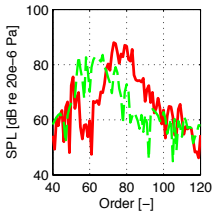	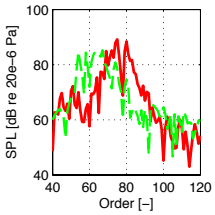	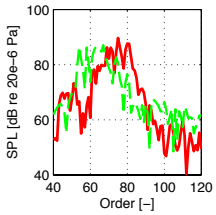	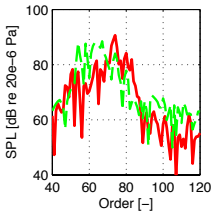	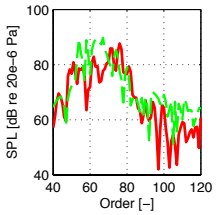
14	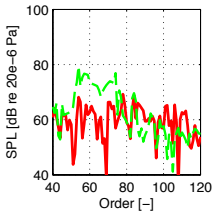	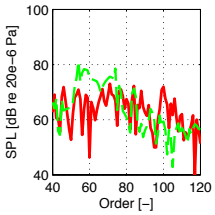	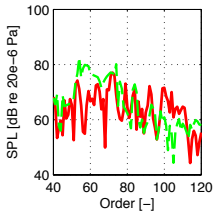	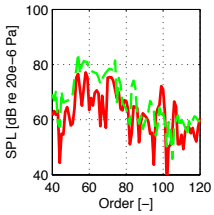	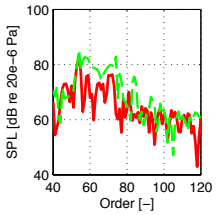
16	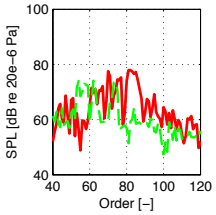	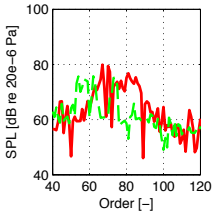	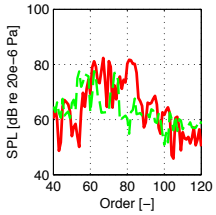	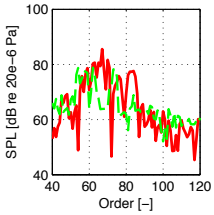	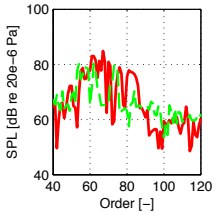
20	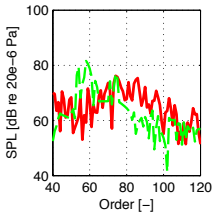	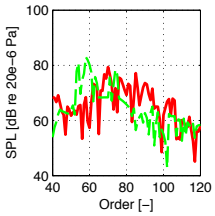	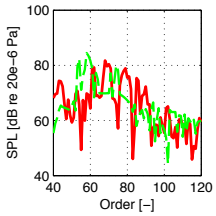	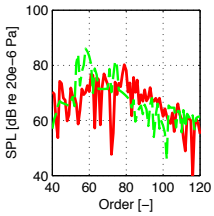	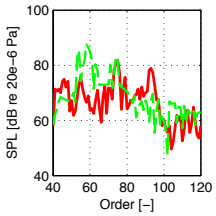

(c) Test Set

09	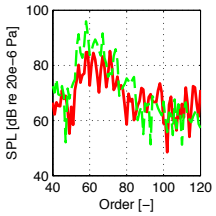	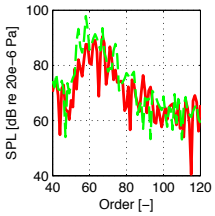	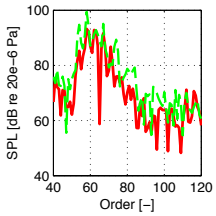	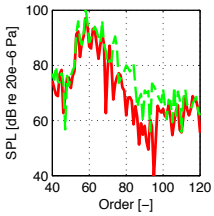	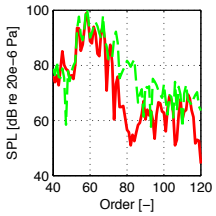
15	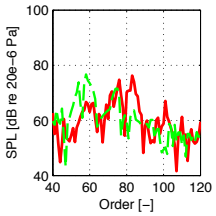	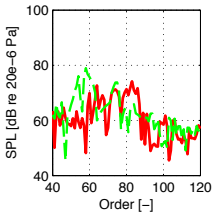	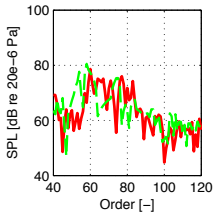	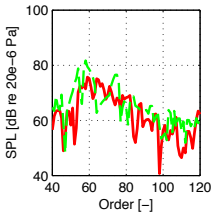	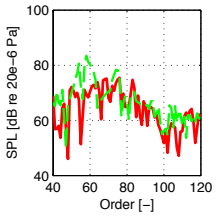

Tire No.	45 mph	50 mph	55 mph	60 mph	65 mph
18	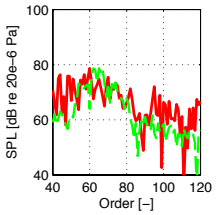	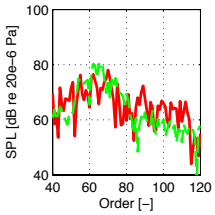	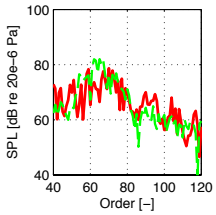	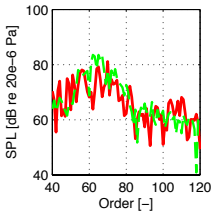	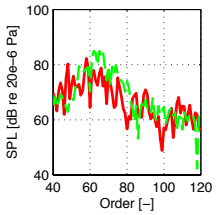
22	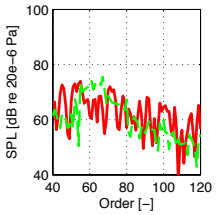	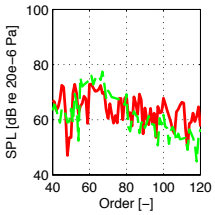	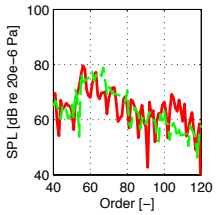	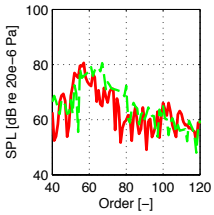	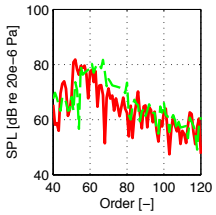
23	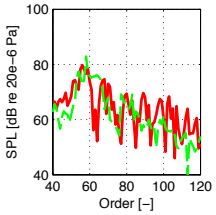	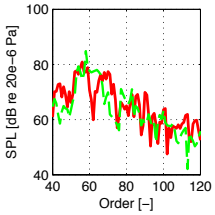	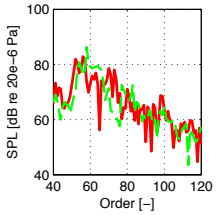	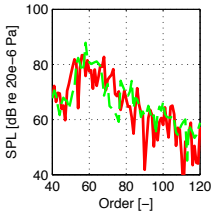	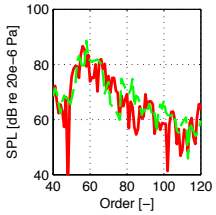

Figure 5.13: Comparison between measured (red) and predicted (green) tread pattern noise spectrums [ANN_1 at different speed]

The measured and predicted sound pressure levels (SPL) at different order are compared and demonstrated in Figure 5.14. A good agreement between the measured and predicted data is shown.

Order Range	Measured and Predicted SPL				
40~44	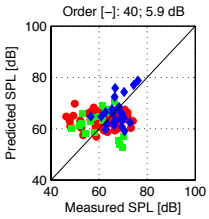	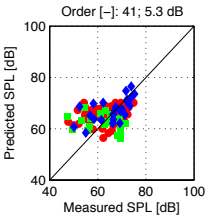	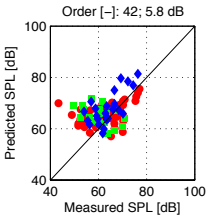	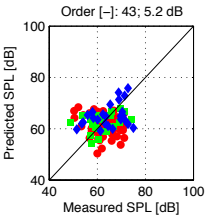	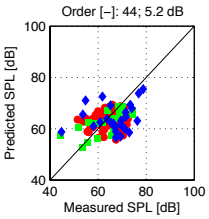

Order Range	Measured and Predicted SPL
45~59	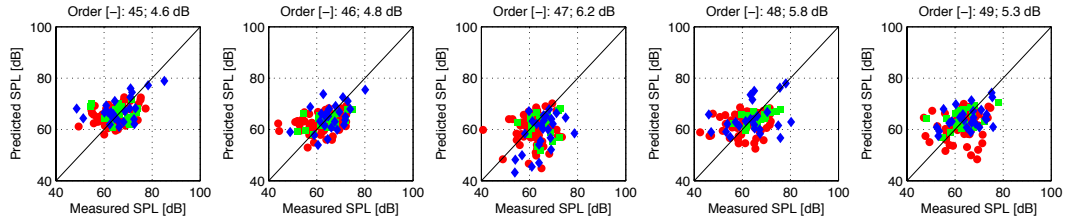
50~54	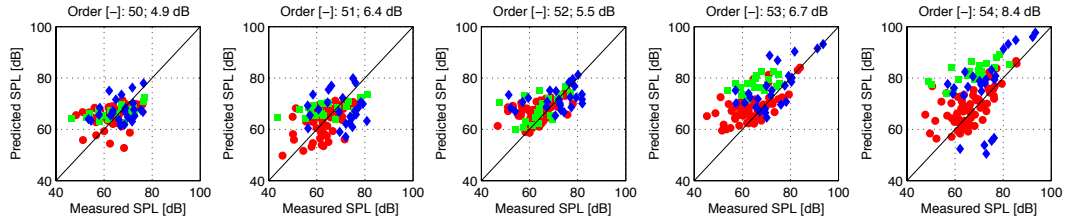
55~59	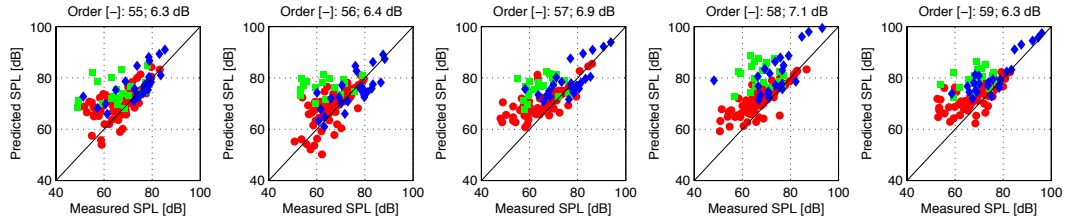
60~64	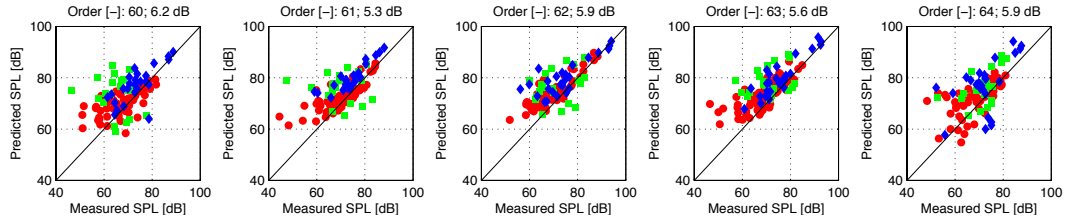
65~69	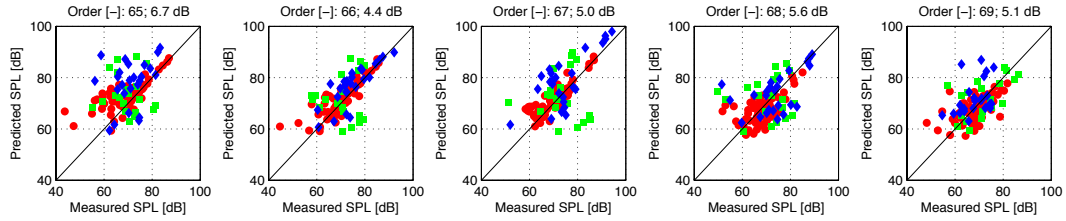
70~74	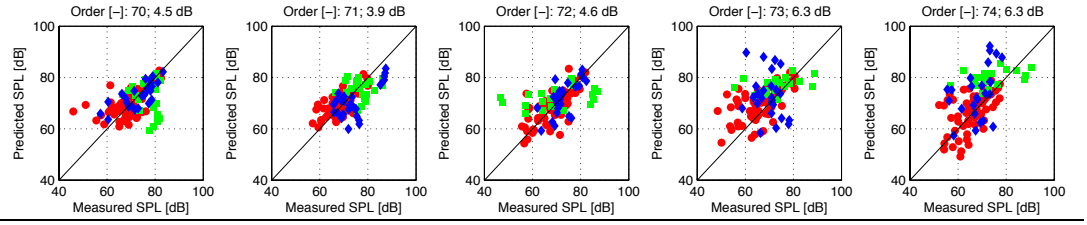

Order Range	Measured and Predicted SPL
75~79	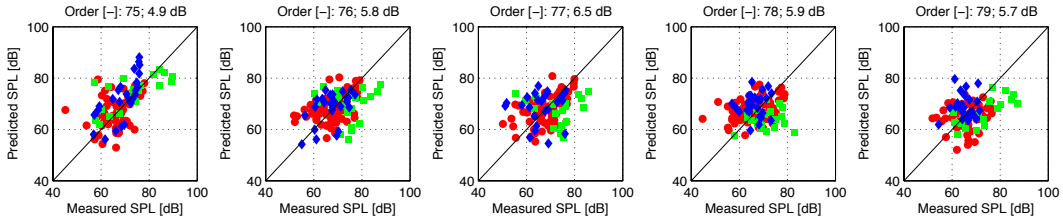
80~84	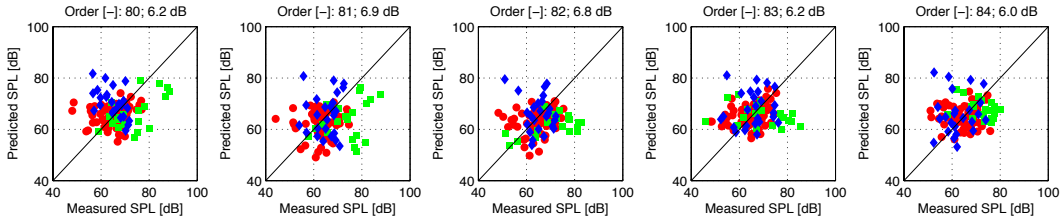
85~89	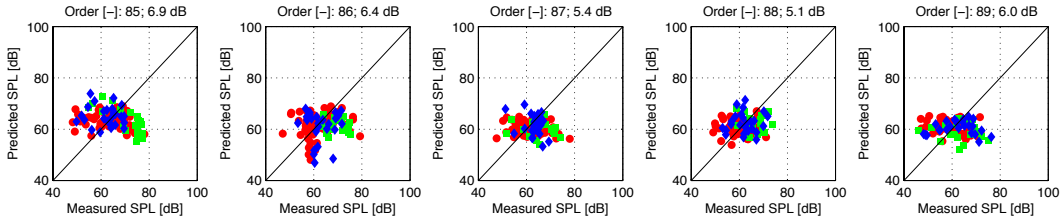
90~94	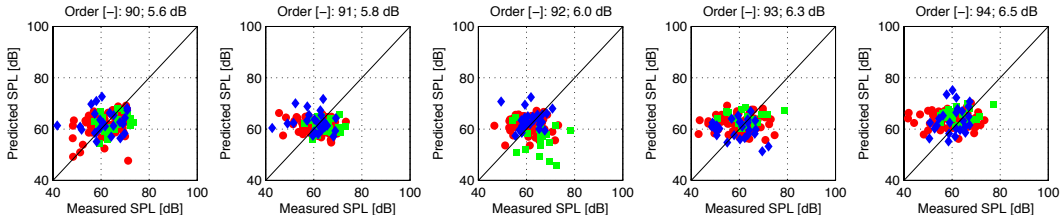
95~99	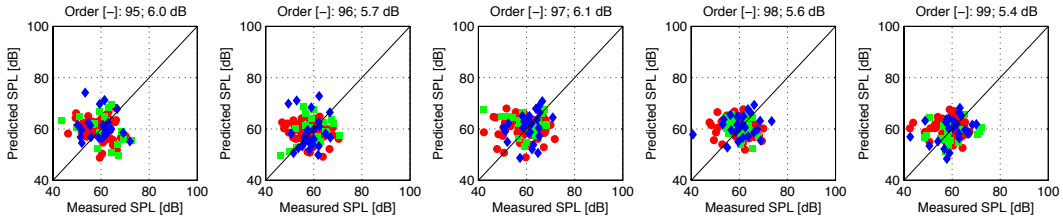
100~104	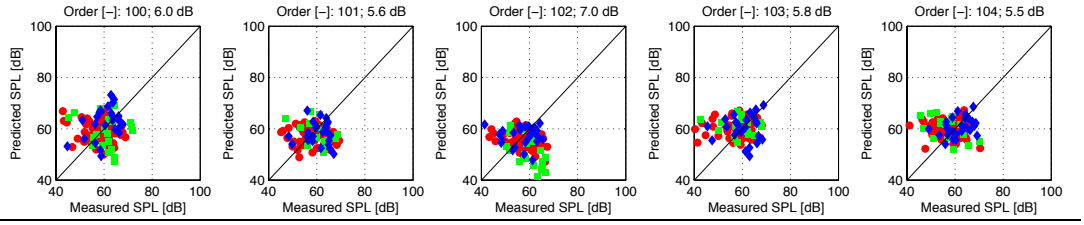

Order Range	Measured and Predicted SPL
105~109	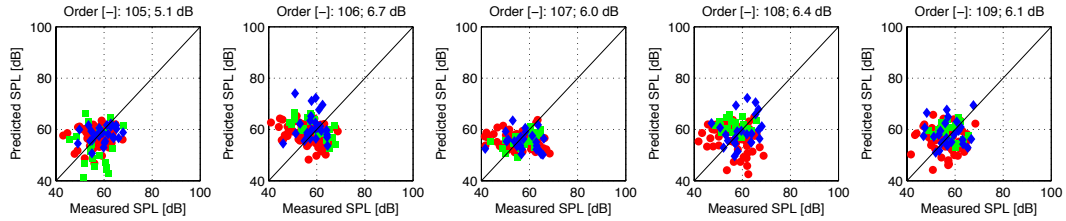
110~114	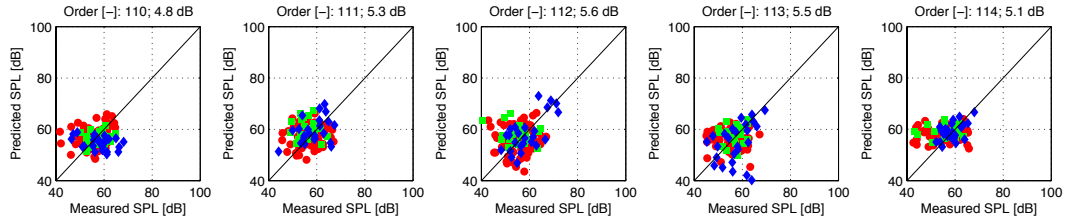
115~119	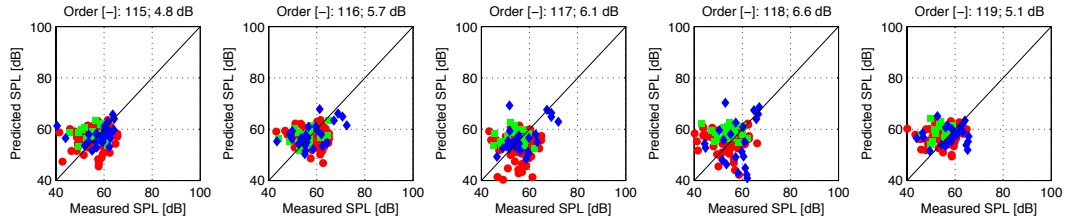
120	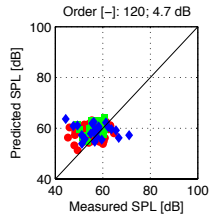

*Red points are samples from train set, green from validation set, and blue from test set. The numbers after the order value in the title of each subplot is the average dB error for the SPL at the specific order.

Figure 5.14: Comparison between measured and predicted SPL at different order [ANN_1 at different speed]

The average absolute dB error for all samples at different order is plotted and displayed in Figure 5.15. It is still shown that, the train set has the smallest dB error, while the validation set has the largest.

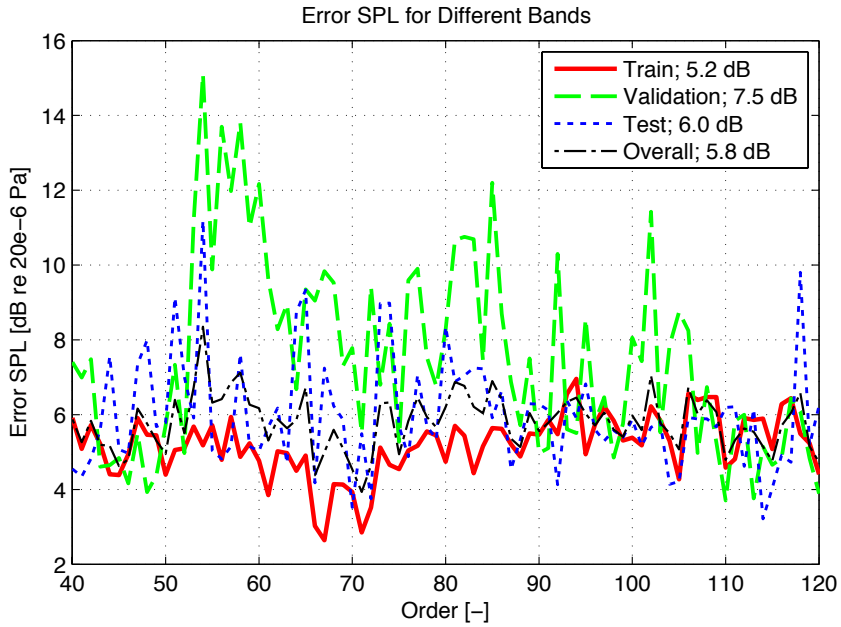

Figure 5.15: Average dB error at different order (the number in the legend is the average value across all the orders for the specific sample set) [ANN_1 at different speed]

The overall sound pressure levels for the measured and predicted tread pattern noise are compared in Figure 5.16. The average dB error for train, validation, and test set is 1.1, 3.5, and 2.1 dB. The average dB error for all the samples at 60 mph is 1.7 dB, which is considered very good in terms of prediction accuracy. It is also interesting to note that, these five blue points on the top are the results for the same tire (Tire 09) at different speed. The best prediction occurs at 60 mph, which makes sense because the ANN is built at 60 mph. The other speeds are obtained using speed exponent scaling. Again, like Figure 5.11, the over-prediction occurs for the test set.

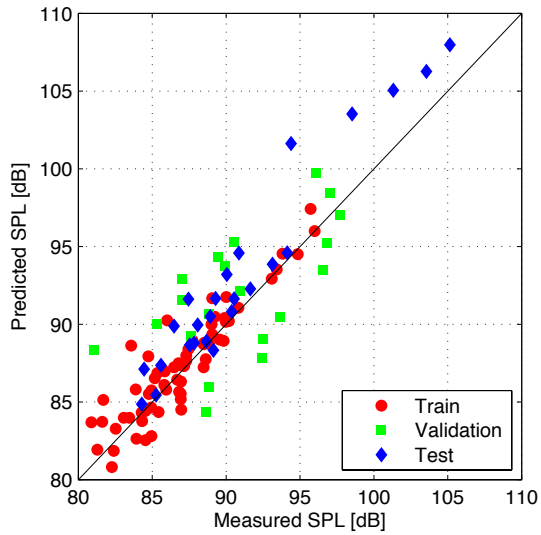

Figure 5.16: Comparison between measured and predicted overall SPL [ANN_1 at different speed]

Figure 5.17 shows the same results as Figure 5.16, but with the data points sorted by tires, so the set of points for a specific tire at different speeds can be identified. The accuracy for predicting different tires is different, and the speed at which best prediction occurs is also different for different tires. However, the overall results look good in general.

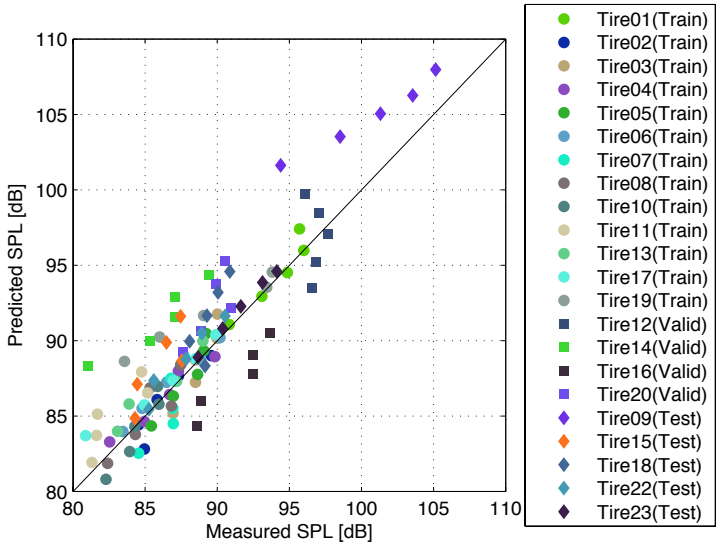

Figure 5.17: Comparison between measured and predicted overall SPL sorted by tires [ANN_1 at different speed]

5.5 Other ANN_1 Configurations

The ANN_1 model discussed above in Section 5.3 and 5.4 is the one with optimized configurations (e.g., speed exponent) and selected in the end. Config. No. 3 in Table 5.3 is the optimized configuration used. In determining the optimized configuration, several other ANN_1 configurations are also investigated and briefly presented below. It is noted that only the tires with the size of 215/60R16 are used in this chapter to exclude the tire size effect.

5.5.1 ANN_1 at 60 mph

As discussed in Section 5.1, the input of ANN_1 is coherent tread profile spectrum and air volume velocity spectrum, while the output of ANN_1 is tread pattern noise spectrum. There are two methods to represent these input and output spectra: (1) original spectral points at all orders (referred to as order), (2) Gaussian parameters (referred to as Gaussian). For the Gaussian method, different number of terms used for curve fitting generates different Gaussian parameters. The following input/output configurations investigated for the ANN_1 at 60 mph are listed in Table 5.3.

Table 5.3: Input/output configurations for ANN_1 at 60 mph

Config.	Input		Output	
No.	Method	Number of Parameters	Method	Number of Parameters
1	Order	162	Order	81
2	Gaussian (one-term)	6	Order	81
3	Gaussian (two-term)	12	Order	81
4	Gaussian (three-term)	18	Order	81
5	Gaussian (four-term)	24	Order	81
6	Gaussian (one-term)	6	Gaussian (one-term)	3
7	Gaussian (two-term)	12	Gaussian (two-term)	6

*Config. No. 3 is the optimized configuration used in Section 5.3 and 5.4.

The results for the different input/output configurations of ANN_1 at 60 mph are shown in Table 5.4. For each configuration, the measured and predicted spectra for two tires in the test set (Tires 09 and 15) are compared. Tire 09 has relatively large tread pattern noise component while for Tire 15 it's much smaller. As shown in Table 5.4, for Configurations No. 1~5 that utilize the original order parameters as the output, the spectral trend is successfully captured

in the prediction. For Configurations No. 6~7 that utilize the Gaussian parameters as the output, the spectral trend is not able to be captured. This is likely because a slight change of the Gaussian parameters, which is common in ANN development, governing the output will have a very large influence on the entire spectrum, leading to a very unstable model. Therefore, an output represented directly by the spectral points is preferred for a robust ANN model. The measured and predicted overall SPL for all tires is also compared in Table 5.4. The average dB error between measured and predicted overall SPL for different input/output configurations of ANN_1 is displayed in Table 5.5. It can be seen that, the best configuration (No. 3) for ANN_1 at 60 mph is input spectra represented by two-term Gaussian parameters while output spectrum represented by original spectral points at all orders. It is also interesting to note that, for Configurations No. 6~7 that have very small number of output parameters, the agreement between measured and predicted for the train set is very good compared to validation and test sets. It is likely because when input parameters/neurons and the hidden neurons are larger than the output parameters/neurons, ANN tends to capture the characteristics in the train set more easily or even over-learn due to more knobs that can adjust.

Table 5.4: Results for different input/output configurations of ANN_1 at 60 mph

Cfg. No.	Narrowband Spectrum (Tire 09) (red: measured; green: predicted)	Narrowband Spectrum (Tire 15) (red: measured; green: predicted)	Overall SPL (All Tires) (red: train; green: validation; blue: test)
1	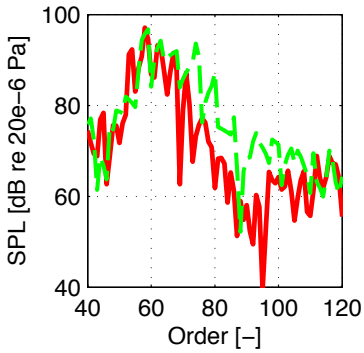	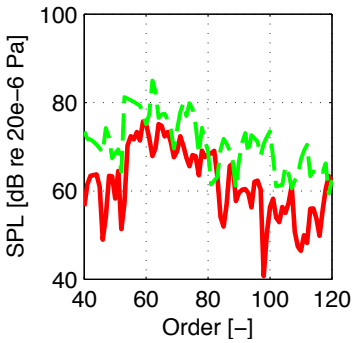	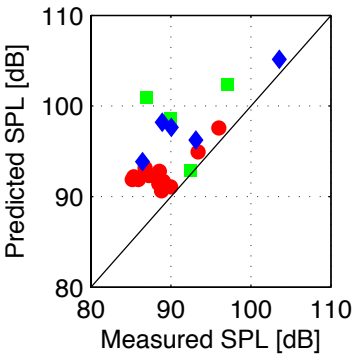

Cfg. No.	Narrowband Spectrum (Tire 09) (red: measured; green: predicted)	Narrowband Spectrum (Tire 15) (red: measured; green: predicted)	Overall SPL (All Tires) (red: train; green: validation; blue: test)
2	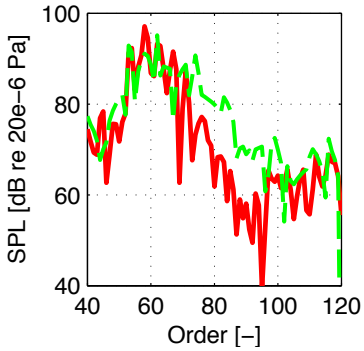	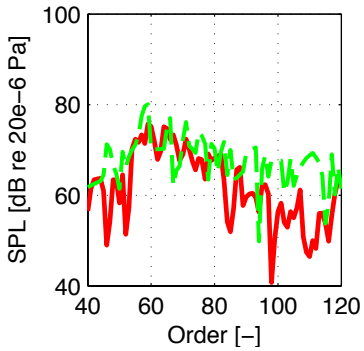	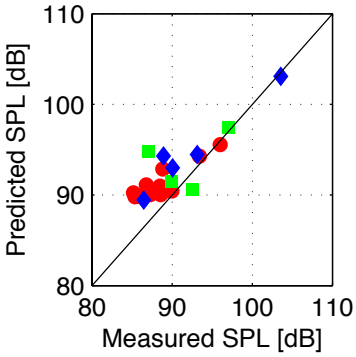
3	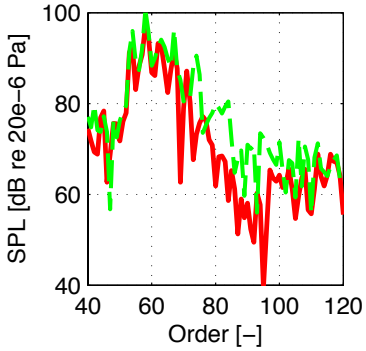	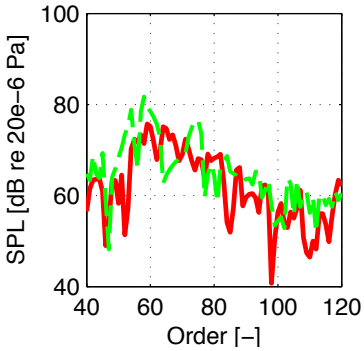	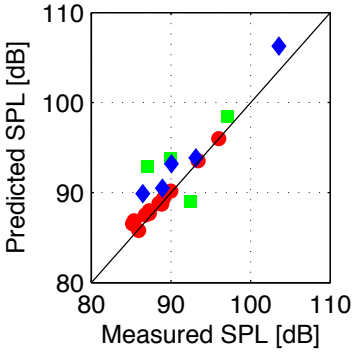
4	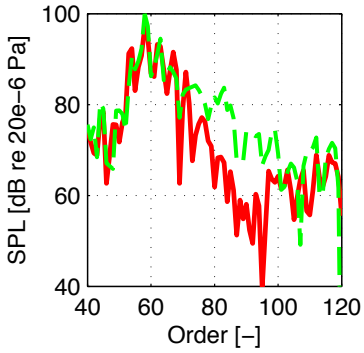	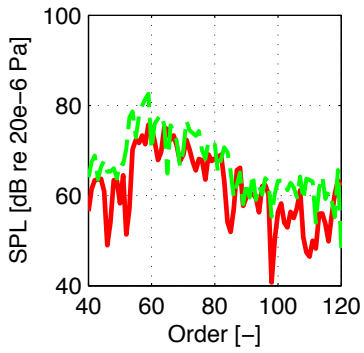	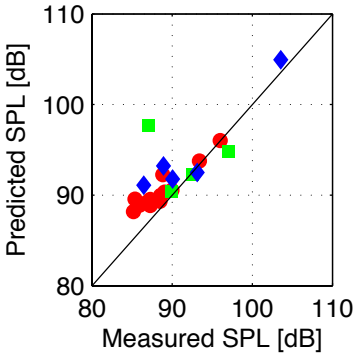

Cfg. No.	Narrowband Spectrum (Tire 09) (red: measured; green: predicted)	Narrowband Spectrum (Tire 15) (red: measured; green: predicted)	Overall SPL (All Tires) (red: train; green: validation; blue: test)
5	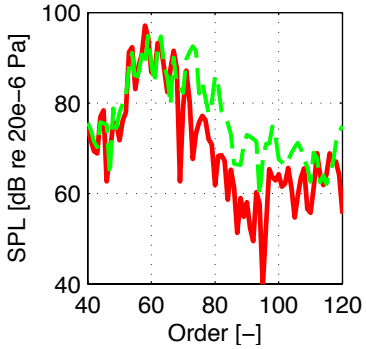	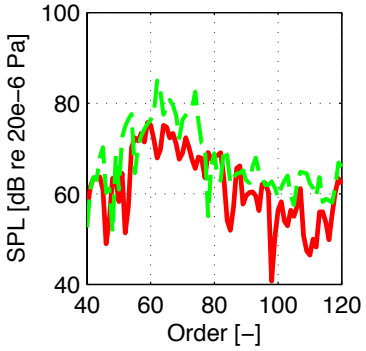	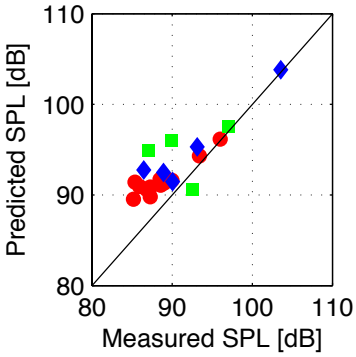
6	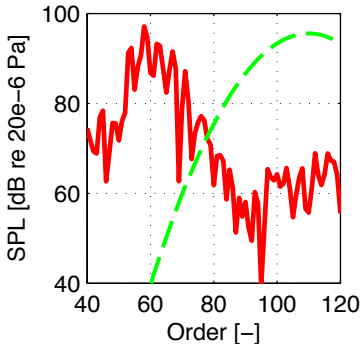	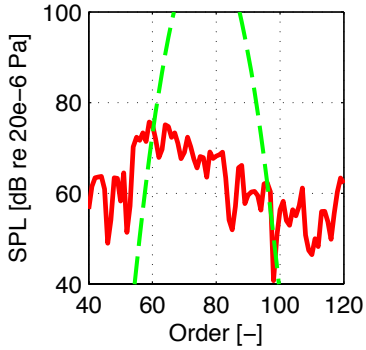	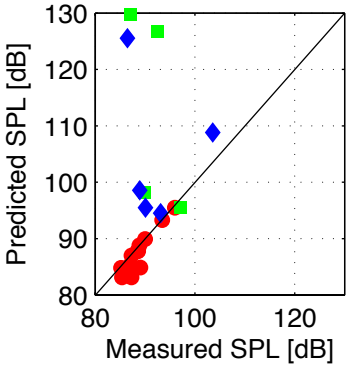
7	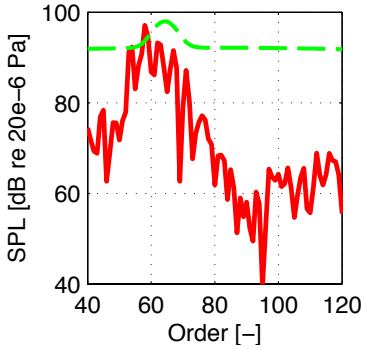	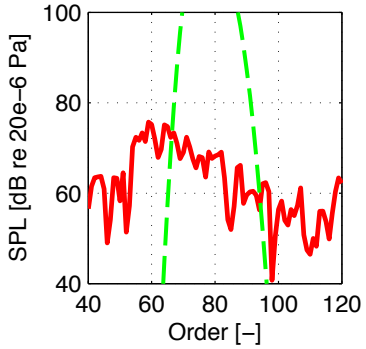	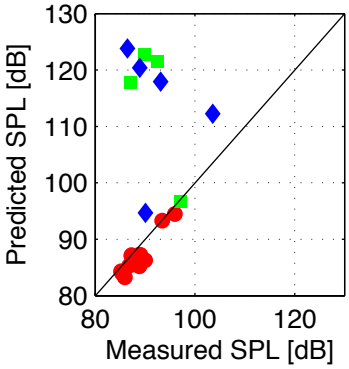

Table 5.5: Overall SPL error for different input/output configurations of ANN_1 at 60 mph (red indicates optimized)

Config.	Average dB Error for Overall SPL [dB]			
No.	Train Set	Validation Set	Test Set	All
1	4.0	7.1	5.8	4.9
2	2.7	2.9	2.6	2.7
3	**0.5**	**3.6**	**2.3**	**1.5**
4	1.9	3.4	2.5	2.3
5	3.0	4.1	2.7	3.1
6	1.3	21.7	12.1	7.5
7	1.6	23.3	21.4	10.0

5.5.2 ANN_1 at Different Speed

To extend the developed ANN_1 at 60 mph to different speed, different speed exponents in the range from 2 to 6 are investigated. The configuration of ANN_1 at 60 mph is the optimized one, Config. No. 3 discussed in 5.5.1. The results for comparisons between measured and predicted at all speeds are shown in Table 5.6 and Table 5.7. In Table 5.6, the narrowband spectra are compared between the measurement and prediction for two tires at 45 mph.

Table 5.6: Results for different speed exponents of ANN_1 at all speeds

n	Narrowband (Tire 09 at 45 mph) (red: measured; green: predicted)	Narrowband (Tire 15 at 45 mph) (red: measured; green: predicted)	Overall SPL (All Tires) (red: train; green: validation; blue: test)
2	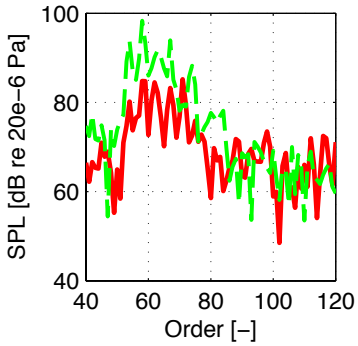	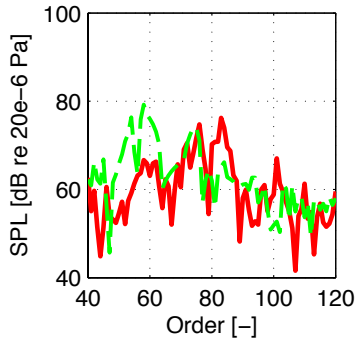	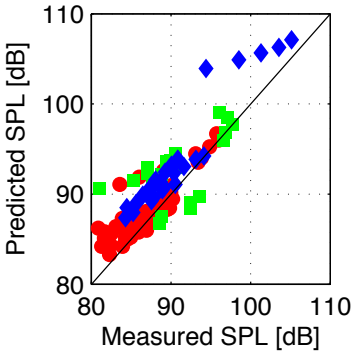

n	Narrowband (Tire 09 at 45 mph) (red: measured; green: predicted)	Narrowband (Tire 15 at 45 mph) (red: measured; green: predicted)	Overall SPL (All Tires) (red: train; green: validation; blue: test)
3	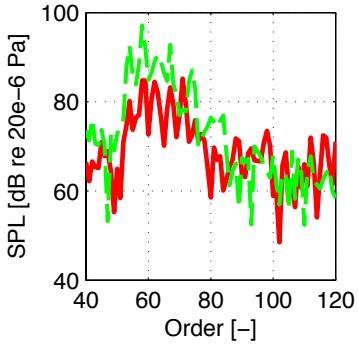	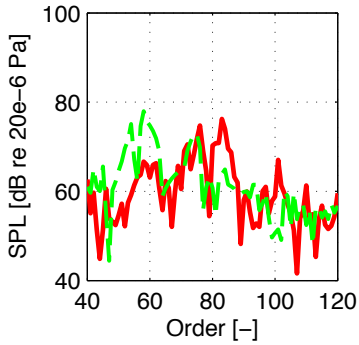	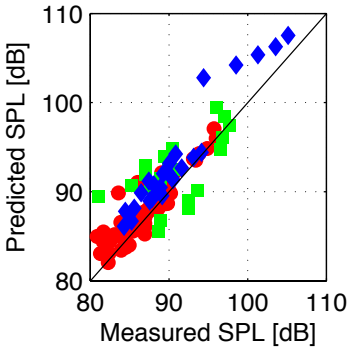
4	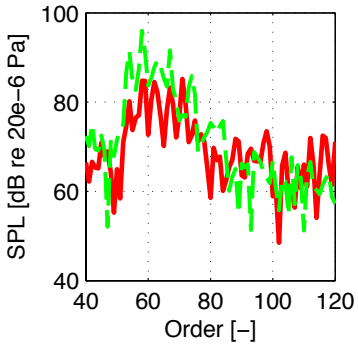	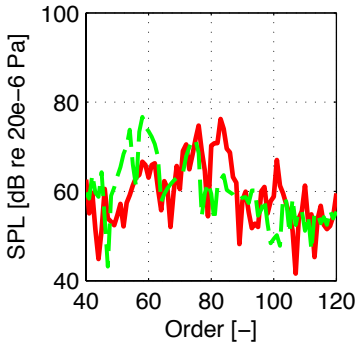	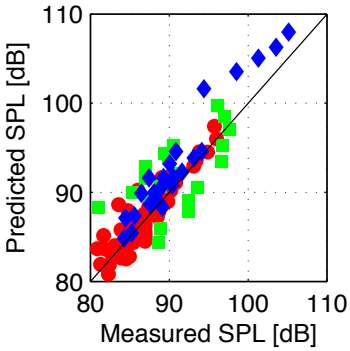
5	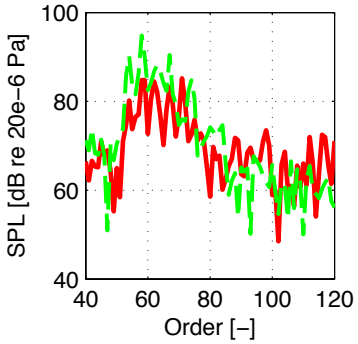	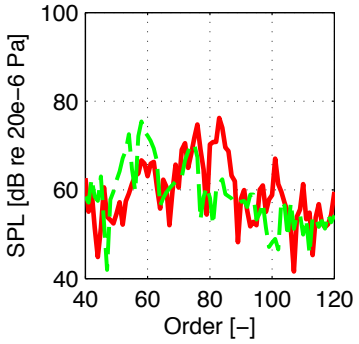	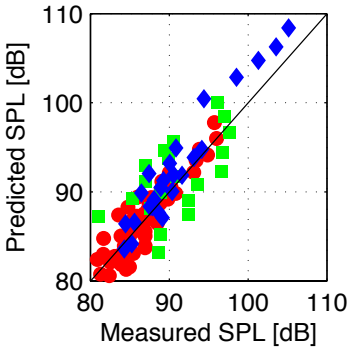

n	Narrowband (Tire 09 at 45 mph) (red: measured; green: predicted)	Narrowband (Tire 15 at 45 mph) (red: measured; green: predicted)	Overall SPL (All Tires) (red: train; green: validation; blue: test)
6	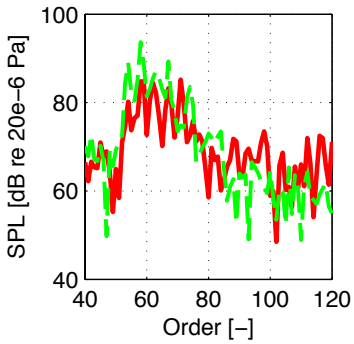	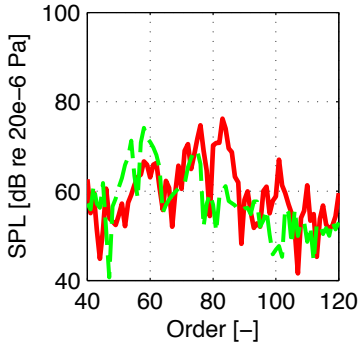	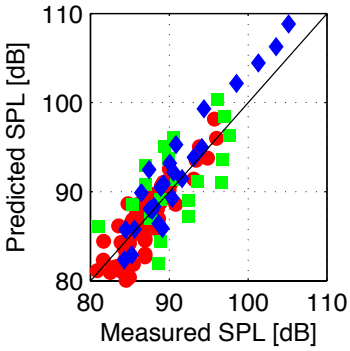

* $n = 4$ is the optimized configuration used in Section 5.4.

It can be seen from Table 5.6 that, as speed exponent n increases from 2 to 6, the agreement for Tire 09 at 45 mph becomes better, especially in the dominant order range from 50 to 70. It is because the real optimized speed exponent for Tire 09 is around 7, as shown in Figure 5.7. This also explains why the top five blue points in the plots on the right column of Table 5.6 align better with the reference line as speed exponent n increases. On the other hand, for Tire 15, as speed exponent n increases from 2 to 6, the agreement for Tire 15 at 45 mph becomes worse, especially in the dominant order range from 70 to 90. It is because the real optimized speed exponent for Tire 15 is around 2, as shown in Figure 5.7. Therefore, the optimized speed exponent should be selected from the balance between all tires. In general, the optimized speed exponent is 4, as seen from Table 5.7.

Table 5.7: Overall SPL error for different speed exponents of ANN_1 at all speeds (red indicates optimized)

n	Average dB Error for Overall SPL [dB]			
	Train Set	Validation Set	Test Set	All
2	1.4	3.4	2.9	2.1
3	1.1	3.4	2.5	1.8
4	**1.1**	**3.5**	**2.1**	**1.7**
5	1.2	3.5	2.1	1.8
6	1.6	3.6	2.2	2.1

For $n = 5$ or 6, the over-prediction for the test set is less obvious though with larger average dB error. This is likely because the larger speed exponent compromises (bends down) the

over-prediction coincidentally, especially for smaller speeds away from 60 mph.

5.5.3 Other Input and Output Data Set

Some other configurations for the input and output data set for ANN_1 development at 60 mph are worth investigating.

5.5.3.1 Input Data Set

The input data set for ANN_1 development at 60 mph can include both tread pattern spectra, or just one of the them, as shown in Table 5.8. All the input data sets are represented by two-term Gaussian parameters, while the output data sets are represented by original spectral points at all orders, which is the optimized case in Section 5.5.1.

Table 5.8: Other input data sets for ANN_1 at 60 mph

Input Set No.	Input Data Set	Number of Parameters	Output Data Set	Number of Parameters
1	Coherent tread profile spectrum	6	Tread pattern noise spectrum at 60 mph	81
2	Air volume velocity spectrum	6	Tread pattern noise spectrum at 60 mph	81
3	Coherent tread profile spectrum and air volume velocity spectrum	12	Tread pattern noise spectrum at 60 mph	81

*Input Set No. 3 is the optimized configuration used in Section 5.3 and 5.4. It is also the same as Config. No. 3 in Section 5.5.1. It is included here for the purpose of comparison and completeness.

The results for comparisons between measured and predicted are shown in Table 5.9 and Table 5.10. It is demonstrated that the spectral shape can be captured if ANN_1 is developed with only one tread pattern spectrum as input, but the accuracy is not as good as the one developed with both tread pattern spectra as input.

Table 5.9: Results for other input data sets of ANN1 at 60 mph

Input Set No.	Narrowband Spectrum (Tire 09) (red: measured; green: predicted)	Narrowband Spectrum (Tire 15) (red: measured; green: predicted)	Overall SPL (All Tires) (red: train; green: validation; blue: test)
1	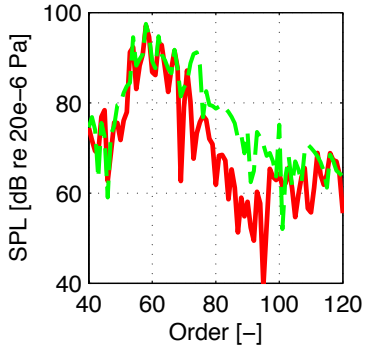	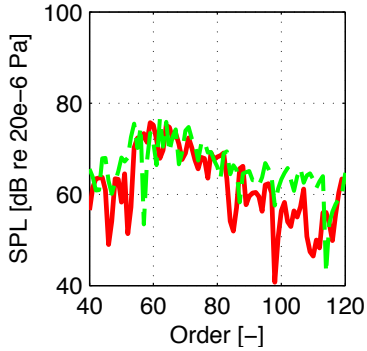	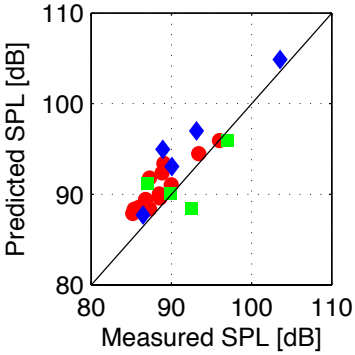
2	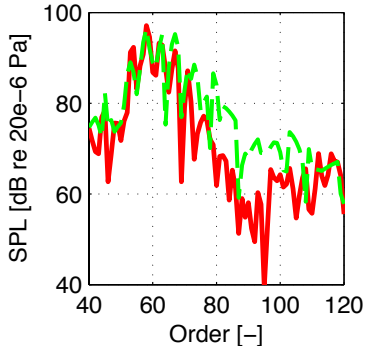	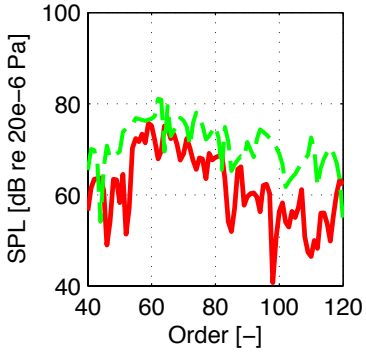	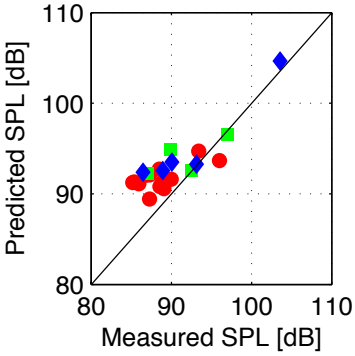
3	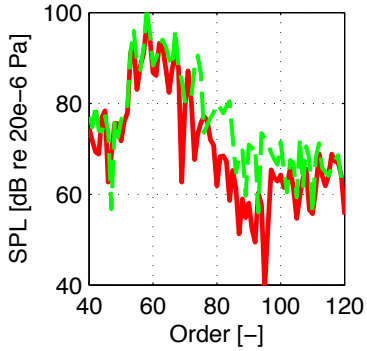	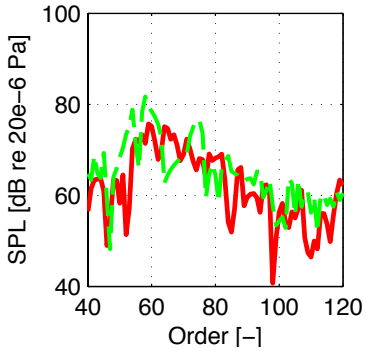	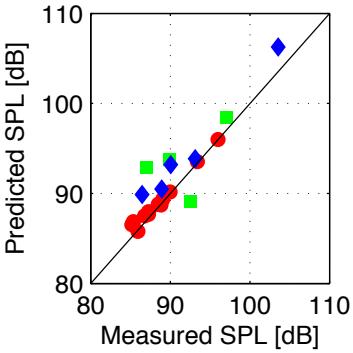

Table 5.10: Overall SPL error for other input data sets of ANN_1 at 60 mph (red indicates optimized)

Input Set No.	Average dB Error for Overall SPL [dB]			
	Train Set	Validation Set	Test Set	All
1	2.2	2.4	3.1	2.5
2	3.5	2.7	2.8	3.2
3	**0.5**	**3.6**	**2.3**	**1.5**

5.5.3.2 Output Data Set

In the development of ANN_1 at 60 mph as discussed in Section 5.3, the output data set used is the tread pattern noise spectrum at 60 mph only. That is to say, the noise data at other speeds are not used for developing ANN_1. In order to take advantage of all the noise data collected, a scaling and averaging process for the data at different speeds is conducted: all the noise spectra at different speeds are scaled to 60 mph using a certain speed exponent n, then the average of the scaled noise spectra is used as the output of ANN_1 at 60 mph. The extension of ANN_1 at 60 mph to different speed should use the corresponding speed exponent in the previous step.

The investigated speed exponent for this output data set is shown in Table 5.11. All the input data sets are represented by two-term Gaussian parameters, while the output data sets are represented by original spectral points at all orders, which is the optimized case in Section 5.5.1.

Table 5.11: Other output data sets for ANN_1 at 60 mph

Output Set No.	Input		Output	
	Data Set	Number of Parameters	Data Set	Number of Parameters
1	Two tread pattern spectra	12	Tread pattern noise spectrum at 60 mph	81
2	Two tread pattern spectra	12	Averaged spectrum using $n = 2$	81
3	Two tread pattern spectra	12	Averaged spectrum using $n = 3$	81
4	Two tread pattern spectra	12	Averaged spectrum using $n = 4$	81
5	Two tread pattern spectra	12	Averaged spectrum using $n = 5$	81
6	Two tread pattern spectra	12	Averaged spectrum using $n = 6$	81

*Output Set No. 1 is the optimized configuration used in Section 5.3 and 5.4. It is also the same as Config. No. 3 in Section 5.5.1. It is included here for the purpose of comparison and completeness.

The results for comparisons between measurement and prediction at all speeds are shown in Table 5.12 and Table 5.13. It is demonstrated that the best accuracy occurs when speed exponent n is 4, however, it is not improved much compared to the original ANN_1 developed only using the data at 60 mph. It should be noted that for Output Set No. 4, the over-prediction for the test set reduces, but the over-prediction for the train set increases, which means the training process is actually not very good.

Table 5.12: Results for other output data sets of ANN_1 at all speeds

Output Set No.	Narrowband (Tire 09 at 45 mph) (red: measured; green: predicted)	Narrowband (Tire 15 at 45 mph) (red: measured; green: predicted)	Overall SPL (All Tires) (red: train; green: validation; blue: test)
1	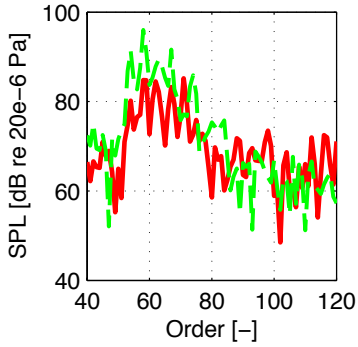	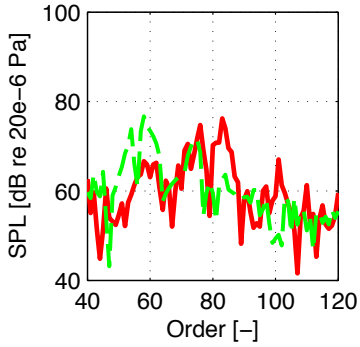	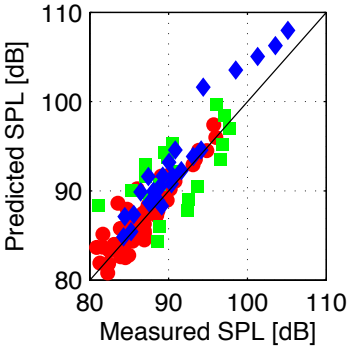
2	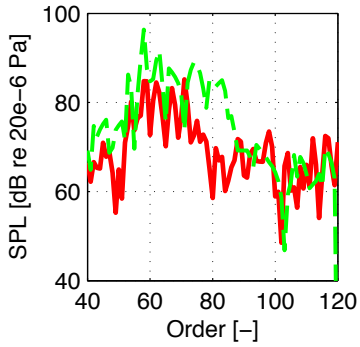	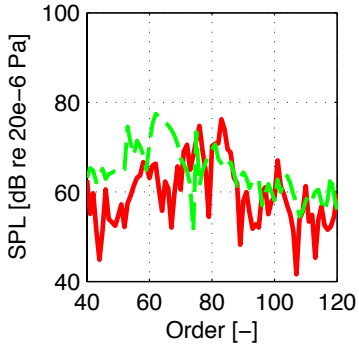	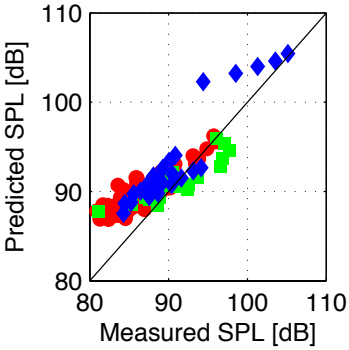

Output Set No.	Narrowband (Tire 09 at 45 mph) (red: measured; green: predicted)	Narrowband (Tire 15 at 45 mph) (red: measured; green: predicted)	Overall SPL (All Tires) (red: train; green: validation; blue: test)
3	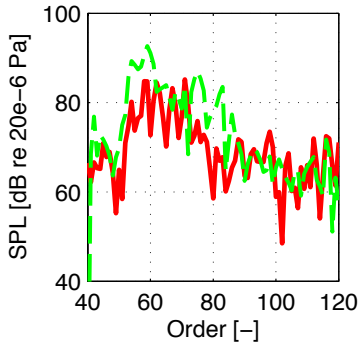	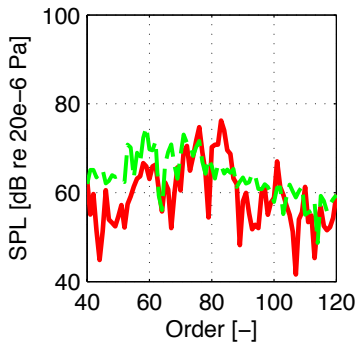	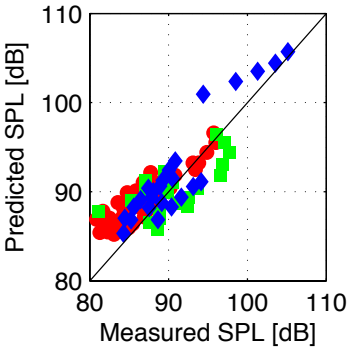
4	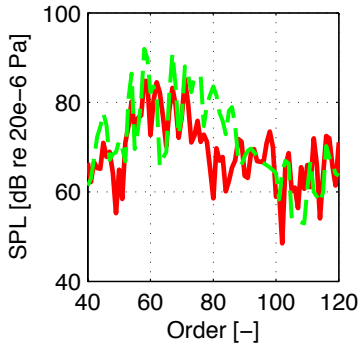	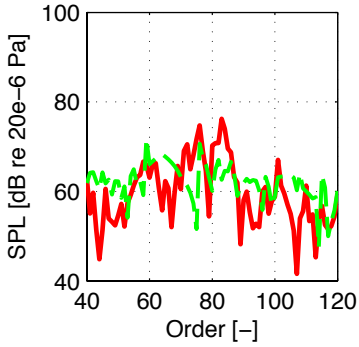	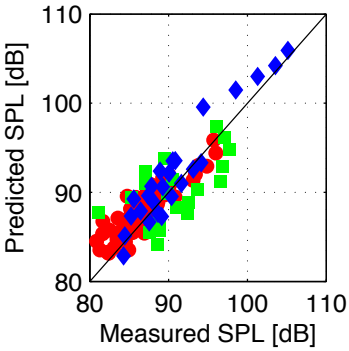
5	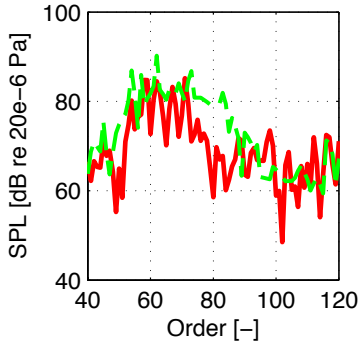	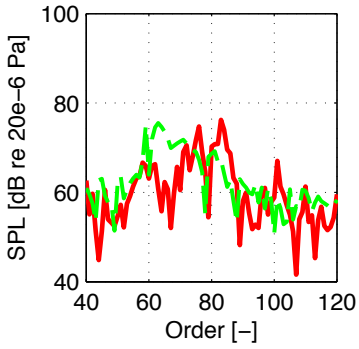	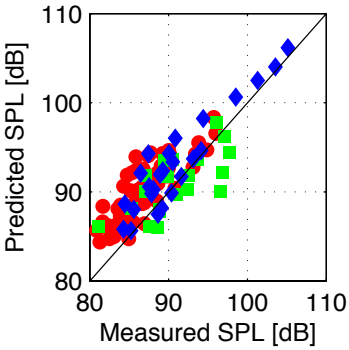

Output Set No.	Narrowband (Tire 09 at 45 mph) (red: measured; green: predicted)	Narrowband (Tire 15 at 45 mph) (red: measured; green: predicted)	Overall SPL (All Tires) (red: train; green: validation; blue: test)
6	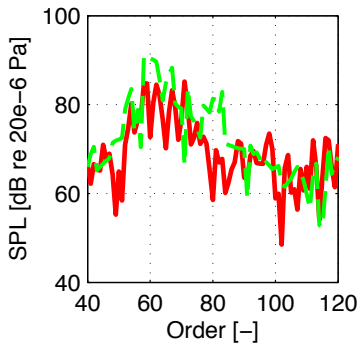	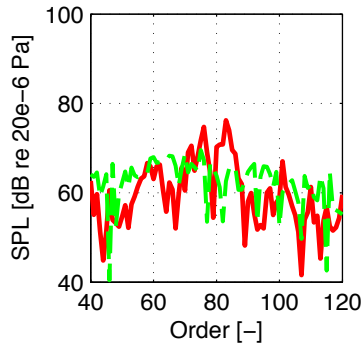	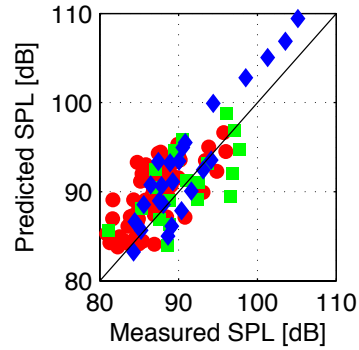

Table 5.13: Overall SPL error for other output data sets of ANN_1 at all speeds (red indicates optimized)

Output Set No.	Average dB Error for Overall SPL [dB]			
	Train Set	Validation Set	Test Set	All
1	**1.1**	**3.5**	**2.1**	**1.7**
2	3.0	2.0	2.6	2.8
3	2.4	2.7	2.1	2.4
4	**1.6**	**3.3**	**1.8**	**2.0**
5	3.3	2.6	2.4	3.0
6	3.2	3.1	2.9	3.1

5.5.4 Summer/All-Season Tires Only

In this subsection, the winter tires (Tires 09, 12, and 19) are excluded for the development of ANN_1, i.e., the ANN_1 is developed for summer/all-season tires only. The other configurations for ANN_1 development are the optimized ones used in Section 5.3 and 5.4.

The results and comparison between the ANN_1 for all tires are shown in Table 5.14. It can be seen that the accuracy for ANN_1 for summer/all-season tires only is as good as ANN_1 for all tires. The ANN_1 for all tires looks a little bit better, likely because with winter tires included, the ANN_1 is better trained due to a broader range of training data.

Table 5.14: Comparison between the ANN_1 for all tires and ANN_1 for summer/all-season tires only

ANN_1 Category	Average dB Error for Overall SPL [dB] at 60 mph			
	Train Set	Validation Set	Test Set	All
All Tires	0.5	3.6	2.3	1.5
Summer/All-Season Tires	1.0	4.2	2.3	1.8
	Average dB Error for Overall SPL [dB] at Different Speed			
	Train Set	Validation Set	Test Set	All
All Tires	1.1	3.5	2.1	1.7
Summer/All-Season Tires	1.1	4.6	2.3	1.9

5.6 Conversion from Order Spectrum to Frequency Spectrum

It is noted that the output of ANN_1, i.e., the predicted tread pattern noise, is in order spectrum discussed above. It will be later converted to frequency spectrum based on the rotational speed of the tire in Hz. To obtain the rotational speed of the tire, the vehicle speed and tire circumference are used. An example is illustrated in Figure 5.18, including the speed exponent scaling from 60 mph. Figure 5.18a shows the tread pattern noise in order spectrum at 60 mph for Tire 09 (215/60R16). The rotational speed at 45 mph is ~9.95 Hz based on the tire circumference. The amplitude in the order spectrum at 45 mph is calculated using the speed exponent scaling, and the spectrum is then converted from order to frequency by multiplying 9.95, as shown in Figure 5.18b (frequency resolution = 9.95). The frequency resolution is then changed from 9.95 Hz to 10 Hz based on interpolation, as shown in Figure 5.18c. Note that the frequency range in Figure 5.18c is not the same as that in Figure 5.18b. In Figure 5.18c, the spectral amplitude of the frequencies out of the range in Figure 5.18b is set to 4e-10. In addition, the amplitude in Figure 5.18c is further adjusted, so that the OASPL in Figure 5.18c is the same as that in Figure 5.18b (summation of p^2_{rms} = 3.3444).

(a) Tread pattern noise in order spectrum at 60 mph (order resolution = 1) in the range of [40, 120]

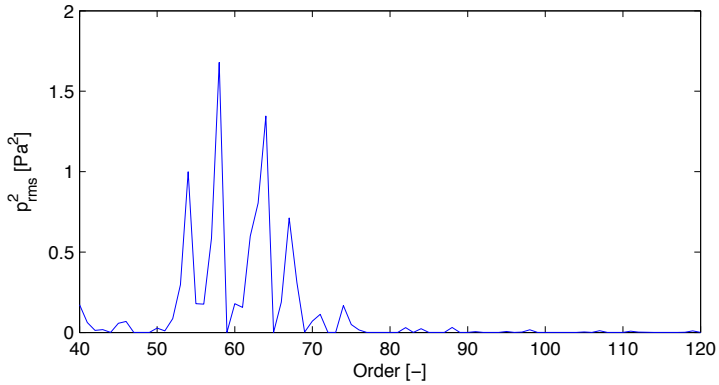

(b) Tread pattern noise in frequency spectrum at 45 mph (frequency resolution = 9.95 Hz) in the range of [398, 1194] Hz

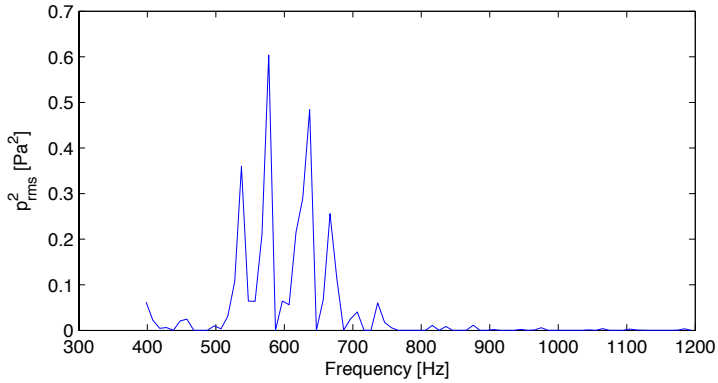

(c) Tread pattern noise in frequency spectrum at 45 mph (frequency resolution = 10 Hz) in the range of [400, 1600] Hz

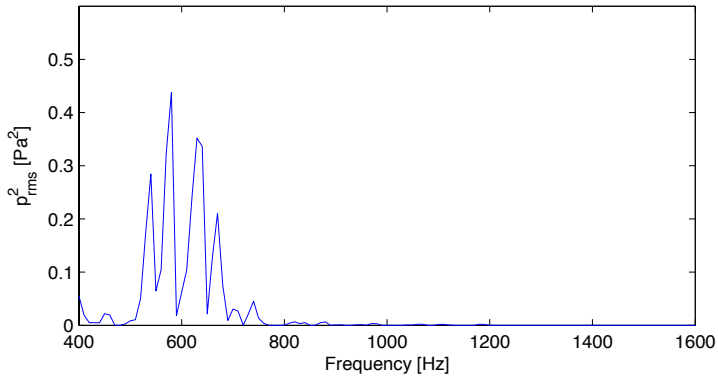

Figure 5.18: Speed exponent scaling and conversion from order domain to frequency domain.

5.7 Summary

The configuration for ANN_1 model on tread pattern noise is optimized. The optimized input is coherent tread profile spectrum and air volume velocity spectrum, both represented by two-term Gaussian parameters. The optimized output is tread pattern noise spectrum represented by original spectral points at all orders. The ANN_1 model is firstly developed at 60 mph, then extended to different speed using a speed exponent of 4. The optimized ANN_1 model is validated using experimental data, and is able to predict tread pattern noise well from typical tread patterns of tire size investigated (215/60R16) at normal highway speeds. In addition, Chapter 7 shows that the ANN_1 is also valid for other tire sizes.

6 ANN Model for Non-Tread Pattern Noise (ANN_2)

The development and validation of the second part of ANN model for TPIN, i.e., ANN_2 on non-tread pattern noise, is discussed in this chapter.

Besides vehicle speed, the non-tread pattern noise depends on the pavement and some tire parameters other than tread pattern, such as the tread rubber hardness and tire size. In the present study, the non-tread pattern noise was investigated only on the same pavement (a non-porous asphalt pavement). For the same pavement, the tread rubber hardness is expected to have effect on the amplitude of the non-tread pattern noise; the tire size is expected to have effect on the dominant frequencies of the non-tread pattern noise.

6.1 Effect of Rubber Hardness

In this section, the effect of the tread rubber hardness is investigated.

6.1.1 Literature Survey

The increase of rubber hardness generally increases the TPIN level, as shown in Table 6.1. The effect varies mostly from 0.1 to 0.3 dB/Shore A, depending on the tire and pavement types.

Oddershede and Kragh (2014) [402] found that the rubber hardness does not significantly influence the TPIN spectral shape in the hardness range of 62-74 Shore A. The rubber hardness influences TPIN mostly in the frequency range of 1-3 kHz (Sandberg and Ejsmont, 2002 [24]). For the aggressive tread, the influence around 2-2.5 kHz might be 10 dB. It is reasonable to speculate that increased hardness amplifies the stick/slip motions. A study attempted to explain the hardness effect by modeling is Wullens and Kropp, 2001 [403]. The frequency range of 400-700 Hz and 1300-1400 Hz was found to match the measurements best (Wullens, 2002 [404]).

Rochoux and Biesse (2010) [405] found that soft rubber has better noise performance at high frequencies, which leads to a paradox: it should give higher air compression because of its higher deformation, since at high texture frequencies, a deeper road cavity is better

because it results in better air drainage which reduces air compression, thus cavity air pumping noise. This might suggest that the air pumping mechanism is insignificant for the tire tested. Rochoux and Biesse (2010) [405] also observed that the decrease of rubber viscosity (hysteretic behavior) will increase the vibrations from texture impact on the tire rubber, especially at the contact center and the trailing edge.

Table 6.1: Effect of rubber hardness on TPIN level

Reference	Rubber Hardness Effect	Condition
Watanabe et al., 1998 [406]	0.26 to 0.42 dB/ Shore A	Cross-bar truck tire from 40 to 59 Shore A tested on a drum facility
Sandberg and Ejsmont, 2000 [94]	Positive correlation with TPIN (R^2 = 0.3)	Especially at high frequencies and on rough road surface (Sandberg and Ejsmont, 2007 [249])
Sandberg and Ejsmont, 2007 [249]	0.1 to 0.25 dB/ Shore A, mainly at high frequencies	General condition
Ho et al., 2013 [407]	Positive correlation with TPIN (R^2 = 0.68~0.98)	Types of pavement are categorized (i.e., results on the same pavement)
Buehlmann et al. (2013) [408]	Up to 0.3 dB/Shore A	ISO road surface
Oddershede and Kragh (2014) [402]	0.09 dB/Shore A	Close Proximity method (CPX) for SRTT tires from 62-74 Shore A
Swieczko-Zurek et al. (2015) [409]	0.15 dB/Shore A for SRTT; 0.19 dB/Shore A for Avon AV4 tires	ISO road surface
Schubert et al. (2016) [410]	-0.03 to 0.14 dB/Shore A	Depending on the tire and pavement

Sandberg and Ejsmont (2007) [249] noted that tire noise is generally more closely related to hardness for rough than for very smooth road surfaces. However, Sandberg and Ejsmont (2002) [24] reported that when running tires with substantial side forces, a totally contrary effect of tread rubber hardness occurred, namely that the softer tread gave higher noise levels above 1 kHz.

Parameters physically similar to tire hardness is the stiffness and storage moduli (Bekke et al., 2013 [241]). The tread compound stiffness (E' or called elastic modulus) measures how much force needed to deform the tire to a certain distance. The loss modulus (E'') measures

the compound's hysteresis reducing the travelling distance of vibrational waves. Their respective ratio ($\tan\delta = E''/E'$) is often used as a design parameter in rubber compounding. It was shown that a higher $\tan\delta$ reduces the TPIN and a maximum effect is around 1.5 dB(A). It means a smaller elastic and a higher loss modulus are in favor of noise reduction. However, the loss modulus should not be too large, because higher hysteresis often increases rolling resistance (Saemann, 2008 [411]).

Schubert et al. (2016) [410] indicated that Shore hardness of the tires is not able to sufficiently describe the acoustically relevant properties of tires. Therefore, the mechanical admittance (mobility) or its inverse (i.e., mechanical impedance) is used instead since it is a direct descriptor for the vibrational behavior of the tire. Aging (or hardening) generally causes a decrease of the tire mobility and a slightly increase of the mode frequencies.

The tire aging and hardening are closed related. The tire degradations include mechanical wear and chemical ageing. Langwieder et al. (2001) [412] reported that 2-5% of tires in actual use had a tread depth of less than the legal minimum 1.6 mm and that 1-4% of the tires were "over-aged". The age effect is the effect which occurs when a tire is stored in a way in which its tread rubber compound undergoes changes due to exposure to moderate or high temperatures, or to certain substances and gasses in the air, for example, oxygen diffusing through the tire composite and reacting with the internal components (Sandberg and Ejsmont, 2007 [249]). Gothié (2001) [413] reported that the ageing effect is around 1 Shore A/year; however, larger the first years and lower in later years. Even though the tire is stored in a professional way (dark and in a relatively cool place), the ageing effect still exists. However, a temperature of -10 °C is able to suppress the aging effect well (Gothié, 2005 [414]).

6.1.2 Regression Analysis

To investigate the influence of the tread rubber hardness on TPIN, the 19 tires (Tires No. 1-19) with different tread patterns but the same size of 215/60R16 were investigated. In terms of the tread pattern noise, the influence of the rubber hardness is marginal compared to the tread pattern parameters. In addition, no tire samples with the same tread pattern but different rubber hardness are available to make further investigations. In the following, the influence of the rubber hardness on the non-tread pattern noise is presented.

The measured data of the non-tread pattern noise for the 19 tires at five speeds (nominal speed of 45, 50, 55, 60, 65 mph) were used to obtain the regression equation below.

$$SPL = p_0 + p_1 \cdot Hardness + p_2 \cdot Speed \tag{5.1}$$

where *SPL* is the overall A-weighted sound pressure level for the non-tread pattern noise in [dB]; *Hardness* is the tread rubber hardness in [Shore A]; *Speed* is the tire rotational speed in [Hz] (exact value calculated from the optical signal); p_0, p_1, and p_2 are coefficients. The 3D fitted surface through two-variable linear regression analysis is displayed in Figure 6.1a. It is shown that $p_1 = 0.11$, indicating non-tread pattern noise increases with rubber hardness, which agrees with most of the literature. The corresponding 2D projected views of the fitted surface are shown in Figure 6.1b-d.

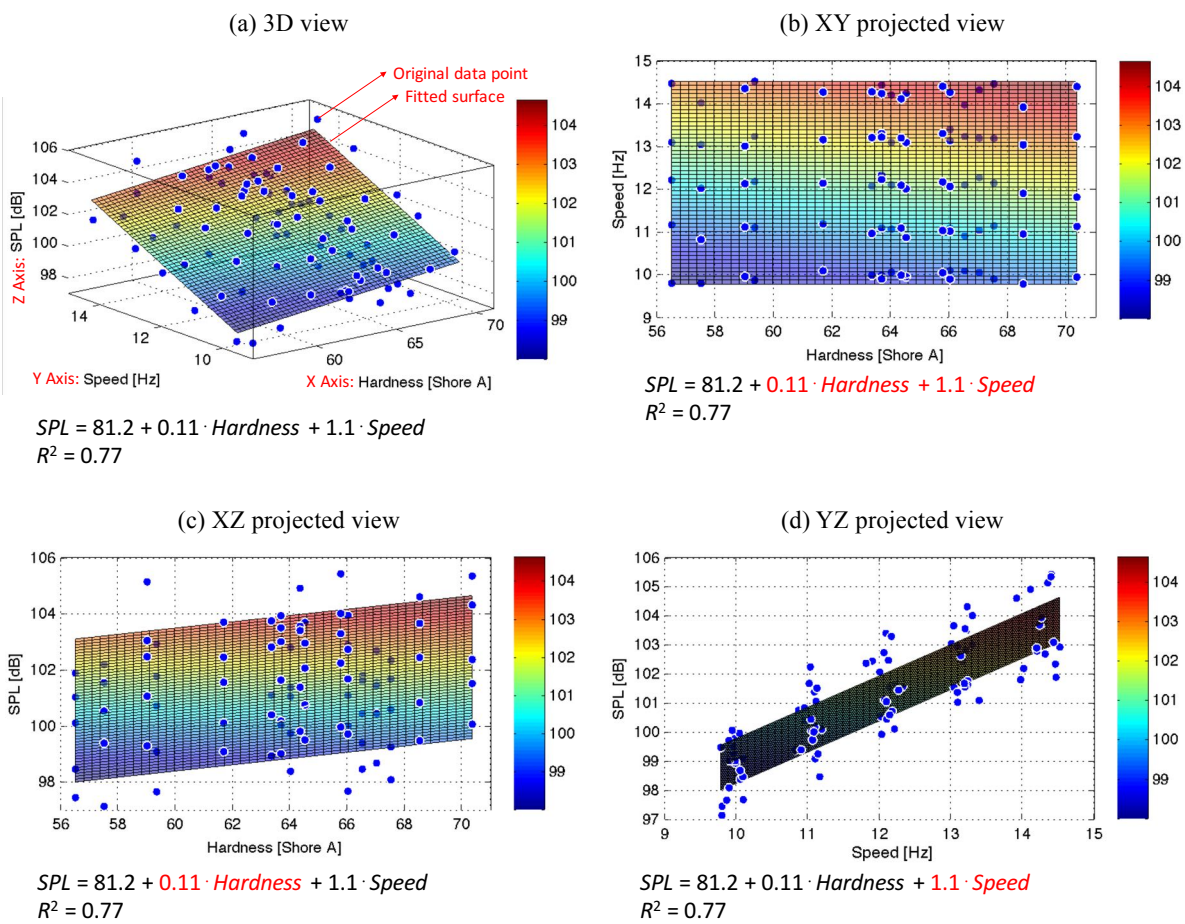

Figure 6.1: Surface fitting for rubber hardness effect

In addition, if the data for all the tires of different sizes are included and the unit of speed is mph, the regression equation obtained becomes $SPL = 74.1 + 0.228 \cdot Hardness + 0.227 \cdot Speed$ where $R^2 = 0.75$, indicating the non-tread pattern noise increases with rubber hardness by 0.228 dBA per Shore A, which agrees with most of the literature.

6.1.3 ANN Model

As a preliminary attempt, artificial neural network (ANN) is used to correlate the non-tread pattern noise with the rubber hardness and the speed for the same test samples in Section 6.1.2 that only includes tires of 215/60R16. The schematic of the ANN model is illustrated in Figure 6.2. The input of the preliminary ANN_2 model is the rubber hardness in [Shore A] and the tire rotational speed in [Hz]; the output is the non-tread pattern noise spectrum in [Pa^2] from 400 to 1600 Hz with resolution of 10 Hz. It is noted that the noise spectral location for the non-tread pattern noise basically doesn't change with speed as shown in Appendix C: Effect of Speed. Therefore, the ANN_2 model can include all the speeds and potentially it is simpler than ANN_1.

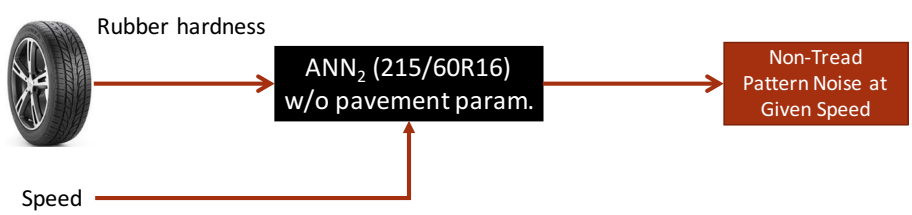

Figure 6.2: Schematic of preliminary ANN_2 (215/60R16)

The subsets of samples for developing the preliminary ANN_2 model is shown in Table 6.2.

The comparisons between the measured and predicted TPIN spectra (A-weighted) are demonstrated in Figure 6.3. The corresponding results for the overall A-weighted sound pressure level (OASPL) is shown in Figure 6.4. It is seen that the agreement is good. The average error between the measured and predicted is 0.6 dB for the train set, 0.8 dB for the validation set, 1.7 dB for the test set, and 0.9 dB on average for all the sets.

Table 6.2: Subsets of samples for developing the preliminary ANN_2 model (215/60R16)

Subset	Train Set	Validation Set	Test Set
Purpose	Train ANN	Stop training ANN and avoid over-training	Examine/validate the accuracy of the trained model
Number of Tires	9	5	5
Tires	05 07 09 12 13 14 15 17 18	01 06 08 11 16	02 03 04 10 19

(a) Train set

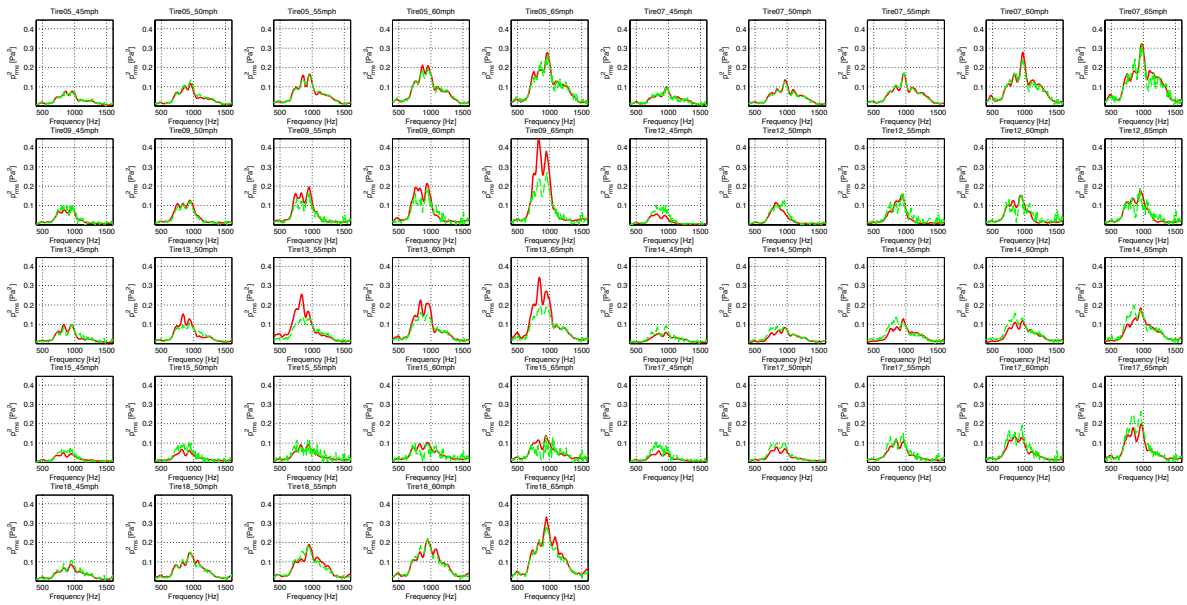

(b) Validation set

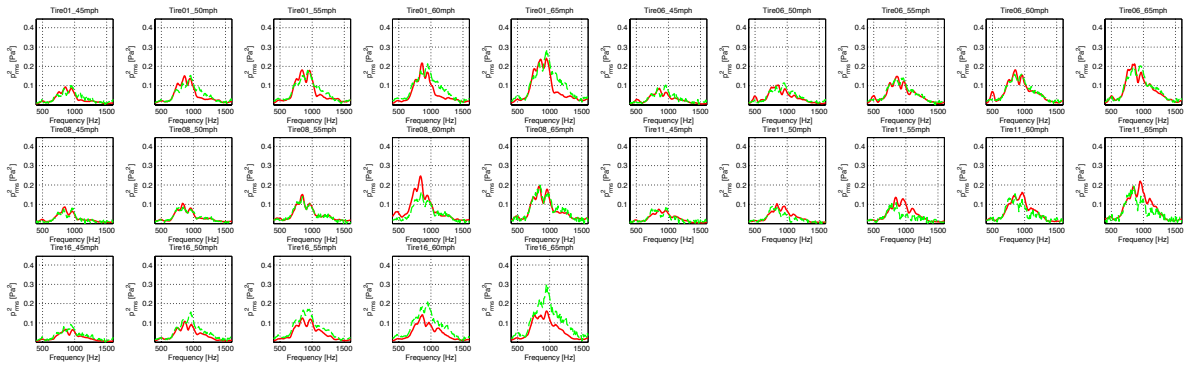

(c) Test set

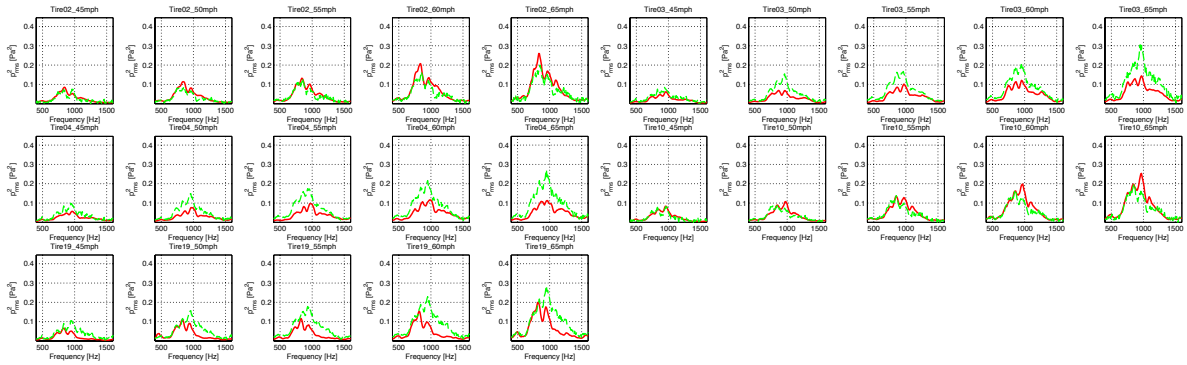

Figure 6.3: Spectral results for preliminary ANN_2 (215/60R16) (red denotes measured, green denotes predicted)

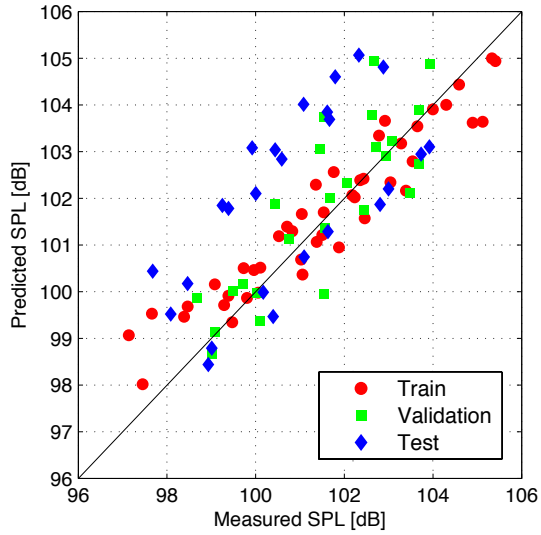

Figure 6.4: OASPL results for preliminary ANN_2 (215/60R16)

This demonstrates that ANN is capable of capturing the relations between the rubber hardness, speed, and the non-tread pattern noise for a specific tire size. In addition, Figure 6.4 shows that, unlike ANN_1, ANN_2 doesn't seem to over predict too much.

It should be noted that, like ANN_1, sometimes the direct ANN_2 output values in linear scale at specific frequencies are negative, which is physically wrong. In addition, for the prediction of the non-tread pattern noise (a broadband noise), the capturing of the spectral shape is most important. Therefore, a moving average (five adjacent points) post-processing is performed,

as illustrated in Figure 6.5, which eliminates the negative values and keeps the spectral shape. Figure 6.5a shows no negative values in this case, but presented just for explaining the approach.

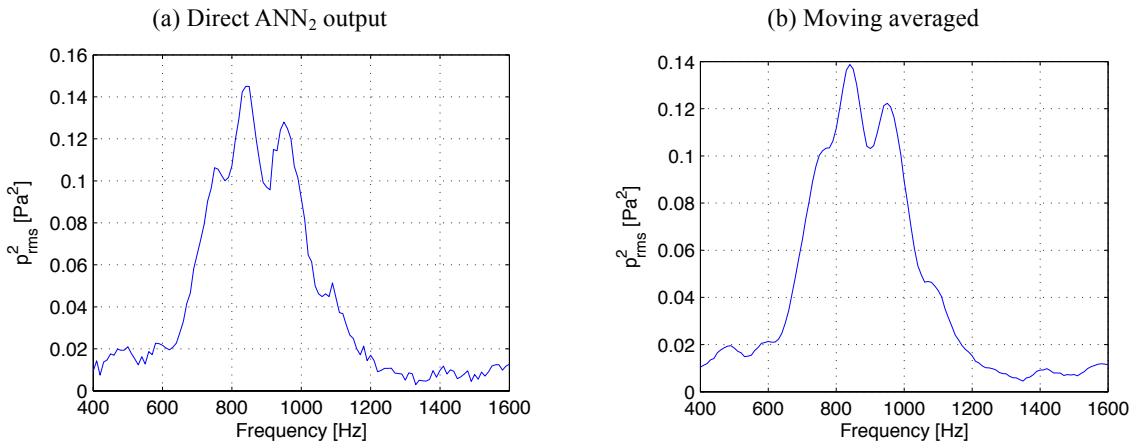

Figure 6.5: Post-processing for ANN_2 output (Tire 09 at 60 mph)

6.1.4 Other ANN_2 Configurations

Five configurations for the preliminary ANN_2 have been tried, as shown in Table 6.3. The results are shown in Figure 6.6.

Table 6.3: Configurations for preliminary ANN_2 (215/60R16)

	Configurations
(a) Spectral lines as output (original)	This is the original configurations discussed in Section 6.1.3, with the non-tread pattern noise spectrum as the output
(b) Overall level as output	The output is the overall noise level directly.
(c) Both as output	The output includes both the non-tread pattern noise spectrum and the overall noise level.
(d) Using speed scaling exponent of 3.5	The preliminary ANN_2 (215/60R16) at 60 mph is developed first using data at 60 mph only; results at other speeds are then obtained using speed scaling exponent of 3.5.
(e) Using error weights	In training/validating the ANN, error weights are applied so that more weights are given to the dominant frequencies.

(a) Spectral lines as output (original)

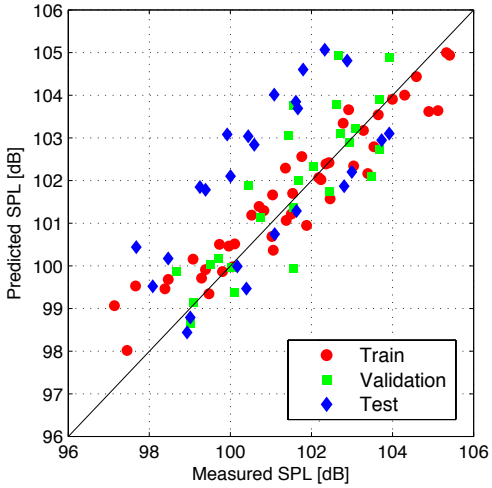

Average dB error
Train: 0.6 dB; Validation: 0.8 dB
Test: 1.7 dB; All: 0.9 dB

(b) Overall level as output

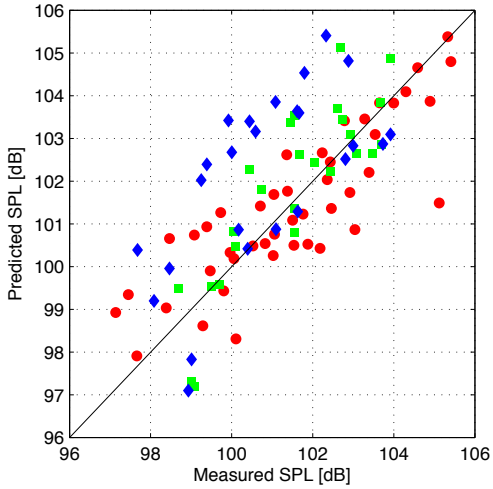

Average dB error
Train: 0.9 dB; Validation: 0.9 dB
Test: 1.8 dB; All: 1.1 dB

(c) Both as output

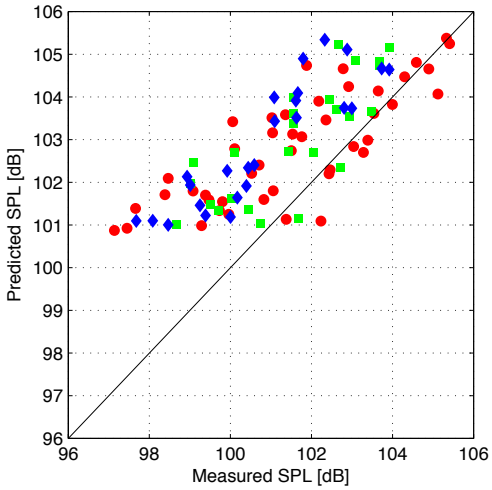

Average dB error
Train: 1.5 dB; Validation: 1.5 dB
Test: 2.1 dB; All: 1.7 dB

(d) Using speed scaling exponent of 3.5

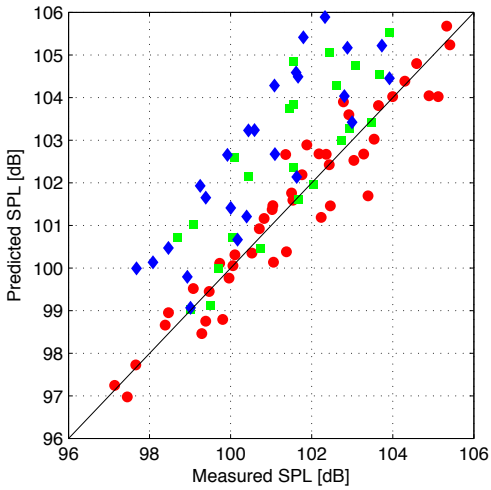

Average dB error
Train: 0.5 dB; Validation: 1.4 dB
Test: 1.9 dB; All: 1.1 dB

(e) Using error weights

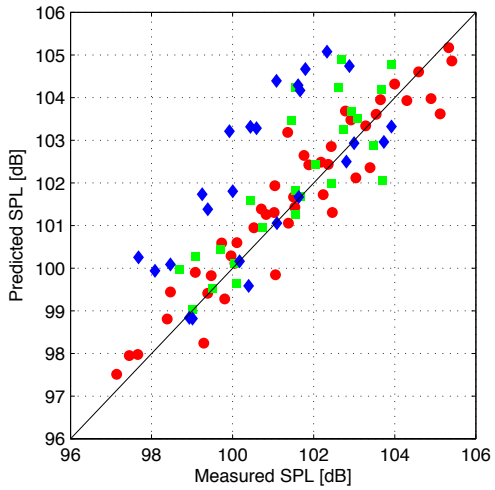

Average dB error
Train: 0.6 dB; Validation: 0.8 dB
Test: 1.6 dB; All: 0.9 dB

(f) Error weights

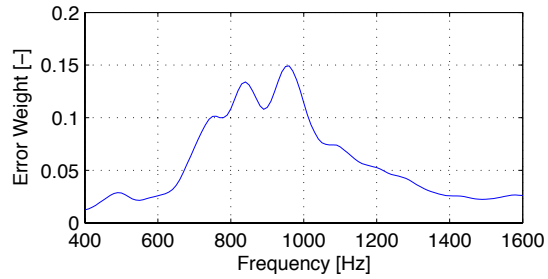

Figure 6.6: Results for different ANN_2 configurations

It can be seen from Figure 6.6b-d that the modified configurations do not improve the prediction accuracy. For example, the decreased performance in Figure 6.6b is likely because the ANN robustness reduces as just one single parameter is chosen as the output; the original outputs in Figure 6.6a are all the spectral lines, so that the overall level can still be predicted well even if several spectral lines fail to capture the trend. Figure 6.6c shows that the inclusion of both spectral lines and overall noise level as the output is actually unnecessary due to duplicate training request. Figure 6.6d shows that the speed exponent scaling is fine but not as good as the one with speed as a direct input, because not all tires have the same speed exponent (e.g., 3.5).

However, the error weights configuration does seem to improve the prediction accuracy a little bit, as shown in Figure 6.6e. In the train/validation process of ANN, the mean squared error between the measured and predicted data with error weights applied is calculated at each epoch, given by

$$MSE = \frac{\sum_{i=1}^{M}\sum_{j=1}^{N} EW_j \times \left(m_{ij} - p_{ij}\right)^2}{M \times N} \tag{5.2}$$

where MSE is mean squared error, M is the number of tires used, N is the number of spectral lines in the output, EW_j is the error weight at specific spectral line denoted by j, m_{ij} is the measured value for a specific tire of i at specific spectral line of j, and p_{ij} is the predicted value for a specific tire of i at specific spectral line of j. The training process of ANN is stopped at the moment when MSE reaches the minimum. The error weights for the spectral lines are shown in Figure 6.6f, which are decided by the average of the non-tread pattern noise for all tires of 215/60R16.

The configuration with error weights is adopted in the final development of ANN_2.

6.2 Effect of Tire Size

In this section, the effect of the tire size is investigated. The illustration for the tire size parameters of interest and an example is displayed in Figure 6.7.

Figure 6.7: Tire size parameters

6.2.1 Literature Survey

The conventional naming for tire size of passenger car tires is like 215/60R16: 215 is tire

section width is mm; 60 is aspect ratio (section height divided by section width) in percentage; 16 is rim diameter in inch.

As the tire width increases, the tread/texture impact becomes more extensive leading to greater vibrations. Stick/slip and stick/snap phenomena are also amplified. A tire with a wider section involves greater displacement of air within the tire-road interface, amplifying both air pumping and air turbulence. In addition, horn shape and Helmholtz resonator are easier to occur with greater tire width (Kumar et al., 2011 [244]).

Generally, wider tire section generates greater TPIN (Sandberg and Ejsmont, 1998 [415]), especially in the low frequency band from 500 to 1000 Hz (Yang et al., 2013 [243]). As such, tire noise regulations usually have step limits for different range of tire width. It was found that TPIN on smooth pavement at the speed of 70 km/h increased by around 0.3-0.4 dB per 10 mm of width increase (Storeheier and Sandberg, 1990 [416]). The width influence may also be expressed as an increase of 4 dB per doubling of width (Sandberg and Ejsmont, 2002 [24]). Ulrich (1984) [417] reported that the sound power P has the relationship with tire width b as $P \propto b^{3/2}$.

However, it was found that the influence of tire width is not linear or consistent, and becomes insignificant when it exceeds 200 mm (Yang et al., 2013 [243]). Only a weak correlation ($R^2 = 0.38$) was found in a set of 276 tires of different widths (Sandberg, 2001 [7]). Actually, it was shown that for the same speeds and number of tires, TPIN of truck tires is only slightly higher than that of car tires, despite the greater widths and much higher loads (Sandberg, 2001 [7]).

Tire width has a small influence on the radial natural frequency but it also depends on the tire diameter which will be discussed below (Kostial et al., 2013 [395]).

It was shown that TPIN decreases with increase in overall tire diameter (Kumar et al., 2011 [244]). As tire diameter increases, the attack angle decreases, leading to less pronounced and abrupt tread/texture impact. On the other hand, the decreased attack angle amplifies the horn effect. Increased tire diameter will reduce the tire cavity resonant frequency (Mohamed and Wang, 2015 [245]). Ulrich (1984) [417] reported that the sound power P has the relationship

with tire radius a as $P \propto 1/a^3$. Pei et al. (2015) [418] found that the increase of the radius of the belt layer or the radius of tire tread will reduce the tire vibrations.

Tire aspect ratio is another important dimensional parameter, defined as the section height divided by the nominal section width multiplied by 100 (expressed as a percentage), but it is not interesting in TPIN analysis. However, it is interesting to point out that the aspect ratio has decreased from 0.8 to 0.4 over the last three decades (Tanaka et al., 2016 [419]) in order to improve the vehicle stability at high speed.

6.2.2 Tire Size Effect on Spectral Distribution

Ten different tire sizes have been tested, as shown in Figure 6.8. Tire 56 (spare tire) is not included considering it is an outlier (too narrow and small).

(a) In ascending order of tire outer diameter

(b) In ascending order of nominal section width

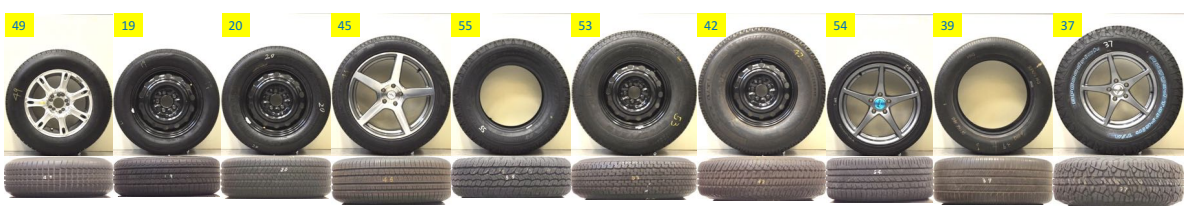

Figure 6.8: Tires of different sizes

The non-tread pattern noise spectra for tires of different sizes are shown in Figure 6.9a. To reduce the fuzziness of the spectral curves, a moving average process is applied to obtain Figure 6.9b and Figure 6.9c. A moving average is used in time signal and strictly speaking is not correct for a spectrum. However, it is used here for convenience. The total spectral energy

is kept constant no loss/gain of energy occurs (constant overall levels). To further investigate the spectral distribution, the one-peak Gaussian curve fitting is performed for Figure 6.9c to obtain Figure 6.9d. As is shown in Figure 6.9b, the central frequencies of the non-tread pattern noise changes with tire size. For example, the central frequency for Tire 37 (265/70R17) is 710 Hz, while 785 Hz for Tire 42 (235/85R16) and 966 Hz for Tire 49 (205/70R15).

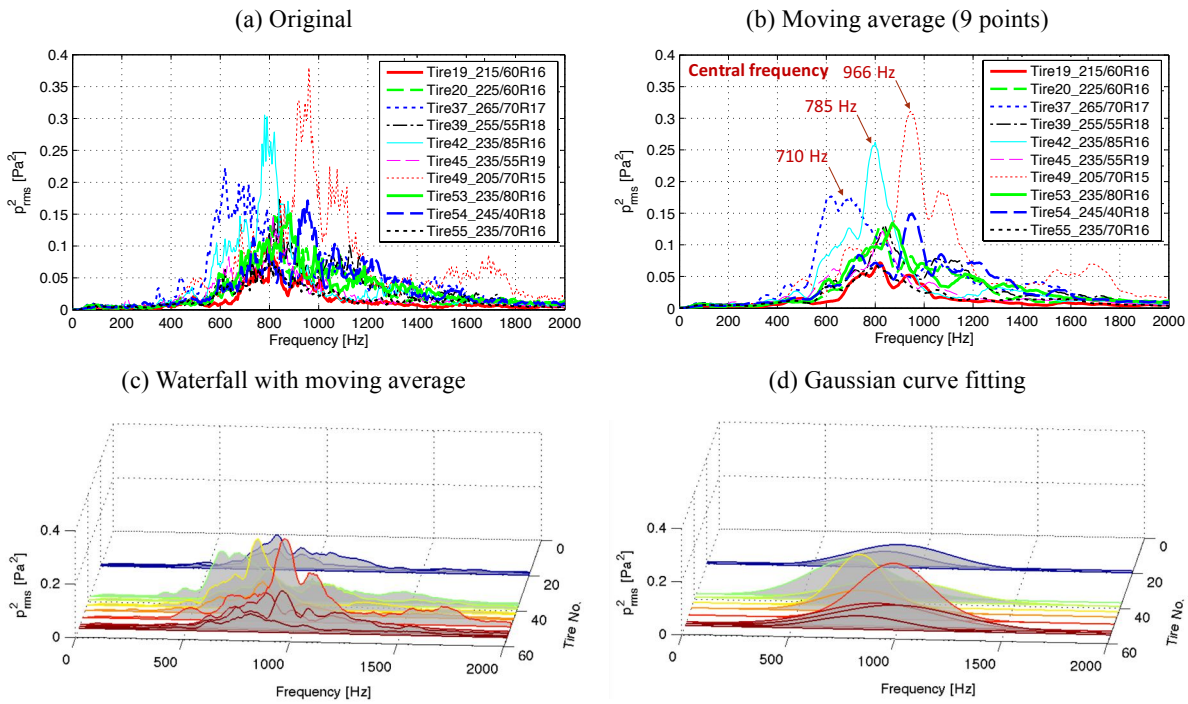

Figure 6.9: Non-tread pattern noise spectra for tires of different sizes (narrowband, 5 Hz resolution)

It is shown from Figure 6.9d that the central frequencies of the non-tread pattern noise changes with tire size. In order to investigate which tire size parameter influences the central frequency, the linear regression analysis is performed between each tire size parameter and the central frequency of the non-tread pattern noise, as shown in Figure 6.10. It is shown that the most influential parameter (R^2 = 0.51) is the carcass width defined as the section width plus two times the section height (tire sidewall). The correlation with respect to circumference or outer diameter also looks good (R^2 = 0.62), but it is likely due to statistical coincidence because larger carcass width usually leads to larger circumference or outer diameter (R^2 = 0.88 according to current data). Therefore, more tires of different carcass

width but the same/similar circumference need to be tested to verify this hypothesis, e.g., very narrow or wide tires but with the same outer diameter. As such, circumference is not used to correlate with the central frequency (physically wrong even though statistically right).

In addition, the amplitude and spread of the non-tread pattern noise spectrum do not correlate well with any of the tire size parameters, as shown in Figure 6.11 and Figure 6.12, respectively, which suggests that the tire size does not have much influence on the amplitude and spread of the non-tread pattern noise spectrum. On the other hand, it is speculated that the amplitude of the non-tread pattern noise spectrum depends on the tread rubber hardness. As is mentioned earlier, some of the bigger tires have very large rubber hardness of over 70 Shore A due to age hardening. As an exception, the only statistically significant correlation between the spread and the tire size is for the ratio of section width to outer diameter (R^2 = 0.56), as shown in Figure 6.12. It shows that as this ratio increases (the tire becomes fatter and shorter), the spread of the non-tread pattern noise spectrum increases. However, this phenomenon is not easy to be justified by physical mechanisms, so it is speculated that the correlation might be just coincidental. In addition, once the spare tire (Tire 56, 125/70D16, the slimmest with the smallest ratio), this correlation is not good any more.

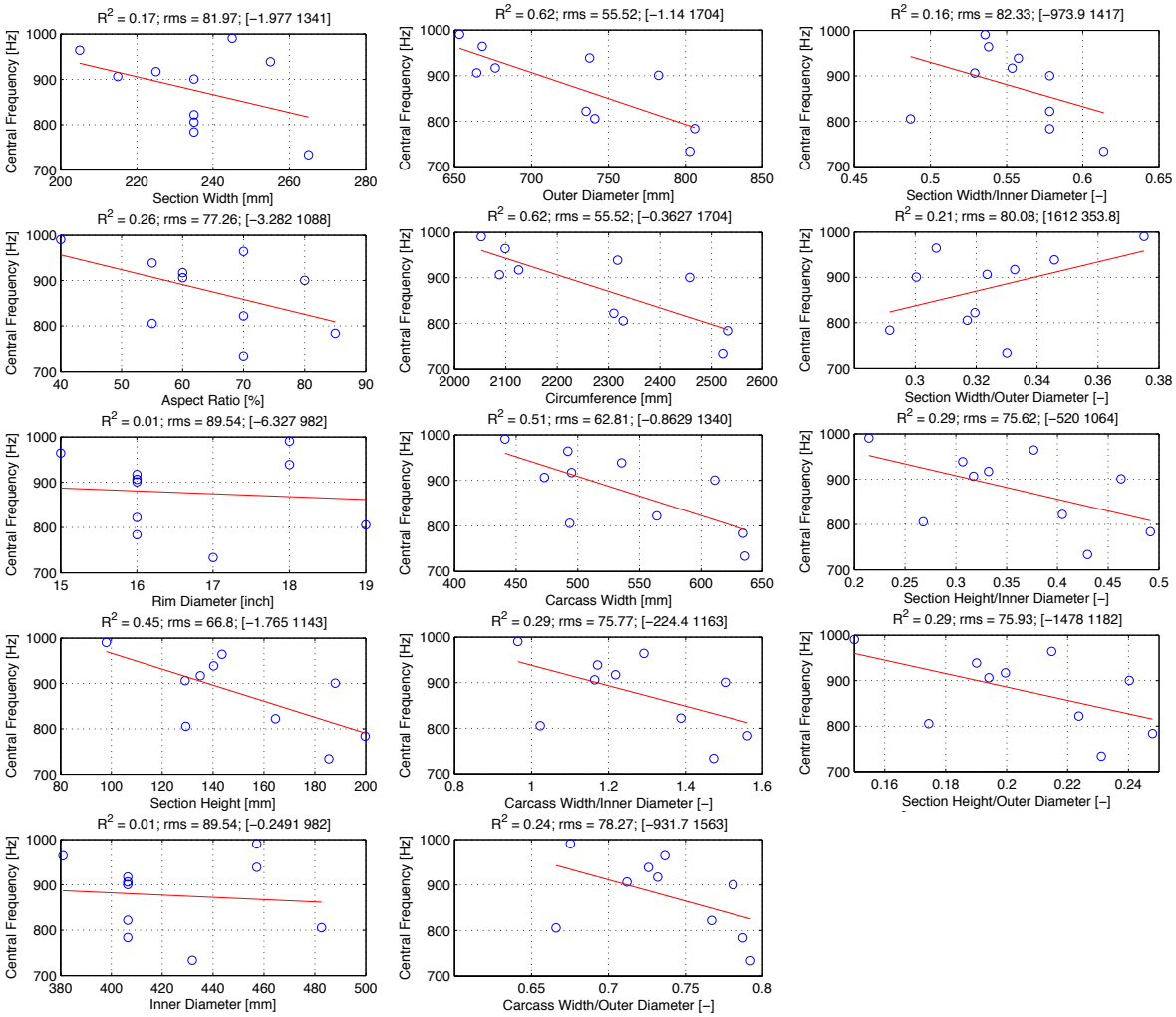

Figure 6.10: Correlation between central frequency and tire size parameters (blue circle denotes original data; red line denotes fitted curve) (the text above each subplot includes: R^2, coefficient of determination; *rms*, root mean squared value; [*a*, *b*], coefficients in regression equation $y = ax+b$)

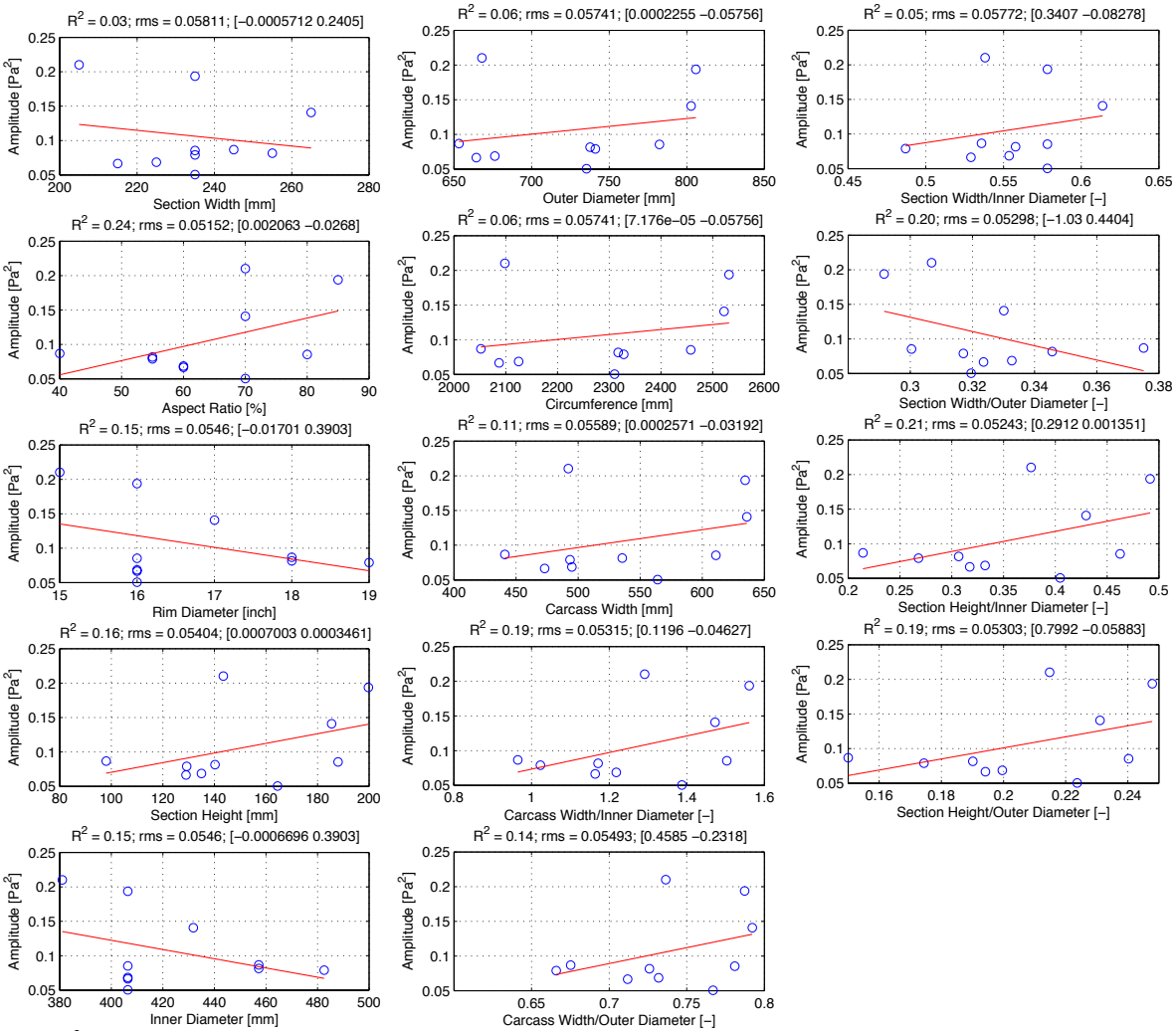

Figure 6.11: Correlation between amplitude and tire size parameters (blue circle denotes original data; red line denotes fitted curve) (the text above each subplot includes: R^2, coefficient of determination; *rms*, root mean squared value; [*a*, *b*], coefficients in regression equation $y = ax+b$)

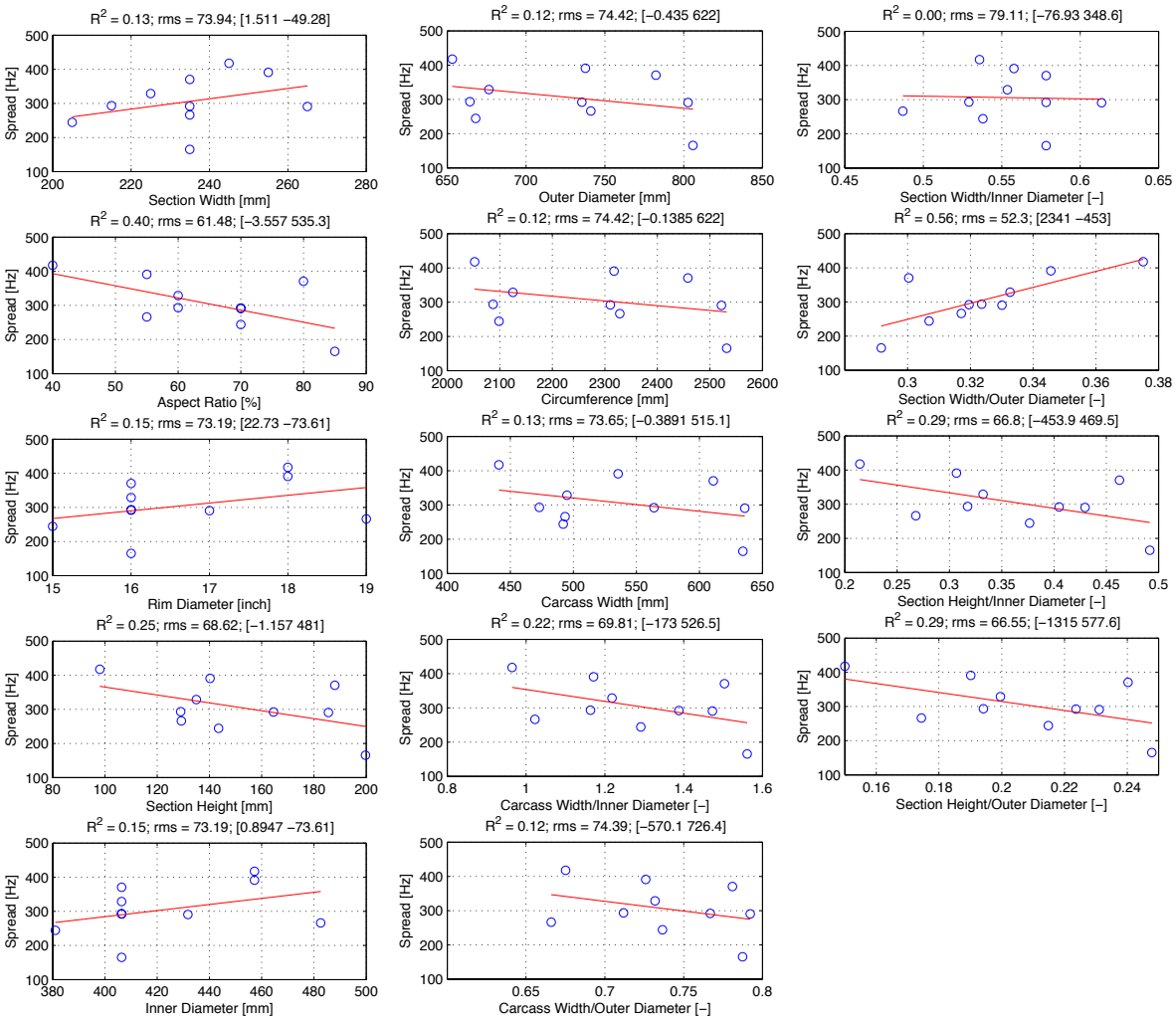

Figure 6.12: Correlation between spread and tire size parameters (blue circle denotes original data; red line denotes fitted curve) (the text above each subplot includes: R^2, coefficient of determination; *rms*, root mean squared value; [*a*, *b*], coefficients in regression equation $y = ax+b$)

6.2.3 Nonlinear Correlation

The correlations between the noise spectral parameters and tire size parameters are linear. The nonlinear curve fitting is also tried for the correlations. The results for the correlation between the central frequency and carcass width are shown in Figure 6.13, including polynomial of different orders, exponential of different terms, and power model. The increased number of predictors in a fitted model will always increase R-squared, even if just due to chance. Therefore, the adjusted R-squared is used instead of R-squared to account for

the number of predictors in the model. In Figure 6.13a, the 1st order polynomial is also called linear correlation. It can be seen that the adjusted R-squared for the nonlinear model (Figure 6.13b-f) is not larger than the linear model (Figure 6.13a). That is to say, the linear model is adequate to correlate the central frequency and the carcass width.

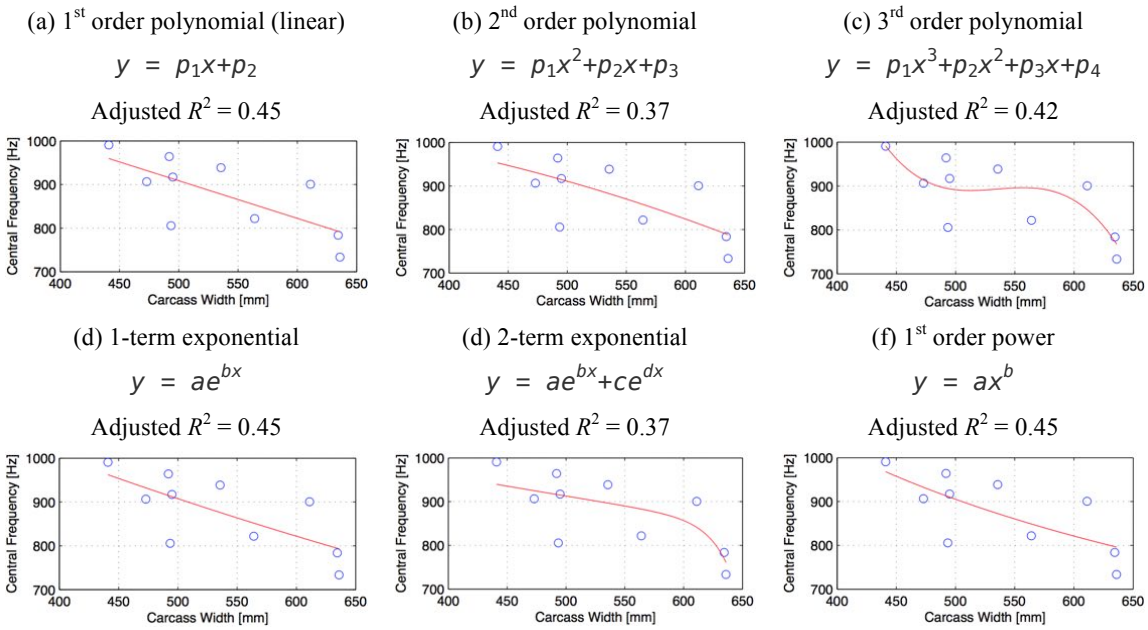

Figure 6.13: Different types of correlations between the central frequency of non-tread pattern noise and the carcass width

6.2.4 Tire Size Scaling

As shown in Figure 6.10, the relation between the central frequency of non-tread pattern noise and the carcass width is given by

$$CF = -0.8629 \cdot CW + 1340 \tag{5.3}$$

where CF is central frequency, and CW is carcass width. Therefore, without considering the amplitude and spread, the non-tread pattern noise spectrum for a given tire size (carcass width) can be obtained by scaling from another tire size (e.g., 215/60R16 with a carcass with of 473 mm). That is also to say, if the non-tread pattern noise spectra for different tire sizes are scaled to one specific tire size, the spectra should basically coincide, which has been validated, as shown in Figure 6.14 where tires of different sizes are scaled to that with a carcass width of

520 mm. It can be seen that, especially from Figure 6.14b after the amplitude is normalized (i.e., all scaled spectra have the same overall energy, to be more specific, the spectral amplitude is divided by its corresponding overall energy for each spectrum), all the scaled spectra have the same or similar central frequencies. It is noted that the data shown in Figure 6.14 are not used to develop the ANN_2, and are just included here for illustration.

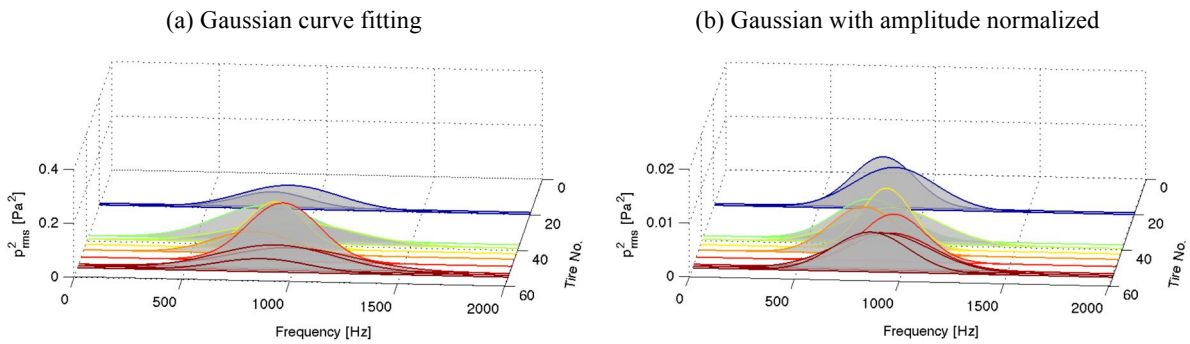

Figure 6.14: Non-tread pattern noise spectra for tires of different sizes after tire size scaling

The tire size scaling process is similar to that in Figure 5.18, including frequency scaling, adjustment of frequency resolution to a constant value (10 Hz here), adjustment of the amplitude so that the overall spectral energy is not lost or added.

6.3 Summary

The tread pattern noise is not much dependent on the tread rubber hardness or tire size while the non-tread pattern noise is. For the non-porous asphalt pavement tested, the non-tread pattern noise increases with rubber hardness by ~0.23 dBA/Shore A. The tire carcass width (section width plus two times section height) influences the central frequencies of the non-tread pattern noise spectrum; the central frequencies decrease as the tire carcass width increases.

In the non-tread pattern noise modeling, the ANN_2 for tire size of 215/60R16 can be developed first for different tread rubber hardness and vehicle speed. Then the non-tread pattern noise for a different tire size can be obtained using tire size scaling.

In developing ANN_2 for tire size of 215/60R16 and in order to take advantage of all the

noise data collected, not only the data for tires of 215/60R16 will be used, but data for tires of other sizes will also be used and scaled to 215/60R16 according to Eq. (5.3).

7 ANN Model of TPIN (AMOT)

In this chapter, the complete tire-pavement interaction noise (TPIN) model using artificial neural network (ANN) is presented. The complete model is named as **A**NN **M**odel **o**f **T**PIN (AMOT). This model includes the ANN_1 sub-model for tread pattern noise, ANN_2 sub-model for non-tread pattern noise, and some other necessary sub-models.

7.1 Structure of AMOT

The structure of AMOT is illustrated in Figure 7.1. As can be seen in Figure 7.1, the inputs of the AMOT model are tire parameters, driving condition parameters, and pavement parameters. However, all the tests have been conducted on the same pavement, therefore, the pavement parameters have not been included into the current version of AMOT. The input tire parameters include the 3D tread profile data obtained from the CTWIST file (Circumferential Tread Wear Imaging System, a 3D laser scanning system) or from a CAD program, the tire size in the format of XXX/XXRXX, and the tread rubber hardness in the unit of Shore A. The driving condition parameter is the vehicle speed in the unit of mph. The temperature is not included as input, because data have shown that its effect is not very significant under normal conditions. In addition, the temperature effect can be reflected from the rubber hardness (temperature affects the tire tread rubber hardness). The outputs of the AMOT model are TPIN narrowband spectrum, TPIN 1/3 octave band spectrum, and the overall A-weighted sound pressure level (OASPL).

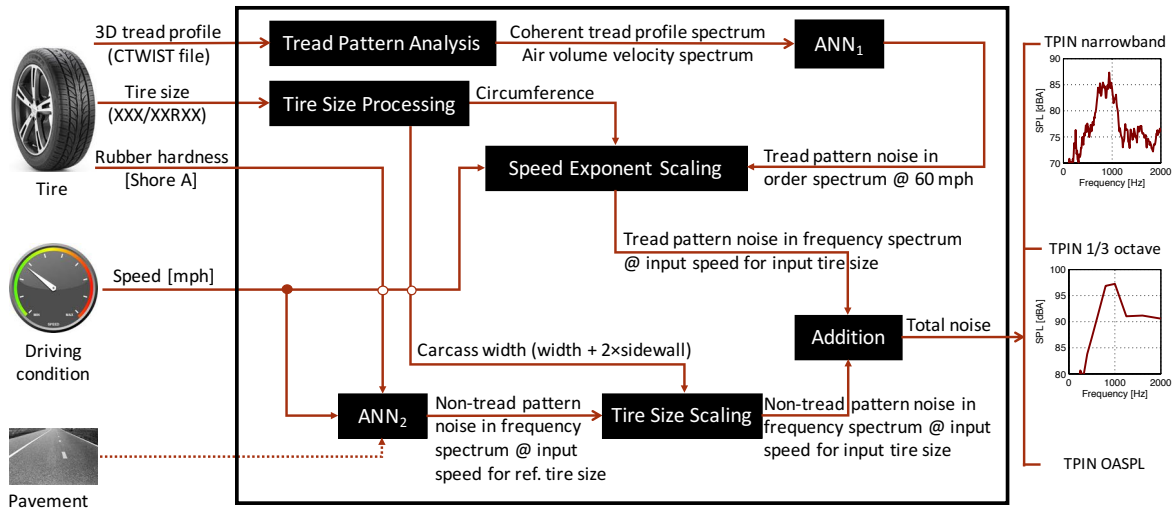

Figure 7.1: Structure of ANN Model of TPIN (AMOT) (the solid circle at the intersection of two lines denotes there is connection while hollow circle denotes no connection)

There are basically two parallel flows of modeling: one to predict the tread pattern noise, the other to predict the non-tread pattern noise. For the tread pattern noise modeling, the tread pattern noise is first predicted at 60 mph in the order domain assuming the tire size has no effect. Next, the tread pattern noise in the order domain at other vehicle speeds is obtained based on speed exponent scaling. Then, the tread pattern noise in the order domain is converted to the frequency domain based on the tire rotational speed in Hz calculated from the tire circumference and vehicle speed. For the non-tread pattern noise modeling, the non-tread pattern noise is first predicted for a reference tire size (215/60R16) in the frequency domain. Then, the non-tread pattern noise for the other tire sizes is obtained by adjusting central frequencies based on the tire size scaling.

The complete AMOT model is comprised of seven sub-models, as listed in Table 7.1. Each sub-model is a MATLAB function.

Table 7.1: Sub-models of ANN Model of TPIN (AMOT)

No.	Sub-model Name	MATLAB Function Name	Input	Output
1	Tread Pattern Analysis	FN_Tread_Pattern_Analysis	3D tread profile from CTWIST file	Coherent tread profile spectrum, air volume velocity spectrum
2	ANN_1	FN_ANN1	Coherent tread profile spectrum, air volume velocity spectrum	Tread pattern noise in order spectrum @ 60 mph
3	Tire Size Processing	FN_Tire_Size_Processing	Tire size in conventional format of XXX/XXRXX	Circumference, carcass width
4	Speed Exponent Scaling	FN_Speed_Exponent_Scaling	Tread pattern noise in order spectrum @ 60 mph, circumference, speed in [mph]	Tread pattern noise in frequency spectrum @ input speed for input tire size
5	ANN_2	FN_ANN2	Rubber hardness in [Shore A], speed in [mph], pavement (not included in current version)	Non-tread pattern noise in frequency spectrum @ input speed for 215/60R16
6	Tire Size Scaling	FN_Tire_Size_Scaling	Non-tread pattern noise in frequency spectrum @ input speed for 215/60R16 (reference carcass width)	Non-tread pattern noise in frequency spectrum @ input speed for input tire size
7	Addition	Simple summation	Tread pattern noise in frequency spectrum @ input speed for input tire size, Non-tread pattern noise in frequency spectrum @ input speed for input tire size	Total noise

7.2 Development of AMOT

The key to the development of the AMOT model is the two sub-models of ANN_1 and ANN_2. The tire samples used to develop the ANN_1 and ANN_2 sub-models were carefully selected, as shown in Table 7.2. It is noted that the train/validation sets for ANN_1 are different from those for ANN_2. This is because some of the tread profile data for some tires are not available, so

those tires cannot be used to develop ANN_1. Another consideration is, either for ANN_1 or ANN_2, both train and validations sets should include tires that cover a large range of the input parameters, e.g., a large range of tread patterns (summer pattern and winter pattern) for ANN_1 and a large range of rubber hardness for ANN_2. However, the test set for ANN_1 and ANN_2 is the same, i.e., Tires 09, 15, 18, 22, 23, 45, 49, and 55 are neither used to train/stop ANN_1 nor ANN_2. Therefore, they can be used to examine/validate the accuracy of the complete model of AMOT.

Table 7.2: Subsets of samples for developing ANN_1 and ANN_2

Subset	Train Set	Validation Set	Test Set
Purpose	Train ANN	Stop training ANN and avoid over-training	Examine/validate the accuracy of the trained model
		ANN_1	
Number of Tires	13	4	8
Tires	01 02 03 04 05 06 07 08 10 11 13 17 19	12 14 16 20	09 15 18 22 23 45 49 55
		ANN_2	
Number of Tires	20	9	8
Tires	02 03 04 05 07 12 13 14 17 19 20 24 25 29 37 39 42 53 54 57	01 06 08 10 11 16 26 27 43	09 15 18 22 23 45 49 55

7.3 Results of AMOT (Test Set)

The results for the tires in the test set exclusively used for the final validation of AMOT are presented in this section.

The results of the comparison between the predicted and measured TPIN for each tire at specific speed in the train set and validation set are demonstrated in Appendix B: Results of AMOT (Train and Validation Set).

7.3.1 Individual Tires

7.3.1.1 Tire 09

The results for Tire 09 are demonstrated in Figure 7.2. Good agreement between the measurement and prediction is shown. It is noted that, in Figure 7.2b, the tread pattern noise results for Tire 09 are good for 60 mph, which makes sense because ANN_1 is trained at 60 mph. However, the tread pattern noise results for lower speed are over-predicted, and the tread pattern noise results for higher speed are under-predicted. This is because the real speed exponent for Tire 09 is about 7 likely due to supersonic air flow, but AMOT uses a speed exponent of 4 to scale results from 60 mph to other speeds. Figure 7.2g-i shows that the tread pattern noise is somewhat over-predicted while the non-tread pattern noise is somewhat under-predicted, which coincidentally ends up with a very good prediction for the total tire noise.

(a) Total tire noise in narrowband

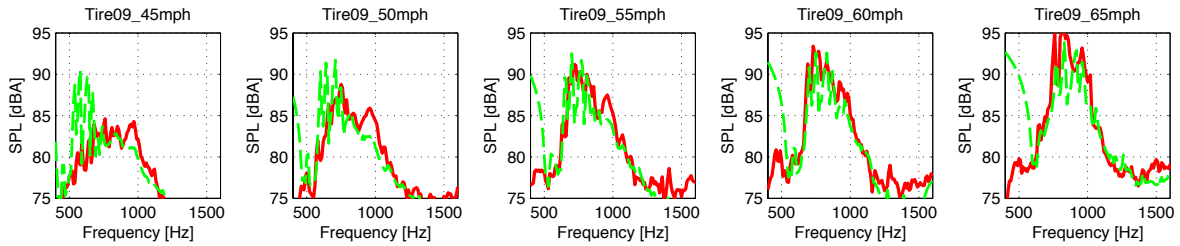

(b) Tread pattern noise in narrowband

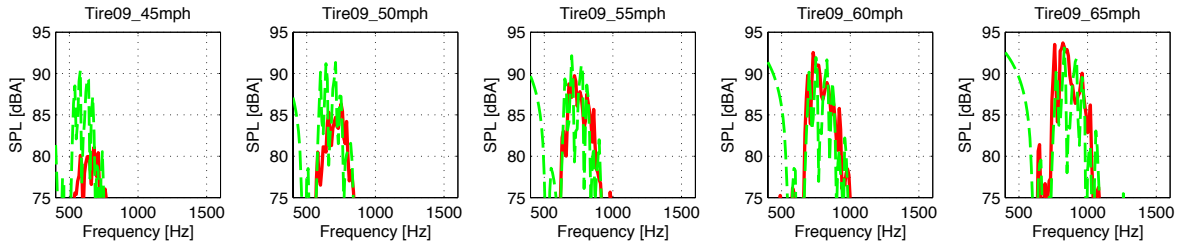

(c) Non-tread pattern noise in narrowband

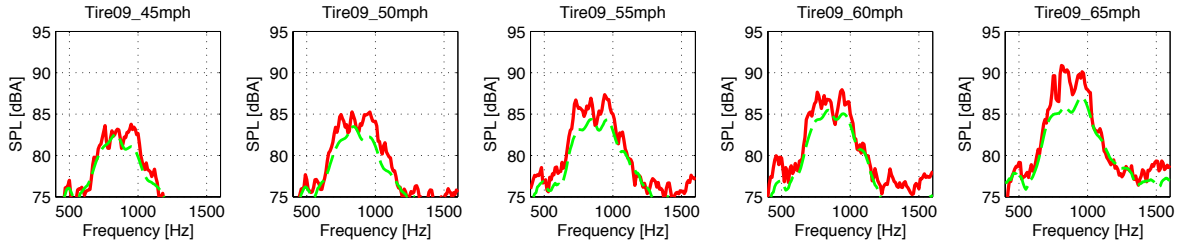

(d) Total tire noise in 1/3 octave band

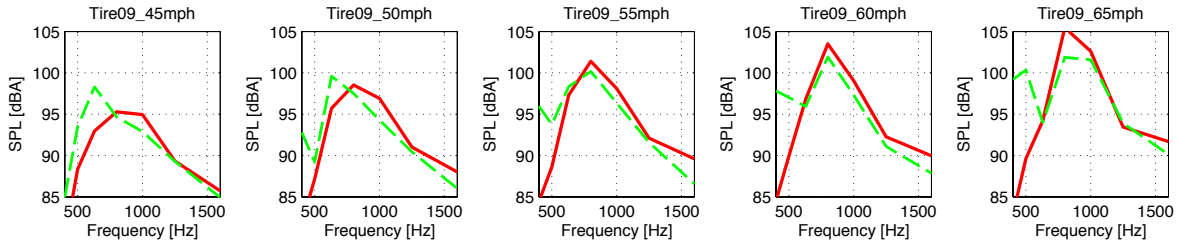

(e) Tread pattern noise in 1/3 octave band

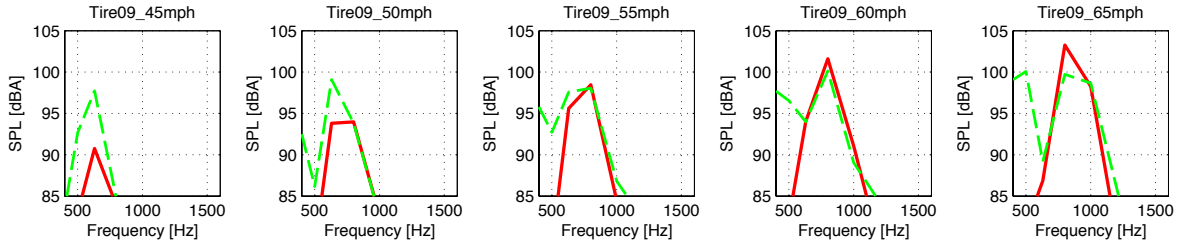

(f) Non-tread pattern noise in 1/3 octave band

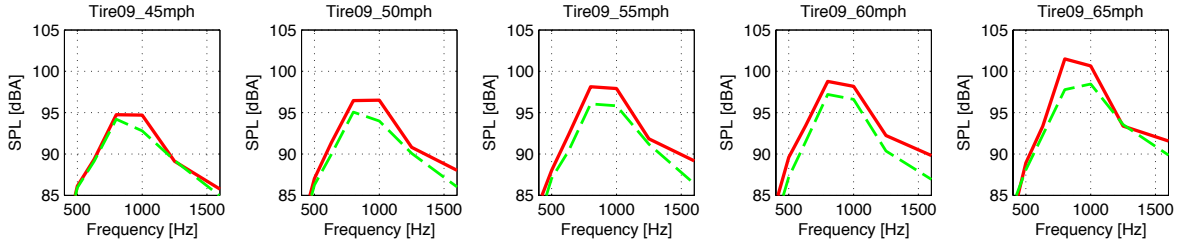

(g) OASPL of total tire noise

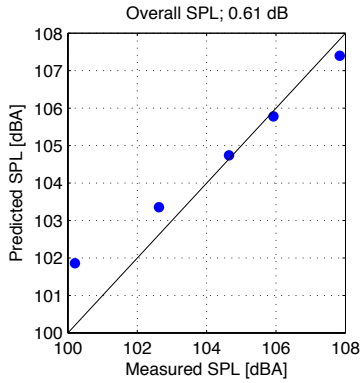

(h) OASPL of tread pattern noise

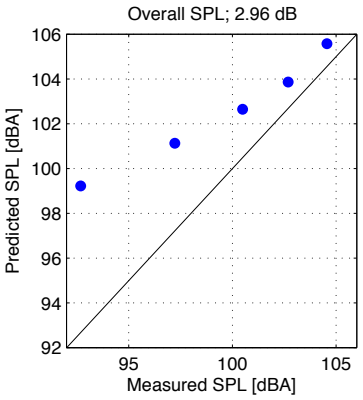

(i) OASPL of non-tread pattern noise

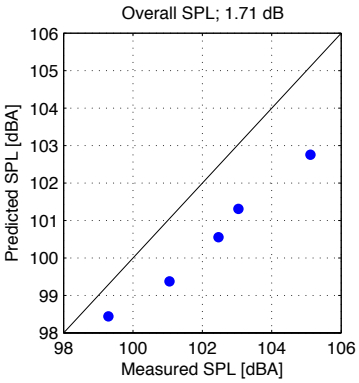

Figure 7.2: Results of AMOT for Tire 09 (in a-f, red denotes measured, green denotes predicted; in g-i, the value above the plot is the average dB error)

7.3.1.2 Tire 15

The results for Tire 15 are demonstrated in Figure 7.3. Good agreement between the measurement and prediction is shown. For this tire, the tread pattern noise is marginal compared to the non-tread pattern noise.

(a) Total tire noise in narrowband

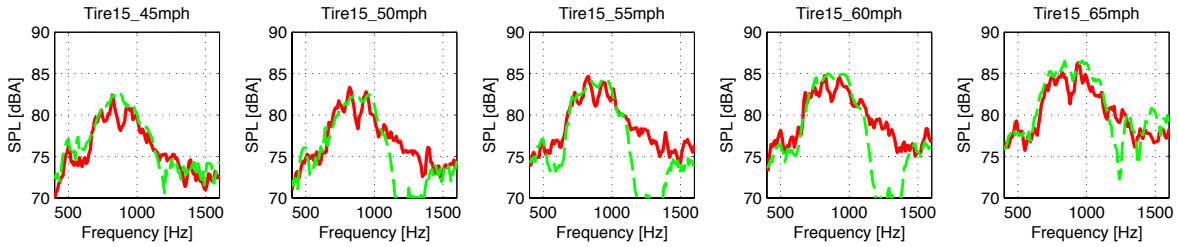

(b) Tread pattern noise in narrowband

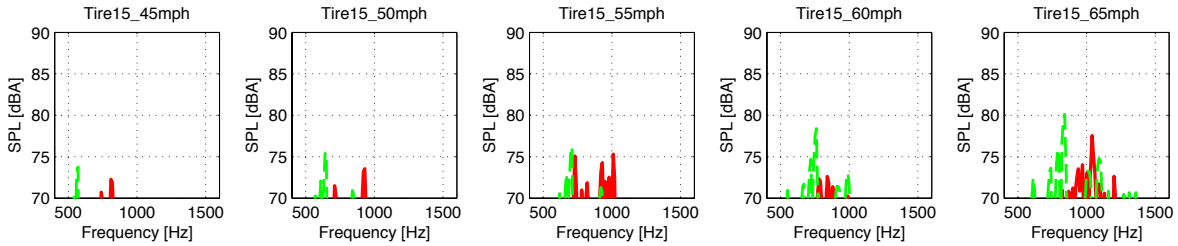

(c) Non-tread pattern noise in narrowband

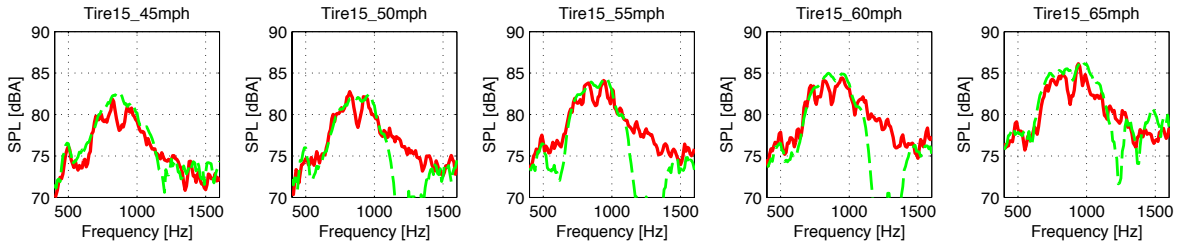

(d) Total tire noise in 1/3 octave band

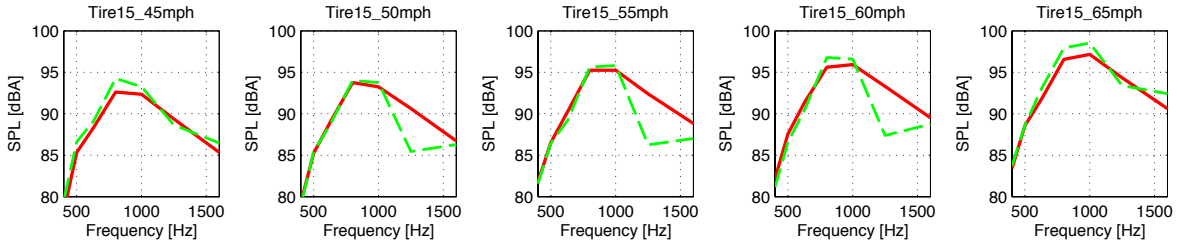

(e) Tread pattern noise in 1/3 octave band

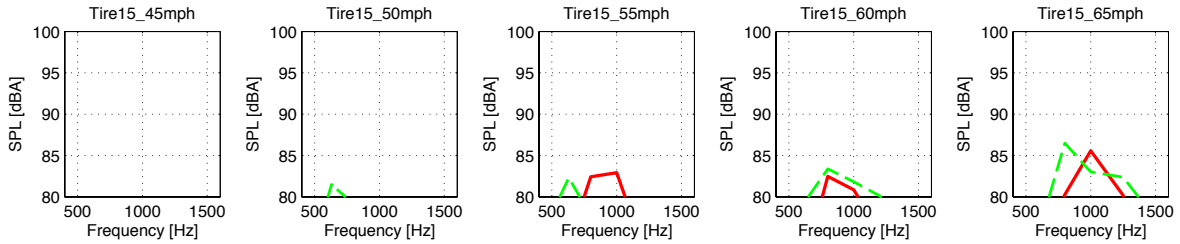

(f) Non-tread pattern noise in 1/3 octave band

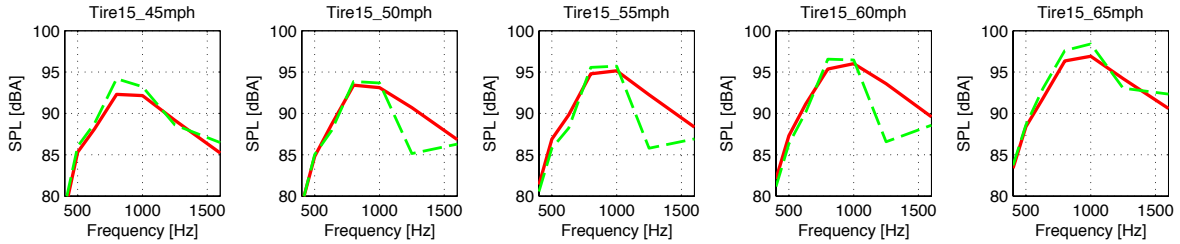

(g) OASPL of total tire noise

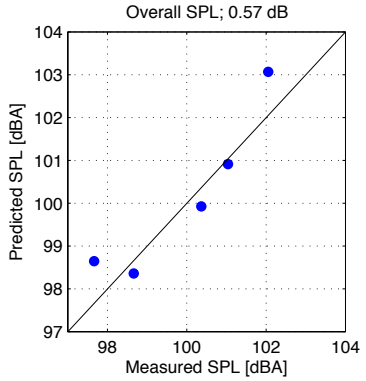

(h) OASPL of tread pattern noise

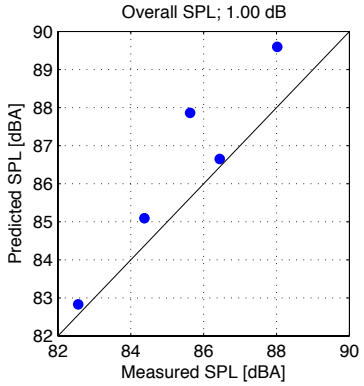

(i) OASPL of non-tread pattern noise

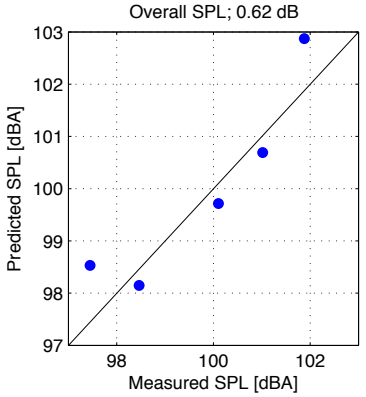

Figure 7.3: Results of AMOT for Tire 15 (in a-f, red denotes measured, green denotes predicted; in g-i, the value above the plot is the average dB error)

7.3.1.3 Tire 18

The results for Tire 18 are demonstrated in Figure 7.4. Good agreement between the measurement and prediction is shown. The non-tread pattern noise is a little bit under-predicted.

(a) Total tire noise in narrowband

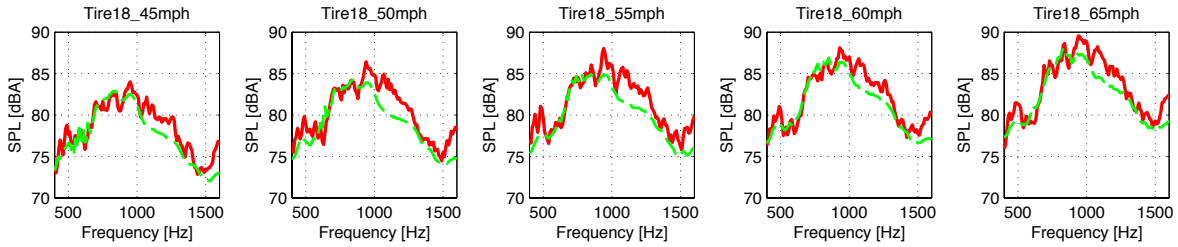

(b) Tread pattern noise in narrowband

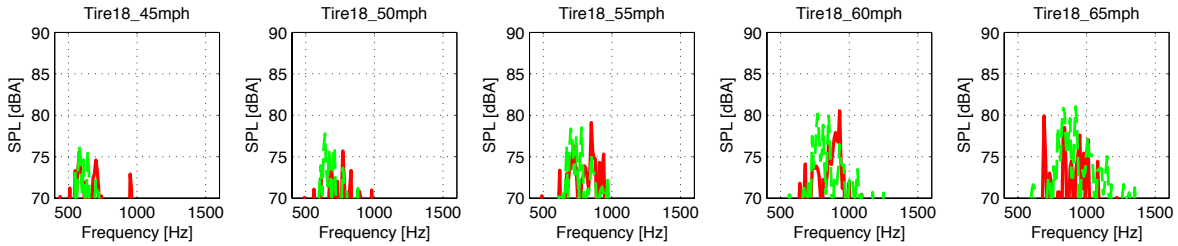

(c) Non-tread pattern noise in narrowband

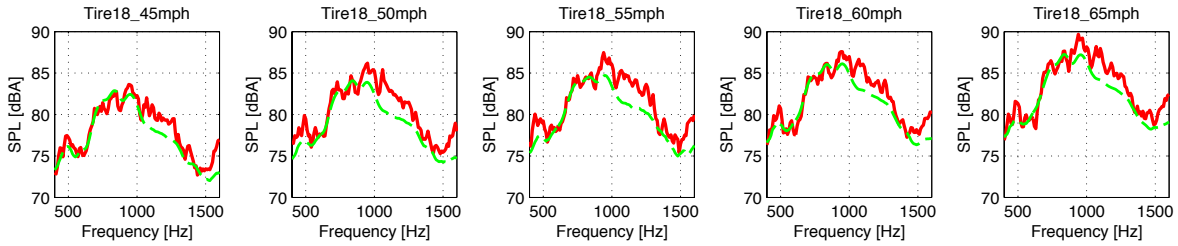

(d) Total tire noise in 1/3 octave band

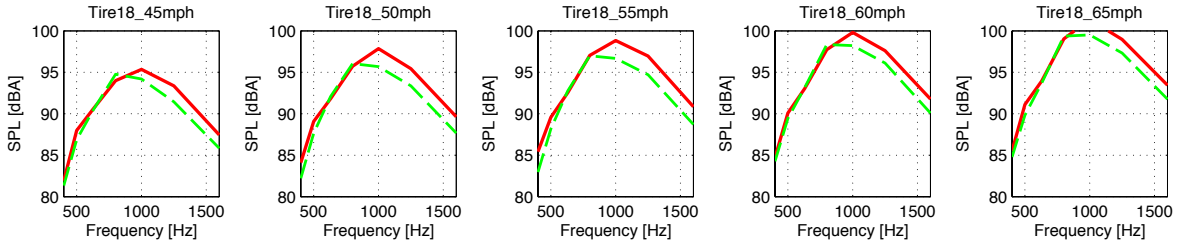

(e) Tread pattern noise in 1/3 octave band

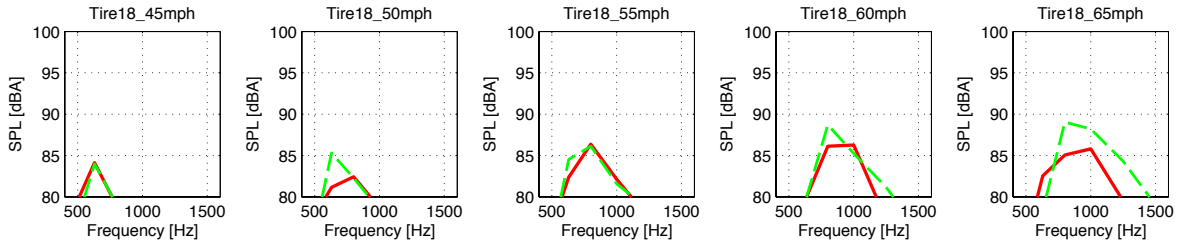

(f) Non-tread pattern noise in 1/3 octave band

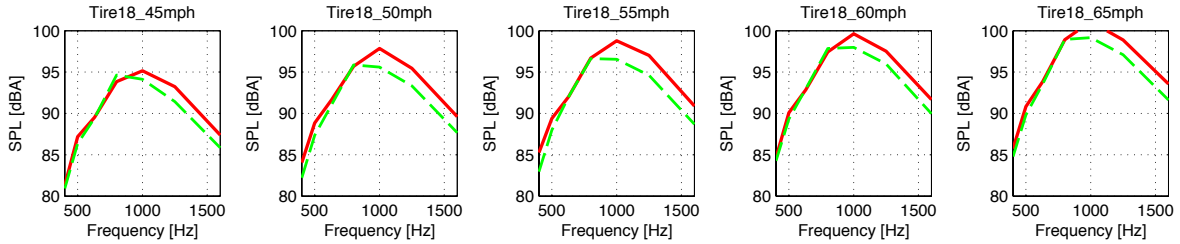

(g) OASPL of total tire noise

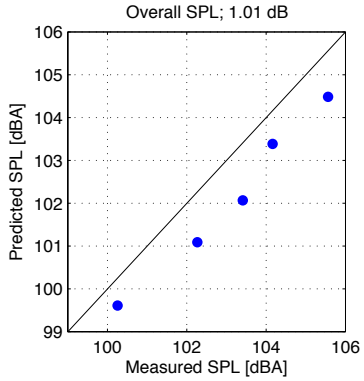

(h) OASPL of tread pattern noise

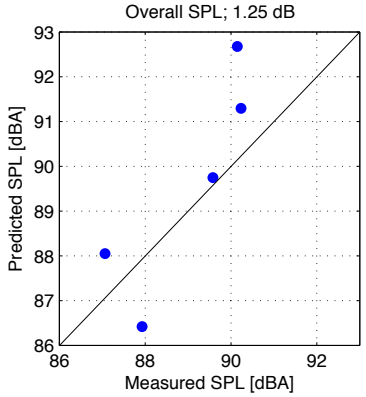

(i) OASPL of non-tread pattern noise

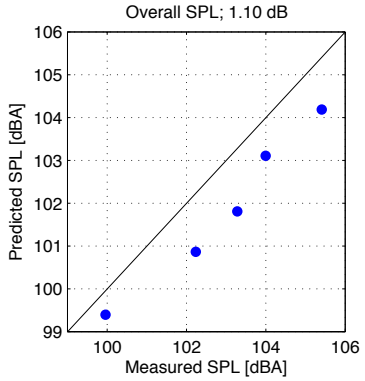

Figure 7.4: Results of AMOT for Tire 18 (in a-f, red denotes measured, green denotes predicted; in g-i, the value above the plot is the average dB error)

7.3.1.4 Tire 22

The results for Tire 22 are demonstrated in Figure 7.5. The tread pattern noise is over-predicted by about 8 dB for all the speeds due to the over-prediction at 60 mph. However, since the tread pattern noise is very small compared to the non-tread pattern noise, the prediction for the total tire noise is still not bad (~1.3 dB error).

(a) Total tire noise in narrowband

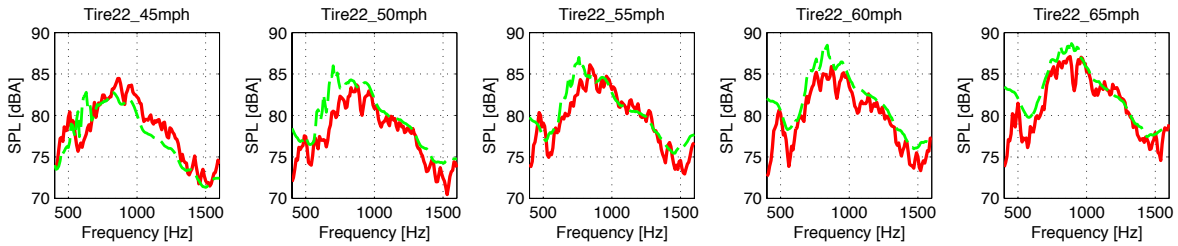

(b) Tread pattern noise in narrowband

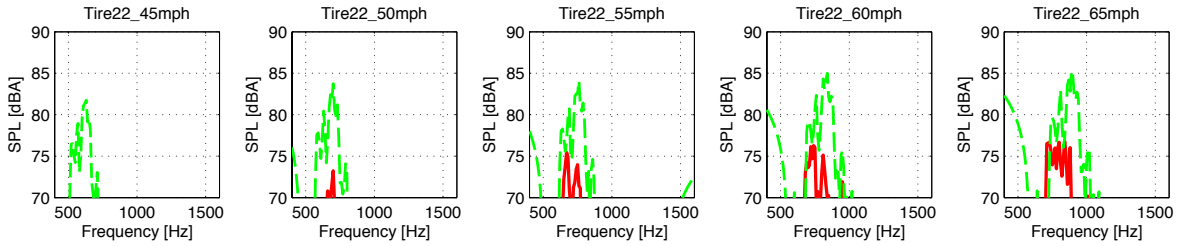

(c) Non-tread pattern noise in narrowband

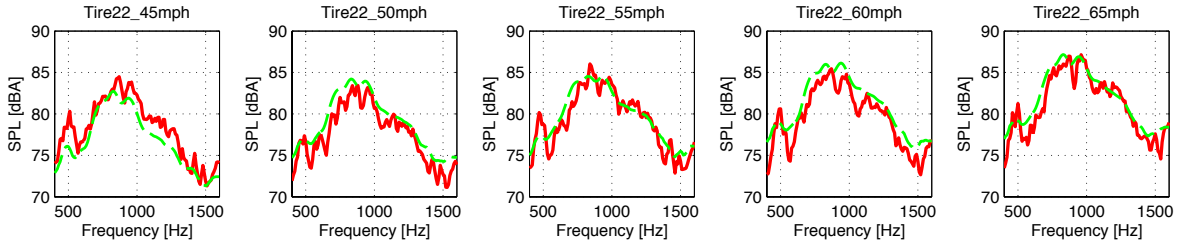

(d) Total tire noise in 1/3 octave band

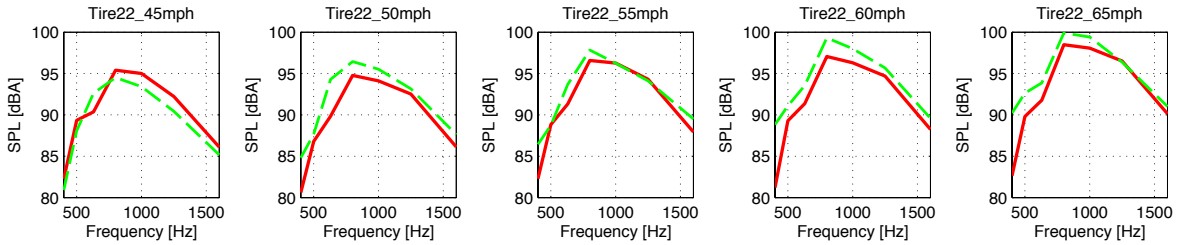

(e) Tread pattern noise in 1/3 octave band

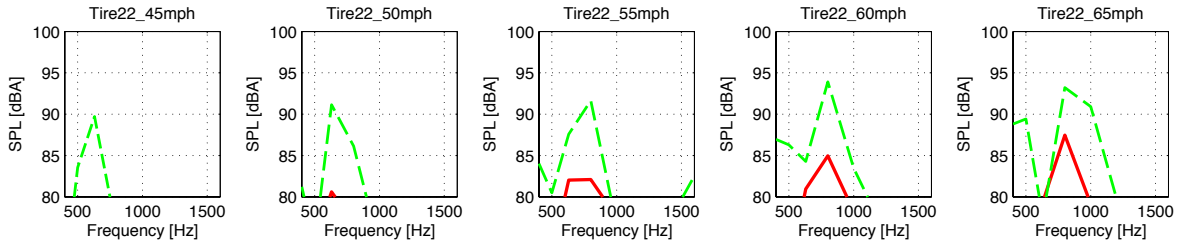

(f) Non-tread pattern noise in 1/3 octave band

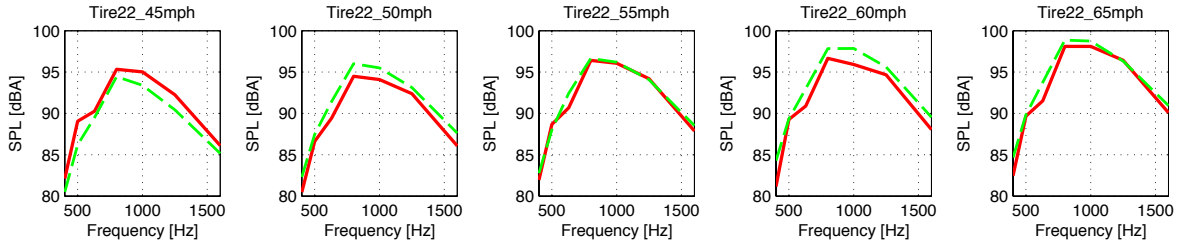

(g) OASPL of total tire noise

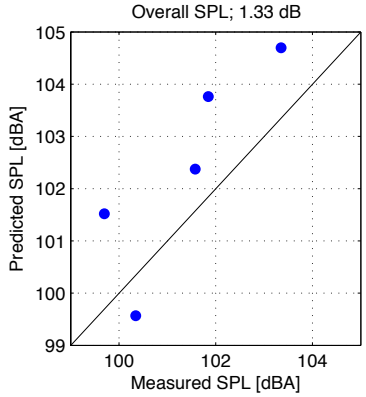

(h) OASPL of tread pattern noise

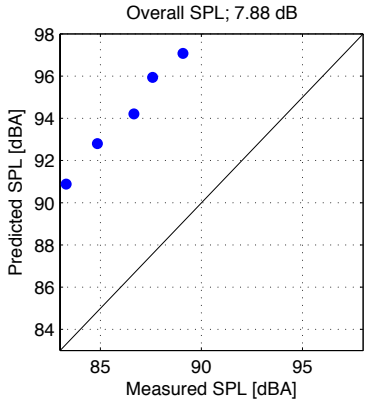

(i) OASPL of non-tread pattern noise

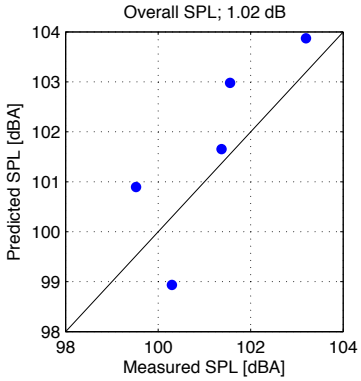

Figure 7.5: Results of AMOT for Tire 22 (in a-f, red denotes measured, green denotes predicted; in g-i, the value above the plot is the average dB error)

7.3.1.5 Tire 23

The results for Tire 23 are demonstrated in Figure 7.6. The tread pattern noise is over-predicted by about 4 dB for all the speeds due to the over-prediction at 60 mph. However, since the tread pattern noise is very small compared to the non-tread pattern noise that is also under-predicted by about 1 dB, the prediction for the total tire noise is still not bad (error < 0.5 dB).

(a) Total tire noise in narrowband

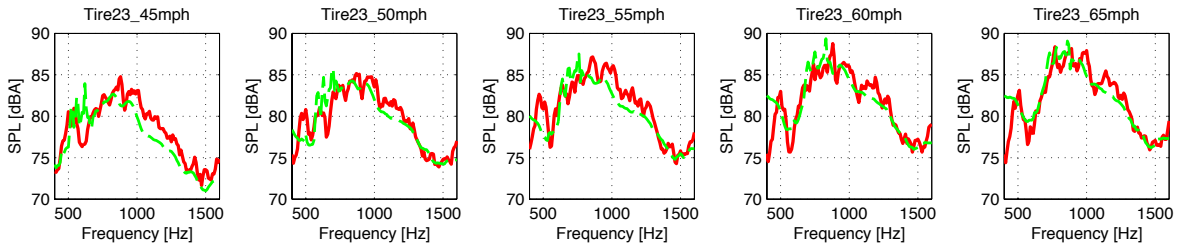

(b) Tread pattern noise in narrowband

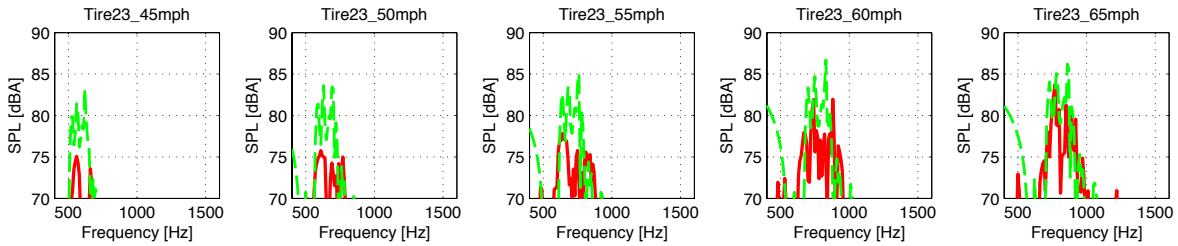

(c) Non-tread pattern noise in narrowband

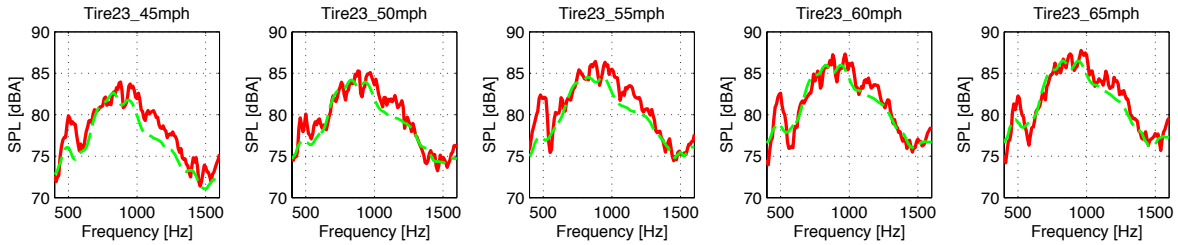

(d) Total tire noise in 1/3 octave band

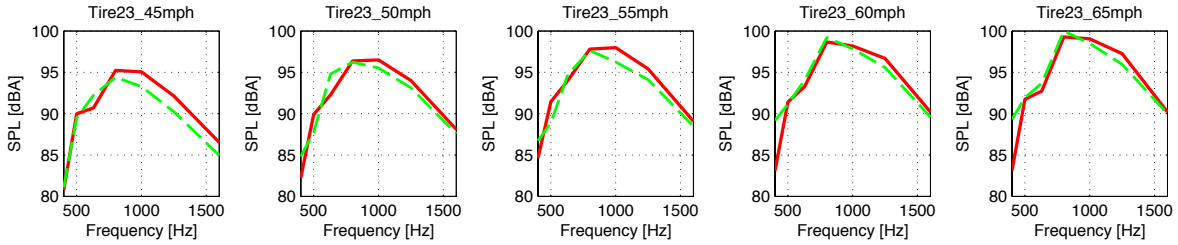

(e) Tread pattern noise in 1/3 octave band

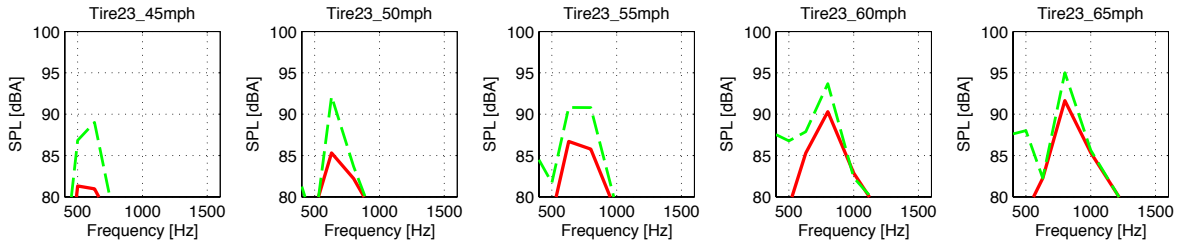

(f) Non-tread pattern noise in 1/3 octave band

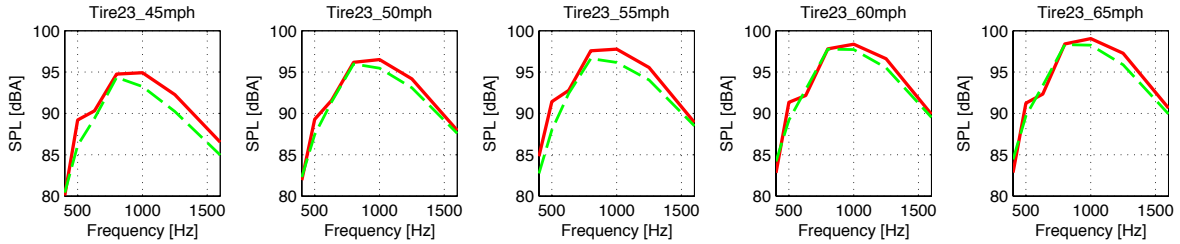

(g) OASPL of total tire noise

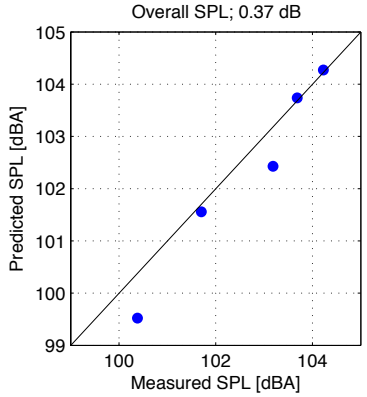

(h) OASPL of tread pattern noise

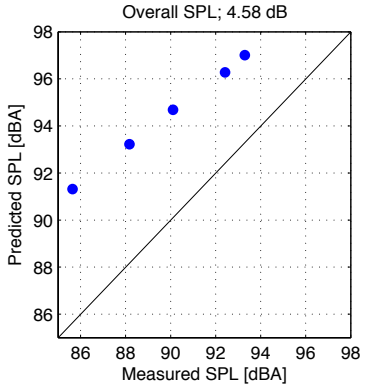

(i) OASPL of non-tread pattern noise

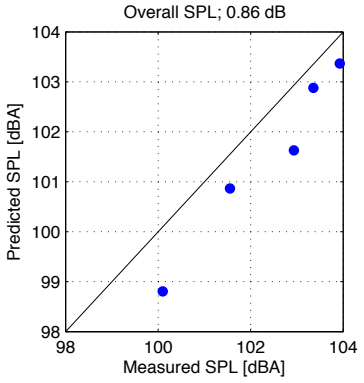

Figure 7.6: Results of AMOT for Tire 23 (in a-f, red denotes measured, green denotes predicted; in g-i, the value above the plot is the average dB error)

7.3.1.6 Tire 45

The results for Tire 45 are demonstrated in Figure 7.7. The tread pattern noise is over-predicted by about 7 dB for all the speeds due to the over-prediction at 60 mph. However, since the tread pattern noise is insignificant compared to the non-tread pattern noise, the prediction for the total tire noise is still not bad (error < 2 dB).

(a) Total tire noise in narrowband

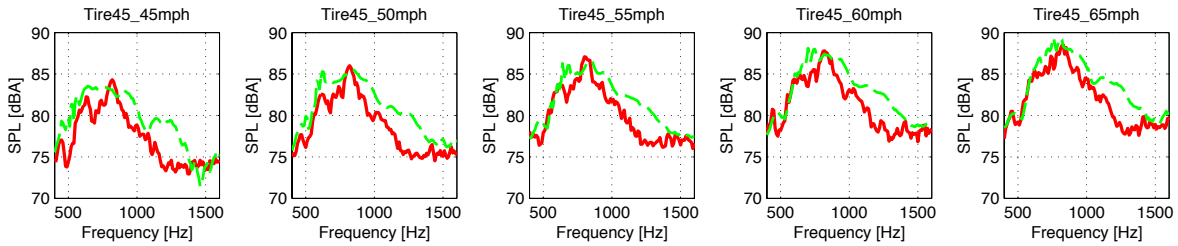

(b) Tread pattern noise in narrowband

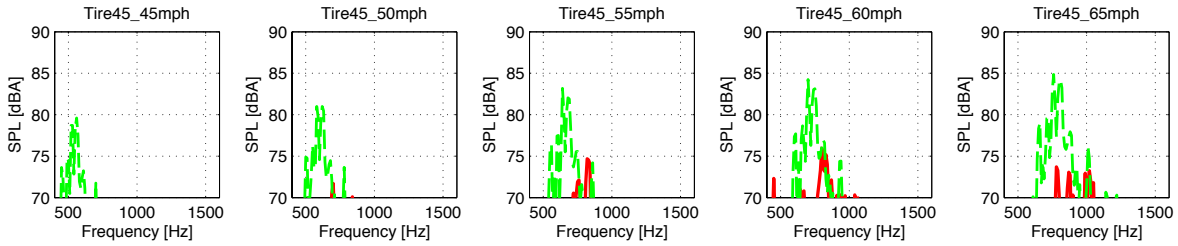

(c) Non-tread pattern noise in narrowband

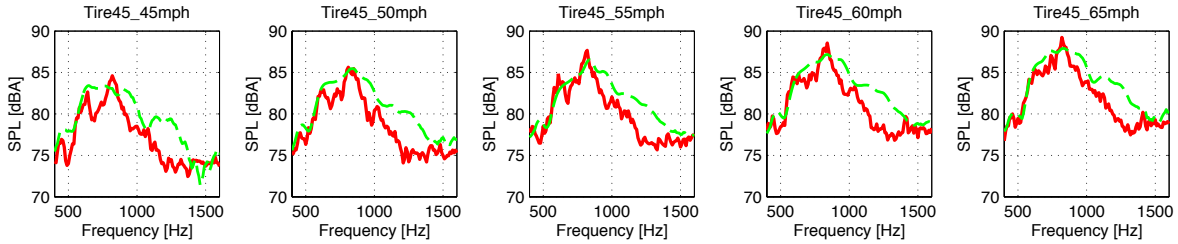

(d) Total tire noise in 1/3 octave band

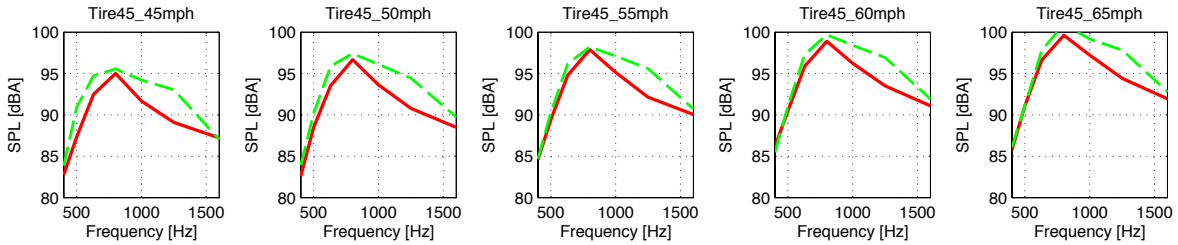

(e) Tread pattern noise in 1/3 octave band

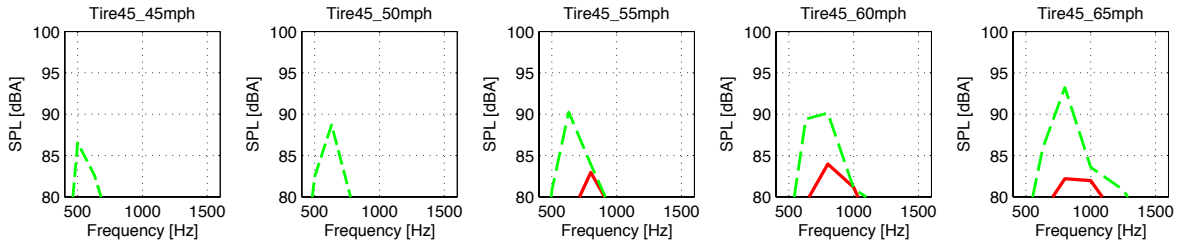

(f) Non-tread pattern noise in 1/3 octave band

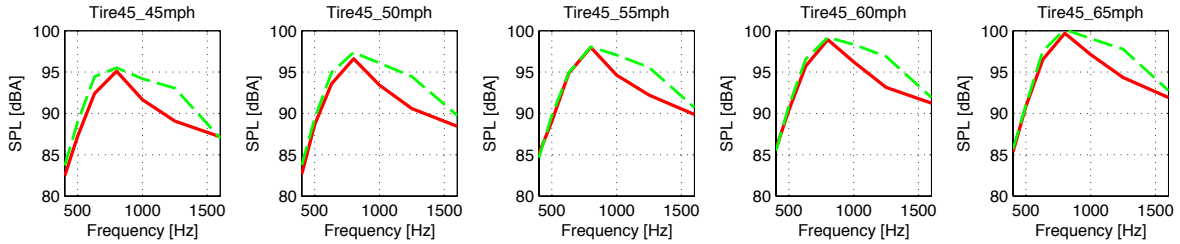

(g) OASPL of total tire noise

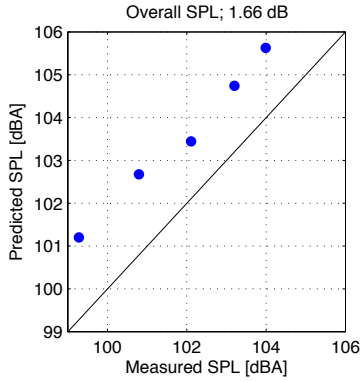

(h) OASPL of tread pattern noise

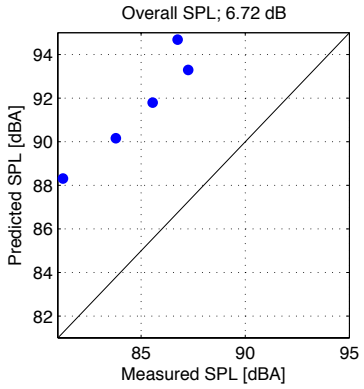

(i) OASPL of non-tread pattern noise

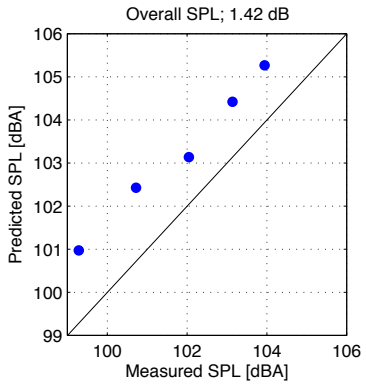

Figure 7.7: Results of AMOT for Tire 45 (in a-f, red denotes measured, green denotes predicted; in g-i, the value above the plot is the average dB error)

7.3.1.7 Tire 49

The results for Tire 49 are demonstrated in Figure 7.8. Good agreement between the measurement and prediction is shown. It is important to note that, the tread pattern noise for this tire is very large, and the AMOT successfully predicts it, including the spectral amplitude and peak location.

(a) Total tire noise in narrowband

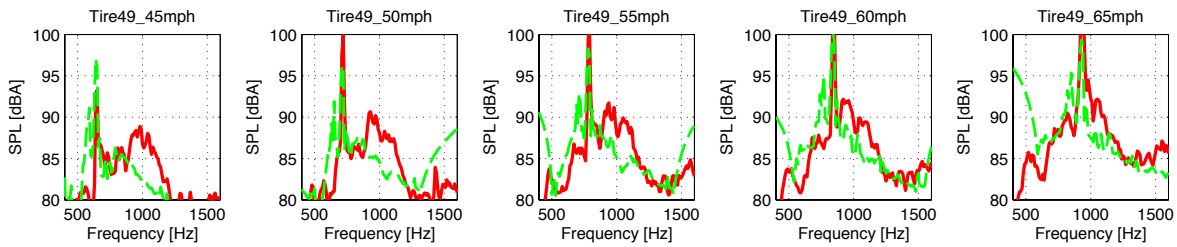

(b) Tread pattern noise in narrowband

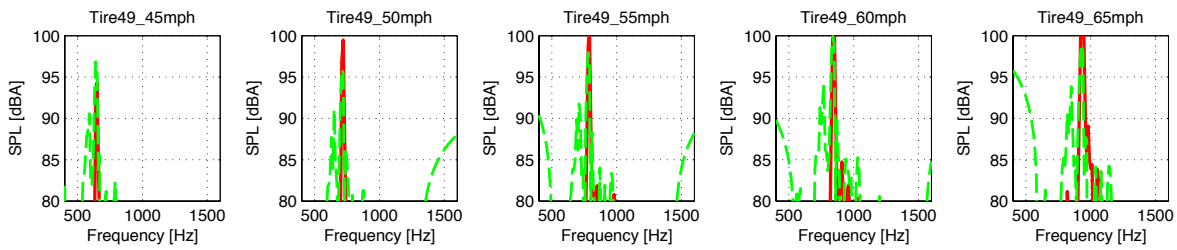

(c) Non-tread pattern noise in narrowband

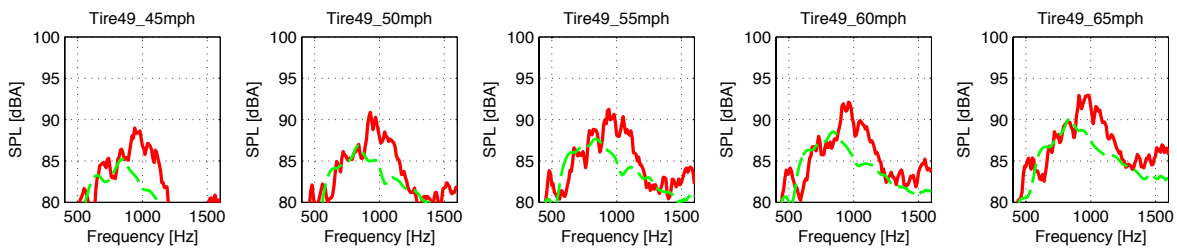

(d) Total tire noise in 1/3 octave band

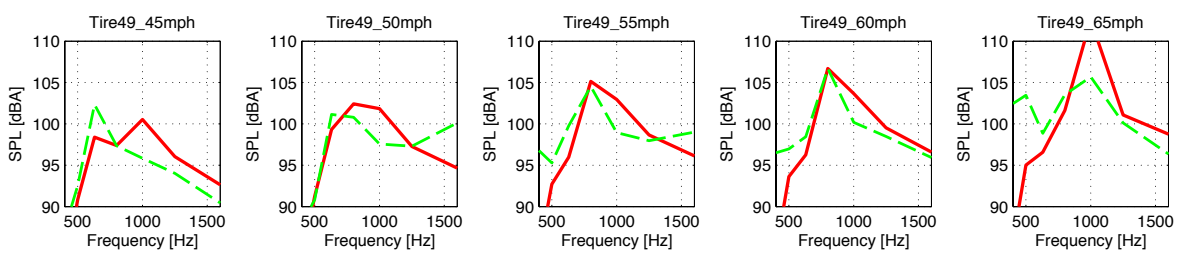

(e) Tread pattern noise in 1/3 octave band

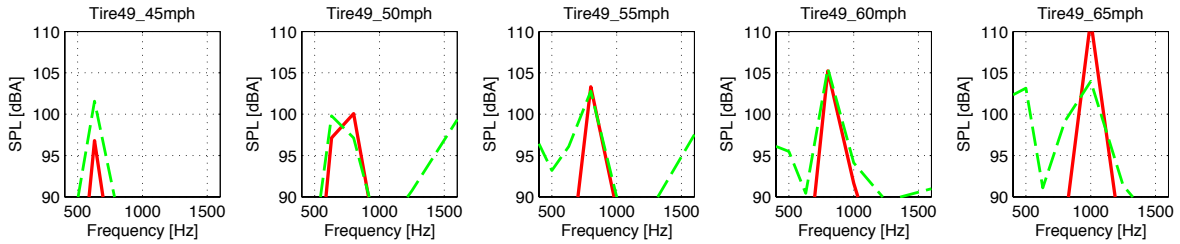

(f) Non-tread pattern noise in 1/3 octave band

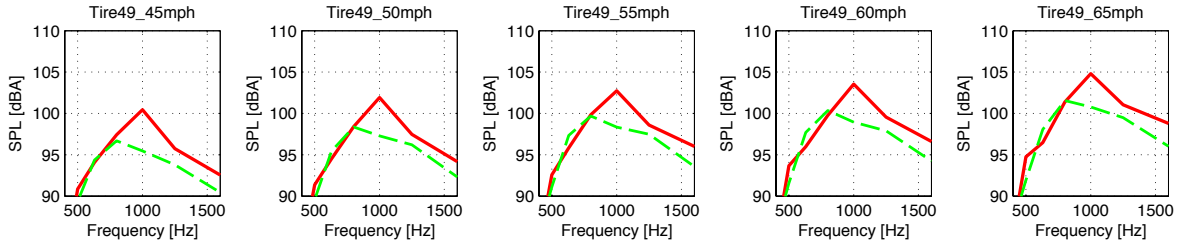

(g) OASPL of total tire noise

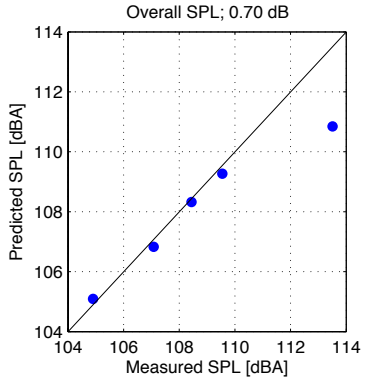

(h) OASPL of tread pattern noise

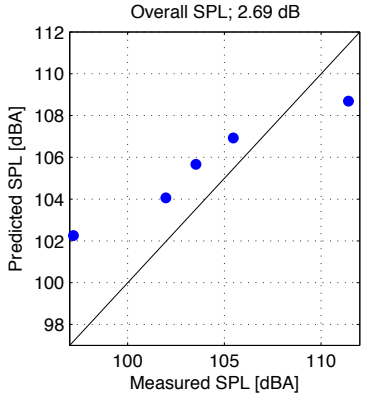

(i) OASPL of non-tread pattern noise

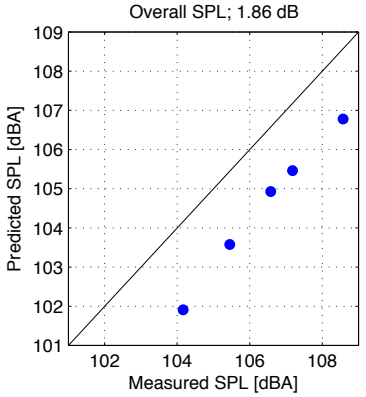

Figure 7.8: Results of AMOT for Tire 49 (in a-f, red denotes measured, green denotes predicted; in g-i, the value above the plot is the average dB error)

7.3.1.8 Tire 55

The results for Tire 55 are demonstrated in Figure 7.9. Good agreement between the measurement and prediction is shown.

(a) Total tire noise in narrowband

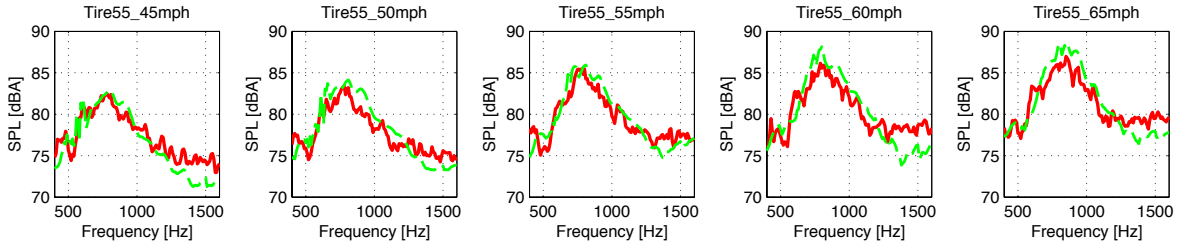

(b) Tread pattern noise in narrowband

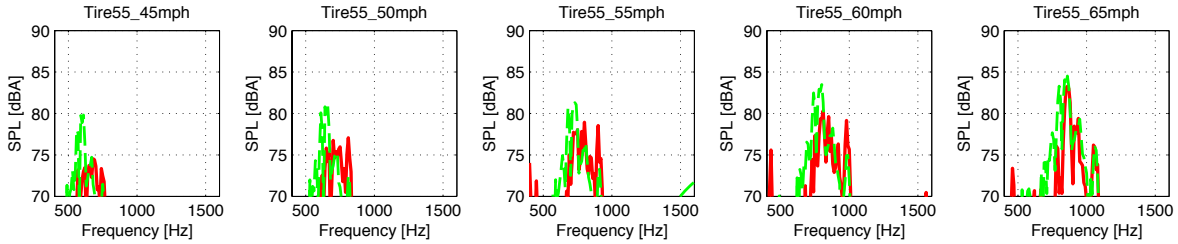

(c) Non-tread pattern noise in narrowband

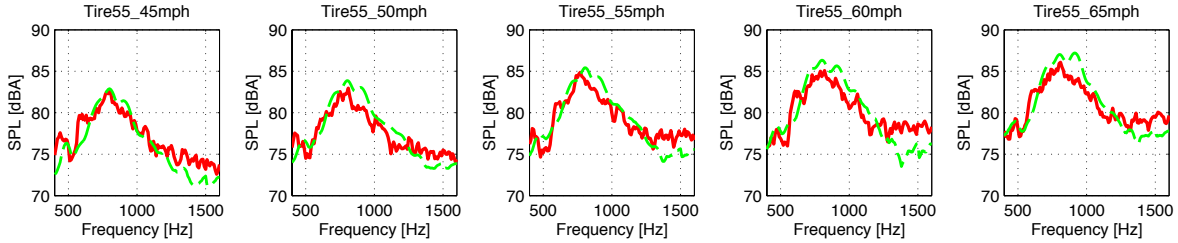

(d) Total tire noise in 1/3 octave band

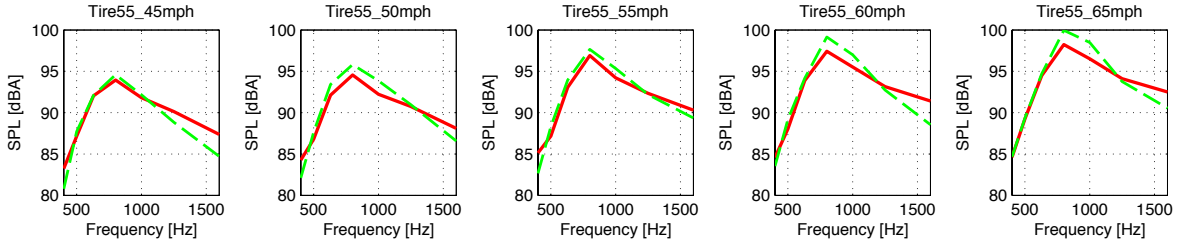

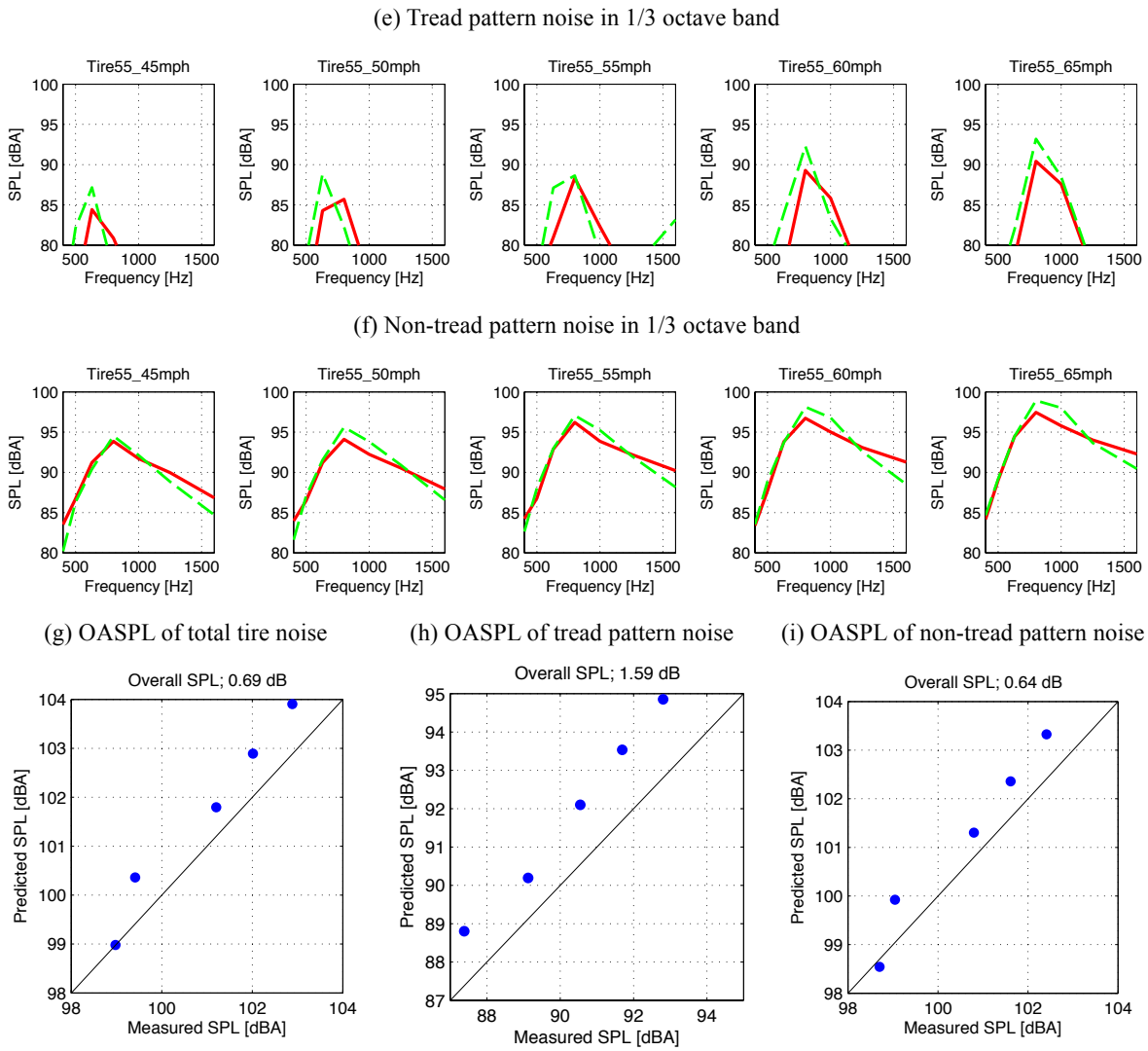

Figure 7.9: Results of AMOT for Tire 55 (in a-f, red denotes measured, green denotes predicted; in g-i, the value above the plot is the average dB error)

7.3.2 All Tires

The results in overall A-weighted sound pressure level (OASPL) for all the tires in the test set are shown in Figure 7.10. Good agreement between the measurement and prediction is shown. The average dB error for the total noise and non-tread pattern noise is about 1 dB, which is very good in acoustics. The average dB error for the tread pattern noise is about 3.6 dB, i.e., only about two times difference in energy linear scale, which is acceptable. There are some over-predictions for the tread pattern noise shown in Figure 7.10b, as discussed before.

In overall, ANN_2 seems to work better than ANN_1.

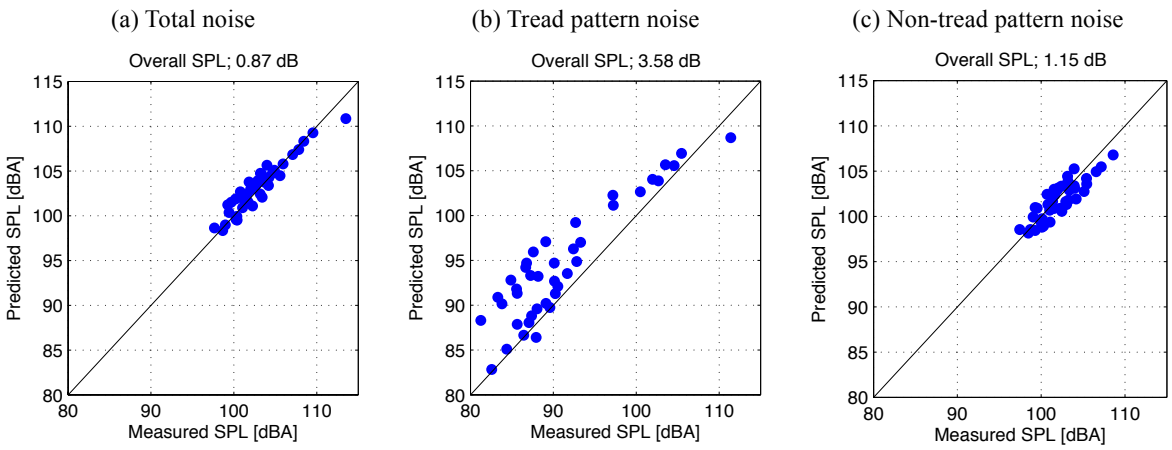

Figure 7.10: Results of AMOT in overall A-weighted sound pressure level (OASPL) (the value above each subplot denotes the average dB error between measurement and prediction)

7.4 Summary

In this chapter, the structure, development, and results for the complete ANN Model of TPIN (AMOT) are presented. The optimized AMOT model is capable of predicting TPIN well in narrowband, 1/3 octave band, and overall noise level.

The new aspects of this model include: (1) it is the first model to predict tread and non-tread pattern noise; (2) it accounts for tire size; (3) it predicts tire noise in narrowband spectrum.

On the other hand, the limitations of this model include: (1) the pavement parameters, e.g., texture and absorption, are not included, so it might not be valid for other type of pavements, e.g., cement concrete pavement. (2) tire pressure, tire load, and temperature are not included. However, the effects of tire pressure and temperature were investigated in this study, but it was found that they are not very influencing in normal conditions. From literature, tire load does not influence TPIN significantly (+1 dB per doubling load). (3) The model might not be able to handle tires with sizes that are out of the normal range for passenger car tires. (4) the tread pattern noise prediction is not accurate for some tires at speeds away from 60 mph, because these tires have different speed exponent other than four that is used in the model. (5)

the tread pattern noise tends to be over-predicted, likely due to the insufficient number of samples to train the ANN or imperfect ANN configurations. (6) The model only predicts the tire noise from the leading edge of the contact patch; the tire noise from the trailing edge might be different.

8 Conclusions and Future Work

In the present study, forty-two tires with different tread patterns and sizes were tested at different speeds on a non-porous asphalt pavement. The On-Board Sound Intensity (OBSI) technique was used to collect the tire noise data at both the leading and trailing edge of the tire contact patch. A wheel sensor (optical sensor recording the once-per-revolution signal of the wheel) was also installed to monitor the vehicle speed and, more importantly, to provide the data needed to perform the order tracking analysis in order to break down the tire noise into two components: the tread pattern and the non-tread pattern noise. Based on the experimental noise data collected, two artificial neural networks (ANN) were developed to predict the tread pattern (ANN_1) and the non-tread pattern noise (ANN_2) components, separately. The inputs of ANN_1 are the coherent tread profile spectrum and the air volume velocity spectrum calculated from the digitized 3D tread pattern. The inputs of ANN_2 are the tire size and tread rubber hardness. The vehicle speed is also included as input for the two ANN's. The optimized ANN's are able to predict the tire-pavement interaction noise well for different tires on the pavement tested.

The main conclusions of the present study are:

(1) Through the separation of the total TPIN into two components, tread pattern noise and non-tread pattern noise component, it is demonstrated that for the commonly used tires (summer or all-season tires), the tread pattern noise is not the dominant noise source (below 5% of total noise), at least for the non-porous asphalt pavement tested, which suggests that the NVH (Noise, Vibration, and Harshness) engineers in the tire industries have done a good job on optimizing the tread pattern to reduce the noise. Considerable tread pattern noise (10~50% of total noise) only exists for some snow tires or directional tires whose tread patterns look aggressive due to traction requirement and are not perfectly randomized. It is implied that, in the future, in order to reduce TPIN for common tire-pavement combinations, reducing the non-tread pattern noise mainly due to tire vibrations excited by pavement is more feasible than reducing the tread pattern noise due to tread pattern. However, tread pattern noise is dominant at some frequencies (well above non-tread pattern noise) and could be easily perceived even when the total level is low compared to non-tread pattern noise. Therefore,

spreading the tread pattern noise to wider frequency range is also the key to improving NVH performance. In addition, once the pavement becomes very quiet as the paving techniques improve, the tread pattern noise might become dominant.

(2) It is generally accepted that the most important TPIN generation mechanisms are tread impact and air pumping. To characterize the two mechanisms, the 3D tread pattern is parameterized using two spectrums: coherent tread profile spectrum and contact patch air volume velocity spectrum. These two spectrums correlate well with the tread pattern noise spectrum, supporting the conclusion that the tread pattern leads to the tread pattern noise. Based on this, the ANN_1 is developed, validated using experimental data, and is able to predict tread pattern noise well from typical tread patterns at normal highway speeds.

(3) For non-tread pattern noise and ANN_2 development, the tread rubber hardness was found to have a positive correlation with the non-tread pattern noise (~0.23 dBA/Shore A). Another finding is that the central frequencies of the non-tread pattern noise decrease as the tire carcass width (i.e., tire section width plus two times tire section height) increases.

(4) The complete ANN Model of TPIN (AMOT), including the ANN_1 for tread pattern noise and ANN_2 for non-tread pattern noise, is capable of predicting TPIN well in narrowband, 1/3 octave band, and overall noise level for tires of different sizes with typical tread patterns at normal highway speed on a non-porous asphalt pavement. The novelty of this model includes: (a) it is the first model to predict tread and non-tread pattern noise; (b) it accounts for tire size, which is the first to reveal the effect of tire size on the tire noise spectrum; (c) it predicts tire noise in narrowband spectrum instead of octave band or fractional octave band that most of other models use.

The recommendations for future work are:

(1) More data samples for different tires (e.g., different tread patterns, tire sizes, and rubber hardness) can be collected to improve the performance of the ANN models. To be more specific, more different and/or less commonly seen tread patterns can be tested to improve ANN_1 so that the over-prediction can possibly be removed; more different tire sizes, including very narrow and very wide tires, can be tested to improve ANN_2, and validate the

tire size scaling hypothesis.

(2) Pavement parameters can be included into the ANN models by conducting tire noise tests on different pavements. This is proposed as the second phase of the project MODL-2015-B3-8 sponsored by CenTiRe. Only preliminary data and results have been collected and analyzed for the moment. The spectral shapes of the tread pattern noise from the same tire tested on different pavements are almost the same while the spectral shapes of the non-tread pattern noise are quite different. The spectral amplitude of the tread pattern noise was slightly larger on smoother pavement while the spectral amplitude of non-tread pattern noise was considerably larger on rougher pavement. Therefore, the relative noise contribution of tread pattern and non-tread pattern noise is a function of pavement.

(3) The ANN model presented in this dissertation is only based on the results of Mic 1 (leading inboard microphone). Similar models can be extended to the other three microphones, the average acoustic energy of microphones, and the intensity probes.

References

[1]M. Heckl, “Tire noise generation,” *Wear*, vol. 113, pp. 157–170, 1986.

[2]L. R. Wayson, “On-Board Sound Intensity (OBSI) Study, Phase 2, Summary,” in *Final Report, FDOT Project No. #BDT06*, 2014, p. 1p-.

[3]W. Jones, “Highway Noise Control with HMA,” *Asphalt*, 2002.

[4]E. Kohler, “OBSI Testing,” in *Presentation at Pavement Evaluation 2010, Roanoke, Virginia*, 2010.

[5]M. E. Braun, S. J. Walsh, J. L. Horner, and R. Chuter, “Noise source characteristics in the ISO 362 vehicle pass-by noise test: Literature review,” *Appl. Acoust.*, vol. 74, no. 11, pp. 1241–1265, 2013.

[6]R. O. Rasmussen, R. J. Bernhard, U. Sandberg, and E. P. Mun, “The Little Book of Quieter Pavements.,” *Rep. No. FHWA-IF-08-004*, 2007.

[7]U. Sandberg, “Tyre / road noise – Myths and realities,” in *The 2001 International Congress and Exhibition on Noise Control Engineering*, 2001.

[8]L. Domenichini, A. Fracassa, F. La Torre, G. Loprencipe, A. Ranzo, and A. Scalamandrè, “Relationship between road surface characteristics and noise emission,” in *First International Colloquium on Vehicle Tyre Road Interaction, Rome, Italy, Paper 99.03*, 1999, pp. 1–22.

[9]U. Sandberg, “Noise emissions of road vehicles effect of regulations: Final Report 01-1,” *Noise News Int.*, vol. 9, no. 3, pp. 147–203, 2001.

[10] M. Harrison, “Vehicle Refinement: Controlling Noise and Vibration in Road Vehicles,” MA, USA: Elsevier, 2004.

[11] C. Chen, Y. Kuan, C. Chen, and M. Sung, “Using CFD Technique to Investigate the Effect of Tire Roiling-noise with Different Pattern Design,” in *Applied Mechanics and Materials*, 2014, vol. 575, pp. 469–72.

[12] J. Jabben, E. Verheijen, and C. Potma, “Noise reduction by electric vehicles in the Netherlands,” in *41st International Congress and Exposition on Noise Control Engineering 2012, INTER-NOISE 2012*, 2012, vol. 3, pp. 2505–2512.

[13] C. Mendonca, E. Freitas, J. P. Ferreira, I. D. Raimundo, and J. A. Santos, “Noise abatement and traffic safety: The trade-off of quieter engines and pavements on vehicle detection,” *Accid. Anal. Prev.*, vol. 51, pp. 11–17, 2013.

[14] NHTSA, “NHTSA sets ‘Quiet Car’ safety standard to protect pedestrians,” 2016. [Online]. Available: https://www.nhtsa.gov/About-NHTSA/Press-Releases/nhtsa_quiet_car_final_rule_11142016. [Accessed: 14-Nov-2016].

[15] National Highway Traffic Safety Administration (NHTSA), *Minimum Sound Requirements for Hybrid and Electric Vehicles*. 2016.

[16] National Highway Traffic Safety Administration (NHTSA), *Minimum Sound Requirements for Hybrid And Electric Vehicles - Final Environmental Assessment*. 2016.

[17] U. Sandberg, “What is the biggest threat to health and safety- Quiet or noisy vehicles,” *J. Acoust. Soc. Am.*, vol. 134, 2013.

[18] D. B. Thrasher, R. F. Miller, and R. G. Bauman, “Effect of pavement texture on tire/pavement interaction noise,” in *SAE Technical Papers*, 1976.

[19] R. F. Miller and D. B. Thrasher, “Passby tire/pavement interaction noise measurement problems,” in *SAE Technical Papers*, 1976.

[20] M. G. Pottinger, K. D. Marshall, J. M. Lawther, and D. B. Thrasher, “Review Of Tire/Pavement Interaction Induced Noise And Vibration,” in *ASTM Special Technical Publication*, 1986, pp. 183–287.

[21] P. R. Donavan, “Assessment of tire/pavement interaction noise under vehicle passby test conditions using sound intensity measurement methods,” *J. Acoust. Soc. Am.*, vol. 103, 1998.

[22] L. Khazanovich and B. I. Izevbekhai, “Implication of time-dependent texture degradation on pavement on board sound intensity patterns in MnROAD test cells,” in *Proceedings of the International Noise Conference, Dearborn Michigan July 2008*, 2008.

[23] A. Syamkumar, K. Aditya, and V. Chowdary, “Development of mode-wise noise prediction models for the noise generated due to tyre-pavement surface interaction,” *Adv. Mater. Res.*, vol. 723, pp. 50–57, 2013.

[24] U. Sandberg and J. A. Ejsmont, *Tyre/road noise reference book*. Kisa, Sweden; Harg, Sweden: INFORMEX, 2002.

[25] U. Sandberg and J. A. Ejsmont, “The Tire/Road noise computerized bibliography,” in *International symposium, Euro noise ’95: software for noise control; 1995; Lyon; France*, 1995, pp. 289–294.

[26] P. Sabiniarz and W. Kropp, “A waveguide finite element aided analysis of the wave field on a stationary tyre, not in contact with the ground,” *J. Sound Vib.*, vol. 329, no. 15, pp. 3041–3064, 2010.

[27] N. Campillo-Davo, R. Peral-Orts, E. Velasco-Sanchez, and H. Campello-Vicente, “An experimental procedure to obtain sound power level of tyre/road noise under Coast-By conditions,” *Appl. Acoust.*, vol. 74, no. 5, pp. 718–727, 2013.

[28] P. Zakelj, “Tire tread noise treatment,” in *US Patent US6112167*, 2000.

[29] J. He, X. Jin, W. Wang, H. Jianfeng, J. Xiaoxiong, and W. Wanying, “Analysis of tire tread pattern’s impact on interior vibration and noise based on Wavelet Transform,” in *Applied Mechanics and Materials*, 2011, vol. 66–68, no. 3, pp. 1755–1761.

[30] Z. He, L. Lu, and L. Luo, “The energy distribution of tire-road noise and noisy speech based on wavelet packet,” in *Key Eng. Mater. (Switzerland)*, 2011, vol. 464, pp. 721–724.

[31] H. SungWook, H. JinHyuk, S. KiDuck, L. SangKwon, H. S. Wook, H. J. Hyuk, S. K. Duck, and L. S. Kwon, “The study of tire pattern noise by using wavelet transform,” in *Applied Mechanics and Materials*, 2012, vol. 105–107, pp. 267–70.

[32] X. Chen, L. Chen, C. xia, and C. Lijun, “Analysis tire tread patterns noise based on Wavelet transform,” in *Advanced Materials Research*, 2013, vol. 823, pp. 180–3.

[33] ISO, “Acoustics - Method for measuring the influence of road surfaces on traffic noise -

Part 1: The Statistical Pass-By Method," *ISO 11819-1*, 1997.

[34] ISO, "Acoustics -- Method for measuring the influence of road surfaces on traffic noise -- Part 4: SPB method using backing board," *ISO/PAS 11819-4*, 2013.

[35] R. McDaniel, A. Shah, T. Dare, and R. Bernhard, "Hot Mix Asphalt Surface Characteristics Related to Ride , Texture , Friction , Noise and Durability," 2014.

[36] G. Wang, R. Shores, J. Botts, and R. Hibbett, "On-Board Sound Intensity Tire-Pavement Noise Study in North Carolina.," no. December, p. 210p-, 2011.

[37] R. O. Rasmussen and R. C. Sohaney, "Tire/Pavement and Environmental Traffic Noise Research Study," p. 147p-, 2012.

[38] E. B. Dick, B. I. Izevbekhai, and T. Casey, "Influence of Pavement on Traffic Noise -- Statistical Pass-By Measurements of Traffic on Several Interstate Pavements," 2010.

[39] "Controlled Pass-By Method," *French Natl. Stand. NF S S1 119-2*, 1999.

[40] ISO, "Measurement of noise emitted by accelerating road vehicles -- Engineering method -- Part 1: M and N categories," *ISO 362-1*, 2015.

[41] ISO, "Measurement of noise emitted by accelerating road vehicles -- Engineering method -- Part 2: L category," *ISO 362-2*, 2009.

[42] ISO, "Acoustics -- Measurement of noise emitted by accelerating road vehicles -- Engineering method," *ISO 362*, 1981.

[43] ISO, "Acoustics -- Measurement of noise emitted by accelerating road vehicles -- Engineering method," *ISO 362/Amd 1*, 1985.

[44] T. J. Copeland and R. Seth Wilhoit, "Tire noise pass-by testing system meets latest standards," in *Sound and Vibration*, 2012, vol. 46, no. 5, pp. 12–16.

[45] T. C. Giorjao, R. Yoneda, A. L. Cherman, and A. R. Morais, "Tire contribution for pass by noise," in *SAE Technical Papers*, 2005.

[46] ISO, "Tyres - Coast-by methods for measurement of tyre-to-road sound emission," *ISO 13325*, 2003.

[47] J. A. Ejsmont and U. Sandber, "Tire/Road Noise: Trailer Measurements in Practice," in *Proc. of INTER-NOISE 85*, 1985.

[48] D. I. Hanson and R. S. James, "Colorado DOT Tire/Pavement Noise Study.," in *Report No. CDOT-DTD-R-2004-5, Colorado Department of Transportation*, 2004.

[49] R. J. Bernhard, R. L. Wayson, J. E. Haddock, N. Neithalath, A. El-Aassar, J. Olek, T. K. Pellinen, and W. J. Weiss, "An Introduction to Tire / Pavement Noise of Asphalt Pavement," 2005.

[50] AASHTO, "Standard Method of Test for Determining the Influence of Road Surfaces on Vehicle Noise Using the Statistical Isolated Pass-By (SIP) Method," *AASHTO TP 98*, 2013.

[51] AASHTO, "Standard Method of Test for Determining the Influence of Road Surfaces on Vehicle Noise Using the Statistical Isolated Pass-By (SIP) Method," *AASHTO TP 98*, 2012.

[52] D. M. Lodico, J. L. Rochat, P. Donavan, and R. O. Rasmussen, "Overview and application

of the Statistical Isolated Pass-By Method (SIP) for determining the influence of road surfaces on vehicle noise (AASHTO TP-98)," in *41st International Congress and Exposition on Noise Control Engineering 2012, INTER-NOISE 2012*, 2012, vol. 3, pp. 2592–2601.

[53] AASHTO, "Standard Method of Test for Determining the Influence of Road Surfaces on Traffic Noise Using the Continuous Flow Traffic Time-Integrated Method (CTIM)," *AASHTO TP 99*, 2013.

[54] AASHTO, "Standard Method of Test for Determining the Influence of Road Surfaces on Traffic Noise Using the Continuous Flow Traffic Time-Integrated Method (CTIM)," *AASHTO TP 99*, 2012.

[55] J. L. Rochat, D. Lodico, P. Donavan, and R. O. Rasmussen, "Overview and application of the Continuous-Flow Traffic Time-Integrated Method (CTIM) for determining the influence of road surfaces on traffic noise," in *41st International Congress and Exposition on Noise Control Engineering 2012, INTER-NOISE 2012*, 2012, vol. 3, pp. 2602–2611.

[56] T. Siddon, "Noise Generation Mechanisms for Passenger Car Tires," in *84th meeting of the ASA*, 1972.

[57] Y. Zhang, J. G. McDaniel, and M. L. Wang, "Pavement macrotexture estimation using principal component analysis of tire/road noise," in *Proc. SPIE, Int. Soc. Opt. Eng. (USA)*, 2014, vol. 9063, p. 90630K (9 pp.)-pp.

[58] R. F. Miller and D. B. Thrasher, "Spectral Analyses in Truck Tire Noise Fields," in *SAE West Coast Meeting, Anaheim, CA, August 1974*, 1974.

[59] W. F. Reiter, A. C. Eberhardt, L. J. Harper, and T. L. Atkinson, "Truck Noise VII-A Experimental Investigation of Truck Tire Sound Vibration," Raleigh, NC, United states, 1974.

[60] S. Landers, G. Richards, and J. Bradisse, "Onboard Tire Sound Level Testing Technique," *Highw. Tire Noise, Soc. Automot. Eng.*, no. 762017, 1977.

[61] S. P. Landers, "A Vibrational Sound Mechanism of Lug Type Tread Designs," *Highw. Tire Noise, Soc. Automot. Eng.*, 1977.

[62] M. C. P. Underwood and P. Nelson, "Lorry Tyre Noise," *Veh. Noise Vib.*, no. C139/84, p. 50p-, 1984.

[63] W. F. Reiter and A. C. Eberhardt, "The Relationship between Truck Tire Vibration and Near and Far Field Sound Levels," *Highw. Tire Noise, Soc. Automot. Eng.*, no. 762021, 1977.

[64] A. C. Eberhardt, "An Experimental and Analytical Investigation of the Vibration Noise Generation Mechanism in Truck Tires," United States, 1981.

[65] SAE, "Sound Level Of Highway Truck Tires," *SAE J 57*, 2014.

[66] SAE, "Sound Level Of Highway Truck Tires," *SAE J 57*, 1977.

[67] U. Sandberg and J. A. Ejsmont, "Selection of Tyres with Regard to Noise Emissions," in *Unpublished, VTI, Sweden*, 1992.

[68] S. Phillips, S. Kollamthodi, and P. Nelson, "Investigations of tyre/road noise – Draft report," in *Project report PR/SE/272/2001 S032J/VB, Transport Research Laboratory, Crowthorne, U.K.*, 2001.

[69] M. M. Osman and D. N. May, "Relative Influence of Pavement Texture and Tire Type on Pavement/Tire Noise," in *Vehicle Noise Regulation and Reduction, SP-456*, 1980, no. 800282.

[70] P. R. Donavan and D. M. Lodico, "Measuring Tire-Pavement Noise at the Source (NCHRP Report 630)," 2009.

[71] E. Ungar and B. Bronsdon, "Tire Noise Data Bank," in *Bolt, Beranek, and Newman, Inc. Report No. 4411, June, 1980, Prepared for the U.S. Environmental Protection Agency, Office of Noise Abatement and Control, EPA Contract No. 68-01-3950.*, 1980.

[72] G. Breyer, "Low-Noise Road Surfaces in Austria," in *Proceedings of the International Tire/Road Noise Conference 1990, Gothenberg, Sweden*, 1990.

[73] M. Springborn, "Measurement of Tire/Road Noise and the Influence of the Road Surface," in *Proceedings of the International Tire/Road Noise Conference 1990, Gothenberg, Sweden*, 1990.

[74] H. Steven, "Investigations on a Measuring Method for the Tyre/Road Noise of Passenger Cars," in *Proceedings of the International Tire/Road Noise Conference 1990, Gothenberg, Sweden*, 1990.

[75] J. D. Chalupnik, "Predicting Roadside Noise Levels from Near Field Trailer Measurements," in *Proceedings of Noise-Con 1996, Seattle, WA*, 1996, vol. 1, pp. 61–66.

[76] Y. Oshino and H. Tachibana, "Relationships between Road Texture and Tire/Road Noise," in *Proceedings of Noise-Con 1996, Seattle, WA*, 1996, vol. 1, pp. 67–72.

[77] Y. Oshino, T. Mikami, and H. Tachibana, "Study of road surface indices for the assessment of tire/road noise," in *Proceedings of Inter-Noise 2001, the Haag, the Netherlands*, 2001.

[78] T. Fujikawa, Y. Oshino, T. Mikami, and H. Tachibana, "Examination on Effects of Road Roughness Parameters for Abating Tire/Road Noise," in *Proceedings of Inter-Noise 2004, Prague, Czech Republic*, 2004.

[79] M. T. McNerney, B. J. Landsberger, T. Turen, and A. Pandelides, "Comparative Field Measurements of Tire/Pavement Noise of Selected Texas Pavements," in *Center for Transportation Research, the University of Texas at Austin, Austin, TX, Report No. 7-2957-2*, 2000, p. 56p-.

[80] J. S. C. Chuang, H.-H. Lin, Y.-Y. Chen, and T.-K. Su, "Study of Tire Noise for Vehicle Noise Control," in *SAE Paper 2005-01-2415, Society of Automotive Engineers Noise and Vibration Conference Proceedings, Traverse City, MI*, 2005.

[81] P. R. Donavan and L. J. Oswald, "The Identification and Quantification of Truck Tire Noise Sources under On-Road Operating Conditions," in *General Motors Research Laboratories*, 1980, no. GMR-3380, pp. 253–8.

[82] P. Donovan and B. Rymer., "Measurement of Tire Pavement Noise Sound Intensity Methodology," in *Proceedings of Asphalt Rubber 2003*, 2003.

[83] K. P. Biligiri, "Asphalt mixtures' properties indicative of tire/pavement noise," in *PhD Dissertation, ARIZONA STATE UNIVERSITY*, 2008.

[84] P. Donavan and L. Oswald, "Quantification of Noise Mechanisms of Blank, Rib, and Cross-Bar Tread Bias-Ply Truck Tires," in *General Motors Research Laboratories*, 1981, no.

GMR-3750.

[85] P. Donavan, “The Role of Acoustic Tube Resonances in the Radiation of Sound from Circumferentially Ribbed Truck Tires,” in *General Motors Research Laboratories*, 1981, no. GMR-3846.

[86] Y. Oshino and H. Tachibana, “Noise Source Identification on Rolling Tires by Sound Intensity Measurement,” in *Proceedings of the International Tire/Road Noise Conference 1990*, 1990, vol. 12, no. 2, pp. 87–92.

[87] O. Bschorr, A. Wolf, and J. Mittmann, “Theoretische und experimentelle Untersuchungen zur Abstrahlung von Reifenlärm,” in *Interim Report, Messerschmitt-Bölkow- Blohm GmbH*, 1981.

[88] O. Krauss and F. Gauterin, “Analysis of tire road noise using a tire cavity sound measurement system,” in *Proceedings - European Conference on Noise Control*, 2012, pp. 911–915.

[89] A. Bennetts and N. Crookes, “Advances in the measurement of road and tyre noise,” *Acoust. Bull.*, vol. 38, no. 4, pp. 35–38, 2013.

[90] J. Masino, B. Daubner, M. Frey, and F. Gauterin, “Development of a tire cavity sound measurement system for the application of field operational tests,” in *2016 Annual IEEE Systems Conference (SysCon). Proceedings*, 2016, p. 5 pp.-pp.

[91] ISO, “Acoustics -- Measurement of the influence of road surfaces on traffic noise -- Part 2: The close-proximity method,” *ISO/DIS 11819-2*, 2014.

[92] ISO, “Acoustics -- Measurement of the influence of road surfaces on traffic noise -- Part 2: The close-proximity method,” *ISO 11819-2*, 2000.

[93] E.-U. Saemann, G. Dimitri, and P. Kindt, “Tire Requirements for Pavement Surface Characteristics,” in *Presented at 7th Symposium on Pavement Surface Characteristics: SURF 2012 Norfolk, VA*, 2012, pp. 1–33.

[94] U. Sandberg and J. A. Ejsmont, “Noise emission, friction and rolling resistance of car tires - summary of an experimental study,” in *Proc. of NOISE-CON 2000, Newport Beach, California*, 2000.

[95] GB, “Acoustics - Measurement of Noise Inside Motor Vehicles,” in *Chinese Standard, GB/T 18697*, 2002.

[96] J. Chang, W. WanYing, J. XiaoXiong, C. Jin, W. Y. Wang, X. X. Jin, J. Chang, W. WanYing, and J. XiaoXiong, “Study on tire noise transfer path identification,” in *2010 10th International Conference on Signal Processing Proceedings (ICSP 2010)*, 2010, pp. 2629–2632.

[97] AASHTO, “Standard Method of Test for Measurement of Tire/Pavement Noise Using the On-Board Sound Intensity (OBSI) Method,” *AASHTO TP 76*, 2013.

[98] ASTM, “New Practice for Measurement of Tire/Pavement Noise Using the On-Board Sound Intensity (OBSI) Method,” *ASTM WK26025*, 2009.

[99] AASHTO, “Standard Method of Test for Measurement of Tire/Pavement Noise Using the On-Board Sound Intensity (OBSI) Method,” *AASHTO TP 76*, 2008.

[100] R. O. Rasmussen, “Tire-Pavement Noise Standards - An Update of Tire-Pavement Noise

Technical Working Group," in *Presentation at Pavement Evaluation 2010, Roanoke, Virginia*, 2010.

[101] L. Khazanovich and B. I. Izevbekhai, "Trend of pavement on board sound intensity with respect to texture degradation patterns in mnroad test cells," in *Institute of Noise Control Engineering of the USA - 23rd National Conference on Noise Control Engineering, NOISE-CON 08 and Sound Quality Symposium, SQS 08*, 2008, vol. 1, pp. 160–172.

[102] L. R. Wayson, M. J. MacDonaldA, and A. Martin, "On-Board Sound Intensity (OBSI) Study: Phase 2," in *Final Report, FDOT Project No. #BDT06*, 2014, p. 145p-.

[103] R. L. Wayson, J. M. MacDonald, and M. Berrios, "On-board sound intensity measurements and results in Florida," in *24th National Conference on Noise Control Engineering 2010, Noise-Con 10, Held Jointly with the 159th Meeting of the Acoustical Society of America*, 2010, vol. 1, pp. 573–584.

[104] P. R. Donavan and D. Lodic, "Applicability of on-board sound intensity (OBSI) method to quantifying the effect of pavement type on tire-pavement noise," in *Institute of Noise Control Engineering of the USA - 23rd National Conference on Noise Control Engineering, NOISE-CON 08 and Sound Quality Symposium, SQS 08*, 2008, vol. 1, pp. 173–184.

[105] R. O. Rasmussen, R. C. Sohaney, P. R. Donavan, and B. C. Rymer, "Improving wayside noise measurements on roadways and at test tracks using on-board sound intensity," in *41st International Congress and Exposition on Noise Control Engineering 2012, INTER-NOISE 2012*, 2012, vol. 3, pp. 2583–2591.

[106] G. Wang, G. Smith, and R. Shores, "Pavement noise investigation on North Carolina highways: An on-board sound intensity approach," *Can. J. Civ. Eng.*, vol. 39, no. 8, pp. 878–86, 2012.

[107] P. R. Donavan and D. M. Lodico, "Evaluation of on-board sound intensity measurement parameters using a tire noise chassis dynamometer," in *41st International Congress and Exposition on Noise Control Engineering 2012, INTER-NOISE 2012*, 2012, vol. 3, pp. 2555–2569.

[108] M. Trevino and T. Dossey, "On-board sound intensity testing of PFC pavements in Texas," in *Institute of Noise Control Engineering of the USA - 22nd National Conference on Noise Control Engineering, NOISE-CON 2007*, 2007, vol. 1, pp. 423–434.

[109] D. E. Mogrovejo, G. W. Flintsch, E. D. de León Izeppi, and K. K. McGhee, "Effect of Air Temperature and Vehicle Speed on Tire/Pavement Noise Measured with On-Board Sound Intensity Methodology," in *The Transportation Research Board (TRB) 92nd Annual Meeting, Washington, D.C., January 13-17, 2013*, 2013.

[110] D. E. M. Carrasco, "Effect of Air Temperature , Vehicle Speed , and Pavement Surface Aging on Tire / Pavement Noise Measured with On-Board Sound Intensity Methodology," Virginia Tech, 2012.

[111] E. Haas, J. Hencken, and T. Bennert, "A statistical evaluation of one-third octave band frequencies measured using the on-board sound intensity method," in *41st International Congress and Exposition on Noise Control Engineering 2012, INTER-NOISE 2012*, 2012, vol. 11, pp. 9464–9475.

[112] R. O. Rasmussen and R. C. Sohaney, “Measuring and visualizing tire-pavement noise using on-board sound intensity,” in *ASTM Special Technical Publication*, 2012, vol. 1555 STP, pp. 160–169.

[113]D. E. Mogrovejo, G. W. Flintsch, E. D. De Leon Izeppi, K. K. McGhee, and R. A. Burdisso, “Short-term effect of pavement surface aging on tire-pavement noise measured with onboard sound intensity methodology,” *Transp. Res. Rec.*, no. 2403, pp. 17–27, 2014.

[114] W. F. Reiter Jr. and A. C. Eberhardt, “Truck tire vibration noise,” in *SAE Technical Papers*, 1974.

[115] T. P. Dare, “Generation mechanisms of tire-pavement noise,” Purdue University, 2012.

[116] JASO, “Test procedures for tire noise,” in *Japanese Automobile Standards Organization JASO C606-81*, 1981.

[117] S. Ullrich, “Drum-measurements of tyre noise as a function of roadway tempera- ture and circumferential forces,” in *Proceedings of INTER-NOISE 93, page 659, Leuven, Belgium*, 1993.

[118] U. Sandberg and J. A. Ejsmont, “Three basic methods for measurement of tire/road noise,” in *Proceedings of INTER-NOISE 84, page 93, Honolulu, HI*, 1984.

[119] U. Sandberg, “Review of comparative study of tire:road noise measurements on drums and road.” 1983.

[120] J. A. Ejsmont, “Tire/road noise: comparison of road and laboratory measurements and influence of some tire parameters on generation of sound,” Linköping, Sweden, 1982.

[121]B. Swieczko-Zurek, J. Ejsmont, G. Ronowski, S. S. Taryma, B. Świeczko-żurek, J. Ejsmont, G. Ronowski, and S. S. Taryma, “Comparison of road and laboratory measurements of tyre/road noise,” in *INTERNOISE 2014 - 43rd International Congress on Noise Control Engineering: Improving the World Through Noise Control*, 2014.

[122] ISO, “Acoustics - Test surface for road vehicle noise measurement,” in *Technical Report ISO 10844, International Organization for Standardization*, 1991.

[123] N.-A. Nilsson, “Principles in the control of external tire/road noise,” in *Proceedings of INTER-NOISE 82, page 123, San Francisco, CA*, 1982.

[124] R. J. Bernhard and W. D. Thornton, “Preliminary results using the tire/pavement test apparatus,” in *Proceedings of INTER-NOISE 03, Jeju, South Korea*, 2003.

[125] K. Ginn, “Tyre Noise Measurements Using Spatial Transformation of Sound Fields,” in *Proceedings of the International Tire/Road Noise Conference 1990, Gothenberg, Sweden, August, 1990*, 1990.

[126] R. J. Ruhala and C. B. Burroughs, “Tire/pavement interaction noise source identification using multi-planar nearfield acoustical holography,” in *SAE Technical Papers*, 1999, no. 724.

[127] S. Dumbacher, J. Blough, D. Hallman, and P. Wang, “Source identification using acoustic array techniques,” in *SAE Technical Papers*, 1995.

[128] B. Kim and T. Lee, “A Study on the Tire Noise,” in *Proceedings of Inter-Noise 2003, Seogwipo, Korea*, 2003.

[129] W. Hendricx and F. Mancosu, “Experimental Determination of the Noise Emitting Parts of a Rotating Tire in the European Research Project TINO,” in *SAE Paper 1999-01-1732, Society of Automotive Engineers Noise and Vibration Conference Proceedings, Traverse City, MI*, 1999.

[130] R. J. Ruhala and C. B. Burroughs, “Application of nearfield acoustical holography to tire/pavement interation noise emissions,” in *SAE Technical Papers*, 1997.

[131] R. J. Ruhala and C. B. Burroughs, “Separation of leading edge, trailing edge, and sidewall noise sources from rolling tires,” in *Proceedings - National Conference on Noise Control Engineering*, 1998, pp. 109–114.

[132] J.-G. Ih and A. Oey, “Effect of patterns on wave propagation and sound radiation over the tire surface,” in *41st International Congress and Exposition on Noise Control Engineering 2012, INTER-NOISE 2012*, 2012, vol. 2, pp. 1436–1441.

[133] D. S. Cho and S. Mun, “Determination of the sound power levels emitted by various vehicles using a novel testing method,” *Appl. Acoust.*, vol. 69, no. 3, pp. 185–195, 2008.

[134] D. S. Cho and S. Mun, “Study to analyze the effects of vehicles and pavement surface types on noise,” *Appl. Acoust.*, vol. 69, no. 9, pp. 833–843, Sep. 2008.

[135] W. D. Fonseca and S. N. Y. Gerges, “Development of a low cost system for pass-by noise beamforming measurements,” in *20th International Congress on Acoustics 2010, ICA 2010 - Incorporating Proceedings of the 2010 Annual Conference of the Australian Acoustical Society*, 2010, vol. 3, pp. 2123–2129.

[136] D. Yang, Z. Wang, B. Li, Y. Luo, and X. Lian, “Quantitative measurement of pass-by noise radiated by vehicles running at high speeds,” *J. Sound Vib.*, vol. 330, no. 7, pp. 1352–64, 2011.

[137] P. A. G. Zavala, J. R. D. F. Arruda, F. G. Bueno, G. Miranda, W. Mothio, and C. A. Adas, “Heavy vehicles pass-by noise beamforming using generalized inverse method and an optimized array,” in *SAE Technical Papers*, 2013, vol. 13.

[138] R. J. Lustberg, “Acoustic beamforming using microphone arrays,” Massachusetts Institute of Technology, 1993.

[139] T. Tanaka, “Identification Methods for Tire/Road Noise during Vehicle Operating Conditions with Acoustic Holography,” in *Proceedings of Inter-Noise 2004, Prague, Czech Republic, August*, 2004.

[140] J. Maillard and J. Jagla, “Auralization of non-stationary traffic noise using sample based synthesis - Comparison with pass-by recordings,” in *41st International Congress and Exposition on Noise Control Engineering 2012, INTER-NOISE 2012*, 2012, vol. 1, pp. 608–619.

[141] G. Tong, Q. Wang, K. Yang, and L. Wang, “Simulation on the radial tire wear noise,” in *Applied Mechanics and Materials*, 2014, vol. 488, pp. 1121–4.

[142] BASt (Federal Highway Research Institute), “Der Prüfstand Fahrzeug/Fahrbahn der BASt (Federal Highway Research Institute’s vehicle-pavement interaction test facility),” *http://www.bast.de/EN/Automotive_Engineering/Technology/Technology_node.html*. .

[143] R. J. Ruhala and C. B. Burroughs, “Localization of tire/pavement noise source regions,” *Noise Control Eng. J.*, vol. 56, no. 5, pp. 318–331, 2008.

[144] N. A. Nilsson, “External Tire/Road Noise from Trailing Contact Edge - The Excitation Process,” in *Report: IFM/TR-6.380.01*, 1980, p. 71p-.

[145] F. Conte and P. Jean, “CFD modelling of air compression and release in road cavities during tyre/road interaction,” in *EURONOISE 2006 - The 6th European Conference on Noise Control: Advanced Solutions for Noise Control*, 2006.

[146] R. J. Bernhard, W. D. Thornton, and J. Baumann, “Effects of Varying the Tire Cap Ply, Sidewall Filler Height and Pavement Surface Texture on Tire/Pavement Noise Generation.,” in *SQDH 2003-1, Final Report, Purdue University*, 2003, p. 90-.

[147] S. Sainty, A. Tawaf, J. J. Richard, Z. Mohamed, and X. Wang, “Analysis of potential solutions to audible tire cavity and rim coupling resonance noise,” in *American Society of Mechanical Engineers, Noise Control and Acoustics Division (Publication) NCAD*, 2012, vol. 6, pp. 4457–4463.

[148] X. Wang, Z. Mohamed, H. Ren, X. Liang, and H. Shu, “A study of tyre, cavity and rim coupling resonance induced noise,” *Int. J. Veh. Noise Vib.*, vol. 10, no. 1–2, pp. 25–50, 2014.

[149] E. M. Negrus and C. Teodorescu, “Testing and evaluation of tyre like component part of motor vehicle,” in *ISBN 973-648-027-5, BREN Publisher, Bucharest*, 2002, p. 102p.

[150] H. Yamauchi and Y. Akiyoshi, “Theoretical analysis of tire acoustic cavity noise and proposal of improvement technique,” *JSAE Rev.*, vol. 23, no. 1, pp. 89–94, 2002.

[151] T. K. Lee, B. S. Kim, and G. J. Kim, “The identification of tyre induced vehicle interior noise,” *Appl. Acoust. (UK)*, vol. 68, no. 1, pp. 134–56, 2000.

[152] W. F. Reiter and A. C. Eberhardt, “Experimental investigation of truck tire noise generated through tire vibration,” in *Proceedings of INTER-NOISE 74, Washington, D.C.*, 1974, p. 467.

[153] M. Bergmann, “Noise generation by tire vibrations,” in *Proceedings of INTER- NOISE 80, Miami, FL*, 1980, p. 239.

[154] K. J. Plotkin, M. L. Montroll, and W. R. Fuller, “The generation of tire noise by air pumping and carcass vibration,” in *Proceedings of INTER- NOISE 80, Miami, FL*, 1980, p. 273.

[155] U. Essers, W. Liedl, R. Eberspacher, E. Kohler, and R. Litschel, “Air-Borne, Structure-Borne and Laser-Optical Measurements of Tyre Noise Generating Mechanisms on Dry and Wet Surfaces,” p. 17p-.

[156] I. Sakamoto, T. Tanaka, T. Murakami, and S. Ogata, “Tire noise reduction by using sound absorbing material,” in *Proceedings of INTER- NOISE 99, Fort Lauderdale, FL*, 1999, p. 137.

[157] F. Anfosso-Lédée, “Modeling the local propagation effects of tire-road noise: Propagation filter between CPX and CPB measurements,” in *Proceedings of INTER-NOISE 04, Prague, Czech Republic*, 2004, p. 2543.

[158] P. Klein and J.-F. Hamet, “Tyre/road noise prediction with the HyRoNE model,” in *Proceedings of INTER-NOISE 07, Istanbul, Turkey*, 2007, p. 191.

[159] K. Yoshihisa, Y. Okada, T. Yokota, and T. Iwase, “Experimental study on the effects of wind and the ground on horizontal propagation of sound,” in *Proceedings of INTER-NOISE 06, Honolulu, HI*, 2006, p. 5540.

[160] U. Sandberg, “Semi-generic temperature corrections for tyre/road noise,” in *Proceedings of INTER-NOISE 04, Prague, Czech Republic*, 2004, p. 3302.

[161] J. L. Rochat, “Investigation of Temperature Correction for Tire/Pavement Noise Measurements.,” p. 70p-.

[162]F. R. Archibald, “An elementary analysis of a vehicle tire tread noise source,” *J. Sound Vib.*, vol. 34, no. 2, pp. 285–6, 1974.

[163] K. Iwao and I. Yamazaki, “A study on the mechanism of tire/road noise,” in *JSAE Review no. 17*, 1996, vol. 17, no. 2, pp. 139–144.

[164] J. A. Ejsmont, U. Sandberg, and S. Taryma, “Influence of tread pattern on tire/road noise,” in *Passenger Car Meeting, October 1, 1984 - October 4, 1984*, 1984, p. 9p-.

[165] U. Sandberg and L. Goubert, “Poroelastic Road Surface (PERS): A review of 30 years of R & D work,” in *Proc. of Inter-Noise 2011, Osaka, Japan*, 2011.

[166] D. A. Kuemmel, J. R. Jaeckel, A. Satanovsky, S. F. Shober, and R. B. Schmiedlin, “Impacts Related to Pavement Texture Selection.,” in *WI/SPR-06-96 MU-CHTE-97-01 Final Report*, 1997.

[167] F. E. Timmons, “An industry viewpoint of tire sound reduction and measurement methodology,” in *SAE Technical Papers*, 1976.

[168] M. Brusarosco, A. Cigada, and S. Manzoni, “Measurement and analysis of tyre and tread block dynamics due to contact phenomena,” *Veh. Syst. Dyn.*, vol. 49, no. 6, pp. 855–869, 2011.

[169] N. Zhang, J. Zhang, and Y. Wang, “Experimental verification of stick-slip motion between two rolling contact surfaces,” in *Advanced Materials Research*, 2011, vol. 230–232, pp. 1362–1366.

[170] A. R. Crowther and R. Singh, “Identification and quantification of stick-slip induced brake groan events using experimental and analytical investigations,” *Noise Control Eng. J.*, vol. 56, no. 4, pp. 235–55, 2008.

[171] N.-A. Nilsson, “Air resonant and vibrational radiation - possible mechanisms for noise from cross-bar tires,” in *Proc. International Tire Noise Conference, Stockholm, Sweden*, 1979, pp. 93–109.

[172] A. Kuijpers and G. van Blokland, “Tyre/road noise models in the last two decades: A critical evaluation,” in *Proceedings of Inter-Noise 2001, The Hague, Holland.*, 2001, p. 2494.

[173] P. Andersson, “Modelling interfacial details in tyre/road contact - Adhesion forces and non-linear contact stiffness,” *Doktorsavhandlingar vid Chalmers Tek. Hogsk.*, no. 2334, pp. 1–136, 2005.

[174] R. E. Hayden, “Roadside noise from the interaction of a rolling tire with the road surface,” in *Proceedings of the Purdue Noise Control Conference, Purdue University, Indiana, USA*, 1971.

[175] S. Kim, W. Jeong, Y. Park, and S. Lee, “Prediction method for tire air-pumping noise using a hybrid technique,” *J. Acoust. Soc. Am.*, vol. 119, no. 6, pp. 3799–3812, 2006.

[176] F. Wullens, “Modelling of the local deformation at the tyre/road contact for the description of air pumping,” *Acta Acust. united with Acust.*, vol. 89, no. SUPP., pp. S84–S84, 2003.

[177] E.-Y. Kim, S.-W. Hwang, and S.-K. Lee, “Image-based approach to optimize the tyre pitch sequence for a reduction in the air-pumping noise based on a genetic algorithm,” *Proc. Inst. Mech. Eng. Part D J. Automob. Eng.*, vol. 226, no. 9, pp. 1171–1184, 2012.

[178] R. C. Chanaud, “Experiment study of aerodynamic sound from a rotating disc,” *J Acoust Soc Am.*, vol. 45, no. 2, 1969.

[179] R. J. Ruhala, “A study of tire/pavement interaction noise using near-field acoustical holography,” in *PhD Dissertation, Pennsylvania State University*, 1999.

[180] I. D. Wilken, L. J. Oswald, R. Hickling, O. L. J., and R. Hickling, “Research on Individual Noise Source Mechanisms of Truck tires: Aeroacoustic Sources,” in *SAE Highway Tire Noise Symposium Proceedings P-70, Paper 762022, Detroit, Ml, Nov. 1976*, 1976, pp. 155–165.

[181] M. G. Richards, “Automotive tire noise: a comprehensive study,” *Sound Vib.*, vol. 8, no. 5, pp. 42–47, 1974.

[182] W. Kropp, K. Larsson, and S. Barrelet, “The influence of belt and tread band stiffness on the tyre noise generation mechanisms,” in *Proc. of the International Congress on Acoustics (ICA) 1998, Seattle, WA, USA*, 1998.

[183] H.-S. Kwon, J. S. Bolton, and D. L. Hallman, “Nearfield acoustical holography applied to sound radiation from tires,” in *Proceedings - National Conference on Noise Control Engineering*, 1998, pp. 103–108.

[184] M. G. Richards, “Cross lug tire noise mechanisms,” in *SAE Technical Papers*, 1976.

[185] O. Bschorr, “Reduction of tire noise,” in *Proc. of INTER-NOISE 85, Munich, Germany*, 1985, pp. 271–274.

[186] J. K. Thompson, “Plane wave resonance in the tire air cavity as a vehicle interior noise source,” *Tire Sci. Technol.*, vol. 23, no. 1, pp. 2–10, 1995.

[187] R. W. Scavuzzo, L. T. Charek, P. M. Sandy, and G. D. Shteinhauz, “Influence of wheel resonance on tire acoustic cavity noise,” in *SAE Technical Papers*, 1994.

[188] R. Gunda, S. Gau, and C. Dohrmann, “Analytical model of tire cavity resonance and coupled tire/cavity modal model,” *Tire Sci. Technol.*, vol. 28, no. 1, pp. 33–49, 2000.

[189]T. Sakata, H. Morimura, and H. Ide, “Effects of tire cavity resonance on vehicle road noise,” *Tire Sci. Technol.*, vol. 18, no. 2, pp. 68–79, 1990.

[190] L. Molisani, “A Coupled Tire Structure-Acoustic Cavity Model,” in *PhD Dissertation, Virginia Tech*, 2004.

[191] A. S. Waisanen and J. R. Blough, “Road noise TPA simplification for improving vehicle sensitivity to tire cavity resonance using helium gas,” in *SAE Technical Papers*, 2009.

[192] M. Kohli, S. N. Moorthy, M. V. Rao, and P. Raghavendran, “Experimental determination of acoustic cavity resonances of vehicle sub-systems,” in *SAE Technical Papers*, 2014, vol. 1.

[193] H. Periyathamby, “Helmholtz resonator for reducing tire cavity resonance and in-vehicle noise,” in *Can. Acoust. (Canada)*, 2004, vol. 32, no. 4, pp. 27–31.

[194] E.-J. Ni, D. S. Snyder, G. F. Walton, N. E. Mallard, G. E. Barron, J. T. Browell, and B. N. Aljundi, “Radiated noise from tire/wheel vibration,” *Tire Sci. Technol.*, vol. 25, no. 1, pp. 29–

42, 1997.

[195] R. Erixon, “Wave propagation in car tyres - A study of the wave types and vibrations of tyre carcass,” in *TRITA-FKT 1998:32, MWL, Royal Inst. of Technology, Stockholm, Sweden*, 1998.

[196] J. Pope and W. C. Reynolds, “Tire noise generation: The roles of tire and road,” in *SAE Technical Papers*, 1976.

[197] H. Koike, T. Fujikawa, Y. Oshino, and H. Tachibana, “Generation Mechanism Of Tire/Road Noise Part 2 Pipe Resonance In Tread Groove Of Tire,” in *Inter-Noise 99*, 1999.

[198] S. Fujiwara, K. Yumii, T. Saguchi, and K. Kato, “Reduction of tire groove noise using slot resonators,” *Tire Sci. Technol.*, vol. 37, no. 3, pp. 207–223, 2009.

[199] J. Eisenblaetter, S. J. Walsh, and V. V. Krylov, “Air-related mechanisms of noise generation by solid rubber tyres with cavities,” *Appl. Acoust.*, vol. 71, no. 9, pp. 854–860, 2010.

[200] A. Kitahara, T. Akashi, Y. Waki, H. Heguri, N. Warning, and C. Copyright, “Interior noise reduction by tire surface geometry and Helmholtz resonators on tread patterns,” in *40th International Congress and Exposition on Noise Control Engineering 2011, INTER-NOISE 2011*, 2011, vol. 1, pp. 608–613.

[201] N. A. Nilsson, S. Soederqvist, and O. Bennerhult, “Air-Resonant Radiation - A Possible Mechanism for High Frequency Noise from Cross-Bar Tires.,” in *Technical Report 6.084.02, IFM Akustikbyran AB, Stockholm, Sweden*, 1979, p. 86p-.

[202] B. Swieczko-Zurek, “Biological hazards in low noise, poroelastic road surfaces,” in *20th International Congress on Sound and Vibration 2013, ICSV 2013*, 2013, vol. 4, pp. 2813–2818.

[203] U. Sandberg, W. Kropp, and K. Larsson, “The Multi-Coincidence Peak around 1000 Hz in Tyre / Road Noise Spectra,” in *Euronoise Naples 2003*, 2003, vol. 89, no. SUPP., pp. 1–8.

[204] N.-A. Nilsson, “Possible method of reducing external tire noise,” in *Proceedings of the International Tire Noise Conference 1979, Stockholm, Sweden*, 1979.

[205] W. R. Graham, “Influence of tire geometry on the horn effect,” in *41st International Congress and Exposition on Noise Control Engineering 2012, INTER-NOISE 2012*, 2012, vol. 8, pp. 6995–7008.

[206] K. M. Li and W. K. Lui, “A study of the horn effect above a porous road pavement,” in *8th International Congress on Acoustics*, p. 4 pp.-pp.

[207] C.-Y. Kuo, R. A. G. Graf, A. P. Dowling, and W. R. Graham, “On the horn effect of a tyre/road interface, Part II: Asymptotic theories,” *J. Sound Vib.*, vol. 256, no. 3, pp. 433–445, 2002.

[208] R. A. G. Graf, C.-Y. Kuo, A. P. Dowling, and W. R. Graham, “On the horn effect of a tyre/road interface, Part I: Experiment and computation,” *J. Sound Vib.*, vol. 256, no. 3, pp. 417–431, 2002.

[209] B. Peeters, I. Ammerlaan, A. Kuijpers, and G. Van Blokland, “Reduction of the horn effect for car and truck tyres by sound absorbing road surfaces,” in *39th International Congress on Noise Control Engineering 2010, INTER-NOISE 2010*, 2010, vol. 5, pp. 3569–3578.

[210] A. D. Virmalwar, S. M. Athavale, and P. R. Sajanpawar, “Application Of Fem And

Experimental Techniques For Simulation Of Tyre/Road Air Pumping Noise, Horn Effect And Vibration Of Tyre Sidewalls," in *Inter-Noise 99*, 1999.

[211] K. Schaaf and D. Ronneberger, "Noise radiation from rolling tires - sound amplification by the 'horn-effect,'" in *Proceedings of Inter-Noise 1982, San Francisco, CA*, 1982, p. 131.

[212] T. Dare, W. Woldemariam, R. McDaniel, J. Olek, and R. Bernhard, "Comparing tests for near-grazing-incidence noise reduction and sound absorption tests for hot-mix asphalt," *Transp. Res. Rec.*, no. 2270, pp. 1–8, 2012.

[213] A. F. Seybert and J. Han, "Measurement of pavement absorption using ISO 13472-2," in *Proceedings - European Conference on Noise Control*, 2008, pp. 4907–4911.

[214] J. Guo, R. Zhang, and R. Wang, "Experimental research on sound absorption performance of low-noise pavement," in *Advanced Materials Research*, 2012, vol. 374–377, pp. 1400–1404.

[215] J. L. Rochat, P. Donavan, A. Seybert, and T. Dare, "Pavement sound absorption measurements in the U.S.," in *41st International Congress and Exposition on Noise Control Engineering 2012, INTER-NOISE 2012*, 2012, vol. 3, pp. 2612–2626.

[216] U. Sandberg, "ROAD TRAFFIC NOISE - THE INFLUENCE OF THE ROAD SURFACE AND ITS CHARACTERIZATION.," *Appl. Acoust.*, vol. 21, no. 2, pp. 97–118, 1987.

[217] F. Anfosso, A. Houari, and M. Ben Tahar, "On a possible influence of road stiffness on tire/road noise generation," *Acta Acust. united with Acust.*, vol. 89, no. SUPP., pp. S81–S82, 2003.

[218] M. J. Crocker, D. Hanson, Z. Li, R. Karjatkar, and K. S. Vissamraju, "Measurement of acoustical and mechanical properties of porous road surfaces and tire and road noise," in *Transportation Research Record*, 2004, no. 1891, pp. 16–22.

[219] U. Sandberg, W. Kropp, and K. Larsson, "The multi-coincidence peak around 1kHz in tyre/road noise spectra," *Acta Acust. united with Acust.*, vol. 89, no. SUPP., pp. S84–S84, 2003.

[220] IEC, "Electroacoustics – Sound Level Meters," *IEC 61672*, 2003.

[221] R. J. Bernhard, "Tire Noise Fundamentals," in *Presented at Universidade Estadual de Campinas, 2005 August 12*, 2005.

[222] T. Dare and R. Bernhard, "Accelerometer Measurements of Tire Tread Vibrations and Implications to Wheel-Slap Noise," *Tire Sci. Technol.*, vol. 41, no. 2, pp. 109–126, 2013.

[223] P. R. Donavan, "Tire-Pavement Interaction Noise Measurement under Vehicle Operating Conditions of Cruise and Acceleration," in *Society of Automotive Engineers Noise and Vibration Conference Proceedings*, 1993.

[224] D. B. Moore, "The Revised ISO 362 Standard for Vehicle Exterior Noise Measurement," *Sound & Vibration*, no. October, pp. 19–23, 2006.

[225] T. Senda, M. Nakai, M. Yokoi, and Y. Chiba, "Tire squeal," *Bull. Jpn. Soc. Mech. Eng.*, vol. 27, no. 231, pp. 2016–23, 1984.

[226] N. M. Trivisonno, J. R. Beatty, and R. F. Miller, "Origin of tire squeal -- 2," *Rubber Chem. Technol.*, vol. 41, no. 4, pp. 953–976, 1968.

[227] W. A. Leasure, D. M. Corley, D. R. Flynn, and J. S. Forrer, "Truck noise - I. peak A-weighted sound levels due to truck tires," in *Report No. OST/TST-72-1, National Bureau of Standards, Building Research Division, Washington, D.C., USA*, 1972.

[228] R. D. Kilmer, "Test Procedures for Future Tire Noise Regulations.," in *Proceedings P-70, SAE Highway Tire Noise Symposium, San Francisco, Soc. of Automotive Engineers, Warrendale, PA, USA*, 1976, p. 6p-.

[229] R. D. Kilmer, M. A. Cadoff, D. E. Mathews, and C. O. Shoemaker, "Effects of Load, Inflation Pressure and Tire Deflection on Truck Tire Noise Levels.," in *DOT-HS-803 874, US Department of Transportation, Washington, D.C.*, 1979, p. 49p-.

[230] M. C. P. Underwood, "THe origins of tire noise," in *University of Southampton, Inst. of Sound and Vibration Research, Southampton, United Kingdom*, 1980.

[231] P. M. Nelson, M. C. P. Underwood, and P. M. Nelson, "Lorry Tire Noise," *Veh. Noise Vib.*, no. C139/84, p. 50p-, 1984.

[232] J. C. Walker, "Noise Generated at the Tire-Road Interface," in *PhD Dissertation TD 1292, Dunlop Ltd., Birmingham, United Kingdom*, 1981.

[233] A. Köllman, "Ermittlung des Standes der Technik hinsichtlich der Geräuschemission von PKW-Reifen," in *Research Report 105 05 144, FIGE GmbH, Herzogenrath, Germany*, 1993.

[234] A. Wolf, B.-M. Schuh, and O. Krauss, "Erfassung des Wissenstandes über Reifen/Fahrbahngeräusche beim Nutzfahrzeug," in *FAT Schriftenreihe Nr. 97, Forschungsvereinigung Automobiltechnik e.v. (FAT), Frankfurt, Germany*, 1992.

[235] A. von Meier, G. J. van Bloklan, and G. Descornet, "The influence of texture and sound absorption on the noise of porous road surfaces," in *Proc. of the Second International Symposium of Road Surface Characteristics, 23-26 Jun 1992, Technical University of Berlin, Berlin, Germany*, 1992.

[236] D. Cantrell, "Airborne Tire Noise Generation – the Effects of Axle Weight, Tire Inflation Pressure, and Suspension Alignment," in *Noise & Vibration Laboratory, General Motors Proving Ground*, 1988.

[237] R. Wozniak, S. Taryma, and P. Mioduszewski, "Tire camber angle influence on tire-pavement noise," *Noise Control Eng. J.*, vol. 63, no. 3, pp. 216–224, 2015.

[238] H. F. Reinink, D. F. de Graaff, A. A. A. Peeters, and H. M. Peeters, "Tyre/road noise measurements of truck tyres," in *Report No. M+P.DWW.03.7.1 (5 February 2005), M+P Raadgevende ingenieurs bv, P.O. Box 2094, NL-5260 CB Vught, The Netherlands*, 2005.

[239] T. Tanizaki, K. Ueda, T. Murabe, H. Nomura, and T. Kamakura, "Discrimination between summer and winter tires using tire/road noises emitted by running vehicles," *IEEJ Trans. Ind. Appl.*, vol. 133, no. 5, pp. 558–565, 2013.

[240] VTI, "Effects of winter tyres – state of the art IN SWEDISH," in *VTI rapport 543*, 2006.

[241] D. Bekke, Y. Wijnant, T. Weegerink, and A. De Boer, "Tire-road noise: An experimental study of tire and road design parameters," in *42nd International Congress and Exposition on Noise Control Engineering 2013, INTER-NOISE 2013: Noise Control for Quality of Life*, 2013, vol. 1, pp. 173–180.

[242] E. U. Seamenn, “Development of low noise tyres in EU project SILENCE,” in *Proceedings of Paris Acoustics*, 2008.

[243] J. S. Yang, T. F. Fwa, G. P. Ong, and C. H. Chew, “Finite-element analysis of effect of wide-base tire on tire-pavement noise,” *Adv. Mater. Res.*, vol. 723, pp. 105–112, 2013.

[244] A. Kumar, A. Tandon, S. Paul, A. Singla, S. Kumar, P. Vijay, and U. D. Bhangale, “Influence of Tyre’s Dimensional Characteristics on Tyre-Pavement Noise Emission,” *Phys. Rev. Res. Int.*, vol. 1, no. 4, pp. 124–137, 2011.

[245] Z. Mohamed and X. Wang, “A study of tyre cavity resonance and noise reduction using inner trim,” *Mech. Syst. Signal Process.*, vol. 50–51, pp. 498–509, 2015.

[246] H. Oldenettel and H. J. Koster, “Test procedure for the quantification of rolling tire belt vibrations,” in *Vehicle System Dynamics*, 1997, vol. 27, no. Suppl.

[247]R. F. Keltie, “Analytical model of the truck tire vibration sound mechanism,” *J. Acoust. Soc. Am.*, vol. 71, no. 2, p. 359, 1982.

[248] A. Ivannikov, U. Haberkorn, and H. Langenberg, “Einflussgrössen auf Riefen/Fahrbahn-Geräusche eines LKW bei unterschiedlichen Fahrbedingunen,” in *FAT Schriftenreihe Nr. 158, Forschungsvereinigung Automobiltechnik e.v. (FAT), Germany (ISSN 0933-050 X)*, 1998.

[249] U. Sandberg and J. A. Ejsmont, “Influence of tyre rubber hardness on tyre/road noise emission,” in *Turkish Acoustical Society - 36th International Congress and Exhibition on Noise Control Engineering, INTER-NOISE 2007 ISTANBUL*, 2007, vol. 1, pp. 394–403.

[250] W.-T. Hung, Y.-K. Lam, C.-F. Ng, and R. C.-K. Leung, “The impacts of tyre hardness and tread depth on tyre/road noise,” in *20th International Congress on Sound and Vibration 2013, ICSV 2013*, 2013, vol. 4, pp. 2846–2852.

[251] D. B. Thrasher, “Effect of tread wear on tire/pavement interaction noise,” in *Inter-Noise 80. Noise Control for the 80’s. Proceedings of the 1980 International Conference on Noise Control Engineering*, pp. 277–80.

[252] R. H. Spelman, “Truck tires - Effects of design and construction on wear and noise,” in *SAE Technical Papers*, 1963.

[253] U. Sandberg and K.-P. Glaeser, “Effect of tyre wear on noise emission and rolling resistance,” in *Proceedings of INTER-NOISE 08, Shanghai, China*, 2008, p. 4066.

[254] R. C. Raabe and I. Burche, “Retreaded truck tire noise tests,” in *BT - Truck Meeting, November 4, 1974 - November 7, 1974*, 1974.

[255] FEHRL (Forum of European National Highway Research Laboratories), “Tyre/road noise,” in *FEHRL Final Report SI2.408210*, 2001.

[256] U. Sandberg, “Survey of noise emission from truck tires,” in *Proc. of Inter-Noise 91, Sydney, Australia*, 1991.

[257] M. Hasebe, “Experimental study of the noise generated by a passenger automobile equipped with studded and regular snow tyres,” *Appl. Acoust.*, vol. 17, no. 4, pp. 247–254, 1984.

[258] AASHTO, “Effects of Studded Tires,” in *TRB/NCHRP/SYN-32, Transportation Research*

Board, Washington, D.C.; Federal Highway Administration, Washington, D.C.;American Association of State Highway and Transportation Officials, Washington, D.C., 1975, p. 58p-.

[259] U. Sandberg, B. Kalman, and A. R. Williams, "The porous tread tire - The quietest pneumatic tire measured so far?," in *International Congress on Noise Control Engineering 2005, INTERNOISE 2005*, 2005, vol. 5, pp. 3996–4005.

[260] J. S. Bolton, H. J. Song, Y. K. Kim, and Y. J. Kang, "Wave number decomposition approach to the analysis of tire vibration," in *Proceedings - National Conference on Noise Control Engineering*, 1998, pp. 97–102.

[261] ISO, "Passenger car, truck, bus and motorcycle tyres -- Methods of measuring rolling resistance," *ISO 18164*, 2005.

[262] R. Stenschke and P. Vietzke, "Noise and use characteristics of modern car tyres (State of the art)," in *7th International Congress on Sound and Vibration, 4-7 July 2000, Garmisch-Partenkirchen, Germany*, 2000.

[263] J. Ejsmont, G. Ronowski, S. Taryma, P. Mioduszewski, S. Sobieszczyk, and B. Swieczko-Zurek, "Relations between tire/road noise and tire rolling resistance on different road pavements," in *41st International Congress and Exposition on Noise Control Engineering 2012, INTER-NOISE 2012*, 2012, vol. 11, pp. 9476–9485.

[264] C. Hoever and W. Kropp, "A simulation-based parameter study of car tyre rolling losses and sound generation," in *Proceedings - European Conference on Noise Control*, 2012, pp. 926–931.

[265] D. I. Hanson, R. S. James C, and C. NeSmith, "Tire/Pavement Noise Study," in *NCAT Report 04-02*, 2004, p. 49p-.

[266] Y. Che, W. Xiao, L. Chen, Z. Huang, C. Yong, X. Wangxin, C. Lijun, and H. Zhichu, "GA-BP Neural Network Based Tire Noise Prediction," *Adv. Mater. Res.*, vol. 443–444, pp. 65–70, 2012.

[267] J. Ge, J. Fan, Q. Gu, R. Qian, and L. Youming, "Design method and application of low noise tire," in *Symposium of International Rubber Conference 2004*, 2004.

[268] P. Cao, X. Yan, W. Xiao, and L. Chen, "A prediction model to coupling noise of tire tread patterns and road texture," in *Proceedings of the 8th International Conference of Chinese Logistics and Transportation Professionals - Logistics: The Emerging Frontiers of Transportation and Development in China*, 2008, pp. 2332–2338.

[269] S. Fong, "Tyre noise predictions from computed road surface texture induced contact pressure," in *Proceedings of INTER-NOISE 98 Christchurch, New Zealand*, 1998, pp. 137–140.

[270] N. Alt, K. Wolff, G. Eisele, and F. Pichot, "Fahrzeug Außen Geräuschsimulation (Vehicle exterior noise simulation)," *Automob. Zeitschrift*, vol. 108, pp. 832–36, 2006.

[271] Y. Liu, T. Li, Y. Liu, and Y. Su, "Optimize the Structure Parameters of Tread Pattern Based on the Fuzzy Genetic Arithmetic," in *2010 International Conference on Measuring Technology and Mechatronics Automation (ICMTMA 2010)*, 2010, vol. 2, pp. 860–3.

[272] P. R. Donavan, "Comparative measurements of tire/pavement noise in Europe and the United States," in *Noise News International 13.2*, 2005, pp. 46–53.

[273] U. Sandberg, J. A. Ejsmont, and E. Gustavsson, "Tire/Road Noise on Rubberized Asphalt and Cement Concrete Surfaces in Sweden.," p. 60p-, 1990.

[274] R. Rasmussen, "Measuring and modeling tire-pavement noise on various concrete pavement textures," *Noise Control Eng. J.*, vol. 57, no. 2, pp. 139–147, 2009.

[275] M. Li, A. Molenaar, M. van de Ven, R. Huurman, and W. van Keulen, "New Approach for Modelling Tyre/Road Noise," in *Inter-Noise 2009*, 2009.

[276] ISO, "Characterization of pavement texture by use of surface profiles -- Part 3: Specification and classification of profilometers," *ISO 13473-3*, 2002.

[277] ASTM, "Standard Test Method for Measuring Pavement Macrotexture Properties Using the Circular Track Meter," *ASTM E2157, ASTM, West Conshohocken, PA*, 2009.

[278] T. Dare and R. Bernhard, "Predicting tire-pavement noise on longitudinally ground pavements using a nonlinear model," in *38th International Congress and Exposition on Noise Control Engineering 2009, INTER-NOISE 2009*, 2009, vol. 1, pp. 405–415.

[279] U. Sandberg and J. A. Ejsmont, "Texturing of cement concrete pavements to reduce traffic noise," *Noise Control Eng. J.*, vol. 46, no. 6, p. 231, 1998.

[280] R. Rasmussen, S. Karamihas, E. Mun, and G. Chang, "Relating pavement texture to tire-pavement noise," in *Institute of Noise Control Engineering of the USA - 35th International Congress and Exposition on Noise Control Engineering, INTER-NOISE 2006*, 2006, vol. 1, pp. 422–431.

[281] FHWA, "Technical Advisory T 5040.36 – Surface Texture for Asphalt and Concrete Pavements," in *FHWA, Washington, DC*, 2005.

[282] ISO, "Characterization of pavement texture by use of surface profiles -- Part 5: Determination of megatexture," *ISO 13473-5*, 2009.

[283] ASTM, "Standard Test Method for Measuring Pavement Macrotexture Depth Using a Volumetric Technique," *ASTM E965*, 2006.

[284] ASTM, "Standard Practice for Calculating Pavement Macrotexture Mean Profile Depth," *ASTM E1845*, 2009.

[285] ISO, "Characterization of pavement texture by use of surface profiles -- Part 1: Determination of Mean Profile Depth," *ISO 13473-1*, 1997.

[286] V. V. Saykin, "Pavement macrotexture monitoring through sound generated by the tire-pavement interaction," in *Northeastern University, Master's Thesis*, 2011.

[287] ASTM, "Standard Practice for Computing International Roughness Index of Roads from Longitudinal Profile Measurements," *ASTM E1926*, 2008.

[288] ASTM, "Standard Test Method for Measuring Road Roughness by Static Level Method," *ASTM E1364*, 2012.

[289] T. Beckenbauer and A. Kuijpers, "Prediction of pass-by levels depending on road surface parameters by means of a hybrid model," in *Proceedings of Inter-Noise 2001, The Hague, Holland*, 2001, pp. 2528–2533.

[290] F. Wullens, W. Kropp, and P. Jean, "Quasi-3D versus 3D contact modelling for tyre/road

interaction," in *Proceedings of INTER-NOISE 04, Prague, Czech Republic*, 2004, p. 3318.

[291] R. O. Rasmussen, S. I. Garber, G. J. Fick, T. R. Ferragut, and P. D. Wiegand, "How to Reduce Tire-Pavement Noise- Interim Better Practices," 2008.

[292] P. Donavan, "Influence of PCC Surface Texture and Joint Slap on Tire/Pavement Noise Generation," in *Proceedings of Noise-Con 2004, Baltimore*, 2004, pp. 251–262.

[293] T. Dare and R. Bernhard, "Noise generation in contraction joints in Portland cement concrete," in *24th National Conference on Noise Control Engineering 2010, Noise-Con 10, Held Jointly with the 159th Meeting of the Acoustical Society of America*, 2010, vol. 1, pp. 561–572.

[294] T. Dare, R. Bernhard, and W. Thornton, "Effects of contraction joint width, fill condition, faulting and beveling on wheel-slap noise," *Noise Control Eng. J.*, vol. 59, no. 3, pp. 228–233, 2011.

[295] D. Marriner and C. Wakefield, "Modular expansion joint noise in B.C.," in *40th International Congress and Exposition on Noise Control Engineering 2011, INTER-NOISE 2011*, 2011, vol. 1, pp. 763–768.

[296] M. Behzad, M. Hodaei, and I. Alimohammadi, "Experimental and numerical investigation of the effect of a speed bump on car noise emission level," *Appl. Acoust.*, vol. 68, no. 11–12, pp. 1346–1356, 2007.

[297] ASTM, "Standard Test Method for Effective Porosity and Effective Air Voids of Compacted Bituminous Paving Mixture Samples," *ASTM D7063/D7063M*, 2011.

[298] U. Sandberg and P. Mioduszewski, "Gaining extra noise reduction and lower rolling resistance by grinding a porous asphalt pavement," in *41st International Congress and Exposition on Noise Control Engineering 2012, INTER-NOISE 2012*, 2012, vol. 8, pp. 6958–6969.

[299] G.-J. Van Blokland and A. Von Meier, "Reducing tyre/road noise with porous road surfaces and the effect of tyre choice," in *SAE Technical Papers*, 1993.

[300] P. Sachakamol and L. Dai, "Impact of porous pavement characteristics on tire/pavement noise emission from ARC roads," in *17th International Congress on Sound and Vibration 2010, ICSV 2010*, 2010, vol. 4, pp. 2464–2473.

[301] ISO, "Acoustics -- Determination of sound absorption coefficient and impedance in impedance tubes -- Part 1: Method using standing wave ratio," *ISO 10534-1*, 1996.

[302] ISO, "Acoustics -- Measurement of sound absorption properties of road surfaces in situ -- Part 1: Extended surface method," *ISO 13472-1*, 2002.

[303] ISO, "Acoustics -- Materials for acoustical applications -- Determination of airflow resistance," *ISO 9053*, 1991.

[304] ANSI/ASA, "American National Standard Method for Determining the Acoustic Impedance of Ground Surfaces," *ANSI/ASA S1.18*, 2010.

[305] C. H. Reyes and J. Harvey, "A method for predicting sound intensity noise levels using laboratory pavement cores," in *Proceedings of Noise-Con 2011, Portland, OR*, 2011, pp. 522–534.

[306] J. Hubelt, W. Bartolomaeus, and F. Wellner, "On the correlation between motor vehicle noise levels and in situ measurement data of airflow resistance, water permeability and sound absorption coefficient of open porous asphalts," in *Institute of Noise Control Engineering of the USA - 35th International Congress and Exposition on Noise Control Engineering, INTER-NOISE 2006*, 2006, vol. 2, pp. 1119–1123.

[307] B. Altreuther and T. Beckenbauer, "Dynamic measurement of air flow resistance," in *EURONOISE 2006 - The 6th European Conference on Noise Control: Advanced Solutions for Noise Control*, 2006, p. 6P–6P.

[308] AASHTO, "Standard Method of Test for Determining Dynamic Modulus of Hot-Mix Asphalt Concrete Mixtures," *AASHTO T 342*, 2011.

[309] U. Sandberg and L. Goubert, "PERSUADE - A European project for exceptional noise reduction by means of poroelastic road surfaces," in *40th International Congress and Exposition on Noise Control Engineering 2011, INTER-NOISE 2011*, 2011, vol. 1, pp. 673–683.

[310] S. A. Storeheier, "Preliminary Investigation on a Poroelastic Material Used as a Low Noise Road Surface.," in *SINTEF Foundation Ofscient and Industrial Research*, 1987, p. 41p-.

[311] N.-A. Nilsson and O. Sylwan, "New vibro-acoustical measurement tools for characterization of poroelastic road surfaces with respect to tire/road noise," in *Proceedings of the Tenth International Congress on Sound and Vibration*, 2003, pp. 4343–4350.

[312] ASTM, "Standard Test Method for Measuring Paved Surface Frictional Properties Using the Dynamic Friction Tester," *ASTM E1911*, 2009.

[313] W. K. Ng, P. S. Ng, and W. T. Hung, "Measurement of tyre/road surface noise with close-proximity method in Hong Kong," in *Proceedings of INTER-NOISE 09, Ottawa, Canada*, 2009, p. 1178.

[314] N. Neithalath, J. Weiss, and J. Olek, "Reducing the Noise Generated in Concrete Pavements through Modification of the Surface Characteristics," 2005.

[315] H. Bendsten, E. Kohler, and Q. Lu, "Acoustic Aging of Asphalt Pavements - A California Danish Comparison," in *Road Directate, Danish Road Institute, Report 171*, 2009.

[316] R. K. Kay, "Pavement Surface Condition Rating Manual," in *Washington State Department of Transportation Report*, 1992.

[317] MNDOT, "MnDOT Distress Identification Manual," in *Report, Minnesota Department of Transportation, Office of Materials and Road Research*, 2003.

[318] R. R. Boullosa and A. P. Lopez, "Tra," *Noise Control Eng. J.*, vol. 29, no. 2, p. 54, 1987.

[319] G. Descornet, "Vehicle noise emission on wet road surfaces," in *Proceedings of INTER-NOISE 00, Nice, France*, 2000, p. 4968.

[320] S. Kocak and M. E. Kutay, "Relationship between Material Characteristics of Asphalt Mixtures and Highway Noise," in *Paper No. 12-4309, TRB 91st Annual Meeting Compendium of Papers, TRB, National Research Council*, 2012.

[321]S. Konishi, T. Fujino, N. Tomita, and M. Sakamoto, "Temperature effect on tire/road noise," in *Proceedings - International Conference on Noise Control Engineering*, 1995, vol. 1, p. 147.

[322] F. Anfosso-LédéE and Y. Pichaud, “Temperature effect on tyre-road noise,” *Appl. Acoust.*, vol. 68, no. 1, pp. 1–16, 2007.

[323] A. Bae, S. M. Stoffels, and S. W. Lee, “Observed Effects of Subgrade Moisture on Longitudinal Profile,” in *Paper No. 06-2312, TRB 85th Annual Meeting Compendium of Papers CD-ROM, TRB, National Research Council, Washington, DC*, 2006.

[324] P. R. Donavan, “Investigations of the influence of lower frequency aerodynamic noise on interior cruise and exterior pass-By sound levels,” in *SAE Technical Papers*, 2012, vol. 5, no. 3.

[325] Z. Lou, “An experimental and numerical study of tire/pavement noise on Asphalt Rubber Concrete pavement,” University of Regina, 2007.

[326] G. Wang, H. Zhou, Z. Mao, and L. Gao, “Boundary element analysis of rolling tire noise,” in *Proceedings 2011 International Conference on Transportation, Mechanical, and Electrical Engineering, TMEE 2011*, 2011, pp. 1970–3.

[327] Y. Nakajima, Y. Inoue, and H. Ogawa, “Application of the boundary element method and modal analysis to tire acoustics problems,” *Tire Sci. Technol.*, vol. 21, no. 2, pp. 66–90, 1993.

[328] J. Biermann, O. von Estorff, S. Petersen, and H. Schmidt, “Computational model to investigate the sound radiation from rolling tires,” in *Tire Science and Technology*, 2007, vol. 35, no. 3, pp. 209–225.

[329] K. J. Plotkin and E. Stusnick, “A Unified Set of Models for Tire/Road Noise Generation,” in *Report: WR-81-26, 63p, Environmental Protection Agency, Arlington, VA. Office of Noise Abatement and Control*, 1981, p. 63p-.

[330] L. E. Kung, W. Soedel, T. Y. Yang, and H. W. Kim, “Free vibrations of a pneumatic tire wheel unit using a ring on a elastic foundation and a finite element model membrane,” *J. Sound. Vib.*, vol. 107, no. 2, p. 181, 1986.

[331] P. Bremner, J. Huff, and J. S. Bolton, “A model study of how tire construction and materials affect vibration-radiated noise,” in *SAE Technical Papers*, 1997.

[332] M. C. Bérengier, M. R. Stinson, G. A. Daigle, and J. F. Hamet, “Porous road pavements: Acoustical characterization and propagation effects,” *J. Acoust. Soc. Am.*, vol. 101, no. 1, p. 155, 1997.

[333] W. Kropp, “A Mathematical model of tyre noise generation,” *Heavy Veh. Syst.*, vol. 6, no. 1–4, pp. 310–329, 1999.

[334] Y.-J. Kim and J. S. Bolton, “Effect of Rotation on the Vibration Characteristics of Tires,” in *InterNoise 2002, The 2002 International Congress and Exposition on Noise Control Engineering Dearborn, MI, USA*, 2002.

[335] L. R. Molisani, R. A. Burdisso, and D. Tsihlas, “A coupled tire structure/acoustic cavity model,” *Int. J. Solids Struct.*, vol. 40, no. 19, pp. 5125–5138, 2003.

[336] B. S. Kim, G. J. Kim, and T. K. Lee, “The identification of sound generating mechanisms of tyres,” *Appl. Acoust.*, vol. 68, no. 1, pp. 114–133, 2007.

[337] P. Gu, Z. C. Feng, Y. Chen, Z. Li, P. Gu, Y. Chen, and Z. Li, “Modeling and experimental investigation of tire cavity noise generation mechanisms for a rolling tire,” in *SAE Technical*

Papers, 2009, vol. 2, no. 1, pp. 1414–1423.

[338] D. J. O'Boy and A. P. Dowling, "Tyre/road interaction noise-A 3D viscoelastic multilayer model of a tyre belt," *J. Sound Vib.*, vol. 322, no. 4–5, pp. 829–850, 2009.

[339]I. Lopez Arteaga, "Green's functions for a loaded rolling tyre," *Int. J. Solids Struct.*, vol. 48, no. 25–26, pp. 3462–3470, 2011.

[340] J. S. Bolton and R. Cao, "Effect of Rotation on the Natural Frequencies of Coupled Tire Structural-Acoustical Mode," in *Publications of the Ray W. Herrick Laboratories. Paper 94.*, 2013.

[341] S. Saigal and T. Y. Yang, "Free vibrations of a tire as a toroidal membrane," *J. Sound Vib.*, vol. 107, no. 1, pp. 71–82, 1986.

[342] C. Wright and G. H. Koopmann, "A Technique to Predict the Acoustic Radiation Characteristics of an Automobile Tire," *Tire Sci. Technol.*, vol. 14, no. 2, pp. 102–115, 1986.

[343] T. L. Richards, "Finite element analysis of structural-acoustic coupling in tyres," *J. Sound Vib.*, vol. 149, no. 2, pp. 235–243, 1991.

[344] W. Kropp, "Ein Modell zur Beschreibung des Rollgeräusches eines unprofiliertenGürtelreifens auf rauher Straβenoberfläche," in *Thesis, Fortschritt-Berichte Reihe 11, Nr 166, VDI Verlag, Düsseldorf*, 1992.

[345] F. De Roo and E. Gerretsen, "TRIAS - tyre road interaction acoustic simulation model," in *InterNoise 2000, The 29th International Congress and Exhibition on Noise Control Engineering 27-30 August 2000, Nice, FRANCE, Volume 4*, 2000, pp. 2488–2496.

[346] C.-M. Nilsson, "Waveguide finite elements applied on a car tyre," in *doctoral thesis, Department of Aeronautical and Vehicle Engineering, Royal Institute of Technology*, 2004.

[347] M. Brinkmeier, U. Nackenhorst, S. Petersen, and O. von Estorff, "A finite element approach for the simulation of tire rolling noise," *J. Sound Vib.*, vol. 309, no. 1–2, pp. 20–39, Jan. 2008.

[348] Y. Waki, K. Kozuki, and H. Heguri, "Estimation of noise radiating parts of a tire using the wave finite element method," in *40th International Congress and Exposition on Noise Control Engineering 2011, INTER-NOISE 2011*, 2011, vol. 1, pp. 577–584.

[349] I. Kido, S. Ueyama, M. Hashioka, S. Yamamoto, M. Tsuchiyama, and H. Yamaoka, "Tire and Road Input Modeling for Low-Frequency Road Noise Prediction," in *SAE Technical Papers*, 2011, vol. 4, no. 2, pp. 1277–1282.

[350] G. Tong, X. Jin, W. Tian, and K. Yang, "Simulation on factors affecting radial tire noise," *J. Converg. Inf. Technol. (South Korea)*, vol. 8, no. 8, pp. 209–16, 2013.

[351] N. Vlahopoulos, G. Zhang, W. Brophy, and M. Ramaswami, "Vehicle airborne noise analysis using the energy finite element method," in *SAE Technical Papers*, 2013, vol. 4.

[352] Y. Wei, X. Feng, Z. Fuqiang, and D. Xiang, "Simulation of rolling noise based on the mixed Lagrangian-Eulerian method," *Tire Sci. Technol.*, vol. 44, no. 1, pp. 36–50, 2016.

[353] L. Banz, H. Gimperlein, Z. Nezhi, and E. P. Stephan, "Time domain BEM for sound radiation of tires," *Comput. Mech.*, vol. 58, no. 1, pp. 45–57, 2016.

[354] M. J. Gagen, “Novel acoustic sources from squeezed cavities in car tires,” *J. Acoust. Soc. Am.*, vol. 106, no. 2, pp. 794–801, 1999.

[355] P. Gautam and A. J. Chandy, “Numerical investigation of the air pumping noise generation mechanism in tire grooves,” *J. Vib. Acoust. Trans. ASME, Pap. No VIB-15-1493*, vol. 138, no. 5, pp. 51002-51002–8, 2016.

[356] R. Rasmussen, T. Ferragut, E. Mun, and P. Wiegand, “A comprehensive field study on concrete pavement solutions for reducing tire-pavement noise,” in *Institute of Noise Control Engineering of the USA - 35th International Congress and Exposition on Noise Control Engineering, INTER-NOISE 2006*, 2006, vol. 1, pp. 412–421.

[357] T. Fujikawa, Y. Oshino, T. Mikami, and H. Tachibana, “Examination of road roughness parameters for abating tire vibration and radiated noise,” *Noise Control Eng. J.*, vol. 57, no. 2, pp. 77–83, 2009.

[358] T. Fujikawa, Y. Oshino, and H. Tachibana, “Effect of road roughness on tire/road noise - Approach by frequency analysis,” in *Turkish Acoustical Society - 36th International Congress and Exhibition on Noise Control Engineering, INTER-NOISE 2007 ISTANBUL*, 2007, vol. 5, pp. 3130–3134.

[359] S. A. Storeheier, “Investigation on road surface texture levels in tyre/road noise mitigation,” in *Proceedings of INTER-NOISE 04, page 3403, Prague, Czech Republic*, 2004.

[360] RLS, “Richtlinien für den Lärmschutz an Strassen,” in *BM für Verkehr, Bonn*, 1990.

[361] A. Cocchi, A. Farina, and G. Lopes, “Modelli matematici per la previsione del rumore stradale: verifica ed affinazione del modello CNR in base a rilievi sperimentali nella città di Bologna,” in *Acta of 19° Convegno Nazionale AIA*, 1991.

[362] Federal Highway Authority, “FHWA Traffic Noise Model Users Guide,” in *US Department of Transportation, Report N. FHWA-PD-96-009 and DOT-VNTSC-FHWA-98-1*, 1998.

[363] S. Kephalopoulos, M. Paviotti, and F. Anfosso-Ledee, “Common Noise Assessment Methods in Europe (CNOSSOS-EU),” in *European Commission Joint Research Centre, Luxembourg publications Office of the European Union*, 2012.

[364] A. Ongel, E. Kohler, and J. Harvey, “Principal components regression of onboard sound intensity levels,” *J. Transp. Eng.*, vol. 134, no. 11, pp. 459–66, 2008.

[365] Y. Zhang, J. G. McDaniel, and M. L. Wang, “Estimation of Pavement Macrotexture by Principal Component Analysis of Acoustic Measurements,” *J. Transp. Eng.*, vol. 140, no. 2, p. 04013004 (11 pp.)-pp., 2014.

[366] M. Li, W. van Keulen, H. Ceylan, G. Tang, M. van de Ven, and A. Molenaar., “Influence of Road Surface Characteristics on Tire-Road Noise for Thin-Layer Surfacings,” *J. Transp. Eng.*, vol. 141, no. 11, 2015.

[367] S. Roychowdhury, “Fuzzy curve fitting using least square principles,” in *Proceedings of the IEEE International Conference on Systems, Man and Cybernetics*, 1998, vol. 4, pp. 4023–4027.

[368] J. Fry, P. Jennings, N. Taylor, and P. Jackson, “Vehicle drive-by noise prediction: A neural networks approach,” in *SAE Technical Paper Series 1999-01-1740*, 1999.

[369] X.-H. Li, J. Liu, D.-Q. Liu, and K.-M. Sun, “Application of tread patterns noise-reduction based on self-adaptive fuzzy genetic algorithm,” *Comput. Eng. Appl.*, vol. 45, no. 22, 2009.

[370] B. Yu and Q. Lu, “Bayesian model for tyre/asphalt pavement noise,” *Proc. Inst. Civ. Eng. - Transp.*, vol. 166, no. 4, pp. 241–252, 2013.

[371] A. Kuijpers and G. van Blokland, “Tyre/road noise modeling: The road from a tyre’s point-of-view,” in *Proceedings of Inter-Noise 2003, The 32nd International Congress and Exposition on Noise Control Engineering Jeju International Convention Center, Seogwipo, Korea, August 25-28, 2003*, 2003, p. 249.

[372] E. Rustighi, S. J. Elliott, S. Finnveden, K. Guly, T. Mocsai, and M. Danti, “Linear stochastic evaluation of tyre vibration due to tyre/road excitation,” *J. Sound Vib.*, vol. 310, no. 4–5, pp. 1112–27, 2008.

[373] G. Dubois, J. Cesbron, F. Anfosso-Lédée, and H. P. Yin, “A Multi-Asperity Tyre/Road Contact Model for Rolling Noise Prediction,” in *Forum Acusticum 2011*, 2011.

[374] G. Dubois, J. Cesbron, H. P. Yin, F. Anfosso-Ledee, and D. Duhamel, “Statistical estimation of low frequency tyre/road noise from numerical contact forces,” *Appl. Acoust.*, vol. 74, no. 9, pp. 1085–1093, 2013.

[375] J. Winroth, C. Hoever, W. Kropp, and T. Beckenbauer, “The contribution of air-pumping to tyre/road noise,” in *Proceedings of AIA-DAGA 2013*, 2013, pp. 1594–1597.

[376] Z. Mohamed and X. Wang, “A deterministic and statistical energy analysis of tyre cavity resonance noise,” *Mech. Syst. Signal Process.*, vol. 70–71, pp. 947–957, 2016.

[377] Department for Transport, “Calculation of Road Traffic Noise,” in *Department for Transport Welsh Office, ISBN 0 11 550847 3*, 1988.

[378] “Bruit des infrastructures de transports terrestres,” *French Stand. XPS 31-133*, 2001.

[379] L. Dai and H. S. Lee, “Ray acoustics approach to quantitative prediction of highway traffic noise,” in *ASME International Mechanical Engineering Congress and Exposition, Proceedings (IMECE)*, 2010, vol. 8, no. PARTS A AND B, pp. 223–228.

[380] Y. Wei, Q. Feng, H. Wang, and M. Kaliske, “A hybrid numerical-experimental analysis for tire air-pumping noise with application to pattern optimization,” *Noise Control Eng. J.*, vol. 64, no. 1, pp. 56–63, 2016.

[381] J. Fry and P. Jennings, “Using Multi-Layer Perceptrons to Predict Vehicle Pass-By Noise,” *Neural Comput Appl*, vol. 11, no. 3, pp. 161–7, 2003.

[382] T. Li, J. Feng, R. Burdisso, and C. Sandu, “The Effects of Tread Pattern on Tire Pavement Interaction Noise,” in *45th International Congress and Exposition on Noise Control Engineering: Towards a Quieter Future, INTER-NOISE 2016 Hamburg, Germany, August 21-24, 2016*, 2016, pp. 2185–2196.

[383] T. Li, J. Feng, R. Burdisso, and C. Sandu, “The Effects of Speed on Tire-Pavement Interaction Noise (Tread-Pattern-Related Noise and Non-Tread-Pattern-Related Noise),” in *35th Annual Meeting and Conference on Tire Science and Technology, September 13-14, 2016, Akron, Ohio, USA*, 2016.

[384] J. A. E. S. Taryma, “Halas Opon Samochodow Osobowych Poruszajacych Sie Posuchych

Nawierzchniach asfaltowych I Betonowych," in *Ph.D Thesis, Technical university of Gdansk, Poland. (In Polish)*, 1982.

[385] L. E. Kinsler, A. R. Frey, A. B. Coppens, and J. V Sanders, "Fundamentals of acoustics," *4th Edition. ISBN 0-471-84789-5. Wiley-VCH*. p. 560, 1999.

[386] A. Schuhmacher, "Blind Source Separation Applied to Indoor Vehicle Pass-By Measurements," *SAE Int. J. Passeng. Cars - Mech. Syst.*, vol. 8, no. 3, pp. 1034–1041, 2015.

[387] L. Tarassenko, *Guide to Neural Computing Applications*. Butterworth-Heinemann, 1998.

[388] J. H. Friedman, R. Tibshirani, and T. Hastie, *The Elements of Statistical Learning*. Springer, Berlin, 2001.

[389] M. H. Beale, M. T. Hagan, and H. B. Demuth, *Neural network toolbox 7*. User's Guide, MathWorks, 2010.

[390] C. Yong, X. Wangxin, and C. Lijun, "Laboratory test and spectrum analysis method of tire noise," in *2009 International Conference on Measuring Technology and Mechatronics Automation (ICMTMA), IEEE Press, Apr. 2009*, 2009, vol. 1, pp. 487–490.

[391] ISO, "Acoustics -- Specification of test tracks for measuring noise emitted by road vehicles and their tyres," *ISO 10844*, 2014.

[392] P. D. Wasserman, *Advanced Methods in Neural Computing*. Van Nostrand Reinhold, New York, 1993.

[393] R. N. Neal, *Bayesian learning for Neural Networks*. Springer-Verlag, 1996.

[394] U. Kumar, J. Prakash, G. Unnikrishnan, and T. Thomas, "Tire Pitch Sequence Optimization using HyperStudy," in *Altair Technology Conference, India*, 2013.

[395] P. Kostial, Z. Jancikova, D. Bakosova, J. Valicek, M. Harnicarova, I. Spicka, P. Kotial, D. Bakoova, and I. picka, "Artificial Neural Networks Application in Modal Analysis of Tires," *Meas. Sci. Rev.*, vol. 13, no. 5, pp. 273–278, 2013.

[396] W. Kongrattanaprasert, H. Nomura, T. Kamakura, and K. Ueda, "Application of neural network analysis to automatic detection of road surface conditions utilizing tire noise from vehicles," in *2009 ICROS-SICE International Joint Conference. ICCAS-SICE 2009*, 2009, pp. 2354–8.

[397] W. Kongrattanaprasert, H. Nomura, T. Kamamura, and K. Ueda, "Automatic detection of road surface states from tire noise using neural network analysis," in *20th International Congress on Acoustics 2010, ICA 2010 - Incorporating Proceedings of the 2010 Annual Conference of the Australian Acoustical Society*, 2010, vol. 4, pp. 2965–2968.

[398] M. Kandpal, V. K. Kakar, and G. Verma, "Classification of ground vehicles using acoustic signal processing and neural network classifier," in *2013 International Conference on Signal Processing and Communication, ICSC 2013*, 2013, pp. 512–518.

[399] Y. Nakajima, H. Kadowaki, T. Kamegawa, and K. Ueno, "Application of a Neural Network for the Optimization of Tire Design," *Tire Sci. Technol.*, vol. 27, no. 2, pp. 62–83, 1999.

[400] M. El-Gindy, H. L. Lewis, and A. S. Lewis, "Development of a tire/pavement contact-stress model based on an artificial neural network," *Am. Soc. Mech. Eng. Des. Eng. Div.*, vol. 101, pp. 25–34, 1999.

[401] M. El-Gindy and H. Lewis, “Development of a Tire/Pavement Contact-Stress Model Based on Artificial Neural Networks,” in *Final Report No. FHWA-RD-99-041*, 2001.

[402] J. Oddershede and J. Kragh, “Changes in noise levels from Standard Reference Test Tyres due to increasing tyre tread hardness,” in *Proceedings of Forum Acusticum, v 2014-January, 2014, Forum Acusticum, FA 2014*, 2014.

[403] F. Wullens and W. Kropp, “Influence of the local stiffness of the rubber layer of the tire on the generation of tire/road noise,” in *Proc. of ICA 2001, Rome, Italy*, 2001.

[404] F. Wullens, “Towards an optimisation of tire/road parameters for noise reduction,” in *Lic Thesis, Report F 02-01, Dept. of Applied Acoustics, Chalmers Univ. of Technology, Gothenburg, Sweden*, 2002.

[405] D. Rochoux and F. Biesse, “Tire/road noise, the tire vibration as the main noise source from road texture,” in *39th International Congress on Noise Control Engineering 2010, INTER-NOISE 2010*, 2010, vol. 5, pp. 3597–3606.

[406] T. Watanabe, N. Tomita, S. Kishinami, H. Yamaguchi, S. Konishi, and A. Kawana, “Noise generation mechanism of cross-bar tyres and countermeasures against it,” *Int. J. Veh. Des.*, vol. 9, no. 6, pp. 641–653, 1988.

[407] K.-Y. Ho, W.-T. Hung, C.-F. Ng, Y.-K. Lam, R. Leung, and E. Kam, “The effects of road surface and tyre deterioration on tyre/road noise emission,” *Appl. Acoust.*, vol. 74, no. 7, pp. 921–925, 2013.

[408] E. Buhlmann, S. Schulze, and T. Ziegler, “Ageing of the new CPX reference tyres during a measurement season,” in *42nd International Congress and Exposition on Noise Control Engineering 2013, INTER-NOISE 2013: Noise Control for Quality of Life*, 2013, vol. 1, pp. 369–376.

[409] B. Swieczko-Zurek, J. Ejsmont, P. Mioduszewski, G. Ronowski, and S. Taryma, “The effect of tire aging on acoustic performance of CPX reference tires,” in *INTER-NOISE 2015 - 44th International Congress and Exposition on Noise Control Engineering*, 2015.

[410] S. Schubert, M. Mannel, M. Ertsey, and C. Hoever, “Influence of the tyre impedance on CPX level used to evaluate tyre/road noise,” in *Proceedings of the INTER-NOISE 2016 - 45th International Congress and Exposition on Noise Control Engineering: Towards a Quieter Future*, 2016, pp. 4945–4954.

[411] E.U. Saemann, “Contribution of the tyre to further lowering tyre/road noise,” in *Proceedings of ParisAcoustics’08*, 2008.

[412] Langwieder et al., “Die Ergebnisse des ReifenCheck 2001 und deren Bedeutung für die Verkehrs- sicherheit (in German),” in *VDI-Berichte Nr. 1632, 2001, VDI, Germany*, 2001.

[413] M. Gothié, “Information presented at the meeting of PIARC/C1 in Copenhagen, Denmark, September 2001,” in *Presentation by by Mr Gothié of LCPC in Lyon, France*, 2001.

[414] M. Gothié, “Presentation at the meeting of PIARC/C1 in Rome, Italy, October 2005,” in *Presentation by Mr Gothié of LCPC in Lyon, France*, 2005.

[415] U. Sandberg and J. Ejsmont, “Tire/road noise - a subject of international concern,” in *Proceedings of INTER-NOISE 88, page 1309, Avignon, France*, 1988.

[416]S. A. Storeheier and U. Sandberg, “Vehicle Related Parameters Affecting Tyre/Road Noise,” in *Proceedings of the International Tire/Road Noise Conference 8-10 August 1990 Gothenburg, STU-information No. 794-1990, NUTEK, Stockholm*, 1990.

[417] S. Ulrich, “Rollgeräuschmessungen der Bundesanstalt für Strassenwesen an Strassen mit unterschiedlichen Decken und an einem Innentrommelprüfstand (Rolling noise measurements of the Federal Highway Research Institute on roads with different ceilings and an indoor drum,” in *Mitteilung Nr. 57, Institut für Strassen- und Eisenbahn- und Felsbau and der E.T.H. Zürich*, 1984, p. 207.

[418] X. Pei, G. Wang, H. Zhou, F. Zhao, and J. Yang, “Influence of tread structure design parameters on tire vibration noise,” in *Proceedings of SAE-China Congress 2015: Selected Papers Volume 364 of the series Lecture Notes in Electrical Engineering*, 2015, pp. 325–338.

[419] Y. Tanaka, S. Horikawa, and S. Murata, “An evaluation method for measuring SPL and mode shape of tire cavity resonance by using multi-microphone system,” *Appl. Acoust.*, vol. 105, pp. 171–178, 2016.

[420]Anonymous, “Truck Tire Noise,” in *Rubber Manufacturers Association (RMA), Washington, D.C., USA*, 1971.

[421] J. C. Walker and A. R. Williams, “The improvement of noise and traction due to road/tire interaction,” in *Proceedings of International Tire Noise Conference 1979, Stockholm, Sweden*, 1979.

[422] D. Tetlow, “Truck tire noise - an initial survey of tire noise variables,” in *General Motors Proving Ground Report*, 1968.

[423] E. Köhler and W. Liedl, “Grenzen der Beeinflussungdes Reifenabrollgerausches bei nasser Fahrbahn,” in *Entwicklungslinien in Kraftfahrzeu-technik und Strassenverkehr, Forschungsbilanz 1981, Verlag TUV Rheinland, Germany*, 1981.

[424] H. Steven and H. Pauls, “Entwicklung eines Messverfahrens für das Reifen-Fahrbahn-Geräusch,” in *Report from FIGE, Herzogenrath, Germany*, 1990.

[425] H. Steven, D. Küppers, G. J. van Blokland, M. H. van Houten, and R. van Loon, “International validation test for the close proximity (CPX) method,” 2000.

[426] Y. J. Kim and J. S. Bolton, “Effects of rotation on the dynamics of a circular cylindrical shell with application to tire vibration,” *Journal of Sound and Vibration*, vol. 275, no. 3–5. pp. 605–621, 2004.

[427] S. C. Huang and W. Soedel, “Effects of coriolis acceleration on the free and forced in-plane vibrations of rotating rings on elastic foundation,” *Journal of Sound and Vibration*, vol. 115, no. 2. pp. 253–274, 1987.

[428] S. C. Huang and W. Soedel, “Effects of Coriolis acceleration on the forced vibration of rotating cylindrical shells,” *J. Appl. Mech.*, vol. 55, pp. 231–233, 1988.

[429] K. Takami and T. Furukawa, “Study of Tire Noise Characteristics With High-Resolution Synchronous Images,” in *EURONOISE, Maastricht, The Netherlands, May 31–June 3*, 2015, pp. 2113–2118.

[430] K. Takami and T. Furukawa, “High-resolution deformation measurement system for fast rotating tires,” in *Proceedings of the ASME Design Engineering Technical Conference*, 2015,

vol. 8, p. 6 pp.

[431]M. J. Gagen, “Nonlinear acoustic sources in squeezed car tyre cavities,” *Noise Vib. Worldw.*, vol. 31, no. 4, pp. 9–19, 2000.

[432] Robert Bosch GmbH, *Automotive Handbook*, 6th ed. SAE, 2004.

[433] S. Samuels, “Recent Australian Tyre/Road Noise Research,” in *Proc. of the International Tire Noise Conference, STU-information No. 168-1980, NUTEK, Stockholm*, 1979, pp. 1–25.

[434] Anonymous, “Foreign Research in TIre Noise,” in *Office of Noise Abatement and Control, U.S., Environmental Protection Agency*, 1980.

[435] M. Muthukrishnan, “Effects of material properties on tire noise,” in *SAE Technical Papers*, 1990.

[436] G. Tong, Q. Wang, K. Yang, and X. C. Wang, “An experiment investigation to the radial tire noise,” in *Advanced Materials Research*, 2013, vol. 694 697, pp. 400–4.

[437] P. Kindt, F. De Coninck, P. Sas, and W. Desmet, “Analysis of tire/road noise caused by road impact excitations,” in *SAE Technical Papers*, 2007.

[438] P. Kindt, F. De Coninck, P. Sas, and W. Desmet, “Experimental modal analysis of radial tires under different boundary conditions,” in *13th International Congress on Sound and Vibration 2006, ICSV 2006*, 2006, vol. 6, pp. 5111–5118.

[439] B. V. S. S. Bharadwaja and P. N. Siva, “A Numerical Study on the Influencing Parameters of Tire-acoustic Cavity,” in *Applied Mechanics and Materials*, 2013, vol. 459, pp. 390–5.

[440] R. S. McDaniel, K. J. Kowalski, A. Shah, J. Olek, and R. J. Bernhard, “Long-Term Performance of a Porous Friction Course,” in *FHWA/IN/JTRP-2009/22, Joint Transportation Research Program, Indiana Department of Transportation and Purdue University, West Lafayette, IN*, 2010.

[441] K. J. Kowalski, R. S. McDaniel, and J. Olek, “Identification of Laboratory Technique to Optimize Superpave HMA Surface Friction Characteristics,” in *FHWA/IN/JTRP-2010/06, Joint Transportation Research Program, Indiana Department of Transportation and Purdue University, West Lafayette, IN*, 2010.

[442] S. E. Paje, M. Bueno, F. Teran, and U. Vinuela, “Monitoring road surfaces by close proximity noise of the tire/road interaction,” *J. Acoust. Soc. Am.*, vol. 122, no. 5, pp. 2636–2641, 2007.

[443] T. Dare, T. Wulf, W. Thornton, and R. J. Bernhard, “Acousti- cal e↵ects of grinding and grooving on Portland cement concrete pavements,” in *Technical report, The Institute for Safe, Quiet and Durable Highways*, 2009.

[444] K. W. Anderson, J. S. Uhlmeyer, T. Sexton, M. Russell, and J. Weston, “Evaluation of Long-Term Pavement Performance and Noise Characteristics of the Next Generation Concrete Surface: Final Report.,” in *Washington (State). Dept. of Transportation, WA-RD 767.2*, 2014, p. 52p-.

[445] J. Hencken, E. Haas, and T. Bennert, “Using Tire/Pavement Interface Noise Results to Define Statistically Similar Bituminous Pavements in Massachusetts,” in *Presented at 7th Symposium on Pavement Surface Characteristics: SURF 2012 Norfolk, VA*, 2012.

[446] J. S. Miller and W. Y. Bellinger., “Distress identification manual for the long-term pavement performance program,” in *FHWA Report No. FHWA-RD-03-031*, 2003.

[447] J.-F. Hamet and P. Klein, “Use of a rolling model for the study of correlation between road texture and tire noise,” in *The 2001 International Congress and Exhibition on Noise Control Engineering, The Hague, The Netherlands*, 2001.

[448] S. Huschek, “Characterization of pavement surface texture and its influence on tire/road noise,” in *Proceedings of the Third International Symposium on Pavement Surface Characteristics: Christchurch, New Zealand 3-4 September 1996*, 1996.

[449] D.-C. He and L. Wang, “Texture features based on texture spectrum,” *Pattern Recognition*, vol. 24, no. 5. pp. 391–399, 1991.

[450] Y. G. Lee, J. H. Lee, and Y. C. Hsueh, “Texture classification using fuzzy uncertainty texture spectrum,” *Neurocomputing*, vol. 20, no. 1–3, pp. 115–122, 1998.

[451] L. Wang and D.-C. He, “Texture classification using texture spectrum,” *Pattern Recognition*, vol. 23, no. 8. pp. 905–910, 1990.

[452] ISO, “Characterization of pavement texture by use of surface profiles -- Part 4: Spectral analysis of surface profiles,” *ISO/TS 13473-4*, 2008.

[453] J.-F. Hamet and P. Klein, “Road texture and tire noise,” in *Proceedings of Inter-Noise 2000, Nice, France*, 2000, pp. 178–183.

[454] P. Gautam and A. J. Chandy, “A Three-Dimensional Numerical Investigation of Air Pumping Noise Generation in Tires,” *J. Vib. Acoust. Trans. ASME*, vol. 138, no. 6, 2016.

Appendix A: Tread Pattern Analysis

A.1 2D Tread Pattern

The digitized two-dimensional tread patterns for the test tires are displayed in Table A.1. Note that the tread profile data of Tire 49 is artificially generated instead of from scanning, but should be similar to real data.

Table A.1: 2D tread patterns of test tires

Tire No.	2D Tread Pattern
01	
02	
03	
04	
05	
06	
07	
08	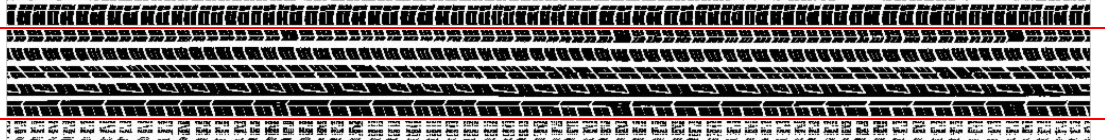
09	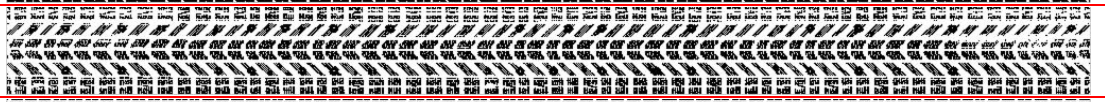
10	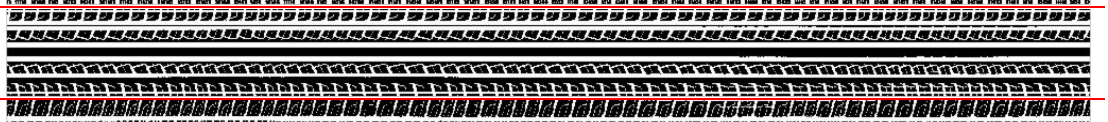
11	

Tire No.	2D Tread Pattern
12	
13	
14	
15	
16	
17	
18	
19	
20	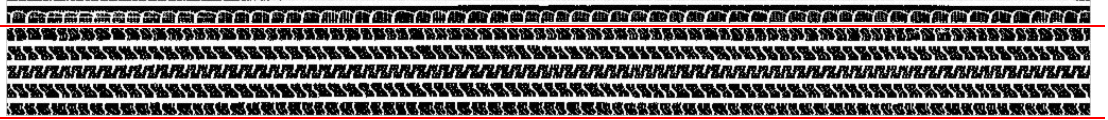
21	N/A (slick tire)
22	
23	
45	
49	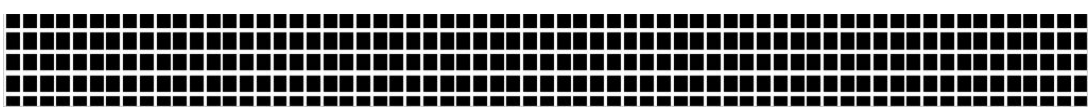
55	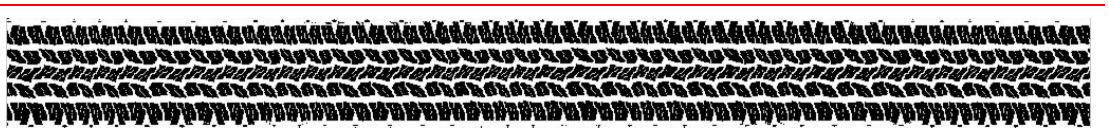

A.2 Tread Profile Spectra for Circumferential Sections

The tread profile power spectra for all circumferential sections are displayed in Figure A.1.

Tire 01

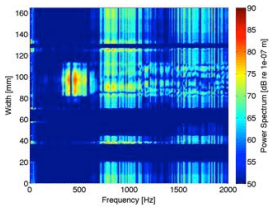

Tire 02

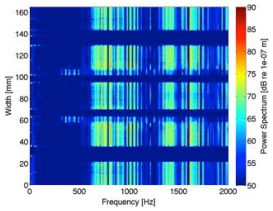

Tire 03

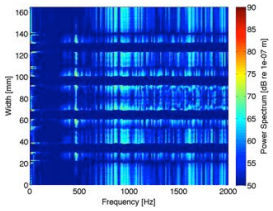

Tire 04

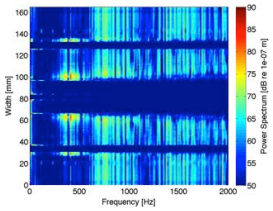

Tire 05

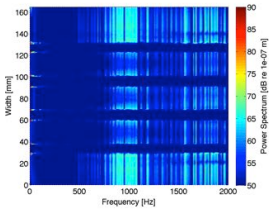

Tire 06

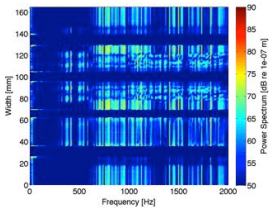

Tire 07

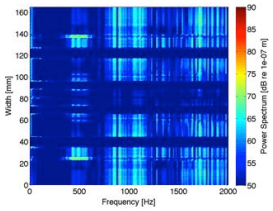

Tire 08

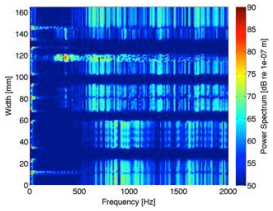

Tire 09

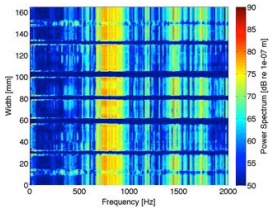

Tire 10

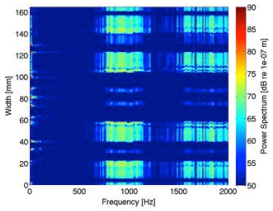

Tire 11

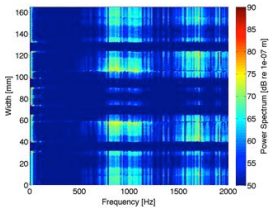

Tire 12

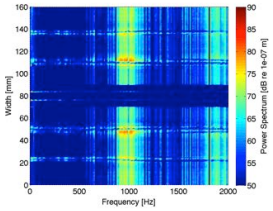

Tire 13

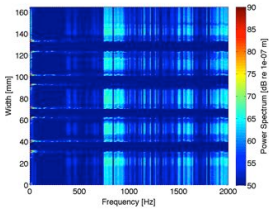

Tire 14

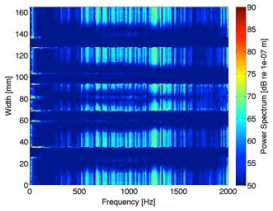

Tire 15

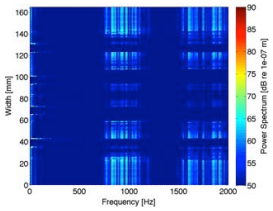

Tire 16

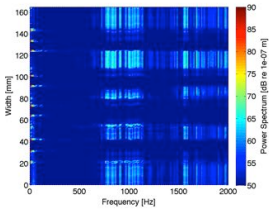

Tire 17

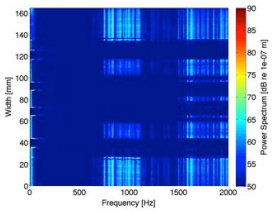

Tire 18

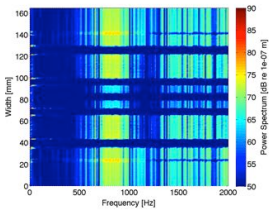

Tire 19

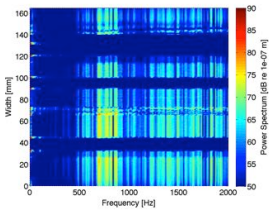

Tire 20

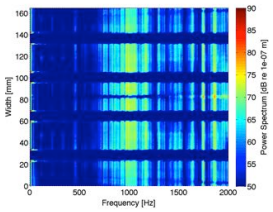

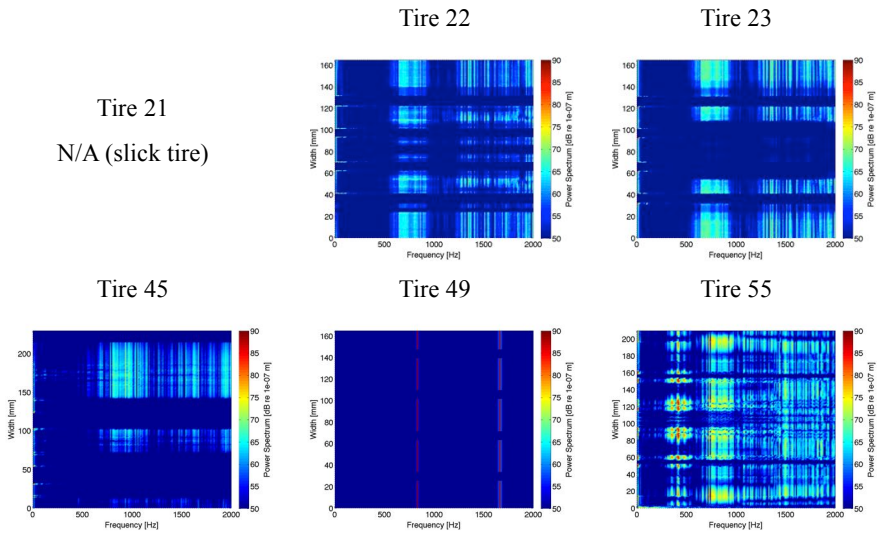

Figure A.1: Tread profile power spectra for all circumferential sections at 60 mph

A.3 Comparisons between Tread Pattern Spectra and TPIN Spectra

In Table A.2, the coherent tread profile spectrum is compared with the total noise spectrum, tread pattern noise spectrum, and non-tread pattern noise spectrum, respectively.

Table A.2: Comparison between coherent tread profile spectrum in red and TPIN spectra in black

Tire No.	Total Noise	Tread Pattern Noise	Non-tread Pattern Noise
01	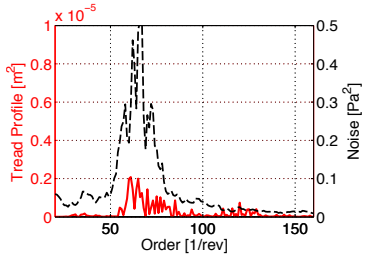	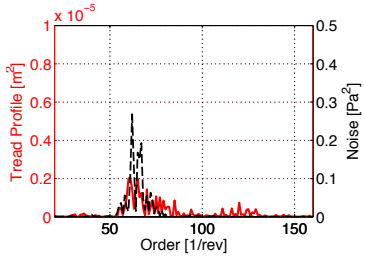	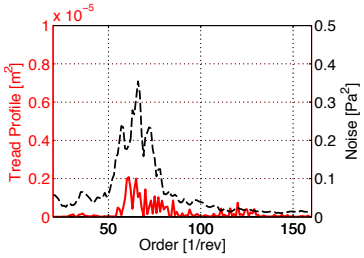
02	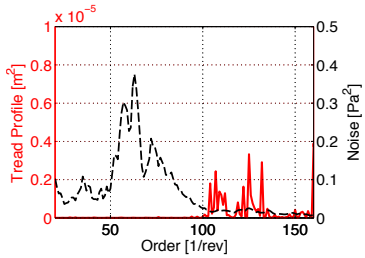	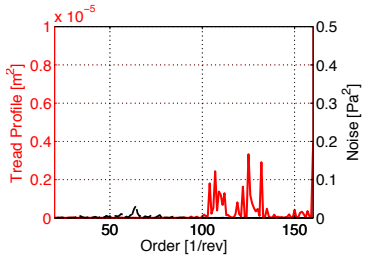	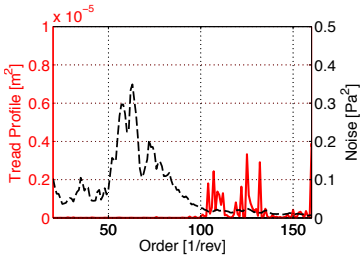

Tire No.	Total Noise	Tread Pattern Noise	Non-tread Pattern Noise
03	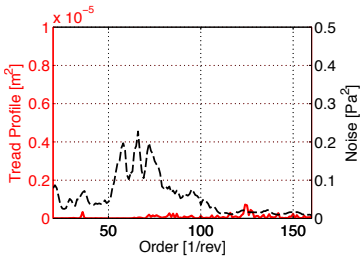	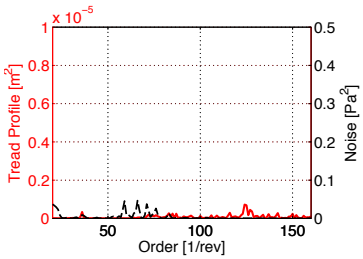	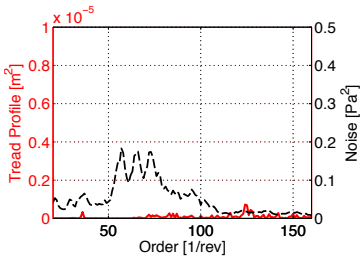
04	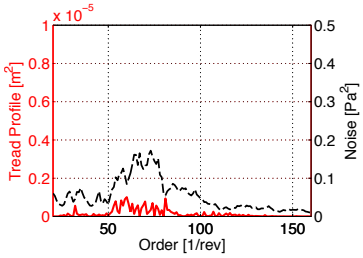	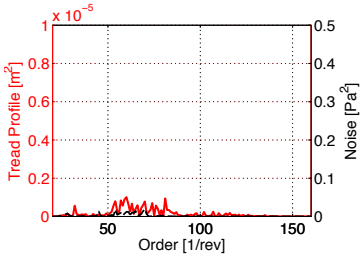	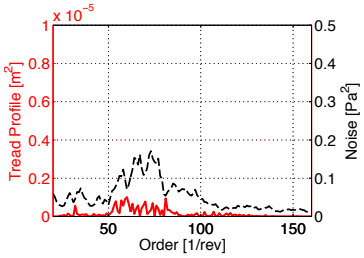
05	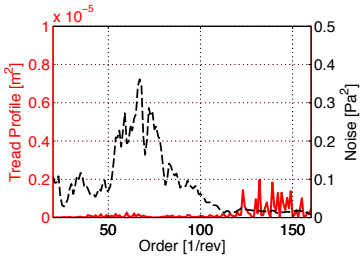	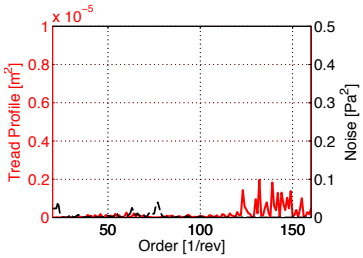	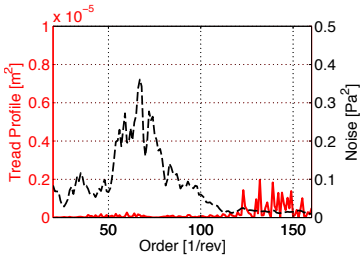
06	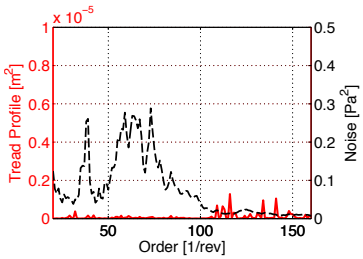	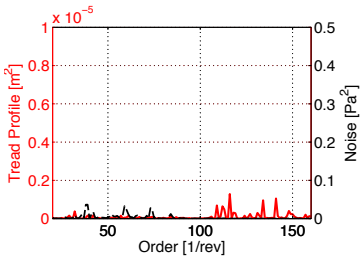	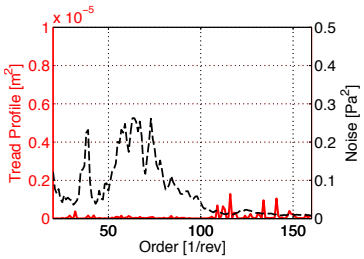
07	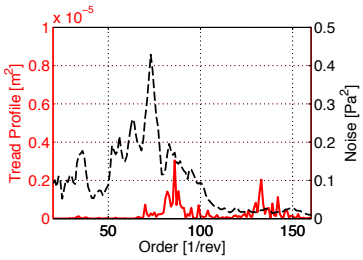	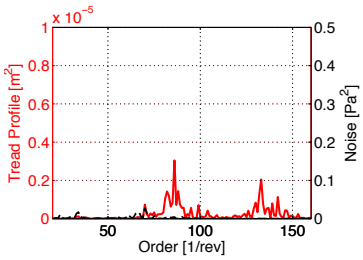	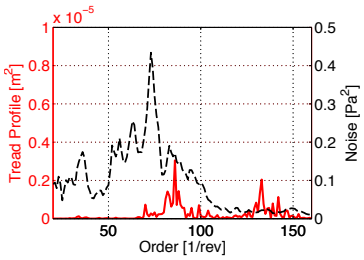

Tire No.	Total Noise	Tread Pattern Noise	Non-tread Pattern Noise
08	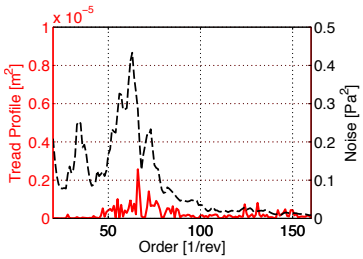	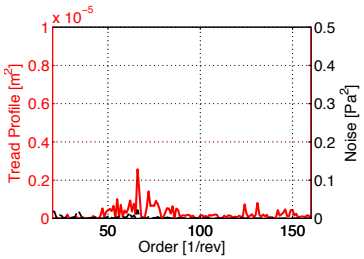	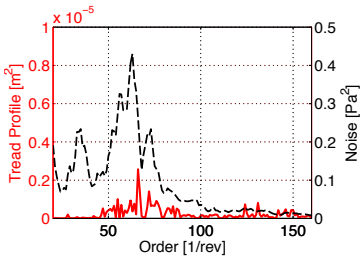
09	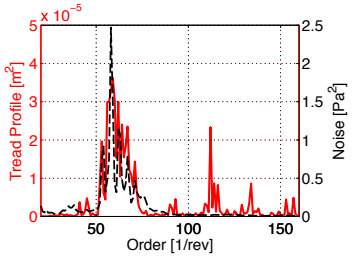	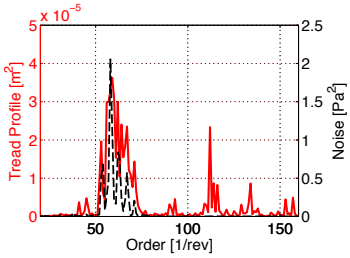	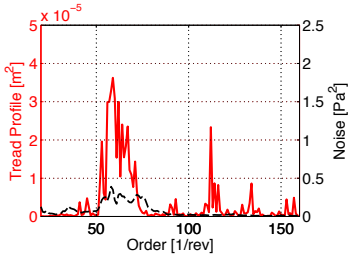
10	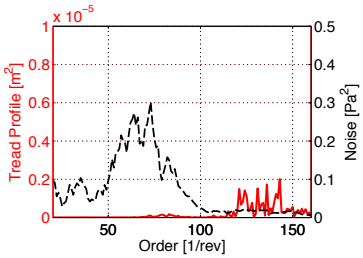	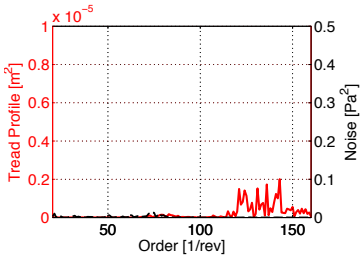	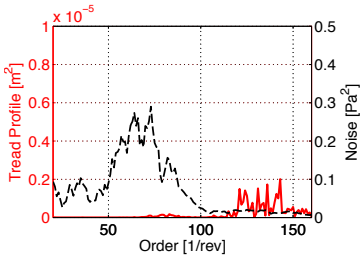
11	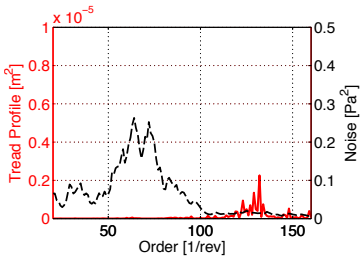	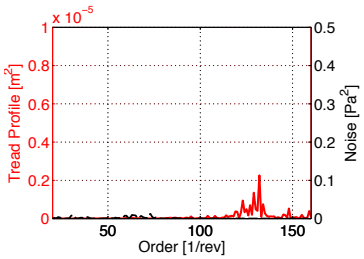	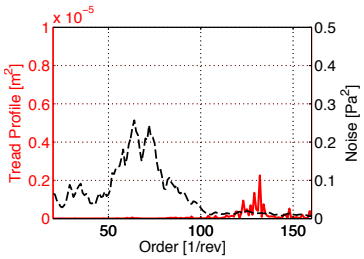
12	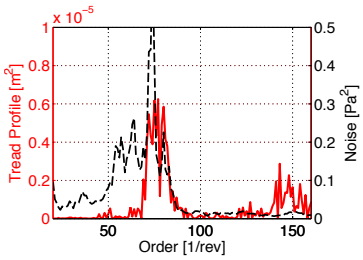	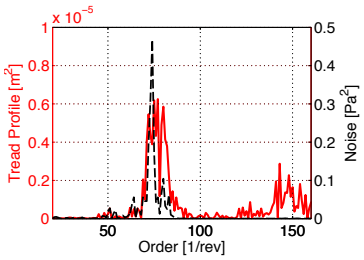	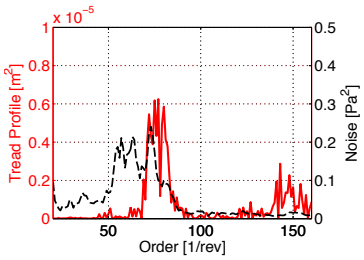

Tire No.	Total Noise	Tread Pattern Noise	Non-tread Pattern Noise
13	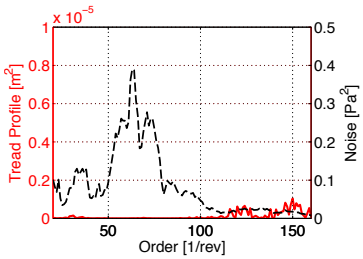	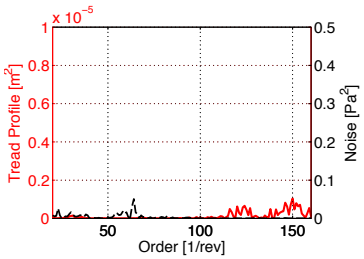	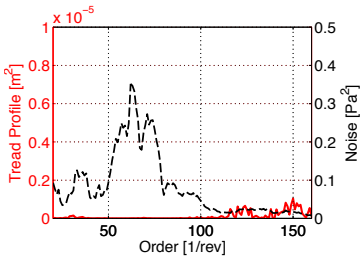
14	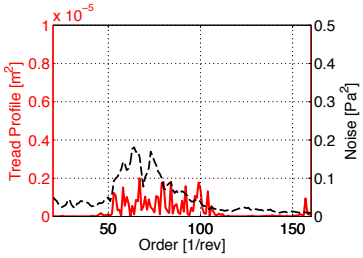	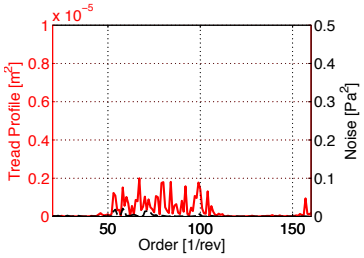	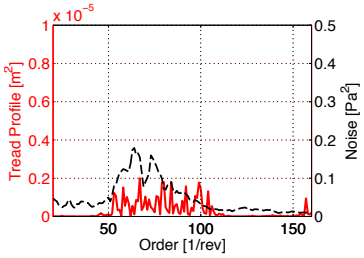
15	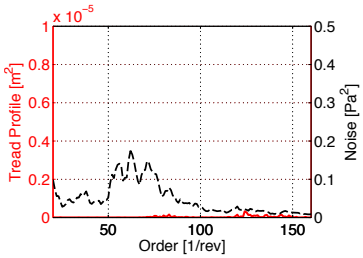	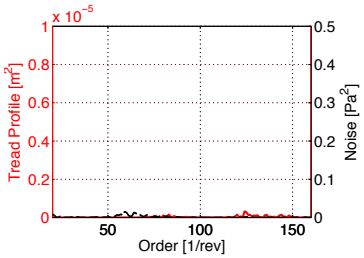	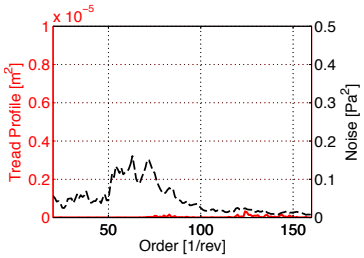
16	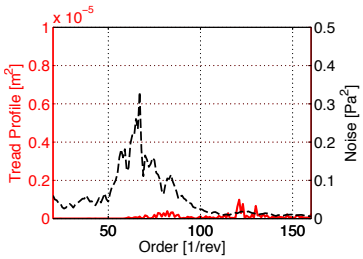	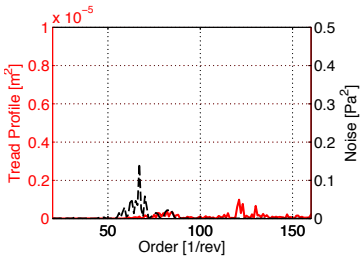	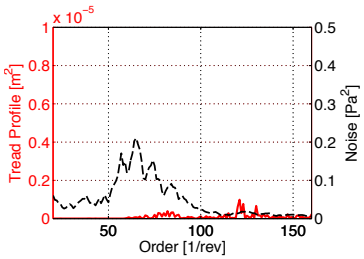
17	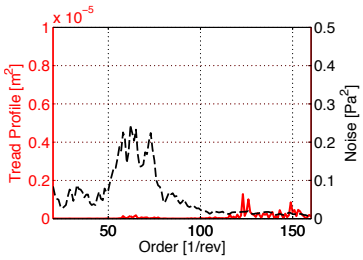	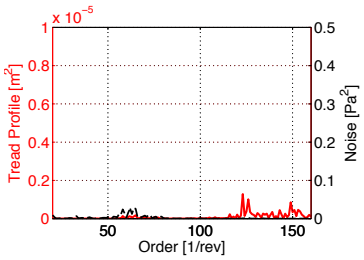	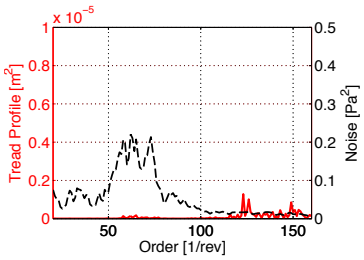

Tire No.	Total Noise	Tread Pattern Noise	Non-tread Pattern Noise
18	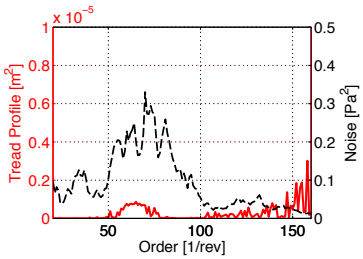	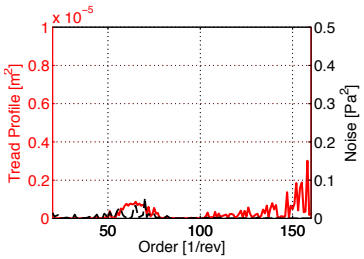	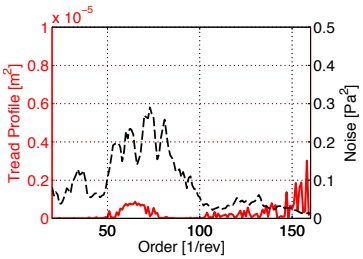
19	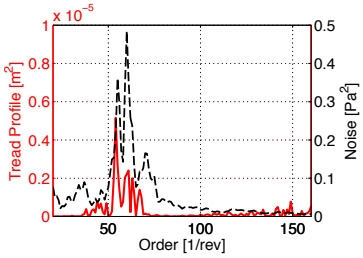	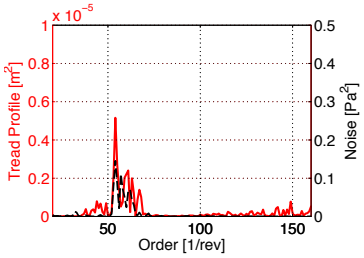	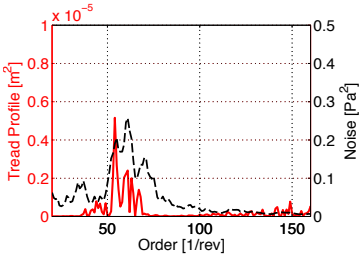
20	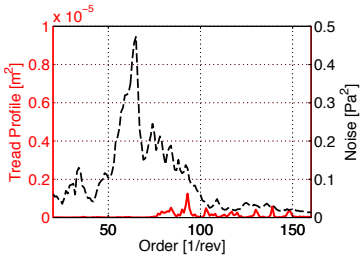	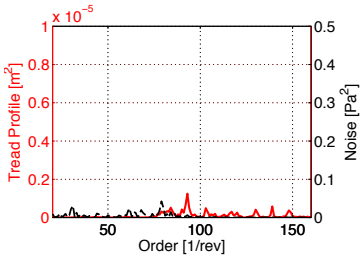	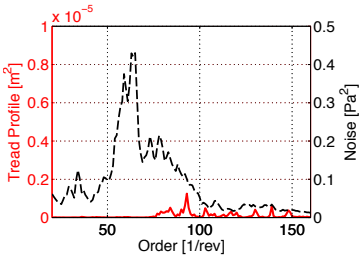
21		N/A (slick tire)	
22	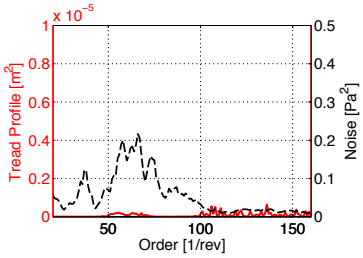	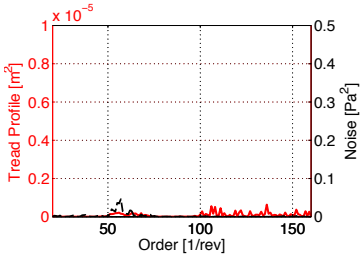	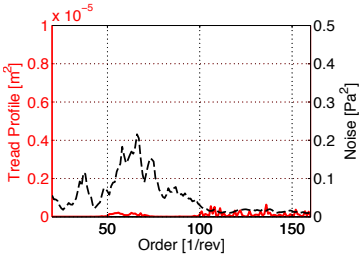
23	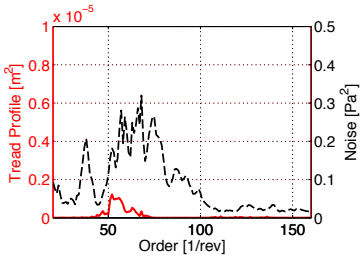	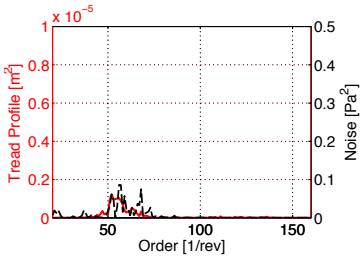	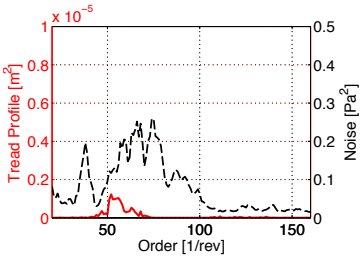

In Table A.3, the air volume velocity spectrum is compared with the total noise spectrum, tread pattern noise spectrum, and non-tread pattern noise spectrum, respectively.

Table A.3: Comparison between air volume velocity spectrum in red and TPIN spectra in black

Tire No.	Total Noise	Tread Pattern Noise	Non-tread Pattern Noise
01	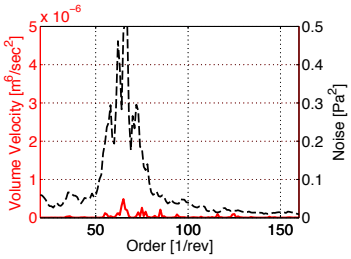	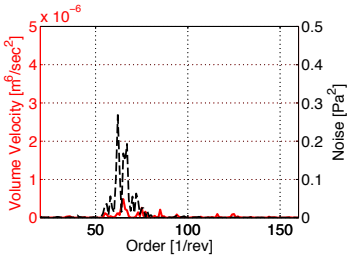	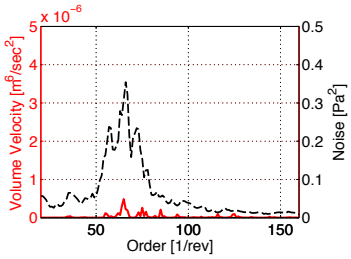
02	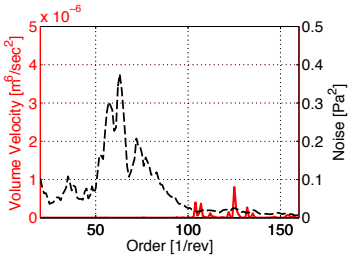	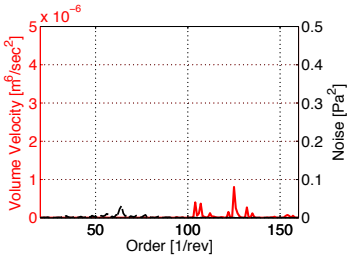	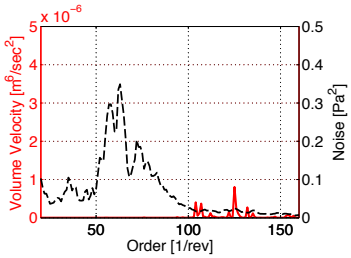
03	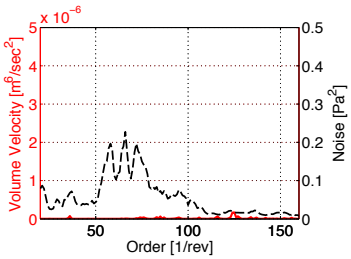	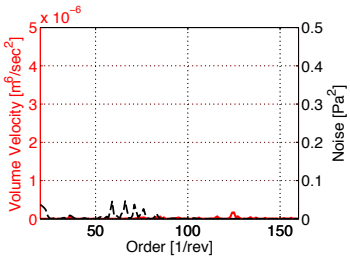	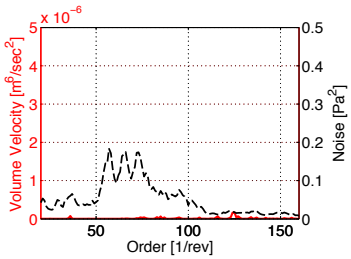
04	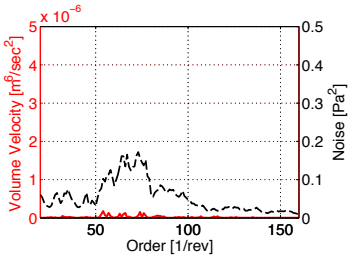	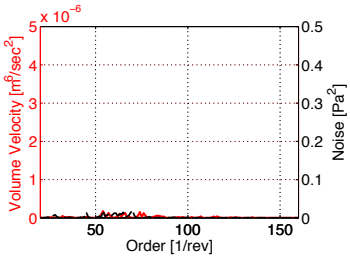	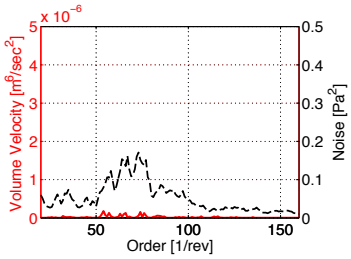
05	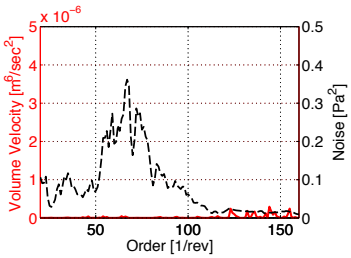	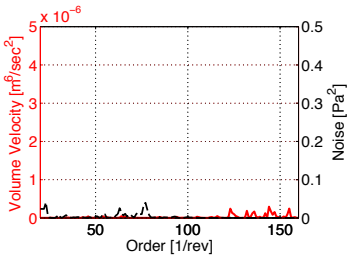	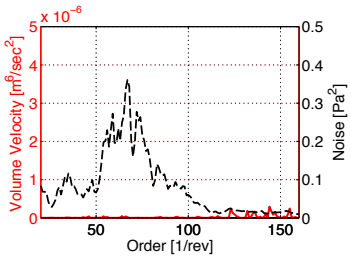

Tire No.	Total Noise	Tread Pattern Noise	Non-tread Pattern Noise
06	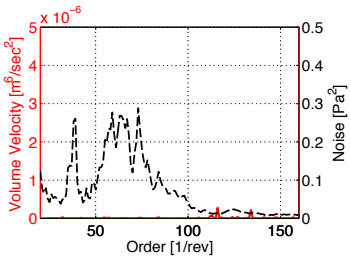	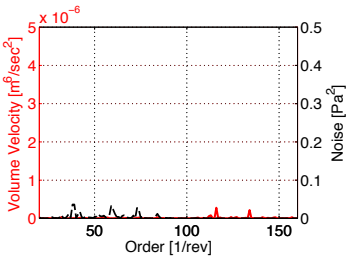	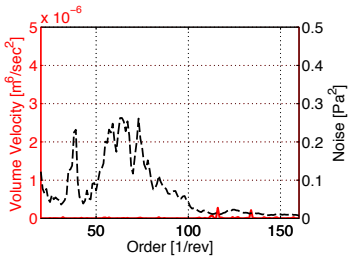
07	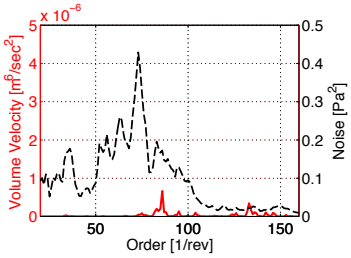	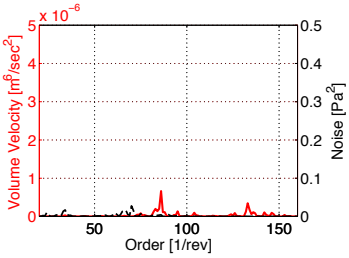	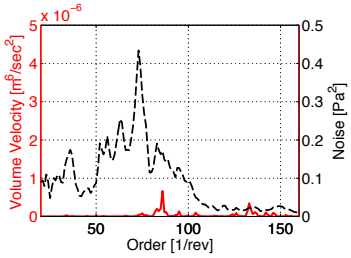
08	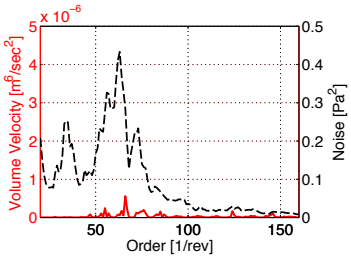	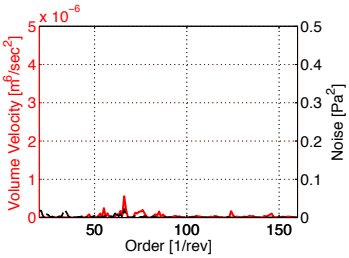	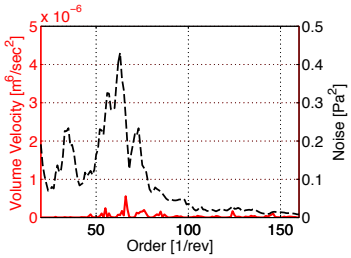
09	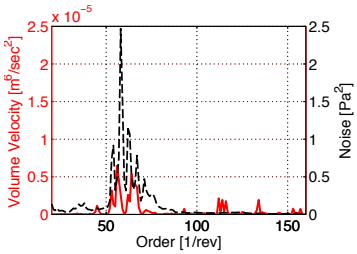	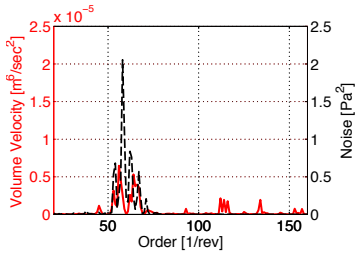	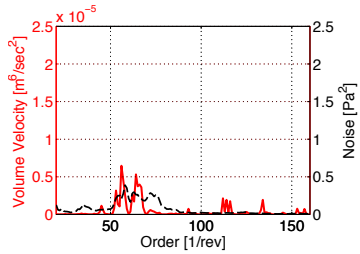
10	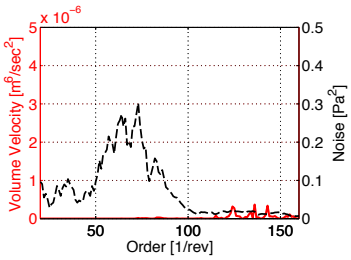	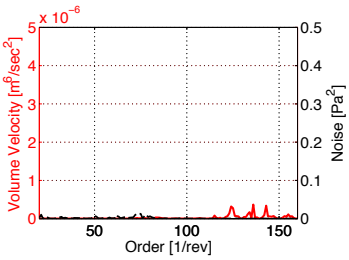	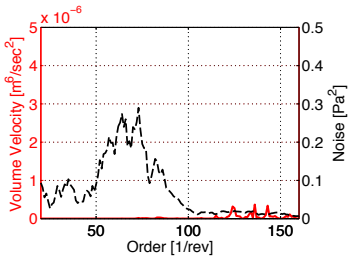

Tire No.	Total Noise	Tread Pattern Noise	Non-tread Pattern Noise
11	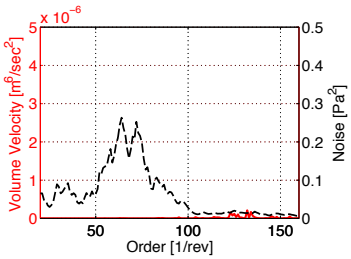	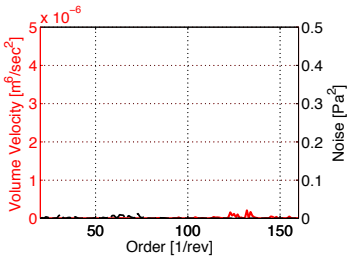	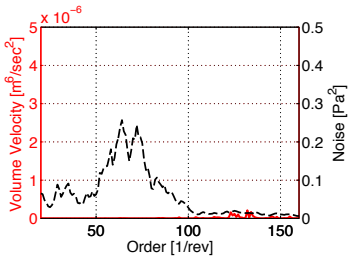
12	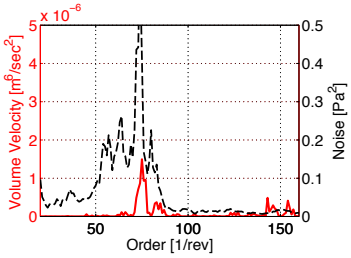	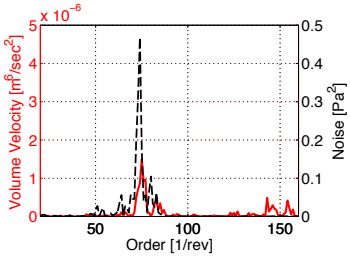	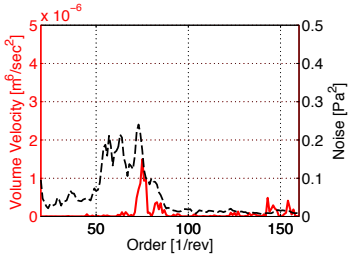
13	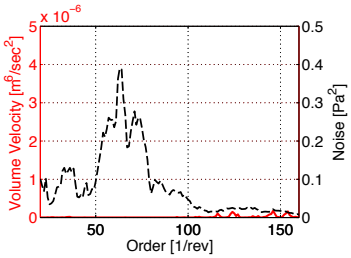	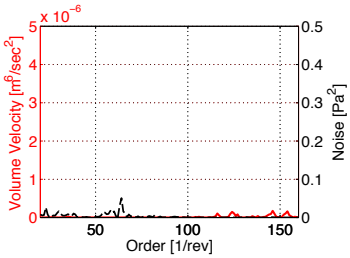	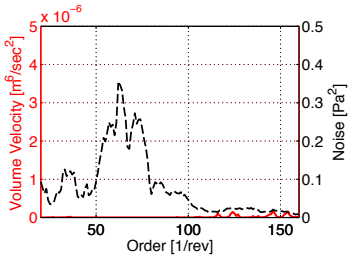
14	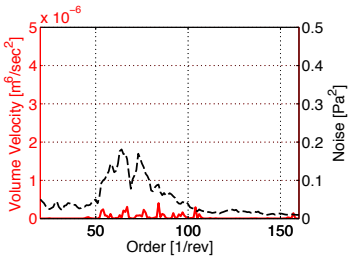	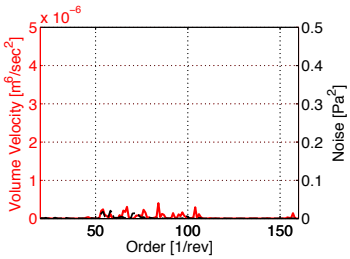	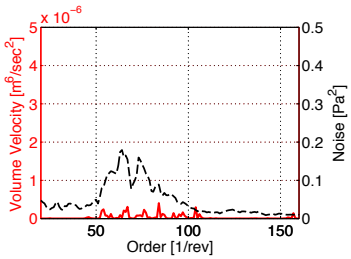
15	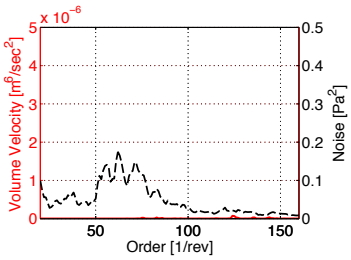	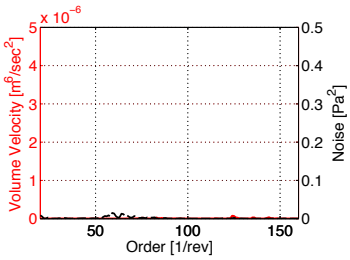	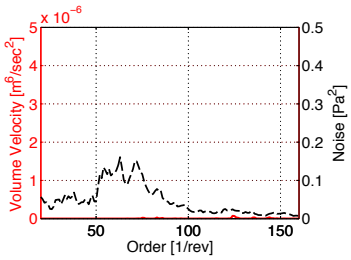

Tire No.	Total Noise	Tread Pattern Noise	Non-tread Pattern Noise
16	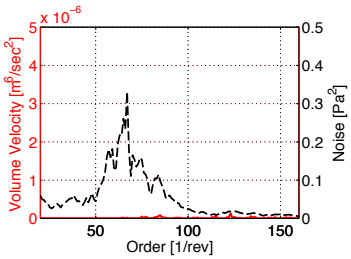	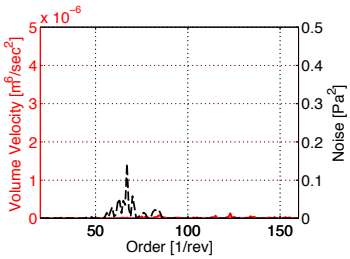	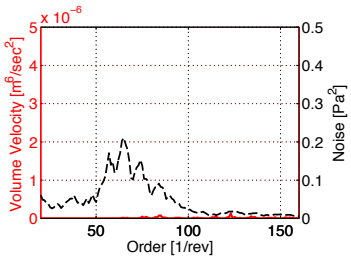
17	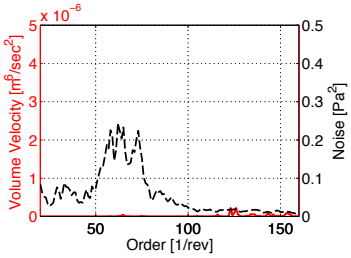	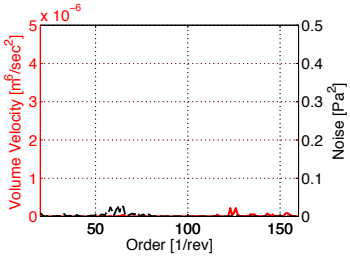	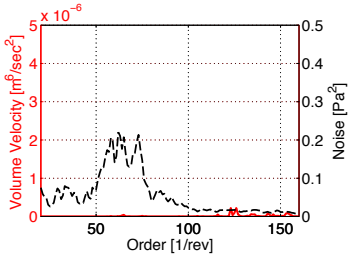
18	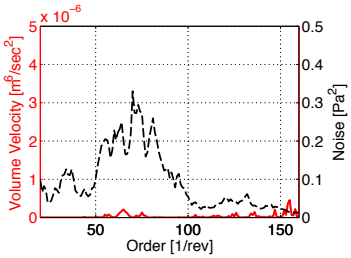	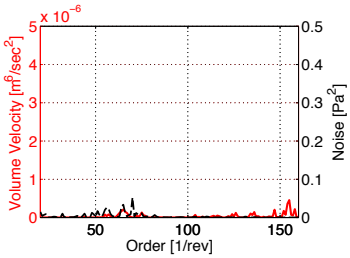	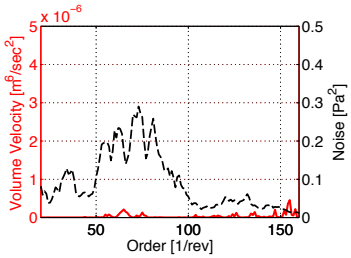
19	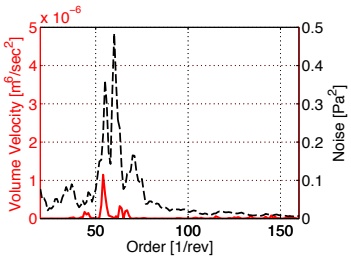	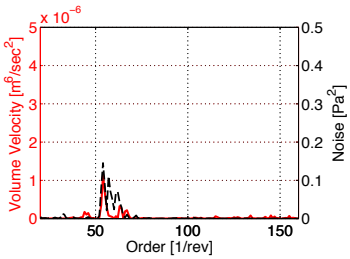	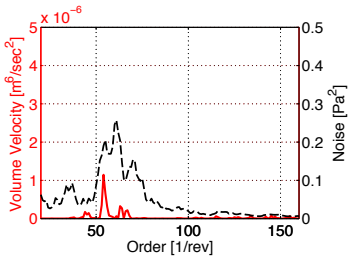
20	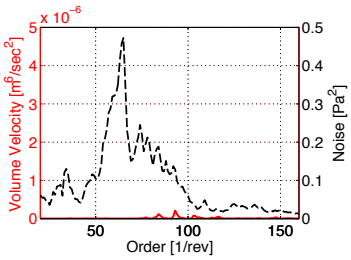	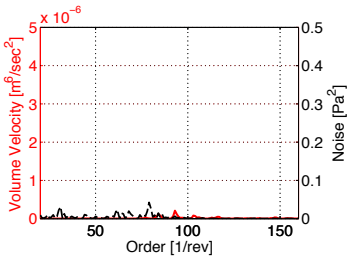	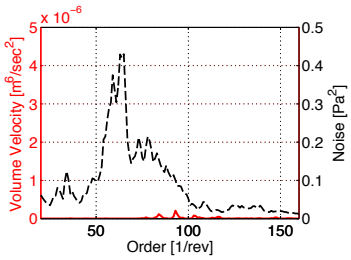
21		N/A (slick tire)	

Tire No.	Total Noise	Tread Pattern Noise	Non-tread Pattern Noise
22	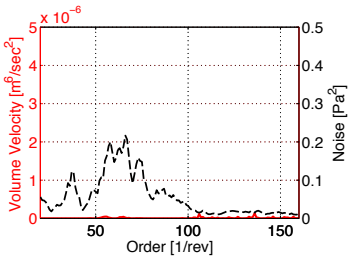	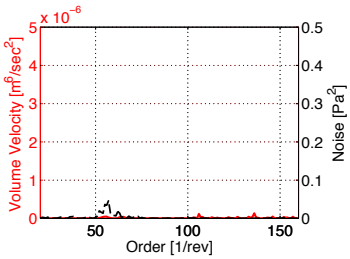	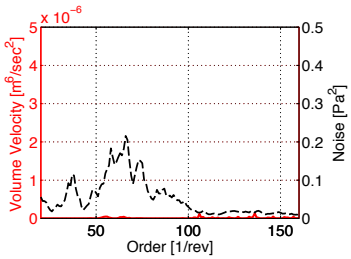
23	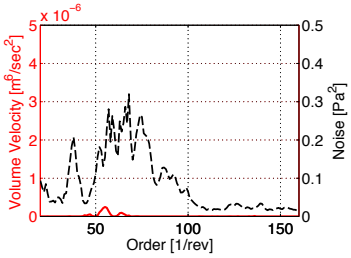	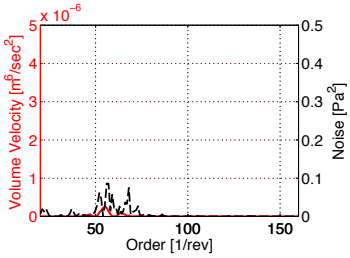	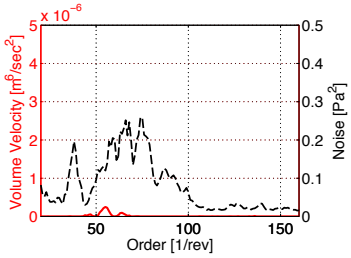

A.4 Tread Pattern Spectra and Gaussian Curve Fitting

The incoherent tread profile spectrum, coherent tread profile spectrum, and volume velocity spectrum for each tire are demonstrated in Table A.4. The corresponding two-term Gaussian fitted curve is superimposed in each corresponding plot.

Table A.4: Incoherent tread profile spectrum, coherent tread profile spectrum, and volume velocity spectrum (blue: original; red: Gaussian)

Tire No.	Tread Pattern Spectra and Gaussian Curve Fitting
01	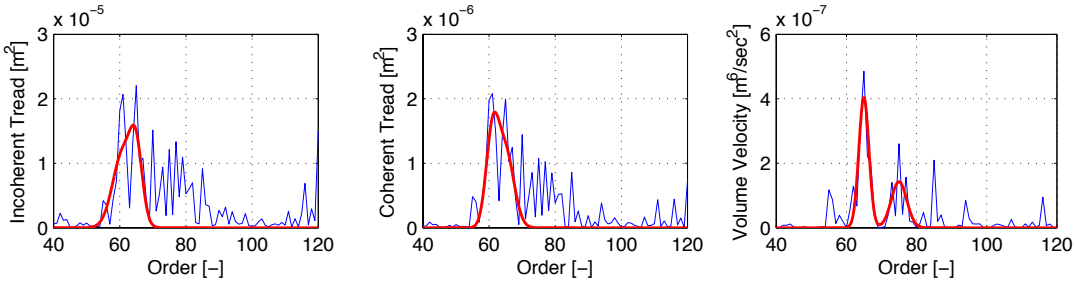

Tire No.	Tread Pattern Spectra and Gaussian Curve Fitting
02	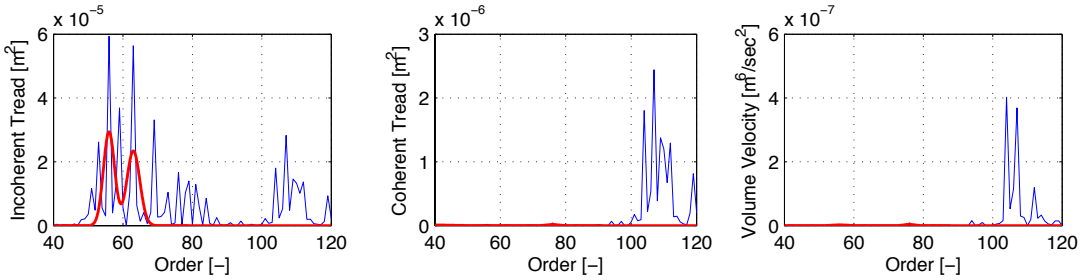
03	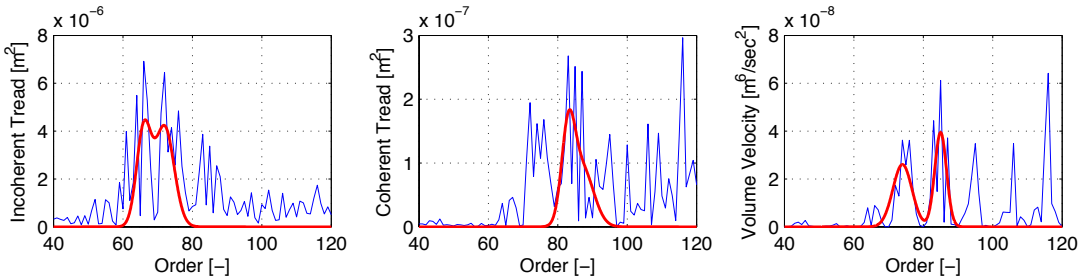
04	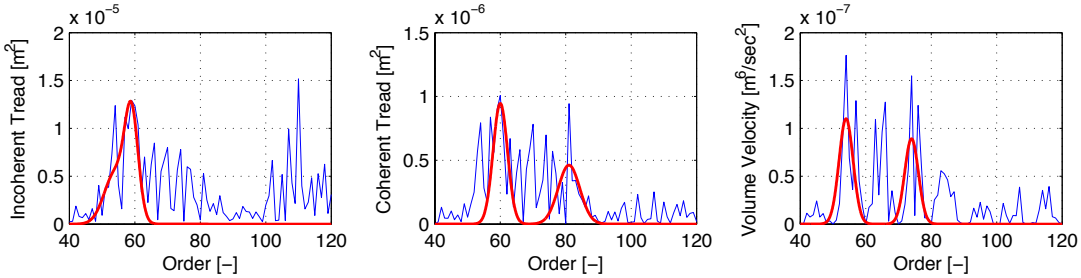
05	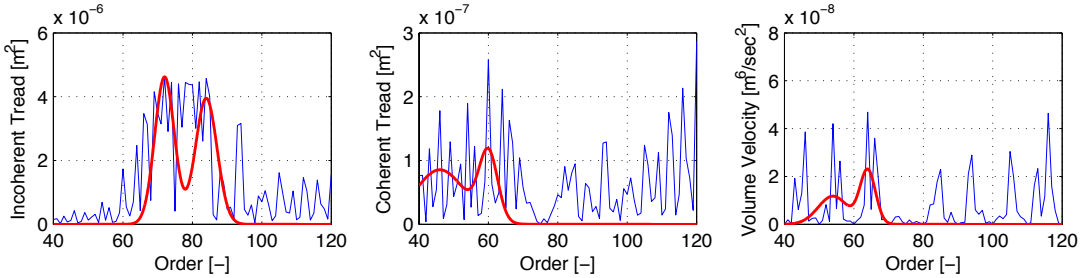

Tire No.	Tread Pattern Spectra and Gaussian Curve Fitting
06	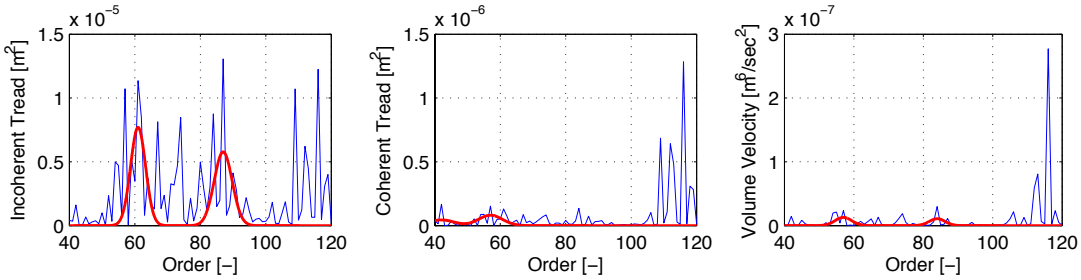
07	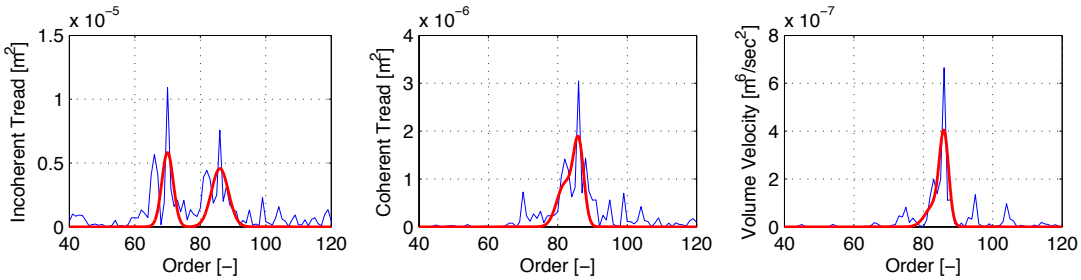
08	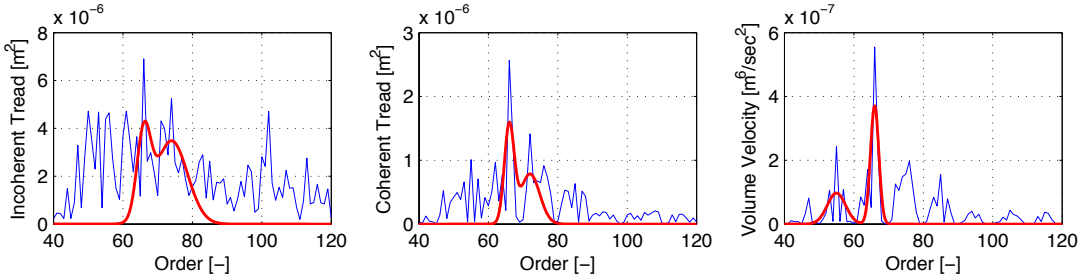
09	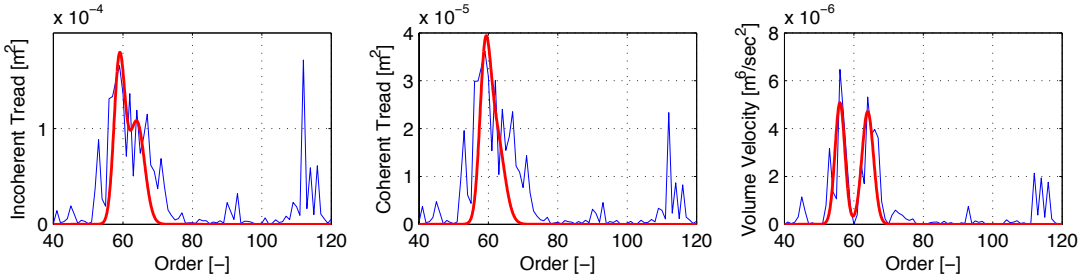

Tire No.	Tread Pattern Spectra and Gaussian Curve Fitting
10	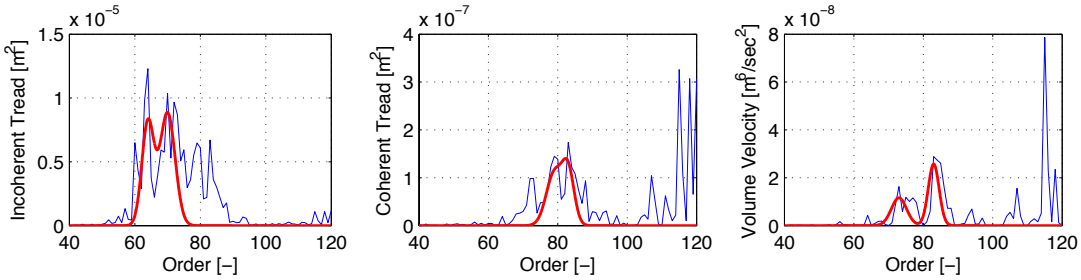
11	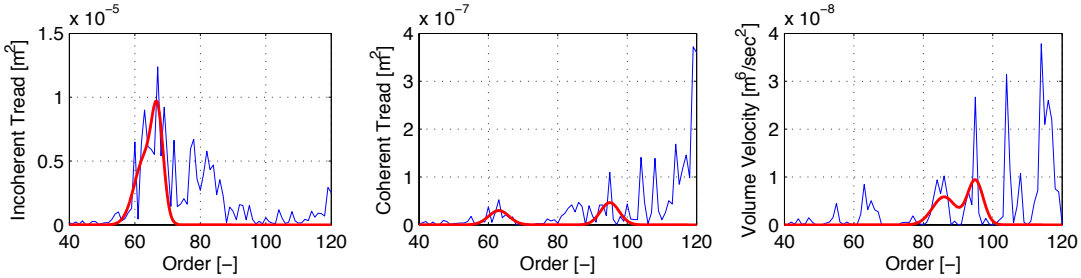
12	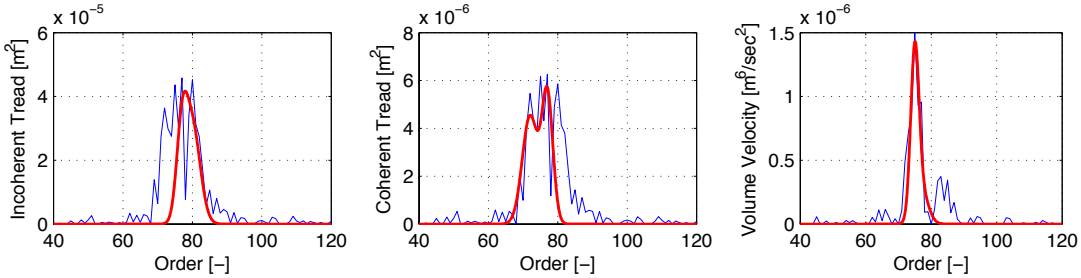
13	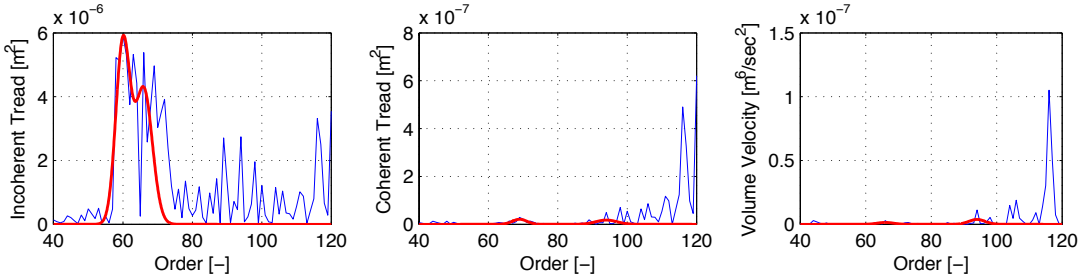

Tire No.	Tread Pattern Spectra and Gaussian Curve Fitting
14	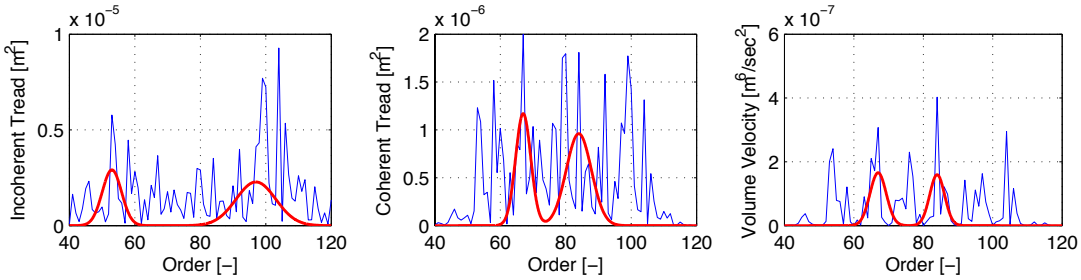
15	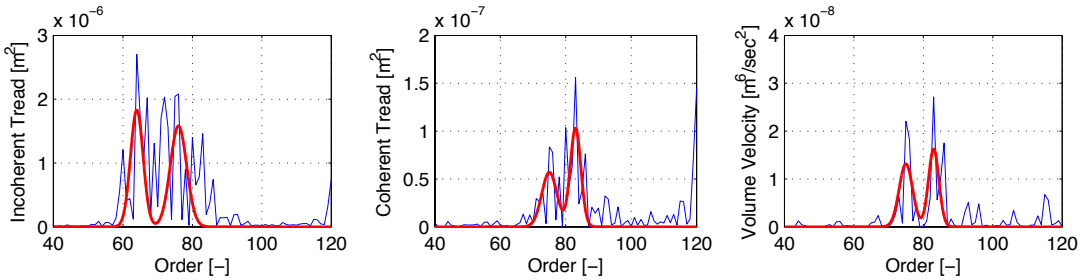
16	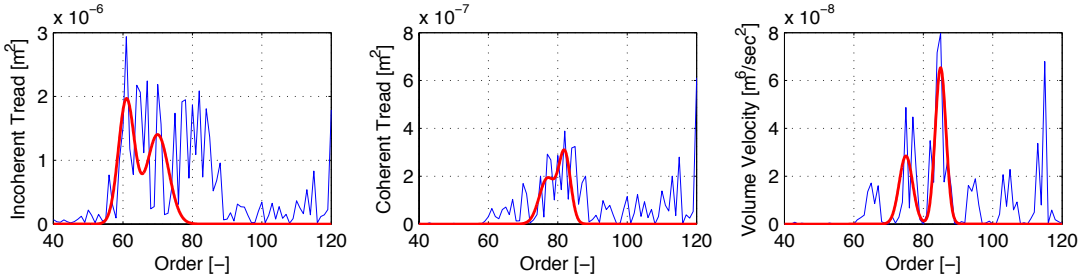
17	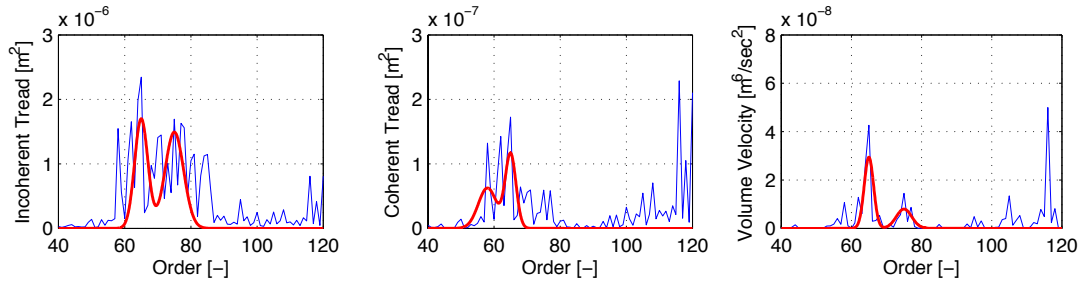

Tire No.	Tread Pattern Spectra and Gaussian Curve Fitting
18	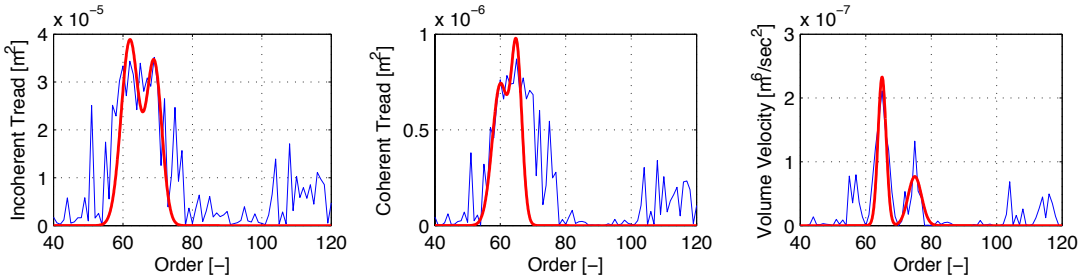
19	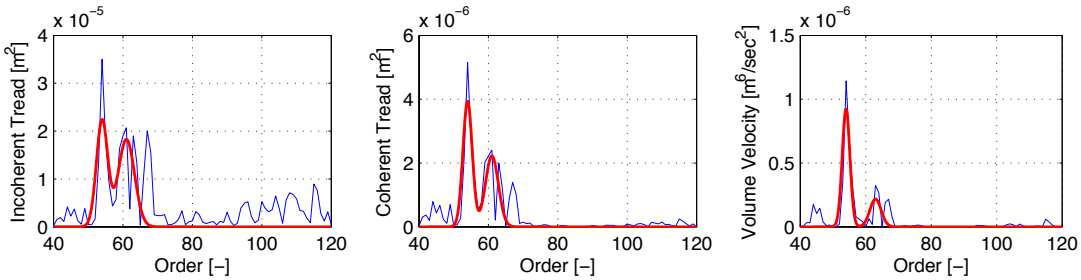
20	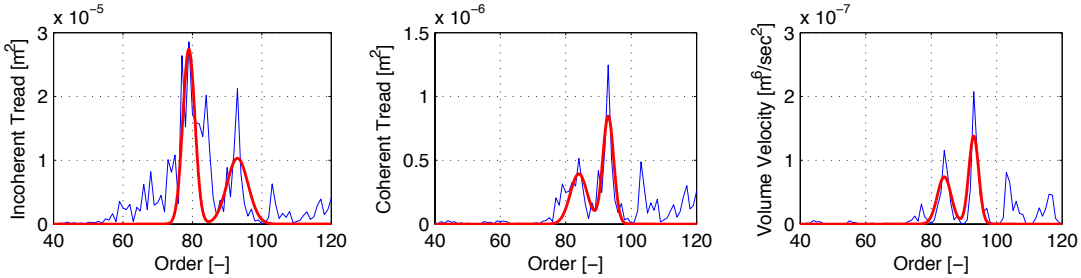
21	N/A (slick tire)
22	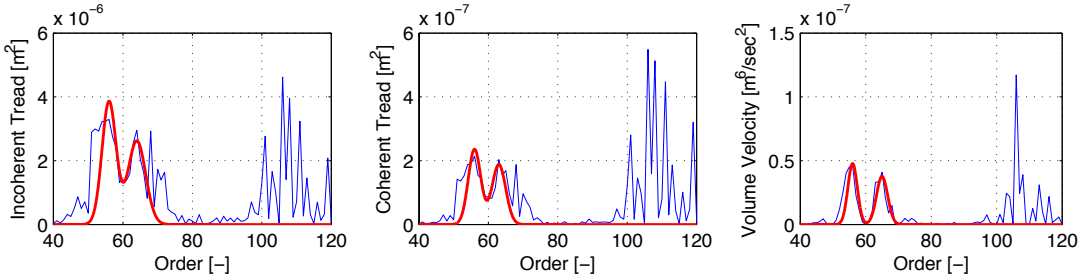

Tire No.	Tread Pattern Spectra and Gaussian Curve Fitting
23	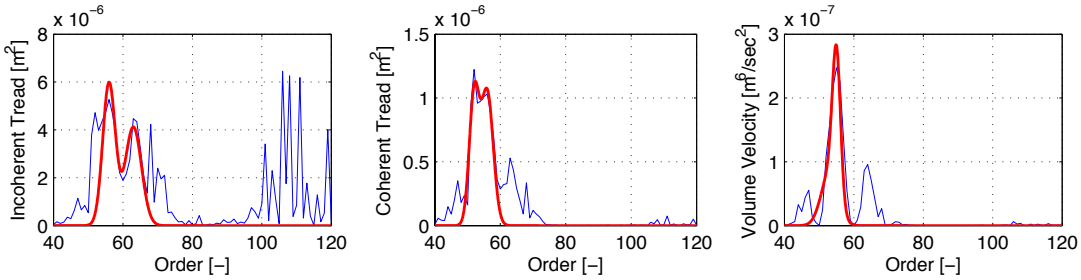
45	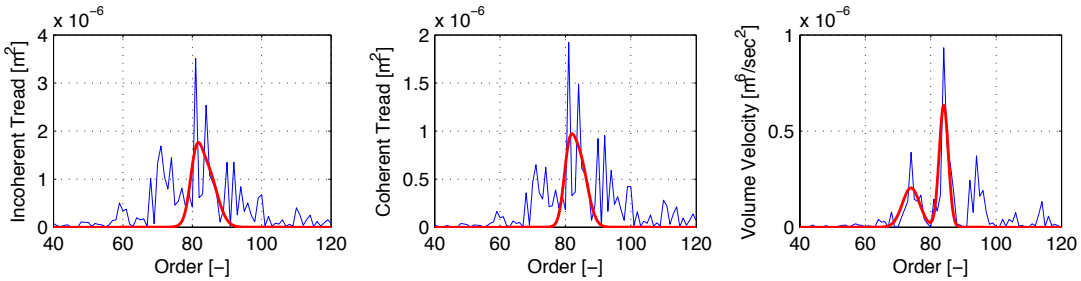
49	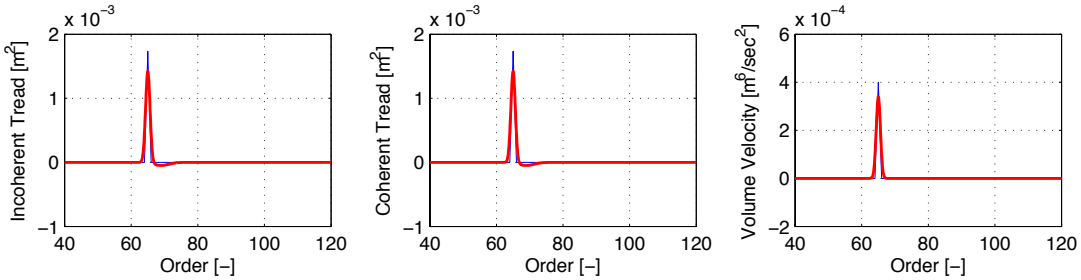
55	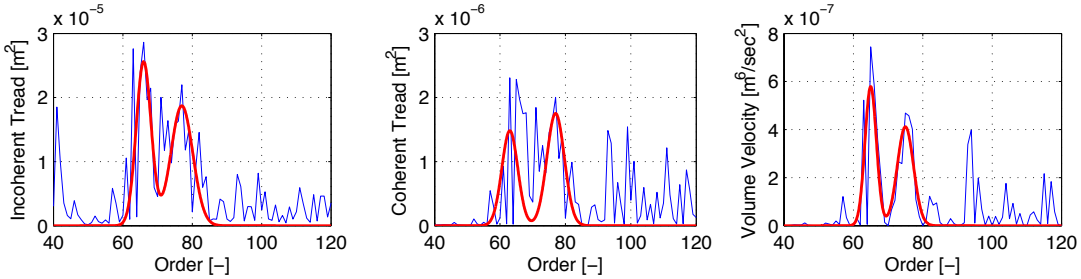

Appendix B: Results of AMOT (Train and Validation Set)

B.1 Narrowband Spectrum in Linear Scale

The results for the total noise in narrowband linear scale are shown in Figure B.1.

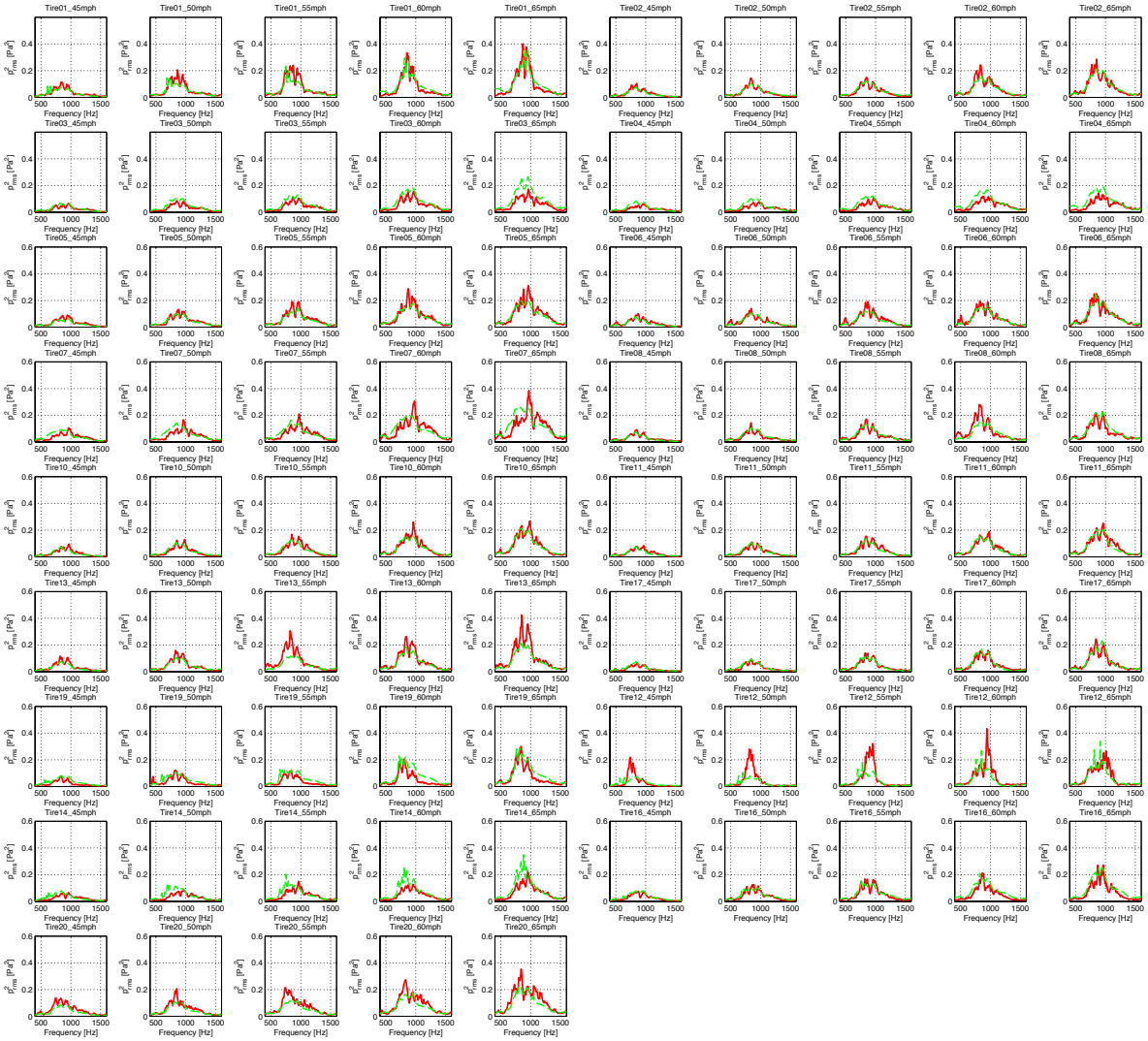

Figure B.1: Total noise in narrowband linear scale (red denotes measured, green denotes predicted)

The results for the tread pattern noise in narrowband linear scale are shown in Figure B.2.

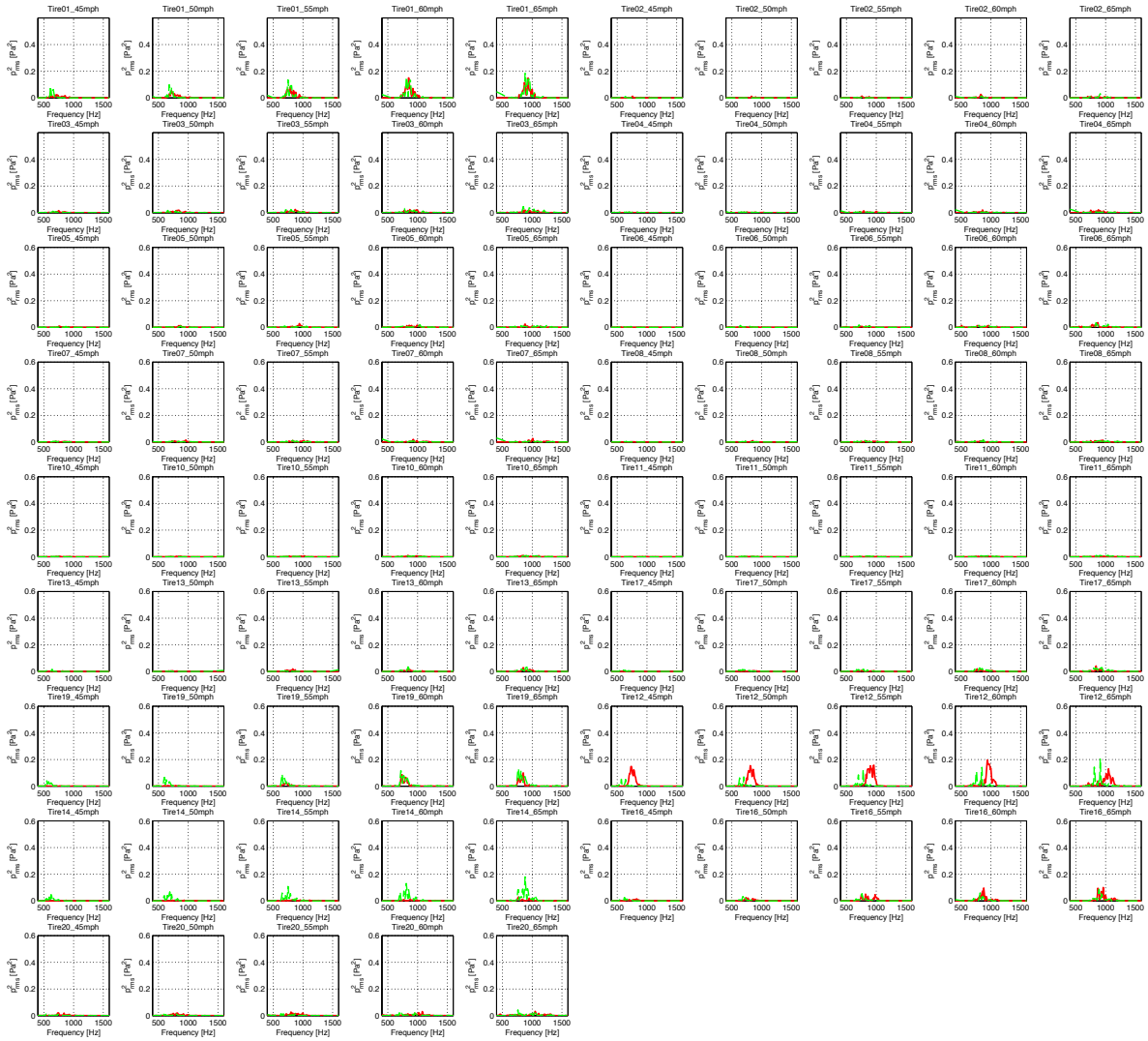

Figure B.2: Tread pattern noise in narrowband linear scale (red denotes measured, green denotes predicted)

The results for the non-tread pattern noise in narrowband linear scale are shown in Figure B.3.

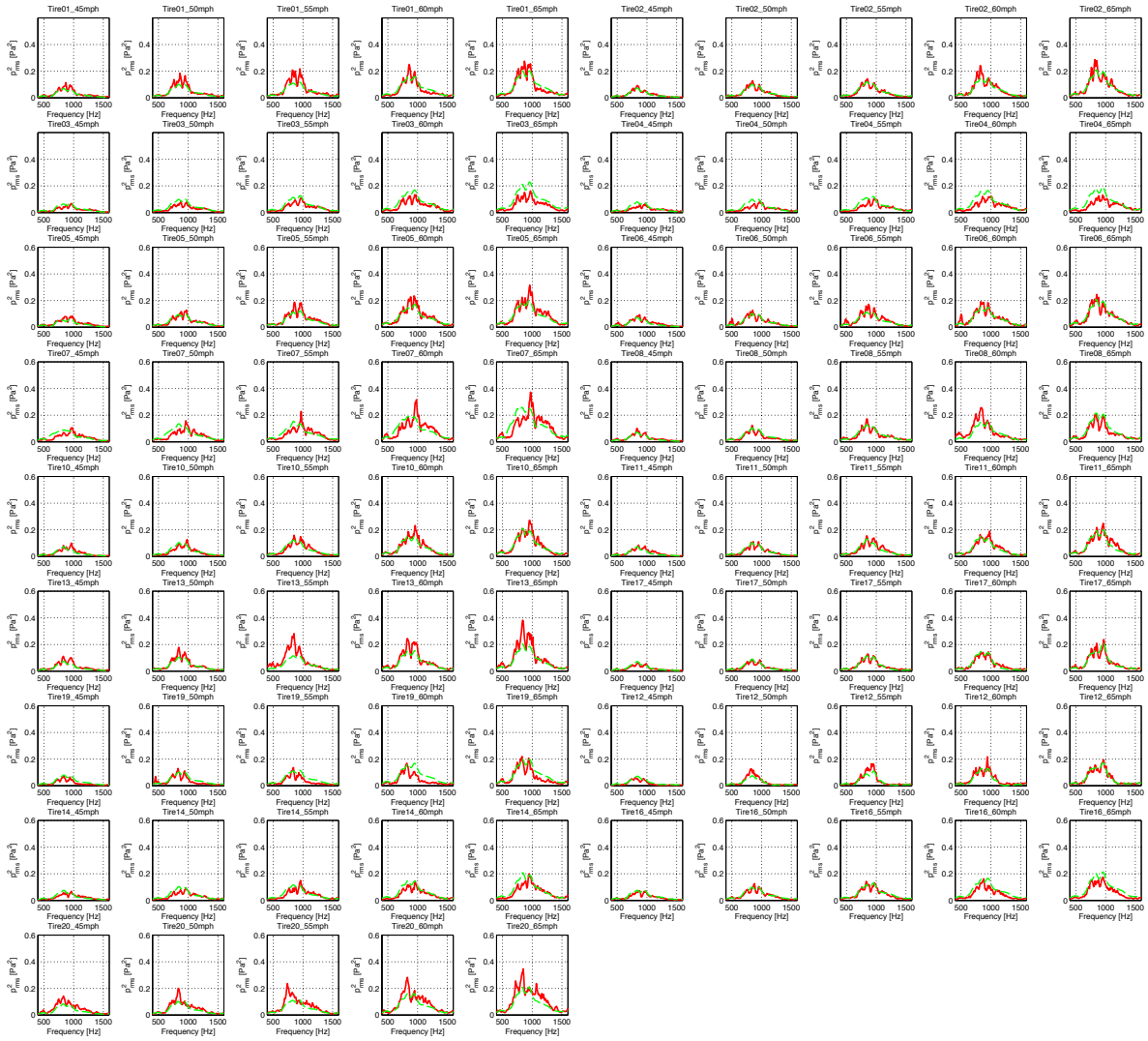

Figure B.3: Non-tread pattern noise in narrowband linear scale (red denotes measured, green denotes predicted)

B.2 Narrowband Spectrum in dB Scale

The results for the total noise in narrowband dB scale are shown in Figure B.4.

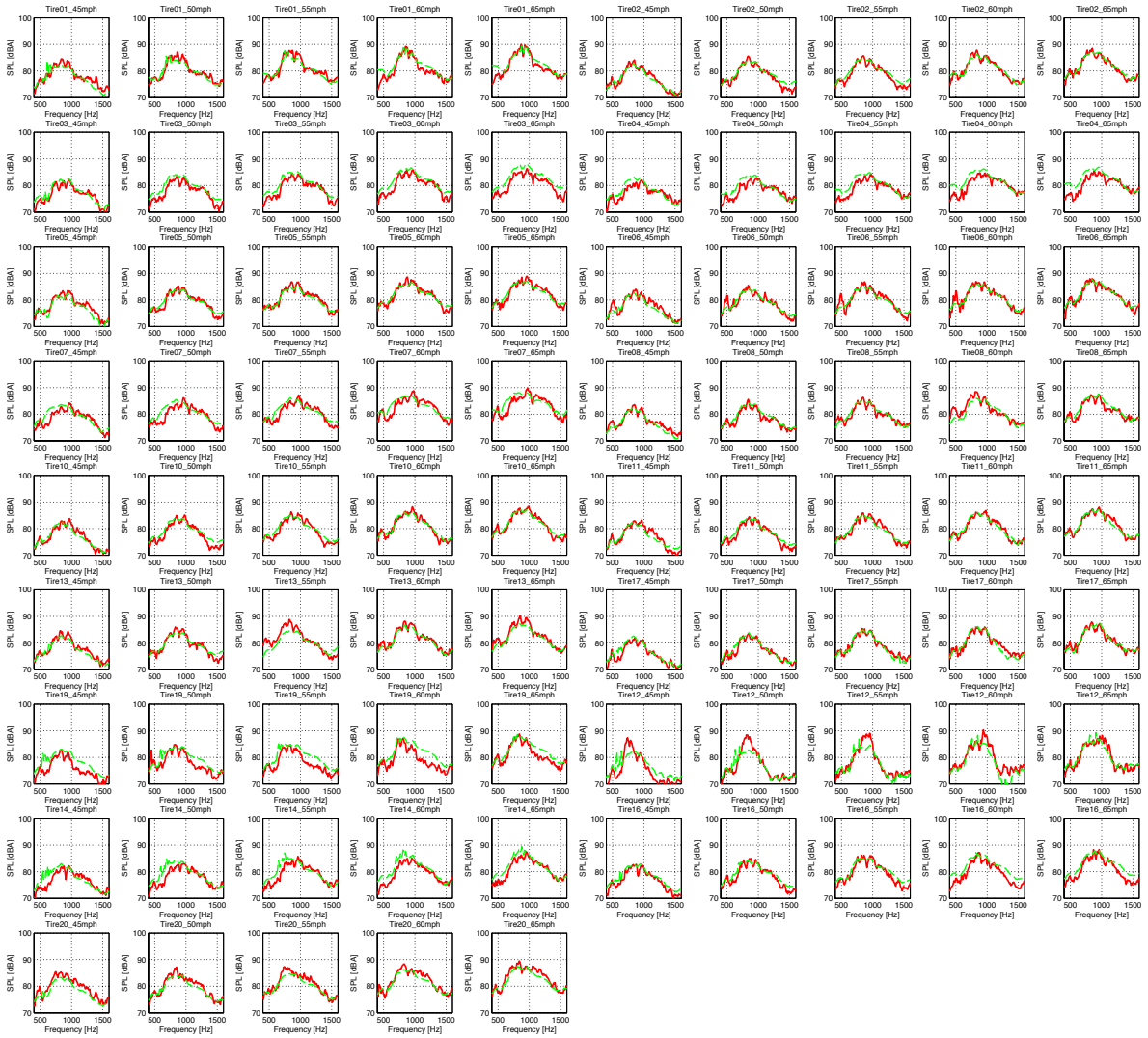

Figure B.4: Total noise in narrowband dB scale (red denotes measured, green denotes predicted)

The results for the tread pattern noise in narrowband dB scale are shown in Figure B.5.

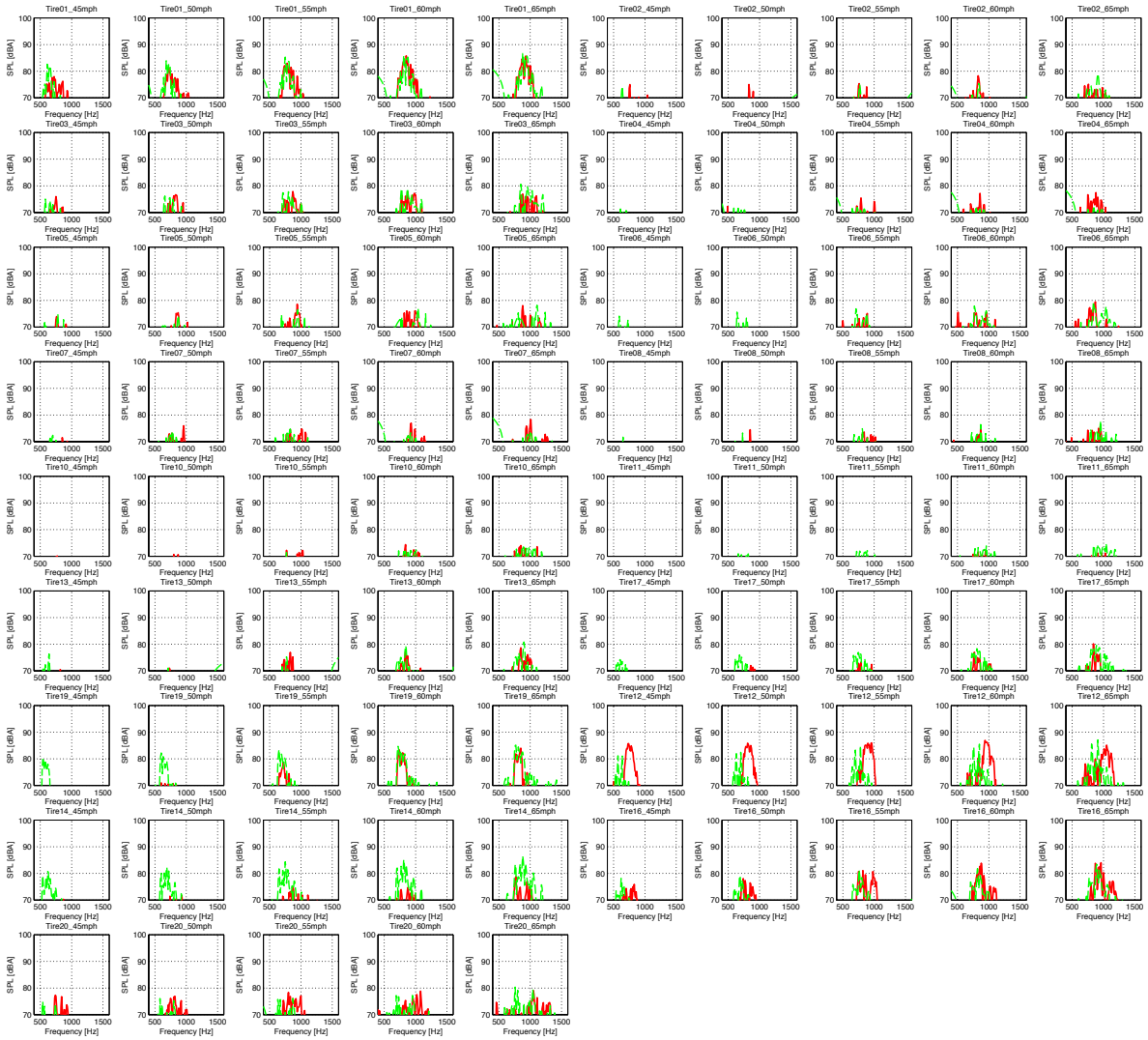

Figure B.5: Tread pattern noise in narrowband dB scale (red denotes measured, green denotes predicted)

The results for the non-tread pattern noise in narrowband dB scale are shown in Figure B.6.

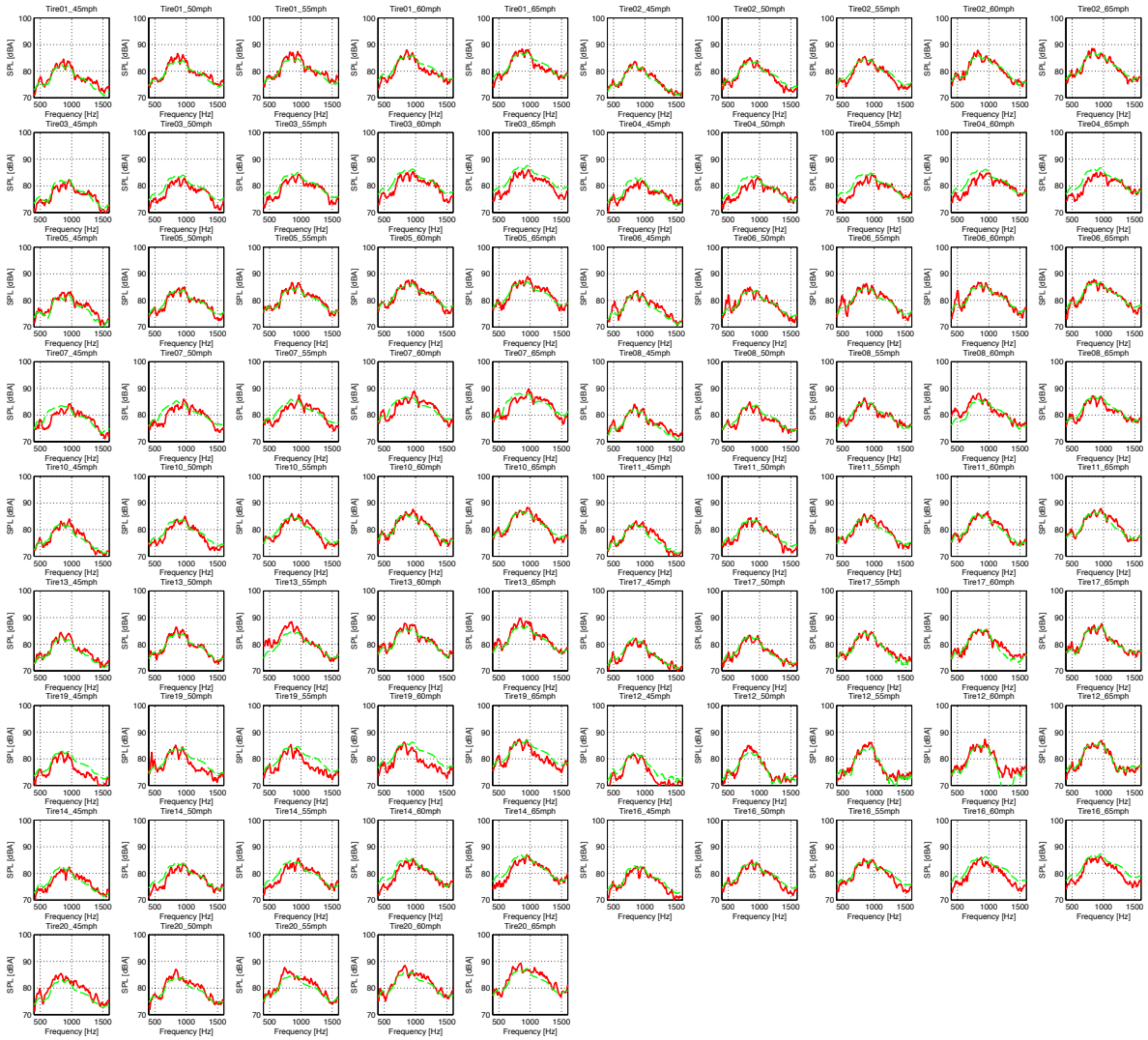

Figure B.6: Non-tread pattern noise in narrowband dB scale (red denotes measured, green denotes predicted)

B.3 1/3 Octave Band Spectrum in Linear Scale

The results for the total noise in 1/3 octave band linear scale are shown in Figure B.7.

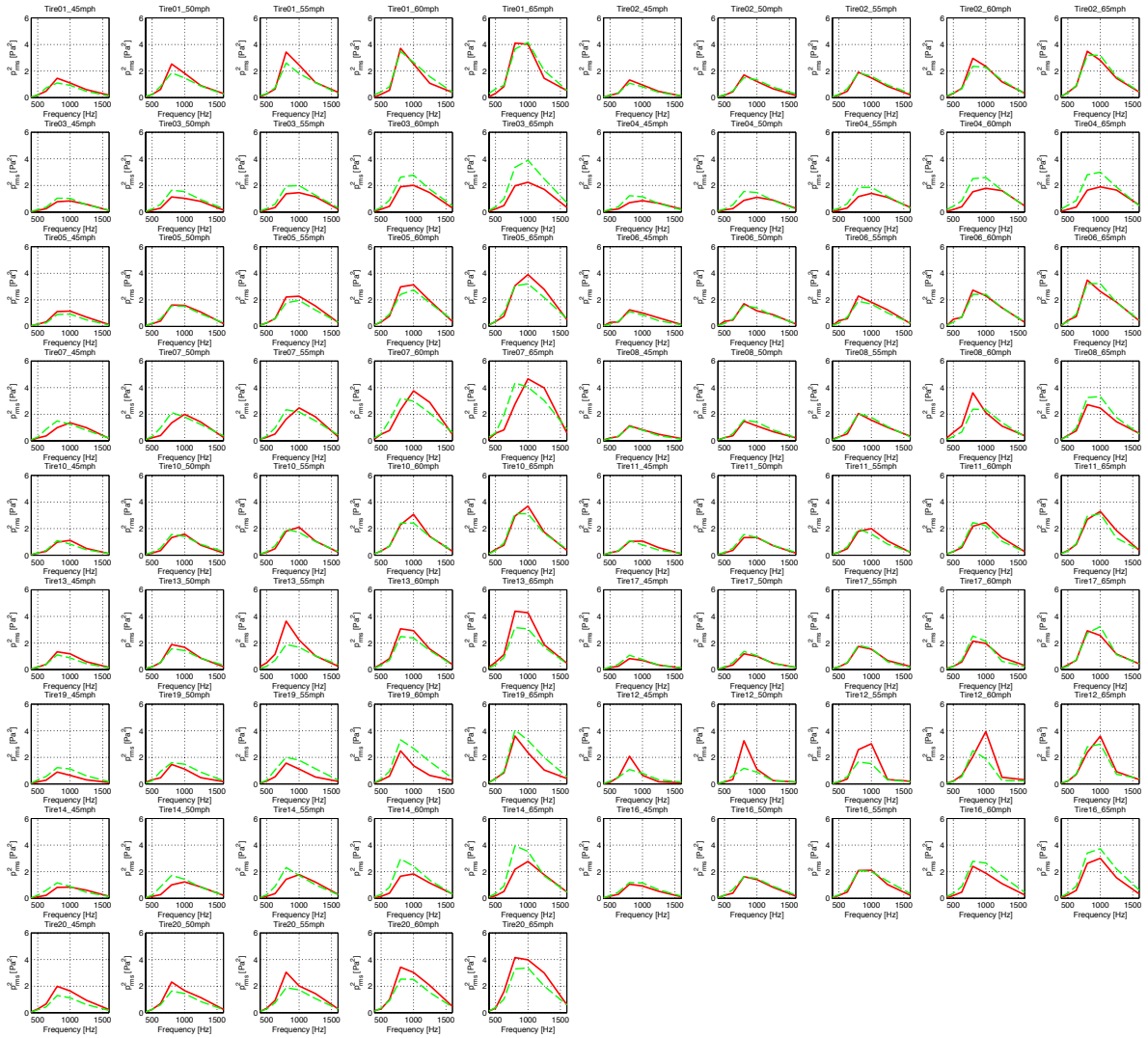

Figure B.7: Total noise in 1/3 octave band linear scale (red denotes measured, green denotes predicted)

The results for the tread pattern noise in 1/3 octave band linear scale are shown in Figure B.8.

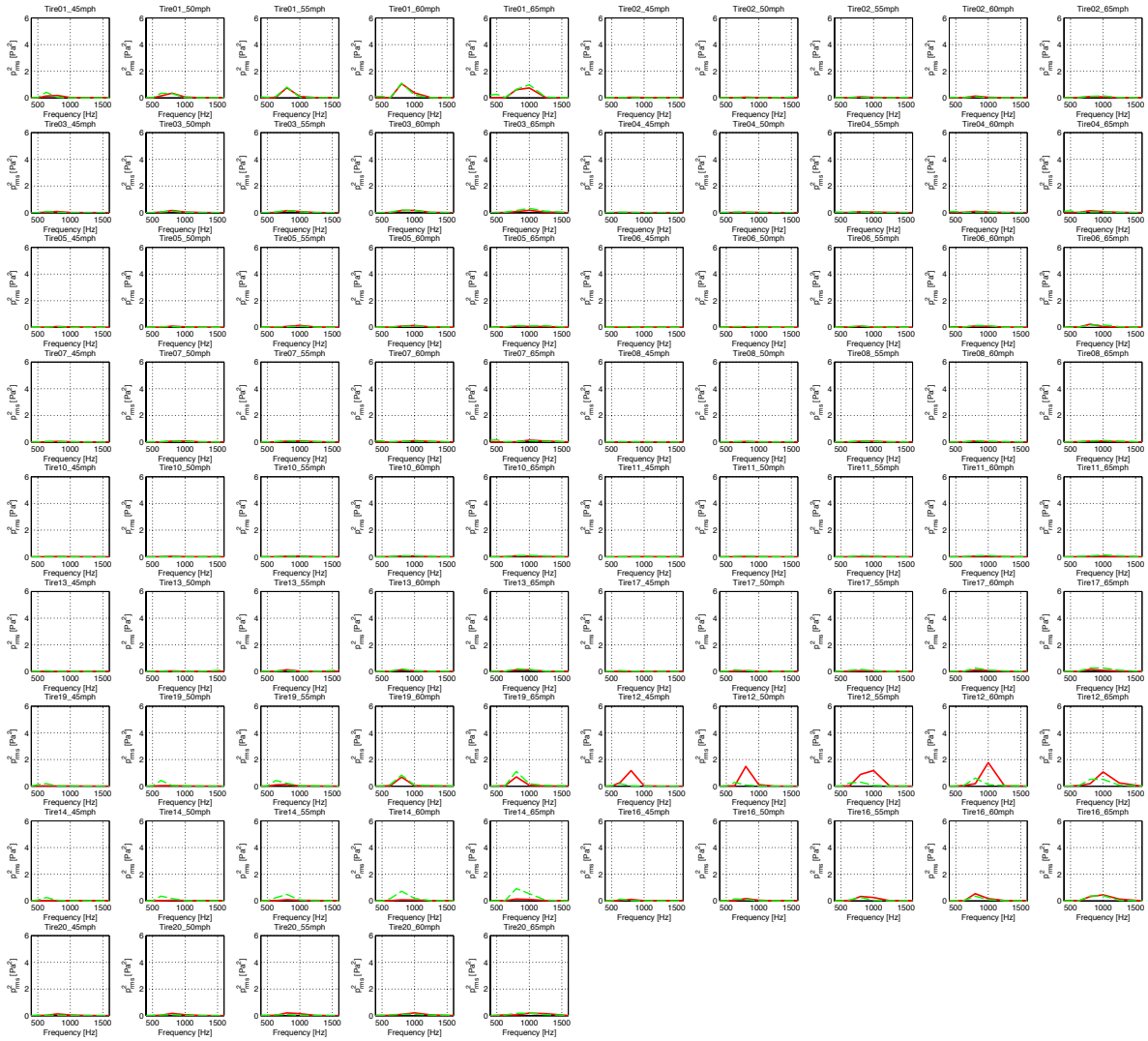

Figure B.8: Tread pattern noise in 1/3 octave band linear scale (red denotes measured, green denotes predicted)

The results for the non-tread pattern noise in 1/3 octave band linear scale are shown in Figure B.9.

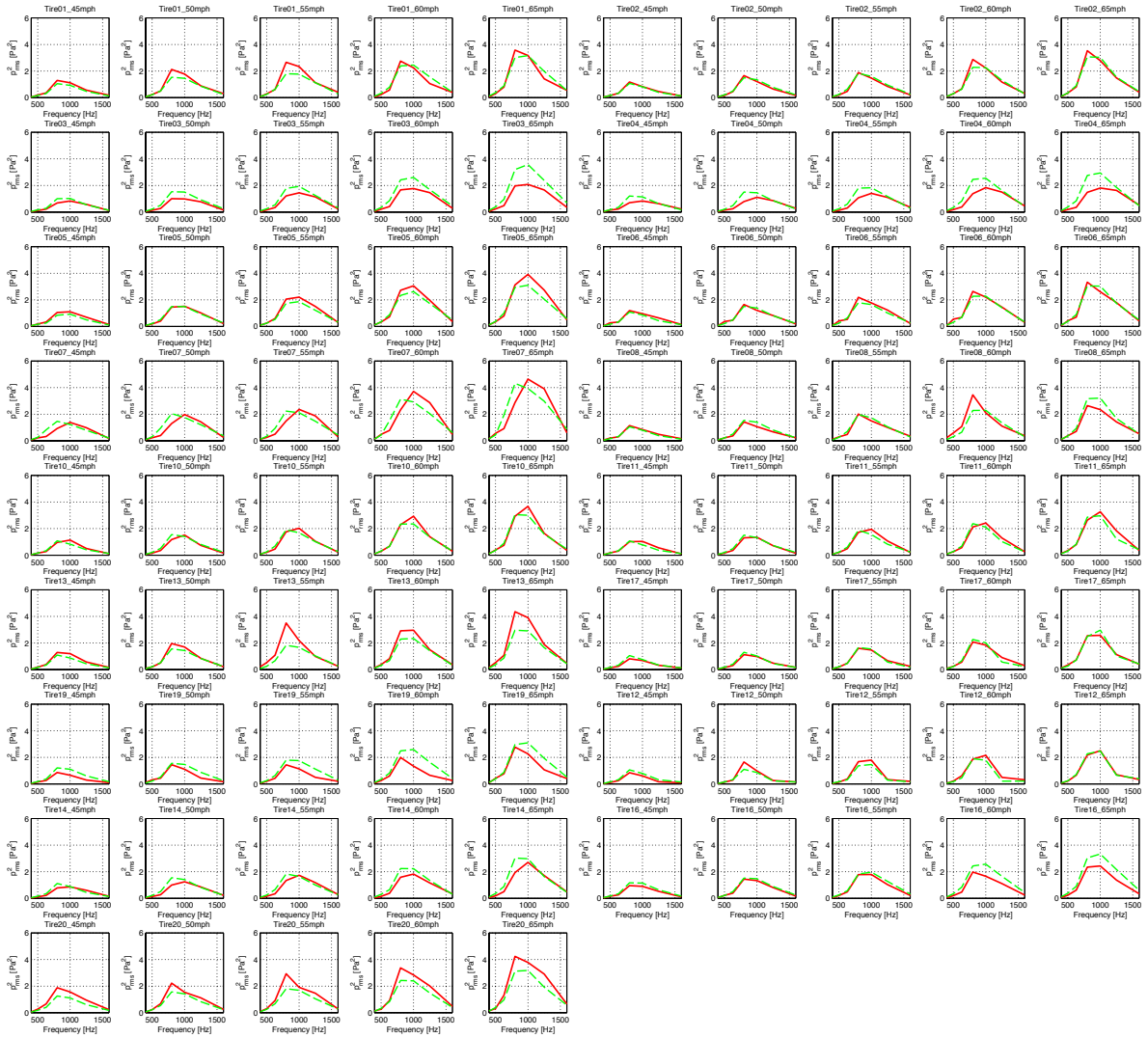

Figure B.9: Non-tread pattern noise in 1/3 octave band linear scale (red denotes measured, green denotes predicted)

B.4 1/3 Octave Band Spectrum in dB Scale

The results for the total noise in 1/3 octave band dB scale are shown in Figure B.10.

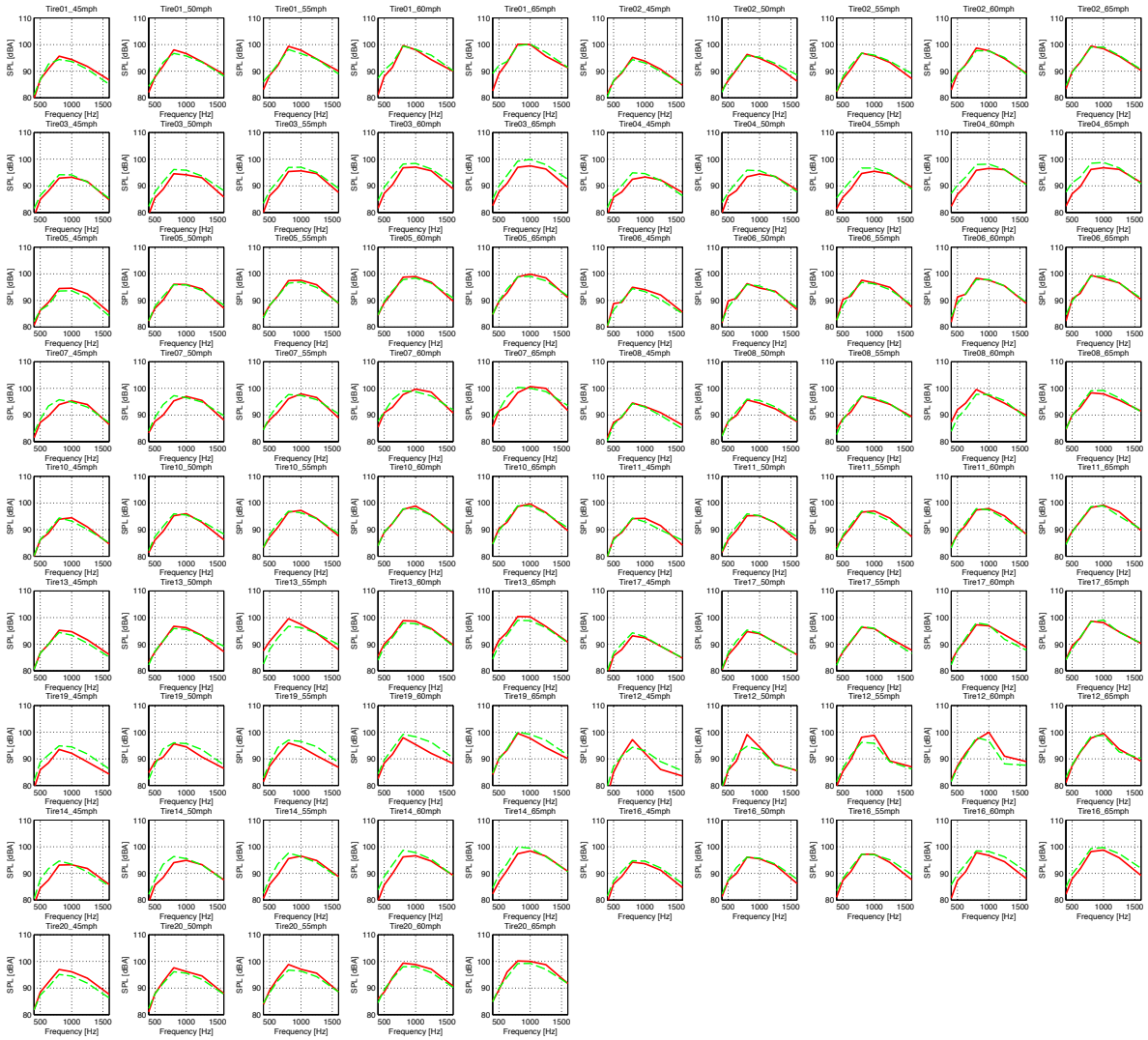

Figure B.10: Total noise in 1/3 octave band dB scale (red denotes measured, green denotes predicted)

The results for the tread pattern noise in 1/3 octave band dB scale are shown in Figure B.11.

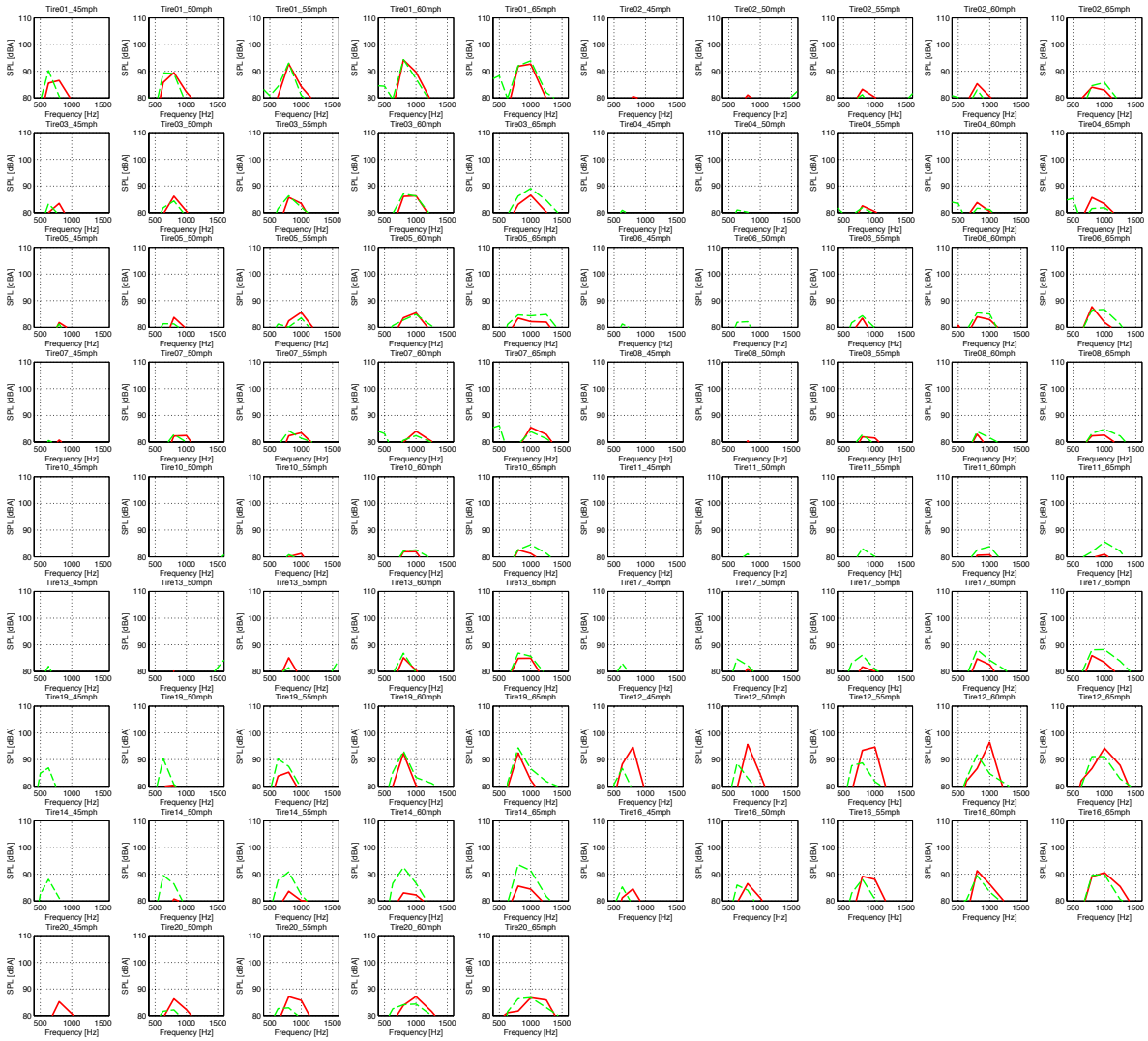

Figure B.11: Tread pattern noise in 1/3 octave band dB scale (red denotes measured, green denotes predicted)

The results for the non-tread pattern noise in 1/3 octave band dB scale are shown in Figure B.12.

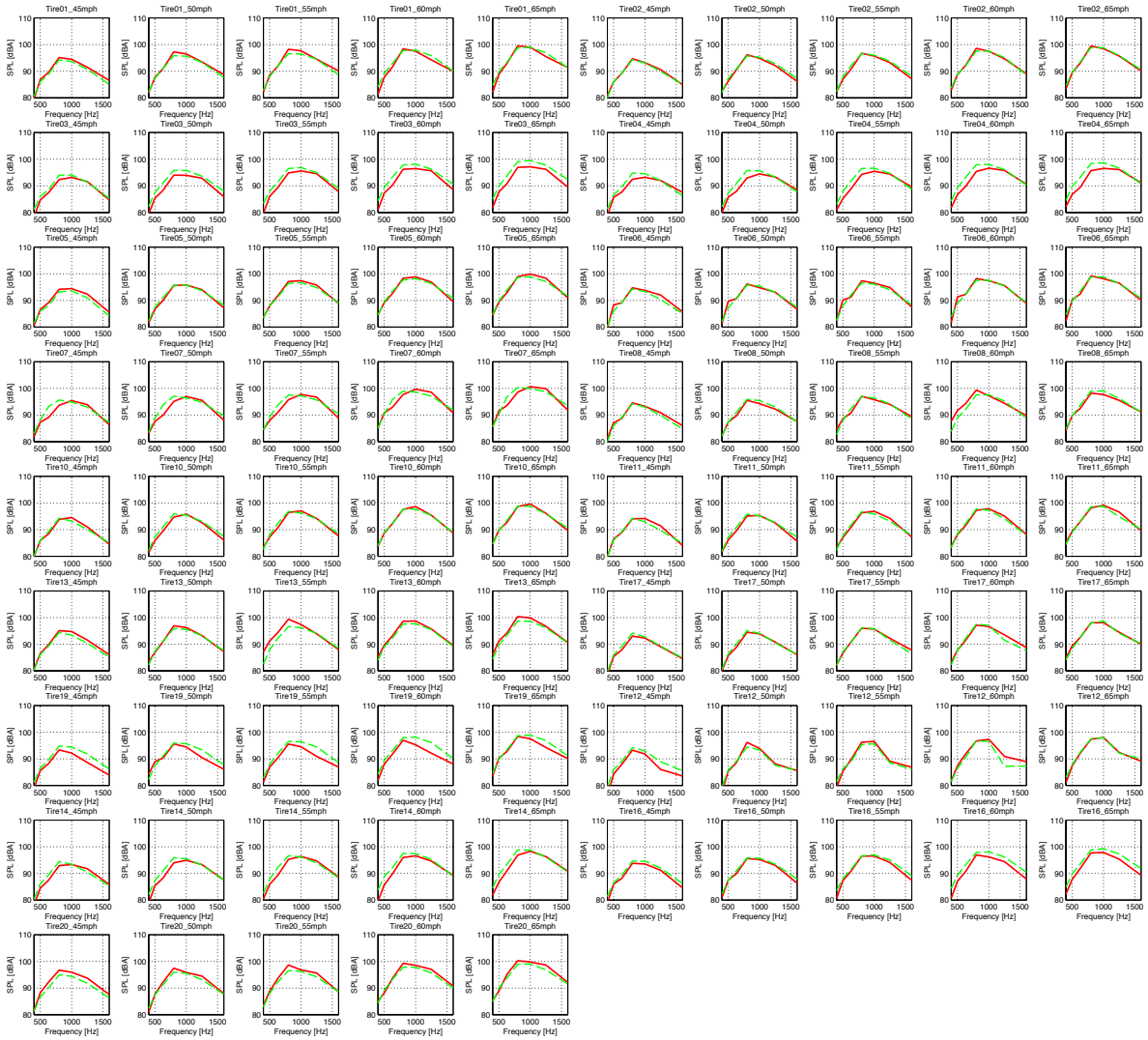

Figure B.12: Non-tread pattern noise in 1/3 octave band dB scale (red denotes measured, green denotes predicted)

B.5 Overall A-weighted Sound Pressure Level (OASPL)

The results for the Overall A-weighted Sound Pressure Level (OASPL) are shown in Figure B.13.

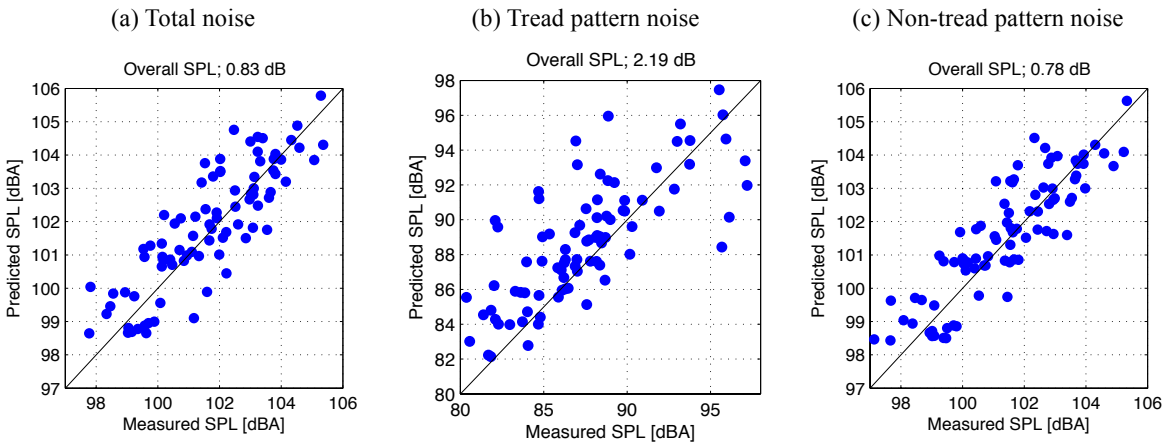

Figure B.13: Overall A-weighted Sound Pressure Level (OASPL) (the value above each subplot denotes the average dB error between measurement and prediction)

Appendix C: Effect of Speed

C.1 Introduction

Tire-pavement interaction noise (TPIN) dominates for passenger vehicles above 40 km/h and 70 km/h for trucks [7]. As the vehicle speed and the number of tire revolutions per unit time increase, the speed with which the tire comes in contact with the pavement surface increases, resulting in higher tire/pavement impact frequency and also an increased pumping in and out of air from the contact edge [23], which increases TPIN.

The approximate relationship between TPIN and speed is typically expressed by $L_p = 10n\log_{10}(v)+b$, where L_p is sound pressure level, n is speed exponent, v is vehicle speed, and b is a speed coefficient [24]. Ejsmont [120] reported that the speed exponent is in the range of 2.7~4.6. The values vary for different tires [420]–[422] and different pavements [423]–[425]. Speed exponents for each frequency ranges were reported by Beckenbauer and Kuijpers [289]. The overall speed exponent is around 4, however, a clear drop is shown around 500-800 Hz for normal tires. It is noted that different mechanisms have different speed exponent, as shown in Table C.1 [172].

Table C.1: Speed exponents for different TPIN mechanisms

TPIN Mechanism	Speed Exponent
Tread impact	2.0-3.0
Texture impact	3.0-3.5
Stick/slip (friction)	3.0-5.0
Stick/snap	3.0-5.0
Air pumping	4.0-5.0
Air turbulence	5.0-6.0
Pipe resonance	0.0
Helmholtz resonance	0.0

It might be instructive to develop a relevant method to differentiate noise-generating mechanisms at different frequencies [172]. A speed exponent of zero means the corresponding mechanisms are independent of speed, such as pipe resonance and Helmholtz

resonance. However, it should be pointed out that these two mechanisms are amplification mechanisms rather than generation mechanisms, which means the corresponding amplifying factors for the two mechanisms are independent of speed. However, the values of speed exponents in Table C.1 are mostly estimated based on the physical mechanisms rather than actually measurements, which have not yet been conclusively proven.

In addition, n and b are not independent of each other. b decreases as n increases [24]. However, Mogrovejo et al. [109], pointed out that extrapolation for the relation between b and n is not recommended since tire-pavement interaction is not the main source of noise at lower speeds.

The speed has an influence on the TPIN spectrum as it affects the tire eigenfrequencies [339]. There are three effects: (1) The stiffening due to the rotation leads to slightly higher structural eigenfrequencies; (2) the Coriolis acceleration leads to the so-called "bifurcation" effect, where the speed of waves propagating in opposite circumferential directions with the same wavelength are different even when observed in the Lagrangian (tire-fixed) reference system [426]–[428]; (3) the Doppler-shift, which appears when the tire is observed from an Eulerian (vehicle-fixed) reference system.

Speed is the most important single parameter in terms of TPIN levels, so nearly all TPIN models include it, mostly using statistical approaches [8], [23], [266], [360]–[363], [377]–[379]. However, few models investigate how speed affects the noise spectrum. Contradictory results were sometimes reported. Alt [270] showed that the dominant frequencies of TPIN do not change with speed while Schumacher [386] indicated that they do. Therefore, the effect of speed on TPIN is not clear, neither are the generating mechanisms. Takami and Furukawa [429], [430] reported that the dominant frequencies of air pumping noise do not change with speed at the leading edge of the contact patch, but increase with increasing speed at the trailing edge.

The main objective of this paper is to investigate the effects of speed on TPIN, including both overall levels and spectrums. Firstly, the experimental setup for collecting tire noise data from five different tires is introduced. Secondly, the total tire noise is separated into two noise components using order tracking analysis: noise component related to tread pattern and noise

component not related to tread pattern. To the best of the authors' knowledge, no previous literature has reported the application of this separation technique to the tire noise. Thirdly, the effects of speed on the total noise and the two noise components are analyzed separately. Finally, the speed exponent and scaling for the total noise and the two noise components are investigated.

C.2 Experiments

Nineteen tires of the same size (215/60R16) but with different tread patterns were tested between March and September, 2016, which are listed in Table C.2. Pictures of their tread patterns are displayed in Figure C.1. The red arrow in Figure C.1 indicates the rotation direction for directional tires in this test. The number of blocks, as shown in Table C.2, is the number of tread elements around the full tire circumference. The values range from 56 to 77. The number of plies in the tread band and the sidewall is different for different tires, indicating that the structure of the tires is different. The tread rubber hardness was measured immediately after the test.

Table C.2: Specifications of the test tires

No.	Condition	Number of Blocks	Number of Plies (Tread/ Sidewall)	Rubber Hardness [Shore A]
01	All season	70	5/2	67
02	All season	64	4/1	62
03	All season	72	4/2	66
04	All season	64	4/1	67
05	All season	76	4/1	69
06	All season	70	4/1	64
07	All season	76	4/1	68
08	All season	56	4/2	64
09	Winter/Snow	62	3/1	59
10	All season	72	4/1	65
11	All season	72	4/1	62
12	Winter/Snow	77	4/1	56
13	All season	66	4/1	64
14	All season	68	4/1	64

No.	Condition	Number of Blocks	Number of Plies (Tread/ Sidewall)	Rubber Hardness [Shore A]
15	All season	72	4/1	55
16	All season	72	4/1	66
17	All season	72	4/1	58
18	All season	65	5/2	65
19	Winter/Snow	60	5/2	64

Figure C.1: Tread patterns of the test tires (arrow indicates rotation direction)

The test pavement is U.S. Route 460 near Virginia Tech (between Toms Creek Rd. and North Main St. with one way distance of around 1.3 mile), as shown in Figure C.1. It is a non-porous asphalt pavement, dense graded hot mix asphalt (HMA), which is commonly seen in the USA. Both eastbound section and westbound section were tested, but only results on westbound section will be discussed in this paper. Part of relevant results on eastbound section were discussed in [382]. For each tire, the noise data were collected under five different vehicle speeds (45, 50, 55, 60, and 65 mph). In addition, an acceleration test was also conducted where the vehicle accelerated from 45 to 65 mph within 10 seconds. Three inflation pressures were tested, i.e., 26, 32 and 40 psi. In this paper, only results at 32 psi will be discussed; same conclusions are drawn for the other inflation pressures. The ambient

temperature range during the test days was 55-86 °F (13-30 °C).

Figure C.2: Test pavement (source from Google Map)

The vehicle used for testing was a 2012 Chevrolet Impala LT (front wheel drive). The equipment used for collecting noise data was an on-board sound intensity (OBSI) system based on standard AASHTO TP-76 [97]. The setup of the OBSI system is shown in Figure C.1. The system was installed at the rear right tire with a camber angle close to zero. The conventional OBSI system has two sound intensity probes, one at the leading edge of the tire-road contact patch, the other at the trailing edge. Each probe consists of two microphones to record the sound pressure. The sound intensity along the direction of the two microphones (away from the tire) is then calculated. The optical sensor, as shown in Figure C.1, radiates a beam onto the side face of the black disk rotating with the tire, and once the beam encounters the retroreflective tape and gets reflected to the optical sensor, the optical sensor generates a pulse. Therefore, a pulse signal is recorded at the exact time the tire completes one revolution. The optical signal can be used to accurately calculate vehicle speed, acceleration, as well as used for the order tracking analysis, which will be discussed later. The microphone and optical signals were recorded simultaneously at 25.6 kHz. The microphones were very close to the noise source of interest, i.e., tire-pavement interaction, therefore, the other noise sources, such as engine and exhaust, have marginal influence on the total noise collected. In addition, a foam ball-type microphone windscreen was wrapped around each probe to eliminate the wind noise.

Figure C.3: On-board sound intensity (OBSI) with optical sensor installed on the test vehicle

C.3 Tire Noise Analysis

A high-pass filter at 20 Hz was applied to the sound pressure time signals to eliminate subfrequency interferences from wind or the electronic system. In this section, only the signal from the leading inboard microphone (Mic 1) will be used for the illustration. However, the same results were observed and the same conclusions were drawn from the other microphones. It should be pointed out that all the results presented in this section are only valid for the pavement tested.

C.3.1 Tire Noise Components

The un-weighted sound pressure level spectrogram (dB) for Tire 12 during the acceleration test (from 45 mph to 65 mph within 10 seconds) is shown in Figure C.4. This figure is used to illustrate that there exist two main noise components in the dominant part of the spectrum, e.g., 600 to 1200 Hz. The first component is clearly associated to the vehicle speed or tire speed with the center band frequency going from 700 to 1000 Hz as the vehicle speed increases from 45 mph to 65 mph. The second component is independent of the vehicle speed (or tire rotation) with the spectral content encompassed always within the fixed frequency range between 600-1200 Hz.

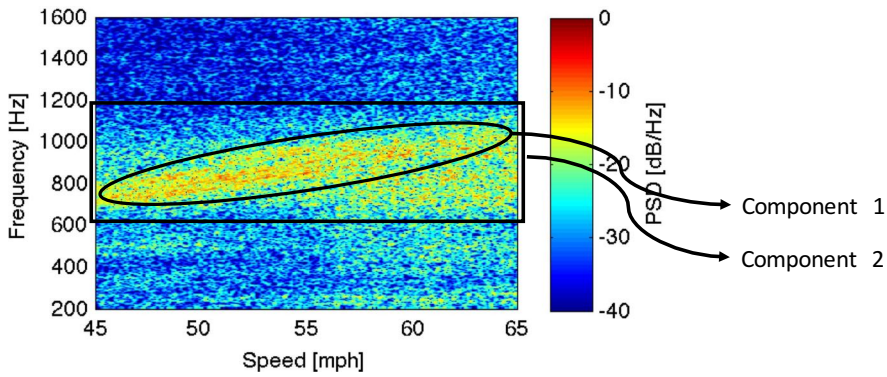

Figure C.4: Spectrogram of microphone 1 (leading inboard) for Tire 12 accelerating from 45 mph to 65 mph

Both, the tread impact and the air pumping, are periodic with the rotation of the tire. It is reasonable to infer that the first component of noise is related to the tread pattern. This noise component is, thus, referred to as tread pattern noise. The second component is clearly not related to the periodic tread pattern and it is most likely due to tire structural vibration excited by the roughness of the pavement. However, for the sake of generality, this second noise component is referred here as non-tread pattern noise. It should be noted that, the tread pattern noise and non-tread pattern noise are categorized by the excitation source (periodic tread pattern or non-periodic pavement) rather than the vibration response position (tire tread or carcass). Both tire tread noise and tire carcass noise consist of both tread pattern noise and non-tread pattern noise. To be more specific, the tire tread noise includes two parts: (1) tread pattern noise that is periodic and related to the geometry/layout of the tread elements, and (2) vibration noise of tread elements that is randomly excited by the pavement and more related to the stiffness of the tread elements, which is not considered as tread-pattern related, thus belongs to the non-tread pattern noise. Likewise, the tire carcass noise also consists of tread pattern noise and non-tread pattern noise.

To investigate the effect of speed on the two noise components separately, these two noise components must be separated. The appendix briefly describes the separation technique using the optical sensor signal. The pipe resonance due to longitudinal tread grooves is considered as a noise amplification mechanism rather than a noise generation mechanism, i.e., the pipe resonance is able to amplify both tread pattern noise and non-tread pattern noise. For some cement concrete pavement tined with evenly spaced lateral slots, a tonal noise whose

frequency scale with speed can be generated due to the periodic pavement texture. However, as long as the pavement texture is not exactly periodic (some errors of slot intervals may inevitably occur), this tonal noise will be separated into the non-tread pattern noise using order tracking analysis, which indicates the separation technique discussed in the present paper is still valid (results not shown here). It should be noted that the results and conclusions on the speed effect in the present paper is only valid for the tested pavement which is isotropic.

C.3.2 Tire Noise Separation

In this section, order tracking analysis utilizing the optical signal is performed to separate the two components of noise signals. The total, tread pattern and non-tread pattern noise spectra for some of the test tires are displayed in Figure C.5. It can be observed that the tread pattern noise component is significant for Tires 12 and 19 (both snow tires). For Tires 15 and 18, the tread pattern noise is significantly lower than the non-tread pattern noise. It also explains why the total noise spectrum coincides to a large degree with the non-tread pattern noise spectrum as shown in Figure C.5b, c. On the other hand, for tires 12 and 19 the tread pattern has a more important contribution to the tire noise. The tread pattern noise is more easily observed in the spectra in Figure C.5a, d. It is important to mention that the relative contribution between tread-pattern and non-tread pattern noise components is a function of the pavement. Thus, the results presented here are valid for the pavement tested. Preliminary data from testing on a newer and smoother asphalt pavement shows that the tread pattern noise contribution increases to 50% of the total tire noise for Tire 12. Two extreme scenarios for a typical patterned tire can be expected: (1) on an extremely smooth pavement, such as the steel surface of the lab drum, the tread pattern noise contribution should be completely dominant, as there is basically no pavement excitation; (2) on an extremely rough pavement, such as the gravel road, the non-tread pattern noise should be overwhelmingly dominant, as the tread pattern has marginal influence on the interaction between the tire (with a gentle tread pattern) and the pavement (with more aggressive texture). It is noted that in the second scenario, the relatively marginal tread pattern noise doesn't necessarily suggest that the tread noise is marginal.

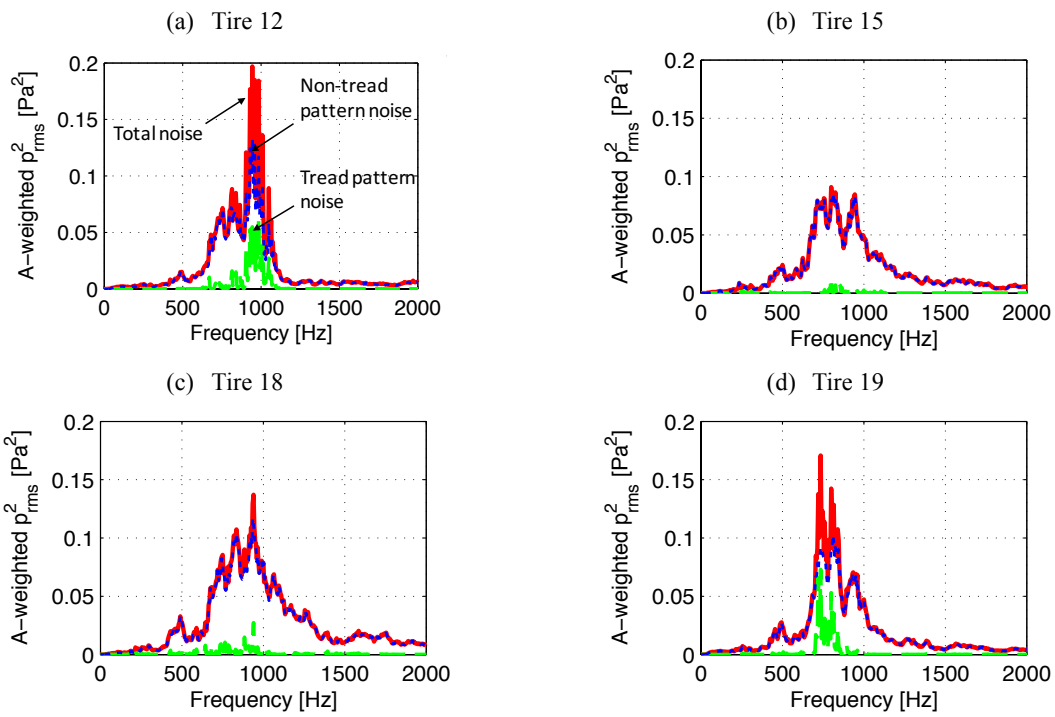

Figure C.5: Total, tread-pattern, and non-tread pattern noise components at 60 mph (5 Hz resolution)

For the tires that have a large component of tread pattern noise, more oblique spectral contents will occur in the spectrogram of acceleration test, as shown in Figure C.4. For the tires that have a small component of tread pattern noise, the spectral contents in the spectrogram of acceleration test will remain nearly level. This explains why the results contradicted each other in some of the literature [270], [386].

The non-tread pattern noise can be potentially considered as the minimum tire noise for a specific tire when the tread pattern is perfectly randomized and the tread pattern noise is reduced to zero. A perfectly randomized tread pattern is similar to a slick tread pattern in perspective of tire pavement interaction noise generation. That is also to say, usually for the tires for which the tread patterns are already well randomized, further optimization of tread patterns will not result in too much noise reduction. An important conclusion of this initial study is that the easier way to reduce tire noise is to reduce the non-tread pattern noise which is shown by the data to be the major component, at least for the pavement used in this field tests. This also explains why sometimes the slick tire is among the noisiest [255], as it is the non-tread pattern noise rather than the tread pattern noise that predominantly determines the

acoustic performance of a tire for a specific pavement.

C.4 Effect of Speed on Noise Spectrum

The effect of speed is analyzed separately for the total noise, the tread pattern noise, and the non-tread pattern noise spectrums, which has not been reported in previous open literature. Both signals from leading inboard microphone (Mic 1) and trailing inboard microphone (Mic 3) are discussed, because different characteristics are shown.

C.4.1 Effect of Speed on Total Noise Spectrum

The total noise spectrums for two representative tires (Tire 12 with large tread pattern noise and Tire 15 with small tread pattern noise) at different speeds are shown in Figure C.6. The noise from the leading edge of the contact patch is shown on the left while the noise from the trailing edge is shown on the right. Five speeds (45, 50, 55, 60, 65 mph) were tested, but for the sake of clarity and concision, only three speeds (45, 55, 65 mph) are presented here.

For Tire 12, the dominant frequencies shift with speed for both leading and trailing edge; the amplitude doesn't change much for the leading edge as the speed increases while it increases significantly for the trailing edge. For Tire 15, however, the results are completely different: the dominant frequencies do not shift with speed for both leading and trailing edge; the amplitude increases as the speed increases for both leading and trailing edge. For Tire 19 (not shown here), the trend looks similar to Tire 15, but the spectral amplitude increases drastically as speed increases from 55 to 65 mph, which cannot be well explained for the moment. Therefore, the effect of speed on the total noise is not clear and general conclusions cannot be drawn.

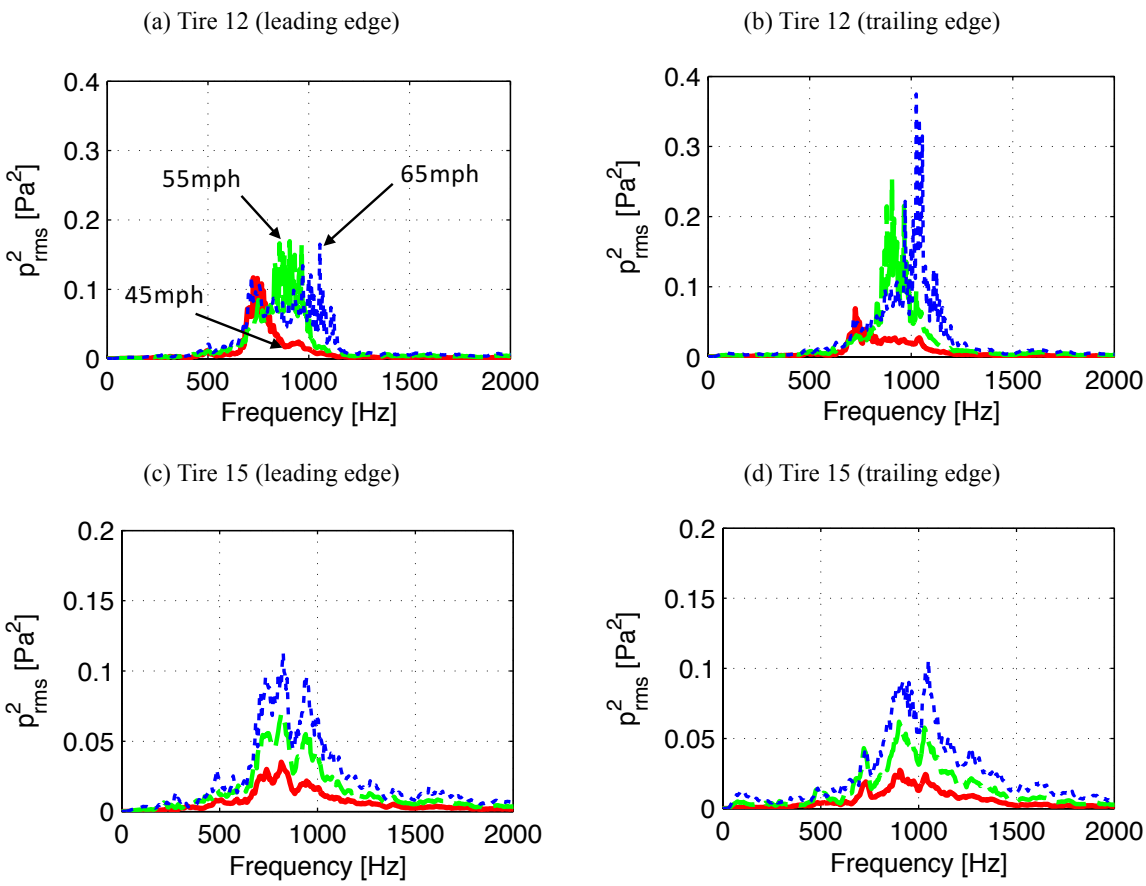

Figure C.6: Total noise spectrums for different speeds

C.4.2 Effect of Speed on Tread Pattern Noise Spectrum

The tread-pattern-noise spectrums for Tires 12 and 15 at different speeds are shown in Figure C.7.

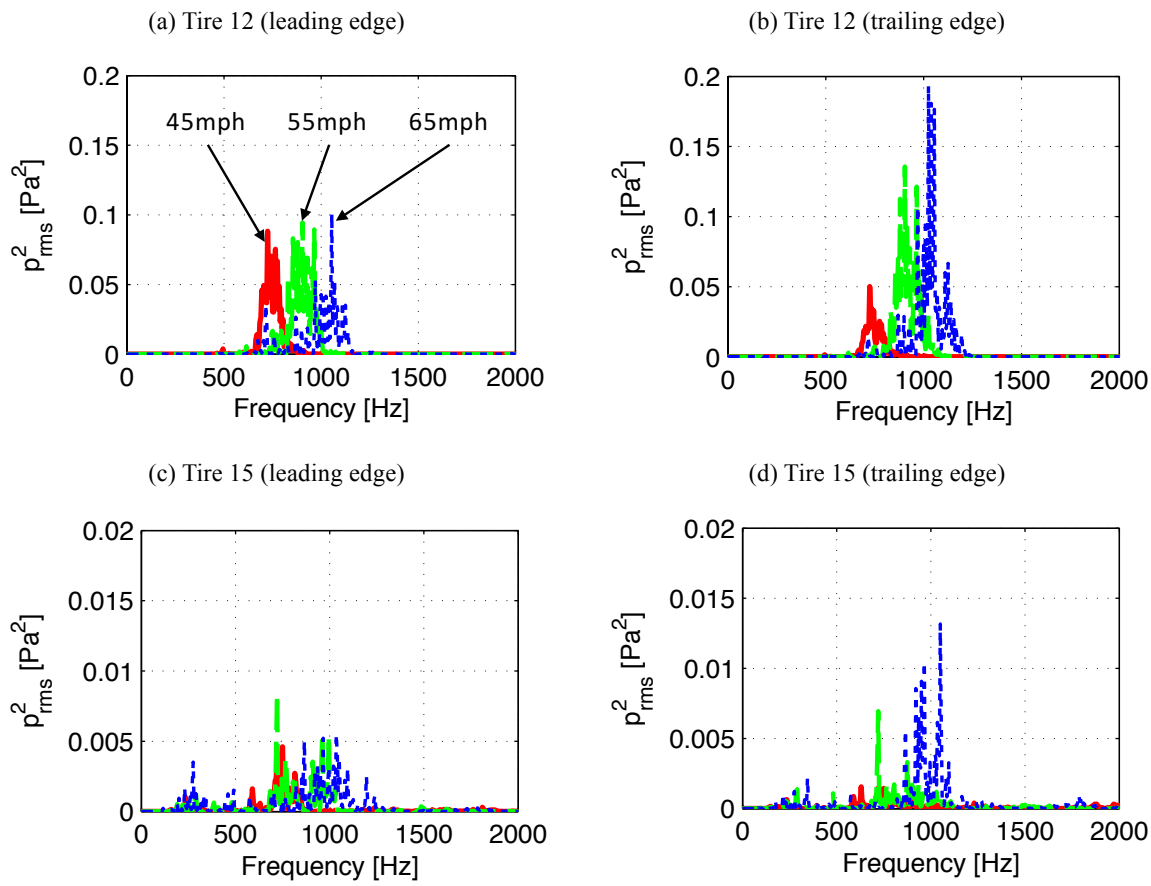

Figure C.7: Tread-pattern-noise spectrums for different speeds

For a specific tire at the specific edge, the spectral contents change with speed. The dominant frequencies increase with speed and are around the block passing frequency (number of blocks times tire rotational speed). For example, it is given that the number of blocks for Tire 12 is 77, and the tire rotational speed at 45, 55, and 65 mph are ~9.7, 12.1, and 14.1 Hz, respectively, according to the optical signal. Through simple calculation, the block passing frequencies at 45, 55, and 65 mph are ~747, 932, and 1086 Hz, respectively, which agrees very well with the dominant frequencies as shown in Figure C.7a and Figure C.7b.

Speed usually has a larger influence on the trailing edge than on the leading edge, e.g., Tires 12 and 15, where the amplitude for the leading edge remains nearly constant as the speed increases while the amplitude for the trailing edge greatly increases. The reason that the spectrums for Tire 15 are fuzzy is that, the spectral amplitude is actually too small (one

order of magnitude smaller than for Tire 12).

C.4.3 Effect of Speed on Non-Tread Pattern Noise Spectrum

The non-tread-pattern-noise spectrums for Tires 12 and 15 at different speeds are shown in Figure C.8.

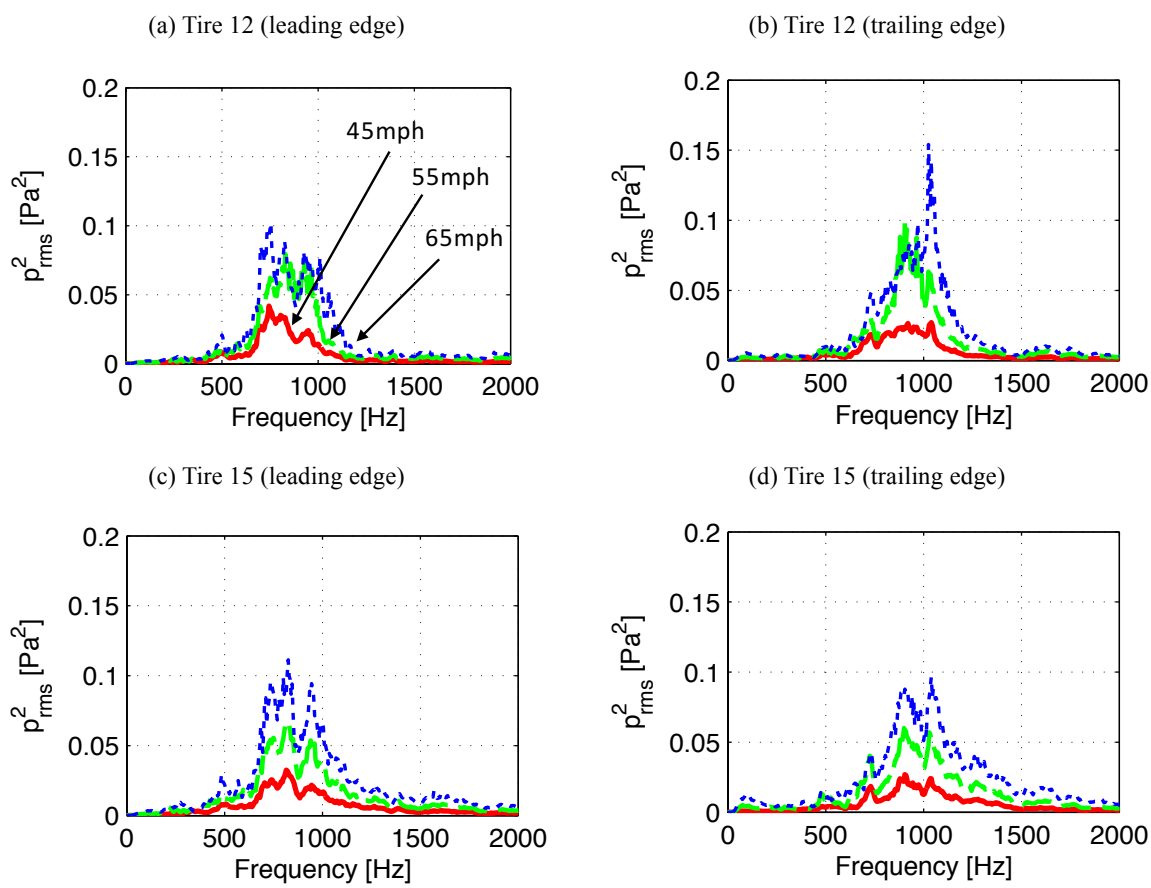

Figure C.8: Non-tread-pattern-noise spectrums for different speeds

For a specific tire at the specific edge, the spectral shape remains the same for different speeds while the amplitude increases with speed. At the leading edge, the dominant frequencies are around 800 Hz where two peaks are usually observed. At the trailing edge, the dominant frequencies are around 1000 Hz where another two peaks are usually observed. It is stipulated that this non-tread pattern noise comes from the structural resonances of other tire components not related to tread pattern, due to the pavement excitation that can be considered

as a broadband spectrum.

C.4.4 Summary

No general trends for the effect of speed on the total tire noise spectrum can be found for different tires. However, after the total tire noise is broken down into the two components, the effect of speed can be generalized: the frequencies of the tread pattern noise component shift with speed while the frequencies of non-tread pattern noise component do not shift with speed (only amplitudes change). From another point of view, this noise separation technique is thus validated.

C.5 Scaling Law for Different Speeds

In addition to the effect of speed on the noise spectrum, the overall A-weighted sound pressure level (OASPL) is also of interest, as shown in Figure C.9. The OASPL is dominated by the noise in the range of 400-1200 Hz. It is shown that the effect of speed on the total noise and the non-tread pattern noise look similar for different tires while the effect of speed on the tread pattern noise look different for different tires.

(a) Tire 12 (leading edge)

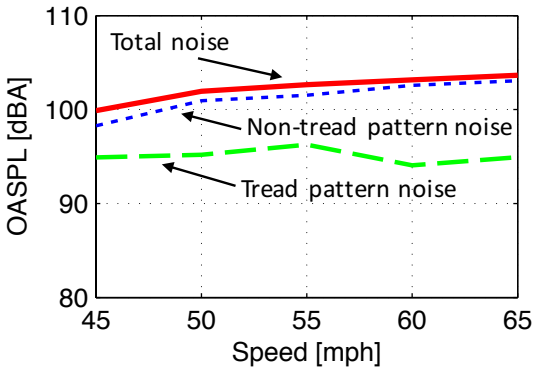

(b) Tire 12 (trailing edge)

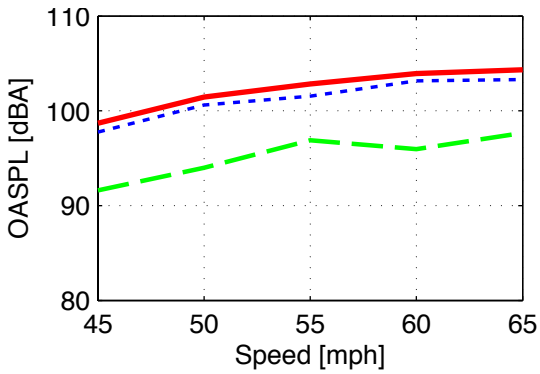

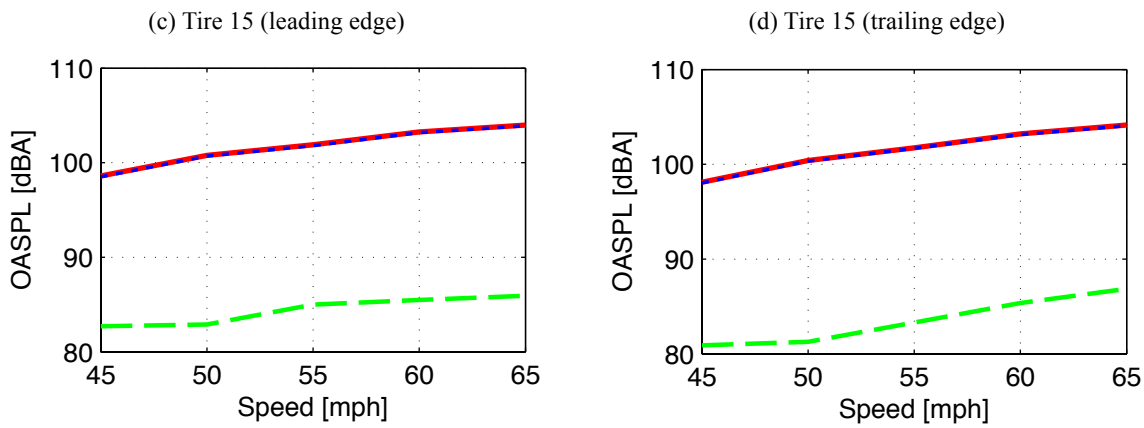

Figure C.9: Effect of speed on the overall A-weighted sound pressure level (OASPL)

The approximate relationship between overall A-weighted tire noise level and speed can be described as the equation below [24].

$$L_{pA} = 10n\log_{10}(v) + b$$

where L_{pA} is overall A-weighted sound pressure level (OASPL) in dB scale, n is scaling law or speed exponent, v is vehicle speed, and b is a speed coefficient. The scaling law can be calculated statistically using a curve-fitting approach. It can also be considered as the sensitivity of noise level to speed. The scaling law can then be used to scale the noise spectrum at a given speed to the reference speed, as given by

$$S_{v_ref} = S_v \times \left(\frac{v_{ref}}{v}\right)^n$$

where v_{ref} is the reference speed (60 mph in this paper), S_v is the noise spectrum at the speed v in the linear scale, S_{v_ref} is the noise spectrum scaled to the reference speed in the linear scale.

The optimized scaling law n for each tire is identified through an iteration process, as shown in Table C.3. The first row (n = 0) shows the overall sound pressure level at different speed; the standard deviation in the rightmost column is computed from the five values. It should be noted that, the standard deviation for dB is mathematically wrong, but here is only

for the purpose of identifying the optimized scaling law. From the second to the last row, SPL at the five speeds are all scaled to 60 mph using Equation above. It can be seen that, as scaling law *n* increases, the standard deviation decreases at first then increases. The optimized scaling law for this tire (Tire 01) is 2.6 when standard deviation is minimum. In addition, the optimized scaling law can also be obtained through nonlinear regression. The results are almost the same for the two algorithms.

Table C.3: Identification of optimized scaling law n for total noise of Tire 01 at leading inboard edge (red indicates optimized n)

Scaling law [-]	45 mph [dB]	50 mph [dB]	55 mph [dB]	60 mph [dB]	65 mph [dB]	Standard Deviation [dB]
0.0	101.8	103.2	104.9	105.0	105.8	1.6
1.0	103.1	103.9	105.2	105.0	105.5	1.0
2.0	104.3	104.5	105.5	105.0	105.1	0.5
2.6	**105.1**	**104.9**	**105.7**	**105.0**	**104.9**	**0.3**
3.0	105.6	105.2	105.8	105.0	104.8	0.4
4.0	106.9	105.9	106.2	104.9	104.4	1.0
5.0	108.1	106.5	106.5	104.9	104.1	1.6
6.0	109.4	107.2	106.8	104.9	103.7	2.2
7.0	110.7	107.9	107.1	104.8	103.3	2.8
8.0	111.9	108.5	107.4	104.8	103.0	3.4
9.0	113.2	109.2	107.7	104.8	102.6	4.1
10.0	114.5	109.9	108.0	104.8	102.3	4.7

C.5.1 Scaling Law for Total Noise

Using the same process in Table C.3, the standard deviation versus scaling law of the total tire noise for different tires is plotted in Figure C.10. The lowest point of each curve indicates the optimized scaling law for each tire. It is also shown that the standard deviation is not very sensitive around the optimized scaling law, indicating that a bit error from the optimized value will still generate good scaling results.

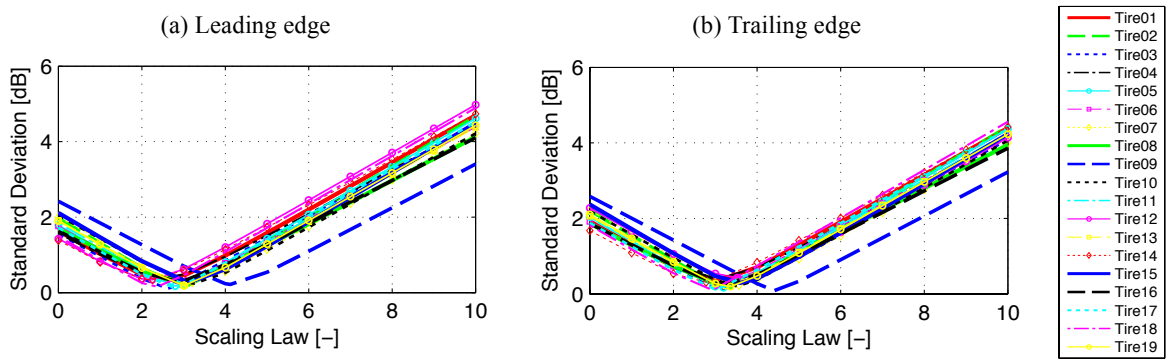

Figure C.10: Standard deviation versus scaling law for the total noise

The optimized scaling law n and coefficient of determination R^2 for the total tire noise is shown in Table C.4. The scaling law of the trailing edge (2.9~4.4) is generally larger than the leading edge (2.3~4.1), indicating that speed has a larger influence on the noise at the trailing edge; one reason might be that at the trailing edge the tread rubber is released from contact with the pavement and larger vibrations occur while at the trailing edge the tread rubber is to be in contact with the pavement and the vibrations are suppressed. This is in accord with the observation that the tread band has a much wider distribution of vibrations at the trailing edge than that at the leading edge [352]. It is also shown in Figure C.6 that the noise spectral amplitude at the trailing edge increases faster with speed than the leading edge.

Table C.4: Scaling law for total tire noise

Tire No.	Leading Edge		Trailing Edge	
	n	R^2	n	R^2
01	2.84	0.94	3.30	0.96
02	3.00	~1.00	3.37	~1.00
03	2.54	~1.00	3.06	0.99
04	2.80	0.99	3.27	0.99
05	3.22	0.94	3.55	0.96
06	2.77	0.97	3.11	0.98
07	3.21	0.98	3.57	0.99
08	2.93	0.97	3.22	0.98
09	4.13	0.99	4.42	~1.00
10	3.25	0.98	3.52	0.99

11	2.94	0.98	3.22	0.98
12	2.25	0.95	3.53	0.96
13	3.03	0.98	3.26	0.99
14	3.11	0.82	3.55	0.86
15	3.20	0.98	3.60	0.99
16	2.82	0.98	3.25	0.99
17	2.80	0.99	3.06	0.99
18	2.37	0.99	2.92	~1.00
19	3.02	0.99	3.37	~1.00

All the noise spectrums at different speeds are scaled to the reference speed using Equation above. The scaled spectrums for Tires 12 and 15 are shown in Figure C.11. It can be seen that the scaling law works well for the total noise spectrum of Tire 15. However, the scaling results are very bad for Tire 12.

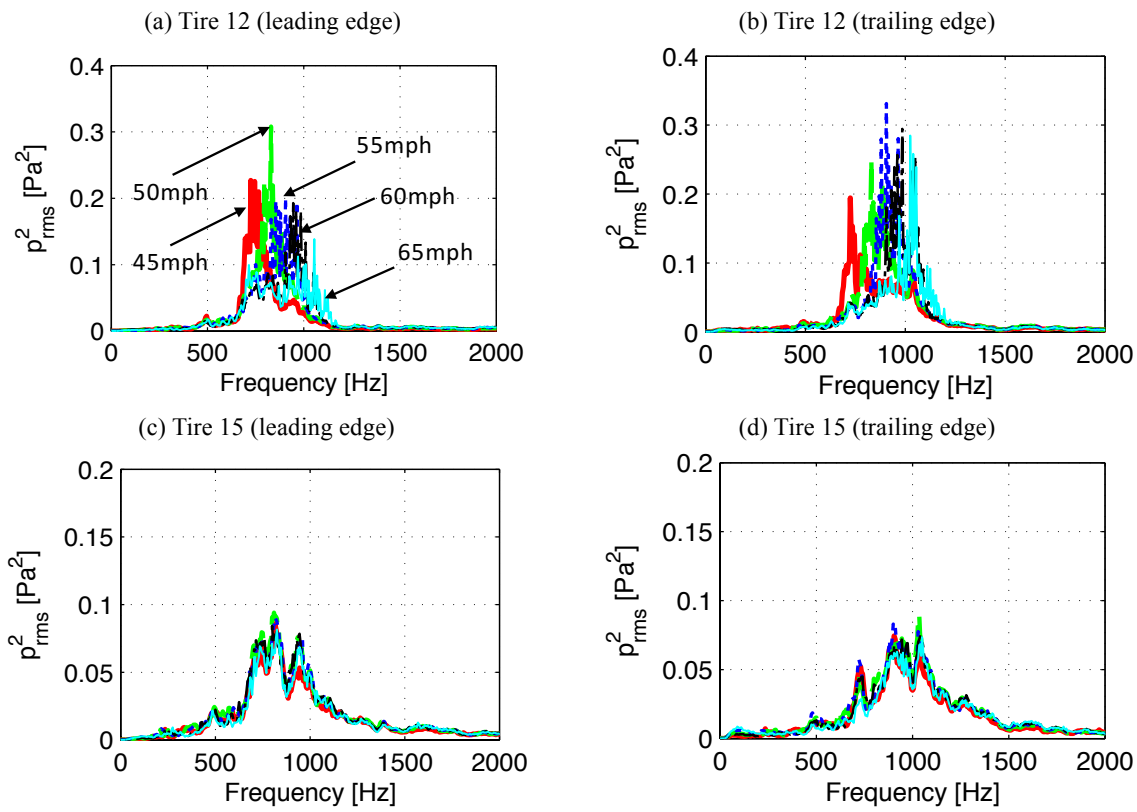

Figure C.11: Scaled total noise spectrums for different speeds

As discussed earlier, the effects of speed on the tread pattern noise component and the non-tread pattern noise component are different, therefore, looking at scaling law of total noise is an inaccurate approach. The better approach used in the following is to separate the two noise components and then look at the scaling laws separately.

C.5.2 Scaling Law for Tread Pattern Noise

The standard deviation versus scaling law of the tread pattern noise for different tires is plotted in Figure C.12. It is shown that the curves for the tread pattern noise do not collapse as well as those for the total tire noise as shown in Figure C.10, suggesting that the optimized scaling law has a broader range for the tread pattern noise of different tires.

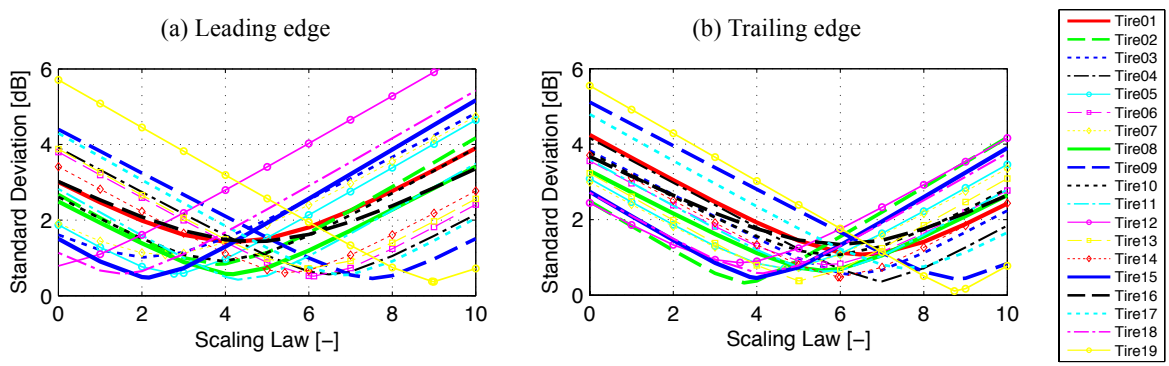

Figure C.12: Standard deviation versus scaling law for the tread pattern noise

The optimized scaling law n and coefficient of determination R^2 for the tread pattern noise is shown in Table C.5. It should be pointed out that the tread-pattern noise for some tires, such as Tire 15, is so small that strong conclusions cannot be made, neither for cases with small values of R^2 such as Tire 01. The range of the scaling law for the tread pattern noise is much wider than the total noise. However, the scaling law at the trailing edge (3.6~8.8) is still generally larger than the leading edge (-0.2~9.0), except for some tires like Tire 19 where the scaling law at both the leading and trailing edge is as large as around 9. It means that, for Tire 19, increasing speed will amplify the tread pattern noise dramatically at both, leading and trailing edges; there is basically no tread pattern noise at low speed (45 mph) while the tread pattern noise is considerably large at high speed (65 mph). Another anomaly is that, for Tire

12, the scaling law at the leading edge is negative, which means increasing speed reduces the tread pattern noise, which is counterintuitive. This is possibly due to the fact that Tire 12 is directional tire and its tread pattern is perfectly symmetric. It is interesting to mention that the tread pattern noise for Tire 12 tested in the reverse direction is reduced by ~6 dB and the scaling law for both leading edge and trailing is positive (leading: 1.64 with R^2 = 0.79; trailing: 5.30 with R^2 = 0.71). This is likely because the noise generation mechanisms are different between the leading edge and trailing edge and in the reverse direction the footprint of the tread pattern is reversed.

Table C.5: Scaling law for tread pattern noise

Tire No.	Leading Edge		Trailing Edge	
	n	R^2	n	R^2
01	1.65	0.07	3.98	0.21
02	3.81	0.79	3.70	0.99
03	1.81	0.62	5.32	0.87
04	5.47	0.84	6.46	0.99
05	2.16	0.78	3.76	0.80
06	5.70	0.97	5.51	0.99
07	2.56	0.56	4.69	0.89
08	4.19	0.92	5.56	0.97
09	7.53	0.99	8.75	~1.00
10	3.90	0.79	5.72	0.81
11	4.30	0.98	5.45	0.99
12	-0.22	0.02	3.60	0.80
13	5.97	0.95	5.02	0.98
14	4.87	0.92	5.44	0.95
15	2.17	0.91	3.83	0.98
16	3.46	0.49	5.24	0.83
17	6.73	0.98	7.50	0.97
18	1.54	0.67	4.16	0.89
19	8.96	0.98	8.74	~1.00

The differences in the scaling law of tread pattern noise for different tires might be due to

the different tread pattern designs. For example, some tread grooves in Tire 19 have very large tortuosity, as shown around the colored lines in Figure C.1, which prevents the air from pumping out smoothly and increases the air pumping noise. At very high speed, the groove volume changes much faster than the air can evacuate from or suck into the squeezed/expanded groove; explosion/implosion phenomenon might occur generating shock waves of which the scaling law can be up to 8 [354], [431].

The scaled spectrums for the different speeds are shown in Figure C.13. It should be noted that, in these spectrums, both the amplitudes and the frequencies are scaled with speed. The scaling of frequency will lead to the variation of A-weighted levels, but not considerably (less than 1 dBA for scaling from 45 mph to 60 mph). It can be seen in Figure C.13 that the scaling results for the tread pattern noise spectrums are pretty good. It is implied that the dominant spectral contents of tread pattern noise do have proportional relation with speed.

(a) Tire 12 (leading edge)

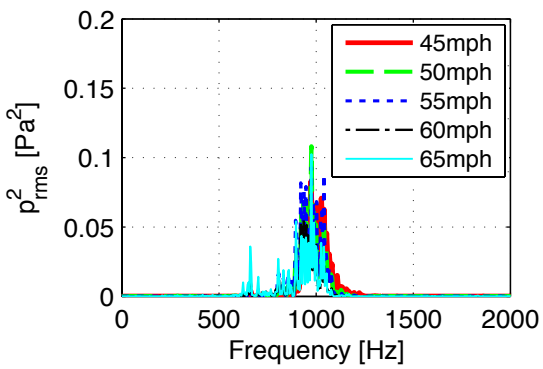

(b) Tire 12 (trailing edge)

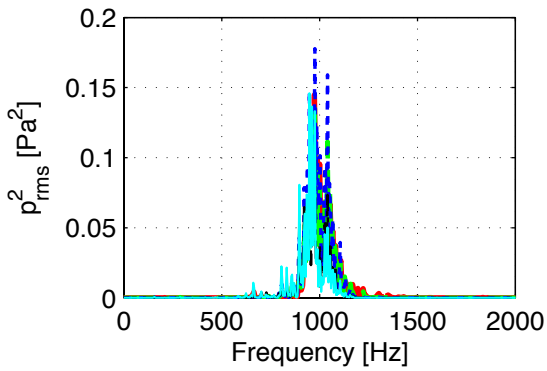

(c) Tire 15 (leading edge)

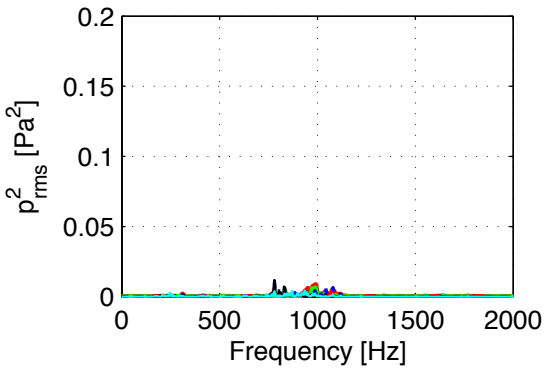

(d) Tire 15 (trailing edge)

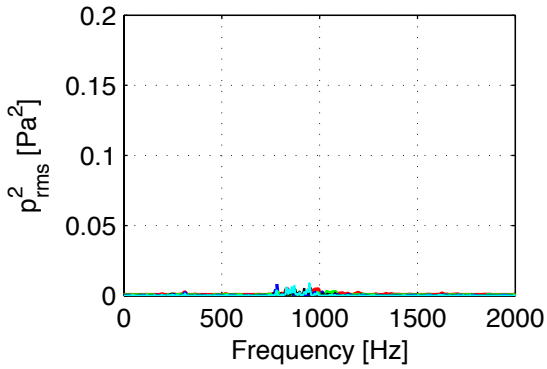

Figure C.13: Scaled tread pattern noise spectrums for different speeds

C.5.3 Scaling Law for Non-Tread Pattern Noise

The standard deviation versus scaling law of the non-tread pattern noise for different tires is plotted in Figure C.14. Compared with Figure C.12, it is shown that the curves for the non-tread pattern noise are much more concentrated than those for the tread pattern noise, indicating that the optimized scaling law of the non-tread pattern noise for different tires is more stable.

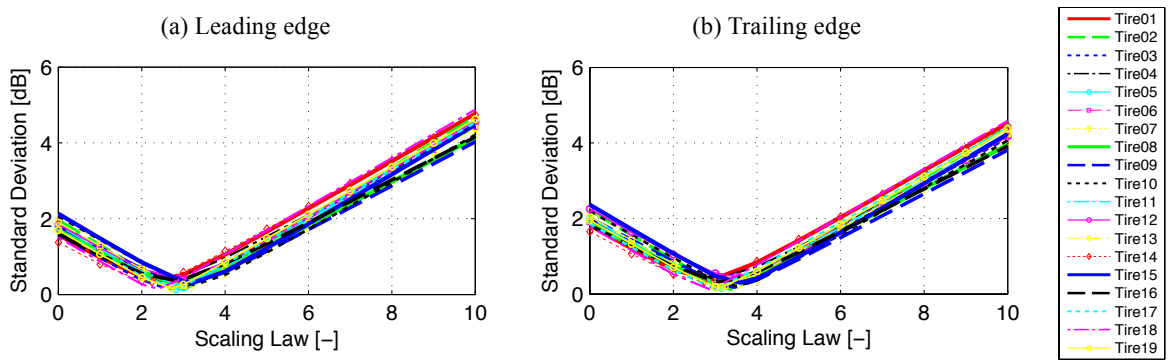

Figure C.14: Standard deviation versus scaling law for the non-tread pattern noise

The optimized scaling law n and coefficient of determination R^2 for the non-tread pattern noise is shown in Table C.6. Likewise, the scaling law at the trailing edge (2.9~3.6) is still larger than the leading edge (2.4~3.3), which is similar to that for the total noise. The differences in the scaling law of non-tread pattern noise for different tires might be due to the different tire structures, such as tire stiffness and rubber hardness. No correlations have been found between the number of plies and the scaling law value based on the current results. For the interest, the non-tread pattern noise for Tire 12 tested in the reverse direction doesn't change, which makes sense because the non-tread pattern noise is not related to the tread pattern.

Table C.6: Scaling law for non-tread pattern noise

Tire No.	Leading Edge		Trailing Edge	
	n	R^2	n	R^2
01	2.86	0.91	3.25	0.93
02	2.98	~1.00	3.39	~1.00
03	2.57	~1.00	3.03	0.99
04	2.78	0.99	3.22	0.99
05	3.26	0.94	3.55	0.96
06	2.70	0.97	3.08	0.99
07	3.22	0.98	3.54	0.98
08	2.92	0.97	3.22	0.98
09	3.09	0.97	3.46	0.99
10	3.27	0.98	3.52	0.99
11	2.91	0.98	3.23	0.98
12	2.89	0.96	3.49	0.94
13	3.01	0.98	3.24	0.98
14	3.11	0.82	3.53	0.86
15	3.22	0.98	3.59	0.99
16	2.80	0.97	3.19	0.98
17	2.77	0.99	3.03	0.99
18	2.40	0.99	2.87	~1.00
19	2.72	~1.00	3.16	~1.00

The scaled spectrums for the different speeds are shown in Figure C.15. Unlike the scaled total noise spectrums, the scaling results are perfect for Tire 15 while fairly good for Tire 12.

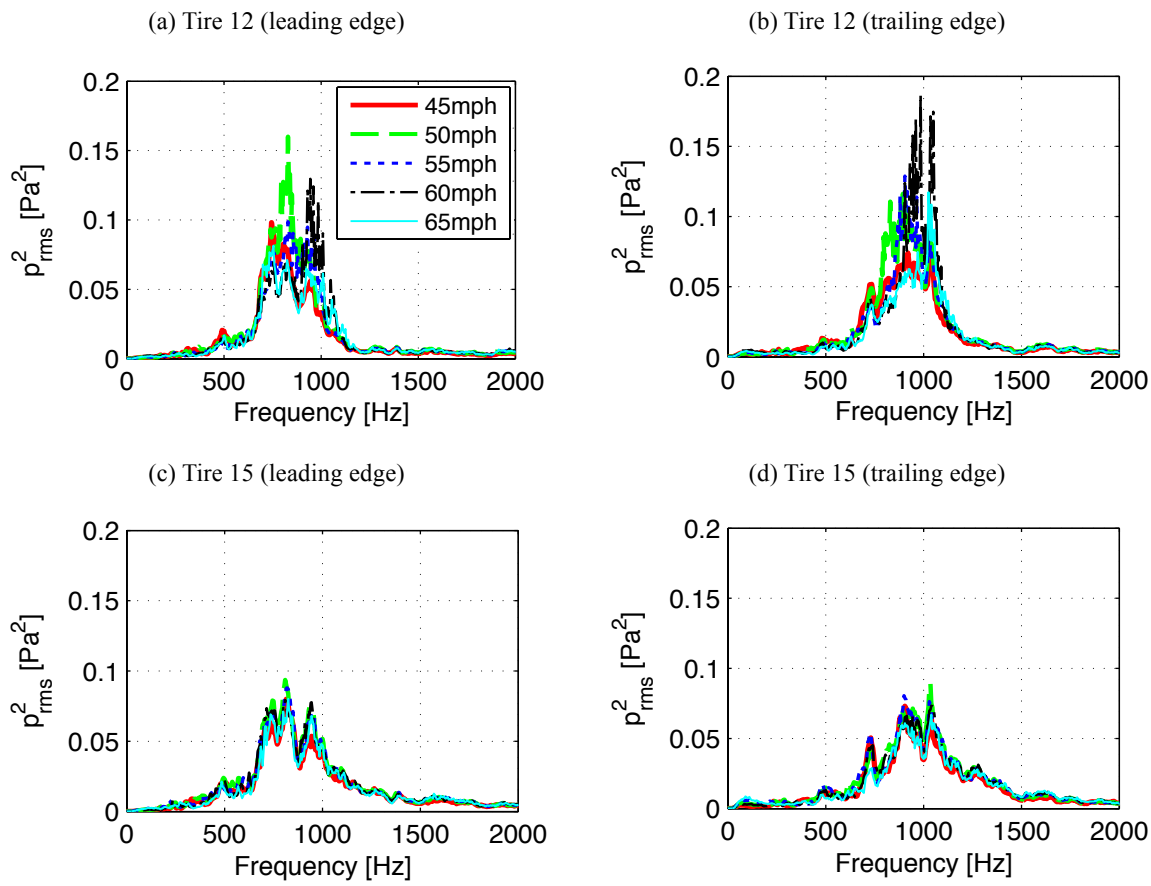

Figure C.15: Scaled non-tread pattern noise spectrums for different speeds

C.5.4 Scaling Law for Leading Edge and Trailing Edge

Figure C.16 shows that the scaling laws for the leading edge and trailing edge are positively correlated. The points are generally above the reference line ($y = x$), indicating that, as discussed before, the scaling law at the trailing edge is larger than that at the leading edge. The points for non-tread pattern noise are less randomly scattered than the other two, which means the results for the leading edge can be a good prediction for the trailing edge.

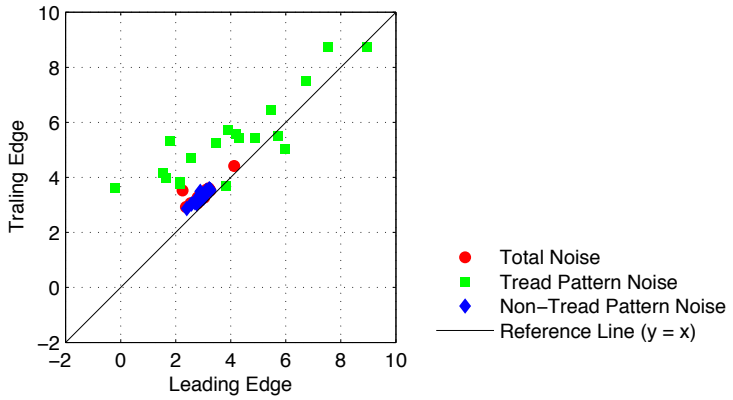

Figure C.16: Scaling laws for the leading edge versus trailing edge

C.6 Conclusions

For the non-porous asphalt pavement tested, there are no clear general trends for the effect of speed on the total tire noise spectrum for different tires. For some tires, the spectral shapes shift with speed, while for others they don't. Order tracking analysis was performed to separate the total tire noise into two components: tread pattern noise component and non-tread pattern noise component. General characteristics for the two noise components can be found. The spectral contents (dominant frequencies) of the tread pattern noise are proportional to speed. On the other hand, the spectral contents of the non-tread pattern noise do not change with speed except for its amplitude.

It was found that the tread pattern noise for different tread pattern designs has different sensitivity with respect to speed. Increasing the tread rubber hardness might decrease the sensitivity of non-tread pattern noise to speed. In addition, speed has greater influence on the noise generated at the trailing edge of the contact patch than at the leading edge.

Appendix D: Effect of Tire Inflation Pressure

D.1 Introduction

For modern passenger-car tires, the recommended cold inflation pressure is usually between 30 and 35 psi while the maximum allowable inflation pressure is typically between 44 and 51 psi. For modern truck tires, the normal inflation pressure is greater than that of passenger-car tires and of larger range, might be 50-70 psi for light-duty truck tires and 80-100 psi for heavy-duty truck tires [432].

Increased inflation could stiffen the tire carcass and change vibration characteristics such as structural resonance frequencies [115]. It could also influence the size and shape of contact patch due to tire deflection, and affect air pumping by changing how the air pockets in the tread grooves deform. It is implied that inflation pressure could affect the same mechanisms as tire load because tire deflection is dependent on both inflation pressure and tire load.

A number of literatures presented the effect of inflation pressure on tire-pavement interaction noise (TPIN) levels. However, contradictory results were usually reported. Bremner et al. (1997) [331] reported that TPIN level increased slightly with the increase of tire inflation pressure. Ulrich (1984) [417] reported that the sound power P has the relationship with tire inflation pressure p_s as $P \propto p_s^{1/2}$. Heckl (1986) [1] also indicated that the sound power increases as the square root of inflation pressure. Iwao and Yamazaki (1996) [163] reported that, with driving torque, TPIN level rises with the inflation pressure. On the other hand, Donavan (1998) [21] and Samuels (1979) [433] reported the opposite results. Keltie (1982) [247] reported that for truck tires the acoustic power generated decreases significantly with the increase of inflation pressure (0.6 dB/psi) while at sufficiently high pressure (above 70 psi) the acoustic power is insensitive to further pressure increases. EPA (Environmental Protection Agency, USA) (1980) [434] also reported that TPIN level from lug type truck tires decreased as inflation increased, especially for pressure in the range of 29-58 psi. It can be inferred that there seems to be no clear or at least no linear dependence between inflation pressure and TPIN levels. Bolton et al. (1998) [260] reported that no clear correlation between the inflation pressure and the vibration patterns of a tire was found.

Muthukrishnan (1996) [435] noted that the noise levels increased with the increase of inflation pressure under lighter tire load, but the trend reversed under higher load. Tong et al. (2013) [436] indicated that the effect of inflation pressure on TPIN levels is very marginal.

The effect of inflation pressure on the TPIN spectrum was also investigated. Bremner et al. (1997) [331] indicated that the effect of increasing inflation pressure is to increase the tire stiffness at lower frequencies without increasing the mass, resulting in the increase of wavespeed and decrease of modal wavenumbers. Increased inflation also increases the tire eigenfrequenicies [395] and the cut-on frequencies for propagating vibration modes [260]. Keltie (1982) [247] demonstrated that acoustic power spectrum is shifted towards higher frequency as the inflation pressure increases from 60 psi to 80 psi for truck tires. Kindt et al. (2007) [437] found that as the inflation pressure increases, the vibration spectrum shows in general a higher amplitude and a positive frequency shift at the structural resonances, which is due to the tire structure stiffening (both tread band and sidewall). The transfer of tire vibrations to the rim is also improved with the sidewall stiffening. To summarize, a consistent conclusion was drawn: the increase of inflation pressure shifts the TPIN spectrum to higher frequencies.

Kindt et al. (2006) [438] pointed out that the frequency change is due to the change of tire structure resonances; the acoustic resonance frequencies in the tire cavity are not affected, because they are dependent on the geometry of the air cavity and the velocity of sound. The velocity of sound for ideal gas is determined by $c = \sqrt{(\gamma p/\rho)} = \sqrt{(\gamma RT)}$ where c is speed of sound, γ is adiabatic index (1.402 for air), p is pressure, ρ is air density, R is gas constant and T is temperature (constant). As such, the velocity of sound is constant and geometry of the air cavity also doesn't change significantly with inflation pressure, so the acoustic cavity resonance frequencies do not change much, except when the pressure change leads to the significant change of tire deflection on the contact patch [439].

Several existing TPIN models included inflation pressure as a parameter [247], [260], [341], [348], [350]. Most of the models investigated tire vibration characteristics at low frequencies below 500 Hz using finite element (FE) method, and few have explicitly presented the effect of inflation pressure on TPIN. In summary, the effects of inflation

pressure on TPIN have not been conclusively demonstrated in prior literature.

D.2 Effect of Inflation Pressure on TPIN Levels

In the following, the effect of inflation pressure on overall A-weighted sound pressure level (OASPL) of total noise, tread pattern noise and non-tread pattern noise will be discussed separately. Only the results for the leading inboard microphone (Mic 1) will be presented; results for other microphones have the same trend.

D.2.1 Total Noise Level

The effect of inflation pressure on OASPL of total noise is shown in Figure D.1. It can be seen that there is no linear dependence between OASPL of total noise and inflation pressure considering all the speeds. The variation of OASPL for different inflation pressures (26-40 psi) is generally less than 1 dBA. On the contrary, the vehicle speed is shown to have much stronger positive correlation with OASPL. It should be noted that at the same nominal speed, e.g., 60 mph, for the three tests at 26, 32, and 40 psi, the actual speed might be 60±2 mph, which is another possible reason for the OASPL variation at different inflation pressures. Therefore, there is no strong evidence showing the inflation pressure has an influence on the OASPL of total tire noise; or its influence is very marginal. However, there seems to be a trend that the OASPL of total noise is minimum at the general manufacturer-recommended inflation pressure (32 psi), e.g., for Tires 18 and 20.

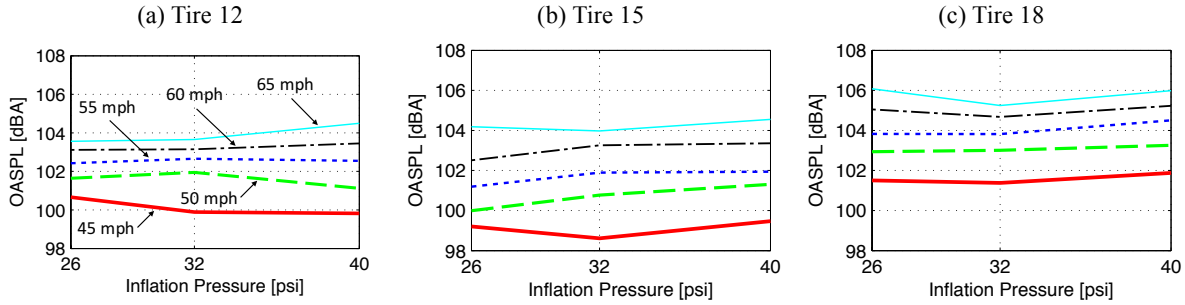

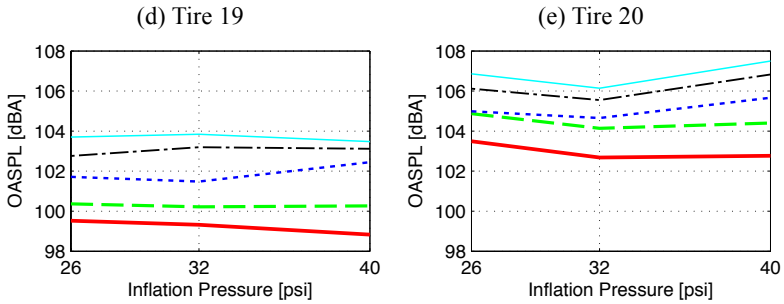

Figure D.1: Effect of inflation pressure on total noise level (OASPL)

D.2.2 Tread Pattern Noise Level

The effect of inflation pressure on OASPL of tread pattern noise is shown in Figure D.2. Similar to the total noise level, there is no clear or linear correlation between the OASPL of tread pattern noise and inflation pressure; or the influence of inflation pressure is of little significance (less than 2 dBA). In addition, for Tires 15, 18, and 20, the OASPL is so small (below 90 dBA) that the values tend to be inaccurate.

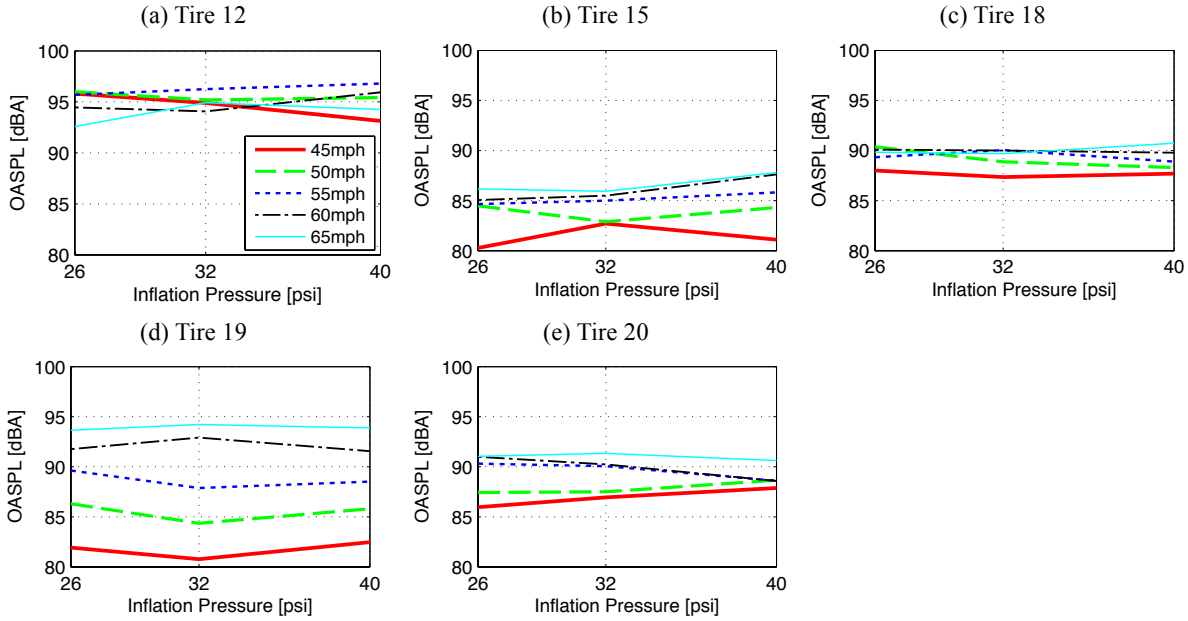

Figure D.2: Effect of inflation pressure on tread pattern noise level (OASPL)

D.2.3 Non-tread Pattern Noise Level

The effect of inflation pressure on OASPL of non-tread pattern noise is shown in Figure

D.3. Since the non-tread pattern noise is usually the dominant noise component of total tire noise, the trend for non-tread pattern noise is almost the same as that for the total noise discussed before.

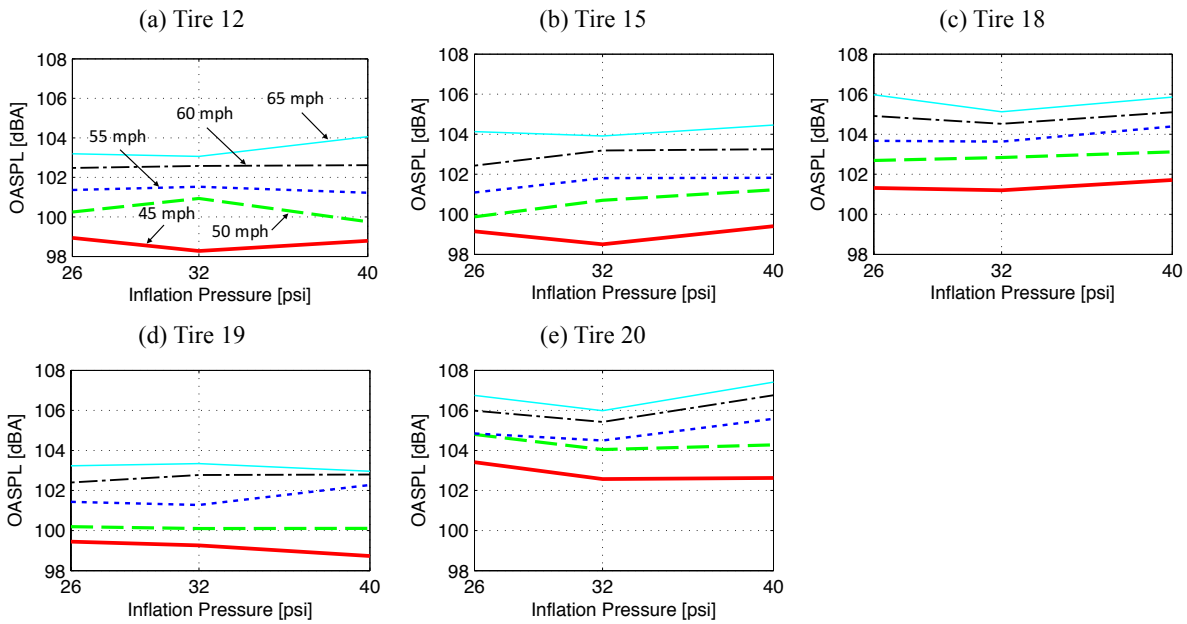

Figure D.3: Effect of inflation pressure on non-tread pattern noise level (OASPL)

D.3 Effect of Inflation Pressure on TPIN Spectrums

The effect of inflation pressure on the tire noise spectrums is discussed below. The effects on total noise, tread pattern noise, and non-tread pattern noise spectrums are analyzed individually.

D.3.1 Total Noise Spectrum

The effect of inflation pressure on total noise spectrum is shown in Figure D.4. It can be seen that as the inflation pressure increases, the dominant spectral contents shift to higher frequencies but the amplitudes tend to decrease. This results in a complex and nonlinear change of OASPL, as discussed before.

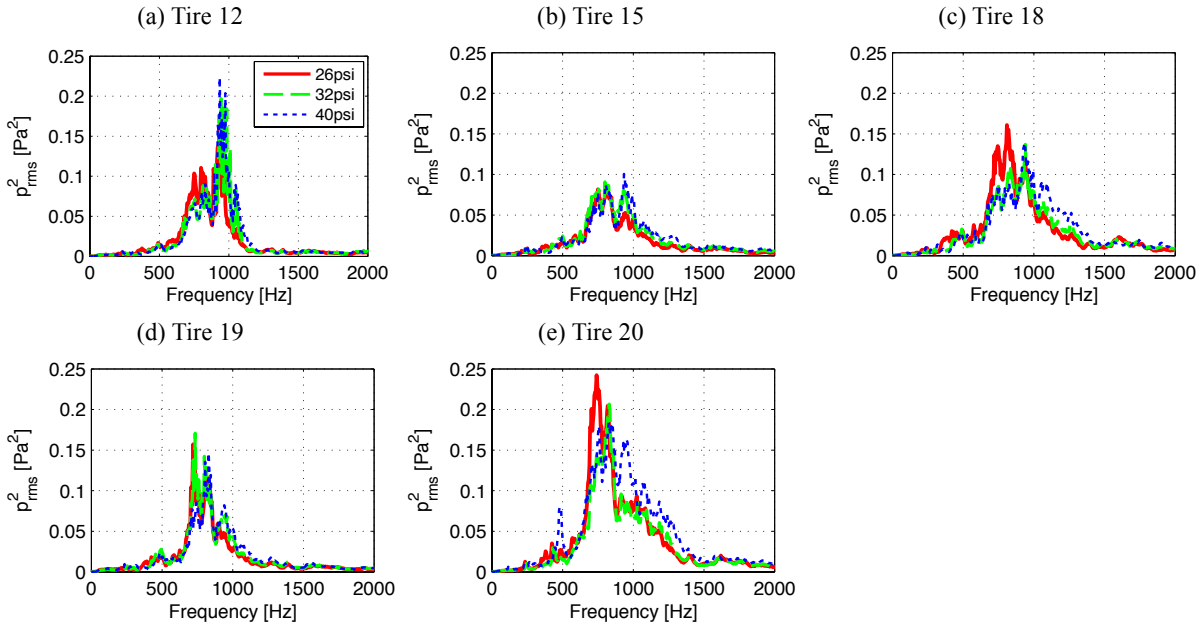

Figure D.4: Effect of inflation pressure on total noise spectrum

D.3.2 Tread Pattern Noise Spectrum

The effect of inflation pressure on tread pattern noise spectrum is shown in Figure D.5. For the tread pattern noise spectrum, there seems to be no such trend of frequency shift or amplitude change as for the total noise spectrum. However, the spectrum change is likely due to the change of tire-road contact patch. As the inflation pressure increases, the contact patch length/width decreases, leading to the change of tread impact and air pumping from the tread blocks and grooves under contact patch.

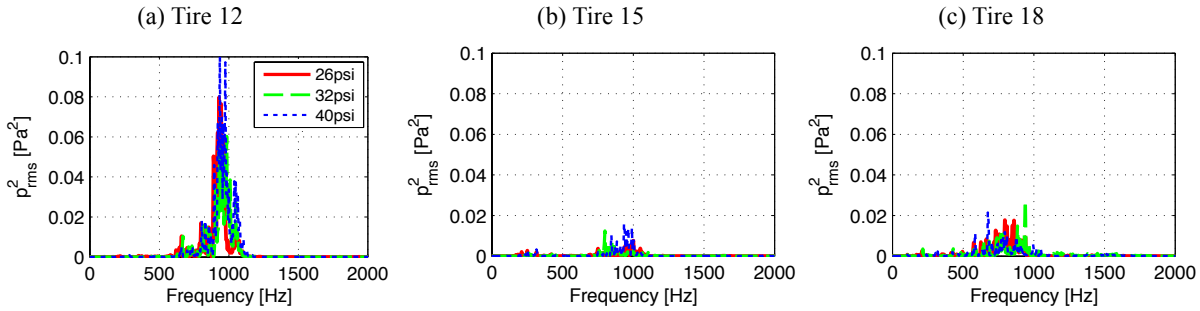

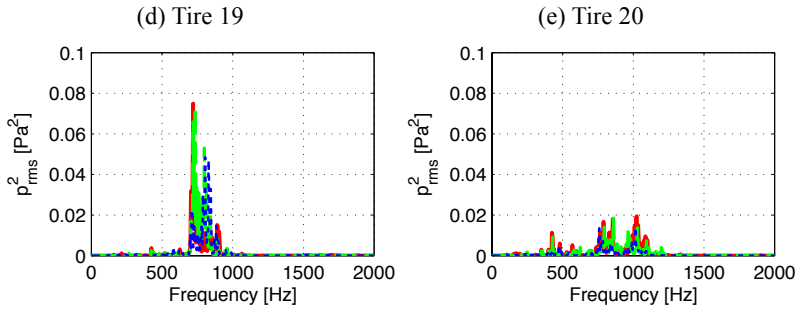

Figure D.5: Effect of inflation pressure on tread pattern noise spectrum

D.3.3 Non-tread Pattern Noise Spectrum

The effect of inflation pressure on non-tread pattern noise spectrum is shown in Figure D.6. It is demonstrated that the trend for non-tread pattern noise spectrum is similar to that for total noise spectrum. The spectral contents shift to higher frequencies with amplitudes decreasing. This is likely due to the fact that larger inflation pressure leads to larger stiffness of tire sidewall and tread band, resulting in higher resonance frequencies of tire structure but with smaller vibrations.

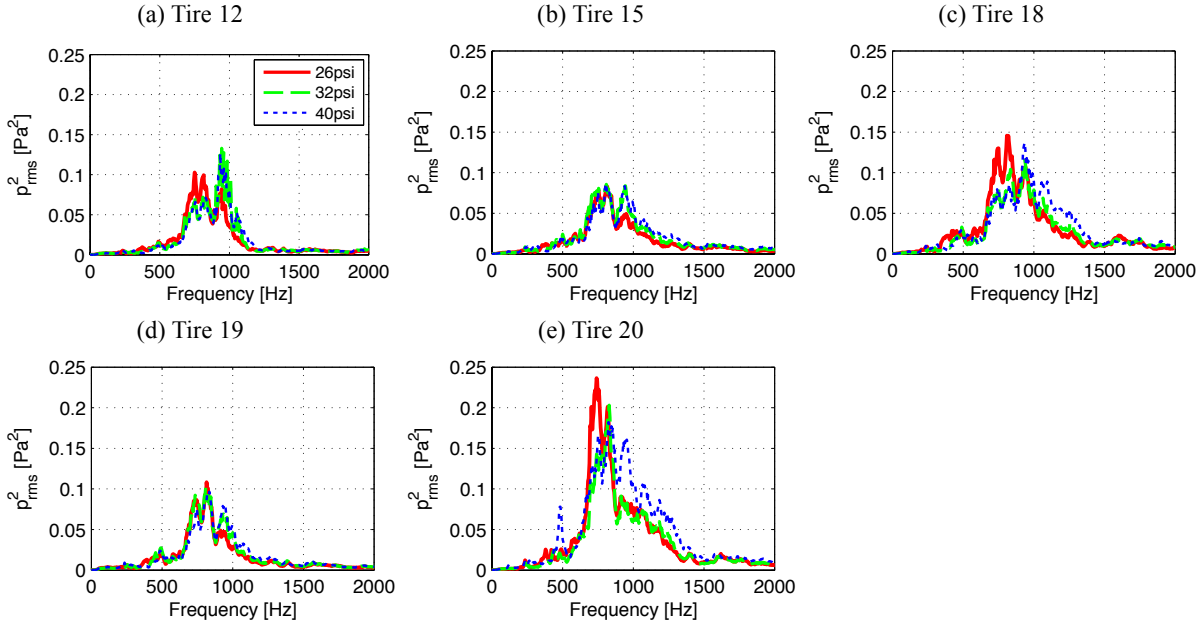

Figure D.6: Effect of inflation pressure on non-tread pattern noise spectrum

D.4 Effect of Inflation Pressure on Speed Exponent

The approximate relationship between overall A-weighted tire noise level and speed can be described as below [24].

$$L_{pA} = 10n\log_{10}(v) + b$$

where L_{pA} is overall A-weighted sound pressure level (OASPL) in dB scale, n is speed exponent or scaling law, v is vehicle speed, and b is a speed coefficient. The speed exponent can be calculated statistically using a curve-fitting approach for a specific tire at a specific inflation pressure. It can also be considered as the sensitivity of noise level to speed. In calculating the speed exponent, the actual speed rather than nominal speed is used.

The effects of inflation pressure on the speed exponent of total noise level, tread pattern noise level, and non-tread pattern noise level are analyzed below.

D.4.1 Total Noise Speed Exponent

The effect of inflation pressure on total noise level speed exponent is shown in Figure D.7. It can be seen that increasing inflation pressure will generally increase the speed exponent for total noise level except for 32-40 psi of Tire 15 and 26-32 psi of Tire 18, which means larger inflation pressure makes the total noise level more sensitive to speed.

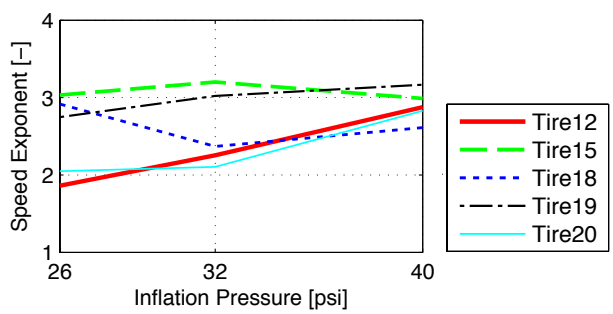

Figure D.7: Effect of inflation pressure on total noise level speed exponent

D.4.2 Tread Pattern Noise Speed Exponent

The effect of inflation pressure on tread pattern noise level speed exponent is shown in Figure D.8. No clear trend is found for the speed exponent of tread pattern noise level,

implying that the inflation pressure has an insignificant influence on tread pattern noise.

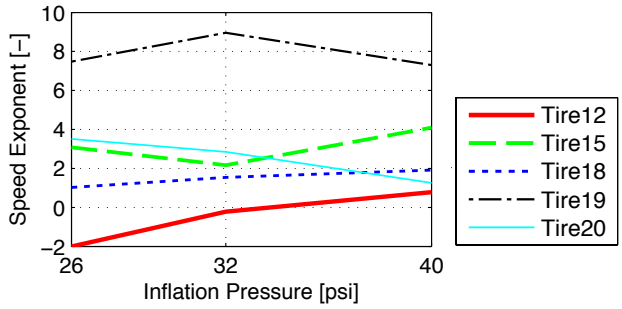

Figure D.8: Effect of inflation pressure on tread pattern noise level speed exponent

D.4.3 Non-tread Pattern Noise Speed Exponent

The effect of inflation pressure on non-tread pattern noise level speed exponent is shown in Figure D.9. Its influence on non-tread pattern noise level speed exponent is almost the same as on total noise level speed exponent.

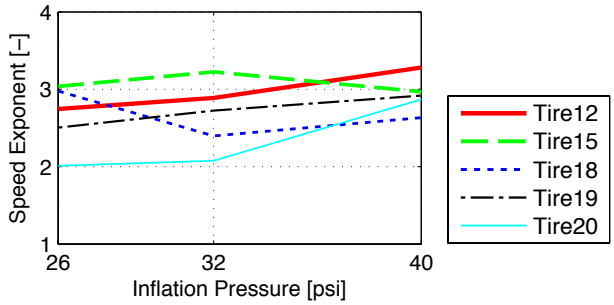

Figure D.9: Effect of inflation pressure on non-tread pattern noise level speed exponent

D.5 Conclusions

For the tested tires and pavement, the inflation pressure within the normal range of 26~40 psi only has a marginal influence on the tire-pavement interaction noise, including both tread-pattern-related noise and non-tread-pattern-related noise, in terms of either overall levels or spectrums.

The non-tread-pattern-related noise spectrum tends to shift to higher frequencies with smaller amplitudes as inflation pressure increases likely due to stiffer tire structure. In

addition, the non-tread-pattern-related noise overall level seems to become more sensitive to vehicle speed with increasing inflation pressure.

Appendix E: Tones due to Pavement Distress

E.1 Introduction

Pavement parameter might be more important than tire parameters (Sandberg and Ejsmont, 2002 [24]) in terms of tire-pavement interaction noise (TPIN). As a matter of fact, two thirds of literature focus on the pavement effects while only one third focus on the tire effects (Sandberg and Ejsmont, 2002 [24]). Fong (1998) [269] indicated that the texture dominated in noise generation for chipseal surfaces. Different pavement parameters affect different generation and propagation mechanisms.

The pavement related parameters could be categorized into primary parameters, secondary parameters and tertiary parameters. The primary parameters are those for pavement design or mixture properties, such as grading size distribution, content of binder and thickness; the secondary parameters are characteristics that show up and remain relatively constant after the pavement is built, such as porosity, texture and impedance (Li et al., 2009 [275]); the tertiary parameters are those that might change with time, such as wetness, wear/age, and surface rating.

For a specific pavement, its acoustic performance might change with time due to wear/age. Traffic wear on pavement can change the micro- and macro-texture, resulting in friction and TPIN changes (McDaniel et al., 2010 [440]). Friction initially increases within a few months as traffic wears off the binder film coating the aggregate particles, and then decreases as the particles are further polished (Kowalski, 2010 [441]). For porous asphalt pavement, after a small decrease within the first months of service (Mogrovejo et al., 2014 [113]), TPIN generally increases over year due to the clogging of air voids (Paje, 2007 [442]), and then begins a steady trend (Mogrovejo et al., 2014 [113]). It is a cumulative process whose rate changes depending on porous mixes and locations. An increase of about 0.5 dB per year in CPX measurements for a porous polymer-modified friction course was found (Ng et al., 2009 [313]). Chalupnik (1996) [75] indicated that the age of pavement was more important than the type of pavement in terms of TPIN. For cement concrete pavement, the influence of wear and aging were relatively small (Sandberg et al., 1990 [273]). Longitudinally grooved

pavements with significant macro-texture can become quieter as macro-textural features are worn down over time (Dare et al., 2009 [443]). The amount of wear can be estimated by traffic volume or single axle loads (ESALs). Winter maintenance operations and the impact of cyclic freezing and thawing (weather wear) are also forms of wearing (Neithalath et al., 2005 [314]). Like traffic wear, TPIN generally increase as pavement ages (Bendsten, 2009 [315]). Acoustic longevity describes how well pavement retains its TPIN level over time. For example, the first Next Generation Concrete Surface (NGCS) built by the Washington State Department of Transportation (WSDOT) showed a very short acoustic longevity (Anderson et al., 2014 [444]). On-board sound intensity (OBSI) levels increased from initial levels of 100.6 dBA to 104.4 dBA in 30 months. However, the effects of age were marginal for some other pavements (Hencken, 2012 [445]).

Surface rating (SR) is a measure of the wear or distress on a pavement surface by counting the number of cracks and joint deterioration on a segment of road, and then applying weighting factors (Kay, 1992 [316]; MNDOT, 2003 [317]). The rating is typically highest immediately after construction or rehabilitation and gradually (or sometimes rapidly) decreases due to the accumulation of cracking, rutting, raveling and other types of distress (Mcdaniel et al., 2014 [35]). Asphalt pavement distress typically includes fatigue (alligator) cracking, block cracking, edge cracks, longitudinal (linear) & transverse cracking, reflection cracking, slippage cracks, corrugations & shoving, rutting, settlement/grade depressions, upheaval/swell, utility cuts/patch failure, pot hole, raveling/weathering, bleeding, polished aggregate, loss of aggregate on surface treatments, and longitudinal/transverse streaking (Miller and Bellinger, 2003 [446]). TPIN increases with the SR dropping as the distress increases the pavement roughness. However, few literatures have reported the effect of pavement distress on the TPIN spectrum.

In this paper, the acoustic characteristics of a pavement section that has transverse corrugation distress are analyzed and compared with a normal pavement section. First, the experimental setup for the tire noise data collection is introduced, including the test pavement and test tires. Second, the comparisons of total tire noise spectrums are conducted between the corrugation section and the normal section. Then, order tracking analysis is performed to separate the total noise into two components, tread-pattern-related noise

component and non-tread-pattern-related noise component. Finally, the two noise components are individually compared between the two pavement sections.

E.2 Experiments

The test pavement is U.S. Route 460 near Virginia Tech (between Toms Creek Rd. and North Main St. It is a non-porous asphalt pavement, dense graded hot mix asphalt (HMA). In the eastbound direction, a segment of the pavement shows appreciable corrugation distress. As such, the total section was divided into two consecutive sub-sections for testing, normal section and corrugation section both with a length of ~100 m, as shown in Figure E.1. It can be seen that the corrugations are in the transverse direction and close to evenly spaced.

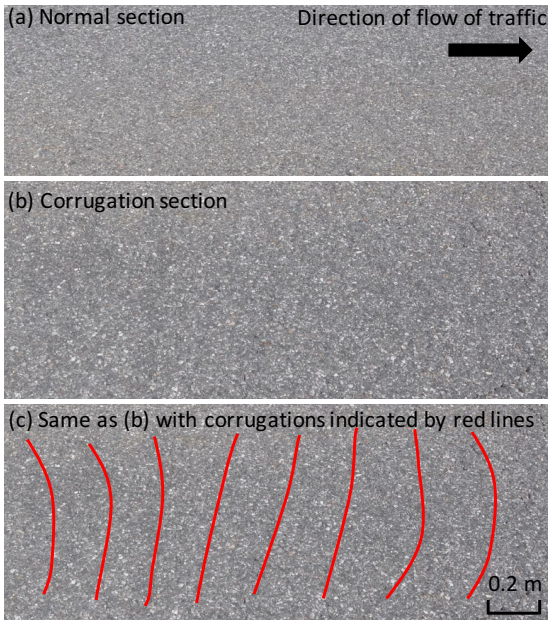

Figure E.1: Two test sections (normal section and corrugation section)

Five different tires were tested on March 7-11, 2016 [382], [383], and they are listed in Table E.1. Pictures of their tread patterns are displayed in Figure E.1. The red arrow in Figure E.1 indicates the rotation direction for directional tires in this test. Tire 20 is the Standard Reference Test Tire (SRTT). The tires have different tread patterns but with the same or very similar size and aspect ratio. The number of blocks, as shown in Table E.1, is the number of tread elements around the full tire circumference. The values range from 60 to 81. The

number of plies in the tread band and the sidewall is different for different tires, indicating that the structure of the tires is different. The tread rubber hardness was measured immediately after the test.

Table E.1: Specifications of the test tires

No.	Size	Condition	Number of Blocks	Number of Plies (Tread/ Sidewall)	Rubber Hardness [Shore A]
12	215/60R16	Winter/Snow	77	4/1	56
15	215/60R16	All season	72	4/1	55
18	215/60R16	All season	65	5/2	65
19	215/60R16	Winter/Snow	60	5/2	64
20	225/60R16	All season	81	3/1	65

Figure E.2: Tread patterns of the test tires (arrow indicates rotation direction)

For each tire, the noise data were collected under five different vehicle speeds (45, 50, 55, 60, and 65 mph). Three inflation pressures were tested, i.e., 26, 32 and 40 psi. Only results at 32 psi are discussed in this paper; same conclusions are drawn for the other inflation pressures. The ambient temperature range during the test days was 55-74° F.

The vehicle used for testing was a 2012 Chevrolet Impala LT (front wheel drive). The equipment used for collecting noise data was an on-board sound intensity (OBSI) system based on standard AASHTO TP-76 [97]. The setup of the OBSI system is shown in Figure 3.4. The system was installed at the rear right tire with a camber angle close to zero. The

conventional OBSI system has two sound intensity probes, one at the leading edge of the tire-road contact patch, the other at the trailing edge. Each probe consists of two microphones to record the sound pressure. The sound intensity along the direction of the two microphones (away from the tire) is then calculated. However, in the present OBSI system, one of the microphones (Mic 4) at the trailing edge was disconnected and the channel was used to record the optical sensor signal. The optical sensor, as shown in Figure E.3, radiates a beam onto the side face of the black disk rotating with the tire, and once the beam encounters the retroreflective tape and gets reflected to the optical sensor, the optical sensor generates a pulse. Therefore, a pulse signal is recorded at the exact time the tire completes one revolution. The optical signal can be used to accurately calculate vehicle speed, acceleration, as well as used for the order tracking analysis, which will be discussed later. The microphone and optical signals were recorded simultaneously at 25.6 kHz.

Figure E.3: On-board sound intensity (OBSI) with optical sensor installed on the test vehicle

E.3 Total Noise Spectrum

As indicated, the OBSI system used in the present study has three microphones since the 4th channel was used to record the optical sensor signal. In each test run, the time duration of data collected for the normal or corrugation section was 5-10 seconds depending on the vehicle speed. A high-pass filter at 20 Hz was applied to the sound pressure time signals to eliminate subfrequency interferences from wind or the electronic system. In this paper, only

the signal from the leading inboard microphone (Mic 1) will be presented. However, the same results were observed and conclusions drawn from the other microphones. It should be pointed out that all the results presented in this section are only valid for the pavement tested.

The total noise spectrums at 60 mph for the normal and corrugation sections are shown in Figure E.4. It can be seen that compared to the normal section, strong tones (sharp peaks) are generated on the corrugation section. This typically increases the overall A-weighted sound pressure level (OASPL) by 0.5~1 dBA, and can be clearly heard inside the vehicle at low speed (45 mph). This agrees with prior literature that the corrugations form transverse texture, and allows coincident impact between tire and pavement along the contact patch width, resulting in high TPIN levels (Wullens et al., 2004 [290]). Uniformly spaced transverse texture can also produce high tonal noise (Hamet and Klein, 2001 [447]). Rasmussen et al. (2008) [291] also reported that anisotropic/orientated pavement texture in the form of periodic features, such as peaks and grooves, leads to higher TPIN than isotropic texture does. Beckenbauer and Kuijpers (2001) [289] demonstrated that positive texture (texture features projected above the mean pavement level such as corrugations in the pavement) typically increases impact and friction mechanisms.

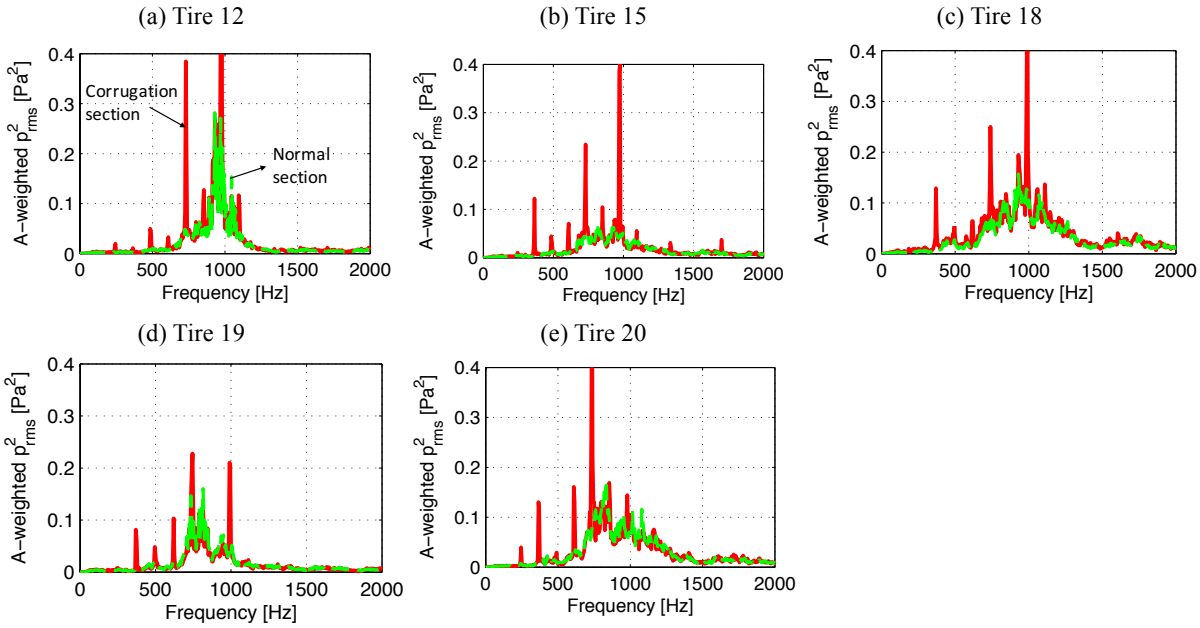

Figure E.4: Total noise spectrums at 60 mph (5 Hz resolution).

It is noted that 1 dBA increase in OASPL might be unnoticeable to human ears if the increase is spread evenly over all the audible frequencies, however, the OASPL increase by 1 dBA centered at certain narrow frequencies generating tones might be very clear and annoying. In order to demonstrate that the tones are related to the pavement rather than the tire tread pattern, the noise separation is performed in the following.

E.4 Tire Noise Separation

In this section, order tracking analysis utilizing the optical signal is performed to separate the two components of noise signals, tread-pattern-related noise and non-tread-pattern-related noise [382], [383].

The total, tread pattern and non-tread pattern noise spectra for each tire are displayed in Figure E.5. The results for the normal section are shown on the left column while the results for the corrugation section are shown on the right column. It is shown that the tones are in the non-tread pattern noise component, indicating that the tones are related to the pavement rather than the tire tread pattern. The tread pattern noise and non-tread pattern noise are analyzed individually for the comparisons between the normal and corrugation sections in the following.

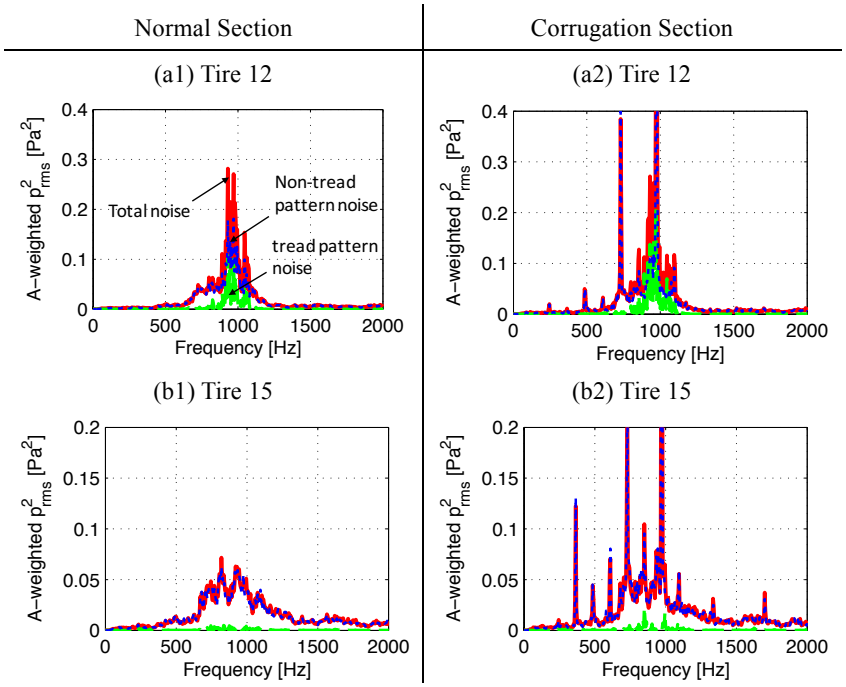

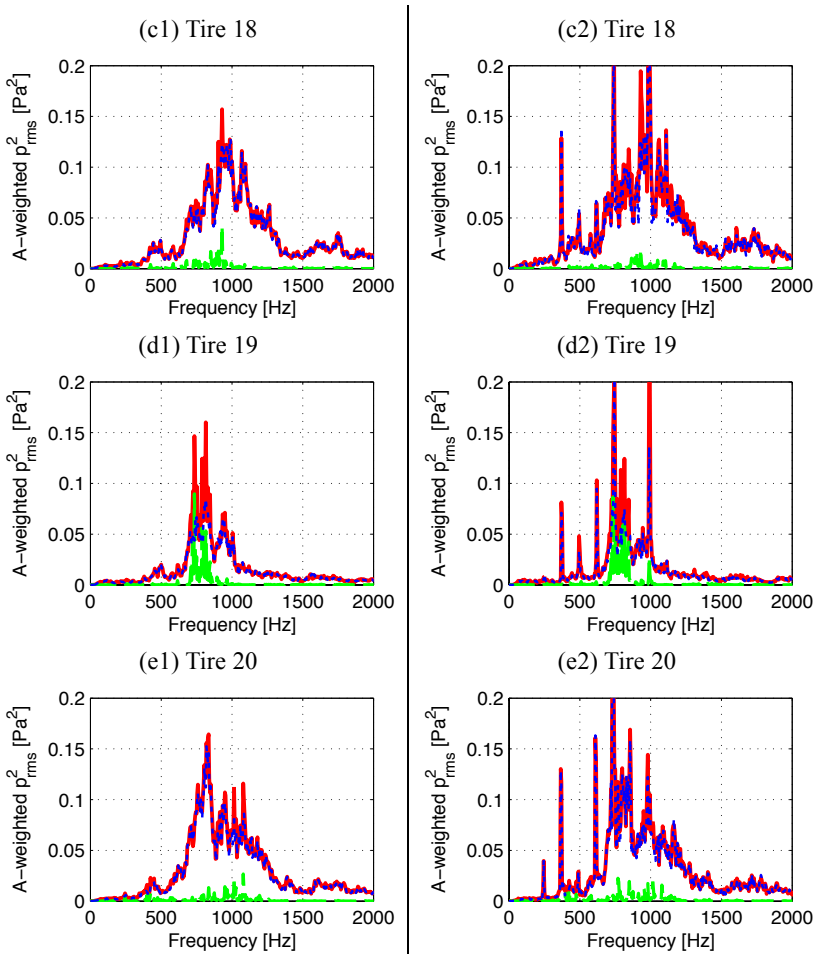

Figure E.5: Total, tread-pattern, and non-tread pattern noise components at 60 mph (5 Hz resolution)

E.5 Tread Pattern Noise Spectrum

The tread pattern noise spectrums at 60 mph for the normal and corrugation sections are shown in Figure E.6. It can be seen that the tread pattern noise component on the two sections is almost the same, which means the corrugation distress on the pavement is independent of and has little influence on the noise generated due to the tread pattern.

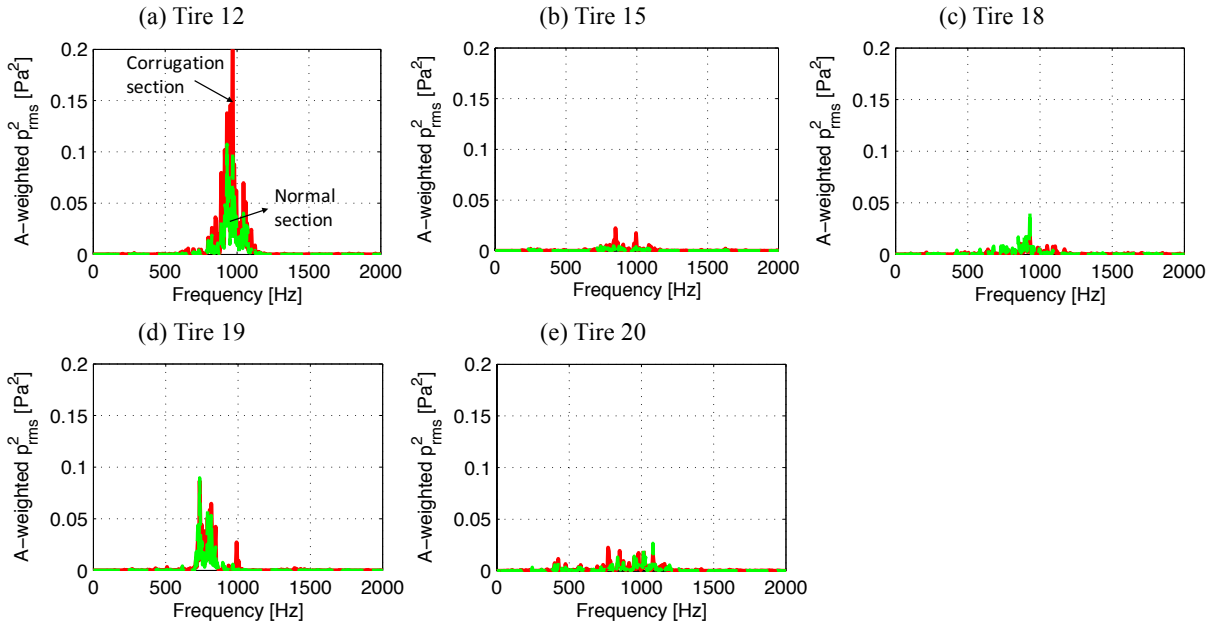

Figure E.6: Tread pattern noise spectrums at 60 mph (5 Hz resolution)

E.6 Non-tread Pattern Noise Spectrum

The non-tread pattern noise spectrums at 60 mph for the normal and corrugation sections are shown in Figure E.7. It is demonstrated that there exist clear tones in the non-tread pattern noise spectrums. For all the tires tested, the frequencies at which the tones occur are the same. The interval between the two adjacent tones is shown to be ~120 Hz, which is also the fundamental frequency. It can be calculated by

$$f_{tone} = f_{tire} l_{tire} / l_{corrugation}$$

where f_{tone} is the fundamental frequency of the harmonic tones, f_{tire} is the tire rotational speed (~13 Hz or rev/sec at 60 mph), l_{tire} is the tire circumference (~2.1 m), and $l_{corrugation}$ is the distance between the two corrugations on the pavement. Using the above equation, the corrugation interval is calculated as $l_{corrugation} \approx 0.23$ m, which matches quite well with the measurement, as shown in Figure E.1. This is strong evidence that the tones are due to the corrugation distress in the pavement. The harmonic overtones are generated because the corrugations are not exactly evenly spaced.

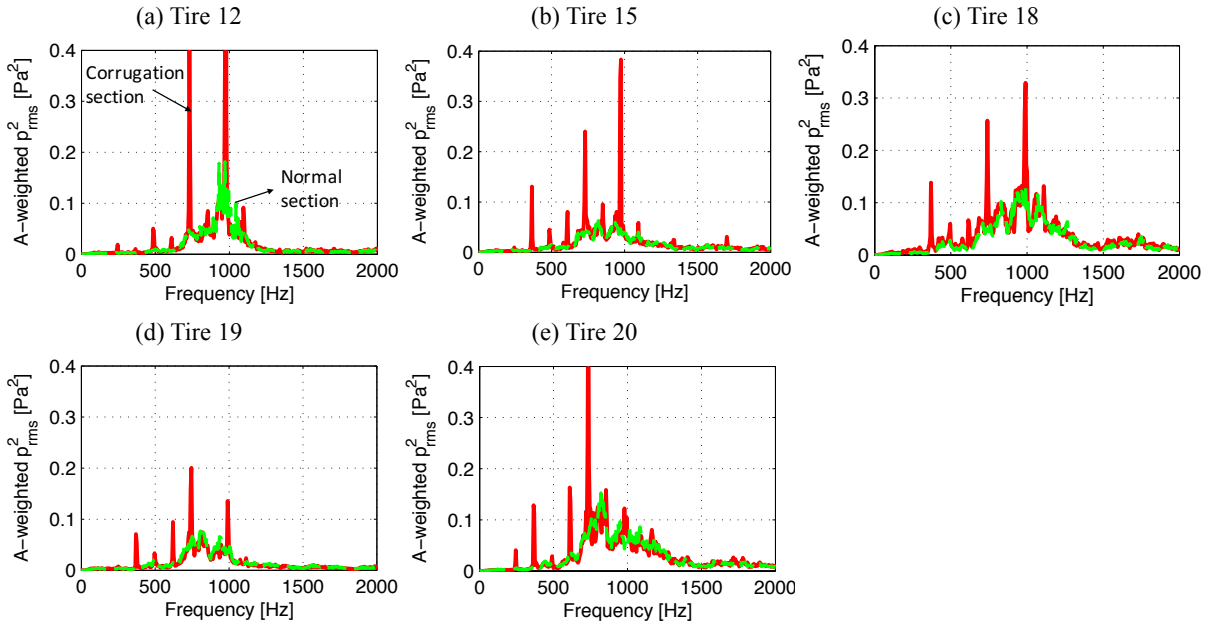

Figure E.7: Non-tread pattern noise spectrums at 60 mph (5 Hz resolution)

Another evidence is that the fundamental frequencies scale quite well with vehicle speed, as shown in Figure E.8. The frequency resolution in this plot is 1 Hz for better accuracy. The fundamental frequencies for 45 mph, 55 mph, and 65 mph are 92 Hz, 113 Hz and 132 Hz, respectively, indicating a perfect proportional relation between the fundamental frequency and speed. It is also shown that the intensity (amplitude) of the tones increases with increasing speed. However, at higher speed, the tone tends to be less audible, at least inside the vehicle, due to the greater increase of the total noise.

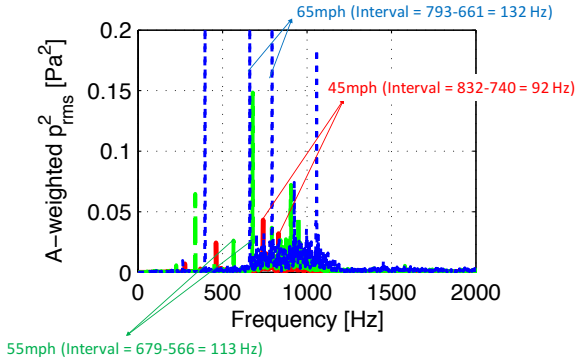

Figure E.8: Non-tread pattern noise spectrums at different speeds for Tire 12 on the corrugation section (1 Hz resolution)

It should be pointed out that, the main non-tread pattern spectral content excluding the tones due to pavement corrugations doesn't shift with speed as it is supposed to be excited by the isotropic pavement texture, which is considered to be random, homogeneous and broadband. As opposed to the non-tread pattern noise, the entire tread pattern noise spectral content shifts with speed as it is excited by the tread pattern blocks/grooves, which is periodic with speed [383].

E.7 Conclusions

The comparisons of acoustic characteristics between normal section and corrugation section reveal that the transverse corrugations close to evenly spaced resulting from pavement fatigue/distress can lead to obvious harmonic tones, which is proved through order tracking analysis. The frequencies of the tones are proportional to the vehicle speed. The tones can increase the overall TPIN levels by up to 1 dBA, which is annoying even inside the vehicle and should be avoided in terms of noise reduction. As a matter of fact, the corrugations in this test are barely distinguishable; it is inferred that a more severe pavement distress of this type will lead to higher tones, which might occur if the pavement keeps on wearing and is not appropriately maintained. One potential application of this study is to quickly detect and identify the distressed pavement section by the tire noise data analysis instead of visual inspection or laser profilometer that is very slow and expensive.

Appendix F: Rough and Smooth Pavement

F.1 Introduction

Pavement texture is defined as "the deviation of a pavement surface from a true planar surface" within a specific wavelength range (ISO, 1997 [285]). Among the pavement related parameters, pavement texture has the greatest influence on the tire-pavement interaction noise (TPIN) (Huschek, 1996 [448]) and is included in nearly all TPIN models. However, texture cannot be described using one single metric. It is divided into a group of parameters representing different aspects of texture based on the wavelength of the texture: micro-texture (<0.5 mm), macro-texture (0.5-50 mm), mega-texture (50-500 mm), unevenness (0.5-50 m) and topographical undulation (>50 m) (Dimitri, 2012 [93]).

Micro-texture is a function of the surface texture of the aggregate particles. High micro-texture provides high frictional resistance and water skid resistance by disrupting the continuity of the water film. It can be analogous to sand paper with a gritty surface. Higher micro-texture increases stick/slip (friction) noise generation mechanism but decreases stick/snap generation mechanism. These conflicting changes might explain why it is difficult to find clear relations between micro-texture and TPIN (Sandberg and Ejsmont, 2002 [24]). Micro-texture was shown to influence TPIN above 1000 Hz (Dare and Bernhard, 2009 [278]; Sandberg and Ejsmont, 1998 [279]).

Macro-texture represents the overall properties of the pavement surface and has the greatest influence on TPIN among texture characteristics. It depends on the type of asphalt surface (e.g., dense versus porous), the gradation of the aggregates in the mixture, and presence of air voids at the surface (Mcdaniel et al., 2014 [35]). Higher macro-texture reduces hydroplaning by providing channels at the surface through which water can travel away from the contact area. Higher macro-texture (10-50 mm) increases texture impact TPIN generation mechanism. It also influences the air pumping generation mechanism by changing the volume of air cavities in the pavement. It has certain influence on the stick/slip, pipe resonance and Helmholtz resonance mechanism. Macro-texture was shown to affect TPIN levels in the range of 630-1000 Hz (Rasmussen et al., 2006 [280]). However, higher

macro-texture (0.5-10 mm) was reported to decrease TPIN levels (FHWA, 2005 [281]).

Generally, mega-texture, unevenness, or topographical undulation has little influence on TPIN, except in cases of extreme roughness such as potholes, joints and bumps.

Texture profile can be measured using a laser profiler standardized in ISO 13473 (2002) [276]. Texture spectrum analysis (He and Wang, 1991 [449]; Lee et al., 1998 [450]; Wang and He, 1990 [451]) can then be applied to pavement texture investigations standardized in ISO/TS 13473-4 (2008) [452].

TPIN has different sensitivities to the different components of texture spectrum, and certain range of spectrum might be ignored or cannot be recognized by the tire (Biermann et al., 2007 [328]). Sandberg and Ejsmont (2002) [24] demonstrated that TPIN at low frequencies (below 1000 Hz) increases with texture amplitude within the texture wavelength range of 10-500 mm. TPIN at high frequencies (above 1000 Hz) decreases with texture amplitude within the texture wavelength range of 0.5-10 mm. Li et al. (2015) [366] reported the similar trends. However, Domenichini et al. (1999) (Domenichini et al., 1999 [8]) reported that the effect TPIN above 1000 Hz decreases with texture amplitude centered on 5 mm only when the total texture spectral line of 4, 5 and 6.3 mm is less than 200. It should be pointed out that the correlation between TPIN and pavement texture of short wavelengths is still uncovered. Many researchers failed to measure texture levels with enough precision at such short wavelengths, so the results were usually debatable (Fong, 1998 [269]). For most of the cases, power spectrum of the texture is used, which will lose the phase information. However, Hamet and Klein (2000) [453] claimed that two pavements with identical power spectrum or amplitude spectrum of the texture do not necessarily show the same acoustical behavior. Both the amplitude and phase information should be taken into account.

To characterize the pavement texture using a single parameter, mean profile depth (MPD) is defined as the average depth of a section of pavement and indicates the pavement texture (mainly macro-texture). TPIN has good correlation with MPD and correlation increases with vehicle speed (Saykin, 2011 [286]). However, some researchers claimed that the correlation is weak, because MPD filters out the spectral contents of short wavelengths and cannot be representative of texture characteristics. A similar term, mean texture depth (MTD) is

traditionally measured and calculated with Sand Patch Method, which is standardized in ASTM E965 (2006) [283]. The MPD is shown to have strong relation (R^2=0.85) with the root mean square (RMS) of the pavement texture, which describes the roughness of the pavement surface or the texture height deviation from the true plane (Reyes and Harvey, 2011 [305]).

In this paper, the acoustic characteristics of a rough pavement section and a smooth pavement section are analyzed and compared. First, the experimental setup for the tire noise data collection is introduced, including the test pavement and test tires. Second, the comparisons of total tire noise spectrums are conducted between the rough section and the smooth section. Then, order tracking analysis is performed to separate the total noise into two components, tread-pattern-related noise component and non-tread-pattern-related noise component. Finally, the two noise components are individually compared between the two pavement sections.

F.2 Experiments

The test pavement is U.S. Route 460 near Virginia Tech (between Southgate Dr. and South Main St. in the eastbound direction. It is a non-porous asphalt pavement, dense graded hot mix asphalt (HMA). Part of the pavement was repaired with smooth patches. As such, the total section was divided into two consecutive sub-sections for testing, rough section (original) and smooth section (patched) both with a length of ~80 m, as shown in Figure F.1.

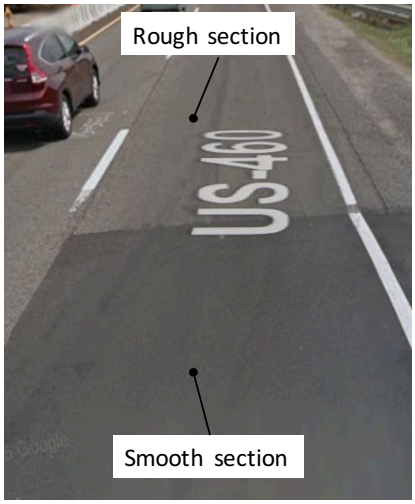

Figure F.1: Two east sections (rough section and smooth section) (Source from Google Street View)

Five different tires were tested, and their tread patterns are displayed in Figure F.2. The red arrow in Figure F.2 indicates the rotation direction for directional tires in this test. The tires have different tread patterns but with the same size and aspect ratio (215/60R16). Tires 07 and 08 are all-season tires; Tires 09, 12, and 19 are snow tires. For each tire, the noise data were collected at 60 mph. The inflation pressure was set to 32 psi.

Figure F.2: Tread patterns of the test tires (arrow indicates rotation direction)

The vehicle used for testing was a 2012 Chevrolet Impala LT (front wheel drive). The equipment used for collecting noise data was an on-board sound intensity (OBSI) system based on standard AASHTO TP-76 [97]. The setup of the OBSI system is shown in Figure F.3. The system was installed at the rear right tire with a camber angle close to zero. The conventional OBSI system has two sound intensity probes, one at the leading edge of the tire-road contact patch, the other at the trailing edge. Each probe consists of two microphones to record the sound pressure. The sound intensity along the direction of the two microphones (away from the tire) is then calculated. In addition, in the present OBSI system, an optical sensor was installed and was used to record the once-per-revolution signal. The optical sensor, as shown in Figure F.3, radiates a beam onto the side face of the black disk rotating with the tire, and once the beam encounters the retroreflective tape and gets reflected to the optical sensor, the optical sensor generates a pulse. Therefore, a pulse signal is recorded at the exact time the tire completes one revolution. The optical signal can be used to accurately calculate vehicle speed, as well as used for the order tracking analysis, which will be discussed later. The microphone and optical signals were recorded simultaneously at 25.6 kHz.

Figure F.3: On-board sound intensity (OBSI) with optical sensor installed on the test vehicle

F.3 Total Noise Spectrum

In each test run, the time duration of data collected for the rough or smooth section was three seconds. A high-pass filter at 20 Hz was applied to the sound pressure time signals to eliminate subfrequency interferences from wind or the electronic system. In this paper, only the signal from the leading inboard microphone (Mic 1) will be presented. However, the same results were observed and conclusions drawn from the other microphones.

The total noise spectrums at 60 mph for the rough and smooth sections are compared and shown in Figure F.4. The differences in TPIN spectrums between rough and smooth sections depend on the tread pattern; no general trends can be found. For Tires 07 and 08, all the TPIN spectral contents increase on the rough section compared to the smooth section, especially for Tire 07. For Tires 09, 12 and 19, the TPIN only increase over part of the frequencies while at certain frequencies the TPIN is larger on the smooth section than on the rough section, e.g., 700-800 Hz for Tire 09, 900-1000 Hz for Tire 12, and 700 Hz for Tire 19.

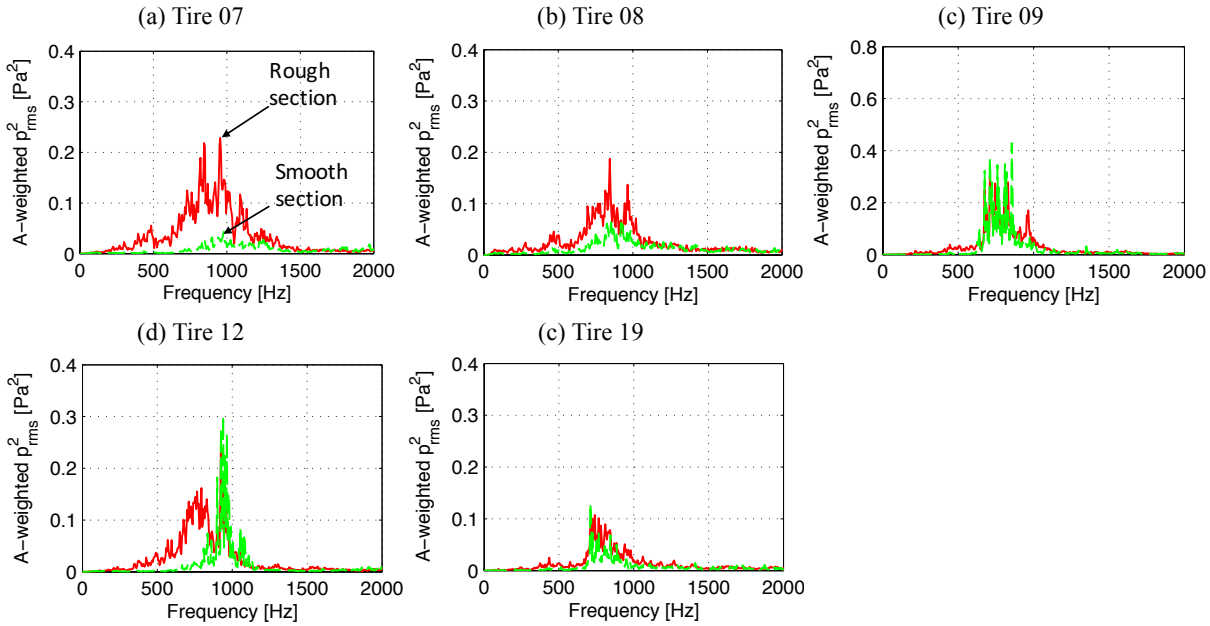

Figure F.4:Total noise spectrums at 60 mph (5 Hz resolution)

The overall A-weighted sound pressure level (OASPL) of the total noise on rough and smooth sections is shown in Table F.1. Generally, the OASPL is 2-3 dBA larger on the rough section than on the smooth section. However, the OASPL difference for Tire 07 is as large as 5.8 dBA while for Tire 09 only 0.9 dBA. In Table F.1, the rank of tires from quietest to noisiest is also displayed. It is interesting to note that Tire 07 is the noisiest tire on the rough section but turns out to be among the quietest on the smooth section.

Table F.1: OASPL of total noise on rough and smooth sections

Tire No.	OASPL [dBA]			Rank (From Quiet to Noisy)	
	Rough	Smooth	Difference (Rough-Smooth)	Rough	Smooth
07	105.5	99.7	5.8	5	2
08	104.3	101.5	2.8	3	4
09	104.9	104.0	0.9	4	5
12	104.1	101.2	2.9	2	3
19	101.7	99.3	2.4	1	1

In order to better explain the differences in total noise due to different pavement sections, the noise separation is performed to identify the noise component due to the tread pattern and the noise component due to the pavement in the following.

F.4 Tire Noise Separation

In this section, order tracking analysis utilizing the optical signal is performed to separate the two components of noise signals, tread-pattern-related noise and non-tread-pattern-related noise [382], [383].

The total, tread pattern and non-tread pattern noise spectra for each tire are displayed in Figure F.5. The results for the rough section are shown on the left column while the results for the smooth section are shown on the right column. The tread pattern noise and non-tread pattern noise are analyzed individually for the comparisons between the rough and smooth sections in the following. It can be seen that, for Tires 07 and 08, the tread pattern noise component is insignificant compared to the non-tread pattern noise component.

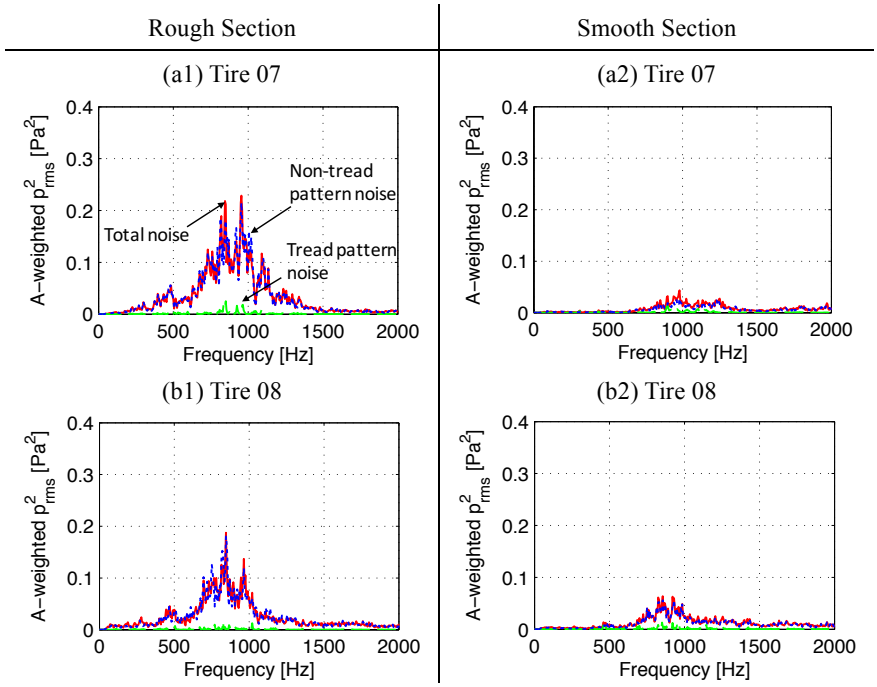

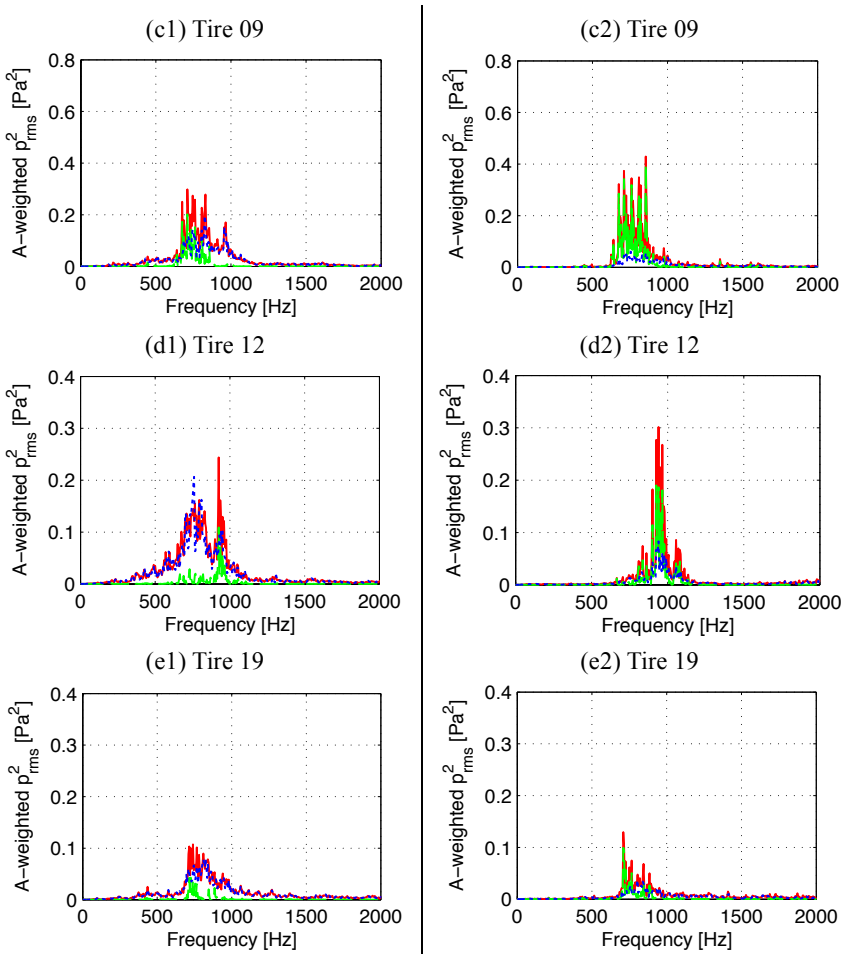

Figure F.5: Total, tread-pattern, and non-tread pattern noise components at 60 mph (5 Hz resolution)

F.5 Tread Pattern Noise Spectrum

The tread pattern noise spectrums at 60 mph for the rough and smooth sections are shown in Figure F.6, and the corresponding OASPL is shown in Table F.2. It can be seen that the spectral shape of the tread pattern noise component on the two sections is almost the same, which makes sense because the tread pattern noise is generated due to the tire tread pattern independent of the pavement. However, it is demonstrated that the amplitude of the tread pattern noise on the smooth section is generally larger (up to 3.6 dBA for Tire 09) than that on the rough section. It is likely because the smoother texture makes the tread pattern noise more distinguishable. The dominant frequencies of the tread pattern noise spectrums are basically where the total noise spectral amplitude of smooth section is larger than that of rough section,

as discussed above and shown in Figure F.4. For Tire 07, the trend is opposite, probably because its tread pattern noise is so small that some error in the values might occur.

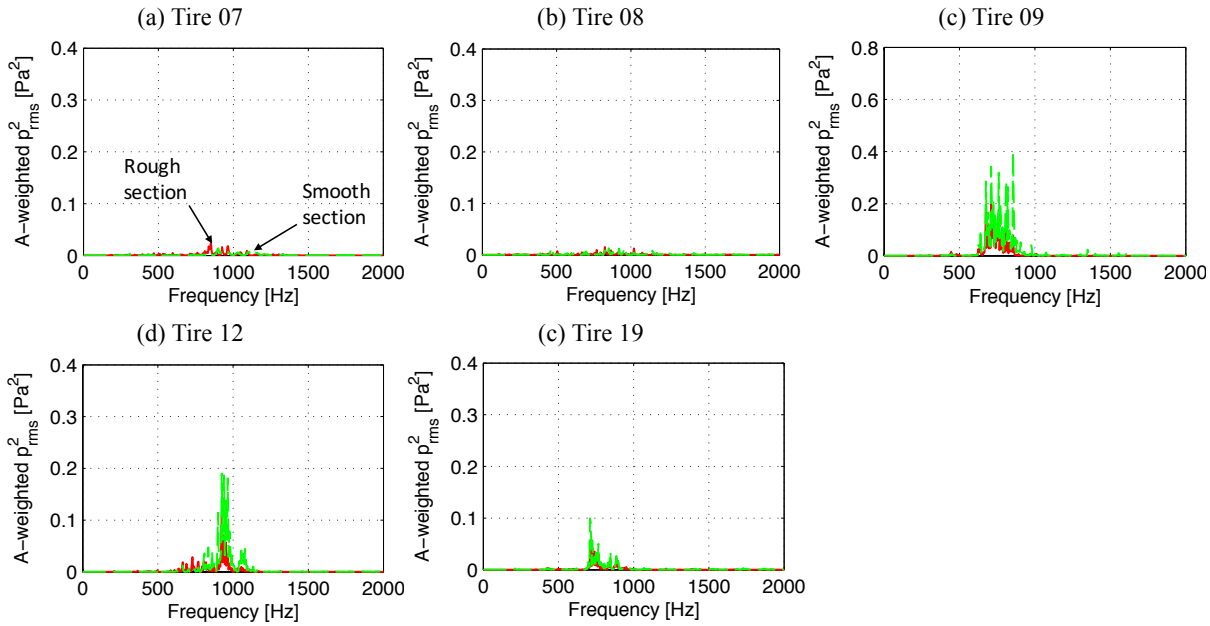

Figure F.6: Tread pattern noise spectrums at 60 mph (5 Hz resolution)

Table F.2: OASPL of tread pattern noise on rough and smooth sections

Tire No.	OASPL [dBA]			Rank (From Quiet to Noisy)	
	Rough	Smooth	Difference (Rough-Smooth)	Rough	Smooth
07	91.0	90.2	0.8	2	2
08	89.0	89.8	-0.8	1	1
09	98.4	102.0	-3.6	5	5
12	94.2	97.6	-3.4	4	4
19	91.9	93.7	-1.8	3	3

As shown in Table F.2, the ranking of the tires is consistent on either rough or smooth pavement. It is implied that the tire with the smallest tread pattern noise has the best tread pattern design in terms of noise reduction, regardless of the pavement.

F.6 Non-tread Pattern Noise Spectrum

The non-tread pattern noise spectrums at 60 mph for the rough and smooth sections are shown in Figure F.7, and its corresponding OASPL is displayed in Table F.3. It can be seen that the amplitude of the non-tread pattern noise on the rough section is generally larger than that on the smooth section over all the frequencies. The non-tread pattern noise is supposed to be excited by the isotropic pavement texture, which is considered to be random, homogeneous and broadband; the non-tread pattern noise increases as the spectral contents (rough > smooth) of the pavement texture increase.

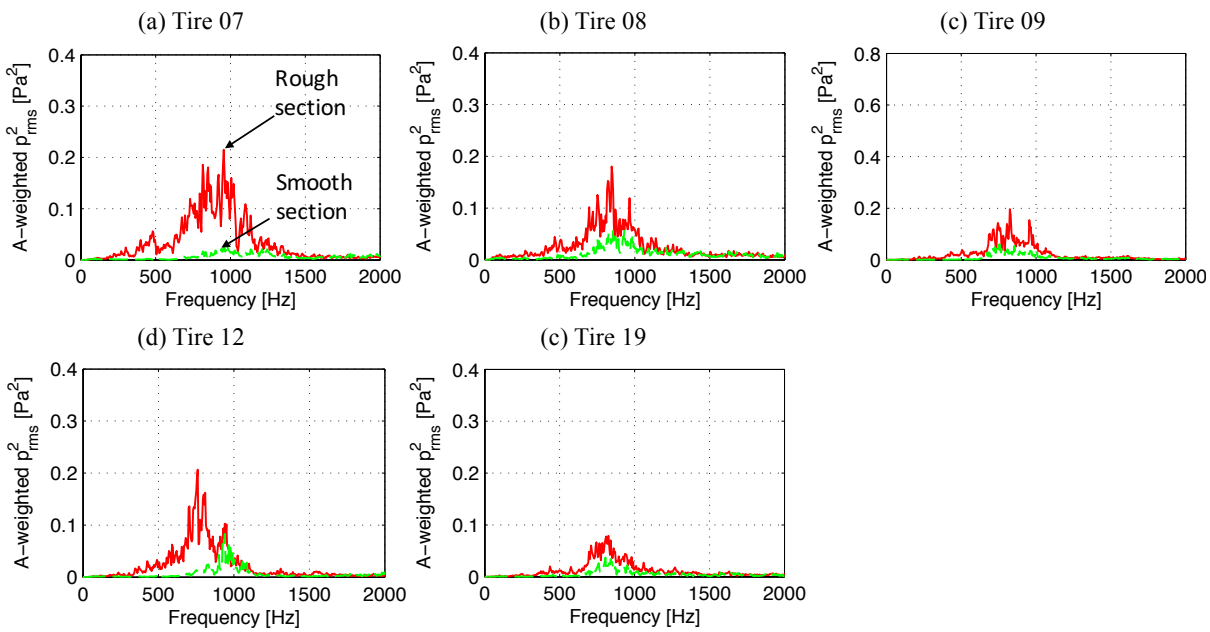

Figure F.7: Non-tread pattern noise spectrums at 60 mph (5 Hz resolution)

Table F.3: OASPL of non-tread pattern noise on rough and smooth sections

Tire No.	OASPL [dBA]			Rank (From Quiet to Noisy)	
	Rough	Smooth	Difference (Rough-Smooth)	Rough	Smooth
07	105.5	99.0	6.5	5	3
08	104.3	101.2	3.1	4	5
09	103.7	99.5	4.2	3	4
12	103.6	98.6	5.0	2	2
19	101.3	97.8	3.5	1	1

The ranking of tires for the non-tread pattern noise is inconsistent on the two pavement sections. For example, Tire 07 is fairly quiet on the smooth section while it becomes the noisiest on the rough section in terms of non-tread pattern noise. This is likely because its tire components not related to tread pattern is more prone to resonate at higher pavement texture excitation.

F.7 Percent Contribution from Two Noise Components

As discussed above, on the smoother pavement, the tread pattern noise increases and the non-tread pattern noise decreases. As such, the percent contribution from tread pattern noise component increases on the smoother pavement (~3 times), as shown in Table F.4. For example, more than half (64%) of the TPIN comes from the tread pattern for Tire 09 on the smoother section while only 23% on the rough section. It is implied that on smoother pavement, the tread pattern is more important in terms of noise reduction. Smoother pavement is more feasible for ranking the quietness of a tire or its tread pattern. For an extreme example, the lab drum with a very smooth steel surface as a pavement is supposed to generate the smallest non-tread pattern noise, and meantime the tread pattern noise is dominant, such as air pumping noise (Gautam and Chandy, 2016 [454]). It also agrees with the observation that the tread pattern noise component that shifts with speed is more easily seen for tires tested on the lab drum (Schumacher, 2015 [386]) than that on real pavement (Alt et al., 2006 [270]).

Table F.4: Percent contribution from tread pattern noise component

Tire No.	Tread Pattern Noise Contribution [%]		Rank (From Small to Large)	
	Rough	Smooth	Rough	Smooth
07	3.4	11.6	2	2
08	2.9	6.8	1	1
09	22.8	64.0	5	5
12	10.3	44.3	3	4
19	10.3	28.0	3	3

In Table F.4, it also exhibits that, for Tires 07 and 08 (all-season tires), the tread pattern contributes marginally to the total tire noise, especially on the rough section (below 5%), which means the tread pattern is well designed and randomized. For Tires 09, 12, and 19 (snow tires), of which the tread pattern looks aggressive, the tread pattern contributes considerably to the total tire noise, especially on the smooth section.

F.8 Conclusions

The comparisons of tire-pavement interaction noise (TPIN) between a rough section and a smooth section were analyzed in this paper. The spectrums of the total noise between the two sections revealed no general trends. Therefore, the total noise was separated into two noise components: tread pattern noise and non-tread pattern noise. It was found that the spectral shapes of the tread pattern noise between the two sections were almost the same while the spectral shapes of the non-tread pattern noise between the two sections were quite different. The spectral amplitude of the tread pattern noise was generally larger on smoother pavement while the spectral amplitude of non-tread pattern noise was generally larger on rougher pavement. It is also reasonable to conclude that the tread pattern is more important on smoother pavement in terms of noise generation.

Appendix G: Characteristics of TPIN from Slick Tire

G.1 Introduction

In the open literature or even in the tire industry, slick tires are believed to be the quietest tires. However, the fact is it likely depends on the pavement: the slick tire is probably quietest on very smooth pavement (e.g., indoor steel drum) but might be the noisiest on rough pavement. Among the ~1000 references related to tire noise the present authors reviewed, only two [255], [269] were found to explicitly make this statement but without reasonable explanations or data.

G.2 Experiments

The tires tested for this topic are shown in Table G.1.

Table G.1: Testing of slick tires (red arrow indicates rotation direction)

	Slick Tire	Patterned Tire	Note
(a)			Tire 21 is racing slick tire for smooth competition track only. When tested on normal highways, stones are picked up due to soft tread as shown on the right, so the noise data might not be valid. Note that no corresponding patterned tire is compared with this slick tire.
(b)			Tires 20 and 46 are identical except that Tire 20 is with normal tread and Tire 46 is with heavily worn tread (towards slick).
(c)			Tires 37 and 35 are identical except that Tire 37 is with normal tread and Tire 35 is with tread intentionally shaved (towards slick).

	Slick Tire	Patterned Tire	Note
(d)			Tires 42 and 41 are identical except that Tire 42 is with normal tread and Tire 41 is with tread intentionally shaved (towards slick).
(e)			Tires 13 and 57 are identical except that Tire 13 is with normal tread and Tire 57 is with worn tread (towards slick). The tire sizes are also slightly different.

G.3 Noise Separation Analysis

For each tire, the total noise is broken down into two components, tread pattern noise and non-tread pattern noise, as shown in Figure G.1.

	Slick Tire	Patterned Tire
	Tire 21	
(a)	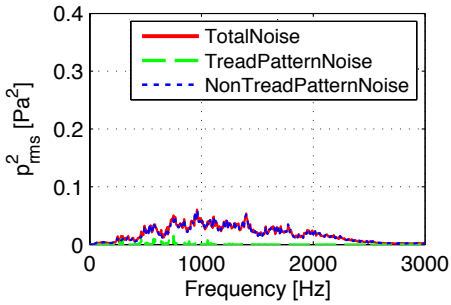	
	Tire 46	Tire 20
(b)	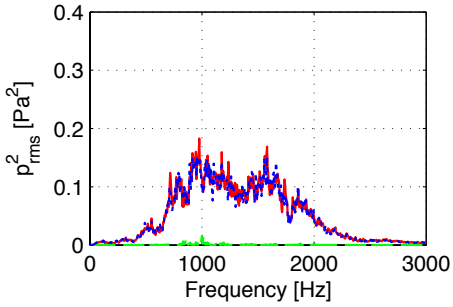	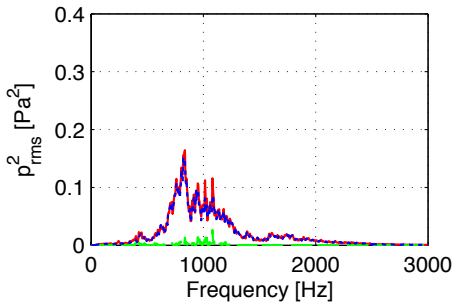

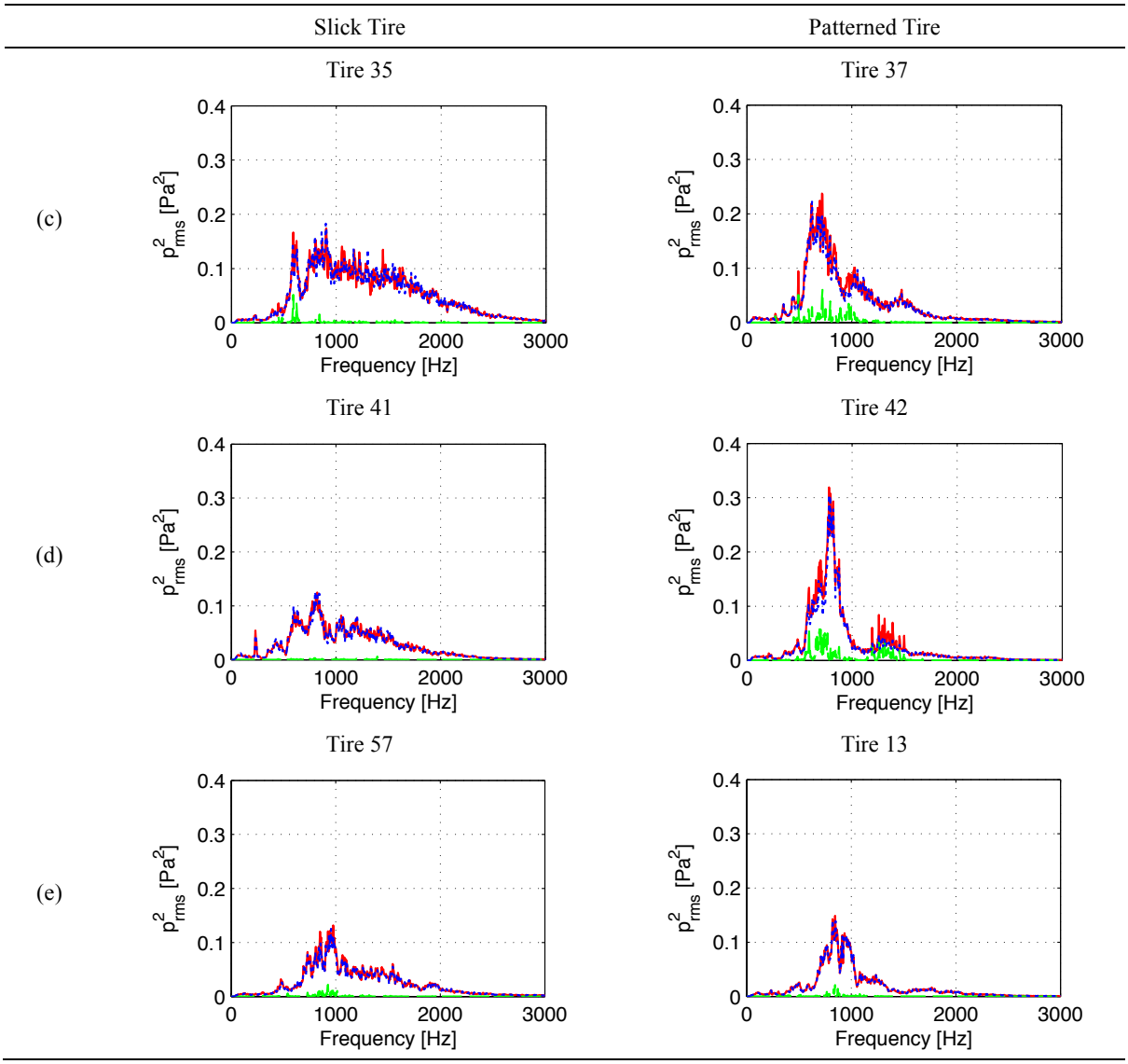

Figure G.1: Noise separation analysis (60 mph, 32 psi, eastbound, leading inboard mic)

G.4 Total Noise Spectrum

The total noise spectral comparisons between slick tire and patterned tire are shown in Figure G.2. Generally, the total noise of slick tire is larger than the corresponding patterned tire, especially over 1000-2500 Hz.

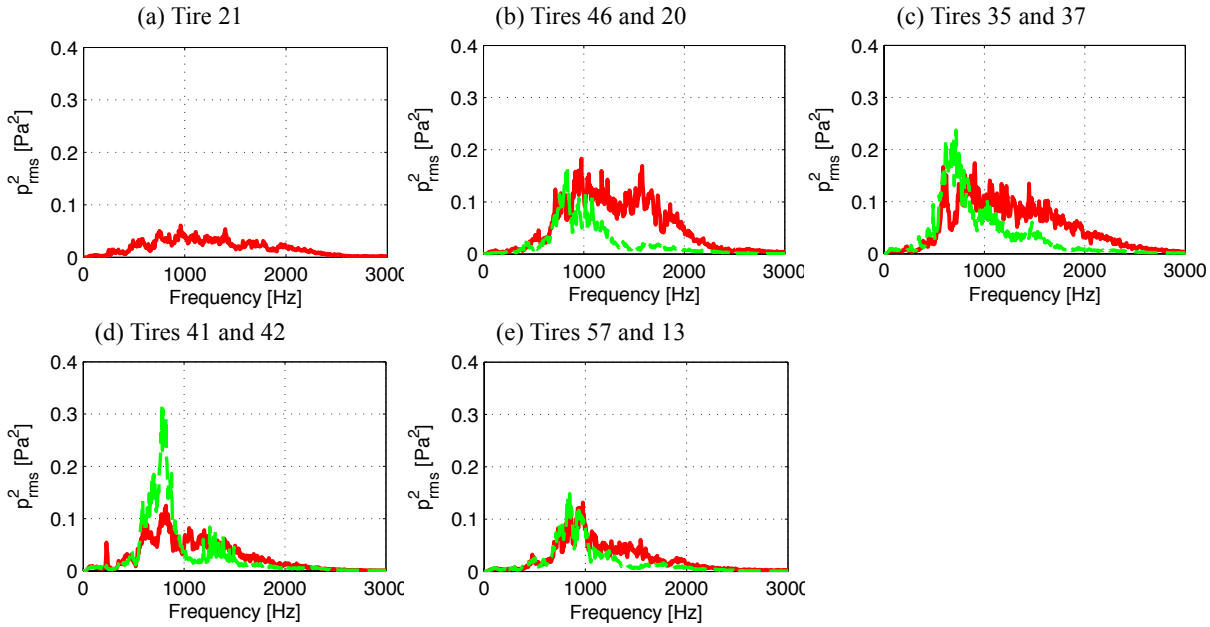

Figure G.2: Total noise spectral comparisons (red: slick tire; green: patterned tire) (60 mph, 32 psi, eastbound, leading inboard mic)

G.5 Tread Pattern Noise Spectrum

The tread pattern noise spectral comparisons between slick tire and patterned tire are shown in Figure G.3. It makes sense that the tread pattern noise from the slick tire is smaller than the corresponding patterned tire.

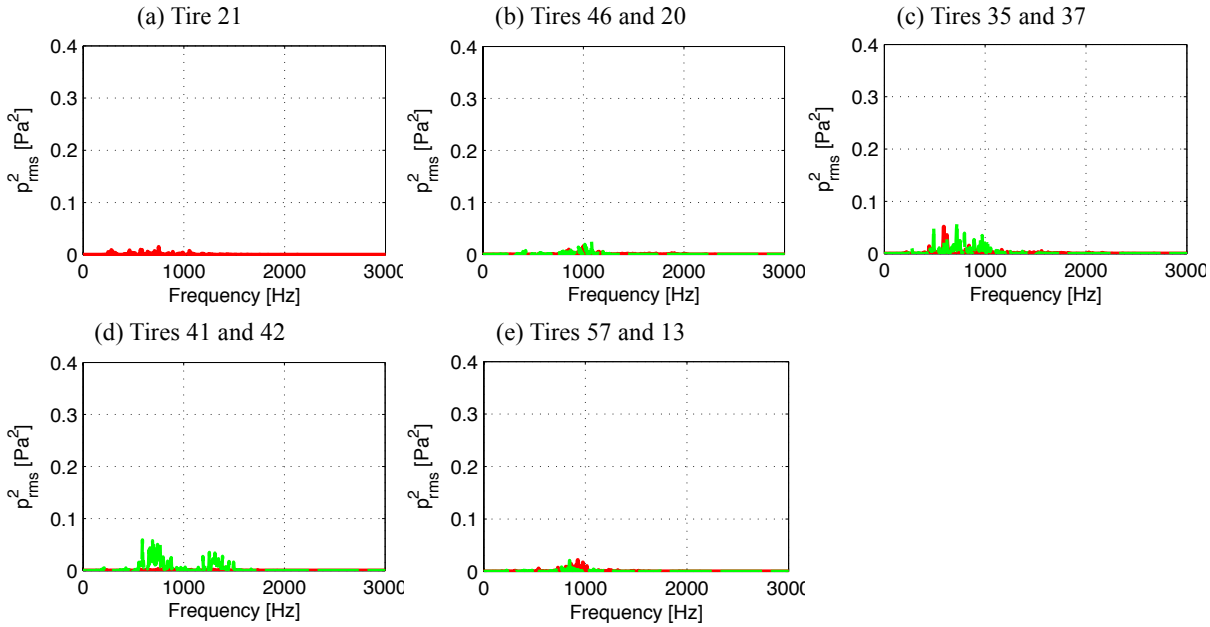

Figure G.3: Tread pattern noise spectral comparisons (red: slick tire; green: patterned tire) (60 mph, 32 psi, eastbound, leading inboard mic)

G.6 Non-Tread Pattern Noise Spectrum

The non-tread pattern noise spectral comparisons between slick tire and patterned tire are shown in Figure G.4. Generally, the non-tread pattern noise of slick tire is larger than the corresponding patterned tire, especially over 1000-2500 Hz for the pavement tested (not very smooth). The reason the non-tread pattern noise of patterned tires at higher frequencies is smaller than that of slick tires is speculated to be that the tread blocks damp out high-frequency tire vibrations due to pavement roughness, e.g., tread block acts like a damper dissipating energy, which it is absent in a slick tire. However, for Figure G.4d, the non-tread pattern noise of the patterned tire is larger than that of the slick tire at around 800 Hz, which is likely due to the resonance of the tread blocks (might coincide with the dominant frequencies of the tire carcass vibrations). That is also to say, the tread blocks might function as a filter, attenuate spectral contents at higher frequencies, and amplify spectral contents at resonance frequencies.

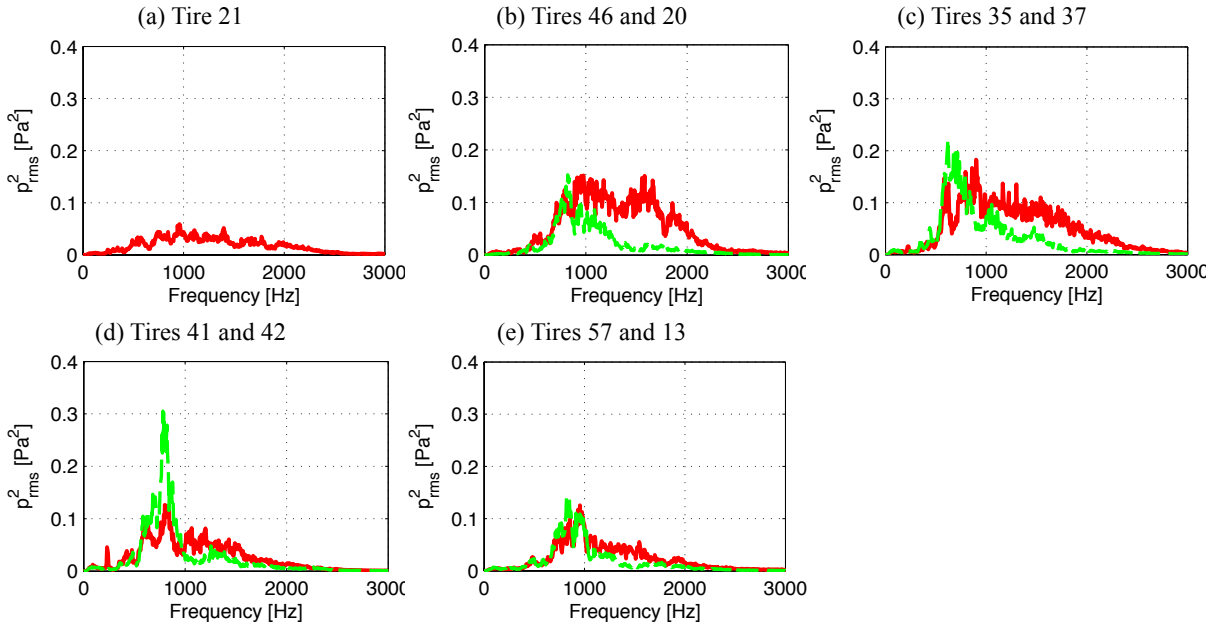

Figure G.4: Non-tread pattern noise spectral comparisons (red: slick tire; green: patterned tire) (60 mph, 32 psi, eastbound, leading inboard mic)

Appendix H: A Literature Review of Tire-Pavement Interaction Noise

The following is a complete literature review on Tire-Pavement Interaction Noise (TPIN). The introduction to TPIN, measurement techniques, physical mechanisms, influencing parameters, existing models, and reduction approaches are included. This can be considered as a separate document from this dissertation. Note that the citations/references in the following literature review are also separate from the main body of the dissertation.

This literature review includes ~1000 references, covering 22 measurement techniques, 15 physical mechanisms, 53 influencing parameters, and 74 existing models.

A Literature Review on Tire-Pavement Interaction Noise

Tan Li
Email: L@vt.edu
Department of Mechanical Engineering, Virginia Tech
Blacksburg, VA 24060, USA

This document is an appendix of the author's Ph.D. dissertation entitled "Tire-Pavement Interaction Noise (TPIN) Modeling Using Artificial Neural Network (ANN)", but can be referenced separately.

Contents

List of Figures **315**

List of Tables **326**

1 Introduction **330**

1.1 Motivation *331*

1.1.1 Pollution 331

1.1.2 Policy 333

1.2 Noise Abatement *337*

1.3 Vehicle Noise *338*

1.4 Noise Categories *345*

1.5 Structure of Work *350*

2 Measurement Techniques **352**

2.1 Introduction *352*

2.2 Roadside Measurement *354*

2.2.1 Statistical Pass-By (SPB) 354

2.2.2 Controlled Pass-By (CPB) 355

2.2.3 Coast-By (CB) 356

2.2.4 Statistical Pass-By and Time-Averaged Wayside (SPB/TA) 357

2.2.5 Statistical Isolated Pass-by (SIP) 359

2.2.6 Continuous-Flow Traffic Time-Integrated Method (CTIM) 360

2.2.7 Coast-By Sound Power Level (CBSWL) 361

2.2.8 Summary 362

2.3 On-board Measurement *364*

2.3.1 Behind the Tire (BTT) 364
2.3.2 Trailer Coast-By (TCB) 365
2.3.3 On-Board Sound Pressure (OBSP) 366
2.3.4 Close Proximity Sound Intensity (CPI) 368
2.3.5 Sound Intensity Field (SIF) 371
2.3.6 Tire Cavity Microphone (TCM) 371
2.3.7 Close-Proximity Trailer (CPX) 373
2.3.8 In Vehicle (IV) 374
2.3.9 On-Board Sound Intensity (OBSI) 375
2.3.10 Summary 379
2.4 Lab Measurement 381
2.4.1 Tire Vibration Measurements (TVM) 381
2.4.2 Laboratory Drum (DR) 382
2.4.2.1 Outer Rotating Drum 383
2.4.2.2 Inner Rotating Drum 384
2.4.2.3 Outer Stationary Drum 384
2.4.3 Near-field Acoustic Array Technology (NAAT) 385
2.4.4 Novel Pass-By (NPB) with Novel Close Proximity (NCPX) 388
2.4.5 Far-field Acoustic Array Technology (FAAT) 390
2.4.6 Traffic Noise Auralization (TNA) 392
2.4.7 Summary 394
2.5 Relationship between Different Measurement Techniques 396
2.6 Conclusions 400
3 Physical Mechanisms 401
3.1 Introduction 401
3.2 Generation Mechanisms 402
3.2.1 Impact (Shock) 403
3.2.2 Adhesion 408
3.2.2.1 Stick/Slip (Friction) 408
3.2.2.2 Stick/Snap 409
3.2.3 Air Displacement 410

3.2.3.1 Air Pumping 410
3.2.3.2 Air Turbulence 413
3.3 Amplification Mechanisms 414
3.3.1 Tire Resonance 415
3.3.1.1 Belt Resonance 415
3.3.1.2 Torus Cavity Resonance 416
3.3.1.3 Sidewall Resonance 421
3.3.1.4 Tire/Rim Assembly Resonance 422
3.3.2 Air Resonance 422
3.3.2.1 Pipe Resonance 423
3.3.2.2 Helmholtz Resonance 424
3.3.3 Horn Effect 426
3.4 Attenuation Mechanisms 428
3.4.1 Acoustical Impedance (Pavement Absorption) 428
3.4.2 Mechanical Impedance (Vibration Transfer) 429
3.5 Summary 429
4 Influencing Parameters 435
4.1 Introduction 435
4.2 Driver Influence Parameters 436
4.2.1 Speed 436
4.2.2 Longitudinal Force/Slip 440
4.2.3 Lateral Force/Slip 441
4.2.4 Tire Load 442
4.2.5 Inflation Pressure 444
4.2.6 Tire Camber Angle 446
4.3 Tire Related Parameters 447
4.3.1 Tire Type/Construction 447
4.3.2 Tire Size 449
4.3.3 Belt Stiffness 452
4.3.4 Damping (Loss Factor) 453
4.3.5 Non-uniformity 454

4.3.6 Rubber Hardness 454
4.3.7 Wear/Aging 459
4.3.8 Retreaded 460
4.3.9 Studded 461
4.3.10 Tread Porosity 462
4.3.11 Tire Cavity Content 462
4.3.12 Rolling resistance 462
4.3.13 Reference Tire 463
4.4 Tread Pattern Parameters 465
4.4.1 Randomization 469
4.4.2 Rotation Direction / Side Asymmetry 474
4.4.3 Ventilation 474
4.4.4 Tread Segment 475
4.5 Pavement Related Parameters 476
4.5.1 Texture 480
4.5.1.1 Micro-texture (below 0.5 mm) 484
4.5.1.2 Macro-texture (0.5-50 mm) 484
4.5.1.3 Mega-texture (50-500 mm) 485
4.5.1.4 Unevenness (0.5-50 m) 485
4.5.2 MPD/MTD/Texture 486
4.5.3 International Roughness Index (IRI) 487
4.5.4 Positive versus Negative Texture 488
4.5.5 Transverse Texture 488
4.5.6 Anisotropic Texture 488
4.5.7 Joints 489
4.5.8 Porosity (Air Void Content) 490
4.5.9 Sound Absorption 493
4.5.10 Airflow Resistance 494
4.5.11 Thickness of Layer 495
4.5.12 Stiffness (Mechanical Impedance) 496
4.5.13 Normal Adhesion 497

4.5.14 Tangential Friction 497
4.5.15 Wear/Age 498
4.5.16 Surface Rating (SR) 499
4.5.17 Wetness 499
4.5.18 Mixture Parameters / Materials 500
4.5.19 Reference Pavement 501
4.6 Environmental Parameters 502
4.6.1 Temperature 502
4.6.2 Air Humidity 505
4.6.3 Wind 505
4.7 Summary 506
5 Existing Models 511
5.1 Introduction 511
5.2 Deterministic Models 513
5.2.1 Introduction 513
5.2.2 Conventional Physics Models 514
5.2.2.1 Hayden (Monopole, 1971) 514
5.2.2.2 Plotkin and Stusnick (Unified, 1981) 515
5.2.2.3 Keltie (Truck Tire, 1982) 521
5.2.2.4 Kung et al. (2D Ring, 1986) 522
5.2.2.5 Heckl (Various Mechanisms, 1986) 523
5.2.2.6 Bremner et al. (Tire Vibration, 1997) 525
5.2.2.7 Bérengier et al. (Porous Pavement, 1997) 526
5.2.2.8 Bolton et al. (Wavenumber Decomposition, 1998) 528
5.2.2.9 Kropp (Orthotropic Plate, 1999) 529
5.2.2.10 Kim and Bolton (Shell, 2002) 533
5.2.2.11 Molisani et al. (Coupled Cavity, 2003) 535
5.2.2.12 Kim et al. (Waveguide, 2007) 536
5.2.2.13 Feng et al. (Cavity, 2009) 538
5.2.2.14 O'Boy and Dowling (3D Multilayer, 2009) 539
5.2.2.15 Arteaga (Green's Function, 2011) 542
5.2.2.16 Bolton and Cao (Coupled Mode, 2013) 543

5.2.3 Finite Element and Boundary Element Models 544
5.2.3.1 Saigal et al. (Toroidal Membrane, 1986) 545
5.2.3.2 Wright and Koopmann (Acoustic Radiation, 1986) 546
5.2.3.3 Richards (FEA Coupling, 1991) 547
5.2.3.4 Larsson and Kropp (3D 2 Plate, 1992) 549
5.2.3.5 De Roo and Gerretsen (TRIAS, 2000) 551
5.2.3.6 Nilsson (WFEM, 2004) 552
5.2.3.7 Biermann et al. (IFEM, 2007) 553
5.2.3.8 Brinkmeier et al. (FEM & BEM, 2008) 554
5.2.3.9 Waki et al. (WFE, 2011) 554
5.2.3.10 Kido et al. (Road Input, 2011) 555
5.2.3.11 Yang et al. (FSI, 2013) 556
5.2.3.12 Tong et al. (Wear, 2013) 557
5.2.3.13 Vlahopoulos et al. (EFEA/EBEA, 2013) 557
5.2.3.14 Mohamed and Wang (Cavity, 2015) 558
5.2.3.15 Wei et al. (MLE, 2016) 559
5.2.3.16 Banz et al. (Time Domain BEM, 2016) 560
5.2.4 Computational Fluid Dynamics Models 561
5.2.4.1 Gagen (Shock Wave, 1999) 561
5.2.4.2 Kim et al. (Hybrid CFD, 2006) 562
5.2.4.3 Chen et al. (CFD, 2014) 563
5.2.4.4 Gautam and Chandy (Air Pumping CFD, 2016) 563
5.2.4.5 Fabrizi (Pipe Resonance, 2016) 564
5.2.5 Summary 566
5.3 Statistical Models 571
5.3.1 Introduction 571
5.3.2 Traditional Regression Models 573
5.3.2.1 RLS (Germany, 1990) 573
5.3.2.2 CNR (Italia, 1991) 574
5.3.2.3 TNM (US, 1998) 575
5.3.2.4 Hanson and James (Dense Graded, 2004) 576
5.3.2.5 Rasmussen (Concrete Texture, 2009) 577
5.3.2.6 Fujikawa et al. (Asperity, 2009) 578

5.3.2.7 Reyes and Harvey (Pavement Core, 2011) 580
5.3.2.8 CNOSSOS (EU, 2012) 581
5.3.2.9 Syamkumar et al. (Mode-wise, 2013) 582
5.3.2.10 Wayson et al. (FDOT, 2014) 583
5.3.3 Principal Component Analysis Models 584
5.3.3.1 Ongel et al. (Asphalt Pavement, 2008) 584
5.3.3.2 Zhang et al. (MTD, 2014) 587
5.3.3.3 Li et al. (Thin Surfacing, 2015) 588
5.3.4 Fuzzy Curve Fitting Models 589
5.3.4.1 Fry et al. (CPB ANN, 1999) 589
5.3.4.2 Khazanovich and Izevbekhai (Pavement Aging, 2008) 592
5.3.4.3 Li et al. (F-GA, 2009) 593
5.3.4.4 Che et al. (ANN, 2012) 593
5.3.4.5 Yu and Lu (Bayesian, 2013) 596
5.3.5 Summary 598
5.4 Hybrid Models 601
5.4.1 Introduction 601
5.4.2 Tire-Pavement Interface Models 601
5.4.2.1 Fong (Truck Contact, 1998) 601
5.4.2.2 Domenichini et al. (DGAC Texture, 1999) 602
5.4.2.3 Beckenbauer and Kuijpers (SPERoN, 2001) 605
5.4.2.4 Kuijpers and Blokland (Enhanced SPERoN, 2003) 608
5.4.2.5 Klein and Hamet (HyRoNE, 2007) 610
5.4.2.6 Rustighi et al. (Road Excitation, 2008) 612
5.4.2.7 Dubois et al. (Viscoelastic Contact, 2011) 615
5.4.2.8 Dubois et al. (Contact Distribution, 2013) 617
5.4.2.9 Klein and Cesbron (3D Envelopment, 2016) 618
5.4.3 Mechanism Separation Models 620
5.4.3.1 Cao et al. (Tire/Road Coupling, 2008) 620
5.4.3.2 Dare (Mechanism Decomposition, 2012) 622
5.4.3.3 Winroth et al. (Air Pumping Separation, 2013) 625
5.4.3.4 Mohamed and Wang (Deterministic SEA, 2016) 626
5.4.3.5 Le Bot et al. (Statistical Vibration, 2017) 627

5.4.3.6 Wang and Duhamel (Network Resonator, 2017) 631
5.4.4 Noise Propagation Models 632
5.4.4.1 CRTN (UK, 1988) 632
5.4.4.2 NMPB (France, 1996) 634
5.4.4.3 Dai and Lee (Highway, 2010) 636
5.4.4.4 Wei et al. (Air Pumping, 2016) 640
5.4.5 Summary 640
5.5 Conclusions 644
6 Noise Reduction 646
6.1 Quiet Tire 646
6.2 Quiet Pavement 657
6.3 Combination of Tires and Pavements 659
6.4 Other Considerations 659
References 661

List of Figures

Figure 1: Literature records count (generated via Engineering Village on Aug 12, 2016, search query for "tire" & "noise" in subject/title/abstract from databases of Compendex, Inspec & NTIS) 331

Figure 2: Strategic noise map for the night-time period (L_{night}) in Dublin, Ireland (source from Murphy and King, 2011 [16], Figure 2; reprinted with permission from Elsevier) 332

Figure 3: Regulation limits for noise emission of passenger cars in European Union (EU), Japan and USA (source from Sandberg, 2001 [22], Figure 1; reprinted under fair use provision) .. 333

Figure 4: Noise emission limits according to Directive 2001/43/EC (source from FEHRL, 2001 [28], Appendices Figure 3; reprinted under fair use provision)..... 334

Figure 5: Noise emission limits according to Regulation (EC) 661/2009 (modified from EC, 2009 [29] ; reprinted under fair use provision)..... 334

Figure 6: Tire labeling information (source from ETRMA, 2011 [36]; reprinted with permission from ETRMA) 335

Figure 7: China Green Tyre Rating Assessment (C-GTRA) (source from RenMinWang, 2016 [35] ; reprinted under fair use provision)..... 336

Figure 8: Noise source ranking for a vehicle during the pass-by noise test (source from Braun et al., 2013 [48], Figure 21; original from Bosch, 2004 [49]; reprinted with permission from Elsevier)..... 339

Figure 9: Engine noise map of sound pressure level versus torque and rotational speed (source from Braun et al., 2013 [48], Figure 11; original from Biermann, 2004 [51]; reprinted with permission from Elsevier)..... 339

Figure 10: Sound pressure level of intake orifice noise versus engine speed and frequency (source from Braun et al., 2013 [48], Figure 14; original from Zeller, 2009 [52]; reprinted with permission from Elsevier)..... 340

Figure 11: Sound pressure level of exhaust noise versus engine speed (source from Braun et al., 2013 [48], Figure 16; original from Alfredson and Davies, 1970 [53]; reprinted with permission from Elsevier) 340

Figure 12: Typical frequency spectrum of exhaust noise measured at 1880 rpm and 0.9 m from the outlet: (a) 0–5000 Hz; (b) 100–600 Hz (source from Braun et al., 2013 [48], Figure 17; original from Alfredson and Davies, 1970 [53]; reprinted with permission from Elsevier)... 341

Figure 13: Vehicle noise components versus speed (source from Rasmussen et al., 2007 [62], Figure 7; reprinted with permission from Dr. Robert Otto Rasmussen of The Transtec Group, Inc., USA) 342

Figure 14: Power spectrum of the microphone signals situated close to the engine (blue) and close to the tire (red) for a pass-by velocity of 70 km/h (source from Bravo et al., 2012 [57], Figure 3; reprinted with permission from ASME)..... 342

Figure 15: Noise emissions from exhaust and intake system (source from Freeman and Cerrato, 2011 [60], Figure 4; reprinted under fair use provision)..... 343

Figure 16: The most important reduction measures employed in a common car in order to satisfy the various steps in tightened noise emission limits in Germany and the EU. Note the curves that indicate how the limits and the sources engine, intake, exhaust and tire have developed over time. (Source from Sandberg, 2001 [22], Figure 3; reprinted under fair use provision) 344

Figure 17: Contributions of the various sub-sources of highway traffic noise (source from Bernhard and Wayson, 2005 [66], Figure 1.1; reprinted with permission from Ms. Amy Miller of Asphalt Pavement Alliance)..... 344

Figure 18: Contribution matrix indicating the relative power contribution from each independent component (column) to each reference microphone (row) (source from Schuhmacher, 2015 [67], Figure 11; reprinted under fair use provision)..... 345

Figure 19 Vehicle interior noise transmission path (source from He et al., 2011 [68], Figure 2; reprinted with permission from Trans Tech Publications Ltd) 345

Figure 20: Interior noise spectrum at speed 80 km/h (source from Chang et al., 2010 [69], Figure 4; reprinted with permission from IEEE)..... 346

Figure 21: Contribution of tire structure-borne and airborne noise for interior noise (source from Kitahara, 2011 [75], Figure 2; reprinted under fair use provision)..... 347

Figure 22: Structure-borne interior noise due to spindle force and moment variations (source from Saguchi et al., 2007 [78], Figure 13; reprinted under fair use provision)..... 348

Figure 23: Coast down measurement of exterior noise at the leading CPX (above) and interior noise at right-ear passenger seat (below) measured simultaneously (source from Bekke et al., 2010 [81], Figure 5; reprinted under fair use provision) 348

Figure 24: Interior noise spectrum versus electric motor rpm (80% accelerator pedal position measured on roller test bench) (source from Fischer et al. 2014 [86], Figure 6; reprinted with permission from Mr. David Landes of Karlsruhe Institute of Technology, Germany)..... 349

Figure 25: Sound qualities in the compartment of a passenger car (source from Lee et al., 2005 [91], Figure 1; reprinted with permission from Mr. Craig Myles on behalf of SAGE Ltd. Permissions Team) 350

Figure 26: Statistical Pass-by (SPB) (Source from Wang et al., 2011 [42], Figure 2.1; reprinted under fair use provision) 354

Figure 27: Controlled Pass-By (CPB) (Source from Copeland and Wilhoit, 2012 [106], Figure 1; reprinted with permission from Mr. Jack Mowry, Editor and Publisher of Sound & Vibration) 356

Figure 28: Coast-By (CB) (Source from Sandberg and Ejsmont, 2002 [7], Fig. 14.3; reprinted with permission from Dr. Ulf Sandberg of VTI, Sweden)..... 357

Figure 29: Statistical Pass-By and Time-Averaged Wayside (SPB/TA) (Source from Bernhard and Wayson, 2005 [66], Figure 6.4; reprinted with permission from Ms. Amy Miller of Asphalt Pavement Alliance, USA; photo courtesy of Judith Rochat, U.S. DOT Volpe Center)..... 358

Figure 30: Statistical Isolated Pass-by (SIP) (Source from Lodico et al., 2012 [109], Figure 1; reprinted under fair use provision)..... 359

Figure 31: Continuous-Flow Traffic Time-Integrated Method (CTIM) (Source from Rochat et al., 2012 [115], Figure 2; reprinted under fair use provision) 360

Figure 32: Coast-By Sound Power Level (CBSWL) (Source from Campillo-Davo et al., 2013 [94], Figure 13; reprinted with permission from Elsevier)..... 361

Figure 33: Behind The Tire (BTT) (Source from Landers et al., 1977 [133], Figure 1; reprinted under fair use provision) 365

Figure 34: Trailer Coast-By (TCB) (Source from Sandberg and Ejsmont, 2002 [7], Fig. 16.30; reprinted with permission from Dr. Ulf Sandberg of VTI, Sweden, Mr. Steve Phillips of CEDR at EU, and Dr. Philip Morgan of TRL, UK)..... 366

Figure 35: On-Board Sound Pressure (OBSP) (Source from Chuang et al., 2005 [150], Figure 4 ; reprinted under fair use provision)..... 367

Figure 36: Close-Proximity Sound Intensity (CPI) (Source from Bernhard and Wayson, 2005 [66], Figure 6.6; reprinted with permission from Ms. Amy Miller of Asphalt Pavement Alliance, USA; photo provided by Dr. Paul Donavan of Illingworth and Rodkin, Inc., USA) 369

Figure 37: Sound Intensity Field (SIF) (Source from Donavan and Oswald, 1981 [160], Figure 11 and Figure 12; reprinted with permission from Dr. Paul Donavan of Illingworth and Rodkin, Inc., USA) 371

Figure 38: Tire Cavity Microphone (TCM) (Source from Bennetts and Crookes, 2013 [164], Figure 1; reprinted with permission from Mr. Charles Ellis, Publicity Officer and Acoustics Bulletin Editor, UK)..... 372

Figure 39: Close-Proximity Trailer (CPX) (Source from Wang et al., 2011 [42], Figure 2.2; reprinted with permission from Dr. Ulf Sandberg of VTI, Sweden) 373

Figure 40: In Vehicle (IV) (Source from He et al., 2011 [68], Figure 3; reprinted with permission from Trans Tech Publications Ltd)..... 374

Figure 41: On-board sound intensity (OBSI) configurations (modified from AVEC, 2012 [176]) 376

Figure 42: Tire Vibration Measurements (TVM) (Source from Dare, 2012 [213], Figure 3.11; reprinted with permission from Dr. Tyler Dare of Pennsylvania State University, USA).. 381

Figure 43: Laboratory Drum (DR) Outer Rotating Drum (Source from Tong et al., 2014 [238], Figure 5; reprinted with permission from Trans Tech Publications Ltd)..... 384

Figure 44: Laboratory Drum (DR) Inner Rotating Drum (Source from BASt website, [240], Federal Highway Research Institute's vehicle-pavement interaction test facility; reprinted with permission from M.Sc. Christopher Gerhard of Federal Highway Research Institute (BASt), Germany) 384

Figure 45: Laboratory Drum (DR) Outer Stationary Drum (Source from Bernhard and Wayson, 2005 [66], Figure 6.9; reprinted with permission from Ms. Amy Miller of Asphalt Pavement Alliance, USA; photo courtesy of Ray W. Herrick Laboratories, Purdue University, USA) 385

Figure 46: Tire/road noise distribution on a measurement plane around 500 Hz under three

driving conditions: (a) accelerating according to ISO 362; (b) constant velocity of 55 km/h; (c) coast down from 55 km/h (source from Park and Kim, 2001 [242], Figure 12, Figure 14, Figure 15; reprinted with permission from AIP Publishing LLC) 386

Figure 47: Near-field Acoustic Array Technology (NAAT) Trailer (Source from Ruhala and Burroughs, 1999 [243], Figure 1 ; reprinted under fair use provision) 388

Figure 48: Near-field Acoustic Array Technology (NAAT) Lab Drum (Source from Dumbacher et al., 1995 [246], Figure 9 ; reprinted under fair use provision) 388

Figure 49: Novel Pass-By (NPB) with Novel Close Proximity (NCPX) (Source from Cho and Mun, 2008 [254], Figure 1 and Figure 3; reprinted with permission from Elsevier) 389

Figure 50: Far-field Acoustic Array Technology (FAAT) Pass-by Acoustic Holography (PAH) (Source from Yang et al., 2011 [56], Figure 5; reprinted with permission from Elsevier) 390

Figure 51: Far-field Acoustic Array Technology (FAAT) Pass-by Noise Beamforming (PNB) (Source from Zavala et al., 2013 [262], Figure 9 ; reprinted under fair use provision) 391

Figure 52: Traffic Noise Auralization (TNA) (Source from Maillard and Jagla, 2012 [265], Figure 2; reprinted under fair use provision) 392

Figure 53: Comparison of spectra for CPX, OBSI, and CPB levels with 24 dB added for Dunlop tire on Section AC S5 at 45 mph (source from Donavan and Lodico, 2009 [139], Figure 7; reprinted with permission from Dr. Paul Donavan of Illingworth and Rodkin, Inc., USA)397

Figure 54: The propagation of active intensity and sound pressure radiated by the special pattern tire to the far field. (a) The active intensity (x and z direction) and sound pressure are visualized on y = 0.5 m plane. (b) Constant velocity condition. (c) Accelerating condition. (d) Coast down condition. (Source from Park and Kim, 2001 [242], Figure 16; reprinted with permission from AIP Publishing LLC) 398

Figure 55: Representation of the physical configuration for the extrapolation of the signals acquired by the microphones in the proximity of the tire (source from Bravo et al., 2012 [57], Figure 4; reprinted with permission from Ms. Beth Darchi on behalf of ASME) 399

Figure 56: The transfer function between the microphone close to the tire and the receiver position for different propagating surfaces (source from Bravo et al., 2012 [57], Figure 6; reprinted with permission from Ms. Beth Darchi on behalf of ASME) 400

Figure 57: The three wave types considered in the model (rings represent points in the rubber tread layer and stars represent points in the stiff belt layer) (source from Larsson and Kropp, 1999 [226], Figure 3; reprinted under fair use provision) 402

Figure 58: Dynamic characteristic of tire vibration (source from Iwao and Yamazaki, 1996 [307], Figure 8; reprinted under fair use provision) 406

Figure 59: Tire sidewall and tread region acceleration signals versus time for approximately one tire revolution (source from Keltie, 1982 [223], Figure 1; reprinted with permission from AIP Publishing LLC) 406

Figure 60: Frequency response function (FRF) amplitude in the tangential direction (vertical load 4 kN: dotted line, tire with tread blocks; solid line, tire without tread blocks) (source from Brusarosco et al., 2011 [341], Figure 4; reprinted with permission from Taylor & Francis) .. 409

Figure 61: Pulse shapes for modeling air pumping noise (source from Chiu and Fu, 2015 [361], Figures 2-4; reprinted with permission from Elsevier) 411

Figure 62: Tire carcass dispersion characteristics under static condition (source from Kwon et al., 1998 [245], Figure 4; reprinted under fair use provision) 416

Figure 63: Torus cavity resonance modes (source from Yamauchi and Akiyoshi, 2002 [299]; reprinted under fair use provision) 418

Figure 64: Frequency of oscillation of trailing edge signals versus distance of the large cavity from the contact patch: (i) frequency measured from period of oscillations (crosses); (ii) predicted frequency assuming 'air resonant radiation' (solid line). (Source from Eisenblaetter et al., 2010 [353], Figure 8; reprinted with permission from Elsevier) 426

Figure 65: Illustration of generation mechanisms 432

Figure 66: Illustration of amplification mechanisms 432

Figure 67: Illustration of attenuation mechanisms 433

Figure 68: Speed exponent in 1/3 octave band (n is speed exponent; f_T is the center frequency of 1/3 octave band) (source from Beckenbauer and Kuijpers, 2001 [487], Figure 4; reprinted under fair use provision) 437

Figure 69: (a) Top figure is vehicle speed versus time; (b) bottom figure is tire noise spectrum versus time (source from Schuhmacher, 2015 [67], Figure 12; reprinted under fair use provision) 440

Figure 70: Changes of TPIN due to driving torque and inflation pressure (source from Iwao and Yamazaki, 1996 [307], Figure 7; reprinted under fair use provision) 441

Figure 71: The effect of vehicle acceleration rate on tire noise as measured with on-board sound intensity (source from Donavan et al., 1998 [4], Figure 2; reprinted with permission from AIP Publishing LLC) 441

Figure 72: Changes of tire noise due to tire load and speed (source from Iwao and Yamazaki, 1996 [307], Figure 6; reprinted under fair use provision) 444

Figure 73: Vertical spindle force spectrum at different inflation pressures; driving over 5 mm high semi-circular cleat at speed of 22.6 km/h (source from Kindt et al., 2007 [525], Figure 8; reprinted under fair use provision) 446

Figure 74: Common tires with year indicated (source from Sandberg and Ejsmont, 2002 [7], Figure 6.5; reprinted with permission from Dr. Ulf Sandberg of VTI, Sweden) 450

Figure 75: Relation between TPIN level and tire width (data based on measurements 1981-1987 on radial car tires in Germany, Sweden and Norway) (source from Storeheier and Sandberg, 1990 [545]; reprinted under fair use provision) 451

Figure 76: Attack angles of tires with different tire diameters ($\alpha_1 > \alpha_2$) 452

Figure 77: Frequency spectra measured at each individual tire on the ISO test track (the numbers in the legend indicate year) (source from Oddershede and Kragh, 2014 [553], Figure 6; reprinted with permission from Mr. Jens Oddershede of Vejdirektoratet, Denmark) 455

Figure 78: Commonly proposed air pumping mechanism: disagreement with measurements from

the tire's point of view (source from Rochoux and Biesse, 2010 [337], Figure 1; reprinted under fair use provision) 456

Figure 79: Example for mobility measurements results (source from Schubert et al., 2016 [559], Figure 5; reprinted under fair use provision) 457

Figure 80: Comparison of measured mobility spectra for SRTT tires of different age (source from Schubert et al., 2016 [559], Figure 8; reprinted under fair use provision) 458

Figure 81: A typical stud pattern (8 stud lines with 16 stud on each line, 128 studs in total) (source from Johnsson and Nykänen, 2013 [572], Figure 3; reprinted under fair use provision) 461

Figure 82: Tread pattern of SRTT (tread surface is white painted) 464

Figure 83: Footprint of old Uniroyal SRTT (4410 N in load, 19 cm in length, 13 cm in width) (source from Ruhala, 1999 [244], Figure 5.2; reprinted with permission from Dr. Richard J. Ruhala of Kennesaw State University) 465

Figure 84: Colourmap plots of different pass-by noise tests: (a) engine switched off and slick tires; (b) engine switched off with standard tires; (c) ISO 362 acceleration test (source from Braun et al., 2013 [48], Figure 7; original from Alt et al., 2006, [584]; reprinted with permission from Elsevier) 466

Figure 85: Waterfall plots of tire/road noise measured on the road with three different tire types: (a) wide summer tire; (b) regular summer tire; (c) slick tire (source from Braun et al., 2013 [48], Figure 20; original from Alt et al., 2006, [584]; reprinted with permission from Elsevier)466

Figure 86: Example of a tread design with low TPIN characteristics (source from Saemann, 2005 [588]; reprinted under fair use provision)..... 469

Figure 87: Noise characteristics in the time domain when lateral groove contacts ground (source from Wei et al., 2016 [366], Figure 3; reprinted under fair use provision) 475

Figure 88: Acoustic performances of typical pavements in Virginia (source from McGhee, 2012 [606], Page 14; reprinted under fair use provision)..... 479

Figure 89: Contour lines of the correlation coefficient between TPIN levels (at 80 km/h) and pavement texture levels for four different tires (source from Sandberg and Ejsmont, 2002 [7], Figure 11.6; reprinted with permission from Dr. Ulf Sandberg of VTI, Sweden)..... 482

Figure 90: Pavement texture PSD and tread profile PSD (source from Bremner et al., 1997 [334], Figure 21; reprinted under fair use provision) 483

Figure 91: Surface texture levels for the thin-layer surfacing sections (source from Li et al., 2015 [613], Figure 3; reprinted with permission from American Society of Civil Engineers)..... 484

Figure 92: Evenness classification according to ISO 8608 (1995) [635] (modified from Barbosa, 2011 [636], Figure 8; reprinted under CC BY-NC 4.0 suggested by Dr. Francisco Ricardo Cunha, Editor-in-Chief of the J. Braz. Soc. Mech. Sci and Engn) 486

Figure 93: Sound absorption coefficients for the thin-layer surfacing sections (source from Li et al., 2015 [613], Figure 4; reprinted with permission from American Society of Civil Engineers) 494

Figure 94: Contour lines of the correlation coefficient between noise level (passenger car tire at

80 km/h) and sound absorption coefficient (source from Li et al., 2015 [613], Figure 6; reprinted with permission from American Society of Civil Engineers) 494

Figure 95: Typical cumulative spectral content of TPIN for different road conditions (source from Kongrattanaprasert et al., 2010 [708], Figure 1; reprinted under fair use provision)..... 500

Figure 96: Difference in levels measured on ISO and SAE test surfaces (SAE less ISO) (source from Donavan et al., 1998 [4], Figure 4; reprinted with permission from AIP Publishing LLC) 502

Figure 97: Shell model geometry and coordinate system (source from Keltie, 1982 [223], Figure 3; reprinted with permission from AIP Publishing LLC)..... 522

Figure 98: Frequency-wavenumber characteristics of tire carcass vibration (source from Bolton et al., 1998 [380], Figure 8; reprinted with permission from Dr. J. Stuart Bolton of Purdue University, USA)..... 529

Figure 99: Schematic of an orthotropic plate tire model (source from Kropp, 1999 [413], Figure 2; reprinted with permission from Dr. Jeanette Brooks on behalf of Inderscience Enterprises Limited)..... 530

Figure 100: Schematic of two multipoles for the sound radiation model (source from Kropp, 1999 [413], Figure 6; reprinted with permission from Dr. Jeanette Brooks on behalf of Inderscience Enterprises Limited) 532

Figure 101: Finite cylinder model (source from Kropp, 1999 [413], Figure 8; reprinted with permission from Dr. Jeanette Brooks on behalf of Inderscience Enterprises Limited) 532

Figure 102: Schematic of measurement facilities (source from Kropp, 1999 [413], Figure 11; reprinted with permission from Dr. Jeanette Brooks on behalf of Inderscience Enterprises Limited)..... 533

Figure 103: Complete viscoelastic cylindrical model of the tire belt (source from O'Boy and Dowling, 2009 [547], Figure 1; reprinted with permission from Elsevier)..... 539

Figure 104: Tire-rim assembly modeled as tensioned string-hard wall (source from Bolton and Cao, 2013 [767]; reprinted with permission from Dr. J. Stuart Bolton of Purdue University, USA) 543

Figure 105: Variation of structural wave speed with frequency for the unloaded tire (source from Wright and Koopmann, 1986 [773], Figure 6; reprinted with permission from Mr. Michael Kaliske of TU Dresden, Germany on behalf of Tire Science and Technology) 547

Figure 106: Tire model consisting of two coupled elastic layers under tension on an elastic bedding (source from Larsson and Kropp, 1999 [226], Figure 1; reprinted under fair use provision) 550

Figure 107: Schematic diagram of the mathematical simulation model TRIAS (Tyre Road Interaction Acoustic Simulation); the supporting model RODAS (ROad Design Acoustic Simulation) is indicated in the upper part of the scheme (source from de Roo and Gerrestsen, 2000 [664], Figure 1; reprinted under fair use provision) 551

Figure 108: Dispersion relations with various symbols indicating different groups of modes (Continental 205/55R16, source from Sabiniarz and Kropp, 2010 [9], Figure 13; reprinted

with permission from Elsevier)..... 553

Figure 109: Left - footprint and contact pressure distribution at 70% load (source from Wei et al., 2016 [798], Figure 6; reprinted with permission from Mr. Michael Kaliske of TU Dresden, Germany on behalf of Tire Science and Technology); right - The acceleration in the footprint at 0.0024 seconds (source from Wei et al., 2016 [798], Figure 7; reprinted with permission from Mr. Michael Kaliske of TU Dresden, Germany on behalf of Tire Science and Technology)..... 560

Figure 110: Schematic diagrams of the piston/sliding-door/cavity source model (source from Kim et al., 2006 [358], Figure 3; reprinted with permission from AIP Publishing LLC)..... 562

Figure 111: Schematic diagram showing different deformation models with (a) piston-like motion of bottom wall (b) side walls bulging inward (source from Gautam and Chandy, 2016 [801], Figure 3; reprinted with permission from Ms. Beth Darchi on behalf of ASME) 564

Figure 112: On the left, A-weighted sound pressure levels of the pressure signals recorded in four probes placed around and inside the contact patch of the tire with the road surface; on the right, the position of the four probes with the reference of the footprint shape (source from Fabrizi, 2016 [419], Figure 12; reprinted with permission from Mr. Michael Kaliske of TU Dresden, Germany on behalf of Tire Science and Technology) 566

Figure 113: Illustration of pavement roughness parameters in Fujikawa et al. Model (source from Fujikawa et al., 2009 [218], Figure 1; reprinted under fair use provision) 578

Figure 114: Two-stage ANN Models for pass-by noise (source from Fry and Jennings, 2003 [847], Figure 3; reprinted with permission from Springer)..... 591

Figure 115: Schematic of a typical artificial neural network (ANN) (source from Che et al., 2012 [586], Figure 2; reprinted with permission from Trans Tech Publications Ltd)..... 594

Figure 116: Example of pavement texture - rolling noise correlation chromatic plot (source from Domenichini et al., 1999 [63], Figure 10; reprinted under fair use provision)..... 603

Figure 117: Texture index (TI) illustration for Domenichini et al. Model (source from Domenichini et al., 1999 [63], Figure 14; reprinted under fair use provision)..... 604

Figure 118: Scheme of SPERoN Model (source from Beckenbauer and Kuijpers, 2001 [487], Figure 1; reprinted under fair use provision)..... 606

Figure 119: Illustration of shape factor (a. asphalt with surface dressing; b. hot rolled asphalt) (source from Beckenbauer and Kuijpers, 2001 [487], Figure 2; reprinted under fair use provision)..... 606

Figure 120: Contact pressure level spectra for different speed (a. stone mastic asphalt 0/8; b. surface dressing 3/5) (source from Beckenbauer and Kuijpers, 2001 [487], Figure 3; reprinted under fair use provision)..... 607

Figure 121: (a) Coefficient of determination R^2, (b) regression coefficient for the shape level c_{gAF} and (c) regression coefficient for the speed term c_{vAF} depending on third-octave canter frequency f_T. Parameter: type of tire. The dashed line in (a) is valid for the statistical model without the variable L_g (shape level) for patterned tires. (Source from Beckenbauer and Kuijpers, 2001 [487], Figure 4; reprinted under fair use provision) 608

Figure 122: 3D contact model in Enhanced SPERoN Model (source from Kuijpers and Blokland, 2003 [865], Figure 1; reprinted under fair use provision) 609

Figure 123: Illustration of envelopment procedure in HyRoNE Model (Beckenbauer et al., 2008 [332], Figure 5; reprinted with permission from Mr. Philippe Herzog on behalf of SFA, France) 611

Figure 124: Mesh used for the tire model. The circles indicate the chosen contact points. (Source from Rustighi et al., 2008 [874], Figure 2; reprinted with permission from Elsevier)..... 613

Figure 125: Root mean squared velocity of the tire elements at 80 km/h. Note that distances ±0.1 m in the radial direction correspond to the tread section of the tire and from ±0.1 to ±0.2 m to the sidewalls. (Source from Rustighi et al., 2008 [874], Figure 7; reprinted with permission from Elsevier) 614

Figure 126: The sound pressure level (SPL) calculated at the surface of the tire elements at 80 km/h (source from Rustighi et al., 2008 [874], Figure 9; reprinted with permission from Elsevier) 614

Figure 127: Sound pressure level at the 8 passenger ears at 20 (continuous line), 40 (dotted line) and 80 (dashed line) km/h (source from Rustighi et al., 2008 [874], Figure 13; reprinted with permission from Elsevier)..... 615

Figure 128: Iso-correlation curves between (a) contact force and noise level; (b) pavement texture and contact force; (c) pavement texture and noise level (source from Cesbron et al., 2009 [884], Figure 17-19; reprinted with permission from Elsevier) 616

Figure 129: Top left: tire tread pattern; top right: pavement roughness; bottom: combined tire/pavement roughness (longitudinal/lateral spatial resolution = 1 mm, source from Klein and Cesbron, 2016 [609], Figure 10; reprinted under fair use provision) 619

Figure 130: Contact pressure distribution (red curve: patterned E3A tire; black curve: slick tire) (source from Klein and Cesbron, 2016 [609], Figure 13; reprinted under fair use provision) 620

Figure 131: Constituent spectra and predicted total spectrum compared to measured spectrum for cell 1, leading probe. Blue: treadband spectrum. Red: sidewall spectrum. Green: tangential spectrum. Dotted black: predicted total spectrum. Solid black: measured spectrum. (Source from Dare, 2012 [213], Figure 5.10; reprinted with permission from Dr. Tyler Dare of Pennsylvania State University, USA) 623

Figure 132: Tyre-road model. Left: the tyre is virtually unwrapped. Right: equivalent prestressed orthotropic plate under visco-elastic foundation. (Source from Le Bot et al., 2017 [887], Figure 1; reprinted with permission from Elsevier) 627

Figure 133: Relative standard deviation of spatial energy repartition in the frequency, damping loss factor plane under a point-excitation. Left side: modal regime with few modes contributing the dynamics. Top right-hand corner (black): free field regime where rays are highly absorbed. Bottom right-hand corner (bright): diffuse field regime. The broken lines are regime boundaries determined by $N(\omega) = n(\omega)\cdot\Delta\omega$ and $m(\omega)$. (Source from Le Bot et al., 2017 [887], Figure 7; reprinted with permission from Elsevier)..... 630

Figure 134: Examples of energy fields corresponding to crosses in Figure 133. (a) Regime of modal field (point A); (b) Regime of diffuse field (point B); (c) Regime of free field (point

C). (Source from Le Bot et al., 2017 [887], Figure 8; reprinted with permission from Elsevier) 631

Figure 135: A network (in red) between a round surface and a rigid plane surface (ABCD indicates the contact patch; 1 is a longitudinal pipe while 2 and 3 are transverse pipes; b_{sq} is half the flange width for pipe 2). (Source from Wang and Duhamel, 2017 [888], Figure 2; reprinted with permission from Elsevier) 631

Figure 136: Comparisons between HPM and SPB, CadnaA, and TNM (source from Dai and Lee, 2010 [909], Figure 1; reprinted with permission from Ms. Beth Darchi on behalf of ASME) 639

Figure 137: Attaching a rubber ring on the inside surface of the center part of the tread surface (source from Iwao and Yamazaki, 1996 [307], Figure 13; reprinted under fair use provision) 648

Figure 138: Tire cross section with seal and foam absorber mounted on a rim (source from Saemann et al., 2011 [914], Figure 1; reprinted under fair use provision) 648

Figure 139: Reduction of fluid drag force and noise by using bypass structure and the bionic tread groove (source from Zhou et al., 2014 [915], Figure 4; reprinted under fair use provision) 648

Figure 140: Illustration of low noise transverse groove (L = 4×P) (source from Kakumu, 1990 [916], Figure 2; reprinted under fair use provision) 648

Figure 141: Illustration of low noise tread pattern (The sum of the groove void (A+B+C+D+E+F+G+H+l) along projection 86 is substantially equal to the sum of groove void (J +K+L+M+N+O+P+Q+R+S) along projection 88) (Source from Cusimano, 1992 [917], Figure 1A; reprinted under fair use provision) 649

Figure 142: (a) Product image of Continental ComfortContact CC6; (b) harmonic comfort chambers; (c) 0' dB-Eaters (Source from Continental AG, 2016 [918]; reprinted under fair use provision) 649

Figure 143: Finite element displacement analysis results for Kühl wheel mode shape at 210 Hz (source from Sainty et al., 2012 [296], Figure 2; reprinted with permission from ASME) 650

Figure 144: CAD model of a tire with three rubber strips extruded into the cavity (source from Sainty et al., 2012 [296], Figure 6; reprinted with permission from ASME) 650

Figure 145: CAD model of proposed elastic ring with the four fins attached (source from Sainty et al., 2012 [296], Figure 10; reprinted with permission from ASME) 651

Figure 146: Incorporation of secondary acoustic cavities to detune and damp out the main tire cavity resonance (source from Molisani, 2004 [344], Figure 4.2; reprinted under fair use provision) 651

Figure 147: Assembling separate thin, lightweight plastic resonators in the wheel well (source from Kamiyama, 2014 [920], Figure 1; reprinted under fair use provision) 652

Figure 148: CAD model fitted with Helmholtz resonator (source from Sainty et al., 2012 [296], Figure 4; reprinted with permission from ASME) 652

Figure 149: Testing tire filled with PU foam prior to the wheel rim and tire assembling (source from Sainty et al., 2012 [296], Figure 7; reprinted with permission from ASME) 653

Figure 150: TireSilencer with white rigid foam support removed from tire after 1,053 miles (source from Schmidt and Majumdar, 2011 [924], Figure 2; reprinted under fair use provision) 653

Figure 151: Pirelli Noise Cancelling System (PNCS) (source from Tire Business, 2013 [925] ; reprinted under fair use provision)..... 653

Figure 152: Installation of the trim onto the rim and tire (a. the trim layer on the rim; b. the trim layer onto the tire) (source from Mohamed and Wang, 2015 [393], Figure 7; reprinted with permission from Elsevier)..... 654

Figure 153: Criteria for the choice of tires by consumers (source from FEHRL, 2001 [28], Figure 49; reprinted under fair use provision)..... 654

Figure 154: Polar diagram illustrating the property profile of a particular tire (source from FEHRL, 2001 [28], Figure 26, kindly obtained from Dr. Saemann, Continental Tyres; reprinted under fair use provision)..... 655

Figure 155: Helmholtz type porous asphalt (left) and laying process (right) (source from Maennel et al. (2013) [932], Figure 7, Figure 8; reprinted with permission from Mr. Manuel Männel of Müller-BBM GmbH, Germany)..... 658

List of Tables

Table 1: Permissible limits on ambient noise standards in India (source from CPCB, 2000 [39]; reprinted under fair use provision) 337

Table 2: Category of TPIN measurement techniques 352

Table 3: Standards for pass-by noise (Siemens, 2014 [95]) 353

Table 4: Summary of roadside measurement techniques 363

Table 5: Various experiments using behind the tire (BTT) approach 364

Table 6: Tests using OBSP method 367

Table 7: Comparisons between sound pressure and sound intensity (Bloemhof, 1986 [156]) 369

Table 8: PI index requirements for each 1/3 octave band (source from AASHTO TP-76, 2013 [112], Table 1; reprinted with permission from Mr. Robert Cullen of AASHTO) 371

Table 9: History of OBSI development 377

Table 10: Summary of on-board measurement techniques 380

Table 11: Comparisons between LDV measurement and accelerometer measurement 382

Table 12: Tests using NAAT method 387

Table 13: Summary of lab measurement techniques 395

Table 14: Relationships between different methods 397

Table 15: Dominant frequencies for different TPIN components 401

Table 16: Typical impact frequencies (source from Sandberg and Ejsmont, 2002 [7], Table 7.2; reprinted with permission from Dr. Ulf Sandberg of VTI, Sweden) 404

Table 17: Impact-induced vibrations 405

Table 18: Review of tire torus cavity resonance (underlined items in green are reduction countermeasures) (source partly from Mohamed et al., 2013 [41]) 419

Table 19: Horn effect experiments (summarized from Sandberg and Ejsmont, 2002 [7]) 427

Table 20: Tire-Pavement Interaction Noise (TPIN) Mechanisms 431

Table 21: Various factors resulting in TPIN spectrum peak around 1000 Hz (car tires at highway speed V = 100 km/h, Sound Speed c = 340 m/s) 434

Table 22: Overview of parameters affecting TPIN (summarized from Sandberg and Ejsmont, 2002 [7]) 435

Table 23: Speed exponents for different TPIN mechanisms (modified from Kuijpers and van Blokland, 2001 [347], Figure 1) 437

Table 24: Coefficients in relationship between speed and TPIN level (source from Sandberg and Ejsmont, 2002 [7], Table 9.1; reprinted with permission from Dr. Ulf Sandberg of VTI,

Sweden)..... 438

Table 25: Influence of tire load on TPIN (summarized from Sandberg and Ejsmont, 2002 [7])... 443

Table 26: General influences of different parameters on TPIN and tire rolling resistance (modified from Ejsmont et al., 2012 [573], Table 1)..... 463

Table 27: Tread element number and length for old SRTT (modified from Ruhala, 1999 [244]) .. 465

Table 28: General influence of tread pattern on TPIN (source from Sandberg and Ejsmont, 2002 [7], Table 10.3; reprinted with permission from Dr. Ulf Sandberg of VTI, Sweden) 467

Table 29: Tread pattern design requirements (modified from Liljegren, 2008 [591], Figure 46) ... 469

Table 30: Different layouts of tire segments and principles of randomization (source from Sandberg and Ejsmont, 2002 [7], Table 10.2; reprinted with permission from Dr. Ulf Sandberg of VTI, Sweden)..... 471

Table 31: Progression of pitch sequencing techniques in historical perspective (Williams, 1995 [592]) 472

Table 32: Illustrations of different types of pavements (modified from NZ Transport Agency, 2014 [54], Figure 1.6 – Figure 1.19; reprinted with permission from Ms. Helen Lane on behalf of NZ Transport Agency) 476

Table 33: Texture parameters and influence on tire/pavement characteristics (red ↑ indicates increase, green ↓ indicates decrease and blue • indicates complex) (modified from Dimitri, 2012 [170]; Wayson, 1998 [612]) 480

Table 34: Examples of different pavement textures (modified from Thrasher et al., 1976 [1]) 481

Table 35: Temperature coefficients of the relationship between pass-by noise level at 90 km/h and air, pavement or tire temperatures, per road pavement category (source from Anfosso-LédéE and Pichaud, 2007 [715], Table 5; reprinted with permission from Elsevier)504

Table 36: Summary of driver influence parameters affecting TPIN..... 508

Table 37: Summary of tire-related parameters affecting TPIN..... 508

Table 38: Summary of tread pattern parameters affecting TPIN 509

Table 39: Summary of pavement-related parameters affecting TPIN 509

Table 40: Summary of environmental parameters affecting TPIN 510

Table 41: Introduction of three categories of TPIN models..... 512

Table 42: Input tire parameters (slick 205/60R15) for Larsson and Kropp model (data in brackets refer to loss factors for the corresponding parameters) (Modified from Andersson and Larsson, 2005 [738], Table 1; reprinted with permission from Ms. Brigitte Badelt of S. Hirzel Verlag on behalf of the European Acoustics Association) 513

Table 43: Nomenclature for Unified Model..... 515

Table 44: Summary of conventional physics models on TPIN..... 568

Table 45: Summary of finite element and boundary element models on TPIN..... 569

Table 46: Summary of computational fluid dynamics models on TPIN..... 570

Table 47: Nomenclature of early models for traffic noise prediction (Quartieri et al., 2009 [810]) 571

Table 48: Early models for traffic noise prediction (Quartieri et al., 2009 [810]) 572

Table 49: Nomenclature of RLS 90 (RLS, 1990 [821]) 573

Table 50: Nomenclature of CNR (Cocchi et al., 1991 [823])..... 574

Table 51: REMEL conditions in TNM (Rochat et al., 2012 [828])..... 575

Table 52: Specifications of pavements measured in Fujikawa et al. Model (source from Fujikawa et al., 2009 [218], Table 2; reprinted under fair use provision) 579

Table 53: Coefficients for Reyes and Harvey Model (source from Reyes and Harvey, 2011 [639], Table 1; reprinted under fair use provision)..... 581

Table 54: Investigated parameters in Syamkumar Model (Syamkumar et al., 2013 [6]) 583

Table 55: Statistical equation coefficients and R^2 for passenger cars in Mode-wise Model (Syamkumar et al., 2013 [6]) 583

Table 56: Initial parameters investigated in Ongel Model (Ongel et al., 2008 [840])..... 585

Table 57: Statistics of parameters in Ongel Model (Ongel et al., 2008 [840])..... 586

Table 58: Correlation matrix for nine input parameters and OBSI output in Ongel Model (source from Ongel et al., 2008 [840], Table 3; reprinted with permission from American Society of Civil Engineers) 586

Table 59: Effects of Pavement Parameters on Different 1/3 Octave Band Frequencies (Modified from Ongel and Harvey, 2010 [662], Table 3)..... 587

Table 60: Input pavement parameter combination of surface texture and sound absorption (modified from Li et al., 2015 [613], Table 3)..... 589

Table 61: Coefficient of determination for the three models (Li et al., 2015 [613])..... 589

Table 62: Metrics for two-stage ANN Models for pass-by noise (Fry and Jennings, 2003 [847]) . 591

Table 63: Exponents for Khazanovich Model (Khazanovich and Izevbekhai, 2008 [5])..... 592

Table 64: Input and output parameters of ANN (Che et al., 2012 [586])..... 595

Table 65: Coefficients for Yu and Lu (Bayesian) Model (Yu and Lu, 2013 [859])..... 597

Table 66: Summary of traditional regression models on TPIN 599

Table 67: Summary of principal component analysis models on TPIN 600

Table 68: Summary of fuzzy curve fitting models on TPIN..... 600

Table 69: Comparison between SPERoN and HyRoNE Models (Beckenbauer et al., 2008 [332]; Klein et al., 2008 [870])..... 612

Table 70: Parameters of the linear regression for speed effect on surface DAC 0/10 (source from Dubois et al., 2013 [61], Table 1; reprinted with permission from Elsevier) 617

Table 71: Parameters for the correlation between noise level and contact force for slick tire (error ε = 1.50%) (source from Dubois et al., 2013 [61], Table 2; reprinted with permission from Elsevier) 618

Table 72: Parameters for the correlation between noise level and contact force for patterned tire (error $\varepsilon = 1.34\%$) (source from Dubois et al., 2013 [61], Table 3; reprinted with permission from Elsevier) 618

Table 73: Recalibrated CRTN Models Proposed by Local Researchers in Hong Kong (Leung and Mak, 2008 [891]) 634

Table 74: Traffic conditions in NMPB 2008 [903] 634

Table 75: Correction for pavement type in NMPB 2008 [903] 635

Table 76: Values for Spectral Correction of each Octave Band [906] 635

Table 77: Nomenclature for Highway Prediction Model (HPM) (Dai and Lee, 2010 [909]) 637

Table 78: Summary of tire-pavement interface models on TPIN 642

Table 79: Summary of mechanism separation models on TPIN 643

Table 80: Summary of noise propagation models on TPIN 643

Table 81: Design concepts for quiet tire (green indicates put into mass production) 646

Table 82: Target conflicts in tire development (red indicates bad; green indicates good; yellow indicates ambiguous) (modified from FEHRL, 2001 [28]) 655

Table 83: Modifications to lower tire noise and the drawbacks (Saemann et al., 2012 [170]) 656

Table 84: General suggestions on noise reduction in terms of pavement characteristics (Rasmussen, 2010 [831]) 657

Table 85: Quiet pavement technologies (McGhee, 2012 [606]; Mogrovejo et al., 2014 [673]) 657

1 Introduction

The term Tire-Pavement Interaction Noise was first found as early as in 1976 (Thrasher et al., 1976 [1] and Miller and Thrasher, 1976 [2]), also later in 1986 (Pottinger et al., 1986 [3]) and 1998 (Donavan et al., 1998 [4]). The acronym TPIN was first found in 2008 (Khazanovich and Izevbekhai, 2008 [5]), later also in 2013 (Syamkumar et al., 2013 [6]). Tire-Pavement Interaction Noise (TPIN) is also known as tire road interaction noise, tire-pavement noise, tire road noise, or tire noise. Tire-pavement interaction noise is defined as the noise emitted from a rolling tire as a result of the interaction between the tire and road surface (Sandberg and Ejsmont, 2002 [7]).

Modern TPIN research started around mid-1970's as engine became less noisy and aerodynamic design of vehicle body were optimized. Sandberg and Ejsmont (1995) [8] have collected a computerized bibliography termed "TRN BIBLIOGRAPHY" totaling 1280 documents as of August 1994. However, most of these references were from special conference proceedings, industrial/government reports rather than archival journals. A large number of literatures have advanced the modeling of tire-pavement interaction noise, as displayed in Figure 1. However, up to date TPIN is still in mystery and difficult to describe or predict accurately, and the findings still seem fragmented probably due to the many complex generation mechanisms. Although a tire seems to be a simple structure at first glance, the combination of its geometrical properties and multi-layer composite structure leads to highly complex vibrational behavior (Sabiniarz and Kropp, 2010 [9]).

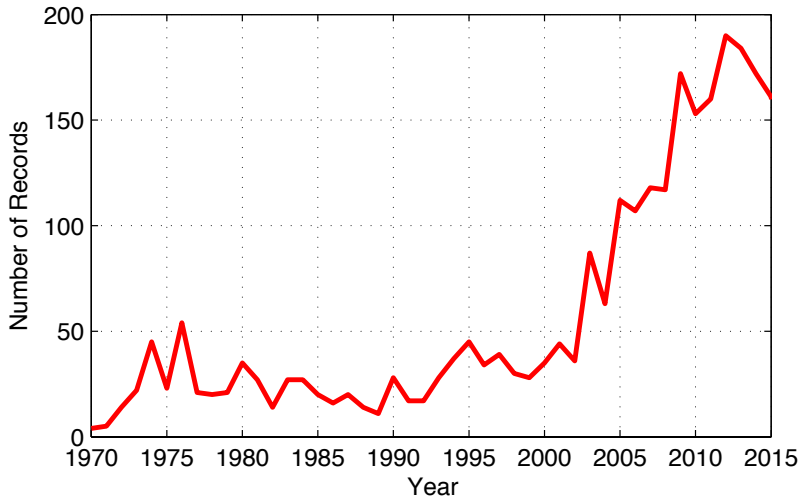

Figure 1: Literature records count (generated via Engineering Village on Aug 12, 2016, search query for "tire" & "noise" in subject/title/abstract from databases of Compendex, Inspec & NTIS)

1.1 Motivation

The motivation for controlling tire-pavement interaction noise is multiple and different across different countries. One is to pass the legal approval for exterior noise level; one is to reduce the annoyance level in car interior space and increase passenger comfort (Harrison, 2004 [10]); one is to boycott foreign tire imports (Chen, 2014 [11]).

1.1.1 Pollution

"Environmental pollution" might suggest, to many people, air pollution, water pollution, or similar concepts. But another pollution, which is not quite visible but encountered by more and more cities, is noise pollution. Noise barriers that are up to 20 feet tall have to be built to shield the neighborhoods from road noise for hundreds of yards along busy highways (Wayson, 2014 [12]). According to many opinion polls traffic noise is considered to be the number one noise nuisance affecting millions of people. Among the different sources of traffic noise (road vehicles, railways and aeroplanes) the sound generated by cars is most important because there are millions of them and because they are almost ubiquitous (Heckl (1986) [13]).

European Commission Green Paper (1996) [14] pointed out it is estimated that 110 million people (22 % of the EU population) are affected by sound pressure level greater than 65 dBA,

and more than 225 million (45 % of the EU population) are exposed to noise levels above 55 dBA. It also indicated that road traffic noise is the most dominant source (over 90%) of environmental noise in Europe, followed by rail traffic noise (Remington et al., 1983 [15]), aircraft noise and industrial noise. As such, traffic noise pollution becomes more and more concerned, as illustrated in Figure 2 (Murphy and King, 2011 [16]).

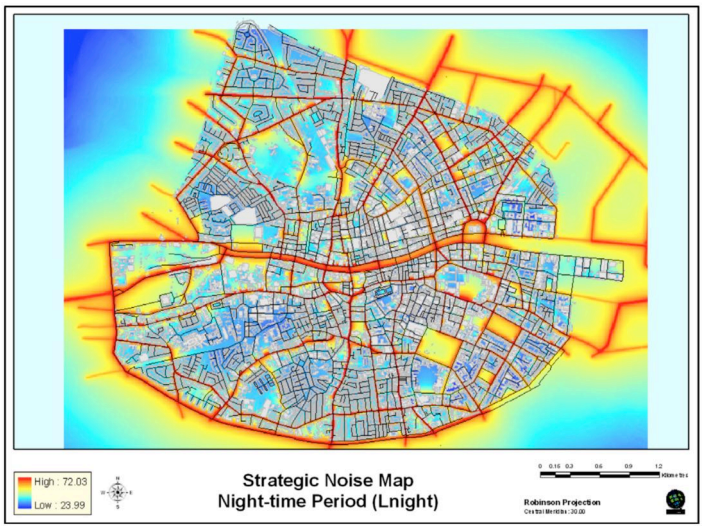

Figure 2: Strategic noise map for the night-time period (L_{night}) in Dublin, Ireland (source from Murphy and King, 2011 [16], Figure 2; reprinted with permission from Elsevier)

According to World Health Organization (WHO), noise is the second largest environmental cause of health issues, just after air quality (particulate matter). Sleepers exposed to night noise levels above long-term average 40 dB can suffer health effects like annoyance, sleep disturbance and awakenings. Above 55 dB, cardiovascular disease, cognitive impairment and tinnitus might be triggered. It was estimated that each year noise pollution leads to about 910 thousand additional prevalent cases of hypertension, 43 thousand hospital admissions, and at least 10 thousand premature deaths related to coronary heart disease and stroke (Kim, 2007 [17]). It was also indicated that 1-1.6 million healthy life years are lost every year from traffic noise in the EU cities.

In addition, truck drivers for long distance travelling exposed to continuous vehicle noise of high levels are easier to have health issues (Pan and Boulet, 2014 [18]). Loud traffic noise also affects animal behavior (Goodwin and Shriver, 2011 [19]; Lengagne, 2008 [20]; Bee and

Swanson, 2007 [21]).

1.1.2 Policy

As traffic noise becomes more of a concern, the global regulations tend to have more and more tightening limits on the noise levels. After the INTER-NOISE 1992 conference in Toronto, the International Institute of Noise Control Engineering (I-INCE) started a global study on the effect of vehicle noise regulations on road traffic noise. The work was conducted by the Working Party on Noise Emissions of Road Vehicles (WP-NERV) including 13 members from 10 countries, of which Ulf Sandberg from Swedish National Road and Transport Research Institute (VTI) was the convener. The final report (2001) [22] presented the changes of vehicle noise emission limits over 30 years (1970-2001), as shown in Figure 3. Recommendations for future noise emission regulations were also given in the report since some regulations had limited effect (Sandberg, 2001 [22]).

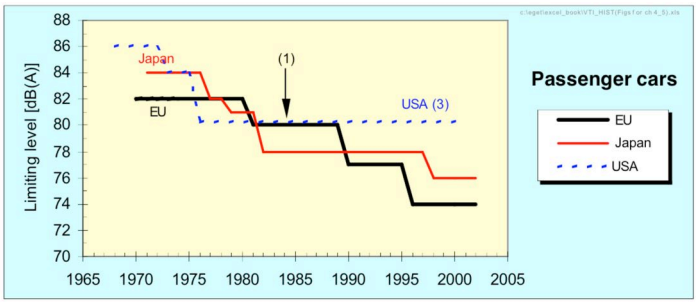

Figure 3: Regulation limits for noise emission of passenger cars in European Union (EU), Japan and USA (source from Sandberg, 2001 [22], Figure 1; reprinted under fair use provision)

In Figure 3, it can be seen that Europe has the most stringent regulations on tire noise. The first relevant policy is Directive 70/157/EEC in 1970 (European Economic Community, 1970 [23]). The main current regulation on environmental noise is Directive 2002/49/EC (2002) [24]. For road traffic noise, the current regulations are Regulation (EU) 540/2014 (2014) [25] for motor vehicles and Regulation (EU) 168/2013 (2013) [26] for motor cycles. For tire noise, Directive 2001/43/EC (2001) [27] indicates the noise emission limits for new tires, as shown in Figure 4 (FEHRL, 2001 [28]). In 2009, Regulation (EC) 661/2009 [29] and Regulation (EC) 1222/2009 [30] requires revised noise limits (more stringent) for tire approval, as shown in Figure 5, and mandatory tire labeling beginning from November 2012 as shown in Figure 6.

The tire approval process is in UN/ECE R117/2011 (2011) [31] and UN/ECE R51/2011 (2011) [32] requiring measurement of rolling resistance, wet grip and pass-by noise. In the future, for M1a vehicles (99% of the current car population) is planned to be limited to 72 dBA in 2016 then to 68 dBA in 2024, affecting roughly 85% of the current car population (ACEA, 2012 [33]). The Dutch national Traffic and Transportation indicated the goal regarding noise nuisance caused by road traffic: decreasing the number of houses exposed to a noise level of >70 dBA by 100%, the number > 65 dBA by 90% and the number > 60 dBA by 50% in 2030 (Nijland et al., 2003 [34]). China also introduces tire labeling system for voluntary tire certification including tire noise, as shown in Figure 7 (RenMinWang, 2016 [35]).

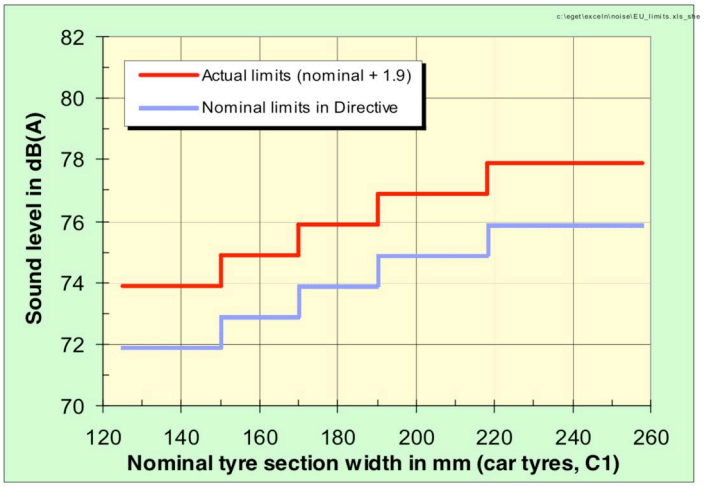

Figure 4: Noise emission limits according to Directive 2001/43/EC (source from FEHRL, 2001 [28], Appendices Figure 3; reprinted under fair use provision)

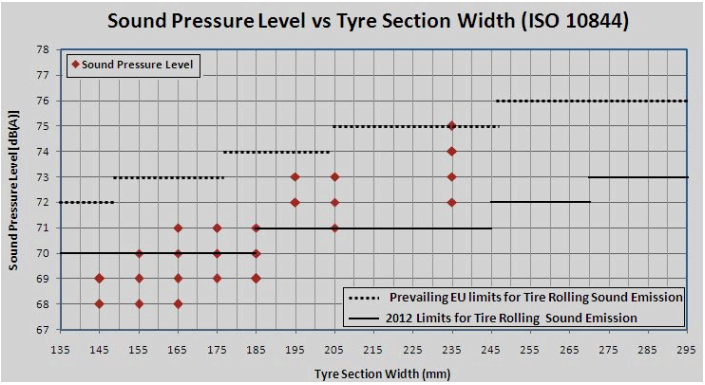

Figure 5: Noise emission limits according to Regulation (EC) 661/2009 (modified from EC, 2009 [29] ; reprinted under fair use provision)

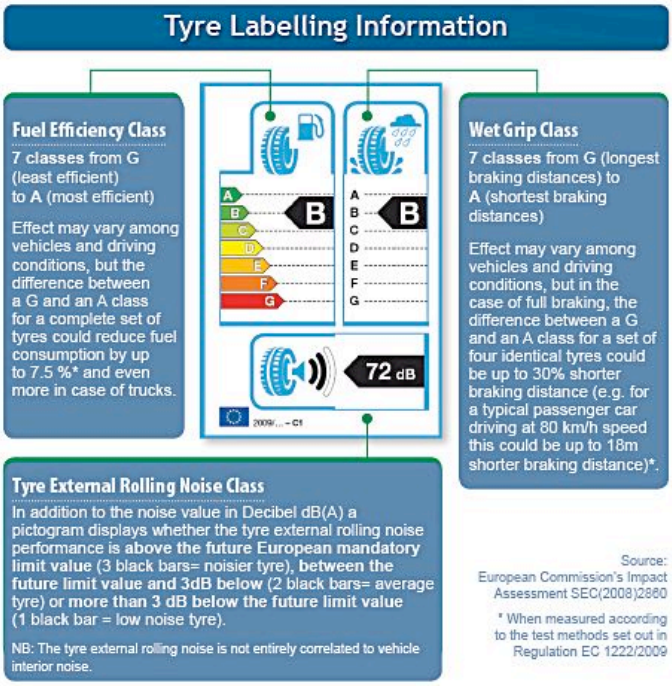

Figure 6: Tire labeling information (source from ETRMA, 2011 [36]; reprinted with permission from ETRMA)

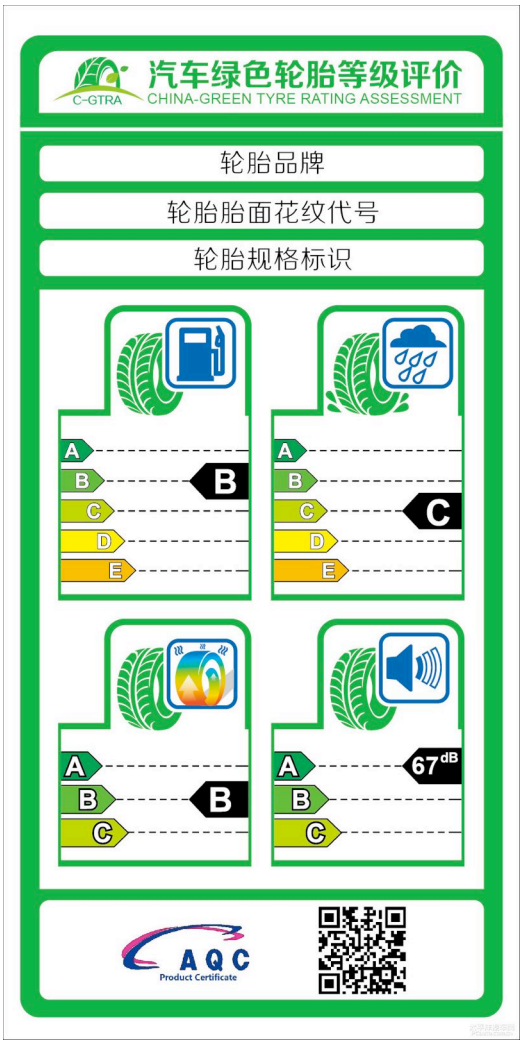

Figure 7: China Green Tyre Rating Assessment (C-GTRA) (source from RenMinWang, 2016 [35] ; reprinted under fair use provision)

In the U.S., National Highway Traffic Safety Administration (NHTSA) requires tire labeling according to Uniform Tire Quality Grading standard (UTQG), including wet braking traction performance, predicted tread wear life, and high temperature endurance without tire noise requirements. The current federal regulation for traffic noise is 23 CFR 772 (2010) [37].

In Canada, the regulation regarding sound levels related to transportation is "Noise Assessment Criteria in Land Use Planning, LU-131" published by Ontario Ministry of the Environment (MOE) in October of 1997 [38].

In India, the noise pollution is also regulated by CPCB (2000) [39] and framed under the

Environment Act 1986 [6], as shown in Table 1.

Table 1: Permissible limits on ambient noise standards in India (source from CPCB, 2000 [39]; reprinted under fair use provision)

Zone Code	Category of Zone	Day (6 am to 10 pm)	Night (10 pm to 6 am)
A	Industrial	75 dB	70 dB
B	Commercial	65 dB	55 dB
C	Residential	55 dB	45 dB
D	Silent	50 dB	40 dB

Most policies are focused on exterior vehicle noise (mostly by coast by method at 7.5 m distance from the vehicle [40]), but for interior noise, it is only regulated by market requirement or consumer oriented (Mohamed, 2013 [41]).

1.2 Noise Abatement

Traffic noise is dependent on traffic volume, traffic speed and the percentage of trucks in the traffic mix [42] (on high-speed road, the dominant noise source is heavy truck tires [43]). In US, federal Code 23, Section 772 (2010) [37] requires transportation projects that receive federal funding to meet noise impacts limits. The U.S. Department of Transportation, Federal Highway Administration (2010) [44] presented five approved methods to mitigate traffic noise, including noise barriers, vegetation screens, traffic management, building insulation and buffer zones, most of which are passive noise control regarding sound transmission path. Usually, noise barrier is the only viable option to mitigate the traffic noise.

The reason why quiet pavement is not included in the approved methods is that pavements can wear out and grow louder with time. Donovan et al. (2013) [45] presented a methodology for evaluating feasibility, reasonableness, effectiveness, acoustic longevity, and economic features of pavement strategies and barriers for noise mitigation. Life cycle cost analysis (LCCA) is utilized to quantify their economic features. It was reported that noise barriers have a higher initial cost ($1.3-3 million per mile [46]) than quieter pavements but have lower ongoing costs due to minimal maintenance requirements. In addition, the noise reduction effect of noise barriers does not diminish with time.

However, as the endurance of pavement acoustic performance improves, more and more transportation agencies are interested in quiet pavement, especially in Europe. Moreover,

noise barriers have some disadvantages: locations such as hillsides and intersections are not suitable for building noise barriers; most noise barriers block the view, which does not look beautiful; barrier on one side will increase reflection to the other side (Kohler, 2010 [47]). Controlling tire-pavement interaction noise at its source, i.e., quiet pavement and quiet tire, might be a more economical and effective approach.

1.3 Vehicle Noise

Noise, vibration, and harshness (NVH), a.k.a., noise and vibration (N&V) represents quality factor in automotive engineering (Mohamed, 2013 [41]). It is generally accepted that there are five major sources of noise for a running vehicle: engine (power train), intake system, exhaust system, aerodynamic turbulence (wind) and tire-pavement interaction (Braun et al., 2013 [48]), as shown in Figure 8 (Bosch, 2004 [49]). The power train noise is generated primarily due to combustion in the engine, gas flow, and mechanical movement of the transmission parts. The aerodynamic noise depends on vehicle geometry and speed of the vehicle, generated due to aerodynamic friction and turbulence caused by the vehicles moving at higher speeds. The combination of engine (power train), intake system, exhaust system is also called propulsion system of which the performance is largely dependent on the engine speed; they are coherent noise sources and interacting with each other but incoherent with tire noise (Fry et al., 1999 [50]). It is reasonable to infer that for the same vehicle speed, lower gear generates more noise since the engine speed is higher, as shown in Figure 9 (Biermann, 2004 [51]). It can be seen that noise level is relatively independent of torque except when rpm is below 1000. The intake orifice noise versus engine speed is displayed in Figure 10 (Zeller, 2009 [52]). The exhaust noise versus engine speed is displayed in Figure 11 and its typical spectrum is shown in Figure 12 (Alfredson and Davies, 1970 [53]). For vehicle noise from trucks, the supplementary braking noise (pneumatic cylinders) and “body slap” are often important (NZ Transport Agency, 2014 [54]).

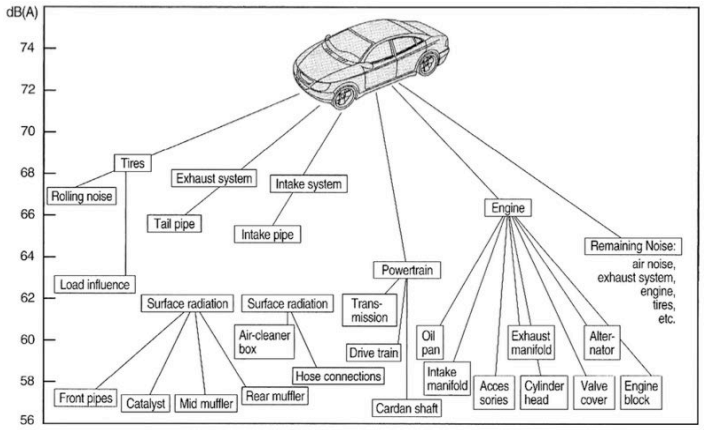

Figure 8: Noise source ranking for a vehicle during the pass-by noise test (source from Braun et al., 2013 [48], Figure 21; original from Bosch, 2004 [49]; reprinted with permission from Elsevier)

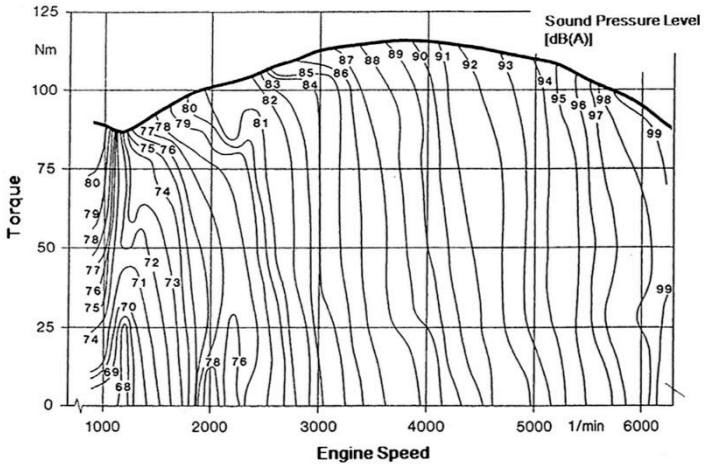

Figure 9: Engine noise map of sound pressure level versus torque and rotational speed (source from Braun et al., 2013 [48], Figure 11; original from Biermann, 2004 [51]; reprinted with permission from Elsevier)

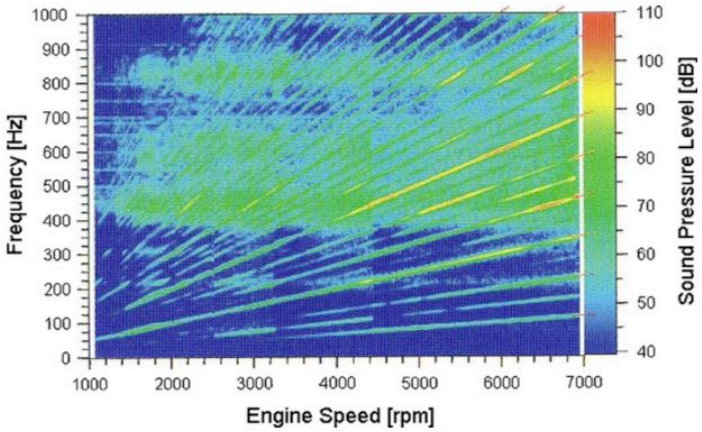

Figure 10: Sound pressure level of intake orifice noise versus engine speed and frequency (source from Braun et al., 2013 [48], Figure 14; original from Zeller, 2009 [52]; reprinted with permission from Elsevier)

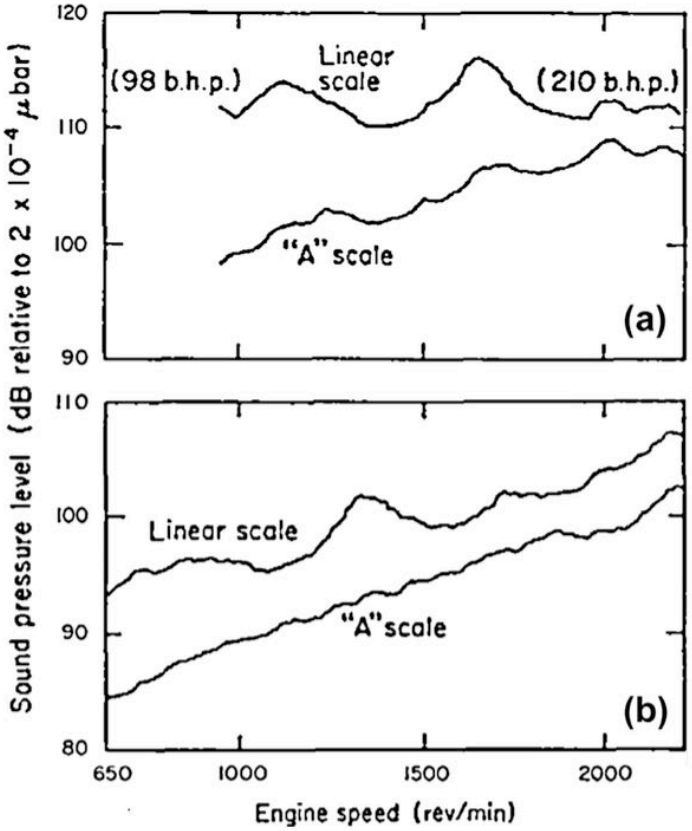

Figure 11: Sound pressure level of exhaust noise versus engine speed (source from Braun et al., 2013 [48], Figure 16; original from Alfredson and Davies, 1970 [53]; reprinted with permission from Elsevier)

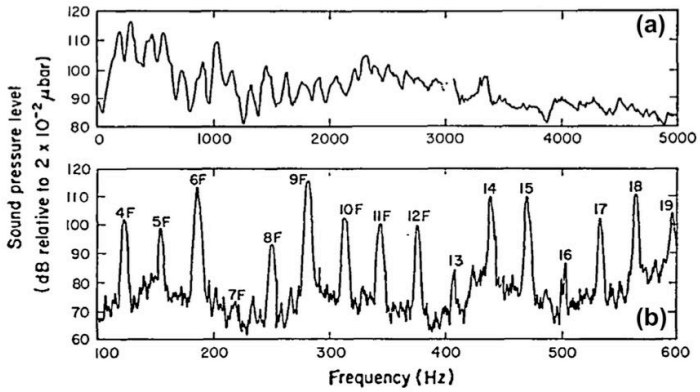

Figure 12: Typical frequency spectrum of exhaust noise measured at 1880 rpm and 0.9 m from the outlet: (a) 0–5000 Hz; (b) 100–600 Hz (source from Braun et al., 2013 [48], Figure 17; original from Alfredson and Davies, 1970 [53]; reprinted with permission from Elsevier)

These noise sources contribute differently for different speed, as illustrated in Figure 13, including propulsion noise, tire-pavement interaction noise and aerodynamic noise. Sandberg (2001) [55] indicated that tire-pavement interaction noise dominates for passenger vehicles above 40 km/h and 70 km/h for trucks. Engine noise is dominant at low speed in low frequencies (Yang et al., 2011 [56]) shown in Figure 14 (Bravo et al., 2012 [57]), while aerodynamic noise is important only at very high speed (15% at 150 km/h [58]) and only at low frequencies (50-400 Hz [59]). The intake and exhaust noise also centers around low frequencies, as shown in Figure 15 (Freeman and Cerrato, 2011 [60]). It was reported that air turbulence noise was still more than 10 dB lower than TPIN even at speed of 90 km/h for frequencies between 315 Hz and 5 kHz, and engine and exhaust noise were negligible (Dubois et al, 2013 [61]).

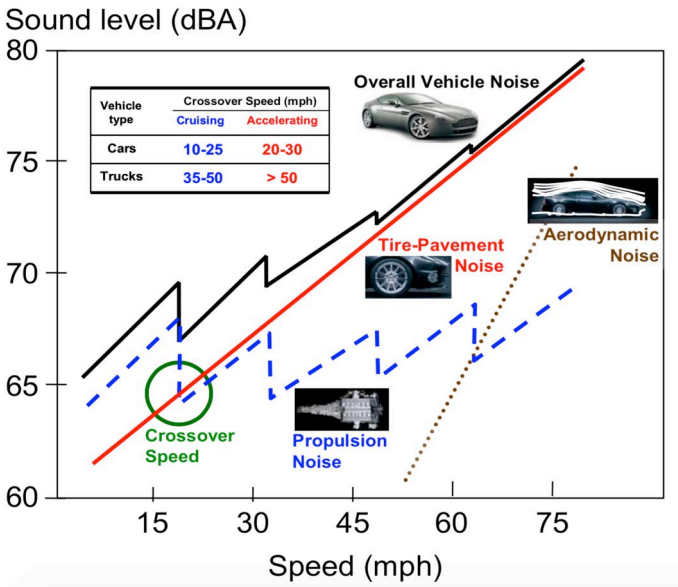

Figure 13: Vehicle noise components versus speed (source from Rasmussen et al., 2007 [62], Figure 7; reprinted with permission from Dr. Robert Otto Rasmussen of The Transtec Group, Inc., USA)

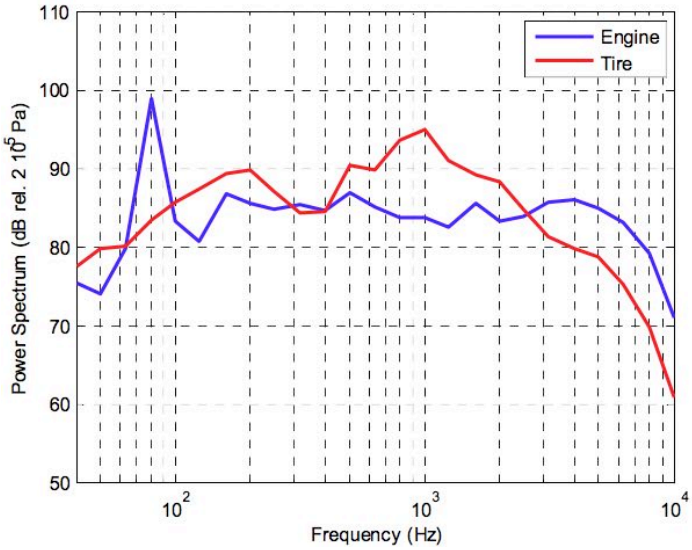

Figure 14: Power spectrum of the microphone signals situated close to the engine (blue) and close to the tire (red) for a pass-by velocity of 70 km/h (source from Bravo et al., 2012 [57], Figure 3; reprinted with permission from ASME)

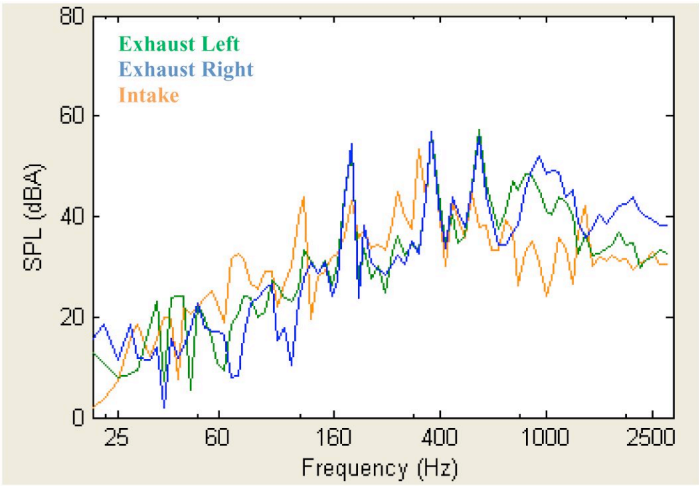

Figure 15: Noise emissions from exhaust and intake system (source from Freeman and Cerrato, 2011 [60], Figure 4; reprinted under fair use provision)

That is to say, at normal highway speed, tire-pavement interaction noise is the most important noise contributor (up to 80-90% at speed of over 70-80 km/h [63]). It seems not to be the common established thought, which is engine is the dominant noise source. It was true before 1970's, however, as engine and exhaust became less noisy and aerodynamic design of vehicle body were optimized (Dechipre et al., 2010 [64]), the tire-pavement interaction noise became more and more dominant, as shown in Figure 16 (Sandberg, 2001 [22]). The trend of electric motor replacing combustion engine is also playing a great role in this change now and in the future (Gasparoni et al., 2014 [65]). Sandberg (2001) [55] further claimed that usually tire noise dominates during almost all types of driving for cars and down to about 40 km/h for trucks (vehicles meeting EU requirements), as shown in Figure 17 (Bernhard and Wayson, 2005 [66]).

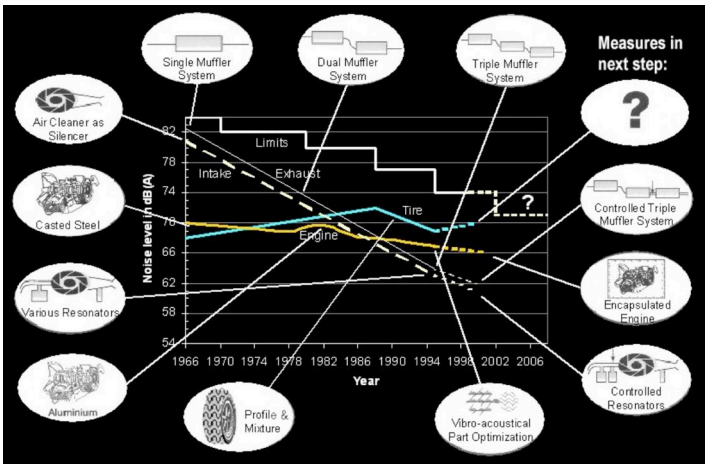

Figure 16: The most important reduction measures employed in a common car in order to satisfy the various steps in tightened noise emission limits in Germany and the EU. Note the curves that indicate how the limits and the sources engine, intake, exhaust and tire have developed over time. (Source from Sandberg, 2001 [22], Figure 3; reprinted under fair use provision)

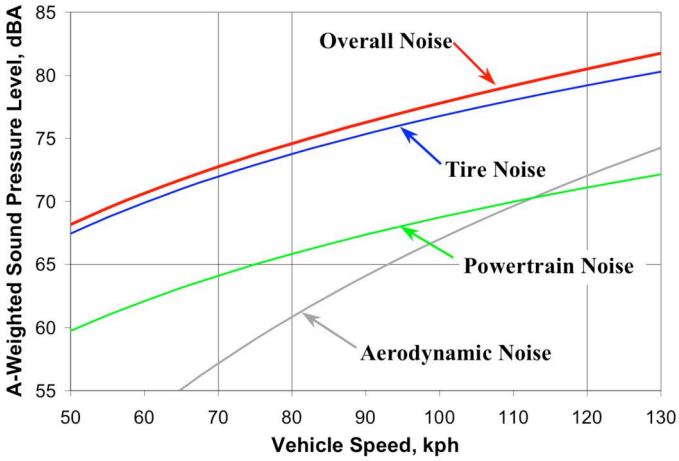

Figure 17: Contributions of the various sub-sources of highway traffic noise (source from Bernhard and Wayson, 2005 [66], Figure 1.1; reprinted with permission from Ms. Amy Miller of Asphalt Pavement Alliance)

Schuhmacher (2015) [67] applied the blind source separation (BSS) technique to the indoor vehicle pass-by noise to separate the contributions from different components of the vehicle using 17 microphones. The results are below in Figure 18.

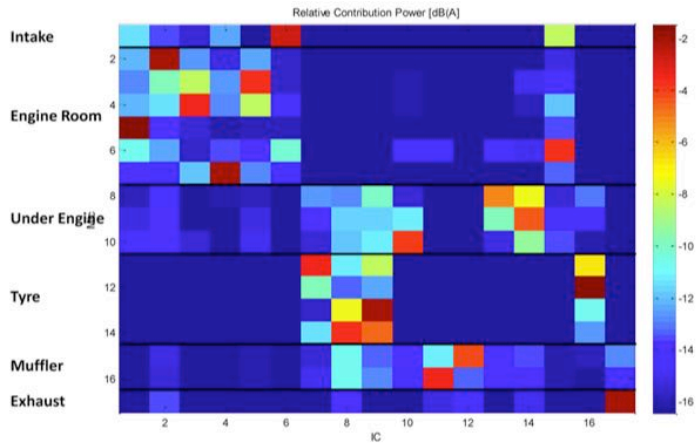

Figure 18: Contribution matrix indicating the relative power contribution from each independent component (column) to each reference microphone (row) (source from Schuhmacher, 2015 [67], Figure 11; reprinted under fair use provision)

1.4 Noise Categories

The three basic elements of noise are source, transmission path and receiver. Based on the noise generation mechanism (source) and the conveying medium (path), tire noise can be classified as structure-borne noise and airborne noise. Based on the position of the receiver, tire noise can be categorized as interior noise (inside the vehicle) and exterior noise (outside the vehicle). As such, there are basically four types of noise combining the two sets of categories, as illustrated in Figure 19 (He et al., 2011 [68]). When it comes to tire-pavement interaction noise, it usually refers to exterior noise, including both structure-borne and airborne.

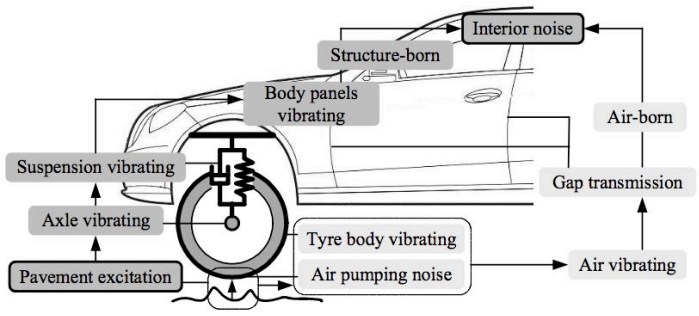

Figure 19 Vehicle interior noise transmission path (source from He et al., 2011 [68], Figure 2; reprinted with permission from Trans Tech Publications Ltd)

Structure-borne noise is generated from a vibrating source, such as tread impact. The acoustic energy created by these vibrations is transmitted into and through solid structure, such as rim, axle, suspension and vehicle body. Air-borne noise is generated directly due to air displacement such as air pumping. It should be noted that the acoustic energy of the structure-borne noise is finally released as airborne noise at the interface between the structure and air and thus can be heard. Airborne noise may also change into structure-borne, and usually back to airborne again, such as air pumping noise transmitted into interior noise through vibrations of windows. Structure-borne noise can be attenuated by vibration isolators, while airborne noise is reduced by absorption materials or through the use of sound barrier. Generally, in acoustics the difference between airborne and structure-borne noise is in the medium of transmission, but in terms of tire noise, the difference is focused on the noise generation mechanism.

Vehicle interior noise is a completely different topic than exterior noise (mainly TPIN). The spectral content of interior noise is focused around low frequencies, as shown in Figure 20 (Chang et al., 2010 [69]). Jen and Lu (2007) [70] reported that the major road excitation input was below 50 Hz and the interior noise resonances caused by modes of tires and suspensions were mainly below 100 Hz.

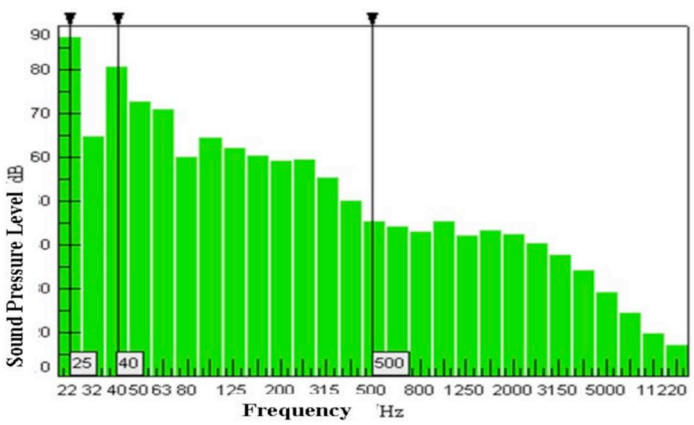

Figure 20: Interior noise spectrum at speed 80 km/h (source from Chang et al., 2010 [69], Figure 4; reprinted with permission from IEEE)

The three primary sources are engine, tire, and wind (Lim et al., 2014 [71]). The secondary sources might be mechanical devices such as ventilation fans (Aissaoui, 2015 [72]) and power

windows (Johnsson and Nykänen, 2013 [73]). Chang et al. (2010) [69] indicated that tire becomes the dominant noise source for interior noise when speed is over 80 km/h, and structure-borne contributes mainly at low frequencies (below 500 Hz) while airborne contributes at high frequencies (500-2000 Hz) (Lopez et al., 2007 [74]). Kitahara et al. (2011) [75] reported the same results, as shown in Figure 21. Since the interior noise is mainly structure-borne noise, transfer path analysis (Tsuji et al., 2015 [76]; Zhao, 2008 [77]) and multiple coherence filtering (MCF) is often utilized (Chang et al., 2010 [69]). Saguchi et al. (2007) [78] investigated the noise and vibration transmissibility for the forces and moments at the spindle, as shown in Figure 22 [78]. Vertical force F_z affects up to 500Hz, overturning moment M_x and aligning moment M_y have influence at around 200Hz, and lateral force F_y is effective for 600Hz. Kido and Ueyama (2005) [79] speculated that it is due to suspension (Geluk et al., 2011 [80]) and wheel resonance. The comparison between the spectra of exterior noise and interior noise is displayed in Figure 23.

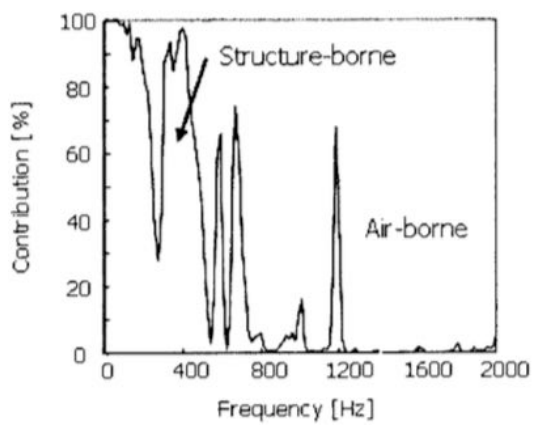

Figure 21: Contribution of tire structure-borne and airborne noise for interior noise (source from Kitahara, 2011 [75], Figure 2; reprinted under fair use provision)

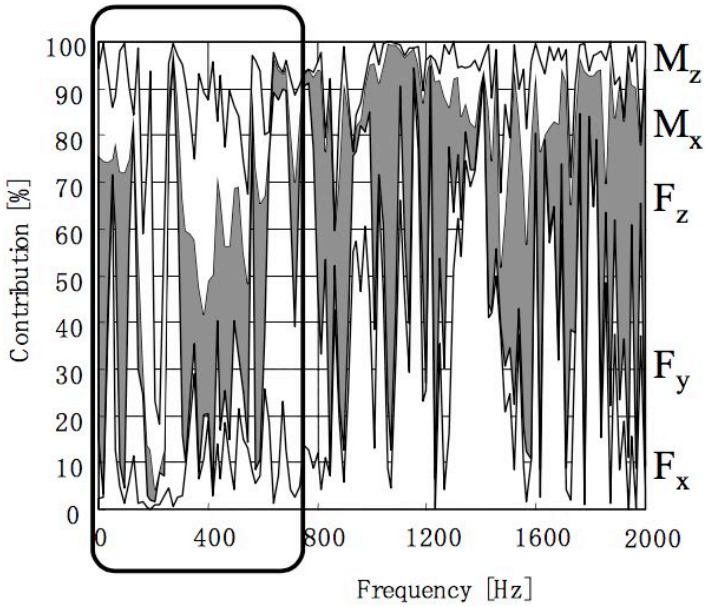

Figure 22: Structure-borne interior noise due to spindle force and moment variations (source from Saguchi et al., 2007 [78], Figure 13; reprinted under fair use provision)

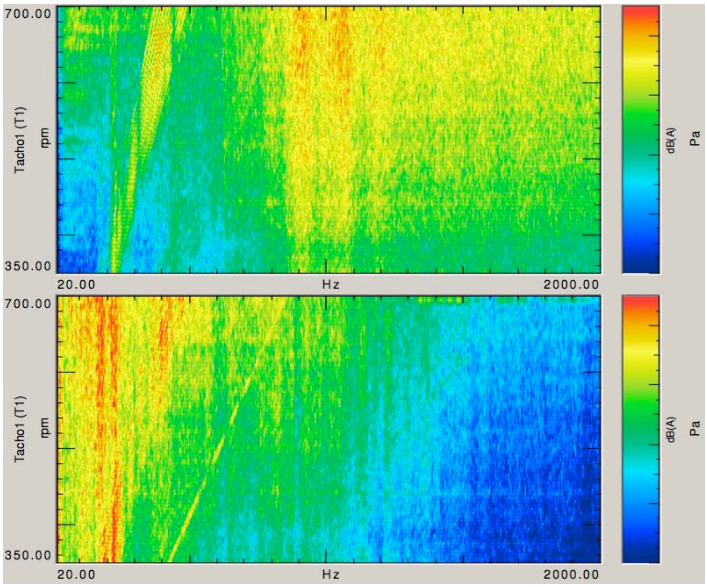

Figure 23: Coast down measurement of exterior noise at the leading CPX (above) and interior noise at right-ear passenger seat (below) measured simultaneously (source from Bekke et al., 2010 [81], Figure 5; reprinted under fair use provision)

Sotteck and Philippen (2010) [82] investigated the separation of airborne and structure-borne tire road interior noise using Operational Path Analysis (OPA). The same authors (2012) [83]

presented an approach combining Operational Transfer Path Analysis (OTPA) and Cross-Talk Cancellation (CTC) to study the interior noise from tire under dynamic driving conditions, such as acceleration and deceleration when the engine noise is of more importance.

Pietrzyk (2001) [84] reported that the structural-borne noise from tire resonances below 400 Hz was believed to be transmitted through spindle and solid parts of the vehicle, and thus the interior noise came from the excited panels and surfaces of the cabin. Molisani et al. (2003) [85] identified that one such tire resonance is due to the tire acoustic cavity (resonance of the air column inside the tire cavity).

He et al. (2011) [68] found that interior noise is greatly influenced by tire tread impact. As such, the dominant frequencies have a strong relation with vehicle speed, which is not the case for exterior noise. It is best shown in electric vehicle, since the rpm of electric motor is also proportional to speed, as shown in Figure 24 (Fischer et al. 2014 [86]).

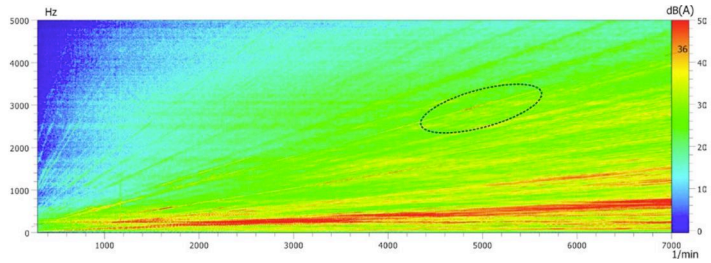

Figure 24: Interior noise spectrum versus electric motor rpm (80% accelerator pedal position measured on roller test bench) (source from Fischer et al. 2014 [86], Figure 6; reprinted with permission from Mr. David Landes of Karlsruhe Institute of Technology, Germany)

The structural-acoustic finite element method is often used for modeling vehicle interior noise (Sung and Nefske, 2010 [87]), but it is only valid at low frequencies. Sung and Nefske (2009) [88] then presented a new statistical regression-based energy method for early vehicle design, which is suitable for high frequencies where Statistical Energy Analysis (SEA) is often utilized in acoustics (Gur et al., 2015 [89]). Langhe et al. (2011) [90] proposed a hybrid modeling process where Finite Element Method (FEM) with Auto Extruding Perfectly Matched Layer (AML) technologies is used for the low to mid frequency range while Fast Multipole Boundary Element Method (FMBEM) for higher frequency range, maintaining both modeling accuracy and computation speed requirements.

For interior noise, sound balance or sound quality (shown in Figure 25 [91]) is more of a concern than just making the vehicle quieter [71]. Due to the complexity of human hearing perception, two different noises with the same A-weighted level are not necessarily equally disturbing, which can be partly explained by psychoacoustics, including loudness, loudness level, sharpness, fluctuation strength, roughness and so on (Peng et al., 2010 [92]). The reduction of tones or addition of harmonics sometimes makes the interior noise more pleasant without changing the overall sound levels. The noise frequency range that mostly affects interior comfort is 50 to 200 Hz (Labor and Priebsch, 2007 [93]).

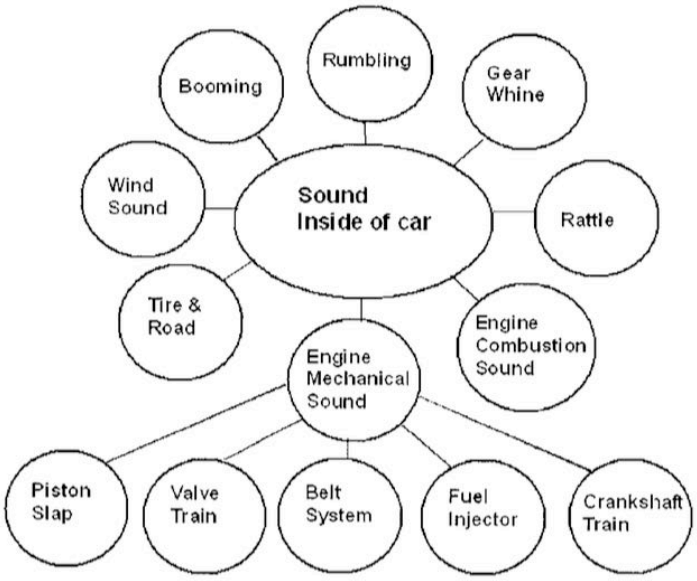

Figure 25: Sound qualities in the compartment of a passenger car (source from Lee et al., 2005 [91], Figure 1; reprinted with permission from Mr. Craig Myles on behalf of SAGE Ltd. Permissions Team)

1.5 Structure of Work

In Chapter 1, an introduction to the topic of tire-pavement interaction noise (TPIN) is given.

In Chapter 2, the measurement techniques of TPIN were reviewed and divided into three categories base on the test environment: roadside, on-board and lab. The relationship between different measurement techniques is also discussed at the end.

In Chapter 3, the physical mechanisms of TPIN were reviewed and divided into three categories: generation mechanisms, amplification mechanisms and attenuation mechanisms.

In Chapter 4, the influencing parameters of TPIN were reviewed and divided into five categories: driver influence parameters, tire related parameters, tread pattern parameters, pavement related parameters, and environmental parameters.

In Chapter 5, the existing models of TPIN were reviewed and categorized into deterministic models, statistical models and hybrid models. Each model was self-contained with key principles, equations, and illustrations included. The deterministic models were divided into three sub-categories: conventional physics models, finite element and boundary element models, and computational fluid dynamics models; the statistical models were divided into three sub-categories: traditional regression models, principal component analysis models, and fuzzy curve-fitting models; the hybrid models were divided into three sub-categories: tire-pavement interface models, mechanism separation models, and noise propagation models.

In Chapter 6, the approaches to reducing TPIN are discussed.

In this literature review work, the present author has endeavored to extract useful, inspiring, and well-validated information from enormous number of references. However, the present author cannot guarantee that this work includes all the relevant knowledge in the public domain. In addition, if some of the opinions in this work are not true to the original due to misinterpretation, I apologize.

2 Measurement Techniques

2.1 Introduction

There are a number of different techniques to measure tire-pavement interaction noise (TPIN). Each method has advantages and disadvantages, and is applied differently under different situations. These methods can be divided into different categories according to different criterion, as listed in Table 2.

Table 2: Category of TPIN measurement techniques

Criterion	Measured Parameter	Sound Field	Acoustic Equipment (Instrumentation)	Test Environment	Measured Noise Source	Standard
Category	Sound pressure, sound intensity, sound power	Near-field, far-field	Microphone, intensity probe, microphone array	Roadside, on-board, lab	TPIN, vehicle, traffic	Standardized, non-standardized

Sound pressure is the quantity utilized by most measurement techniques, but it is also dependent of some other external factors for a given tire-pavement combination, such as measurement position. Sound power is able to deal with this problem perfectly. Sound intensity have not been widely used, partly because some researchers claimed that they require a noise source emitting stationary noise, which is not the case of the tire pavement interaction noise (Campillo-Davo et al., 2013 [94]).

Far-field noise is also called Pass-by Noise (PBN) that corresponds to several measurement techniques, such as Statistical Pass-By (SPB), Controlled Pass-By (CPB), Coast-By (CB) and such. A list of standards for pass-by noise is displayed in Table 3 (Siemens, 2014 [95]).

Table 3: Standards for pass-by noise (Siemens, 2014 [95])

	Standard	Name
Light Vehicles (Passenger and Goods)	ISO 362-1: 2015	Measurement of noise emitted by accelerating road vehicles -- Engineering method -- Part 1: M and N categories
	SAE J986: 2013	Sound level for passenger cars and light trucks
	SAE J1470: 2013	Measurement of noise emitted by accelerating highway vehicles
Heavy Vehicles (HGV and Bus)	ISO 362-1: 2015	Measurement of noise emitted by accelerating road vehicles -- Engineering method -- Part 1: M and N categories
	SAE J1470: 2013	Measurement of noise emitted by accelerating highway vehicles
	SAE J366: 2011	Exterior sound level for heavy trucks and buses
Motorcycles	ISO 362-2: 2009	Measurement of noise emitted by accelerating road vehicles -- Engineering method -- Part 2: L category
	ASEP Regulation 41	Motorcycle noise emissions (UN/ECE Regulation No. 41)
	F76A US	American standard for motorbikes acceleration noise
Exhaust Noise	ISO 5130: 2007	Acoustics -- Measurements of sound pressure level emitted by stationary road vehicles

The instrumentation for vehicle noise and vibration measurements includes microphones, accelerometers, Laser scanning vibrometry, force gauges, or load cells. However, when it comes to acoustical noise, it basically refers to only one sensor: microphone. It should be noted that most of the data analysis in the current literature are focused on overall sound levels, octave band levels or 1/3 octave band levels while few of them are in narrowband.

Although the measurement techniques vary, the digital processing methods are almost the same. The first step is to acquire a certain period of sound level data. The second step is transforming the time domain data to frequency domain data using Fast Fourier Transform (FFT) or Short-Time Fourier Transform (STFT). Conventional Fourier Transform (FT) is good at analyzing frequency domain signal but loses time information. Short Term Fourier Transform (STFT) is able to analyze the frequency domain in local time range (Zakelj, 2000 [96]), but is not able to analyze variety of time-varying signals [68] (He et al., 2011). Another transform is Wavelet Transform (WT), which does better job in handling non-stationary random signal and becomes popular recently (He et al., 2011 [97]; He et al., 2011 [68]; SungWook et al., 2012 [98]; Chen et al., 2013 [99]).

In this paper, the measurement techniques on TPIN were reviewed and divided into three categories based on the test environment: roadside, on-board and lab. The relationship between different measurement techniques is discussed at the end.

2.2 Roadside Measurement

The roadside measurement technique measures the far-field noise of the moving vehicle at the roadside with the measurement equipment stationary.

2.2.1 Statistical Pass-By (SPB)

The statistical pass-by (SPB) method, as described in ISO 11819-1 (1997) [100], is a technique for measuring the average total traffic noise for a given section of pavement. This approach is commonly used for comparing acoustic properties of different pavements. An example of measurement setup is shown in Figure 26.

Figure 26: Statistical Pass-by (SPB) (Source from Wang et al., 2011 [42], Figure 2.1; reprinted under fair use provision)

A tripod-mounted microphone is placed 7.5 m (mainly in Europe and ISO) or 15 m (mainly in USA and SAE in earlier times) from the center of the lane of traffic to be tested and 1.2 m above the pavement. Maximum sound pressure level (SPL), vehicle type, and vehicle speed are recorded for at least 100 passenger cars and 80 heavy vehicles randomly and individually,

which are statistically significant. A speed correction is performed to determine the average SPL at the desired same speed. Then statistical pass-by index (SPBI) is calculated using the weighting factors of 70.0% cars, 7.5% dual-axle heavy vehicles, and 22.5% multi-axle heavy vehicles. Thus it best represents actual traffic noise emissions and provide the best available measurement of the impact of traffic noise on properties adjacent to highways (Rasmussen and Sohaney, 2012 [101]).

A slightly modified SPB method, which is SPB method using backing board in ISO/PAS 11819-4 (2013) [102], was developed for measurement sites where there is a potential influence of acoustic reflections from the rear of the measurement position or other acoustic environment issues. The configurations are the same as the original SPB except that the microphone is mounted on a rectangular hard reflective board. However, it should be noted that this method would inevitably reduce the accuracy of results compared to a true free-field measurement.

This technique is in general compliance with Statistical Isolated Pass-By Method (SIP) and Continuous-Flow Traffic Time-Integrated Method (CTIM).

2.2.2 Controlled Pass-By (CPB)

This technique was first introduced by French National Standard NF S S1 119-2 (1999, previously AFNOR S 31 119-1 in 1993) [103] (constant speed) and the similar standard is ISO 362 [104,105] (accelerate). This method is similar to the SPB method except that it uses a test vehicle instead of the existing uncontrolled traffic stream. Maximum pass-by SPL is recorded for several passes of the same test vehicle under the same operating conditions. The maximum SPL is usually obtained when the vehicle shortly passed the microphone. There might be two reasons: (1) the vehicle is accelerating; (2) the noise source of exhaust system has strong directivity for radiating backwards. An example of the measurement setup is shown in Figure 27.

Figure 27: Controlled Pass-By (CPB) (Source from Copeland and Wilhoit, 2012 [106], Figure 1; reprinted with permission from Mr. Jack Mowry, Editor and Publisher of Sound & Vibration)

The operating conditions of the test vehicle could be drive-by (accelerate), cruise-by (constant speed) or coast-by (decelerate). Its flexibility and repeatability provides a good solution to evaluate vehicle noise for homologation purposes. Automotive or tire companies might have individual but similar standards for product development (Copeland and Wilhoit, 2012 [106]).

2.2.3 Coast-By (CB)

The coast-by method, as described in ISO 13325 (2003) [107], is similar to the CPB method, but the engine of the test vehicle equipped with test tires is switched off as the vehicle reaches the test area. In this method, power train noise is practically eliminated and the measured noise will be mainly from all the tires. An example of the measurement setup is shown in Figure 28.

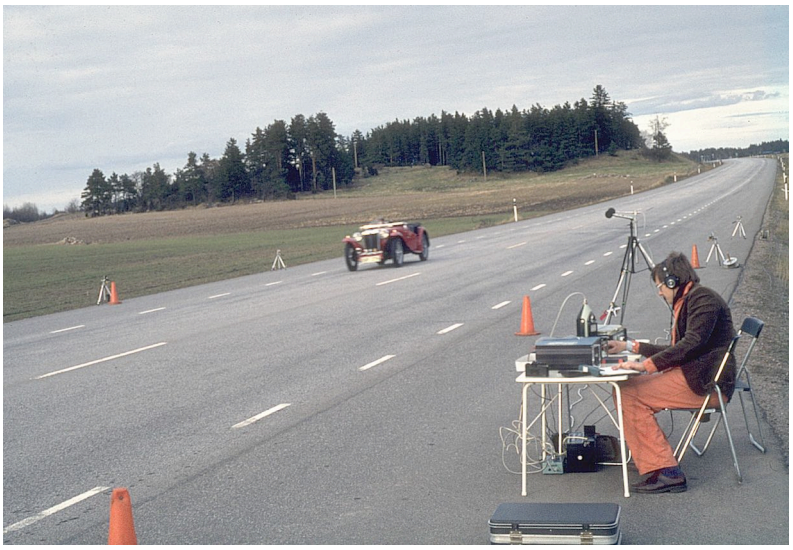

Figure 28: Coast-By (CB) (Source from Sandberg and Ejsmont, 2002 [7], Fig. 14.3; reprinted with permission from Dr. Ulf Sandberg of VTI, Sweden)

The overall A-weighted sound pressure level (OASPL) at 15 m distance for automobiles and light trucks under cruising conditions is given by

$$L_A = 32\log(v/88) + 71 \tag{1}$$

where L_A is OASPL, v is speed in km/h (the reference speed is 88 km/h). The OASPL for motorcycles is

$$L_A = 25\log(v/88) + 78 \tag{2}$$

and for trucks

$$L_A = \begin{cases} 84 & v \le 48 \text{ km/h} \\ 20\log(v/88) + 88 & v > 48 \text{ km/h} \end{cases} \tag{3}$$

2.2.4 Statistical Pass-By and Time-Averaged Wayside (SPB/TA)

This method is a modified version of SPB applied under heavy traffic conditions when SPB cannot be used to measure noise from isolated vehicle. This is seen to be a precursor to CTIM. An example of the measurement setup is shown in Figure 29.

Figure 29: Statistical Pass-By and Time-Averaged Wayside (SPB/TA) (Source from Bernhard and Wayson, 2005 [66], Figure 6.4; reprinted with permission from Ms. Amy Miller of Asphalt Pavement Alliance, USA; photo courtesy of Judith Rochat, U.S. DOT Volpe Center)

A microphone is placed at 15 m from and 1.5 m (lower than CTIM) higher than the center of the outside lane. In 2009 and 2011, additional measurements were made at a 15/3.7 m (same as CTIM) and 7.6/1.2 m (nearer and lower than CTIM) (Rasmussen and Sohaney, 2012 [101]). Measurement sites should be selected where background noise is at least 10 dB(A) lower than the tested traffic noise. Sound pressure is measured continuously for a period of time and converted to equivalent SPL (L_{peq}). This method is best applied for evaluation of noise change of a particular section with time. It is difficult to normalize the data to make comparisons between different pavements (Bernhard and Wayson, 2005 [66]).

SPB/TA is not a standardized method; the same situation is for Environmental Wayside Method or SPBI+ by Colorado Department of Transportation (CDOT) (Hanson and James, 2004 [108]). The microphone locations for SPBI are 15/1.5 m, 30/1.5 m and 60/1.5 m. Such far locations are chosen because the noise levels at these distances would correspond to locations of residences in these areas (Rasmussen and Sohaney, 2012 [101]). However, industry experts have questioned the accuracy and usefulness of measurements over 60 m. Additionally, conducting practical SPBI+ tests was often difficult due to the inability to obtain approvals for adjacent land access and/or contamination from other sound sources.

2.2.5 Statistical Isolated Pass-by (SIP)

This measurement technique is very similar to SPB, but stricter on testing requirements (Lodico et al., 2012 [109]). The SIP Method is used to measure noise from isolated vehicle pass-by (constant-speed cruise-by) within existing traffic without noise contamination from other vehicles. More considerations for measurement site and vehicle selection are needed. Besides maximum SPL, vehicle speed and vehicle category, meteorological data including air temperature and wind conditions will also be recorded in the vicinity of microphone position for later elimination of unacceptable samples. The desirable number of acceptable vehicles for each category is 100. An example of the measurement setup is shown in Figure 30.

Figure 30: Statistical Isolated Pass-by (SIP) (Source from Lodico et al., 2012 [109], Figure 1; reprinted under fair use provision)

Like SPB, speed correction is applied using linear regression, but the designated speed for SIP is the average test speed for all vehicles within a vehicle category, not a pre-specified speed for SPB. The speed-adjusted value of L_{veh} is compared to the Reference Vehicle Sound Level $L_{veh,ref}$, both at the designated speed. The difference between L_{veh} and $L_{veh,ref}$ is calculated and reported as the Statistical Isolated Pass- by Index (SIPI). It is a good method to evaluate and compare the noise levels of pavements with different parameters.

SIP for evaluating vehicle noise, as is standardized in AASHTO TP-98 (2013) [110], is one of the three TPIN-related standards published by American Association of State Highway and Transportation Officials (AASHTO) (2010) [111]. The other two are the On-Board Sound Intensity Method (AASHTO TP-76-2013 [112]) for evaluating tire/pavement noise, and the Continuous-Flow Traffic Time Integrated Method (AASHTO TP-99-2013 [113]) for evaluating

traffic noise. These three standards provide good correlation with data from Traffic Noise Model (TNM) developed by U.S. Department of Transportation (DoT) Federal Highway Administration (FHWA) (Rochat et al., 2012 [114]), such as Reference Energy Mean Emission Levels (REMELS).

2.2.6 Continuous-Flow Traffic Time-Integrated Method (CTIM)

This method, as described in AASHTO TP-99 (2013) [113], is applied to roadways where measuring single isolated vehicle pass-by events (SIP method) would be difficult due to continuously flowing, relatively dense traffic. An example of the measurement setup is shown in Figure 31.

Figure 31: Continuous-Flow Traffic Time-Integrated Method (CTIM) (Source from Rochat et al., 2012 [115], Figure 2; reprinted under fair use provision)

One microphone is placed 15 m from the center of the nearest travel lane, at a height of 3.7 m above the center of the nearest travel lane (Rochat et al, [115]). A-weighted sound pressure levels from the existing traffic for all vehicles on all roadway lanes are measured continuously for a time block of 5 or 15 minutes and then calculated to generate an average SPL (L_{peq}). Traffic count, vehicle type, speed and meteorological data are also collected in the meantime. A traffic noise prediction model is used to normalize sound levels to account for traffic variation such as percentage of heavy trucks. The method helps state highway agencies to compare varying pavement surfaces on a single roadway or to evaluate the effects of quieter pavements (Illingworth & Rodkin, 2011 [116]; Donavan et al., 2012 [117]).

In some sense, SIP and CTIM can be considered as special cases of SPB method applied under different conditions.

2.2.7 Coast-By Sound Power Level (CBSWL)

Like NPB with NCPX, the final measurement of this method is sound power level of TPIN converted from the average coast-by SPL (Campillo-Davo et al., 2013 [94]). Based on the procedure described in the Directive 2001/43/EC (EC, 2001 [118]) and ISO 3744 (ISO, 1994 [119]), it is assumed that all SPL measurement positions comply with far field requirements according to the ISO 12001 [120] and that each tire is an omnidirectional point source moving over a reflecting plane. Doppler Effect can be neglected in third-octave band analysis (from 100 Hz to 10 kHz) with an error of only 0.015 dB for a speed of 100 km/h (Heijden and Son, 1982 [121]). An example of the measurement setup is shown in Figure 32.

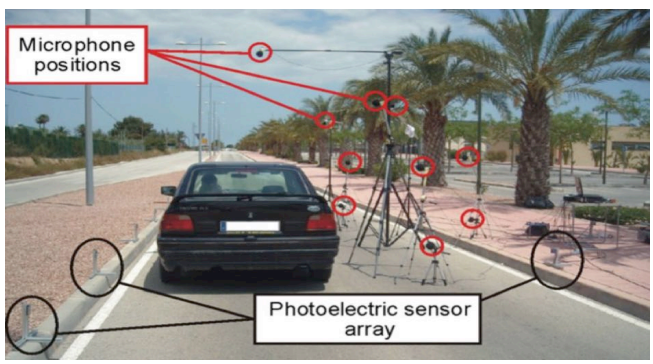

Figure 32: Coast-By Sound Power Level (CBSWL) (Source from Campillo-Davo et al., 2013 [94], Figure 13; reprinted with permission from Elsevier)

10 microphones are distributed on a hemispheric surface and placed in the center of the testing area. The radius of the hemispheric surface should satisfy,

$$r > 2d_0 \tag{4}$$

where d_0 is the characteristic dimension of a imaginary parallelepipedic surface that exactly encompasses the four tires installed on the vehicle and can be calculated as,

$$d_0 = \sqrt{(l_1/2)^2 + (l_2/2)^2 + l_3^2} \tag{5}$$

where l_1 is the longitudinal dimension, l_2 is the lateral dimension and l_3 is the vertical

dimension.

Average SPL at the 10 microphones are calculated at the instant the vehicle is located at measurement surface center,

$$L_p'^{(\mathrm{avg})} = 10 \cdot \log_{10}\left[\frac{1}{10} \cdot \sum_{i=1}^{10} 10^{\frac{1}{10}L'_{pi}}\right] \mathrm{dB} \tag{6}$$

where $L_p'^{(\mathrm{avg})}$ is the SPL averaged over the measurement surface in each frequency band, and L_{pi}' is the SPL measured in each frequency band at the ith microphone position. If the background noise level is not over 15 dB less than $L_p'^{(\mathrm{avg})}$, it is necessary to apply any background noise correction factor K in accordance with ISO 3744 (ISO, 1994 [119]). The corrected SPL $L_{pf}^{(\mathrm{avg})}$ is

$$L_{pf}^{(\mathrm{avg})} = L_p'^{(\mathrm{avg})} - K \tag{7}$$

The SWL of the TPIN L_{Wri} is calculated by

$$L_{Wri} = L_{pf}^{(\mathrm{avg})} + 10 \cdot \log_{10}\left(\frac{S}{S_0}\right) \mathrm{dB} \tag{8}$$

where S is the area of the measurement surface ($S = 2\pi r^2$) in square meters, and $S_0 = 1\ \mathrm{m}^2$.

2.2.8 Summary

The roadside measurement techniques described above are summarized in Table 4. Most of the techniques have corresponding standards where typically the maximum sound pressure level ($L_{p\max}$) is measured as the vehicle passes by. The advantage is the measurement equipment is usually just one microphone, which is very simple. However, the TPIN cannot be isolated from the total vehicle noise or traffic noise.

Table 4: Summary of roadside measurement techniques

No.	Method	Acronym	Current Standard	First Version	Equipment	Measured Parameter	Main Noise Source	Category	Advantage	Disadvantage	References
1	Statistical Pass-By	SPB	ISO 11819-1 [100], ISO 11819-4 [102]	ISO (1997) [100], ISO (2013) [102]	1 Mic	$L_{p\max}$	Traffic	Roadside, far-field	Minimal equipment, no traffic control, good to evaluate pavements at receiver	Time-consuming, weather sensitive, noise source isolation not possible	42,101,122,123
2	Controlled Pass-By	CPB	NF S S1 119-2 [103], ISO 362 [104,105]	NF (1999) [103], ISO (1981) [124], ISO (1985) [125]	1 Mic	$L_{p\max}$	Vehicle	Roadside, far-field	Flexible and repeatable, less time needed	Traffic control required, TPIN not isolated	106,126
3	Coast-By	CB	ISO 13325 [107]	ISO (2003) [107]	1 Mic	$L_{p\max}$	All tires	Roadside, far-field	TPIN isolated	Speed not constant	7,127
4	Statistical Pass-By and Time-Averaged Wayside	SPB/TA	N/A	Hanson and James (2004) [108]	1-3 Mic's	L_{peq}	Traffic	Roadside, far-field	Similar to CTIM, not standardized	Similar to SPB, TPIN not isolated	66,101,108
5	Statistical Isolated Pass-by	SIP	AASHTO TP-98 [110]	AASHTO (2012) [128]	1 Mic or 2	$L_{p\max}$	Vehicle	Roadside, far-field	Similar to SPB, one vehicle isolated	Similar to SPB, TPIN not isolated	109
6	Continuous-Flow Traffic Time-Integrated Method	CTIM	AASHTO TP-99 [113]	AASHTO (2012) [129]	1 Mic	L_{peq}	Traffic	Roadside, far-field	Similar to SPB	Similar to SPB/TA	115
7	Coast-By Sound Power Level	CBSWL	N/A	Campillo-Davo et al. (2013) [94]	10 Mic's	L_W	All tires	Roadside, far-field	Similar to NCPX, easy procedure	Not capable of isolating TPIN from one tire	94

"First Version" refers to the first standard if the method has been standardized; otherwise it refers to the first measurement attempt.
Some of the references in "First Version" are the same as in "Current Standard", except the published year.
For the column of "Main Noise Source":

"One tire" means the main noise comes from the only tested tire on which the testing equipment is mounted.
"All tires" means the main noise comes from all the tires (usually four) of the tested vehicle or trailer.
"Vehicle" means the main noise comes from the tested vehicle (TPIN, powertrain, air intake and outlet and aerodynamics noise).
"Traffic" means the main noise comes from all the vehicles on the road.

The advantage and disadvantage are evaluated in terms of TPIN investigation.

2.3 On-board Measurement

The on-board technique measures the near-field tire noise with the measurement equipment fixed on the running vehicle.

2.3.1 Behind the Tire (BTT)

This measurement technique was mostly employed on truck tires between the 1970's and 1980's. Sound pressure level (SPL or L_p) was measured directly behind the test tire with one microphone, the position of which varied (as show in Table 5) due to the lack of standard, but was without exception relatively close to the pavement and tire. An example of the measurement setup is shown in Figure 33.

Table 5: Various experiments using behind the tire (BTT) approach

Reference	Author	Year	Tire Type	Microphone Position	Correlation with Pass-By Noise (PBN)
[130]	Siddon	1972	Passenger car tires	Not reported	Not reported
[131]	Miller & Thrasher	1974	Truck tires (lug-type)	Height: 150 mm; distance from the rear edge of the tire contact patch: 460 mm	Same frequency content, difference range: 8-37 dB
[132]	Reiter et al.	1974	Truck tires (5 tread patterns)	Height: 200 mm; distance from closest point of the tire: 150 mm	Not reported
[133,134]	Landers et al.	1977, 1977	Both light and heavy-duty tires	Dead air pocket: as close as possible	Not reported
[135]	Underwood et al.	1984	Lorry tires	Height: 560 mm; behind the tire: 240 mm	Not reported
[136,137]	Eberhardt et al.	1977, 1981	Truck tires	Height: 200 mm; distance from closest point of the tire: 150 mm	R^2 = 0.7, error 3-4 dB
[138]	Zhang et al.	2014	Passenger car/van tires	Behind the driver side rear tire under the vehicle	Not reported

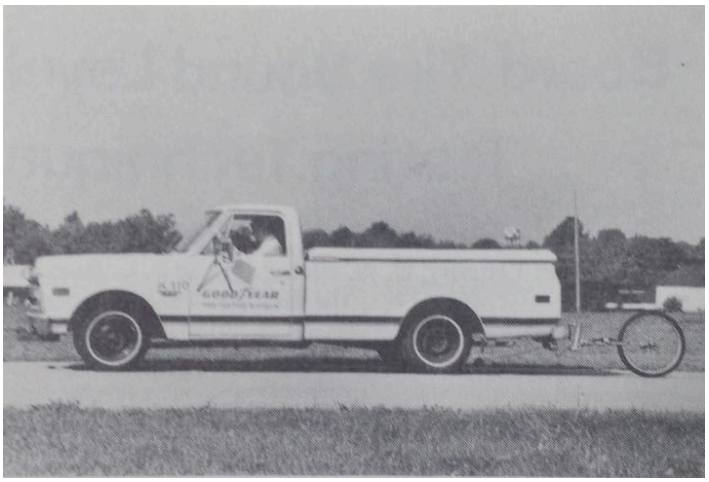

Figure 33: Behind The Tire (BTT) (Source from Landers et al., 1977 [133], Figure 1; reprinted under fair use provision)

It was probably the first on-board approach to testing the TPIN. However, since there was limited evidence (Table 5) showing acceptable correlation between the far field pass-by sound levels and BTT near field levels, this approach was seldom used after the 1980's (Donavan and Lodico, 2009 [139]). Having said that, due to its simple setup and configurations, BTT method is now and then employed when measurement equipment is limited, such as Zhang et al. (2014) [138].

2.3.2 Trailer Coast-By (TCB)

This method is a hybrid of CPX method and CB method. The test tires are mounted on a trailer with a very long drawbar (10 m) connecting the towing vehicle. As the trailer coasts by the test section, SPL is measured by a microphone located wayside. TCB method is strongly supported by US engineers for truck tire noise; for example, SAE J57 (2014) [140] specifies this method. The second part of ISO 13325 (2003) [107] also indicates this method. An example of the measurement setup is shown in Figure 34.

Figure 34: Trailer Coast-By (TCB) (Source from Sandberg and Ejsmont, 2002 [7], Fig. 16.30; reprinted with permission from Dr. Ulf Sandberg of VTI, Sweden, Mr. Steve Phillips of CEDR at EU, and Dr. Philip Morgan of TRL, UK)

In this method, quiet tires (-6 dB relative to test tires) are needed for the towing vehicles. Closer microphone position is preferred (7.5 m instead of 15 m) (Sandberg and Ejsmont, 1992 [141]). Enclosure around the towing vehicle tires might be used to screen the sound contamination (Phillips et al., 2001 [142]).

2.3.3 On-Board Sound Pressure (OBSP)

This method is a transient version of TPIN SPL measurement from BTT method to the standardized Close-Proximity Trailer (CPX) method. Various microphone locations and configurations have been tried, as listed in Table 6. An example of the measurement setup is shown in Figure 35.

Table 6: Tests using OBSP method

Reference	Author	Year	Trailer Used	Number of Microphones	Angle to the Direction of Travel	Microphone Configuration	Correlation with Pass-By Noise (PBN)	Conclusion
[143]	Osman & May	1980	No	1	145 °	Fitted with nose cone	N/A	A-weighting to diminish wind effects in 30-300 Hz
[144]	Ungar & Bronsdon	1980	No	1	90 °	Fitted with windscreen	N/A	Windscreen worked better than a noise cone
[145]	Breyer	1990	Yes	2	90°, 180 °	Not reported	N/A	Measuring conditions had been recently standardized
[146]	Springborn	1990	Yes	3	0°, 90°, 180 °	Not reported	Scatter of 2 to 4 dB	Rating of road surfaces was independent of test tire
[147]	Steven	1990	No	4	0°, 45°, 135°, 180 °	Windscreen	Error ± 2 dB	Best correlation: 45° Worst correlation: 180°
[148]	Chalupnik	1996	Yes	2	90°, 135°	Windscreen	1/3 octave band 90° error: 8-10 dB; 135° error: 5-6 dB	Neither position completely recorded the tire noise as measured on the roadside
[149]	McNerney et al.	2000	Yes	2	135°, 180 °	Nose cone Windscreen	135° $R^2 = 0.52$; 180° $R^2 = 0.58$; average $R^2 = 0.57$	The correlation of the two onboard microphones: $R^2 = 0.93$
[150]	Chuang et al.	2005	No	1	90°	Windscreen	$R^2 = 0.99$	In-lab levels were lower for same microphone position

Figure 35: On-Board Sound Pressure (OBSP) (Source from Chuang et al., 2005 [150], Figure 4 ; reprinted under fair use provision)

No standards were applied to these tests, which might be on-vehicle or on-trailer. Correlation to pass-by levels was reported with varying degrees of success. Most cases failed to present good correlation except Chuang et al. (2005) [150]. However, it is not practical to use such microphone location, 500mm away from the sidewall, for in-situ TPIN measurement (Donavan and Lodico, 2009 [139]). It is not even allowed in Japan for the use of any objects protruding from the vehicle (Sandberg and Ejsmont, 2002 [7]).

Ibarra et al. (2016) [151] applied on-board sound pressure system to obtain the parameters of ground surfaces in real time at different speeds. That is to say, it was not intended for tire noise measurement, but for the measurement of ground impedance based on the sound level difference of two microphones vertically aligned at different heights (ANSI S1.18, 2010 [152]). As such, the sound source is not from the tire but from a small directional speaker attached to the system.

2.3.4 Close Proximity Sound Intensity (CPI)

Unlike the joint effort in development and widespread popularity of trailer to measure the TPIN sound pressure level (SPL) at the source in Europe, the researchers in US endeavored to develop techniques to measure the sound intensity level (SI level, SIL or L_I). This work was done almost exclusively and privately at the General Motors Corporation (GM) throughout the 1980's. An example of the measurement setup is shown in Figure 36.

Figure 36: Close-Proximity Sound Intensity (CPI) (Source from Bernhard and Wayson, 2005 [66], Figure 6.6; reprinted with permission from Ms. Amy Miller of Asphalt Pavement Alliance, USA; photo provided by Dr. Paul Donavan of Illingworth and Rodkin, Inc., USA)

Physically, sound pressure and sound intensity are significantly different quantities, as shown in Table 7, even though in many practical cases their behavior and level (with appropriate reference levels) are similar to each other.

CPI method is similar to CPX except that the intensity probe is used instead of microphones. In addition, the intensity probe is placed in such a way that only sound radiating from the test tire can be detected, it is not necessary to shield the probe from wind or traffic noise, so generally trailer is not needed either. The intensity probe is usually mounted close to the test tire of the test vehicle itself (Bernhard and Wayson, 2005 [66]; Donovan and Rymer, 2003, [153]; Biligiri, 2008 [154]). Thus, the present author argue that CPI is more a predecessor to OBSI than a modified version of CPX.

It should also be noted that sound intensity measurements would have significant errors if a high reactive component is present or the indicated sound intensity level is much smaller than the sound pressure level. Donavan (1995) [155] noted that Large sound intensity measurement errors might occur for even very small phase mismatch between microphone channels when the intensity vector does not coincide with the sensitive axis of the probe. As a result, probe/microphone configurations are very important in sound intensity measurements.

Table 7: Comparisons between sound pressure and sound intensity (Bloemhof, 1986 [156])

	Sound Pressure (SP)	Sound Intensity (SI)
Physical Meaning	Local pressure deviation from the ambient (average, or equilibrium) atmospheric pressure	Sound power (average rate of flow of acoustic energy or sound energy per time unit) per unit area
Quantity Type	Scalar quantity	Vector quantity; direction: same as acoustic energy flow
Measurement Equipment	One microphone	One intensity probe (two phase-matched and closely spaced microphones) (Crocker, 1997 [157])
At Acoustic Near Field	Very sensitive to position; cannot detect energy flow	A Smoother function of position; capable of detecting the propagating energy
Advantage	Easy to process data	Able to localize noise sources and reject background noise
Relation	$\mathbf{I} = p\mathbf{v}$ where $\mathbf{I}$ is sound intensity, p is sound pressure, and $\mathbf{v}$ is acoustic velocity at that point	

Sound intensity can be calculated using two different methods. The first is in the temporal

domain by Fahy (1995) [158]. The sound pressures corresponding to the two microphones on a given probe are used to calculate the instantaneous particle velocity and intensity at each sample point. The second method used for SI calculation is in the frequency domain. The corresponding equation is given by (Waser and Crocker, 1984 [159])

$$I_r = \frac{\mathrm{Im}\left[p_A p_B^*\right]}{2\omega\rho\Delta r} = \frac{\mathrm{Im}\left[G_{AB}\right]}{\omega\rho\Delta r} \tag{9}$$

$$G_{AB}(\omega) = \left\langle FFT\left(p_A(t)\right) \times FFT\left(p_B(t)\right)^* \right\rangle / 2 \tag{10}$$

where I_r is the sound intensity with the direction from A to B, p_A and p_B are sound pressures at microphone A and B, respectively, asterisk * means the complex conjugate of corresponding value, Im means the imaginary part of the complex number, ω is the radian frequency, ρ is the air density, Δr is the distance between the two microphones, G_{AB} is the cross spectrum of the two sound pressure signals, *FFT* is fast Fourier transform.

An important parameter relating sound pressure and sound intensity is Pressure Intensity Index (*PI*), as defined by

$PI = SPL - SIL$

where *SPL* is sound pressure level, and *SIL* is sound intensity level, given by

$$SPL = 10\log_{10}\left(\frac{p_{rms}^2}{p_{ref}^2}\right) \tag{11}$$

$$SIL = 10\log_{10}\left(\frac{I}{I_{ref}}\right) \tag{12}$$

where p_{rms} is the root mean square of sound pressure signal, p_{ref} is reference sound pressure (20 μPa); I is sound intensity, I_{ref} is reference sound intensity (1 pW/m^2). Pressure Intensity Index is the difference between the sound pressure level and the sound intensity level, and is a good indicator for the quality of the acoustic measurement. A high value of *PI* means that accurate sound Intensity measurements will be difficult. For the TPIN, the PI Index should satisfy the requirements in Table 8 to guarantee the accuracy of sound intensity measurements, which is described by OBSI standard AASHTO TP-76 (2013) [112].

Table 8: PI index requirements for each 1/3 octave band (source from AASHTO TP-76, 2013 [112], Table 1; reprinted with permission from Mr. Robert Cullen of AASHTO)

1/3 Octave Band Center Frequency [Hz]	Minimum PI Index [dB]	Maximum PI Index [dB]
400	-1.0	5.0
500	-1.0	4.5
630	-1.0	3.5
800	-1.0	2.5
1000	-1.0	2.5
1250	-1.0	3.0
1600	-1.0	3.0
2000	-1.0	3.0
2500	-1.0	3.5
3150	-1.0	4.0
4000	-1.0	4.5
5000	-1.0	5.0

2.3.5 Sound Intensity Field (SIF)

Some of the studies used multiple SI probes or put the probes at other positions besides leading/trailing edges to generate the entire sound intensity contours near the tire to localize the TPIN source (Donavan and Oswald, 1981 [160]; Oswald and Donavan, 1980 [161]; Donavan, 1981 [162]; Oshino and Tachibana, 1990 [163]), as shown in Figure 37. It can be easily seen from the intensity mapping that the stronger source regions are at the leading and trailing edges of the contact patch for normal tire-pavement combination, at least in the range from 400 to 2500 Hz.

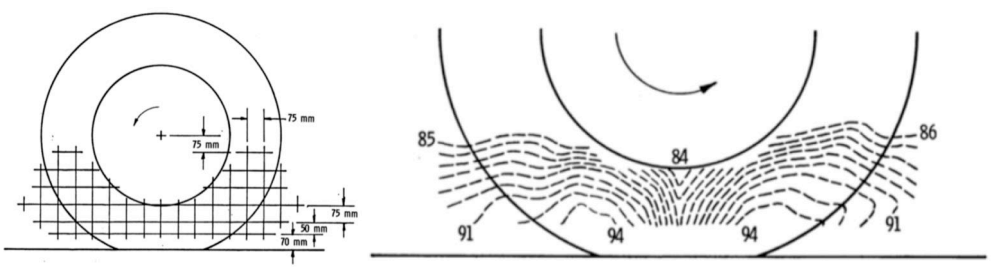

Figure 37: Sound Intensity Field (SIF) (Source from Donavan and Oswald, 1981 [160], Figure 11 and Figure 12; reprinted with permission from Dr. Paul Donavan of Illingworth and Rodkin, Inc., USA)

2.3.6 Tire Cavity Microphone (TCM)

As opposed to all other measurement techniques, TCM measures the noise inside the tire instead of outside. The TCM fits on the wheel and is approximately the same size as the original Tire Pressure Monitoring System (TPMS). TPMS has been reduced greatly in size and modularized to fit in different tires, which is not the case for TCM. An example of the

measurement setup is shown in Figure 38.

Figure 38: Tire Cavity Microphone (TCM) (Source from Bennetts and Crookes, 2013 [164], Figure 1; reprinted with permission from Mr. Charles Ellis, Publicity Officer and Acoustics Bulletin Editor, UK)

It has been proved that the noise inside the tire is correlated with the near-field noise radiated outside the tire (CPX) by means of surface-type specific ratios (Krauss and Gauterin, 2012 [165]) and tracks the level and frequency content of the far-field radiated noise from the tire (SPB) (Bennetts and Crookes, 2013 [164]). Different road surfaces can be distinguished using this method, especially at the cavity mode frequencies (100 Hz - 1 kHz).

This technique was performed for the first time at University of Stuttgart, Germany in 1981 (Bschorr, 1981 [166]), after which several approaches were made to carry over the basic idea into a practicable method (Bschorr, 2001 [167]; Wolf, 1997 [168]). It has been further enhanced by Cooper Tire in the UK after 2005 (Bennetts and Crookes, 2013 [164]). A microphone and radio link system was developed that solved the problem of data overload at a speed of over 30 km/h. In the meantime, another German university, Karlsruhe Institute of Technology, developed a similar method, i.e., Tire Cavity Sound Measurement Method (TCSMM) (Krauss and Gauterin, 2012 [165]).

It is a highly research oriented technique, as it well screens background noise (wind, traffic etc.) due to the sound insulation of the tire. However, it is shown that internal tire noise is

more sensitive to pavement roughness than speed, which is not the case for external noise (Bennetts and Crookes, 2013 [164]). More research needs to be conducted to better interpret the tire cavity noise and identify correction factors for different tires and speeds.

Masino et al. (2016) [169] developed a lower cost acoustic sensor (200 USD) to measure sound level up to 161 dB. The common MEMS microphone is about 7000 USD with a maximum sound pressure level of below 133 dB.

2.3.7 Close-Proximity Trailer (CPX)

The Close Proximity method (CPX) was a very favorable technique to measure the TPIN at the source in the 1980's in Europe (Sandberg and Ejsmont, 2002 [7]; Dimitri, 2012 [170]; Sandberg and Ejsmont, 2000 [171]), and was the first on-board method having good correlation with pass-by methods and OBSI method (Donavan and Lodico, 2009 [139]). An example of the measurement setup is shown in Figure 39.

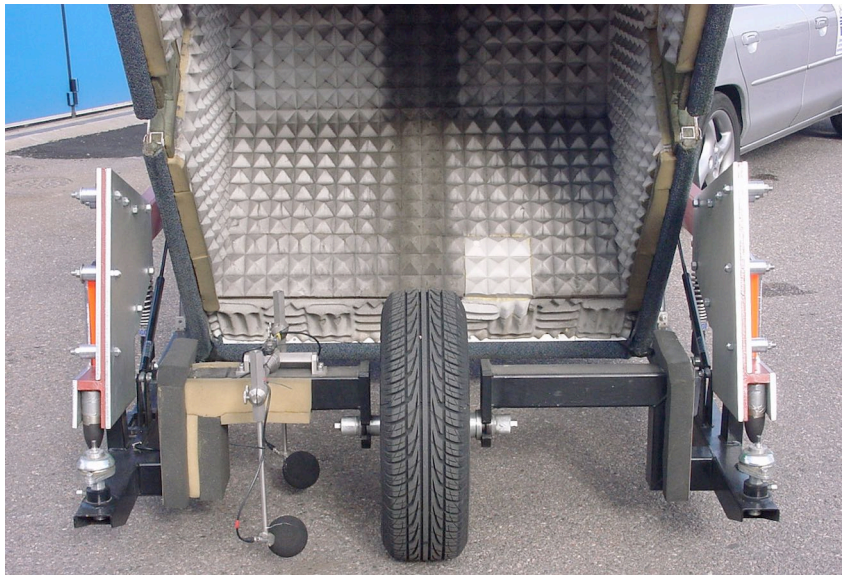

Figure 39: Close-Proximity Trailer (CPX) (Source from Wang et al., 2011 [42], Figure 2.2; reprinted with permission from Dr. Ulf Sandberg of VTI, Sweden)

The test tire is mounted on a trailer, which is towed behind a test vehicle at target speeds. Usually two microphones are located near the tire (100-450 mm, one at the leading edge, the other at the trailing edge of contact patch) to measure the average SPL for a period of time

(4-60 s). Sometimes more microphones are employed around the tire and thus additional data processing equipment is needed. The trailer has an enclosure with sound-absorbing material attached inside around the microphones and test tire in order to provide screening from wind and traffic noise.

In the early studies, no standards, such as microphone numbers and locations, for this method were presented. In the mid 1990's, standardization of the CPX method began when interest of measuring the effect of pavement on traffic noise emission grew (Donavan and Lodico, 2009 [139]). By 2000, the first ISO standard was published, i.e., ISO 11819-2 (2000) [172]. However, considerable uncertainty, expected or unexpected, still exists (CROW, 2012, [173]).

CPX is a good and quick method to measure the TPIN across a pavement network and to monitor pavement condition. However, the near-field feature causes some error for low frequency noise from highly directive sources and pavement absorption might be underestimated (Bernhard and Wayson, 2005 [66]). Buytaert (2014) [174] investigated the noise level difference between the left tire and right tire of a CPX-trailer and found that the right wheel track is usually higher, especially for heavy vehicle reference tire AVON AV4.

2.3.8 In Vehicle (IV)

Besides wayside or at the source, noise measurements can also be conducted in-vehicle, with microphones (sometimes also accelerometers) placed inside the passenger compartment (Rasmussen, 2007 [62]). Data is collected as the vehicle is in motion, but potential sources such as the air conditioning or radio are excluded. The measurement positions are determined through path analysis of tire tread pattern's impact on interior vibration and noise [68] according to GB/T 18697-2002 (GB, 2002 [175]). An illustration of the measurement setup is shown in Figure 40.

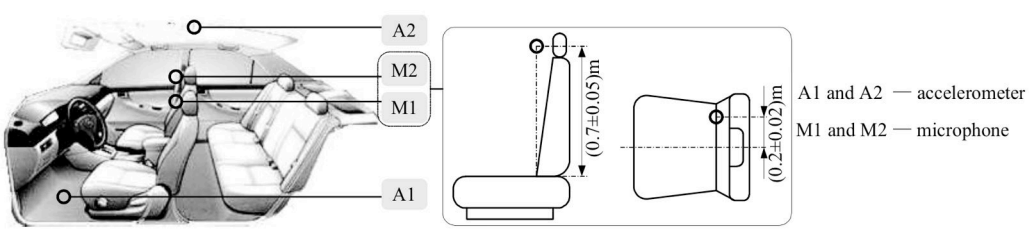

Figure 40: In Vehicle (IV) (Source from He et al., 2011 [68], Figure 3; reprinted with permission from Trans Tech Publications Ltd)

It should be noted that in-vehicle noise frequency is commonly much lower than outside noise. The vehicle attenuates the high frequency sound and amplifies it at low frequencies. Since in-vehicle noise is greatly dependent on the vehicle type and condition, the present author do not suggest using this method (interior noise) to interpret TPIN (Chang et al., 2010 [69]).

2.3.9 On-Board Sound Intensity (OBSI)

Like CPI, OBSI method measures sound intensity near the tire but uses two SI probes (leading edge and trailing edge respectively) held by a fixture attached to the wheel studs, as shown in Figure 41 (AVEC, 2012 [176]). It was originally developed and refined at General Motors as specification GMN7079TP (GM, 2004 [177]). It took about thirty years (1980's – 2010's) for the first CPI application at GM to grow mature and be standardized as OBSI method (AASHTO TP-76-2013 and ASTM WK26025-2009) [112,178]. Relevant proprietary technical documents from GM were released to public domain as OBSI became more and more popular, especially as an advanced way to study the performance of pavements for tire noise generation (Kohler, 2010 [47]; Rasmussen, 2010 [111]). It is worthwhile to do a literature review and understand the OBSI development history, as shown in Table 9. The current standard AASHTO TP-76 (2013) [112] also indicated that two intensity probes might be installed and measure concurrently (dual-probe), or just one probe at a time (single-probe, first at leading edge, then at the trailing edge) and measure separately. However, most of the OBSI the authors are aware of are dual-probe configurations.

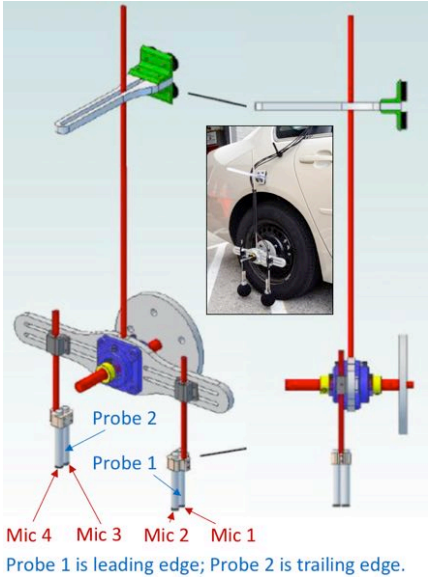

Figure 41: On-board sound intensity (OBSI) configurations (modified from AVEC, 2012 [176])

Table 9: History of OBSI development

Reference	Author	Year	Test Content	Probe Location	Number of Probes	Probe Configuration	Correlation with Pass-By Noise (PBN, y for here)	Conclusions
Early Technique Development in 1980's								
[161]	Oswald & Donavan	1980	Probe flow noise (self- and turbulence-induced)	In an anechoic, open jet wind tunnel	1	Microphone diameter: 1⁄4, 1⁄2, and 1 inch; Microphone spacing: 0 to 1 diameter; Fitted with nose cones	N/A	SI levels not sensitive to flow with high signal to noise ratio (SNR); Optimum probe design: 1⁄2 inch diameter microphones spaced 16mm apart
[160,179]	Donavan & Oswald	1981, 1980	3 truck tires (blank, zigzag rib, and cross-bar tread); 2 AC pavements	0.6 m behind and 0.6 m below the centerline of tire; Distance from tire sidewall: 30, 50, 100, 200, and 400mm	1; SIF; 75x75 mm grid; 58-60 points	Diameter: 1⁄2 inch; Spacing: 16 mm; Side-by-side; Nose cones; High pass filter 150 Hz	N/A	Optimal probe distance from the tire sidewall (maximizing tire noise while minimizing wind noise): 100 mm
[162]	Donavan	1981	4 different "all seasons" passenger car tires	Front tire (non-driven); Distance from tire sidewall: 100 mm	1; SIF; 75x75 mm grid	Diameter: 1⁄2 inch; Spacing: 16 mm; Side-by-side; Nose cones	N/A	NA
[180]	Hamill	1985	6 Treaded and blank tread tires; DGAC and PCC pavements	Right rear tire (non-driven); Height: 50, 100mm; Distance from tire sidewall: 100 mm	2	Diameter: 1⁄2 inch; Spacing: 16 mm; Side-by-side; Nose cones; High pass filter 350 Hz	With interior SPL; Same rank ordering from750-2500 Hz	Optimum height: 60 mm; Logarithmical/energy average of 2 SI levels as total TPIN level
[181]	Cantrell	1988	Uniroyal Tiger Paw Tire DAC pavements; Loading: 1200-2000 lbs; Inflation: 20-40 psi; Toe: 0°, ±1°, ±2°; Camber: 0°, ±1°, ±2°	Trailer; Height: 60 mm; Distance from tire sidewall: 100 mm	2	Diameter: 1⁄2 inch; Spacing: 16 mm; Side-by-side; Nose cones; High pass filter 350 Hz	N/A	SI sensitivity: toe > inflation > camber > load; Compact SUV instead of passenger van as towing vehicle eliminated wind noise contamination
Applications in Test Tracks in 1990's								
[163]	Oshino & Tachibana	1990	3 truck and bus tires (wavy rib, crossbar lug, and discrete block rib)	Trailer; Distance from tire sidewall: 100 mm	1; SIF; 50x50 mm grid	Side-by-side; Nose cones	N/A	Noise source region extended over the entire contact patch for the crossbar tire
[182]	Rasmussen	1990	2 different pavements	Not reported	2	Face-to-face; "Football" shaped windscreen	N/A	First application of the time domain approach to measuring SI instead of fast Fourier transform (FFT) approach
[183]	Stumpf	1990	Lab road wheel	Multi-locations enclosing a tire	1	Not reported	N/A	Correlating sound power [184]; Trailing edge level ~1dB higher than leading edge level
[185]	Donavan	1993	7 tires; DGAC pavement	Height: 60 mm; Distance from tire sidewall: 100 mm	2	High pass filter 500 Hz	$y = 0.94x - 19.19$	Good spectrum correlation with CPB

Reference	Author	Year	Test Content	Probe Location	Number of Probes	Probe Configuration	Correlation with Pass-By Noise (PBN, y for here)	Conclusions
[186,187]	Hall & Bolton	1994, 1995	14 test tracks of; ISO 10844 porous AC; SAE J1470 asphalt	Front tire (driven); Height: 66 mm; Distance from tire sidewall: 100 mm	2	Not reported	$y = 0.90x - 16.34$	Wind noise contamination present for the trailing edge
[188]	Donavan	1997	5 tires; ISO 10844 and SAE J1470 pavements	Height: 60 mm; Distance from tire sidewall: 100 mm	2	High pass filter 500 Hz	$y = 0.87x - 11.45$	SAE pavements were 2 dB greater than ISO pavements.
[189]	Sakamoto et al.	2003	2 car tires (one blank); ISO 10844 and ISO replica on road wheel	Height: 150 mm; Distance from tire sidewall: 200 mm	7	Three dimensional (four microphones)	N/A	3D OBSI vectors all had a definite upward component
[190]	Sakamoto et al.	2004	4 tires (one blank)	Height: 150 mm; Distance from tire sidewall: 200 mm	7	3D from Brüel & Kjaer; Wrapped with two layers of "windbreak netting"	N/A	Tire noise increased with applied torque.
In-Situ Pavement Noise Evaluation in 2000's								
[191]	Donavan & Rymer	2003	2 tires; Highway AC pavement	Height: 75 mm; Distance from tire sidewall: 100 mm	2	Diameter: 1⁄2 inch; With preamplifiers; Spacing: 16 mm; Face-to-face; Nose cones; Spherical foam windscreen	$y = 1.09x - 32.25$	Protocol refined sponsored by Caltrans; Standard test speed: 60 mph; Standard test tire: Goodyear Aquatred 3 P205/70R15
[192]	Donavan & Scofield	2003	PCC pavements (longitudinally, uniformly, and randomly transversed)	Same as above	2	Same as above	$y = 1.07x - 30.25$	Level differences between pavements were identical for all vehicles
[193]	Donavan & Rymer	2004	6 AC and 6 PCC pavements	Same as above	2	Same as above	$y = 1.09x - 31.99$	Good spectrum correlation
[194]	Donavan	2006	Exposed to air flow	Not reported	1 & 2	Single horizontal probe & dual vertical probe	N/A	Best for horizontal single probe with nose cones and a windscreen or dual vertical configuration with windscreens and no nose cones

It can be concluded that OBSI is suitable for measuring both truck and light vehicle tires with an excellent correlation with pass-by levels (R^2 generally greater than 0.95). Although OBSI needs a more sophisticated data processor, easy-to-us functions are usually available on professional acoustic software and real-time recording/analyzing can be achieved. OBSI data are usually filtered (third-octave band numerical filtering) to only include energy within the third-octave bands of 500 Hz to 5 kHz by employing a bandpass filter or 400-5000 Hz according to AASHTO TP-76 (2013) [112].

It is interesting to note that in US, during the standardization of at-the-source TPIN measurement, two candidates are chosen, OBSI and CPX. Finally, OBSI won in the field tests with a better and more stable correlation both in overall and spectrum level with pass-by methods. It turns out to be the only near field TPIN measurement standard published by US government. The authors believe that OBSI method has great potential to be further developed as a universal research oriented standard and win more attention from both automotive/tire industries and transportation authorities, which is why so much effort is put on this review.

2.3.10 Summary

The on-board measurement techniques described above are summarized in Table 10. This type of measurement techniques has emerged since 1972, but few of them have been standardized, probably because the equipment used is complex and difficult to standardize, especially when trailer is needed. The advantage is the noise components other than the tire noise are basically excluded or can be ignored.

Table 10: Summary of on-board measurement techniques

No.	Method	Acronym	Current Standard	First Version	Equipment	Measured Parameter	Main Noise Source	Category	Advantage	Disadvantage	References
1	Behind The Tire	BTT	N/A	Siddon (1972) [130]	1 Mic	L_p	One tire	On-board, near-field	First on-board approach, easy	Bad correlation with CPB, inaccurate	130–138
2	Trailer Coast-By	TCB	SAE J57 [140], ISO 13325 [107]	SAE (1977) [195], ISO (2003) [107]	1 Mic	$L_{p\max}$	All tires on trailer	Trailer, far-field	Similar to CB	Expensive, towing vehicle noise	141,142
3	On-Board Sound Pressure	OBSP	N/A	Osman and May (1980) [143]	1-4 Mic's	L_p	One tire	On-board, near-field	TPIN isolated	Similar to BTT	139,143–150,196–198
4	Close Proximity Sound Intensity	CPI	N/A	Donavan and Oswald (1980) [179]	1 Probe	L_I	One tire	On-board, near-field	Same as CPX, trailer not necessary	Real vehicle but not account for all types	66,153,154
5	Sound Intensity Field	SIF	N/A	Donavan and Oswald (1981) [160]	>=1 Probes	L_I	One tire	On-board, sound field	Capable of locating sound source	Time-consuming, asynchronous tests	160,162,163,179
6	Tire Cavity Microphone	TCM	N/A	Bschorr et al. (1981) [166]	1 Mic	L_p	One tire	Inside tire, near-field	Not sensitive to background noise	Bad/complex correlation with external TPIN	164,165,169
7	Close-Proximity Trailer	CPX	ISO 11819-2 [172]	ISO (2000) [199]	>=2 Mic's 1 Trailer	$L_{p\mathrm{avg}}$	One tire	Trailer, near-field	Less sensitive to weather/traffic	Trailer cost/space, not typical/real vehicle	7,66,139,170,171
8	In Vehicle	IV	GB/T 18697 [175]	GB (2002) [175]	1-4 Mic's	$L_{p\mathrm{avg}}$	Vehicle	Interior, near-field	Easiest way	Worst correlation with TPIN	62,69
9	On-Board Sound Intensity	OBSI	AASHTO TP-76 [112], ASTM WK26025 [178]	AASHTO (2008) [200], ASTM (2009) [178]	1 or 2 Probes	L_I	One tire	On-board, near-field	Same as CPI, more accurate	Device protrusion out of vehicle subject to law	5,42,47,111,201–212

"First Version" refers to the first standard if the method has been standardized; otherwise it refers to the first measurement attempt.
Some of the references in "First Version" are the same as in "Current Standard", except the published year.
For the column of "Main Noise Source":

"One tire" means the main noise comes from the only tested tire on which the testing equipment is mounted.
"All tires" means the main noise comes from all the tires (usually four) of the tested vehicle or trailer.
"Vehicle" means the main noise comes from the tested vehicle (TPIN, powertrain, air intake and outlet and aerodynamics noise).
"Traffic" means the main noise comes from all the vehicles on the road.

The advantage and disadvantage are evaluated in terms of TPIN investigation.

2.4 Lab Measurement

The roadside and on-board measurement techniques are intended for field test or road test. As far as the more sophisticated and accurate measurement, lab environment is usually necessary, or the outdoor test environment needs to be carefully controlled.

2.4.1 Tire Vibration Measurements (TVM)

This method can only interpret the structural borne part of TPIN. Tire vibration modeling is usually the fundamental step in deterministic TPIN models. The measurements of tire vibrations are used to verify TPIN models and investigate into noise generation mechanisms (Dare, 2012 [213]). There are many different methods coupled with different post-processing techniques for such measurements. An example of the measurement setup is shown in Figure 42.

Figure 42: Tire Vibration Measurements (TVM) (Source from Dare, 2012 [213], Figure 3.11; reprinted with permission from Dr. Tyler Dare of Pennsylvania State University, USA)

A Laser-Doppler Vibrometer (LDV) makes non-contact vibration measurements of a surface. The laser beam with known frequency from the LDV is directed at the surface of interest, and the vibration amplitude and frequency are calculated based on the Doppler shift of the reflected laser beam frequency due to the motion of the surface. LDV method is frequently used for structural modal analysis and able to applied for tire vibration measurements on lab drums (Nilsson, 1980 [214]; Cvar and Bernhard, 2000 [215]). Another non-contact device is called electronic speckle pattern interferometry (ESPI) (Kostial et al.,

2013 [216]). It also has the advantage of full field tire measurements. It can be used in real time based on video recording and display to measure dynamic displacement.

Accelerometer is an alternative method to measure tire vibrations. Accelerometers can be glued to tire sidewalls (Reiter and Eberhardt, 1974 [217]), embedded in tire treads or placed between tread elements (Fujikawa et al., 2009 [218]; Burroughs and Dugan, 2002 [219]), or mounted inside the tire cavity (Plotkin et al., 1980 [220]; Bergmann, 1980 [221]).

The advantages and disadvantage of the two measurement methods above are listed in Table 11.

Table 11: Comparisons between LDV measurement and accelerometer measurement

	Advantages	Disadvantages	References
LDV	(1) Laser does not influence the vibrations. (2) Laser can measure a fixed point near contact patch.	(1) Wheel assembly has to be stationary. (2) System is expensive. (3) Measurements can only be made in the direction of the laser.	215,221
Accelerometer (or micro-accelerometer [222])	(1) It can measure one material point on a tire. (2) It can measure tangential and axial vibrations.	(1) Tire has to be modified to attach the accelerometer, such as glue or mounting hole. (2) The mass of equipment can alter the vibration properties of the tire. (3) Measurement chain between the transducer and computer has to be used, such as slip rings or wireless system [192].	221,223,224

TVM is usually conducted indoors for high-frequency modal characterization of tires under both static (unloaded & loaded) and rotating conditions (Rocca et al., 2011 [225]). Generally radial and tangential vibrations (Larsson and Kropp, 1999 [226]; Kropp et al., 2001 [227]) are included in the vibration models while axial vibrations are often neglected, either by reducing to a two- dimensional system (Perisse and Hamet, 2000 [228]) or by assuming tread pattern and pavement texture are uniform in the axial direction (Fujikawa, et al., 1999 [229]).

2.4.2 Laboratory Drum (DR)

Laboratory drum method is also called roadwheel method. Generally, lab tests are able to precisely control test parameters, such as speed and loading, and eliminate unwanted factors maximally, such as atmospheric condition changes (Ullrich, 1993 [230]). This method can be conducted in a very fast and accurate manner. In the lab environment, a lot of other

sophisticated devices, such as accelerometer and laser-Doppler vibrometer, are practicable to be applied to conduct deeper investigations. SPL, sound intensity, or even sound field is relatively easy to be measured. As drum method is flexible, very few standards are presented, except JASO C606-81 in Japan (JASO, 1981 [231]), and GB/T 32789-2016 in China (GB, 2016 [232]).

However, laboratory techniques are by no means perfectly representative of actual pavements (Sandberg and Ejsmont, 1984 [233]). The curvature of the drum, driver noise, or the residuals on the drum might lead to unavoidable errors compared to in-situ TPIN (Sandberg, 1983 [234]; Ejsmont, 1982 [235]; Swieczko-Zurek et al., 2014 [236]). For example, GB/T 32789-2016 in China (GB, 2016 [232]) requires the drum surface be smooth steel. Based on the types of drum, this method is divided into three categories: outer rotating drum, inner rotating drum and outer stationary drum. The authors have never seen an inner stationary drum.

2.4.2.1 Outer Rotating Drum

In this configuration, a fixed wheel assembly rolls against the outside surface of the drum. Microphones are mounted at locations similar to CPX or OBSI method. The disadvantage is that in most cases the surface of the drum is purely smooth steel, which is greatly different from actual pavements. Even though replicas can be fabricated and mounted on the drum, the type of replicas are often limited to one or two idealized surfaces, such as ISO replica made of polyester and fiberglass (ISO, 1991 [237]). An example of the measurement setup is shown in Figure 43.

Figure 43: Laboratory Drum (DR) Outer Rotating Drum (Source from Tong et al., 2014 [238], Figure 5; reprinted with permission from Trans Tech Publications Ltd)

2.4.2.2 Inner Rotating Drum

In this configuration, a fixed wheel assembly rolls against the inside surface of the drum. Actual pavements are possible to be mounted on this kind of apparatus, but it is very time-consuming to construct (Nilsson, 1982 [239]). An example of the measurement setup is shown in Figure 44.

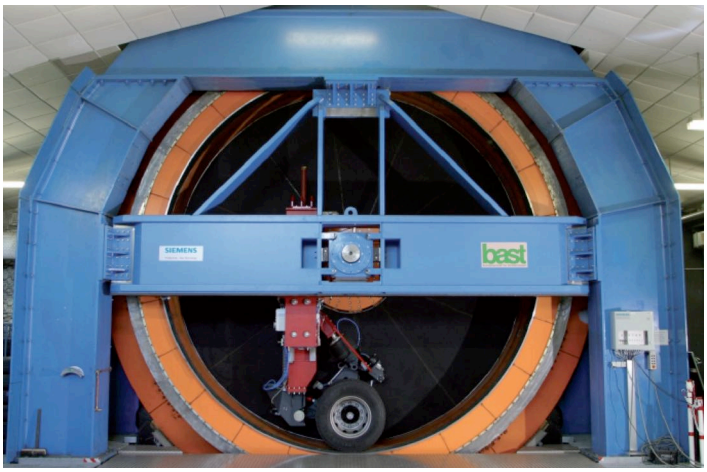

Figure 44: Laboratory Drum (DR) Inner Rotating Drum (Source from BASt website, [240], Federal Highway Research Institute's vehicle-pavement interaction test facility; reprinted with permission from M.Sc. Christopher Gerhard of Federal Highway Research Institute (BASt), Germany)

2.4.2.3 Outer Stationary Drum

This configuration includes a stationary drum with revolving wheel assemblies rolling

against it. The only apparatus of this type, as far as the authors are aware, is the Tire-Pavement Test Apparatus (TPTA) at the Institute for Safe, Quiet, and Durable Highways (ISQDH) at Purdue University (Bernhard and Thornton, 2003 [241]). This is also the only TPIN lab apparatus known in US (Rasmussen et al., 2007 [62]). The microphones are mounted to the arms to which the revolving tires are attached. An example of the measurement setup is shown in Figure 45.

Figure 45: Laboratory Drum (DR) Outer Stationary Drum (Source from Bernhard and Wayson, 2005 [66], Figure 6.9; reprinted with permission from Ms. Amy Miller of Asphalt Pavement Alliance, USA; photo courtesy of Ray W. Herrick Laboratories, Purdue University, USA)

The advantage of this drum is that it allows actual pavements samples to be quickly mounted or replaced and the pavements are also very easy to be fabricated (Dare, 2012 [213]). The disadvantage is that due to rotational force of the wheel assembly, the maximum speed is only 60 km/h, as compared to rotating drums that can reach over 200 km/h.

2.4.3 Near-field Acoustic Array Technology (NAAT)

NAAT method has been applied exclusively in the research domain with array or grid of microphones surrounding the tire measuring TPIN (mostly SPL) simultaneously to generate the sound field, as illustrated in Figure 46 (Park and Kim, 2001 [242]). Fields of sound pressure, active intensity, and reactive intensity fields can be computed (Ruhala and Burroughs, 1999 [243]). Reference microphones are needed to calibrate the magnitude and phase of the response

of all microphones.

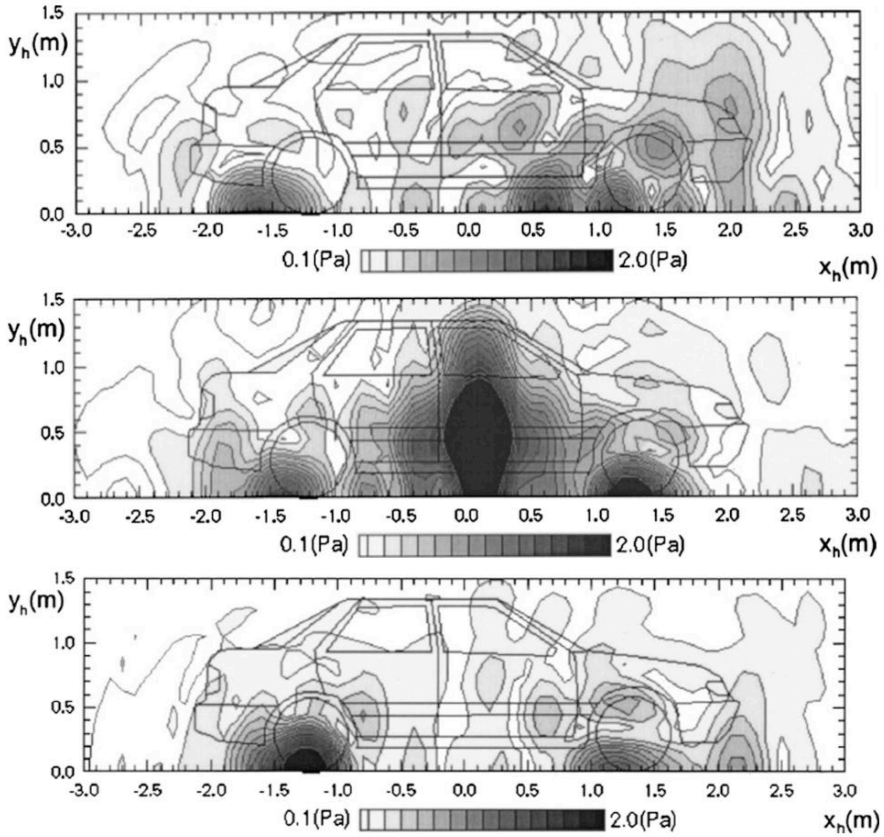

Figure 46: Tire/road noise distribution on a measurement plane around 500 Hz under three driving conditions: (a) accelerating according to ISO 362; (b) constant velocity of 55 km/h; (c) coast down from 55 km/h (source from Park and Kim, 2001 [242], Figure 12, Figure 14, Figure 15; reprinted with permission from AIP Publishing LLC)

Due to the lack of considerable development and streamlining, the use of this method is highly limited to lab environment or test track trailer rather than in-situ highway environment. In addition, there have been few literatures correlating the NAAT measurements with actual vehicle pass-by's. Theoretically, however, Spatial Transformation of Sound Fields (STSF) technique can be used to predict far-field sound. STSF is essentially a Near-field Acoustic Holography (NAH) technique coupled with a routine to propagate the sound to the far field using the Helmholtz integral (Donavan and Lodico, 2009 [139]).

Based on how to measure and localize sources on tires, NAAT can be divided into three

categories: (1) traditional near-field acoustical holography (NAH, efforts largely done at Penn State University [243,244] and Purdue University [245]), (2) temporal array (TA) techniques (summing signals with time delays to converge on source points), and (3) inverse frequency response function (IFRF) techniques (where path transfer function from artificial point sources to the array microphones are measured) (Dumbacher et al., 1995 [246]). A review of these methods is listed in Table 12. Examples of the measurement setup are shown in Figure 47 and Figure 49.

Table 12: Tests using NAAT method

Reference	Author	Year	Facility	Method	Microphone Array	Array Plane
[247]	Ginn	1990	Lab drum	NAH with STSF	A vertical rake of 12 with 20 horizontal increments	Parallel to the tire side wall, 70 mm outboard
[246]	Dumbacher et al.	1995	Lab drum	NAH [245]	A vertical rake of 16 with 32 horizontal increments	Parallel to the tire side wall, 50 mm outboard
[246]	Dumbacher et al.	1995	Lab drum	TA or beam forming	2 microphones spaced 800 mm apart traversed in a circular direction in 18° increments, thus 10 pairs	Parallel to the tire side wall, 1440 mm outboard
[246]	Dumbacher et al.	1995	Lab drum	IFRF	7 by 8 grid	Parallel to the tire side wall, 180 mm outboard
[248]	Hendricx and Mancosu	1999	Lab drum	IFRF	U-shaped fixture holding 16 microphones	Surrounding the tread band and sidewalls with each microphone 30mm from the nearest point of the tire
[249,250]	Ruhala and Burroughs	1997, 1998	Trailer	NAH	A vertical rake of 5 with 24 horizontal increments	Parallel to the tire side wall, 100 mm outboard
[243]	Ruhala and Burroughs	1999	Trailer	NAH	A vertical rake of 9	Three planes (front, rear and side), 120 mm from tire
[251]	Kim and Lee	2003	Lab drum	NAH with STSF	A vertical rake of 12 with 20 horizontal increments	Parallel to the tire side wall, 70 mm outboard
[252]	Ih and Oey	2012	Lab hammer impact	NAH	17 microphones surrounding tread (7) and side wall (5 each side), sweep around the tire with 44 increments	10 mm from tire
[253]	Vercammen et al.	2015	Lab drum	NAH	Two techniques: (1) sound pressure measurements with 7 mic's around tire; (2) LMS Soundbrush, sound intensity measurements with a scanning intensity probe (4 phase-matched mic's)	Half-hemisphere (r = 1.5 m) around the tire/road contact point

Figure 47: Near-field Acoustic Array Technology (NAAT) Trailer (Source from Ruhala and Burroughs, 1999 [243], Figure 1 ; reprinted under fair use provision)

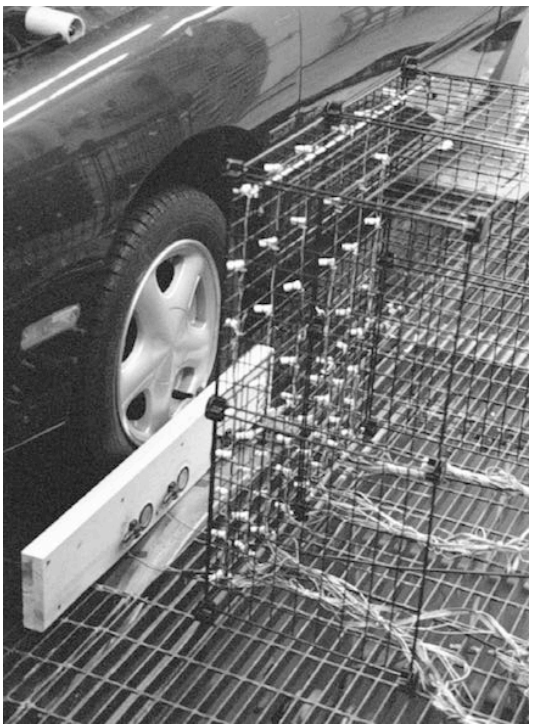

Figure 48: Near-field Acoustic Array Technology (NAAT) Lab Drum (Source from Dumbacher et al., 1995 [246], Figure 9 ; reprinted under fair use provision)

2.4.4 Novel Pass-By (NPB) with Novel Close Proximity (NCPX)

This integrated method is used to measure the sound power level (PWL, SWL or L_W) of TPIN or combined noise of TPIN and power train noise (Cho and Mun, 2008 [254]). If the vehicle coasts by, only TPIN will be measured (Cho and Mun, 2008 [255]). PWL is independent

of the environment in which flowing traffic is located. However, there is little instrumentation available for measuring PWL directly. Most suggested techniques are based on SPL conversion and correction factor (Bloemhof, 1986 [156]; Moir and Stevens, 1974 [256]; ISO, 1981 [257]; Jacobsen, 1992 [258]; Fahy, 1997 [259]), which is also the NPB with NCPX method is based on. An example of the measurement setup is shown in Figure 49.

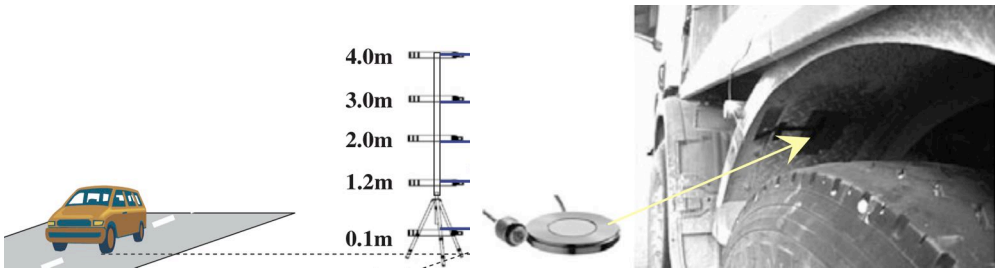

Figure 49: Novel Pass-By (NPB) with Novel Close Proximity (NCPX) (Source from Cho and Mun, 2008 [254], Figure 1 and Figure 3; reprinted with permission from Elsevier)

The measurement procedure is as follows (Cho and Mun, 2008 [254]).

(1) NPB method is used to obtain the A-weighted maximum SPL ($L_{pA\mathrm{max,NPB}}$). Similar to SPB, the microphones are set up at the roadside 7.5 m from the center of the lane in which the individual vehicle is driven. In addition, to evaluate the effect of noise directivity, five microphones are installed at different heights.

(2) NCPX method is used to measure the A-weighted square mean value of the near-filed TPIN sound pressure ($L_{pA\mathrm{avg,NCPX}}$). The equipment is a surface microphone, which can be directly mounted on the vehicle's wheel arch or the flat surface located over the truck tires of a tandem axle; this location allows the maximum elimination of the influence of the turbulent airflow.

(3) The total attenuation (A_{total}), such as geometrical divergence, atmospheric absorption, ground effect and screening structures, is calculated based on ISO 9613-2 (1996) [260].

(4) Finally, L_W can be determined using the relationships of $L_{pA\mathrm{max,NPB}}$, $L_{pA\mathrm{avg,NCPX}}$ and A_{total}.

$$L_W = L_{pA\mathrm{avg,NCPX}} + C \tag{13}$$

where C is correction factor, which is constant and converts SPL to PWL. C can be identified at the reference microphone location where directivity correction (D_I) can be set to

zero.

$$C = L_{pA\max,\mathrm{NPB}} - L_{pA\mathrm{avg},\mathrm{NCPX}} + A_{total} - D_I \tag{14}$$

where $L_{pA\max,\mathrm{NPB}}$, A_{total} and D_I (set to zero) are measured at reference location.

2.4.5 Far-field Acoustic Array Technology (FAAT)

Like NAAT, Far-field Acoustic Array Technology utilizes array of microphones to generate sound field, except that the microphones are located on the roadside instead of on-board and the measurement scope is the entire vehicle. It provides a solution to accurately locating and quantifying the pass-by noise source of the running vehicle.

As far as the authors are aware, three specific methods of FAAT have been published: Pass-by Acoustic Holography (PAH) method (Yang, 2011 [56]), Pass-by Noise Beamforming (PNB) method (Fonseca and Gerges, 2010 [261]; Zavala et al., 2013 [262]) and moving frame acoustic holography (MFAH) (Park and Kim, 2001 [242]). An example of the measurement setup is shown in Figure 50 and Figure 52.

Figure 50: Far-field Acoustic Array Technology (FAAT) Pass-by Acoustic Holography (PAH) (Source from Yang et al., 2011 [56], Figure 5; reprinted with permission from Elsevier)

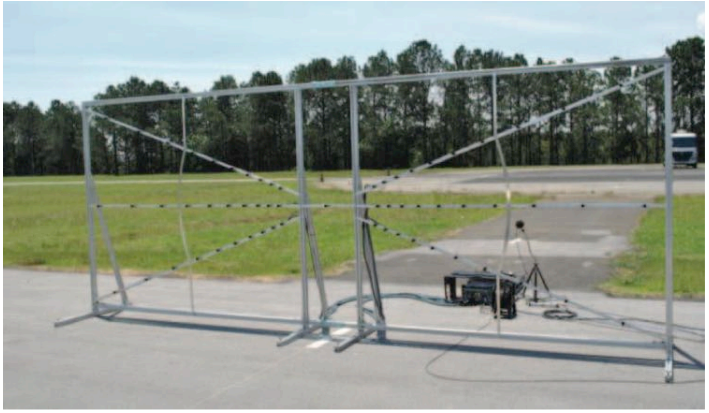

Figure 51: Far-field Acoustic Array Technology (FAAT) Pass-by Noise Beamforming (PNB) (Source from Zavala et al., 2013 [262], Figure 9 ; reprinted under fair use provision)

PAH system utilizes acoustic holography method coupled with nonlinear time mapping to eliminate the Doppler effect effectively in the time domain. The effective sound pressure distribution is reconstructed on the surface of a running vehicle. The method is also validated by the tests with known moving speakers (Yang, 2011 [56]). The applicable vehicle speed is limited to 0.2 Ma (244 km/h).

Beamforming is an acoustic imaging technique that can map noise sources by differentiating sound levels based on the direction from which they originate (Lustberg, 1993 [263]; Tanaka, 2004 [264]). PNB method aims to evaluate the noise source distribution of the entire pass-by vehicle. The system is composed of low cost electret microphones mounted in a metallic array that are connected by a coaxial cable to the acquisition system (Fonseca and Gerges, 2010 [261]) coupled with advanced tracking systems. The same research group later presented a modified technique based on generalized Inverse and an array of microphones optimized for low frequencies, showing advantages compared to the conventional method (delay-and-sum algorithm) and obtaining better separation of coherent sources with better dynamic range in a wide frequency range (50 Hz - 7 kHz) (Zavala et al., 2013 [262]).

Moving frame acoustic holography (MFAH) (Park and Kim, 2001 [242]) arranged 16 microphones in a vertical array spaced 10 cm with the lowest microphone 5 cm above the ground. It visualized the sound intensity maps of tire and engine noise during pass-by test. It also employed magnitude correction method.

2.4.6 Traffic Noise Auralization (TNA)

This method developed in France generates real time synthetic TPIN noise and engine noise signals at the source based on the vehicle speed and acceleration data in the non-stationary traffic (Maillard and Jagla, 2012 [265]). Propagation effects are then applied to predict the pass-by noise at specific positions. As far as the authors are aware, it is probably the most advanced model of traffic noise (Dutilleux et al., 2008 [266]; Dutilleux et al., 2010 [267]; Salomons et al., 2010 [268]; van Maercke and Defrance, 2007 [269]; Can et al., 2008 [270]) and can be well served as an evaluation tool for urban planning (EU, 2009 [271]; EU, 2012 [272]). An example of the measurement setup is shown in Figure 52.

Figure 52: Traffic Noise Auralization (TNA) (Source from Maillard and Jagla, 2012 [265], Figure 2; reprinted under fair use provision)

Auralization synthesizes an artificial sound environment that is exactly the same as the target sound field that perceptually you cannot distinguish it is virtual or real (Kleiner et al., 1993 [273]; Funkhouser et al., 2004 [274]; Funkhouser et al., 1998 [275]; Laine et al., 2009 [276]). In the case of traffic noise, the auralization process involves three main steps: (1) the synthesis of the source signals (such as TPIN and engine noise), (2) their filtering to model the sound propagation along a single contribution and (3) the spatial rendering of each individual contribution.

The first step requires real world sound samples. TPIN and engine noise signal samples are obtained either from pass-by audio recordings of individual vehicles (Nilsson et al., 2011 [277]; Kaczmarek, 2007 [278]; Maillard and Martin, 2008 [279]) or recorded directly at the source (contact patch for TPIN and engine compartment for engine noise) (Jagla et al., 2012 [280]; Maillard, 2009 [281]). For the latter one, the two sound components are sampled at different vehicle speed and engine speed with gear position. Auralization is generated by overlapping and adding the selected two sound samples according to the target speed in the real world. Based on this principle, hundreds of vehicles in the traffic can be auralized at the same time.

In the first step, calibration needs to be done to make sure the output signal of the synthetic noise represents the sound pressure of the target source in free field at a distance of 1 m.

The second step feeds the synthesized signal to a delay line modeling the propagation delays of each path. The delayed signal of a given propagation path together with the original source noise is then fed to a FFT-based octave band equalizer with gains calculated from the propagation path and source directivity data.

The third step feeds the equalized propagation path contributions to the 3D sound module and then mixes all contributions to generate a multi-channel output signal suited for the exact representation of the target sound field. It shows good correlation with actual pass-by noise (Maillard and Jagla, 2012 [265]).

A similar method, Traffic Noise Synthesizer (TNS), was developed in Germany [282] and has been successfully applied in auralization of noise generated by electric and combustion-powered scooters and the subjective evaluation of the resulting annoyance (Fiebig et al., 2012 [283]).

Auralization model was also used to investigate structure-borne tire noise in vehicle to correlate recordings and simulations based on the hub forces (Löfdahl et al., 2015 [284]).

A more relevant technique of tire noise auralization (TNA) is the substitution monopole models for tire noise sound synthesis (Berckmans, 2010 [285]). The running tire was modeled by a monopole distribution covering the static tire. The relative phase and magnitude of these monopoles were quantified by an inverse ASQ technique. It was shown that the dominant factor in the accuracy of the model is the number of monopoles in the model.

Auralization might be categorized into two types: (1) rough sound sketch without details; (2) precise auralization indistinguishable from a real recording (Nykänen, 2008 [73]).

2.4.7 Summary

The lab measurement techniques described above are summarized in Table 13. The measurement equipment is various and flexible, such that no standards have been found except for laboratory drum method. However, multiple sound parameters are possible to be measured, including the sound field. In addition, the effect of environmental parameters, such as air temperature and wind speed, can be greatly reduced if the test is conducted in the lab.

Table 13: Summary of lab measurement techniques

No.	Method	Acronym	Current Standard	First Version	Equipment	Measured Parameter	Main Noise Source	Category	Advantage	Disadvantage	References
1	Tire Vibration Measurements	TVM	N/A	Reiter and Eberhardt (1974) [286]	LDV or accelerometer	Vibration velocity	One tire	N/A	Analysis of TPIN mechanisms	Interpretation of structure borne TPIN only	213
2	Laboratory Drum	DR	JASO C606-81 [231]	JASO (1981) [231]	Various	Various	One tire	Lab, near/far-field	Precise control of parameters	Not real pavements	62,213,230,233–237,239,241
3	Near-field Acoustic Array Technology	NAAT	N/A	Ginn (1990) [247]	Mic array	Generally $L_{p\mathrm{avg}}$	One tire	Lab/trailer, near-field	Capable of detecting TPIN source	Expensive, no correlation to CPB reported	243,246–252
4	Novel Pass-By with Novel Close Proximity	NPB with NCPX	N/A	Cho and Mun (2008) [254]	5 Mic's, 1 surface mic	$L_{p\mathrm{max}}$, $L_{p\mathrm{avg}}$, L_W	One tire	On-board/road side, near/far-field	Sound power is independent of environment	Complex procedure, correction factor	254,255
5	Far-field Acoustic Array Technology	FAAT	N/A	Fonseca and Gerges (2010) [261]	Mic array	$L_{p\mathrm{max}}$	Vehicle	Roadside, far/sound field	Capable of distinguishing vehicle noise sources	Doppler effect limitation	56,261–264
6	Traffic Noise Auralization	TNA	N/A	Maillard and Jagla (2012) [265]	Auralization equipment	L_p	Traffic	Virtual sound	Capable of non-stationary traffic evaluation	TPIN not isolated	265

"First Version" refers to the first standard if the method has been standardized; otherwise it refers to the first measurement attempt.
Some of the references in "First Version" are the same as in "Current Standard", except the published year.
For the column of "Main Noise Source":

"One tire" means the main noise comes from the only tested tire on which the testing equipment is mounted.
"All tires" means the main noise comes from all the tires (usually four) of the tested vehicle or trailer.
"Vehicle" means the main noise comes from the tested vehicle (TPIN, powertrain, air intake and outlet and aerodynamics noise).
"Traffic" means the main noise comes from all the vehicles on the road.

The advantage and disadvantage are evaluated in terms of TPIN investigation.

2.5 Relationship between Different Measurement Techniques

Several studies have attempted to discover relationships between the different measurement techniques of TPIN [7,101,127,187,234–236]. Some of relevant studies are listed in Table 5, Table 6, and Table 14. Generally, it is shown that measurement techniques within the same category have better correlation with each other than those outside the category. For example, CPX (near-field) has better correlation with OBSI (near-field, $R^2 = 0.93$) than CPB (far-field, $R^2 = 0.79$) (Donavan and Lodico, 2009 [139]). This is largely due to the uncontrolled propagation environment for far-field measurements (Donavan et al., 2013 [45]), especially for porous pavements (Donavan, 2011 [287]).

It stands to reason that standardized methods have better correlation with each other thus are more valuable for information exchange between studies than non-standardized methods. Specifically, it was found that OBSI data could predict CPB data for a variety of pavement types within 0.5 dB on average when considering overall sound pressure levels (OASPL) (Donavan and Rymer, 2004 [193]), and their frequency spectrum correlates well too, better than CPX, as shown in Figure 53 (Donavan and Lodico, 2009 [139]). Donavan et al. (1998) [4] found the same rank ordering of tires using OBSI and CB methods. The coefficient of determination R^2 between OBSI and Pass-by Noise (PBN) is generally over 0.95 (see Table 9), while R^2 between CPX and PBN is usually only 0.8 (see Table 14). The laboratory drum method (DR) shows no better correlation with PBN either with R^2 around 0.8 (see Table 14). As a result, the authors would argue OBSI seems to be the best trade-off method taking both accuracy and cost effectiveness into account, although each method has its own benefits and drawbacks and should be carefully selected based on practice. However, the principle is to try to use a single technique to reduce measurement errors. In addition, the reason why OBSI has good correlation with PBN is that tire noise has a good directivity sideways, as illustrated in Figure 54 (Park and Kim, 2001 [242]).

Table 14: Relationships between different methods

Reference	Author	Year	Methods	Coefficient of Determination R^2
[288]	Sandberg	1997	CPX versus SPB	0.80
[289]	Steven et al.	2000	CPX versus SPB	0.80
[290]	Konishi et al.	1996	DR versus CB	0.29 for Safety Walk (very smooth drum)
[7]	Sandberg & Ejsmont	2002	DR versus CB	0.98 for 35 km/h 0.77 for 50 km/h 0.81 for 80 km/h
[171]	Sandberg & Ejsmont	2000	CPX versus DR	0.65 for SMA 8 versus ISO replica (medium) 0.86 for DAC 16 versus GRB-S replica (smooth) 0.84 for CS 12 versus GRB-R replica (rough)

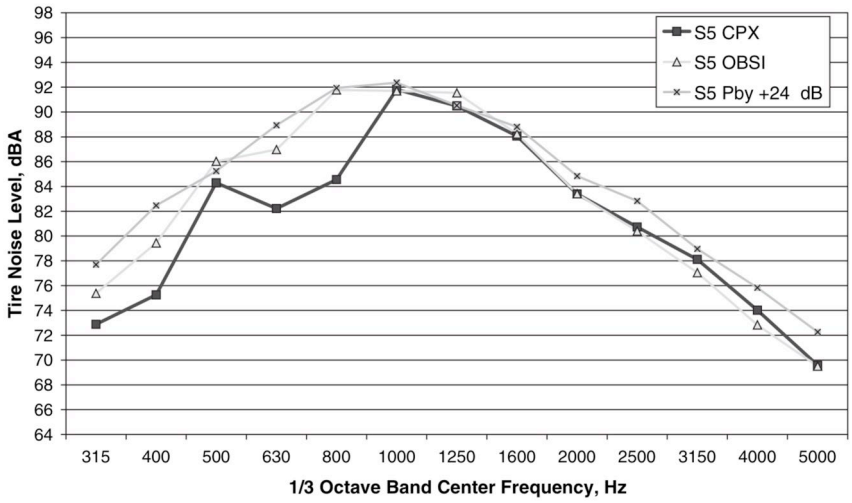

Figure 53: Comparison of spectra for CPX, OBSI, and CPB levels with 24 dB added for Dunlop tire on Section AC S5 at 45 mph (source from Donavan and Lodico, 2009 [139], Figure 7; reprinted with permission from Dr. Paul Donavan of Illingworth and Rodkin, Inc., USA)

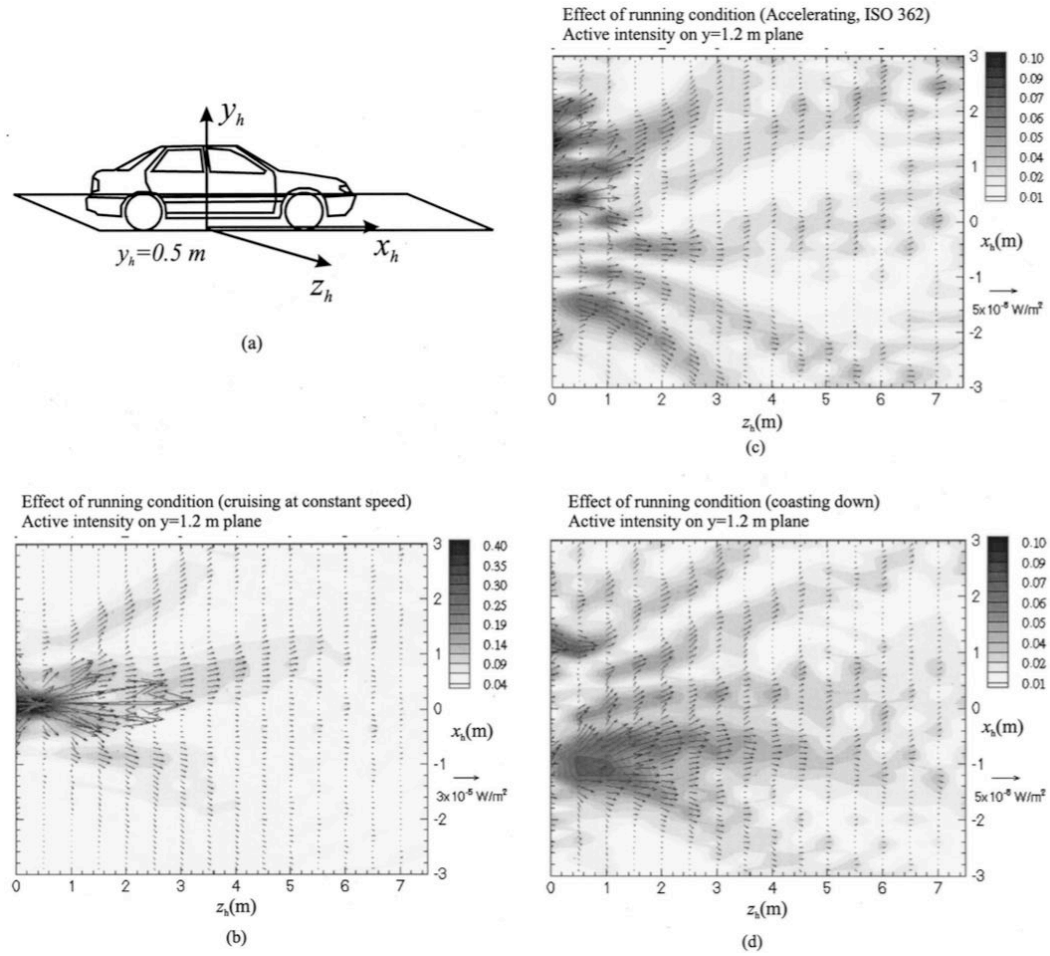

Figure 54: The propagation of active intensity and sound pressure radiated by the special pattern tire to the far field. (a) The active intensity (*x* and *z* direction) and sound pressure are visualized on *y* = 0.5 m plane. (b) Constant velocity condition. (c) Accelerating condition. (d) Coast down condition. (Source from Park and Kim, 2001 [242], Figure 16; reprinted with permission from AIP Publishing LLC)

The procedure of predicting far-field TPIN from near-field levels is essentially an extrapolation process (Bravo et al., 2012 [57]). The difference between the near-field levels L_{nf} and the levels at the receiver position L_{ff} is also called propagation filter ΔL, expressed as

$$\Delta L = L_{nf} - L_{ff} \tag{15}$$

The four individual noise sources corresponding to the four tires are replaced by one equivalent source situated at the center of the vehicle, as seen in Figure 55. The near-field levels due to each tire source can be expressed as

$$L_{nf,i} = L_{W,i} - 10\log_{10}\left(4\pi r_{nf,i}^2\right) + Att_{nf,i} \tag{16}$$

where L_W is the sound power level due to one tire, r_{nf} is the distance from the tire to the near-field receiver, Att_{nf} is the attenuation level in the near-field propagation path, and i is the tire index that can be 1, 2, 3 or 4. Similarly, the sound level at the far-field receiver corresponding to the equivalent source can be expressed as

$$L_{ff} = L_{W\mathrm{eq}} - 10\log_{10}\left(4\pi r_{eq}^2\right) + Att_{ff} \tag{17}$$

where $L_{W\mathrm{eq}}$ is the sound power level due to the equivalent source (four tires), r_{eq} is the distance from the equivalent source to the far-field receiver, and Att_{ff} is the attenuation level in the far-field propagation path.

In addition, the levels at the far-field receiver due to each tire can be expressed as

$$L_{ff,i} = L_{W,i} - 10\log_{10}\left(4\pi r_i^2\right) + Att_i \tag{18}$$

where r is the distance from each tire to the far-field receiver, and Att is the attenuation level in the propagation path. Lastly, the propagation filter can be calculated as [291]

$$\Delta L = Att_{nf} - Att_1 - 20\log_{10}\left(\frac{r_{nf}}{r_1}\right) - 10\log_{10}\left(1 + \left(\frac{r_1}{r_3}\right)^2 \cdot 10^{\frac{Att_3 - Att_1}{10}}\right) - 10\log_{10}(2) \tag{19}$$

which is for the overall sound level. The corresponding frequency spectrum is shown in Figure 56. It can be seen that the difference between near-field and far-field level varies at different frequencies for different pavements.

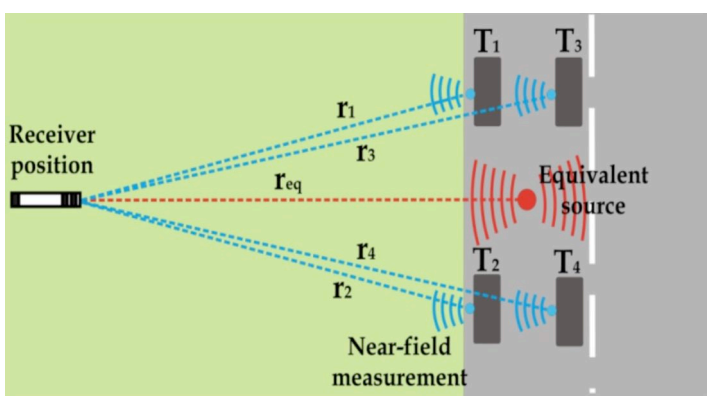

Figure 55: Representation of the physical configuration for the extrapolation of the signals acquired by the microphones in the proximity of the tire (source from Bravo et al., 2012 [57], Figure 4; reprinted with permission from Ms. Beth Darchi on behalf of ASME)

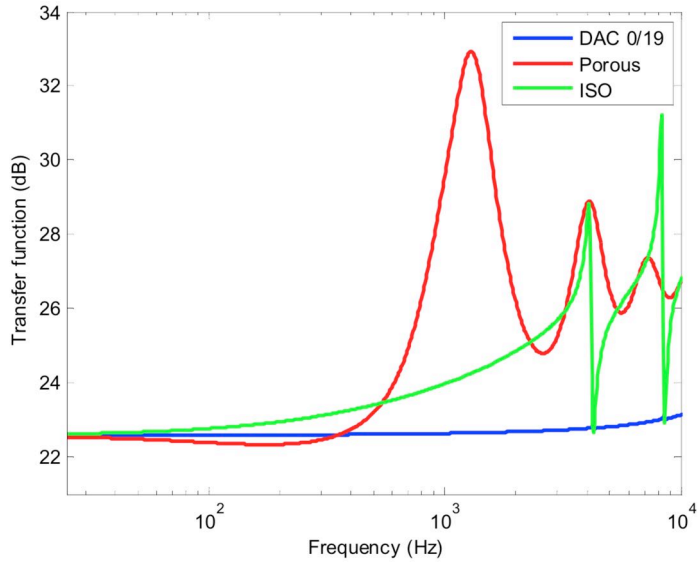

Figure 56: The transfer function between the microphone close to the tire and the receiver position for different propagating surfaces (source from Bravo et al., 2012 [57], Figure 6; reprinted with permission from Ms. Beth Darchi on behalf of ASME)

2.6 Conclusions

The measurement techniques on TPIN have evolved from simple overall sound pressure level test, to the more accurate on-board sound intensity test, then to the sound field holography in the lab. Each technique has advantages and disadvantages. The roadside measurement is very easy, but not accurate or informative; the lab measurement is very flexible and inspiring, but usually unaffordable in equipment and sometimes fails to represent the actual driving conditions on the road; the on-board measurement is intermediate between the above two. In summary, the selection of the measurement technique should be based on the equipment available, measurement goals, and test environment.

3 Physical Mechanisms

3.1 Introduction

Tire-pavement interaction occurs under fairly harsh and complex conditions, inherently making noise mechanisms very difficult to identify. Numerous mechanisms take place simultaneously, to varying degrees, depending on specific tire-pavement combination (Rasmussen et al., 2007 [62]). In this work, these physical mechanisms are divided into three categories: generation mechanisms, amplification mechanisms and attenuation mechanisms.

Different mechanisms take place at different tire components, all as noise sources contributing to the total tire-pavement interaction noise (TPIN). A summary of dominant frequencies for different TPIN components is listed in Table 15.

Table 15: Dominant frequencies for different TPIN components

	Dominant Frequency [Hz]	References
Leading Edge of Contact Patch	500-2000	250,292
Trailing Edge of Contact Patch	500-2000	292–294
Tire Side Wall	500-1000	252,295
Rim	200-400	296
Tire/Rim Assembly	220-280	297
Wheel Housing	500-600	298
Interior	250	299,300

It should be noted that even though a large body of literature has attempted to uncover and distinguish these mechanisms since mid 1970's (Reiter and Eberhardt, 1974 [217]; Bergmann, 1980 [221]; Plotkin et al., 1980 [220]), they are by no means clear-cut. Too many speculations still exist and never reach an agreement. As Sandberg and Ejsmont (2002) [7] indicated, "perhaps the most obvious example of risks of a certain bias or too much speculation is the topic of generation mechanisms, sometimes leading to rather heated discussions." In addition, the mechanisms themselves may have changed over time due to changes in tire and pavement technology (Dare, 2012 [213]). However, all the possible mechanisms are detailed below to the best knowledge of the present author. A summary table could be found in Table 20 at the end.

3.2 Generation Mechanisms

Generation mechanisms are fundamental mechanisms that make sound and explain where sound begins. Sound pressure maps (a damped progressive wave field) indicate that TPIN mainly generates in the vicinity of the applied force on the contact patch (Lee et al., 2000 [300]).

The noise generated includes two types: structure-borne noise and airborne noise [301]. The former corresponds to impact mechanism and adhesion mechanism; the latter corresponds to air displacement mechanism.

Structure-borne noise is induced by structural vibrations, of which the wave types existing in a vibrating tire have three forms (Larsson and Kropp, 1999 [226]; Larsson and Kropp, 2002 [302]): (1) membrane/bending or flexural waves at low frequencies (dominant between 500-1000 Hz) due to the pre-stress in the material (Ishihama and Kagaya, 2012 [303]); (2) longitudinal waves like in coil spring; and (3) shear waves where the stiff steel belt moves against and parallel to the soft rubber tread (Erixon, 1998 [304]). The shapes of the three wave types are shown in Figure 57 (Larsson and Kropp, 1999 [226]). Heckl (1986) [13] also noted that the motion of a tire surface consists of three wave types and each type of wave is running in the positive or negative direction allows the representation of the whole vibration pattern in six terms.

Figure 57: The three wave types considered in the model (rings represent points in the rubber tread layer and stars represent points in the stiff belt layer) (source from Larsson and Kropp, 1999 [226], Figure 3; reprinted under fair use provision)

For tire modeling, Heckl (1986) [13] developed a tension-stiffened, flexural ring model to predict the wavespeeds and modes of tire vibrations. The sidewalls were modeled as elastic

support to the ring. Heckl (1986) [13] showed that the speed of longitudinal waves in the ring material is given by $c_L = (E/\rho)^{1/2}$ where E is Young's modulus and ρ is density; the ring frequency is given by $f_0 = c_L/2\pi a$ where a is the radius of the tire. The circumferential waves in the tire tread were validated by Kropp (1989) [305]. However, the one-dimensional ring bending model was limited below 400 Hz for the prediction of drive point admittance of the tire tread. Above 400 Hz, it was better predicted by two-dimensional plate waves. Lee and Ni (1997) [306] included bending waves and in-plane (extension/shear) waves and indicated that in-plane waves should be important at higher frequencies.

3.2.1 Impact (Shock)

Impact mechanism is also called shock mechanism, which is the sudden impulse contact between tire tread and pavement. This is analogous to a rubber hammer striking against a surface. The resulting sound can be seen to come from hundreds of small hammer strokes each second (Rasmussen et al., 2007 [62]). At the leading edge, impact mechanism occurs as the tread element is pushed in toward the tire center; at the trailing edge, the release of tread element can be considered as an inverse impact (Negrus and Teodorescu, 2002 [298]; Iwao and Yamazaki, 1996 [307]). The local deformations of the tread can cause air volume displacement acting as monopoles (Ronneberger, 1985 [308]; Ronneberger, 1989 [309]).

This mechanism is caused by the inhomogeneities of the tire tread and/or the pavement surface. If the pavement is extremely smooth (low macrotexture), it will be mainly tread impact as tread blocks/elements hit the pavement. Likewise, if the tire has smooth pattern, it will be mainly texture impact as the pavement asperities impact the tire tread. However, most of the time, these two mechanisms occur simultaneously and cannot be separated. It stands to reason that there will be little impact if both tires and pavements are smooth.

Impact-induced vibrations are responsible for a major source of TPIN. The frequency of impact depends on the distance between the tread elements or the texture asperities as well as the vehicle speed.

$$f = \frac{v}{\lambda} \tag{20}$$

where f is impact frequency, v is vehicle speed and λ is the distance/wavelength for tread or texture periodicities. f is usually below 1000 Hz (Nilsson et al., 1980 [214]; Descornet and

Sandberg, 1980 [310]), as shown in Table 16 (Sandberg and Ejsmont, 2002 [7]). An unexpected frequency was also found being 14th times the tire rotation frequency, corresponding to the tire molding repetitions (Saemann and Schmidt, 2002 [311]).

Table 16: Typical impact frequencies (source from Sandberg and Ejsmont, 2002 [7], Table 7.2; reprinted with permission from Dr. Ulf Sandberg of VTI, Sweden)

		λ [mm]	Speed v [km/h]				
			30	50	70	90	110
Tread Impact	Car Tire	20-40	210-420	350-700	490-970	625-1250	770-1540
		Average: 30	275	465	650	830	1025
	Truck Tire	45-65	130-185	215-310	300-430	380-560	470-680
		Average: 55	150	250	350	450	550
Texture Impact		8-20	420-1040	700-1740	970-2430	1250-3125	1540-3825
		Average: 14	600	990	1390	1790	2180

Tread pattern and pavement macrotexture (smoothness/roughness) play great roles in the impact-induced vibrations. Tire rubber hardness (Doan et al., 1995 [312]) and pavement mechanical impedance (or stiffness) (Nilsson, 1982 [239]; Sandberg and Goubert, 2011 [313]) are another two main influencing factors. The induced vibrations at the tread band can be classified into different wave types or modes (Kim and Bolton, 2001 [314]; Campanac et al., 1999 [315]; Yum and Bolton, 2004 [316]; Yum et al., 2006 [317]), and can exist in the radial, tangential, or axial directions as listed in Table 17 (Bergmann, 1980 [221]). Vibrations can also be excited by circumferential tube resonances (Ruhala and Burroughs, 1998 [250]) at the tire sidewall (Reiter and Eberhardt, 1974 [217]; Keltie, 1982 [223]). These vibrations are commonly measured with embedded accelerometers (Dare, 2012 [213]).

Table 17: Impact-induced vibrations

Direction		Importance	Measurement Device	Notes
Tread Band	Radial	High	Laser-Doppler vibrometer (LDV) or embedded accelerometers	(1) Radiation (above 500 Hz [215]) limited to around contact patch (Yum et al., 2006 [317]; Kuijpers and van Blokland, 2001 [318]) due to damping within tire carcass (Eberhardt, 1980 [319]) (2) Ineffective radiator below 400 Hz due to flexural mode shapes of the tire (Yum and Bolton, 2004 [316]; Yum et al., 2006 [317]) (3) Only low ordered radiation modes (first four, either s-modes or a-modes) are efficient radiators between 0-1600 Hz (Ji and Bolton, 2015 [320]) (4) Reduction methods: soft tread compound (Sandberg, 2005 [321]), thin or worn tread (Sandberg and Glaeser, 2008 [322]), compliant pavement (Nilsson, 1982 [239]) (5) There is a large radial deceleration as it enters the contact area and a very large acceleration as it leaves it, however, it does not radiate efficiently; the accelerations in the middle of contact patch are small but radiated efficiently (Heckl, 1986 [13]).
	Tangential	Medium	Embedded accelerometers	(1) Difficult to apply LDV measurements near the contact patch (2) Also resulting from stick/slip mechanism (a.k.a. friction) (Larsson, 1999 [323])
	Axial	Low	Embedded accelerometers	(1) Levels much lower than those in other directions (Bergmann, 1980 [221]; Dugan and Burroughs, 2003 [224]) (2) Texture measurements in the axial direction unnecessary for modeling (Hamet and Klein, 2000 [324]; Wullens et al., 2004 [325]) (3) Excited by pavement that is not uniform axially (Dare, 2012 [213])
Side Wall		Fair	Laser-Doppler vibrometer (LDV) or embedded accelerometers	(1) Important between 500-1000 Hz (Eberhardt, 1984 [326]; Donavan and Oswald, 1980 [179]; Ruhala and Burroughs, 2008 [292]) (2) Loudest near the trailing edge (Phillips et al., 1999 [327]) (3) Little or no sound radiation (Plotkin et al., 1980 [220]) other than adjacent to contact patch

In fact, tire side wall acts like a low pass filter and attenuates vibrations over frequencies of 1000 Hz (cut-off frequency [328]) due to its damping characteristics, as shown in Figure 58 (Iwao and Yamazaki, 1996 [307]). It was concluded that sidewall vibrations are largely dependent on tread vibrations and the contributions to emitted sound are about 10 dB lower than tread band (Eberhardt, 1981 [329]). The acceleration levels on the sidewall were also measured to be 10 dB lower than in the tread center (Doan et al., 1995 [312]). Bergmann (1984) [330] showed that the radiation from the side walls of a tire is of minor importance. In addition, the sound radiation abilities of shoulder regions are between tread band and sidewall (Doan et al., 1995 [312]). Axial motion as well as motion of the side walls is of minor importance (Jennewein and Bergmann, 1985 [331]).

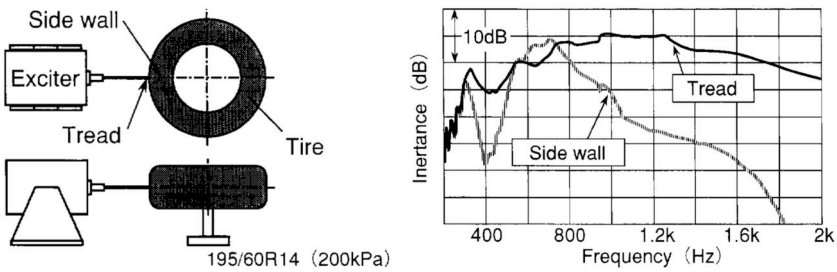

Figure 58: Dynamic characteristic of tire vibration (source from Iwao and Yamazaki, 1996 [307], Figure 8; reprinted under fair use provision)

The typical sidewall and tread band accelerations is shown in Figure 59 (Keltie, 1982 [223]). It was seen that the vibrations in the sidewall is centered at the contact region while the vibrations in the tread band is centered at the entry and exit of the contact region.

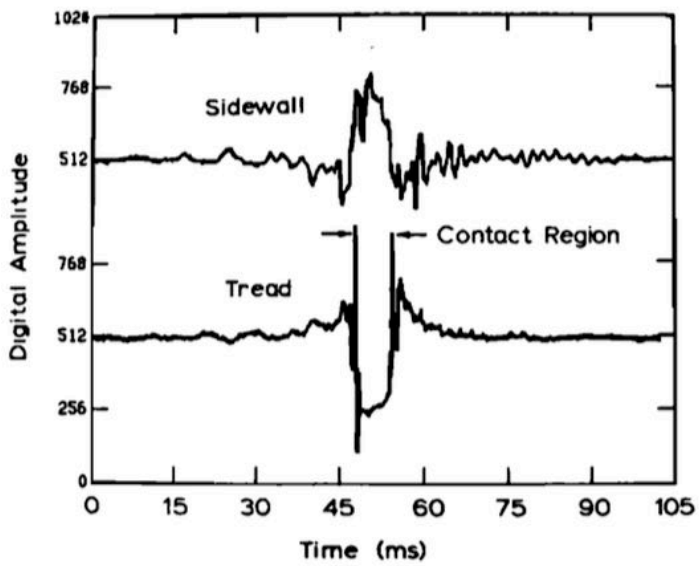

Figure 59: Tire sidewall and tread region acceleration signals versus time for approximately one tire revolution (source from Keltie, 1982 [223], Figure 1; reprinted with permission from AIP Publishing LLC)

It is worth noting that all the vibrations mentioned above are related to tire. Pavement is also vibrated when impacted by the tire, but nearly unnoticeable due to its much larger stiffness than tire. Thus it is argued that pavement is not a significant contributor to TPIN in any way.

Beckenbauer et al. (2008) [332] considered the impact mechanism as the varying contact

forces exciting the tire to vibrations. As such, the spectrum of contact pressure in the frequency domain was analyzed as an input parameter.

Some researchers (Liu et al., 2008 [333]; He et al., 2011 [68]; Chen et al., 2013 [99]; He et al., 2011 [97]; SungWook et al., 2012 [98]) used Wavelet Transform (WT) to analyze tread pattern noise signals in time-frequency domain instead of conventional Fourier Transform (FT) or Short-Time Fourier Transform (STFT). Wavelet Transform is more efficient to deal with and identify non-stationary signal and pattern noise has impulsive characteristics since it's generated by tread block impact. Wavelet Transform can provide adjustable window size to obtain more time resolution in the high frequency, and more frequency resolution in the low frequency range, thus more information of signal can be acquired (SungWook et al., 2012 [98]).

It was reported that the input power into tire vibrations due to impact has cubic dependence on the speed (Heckl, 1986 [13]; Bremner et al., 1997 [334]).

Heckl (1986) [13] indicated that radiation of tire vibrations is a very inefficient process (given a certain vibratory velocity a tire radiates at least one order of magnitude less sound than a thick plate of the same area) with a strong "hydrodynamic short-circuiting" effect because the wavelengths of waves on tires are, apart from the longitudinal mode, much smaller than the wavelengths in air (speed of sound in air = 340 m/s; on a tire = 60-100 m/s).

Tread impact noise and texture impact noise can be separated if signal-averaging methods are applied (i.e. if the sound signals are added over a long time in the rhythm of the tire revolutions or in the rhythm of the test drum revolutions) (Walker, 1984 [335,336]).

Rochoux and Biesse (2010) [337] observed that the speed effect of texture impact has an influence at a power of approximately 2 using indenter experiments. High frequency noise is higher for the stiffer tire than for the softer one. It was also found that the sharper the pavement texture is, the lower noise will be generated. The maximum force developed under the impact of the spherical indenter was found to be

$$F_{\max} = \left[\frac{4}{3\left(1-v^2\right)}\right]^{\frac{2}{5}} \left(\frac{5}{4}\right)^{\frac{3}{5}} R^{\frac{1}{5}} E^{\frac{2}{5}} m^{\frac{3}{5}} V^{\frac{6}{5}} \tag{21}$$

where v is rubber Poisson's ratio, R is the radius of spherical indenter, E is rubber stiffness, m is indenter mass, V is speed.

3.2.2 Adhesion

Adhesion mechanism happens mostly when the pavement texture is smooth (low macrotexture), including Stick/Slip for harsh pavement (high microtexture) and Stick/Snap for polished pavement (low microtexture).

3.2.2.1 Stick/Slip (Friction)

As the rubber tread element enters the contact patch, it will be deformed stick with the pavement due to the normal tire force, but also periodically slip once tangential force reaches the critical limit (static friction coefficient) [62]. Shear forces are built up in the tread blocks and released as the treads leave the contact patch (Ejsmont, 1990 [338]), free vibration of tread blocks generating sound (Wozniak, 2001 [339]; Wozniak and Taryma, 2004 [340]). These phenomena happen thousands of time each time, thus generating high frequency stick/slip sound (in the 1000-2500 Hz range and above) (Nilsson et al., 1980 [214]; Wozniak, 2001 [339]; Brusarosco et al., 2011 [341]). In some sense, this effect is due to the difference between the coefficient of static friction and the coefficient of kinetic friction at the tire/pavement interface.

It is similar to the distinctive squeaking of shoes on a basketball court or the hissing sound of hand moving against a very smooth desk board. In early years like 1950's, tire squeal is a big problem especially during cornering and braking (Crowther and Singh, 2008 [342]), such that it was considered normal. This issue was eventually solved through the development of synthetic rubber compounds that have favorable damping characteristics and was almost forgotten after 1970's (Timmons, 1976 [343]). The pure tone of squeal is analogous to many musical instruments where self-resonant excitation occurs due to friction such as the translator motion of the bow against the string of violin.

This mechanism mainly contributes to tangential vibrations, also called "scrubbing" (Molisani, 2004 [344]). Friction is affected by both tire tread and pavement characteristics, such as rubber hardness which itself is also affected by temperature for the former, and pavement texture probably at all wavelengths and whether it is positive or negative for the latter. It is proven that the normal tire force applied is one of the key parameters affecting stick/slip motion (amplitude/strength) and there exists an upper limit beyond which stick or lock remains at all time but normal tire force doesn't influence its frequency (Zhang et al., 2011 [345]). Kröger and Moldenhauer (2010) [346] investigated the stick/slip vibration frequencies

based on the parameters of tread blocks.

For such high frequencies as above 1000 Hz, numerical models such as FEA will be helpless due to its inherent limitations and unreliability in that range. Micro-electro-mechanical system accelerometers are usually applied inside the tire to conduct vibration measurements and reduce noise. It is shown that tread blocks have great influence on this mechanism under sliding conditions, as shown in Figure 60 (Brusarosco et al., 2011 [341]).

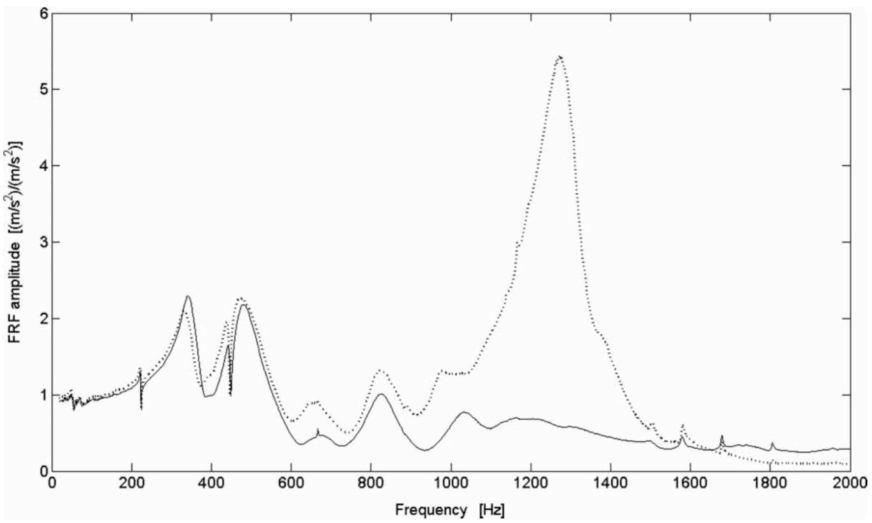

Figure 60: Frequency response function (FRF) amplitude in the tangential direction (vertical load 4 kN: dotted line, tire with tread blocks; solid line, tire without tread blocks) (source from Brusarosco et al., 2011 [341], Figure 4; reprinted with permission from Taylor & Francis)

3.2.2.2 Stick/Snap

Stick/Snap mechanism occurs when tread blocks stick to the pavement due to adhesion bonding or vacuum and then are pulled away and released at the trailing edge of the contact patch (Ruhala and Burroughs, 1998 [250]; Kuijpers and van Blokland, 2001 [347]). Specifically, this mechanism happens for "winter" treads at high temperature when the tread surface becomes sticky and the pavement is very clean (Sandberg and Ejsmont, 2002 [7]). This can be seen as similar to the pop sound when a suction cup releases from a smooth surface (Rasmussen et al., 2007 [62]).

The mechanism can cause both radial and tangential (Nilsson, 1980 [348]) carcass vibrations with the dominant frequency above 1000 Hz [214]. Vibrations can be reduced by increasing

pavement wetness and by increasing microtexture (Kroger et al., 2004 [349]). Temperature is also an influencing factor. The frequencies increase with the reduction of the height of tread blocks.

Hydrophobic materials have stronger adhesive attractions to each other than hydrophilic materials. In drum test, Stick/Snap usually happens when the drum surface becomes sticky due to the rubber deposits (hydrophobic) on it (Sandberg and Ejsmont, 2002 [7]). As opposed to that, it is shown by experiments that adhesion forces are reduced when talc (hydrophilic) is injected into the contact patch (Pottinger et al., 1986 [3]). As a matter fact, the mechanism also contributes to rolling resistance of tires (Taryma, 1998 [350]).

In addition, an interesting theorem has attempted to explain this mechanism that electrostatic charges resulting from friction affect adhesion and discharge of electric charges can generate sound [351]. However, this theorem is fairly questionable.

3.2.3 Air Displacement

All the mechanisms above are related to structure-borne (or structural vibrations) noise. The airborne mechanism (El-Sebai et al., 1999 [352]) will be discussed below, i.e., air displacement mechanism, which includes air turbulence and air pumping (Eisenblaetter et al., 2010 [353]).

3.2.3.1 Air Pumping

At the contact patch, a volume of air is enclosed in between the cavities and pores constituted by the tread grooves and pavement texture. As the tire and pavement roll together at the leading edge, the air is rapidly compressed and squeezed out, generating air pumping noise (Rasmussen et al., 2007 [62]). It could be considered similar effect as hands clapping where the air is pressed away at the edges of hands (Mcdaniel, 2014 [122]). Whistling is also physically analogous to this where air is forced out of a small opening. At the trailing edge, the air is expanded and sucked back into cavities, also generating sound. All of these happen thousands of times each second. To be more exact, the acceleration of air leads to the sound generation (Beckenbauer et al., 2008 [332]).

Air pumping was first investigated as early as 1971 by Hayden: the air pressed out was assumed to feed an acoustic monopole (Hayden, 1971 [354]). Before that in the 1960's, there was a special retreaded truck tire having pockets in its tread in the USA (NBS, 1970 [355]). This

tire turned out to so noisy that it was nicknamed "Singing Sam" and withdrawn from the market in the early 1970's (Leasure and Corley, 1974 [356]). Air pumping also occurs for slick tire due to the pavement voids. Donavan and Oswald (1981) [160] stated that the noise over 1000 Hz at the trailing edge of a slick tire might be from air pumping.

Air pumping is a major source of TPIN and generally highest around 1000-2500 Hz or higher (Donavan and Oswald, 1980 [179]; Donavan and Lodico, 2009 [357]; Kim et al., 2006 [358]). Sandberg and Ejsmont (2002) [7] indicated that there exists a transition frequency after which air pumping noise dominates the structure-borne noise; this transition frequency is around 800-1000 Hz for a passenger car tire while it is around 600-800 Hz for a truck and bus tire. It is found that increasing pavement porosity and macro-texture can reduce air pumping noise by creating extra channels to ventilate the compressed air (Descornet and Sandberg, 1980 [310]; Nilsson, 1982 [239]; Sandberg et al., 2005 [321]; Fujikawa et al., 2006 [359]). Experiments of hand-cut pattern tires also showed that transverse pockets cut in the smooth tire increased the noise by up to 15 dB within the range 1000-6300 Hz (Ejsmont et al., 1984 [360]). It was also shown that inclined grooves generate less air pumping noise than transverse grooves (Chiu and Fu, 2015 [361]). The pulse pressure of air pumping can be modeled as unit pulse, bell-shaped pulse, and N-shaped pulse (Chiu and Fu, 2015 [361]), as shown in Figure 61.

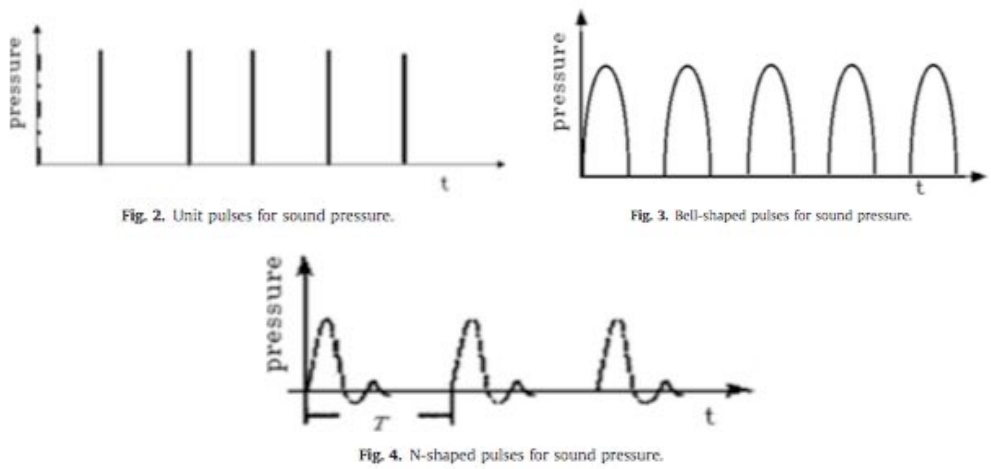

Figure 61: Pulse shapes for modeling air pumping noise (source from Chiu and Fu, 2015 [361], Figures 2-4; reprinted with permission from Elsevier)

The monopole theory models a vibrating point source as a small spherical emitter (Gagen,

1999 [362]; Gengen, 2000 [363]) and agrees well with experiments (Samuels, 1979 [364]; Plotkin et al., 1980 [365]).

$$
\begin{aligned}
V &= \frac{4}{3}\pi R^3 \\
V' &= 4\pi R^2 R' \\
V'' &= 4\pi\left(2RR'^2 + R^2 R''\right) \\
p &= \frac{\rho V''}{4\pi r} = \frac{\rho R\left(2R'^2 + RR''\right)}{r}
\end{aligned}
\tag{22}
$$

where R is the radius of the emitter, R' and R'' is first and second derivative of R with respect to time, V is the volume of the spherical emitter, V' and V'' are the first and second derivative of V with respect to time, ρ is the air density, r is the distance between source and receiver, and p is the sound pressure at the receiver. It is implied that the properties of the mechanism are related to the second derivative of the volume with respect to time (Wei et al., 2016 [366]). Air pumping noise will also be reduced in the form of dipoles if positive and negative pulses cancel when the phase of popping in and popping out match (Plotkin and Stusnick, 1981 [43]).

Another theory in (Ronneberger, 1989 [309]) simplified the tire with slick tread. A more detailed model was presented in (Hamet et al., 1990 [367]).

Gagen (1999) [362,363] also argued that Hayden's monopole model where local air movements were exactly equated with the volume changes of the system is too simple to represent the complex air squeezing process at the tire/pavement interface. Gagen assumed that the change of local volume corresponds to a damped oscillator. The kinetic energy of air expelled from a linearly squeezed groove is

$$
E = \frac{\rho w A^3 l^3 v^2}{2\left(1 - \frac{A}{d_0}\right) d_0^4}
\tag{23}
$$

where ρ is air density, w is the groove depth, A is the new length of the cavity when it is fully compressed, l is groove width, v is vehicle speed, and d_0 is groove length (Eisenblaetter et al., 2010 [353]). The air volume displacement is calculated as

$$\begin{cases} \ddot{V} = \dfrac{\partial^2 V}{\partial t^2} = \dfrac{p \cdot 2\pi \cdot r}{\rho} \\ V'' = \dfrac{\partial^2 V}{\partial x^2} = \dfrac{p \cdot 2\pi \cdot r}{\rho \cdot v^2} \end{cases} \tag{24}$$

The "pseudo-intensity" is given by (Fahy and Elliott, 1981 [368])

$$I_T = \frac{1}{\rho c} \int_0^t p^2 \, dt \tag{25}$$

where c is sound speed in air.

Eisenblaetter (2010) [353] found more air pumping noise at the trailing edge than the leading edge of the contact patch. The air pumping noise is centered around 4000 Hz. However, some researchers found that the air pumping is only important at the leading edge (Nilsson et al., 1980 [214]; Plotkin et al., 1980 [220]) while some others suggested that this mechanism is important at both the leading and trailing edge (Ruhala and Burroughs, 2008 [292]).

Gautam and Chandy (2015) [369] investigated the air pumping phenomenon for one deformed groove using computational fluid dynamics (CFD) and found that at the vehicle speed of 40 km/h the acoustic pressure can be up to 4000 Pa but for less than 1 ms. The main spectral content is centered around 4000-6000 Hz.

The air pumping model in Heckl (1986) [13] is based on Hayden (1971) [354],

$$P = \frac{\rho_0}{4\pi c_0} \left(\frac{\partial q}{\partial t} \right)^2 \tag{26}$$

where P is sound power, ρ_0 is air density, c_0 is sound speed in air, q is the volume flow from the grooves, and t is time. Since $q \propto V$ where V is the vehicle speed, and $\partial/\partial t \propto V$, the relationship between air pumping sound power and vehicle speed is found as $P \propto V^4$, which agrees well with measured results.

Rochoux and Biesse (2010) [337] found that the air pumping is relatively weak compared to the dominant vibratory noise source (vibration of tire belt and sidewall). It was observed that the air pumping noise is in the experiment about 10 dB lower than the modal noise.

3.2.3.2 Air Turbulence

Air turbulence is potentially caused by the tire displacing air when it rotates (rotational turbulence noise) and moves forward (displacement turbulence noise) (Sandberg and

Ejsmont, 2002 [7]). It can be seen as spinning disk mechanism, which was first studied in 1969 (Chanaud, 1969 [370]). It was found to be unimportant at normal highway speeds, but Heckl (1979) [371] noted that significant (especially around 300 Hz and above 3000 Hz [372]) at higher speeds over 0.2 Mach (250 km/h) as the noise was proportional to the 6th power of speed (Hayden, 1972 [354]).

With the help of Near-field Acoustic Holography (NAH) technique, a certain noise radiation was found from the rotating rim with five vents acting like a fan (Ruhala and Burroughs [243], 1999; Ruhala, 1999 [244]). However, the main frequency was around 40 Hz, which was too low to be explained by air turbulence mechanism. It was concluded that it might came from vibrations of the wheel. Noise around tire might also be induced by the hub bearing, which is difficult to be separated from air turbulence (Sandberg and Ejsmont, 2002 [7]).

In addition, the sudden release of a rubber block from the surface (stick/snap) may also cause a transient airflow through the opening slit, generating air turbulence noise (Sandberg and Ejsmont, 2002 [7]).

It should be pointed out that compared to air pumping or vibrational mechanisms, air turbulence is much less significant (Nilsson et al., 1980 [214]; Eberhardt, 1984 [326]; Donavan and Oswald, 1980 [179]; Leasure and Bender, 1973 [373]) in highway noise considerations as concluded in (Wilken et al., 1976 [374]) where careful experiments with a single-wheel trailer in order to assess both mechanism noise at the contact patch. It was shown by aid of a flow visualization technique (an array of tufts suspended from a screen in the wake of the test tire) that vortex shedding did not appear in any pronounced way that might generate significant air turbulence noise. Wilkin et al. (1976) [374] also installed streamline apparatus, a splitter board, and an air shield to reduce the aeroacoustic noise, but no significant noise reduction was found. Ronneberger et al. (1982) [375] indicated that since the speed of tires is still small compared with the speed of sound, purely aerodynamic source mechanisms (turbulence, vortex shedding etc.) are insignificant and can be neglected.

3.3 Amplification Mechanisms

The mechanisms in this subsection amplify the sound produced by the above generation mechanisms, making TPIN even louder. The amplification mechanisms are mostly based on

resonance (like many musical instruments [62]), so different mechanisms will play different roles at different frequencies, as shown in Table 20.

The amplification mechanisms are no less simple than generation mechanisms and are influenced by different parameters to various degrees. As a result, to reduce the TPIN that is heard, not only should the generation be restrained, but also the amplification should be avoided, especially at those frequencies sound is amplified the most (Rasmussen et al., 2007 [62]).

Amplification Mechanisms include tire resonances, air resonances and horn effect mechanisms.

3.3.1 Tire Resonance

Modern tire is very complex system. Typical radial tire is composed of 19 components, 12 compounds, fabrics, 2 steels and 60 raw materials (Gent and Walter, 2006 [376]). Each part of the tire could be excited resonantly at certain frequencies. The most important resonances relating to noise come from the belt, torus cavity, sidewall and tire/rim assembly. It is found that most of these vibrations radiate noise primarily close to the contact patch (Sandberg and Ejsmont, 2002 [7]).

3.3.1.1 Belt Resonance

Almost every TPIN spectrum has a peak around 700-1300 Hz, probably because various generation mechanisms dominate in this region, as shown in Table 20, such as tread/texture impact, stick/slip and air pumping, which are all related to tread pattern or pavement profile. However, the peak around 1000 Hz still exists for non-patterned tire or on surfaces with a pronounced macrotexture (Sandberg and Ejsmont, 2002 [7]; Doan et al., 1995 [312]). In addition, the peak is fairly independent of speed, which cannot be explained by the normal generation mechanisms.

This is speculated to be a belt or carcass resonance [66], whose frequency is only dependent on the structure itself. It was found that increasing tread bending stiffness reduced shoulder tread vibrations and the generated noise, particularly at 500-1000 Hz. Changing the belt mass also largely affects the radiated sound (Kropp et al., 1998 [377]).

Kwon et al., 1998 [245] demonstrated that tire carcass vibration is composed of superposition of waveguide modes. The circumferential modes occur when

$$k_\theta \pi d = 2n\pi \tag{27}$$

where k_θ is circumferential wavenumber, d is tire diameter. Some lower order modes are displayed in Figure 62.

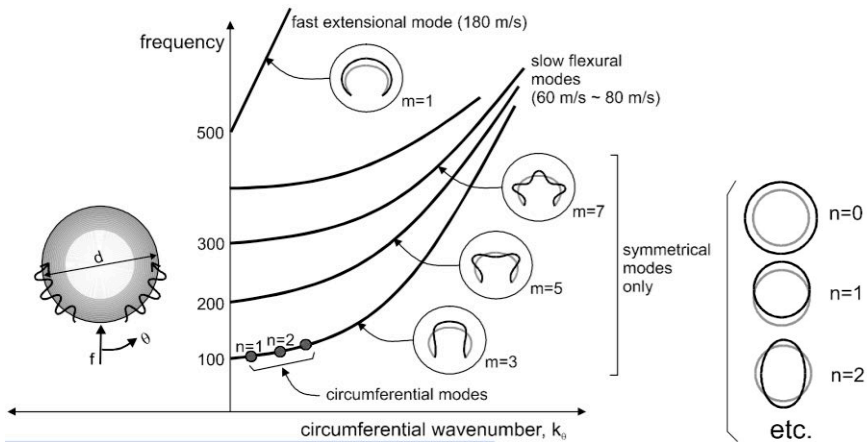

Figure 62: Tire carcass dispersion characteristics under static condition (source from Kwon et al., 1998 [245], Figure 4; reprinted under fair use provision)

There are both slow (60-80 m/s at 128 Hz, flexural mode) and fast (180 m/s at 550 Hz, extensional mode) propagating waves existing in the belt of car tires. The fast waves are considered to be more efficient radiators (Kwon et al., 1998 [245]). Another earlier experiment found peaks in noise emission at 210, 320 and 400 Hz (slow modes) by exciting a truck tire hanging in the air utilizing a shaker with a swept sine input to it. A major peak around 600-750 Hz (lowest fast mode) was also found (Richards, 1976 [378]). For car tires, the same method found slow modes possibly at 200-400 Hz and fast mode at 1000 Hz (Richards, 1974 [379]). It was also suggested that truck tires are more efficient radiators than car tires. Bolton et al. (1998) [380] also noted that at high frequencies, waves propagate from the drive point to both ways and damp quickly without meeting each other while at lower frequencies the two opposite waves interfere with each other and might create standing wave patterns.

Standing waves might occur due to flexural (bending) waves propagating from the contact patch in both directions along the circumference of the tire (Sandberg and Ejsmont, 2002 [7]).

3.3.1.2 Torus Cavity Resonance

Every pneumatic tire since invented by John Boyd Dunlop in 1888 has a torus cavity filled

with air enclosed by tire carcass and rim (Rhyne and Cron, 2006 [381]). The cavity resonance sound is like the distinctive ringing sound generated by a balloon when being thumped (Rasmussen et al., 2007 [62]). The sound (dominantly at 200-250 Hz for passenger car, 150 Hz for heavy trucks) has more influence on interior as structure-borne noise that can be amplified by the vehicle itself at this frequency range but also can be heard outside the vehicle. The cavity resonant noise is transmitted through the wheel hub into the vehicle cabin where a tonal sound could be clearly heard. The first published research regarding torus cavity was found in 1985 (Bschorr, 1985 [382]), after which a lot of researchers investigated this phenomenon since it has huge impact on ride comfort, as shown in Table 18.

For undeformed tire, the acoustic pressure p at any point can be written as (Tanaka et al., 2016 [383])

$$\begin{cases} p_r(x,t) = Ae^{j(\omega t - kx)} \\ p_l(x,t) = Ae^{j(\omega t + kx)} \\ p(x,t) = p_r(x,t) + p_l(x,t) = 2A\cos(kx)e^{j\omega t} \end{cases} \tag{28}$$

where x is coordinate along the tire circumference, t is time, p_r and p_l are acoustics pressure propagating to the two opposite directions (right and left, assuming positive direction is to the right), A is acoustic pressure amplitude, ω is radian frequency of the acoustic wave, k is wavenumber.

The resonant frequency can be calculated as (Sakata et al., 1990 [384]; Thompson, 1995 [385]; Walker and Cortés, 1989 [386]; Richards, 1991 [387])

$$f_i = i \times \frac{c}{L_c} = \frac{2ic}{\pi(D_o + D_i)} \tag{29}$$

where i is the order of cavity resonance mode, f_i is the ith modal frequency, c is the sonic speed in the cavity medium, and L_c is the torus circumferential length, D_o is outer diameter of tire torus, D_i is outer diameter of tire torus. The speed of sound (40°) is around 349 m/s in the air and around 1039 m/s in the helium, so the car tire cavity resonance resides in range of 230-280 Hz for air while 680-830 Hz for helium (Sandberg and Ejsmont, 2002 [7]). A helium tire will avoid coupling with other structure-borne resonances such as from tire/rim assembly and reduce the noise.

For deformed tire, the deflection at the contact patch breaks the symmetry of the tire, thus

splits the frequency at each mode into two corresponding frequencies (low frequency mode and high frequency mode) (Gunda et al., 2000 [388]). The two resonance frequencies f_l and f_u are calculated as (Tanaka et al., 2016 [383])

$$\begin{cases} f_l = \dfrac{c}{L_c + (1-m)L_{cp}} \\ f_u = \dfrac{c}{L_c - (1-m)L_{cp}} \end{cases} \tag{30}$$

where m is the ratio of the smaller tire cross section at the contact patch to the undeformed cross section ($m < 1$), L_{cp} is the contact patch length. Therefore, the relationship can be obtained as $f_l < f_1 < f_u$.

The low frequency mode (shift down) excites the spindle horizontally while the high frequency mode (shift up) vertically (Yamauchi and Akiyoshi, 2002 [299]) as shown in Figure 63. The resonances have very narrow bandwidth characteristic of systems with very low damping (around 0.01, an order of magnitude lower than that of the structural modes). Thus, one approach to reduce the resonance is to add damping material to the tire cavity such as glass fiber or foam rubber (Gu et al., 2002 [389]).

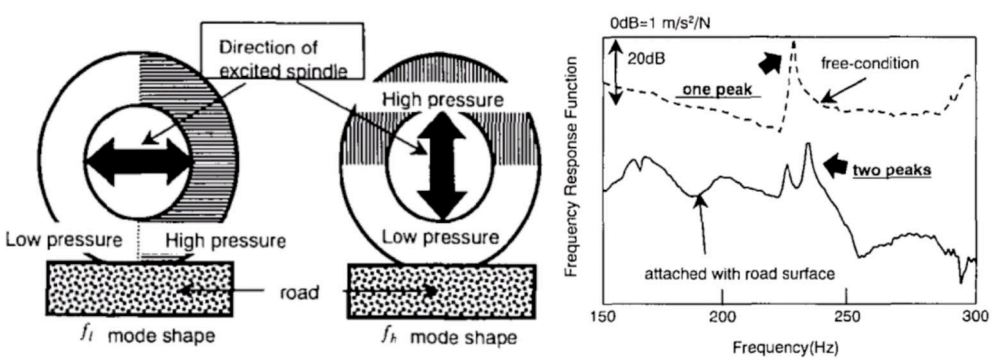

Figure 63: Torus cavity resonance modes (source from Yamauchi and Akiyoshi, 2002 [299]; reprinted under fair use provision)

Various methods such as point excitation, drop test, and acoustic excitation test can be used to identify the resonance mode in the lab (Mohamed et al., 2013 [41]). Internal wireless speakers are preferred to excite the tire cavity (Kim et al., 2007 [390]; Gu et al., 2009 [391]; Hayashi, 2007 [392]).

It is shown that tire structure and cavity geometry have influence on the cavity resonance. Cavity noise peak frequency also depends on the tire load and vehicle speed (Gu et al., 2009 [391]). A lot of countermeasures to reduce cavity resonance were proposed such as different inflated air, absorbent material, tire/wheel structure redesign, as shown in Table 18, but all of these are difficult to be implemented or maintained from the perspective of cost, durability and reliability (Mohamed et al., 2013 [41]).

It is noted that only the first cavity mode (or the two lowest modes, fore/aft and vertical, due to splitting when rotating) resonance was reported to have an adverse effect to vehicle interior noise and force transmissibility, so the cavity resonance frequency often refers to the first order frequency (Mohamed and Wang, 2015 [393]).

Table 18: Review of tire torus cavity resonance (underlined items in green are reduction countermeasures) (source partly from Mohamed et al., 2013 [41])

Reference	Author	Year	Conclusions
[382]	Bschorr	1985	(1) Absorbing material fitted on the rim inside the tire reduced internal tire SPL from 140 dB to 130 dB. Outside the tire, the reduction was 0.8 dB.
[386]	Walker & Cortés	1989	(1) A decrease of noise around 250 Hz was seen for tire inflated with CO_2 compared to normal tire.
[384]	Sakata	1990	(1) Cavity resonance was first defined as an acoustic resonant mode existing inside the tire cavity. (2) Deformed tire has two acoustic modes as compared to one for undeformed tire. (3) Filling with polyurethane foam inside the tire cavity would eliminate the cavity resonance at 230 Hz.
[387]	Richards	1991	(1) Cavity resonances at 240 Hz affected the force transmissibility for structure-borne interior noise.
[394]	Nakajima et al.	1993	(1) Cavity resonances at 470 Hz, 700 Hz, 920 Hz were found for a passenger car tire (185/70R14).
[395]	Scavuzzo et al.	1994	(1) Coupling between the tire cavity acoustic resonance and the tire structural resonance increased the vehicle interior noise. (2) Cavity acoustic resonance occurred at 229 Hz and 232 Hz while the tire/wheel structural resonance occurred at 208 Hz. (3) The use of aluminum wheel instead of steel could avoid the structural-acoustic coupling for the tire-wheel system.
[396]	Ni et al.	1997	(1) The two first cavity modes were found to be 223 Hz and 227 Hz.
[380]	Bolton et al.	1998	(1) Cavity resonances were not important to tire vibrations. (2) Cavity resonances are only important at pavement discontinuities, such as contraction joints.
[397]	Mioduszewski	1999	(1) A decrease of noise around 250 Hz was clearly seen for helium tire compared to normal tire.
[398]	Haverkamp	1999	(1) It was hypothesized from that the frequency of the tone is nearly independent of wheel rotation speed. (2) Using bitumen coating on the rim to change the damping characteristic increased the resonance due to increase of the impedance of the wall, therefore amplifying the resonance mode.

Reference	Author	Year	Conclusions
[399]	Haverkamp	2000	(1) Torus cavity resonance sound at 230 Hz can be heard as a pure tone from the inside of the passenger compartment as air-borne sound. (2) Filling the mineral fibers into the tire cavity could reduce the transmitted energy by more than 20 dB.
[388]	Gunda et al.	2000	(1) Helium-inflated tire shifted cavity resonant frequency to a higher range, consequently caused lesser effect to interior noise.
[299]	Yamauchi & Akiyoshi	2002	(1) Sharp peaks around 250 Hz inside the vehicle in running condition were detected. It was believed to be due to air cavity resonances. (2) Cavity resonance could be reduced by using an oval cross-section torus.
[85,344]	Molisani et al.	2003, 2004	(1) The relative high damping of the tire structure is not effective in damping out the energy in the acoustic resonance. (2) Incorporation of secondary acoustic cavities was found to detune and damp out the main tire cavity resonance. (3) Addition of damping directly into the tire cavity by viscoelastic screen was shown effective to absorb the cavity acoustic energy and reduce forces at the spindle.
[400]	Periyathamby	2004	(1) Installing a sound-damping Helmholtz resonator on the wheel assembly reduced the cavity resonance.
[401]	Fernandez	2006	(1) Helmholtz resonator and quarter-wavelength resonator for reducing cavity resonance were ineffective. (2) Placing certain material with 30 to 40 cm in thickness inside the tire cavity could reduce the SPL at the cavity by up to 11 dB for interior and 1 dB for exterior. Perforated plate over foam or aluminum foam were shown not satisfactory while a type of acoustic wool was found to give the best result.
[402]	Douville et al.	2006	(1) Scanning laser Doppler vibrometer was used to identify the air cavity resonances. (2) On-resonance force transmissibility factors (ORTF, percentage of transmission of vibrations) method was introduced to identify the contribution of the cavity resonance mode to the suspension vibration.
[300]	Kim et al.	2007	(1) The cavity mode coincides with the structural mode when the two modes share the same circumferential wave number. (2) The high air pressure inside the tire cavity made the cavity prone to receive the sound energy from the tire wall. (3) There is no clear resonance peaks for interior noise in high frequency except at the frequencies of the cavity resonance. (4) The frequency response curves tend to be smooth over 300 Hz due to the high damping properties of tire rubber and the high modal density of the tire construction.
[392]	Hayashi	2007	(1) Tire cavity resonance noise could be mitigated by increasing the out of plane torsional stiffness of the wheel, such as adopting smaller rim area, and modifying the wheel spoke section.
[403]	Gu et al.	2008	(1) It was shown by experiments that the coupling between wheel mode and cavity mode could significantly affect the magnitude of vehicle interior noise, depending on whether the wheel mode frequency is higher or lower than the tire cavity frequency.
[404]	Waisanen & Blough	2009	(1) Helium-filled tire could simplify the transfer path analysis due to the gas ability to eliminate excitation sources at the cavity resonance frequency.
[405]	Kindt et al.	2009	(1) Longitudinal and vertical acoustic resonance modal frequencies were identified at 220.7 Hz and 227.6 during cleat test (2) Driving speed, cleat dimension, and tire pressure did have an effect on the structural resonance modes but not on the tire acoustic cavity resonance modes [406].
[407]	Bekke et al.	2010	(1) Torus cavity resonance could be coupled with hub vibration and tire/wheel vibration.

Reference	Author	Year	Conclusions
[408]	Jessop & Bolton	2011	(1) Force exerted on the wheel hub transmits the structure-borne noise to the vehicle interior. (2) Acoustic cavity resonance at 212 Hz mode can be externally detected by microphones or laser vibrometers based on wave number decomposition of the frequency response. (3) When the tire is filled with fibrous, sound- absorbing material, the tire vibrations (driven by both steady-state point input and uniform impact using drop test) associated with the tire cavity mode are suppressed.
[409]	Choi	2011	(1) The cavity resonance became more visible if a large excitation force was applied to the tire due to the suppression of the structurally related higher wave number. (2) A clear dipole-like pattern was observed on the tire surface from the effect of the tire acoustical cavity mode.
[410]	Bharadwaja & Siva	2013	(1) A non-linear finite element (FE) model using Abaqus was developed for determining the acoustic pressure in the torus cavity, when subjected to harmonic excitation. (2) The influence of inflation pressure and the load of the vehicle on the tire acoustic cavity resonance is not significant.
[297]	Wang et al.	2014	(1) The modal frequencies of the tire cavity are closer and more easily coupled with those of the rim structure than those of the tire structure. (2) Adding textures onto the inner tire surface or adding ribs and slots onto the wheel rim circumference surface was found not satisfactory. Nitrogen gas inflated tire was also found marginally effective while helium gas was found effective. (3) Dividing the tire air cavity into four quarters by use of a rubber band with four evenly distributed light weight thin polymer flaps attached on the rim circumference surface was found effective.
[393]	Mohamed & Wang	2015	(1) Installation of trim layer onto the inner surface of the tire tread reduced cavity resonance by adding a damping loss term in the sound pressure frequency response function. (2) The reduction ability depends on the material and thickness of the trim layer.
[411]	Mohamed & Wang	2016	(1) The first cavity resonance was around 200-300 Hz. (2) Tire cavity coupling (strong coupling) causes the resonance frequency to shift depending on the tire structure material and geometry. (3) Sound absorbent materials applied in the tire cavity can reduce the coupling effect as well by suppressing the cavity mode.
[383]	Tanaka et al.	2016	(1) Tire cavity resonance was suppressed with polyurethane foam mounted on the tire's inner liner.

3.3.1.3 Sidewall Resonance

Vibrational energy propagates in the tread band and is transferred to the sidewall where sound can be amplified. Also the tire deflection against the contact patch not only deflects the tread band radially, but also pushes out the sidewalls laterally especially around the shoulder at the leading edge (Ruhala, 1999 [244]; Kwon et al., 1998 [245]).

The sidewalls can be considered as a "sounding board" for tread vibrations up to a frequency of about 800 Hz (Sandberg and Ejsmont, 2002 [7]). It can be thought of as a vibrating phone on a tabletop or a thinner aluminum pie plate (Rasmussen et al., 2007 [62]) enhancing the

response. Actually, the speaker membrane works in a similar way. In other words, although vibrations of tread band dominate over the sidewall, the sidewall behaves better as a radiator if excited resonantly, especially when tread shoulder is excited (Waki et al., 2011 [412]).

The sidewall resonance was found to be the most significant mechanism in the frequency band of 500-1000 Hz under certain conditions (Donavan and Oswald, 1981 [160]). In low frequencies the sidewall acts like a lumped-spring system (Kropp, 1999 [413]) and radiates noise like a piston more efficiently than the tread band but in high frequencies it behaves as a wave guide and attenuate the vibrations (Ruhala, 1999 [244]), just like a low-frequency band-pass filter (Nelson and Phillips, 1997 [414]; Morgan, 2003 [415]; Keulen and Duskov, 2005 [416]). Eberhardt (1979) [417] noted that the vibration levels on the sidewall surface were much lower than the tread band surface.

The sidewall resonance radiates sound to the side, which means it has greater influence on pass-by noise. However, Kwon et al., 1998 [245] indicated that the effective radiation only exists close to the contact patch based on the active intensity plot.

3.3.1.4 Tire/Rim Assembly Resonance

The vibrations transmitted from the tire to the rim are mostly below 100 Hz, which is a main cause of interior noise in vehicles but can also be measured outside. At low frequencies the sidewall acts like a spring with inner tension created by the air inflation, while at high frequencies the sidewall behaves as a wave guide and attenuates the vibration transfer (Erixon, 1998 [304]).

However, a pronounced peak as high as 290-300 Hz is also found, which is believed to be the first bending wave mode of tire/rim assembly (Ni et al., 1997 [396]).

In addition, the rim can also radiate noise (200-400 Hz) separately caused by vibrations transferred from the tire or the air torus (Ni et al., 1997 [396]). Tire/rim assembly resonance (250-300 Hz) and torus cavity resonance (200-300 Hz) are believed to play a big role here (Sandberg and Ejsmont, 2002 [7]). However, Kwon et al. (1998) [245] indicated that the vibrated wheel hub or hubcap was found not to be a significant noise source.

3.3.2 Air Resonance

Air resonance can be considered as special case for air pumping when resonance occurs, so it cannot be investigated separately (Kim et al., 2006 [358]). The two major resonances are pipe

resonance and Helmholtz resonance. Tread pattern design play a great role in air resonance, sometimes small changes to tread pattern may reduce the resonance to a great extent.

3.3.2.1 Pipe Resonance

When you blow across an organ pipe, a pure tone sound will be created with a unique frequency determined by the length of the pipe, its shape and the number of openings (Rasmussen et al., 2007 [62]). The resonances of the air-filled channels ("pipes") in the contact patch give a selective "amplification" especially on an nonporous smooth road or on a test drum, and the effect can be approximately 10 dB in the frequency range 0.8-3 kHz (Jennewein and Bergmann, 1985 [331]).

It is caused by the standing wave with anti-nodes (maximum frequency) at the open ends (Sandberg and Ejsmont, 2002 [7]). If the pipe has openings at both two ends ($\lambda/2$ resonator), the resonance frequency f is (Bruneau, 2010 [418])

$$f_n = \frac{nc}{2(L+0.8d)} \tag{31}$$

where n is an integer indicating the order of resonance, c is the speed of sound, L is the length of pipe and d is the diameter of the pipe. The first order wavelength of $\lambda/2$ resonator is about $2L$.

If the pipe is closed at one end and open at the other ($\lambda/4$ resonator), the resonance frequency f is

$$f_n = \frac{(n-1/2)c}{2(L+0.8d)} \tag{32}$$

The first order wavelength of $\lambda/4$ resonator is about $4L$.

Fabrizi (2016) [419] identified three phenomena related to the aerodynamic noise in the longitudinal tread grooves: (1) at the pipe inlet, the air flow is squeezed laterally into the groove from both sides, each with a high swirl component (counter rotating vortices); (2) at the pipe outlet, the flow creates jets that develop inside the recirculation bubble of the wake; (3) the flow accelerates laterally to the speed of ~300 km/h, and detaches, generating a high-energy shear layer. The aeroacoustic energy of pipe resonance is to the eighth power of the flow velocity (Lassiter, 1952 [420]; Fitzpatrick 1952 [421]).

Similar pipe resonators can be found in the tread pattern as the grooves and sipes contact

the ground and amplify the sound (dominantly at 1000-3000 Hz [245,422]) created by air pumping or other generation mechanisms. This phenomenon is found significant for cross-lugged (Oswald and Arambages, 1985 [423]) or longitudinally/laterally grooved tires (Koike et al., 1999 [424]), especially on such a smooth road surface as specified in ISO 10844 (ISO, 2014 [425]). 3.5 dB increase was found for cutting longitudinal grooves into slick tires (Saemann and Schmidt, 2002 [311]). The calculated frequencies had a good fit with experimental measurements showing the importance of this mechanism at high frequencies (Wilken et al., 1976 [374]; Richards, 1976 [378]; Favre, 1979 [426]). Filling foams into grooves were proven to reduce the noise at 800-2000 Hz (Wilken et al., 1976 [374]). Donovan (1982) [427] also noted that besides air pumping, the source for pipe resonance was the vibration of the groove walls.

It was shown that rough texture and high porosity can reduce the pipe resonance (Koike et al., 1999 [424]). Others ways to suppress this resonance is to build reasonable channels on the tread to efficiently ventilate the air or to apply Helmholtz resonators to the tread pattern design (Fujiwara et al., 2009 [428]). The interior noise was also found to be reduced using Helmholtz resonators (Kitahara, 2011 [75]). The pipe resonance is only dependent on the geometries and independent of vehicle speed, load or inflation pressure, or to a limited degree if dependent.

It is interesting to note that there could be constructive or destructive interference of the sound coherently radiated from the two ends of the pipe (Donavan, 1981 [162]). In particular, there is noticeable interference (2000-2500 Hz on a very smooth surface) in the middle of the contact patch where the distances to both ends are equal (Sandberg and Ejsmont, 2002 [7]). But for rough-textured surface, this phenomenon completely disappeared.

3.3.2.2 Helmholtz Resonance

When air is blown across a pop bottle, a unique tone can be heard. This is called Helmholtz resonance, which is basically a mass-spring vibration effect (Bruneau, 2010 [418]). The air in the bottle neck acts as the mass, and the air in the bottle cavity acts as the spring. When you blow the air in the neck (mass), it is excited and vibrates up and down on the air in the cavity (spring). As such, the Helmholtz resonance is also called “air resonant radiation”. The resonance frequency is determined by the cavity volume and neck dimensions. Nilsson (1979) [429] reported that Helmholtz resonances usually occur when tread grooves open at the

trailing edge of the contact patch.

Similar phenomenon can be found around the trailing edge of the tire contact patch. When the tread lifts off the pavement, a narrow channel forms and connects to the cavity where the air is trapped and enclosed by the tread grove and the pavement. A chirp-like resonant ringdown associated with each cavity occurs, starting at a medium frequency with large amplitude and fading-off at a higher frequency, as the channel grows wider. It was shown that the chirp noise reduced when helium was flooded into the trailing edge to change the sound speed (Nilsson et al., 1980 [348]).

The Helmholtz resonance phenomenon was first investigated in 1979 (Nilsson et al., 1979 [430]) and named as "air resonant radiation". It was concluded that this phenomenon is responsible for the main contribution the A-weighted SPL for tires with transversal grooves. The equation governing the resonance frequency f at the trailing edge for the transversally grooved tires was also presented.

$$\frac{V_0}{s_1 x_1} = \frac{1+(kx_1)^2}{\beta(kx_1)^2\left[1+\left(\frac{\gamma k x_1}{2\beta}\right)^2\right]} - \frac{1-\frac{kx_1}{\tan(kx_1)}}{(kx_1)^2} \tag{33}$$

$$k = \frac{2\pi f}{c} \tag{34}$$

where V_0 is groove volume, x_1 is distance between contact trailing edge and groove edge, k is wave number, c is sound speed, s_1 is area between groove edge and road surface, β_1 is correction coefficient to account for the opening for the opening of the horn sideways and its influence on mass impedance, γ is correction coefficient to account for the opening of the horn sideways and its influence on resistive impedance. The equation was shown to have a good fit with experiments, as shown in Figure 64 (Eisenblaetter et al., 2010 [353]). The dominant frequency of the resonance is generally around 1000-2500 Hz.

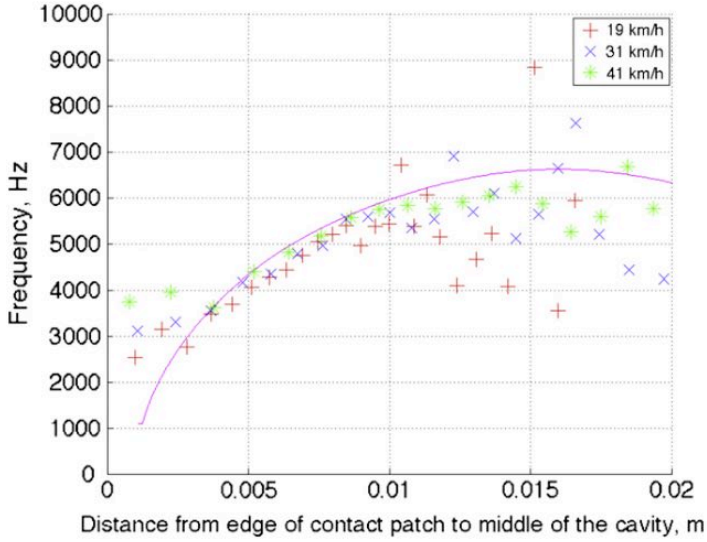

Figure 64: Frequency of oscillation of trailing edge signals versus distance of the large cavity from the contact patch: (i) frequency measured from period of oscillations (crosses); (ii) predicted frequency assuming 'air resonant radiation' (solid line). (Source from Eisenblaetter et al., 2010 [353], Figure 8; reprinted with permission from Elsevier)

A similar but reverse effect can also occur at the leading edge, as the tread is about to contact the pavement. In addition, for smooth tire with no groves the Helmholtz resonance might still occur as the cavity can be formed by pavement macrotexture. Resonance amplitude can be reduced by good ventilation of the cavities, such as porous pavement, porous tread, or ventilated tread pattern design. The volume of the cavity and the shape of the channel (determined by the tire diameter and contact patch length) can change the resonant frequency (Sandberg and Ejsmont, 2002 [7]).

3.3.3 Horn Effect

At the leading edge and trailing edge of the contact patch, the tire and the pavement form a wedge-shaped structure. At the narrow throat, multiple reflections of sound generated occur, much like the acoustic horn or megaphone (Rasmussen et al., 2007 [62]). The horn shape acts as an impedance matching device between sound sources at the contact patch and the surrounding air (Schaaf and Ronneberger, 1982 [431]), thus amplify the sound above 700 Hz (Yum and Bolton, 2004 [316]), especially in range of 2000-3000 Hz (Schaaf and Ronneberger, 1982 [431]) determined by the shape and size of the horn (Iwao and Yamazaki, 1996 [307]). A lot of clever experiments have been conducted to confirm this effect, as shown in Table 19

(Sandberg and Ejsmont, 2002 [7]).

Table 19: Horn effect experiments (summarized from Sandberg and Ejsmont, 2002 [7])

Reference	Author	Year	Test	Conclusions
[431]	Schaaf & Ronneberger	1982	A sound source was put far from the tire and the sound pressure was measured near the throat.	5-20 dB increase between 1-5 kHz was observed with tire present as compared to without tire.
[309]	Ronneberger	1989	Image source model was developed for a 15° tire/pavement contact angle.	11 image sources were needed to produce a 22 dB amplification.
[307]	Iwao & Yamazaki	1996	A loudspeaker was buried at the throat.	Radiated sound was 10 dB increase over 300 Hz under the conditions with a tire compared to without a tire.
[307]	Iwao & Yamazaki	1996	A loudspeaker was buried at the center of the tread but different angular position (0° is along the vertical axis).	Radiating efficiency is the highest at 10° position regardless of the position of the measuring microphone.
[432]	Graf et al.	1999	Efficiency of the horn was tested for tires with different widths (200, 260, 400 mm).	The wider the tire was, the higher the efficiency would be, especially at low frequencies.
[433]	Kropp et al.	2000	Horn amplification was measured in the plane of the tire with different source distance from the contact edge.	Most prominent location of source is 10 mm where air pumping is significant.
[433]	Kropp et al.	2000	Horn amplification was measured out of the plane of the tire (0° is in the plane of the tire).	The larger the angle, the smaller the amplification.
[433]	Kropp et al.	2000	Sound was measured for pass-by situation where distance attenuation was considered.	The optimum occurred at angles of 60-75°.
[434]	Graf et al.	2002	A 200 mm wide tire with shoulder curve radius of 70 mm was compared to curve radius of 0 mm.	5 dB decrease around 1 kHz was observed for the radiusing tire.
[435]	Schutte et al.	2015	The influence of the horn was analyzed at 1 m distance from the horn's center.	Horn effect amplified structure-born noise by up to 14 dB around 1 kHz.

The amplification is also a function of location of the tire excitation, which is dependent on the tire load (Iwao and Yamazaki, 1996 [307]). The horn effect can be reduced if the pavement is porous (Iwai et al., 1994 [436]) or the tread is porous (Sandberg et al., 2005 [321]), due to the sound absorption effect (Lui and Li, 2004 [437]). Decreasing the tire width or radiusing the tire can also reduce the horn effect, as the horn leaks to the side, which means radiation directivity properties are changed (Mioduszewski and Ejsmont, 2009 [438]; Mioduszewski and Ejsmont, 2006 [439]). Tire radius has less influence than tire width, which only influences the pattern of the varying amplification around the belt, rather than its absolute level (Graham, 2012 [440]).

Kropp (1999) [413] reported that the horn effect amplification factor at high frequencies increases with the decrease of the distance between the source and the edge of the horn.

3.4 Attenuation Mechanisms

The sound must travel from the tire to the receiver or measurement device after it has been generated and amplified. During the propagation, attenuation or reduction mechanisms occur [213], such as car body interferences (Sakamoto et al., 1999 [441]; Anfosso-Lédée, 2004 [442]), propagation over pavement (Klein and Hamet, 2007 [443]), and atmospheric conditions (wind [444] and temperature [445,446]).

Most of those mechanisms are much more important for far field measurements such as pass-by tests than near field measurements such as CPX or OBSI. However, there are two major attenuation mechanisms are also very important for near field sound, i.e., pavement Absorption (acoustical impedance) and vibration transfer (mechanical impedance), which are discussed in detail below.

3.4.1 Acoustical Impedance (Pavement Absorption)

Acoustic impedance Z is defined as the ratio of acoustic pressure p to acoustic volume flow U (Bruneau, 2010 [418]).

$$Z = \frac{p}{U} \tag{35}$$

Acoustic impedance usually varies strongly with the frequency. The acoustic impedance at a particular frequency indicates how much sound pressure is generated by a given air vibration at that frequency, which means the higher the acoustic impedance is, the less air vibration will be needed to generate sound.

Communicating voids in porous pavements reduce acoustic impedance, acting like sound absorbing material and affecting the source strength (Sandberg, 1999 [447]). The pavement absorption is dependent on ground impedance (Taherzadeh and Attenborough, 1999 [448]), porosity, tortuosity, and flow resistivity of the pavement (Bérengier, 1997 [449]). The radiated acoustic power level L_w (dB) is calculated by (Nilsson, 1986 [450])

$$L_w = 10 \cdot \log\left(u^2 \cdot Z_r \cdot A_c\right) + 120 \text{ dB} \tag{36}$$

where u is particle velocity in m/s, Z_r is resistive part of the acoustic impedance in N·s/m^3, A_c is horn mouth area (sample area in calculations) in m.

In addition, tire rubber itself is a good acoustic absorption material (Maderuelo-Sanz, 2012 [451]; Venslovas et al., 2011 [452]; Misik and Radvanska, 2008 [453]) that can attenuation sound at the near field.

3.4.2 Mechanical Impedance (Vibration Transfer)

It has been shown that a stiffer pavement with a larger mechanical impedance gives more noise generation than a softer pavement (Sandberg and Ejsmont, 2002 [7]). The tread block elements may be damped when impacted against the soft surface that is like a cushion. A good example is Poroelastic Road Surface (PERS) where the impact deflection is shared among the tire and the pavement rather than just an abrupt deflection in the tire (Sandberg and Goubert, 2011 [313]).

This vibration transfer depends on the dynamic tire/pavement stiffness proportions (Sandberg, 1999 [447]). If the mechanical impedance of the pavement is much higher than the tire, the structural vibration energy will stay within the tire where some of the energy is radiated as sound energy. On the other tire, if the impedances of pavement and tire are comparable, some of the structural vibration energy will be transferred to the pavement, absorbed by the ground, or radiated as sound energy from the pavement.

It is also speculated that sound can be radiated from the vibrated pavement such as elevated road structures (Hidaka and Tachibana, 1992 [454]). According to (Michishita et al., 2000 [455]), the steel plate girders were found to generate a significant sound in range of 500-1000 Hz from elevated motorway. Low frequency sound radiation has been found to be around 25 Hz (Goromaru et al., 2000 [456]). The sound emission from concrete railway bridges is no lower than that from the train and rail up to about 1 kHz (van Haaren, 1999 [457]).

3.5 Summary

A summary of TPIN mechanisms of generation, amplification and attenuation is listed in Table 20. The earliest reference found for the investigation of each mechanism is included. The dominant frequency and potential noise influence are generally for near field TPIN from lightweight passenger cars in the exterior at normal highway speed. Each mechanism also

includes the parameters that have influence, and an analogous example that has similar physics. The illustrations of the mechanisms are shown in Figure 65, Figure 66, and Figure 67.

Table 20: Tire-Pavement Interaction Noise (TPIN) Mechanisms

				Earliest Investigation	Dominant Frequency [Hz]	Potential Influence [dB]	Major Influencing Parameters (red ↑ or green ↓)	Physical Analogy	References
Generation Mechanisms	Structure-borne	Impact (Shock)	Tread Impact	Archibald (1974) [458]	800-1000	7	Tread depth, groove width, rubber hardness	Rubber hammer	68,298,307,360
			Texture Impact	Thrasher et al. (1976) [1]	800-1200	5	Mechanical impedance, macrotexture		239,313,459
		Adhesion	Stick/Slip (Friction)	Timmons (1976) [343]	1000-3000	2	Normal tire force, temperature, pavement texture at all wavelengths and whether it is positive	Sneaker	341,342,345
			Stick/Snap	Nilsson (1979) [429]	2500-4000	2	Pavement wetness, microtexture	Suction cup	250,347,460
	Airborne	Air Displacement	Air Pumping	Hayden (1971) [354]	1000-2500	10	Porosity, macrotexture	Clapping	220,294,358,461,462
			Air Turbulence	Chanaud (1969) [370]	~300 & >3000	2	Speed, tread pattern	Spinning disk	243,244,374
Amplification Mechanisms	Tire Resonance		Belt Resonance	Richards (1974) [379]	600-1300	4	Tread bending stiffness	Circular belt	245,377,378
			Torus Cavity Resonance	Bschorr (1985) [382]	200-250	3	Cavity geometry, tire load, vehicle speed, inflated gas	Balloon	296,344,384,385,388,395,400,404,463
			Sidewall Resonance	Reiter et al. (1974) [132]	500-1000	2	Tire construction	Speaker membrane	160,244,245,250,295
			Tire/Rim Assembly Resonance	Ni et al. (1997) [396]	250-300	Unknown	Tire mass, rim mass	Sanding disk	296,304,396
	Air Resonance		Pipe Resonance	Pope and Reynolds (1976) [464]	1000-3000	6	Porosity, macrotexture, tread pattern	Organ pipe	75,353,424,428
			Helmholtz Resonance	Nilsson et al. (1979) [430]	1000-2500	Unknown	Porosity, macrotexture, tread pattern	Pop bottle	55,298,465,466
	Horn Effect		Horn Effect	Nilsson (1979) [467]	1500-3000	10	Porosity, sound absorption, tire width	Megaphone	431,434,440,468–471
Attenuation Mechanisms	Acoustical Impedance		Pavement Absorption	Underwood and Nelson (1984) [135]	300-2000	7	Porosity	Foam	472–475
	Mechanical Impedance		Vibration Transfer	Sandberg (1987) [476]	500-1000	2	Pavement stiffness	Cushion	477,478

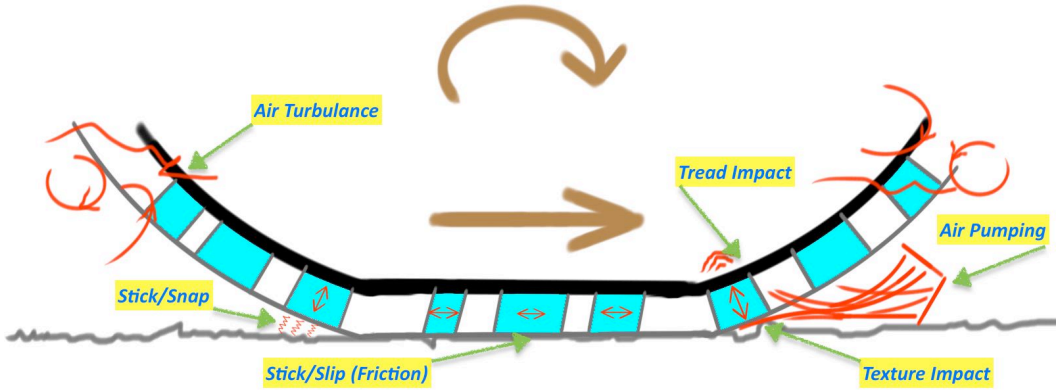

Figure 65: Illustration of generation mechanisms

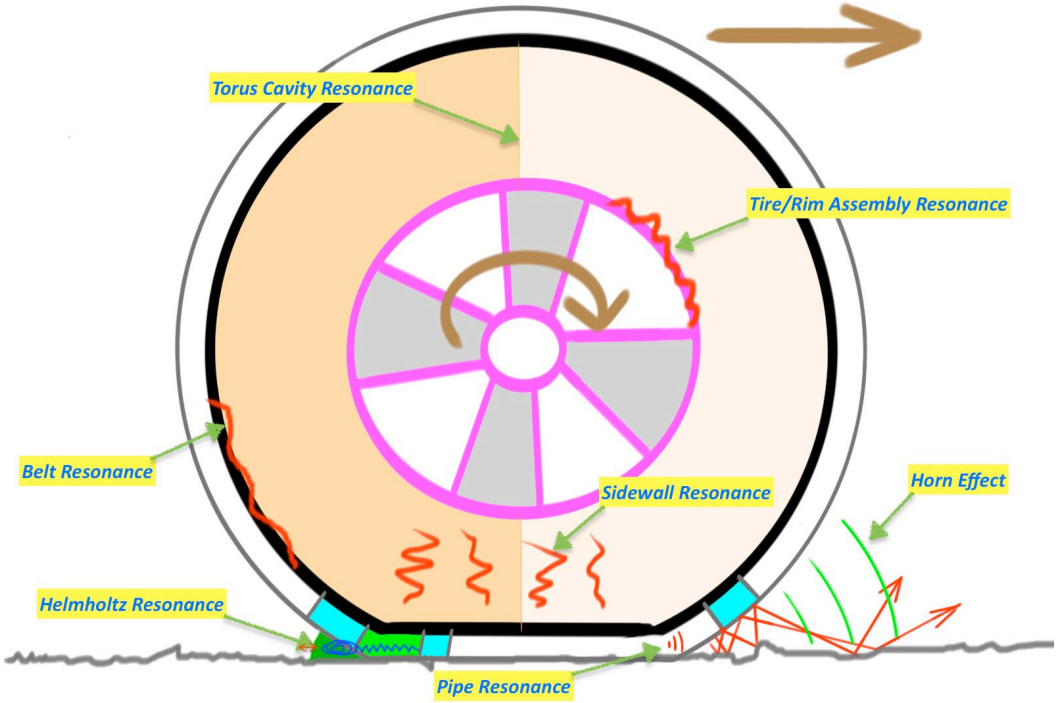

Figure 66: Illustration of amplification mechanisms

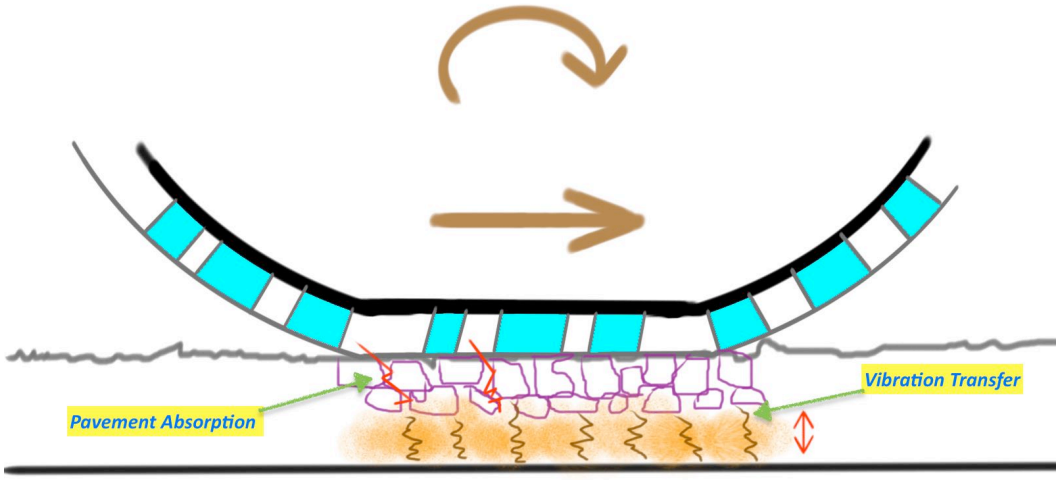

Figure 67: Illustration of attenuation mechanisms

Most frequency spectra of exterior tire-pavement interaction noise have prominent peak in the range of 700-1300 Hz (sometimes might be shifted within the range 630-2000 Hz), especially for car tires after A-weighting (Sandberg, 2003 [479]). A-weighting is the most commonly used procedure when considering human hearing perception (loudness and annoyance) defined in the International standard IEC 61672 (IEC, 2003 [480]). A-weighting gives the most weight to frequency range of 1000-5000 Hz. It somewhat explains the TPIN spectrum peak around 1000 Hz, but not completely.

It is believed that the peak is mostly due to the fact that dominant frequencies for many mechanisms fall under this range (Bernhard, 2005 [481]), as shown in Table 20. A more detailed table elaborates this phenomenon, named multi-coincidence peak (Sandberg, 2003 [479]), as shown in Table 21.

Table 21: Various factors resulting in TPIN spectrum peak around 1000 Hz (car tires at highway speed V = 100 km/h, Sound Speed c = 340 m/s)

	Pertinent Parameters	Equation	Dominant Frequency f [Hz]
Tread Impact	Pattern pitch l: 20-40 mm	$f = V/l$	694-1389
Texture Impact	Prominent wavelength l: 16-25 mm	$f = V/l$	1111-1736
Stick/Slip (Friction)	Tread block properties	NA	1000-3000
Air Pumping	Groove pitch l: 10-30 mm	$f = V/l$	926-2778
Belt Resonance	Belt properties	NA	600-1300
Pipe Resonance	Groove length l: 50-150 mm	$f = c/2l$	1133-3400
Helmholtz Resonance	See 3.3.2.2	See 3.3.2.2	1000-2500
Horn Effect	Horn geometries	NA	700-3000

Scattering or decentralization of these dominant frequencies will be a promising approach to effectively reduce tire-pavement interaction noise. For truck tires, the peak is usually at about two third-octave bands lower frequency than for car tires due to larger tire tread pitch, which is within 500-1000 Hz (Sandberg, 2003 [466]).

4 Influencing Parameters

4.1 Introduction

Generally, the types of vehicles play major roles in the tire-pavement interaction noise (TPIN), such as heavy commercial vehicle (HCV), bus, light commercial vehicle (LCV), car, auto-rickshaw (AR), and two-wheeler (2W). Overall noise level increases with increase in size of the vehicles. That is, the noise produced by heavy commercial vehicle and bus is 10 dB higher than that produced by a two-wheeler when all these vehicles were driven at 70 km/h (Syamkumar et al., 2013 [6]). There are also some vehicle construction related parameters that might influence TPIN (Sandberg and Ejsmont, 2002 [7]), such as vehicle geometry, rim effect, wheel housing (for example, acoustically absorbing honeycomb panel treatment of Jonza et al., 2017 [482]) and underbody screening, but these vehicular parameters are not of interest in this work. Instead, it is assumed that the tested vehicle is of the same type or at least similar.

Different parameters affect TPIN to different degrees, as shown in Table 22 (Sandberg and Ejsmont, 2002 [7]).

Table 22: Overview of parameters affecting TPIN (summarized from Sandberg and Ejsmont, 2002 [7])

Parameters	Potential Noise Variation [dB]	
Speed	25	
Pavement	10	
Tire	10	
Studs in Tire	8	
Load & Inflation	5	
Road Condition	5	
Temperature	4	
Wheel Torque	3	
	Cars	Trucks
Due to Vehicles	7	12
Due to Pavements	9	6

Some other parameters, such as the geometry of the vehicle and wheel shielding, exterior absorption fender around the tire (Sorenson and Jorro, 2012 [483]) and sound absorbing body

undershields (Bückers and Stöckert, 2012 [484]), might have some influence, but very marginally. Biermann and Viehofer (2012) [485] researched on development of cars specified for tire-road noise measurement to reduce vehicle noise other than TPIN and avoid variations due to vehicle. Kim (2015) [486] developed a wheel guard to reduce the high frequency (500-4000 Hz) road noise by 0.5~1 dB.

In this work, the influencing parameters were divided into five categories: driver influence parameters, tire related parameters, tread pattern parameters, pavement related parameters, and environmental parameters. The pertinent frequency, relation with tire noise, potential noise contribution, measurement equipment and relevant mechanism of each parameter are listed in the table as a summary at the end of each corresponding section.

4.2 Driver Influence Parameters

Driver influence parameters are those that can be changed by drivers after tire/pavement combination has been determined. A lot of parameters of this type are difficult to quantify, such as steering speed. A few most important factors are discussed below.

4.2.1 Speed

Speed is the most important single parameter in terms of TPIN levels, so nearly all TPIN models include it. As the vehicle speed and the number of tire revolutions per unit time increase, the speed with which the tire comes in contact with the pavement surface increases resulting in higher tire/pavement impact and also an increased pumping in and out of air from the contact edge (Syamkumar et al., 2013 [6]).

As shown in Table 22, no other single factor has such a prominent influence on TPIN as speed. The speed influence is large but not very interesting (Sandberg, 2001 [55]), since the speed can be easily changed and the range is wide. The approximate relationship between TPIN and speed is shown in Eq. (37) (Dare and Bernhard, 2013 [222]).

$$L_p = 10n\log_{10}(v) + b \tag{37}$$

where L_p is sound pressure level, n is speed exponent, v is vehicle speed, and b is a speed coefficient. It is noted that different mechanism has different speed exponent, shown in Table 23. It might be instructive to develop a relevant method to differentiate mechanisms at

different frequencies. A speed exponent of zero means the corresponding mechanisms are independent of speed, such as pipe resonance and Helmholtz resonance, however, it should be pointed out that these two mechanisms are amplification mechanisms rather than generation mechanisms, which means the corresponding amplifying factors for the two mechanisms are independent of speed. The speed exponent for each frequency ranges was reported by Beckenbauer and Kuijpers (2001) [487], as shown in Figure 121. The overall speed exponent is around 4, however, we can see a clear drop around 500-800 Hz for normal tires.

Table 23: Speed exponents for different TPIN mechanisms (modified from Kuijpers and van Blokland, 2001 [347], Figure 1)

TPIN Mechanism	Speed Exponent
Tread Impact	2.0-3.0
Texture Impact	3.0-3.5
Stick/Slip (Friction)	3.0-5.0
Stick/Snap	3.0-5.0
Air Pumping	4.0-5.0
Air Turbulence	5.0-6.0
Pipe Resonance	0.0
Helmholtz Resonance	0.0

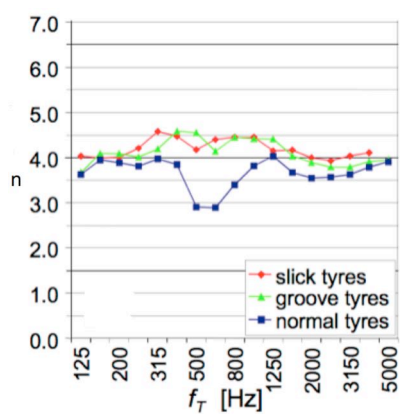

Figure 68: Speed exponent in 1/3 octave band (*n* is speed exponent; f_T is the center frequency of 1/3 octave band) (source from Beckenbauer and Kuijpers, 2001 [487], Figure 4; reprinted under fair use provision)

In practice, a more general and easier equation is used (Sandberg and Ejsmont, 2002 [7]).

$$L = A + B \cdot \log(V) \tag{38}$$

where L is the sound pressure level (SPL) in [dB], A and B are speed coefficients (constants), and V is speed in [km/h]. A and B vary with different measurement specifications,

as shown in Table 24. However, it is shown that *A* and *B* are not independent of each other. *A* decreases as *B* increases. It should be pointed out that extrapolation is not recommended since tire-pavement interaction is not the main source of noise at lower speeds (Mogrovejo et al., 2013 [209]).

Table 24: Coefficients in relationship between speed and TPIN level (source from Sandberg and Ejsmont, 2002 [7], Table 9.1; reprinted with permission from Dr. Ulf Sandberg of VTI, Sweden)

Reference	Author	Year	*A*	*B*	Method	Notes
[235]	Ejsmont	1982	=98.2-1.95B	27…46	CPX and DR	Passenger car tires
[488]	Landers	1976	N/A	40	CPX	Passenger car tires
[489]	Nilsson	1976	=77-1.95B	14...32	CB	Incl. wet road
[490]	Anonymous	1971	24.1 9.3	30.5 41.6	CB	Truck, rib Truck, lug
[491]	Corcoran	1972	N/A	40	CB	Truck tires
[492]	Walker & Williams	1979	N/A	30…40 33	CB	Passenger car tires Truck tires
[493]	Tetlow	1968	N/A	36.5 30 20	CB	Truck, rib Truck, lug Wet road
[494]	Hamet	1988	N/A	26…41	CB	Car tires; power levels
[495]	Köhler & Liedl	1981	N/A	30…45 20…40	CB	Dry road Wet road
[496]	Steven & Pauls	1990	26.2 27.3 23.4 24.4 24.6 21.9 27.9 27.1	32.9 33.5 37.3 36.9 37.2 39.9 35.5 36.7	CPX	Porous AC 0/5 Porous AC 0/8 ISO-S SMA 0/5 Surface dressing PCC AC 0/11 Asphalt 0/11
[497]	Ivannikov et al.	1998	7.1 11.8 10.7	37.6 36.3 36.8	CB	Average of 10 truck tires, ISO surface Average of 10 truck tires, SMA surface Average of 10 truck tires, porous surface
[289]	Steven et al.	2000	30.6 33.5 34.2 30.4 27.8 39.5 37.1 34.4 38.9 20.3 32.7 24.3 27.6	34.9 33.0 32.6 34.9 37.0 29.2 29.0 29.2 30.9 42.0 34.2 37.8 36.9	CPX	AC 0/16 with chippings spread on surface SMA 0/4 SMA 0/6 SMA 0/8 Surface dressing 5/8 Porous AC 6/16 Porous AC 4/8+11/16 double layer Porous AC 2/4+11/16 double layer Gussasphalt 0/11+2/5+5/8 Cement concrete transversely brushed Cement concrete with epoxy-durop 3/4 Cement concrete burlap drag Cement concrete exposed aggregate

A similar equation is often used to normalize TPIN to a specified speed,

$$L_{norm} = L_{meas} + B \cdot \log\left(\frac{V_{ref}}{V}\right) \tag{39}$$

where L_{norm} is the normalized TPIN level at reference speed V_{ref}, L_{meas} is the measured level at actual speed V, B is speed coefficient. B is taken as 35 in CPX measurements (Steven et al., 2000 [498]).

The speed has an influence on the TPIN spectrum as it affects the tire eigenfrequencies (Lopez Arteaga, 2011 [499]). There are three effects: (1) The stiffening due to the rotation leads to slightly higher eigenfrequencies; (2) the Coriolis acceleration leads to the so-called 'bifurcation' effect, where the speed of waves propagating in opposite circumferential directions with the same wavelength are different even when observed in the Lagrangian reference system (tire-fixed) (Kim and Bolton, 2004 [500]; Huang and Soedel, 1987 [501]; Huang and Soedel, 1988 [502]); (3) the Doppler-shift, which appears when the tire is observed from an Eulerian (vehicle-fixed) reference system. Following one particular particle is the Lagrangian description and looking at a particular location in the ambient space is the Eulerian description of motion.

Schuhmacher (2015) [67] investigated the effect of vehicle speed on spectrogram of tire noise, as shown in Figure 69. It can be seen that some of the spectral content (e.g. around 400-500 Hz) doesn't change with speed, but some of the spectral content does change with speed.

Ulrich (1984) [503] reported that the sound power P has the relationship with tire rolling speed V as $P \propto V^n$ where $n = 3\sim4$.

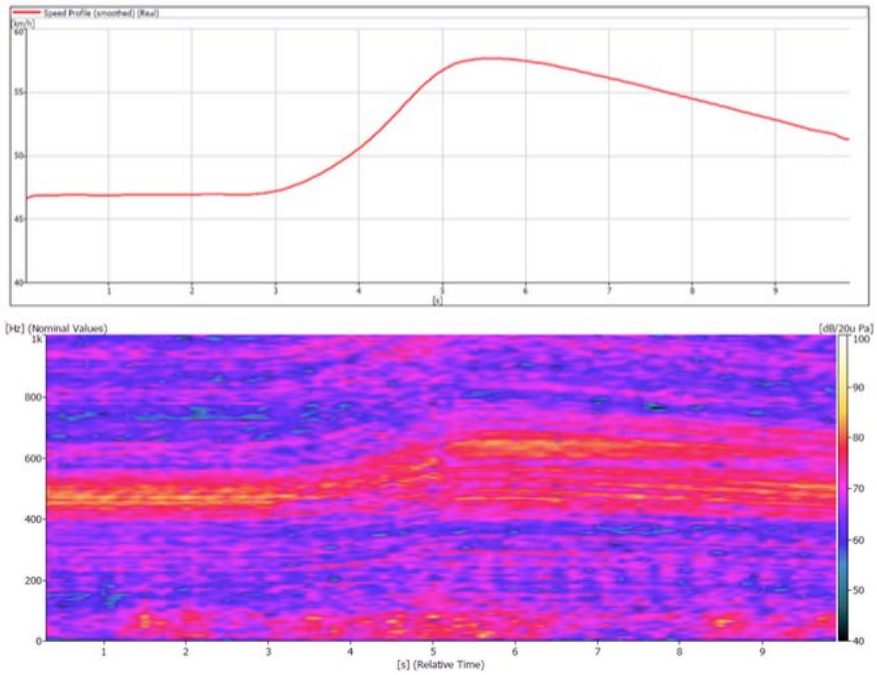

Figure 69: (a) Top figure is vehicle speed versus time; (b) bottom figure is tire noise spectrum versus time (source from Schuhmacher, 2015 [67], Figure 12; reprinted under fair use provision)

4.2.2 Longitudinal Force/Slip

During accelerating (driving condition) and decelerating (braking condition), extra longitudinal force/slip is generated leading to greater stick/slip and increasing TPIN. Driving/breaking torque and slide/skid ratio (slip ratio) are also physically equal to longitudinal force/slip.

However, the magnitude of this effect is highly dependent on the type of tires. Some tires such as high performance sporty tires are marginally affected, while TPIN levels for some tires vary by 9dB using OBSI method (Donavan, 1993 [185]). It is found that the dominant frequency range is from 800 Hz to 1.6 kHz, which is similar to that of the vertical tire load (Iwao and Yamazaki, 1996 [307]).

The driving torque effect on TPIN is also dependent on inflation pressure. Generally, the higher the inflation is, the greater the effect will be, as shown in Figure 70.

TPIN measurement in driving conditions is standardized in ISO 362-1 (2015) [104,504].

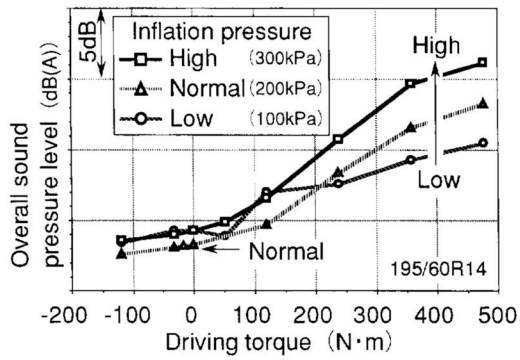

Figure 70: Changes of TPIN due to driving torque and inflation pressure (source from Iwao and Yamazaki, 1996 [307], Figure 7; reprinted under fair use provision)

The acceleration effect depends on the type of tires, as show in Figure 71 (Donavan et al., 1998 [4]). It can be seen the noise from Tire A is completely independent of acceleration.

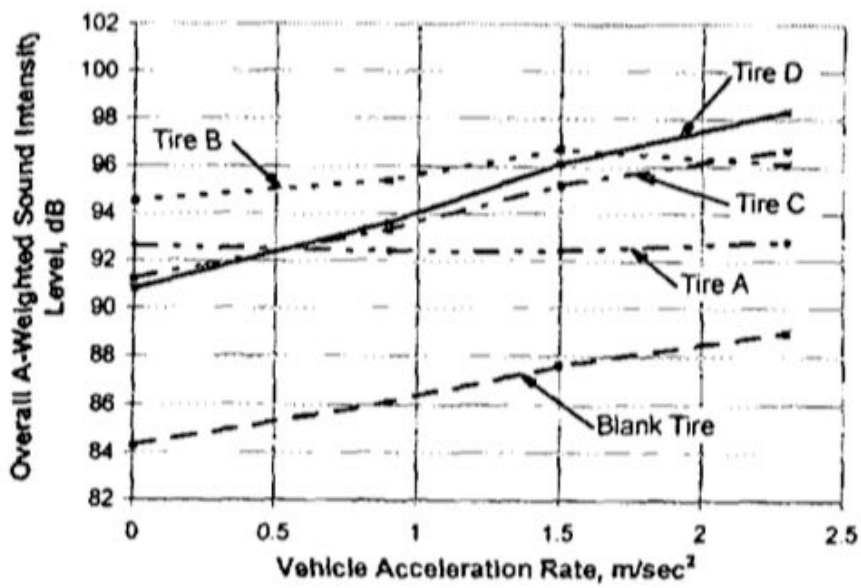

Figure 71: The effect of vehicle acceleration rate on tire noise as measured with on-board sound intensity (source from Donavan et al., 1998 [4], Figure 2; reprinted with permission from AIP Publishing LLC)

4.2.3 Lateral Force/Slip

In practical driving conditions, the lateral acceleration distribution is around 60% for <0.5 m/s^2, 30% for 0.5-1.5 m/s^2, and 10% for 1.5-2.5 m/s^2 (Yamazaki et al., 1989 [505]). Under the 10% of conditions (cornering speed 40-60 km/h with radius R=100 m), the lateral force will

be around 4-8 kN and the slip angle will be 1-2°. In addition, the slip angle is also caused by road crossfall and wheel alignment toe angle but is relatively small. Commonly, 2% crossfall leads to 0.1° slip angle, and normal toe angle leads to 0-0.5° slip angle. Ejsmont (1990) [506] reported that there was a sharp increase of noise and rolling resistance with a slip angle above only 0.5°. Donavan (1982) [427] also indicated that tire noise was higher under a curved path than under a straight path.

Cornering increases SPL essentially equally much up to 1 kHz, but creates higher increases with up to 10dB at 5-8 kHz [7]. It was found that the non-patterned tire is most sensitive to this effect. It is interesting to compare the outside tire (increased load) and inside tire (decreased load) in terms of TPIN spectrum during cornering. It was shown that for the outside tire (increased load), the TPIN level is larger at high frequencies (>2 kHz) but smaller at low frequencies (<1 kHz) than inside tire (decreased load). The larger level at high frequencies (>2 kHz) is due to the increased stick/slip phenomenon; while the smaller level at low frequencies (<1 kHz) is probably due to the movement difficulty of tread elements under large load.

Squeal phenomenon is often observed when cornering (Senda et al., 1984 [507]; Trivisonno et al., 1968 [508]); for example, very pronounced peaks at frequencies 1.2 kHz and 2.5 kHz were shown in a replica drum test. The squeal characteristics were independent on the tread patterns but highly dependent on the pavements.

Tread compound properties have major influence here. Stiffer rubber can reduce this cornering effect by reducing stick/slip. It also explains why tire squeal is more common in summer than in winter, which is probably because the hot weather in summer makes the tire rubber softer. However, under non-slip conditions, stiffer rubber is not preferable from the point of view of noise reduction.

It should be pointed out that it is very difficult to quantify this effect due to the transient characteristics of cornering/steering. The tangential force generally includes longitudinal force and lateral force, which both influence TPIN at high frequencies.

4.2.4 Tire Load

Tire load could affect several different TPIN mechanisms. Sidewall vibrations increased with load (Reiter and Eberhardt, 1974 [217]). Tread/texture impact could be enlarged as loading

changes the shape of the tire near the contact patch [6]. More deformation of air pockets in the contact patch increased air pumping (Dare, 2012 [213]). Generally, for passenger car radial tires TPIN increased by 1 to 2 dBA per doubling of wheel load when inflation pressure was adjusted to the load; by 0.7 to 1.5 dBA if inflation pressure was not adjusted (Taryma, 1982 [509]). For truck tires TPIN increased 8-15 dB per tripling of the load on each tire (Leasure and Bender, 1975 [510]). Results from other researchers are listed in Table 25 (Sandberg and Ejsmont, 2002 [7]). It was shown that tire load has much larger influence on crossbar tires than ribbed tires.

Table 25: Influence of tire load on TPIN (summarized from Sandberg and Ejsmont, 2002 [7])

Reference	Author	Year	Results (Increase per Doubling of Load)		Tire
490	Anon	1971	5 dBA Some tenths of 1 dBA		Cross-ply truck tires with lugged pattern Cross-ply truck tires with rib pattern
511	Leasure et al.	1972	3-6 dBA 0-2.5 dBA		Cross-bar and pocket tread truck tires Ribbed truck tires
512	Kilmer	1976	2-3 dBA Negligible		Cross-ply truck tires with crossbar pattern Cross-ply truck tires with ribbed pattern
513	Kilmer	1979	5 dBA 1 dBA		Cross-ply truck tires with crossbar pattern Cross-ply truck tires with ribbed pattern
514,515	Underwood	1980 1984	6.5 dBA 0.5 dBA		Cross-ply truck tires with crossbar pattern Cross-ply truck tires with ribbed pattern
516	Walker	1981	Does not change appreciably		Cross-ply truck tires
517	Köllman	1993	2.4 dBA		More than 100 car tires
518	Wolf et al.	1992	1-1.5 dBA 5 dBA 4.4 dBA		Trucks and buses Traction truck tires Ribbed truck tires
519	von Meier	1992	3.8 dBA between 70% and 100% max load 1.2 dBA between 70% and 100% max load		Traction truck tires Ribbed truck tires
7	Sandberg & Ejsmont	2003		ISO Surface (Smooth)	GRB-R Surface (Rough)
			Slick Tire	2.4 dBA	0.5 dBA
			Summer Tire	1.4 dBA	-0.1 dBA
			Winter Tire	1.4 dBA	0.9 dBA
			Average	1.7 dBA	0.4 dBA

It should be noted that heavy trucks might emit similar or even lower TPIN than some cars (Sandberg, 2001 [55]) despite that tires of trucks carry a load 5-7 times that of car tires (Sandberg, 2003 [479]). One research found heavy trucks carrying 10-20 tons gross vehicle weight (GVW) emitted lower TPIN than some high-performance cars with wide tires (Sandberg, 2001 [55]). This unexpected phenomenon might be due to the fact that the peak for truck tires is shifted to lower frequencies, which will be greatly reduced after A-weighting filtering. It may also be due to the less pronounced peak character resulting from higher belt stiffness and larger contact patch in the tire/pavement interface (Sandberg, 2003 [479]).

Tong et al. (2013) [520] concluded that TPIN increases as vertical load increases, but the

variation is marginal. It was also shown that the sound pressure level tends to show a peak value at a certain value of vertical tire load (3000 N, shown in Figure 72) as the tire speed increases (Iwao and Yamazaki, 1996 [307]).

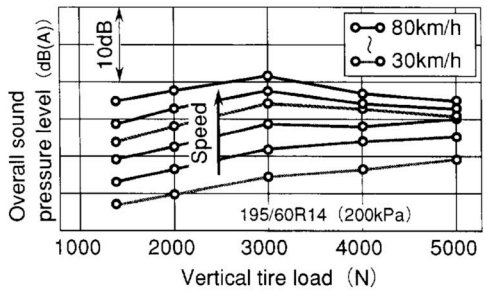

Figure 72: Changes of tire noise due to tire load and speed (source from Iwao and Yamazaki, 1996 [307], Figure 6; reprinted under fair use provision)

Heckl (1986) [13] indicated that sound power increases as the 1/3 power of the tire load. Tire load can influence the size, shape and pressure distribution of contact patch. It was generally agreed that the larger the contact patch, the greater the tire noise. The vehicle load also has marginal influence on the tire acoustic cavity (Bharadwaja and Siva, 2013 [410]) and interior noise (Beniguel and Pen, 2012 [521]). Similarly, it has very small influence on the eigenfrequency (Lopez Arteaga, 2011 [499]).

Ulrich (1984) [503] reported that the sound power P has the relationship with tire static load p_L as $P \propto p_L^{1/3}$.

4.2.5 Inflation Pressure

Inflation pressure could affect the same mechanisms as tire load because tire deflection is dependent on both inflation pressure and tire load [213]. Increased inflation could stiffen the tire carcass and change vibration characteristics such as structural resonance frequencies. It could also influence the size and shape of contact patch, and affect air pumping by changing how the air pockets deform.

Although inflation pressure is usually included as a parameter in TPIN models (Kropp et al., 2001 [227]; Keltie, 1982 [223]), few literature have investigated its effect (Tong et al., 2013 [522]). There seems to be no clear or at least no linear dependence between inflation pressure and the

vibration patterns of a tire (Bolton et al., 1998 [380]). It was reported that TPIN increased slightly with the increase of tire inflation pressure (Bremner et al., 1997 [334]). Heckl (1986) [13] indicated that the sound power increases as the square root of inflation pressure. However, Donavan (1998) [4] and Samuels (1979) [364] reported the opposite results. Muthukrishnan (1996) [523] noted that the noise levels increased with the increase of inflation pressure under lighter tire load, but the trend reversed under higher load.

Keltie (1982) [223] (for truck tires) demonstrated that acoustic power spectrum is shifted towards higher frequency as the inflation pressure increases from 60 psi to 80 psi. It was also reported that the acoustic power generated decreases significantly with the increase of inflation pressure (0.6 dB/psi) while at sufficiently high pressure (above 70 psi) the acoustic power is insensitive to further pressure increases.

Generally, inflation pressure affects TPIN and tire acoustic cavity (Bharadwaja and Siva, 2013 [410]), but the variation is marginal (Tong et al., 2013 [520]). However, with driving torque, TPIN rises with the inflation pressure (Iwao and Yamazaki, 1996 [307]), as shown in Figure 70. Increased inflation also increases the tire eigenfrequenicies (Kostial et al., 2013 [216]) and the cut-on frequencies for propagating vibration modes (Bolton et al., 1998 [380]). However, TPIN from lug type truck tires was shown to decrease as inflation increased, especially for pressure in the range of 200-400 kPa (EPA, 1980 [524]).

Bremner et al. (1997) [334] indicated that the effect of increasing inflation pressure is to increase the tire stiffness at lower frequencies without increasing the mass, resulting in the increase of wavespeed and decrease of modal wavenumbers. Kindt et al. (2007) [525] found that as the inflation pressure increases, the vibration spectrum shows in general a higher amplitude and a positive frequency shift at the structural resonances, which is due to the tire structure stiffening (both tread band and sidewall), shown in Figure 73. The transfer of tire vibrations to the rim is also improved with the sidewall stiffening. However, the acoustic resonance frequencies are not affected, because they are dependent on the geometry of the air cavity and the velocity of sound (Kindt et al., 2006 [526]). The velocity of sound for ideal gas is determined by

$$c = \sqrt{\gamma \frac{p}{\rho}} = \sqrt{\gamma RT} \tag{40}$$

where c is speed of sound, γ is adiabatic index (1.402 for air), p is pressure, ρ is air density,

R is gas constant and T is temperature (constant). As such, the velocity of sound is constant and geometry of the air cavity also doesn't change significantly with inflation pressure, so the acoustic resonance frequencies do not change much, except when the pressure change leads to the change of tire deflection on the contact patch.

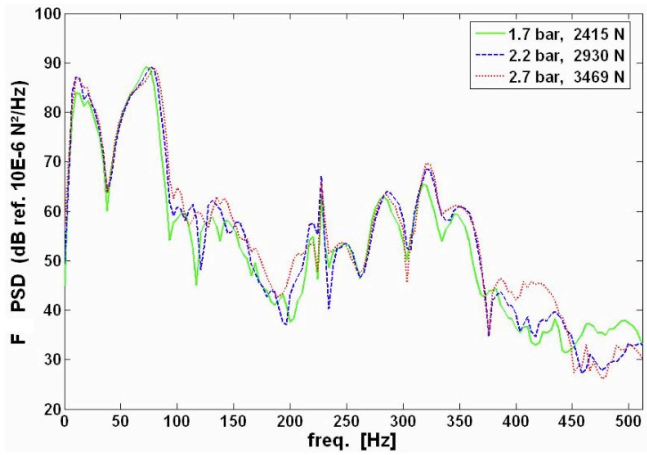

Figure 73: Vertical spindle force spectrum at different inflation pressures; driving over 5 mm high semi-circular cleat at speed of 22.6 km/h (source from Kindt et al., 2007 [525], Figure 8; reprinted under fair use provision)

Inflation pressure is sometimes or more often considered as tire-related parameter. However, the present author include it into the driver influence parameters because the driver can easily change it.

Ulrich (1984) [503] reported that the sound power P has the relationship with tire inflation pressure p_s as $P \propto p_s^{1/2}$.

4.2.6 Tire Camber Angle

Camber angle is the angle between the vertical axis of the wheel and the vertical axis of the vehicle when viewed from the front or rear. It is one of the parameters indicating wheel/tire alignment (others include caster angle and toe angle). The positive camber angle is where the top of the wheel tilts outwards from the vehicle.

Camber angle was found to have larger influence on TPIN for asymmetric tire on smooth surface at negative camber angles for middle range of speeds (50-90 km/h) (Wozniak et al., 2015 [527]). TPIN increases by about 5 dB with camber angle from +3° to -6° at 90 km/h.

Impact mechanism and stick/slip mechanism were thought to contribute most to this change. Change of camber angle can change the cross-section of the tire, footprint, and load distribution. The change of footprint geometry leads to the change of channels between the tread elements, thus influences air pumping and pipe resonance mechanism. Also at negative camber angles, two additional “horns” occur near the leading edge and trailing edge directed with their outlets outwards, which somewhat explains why negative camber angle increases TPIN.

It should be noted that the proper camber angle for testing using laboratory drum method (DR) or close-proximity trailer method (CPX) should be 0°, but no formal requirements are indicated in the standards. However, when experiments are conducted using CPX method, the camber angle is usually in the range from -1.5° to -0.5° due to a compromise between good traction performance (0°) and cornering grip (-3° to -2°), so the TPIN measurement might be influenced by this angle (Wozniak et al., 2015 [527]).

4.3 Tire Related Parameters

Tire properties have major influence on TPIN emission, especially for truck tires (Reinink et al., 2005 [528]). The spread between the noisiest and the quietest tire might be 10 dB, irrespective of pavement type (Sandberg and Ejsmont, 2000 [171]).

The relationships between tire parameters and TPIN from a single tire are presented in this subsection. TPIN from multiple tires (Takahashi et al., 1995 [529]; Mioduszewski, 1995 [530]) in the vehicle is not discussed here.

4.3.1 Tire Type/Construction

It is not easy to identify which type of tire is noisiest/quietest. One research found that on the same pavement, the maximum TPIN occurs on winter tire, followed by slick tire, and the minimum TPIN occurs on summer tire (Chang, 2012 [531]). However, another research claimed that winter tires (not studded) appear to be somewhat less "noisy" than the tires for summer use (Sandberg and Ejsmont, 2000 [171]). It might be reasonable to argue that nowadays the overall TPIN levels from summer tires and winter tires are similar (VTI, 2006 [532]). Having said that, the TPIN spectrum of these two types of tires is still different (Tanizaki et al., 2013 [533]).

The influence of tire construction on tire stiffness is limited since roughly 90% of the tire stiffness originates from the air pressure inside the tire-rim cavity (Bekke et al., 2013 [534]). A maximum influence of tire construction including changing from summer to winter compound was found to be just around 3 dBA (Seamenn, 2008 [535]). It was shown that tires with different sidewall filler height all produce similar overall sound pressure level and frequency spectra for a specific test surface (Bernhard, 2003 [295]). Whether the tire has cap ply or not doesn't influence the results either. It was also indicated that angle of cord either in the carcass or the belt does not have much influence.

For the same types of tread design and rolling speed on the same pavement, the TPIN of radial tire is lower than that of bias tire. It is often assumed the difference is about 2 dBA in favor of radial tires (Sandberg and Ejsmont, 2002 [7]). Leasure and Bender (1975) [510] indicated that radial tires are 1-3 dB quieter than bias-ply tires. A more important benefit of radial tire is 20-30% reduction of rolling resistance (Ejsmont, 1990 [506]). The difference between radial tire and bias tire is the crown angle (90° for radial tire), which is the angle between the ply cord and the circumferential tire centerline. In general, smaller crown angle leads to better cornering performance but harsher ride (El-Gindy et al., 1999 [536]). Most tires in the market right now are radial tires due to low energy dissipation (60% of that of bias tire) and long durability (twice as long as that of bias tire) (Moore, 1975 [537]).

Different tire components (including apex, bead, belt coat, belt wedge, belt wire, cap ply coat, cap ply cord, chafer, liner, ply coat, ply cord, rimstrip, sidewall, tread and undertread) have different influence on structure-borne TPIN (Aboutorabi and Kung, 2012 [538]). The stiffness and mass of tread were found to be the most importance for the tire mode frequencies and generalized mass. Ejsmont (1990) [506] reported that the reinforcement material and tread material in radial tires do not have much influence on TPIN.

Leasure and Bender [510] (1975), and Staadt (1974) [539] indicted that truck tire noise was a major contributor to traffic noise. Fong (1998) [540] reported that the contact pressure for truck tires are usually a magnitude higher than passenger car tire due to higher tread rubber stiffness and inflation pressure. It was also indicated that truck tires radiated greater noise below 100 Hz up to 10 dBA than passenger tires, as well as above 1000 Hz, but similar noise levels between 100 to 1000 Hz.

Bremner et al. (1997) [334] reported that the increase of tire damping loss factor reduces

noise above 300 Hz. Bremner et al. also indicated that the increase of tread thickness will increase its mass per unit area as well as the bending stiffness, resulting in the increase of power input from the pavement and noise radiation especially at the higher frequencies. The increase of the equivalent isotropic modulus of the rubber/fabric matix was reported to increase noise radiation. Adding the steel belting was shown to increase the tread mass, leading to two contradictory effects, i.e., the increase of input power from impact mechanism but decrease of radiation coupling. The total effect is a small decrease in the noise radiation. Adding the radial ply stiffness with lightweight materials such as Kevlar crossply was reported to increase noise radiation.

Pei et al. (2015) [541] investigated the Influence of tread structure design parameters on tire vibration noise using boundary element method (BEM) and modal acoustic transfer vector (MATV). It was found that the contact force spectrum is flat between 0-5000 Hz. It was observed that there is no clear trend for influence of the ratio of radial contact force between belt and carcass to inflation pressure on the tire vibrations, but there seems to be an optimized point.

4.3.2 Tire Size

The conventional naming for tire size of passenger car tires is like 215/60R16: 215 is tire section width is mm; 60 is aspect ratio (section height divided by section width) in percentage; 16 is rim diameter in inch.

There seems to be a persistent trend for tires to be wider and wider over time, especially for sports cars (Dimitri, 2012 [170]), as is shown in Figure 74 (Sandberg and Ejsmont, 2002 [7]). Survey showed that in the last 15 years of the 20th century, the average tire width of cars on market increased from 165 to 195 mm (Sandberg and Ejsmont, 2002 [7]). However, it might not be a good practice from the perspective of noise reduction.

As the tire width increases, the tread/texture impact becomes more extensive leading to greater vibrations. Stick/slip and stick/snap phenomena are also amplified. A tire with a wider section involves greater displacement of air within the tire-road interface, amplifying both air pumping and air turbulence. In addition, horn shape and Helmholtz resonator are easier to occur with greater tire width (Kumar et al., 2011 [542]).

Generally, wider tire section generates greater TPIN (Sandberg and Ejsmont, 1998 [543]),

especially in the low frequency band from 500 to 1000 Hz (Yang et al., 2013 [544]). As such, tire noise regulations usually have step limits for different range of tire width. It was found that TPIN on smooth pavement at the speed of 70 km/h increased by around 0.3-0.4 dB per 10 mm of width increase (Storeheier and Sandberg, 1990 [545]), as shown in Figure 75. The width influence may also be expressed as an increase of 4 dB per doubling of width (Sandberg and Ejsmont, 2002 [7]). Ulrich (1984) [503] reported that the sound power P has the relationship with tire width b as $P \propto b^{3/2}$.

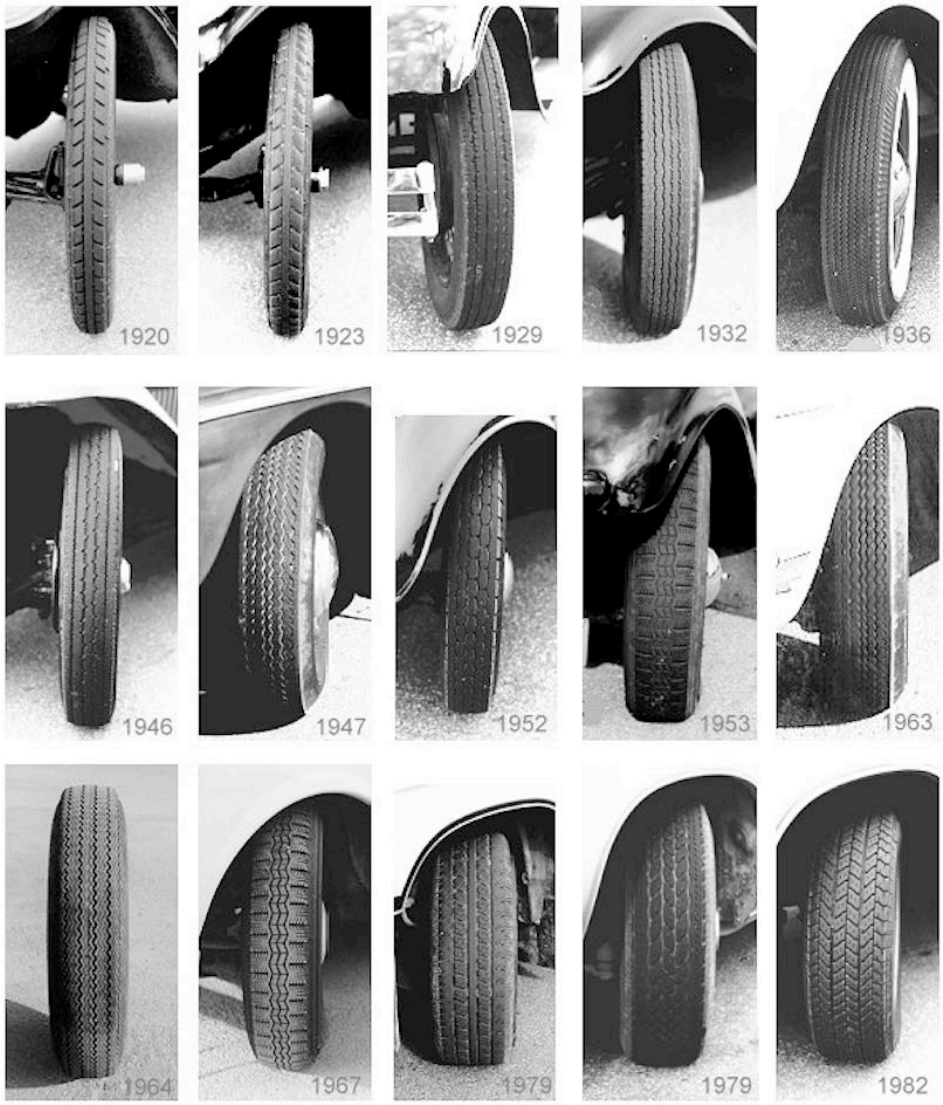

Figure 74: Common tires with year indicated (source from Sandberg and Ejsmont, 2002 [7], Figure 6.5; reprinted with permission from Dr. Ulf Sandberg of VTI, Sweden)

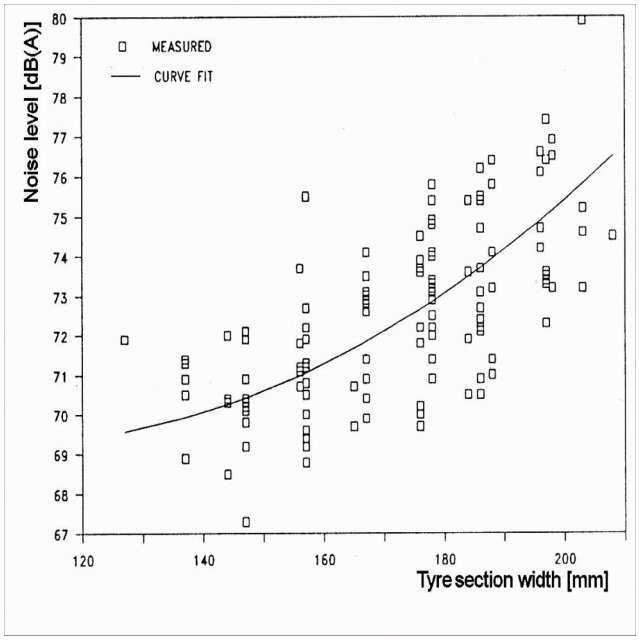

Figure 75: Relation between TPIN level and tire width (data based on measurements 1981-1987 on radial car tires in Germany, Sweden and Norway) (source from Storeheier and Sandberg, 1990 [545]; reprinted under fair use provision)

However, it was found that the influence of tire width is not linear or consistent, and becomes insignificant when it exceeds 200 mm (Yang et al., 2013 [544]), which contradicts with the results shown in Figure 75. Only a weak correlation ($R^2 = 0.38$) was found in a set of 276 tires of different widths (Sandberg, 2001 [55]). Actually, it was shown that for the same speeds and number of tires, TPIN of truck tires is only slightly higher than that of car tires, despite the greater widths and much higher loads (Sandberg, 2001 [55]).

Tire width has a small influence on the radial natural frequency but it also depends on the tire diameter which will be discussed below (Kostial et al., 2013 [216]).

It was shown that TPIN decreases with increase in overall tire diameter (Kumar et al., 2011 [542]). As tire diameter increases, the attack angle decreases, as shown in Figure 76, leading to less pronounced and abrupt tread/texture impact. On the other hand, the decreased attack angle amplifies the horn effect. Increased tire diameter will reduce the tire cavity resonant frequency (Mohamed and Wang, 2015 [393]). Ulrich (1984) [503] reported that the sound power P has the relationship with tire radius a as $P \propto 1/a^3$. Pei et al. (2015) [541] found that the increase of the radius of the belt layer or the radius of tire tread will reduce the tire vibrations.

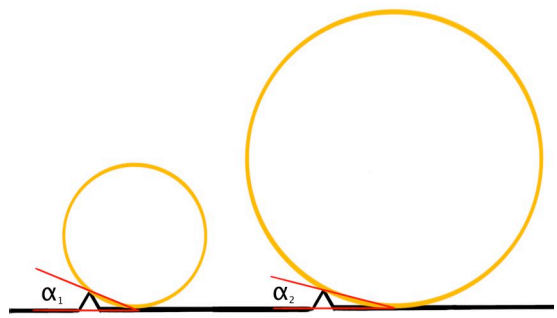

Figure 76: Attack angles of tires with different tire diameters ($\alpha_1 > \alpha_2$)

Tire aspect ratio is another important dimensional parameter, defined as the section height divided by the nominal section width multiplied by 100 (expressed as a percentage), but it is not interesting in TPIN analysis. However, it is interesting to point out that the aspect ratio has decreased from 0.8 to 0.4 over the last three decades (Tanaka et al., 2016 [383]) in order to improve the vehicle stability at high speed.

4.3.3 Belt Stiffness

Belt stiffness also refers to belt bending stiffness or the stiffness of tread band (Wolfgang et al., 1998 [377]). The bending stiffness of a plate is also called flexural rigidity representing the moment per unit length per unit of curvature, given by

$$D = \frac{Eh_e^3}{12\left(1-v^2\right)} \tag{41}$$

where D is flexural rigidity in [Pa·m3] or [N·m], E is Young's Modulus, h_e is elastic thickness and v is Poisson's ratio (Landau and Lifshitz, 1986 [546]). The normal values of standard tires are in the order of 2-5 N·m for circumferential bending stiffness and 1-3 N·m for lateral bending stiffness. When it comes to belt stiffness, it usually refers to circumferential bending stiffness. O'Boy and Dowling, 2009 [547] reported that for the tire belt without the layer of tread rubber, the equivalent bending stiffness is 7.6 N·m with an area density of 14 kg/m^2, while for the tire belt with the layer of tread rubber, the equivalent bending stiffness is 13.6 N·m with an area density of 21.8 kg/m^2.

The radial belt bending stiffness can also be measured by the following method. The

non-inflated tire tread was deflected by a spherically shaped narrow bar. The force required to produce a certain deflection of the tread area was considered the radial belt bending stiffness with the unit of kN/mm (Sandberg and Ejsmont, 2002 [7]). It generally depends on the construction of tread, such as the number of layer and materials.

It was found that the increased carcass stiffness reduces the shoulder tread vibration and the TPIN (Ejsmont, 1982 [235]; Watanabe et al., 1988 [548]). Increasing tread belt stiffness will reduce air pumping (Plotkin and Stusnick, 1981 [43]). It was also indicated that tire with a high tension at the shoulder and/or a lower belt tension at the center of the tread reduces TPIN by up to 2 dB (Doan, 1996 [549]). Bremner et al. (1997) [334] reported that increasing damping or adding steel belts would decrease tire noise. However, increasing bending stiffness of the belt will result in the increase of its mass, which is not good from the dynamics perspective (Kropp et al., 1998 [377]). Wolfgang et al., 1998 [377] indicated that the radial driving point mobility decreases with the increase of belt bending stiffness, resulting in the decrease of velocity amplitude. However, the radiated sound does not change much, because the radiation efficiency increases with the increase of belt bending stiffness. It was pointed out the to avoid this compensation, the surface density (mass per square meter of the belt) should be increased at the same time. It should be noted that large numbers of researches on such construction parameters as belt stiffness, belt angle are proprietary to tire companies and have not been published. However, it is reasonable to assume these parameters have much smaller influence on TPIN than tire dynamics.

Belt stiffness can also refer to circumferential stiffness, lateral stiffness, and torsional stiffness (Kostial et al., 2013 [216]). Generally, they all have similar effect on TPIN as radial stiffness, but to different degrees.

However, Keltie (1982) [223] demonstrated that for truck tires, the sound power is dominated by in-plane or membrane effects rather than bending effects. As such, bending stiffness has little effects on the tire noise (less than 1 dB when doubling the bending stiffness). In addition, it was also shown that as the inflation pressure increases, the effects of the bending stiffness on the radiated sound power decrease.

4.3.4 Damping (Loss Factor)

The damping effect is usually combined with Young's modulus E to form a complex

Young's modulus E with bar above, as given by

$$\bar{E} = E(1 + j\delta_E) \tag{42}$$

where j is imaginary unit, δ_E is loss factor.

The damping is shown to have very small effect on the radiated sound power, indicating that the tire vibration is a forced acoustic radiation problem below acoustic coincidence (Keltie, 1982 [223]). It was reported that only the bands between 250 and 500 Hz show an appreciable (1-2 dB) decrease as the loss factor is increased from 0.7 to 1.05. The decrease for overall sound power level is only about 0.6 dB.

4.3.5 Non-uniformity

Tire non-uniformity or unbalance could result in large self-generated resonant vibrations and a dramatic modulation of low frequencies below 100 Hz (Eberhardt, 1979 [417]). A study on truck tires found that the modulation frequency depended on tire rotation speed (a circumferce of 3.3 m corresponded to 3.8 Hz at 50 km/h). This increased the 200 Hz third-octave band by 15-20 dB and increased the axle vibration amplitude by 1 mm (Ivannikov et al., 1998 [497]). Another study on car tires found that then non-uniformity increased the 80 Hz third-octave band by 7 dB and increased the radial force variation from 70 N to 180 N (Ejsmont, 1982 [235]). However, due to the A-weighting on these frequencies, the overall TPIN increase was only around 1dB. While negligible for exterior noise, it causes major low frequency noise and infrasound inside vehicle, which is not neutral to human health and feeling.

4.3.6 Rubber Hardness

In general, rubber hardness has a positive correlation with TPIN (R^2 = 0.3) (Sandberg and Ejsmont, 2000 [171]), especially at high frequencies and on rough road surface (Sandberg and Ejsmont, 2007 [550]). If the types of pavement are categorized, the coefficient of determination is much higher with R^2 = 0.68~0.98 (Ho et al., 2013 [498]).

A cross-bar truck tire with a tread rubber hardness of 59 Shore A tested on a drum facility was shown to be 5-8 dB noisier than a tire with softer rubber (40 Shore A). However it should be noted that in practice such soft rubber as 40 Shore A (rubber hardness unit according to ISO 868 [551], also in ASTM D2240 - 05(2010) [552]) is not suitable for truck tires due to the

deterioration of other parameters such as wear resistance (Watanabe et al., 1998 [548]) and steering/handling performance. In general, TPIN increases by 1-2.5 dB per 10 unit increase in Shore A hardness (Sandberg and Ejsmont, 2007 [550]). Similarly, Oddershede and Kragh (2014) [553] found that noise levels using Close Proximity method (CPX) increase by approximately 0.09 dB per Shore A for SRTT tires with tread hardness ranging from 62-74 Shore A, as shown in Figure 77 where it also demonstrates that rubber hardness does not significantly influence the TPIN spectral shape in that hardness range. They also found that tire rubber hardness increases with the tire age (2006-2012), called rubber hardening.

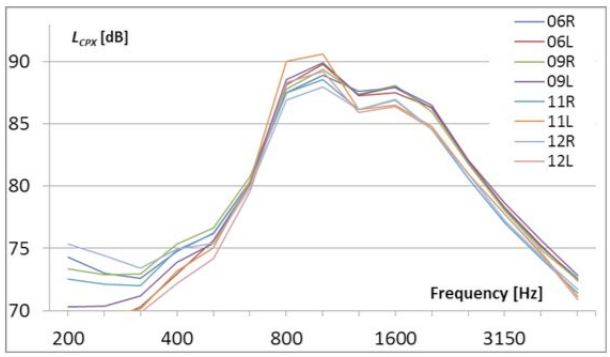

Figure 77: Frequency spectra measured at each individual tire on the ISO test track (the numbers in the legend indicate year) (source from Oddershede and Kragh, 2014 [553], Figure 6; reprinted with permission from Mr. Jens Oddershede of Vejdirektoratet, Denmark)

The rubber hardness influences TPIN mostly in the frequency range of 1-3 kHz (Sandberg and Ejsmont, 2002 [7]). For the aggressive tread, the influence around 2-2.5 kHz might be 10 dB. It is reasonable to speculate that increased hardness amplifies the stick/slip motions.

A study attempted to explain the hardness effect by modeling is Wullens and Kropp, 2001 [554]. The frequency range of 400-700 Hz and 1300-1400 Hz was found to match the measurements best (Wullens, 2002 [555]).

Parameters physically similar to tire hardness is the stiffness and storage moduli (Bekke et al., 2013 [534]). The tread compound stiffness (E' or called elastic modulus) measures how much force needed to deform the tire to a certain distance. The loss modulus (E'') measures the compound's hysteresis reducing the travelling distance of vibrational waves. Their respective ratio ($\tan\delta = E''/E'$) is often used as a design parameter in rubber compounding. It was shown that a higher $\tan\delta$ reduces the TPIN and a maximum effect is around 1.5 dB(A). It

means a smaller elastic modulus and a higher loss modulus are in favor of noise reduction. However, the loss modulus should not be too large, because higher hysteresis often increases rolling resistance (Saemann, 2008 [556]).

Compared to sidewall modulus, Muthukrishnan (1996) [523] concluded that tread modulus has a much larger influence on TPIN but they have to be taken into consideration together. Other properties of tread material also have influence on TPIN but the effect is complicated. It was shown high-hysteresis rubber increased TPIN on rough pavements but decreased TPIN on smooth pavement (Underwood and Nelson, 1984 [135]) (the present author questions this remark). Bremner et al. (1997) [334] reported that increasing tread thickness (tread depth) and rubber stiffness would increase noise.

Rochoux and Biesse (2010) [337] found that soft rubber has better noise performance at high frequencies, which leads to a paradox: it should give higher air compression because of its higher deformation, since at high texture frequencies, a deeper road cavity is better because it results in better air drainage which reduces air compression, thus cavity air pumping noise, as illustrated in Figure 78. This might suggest that the air pumping mechanism is insignificant for the tire tested. Rochoux and Biesse (2010) [337] also observed that the decrease of rubber viscosity (hysteretic behavior) will increase the vibrations from texture impact on the tire rubber, especially at the contact center and the trailing edge.

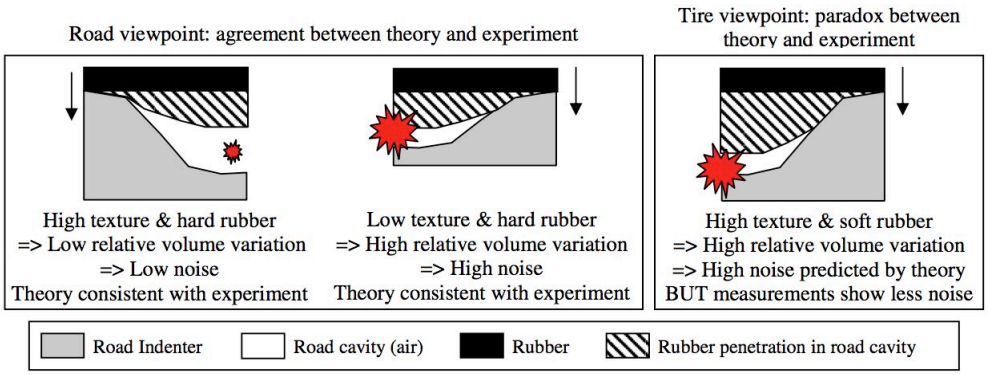

Figure 78: Commonly proposed air pumping mechanism: disagreement with measurements from the tire's point of view (source from Rochoux and Biesse, 2010 [337], Figure 1; reprinted under fair use provision)

Swieczko-Zurek et al. (2015) [557] showed 0.15 dB/Shore A for SRTT and 0.19 dB/Shore A for Avon AV4 tires on ISO road surface while Buehlmann et al. (2013) [558] showed up to 0.3

dB/Shore A.

Schubert et al. (2016) [559] reported that the values are in the range from -0.03 to 0.14 dB/Shore A depending on the tire and pavement, indicating Shore hardness of the tires is not able to sufficiently describe the acoustically relevant properties of tires. Therefore, the mechanical admittance (mobility) or its inverse (i.e., mechanical impedance) is used instead since it is a direct descriptor for the vibrational behavior of the tire. The study was conducted on 11 CPX tires (six Uniroyal SRTT tires and five Avon AV4 tires) manufactured between 14th week in 2014 and 42th week of 2006.

The tires inflated at 200 kPa were mounted on rims suspended by a hub without any load, so the vibrations could propagate unaffected. The shaker was preloaded at 2 kg against the center of the tread. The excitation signal was a band-limited white noise (15 Hz to 4 kHz). The exemplary results of the tire mobility measurements are shown in Figure 79.

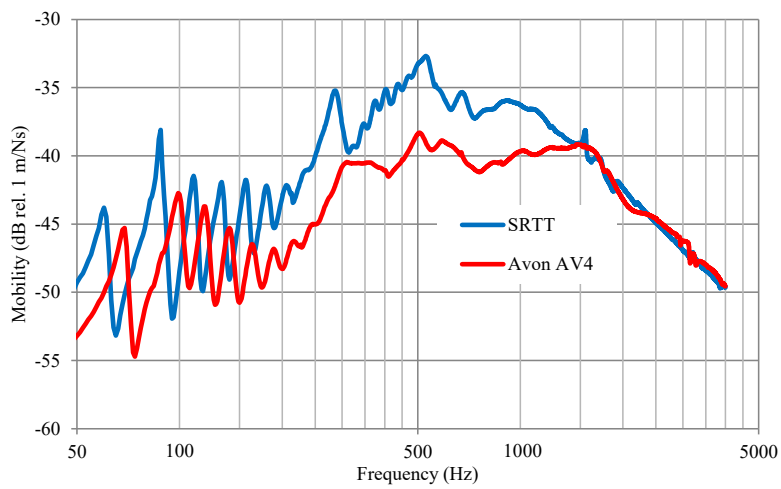

Figure 79: Example for mobility measurements results (source from Schubert et al., 2016 [559], Figure 5; reprinted under fair use provision)

As shown in Figure 80, aging (or hardening) generally causes a decrease of the tire mobility and a slightly increase of the mode frequencies, based on which Schubert et al. (2016) [559] suggested an adjustment of the Young's modulus of the tread layer (-20% for a younger tire and +50 % for an older tire), and of the stiffness of the additional contact springs (-5 % for a younger tire , +10 % for an older tire).

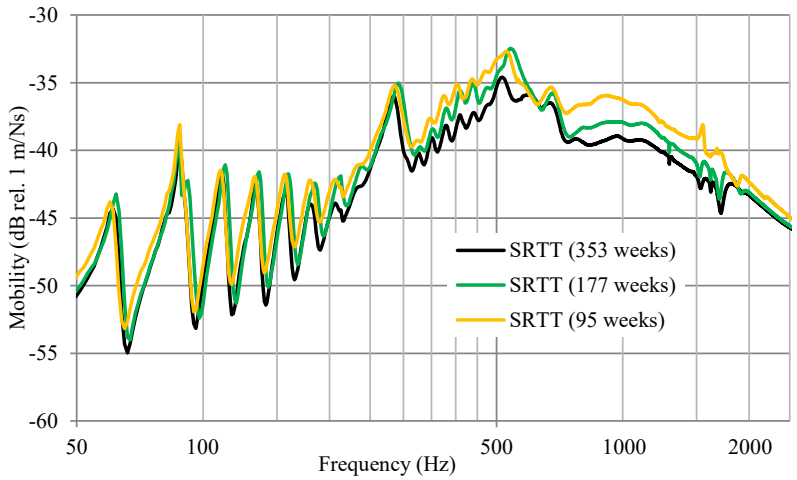

Figure 80: Comparison of measured mobility spectra for SRTT tires of different age (source from Schubert et al., 2016 [559], Figure 8; reprinted under fair use provision)

The tire degradations include mechanical wear and chemical ageing. Langwieder et al. (2001) [560] reported that 2-5% of tires in actual use had a tread depth of less than the legal minimum 1.6 mm and that 1-4% of the tires were "over-aged". The age effect is the effect which occurs when a tire is stored in a way in which its tread rubber compound undergoes changes due to exposure to moderate or high temperatures, or to certain substances and gasses in the air, for example, oxygen diffusing through the tire composite and reacting with the internal components (Sandberg and Ejsmont, 2007 [550]). Gothié (2001) [561] reported that the ageing effect is around 1 Shore A/year; however, larger the first years and lower in later years. Even though the tire is stored in a professional way (dark and in a relatively cool place), the ageing effect still exists. However, a temperature of -10 °C is able to suppress the aging effect well (Gothié, 2005 [562]).

Sandberg and Ejsmont (2007) [550] reported that the rubber hardness of individual tires may increase by up to 15 Shore A in its lifetime, which is an equally large range as new tires may differ in hardness due to construction and material design differences. The summer tires seem to age approximately as much as the winter tires, but take longer time to do so, given the same high temperature exposure, which is logical since summer tires are optimized for higher temperatures. The hardness increase usually results in a noise emission increase, mainly at high frequencies; often as high as 0.2-0.25 dB(A)/Shore A in overall noise level. Hardness is one of the most influential parameters in low-noise tires design. It was also noted that tire

noise is generally more closely related to hardness for rough than for very smooth road surfaces.

However, Sandberg and Ejsmont (2002) [7] reported that when running tires with substantial side forces, a totally contrary effect of tread rubber hardness occurred, namely that the softer tread gave higher noise levels above 1 kHz.

4.3.7 Wear/Aging

Tire wear and aging can be affected by tire storage, tire mounting and vehicle maintenance (ETRTO, 2002 [563]). Thiriez and Subramanian (2001) [564] reported that nine percent of vehicles had at least one tire that was bald (tread depth of 2/32^{nds} of an inch or less).

Tire wear might be the most important single tire-related parameter in terms of TPIN (Tong et al., 2013 [520]). Leasure and Bender (1975) [510] reported that tire noise often increases then decreases with wear due to initial flattening of tire curvature and edges, then tread depth reduction.

When a tire in operation or in storage ages due to oxidization, the rubber hardness both in the tread and the sidewall increases. The aging effect is around 6 Shore A per year (Ho et al., 2013 [498]). The TPIN level increases by 0.08-0.48 dB(A) per shore A value increase, depending on the pavement. Thus, TPIN increases by 0.5-2.5 dB(A) per year due to this effect.

Tire wear/aging not only leads to hardness increase, but also results in cracks in the rubber due to cyclic deflection and kneading, which will affect the carcass vibrational characteristics. In addition, most importantly, there is a loss of tread rubber, leading to a thinner tread and smaller tread depth. As a result, the wear influence on TPIN is very complicated. Generally, TPIN increases with tire wear then decreases, which means the peak occurs when the tire is half worn for both truck tires (Walker and Major, 1974 [565]; Walker, 1975 [566]; Flanagan, 1972 [567]) and car tires (Hillquist and Carpenter, 1973 [568]). It was suggested that changes to tread curvature (crown radius) due to tire wear might explain the TPIN increase (Tetlow, 1971 [569]). It was also found that this effect is more pronounced on smooth pavement than rough pavement (Underwood and Nelson, 1984 [135]). The later decreased TPIN for further wear might be due to the thinner and smoother tread, especially on smooth surface. However, this effect was not easy to be observed on rough pavement, probably because the thinner rubber

layer reduced dynamic stiffness and made the tread band vibrate more easily due to the tread/texture impact (Iwao and Yamazaki, 1996 [307]).

In practice, the wear is seldom even around the tire resulting in tire unbalance, which will cause the problems discussed in the Section 4.3.5 Non-uniformity. The Archard wear theory (Archard, 1953 [570]) could be used to model and calculate the sliding/adhesive tire wear (Tong et al., 2013 [522]; Tong et al., 2014 [238]). The fundamental equation is as follows.

$$V = K\frac{F_N}{H}L \tag{43}$$

where V is the total volume of wear amount, K is the wear coefficient, F_N is the normal load of contact pair, H is the hardness of the softer material in the contact pair, L is the slip distance. The ratio of wear volume $\dot{h}$ for a tire (Tong et al., 2013 [522]) is

$$\dot{h} = \frac{\frac{K}{H}\sum_{i=1}^{N} P_i \gamma_i T_i}{\sum_{i=1}^{N} A_i} \tag{44}$$

where subscript i is the node index, P_i is normal contact pressure at node i, γ_i is the slip ratio, T_i is the width of contact node, A_i is the contact area near node i.

4.3.8 Retreaded

Retreading is the process of replacing the worn-out tread with a new one. The same carcass might be retreaded several times because the life span of tire carcass largely exceeds the tread. Roughly half of the truck tires in Europe are retreaded (FEHRL, 2001 [28]). High quality retreading meets certain national criteria (such as tire balance and randomized pattern), which guarantees no compromise for safety. However, there exists a prejudice that retreaded tires are noisier than the corresponding brand new tire.

A study on 20 truck tires using CPX method revealed that retreaded tires were equally quiet or noisy as "ordinary" new tires (Sandberg, 1991 [571]). The TPIN level differences were within ±1 dB. It was also shown that retreaded tires were less noisy than new tires on the rough pavement but noisier on the smooth pavement. It is probably because the retreaded patterns are often more aggressive and the rubber is softer. Another study on 11 retreaded car tires using Trailer Coast-By (TCB) method showed the same results (Köllman, 1993 [517]).

4.3.9 Studded

A lot of winter tire (snow tire) are fitted with studs (steel or aluminum pins) into the tread to enhance traction performance. However, this generally makes studded tire the noisiest tire. It is very easy to identify studded tires based on the tire noise characteristics (higher levels and more annoying than non-studded winter tires and summer tires). At low speed, the sound is a clatter originating from the metal pin impacting the pavement; at higher speed (above 50 km/h), the individual impacting sound turns into a high frequency hissing sound (Sandberg and Ejsmont, 2002 [7]).

TPIN above 5000 Hz largely increased, probably due to the impact and the associated scratching (when tangential movement occurs) of the pin on the pavement. Studs also produce more noise in the middle frequency range of 400-3000 Hz, which is likely to be caused by the rubber being pressed-in by the studs, thus causing the tire vibrations (Sandberg and Ejsmont, 2002 [7]). Sandberg and Ejsmont (2000) [171] indicated that on average the studded winter tires are about 2 dBA louder than summer tires and about 3 dBA louder than the non-studded winter tires. The studded tire is limited in Japan and Norway, but mostly due to dust generation and pavement damage rather than noise issues (Sandberg, 2001 [22]).

Johnsson and Nykänen (2013) [572] developed a model to predict/auralize the tire stud noise in the vehicle compartment based on the stud pattern and stud/tire response at any desired speed. A typical stud pattern is illustrated in Figure 81 (Johnsson and Nykänen, 2013 [572]). It was also indicated that even though annoyance (human perception) has strong correlation (R^2 = 0.81) with loundness (analytical quantity), listening test is still preferred to evaluate the stud effects.

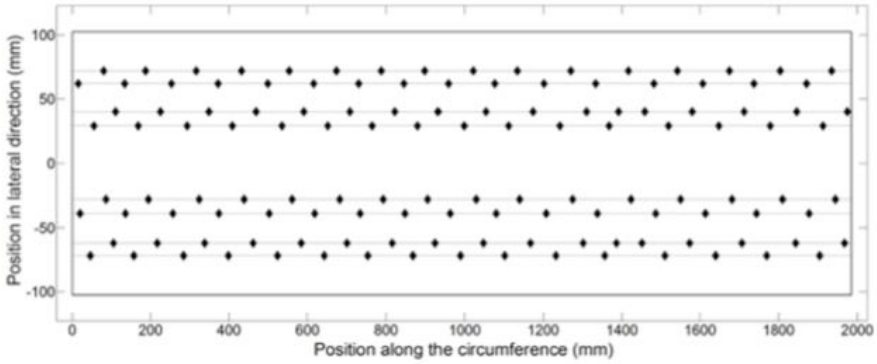

Figure 81: A typical stud pattern (8 stud lines with 16 stud on each line, 128 studs in total) (source from Johnsson and Nykänen, 2013 [572], Figure 3; reprinted under fair use provision)

4.3.10 Tread Porosity

Like porous pavement as a quiet pavement, porous rubber has been used as one of the changes in prototype quiet tires (Nilsson, 1982 [239]). Rubber granules bound with polyurethane are used in the tread to create a porous structure with interconnecting air voids (Sandberg et al., 2005 [321]). This will mitigate air pumping and the horn effect by sound absorption.

A Swedish research found that porous rubber tires reduce TPIN by about 7 dBA on rough pavements. On smoother pavements, this reduction is a bit lower. Besides, rolling resistance was not compromised by the porous rubber, but wet friction performance was poorer (Sandberg et al., 2005 [321]).

4.3.11 Tire Cavity Content

As discussed above, multiple attempts have been successful to mitigate the cavity acoustic resonance by filling the tire with extra materials. For example, filling the test tire with soft dense rubber reduces TPIN by some 8 dB over a frequency range from about 400 to about 1100 Hz (Pottinger et al., 1986 [3]). Results from foam-filled cavities are similar. However, even though vibration amplitudes were reduced, TPIN did not seem to be reduced.

Another method is to fill the cavity with other gases than air such as nitrogen or helium (Wang et al., 2014 [297]). It did shift the resonant frequency a bit, it was shown that acoustic resonances do not affect vibration and the cavity content changes do not affect TPIN very much (Bolton et al., 1998 [380]).

It should be pointed out that changing tire cavity content is definitely not common practice due to cost and durability issues.

4.3.12 Rolling resistance

TPIN and tire rolling resistance (corresponding to fuel consumption and exhaust emission) are two of the most important environmental problems in beginning the 21st century (Ejsmont et al., 2012 [573]).

Results from many studies indicated that there is only weak positive correlation ($R^2 = 0.08$ [171]) between TPIN and tire rolling resistance (Sandberg and Ejsmont, 2000 [171]; Ejsmont et al., 2012 [573]; Stenschke and Vietzke, 2000 [574]; Hoever and Kropp, 2012 [575]). It means it is

possible to reduce TPIN and rolling resistance at the same time without compromising each other, as shown in Table 26.

The method for measuring rolling resistance is standardized in ISO 18164 (2015) [576] combining three individual standards ISO 8767 (1992) [577], ISO 9948 (1992) [578], and ISO 13327 (1998) [579].

Table 26: General influences of different parameters on TPIN and tire rolling resistance (modified from Ejsmont et al., 2012 [573], Table 1)

	Relation with TPIN (↑↗•↘ ↓)	Relation with Rolling Resistance (↑↗•↘ ↓)
Speed	↑	↗
Tire Load	↗	↑
Inflation Pressure	•	↓
Rubber Hardness	↗	↘
Wear/Aging	↗	↘
Studded	↑	↗
Surface Rating (IRI)	•	↗
Porosity	↓	•
Stiffness (Impedance)	↗	N/A
MTD/MPD/Texture	↑	↗
Wetness	↑	↑

4.3.13 Reference Tire

Some sort of reference tires are desired in many studies, such as comparing performances of different vehicles and/or pavements, constructing reference pavement [425]. A reference tire should have well documented specifications, be commercially available over time and represent common tires in market. A previous reference tire was Goodyear Aquatred III (Rasmussen, 2009 [580]). Currently, the P225/60R16 97S Radial Standard Reference Test Tire (SRTT) is the commonly accepted referenced tire described in ASTM F2493 (2014) [581]. Besides noise tests, the SRTT is also used as a reference tire for braking and wear performance. The sole source of supply of SRTT known to the authors at this time is Michelin Passenger and Light Truck Tire Manufacturing (P225/60R16 97S SRTT Uniroyal Tiger Paw AWP) (2014) [581]. The tread pattern is shown in Figure 82. The previous SRTT in 1990s' used to be Uniroyal Tiger Paw XTM P195/75R14 (Ruhala, 1999 [244]), with footprint illustrated in Figure 83. It had 56 circumferential tread elements with 9 varied sizes as shown in Table 27.

The sequence of the 56 tread elements is below.

1, 2, 4, 6, 8, 8, 6, 4,

2, 2, 4, 6, 6, 4, 2, 1,

2, 4, 6, 8, 9, 8, 6, 4,

4, 6, 6, 4, 3, 5, 7, 5,

3, 5, 7, 9, 9, 7, 5, 3,

1, 1, 3, 5, 7, 5, 3, 1,

3, 5, 7, 9, 7, 5, 3, 1.

Even though the reference tire has strict specifications, there still exist variations from test to test (Donavan and Lodico, 2013 [582]). The variation for a single new SRTT tested on the same pavement for multiple times might be 0.7 dB. The variation for multiple new SRTT's tested on the same pavement for multiple times is 1.1 dB on average. Another issue is the variation in TPIN for one tire over time, i.e. wear/aging. TPIN of the older tires was shown to be 0.5 dB higher than the new tires when averaged for all pavements. As a result, a strategy for deciding when test tires should be retired is needed based on the rubber hardness, reduced tread depth, accumulated mileage, and in-service years (Donavan and Lodico, 2013 [582]).

Figure 82: Tread pattern of SRTT (tread surface is white painted)

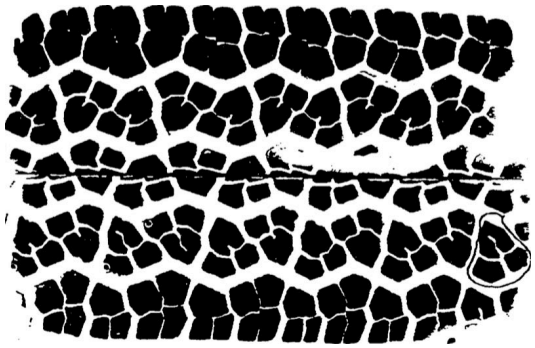

Figure 83: Footprint of old Uniroyal SRTT (4410 N in load, 19 cm in length, 13 cm in width) (source from Ruhala, 1999 [244], Figure 5.2; reprinted with permission from Dr. Richard J. Ruhala of Kennesaw State University)

Table 27: Tread element number and length for old SRTT (modified from Ruhala, 1999 [244])

Element Number	Element Length [inch]
1	1.152
2	1.224
3	1.297
4	1.368
5	1.439
6	1.513
7	1.584
8	1.655
9	1.727

4.4 Tread Pattern Parameters

Tread pattern is considered to be the most important tire parameters influencing TPIN, and it is also the one that is easiest to modify. Pope and Reynolds (1976) [464] have correlated the tread pattern with tire noise below 1 kHz.

It is believed among general public that TPIN comes mainly from the effect of tread pattern impact on the pavement (Cao et al., 2008 [583]) and the non-patterned tire is the quietest tire. However, this is not the case. In fact, non-patterned tire might be the noisiest tire if tested on the rough pavement (FEHRL, 2001 [28]). Fong (1998) [540] found that the sound levels from smooth tires (P175/70R13) were slightly greater than the patterned tire over all the chipseal pavements. Generally, for the same tire construction and rolling speed, the lowest TPIN is produced by a rib tread design (FEHRL, 2001 [28]). Having said that, tread pattern is an important factor that is easy to modify for TPIN reduction. It affects nearly all mechanisms, especially on smooth pavement (Sandberg and Ejsmont, 2002 [7]). In addition, it was found

that the noise spectra from slick tire and standard patterned tire were different, especially around 1000 Hz, as shown in Figure 84 and Figure 85 (Alt et al., 2006, [584]).

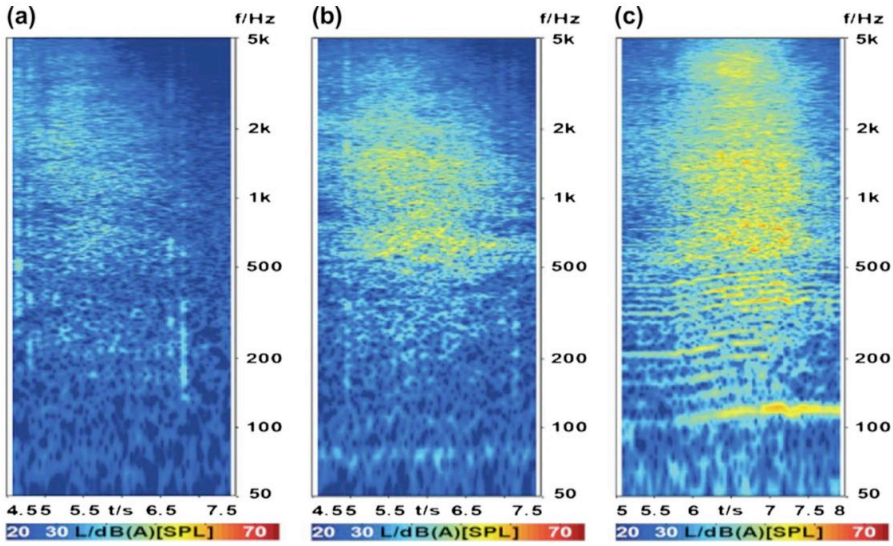

Figure 84: Colourmap plots of different pass-by noise tests: (a) engine switched off and slick tires; (b) engine switched off with standard tires; (c) ISO 362 acceleration test (source from Braun et al., 2013 [48], Figure 7; original from Alt et al., 2006, [584]; reprinted with permission from Elsevier)

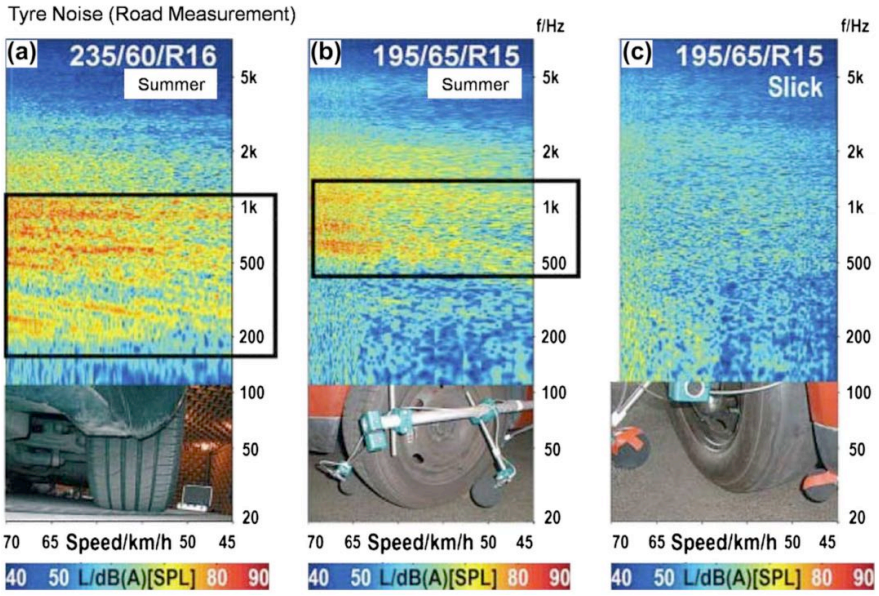

Figure 85: Waterfall plots of tire/road noise measured on the road with three different tire types: (a) wide summer tire; (b) regular summer tire; (c) slick tire (source from Braun et al., 2013 [48], Figure 20; original from Alt et al., 2006, [584]; reprinted with permission from Elsevier)

There are approximately 16,000 different tire tread patterns used on tires (Hanson et al., 2004 [585]). It is not an easy task to parameterize the tread pattern. A lot of parameters are just qualitative, as shown in Table 28 (Sandberg and Ejsmont, 2002 [7]), making the results questionable in some sense. A alternative and smart method to parameterize 2D tread pattern is through image processing (Che et al., 2012 [586]). The drawback of 2D tread pattern is the loss of tread/groove depth information. Ge et al. (2004) [587] found that sound pressure level increased by 10 dBA as the groove depth increased from 0 to 12 mm for a single groove tire. As such, 3D tread profile is an alternative and often applied with 3D laser scanner (CTWIST).

The tread patterns under investigation were usually hand-cut from slick tires, so it might not represent the industrious tires on the market, for example unwanted reduction of dynamic stiffness of the tread might occur (Iwao and Yamazaki , 1996 [307]).

Tire tread pattern design is a compromise between traction, handling, ride, noise, safety and tire longevity (Hanson et al., 2004 [585]). Example of a tread design with low noise characteristics is shown in Figure 86 (Saemann, 2005 [588]). Xie (2003) [589] presented a method to design a tread unit that may be repeated in succession about the circumference of a tire to produce an acoustically acceptable tread pattern, mainly focusing on impact mechanism.

Table 28: General influence of tread pattern on TPIN (source from Sandberg and Ejsmont, 2002 [7], Table 10.3; reprinted with permission from Dr. Ulf Sandberg of VTI, Sweden)

Changes in Tread Pattern			A-weighted SPL	Low to Mid Frequency (Tread Impact)	Mid to High Frequency (Air Resonance)	Highest Frequency (4-16 kHz)
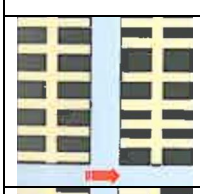	Randomization	Tread randomization	↓	↓	•	•
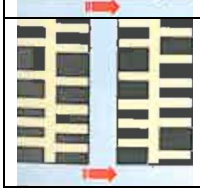		Introduction of an "offset" between left and right side of the tread or introduction of asynchronous randomization	↓	↓	↓	•

Changes in Tread Pattern			A-weighted SPL	Low to Mid Frequency (Tread Impact)	Mid to High Frequency (Air Resonance)	Highest Frequency (4-16 kHz)
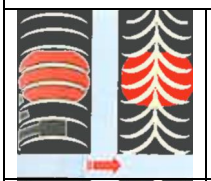		Elimination of grooves that coincide with the contour of the tire footprint	↓	↓	•	•
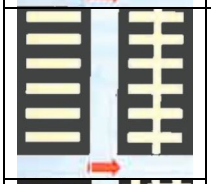	Ventilation	Ventilation of air pockets	↓	•	↓	↓
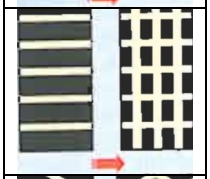		Addition of circumferential grooves to a transverse groove pattern	↓	•	↓	↓
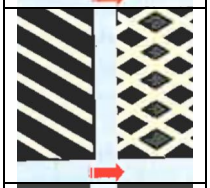		Addition of “mirror Image” grooves	•	•	•	↓
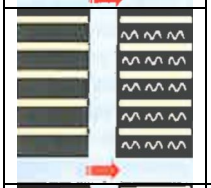		Addition of lamellae	↓•	↓	•	•
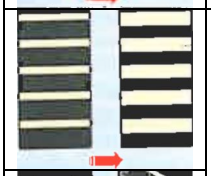	Tread Segment	Increasedo of groove width 2 → 9 mm 9 → 12 mm	↑ ↓	↑ ↓	↑ •	↓ ↓
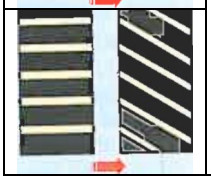		Increase of groove angle (relative to lateral axis) ([423,590]) 0 → 20° 20 → 90°	↓ •	↓ ↓	↓ •	• •

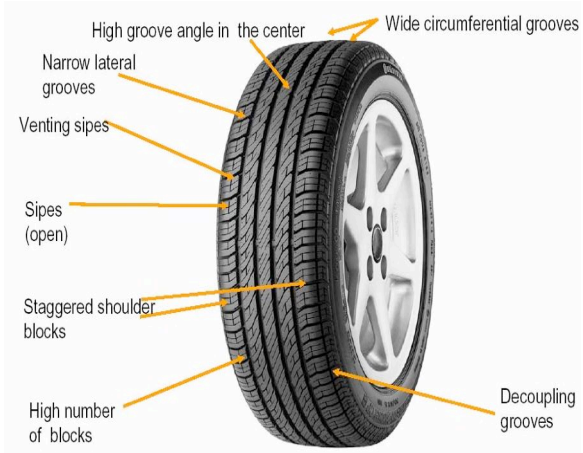

Figure 86: Example of a tread design with low TPIN characteristics (source from Saemann, 2005 [588]; reprinted under fair use provision)

A study applied weighting functions to the grooves and blocks in the contact patch using particle swarm algorithm to correlate tread patterns with TPIN, where the average errors were found to be within 2.5 dB (Chiu and Tu, 2015 [361]).

In addition, tread pattern design is a compromise between several tire performance requirements, as shown in Table 29 (Liljegren, 2008 [591]). Tread pattern design is not only a science but also a creative art (Williams, 1995 [592]).

Table 29: Tread pattern design requirements (modified from Liljegren, 2008 [591], Figure 46)

↑ Positive Effect ↓ Negative Effect	Dry Handling	Dry Braking	Track Performance	Noise and Comfort	Wet Performance	Regular Wear	Rolling Resistance	Mileage
Priority (A is highest)	A	A	A	B	B	B	C	C
Large Shoulder Groove Angle	↓	↓	↑	↑	↑	0	↑	0
Large Number of Sipes	↓	↓	↑	↑	0	↓	↓	↓
Large Shifts	0	0	↑	↑	0	↑	↑	0
Randomization	0	0	0	↑	0	↓	0	↓
Wide Blocks	↑	↑	↑	↑	↓	0	↓	↓
Large Part Horizontal Void	↑	↑	↓	↓	↓	0	↓	↓

4.4.1 Randomization

The randomization process is also called “pitch sequencing” (Bandel et al., 1994 [593];Williams, 1995 [592]). Tread pattern is compromised of sequence of tread segments (or elements) around the tire circumference. That is to say, usually the tread pattern is

randomized, but not completely; the tread pattern segments follow a specific sequence with limited number of elements (3~9).

The tread segment is a combination of the block/lug and the groove/sipe in between. Before 1960's, the tread segments were identical with constant pitch. This resulted in a very objectionable tonal noise. One of the solutions is to vary the segment pitches (patented Michelin in 1929). Usually the segments are stretched or compressed circumferentially to form two to four different lengths. The next step is to spread different pitches around the tire, which is called tread randomization. This process was done manually in earlier years then taken over by computer programs. The latter have been doing a better job. Purely random spacing (within given limits) seems to be not as good as the optimized spacing (found by trial and error) on good commercial tires (Heckl, 1986 [13]). It should be noted that randomization often does not reduce overall TPIN levels, but it distributes the spectrum energy to a larger range and makes the sound more pleasant (ISO, 2007 [594]). For a car with speed of 56 km/h, the sound corresponding to the first-order component (excites the side wall having low dynamic stiffness) of the pattern with a central frequency of 500 Hz is dispersed into the frequency range from 400 Hz to 600 Hz, and the sound corresponding to the second-order component (excites the tread surface) of the pattern with a central frequency of 1000 Hz is dispersed into the frequency range from 800 Hz to 1.2 kHz (Iwao and Yamazaki, 1996 [307]).

The different layouts of tire segments and principles of randomization are shown in Table 30 (Sandberg and Ejsmont, 2002 [7]).

An optimized randomization (such as asynchronous randomization in Table 30) can also be favorable to the uniform distribution of mass and hardness around the tire. A smooth rib or groove is often placed in the central part to avoid segment conflicts between two sides of the tire tread.

Tread randomization might often increase the cost of tire molds, especially more different pitches, or continuous variation of pitch and changing pattern along the circumference are needed.

Another practice to reduce structure-borne TPIN is to avoid abrupt and coherent tread impact over a large part of the tire width (Sandberg and Ejsmont, 2002 [7]). It means the shape of tread pattern should not coincide with the contour of contact patch, which is to say the contour of the tread elements should be longitudinal at the center area but transversal near the

shoulder.

Table 30: Different layouts of tire segments and principles of randomization (source from Sandberg and Ejsmont, 2002 [7], Table 10.2; reprinted with permission from Dr. Ulf Sandberg of VTI, Sweden)

Randomization	Constant Pitch	All segments are of the same length (no randomization)	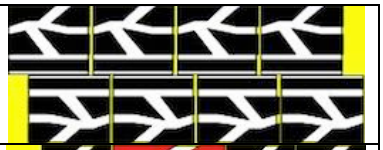
	Synchronous	Segments differ in length, but the order of their placement is the same on the left and right side	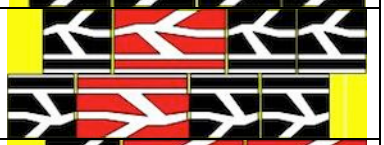
	Asynchronous	Segment differ in length and their order is different on left and right side of the tire	
Symmetry	Symmetric	Segments on the left side of the tire are identical to segments on the right side (but there is an offset in this case)	
	Asymmetric	Segments on the left side have different pattern in relation to right side	
Directivity	Bi-directional	Segments on the left side of the tire are rotated 180° in relation to segments on the right side	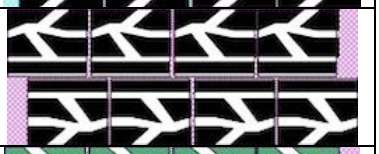
	Directional	Segments on the right side are mirror images of the segments on the left side. Other special properties possible, for example tilted lamellae.	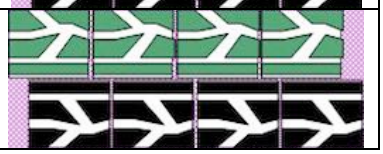

Specific pitch sequences were usually proprietary of tire companies and not released to public. Many of those were patented, the earliest one of which dates back to 1935 (Ewart, 1935 [595]). Varterasian (1969) [596] developed a mathematical method based on mechanical frequency modulation to optimize the tread spacings.

Pitch sequencing has been investigated to reduce tire noise since 1930's. All tire tread element pitch sequences can be defined with five basic parameters: (1) total number of pitches which roughly determines the average pitch size; (2) actual pitch arrangement usually determined by a computer program that uses mathematical algorithms to determine the best

possible order; (3) number of different pitch sizes determining the complexity of a pitch sequence; (4) ratio for each pitch size with the largest pitch divided by the smallest pitch usually ranging from 1.4 to 1.6; (5) total pitches of each size (Williams, 1995 [592]). Table 31 Shows the progression of pitch sequencing techniques in historical perspective.

Table 31: Progression of pitch sequencing techniques in historical perspective (Williams, 1995 [592])

No.	Reference	Tread pattern harmonic spectrum distribution	Notes
1	Mono-space sequence	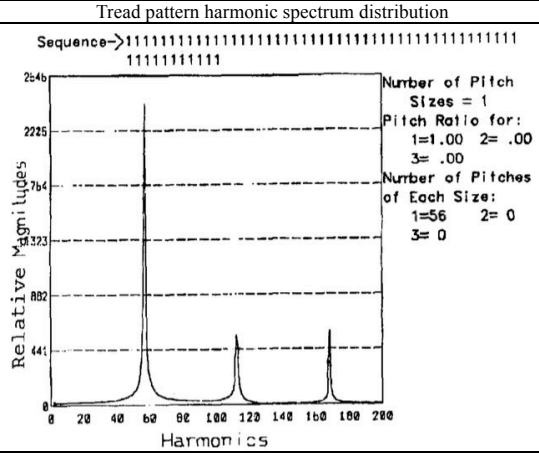	A mono-space sequence would actually be very noisy. A good example of the sound made would be a car going over a metal bridge grating.
2	Ewart, 1935 [595] (US Patent 2006197)	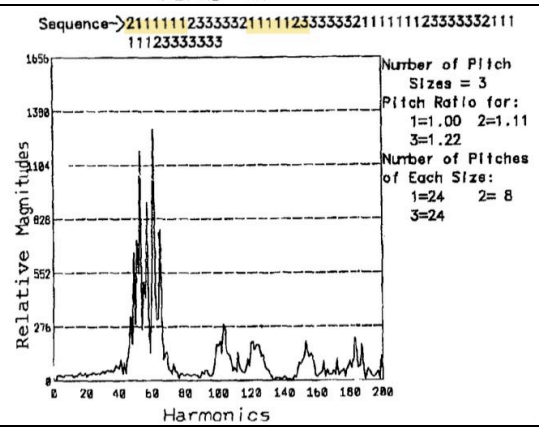	A pitch sequence typically provides an improvement if it can lower the overall magnitude and spread the Fourier spectrum over a broader bandwidth. Mr. Ewart's basic approach is relatively simple. The tire is divided into 8 main sections that are each separated by a small 7-degree section. The main sections are composed of pitch lengths of the same sizes arranged so that the main sections have different lengths. The sequence is further constrained to vary from small to medium to large pitches and back down. This basic concept of cycling from small to medium to large and back down is still in use today, 60 years later (1995).

No.	Reference	Tread pattern harmonic spectrum distribution	Notes
3	Buddenhagen, 1952 [597] (US Patent 2612928)	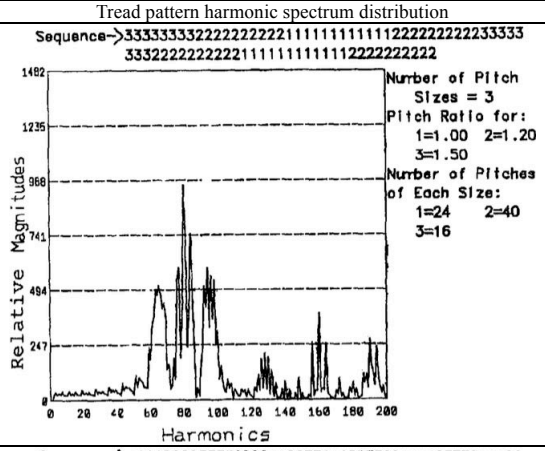	Mr. Buddenhagen again used a division of the tire into 8 segments. In this technique, each segment comprises 45 degrees of the tire circumference. Each segment is however made up of different pitch lengths. There are 2 "A" segments made up of eight large pitches, 4 "B" segments made up of ten medium segments and2"C" segments made up of twelve small pitches.
4	Landers, 1982 [598] (US Patent 4327792)	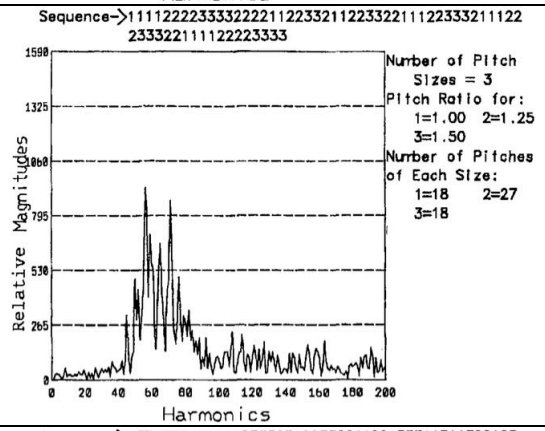	Mr. Landers makes a major change in the pitch sequencing process by breaking the segments into groupings of the same size pitch that in turn make up segments of the tire circumference that are different sizes.
5	Williams, 1994 [599] (US Patent 5314551)	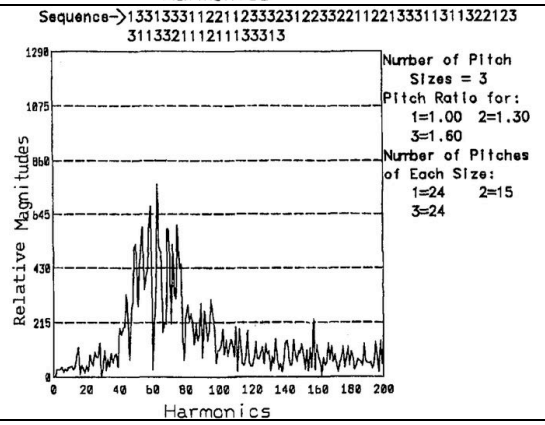	One of the primary departures of this technique from the previous examples is the consistency of the previous techniques to always progress from a small pitch to a medium and then to a large before progressing back down to a small. The General Tire patent in fact encourages going directly from a small pitch to a large pitch. The patent defines any change between two pitches as a transition. The Patent claims that the best frequency distribution is obtained when between 15 to 30 percent of the total transitions between pitches are between a small and a large pitch.

Wei et al. (2016) [366] indicated that the relative phase of the tread pattern pitch, or the offset of the two halves of tire molds, plays a great role in tire noise reduction up to 0.7 dB. The Michelin Primacy 3 ST tires are “Silence Tuned” (ST) to be extra quiet by having tread blocks of varying sizes [600].

4.4.2 Rotation Direction / Side Asymmetry

Asymmetric tread pattern becomes more and more popular due to many reasons (Sandberg and Ejsmont, 2002 [7]). It can optimize traction, braking, handling and safety at the same time. For example, good traction performance is desired for inboard side while handling is valued for outboard side where more side force is carried. As a result, the outboard side needs more rigid blocks or ribs with less lamellae than inboard side (Sandberg and Ejsmont, 2002 [7]).

From the perspective of TPIN reduction, quieter pattern is preferred for outboard side in terms of noise emission. TPIN from inboard side is better damped by vehicle underbody screening or pavement absorption. As a result, the direction of rotation of asymmetric patterned tire matters, especially on smooth pavement.

4.4.3 Ventilation

Air pumping and air resonance contribute largely to TPIN. Good ventilation can keep acoustic pressure from building up or resonating, so it is good practice to avoid closed pockets (air pumping), cavities with narrow outlets and long grooves without ventilated side channels (pipe resonance) (Sandberg and Ejsmont, 2002 [7]). This is also favorable to water drainage (Dong et al., 2010 [601]; Oshino et al., 1999 [602]) and anti-skid (Wang et al., 2013 [603]) properties of tire tread.

A shorter groove might increase the TPIN level at higher frequency, but it is still preferred as long as it avoids the concentration around 1000 Hz. Another way to reduce pipe resonance is to block the grooves using “groove fence” developed by Bridgestone (Sandberg and Ejsmont, 2002 [7]).

Wei et al. (2016) [366] suggested that the long longitudinal groove across the tire circumference has little contribution to the overall tire noise (< 1 dB), because no air volume change is caused. On the other hand, the lateral groove can increase the tire noise by over 4 dB and the wider the groove is, the larger the increase. Wei et al. (2016) [366] observed that the time signal for the lateral groove air pumping occurring at the leading edge and trailing edge is damped sinusoidal, as illustrated in Figure 87.

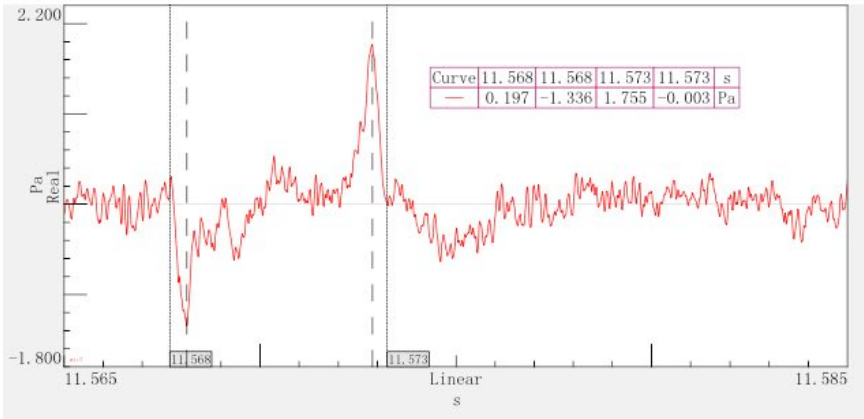

Figure 87: Noise characteristics in the time domain when lateral groove contacts ground (source from Wei et al., 2016 [366], Figure 3; reprinted under fair use provision)

4.4.4 Tread Segment

Most of the parameters about tread pattern discussed above are layout or sequence of tread segments, which are difficult to quantify. For tread segment parameterization, the quantification process is easier. The most important factors are block/groove width, block/groove depth, block/groove length, and block/groove angle (relative to the lateral axis).

It was shown that as groove width increases, TPIN increases due to increased air cavity between blocks. However, after the groove width reaches beyond 9 mm, TPIN decreases, probably due to the tread stiffness reduction (Sandberg and Ejsmont, 2002 [7]).

Increased groove depth also increased air pumping. It was indicated that groove depth is more important than groove width (Zhou, 2013 [604]).

Increased groove length reduces the frequency of pipe resonance but will usually cause higher amplitude due to the coincidence with the impact frequency (Ejsmont et al., 1984 [360]).

TPIN decreases with the increased groove angle, because it avoids simultaneous impact over the tread width. However, it cannot explain why TPIN is not sensitive to groove angle after it is over 20°. There was another study showing that the lowest TPIN occurred when the groove angle is 0°. The groove angle was shown to be the least important parameter (Zhou, 2013 [604]).

Tread pattern redistributes structural stiffness and mass concentration that affect the vibration characteristics of tire (Ih and Oey, 2012 [252]). The groove structure behaves as filter

that mitigates some vibration energy components and causes delay. It takes some time to dissipate the vibration and to excite the adjacent block after one block is excited.

4.5 Pavement Related Parameters

The requirements of pavement have been changed from traffic load support only to multiple aspects, including structural (bearing capacity), environmental (noise and vibration generation, water pollution), safety (friction, aquaplaning, water spray, durability), and hydrological (surface water discharge) (Domenichini et al., 1999 [63]). As such, different criteria need to be accounted for during pavement design.

As mentioned above, pavement parameter might be more important than tire parameters (Sandberg and Ejsmont, 2002 [7]) in terms of tire noise. As a matter of fact, two thirds of literature focus on the pavement effects while only one third focus on the tire effects (Sandberg and Ejsmont, 2002 [7]). Fong (1998) [540] indicated that the texture dominated in noise generation for chipseal surfaces. Different parameters affect different generation and propagation mechanisms.

Generally, pavement can be categorized into two major types: cement concrete pavement and asphalt concrete pavement. The illustrations of different types of pavements are displayed in Table 32 (NZ Transport Agency, 2014 [54]). Different types of pavements have different acoustic performance (Donavan, 2005 [605]), as shown in Figure 88 (Mcghee, 2012 [606]). It was found TPIN levels on cement concrete pavements are 2 dB higher than TPIN levels on asphalt pavements (Syamkumar et al., 2013 [6]). The high frequency noise (over 1 kHz) and low frequency noise (below 250 Hz) was found to be much higher on the cement concrete pavements than on the asphalt pavements (Sandberg et al., 1990 [607]). Asphalt pavements characteristics are affected largely by the mixture design whereas for concrete pavements, the texturing pattern is the key contributor (Rasmussen, 2009 [580]).

Table 32: Illustrations of different types of pavements (modified from NZ Transport Agency, 2014 [54], Figure 1.6 – Figure 1.19; reprinted with permission from Ms. Helen Lane on behalf of NZ Transport Agency)

Pavement Type	Sub-Type	Illustration
Traditional	Gravel	

Pavement Type	Sub-Type	Illustration
	Chipseal	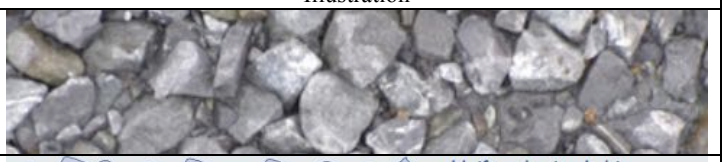
Asphalt Concrete (AC)	Single Coat Seal	
	Reseal	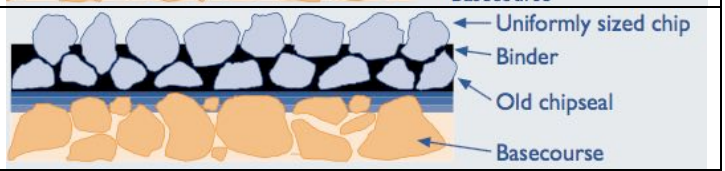
	Two-coat Seal	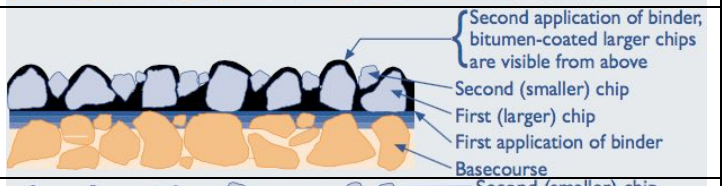
	Racked-in Seal	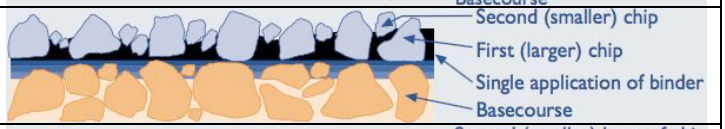
	Sandwich Seal	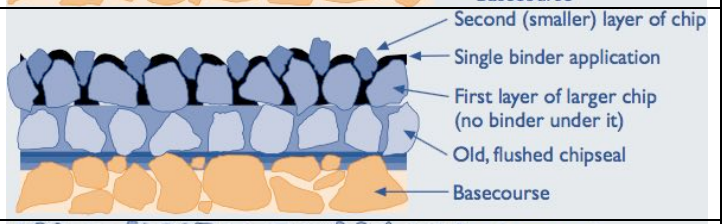
	Slurry Seal	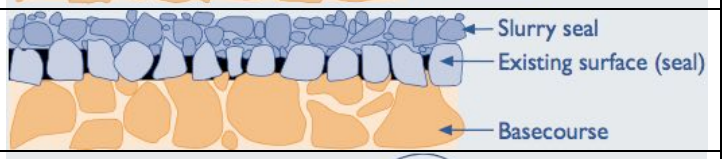
	Cape Seal	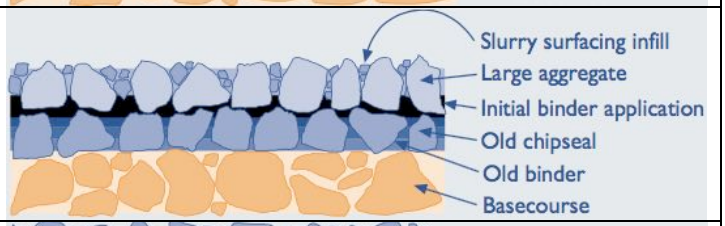
	Asphaltic Concrete	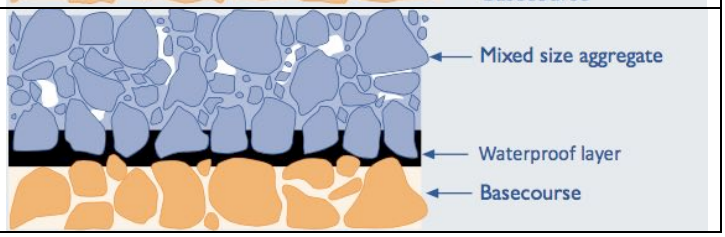

Pavement Type	Sub-Type	Illustration
	Open Graded Porous Asphalt (OGPA)	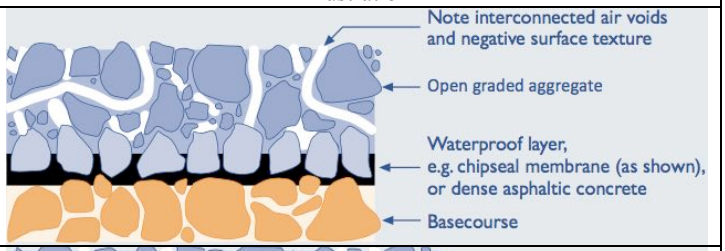
	Stone Mastic Asphalt (SMA)	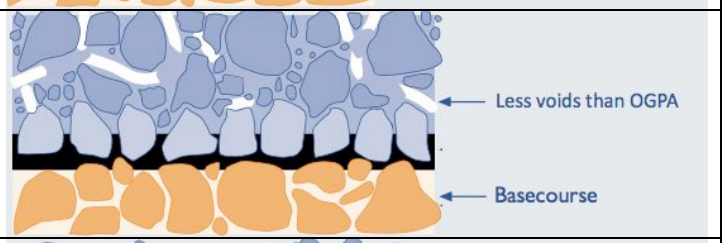
	Macadam	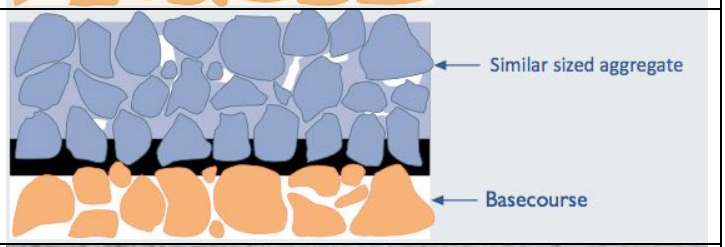
Cement Concrete (CC)	Transvers Grooves	
	Longitudinal Grooves	
	Artificial Turf Drag	
	Burlap Drag	

Pavement Type	Sub-Type	Illustration
	Diamond Grinding	
	Exposed Aggregate	

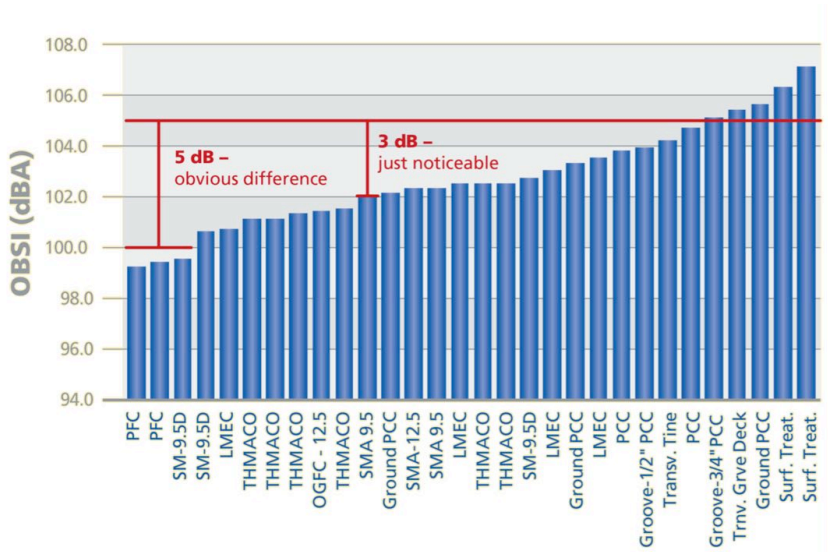

Figure 88: Acoustic performances of typical pavements in Virginia (source from McGhee, 2012 [606], Page 14; reprinted under fair use provision)

The pavement related parameters could be categorized into primary parameters, secondary parameters and tertiary parameters. The primary parameters are those for pavement design or mixture properties, such as grading size distribution, content of binder and thickness; the secondary parameters are characteristics that show up and remain relatively constant after the pavement is built, such as porosity, texture and impedance (Li et al., 2009 [608]); the tertiary parameters are those that might change with time, such as wetness, wear/age, and surface rating.

4.5.1 Texture

The pavement texture is acknowledged to have a significant influence on tire-pavement interaction noise where the tread pattern is not too aggressive (Klein and Cesbron, 2016 [609]).

Pavement texture is defined as "the deviation of a pavement surface from a true planar surface" within a specific wavelength range (ISO, 1997 [610]). Among the pavement related parameters, pavement texture has the greatest influence on TPIN (Huschek, 1996 [611]) and is included in nearly all TPIN models. However, texture cannot be described using one single metric. It is divided into a group of parameters representing different aspects of texture based on the wavelength of the texture. They have different impacts on TPIN and other tire characteristics, as shown in Table 33 (Dimitri, 2012 [170]; Wayson, 1998 [612]).

Table 33: Texture parameters and influence on tire/pavement characteristics (red ↑ indicates increase, green ↓ indicates decrease and blue • indicates complex) (modified from Dimitri, 2012 [170]; Wayson, 1998 [612])

	Micro-texture	Macro-texture	Mega-texture	Unevenness	Topographical Undulations
Wavelength	<0.5 mm	0.5-50 mm	50-500 mm	0.5-50 m	>50 m
Road Roughness			↑	↑ ↑	↑ ↑
Rolling Resistance		↑	↑ ↑	↑	
Tire Road Friction	↑ ↑	↑ ↑	↓ ↓		
Adhesion	↓ ↓				
Drainage		↑ ↑			
Water Skid Resistance	↑ ↑	↑ ↑			
Ride Comfort			↓	↓ ↓	
Optical Property		• •			
Road Hold			↑	↑ ↑	
Splash & Spray		↓ ↓			
Dynamic Loads				↑ ↑	↑
Tire Wear	↑ ↑				
Vehicle Wear			↑	↑	
TPIN		↑	↑		
Interior Noise			↑	↑	

The common pavement textures are shown in Table 34 (Thrasher et al., 1976 [1]).

Table 34: Examples of different pavement textures (modified from Thrasher et al., 1976 [1])

Pavement Texture	Macro-texture (Roughness/Smoothness)	Micro-texture (Harshness/Polishedness)	Dominant Mechanism
	High (rough)	High (harsh)	Impact & stick/slip
	High (rough)	Low (polished)	Impact
	Low (smooth)	High (harsh)	Stick/slip
	Low (smooth)	Low (polished)	Stick/snap

The influence of pavement texture on TPIN is shown in Figure 89 (Sandberg and Ejsmont, 2002 [7]). It shows that TPIN at low frequencies (below 1000 Hz) increases with texture amplitude within the texture wavelength range of 10-500 mm. TPIN at high frequencies (above 1000 Hz) decreases with texture amplitude within the texture wavelength range of 0.5-10 mm. Li et al. (2015) [613] reported the similar trends. However, Domenichini et al. (1999) (Domenichini et al., 1999 [63]) reported that the effect TPIN above 1000 Hz decreases with texture amplitude centered on 5 mm only when the total texture spectral line of 4, 5 and 6.3 mm is less than 200. It should be pointed out that the correlation between TPIN and pavement texture of short wavelengths is still uncovered. Many researchers failed to measure texture levels with enough precision at such short wavelengths, so the results were usually debatable (Fong, 1998 [540]).

It means TPIN has different sensitivities to the different components of texture spectrum, and certain range of spectrum might be ignored or cannot be recognized by the tire (Biermann et al., 2007 [614]). Most of the cases, power spectrum of the texture are used, which will lose the phase information. However, Hamet and Klein (2000) [615] claimed that two pavements with identical power spectrum or amplitude spectrum of the texture do not necessarily show the same acoustical behavior. Both the amplitude and phase information should be taken into account.

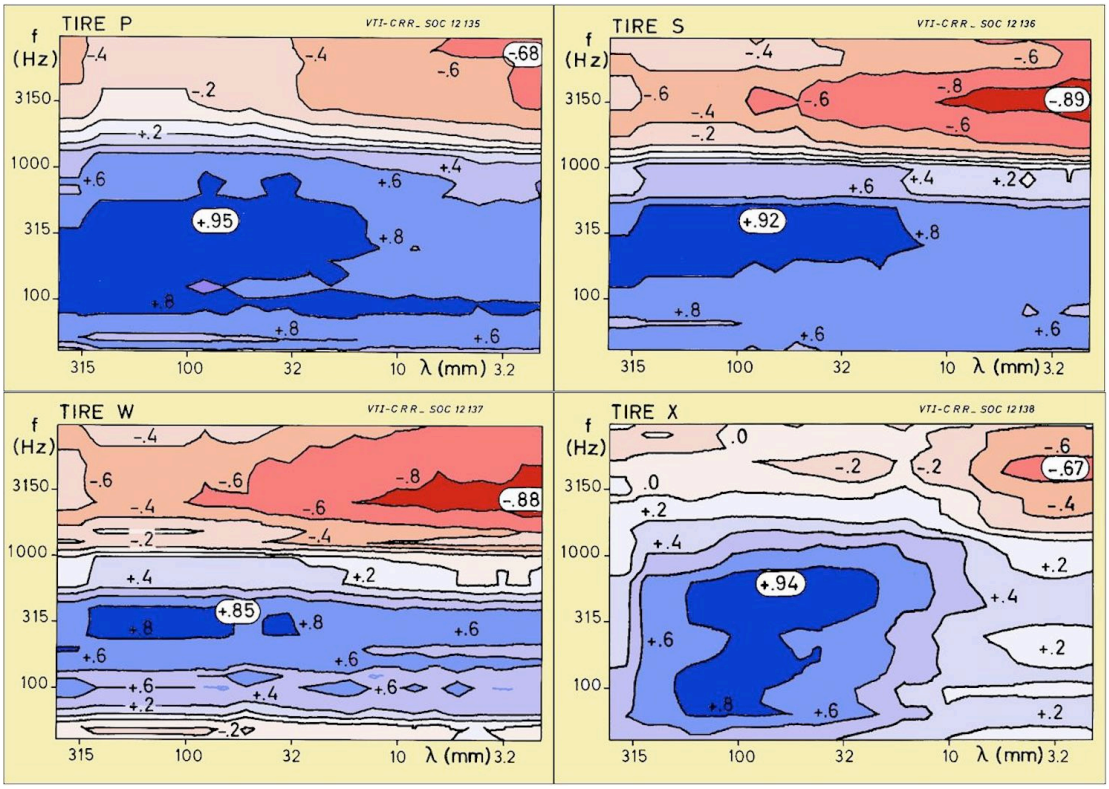

Figure 89: Contour lines of the correlation coefficient between TPIN levels (at 80 km/h) and pavement texture levels for four different tires (source from Sandberg and Ejsmont, 2002 [7], Figure 11.6; reprinted with permission from Dr. Ulf Sandberg of VTI, Sweden)

Concrete pavements texturing is conducted while the concrete is still in fresh (plastic) state. There are basically three techniques: (1) Burlap drag; (2) rake tining; (3) diamond grinding (Rasmussen, 2009 [580]). Different pavement textures or finishes often result from different approaches of paving, leading to different TPIN performance. For example, it was shown that astro-drag pavements are quieter than tined and diamond ground pavements (Hanson and Waller, 2005 [616]).

There are different texture modeling for tire-pavement interaction including friction, vibration and TPIN (Pinnington, 2012 [617]; Pinnington, 2013 [618]). Particles of different orders of magnitude, e.g. atoms, crystals, and stones, are arranged in what are called roughness orders representing a size distribution of the particles. An eight-term truncated Fourier series describes the particle shapes and the envelope of particle peaks [617]. Texture spectrum analysis (He and Wang, 1991 [619]; Lee et al., 1998 [620]; Wang and He, 1990 [621]) can also be applied to

pavement texture investigations standardized in ISO/TS 13473-4 (2008) [622].

Texture profile can be measured using a laser profiler standardized in ISO 13473 (2002) [623]. Multiple lasers are used to measure the depth of the pavements at regularly spaced points along the direction of travel to collect three-dimensional texture data for all wavelengths (Dubois et al., 2013 [61]). An alternative method for texture measurement is the Circular Track Meter (CTM) or Circular Texture Meter standardized in ASTM E2157 (2009) [624]. It is a portable device and much cheaper than laser-based device but only applicable for macro-texture measurements. 2D profile can also be used to if it is sufficient enough to represent pavement texture characteristics (Hamet and Klein, 2001 [625]).

The power spectral density of texture levels Φ^2, as shown in Figure 90, can be typically expressed as (Bremner et al., 1997 [334])

$$\Phi^2(k) = 0.0001 \cdot k^{-4} \tag{45}$$

where k spatial roughness wavenumber defined by

$$k = \frac{\omega}{V} \tag{46}$$

where ω is temporal frequency of vibration, V is the tire rolling speed. Figure 90 also shows a typical tread profile spectrum, which explains why the noise from patterned tire is usually higher than the smooth tire mainly from 300 to 1000 Hz.

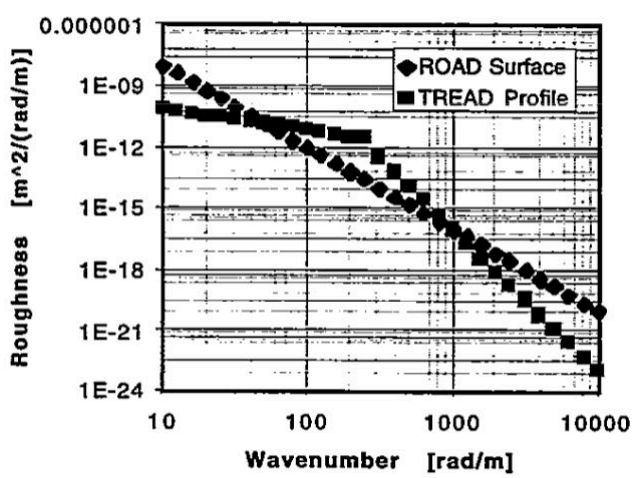

Figure 90: Pavement texture PSD and tread profile PSD (source from Bremner et al., 1997 [334], Figure 21; reprinted under fair use provision)

Typical surface texture levels are shown in Figure 91 (Li et al., 2015 [613]).

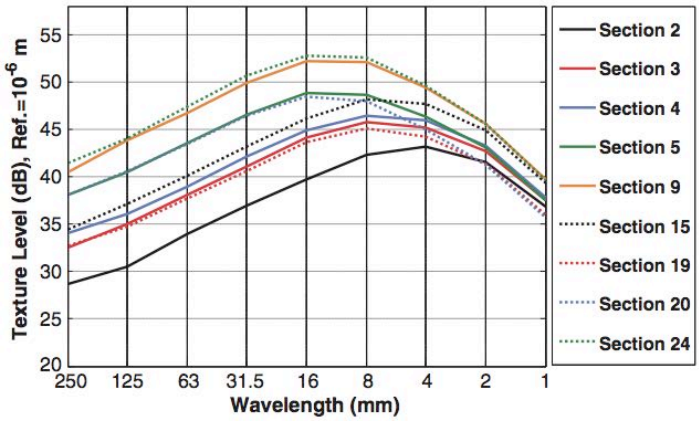

Figure 91: Surface texture levels for the thin-layer surfacing sections (source from Li et al., 2015 [613], Figure 3; reprinted with permission from American Society of Civil Engineers)

4.5.1.1 Micro-texture (below 0.5 mm)

Pavement micro-texture is defined as "a deviation of a pavement surface from a true planar surface with characteristic dimensions along the surface of less than 0.5 mm" (Mcdaniel et al., 2014 [122]). It is a function of the surface texture of the aggregate particles. High micro-texture provides high frictional resistance and water skid resistance by disrupting the continuity of the water film. It can be analogous to sand paper with a gritty surface.

Higher micro-texture increases stick/slip (friction) noise generation mechanism but decreases stick/snap generation mechanism. These conflicting changes might explain why it is difficult to find clear relations between micro-texture and TPIN (Sandberg and Ejsmont, 2002 [7]). Micro-texture was shown to influence TPIN above 1000 Hz (Dare and Bernhard, 2009 [626]; Sandberg and Ejsmont, 1998 [627]).

4.5.1.2 Macro-texture (0.5-50 mm)

Macro-texture is in the same order of size as coarse aggregate or tire tread elements, with spatial wavelengths between 0.5 mm and 50 mm. Indentations made into the tire tread surface generate fluctuating force (Fong, 1998 [540]). Macro-texture represents the overall properties of the pavement surface and has the greatest influence on TPIN among texture characteristics. It depends on the type of asphalt surface (e.g., dense versus porous), the gradation of the aggregates in the mixture, and presence of air voids at the surface (Mcdaniel et al., 2014 [122]).

Higher macro-texture reduces hydroplaning by providing channels at the surface through which water can travel away from the contact area.

Higher macro-texture (10-50 mm) increases texture impact TPIN generation mechanism. It also influences the air pumping generation mechanism by changing the volume of air cavities in the pavement. It has certain influence on the stick/slip, pipe resonance and Helmholtz resonance mechanism. Macro-texture was shown to affect TPIN levels in the range of 630-1000 Hz (Rasmussen et al., 2006 [628]). However, higher macro-texture (0.5-10 mm) was reported to decrease TPIN levels (FHWA, 2005 [629]).

The engineering applications of macro-texture are to measure pavement skid resistance relating to crash rate on rainy days (Henry, 2000 [630]), and to evaluate construction segregation or non-uniformity relating to pavement condition rating (Flintsch et al., 2003 [631]). An alternative metric for macro-texture is Mean Profile Depth (MPD), which will be discussed later.

The macro-texture can be measured manually or automatically. The former corresponds to sand patch method (ASTM, 2006 [632]), the outflow meter, and the circular texture meter (Flintsch et al., 2003 [631]). The latter corresponds to vehicle-mounted laser profilometer (ASTM, 2009 [633]).

4.5.1.3 Mega-texture (50-500 mm)

Generally, mega-texture has little influence on TPIN, except in cases of extreme roughness such as potholes, joints and bumps. However, higher mega-texture normally increases interior noise (FHWA, 2005 [629]). High mega-texture usually indicates construction defect or the end of pavement service life. The determination of pavement mega-texture is standardized in ISO 13473-5 (2009) [634].

4.5.1.4 Unevenness (0.5-50 m)

Pavement texture of higher wavelengths such as unevenness (0.5-50 m) and topographical undulations (> 50 m) is considered to have no influence on TPIN. However, it was found TPIN increased with unevenness in the range 0.5-0.8 m (Domenichini et al., 1999 [63]). The same study also reported that TPIN in the frequency range of 200-1500 Hz decreased with increasing unevenness in the 10-80 m wavelength range (Domenichini et al., 1999 [63]), which was highly questionable because only 11 surfaces were tested.

Unevenness has great influence on the traffic induced vibrations according to unevenness

classification standard ISO 8608 (1995) [635]. The classification is based on the power spectral density (PSD) of the pavement profile with reference to the special frequency value of 0.1 cycle/m or at the wavelength of 10 m. The evenness is classified in eight classes, from A (the best) to H (the worst).

The unevenness also has great correlation with International Roughness Index (IRI), which will be discussed later.

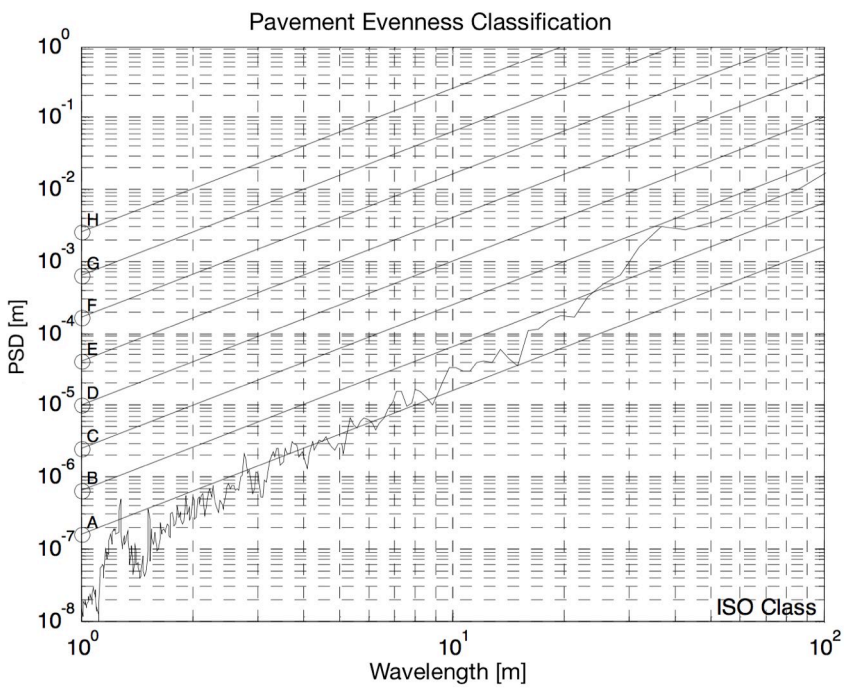

Figure 92: Evenness classification according to ISO 8608 (1995) [635] (modified from Barbosa, 2011 [636], Figure 8; reprinted under CC BY-NC 4.0 suggested by Dr. Francisco Ricardo Cunha, Editor-in-Chief of the J. Braz. Soc. Mech. Sci and Engn)

4.5.2 MPD/MTD/Texture

Mean profile depth (MPD) is defined as the average depth of a section of pavement and indicates the pavement texture (mainly macro-texture). MPD is evaluated based on the pavement profiles mostly measured by laser profilometers according to ASTM E1845 (2009) [633] and ISO 13473-1 (1997) [610]. It is related to wet friction of tire pavement interaction, and the severity of segregation, which will lead to pavement distress such as raveling (Stroup-Gardiner and Brown, 2000 [637]). High MPD means rough pavement and low pavement

condition index (PCI, R^2 = 0.99 [138]). It has almost the same influence on TPIN as macro-texture. TPIN has good correlation with MPD and correlation increases with vehicle speed (Saykin, 2011 [638]). However, some researchers claimed that the correlation is weak, because MPD filters out the spectral contents of short wavelengths and cannot be representative of texture characteristics.

A similar term, mean texture depth (MTD) is traditionally measured and calculated with Sand Patch Method, which is standardized in ASTM E965 (2006) [632]. In the test, a known volume of sand is spread out and allowed to infiltrate the surface. The diameter of the patch is measured to calculate the MPD or mean texture depth (MTD) using the equation below.

$$MPD = \frac{4V}{\pi D^2} \tag{47}$$

where V is the sampling volume, D is the diameter of the area covered by sand. MTD has strong correlations with MPD ($R^2 \approx 0.95$ [63]), and usually they are indicating the same thing (sometimes they are just called texture).

The MPD is shown to have strong relation ($R^2 = 0.85$) with the root mean square (RMS) of the pavement texture, which describes the roughness of the pavement surface or the texture height deviation from the true plane (Reyes and Harvey, 2011 [639]).

4.5.3 International Roughness Index (IRI)

The International Roughness Index (IRI) is the roughness index and a measure of ride and comfort quality calculated from longitudinal pavement profile. A quarter-car vehicle math model is used to yield a roughness index with units of slope (m/km). Most of the texture is in the wavelength range of 1.25-30 m, which represents the pavement unevenness. It was shown IRI has marginal correlation with TPIN (Kohler, 2010 [47]).

IRI is measured with profilometers, which is standardized in ASTM E1926 (2008) [640] and ASTM E1364 (2012) [641]. The standardization work was originally conducted by the World Bank Group (WBG, specification WB TP 46) to determine how to compare or convert data obtained from different countries initiated by The United States National Cooperative Highway Research Program (NCHRP) in the 1980's (Sayers et al., 1986 [642]).

4.5.4 Positive versus Negative Texture

Positive texture is texture features projected above the mean pavement level such as chip seal. Negative texture is texture features with channels or air voids below the mean pavement level such as fine graded asphalt mixture. Positive texture increases impact and friction mechanisms while negative texture reduces air pumping and resonance mechanisms.

It was shown two pavements with identical texture spectra, but one with primarily positive texture and the other with negative texture, have different TPIN levels (Beckenbauer and Kuijpers, 2001 [487]). Positive and negative textures can be addressed by envelopment process where negative texture features can be filtered out.

Texture skewness is often used to quantify positive/negative textures (Rasmussen, 2009 [580]), using the equation below according to ASME B46.1 (2009) [643].

$$\gamma = \frac{1}{N\sigma^3}\sum_{n=1}^{N} z_n^3 \tag{48}$$

where γ is the texture skewness, N is the number of samples along the longitudinal texture line measured, z_n is the texture height at sample point n (the mean value of z_n is 0), σ is the standard deviation of z_n. Most of the pavements have negative skewness, indicating that most of the texture is negative (Dare, 2012 [213]).

4.5.5 Transverse Texture

When speaking of pavement texture, it usually means longitudinal texture. However, transverse texture is also important (Wullens et al., 2004 [325]), especially on cement concrete or grooved asphalt pavements. Transverse texture allows coincident impact between tire and pavement along the contact patch width, resulting in high TPIN levels.

Tined transverse texture can be uniformly spaced or randomly spaced (Rasmussen et al., 2008 [644]). The former can also produce high tonal noise (Hamet and Klein, 2001 [625]).

4.5.6 Anisotropic Texture

Texture on conventional asphalt surfaces without grooving is typically isotropic, but most concrete pavement textures are anisotropic/orientated, which means the texture is different in the longitudinal and transverse directions (Rasmussen et al., 2008 [644]).

Anisotropic texture is often in the form of periodic features, such as peaks and grooves. If

they are transverse, it will be transverse texture mentioned above and increase impact mechanism. If they are longitudinal, it will increase the air displacement mechanism and pipe resonance. Generally, transverse textures shall be avoided from the perspective of TPIN reduction.

4.5.7 Joints

Contraction joints between slabs are often used on Portland cement concrete (PCC) pavements to control cracking caused by the curing process, temperature fluctuations, and vehicle loading (Kane, 1990 [645]). However, the joints will usually cause high tonal "clap" sound called wheel-slap noise or joint-slap noise (Dare and Bernhard, 2013 [222]), increasing the TPIN level by up to 3 dB concentrated in the 800-1000 Hz at highway speed (Donavan, 2004 [646]; Meiarashi et al., 1998 [647]). The joint had little impact on TPIN frequencies above 1600 Hz and below 500 Hz. The wheel-slap noise usually decays within 15 ms (Dare et al., 2011 [648]).

The noise was found to be related to the structural vibration induced by the joints (Dare and Bernhard, 2013 [222]). However, the speed coefficient of increased noise cannot be well explained, since the frequency of excess noise did not depend on vehicle speed. In addition, the wave speed of the vibration induced wave was found to be around 1.7 m/s, which is not efficient sound radiator (Bolton et al., 1998 [380]).

Therefore, increased tread/texture vibration is not a major cause of increased noise at contraction joints, and other mechanisms have been proposed (Dare and Bernhard, 2013 [222]). (1) The contraction joint changes the loading condition at the contact patch and the vibration characteristics. (2) Air is forced out from the joint, i.e., air pumping mechanism. (3) A pipe-like structure is formed as tire rolls over the joint, i.e., pipe resonance, which is shown for slick tires but not significant for treaded tires (Dare and Bernhard, 2010 [649]).

Even though these mechanisms have not been proved by direct experiments, empirical relationships between joint parameters such as width (typically 8 mm) and depth have been found (Dare et al., 2011 [648]). Dare et al., 2011 [648] did a comprehensive investigation on the influences of contraction joint parameters. It was shown that the wheel-slap noise increases by 0.5 dB/mm (R^2 = 0.95~0.98) as the joint width increases from 5 to 24 mm at speed range of 16-48 km/h. The silicone sealant in the joint can reduce the noise substantially for wide

joints, but only marginally for narrow joints. The SPL increases by 1.7 dB/mm as the step-down faulting increases from 0 to 6 mm, while the SPL increases by 2.2 dB/mm as the step-up faulting increases from 0 to 6 mm (R^2 = 0.89~0.99). The beveled joint has similar effect to the standard joint with the same width at the top of the bevel.

Contraction joint is also called Modular Expansion Joint (MEJ) in Canada (Marriner and Wakefield, 2011 [650]). For general traffic with speed of 100 km/h, the dominant MEJ emission frequency was found to be centered at the 630 Hz one-third octave band in 73% of cases. For heavier vehicles, MEJ emission levels were increased by 3.2 to 8.7 dB (Marriner and Wakefield, 2011 [650]).

For the directionality of the joint noise, the MEJ emission level 100 m behind the test vehicle was 8.6 dBA higher than 100 m ahead of the vehicle, but the joint emission level received 7 m behind the vehicle was approximately the same as that received 7 m ahead (Marriner and Wakefield, 2011 [650]).

There are some other common types of faults in road: joint is negative texture and speed bump is positive texture. It was shown that for a bump of height 0.04 m, the peak noise level is increased by 1 to 14 dBA depending on the vehicle speed (20-60 km/h) (Behzad et al., 2007 [406]).

The joints also occur between a road and a bridge, sometimes increasing the overall TPIN by about 10 dBA (Sexton, 2011 [651]; Glaeser et al., 2011 [652]; Wakefield and Marriner, 2011 [653]). It is worth mentioning that the bridge deck surfaces made of open grid steel structures also produce great vibration and noise (Tournour and Cuschieri, 1994 [654]; Cuschieri et al., 1996 [655]; Tournour and Cuschieri, 1994 [656]).

Kindt et al. (2007) [525] investigated the cleat height effect on the tire vibrations. The tire stiffness decreases with the increase of cleat height due to Payne effect where increasing deformation amplitude leads to the decrease of the number of physical bonds in the filler network decreases, resulting in a decrease of stiffness and increase of vibrations (Payne and Scott, 1960 [657]).

4.5.8 Porosity (Air Void Content)

High pavement porosity can greatly reduce TPIN levels, which might explain why porous asphalt pavement with porosity exceeding 20% is quietest pavement. Porous pavements

(a.k.a. drainage asphalt or pervious macadam) have been widely used in Europe and are increasingly used in the United States to mitigate TPIN and improve safety. Donavan (2014) [658] reported that the open-graded asphalt concrete (OGAC, a porous pavement) in the U.S. Highway 101 reduced the traffic noise by over 10 dB.

Pavement porosity can reduce nearly all TPIN generation and amplification mechanisms as sound pressure energy can be absorbed and dissipated through fluid friction within these tortuous channels. Air pumping, pipe resonance, Helmholtz resonance and horn effect are mitigated by interconnected voids providing channels for air pressure to travel away. It also reduces the contact area between the tire and pavement, leading to less stick/slip and stick/snap. It reduces TPIN in the middle and high frequencies but might increase TPIN at low frequencies such as below 1000 Hz due to higher macro-texture (Bernhard et al., 2003 [295]).

A measure of pavement porosity is air void content, including the air voids at the surface and interconnected voids within the mixture. The pores are generated due to the discontinuous granular formulation (Bérengier et al., 1997 [449]). As such, pavement porosity or air void content is largely dependent on the type of mixture such as the size of aggregates. The bigger the aggregates are, the larger the pore size and porosity are. For example, open-graded mixtures tend to have more interconnected voids than dense-graded mixtures. Reyes and Harvey (2011) [639] found that air void content has a positive relation (R^2 = 0.64) with mean profile depth (MPD) which also increases as the size of aggregates increase.

The measurement of the air void content is standardized in ASTM D7063/D7063M (2011) [659] and can be calculated using the pavement core sample with the equation below.

$$V_A = \frac{G_{mm} - G_{mb}}{G_{mm}} \times 100\% \tag{49}$$

where V_A is air void content, G_{mm} is theoretical maximum specific gravity standardized in AASHTO T 209 (2011) [660], G_{mb} is the bulk specific gravity standardized in AASHTO T 331 (2010) [661]. Asphalt pavement can be divided into three categories based on the air void content: dense asphalt (<10%), semi-porous asphalt (10-15%), and porous asphalt (>15%). The effect of air void content is dependent on the type of pavements. Ongel and Harvey (2010) [662] reported that sound intensity levels decrease as V_A increases from 5% to 15% for dense-graded asphalt concrete mixes (DGAC) and gap-graded rubberized asphalt concrete

mixes (RAC-G), while sound intensity levels increase as V_A increases from 10% to 20% for conventional open-graded mixes (OGAC) and open-graded rubberized asphalt concrete mixes (RAC-O).

Cement concrete pavement can also be porous, such as modified Portland cement concrete with porosity of 15%-25% (Neithalath et al., 2005 [663]). Two methods have been explored, one using non-aggregate component of the mixture resulting in Enhanced Porosity Concrete (EPC), and the other using soft inclusions in the matrix (Neithalath et al., 2005 [663]).

The porosity can also be express as

$$\Omega = 1 - \frac{\rho_p}{\rho_a} \tag{50}$$

where ρ_p is the average density of the pavement, ρ_a is the average density of the aggregate. However, in most cases the empirical expression below will be more practical (De Roo and Gerretsen, 2000 [664])

$$\Omega(\text{in } \%) = 0.26 \cdot \left(100 - s_{\%} - f_{\%}\right) + 2.5 \cdot \frac{\Delta d_{st}}{d_{average}} - 9 \cdot \left(1 - e^{-0.00001 b_{\%}^{5}}\right) \tag{51}$$

where $s_{\%}$ is percentage of sand, $f_{\%}$ is percentage of filler, $b_{\%}$ is percentage of binder, Δd_{st} is difference between maximum and minimum grain size of the aggregate, $d_{average}$ is average grain size of the aggregate. The deviations between predicted and measured values range from -9% to +13%, which is pretty accurate.

Another term describing porosity is tortuosity (Olek et al., 2003 [665]). It should be noted that porosity is in conflict with the mechanical strength and durability (Sandberg and Ejsmont, 2002 [7]). High quality binders are often used when designing high porosity pavements. The structure factor measuring the tortuosity of the pores can only be assessed theoretically for idealized geometries [664]. For perpendicular uniform channels, the value can be set to 1. For diffusely oriented uniform channels, a value of 3 would be valid. In granular materials the structure factor appears to be an approximate function of the porosity, as shown below (De Roo and Gerretsen, 2000 [664]).

$$s_f \simeq \Omega^{-1} \tag{52}$$

where s_f is the structure factor, and Ω is the porosity. However, until now, many assumptions and simplifications still exist due to the complexity of the sound wave

propagating in the porous media.

The air void content associated with porous pavement is just a measure of the proportion, but does not consider how much the pores are interconnected, which is more acoustically relevant. Airflow resistance accounts for this effect, which will be discussed later.

4.5.9 Sound Absorption

Sound absorption is highly correlated with porosity. Generally, sound absorption is determined using impedance tube with either standing wave ratio method standardized in ISO 10534-1 (1996) [666] or transfer function method standardized in ISO 10534-2 (1998) [667]. However, core samples need to be extracted from the pavement. A Similar measurement standard in lab for pavement sound absorption is described in ASTM E1050 (2012) [668].

In-situ measurement allows non-destructive tests of absorption standardized in ISO 13472-1 (2002) [669] and ISO 13472-2 (2010) [670], in which diameter and length of the impedance tube within close tolerances are specified and procedure to seal between the pavement and the impedance tube is provided. Sound absorption data are usually reported as narrow-band spectra. However, absorption data are valid only up to approximately 1600 Hz for the most common size of pavement specimen tested. The sound absorption is usually reported in one-third octave bands from 500-1600 Hz. Different types of pavements have absorption spectra of different shapes. Some have low absorption with maximum below 0.1 across all frequencies while porous asphalt has absorption coefficient of 0.5-0.6 for all frequencies. Some pavement has a sharp peak at 800 Hz (Dare, 2012 [213]).

Sound absorption is a function of the acoustic impedance, as shown below (De Roo and Gerretsen, 2000 [664]).

$$\alpha(\phi_0) = 1 - \left| \frac{Z'(\phi_0)\cos\phi_0 - 1}{Z'(\phi_0)\cos\phi_0 + 1} \right|^2 \tag{53}$$

where Z' is acoustic impedance, ϕ_0 is the angle of incidence. Acoustic impedance Z' is considered to be a function of the layer thickness, the porosity of the layer, the specific flow resistance of the material and the structure factor, which is a measure for the tortuosity of the pores (De Roo and Gerretsen, 2000 [664]).

Typical sound absorption coefficients for thin-layer surfacings are shown in Figure 93 (Li et al., 2015 [613]). In the same study, Li et al., 2015 [613] presented the correlation coefficient

between noise levels and sound absorption coefficient, both in frequency domain, as illustrated in Figure 94. As expected, sound absorption reduces tire noise maximally when the frequencies of both coincide, especially around 800 Hz and 2000 Hz.

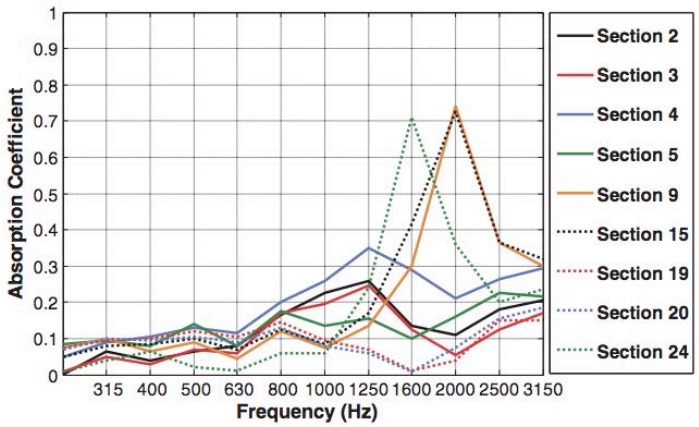

Figure 93: Sound absorption coefficients for the thin-layer surfacing sections (source from Li et al., 2015 [613], Figure 4; reprinted with permission from American Society of Civil Engineers)

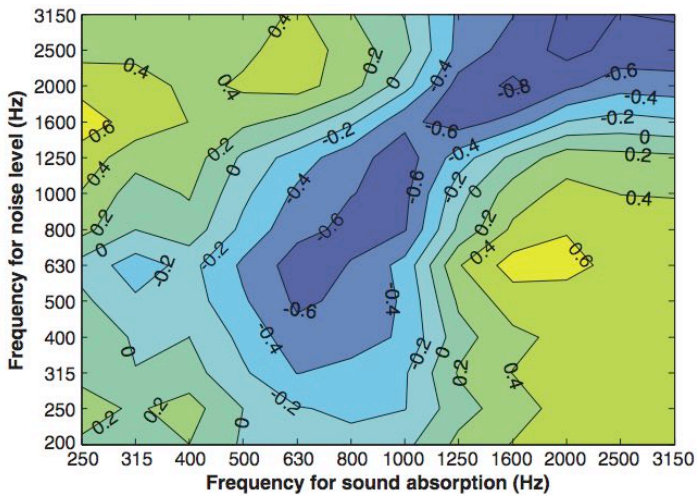

Figure 94: Contour lines of the correlation coefficient between noise level (passenger car tire at 80 km/h) and sound absorption coefficient (source from Li et al., 2015 [613], Figure 6; reprinted with permission from American Society of Civil Engineers)

4.5.10 Airflow Resistance

Airflow resistance is considered to be a more relevant measure of absorption, because it is measured at a shallow angle rather than perpendicular to the pavement surface (Rasmussen et

al., 2007 [62]). It indicates how difficult it is for air to flow through a pavement. According to ISO 9053 (1991) [671] and ANSI/ASA S1.18 (2010) [152], air is forced through a pavement sample, the pressure difference and flow rate are both measured, and airflow resistance is then calculated.

Airflow resistance as acoustic impedance is related to TPIN air pumping and resonance mechanisms. The specific flow resistance of a granular material may be expressed as (De Roo and Gerretsen, 2000 [664])

$$\sigma = \frac{C}{\langle d^2 \rangle}\left(\frac{1}{\Omega} - 1\right)^2 \tag{54}$$

where C is a constant (2.8×10^4 in the literature to best fit the measurement), d is the effective diameter of the aggregate granules (in mm), Ω is the porosity. Nevertheless, the errors between prediction and measurements are fairly large. However, flow resistance is not very important for calculation of sound absorption, variations up to a factor of 2 may be acceptable.

Another expression for specific airflow resistance is

$$R_f = \frac{\Delta p}{u} \tag{55}$$

where R_f is specific airflow resistance, Δp is the difference of pressure across the specimen, and u is the flow velocity (Reyes and Harvey, 2011 [639]). The specific airflow resistance has strong negative relation with air void content. Reyes and Harvey (2011) [639] found that specific airflow resistance of 2000 Pa·s/Pa corresponds to 15% air void content for porous asphalt pavement. It was also found that airflow resistance has good negative relation with water permeability.

A porous pavement with low airflow resistance implies that the airflow generated at the tire-pavement interaction due to air pumping is able to penetrate the pavement without much resistance, leading to the noise reduction from the airborne mechanisms. In contrast, if the airflow resistance is high, the airflow will not pass easily, leading to the increase of the turbulent flow at the contact path and noise increase (Reyes and Harvey, 2011 [639]).

4.5.11 Thickness of Layer

For porous pavement, sound absorption has positive correlation (R^2 = 0.74 [7]) with the

product of layer thickness and air void content (Sandberg and Ejsmont, 2002 [7]). Ren and Gao (2009) [672] reported that void content and pavement depth are the main contributing factors to the noise reduction. The frequency at the peak absorption is related to the thickness of the pavement, which can be used to calculate the optimal thickness based on the frequency of interest (Neithalath et al., 2005 [663]). However, Mogrovejo et al. (2014) [673] reported that the thickness was effective up to a certain degree, but declining benefits then occurred.

The thickness of layer can influence both acoustic impedance and mechanical impedance to be discussed below.

4.5.12 Stiffness (Mechanical Impedance)

The pavement stiffness or modulus has a profound impact on the structural strength of the pavement. It also has impact on TPIN levels by affecting impact mechanism and discharging high frequency tire vibrations into pavement. Rigid pavements are generally louder than flexible pavements (Berge and Storeheier, 1936 [674]), especially around 630-1600 Hz (Li et al., 2012 [675]). For example, Poro-Elastic Road Surface (PERS) containing epoxy-bound shredded rubber was shown to be quieter than conventional pavements (Sandberg and Goubert, 2011 [676]; Storeheier, 1987 [677]; Nilsson and Sylwan, 2003 [678]; Sandberg and Goubert, 2011 [313]; Swieczko-Zurek, 2013 [465]). It is analogous to the running shoes on a flexible running track. Bilawchuk (2005) [679] reported that noise levels on asphalt pavement constructed using crumb rubber binder were lower than normal asphalt pavement when test vehicle was driven at relatively higher speeds. Ponniah et al. (2010) [680] observed that addition of rubber to open graded mixes reduced TPIN by 2 dBA. Beckenbauer (2001) [681] tested two surfaces (one glued with sandpaper on top, one inserted a rubber sheet between the sandpaper and pavement surface), and found that the latter is 3dBA lower than the former. It is reasonable to argue that softer tire/road contact, with softer tire tread as well as road surface, will have better noise reduction (Sandberg, 2003 [479]).

The stiffness is affected by mixture type, aggregate gradation, mixture volumetrics and binder properties. It was shown that pavement with plastic binder could give 1 dBA TPIN reduction (Stenschke, 1990 [682]). Stiffness changes with temperature and moisture, so the pavement stiffness changes over the course of a day or seasonally, and over the service life due to aging and mixture stiffening (Mcdaniel et al., 2014 [122]). Liao et al. (2015) [683] reported

that the stiffness may reduce substantially when pavement temperature increases by 10 °C.

The stiffness/modulus can be measured in lab with Mechanistic-Empirical Pavement Design Guide and the Asphalt Mixture Performance Tester (AMPT), which is standardized in AASHTO T 342 (2011) [684]. It can also be measured in situ with Falling Weight Deflectometer (FWD) (Rao and Von Quintus, 2012 [685]). Stiffness measured is often affected by the loading type, rate, and amount applied in the test, most of the loads used today are impact loads (Li et al., 2012 [675]) described in ASTM C1383 (2010) [686].

Another physically similar and more commonly used parameter is mechanical impedance, defined as the ratio of the driving force to the induced velocity, so it measures the ability of a structure to resist motion when subjected to a given force. It is an overall indicator for the flexibility and energy dissipation properties of the pavement.

Besides the stiffness, mechanical impedance also account for the damping properties, which is dependent on the pavement mixture. Biligiri (2013) [687] reported that asphalt rubber friction course (ARFC) mixes provided higher noise-damping response than the conventional dense graded asphalt (DGA) mixes due to the extra binder, higher porosity, rubber inclusions.

4.5.13 Normal Adhesion

Normal adhesion is correlated with micro-texture. It was shown the pavement sprayed with a layer of anti-adhesion paint has lower TPIN at high frequencies due to less stick/snap (Sandberg and Ejsmont, 2002 [7]).

4.5.14 Tangential Friction

Pavement friction is highly correlated with micro-texture and often used as a measurement for safety and braking distance. It can also impact TPIN by slip/stick mechanism at high frequencies. However, no statistically significant relationship ($R^2 < 0.3$) was found between noise and wet friction both for optimum slip and blocked wheel (Sandberg and Ejsmont, 2000 [171]; Oshino et al., 2001 [197]).

Friction (or wet skid resistance) can be measured with three methods. (1) Towed skid trailer standardized in ASTM E274/E274M (2011) [688] can be used for field testing but very time consuming. The tested tire can be standard ribbed tire (ASTM E501, 2008 [689]) or standard smooth tire (ASTM E524, 2008 [690]). The skid number (SN), locked wheel

longitudinal friction value is reported. (2) Dynamic Friction Tester (DFT) standardized in ASTM E1911 (2009) [691] is a portable device tested in situ. It can be combined with Circular Track Meter (CTM) to calculate the International Friction Index (IFI) standardized in ASTM E1960 (2011) [692]. (3) British Pendulum Tester standardized in ASTM E303 (2013) [693] can be used in lab. The British Pendulum Number (BPN) is reported. The skid number SN_V and British Pendulum Number *BPN* were reported to have relations below (Domenichini et al., 1999 [63]) given the mean texture depth *MTD* and velocity *V*.

$$\begin{cases} SN_0 = -31 + 1.38 \cdot BPN \\ PSNG = 4.1 \cdot \left(\dfrac{MTD}{0.0254} \right)^{-0.47} \\ SN_V = SN_0 \cdot \exp\left(\dfrac{-PSNG \cdot V}{100} \right) \end{cases} \tag{56}$$

where the equations are valid on a wet surface with a nominal water depth of 0.5 mm. In general, skid number SN_V decreases with the increase of velocity *V*. Khaki et al. (2015) [694] reported that tire noise decreases as *BPN* increases for both conventional asphalt and porous asphalt.

4.5.15 Wear/Age

Traffic wear on pavement can change the micro- and macro-texture, resulting in friction and TPIN changes (McDaniel et al., 2010 [695]). Friction initially increases within a few months as traffic wears off the binder film coating the aggregate particles, and then decreases as the particles are further polished (Kowalski, 2010 [696]). For porous asphalt pavement, after a small decrease within the first months of service (Mogrovejo et al., 2014 [673]), TPIN generally increases over year due to the clogging of air voids (Paje, 2007 [697]), and then begins a steady trend (Mogrovejo et al., 2014 [673]). It is a cumulative process whose rate changes depending on porous mixes and locations. An increase of about 0.5 dB per year in CPX measurements for a porous polymer-modified friction course was found (Ng et al., 2009 [698]). Chalupnik (1996) [148] indicated that the age of pavement was more important than the type of pavement in terms of TPIN. For cement concrete pavement, the influence of wear and aging were relatively small (Sandberg et al., 1990 [607]). Longitudinally grooved pavements with

significant macro-texture can become quieter as macro-textural features are worn down over time (Dare et al., 2009 [699]).

The amount of wear can be estimated by traffic volume or single axle loads (ESALs). Winter maintenance operations and the impact of cyclic freezing and thawing (weather wear) are also forms of wearing (Neithalath et al., 2005 [663]). Like traffic wear, TPIN generally increase as pavement ages (Bendsten, 2009 [700]). Acoustic longevity describes how well pavement retains its TPIN level over time. For example, the first Next Generation Concrete Surface (NGCS) built by the Washington State Department of Transportation (WSDOT) showed a very short acoustic longevity (Anderson et al., 2014 [701]). On-board sound intensity (OBSI) levels increased from initial levels of 100.6 dBA to 104.4 dBA in 30 months. However, the effects of age were marginal for some other pavements (Hencken, 2012 [702]).

4.5.16 Surface Rating (SR)

Surface rating (SR) is a measure of the wear or distress on a pavement surface by counting the number of cracks and joint deterioration on a segment of road, and then applying weighting factors (Kay, 1992 [703]; MNDOT, 2003 [704]). The rating is typically highest immediately after construction or rehabilitation and gradually (or sometimes rapidly) decreases due to the accumulation of cracking, rutting, raveling and other types of distress (Mcdaniel et al., 2014 [122]). TPIN increases with the SR dropping as the distress increases the pavement roughness.

Asphalt pavement distress typically includes fatigue (alligator) cracking, block cracking, edge cracks, longitudinal (linear) & transverse cracking, reflection cracking, slippage cracks, corrugations & shoving, rutting, settlement/grade depressions, upheaval/swell, utility cuts/patch failure, pot hole, raveling/weathering, bleeding, polished aggregate, loss of aggregate on surface treatments, and longitudinal/transverse streaking (Miller and Bellinger, 2003 [705]).

4.5.17 Wetness

As one of the most common pavement conditions, wetness can increase TPIN by up to 3 dBA for heavy commercial vehicles (Syamkumar et al., 2013 [6]). The increase frequency range are found to be above 1000 Hz (Boullosa and Lopez, 1987 [706]; Descornet, 2000 [707])

probably due the water splash effect. It was also found that TPIN decreases at low and middle frequencies, which might be attributed to less adhesion. The tire vibrations on the wet road are slightly lower than those on a dry road, indicating that there must be a separate noise generating mechanism independent of the tire vibrations (Heckl, 1986 [13]). Bergmann (1980) [221] found a 10 dB increase over 1 kHz on wet pavement and speculated it was due to the acceleration of water particles at the leading edge. Heckl (1986) [13] also indicated that some of the noise on a very wet road does not come from the tire but from the water. The influence to pavement moisture was found to be independent on speed (Descornet, 2000 [707]). Porous pavements are more sensitive to wetness, as the voids can be saturated with moisture in the pavement.

There are some other pavement conditions, such as ice and/or snow. However, few literatures address such topics on TPIN. TPIN on snowy surface has more spectral contents at low frequencies (below 1.5 kHz) while TPIN on wet surface has more spectral contents at high frequencies (above 1.5 kHz), as illustrated in Figure 95 (Kongrattanaprasert et al., 2010 [708]).

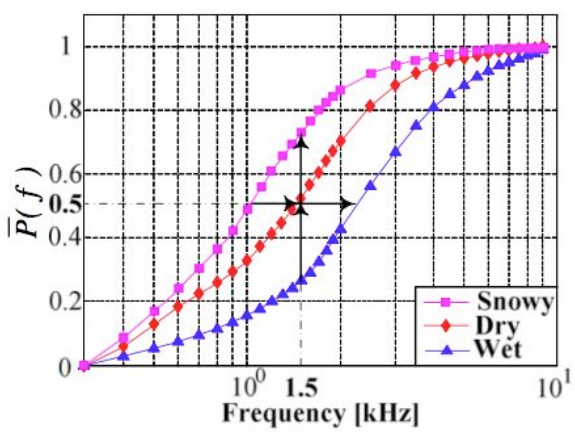

Figure 95: Typical cumulative spectral content of TPIN for different road conditions (source from Kongrattanaprasert et al., 2010 [708], Figure 1; reprinted under fair use provision)

4.5.18 Mixture Parameters / Materials

Various pavement parameters discussed above are determined by the mixture parameters such as nominal maximum aggregate sizes, aging conditions, air void contents, binder types, mixture types, aggregates and gradations. It was reported that mixture parameters that had

great impact on tire-pavement noise (Kocak and Kutay, 2012 [709]; Biligiri, 2008 [154]).

It was found that voids in the mineral aggregate (VMA) and binder content are in favor of TPIN reduction, while coefficient of uniformity of the aggregate gradation is not (Kocak and Kutay, 2012 [709]).

4.5.19 Reference Pavement

Standard pavement is required for measuring exterior vehicle noise or TPIN. The current globally accepted standard is ISO 10844 (2014) [425], which is basically a dense asphalt concrete surface with maximum aggregate size of 8 mm. A lot of attempts have been done to improve the repeatability and reproducibility for both on-board and pass-by noise (Sohaney et al., 2012 [710]; Moore, 2011 [711]). Specifications and measurement procedures for texture, roughness, acoustic absorption, planarity, and asphalt mix have been provided in the standard to reduce the variation of noise generation and propagation from track to track. However, it was argued that the ISO surface is too smooth to be representative of general pavements (FEHRL, 2001 [28]). As such, it is of interest to compare the tire ranking on ISO surface with that on normally used roads, or attempt to select more commonly used surface as reference pavement in the future. On the other hand, compared to rougher pavements, the current ISO surface can better distinguish acoustic behavior between tires, providing more accurate acoustic ranking of a tire (Blokland and Leeuwen, 2010 [712]).

Another standard pavement is SAE test surfaces. Donavan et al., 1998 [4] reported that tire noise from SAE test surfaces is larger than ISO surfaces, as shown in Figure 96.

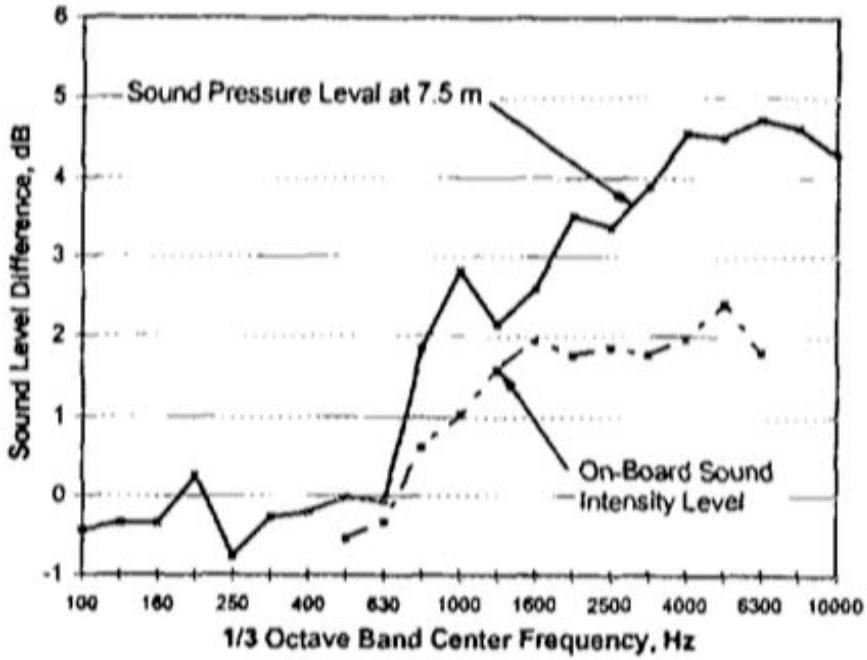

Figure 96: Difference in levels measured on ISO and SAE test surfaces (SAE less ISO) (source from Donavan et al., 1998 [4], Figure 4; reprinted with permission from AIP Publishing LLC)

4.6 Environmental Parameters

Environmental or atmospheric parameters can influence tire-pavement properties and the characteristics of the transmission path. Therefore, they cannot be neglected and have been included in many TPIN models.

4.6.1 Temperature

There are three relevant temperatures, i.e., tire temperature, pavement temperature and air temperature. Tire temperature is influenced by pavement temperature via interaction, but it is very difficult to measure when moving and might heat up or cool down over the course of test (Sandberg, 2004 [445]). Tire temperature has less strong correlation with TPIN than pavement temperature or air temperature (Sandberg and Ejsmont, 2002 [7]). Therefore, tire temperature was seldom included in TPIN models. Kindt et al. (2007) [525] investigated the tire temperature effect on the tire structural vertical resonance and found that the resonant frequency decreases by 0.12 Hz/°C with the increase of tire temperature, probably due to the viscoelastic property change of tire materials. It was also suggested that the tire cavity

acoustic resonance frequency increases at 0.16 %/°C with the increase of temperature.

Pavement temperature is generally highly correlated with air temperature. In general, air temperature equals about 65% of pavement temperature in °C (Kuijpers, 2001 [713]). Liao et al. (2015) [683] reported the following regression equation,

$$T_{pavement} = 1.3591 T_{air} - 2.2902 \tag{57}$$

where R^2 = 0.9506. Pavement properties change with pavement temperature. Asphalt exhibits brittle elastic behavior at lower temperatures while at higher temperatures, the material exhibits a significant viscous behavior resulting in TPIN reduction (Syamkumar et al., 2013 [6]).

Pavement temperature is also related to surface color, but it might also be a psychological effect [7]. For example, a black asphalt pavement might easily become 10 °C warmer than a bright cement concrete pavement in sunshine, which corresponds to 1 dBA in TPIN, but black asphalt pavement normally leaves an impression of quiet surface (Sandberg and Ejsmont, 2002 [7]).

Since air temperature is much easier to measure, it is most commonly included. It was shown that TPIN decreases about 0.04-0.1 dBA/°C with the increase of air temperature (Konishi et al., 1995 [714]; Anfosso-LédéE and Pichaud, 2007 [715]). The temperature coefficient also depends on the tire type and pavement type. The temperature effect is relatively larger for a rough-textured surface than for a smooth-textured surface (Sandberg and Ejsmont, 2002 [7]). Asphalt pavements are more sensitive to temperature than cement concrete because asphalt mixtures are viscoelastic materials whose moduli change with temperature. Liao et al. (2015) [683] investigated four types of asphalt pavements and concluded that air temperature influenced the correlations between noise levels and surface characteristics. They also analyzed the temperature effect on different frequencies and indicated that the effect was most obvious around 2000 Hz for the correlation between sound levels and surface roughness.

It has been found that increased temperature causes TPIN decrease in low-frequency due to the less stiffness of pavement and less hardness of tire rubber, but increase in high-frequency probably due to the more adhesion mechanism (Nilsson, 1980 [214]).

Air temperature or ambient temperature can affect both TPIN generation mechanisms and sound propagation. Therefore, pass-by noise measurements of TPIN are more sensitive to air

temperature than near field measurements such as OBSI.

Many TPIN measurement standards provide temperature correction equations to normalize data to a reference temperature (EEC, 2001 [716]; SAE, 2014 [140], AASHTO, 2013 [112]). The On-Board Sound Intensity (OBSI) Standard AASHTO TP 76 (AASHTO, 2013 [112]) provides the following correction for temperature effects.

$$IL_{Normalized} = IL_{Measured} + 0.072 \times (AirTemp - 20) \tag{58}$$

where $IL_{Normalized}$ is the normalized sound intensity level (dBA) for the reference temperature of 20°C, $IL_{Measured}$ is the measured sound intensity level (dBA) at temperature of $AirTemp$ (°C).

Anfosso-LédéE and Pichaud, 2007 [715] reported the following relationship between air temperature, pavement temperature and tire surface temperature.

$$\begin{cases} T_{pavement} = 1.7T_{air} - 4.5(^{o}\mathrm{C}) \\ T_{tire} = 1.05T_{air} + 15.8(^{o}\mathrm{C}) \end{cases} \tag{59}$$

where both have good correlations (R^2 = 0.94). The data were from two normal tires (165/65R13) on seven different pavements using Controlled Pass-By (CPB) method. The temperature coefficients were listed in Table 35. It was indicated that cement concrete pavements have little temperature effect and correlation is not good. It was also shown that the temperature effect is highest in low and high frequency range (below 500 Hz and above 2000 Hz), which can be explained by generating mechanisms rather than propagation. Therefore, temperature has relatively smaller effect on the overall noise level after A-weighting since spectral content in low and high frequencies is reduced.

Table 35: Temperature coefficients of the relationship between pass-by noise level at 90 km/h and air, pavement or tire temperatures, per road pavement category (source from Anfosso-LédéE and Pichaud, 2007 [715], Table 5; reprinted with permission from Elsevier)

Temperature Coefficient	Dense Asphalt	Porous Asphalt (Porosity > 10%)	Cement Concrete
α_{air} (ref. T_{air}) [dBA/°C]	-0.10	-0.06	-0.03
$\alpha_{pavement}$ (ref. $T_{pavement}$) [dBA/°C]	-0.06	-0.04	-0.02
α_{tire} (ref. T_{tire}) [dBA/°C]	-0.09	-0.05	-0.03

The temperature coefficients also depend on the type of tires. Sandberg (2004) [445] reported a positive coefficient has been observed with a specific tire. Jabben and Potma (2013) [717] also

reported that α is generally negative but can be positive in some special case, such as for a lug pattern of commercial vehicle tire in frequencies of 315 and 630 Hz.

For different speeds, the temperature coefficient can be also different. Jabben and Potma (2013) [717] reported that for the dense asphalt concrete (DAC), the temperature coefficient for statistical pass-by measurements (SPB) varies from -0.03 to -0.12 dB/°C as the vehicle speed increases from 50 to 140 km/h. The average temperature coefficient for trucks is -0.02 dB/°C. The temperature coefficient used by Dutch standard is -0.05 dB/°C for passenger cars and -0.03 dB/°C for trucks.

Konishi et al. (1995) [714] correlated the temperature coefficient with the elastic modulus change of the tread compound, as given by

$$\begin{aligned}\alpha &= kr \times \Delta T \times \Delta E30 \\ &= -5.63 \times 1.20 \times \Delta E30 \text{ (Air Temperature)} \\ &= -5.63 \times 0.82 \times \Delta E30 \text{ (Pavement Temperature)}\end{aligned} \tag{60}$$

where α is temperature coefficient for air or pavement temperature, kr is a coefficient, ΔT is the correction coefficient from air or pavement temperature change to tire temperature change, $\Delta E30$ is the tread rubber elastic modulus change rate at 30 °C (tire temperature).

4.6.2 Air Humidity

Air humidity or moisture is related to pavement wetness discussed above. Moisture can change the structural strength of unbound materials in the pavement layers. Longitudinal profile can also be affected by subgrade moisture (Bae et al., 2006 [718]). Higher humidity or rainfall may clean the pavement and change the texture (Mcdaniel et al., 2014 [122]). On the other hand, distresses or damages such as potholes, stripping, swelling or depressions may also be caused. In addition, higher air humidity reduces sound propagation.

4.6.3 Wind

It was shown that even for near-field OBSI measurements with windscreen, some contribution from aerodynamically generated background noise is present mainly at low frequencies (Donavan, 2012 [59]), decreasing the signal to noise ratio (SNR) especially when the vehicle speed is slow. Therefore, many TPIN measurement standards require that wind speed should be less than 5 m/s, e.g., 3.5 m/s in OBSI standard (AASHTO, 2013 [112]).

Besides wind speed, the wind contamination noise is also related to wind direction. The noise levels increased by 1 to 2 dBA when the wind direction is towards the measurement instrument and decreased by 1 to 2 dBA when the wind direction is away from the measurement instrument (Syamkumar et al., 2013 [6]).

4.7 Summary

The driver influence parameters affecting TPIN are summarized in Table 36. It can be seen that vehicle speed is the most important single parameter influencing TPIN over all frequencies. Accelerating, braking or cornering also largely increases TPIN due to the increase of stick/slip mechanism, especially at higher frequencies. The effects of tire load and inflation pressure are insignificant. Positive camber angle is favorable for TPIN reduction at higher frequencies.

The tire-related parameters affecting TPIN are summarized in Table 37. The tire type (radial/biased) and size can influence TPIN, however, the most important tire parameters are those affecting the contact characteristics between the tire treadband and the pavement, such as tread porosity, embedded stud, wear/aging, and rubber hardness. The parameters that affect the mechanical characteristics of the tire, such as belt stiffness, damping loss factor, non-uniformity, tire cavity content, and rolling resistance, are less influential. The tire width has a greater influence on TPIN than tire diameter.

The tread pattern parameters affecting TPIN are summarized in Table 38. It is shown that appropriate tread pattern optimization is able to reduce TPIN, such as increasing the offset between the tread blocks, and increasing the tread groove ventilation. However, the effects of many other tread pattern design techniques are marginal, such as normal randomization, addition of small sipes. It should be noted that, very few literatures have conclusively and quantitatively reported the effect of tread pattern on TPIN, even though the general public considered the tread pattern as an important factor influencing TPIN.

The pavement-related parameters affecting TPIN are summarized in Table 39. It can be seen that the most important factor is the pavement texture, especially the macro- and mega-texture; so are the related or derivative parameters, such as mean profile depth, IRI, positive or transverse or anisotropic texture, joints, wear/age, and surface rating. Some parameters have an effect on the air pumping mechanism, such as porosity, sound absorption,

and airflow resistance; some parameters have an effect on the impact mechanism, such as thickness of the pavement layer, and stiffness. However, the normal adhesion or tangential friction of the pavement is shown to be of little influence. In addition, it is widely known that wet pavement is noisier than dry pavement.

The environmental parameters affecting TPIN are summarized in Table 40. The environmental parameters have an influence on the sound propagation and thus on the noise level measured in the far field. However, if these parameters are within the normal range when at least the field tests can be successfully conducted, they can be ignored.

Table 36: Summary of driver influence parameters affecting TPIN

No.	Parameter	Pertinent Frequency [Hz]	Relation (↑↓)	Potential Noise Variation [dB]	Measurement Equipment	Relevant Mechanism	References
1	Speed	250-8000	↑	25	Speedometer, wheel/axle-mounted encoder, GPS	Various: impact, air pumping	[6,55,222]
2	Longitudinal Force/Slip	800-1600	↑	10	Accelerometer	Stick/slip	[104,185,307,504]
3	Lateral Force/Slip	1000-8000	↑	7	Accelerometer, gyroscope	Stick/slip	[7,507,508]
4	Tire Load	800-1600	↑	2	Dynamometer	Impact, air pumping	[511–519]
5	Inflation Pressure	1600-3200	Complex	1	Tire pressure gauge/sensor	Impact, air pumping	[181,513]
6	Tire Camber Angle	1000-3000	↓	5	Protractor	Impact, stick/slip	[527]

Table 37: Summary of tire-related parameters affecting TPIN

No.	Parameter	Pertinent Frequency [Hz]	Relation (↑↓)	Potential Noise Variation [dB]	Measurement Equipment	Relevant Mechanism	References
1	Tire Type/Construction	N/A	Complex	3	N/A	Various	[295,532–535]
2	Tire Width	500-1000	↑	3	Measure tape	Various	[440,544]
3	Tire Diameter	N/A	↓	1	Measure tape	Impact, horn	[393,440,542]
4	Belt Stiffness	500-8000	↓	2	Loading test rig with bar	Tire resonance	[235,377,719]
5	Damping (Loss Factor)	250-500	↓	1	N/A	Tire resonance	[223]
6	Non-uniformity	20-200	↑	1	Wheel balancing machines	Tire resonance	[235,497]
7	Rubber Hardness	1000-3000	↑	3	Durometer	Stick/slip	[550,720]
8	Wear/Aging	1000-3000	↑ (then ↓)	5	N/A	Various	[238,322,721,722]
9	Retreaded	500 & 2000-3000	Complex	2	N/A	Impact	[28,571,723]
10	Studded	400-3000 & above 5000	↑	6	N/A	Impact, stick/slip	[724,725]
11	Tread Porosity	N/A	↓	7	N/A	Air pumping, horn effect	[239,321]
12	Tire Cavity Content	400-1100	Complex (↓)	2	N/A	Cavity resonance	[3,297,380]
13	Rolling Resistance	N/A	↑ (Weak correlation)	0	Dynamometer drum: ISO 18164 [576]	N/A	[171,573–575]

Table 38: Summary of tread pattern parameters affecting TPIN

No.	Parameter	Pertinent Frequency [Hz]	Relation (↑↓)	Potential Noise Variation [dB]	Measurement Equipment	Relevant Mechanism	References
1	Randomization	600-1000	↓	0 or marginal	N/A	Tread impact	[7,360]
	Elimination of Groove Footprint Coinciding	800-1000	↓	N/A	N/A	Tread impact	[7,360]
	Offset between Left and Right Side	N/A	↓	5	Caliper	Tread impact	[7,360,726]
2	Rotation Direction / Side Asymmetry	N/A	↑	3	N/A	Various	[7,360]
3	Ventilation	800-1000 & 1600-4000	↓	2	N/A	Air pumping, air resonance	[7,28,360]
4	Addition of Mirror Image Grooves	Above 4000	↓	0	N/A	Air pumping, air resonance	[7,360]
	Addition of Lamellae	800-1000	↓	N/A	N/A	Air pumping, air resonance	[7,360]
	Groove Width	800-2000	↑ 9 mm ↓	N/A	Caliper	Air pumping	[7,28,360]
	Groove Angle (Relative to Lateral)	800-2000	↓	N/A	Protractor	Tread impact	[7,28,360]

Table 39: Summary of pavement-related parameters affecting TPIN

No.	Parameter	Pertinent Frequency [Hz]	Relation (↑↓)	Potential Noise Variation [dB]	Measurement Equipment	Relevant Mechanism	References
1	Micro-texture (below 0.5 mm)	2000-4000	↓	N/A but Marginal	Laser profiler: ISO 13473 [623]; Circular Track Meter (CTM): ASTM E2157 [624] for macro-texture only	Stick/slip, stick/snap	[626,627]
	Macro-texture (0.5-50 mm)	100-1000 & 2000-4000	↓ & (10 mm) ↑	N/A but Significant		Texture impact, air pumping	[122,628,629]
	Mega-texture (50-500 mm)	100-1000	↑	N/A but Significant		Texture impact	[629,634]
	Unevenness (500-800 mm)	N/A	↑	4		N/A	[63]
	Unevenness (10-50 m)	200-1500	↓	1			
2	MPD/MTD/ Texture	N/A	Complex	10	Sand patch method: ASTM E965 [632], ASTM E1845 [633] and ISO 13473-1 [610]	Same as macro-texture	[638]
3	International Roughness Index (IRI)	Same as unevenness	Same as unevenness	Same as unevenness	Profilometer: ASTM E1926 [640] and ASTM E1364 [641]	Same as unevenness	[47]
4	Positive versus Negative Texture	N/A	↑	N/A	Laser profiler	Texture impact, air pumping	[487]
5	Transverse Texture	N/A	↑	N/A	Laser profiler	Texture impact	[325]
6	Anisotropic Texture	N/A	↑	N/A	Laser profiler	Texture impact, air pumping	[644]

No.	Parameter	Pertinent Frequency [Hz]	Relation (↑↓)	Potential Noise Variation [dB]	Measurement Equipment	Relevant Mechanism	References
7	Joints	800-1000	↑	3	Laser profiler	Texture impact, air pumping	222,406,646,648–650
8	Porosity	500-1600 & 3000	↓	7	Pavement core sample: ASTM D7063/D7063M [659]	Various	478,727–729
9	Sound Absorption	Similar to Porosity	Similar to Porosity	Similar to Porosity	Impedance tube: ISO 10534-1 [666] and ISO 13472-1 [669]	Pavement Absorption	473,475,519
10	Airflow Resistance	N/A	↑	N/A	Impedance tube: ISO 9053 [671] and ANSI/ASA S1.18 [152]	Air pumping, air resonance	639,730,731
11	Thickness of Layer	500-1600	↓	5	Measure tape	Acoustic and mechanical impedance	7
12	Stiffness (Mechanical Impedance)	800-1250	↑	1	Impact hammer device: AASHTO T 342 [684]	Vibration Transfer	313,465,676–678
13	Normal Adhesion	2000-4000	↑	1	N/A	Stick/snap	7
14	Tangential Friction	2500-6300	↑	0	Dynamic Friction Tester (DFT): ASTM E1911 [691]	Stick/slip	171
15	Wear/Age	1000-4000	↑	2	N/A	Impact, absorption	663,673,698,700
16	Surface Rating (SR)	N/A	↓	N/A	N/A	Impact	703,704
17	Wetness	Above 1000 Hz	↑	3	N/A	Water splash effect	6,706,707
18	Mixture Parameters/Materials	N/A	Complex	Significant	N/A	Various	154,709

Table 40: Summary of environmental parameters affecting TPIN

No.	Parameter	Pertinent Frequency [Hz]	Relation (↑↓)	Potential Noise Variation [dB]	Measurement Equipment	Relevant Mechanism	References
1	Temperature	1000-4000	↓	3	Thermometer	Impact	714,715
2	Air Humidity	N/A	↓	1	Air humidity meter	Sound propagation	718
3	Wind	300 & 2000	↑	N/A	Wind meter	Air Turbulence	6,59

5 Existing Models

5.1 Introduction

TPIN is dominant noise source for passenger vehicles above 40 km/h and 70 km/h for trucks. The motivation for reducing tire-pavement interaction noise is multiple and different across different countries. One is to pass the legal approval for exterior noise level; one is to reduce the annoyance level in car interior space and increase passenger comfort (Harrison, 2004 [10]); one is to boycott foreign tire imports (Chen, 2014 [11]). It is certain that accurate and reliable models on tire-pavement interaction noise (TPIN) are desirable to vehicle manufacturers and tire companies, since these models will be able to reduce development time (Mohamed et al., 2013 [41]).

A lot of relevant models have been developed to describe and predict tire vibrations and TPIN. However, all of these models are restricted in some sense (Dare, 2012 [213]). For example, some models only describe one or two particular generation mechanisms; some assume two-dimensional tire and pavement; some only include limited tire/pavement combinations, such as slick tire on rough road; some only calculate noise level at the source without considering sound propagation; some are only concerned on tire structural dynamics, and neglect the effect of the nonlinear aerodynamics surrounding the tire.

Generally speaking, it is difficult to evaluate the accuracy of specific models due to different model objectives and the lack of validation (Kuijpers and van Blokland, 2001 [347]). In addition, most of current models only focus on passenger car tires. Very few literatures reported noise models for truck tires that might have more influence on traffic noise. As the increased popularity of porous asphalt pavement, more and more models include pavement absorption and mechanical impedance as parameters of interest.

In general, there are three acoustic modeling approaches: wave, energy and ray acoustics (Crocker, 2007 [732]). The wave acoustics approach commonly adopted by finite element software is used for a small enclosed space, especially if its shape is simple and has well-defined boundary conditions. The energy acoustics approach is often used as a statistical approach for sound intensity. The ray acoustics approach, together with the multiple-image-source concept for reflection calculations, can be used to investigate sound

propagation in the atmosphere. Most of current TPIN models used one or two approaches described above.

In this literature review work, the present author exhaustively collected over 2000 references related to tire noise dated from 1960's to 2010's. The present author cannot guarantee all the references have been covered but vast majority. In the end, 74 models were reviewed from ~300 selected references. The models are divided into three categories based on the characteristics of the approach used: deterministic model, statistical model and hybrid model. A brief introduction of the three categories is shown in Table 41.

Table 41: Introduction of three categories of TPIN models

	Deterministic	Statistical	Hybrid
Method	Physics without experimental data	Correlation of measured noise data and tire-pavement parameters	Incorporating physical principles into empirical model
Example	Brinkmeier et al., 2008 [733]: structurally and aerodynamically radiated noise components	Khazanovich et al., 2008 [5]: different pavements and same tire with curve fitting	Domenichini et al., 1999 [63]: effect of pavement texture on TPIN
Drawback	Low frequency only, computationally intensive, 17 dB error	No knowledge of noise generation mechanism	Mostly pavement parameters only without knowledge of tire inputs, intensive data for training
Major Application [347]	Tire design (qualitative)	Pavement design (quantitative)	Optimization of combination of tire and pavement

The deterministic models are usually focused on low frequencies (below 500 Hz). However, the main spectral content of real tire noise is located from 600-1200 Hz. Therefore, these models tend to have considerable errors. The statistical and hybrid model usually cover the entire dominant frequency of tire noise, resulting in better accuracy. However, most of the models only investigate pavement parameters. Advantages and disadvantages both exist for the three categories of TPIN models. As a matter of fact, one specific model generally focuses on only a few points of interest (physics or parameters) due to the complexity of TPIN mechanisms. For different research purposes and/or under different conditions, one model might have advantages over another in the same category of models.

The purpose of this paper is to present the existing models from literature, compare these models, state their strength and weakness, and provide insights into future research directions in this area. The organization of this paper is as follows. In Section 5.2, the deterministic models were reviewed. In Section 5.3, the statistical models were reviewed. In Section 5.4, the hybrid models were reviewed. In Section 5.5, conclusions of this literature review were given. The present author have endeavored to paraphrase each model to the maximum

accuracy. However, it is also believed that errors and biases might inevitably occur; if so, I apologize.

5.2 Deterministic Models

5.2.1 Introduction

Deterministic models are also called analytical or numerical models. Recent methods, such as finite element method (FEM) (Lou, 2007 [734]) and boundary element method (BEM) (Wang et al., 2011 [735]; Nakajima et al., 1993 [394]), require large computational effort. A large number of parameters are also required, including tire geometry, deformation of the tire, material parameters, boundary conditions and so on (Yang et al., 2013 [544]). On the other hand, generally, the influence of single parameters on TPIN is possible to be investigated only by deterministic models (Biermann et al., 2007 [614]).

Generally, deterministic models need a lot of material or construction parameters as input for tire modeling. For example, Larsson and Kropp model (1992) [226,302,736] includes 24 input parameters (6 geometry parameters and 18 material parameters), some of which are presented below as an example and reference in Table 42. Anderson et al. (2001) [737] also presented a measurement method for collecting these tire material data.

Table 42: Input tire parameters (slick 205/60R15) for Larsson and Kropp model (data in brackets refer to loss factors for the corresponding parameters) (Modified from Andersson and Larsson, 2005 [738], Table 1; reprinted with permission from Ms. Brigitte Badelt of S. Hirzel Verlag on behalf of the European Acoustics Association)

Category	Parameter	Value
Geometry	Length of tread plate	$2\pi\times0.314$ m
	Width of tread plate	0.355 m
	Thickness of tread layer	0.010 m
	Thickness of belt layer	0.001 m
Tread Layer	Density	1175 kg/m^3
	Young's modulus (real part)	25 MPa [0.05~0.70]
	Poisson's ratio	0.499
Belt Layer	Density	3720 kg/m^3
	Young's modulus (real part)	580 GPa [0.02]
	Poisson's ratio	0.4
	Radial bedding	1.02×10^6 N/m^3 [0.09]
	Circumferential bedding	1.02×10^6 N/m^3 [0.09]
	Lateral bedding	1.02×10^6 N/m^3 [0.09]
	Circumferential tension	42000 N/m^2 [0.055]
	Lateral tension	42000 N/m^2 [0.055]

In this section, 37 deterministic models were reviewed, including 16 conventional physics models, 16 finite element and boundary element models, and 5 computational fluid dynamics models. The model name, method, output noise parameter with noise measurement technique, investigated noise generation mechanisms, and investigated input parameters of each model are listed and compared in tables as a summary in Section 5.2.5. The summary tables can be used as a reference for readers to direct to models of interest.

5.2.2 Conventional Physics Models

The conventional physics models typically utilize traditional analytical methods and classic mathematics, such as modal analysis, to present and investigate the dynamical behavior of the tire that is usually modeled as a ring, shell or plate. Traditional acoustic equations are sometimes applied to analyze the structural wave propagation mode in the tire tread and wall, as well as the acoustical mode in the tire cavity. Sixteen models were reviewed in this subsection. In this paper, the heading for the corresponding model follows the structure as authors (model name, year), and the models in each subsection are ordered chronologically.

5.2.2.1 Hayden (Monopole, 1971)

Hayden (1971) [354] developed the first air pumping model focusing on the noise generation at the leading edge of the tire contact patch where the tread is compressed. The model is based on the monopole theory whose governing equation is below.

$$p(r,\omega) = \frac{\rho \omega Q}{4\pi r} \tag{61}$$

where p is the sound pressure (root mean square value), r is the distance between receiver and monopole, ω is radian frequency, ρ is air density, Q is air volume change rate (root mean square value). The initial groove volume V_0 is

$$V_0 = L \cdot D \cdot W \tag{62}$$

where L is groove length in the circumferential direction, D is groove depth, W is groove width. The air volume change rate Q is calculated by

$$Q(v) = \frac{\Delta V}{\Delta t} = \frac{\delta \cdot V_0}{\Delta t} = \frac{\delta \cdot L \cdot D \cdot W}{L / v} = \delta \cdot D \cdot W \cdot v \tag{63}$$

where v is tire forwarding speed, ΔV is the volume change, Δt is the time duration, δ is the fractional change of the initial volume. The radian frequency ω is determined by the repetition between consecutive groove cavities.

$$\omega(v) = 2\pi \cdot v / l_p \tag{64}$$

where l_p is the pitch distance between groove cavities. Combining the above equations gives

$$p(r,v) = \frac{\rho \cdot v^2 \cdot \delta \cdot D \cdot W}{2 \cdot l_p \cdot r} \cdot n \tag{65}$$

where n is the number of groove cavities along the tire width.

5.2.2.2 Plotkin and Stusnick (Unified, 1981)

Plotkin and Stusnick (1981) [43] presented a unified set of analytical models to investigate the major noise generation mechanisms (impact and air pumping) systematically with basic tire structural properties.

Bohm's thin-shell equations (Bohm, 1967 [739]) were used to model the motion of a tire. The air pumping mechanism was analyzed based on the physical behavior (Plotkin et al., 1980 [740]). The influence of pavement texture was also included using Nilsson's linear excitation model (Nilsson, 1976 [741]). Then the sound radiation analysis was employed using Eberhardt's model (Eberhardt, 1979 [417]). The nomenclature for the model is listed in Table 43.

Table 43: Nomenclature for Unified Model

Denotation	Meaning
a	Speed of sound in air
A	Tread area function
A_b	Cross-sectional area of belt
A_c	Cross-sectional area of cords in belt
$A(\phi_0)$	Function describing tread area
A_n, B_n, C_n, D_n	Coefficients of Fourier series describing tire shape
C_p	Phase velocity in belt
d	Tread depth
d_r, d_t	Radial and tangential damping, per unit length
|det|	Magnitude of determinant
E, F, G, H	Coefficients of inverted matrix
E_R	Elastic modulus of rubber
E_s	Elastic modulus of steel

Denotation	Meaning
EA	Extensional stiffness of tread and belts
EI	Bending stiffness of tread and belts; $(EI)_b$ is for the belt plies alone, and $(EI)_t$ is for the tread alone
$f(\phi_1\text{-}\phi)$	Function defining radial displacement at ϕ due to unit force at ϕ_1
$F(\phi)$	Force associated with tread/road interface
G	Geometric amplification factor
$G(\mathbf{r}\|\mathbf{r}')$	Green's function
G_R	Shear modulus of rubber
h	Distance from neutral surface of bending to center of tread
$H(\phi_1\text{-}\phi)$	Unit step function
k_r, k_t	Radial and tangential bedding coefficients
k_A, k_T	Wave number in air and tire
l	Tread pitch length
l_b	Tread block length
l_s	An invariant calculating bedding stiffness
l_v	Tread void length
n	Circumferential mode number
N	Number of belt plies
N_v	Number of voids
p	Acoustic pressure
p_i	Inflation pressure
$p_0(t)$	Sound pressure for a tread void with pitch l_0, depth d_0 and width w_0
p_r, p_t	Radial and tangential external pressures
p_{rs}, p_{rc}, p_{ts}, p_{tc}	Sine and cosine integrals of p_r and p_t, e.g., $p_{rs} = 1/\pi\cdot\int_0^{2\pi} p_r \sin n\phi \mathrm{d}\phi$
P	Point force
P_{avg}	Average contact force pressure
Q	Resonant Q factor; inverse of loss factor
$\mathbf{r}$	Vector from source to receiver; $\|\mathbf{r}\| = \mathrm{r}$
R	Local radius of curvature
R_0	Unperturbed radius of tire
s	Circumferential distance coordinate, measured from contact patch edge
s_0	Coordinate on pavement
S	Surface area
t	Time
t_b	Thickness of belt ply
t_s	Sidewall thickness
t_t	Tread thickness
T_0	Tension in belt due to inflation pressure
U	Speed of tire
u_n	Normal velocity
V	Tread void volume
v, w	Tangential and radial displacement of belt
w_b	Width of belt
w_t	Effective width of tread
w_v	Width of tread void
W	Amplitude of harmonic component of radial displacement w, determined from the forced motion of the contact patch edge
x, y, z	Cartesian coordinates with respect to contact patch center
y_g	Shape of tread groove
y_{gi}	Shape of i'th groove in full tread pattern
z_s	Pavement texture profile
Δz	Average vertical compression of rubber
α	Cord angle
α, β, γ, δ, ε	Matrix coefficients
$\delta(\phi\text{-}\phi_1)$	Dirac delta function
ε_b	Flow blockage factor

Denotation	Meaning
ζ	Load distribution due to pavement texture
η	Damping coefficient
θ_0	Angle between sidewall and belt
κ	Local belt curvature = l/R
κ_0	Curvature of unperturbed belt = l/R_0
μ	Mass density (per unit length) of tread and belts
ρ	Density of air
ϕ	Circumferential coordinate
ϕ_a, ϕ_b	Coordinate of leading edge and trailing edge of contact patch
ϕ_0	Circumferential coordinate fixed to tire; corresponds to ϕ at $t = 0$
$\Delta\phi$	Angle with respect to contact patch center
$\Delta\phi_{cp}$	Angle from center to edge of contact patch
ω	Radial frequency
Ω	Angular velocity of tire
$(\dot{\ })$	Time derivative
$()'$	Spatial derivative; either $\partial/\partial\phi$ or $\partial/\partial s$

5.2.2.2.1 Thin Shell Equations for the Motion of the Tire

The radial tire belt was modeled as a uniform shell on a uniform elastic foundation. The two-dimensional shell equations for the tangential and radial displacements of the belt are as follows (Bohm, 1967 [739]).

$$\begin{cases} \mu\left(\ddot{v}+2\Omega\left(\dot{v}'+\dot{w}\right)+\Omega^2\left(v''+2w'-v\right)\right)-\dfrac{EA}{R_0^2}\left(v''+w'\right)+k_t v-d_t\left(v'\Omega+\dot{v}\right)=p_t\left(\phi,t\right) \\ \mu\left(\ddot{w}+2\Omega\left(\dot{w}'-\dot{v}\right)+\Omega^2\left(w''-2v'-\left(w+R_0\right)\right)\right)+\dfrac{EA}{R_0^2}\left(v'+w\right)+\dfrac{EI}{R_0^4}\left(w^{\text{iv}}+2w''+w\right)-\dfrac{T_0}{R_0^2}\left(w+w''\right)+k_r w+d_r\left(w'\Omega+\dot{w}\right)=p_r\left(\phi,t\right) \end{cases} \tag{66}$$

For stationary tire, after setting all time derivatives to zero, the solutions of the above linear equations are

$$\begin{cases} v=\sum_{n=0}^{\infty}\left(A_n\sin n\phi+B_n\cos n\phi\right) \\ w=\sum_{n=0}^{\infty}\left(C_n\sin n\phi+D_n\cos n\phi\right) \end{cases} \tag{67}$$

where the coefficients are calculated as the following matrix format,

$$\begin{bmatrix} A_n \\ B_n \\ C_n \\ D_n \end{bmatrix}=\frac{1}{|\det|}\begin{bmatrix} E & F & G & H \\ -F & E & -H & G \\ -G & -H & I & J \\ H & G & -J & I \end{bmatrix}\begin{bmatrix} p_{ts} \\ p_{tc} \\ p_{rs} \\ p_{rc} \end{bmatrix} \tag{68}$$

where the parameters in capital letters are given by

$$\begin{cases} E = \alpha\left(\delta^2+\varepsilon^2\right)-\delta\gamma^2 \\ F = \beta\left(\delta^2+\varepsilon^2\right)+\varepsilon\gamma^2 \\ G = \left(\beta\delta+\alpha\varepsilon\right)\gamma \\ H = \left(\gamma^2-\alpha\delta+\beta\varepsilon\right)\gamma \\ I = \delta\left(\alpha^2+\beta^2\right)-\alpha\gamma^2 \\ J = \varepsilon\left(\alpha^2+\beta^2\right)+\beta\gamma^2 \\ \left|\det\right| = \left(\alpha^2+\beta^2\right)\left(\delta^2+\varepsilon^2\right)+2\gamma^2\left(\beta\varepsilon-\alpha\delta\right)+\gamma^4 \end{cases} \tag{69}$$

where the parameters in Greek letters are in terms of tire properties as

$$\begin{cases} \alpha = \left(\dfrac{EA}{R_0^2}-\mu\Omega^2\right)n^2+\left(k_t-\mu\Omega^2\right) \\ \beta = d_t\Omega n \\ \gamma = \left(\dfrac{EA}{R_0^2}-2\mu\Omega^2\right)n \\ \delta = \dfrac{EI}{R_0^4}n^4-\left(\dfrac{2EI}{R_0^4}+\mu\Omega^2-\dfrac{T_0}{R_0^2}\right)n^2+\left(\dfrac{EA}{R_0^2}+\dfrac{EI}{R_0^4}-\dfrac{T_0}{R_0^2}-\mu\Omega^2+k_r\right) \\ \varepsilon = d_r\Omega n \end{cases} \tag{70}$$

The study also presented equations to calculate extensional stiffness, bending stiffness and bedding stiffness of tread belt.

$$EA = 4\left(A-A_c\right)G_R\left(1-\cot^2\alpha-\cot^4\alpha\right) \tag{71}$$

$$\begin{cases} \left(EI\right)_b = \dfrac{EA}{t_b w_b}w_b\dfrac{\left(Nt_b\right)^3}{12} \\ \left(EI\right)_t = E_R w_t\dfrac{t_t^3}{3} \end{cases} \tag{72}$$

$$\begin{cases} k_r = \dfrac{\cos\theta_0+\theta_0\sin\theta_0}{\sin\theta_0-\theta_0\cos\theta_0}p_i \\ k_t = \dfrac{G_R t_s}{l_s}+p_0\cot\theta_0 \end{cases} \tag{73}$$

The damping coefficients for truck tires are approximately calculated by

$$\begin{cases} d_r = \dfrac{\sqrt{k_r \mu}}{10} \\ d_t = \dfrac{\sqrt{k_t \mu}}{10} \end{cases} \tag{74}$$

5.2.2.2.2 Air Pumping

It was found that the tread void compression take place mainly through lateral motion of tread elements entering and leaving the contact patch instead of vertical compression of the tread rubber (Plotkin et al., 1980 [365]; Samuels, 1979 [364]). The reflection from the ground and tire sidewall plays a great role in generating noise by increasing the pressure by a factor of 4, i.e., geometric radiation factor G. Air pumping also depends on the flow blockage factor ε_b, e.g., for rib tires with continuous grooves, some of the displaced air moves within grooves rather than being pumped out where $\varepsilon_b \approx 0.35$, but for cross-bar tires, $\varepsilon_b \approx 1$, which generates more air pumping noise.

To analyze air pumping noise, the volume of a single void is given by

$$V = w_v d\left[l_v - l_b h\kappa_0 + \left(l_v + l_b\right)h\kappa\right] \tag{75}$$

The equation for sound pressure for a monopole source is

$$p = \frac{\rho \ddot{V}}{4\pi r} \tag{76}$$

Assuming κ is a function of ϕ, and all the other parameters in V are constant,

$$\ddot{V} = V''(\phi)\Omega^2 = w_v d\left(l_v + l_b\right)h\frac{d^2\kappa}{d\phi^2}\Omega^2 \tag{77}$$

The final equation for the sound pressure is

$$p(\phi) = -\frac{G\varepsilon_b \rho}{4\pi r}\left(\frac{U}{R_0}\right)^2 w_v dh\left(l_v + l_b\right)\frac{l}{R_0^2}\sum_{n=1}^{\infty} n^2\left(n^2 - 1\right)\left(C_n \sin n\phi + D_n \cos n\phi\right) \tag{78}$$

The sound pressure for a tread void with pitch l_l, depth d_l and width w_l is

$$p_l(t) = \frac{l_l d_l w_l}{l_0 d_0 w_0} p_0(t) \tag{79}$$

where $p_0(t)$ is sound pressure for a tread void with dimensions l_0, d_0 and w_0. The sound pressure of air pumping for a full tread pattern is given by

$$p(\phi)=\frac{1}{w_t}\sum_{i=1}^{N_v}\int_{\frac{-w_t}{2}}^{\frac{w_t}{2}} p_0\left(\phi-\frac{y_{gi}(x)}{R_0}\right)dx \tag{80}$$

5.2.2.2.3 Carcass Vibration

The models are only for steady uniform carcass on a smooth pavement. For the vibration of tire carcass on a textured surface, the circumferential coordinate was changed from ϕ to $s = R_0\phi$, and $()'$ denotes $\partial/\partial s$. For the contact patch edge excitation, the radial displacement of belt is

$$w = We^{i(k_t s-\omega t)}e^{-\eta s} \tag{81}$$

where

$$\begin{cases} k_T=\dfrac{\omega}{C_p} \\ C_p^2=\dfrac{1}{\mu}\left(EIk_T^2+T_0+\dfrac{k_r}{k_T^2}\right) \\ \eta=\dfrac{C_p k_r}{4EIk_T^2+2T_0} \end{cases} \tag{82}$$

The motion at the leading edge ϕ_a and trailing edge ϕ_b due to excitation of tread pattern are

$$\begin{cases} \ddot{w}(\phi_a)=P\Omega^2 f(0)A'(\phi_a-\Omega t) \\ \ddot{w}(\phi_b)=P\Omega^2 f(0)A'(\phi_b-\Omega t) \end{cases} \tag{83}$$

For the pavement texture excitation, the load at point (x, y) is

$$p_r(x,y)=P\left(1+\frac{z_s(x,y)}{\Delta z}\right)=P\left(1+\zeta(x,y)\right) \tag{84}$$

Then the equation for the motion at the trailing edge ϕ_b due to excitation of pavement texture is

$$\ddot{w}(\phi_b)=P\Omega^2 f(0)\left[A'(\phi_b-\Omega t)+A\zeta'\left(s_0+R(\phi_b-\Omega t)\right)R\right] \tag{85}$$

5.2.2.2.4 Sound Radiation

The sound pressure from a moving surface S is (Morse, 1970 [742])

$$p(\mathbf{r})=\int_S G(\mathbf{r}\,|\,\mathbf{r}')\left(\vec{\nabla}p\cdot\hat{n}\right)'dS \tag{86}$$

Using Eberhardt's model (Eberhardt, 1979 [417]) employing Green's function of a vibrating plate corresponding to the flat tread area of tire into an infinite baffle, the final equation leads to

$$p(\mathbf{r},\omega)=\frac{\rho W}{2\pi}\omega^2 e^{-i\omega t}\int_{\frac{-w_b}{2}}^{\frac{w_b}{2}}\int_0^{\infty}\frac{e^{ik_a r}}{r}e^{ik_t s}e^{-\eta s}\,ds \tag{87}$$

5.2.2.3 Keltie (Truck Tire, 1982)

Keltie (1982) [223] modeled the truck tire as an infinitely long incomplete circular cylindrical shell to predict sound power generated, as illustrated in Figure 97. The infinite length assumption is based on the fact that the waves propagating circumferentially are effectively damped out before they can "see" each other near the top of the tire. The tire is basically both nonisotropic and nonhomogeneous material due to the composite structure of the rubber and laminated plies. However, the model considered it as homogeneous and isotropic material with only ply region taken into account, since the ply contributes most of the carrying ability. The boundary conditions of the tire model are pinned connections with the rim along the line $\theta = 0$ and $\theta = \theta_0$.

Based on Flügge's thin shell theory including both bending and extensional effects, the equation of motion for the shell surface is given by

$$\begin{bmatrix} L_{11} & L_{12} & L_{13} \\ L_{12} & L_{22} & L_{23} \\ L_{13} & L_{23} & L_{33} \end{bmatrix}\begin{bmatrix} u(s,\theta,t) \\ v(s,\theta,t) \\ w(s,\theta,t) \end{bmatrix}=\frac{R^2\left(1-\nu^2\right)}{\bar{E}h}\begin{bmatrix} q_x(s,\theta,t) \\ q_\theta(s,\theta,t) \\ q_z(s,\theta,t) \end{bmatrix} \tag{88}$$

where L_{ij} are differential operators, u, v, w and q_x, q_θ, q_z are the deformations and externally applied pressures along x, θ, z directions, s is normalized coordinate given by $s = x/R$, ν is Poisson's ratio, $\bar{E}$ is complex Young's modulus. In order to compute the acoustic radiation, the radial displacement needs to be obtained based on the radial load, written by

$$\begin{cases} q_z(s,\theta,t)=e^{-j\omega t}q(s)H(s) \\ w(s,\theta,t)=e^{-j\omega t}w(s,\theta)=e^{-j\omega t}\sum_{n=1}^{\infty}w_n(s)\left(\frac{2}{\theta_0}\right)^{\frac{1}{2}}\sin\left(\frac{n\pi\theta}{\theta_0}\right) \end{cases} \tag{89}$$

where $q(s)$ and $H(\theta)$ are polynomials that satisfy the differentiability and continuity conditions.

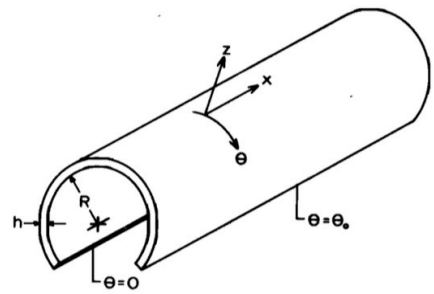

Figure 97: Shell model geometry and coordinate system (source from Keltie, 1982 [223], Figure 3; reprinted with permission from AIP Publishing LLC)

The sound pressure $p(x, r, \theta)$ is governed by

$$\left(\frac{\partial^2}{\partial r^2}+r^{-1}\frac{\partial}{\partial r}+r^{-2}\frac{\partial^2}{\partial \theta^2}+\frac{\partial^2}{\partial x^2}+K_a^2\right)p(x,r,\theta)=0 \tag{90}$$

where r is the radial coordinate, K_a is acoustic wavenumber. The normal velocity of the shell surface $v^s(x, \theta)$ is related to the sound pressure $p(x, r, \theta)$ through the boundary condition and Euler's equation by

$$j\omega\rho_0 v^s(x,\theta)=\left.\frac{\partial p(x,r,\theta)}{\partial r}\right|_{r=R} \tag{91}$$

Where ω is radian frequency, ρ_0 is the air density. The surface acoustic intensity $J(x, \theta)$ is calculated by

$$J(x,\theta)=\frac{1}{2}\mathrm{Re}\left\{\left[p(x,R,\theta,t)\right]\left[v^s(x,\theta,t)\right]^*\right\} \tag{92}$$

where Re indicates real part of the complex value, * indicates complex conjugate. The total radiated sound power Π is given by

$$\Pi=\int_{-\infty}^{\infty}\int_0^{2\pi}J(x,\theta)R\,d\theta\,dx \tag{93}$$

Tire parameters such as bending stiffness, inflation pressure and structural damping were analyzed for their effects on the sound power level both in 1/3 octave band and overall levels.

5.2.2.4 Kung et al. (2D Ring, 1986)

Kung et al. (1985 [743]; 1986 [744]; 1986 [745]), Huang and Soedel (1987) [746,747] considered the tire belt as a 2-demensional rolling ring and the sidewalls as an elastic foundation with radial

and tangential stiffnesses. The equations of motion are given as below (Huang and Soedel, 1987 [746]).

$$\begin{cases} \frac{D}{a^4}\left(u_r''''-u_\theta''\right)-\frac{K}{a^2}\left(u_r'+u_\theta''\right)+\left(\rho h\Omega^2+\frac{p_0}{a}\right)\left(-2u_r'-u_\theta''\right)+\left(\frac{p_0}{a}+k_\theta\right)u_\theta+\rho h\left(\ddot{u}_\theta+2\Omega\dot{u}_r\right)=q_\theta(\theta,t) \\ \frac{D}{a^4}\left(u_r''''-u_\theta'''\right)+\frac{K}{a^2}\left(u_r+u_\theta'\right)+\left(\rho h\Omega^2+\frac{p_0}{a}\right)\left(2u_\theta'-u_r''\right)+\left(\frac{p_0}{a}+k_r\right)u_r+\rho h\left(\ddot{u}_r-2\Omega\dot{u}_\theta\right)=q_r(\theta,t) \end{cases} \tag{94}$$

where k_r is radial stiffness, k_θ is tangential stiffness, u_r is radial displacement, u_θ is tangential displacement, q_r and q_θ are external forces per unit area in the radial and tangential, $D = Eh^3/12(1-v^2)$ is the bending stiffness, $K = Eh/12(1-v^2)$ is the membrane stiffness, E is Young's modulus, ρ is ring density, v is Poisson's ratio, a is the mean radius of the tire, h is the thickness of the tread, p_0 is the internal pressure, Ω is rotational speed. The dots and primes denote differentiation with respect to time t and circumferential coordinate θ, respectively.

Modal analysis showed good agreement between theory and measurement in the range from 0-400 Hz. At higher frequency when the wavelength is close to the tread width of the tire, the model fails, because the tire treadband should be modeled as a 3D plate instead of a 2D ring. For the interest, the naming convention for the mode shapes can be found in Wheeler et al. (2005) [748].

The fundamental 2D circular ring model was developed by Böhm (1966) [749] where the tire was modeled as a ring under the tension caused by the inflation pressure.

5.2.2.5 Heckl (Various Mechanisms, 1986)

Heckl (1986) [13] investigated multiple tire noise generation mechanisms, including tire vibrations, air pumping, pavement texture impact, stick/slip as well as sound radiation from the tire.

The circular ring model for tire vibrations excluding tread block motion is based on Boehm (1966) [750],

$$\begin{cases} \frac{ES}{a^2}\left(u''+v'\right)-\frac{B}{a^4}\left(v'''+v'\right)=\rho S\ddot{u}+k_T u \\ \frac{T_0}{a^2}\left(v''+v\right)-\frac{ES}{a^2}\left(u'+v\right)-\frac{B}{a^4}\left(v''''+v''\right)=\rho S\ddot{u}+k_a v-q \end{cases} \tag{95}$$

where a is the radius, E is Young's modulus of tire material, B is the bending stiffness, ρ is the tire density, k_T is the stiffness of tangential bedding, k_a is the stiffness of radial bedding, T_0

is the tension, S is the cross-sectional area, q is the outside driving pressure in the radial direction, v is the radial displacement, u is the tangential displacement; time derivatives are indicated by dots and derivatives with respect to the angle ϕ by primes. The circular ring model seems to be more useful than usual modal analysis especially when the frequencies and/or the damping is high. However, the wavelength on the tire surface must be longer than approximately four times the tread thickness h or the tread block distance d (whichever is larger). For typical tires ($a \approx 0.28$ m, $d \approx 25$ mm, $c_I \approx 80$ m/s) this gives an upper frequency limit of 800 Hz. Above that frequency tread blocks have to be considered individually.

The air pumping model is based on Hayden (1971) [354],

$$P = \frac{\rho_0}{4\pi c_0}\left(\frac{\partial q}{\partial t}\right)^2 \tag{96}$$

where P is sound power, ρ_0 is air density, c_0 is sound speed in air, q is the volume flow from the grooves, and t is time. Since $q \propto V$ where $V$is the vehicle speed, and $\partial/\partial t \propto V$, the relationship between air pumping sound power and vehicle speed is found as $P \propto V^4$.

The pavement texture impact model represented the tread blocks by little springs of stiffness s. Each of them indexed as v generates a force

$$F_v = s\left(v_{Tv} - v_{Rv}\right) \tag{97}$$

at the point ϕ_v which is determined by the difference between the tire displacement v_T and the road surface amplitude v_R at the vth point. Then the resulting deflection at point ϕ_i is

$$v_{Ti} = \sum_{v=1}^{N} F_v g\left(\phi_i - \phi_v\right) \tag{98}$$

where N is the number of springs and g is the Green's function for a unit force. For the direct air-borne sound excitation of a blank tire on a rough road a theory was also mentioned (Ronneberger, 1984 [751]).

Stick/slip at the trailing edge was discussed but no detailed quantitative theory was provided.

The author also indicated that spatial changes in the bending stiffness of the tire from tread block to tread block are transformed into temporal changes and therefore can also be found in the sound signal, but for a slick tire (homogeneous) there is no such effect.

5.2.2.6 Bremner et al. (Tire Vibration, 1997)

Bremner et al. (1997) [334] developed a tire vibration model to correlate the vibration-radiated noise with tire construction and material properties. The tire was modeled as an orthotropically stiffened and pressurized cylindrical shell with boundary conditions as simply supported. This model was based on the model developed by Mikulas and McElman (1965) [752] and extended by Rennison et al. (1979) [753] (geometric tension stiffness included). As such, this tire vibration model included membrane waves in lower frequency range [754] and bending waves in higher frequency range.

Statistical Energy Analysis (SEA) with modal joint acceptance formulations was used to calculate the wavespeed and radiation efficiency. All main tire design parameters were analyzed for sensitivity study. Wavenumber decomposition was utilized to determine the dispersion characteristics of a stationary tire under radial point force excitation for experimental validation.

The mode shapes for the tread and sidewall considered as a uniform construction are

$$\begin{cases} \Psi_{mn}(x,\theta) = \sin(k_m x)\sin(k_n R\theta) \\ k_m = \dfrac{m\pi}{L} \\ k_n = \dfrac{n}{R} \end{cases} \tag{99}$$

where L is the circumference of the wheel rim, R is the smaller radius of tire cross section, m and n are mode index. It was found that tension stiffness dominates where natural frequency is proportional to circumferential wavenumber below 300 Hz. Above 300 Hz, bending stiffness begins to show dominating trend where natural frequency is proportional to circumferential wavenumber squared.

Statistical Energy Analysis (SEA) gives the following relation

$$\bar{\Pi}_{\Delta\omega}^{in} = \omega(\eta_t + \eta_{rad})\bar{E}_{t,\Delta\omega} \tag{100}$$

where $\Pi_{\Delta\omega}^{in}$ with bar above is the time-averaged power input to the tire in each frequency band $\Delta\omega$, ω is temporal frequency of vibration, η_t is the structural and material damping coefficient, η_{rad} is the radiation coupling loss factor (much smaller than η_t). Without considering the direct vibration field (valid up to 700 Hz), the SEA energy level is

$$\bar{E}_{t,\Delta\omega} = M_t \left\langle \bar{v}_t^2 \right\rangle_{sp,\Delta\omega} \tag{101}$$

where M_t is the tire mass, $<v_t^2>_{sp,\Delta\omega}$ with bar above is the space-averaged and time-averaged reverberant vibration level (particle velocity in the sound field). The power input was based on Remington et al. (1983) [15] that the contact point velocity is determined by the roughness profile of the two contact surfaces and their relative contact point impedances. Assuming the pavement impedance is much larger than the tire, the power input is

$$\bar{\Pi}_{\Delta\omega}^{in} = \bar{v}_{i,\Delta\omega}^2 \operatorname{Re}\left[Z_{ii}^{\infty} \right] \tag{102}$$

where $v_{i,\Delta\omega}^2$ with bar above is the mean squared vibration velocity at the tire contact point, and Z_{ii}^{∞} is the point infinite impedance of tire. $v_{i,\Delta\omega}^2$ with bar above is given by

$$\bar{v}_{i,\Delta\omega}^2 = \frac{\omega^2 \left\langle \Phi_{road}^2(k) + \Phi_{tread}^2(k) \right\rangle}{V} \cdot \Delta\omega \tag{103}$$

where $\Phi^2_{road}(k)$ and $\Phi^2_{tread}(k)$ are power spectral density (PSD) of road roughness and tread roughness (the two spectra are uncorrelated), k is the spatial roughness wavenumber defined by

$$k = \frac{\omega}{V} \tag{104}$$

where V is the tire rolling speed.

The model showed a good agreement with experiments for far-field noise measurements (sound pressure level or SPL at 7.5 m), including effects of rolling speed, rubber damping, inflation pressure, tread thickness, and tread materials.

5.2.2.7 Bérengier et al. (Porous Pavement, 1997)

Bérengier et al. (1997) [449] studies the acoustical performance of porous pavement and developed analytical models describing the surface impedance and sound propagation. Two different models were developed for the impedance characterization, i.e., a phenomenological model and a microstructural model, both including viscous and thermal effects in the porous structure. The two models have a general formulation as below.

$$\begin{cases} k = \omega \left[\dfrac{\rho_g(\omega)}{K_g(\omega)} \right]^{\frac{1}{2}} \\ Z_c = \dfrac{\left[\rho_g(\omega) K_g(\omega) \right]^{\frac{1}{2}}}{\Omega} \end{cases} \tag{105}$$

where k is the complex wavenumber, Z_c is the characteristic impedance; ω is radian frequency, Ω is porosity; ρ_g is complex dynamic density, K_g is bulk modulus.

In the phenomenological model, three physical input parameters are included: airflow resistivity of the porous structure R_s, porosity of air-filled connected pores Ω, and tortuosity q^2. More specifically, the complex dynamic density and bulk modulus are given by

$$\begin{cases} \rho_g(\omega) = \rho_0 q^2 \left(1 + i \dfrac{f_\mu}{f} \right) \\ K_g(\omega) = \gamma P_0 \left[1 + \dfrac{(\gamma - 1)}{\left(1 - i \dfrac{f}{f_\theta} \right)} \right]^{-1} \end{cases} \tag{106}$$

where ρ_0 is air density, γ is specific heat ratio, P_0 is atmospheric pressure, i is imaginary unit, f is frequency; f_μ and f_θ describe the viscous and thermal dependencies, given by

$$\begin{cases} f_\mu = \dfrac{\Omega R_s}{2\pi \rho_0 q^2} \\ f_\theta = \dfrac{R_s}{2\pi \rho_0 N_{pr}} \end{cases} \tag{107}$$

where N_{pr} is Prandtl number.

In the microstructural model, five physical input parameters are included: besides R_s, Ω and q^2, the other two pore shape parameters are s_ρ associated with viscous dependency and s_k associated with thermal dependency. More specifically, the complex dynamic density and bulk modulus are given by

$$\begin{cases} \rho_g(\omega) = \rho_0 q^2 + i\dfrac{R_s \Omega F(\lambda_p)}{\omega} \\ K_g(\omega) = \gamma P_0 \left[1 + 2\dfrac{(\gamma - 1)T(\Lambda_k)}{\Lambda_k} \right]^{-1} \end{cases} \tag{108}$$

where $F(\lambda_p)$ is a function of s_ρ, and $T(\Lambda_k)$ is a function is s_k.

It was found that the phenomenological model with only three input parameters is accurate enough for the acoustic characterization. In addition, R_s and Ω are more importance than q^2. The models can also be used for the pavement clogging detection.

5.2.2.8 Bolton et al. (Wavenumber Decomposition, 1998)

Bolton et al. (1998) [380,755] represented the tire vibration in the form of propagating waves instead of traditional modal form. The authors claimed that the wavenumber domain form might be more closed tied to the physics of wave propagation in tires. The radial vibration of tire carcass is given by

$$u_r = \sum_{m=1}^{N} A_m \Psi_m(s_c, \omega) e^{\pm i k_{\theta m} s} \tag{109}$$

where u_r is the radial velocity, m is the wave type number, N is the number of contributing wave types, A_m is the wave type participation coefficient, $\Psi_m(s_c, \omega)$ is the cross-sectional mode shape, s is the path variable in the circumferential direction, s_c is the path variable in the cross-sectional direction, and $k_{\theta m}$ is the circumferential wave number (real part indicating the propagation speed, and imaginary part indicating the spatial damping). The wave type number of $m = 1$ is fast extensional mode (180 m/s) while $m = 3, 5, 7$ are slow flexural modes (60-80 m/s), as shown in Figure 98. As seen, each curving trajectory indicates a single wave type (slope being propagating speed). The model on the radial tire velocity can then be applied as boundary condition to the acoustic radiation model.

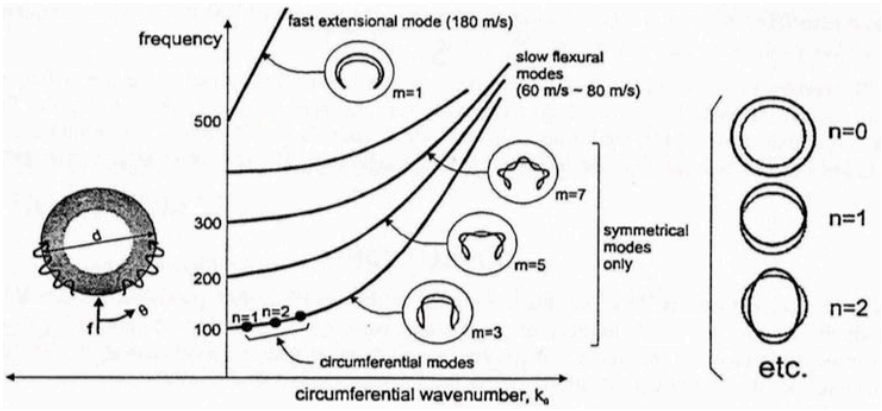

Figure 98: Frequency-wavenumber characteristics of tire carcass vibration (source from Bolton et al., 1998 [380], Figure 8; reprinted with permission from Dr. J. Stuart Bolton of Purdue University, USA)

The study investigated a stationary passenger car tire suspended horizontally and driven radially by a shaker at a point on the tread band. It was reported that at low frequencies a small number of slowly propagating flexural modes dominate, while at higher frequencies the fast modes of tread band extension are dominant. The type of gas (helium, carbon dioxide, and air) inflated into tire cavity was seen to have no effect on carcass vibration while the inflation pressure (20 psi and 40 psi) had major effects. The cut-on frequencies increase with inflation pressure. It was also noted that only the mode of m = 3 and n = 1 (cut-on circumferential mode of first propagational flexural mode) can deliver a net transverse force to the wheel hub and contributes to the structure-borne vibration transmission.

5.2.2.9 Kropp (Orthotropic Plate, 1999)

The model was also developed by Dr. Kropp (1999, Department of Applied Acoustics, Charlmers University of Technology, Sweden) [413]. The model analyzes a smooth tire rolling on a rough pavement. It also consists of three sub-models very similar to Kropp (3D 2 Plate) (1992) [226,736] and also only addresses structure-borne noise. The differences are: (1) In the first sub-model (Tire Model), the tire was simplified as 2D orthotropic plate for vibration calculations; (2) in the second sub-model (Contact Model), a bedding model was used for the tread together with a time iterative solution method to solve the non-linear problem; (3) in the third sub-model (Sound Radiation Model), not only was the vibration of the tire belt accounted for, but the geometrical condition of horn effect and local deformations of the tread were also included by the multipole synthesis method (Cremer, 1984 [756]; Heckl, 1989 [757]).

The advantage of this model is it maintains sufficient accuracy as the Kropp (3D 2 Plate) model and decreases the computational effort. As a result, the measurement and calculation showed a better agreement for a broader frequency range (125-2500 Hz). Below are the brief introductions to the three sub-models.

The tire model considered the belt and the two sidewalls as a flat plate with different bending stiffness in the longitudinal and lateral direction, as illustrated in Figure 99. The differential equation for the vertical motion of the plate is

$$\begin{cases} -T_0\left(\dfrac{\delta^2\xi}{\delta x^2}+\dfrac{\delta^2\xi}{\delta y^2}\right)+B_x\dfrac{\delta^4\xi}{\delta x^4}+2B_{xy}\dfrac{\delta^4\xi}{\delta x^2\delta y^2}+B_y\dfrac{\delta^4\xi}{\delta y^4}-m''\omega^2\xi+s\xi=F_0'' \\ B_{xy}=\sqrt{B_xB_y} \end{cases} \tag{110}$$

where T_0 the tension caused by the he inflation pressure, B_x, B_y and B_{xy} are circumferential, axial, and cross stiffness respectively, ξ is the vertical displacement, s is the spring stiffness of the elastic foundation, m'' is the mass per square meter, F_0'' is the acting force per square meter. The sub-model was validated based on the measurements on a smooth, unloaded, stationary tire, such as the complex point mobility (or admittance, velocity divided by force). One drawback of this model is the negligence of the tire curvature and the thickness of the plate, so there is shift of resonance frequencies below the ring frequency of 400 Hz (circular structure) and large errors for above 3000 Hz (wavelength is comparable to plate thickness) (Übler, 1994 [758]).

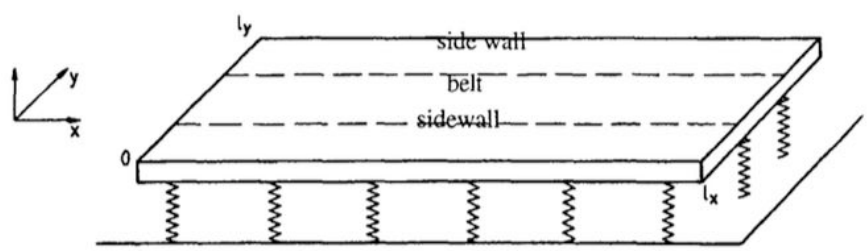

Figure 99: Schematic of an orthotropic plate tire model (source from Kropp, 1999 [413], Figure 2; reprinted with permission from Dr. Jeanette Brooks on behalf of Inderscience Enterprises Limited)

The Contact Model utilized Green's function to calculate the displacement response at a given location due to the force applied at another arbitrary location. The discrete time domain equation is

$$\xi_e(N\Delta t)=\sum_m F_m(N\Delta t)g_{m,e}(0)+\sum_m\sum_{n=0}^{N-1}F_m(N\Delta t)g_{m,e}\left[(N-n)\Delta t\right] \tag{111}$$

where $\xi_e(t)$ is the displacement at the discrete point e at the time t, $F_m(t)$ is the driving force at the discrete point m at the time t, $g_{m,e}(t)$ is the Green's function representing the relation between the input at the discrete point m and an output at the discrete point; Δt is the time increment, N is the time step index. The local deformation of the tread is not considered by the Green's functions but will be compensated for later.

The Sound Radiation Model assumed two multipoles located symmetrically on either side of the road surface, as illustrated in Figure 100. The sound pressure at the point E is

$$p(x_E,y_E,t)=\sum_v a_v H_v^{(2)}(kr_1)e^{jv\phi_1}+\sum_v b_v H_v^{(2)}(kr_2)e^{jv\phi_2} \tag{112}$$

where r_1, ϕ_1 and r_2, ϕ_2 are the coordinates of point $E(x_E, y_E)$ with regard to the two coordinate systems. $H_v^{(2)}$ is the Hankel function 2nd kind, vth order and a_v, b_v are unknown coefficients, k is the wavenumber, j is imaginary unit, v is the circumferential mode index. The particle velocity at the point E is

$$v_E(r_1,\phi_1)=-\frac{1}{j\omega\rho}\sum_v a_v k H_v^{(2)\prime}(kr_1)e^{jv\phi_1}+\frac{1}{j\omega\rho}\sum_v r_n a_v\left\{k\frac{r_1-b\cos\phi_1}{r_2}H_v^{(2)\prime}(kr_2)+jvH_v^{(2)\prime}(kr_2)\frac{\frac{\sin\phi_1}{r_2}-r_1\sin\phi_1\left(\frac{r_1-b\cos\phi_1}{r_2^3}\right)}{\sqrt{1-\left(\frac{r_1\sin\phi_1}{r_2}\right)^2}}\right\}e^{jv\phi_2} \tag{113}$$

where $H_v^{(2)\prime}(kr)$ is derivative of the Hankel function with respect to its argument, b is the distance between the multipoles, r_n is the reflection factor of the road surface for normal incidence, ρ is air density, ω is radian frequency. The boundary conditions, i.e., the velocities normal to the tire surface v_{zn} are determined by the velocity distribution calculated by the Tire Model and Contact Model.

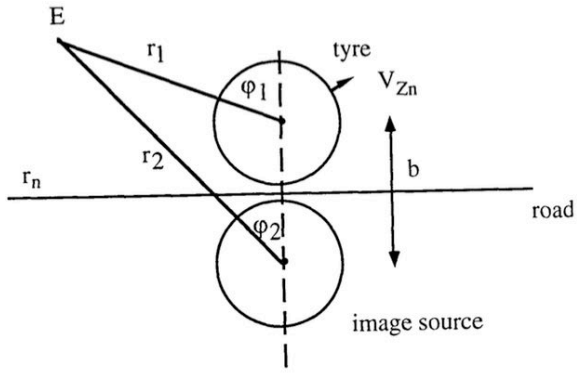

Figure 100: Schematic of two multipoles for the sound radiation model (source from Kropp, 1999 [413], Figure 6; reprinted with permission from Dr. Jeanette Brooks on behalf of Inderscience Enterprises Limited)

To calculate the sound power $P(\omega)$, the tire was modeled as a finite cylinder of the width b, as shown in Figure 101. The equation is

$$P(\omega)=\frac{\rho ca}{8\pi^2}\sum_{v=-\infty}^{\infty}\int_{-\infty}^{\infty}\left|v_{rv}(\omega,k_z)\right|^2\sigma_v(\omega,k_z)dk_z \tag{114}$$

where a is tire radius, c is speed of sound in air, k_z is the wavenumber in the axial direction, $v_{rv}(\omega,\ k_z)$ is the Fourier coefficients of the radial velocity given by $v_{rv}(\omega,\ k_z) = v_{rv}(\omega)\cdot\sin(k_z b)/b$, $\sigma_v(\omega,\ k_z)$ is the sound radiation efficiency given by

$$\sigma_v(\omega,k_z)=\frac{2\omega}{a\pi c}\frac{1}{\sqrt{\frac{\omega^2}{c^2}-k_z^2}}\frac{1}{\left|H_v^{(2)\prime}\left(a\sqrt{\frac{\omega^2}{c^2}-k_z^2}\right)\right|^2} \tag{115}$$

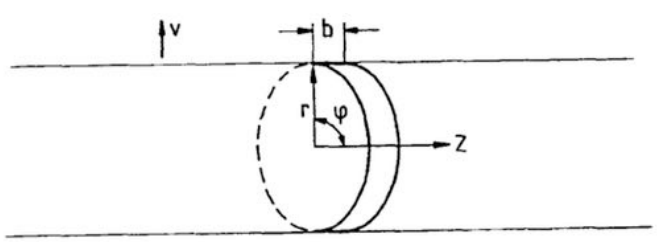

Figure 101: Finite cylinder model (source from Kropp, 1999 [413], Figure 8; reprinted with permission from Dr. Jeanette Brooks on behalf of Inderscience Enterprises Limited)

The full model was validated on the test drum (laboratory drum method, DR) as illustrated

in Figure 102, with three different quantities measured: (1) accelerometers mounted in the tread grooves measured the radial accelerations (Tire Vibration Measurement, TVM) in the Lagrange reference where Doppler shift occured; (2) the laser Doppler vibrometer (LDV) measured local velocities in the Euler reference; (3) the microphone measured the radiated sound pressure level. The first measurement showed higher values than the calculation, but the other two measurements showed good agreement. However, deviation begins to occur above 1500 Hz, because the local deformation of the tread acting like small volume sources becomes more dominant than the belt vibrations. After adding the radiated sound calculated as the integral over the displaced volume, the total third octave band showed very good agreement between 125 to 2500 Hz.

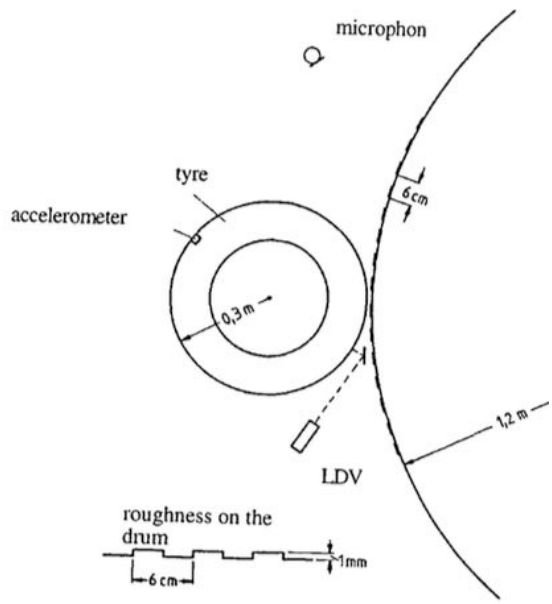

Figure 102: Schematic of measurement facilities (source from Kropp, 1999 [413], Figure 11; reprinted with permission from Dr. Jeanette Brooks on behalf of Inderscience Enterprises Limited)

In the present author's opinion, the Kropp model (orthotropic plate) might be currently the most advanced and suitable approach for tire vibration modeling in tire noise studies.

5.2.2.10 Kim and Bolton (Shell, 2002)

Kim and Bolton (2002) [500,759] analyzed the potential of a rotating tire to radiate sound from static tire dispersion through kinematic compensation. The treadband of the tire was modeled as a simply supported, rotating circular cylindrical shell (Matsubara et al., 2015 [760]) having

finite width in order to identify the effects of rotation.

The governing equations for treadband model is

$$\frac{D}{Dt} = \frac{\partial}{\partial t} + \Omega \frac{\partial}{\partial \phi} \tag{116}$$

$$\begin{cases} L_x\left(u_x, u_\phi, u_r\right) + \lambda \dfrac{Du_x}{Dt} + \rho h \dfrac{D^2 u_x}{Dt^2} = q_x\left(x, \phi, r\right) \\ L_\phi\left(u_x, u_\phi, u_r\right) + \lambda \dfrac{Du_\phi}{Dt} + \rho h \left(\dfrac{D^2 u_\phi}{Dt^2} + 2\Omega \dfrac{Du_r}{Dt} - \Omega^2 u_\phi \right) = q_\phi\left(x, \phi, r\right) \\ L_r\left(u_x, u_\phi, u_r\right) + \lambda \dfrac{Du_r}{Dt} + \rho h \left(\dfrac{D^2 u_r}{Dt^2} - 2\Omega \dfrac{Du_\phi}{Dt} - \Omega^2 u_r \right) = q_r\left(x, \phi, r\right) \end{cases} \tag{117}$$

$$\begin{cases} L_x\left(u_x, u_\phi, u_r\right) = -\dfrac{\partial N_{xx}}{\partial x} - \dfrac{1}{a}\dfrac{\partial N_{\phi x}}{\partial \phi} \\ L_\phi\left(u_x, u_\phi, u_r\right) = -\dfrac{\partial N_{x\phi}}{\partial x} - \dfrac{\partial N_{\phi\phi}}{\partial \phi} - \dfrac{Q_{\phi r}}{a} \\ L_r\left(u_x, u_\phi, u_r\right) = -\dfrac{\partial Q_{xr}}{\partial x} - \dfrac{1}{a}\dfrac{\partial Q_{\phi r}}{\partial \phi} + \dfrac{N_{\phi\phi}}{a} - N_{xx}^r \dfrac{\partial^2 u_r}{\partial x^2} - \dfrac{N_{\phi\phi}^r}{a^2}\dfrac{\partial^2 u_r}{\partial \phi^2} \end{cases} \tag{118}$$

where the subscripts x, ϕ, r denote axial, circumferential and radial direction of the tire respectively, the superscript r denotes residual force. Ω is angular rotational speed, ϕ is circumferential angle in the reference frame, u is the displacement in the corresponding direction, N and Q are resultant normal and shear forces respectively, q is the external force applied in the corresponding direction, ρ is the density of the treadband, h is its thickness, λ is the damping constant, and a is the tire radius. $N_{\phi\phi}{}^r$ is the circumferential resultant normal force given by

$$N_{\phi\phi}^r = ap + \rho h a^2 \Omega^2 \tag{119}$$

where p is the inflation pressure. The linear operators $L_i (i = x, \phi, r)$ are related to the system's stiffness. Rotation was found to have two effects: stiffening of the treadband and "tilting" of the dispersion curves. However, at normal speed inflation pressure has greater influence on the stiffness than rotation. In contrast, the second effect (kinematic tilting effect) was found to be significant. The kinematics relation is

$$\tilde{\omega}_{mn} = \omega_{mn} - n\Omega \tag{120}$$

where $\tilde{\omega}_{mn}$ is the natural frequency in local (Lagrangian, tire-fixed) coordinates, ω_{mn} is the natural frequency in global (Eulerian, vehicle-fixed) coordinates, n is the wave mode number in the circumferential direction.

5.2.2.11 Molisani et al. (Coupled Cavity, 2003)

Molisani et al. (2003) [85] modeled the tire as two shells of revolution and two annular plates where only the outside shell is flexible, i.e. tire sidewalls and rim are assumed rigid. The boundary conditions for the outer shell were assumed to be simply supported. This model provided an efficient tool to investigate the physical coupling mechanisms between the acoustic cavity and the tire structure without complicated computation such as FEA (Richards, 1991 [387]) where these mechanisms were often hidden in the large numerical models.

For the structural equation, the displacement vector of the outer shell was obtained by solving the eigenvalue problem of the self-adjoint Donnel-Mushtari operator. For the acoustic equation, a finite cylindrical cavity with rigid boundary conditions was developed. This model investigated the interaction between the acoustic mode and the structural radial mode. The equation of motion for the system including the fluid loading is

$$\left\{\left[L_c - \Omega^2[I]\right]\right\} \cdot \begin{Bmatrix} u \\ v \\ w \end{Bmatrix} = \begin{Bmatrix} 0 \\ 0 \\ f_w \end{Bmatrix} - \begin{Bmatrix} 0 \\ 0 \\ p(a, x', \theta') \end{Bmatrix} \tag{121}$$

where L_c is shell differential operator, Ω is normalized frequency, I is identity matrix, $\{u, v, w\}^T$ is displacement vector where the components are the axial, tangential and radial, respectively; f_w is vertical load, $p(a, x', \theta')$ is the cavity acoustic pressure acting on the tire. The equation of the coupled system is

$$\left\{[K] - \Omega^2[M]\right\} \cdot \left\{A_{mn}\right\} = \left\{f_{mn}\right\} - \Omega^2[\alpha] \cdot \left\{A_{mn}\right\} \tag{122}$$

where $[K]$ and $[M]$ are diagonal matrices and their elements represents the modal stiffness and mass of the radial modes, $\{A_{mn}\}$ is the vector of modal amplitudes, $\{f_{mn}\}$ is the vector of modal forces, and $[\alpha]$ is the fluid coupling matrix. $[\alpha]$ indicates how much the acoustic mode will affect the structural mode.

It was shown that the tire cavity resonance could largely increase the forces at the spindle and thus increase the vehicle interior noise. It was also found that relatively high damping of the tire structure does not effectively damp out the energy in the acoustic resonance. However, the tire was assumed to be stationary without rotation and the external excitation was a point force acting normal to the shell, so it might be able to represent actual cavity resonances when tire is in motion on real road.

5.2.2.12 Kim et al. (Waveguide, 2007)

Kim et al. (2007) [390] developed an analytical model for the tire vibration and structure-borne noise. Three models were developed to represent different vibration or wave types (waveguide characteristics) at different frequencies: (1) spring-mass model for low frequency below 80 Hz; (2) elastically supported beam model for 80-300 Hz; (3) cylindrical shell for 300-2000 Hz.

Below 80 Hz, spring-mass model considers the tire sidewall as a spring and the tread band as a mass. Four modes are found to be mostly related to sidewall stiffness. The eigen-frequencies of the first radial, lateral and tractive modes ω_r, ω_x and ω_t are given by

$$\begin{cases} \omega_r = \sqrt{\dfrac{\pi R_0 \left(K_r + K_t\right)}{M}} \\ \omega_x = \sqrt{\dfrac{2\pi R_0 K_x}{M}} \\ \omega_t = \sqrt{\dfrac{2\pi R_0 K_t}{I}} \end{cases} \tag{123}$$

where R_0 is tire radius, K_r, K_x and K_t are sidewall spring constants in the radial, lateral and tractive direction, M is tire tread band mass, I is polar moment of inertia of tire tread band.

For 80-300 Hz, the tire tread band is modeled as a tensioned beam ($R_0 = \infty$) supported elastically by sidewall springs with flexural waves propagating in the circumferential direction. The dispersion relation of the free flexural waves is given by

$$\begin{cases} \Omega^2 = \beta^2 \left(R_0 k\right)^4 + \gamma^2 \left(R_0 k\right)^2 + \Omega_r^2 \\ \Omega = \dfrac{\omega}{\omega_0} \\ \beta = \dfrac{h}{\sqrt{12} R_0} \end{cases} \tag{124}$$

where Ω is the non-dimensional frequency and β is the non-dimensional thickness, h is the tread band thickness, ω_0 is the ring frequency.

For over 300 Hz, the second and third radial modes occur and the one-dimensional waveguide turns into two-dimensional, i.e., cylindrical shell/plate. Waveguide behavior and shell curvature are the two important properties that determine the characteristics of the 2D flexural waves. The approximate dispersion relation is written by

$$\begin{cases} \Omega^2 = \left(1-\nu^2\right) \dfrac{m^4}{\left(m^2+n^2\right)^2} + \beta^2 \left[\left(m^2+n^2\right)^2 - \dfrac{n^2(4-\nu)-2-\nu}{2(1-\nu)} \right] \\ m = k_z R_0 \\ n = k_s R_0 \end{cases} \tag{125}$$

where ν is Poisson's ratio, k_z and k_s are circumferential and axial wavenumber. The cross-sectional resonant frequencies (cut-off frequency) are given by apply $k_z = 0$ to the equation above. The dispersion relation accounting for the shell curvature that results in the coupling between radial, axial and circumferential motion is given by the following equations.

$$\begin{cases} \Omega^2 = \beta^2 \left(R_0 k_{cs}\right)^4 + \cos^4 \phi \\ k_{cs}^2 = k_z^2 + k_s^2 \\ \phi = \tan^{-1}\left(\dfrac{k_s}{k_z}\right) \end{cases} \tag{126}$$

It was also concluded that the tire waves discussed above are inefficient sound radiators since their wavenumbers are larger than the acoustic wave number. Acoustically excited wave motion of the tire tread band is an important factor for sound radiation.

5.2.2.13 Feng et al. (Cavity, 2009)

Feng et al. (2009) [391,761] investigated the effects of tire rotating speed and tire load on the cavity resonance mechanism. The lowest two cavity modes (splitting into two modes due to tire load) for a non-rotating tire are defined as horizontal (fore/aft) acoustic mode and vertical acoustic mode. The equations of motion for the two modes are

$$\begin{cases} \ddot{X} + 2\zeta\omega_0\dot{X} + \left(\omega_0^2 + af_0\right)X = 0 \\ \ddot{Z} + 2\zeta\omega_0\dot{Z} + \left(\omega_0^2 + bf_0\right)Z = 0 \end{cases} \tag{127}$$

where X and Z are the coordinates of the center of mass of the air molecules, ω_0 is the natural frequency of the acoustic cavity of the unloaded tire, ζ is the damping ratio, f_0 is the static load on tire outer surface along Z direction, a (negative) and b (positive) represent the effects on the natural frequencies of the two acoustic modes by the tire load. The equations for the natural frequencies of the two modes are

$$\begin{cases} \omega_H = \sqrt{\omega_0^2 + af_0} \\ \omega_V = \sqrt{\omega_0^2 + bf_0} \end{cases} \tag{128}$$

where ω_H and ω_V ($\omega_H < \omega_V$) are resonance frequencies for the horizontal and vertical directions respectively. For a rotating tire with the rotation angle ϕ, the transformation between the tire-fixed coordinate (X, Z) and the vehicle-fixed coordinate (x, z) is

$$\begin{cases} x = X\cos\phi + Z\sin\phi \\ z = -X\sin\phi + Z\cos\phi \end{cases} \tag{129}$$

It is noted that the rotation rate is slow compared to the lowest acoustic mode frequencies. The equations for the natural frequencies for the rotating tire are

$$\begin{cases} \omega_1^2 = \omega_0^2 + \Omega^2 + \dfrac{a+b}{2}f_0 - \sqrt{\left(\dfrac{a-b}{2}f_0\right)^2 + \left[2(a+b)f_0 + 4\omega_0^2\right]\Omega^2} \\ \omega_2^2 = \omega_0^2 + \Omega^2 + \dfrac{a+b}{2}f_0 + \sqrt{\left(\dfrac{a-b}{2}f_0\right)^2 + \left[2(a+b)f_0 + 4\omega_0^2\right]\Omega^2} \end{cases} \tag{130}$$

where Ω is the rotation speed of the tire. Even though the natural frequencies of the two modes vary with Ω, they have the constant average frequency $\tilde{\omega}_0$ as below where the peak SPL occurs.

$$\tilde{\omega}_0 = \sqrt{\omega_0^2 + \frac{1}{2}(a+b) f_0} = \sqrt{\frac{1}{2}\left(\omega_H^2 + \omega_V^2\right)} \tag{131}$$

Further, Lagrange's equations were implemented into the model (Feng and Gu, 2011 [761]).

5.2.2.14 O'Boy and Dowling (3D Multilayer, 2009)

O'Boy and Dowling (2009) [547,762] provided a multilayer viscoelastic cylindrical representation of the tire belt consisting of thin orthotropic layers of different materials of varying thicknesses laid on each other, as illustrated in Figure 103. It overcame the disadvantage of high frequency inaccuracy when the shortest wavelength in the tire becomes comparable to the thickness. Each layer is considered to be isotropic in the circumferential and axial directions, but orthotropic in the radial direction. The model assumed the tire side walls to be pinned and tire belt to be periodic in the axial direction.

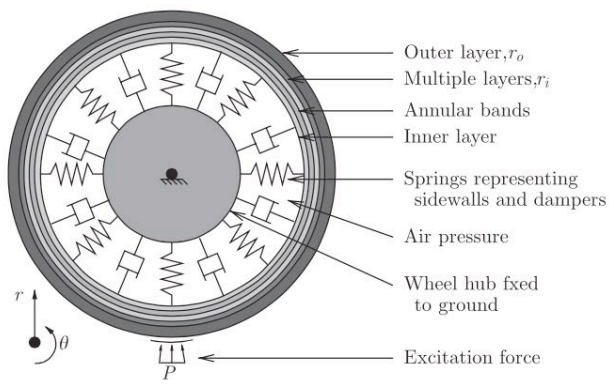

Figure 103: Complete viscoelastic cylindrical model of the tire belt (source from O'Boy and Dowling, 2009 [547], Figure 1; reprinted with permission from Elsevier)

The model made it possible to understand the vibration characteristics of a stationary tire, including resonant frequencies, mode shapes and wave speeds, using the belt layer structure parameters (density, Young's modulus, Poisson's ratio, thickness) defined solely by design data without experimental testing. The stress σ and displacement **u** on the lower surface of layer j are related to the coefficients within that layer (O'Boy and Dowling, 2009 [762]).

$$\begin{pmatrix} \tilde{\sigma} \\ \tilde{\mathbf{u}} \end{pmatrix}_{r_j} = \begin{pmatrix} \mathbf{G} \\ \mathbf{H} \end{pmatrix}_{r_j} \mathbf{W}_{r_j} \mathbf{S}_{r_j} \mathbf{C}_{r_j} \tag{132}$$

where ~ denotes Fourier transformed in the frequency domain, **G** and **H** contain all

information on how the material properties in the viscoelastic layer affect the stresses and displacements for all wavenumbers and frequencies, **W** has only diagonal terms depending on the Wronskian expressions for the Bessel functions, **S** is a summation matrix. Furthermore, components of stress and displacement on one face of the elastic layer can be related to the components on the other face, as shown below.

$$\begin{pmatrix} \tilde{\sigma} \\ \tilde{\mathbf{u}} \end{pmatrix}_{r_{N+1}} = \prod_{j=1}^{N} \mathbf{X}_j \begin{pmatrix} \tilde{\sigma} \\ \tilde{\mathbf{u}} \end{pmatrix}_{r_1} \tag{133}$$

where $\mathbf{X}_j$ is overall material matrix of layer j, which is a function of frequency, wavenumber, material properties of the layer and its inner and outer radii. $\mathbf{X}_j$ is expressed as

$$\mathbf{X}_j = \begin{pmatrix} \mathbf{G} \\ \mathbf{H} \end{pmatrix}_{r_{j+1}} \mathbf{W}_{r_{j+1}} \mathbf{S} \mathbf{M}_{r_{j+1,j}} \mathbf{S}^{-1} \mathbf{W}_{r_j}^{-1} \begin{pmatrix} \mathbf{G} \\ \mathbf{H} \end{pmatrix}_{r_j}^{-1} \tag{134}$$

where $\mathbf{M}_r$ is scaling factor dependent on the thickness of the layer. The most useful vibration data for noise prediction, the displacement u can be obtained by inverse Fourier transform of $\tilde{u}$ as below

$$u(r,t,\theta,y) = \frac{1}{(2\pi)^3} \int_{-\infty}^{\infty} \int_{-\infty}^{\infty} \sum_{n=-\infty}^{\infty} \tilde{u}(r,n,k_y,\omega) e^{in\theta} e^{ik_y y} e^{i\omega t} \mathrm{d}k_y \mathrm{d}\omega \tag{135}$$

where r is radius of the belt layer; t is time, θ is circumferential angle, y is the axial position; ω, n and k_y are the corresponding variable in the frequency domain, which are radian frequency, angular order and axial wavenumber respectively.

The model can provide the displacement or velocity response of the tire belt when excited by radial or tangential force. The response can be displayed in both the frequency-wavenumber and time-spatial domains. It was shown the dominant flexural wave under radial excitation travelled at 50-65m/s, while compression wave under tangential excitation travelled at 150m/s.

O'Boy and Dowling (2009) [547] also introduced a flat bending plate approximation for the tire belt. The vertical displacement $w(x, y, t)$ at position (x, y) at time t is governed by (Graff, 1991 [763])

$$T\nabla^2 w - D\nabla^4 w + p + \eta_p \sqrt{DM} \frac{\partial}{\partial t} \nabla^2 w = M \frac{\partial^2 w}{\partial t^2} \tag{136}$$

where T is in-plane tension in unit of [N/m], $p(x, y, t)$ is load per unit area, M is mass per unit area (area density), η_p is a constant representing an additional damping, ∇ is the gradient operator resulting in a vector like $(\partial/\partial x_1, \partial/\partial x_2)$, ∇^2 is Laplace operator resulting in a scalar like $\partial^2/\partial x_1^2$, $\partial/\partial x_2^2$, D is bending stiffness written by

$$D = \frac{Eh^3}{12\left(1-\nu^2\right)} \tag{137}$$

where E is Young's modulus, ν is Poisson's ratio. This is the case for tire belt without the tread rubber layer. For the case with tread layer included, the equation becomes

$$T\nabla^2 w + \left(\nabla^2 - \frac{\rho}{\kappa^2\mu}\frac{\partial^2}{\partial t^2}\right)\left(\frac{\rho h^3}{12}\frac{\partial^2}{\partial t^2} - D\nabla^2\right)w + k_s w - \eta_p\sqrt{DM}\frac{\partial}{\partial t}\nabla^2 w + \left(1 - \frac{D\nabla^2}{\kappa^2\mu h} + \frac{\rho h^2}{12\kappa^2\mu}\frac{\partial^2}{\partial t^2}\right)p = M\frac{\partial^2 w}{\partial t^2} \tag{138}$$

where κ is the Timoshenko shear coefficient accounting for the shear deformation, μ is the Lamé constant accounting for the rotary inertia, k_s is the stiffness of the equivalent distributed springs representing tire sidewalls, ρ is rubber density. Then the transfer function in the frequency domain between displacement w with tilde above and pressure p with tilde above is expressed as

$$\left.\frac{\tilde{w}}{\tilde{p}}\right|_{(\omega,n,k_y)} = \frac{I_0 k_y^2 + I_1}{\Psi_1 k_y^4 + \left(\Psi_2 + I_2\right)k_y^2 + \left(\Psi_3 + I_3\right)} \tag{139}$$

where Ψ is material terms associated with the bending plate, I is correction terms accounting for the shear deformation and rotary inertia, which are given by

$$
\begin{cases}
\Psi_1 = D \\
\Psi_2 = \dfrac{2Dn^2}{R^2} + T + i\omega\eta_p\sqrt{DM} \\
\Psi_3 = \dfrac{Dn^4}{R^4} + \dfrac{Tn^2}{R^2} + \dfrac{i\omega\eta_p\sqrt{DM}\,n^2}{R^2} + k_s - M\omega^2 \\
I_0 = \dfrac{D}{\kappa^2\mu h} \\
I_1 = 1 + \dfrac{Dn^2}{\kappa^2\mu h R^2} - \dfrac{\omega^2\rho h^2}{12\kappa^2\mu} \\
I_2 = -\omega^2\left(\dfrac{\rho h^3}{12} + \dfrac{D\rho}{\kappa^2\mu}\right) \\
I_3 = -\omega^2\left(\dfrac{\rho h^3}{12} + \dfrac{D\rho}{\kappa^2\mu}\right)\dfrac{n^2}{R^2} + \dfrac{\omega^4\rho^2 h^3}{12\kappa^2\mu}
\end{cases}
\tag{140}
$$

A numerical method was also presented to determine the parameters for the equivalent plate model which best matches the multilayer viscoelastic cylindrical.

5.2.2.15 Arteaga (Green's Function, 2011)

Arteaga (2011) [499] derived a closed-form expression for the Green's functions (Arteaga, 2011 [499]; Hamet, 2001 [764]; Meftah et al., 2013 [765]; Meftah and Duhamel, 2011 [766]) of a loaded rotating tire expressed in the Eulerian reference coordinate based on the Modal-Arbitrary Lagrangian Eulerian (M-ALE) approach (Lopez et al., 2007 [74]). It addresses the contact problem directly in the Eulerian reference frame and includes local tire softening due to non-linear deformation without increasing computational cost.

The expression for the Green's function g_{jl} between the excitation at a given location and direction l and the response at another location and direction j in the Eulerian reference frame is as below.

$$
g_{jl}(\Omega,t) = \sum_{k=1}^{N}\Phi_{jk}\left[\sum_{r=1}^{2N} v_{kr}\frac{\sum_{p=1}^{N} w_{pr}\Phi_{lp}}{a_r}e^{s_r t}\right]
\tag{141}
$$

where Ω is the rotating velocity of the tire, t is time, Φ_{jk} and Φ_{lp} are the corresponding elements of the eigenvector matrix, v_{kr} and w_{pr} are the corresponding elements of the relative eigenvectors of transformed uncoupled first order differential equations, s_r is the

corresponding eigenvalue (same for v_{kr} and w_{pr}), a_r is an intermediate variable.

It should be noted that the only information needed to actually compute these Green's functions are the eigenvalues and eigenvectors of the statically loaded tire in the tire reference frame and the mass matrix that can be easily obtained from a standard FE modeling. The full excitation response of the tire is then calculated from the convolutions between Green's functions and contact forces.

It was shown modal density increases as the rotation speed increases for both the unloaded and the loaded tire.

5.2.2.16 Bolton and Cao (Coupled Mode, 2013)

Bolton and Cao (2013) [767] investigated the coupled tire structural-acoustic mode. The tire tread band is unwrapped and modeled as a tensioned 1D string while the rim is modeled as a hard wall, as illustrated in Figure 104 where R is the tire radius, H is tire section height, and L is circumferential length. The tire cavity is between the string and hard wall.

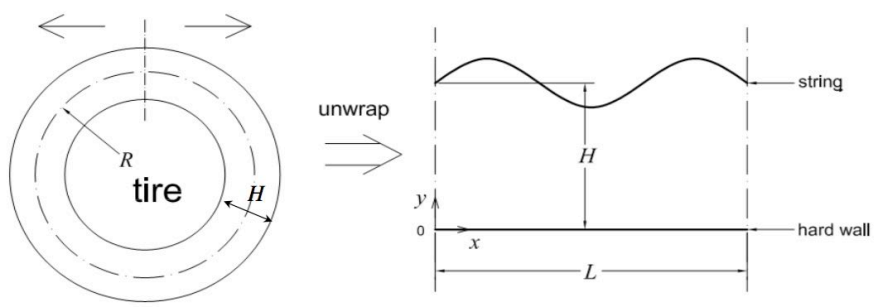

Figure 104: Tire-rim assembly modeled as tensioned string-hard wall (source from Bolton and Cao, 2013 [767]; reprinted with permission from Dr. J. Stuart Bolton of Purdue University, USA)

The air rotating with the tire in the cavity is assumed to be uniform and inviscid flow, governed by the following linearized acoustic wave equation.

$$\frac{\partial^2 p}{\partial t^2} = \left(c^2 - v^2\right)\frac{\partial^2 p}{\partial x^2} + c^2\frac{\partial^2 p}{\partial y^2} - 2v\frac{\partial^2 p}{\partial x \partial t} \tag{142}$$

where p is the sound pressure, c is adiabatic sound speed, v is flow speed, t is time, x and y are circumferential and radial coordinates shown in Figure 104. The wave equation for a tensioned moving string is below.

$$\rho_L\left(\frac{\partial^2\xi}{\partial t^2}+2v\frac{\partial^2\xi}{\partial t\,\partial x}\right)+\left(\rho_L v^2-T\right)\frac{\partial^2\xi}{\partial x^2}=0 \tag{143}$$

where ρ_L is the linear density of string, ξ is the radial displacement of the string in the y direction, T is the string tension force, v is the speed of the moving string assumed to be the same as the air flow speed above. The assumed solutions are

$$\begin{cases} p=\left(Ae^{-jk_y y}+Be^{jk_y y}\right)e^{-jk_x x}e^{j\omega t} \\ \xi=Ce^{-jk_s x}e^{j\omega t} \end{cases} \tag{144}$$

where A, B and C are amplitudes, j is imaginary unit, k_x and k_y are acoustic wavenumber of the air flow in the x and y direction, k_s is the wavenumber of the string, ω is radian frequency. Assuming $k_x = k_s$ and with boundary conditions applied to the fluid-rigid body coupled system, the characteristic equation is given by

$$\omega^2-2v\omega k_x+\left(v^2-\frac{T}{\rho_L}\right)k_x^2=\frac{\rho_0\omega^2}{\rho_L k_y\tan\left(k_y H\right)} \tag{145}$$

The dispersion equation is given by

$$\frac{\omega^2}{c^2}=\left(1-\frac{v^2}{c^2}\right)k_x^2+k_y^2-2\frac{v\omega}{c^2}k_x \tag{146}$$

In this study, frequency-split phenomenon was shown in the effect of tire rotation on the coupled mode. The phase velocity of each mode is approximately the associated static phase velocity plus/minus flow velocity. It was found that the plane wave mode is significantly influenced by the coupling effect while higher modes are less influenced.

In the further study, Cao and Bolton (2015) [768–770] greatly improved this model by considering the tread band as a 2D ring including flexural and longitudinal waves. The displacement of the ring includes both circumferential and radial directions. The solution of acoustic pressure in the air cavity is assumed to be harmonic in circumferential direction and Bessel function in radial direction. Bolton and Cao (2015) [771] verified this model by applying harmonic point input excitation both radially and circumferentially.

5.2.3 Finite Element and Boundary Element Models

The finite element method (FEM), also known as finite element analysis (FEA) or finite

element (FE) for short, is a numerical technique for solving problems in partial differential form. FEM subdivides the entire body, including the surrounding boundary, into smaller/simpler parts called finite elements. A system of linear equations that model these finite elements are then integrated to generate the solution equations of the entire body. Unlike the FEM, boundary element method (BEM) only subdivides the boundary of the body into finite elements, which is generally more computationally efficient.

With the advancement of computers, BEM and FEM have become the two dominant numerical techniques in computer-aided engineering (CAE). BEM and FEM are often coupled with other methods and have several derivations, such as waveguide finite element method (WFEM), infinite/finite element method (IFEM), wave finite element (WFE), energy boundary element analysis (EBEA), and energy finite element analysis (EFEA), which will be discussed in the following. It is often used to calculate the vibrations of the tire, and then together with fluid-structure interaction (FSI) method to analyze the sound generation and propagation into the air. Sixteen models were reviewed in this subsection.

5.2.3.1 Saigal et al. (Toroidal Membrane, 1986)

Saigal et al. (1986) [754] modeled the tire as a toroidal membrane under low internal pressure and mounted on the rim to investigate its free vibrations. A 12 degree-of-freedom (DOF) membrane finite element (FE) was used. To verify validity of the finite element formulations, the study presented the analytical solutions for three types of modeling: a flat rectangular membrane, a circular cylindrical membrane, and a toroidal membrane. The final solution of mode shapes and natural frequencies for the toroidal membrane model is

$$\begin{cases} w(\theta,\phi,t)=\sum_m\sum_n A_{mn}\cos(m\theta)\sin\left[\left(\frac{n}{10}(6\phi-\pi)\right)\right]e^{i\omega_{mn}t} \\ \omega_{mn}=\frac{1}{\xi}\sqrt{\left(\frac{m}{\eta}\right)^2+\left(\frac{6\sqrt{2}n}{10}\right)^2+\Gamma} \end{cases} \tag{147}$$

where w is the displacement normal to the tire surface, θ is the coordinate along the toroid circle, ϕ is the coordinate along the meridian circle, t is time; m and n are mode numbers, ω is natural frequency; ξ, η and Γ are coefficients given by

$$\begin{cases} \xi = \dfrac{a^2 \rho h}{T_\theta} \\ \eta = \dfrac{b}{a} \\ \Gamma = \dfrac{Eh}{T_\theta \left(1 - \nu^2\right)} \end{cases} \tag{148}$$

where a is radius of the meridian circle, b is radius of the toroid circle, ρ is the mass density, h is the thickness of the element; E is the Young's modulus, ν is Poisson's ratio; T_θ is the internal tension force per unit length along the direction of θ given by $pa/2$ where p is the internal pressure.

The equations above were derived under the assumption that b is much greater than a, such that the toroid can be considered as a cylindrical shell of radius of a and length $2\pi b$ where the two ends are attached to each other.

Good agreement with measurements was shown for the symmetrical and twisting modes of vibration. It should be noted that this model is only restricted to lower frequencies since the membrane model cannot account for bending waves in higher frequencies, so it will probably not apply to a steel belted radial tire, but might apply to certain bias ply tires and aircraft tires. In addition, the modeling tire is nonrotating and unloaded. Diaz et al. (2016) [772] developed an analytical tire model including all the material behavior for modal analysis under different operating conditions such as speed, load and inflation pressure. In this study, the effect of the Coriolis accelerations was confirmed; real and standing waves are dominant for nonrotating tire while complex and travelling waves occur due to speed bifurcation effect. Tire loading generally shift down the respective modal frequencies. Increasing inflation pressure shifts up structural modal frequencies but doesn't influence acoustic modes.

5.2.3.2 Wright and Koopmann (Acoustic Radiation, 1986)

This model (Wright and Koopmann, 1986 [773]) predicted the sound pressure and intensity field around the stationary point-excited tire. First, the surface velocity field of the tire was obtained through conventional modal analysis methods. Then, the sound field was numerically calculated using Helmholtz integral formulation with the information of the tire geometry.

The modal analysis is conducted with finite element method. The number of elements is

336, which is determined by the wavelength of the structural vibrations being investigated. The wave speeds of the modes are shown in Figure 105. It is shown that the wave speed decreases exponentially with increasing mode number. In addition, the structural wave speeds are all well below the speed of sound in air, indicating that at these modes the tire is an inefficient acoustic radiator as the tire surface vibrations will not couple very well with the surrounding air.

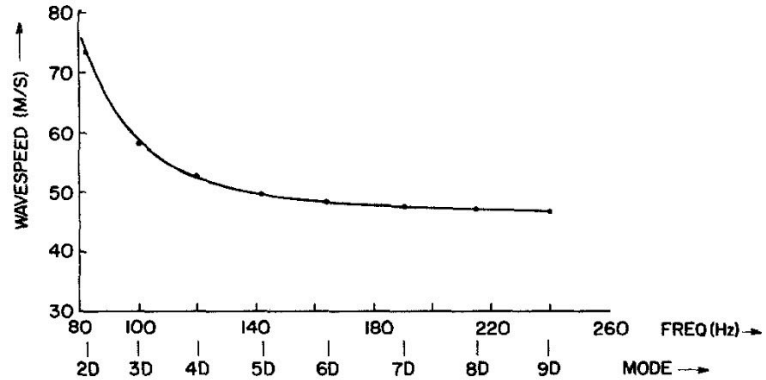

Figure 105: Variation of structural wave speed with frequency for the unloaded tire (source from Wright and Koopmann, 1986 [773], Figure 6; reprinted with permission from Mr. Michael Kaliske of TU Dresden, Germany on behalf of Tire Science and Technology)

The Helmholtz integral formulation considers the tire vibrating body as a continuous series of monopole and dipole sources. It is shown that the sound intensity field has both positive and negative values, meaning that the tire is absorbing as well as generating sound. This, again, proves that the non-propagating responses of the tire are very inefficient at radiating sound. It is suggested that it is the decaying, propagating flexural wave field on the tire that generates the majority of the structure-borne sound. Therefore, the most effective method of reducing structure-borne tire noise is to reduce the forcing inputs at the tire-road interface.

5.2.3.3 Richards (FEA Coupling, 1991)

Richards (1991) [387] numerically analyzed the structural-acoustic coupling cavity using FEA. The structural formulation was based on an existing FEA model for various aspects of tire analysis (Richards, 1987 [774]), consisting of isotropic rubber, cord layers, inflation loading and forces at fixed nodes. The cylindrical space co-ordinates of each of the nodes are

expressed as r, θ and z, while the material coordinate which is attached to the structure is expressed as ϕ. The governing equation is

$$\left(\left[K_0\right]+\mathrm{i}n\left[K_1\right]+n^2\left[K_2\right]-\omega^2\left[M\right]\right)\{a\}=0 \tag{149}$$

where $[K_0]$, $[K_1]$ and $[K_2]$ are stiffness matrices, $[M]$ is mass matrix, i is imaginary unit, n is integer circumferential wavenumber, ω is natural frequency, $\{a\}$ is mode shape containing nodal displacement, element stresses and the reactions at fixed degrees of freedom.

The acoustic formulation is governed by the wave equation,

$$\nabla^2\psi-\frac{1}{c^2}\frac{\partial^2\psi}{\partial t^2}=0 \tag{150}$$

where c is the sound speed, ψ is the velocity potential (particle velocity $\mathbf{v} = \nabla\psi$), which is related to the acoustic pressure p, by

$$p=-\rho\frac{\partial\psi}{\partial t} \tag{151}$$

where ρ is the gas density. Employing weight residual method is to obtain an approximate solution leads to

$$\int_S\frac{\partial\mathbf{u}}{\partial t}\cdot dS+E_2\frac{\partial^2\psi}{\partial\theta^2}-\frac{E_0}{c^2}\frac{\partial^2\psi}{\partial t^2}=0 \tag{152}$$

where S is the part of the thin slice $[\theta, \theta + \delta\theta]$ on the cavity surface, $\mathbf{u}$ is the displacement of the enclosing structural surface; E_0 and E_2 are calculated as

$$\begin{cases} E_0=\int_V dV \\ E_2=\int_V\frac{1}{r^2}dV \end{cases} \tag{153}$$

The resonance frequencies are

$$\omega_n=nc\sqrt{\frac{E_2}{E_0}} \tag{154}$$

where $\sqrt{(E_2/E_0)}$ is considered as the effective radius of the cavity.

The modified equation for the structural-acoustic coupling is

$$\left(\left[K_0\right]+\mathrm{i}n\left[K_1\right]+n^2\left[K_2\right]-\omega^2\left[M\right]\right)\{a\}-\{R\}P=0 \tag{155}$$

where $\{R\}$ includes the complex transformation from ϕ to θ, and depends on the circumferential wavenumber n; P is scaling factor for acoustic pressure. The two extra two equations are

$$\begin{cases} -\{R\}^{+}\{a\} - \dfrac{E_0}{\rho c^2} P - \mathrm{i} n E_0 \chi_0 = 0 \\ \mathrm{i} n E_0 P - \omega^2 \rho \dfrac{E_0^2}{E_2} \chi_0 = 0 \end{cases} \tag{156}$$

where χ_0 is the average angular displacement of gas particles in the cavity, and has the following relation

$$\frac{\partial \chi}{\partial t} = \frac{\partial}{\partial t} \chi_0 e^{in\theta} \cos \omega t = \frac{E_2}{E_0} \frac{\partial \psi}{\partial \theta} \tag{157}$$

It was found that fluids with high density and pressures may have a significant effect on structural resonances.

5.2.3.4 Larsson and Kropp (3D 2 Plate, 1992)

Larsson and Kropp model (1992) [226,302,736] combines three different modules: (1) A tire model where the dynamic properties of the tire are considered; (2) a contact model where the non-linear contact forces (both radial and tangential) and the corresponding vibration velocities on the tire are calculated; (3) a radiation model where the sound radiation from the tire due to the velocity field on the tire surface is calculated. It is one of the most commonly used TPIN models (Dare, 2012 [213]).

As is known, at higher frequency (above 500 Hz), curvature of the tire can be neglected while the importance of the internal structure (i.e. multi-layers of steel and rubber) increases (Larsson and Kropp, 1999 [226]). As a result, Kropp suggested a model of two coupled elastic orthotropic layers/plates (top layer is tread and bottom layer is belt) under tension supported by a linear bedding in the x-, y- and z- directions, as shown in Figure 106. The tension in the layer/plate is caused by the internal inflation pressure and the bedding represents both the side walls and the enclosed air in the tire cavity. The model shows good agreement with measurements up to 2 kHz for a slick 205/60R15 tire (Larsson and Kropp, 1999 [226]).

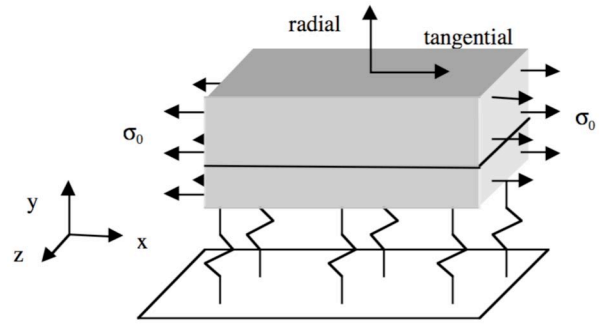

Figure 106: Tire model consisting of two coupled elastic layers under tension on an elastic bedding (source from Larsson and Kropp, 1999 [226], Figure 1; reprinted under fair use provision)

Based on Hamilton's principle (conservation of kinetic and the potential energies of the system), the equations of motion for each of the layers is given by

$$\begin{cases} G\left[\frac{\partial^2\xi}{\partial x^2}+\frac{\partial^2\xi}{\partial y^2}+\frac{\partial^2\xi}{\partial z^2}+\frac{1}{1-2\nu}\frac{\partial}{\partial x}\left(\frac{\partial\xi}{\partial x}+\frac{\partial\eta}{\partial y}+\frac{\partial\zeta}{\partial z}\right)\right]+\sigma_0\frac{\partial^2\xi}{\partial x^2}=\rho\frac{\partial^2\xi}{\partial t^2} \\ G\left[\frac{\partial^2\eta}{\partial x^2}+\frac{\partial^2\eta}{\partial y^2}+\frac{\partial^2\eta}{\partial z^2}+\frac{1}{1-2\nu}\frac{\partial}{\partial y}\left(\frac{\partial\xi}{\partial x}+\frac{\partial\eta}{\partial y}+\frac{\partial\zeta}{\partial z}\right)\right]+\sigma_0\frac{\partial^2\eta}{\partial x^2}=\rho\frac{\partial^2\eta}{\partial t^2} \\ G\left[\frac{\partial^2\zeta}{\partial x^2}+\frac{\partial^2\zeta}{\partial y^2}+\frac{\partial^2\zeta}{\partial z^2}+\frac{1}{1-2\nu}\frac{\partial}{\partial z}\left(\frac{\partial\xi}{\partial x}+\frac{\partial\eta}{\partial y}+\frac{\partial\zeta}{\partial z}\right)\right]+\sigma_0\frac{\partial^2\zeta}{\partial x^2}=\rho\frac{\partial^2\zeta}{\partial t^2} \end{cases} \quad (158)$$

where G is Young's modulus, ν is Poisson's ratio, ξ, η and ζ is the displacement inside the material in the x-, y- and z- directions, σ_0 is the constant external tension (here only in the x direction), ρ_0 is the density of each layer, t is time.

Modal superposition method is used to calculate the response of a finite structure. However, for high frequencies, great number of modes is needed, which makes the calculation time consuming and the damping difficult to model. The model was used to compare TPIN on stone mastic asphalt (SMA) and ISO surfaces. SMA surface was predicted to be 2-3 dB louder than the ISO surface, while it was 7-8 dB louder in reality [775]. Another study on pass-by TPIN on four different pavements showed accurate results within 5 dB only from 500-1250 Hz.

The model was validated against measured radial and tangential point and transfer mobilities where good agreement in both magnitude and phase was shown (Andersson and Larsson, 2005 [738]).

5.2.3.5 De Roo and Gerretsen (TRIAS, 2000)

TRIAS (Tyre Road Interaction Acoustic Simulation, 2000) [664,776–780] includes generation mechanism modeling for both structure-borne (tread/texture impact) and airborne (air pumping) noise and sound radiation modeling. The generation mechanism model uses finite and boundary element method to predict one-third octave band pressure spectra near the tire.

The model includes multiple pavement parameters such as texture depth, porosity, structure factor, flow resistance and/or sound absorption, which can be measured experimentally or acquired by the supporting simulation model RODAS (ROad Design Acoustic Simulation) which generates the physical pavement characteristics from the material composition of the mixture (chipping size, binder content, layer thickness) and analyzes texture spectrum. The schematic of the full model is shown in Figure 107. The input pavement parameters include 1 dimensional texture profiles measured along direction of the road, 2 dimensional texture field, wavelength spectrum, mean profile depth, sound absorption coefficient, distribution of the dimensions of the aggregate particles, binder type and quantity (for porous pavement), thickness of the surface layer, porosity of the surface layer, and specific air flow resistance (de Roo et al., 1999 [776]).

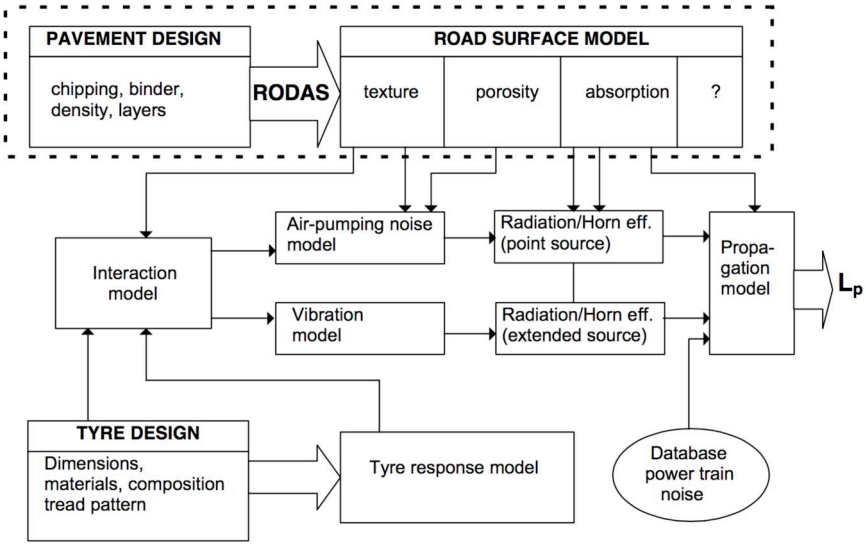

Figure 107: Schematic diagram of the mathematical simulation model TRIAS (Tyre Road Interaction Acoustic Simulation); the supporting model RODAS (ROad Design Acoustic Simulation) is indicated in the upper part of the scheme (source from de Roo and Gerrestsen, 2000 [664], Figure 1; reprinted under fair use provision)

Another supporting submodel, TYDAS (TYre Design Acoustic Simulation) generates model inputs from known tire parameters if all necessary inputs are not known. The input tire parameters include cross section drawing with dimensions (unloaded and loaded), tread pattern, tread depth, total mass of tire, density per layer or the average density of the tire, inflation pressure, load, rolling speed, overall stiffness of the tire, and bending stiffness of the combination of tread and carcass in the *x* (circumferential) and *y* (axial) direction (de Roo et al., 1999 [776]).

The TRIAS model was validated on dense and porous HMA pavements and ISO test tracks. Overall TPIN on the dense asphalt pavements was predicted to within 2 dB overall. TPIN on porous pavements was predicted to be within 5 dB, and the model mostly over-predicted the noise. Measured and predicted TPIN spectra have not been presented.

5.2.3.6 Nilsson (WFEM, 2004)

The application of Waveguide Finite Element Method (WFEM) to tire vibration analysis was firstly presented by Nilsson (2004) [781], then later by Fraggstedt (2006) [782], both at Royal Institute of Technology (KTH), Sweden. The analysis of the wave field on a stationary tire (no contact with ground) was presented by Sabiniarz and Kropp (2010) [9] at Chalmers University of Technology, Sweden.

A waveguide is a structure that guides waves along a single direction with constant physical properties in that direction, such as the circumferential direction of tire. The WFEM method uses a 2D Finite Element (FE) model [783] over the cross-section of the waveguide and describe the response of the tire in terms of a set of waves along this direction (Sabiniarz and Kropp, 2010 [9]). The response of the nodes in this direction X at time t is governed by

$$\left[\mathbf{K}_2\frac{\partial^2}{\partial X^2}+\mathbf{K}_1\frac{\partial}{\partial X}+\mathbf{K}_0+\mathbf{M}\frac{\partial^2}{\partial t^2}\right]\mathbf{V}(X,t)=\mathbf{F}(X,t) \tag{159}$$

where $\mathbf{K}_i$ is stiffness matrices, $\mathbf{M}$ is mass matrix, $\mathbf{F}(X, t)$ is a vector originating from the external load, and $\mathbf{V}(X, t)$ contains all nodal degrees of freedom (DOF).

The results of dispersion relations for waves in the tire are shown in Figure 108 (Sabiniarz and Kropp, 2010 [9]). There are basically three groups of modes: (1) cross-section modes involving strong out-of-plane motion (Group 1 corresponding to symbols '⊥', '×', '▲', '▼',

‘◇’, ‘□’); (2) waves involving significant extensional deformation of either the whole cross-section (Group 2 corresponding to symbols ‘◄’); (3) waves with strong in-plane motion of the sidewalls and rather weak out-of-plane motion of the belt (Group 3 corresponding to symbols ‘○’, ‘+’, ‘►’). It was also concluded that Group I has a rather low wave speed; Group II would be much better radiators; Group III has a higher phase speed, but very low response in the normal direction to the tire surface.

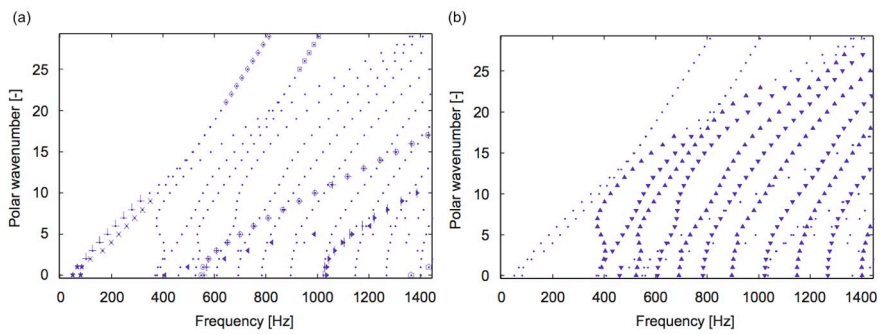

Figure 108: Dispersion relations with various symbols indicating different groups of modes (Continental 205/55R16, source from Sabiniarz and Kropp, 2010 [9], Figure 13; reprinted with permission from Elsevier)

5.2.3.7 Biermann et al. (IFEM, 2007)

Biermann et al. (2007) [614] developed a computational tool to predict the sound radiation from rolling tires and could be divided into three steps: (1) computation of the nonlinear tire stationary rolling process; (2) analysis of tire dynamics caused by the road texture; (3) computation of the sound radiation using infinite/finite element method (IFEM). The third step employed the structural response calculated from the first two steps as boundary conditions.

For the sound radiation analysis, the inner region close to and enveloping the tire was discretized with finite elements, while the outer region was discretized with infinite elements. The governing equation for the elements (Astley-Leis elements) is

$$\left[\mathbf{K}_A + (i\omega)\mathbf{C}_A - \omega^2\mathbf{M}_A\right]\mathbf{p} = \mathbf{f}_A \tag{160}$$

where $\mathbf{K}_A$, $\mathbf{C}_A$ and $\mathbf{M}_A$ are frequency-independent acoustic system matrices referred to as inverse mass, admittance, and compressibility operator, respectively; $\mathbf{p}$ is the unknown pressure at the nodes of acoustical mesh, $\mathbf{f}_A$ is the load vector representing the excitation of acoustic fluid due to tire vibration. The model was validated with two tests, a standing tire

excited by a shaker and a tire rolling on a drum, where a good agreement was shown up to 600 Hz.

5.2.3.8 Brinkmeier et al. (FEM & BEM, 2008)

Brinkmeier et al. model (2008) [733,784–788] is composed of a finite element model of the nonlinear stationary rolling tire and a boundary element model to predict radiated sound with a modal superposition approach. The overall model utilizes combined finite/infinite element approach, where the Astley–Leis elements method employed, which ensures a stable and extremely computationally efficient solution process.

The finite element model uses the arbitrary Lagrange-Eulerian formulation (ALE). The final equation is

$$\left({}^{t}\mathbf{K}-\mathbf{W}\right)\Delta\hat{\phi}={}^{t+\Delta t}\hat{\mathbf{f}}_{e}+{}^{t}\hat{\mathbf{f}}_{i}-{}^{t}\hat{\mathbf{f}}_{\sigma} \tag{161}$$

where ${}^{t}\mathbf{K}$ is the stiffness matrix, $\mathbf{W}$ is ALE-inertia matrix, $\Delta\phi$ with hat above is the incremental displacement, ${}^{t+\Delta t}\mathbf{f}$ with hat above is the forces of external loads, ${}^{t}\mathbf{f}_{i}$ with hat above is the ALE-inertia, ${}^{t}\mathbf{f}_{\sigma}$ with hat above is the internal stresses.

The equation for the boundary element model is

$$\mathbf{A}(\omega)\mathbf{p}:=\left[\mathbf{K}_{A}+(i\omega)\mathbf{C}_{A}-\omega^{2}\mathbf{M}_{A}\right]\mathbf{p}=\mathbf{f}_{A} \tag{162}$$

where $\mathbf{K}_A$ is inverse mass operator or acoustic stiffness, $\mathbf{C}_A$ is admittance operator or acoustic damping, $\mathbf{M}_A$ is compressibility operator or acoustic mass matrix, $\mathbf{p}$ is the sound pressure, $\mathbf{f}_A$ is the load vector representing the tire dynamics on the surface.

The model successfully predicted the acoustic ranking of tires, but the error between prediction and experiment values are 6-17 dB, probably because the model only considers structural-borne noise at low frequency (100-850 Hz) and ignores pavement absorption. In addition, only vertical contact forces are taken into consideration, and friction forces are not included.

5.2.3.9 Waki et al. (WFE, 2011)

Waki et al. (2011) [412] applied the wave finite element (WFE) method (Waki et al., 2009 [789]; Bin Ahmad et al., 2009 [790]) to the primitive estimation of tire vibration and noise radiation. It provided insights into the locations of radiating parts on tire. In contrast to FEA which could only investigate vibrations at low frequencies, WFE could predict up to high frequencies

around 1 kHz.

A short section of a uniform structure such as tire was modeled using FE (Díaz et al., 2012 [791]). The equation of motion is

$$\begin{cases} \mathbf{Dq} = \mathbf{f} \\ \mathbf{D} = \mathbf{K} + j\omega\mathbf{C} - \omega^2\mathbf{M} \end{cases} \tag{163}$$

where **D** is the dynamic stiffness matrix, **q** is the nodal displacement vector, **f** is the nodal forces vector, **K**, **C** and **M** are the stiffness, damping and mass matrices, respectively. Then periodicity condition, as shown below, was applied to the equations of motion of the short section to formulate the eigenproblems.

$$\begin{cases} \mathbf{q}_R = \lambda\mathbf{q}_L \\ \mathbf{f}_R = -\lambda\mathbf{f}_L \end{cases} \tag{164}$$

where the superscripts L and R indicate the left and right-hand side of the section. λ is related to the wavenumbers k, as below.

$$\lambda_i = \exp\left(-jk_i\Delta\right) \tag{165}$$

where Δ is the length of the short section.

It was found that the sound emission field could be very different from the vibration field.

5.2.3.10 Kido et al. (Road Input, 2011)

Kido et al. (2011) [792] correlated the actual road profile with the excitation at the tire contact patch. The spatial road profile was transformed into time domain profile taking into account the driving speed, and then transformed into frequency domain data. The profile data was 2-demensional, which means the entire 2-demensional tread area could be considered.

Further, a FE model was developed to correlate the tire patch excitation and the axle forces on steady-state conditions. The Coriolis force and centrifugal force due to tire rotation were both taken into account. Response of the wheel assembly **x** excited by the external force **f** with tire rotational angular velocity of ω_r (rad/sec) is represented by the following equation.

$$\mathbf{M}\ddot{\mathbf{x}} + \left(\mathbf{C} + \omega_r\mathbf{M}_1\right)\dot{\mathbf{x}} + \left(\mathbf{K} - \omega_r^2\mathbf{M}_2\right)\mathbf{x} = \mathbf{f} \tag{166}$$

where **M**, **K** and **C** are mass matrix, stiffness matrix and viscous damping matrix based on the tire vibrational properties, respectively; $\mathbf{M}_1$ is the skew-symmetric matrix, $\mathbf{M}_2$ is the symmetric matrix depending on the inertia property and rotational axis of the tire. The

Coriolis force is in proportion to the velocity $\omega_r \mathbf{M}_1 \dot{\mathbf{x}}$ and centrifugal force is in proportion to displacement $\omega_r^2 \mathbf{M}_2 \mathbf{x}$. The model also considered the tire stiffness drop caused by tire rotation.

The calculations of axle longitudinal/lateral forces and accelerations at low frequencies (0-120) were found to have good agreement with experimental measurements. It was also found that the influences of Coriolis force and centrifugal force are especially important in the frequency band range of 80 to 100Hz.

5.2.3.11 Yang et al. (FSI, 2013)

Yang et al. model (2013) [544] consists of two sub-models: the rolling tire-pavement interaction sub-model and the near-field sound propagation sub-model. The two sub-models are coupled with fluid-structure-interface (FSI), where the equilibrium conditions of displacement and stress are fulfilled.

Tire and pavement interaction is assumed to be a two-body contact problem where the pavement surface is assumed to be rigid and body forces are ignored. The equation is shown in Eq. (167).

$$\int_{{}^tV} \rho_T \ddot{\mathbf{u}}_T \cdot \delta \mathbf{u}_T \mathrm{d}^tV + \int_{{}^tV} c_T \dot{\mathbf{u}}_T \cdot \delta \mathbf{u}_T \mathrm{d}^tV + \int_{{}^tV} {}^t\tau_T \, \delta \mathbf{e}_T \mathrm{d}^tV = \int_{{}^tS_f} {}^t\mathbf{f}_T^S \cdot \delta \mathbf{u}^S \mathrm{d}^tV - \int_{{}^tS_c} {}^t\mathbf{f}^C \cdot \delta \mathbf{u}^T \mathrm{d}^tS \tag{167}$$

where T represents tire, ρ_T is tire density, c_T is the tire damping ratio, ${}^t\tau_T$ is the stress tensor, $\delta \mathbf{e}_T$ is the strain corresponding to the virtual displacement $\delta \mathbf{u}_T$, ${}^t\mathbf{f}_T^S$ is the surface force per unit area, ${}^t\mathbf{f}^C$ is the surface force per unit area on contact surface.

Near-field sound propagation sub-model is described by the large eddy simulation (LES) model (Wagner et al., 2007 [793]). The LES governing equations for an arbitrary moving cell with a volume of $V(t)$ and a cell-face area of $S(t)$ are given by

$$\frac{\mathrm{d}}{\mathrm{d}t} \iiint_{V(t)} \rho \, dV + \iint_{S(t)} \rho (\mathbf{U} - \mathbf{W}) \cdot dS = 0 \tag{168}$$

$$\frac{\mathrm{d}}{\mathrm{d}t} \iiint_{V(t)} \rho \mathbf{U} \, dV + \iint_{S(t)} \left[\rho \mathbf{U} (\mathbf{U} - \mathbf{W}) - \sigma \right] \cdot dS = \iiint_{V(t)} \mathbf{f}^B \, dV \tag{169}$$

where ρ is the air density, $\mathbf{U}$ is the flow velocity vector, $\mathbf{W}$ is the moving mesh velocity vector, $\mathbf{f}^B$ is the air body force and σ is the total stress tensor.

This model only focuses on PIARC passenger car tire (PIARC, Permanent International

Association of Road Congresses) (Sandberg, 1990 [607]; PIARC, 2004 [794]). The A-weighted one-third octave band sound pressure level showed good agreement between simulation and experiment in the range of 500-2500 Hz with vehicle speed from 50-90 km/h.

5.2.3.12 Tong et al. (Wear, 2013)

Tong et al. (2013) model [238,520,522,795] is composed of steady rolling tire model, tire wear model and tire acoustic model.

The steady rolling tire model utilized Arbitrary Lagrangian Eulerian (ALE) approach decomposing motion into a pure rigid body motion and the superimposed deformation. The expressions of the velocity and acceleration of the particle in both Lagrangian and Eulerian reference frame were derived.

Tire wear model included a 3D tread pattern FE model using Pro/E and Abaqus FE software. The tire acoustic model perceived the sound field as ideal homogeneous fluid medium with small amplitude wave. The acoustic excitation is obtained from steady rolling tire model.

Modal test with random signal excitation was performed to compare measured modal frequency with simulations. The results showed good agreement with maximum deviation of 4.48% from 0-500 Hz. The model investigated four factors that potentially influenced TPIN: speed, tire load, inflation pressure, and tire wear.

5.2.3.13 Vlahopoulos et al. (EFEA/EBEA, 2013)

Vlahopoulos et al. (2013) [796] investigated the airborne noise inside vehicle originating from exterior components including tires, engine and exhaust. These exterior components were assumed to be prescribed acoustic source, and then Energy Boundary Element Analysis (EBEA) was applied to compute the exterior acoustic loading on the vehicle. Further, Energy Finite Element Analysis (EFEA) simulation was employed to calculate interior airborne noise with the exterior acoustic loading as the excitation, i.e., EFEA dealt with acoustic transmission through the vehicle mass panel, Constraint Layer Damping (CLD) and acoustic absorption treatment (or noise reduction) from exterior to interior.

The power transfer mechanism is accounted for by the mass barrier effect of the panel. The governing equation is as below.

$$\tau_{normal} = \frac{\rho_i c_i}{\rho_j c_j}\left[\frac{4}{\left(1+\frac{\rho_i c_i}{\rho_j c_j}\right)^2 + \left(\omega\frac{\rho_s t_s + m_B}{\rho_j c_j}\right)^2}\right] \tag{170}$$

where τ_{normal} is the normal mass barrier transmission coefficient from acoustic enclosure i to acoustic enclosure j through the panel; ρ_i, ρ_j, and ρ_s are the densities of the acoustic enclosure i, acoustic enclosure j, and panel s, respectively; c_i and c_j represent the sound speed in acoustic enclosures i and j; t_s is the thickness of the panel separating the two acoustic spaces; ω is the radial frequency, m_B is the surface mass density of the mass barrier.

As is known, FEA typically only models structure-borne noise at low frequencies, and needs detailed FE model in the path between the excitation and the receiver. As compared to FEA, EFEA captures the physics associated with the path between the exterior acoustic excitation and the interior acoustic cavity, and covers the entire frequency range of 200-8000 Hz. In this vehicle model, the contribution analysis expressed in terms of the power flow into the interior acoustic space of the vehicle found that front floor contributed the most up to 70.8%.

5.2.3.14 Mohamed and Wang (Cavity, 2015)

Mohamed and Wang (2015) [393] focuses on the noise generated from tire torus cavity resonance. The tread plate is assumed to be flexible while the other walls rigid. A modal series solution of the sound pressure frequency response inside the tire cavity is derived from the wave equation using modal superposition. This work also provides a noise reduction method, which is placing a trim layer onto the inner surface of the tire tread plate by adding a damping loss term in the sound pressure frequency response function (sound pressure peak reduction is 10-15 dB).

The cavity natural frequencies can be approximated by the equation below.

$$f_{mnl} = \frac{c}{2\pi}\sqrt{\left(\frac{l\pi}{W}\right)^2 + \left(\frac{2n\pi}{D_o - D_i}\right)^2 + \left(\frac{4m}{D_o + D_i}\right)^2} \tag{171}$$

where f_{mnl} is the cavity natural frequency at corresponding mode with index m, n, l in the axial, radial, azimuthal direction, respectively, c is the speed of sound, W is tire width, D_o is outer diameter of tire torus, D_i is outer diameter of tire torus. FEM is also used as comparison.

It is noted that only a minimum of six elements per wavelength in acoustic space is required, so FEM is relatively computational light.

The Donnel shell theory [797] is used for tire tread vibration calculation. The tread surface particle velocity is defined by

$$u_{pr} = i\omega \frac{F_0 e^{i\omega t}}{\rho h_t} \sum_{m=0,l=0}^{\infty} \frac{B_{ml}^2 \sin(l\pi z_0 / W)\cos(m\theta_0)\sin(l\pi z / W)\cos(m\theta)}{\omega_{lm}^2 (1 + i\eta_p) - \omega^2} \tag{172}$$

where u_{pr} is the plate surface solid particle velocity in the r direction, ρ is top tyre tread pattern plate mass density, h_t is plate thickness, m and l are the plate wave numbers in the θ and z directions, θ_0 and z_0 are location coordinate of the harmonic point excitation force, F_0 is the amplitude of the harmonic point excitation force, ω_{lm} is the natural circular frequency of the annular outer plate, η_p is the plate damping loss factor, B_{ml} is the normalized plate mode shape coefficient.

5.2.3.15 Wei et al. (MLE, 2016)

Wei et al. (2016) [798] developed a model using Mixed Lagrangian-Eulerian (MLE) method to predict the tire noise in the time domain. It was pointed out that the tire vibrations must be analyzed in the Lagrangian reference while the acoustic analysis is usually performed in the Eulerian reference. The model (MLE) transformed the tire vibration data (velocity/acceleration) in the Lagrangian mesh to the Eulerian mesh (finite element model). The radiated noise is then calculated from the vibration information of tire outer surface (tread pattern and groove surface) using acoustic boundary element method (BEM).

It was found that the accelerations are largely distributed near the footprint (about double the contact length). The accelerations at the trailing edge are smaller than those at the leading edge but with a much wider distribution, as shown in Figure 109, which explains why the noise near the trailing edge is greater than at the leading edge.

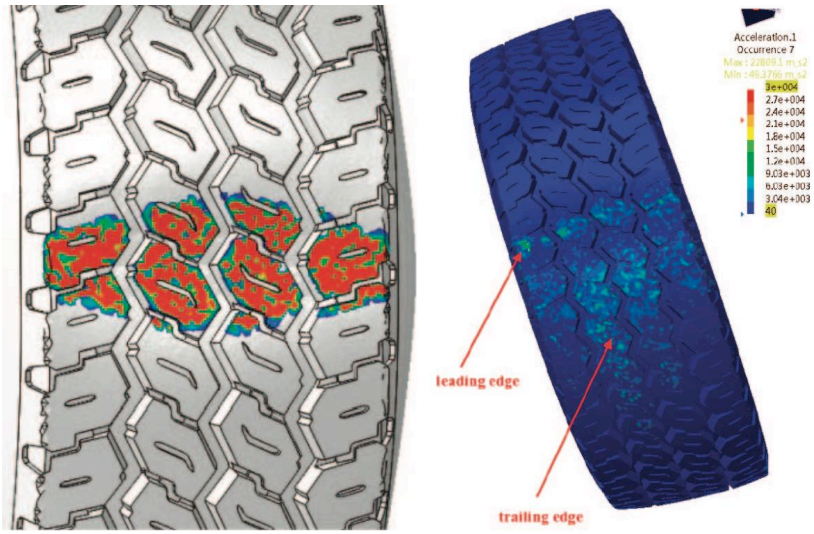

Figure 109: Left - footprint and contact pressure distribution at 70% load (source from Wei et al., 2016 [798], Figure 6; reprinted with permission from Mr. Michael Kaliske of TU Dresden, Germany on behalf of Tire Science and Technology); right - The acceleration in the footprint at 0.0024 seconds (source from Wei et al., 2016 [798], Figure 7; reprinted with permission from Mr. Michael Kaliske of TU Dresden, Germany on behalf of Tire Science and Technology)

The model only accounted for the tire noise due to vibrations, such as impact between tread pattern and road texture, and did not include the air pumping noise.

5.2.3.16 Banz et al. (Time Domain BEM, 2016)

This model [799] (Banz et al., 2016) used a time domain Galerkin boundary element method based on a time-dependent integral equation of the second kind to formulate the acoustic wave equation for the tire noise radiation with the tire dynamics given. The governing equation to be solved is below.

$$(-I+K')\varphi(t,x)=2\frac{\partial p}{\partial n}(t,x)=-2\rho c^2\frac{\partial^2 u_n}{\partial t^2}(t,x)-2\frac{\partial p^I}{\partial n}(t,x) \tag{173}$$

where $-I+K'$ is an operator accounting for the partially absorbing, acoustic boundary conditions on the road, φ is the unknown density, t is the scaled time given by $t=c\tau$ in which c is the sound speed and τ is real time, x is the 3D spatial coordinate vector; p is the sound pressure, n is the normal direction of the tire surface; ρ is air density, u_n is the displacement of the tire in the outer normal direction, and p^I describes an incident wave.

The model was validated in three applications: (1) the sound emission of steady-state vibrating tires (205/55R16 passenger car tire and 315/80R22.5 rib truck tire); (2) noise

amplification in the horn-like geometry between the road and the tire (205/55R16 slick tire); (3) Doppler effect (2% shift) of a moving tire (artificial signal).

5.2.4 Computational Fluid Dynamics Models

Computational fluid dynamics (CFD) uses numerical algorithms to solve and analyze fluid flow problems in computer-aided engineering (CAE). It can be applied to the modeling of airborne TPIN. Five models were reviewed in this subsection.

5.2.4.1 Gagen (Shock Wave, 1999)

Gagen (1999 [362], 2000 [363]) modeled the acoustic sources of air pumping from the squeezed tread groove cavities using shock wave theory (Kinsler et al., 1999 [800]) instead of usual monopole theory (Hayden, 1971 [354]).

It was pointed out that at high speeds as tire/pavement impact causes the groove walls to move with velocities of order 1 m/s, and with accelerations of 10^3 m/s^2 over about 1 ms, the groove volume decreases (then increases at the trailing edge) rapidly by around 10%, which is much faster than the air can evacuate from or suck into the squeezed/expanded groove. This leads to significant pressure and density fluctuations, which makes the usual linear approximations (small amplitude monopole theory) invalid. It is in accord with the nonlinear acoustic phenomenon that both thin width grooves and large width grooves generate small noise while medium width grooves generate large noise (Ejsmont et al., 1984 [360]).

The usual monopole equation for simple harmonic source is expressed as

$$p_1(r,t) \approx \frac{\gamma\rho\ddot{V}}{4\pi r} = -\frac{\gamma\rho\omega^2 V}{4\pi r} \tag{174}$$

where p_1 is the sound pressure, r is the distance between the sound source and receiver, t is time, γ is the ratio of specific heats (1.4 for air), ρ is the air density, V is the air volume, V with double dots above is second order derivative of the air volume with respect to time, ω is the sound frequency. All the parameters are normalized to be dimensionless so that the speed of sound is unit velocity. For non-simple harmonic source, Fourier decomposition into frequency components should be performed before applying monopole theory. The shock wave equation for propagation of density disturbance is given by

$$0=\partial_{tt}\rho-\frac{\partial_{xx}\rho^{\gamma}}{\gamma}-\frac{\partial_{\chi\chi}\rho^{\gamma}}{\gamma f^{2}}-\partial_{xx}\left(\rho v_{x}^{2}\right)-\partial_{x\chi}\left(\rho v_{x}v_{\chi}\right)-\frac{\partial_{\chi x}\left(\rho v_{x}v_{y}\right)}{f}-\frac{\partial_{\chi\chi}\left(\rho v_{y}v_{\chi}\right)}{f}+\frac{\ddot{f}}{f}\rho+\frac{2\dot{f}\partial_{t}\rho}{f}-\frac{\partial_{\chi t}\left(\rho\dot{f}\chi\right)}{f}-\frac{\dot{f}\partial_{\chi}\left(\rho v_{y}\right)}{f^{2}} \quad (175)$$

where ∂ is derivative symbol, v_x and v_y are fluid velocities in the x, y coordinates, χ is computational coordinate where the groove walls are stationary given by $y = f(t)\chi$ and $v_\chi = (v_y - \dot{f}\chi)/f$.

In this study, the kinetic energy of the emitted jet was also investigated to obtain the sound intensity in the far field.

5.2.4.2 Kim et al. (Hybrid CFD, 2006)

Kim et al. model (2006) [358] consisted of three sub-models: (1) small scale noise generation sub-model; (2) noise propagation sub-model; (3) far-field acoustic pressure prediction sub-model.

In the first sub-model, the air-pumping noise source was simulated as piston/sliding-door/cavity geometry, as shown in Figure 110 (Kim et al., 2006 [358]), using Navier-Stokes finite volume solver (CFD), which takes into account the relative motion of the road surface to the tire.

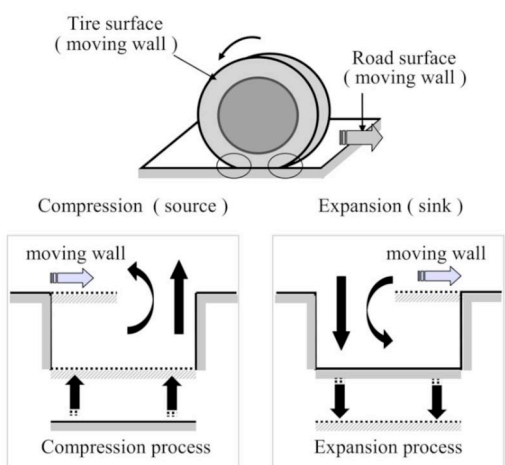

Figure 110: Schematic diagrams of the piston/sliding-door/cavity source model (source from Kim et al., 2006 [358], Figure 3; reprinted with permission from AIP Publishing LLC)

The second sub-model transferred flow properties in the tire grooves as nonlinear air-pumping sources obtained in the first sub-model to the flow simulation of the full tire/road domain considering mid-scale acoustic scattering process.

Finally, the third sub-model predicted the far-field acoustic pressure by the linear Kirchhoff integral method with the acquired flow properties from CFD calculation around rolling tire and road surface geometry. The linear Kirchhoff integral equation is as follows.

$$p'(\mathbf{x},t)=\frac{1}{4\pi}\int_S\int\left[\frac{\cos\theta}{r^2}p'-\frac{1}{r}\frac{\partial p'}{\partial n}+\frac{\cos\theta}{cr}\frac{\partial p'}{\partial \tau}\right]\times \mathrm{d}S(\mathbf{y},\tau) \tag{176}$$

where Here, p' is the perturbed pressure, ($\mathbf{x}$, t) are the observer's location vector and time, ($\mathbf{y}$, τ) are the source location vector and retarded time variables, θ is the angle between the normal vector ($\mathbf{n}$) on the surface and the radiation vector ($\mathbf{r}$), and r is the distance between an observer and a source at the retarded time. The pressure and its derivatives are calculated at the retarded time.

It was found that TPIN at frequencies 3-8 kHz was suppressed by a ventilation of the tire groove.

5.2.4.3 Chen et al. (CFD, 2014)

Chen et al. (2014) [11] used computational fluid dynamics (CFD) to investigate airborne TPIN, such as air pumping, air resonant radiation and pipe resonance. Different tread patterns (hand carved) were simulated and compared with measured near-field noise using laboratory drum method, with the deviation to be a maximum of 4.1% in the frequency range from 0-2000 Hz.

5.2.4.4 Gautam and Chandy (Air Pumping CFD, 2016)

Gautam and Chandy (2016) [801] investigated the air pumping noise generation due to the compression and expansion of air in the tread grooves using the large eddy simulation (LES)-based approach. The compression and expansion of air was assumed to result from the groove volume change. The study suggested two types of tire groove deformation resulting in the groove volume change: (1) a commonly used piston-type motion of the bottom wall and (2) a more realistic bulging in/out of the side walls of a tire groove, as shown in Figure 111. In Figure 111, the white box is the groove, and the black box is the road. Numerical CFD analysis was performed using ANSYS FLUENT™ for both deformation types.

It was found that the piston deformations result in a distinct frequency peak around 2-4 kHz while the side wall deformations result in a more broadband noise spectrum. However, the study assumed that the expansion period begins immediately after the compression period,

which is not the case in reality.

A further study by Gautam and Chandy (2016) [802] investigated both the near-field and far-field acoustic characteristics using LES and Ffowcs-Williams and Hawkings (FW-H) approach respectively, taking into account several airborne mechanisms, including air pumping, pipe resonance, Helmholtz resonance, and rotational turbulence. The simulation environment is a slick tire (215/60R16) with two transverse slots closely spaced in the tread rotating on a smooth drum at 40 km/h in a semi-anechoic chamber. The slot volume change is assumed to be 22% (Takami and Furukawa, 2015 [803,804]) at the tire-pavement interface.

It was concluded that the air pumping noise is focused at higher frequencies around 3-5 kHz, especially at the trailing edge of contact patch. The horn amplification effect can be up to 20 dBA starting from 1.6 kHz, which is proved by the acoustic directivity analysis. However, validation experiments corresponding to the same conditions of simulation were not reported.

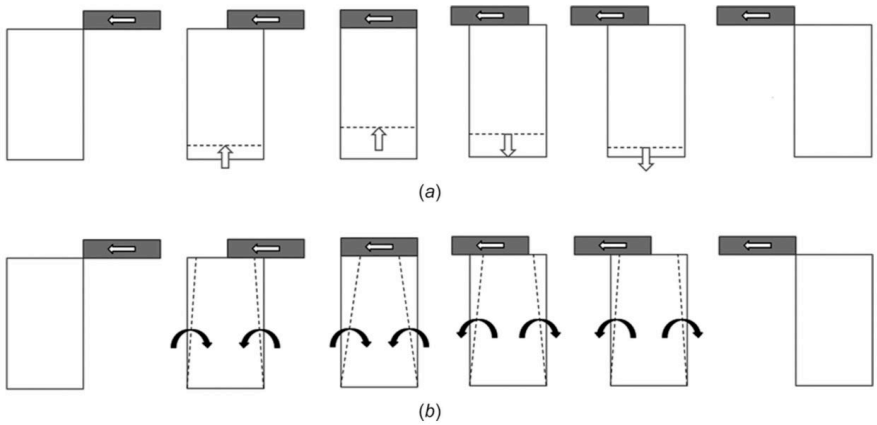

Figure 111: Schematic diagram showing different deformation models with (a) piston-like motion of bottom wall (b) side walls bulging inward (source from Gautam and Chandy, 2016 [801], Figure 3; reprinted with permission from Ms. Beth Darchi on behalf of ASME)

5.2.4.5 Fabrizi (Pipe Resonance, 2016)

This study (Fabrizi, 2016 [419]) modeled the pipe resonance mechanism with computational fluid dynamics (CFD) and computational aeroacoustics. Only the aeroacoustic noise-generation mechanism of the pipe resonance phenomenon was covered, i.e., this is different than the amplification mechanism of pipe resonance that is commonly referred to as where vibroacoustic waves are also taken into account.

The analysis of aeroacoustics in the longitudinal tread grooved is based Lighthill acoustic analogy (Lighthill, 1952 [805]; Lighthill, 1954 [806]),

$$\begin{aligned}
&\frac{1}{c_0^2}\frac{\partial^2 p'}{\partial t^2}-\frac{\partial^2 p'}{\partial x_i^2}=\frac{\partial^2}{\partial x_i \partial x_j}\left(\rho u_i u_j-\tau_{ij}\right)-\frac{\partial f_i}{\partial x_i}+\frac{\partial^2}{\partial t^2}\left(\frac{p'}{c_0^2}-\rho'\right)\\
&p'=p-p_0\\
&\rho'=\rho-\rho_0
\end{aligned} \tag{177}$$

where c_0 is sound speed, t is time, p and p_0 are the instantaneous and equilibrium air pressure, ρ and ρ_0 are the instantaneous and equilibrium air density, u_i and u_j are air velocity in the i direction (flow direction) and j direction (perpendicular to flow direction), τ_{ij} is shear stress tensor, f_i is fluctuating external force per unit volume.

Assuming that the flow can produce sound only at high velocities, it gives that

$$\begin{aligned}
&\rho(\mathbf{x},t)\approx\frac{1}{4\pi c_0^4}\frac{x_i x_j}{\|\mathbf{x}\|^3}\iiint\frac{\partial T_{ij}(\mathbf{y},\tau)}{\partial\tau^2}\mathrm{d}V_y\\
&T_{ij}=\rho u_i u_j+\left(p-\rho c_0^2\right)\delta_{ij}-\tau_{ij}
\end{aligned} \tag{178}$$

where τ is time, $\mathbf{x}$ is the observer point (x_i, x_j) and $\mathbf{y}$ is the source point, T_{ij} is the stress tensor of Lighthill or quadrupole strength density, δ_{ij} is compressive stress tensor coefficient.

The tire model used in the aerodynamic analysis is of size 205/55R16 with two longitudinal tread grooves at rotating speed of 80 km/h. Through Large Eddy Simulation (LES), three phenomena related to the tire aerodynamic noise have been identified: (1) at the pipe inlet, the air flow is squeezed laterally into the groove from both sides, each with a high swirl component (counter rotating vortices); (2) at the pipe outlet, the flow creates jets that develop inside the recirculation bubble of the wake; (3) the flow accelerates laterally to the speed of ~300 km/h, and detaches, generating a high-energy shear layer.

The sound pressure at four positions were analyzed, as shown in Figure 112. For and only for positions of pipe and wake, a clear resonance peak was shown at 1700 Hz, which matches the theory if correction length is set to 10 mm (two times the pipe's section). It also suggests that the resonant acoustic wave could propagate (acoustic energy) only in the flow direction (fluid energy). This directivity is similar to that of a dipole oriented in the longitudinal direction. The peak at 2100 Hz for positions of leading edge side is possibly due to the jet flow generated at the shoulder rib by the air lateral squeezing of the rolling tire. It is noted

that a peak around 600-800 Hz occurs for all positions, which is likely from the vibrations of the tire structure.

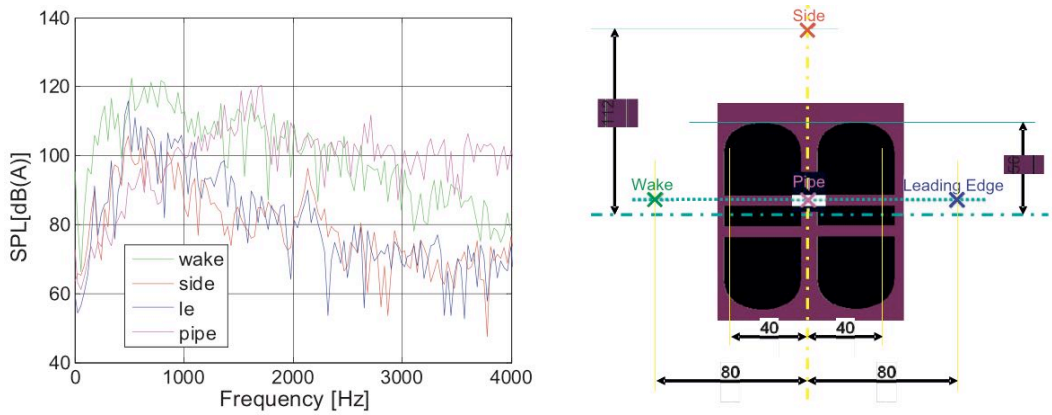

Figure 112: On the left, A-weighted sound pressure levels of the pressure signals recorded in four probes placed around and inside the contact patch of the tire with the road surface; on the right, the position of the four probes with the reference of the footprint shape (source from Fabrizi, 2016 [419], Figure 12; reprinted with permission from Mr. Michael Kaliske of TU Dresden, Germany on behalf of Tire Science and Technology)

5.2.5 Summary

The conventional physics models are summarized in Table 44. It can be seen that this type of modeling has been steadily improved since 1971. The tire was usually modeled as a ring, shell, or plate for vibration investigation; the tire/rim assembly could be modeled as a structure coupled with an air cavity; the sound source was modeled as monopole. However, most models only focused on structure-borne noise, especially that due to the impact between the tire and pavement. Therefore, the tire vibration was usually the output parameter rather than sound pressure level. The frequency range was typical below 500 Hz; some models claimed to be able to predict higher frequencies, but still limited to structure-borne noise. In addition, a large part of the models only considered stationary tire, which is quite different from the normal driving conditions. Only one specific tire or one specific pavement was investigated in some of the models.

The finite element and boundary element models are summarized in Table 45. The finite element method has been applied to TPIN modeling since 1986. Similar to the conventional physics model, the finite element and boundary element model also generally focused on structure-borne noise, and considered the tire carcass as a membrane or plate. However, the near field or far field sound pressure level could be easily predicted with the structure-fluid

coupling technique. The frequency range was almost exclusively below 500 Hz or even lower, such as 150 Hz, due to the inherent drawback of the finite element method. Vehicle speed was typically included in the modeling as an input. Tire parameters were heavily investigated, but the pavement parameters seemed not to be of much interest.

The computational fluid dynamics models are summarized in Table 46. The CFD models started in 1999, somewhat later than the previous two categories. With the help of CFD, the TPIN modeling was extended from structure-borne noise only to airborne noise (air pumping mechanism). Near field sound pressure level was widely accepted as the output parameter of the model. The tire tread pattern was the most important input parameter investigated. However, none of the current models have included pavement parameters that the authors believe are also important, because the air voids within the contact patch are formed between the tread pattern and the pavement texture.

Table 44: Summary of conventional physics models on TPIN

No.	Author	Model Name	Year	Ref.	Method	Output	Frequency Range [Hz]	Mechanism	Driver Parameter	Tire Parameter	Pavement Parameter	Environment Parameter
1	Hayden	Monopole	1971	354	Monopole	Sound pressure, pure tone	N/A	Air pumping	Speed	Groove geometry	N/A	N/A
2	Plotkin and Stusnick	Unified	1981	43	Thin shell	Near field, normalized radiation	0-8000	Impact, air pumping	Speed, tire load	Various	Texture	N/A
3	Keltie	Truck Tire	1982	223	Thin shell	1/3 octave band sound power level	100-2000	Structure-borne	Inflation	Damping, bending stiffness	N/A	N/A
4	Kung et al.	2D Ring	1986	744	Modal expansion	Near field, SPL	0-400	Structure-borne	Tire load	Various	Texture	N/A
5	Heckl	Various Mechanisms	1986	13	Various	LDV, vibration, SPL	0-2000 Hz	Various	Rotating, loaded	Tread pattern	Roughness	N/A
6	Bremner et al.	Tire Vibration	1997	334	SEA, wavenumber decomposition	Far field (7.5 m), 1/3 octave band SPL	100-4000	Impact	Speed, 40 psi	Tread pattern, materials	Texture	N/A
7	Bérengier et al.	Porous Pavement	1997	449	Image source	Impedance, absorption	100-5000	Pavement absorption	N/A	N/A	Airflow resistivity, porosity, tortuosity	N/A
8	Bolton et al.	Wavenumber Decomposition	1998	380	Wavenumber decomposition	Point mobility, wavenumber	0-1000	Structure-borne	Stationary, inflation, gas type	215/70R14	N/A	N/A
9	Kropp	Orthotropic Plate	1999	413	Multipole synthesis	DR, TVM, LDV, acc., 1/3 octave band SPL	125-2500	Structure-borne	Unloaded	Slick	Rough, 1×30 mm step	N/A
10	Kim and Bolton	Shell	2002	759	Wave number decomposition	Vibration	0-4000	Point impact	Speed	N/A	N/A	N/A
11	Molisani et al.	Coupled Cavity	2003	85	Donnell-Mushtari theory, structural acoustic	Modal amplitude, force at spindle	0-1250	Cavity resonance	Stationary without rotating	100/50R12	N/A	N/A
12	Kim et al.	Waveguide	2007	390	Spring-mass, elastically supported beam, cylindrical shell	Vibration, flexural wave, eigen-frequency	0-2000	Structure-borne	Stationary	Geometry, structure	N/A	N/A
13	Feng et al.	Cavity	2009	391	Coordinate transform	Cavity SPL, narrowband	100-300	Cavity resonance	Speed, tire load	N/A	N/A	Temperature
14	O'Boy and Dowling	3D Multilayer	2009	762	Bessel equation	Vibration	0-2000	Structure-borne	Tire load, break/acc.	225/45ZR17	N/A	20 °C
15	Arteaga	Green's Function	2011	499	Modal-ALE	Vibration	0-300	Impact	Tire load, speed	185/70SR14	N/A	N/A
16	Bolton and Cao	Coupled Mode	2013	767	Structural-acoustic coupling	LDV, vibration	0-6000	Structure-borne	Stationary & 50 m/s, 3 bar	225/55R17	N/A	N/A

Table 45: Summary of finite element and boundary element models on TPIN

No.	Author	Model Name	Year	Ref.	Method	Output	Frequency Range [Hz]	Mechanism	Driver Parameter	Tire Parameter	Pavement Parameter	Environment Parameter
1	Saigal et al.	Toroidal Membrane	1986	754	Membrane FE	Vibration	Low	Structure-borne	Inflation, nonrotating, unloaded	Geometry, structure	N/A	N/A
2	Wright and Koopmann	Acoustic Radiation	1986	773	FE, Helmholtz integral	Near field, sound pressure, intensity	80-200	Vibration, radiation	Stationary, point-excited	N/A	N/A	N/A
3	Richards	FEA Coupling	1991	387	Weighted residual approximation	Vibration	0-400	Cavity resonance	N/A	185/70R14	N/A	N/A
4	Larsson and Kropp	3D 2 Plate	1992	736	FE	Pass-by, SPL	0-2000	Structure-borne	Tire load	Various, slick 205/60R15	Texture	N/A
5	De Roo and Gerretsen	TRIAS	2000	664	FEA, BEM	Near field, 1/3 octave band SPL Pass-by, SPL	N/A	Impact, air pumping	N/A	Various, TYDAS	Various, RODAS	N/A
6	Nilsson	WFEM	2004	781	WFEM	Point mobility, wavenumber	0-1500	Structure-borne	Stationary	Geometry, structure	N/A	N/A
7	Biermann et al.	IFEM	2007	614	IFEM, Astley-Leis elements	Far field (1 m), 1/3 octave band SPL	0-1400	Impact	Speed	Slick	Texture	N/A
8	Brinkmeier et al.	FEM & BEM	2008	733	FEA, BEM, ALE	Pass-by, 1/3 octave band SPL	100-850	Structure-borne	40-120 km/h	N/A	Texture spectrum	N/A
9	Waki et al.	WFE	2011	412	FE, modal decomposition	Vibration	0-1500	Impact	Inflation: 220/180 kPa	225/45R17 265/70R17	N/A	N/A
10	Kido et al.	Road Input	2011	792	FE	Axle vibration	0-150	Texture impact	Speed, tire load	Patch area	Texture	N/A
11	Yang et al.	FSI	2013	544	FEA	Near field, 1/3 octave band SPL	500-2500	TPIN	70-90 km/h	PIARC	N/A	N/A
12	Tong et al.	Wear	2013	522	Acoustic FE	Near field, SPL	0-500	Impact	Tire load, speed, inflation	Wear	N/A	N/A
13	Vlahopoulos et al.	EFEA/EBEA	2013	796	EFEA, EBEA, panel contribution analysis	Interior noise	200-8000	Airborne	N/A	N/A	N/A	N/A
14	Mohamed and Wang	Cavity	2015	393	FEM, Bessel root method	Tire cavity SPL	150-500	Torus cavity resonance	N/A	Tire size	N/A	N/A
15	Wei et al.	MLE	2016	798	Mixed Lagrangian-Eulerian, FE, BEM	Near field, 1/3 octave band SPL	Time domain, 0-1250	Vibration	70 km/h	Truck/bus, 315/60R22.5 385/65R22.5	N/A	N/A
16	Banz et al.	Time Domain BEM	2016	799	BEM	1/3 octave band SPL	200-2000	Radiation	Steady-state moving	Pass./truck, slick	N/A	N/A

Table 46: Summary of computational fluid dynamics models on TPIN

No.	Author	Model Name	Year	Ref.	Method	Output	Frequency Range [Hz]	Mechanism	Driver Parameter	Tire Parameter	Pavement Parameter	Environment Parameter
1	Gagen	Shock Wave	1999	362	CFD	Near field, sound pressure/energy	N/A, time domain	Air pumping	Speed	Groove angle, geometry	N/A	N/A
2	Kim et al.	Hybrid CFD	2006	358	CFD, Kirchhoff integral	Far field, 1/3 octave band SPL	250-8000	Air pumping, pipe resonance	100 km/h	Ventilation groove, 165/70SR13	N/A	N/A
3	Chen et al.	CFD	2014	11	CFD	Near field, 1/3 octave band SPL	0-2000	Airborne	N/A	Tread pattern	N/A	N/A
4	Gautam and Chandy	Air Pumping CFD	2016	801	CFD	Near/far field, drum, narrowband SPL	1000-10000	Airborne,air pumping	40 km/h	215/60R16, transverse slots	N/A	N/A
5	Fabrizi	Pipe Resonance	2016	419	CFD, LES, aeroacoustics	Pass-by/in-groove, narrowband SPL	1500-2000 Hz	Pipe resonance	80 km/h	205/55R16, longitudinal grooves	Drum with Safety Walk	N/A

5.3 Statistical Models

5.3.1 Introduction

Due to the fact that much of the physics of tire-pavement interaction noise (TPIN) generation is uncovered, statistical models are more common, especially in industry. Statistical or semi-empirical models are based on correlating measured noise data to tire-pavement parameters. For example, measured TPIN can be correlated with pavement texture, including texture levels at different wavelengths in the longitudinal direction (Rasmussen et al., 2006 [628]; Rasmussen et al., 2006 [807]; Dare and Bernhard, 2009 [626]) and overall texture mean profile depth (MPD) (Fujikawa et al., 2004 [198]; Fujikawa et al., 2009 [218]; Fujikawa et al., 2007 [808]; Storeheier, 2004 [809]).

The early models, as shown in Table 47 and Table 48, were used to predict pass-by traffic noise. It usually used L_{50} as indicator between 1950's and 1960's, then L_{eq} prevailed (Quartieri et al., 2009 [810]).

Table 47: Nomenclature of early models for traffic noise prediction (Quartieri et al., 2009 [810])

Symbol	Meaning	Unit
L_{XX}	Noise level exceeded for *XX*% of the measurement period	[dB] or [dBA]
L_{eq}	Equivalent (energy) sound level	[dB] or [dBA]
Q	Traffic volume (Q_M for motorcycles, Q_{BUS} for buses)	[Vehicles per hour]
Q_{eq}	Equivalent vehicular flows	[Vehicles per hour]
d	Distance from the traffic lane center to the receiver	[ft]
v	Vehicle speed	[mph]
P	Percentage of heavy vehicles in the traffic	[%]
n	Acoustical equivalent of heavy vehicles, indicating the number of light vehicles that generate the same acoustic energy of an heavy vehicle	[-]

Table 48: Early models for traffic noise prediction (Quartieri et al., 2009 [810])

No.	Reference	Author	Year	Equation
1	[811]	Anonymous	1952	$L_{50} = 68 + 8.5\log_{10}(Q) - 20\log_{10}(d)$, for speed of 55-75 km/h and d > 20
2	[812]	Nickson	1965	$L_{50} = C + 10\log_{10}(Q/d)$ where C is a constant that is determined by experimental data under given traffic conditions (vehicle and pavement types)
3	[813]	Johnson and Saunders	1968	$L_{50} = 3.5 + 10\log_{10}(Qv^3/d)$
4	[814]	Griffiths and Langdon	1968	$L_{eq} = L_{50} + 0.018(L_{10} - L_{90})^2$ $L_{10} = 61 + 8.4\log_{10}(Q) + 0.15P - 11.5\log_{10}(d)$ $L_{50} = 44.8 + 10.8\log_{10}(Q) + 0.12P - 9.6\log_{10}(d)$ $L_{10} = 39.1 + 10.5\log_{10}(Q) + 0.06P - 9.3\log_{10}(d)$
5	[815]	Galloway	1969	$L_{50} = 20 + 10\log_{10}(Qv^2/d) + 0.4P$
6	[816]	Burgess	1977	$L_{eq} = 55.5 + 10.2\log_{10}(Q) + 0.3P - 19.3\log_{10}(d)$
7	[817]	Centre Scientifique et Technique du Batiment (France)	1991	$Q_{eq} = Q[1 + P(n - 1)/100]$ $L_{50} = 11.9\log_{10}(Q_{eq}) + 31.4$ $L_{eq} = 0.65L_{50} + 28.8$
8	[818]	Fagotti and Poggi	1995	$L_{eq} = 10\log_{10}(Q_L + Q_M + 8Q_P + 88Q_{BUS}) + 33.5$

All these models essentially have the following format (Murphy and King, 2014 [819]).

$$L_p = E - A_{tot} + C \tag{179}$$

where L_p is the noise level to be predicted ($L_{10,18h}$, L_{Aeq}, L_{den}), E is the emission of the source (sound power of a single point source, sound power per unit length of a line source), A_{tot} is the total sound attenuation (geometric divergence, atmospheric absorption, ground absorption, the barrier, miscellaneous effects), C is the correction factors (façade reflection, different pavement/vehicle types).

These statistical models have better accuracy than deterministic ones since the model parameter values are obtained by actual measured data. However, empirical measurements can never account for all potential conditions, so statistical confidence level and confidence interval are usually analyzed in the meantime. In addition, some of the parameters in these models are not real physical parameters but derived parameters such as a texture spectrum [347], which means they are not adjustable directly. In order to change these parameters, the parameters have to be translated back to original physical parameters, which is not always explicit or even impossible for nonlinear relationships.

A couple of different statistical analysis algorithms can be used. In this section, 18 statistical models were reviewed, including 10 traditional regression models, 3 principal component analysis models, and 5 fuzzy curve-fitting models. The model name, method,

output noise parameter with noise measurement technique, investigated noise generation mechanisms, and investigated input parameters of each model are listed and compared in tables as a summary in Section 5.3.5. The summary tables can be used as a reference for readers to direct to models of interest.

5.3.2 Traditional Regression Models

In this subsection, the traditional regression models include linear regression models and non-linear regression models. The linear regression is easier to model while the non-linear regression is more flexible.

5.3.2.1 RLS (Germany, 1990)

The first version of RLS (Richtlinien für den Lärmschutz an Strassen, or Guideline for Noise Protection on Streets) was released by Der Bundesminister für Verkehr (now is BMVI, Federal Ministry of Transport and digital Infrastructure) in 1981 [820]. The current version is RLS 90 [821] released in 1990. It is used to predict the sound level at a distance of 25 m from the center of the traffic lane. The nomenclature for this model is in Table 49 (RLS, 1990 [821]).

Table 49: Nomenclature of RLS 90 (RLS, 1990 [821])

Symbol	Meaning	Unit
$L_{m,E}^{(25)}$	Reference average sound level at 25 m distance under prescribed/idealized conditions	[dB]
L_m	Real average sound level at 25 m distance under given conditions	[dB]
Q	Traffic volume	[vehicles per hour]
P	Percentage of heavy vehicles in the traffic (weight > 2.8 t)	[%]
R_{SL}	Correction for the speed limit	[dB]
R_{RS}	Correction for the pavement	[dB]
R_{RF}	Correction for the rises and falls along the road	[dB]
R_E	Correction for the absorption characteristics of building surfaces	[dB]
R_{DA}	Correction for the propagation absorption due to the receiver distance	[dB]
R_{GA}	Correction for the attenuation due to the ground and atmospheric conditions	[dB]
R_{TB}	Correction for the attenuation due to the topography and buildings dimensions	[dB]
g	Road gradient	[%]
v_{Lkw}	Speed limit for light vehicles (usually 30-130 km/h)	[km/h]
v_{Pkw}	Speed limit for heavy vehicles (usually 30-80 km/h)	[km/h]

Firstly, the reference average level is calculated as

$$L_{m,E}^{(25)} = 37.7 + 10\log_{10}\left(Q\left(1+0.082P\right)\right) \tag{180}$$

Accounting for the vehicle and pavement conditions, the real average sound level at 25 m

distance is

$$L_m = L_{m,E}^{(25)} + R_{SL} + R_{RS} + R_{RF} + R_E + R_{DA} + R_{GA} + R_{TB} \tag{181}$$

where $R_{RS} = 0.6|g| - 3$ (set to 0 if negative). And R_{SL} is given by

$$R_{SL} = L_{Pkw} - 37.3 + 10\log_{10}\left(\frac{100 + \left(10^{0.1D} - 1\right)P}{100 + 8.23P}\right) \tag{182}$$

where

$$\begin{cases} L_{Lkw} = 23.1 + 12.5\log_{10}\left(V_{Lkw}\right) \\ L_{Pkw} = 27.7 + 10\log_{10}\left[1 + \left(0.02v_{Pkw}\right)^3\right] \\ D = L_{Pkw} - L_{Lkw} \end{cases} \tag{183}$$

5.3.2.2 CNR (Italia, 1991)

The Italian CNR model (Consiglio Nazionale delle Ricerche, or National Research Council in English) was published in 1983 (Canelli et al., 1983 [822]) and then improved by Cocchi et al. in 1991 [823]. The model is a modification of the RLS (Germany) model where the traffic flow is considered as a line source. The nomenclature for this model is in Table 50 (Cocchi et al., 1991 [823]).

Table 50: Nomenclature of CNR (Cocchi et al., 1991 [823])

Symbol	Meaning	Unit
L_{Aeq}	A-weighted equivalent sound level for the given traffic	[dBA]
Q_L	Light vehicles in one hour	[vehicles per hour]
Q_P	Heavy vehicles in one hour	[vehicles per hour]
d	Distance between the lane center and the observer	[m]
d_0	Reference distance (25 m)	[m]
ΔL_V	Correction for the mean flux velocity (0 for 30-50 km/h; +1 for 60km/h; +2 for 70 km/h; +3 for 80km/h; +4 for 100 km/h)	[dBA]
ΔL_F	Correction for the presence of reflective facade near the observer (+2.5)	[dBA]
ΔL_B	Correction for the presence of reflective facade in the opposite direction (+1.5)	[dBA]
ΔL_S	Correction for the pavement type (-0.5 for smooth asphalt; 0 for rough asphalt; +1.5 for cement; +4 for rough pavement)	[dBA]
ΔL_G	Correction for the road gradient	[dBA]
ΔL_{VB}	Correction for the presence of traffic lights (+1) or slow traffic (-1.5)	[dBA]
α	Coefficient related to noise emission from a single vehicle (default =35.1 in Italy)	[dBA]
β	Coefficient related to the weighting factor that heavy vehicles emit more noise (default =6 in Italy)	[-]

The A-weighted equivalent sound level for the traffic is given by

$$L_{Aeq} = \alpha + 10\log_{10}\left(Q_L + \beta Q_P\right) - 10\log_{10}\left(\frac{d}{d_0}\right) + \Delta L_V + \Delta L_F + \Delta L_B + \Delta L_S + \Delta L_G + \Delta L_{VB}$$

5.3.2.3 TNM (US, 1998)

The Traffic Noise Model (TNM) is a software model to predict pass-by noise levels (at a distance of 15 m) near highways. It is the only validated model approved by Federal Highway Administration (FHWA, USA) to test compliance with Code of Federal Regulations "Traffic Noise Prediction" (23 CFR 772.9(a)) (FHWA, 2012 [824]). The first version of TNM was released in 1998 (FHWA, 1998 [825]) based on extensive measurement data (over 6000 pass-by events) taken from 1993 to 1995 (Fleming et al., 1995 [826]). After several revisions, the most current and mature version is TNM 2.5 (software) released in 2004. TNM Version 3.0 is being under development with 2D graphics and GIS functionality implemented (FHWA, 2013 [827]).

The SPL at the receiver is adjusted from a reference sound level termed as Reference Energy Mean Emission Level (REMEL) that describes the maximum sound level from a vehicle under given conditions. The possible conditions are listed in Table 51 (Rochat et al., 2012 [828]).

Table 51: REMEL conditions in TNM (Rochat et al., 2012 [828])

Category	Condition
Vehicle Type	Automobile; medium truck; heavy truck; bus; motorcycle
Pavement Type	Dense-graded asphalt concrete (DGAC); open-graded asphalt concrete (OGAC); Portland cement concrete (PCC); average (a combination of DGAC and PCC)
Operating Condition	Cruise; full-throttle

The energy mean overall A-weighted level associated with the maximum level during pass-by (REMEL, for one vehicle) is

$$L_{A,\max}(S) = 10\log_{10}\left[\left(S^{A/10}\right)\left(10^{(B+\Delta E_B)/10}\right) + 10^{(C+\Delta E_C)/10}\right] \tag{184}$$

where S is vehicle speed in mph; A, B and C are coefficients related to vehicle type, pavement type and operating condition; ΔE_B and ΔE_C are corrections to convert the level mean to the energy mean, as given by

$$\Delta E = 10\log_{10}\left(\frac{1}{N}\sum_{i=1}^{N}10^{\frac{L_i - L_{avg}}{10}}\right) \tag{185}$$

where N is the number of samples, L_i is the overall A-weighted level for the ith sample, L_{avg} is the linear average over all samples. The energy mean REMEL for one-third octave band spectra is

$$\begin{aligned} L_{A,\max}(S,f) = {} & 10\log_{10}\left[\left(S^{A/10}\right)\left(10^{(B+\Delta E_B)/10}\right)+10^{(C+\Delta E_C)/10}\right]-\left(K_1+K_2S\right)+\left(D_1+D_2S\right) \\ & +\left(E_1+E_2S\right)\log_{10}(f)+\left(F_1+F_2S\right)\log_{10}(f)^2+\left(G_1+G_2S\right)\log_{10}(f)^3 \\ & +\left(H_1+H_2S\right)\log_{10}(f)^4+\left(I_1+I_2S\right)\log_{10}(f)^5+\left(J_1+J_2S\right)\log_{10}(f)^6 \end{aligned} \tag{186}$$

where f is the nominal center frequency of the one-third octave band; D_1 and D_2 through K_1 and K_2 are REMEL model coefficients.

The adjusted sound level at the receiver is calculated by the following equation accounting for traffic flow $A_{traffic,i}$, propagation distance A_d and shielding A_s.

$$L_{Aeq,\text{lh}} = EL_i + A_{traffic,i} + A_d + A_s \tag{187}$$

where EL_i is the vehicle noise emission for each vehicle type i depending on $L_{A,\max}$; $A_{traffic,i}$ for each vehicle type i is

$$A_{traffi,i} = 10\log_{10}\left(\frac{V_i}{S_i}\right) - 13.2 \tag{188}$$

5.3.2.4 Hanson and James (Dense Graded, 2004)

Hanson and James (2004) [108,585] was developed by National Center for Asphalt Technology (NCAT) in Auburn University sponsored by Colorado Department of Transportation (CDOT) and Federal Highway Administration (FHWA). 46 different pavements (each 61 m in length, 2.7 km in total) in the NCAT Test Track were tested, most of which were dense graded Hot Mix Asphalt (HMA). Sound levels were measured with two approaches, Close-Proximity Trailer (CPX) and Close-Proximity Sound Intensity (CPI).

The study focused on the mixture properties of the pavements. For each pavement, seven tires at the same speed of 72 km/h were tested and the average noise level was calculated as the model output. The final regression equation for the tire noise level is

$$L_A = 93.4 - 2.56 \times AirVoids + 0.53 \times FinenessModulus \times AirVoids \tag{189}$$

where L_A is the overall A-weighted sound pressure level (OASPL), and R^2 = 0.64. The fineness modulus (FM) is an empirical factor obtained by adding the total percentages of a sample of the aggregate retained on each of a specified series of sieves, and dividing the sum by 100 (TXDOT, 1999 [829]; ASTM, 1980 [830]). The sieve sizes used are No. 100 (150 μm), No. 50 (300 μm), No. 30 (600 μm), No. 16 (1.18 mm), No. 8 (2.36 mm), and No. 4 (4.75 mm), and 3/8 in. (9.5 mm), 3/4 in. (19.0 mm), 1-1/2 in. (38.1 mm), and larger, increasing in the ratio of 2 to 1. Fine aggregates are usually in the range between 2.00 and 4.00, while course aggregates smaller than 38.1 mm between 6.50 and 8.00. The pavements tested in the NCAT study have combinations of fine and coarse aggregates, so they have intermediate values (4.07-5.06).

In addition, the separate influences of different parameters were analyzed: fineness modulus (R^2 = 0.51), air voids (%) (R^2 = 0.11), and pavement age (R^2 = 0.78). The study also ranked the noise levels for four types of pavements as open-graded mixes (coarse gradations) > stone matrix asphalt matrix > dense graded HMA > open-graded mixes (fine gradations).

5.3.2.5 Rasmussen (Concrete Texture, 2009)

Rasmussen (2009) [580] correlated TPIN with typical concrete pavement textures such as burlap drag, rake tining and diamond grinding. 3D texture profiles were measured over 1000 sections representing about 400 nominal textures and totaling 70 km with RoboTex laser measurement system. Enormous amount of data (1 GB for 1.6 km) were collected due to high sampling frequency (1000 Hz) and high resolution (spatial resolution of approximately 0.4 mm^2 and height resolution of 0.01 mm). 3D texture bridging (envelopment) filter was employed to achieve data reduction.

Noise data was collected using OBSI method (96 kHz), except that there were two additional channels for the Data Acquisition System (DAQ). One of the channels was used to record event markers, i.e., signal from an optical transceiver (reflective delineator) indicating the start and end of the test section. Thus, the texture data and noise data could be synchronized after compensating for the travel time between the optical transceiver (at the road side) and the OBSI microphone (at the tire). The study measured frequency range of 500-5000 Hz but focused much on 630, 800 and 1000 Hz third-octave bands.

Different equations were developed for different types of concrete pavements, i.e., they

have different input texture parameters and coefficients, as shown below. It was also concluded that noise cannot be predicted by texture depth (Rasmussen, 2010 [831]).

$$\begin{cases} OBSI_{TT} = f\left(L_{tx,160}, L_{tx,25}, R_{k,tr}\right) \\ OBSI_{LT} = f\left(L_{tx,40}\right) \\ OBSI_{DG} = f\left(L_{tx,80+63+50+40}, Skew_{tr}\right) \\ OBSI_{D} = f\left(L_{tx,50+40}, Skew_{tr}, R_{k,tr}\right) \end{cases} \tag{190}$$

where *OBSI* is overall A-weighted sound intensity level (OASIL), the subscripts *TT*, *LT*, *DG*, *D* indicate transverse tining, longitudinal tining, diamond grinding, and drag; $L_{tx,XX}$ is texture level for third-octave band centered at a texture wavelength of *XX* (mm) according to ISO 13473-4 (2008) [622]; $Skew_{tr}$ is texture skew in transverse direction (unitless) according to ASME B46.1 (2009) [643]; $R_{k,tr}$ is core roughness depth in transverse direction (mm) accoding to ISO 13565-2 (1996) [832]. The complete equation for drag concrete pavement is

$$OBSI_D = 91.0 + 0.315\left(L_{tx,40} + L_{tx,50}\right) - 1.37 Skew_{tr} - 3.11 R_{k,tr} \tag{191}$$

where R^2 is 0.57, and standard error is 0.6 dBA. It should be noted that the tire used is not the current SRTT, but a Goodyear Aquatred III test tire.

5.3.2.6 Fujikawa et al. (Asperity, 2009)

Fujikawa et al. (2009) [218,833–838] developed a statistical model correlating near field TPIN levels with pavement roughness parameters. The roughness parameters in the final model are asperity spacing x_A and asperity height unevenness h_d, as illustrated in Figure 113. Thirteen pavement profiles were measured with single-head laser profile meter accounting for 2-4 m covering no less than 80 asperities for each sample. The specifications of the thirteen pavements are listed in Table 52.

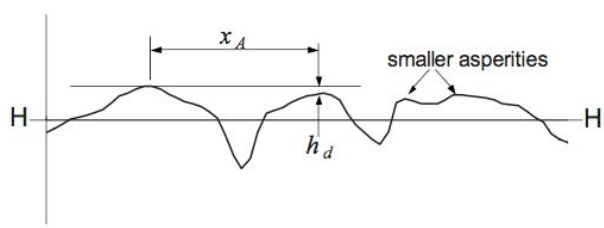

Figure 113: Illustration of pavement roughness parameters in Fujikawa et al. Model (source from Fujikawa et al., 2009 [218], Figure 1; reprinted under fair use provision)

Table 52: Specifications of pavements measured in Fujikawa et al. Model (source from Fujikawa et al., 2009 [218], Table 2; reprinted under fair use provision)

				Asperity Spacing		Asperity Height Unevenness		
No.	Pavement	Max. Aggregate Size [mm]	Age [year]	Average x_A [mm]	95% Confident Range [mm]	Average h_d [mm]	95% Confident Range [mm]	Remarks
B0	Resin crushed stone pavement	13	3	16.7	1.2	2.73	0.28	Sharp-edged aggregates are bound with resin.
B1	Shot blasted dense asphalt	20	3	22.2	1.8	0.74	0.09	Asphalt matrix is roughened by shot blasting.
B2	Semi-flexible pavement	13	6	17.4	1.5	0.51	0.07	Open graded aggregates
B3	Semi-flexible pavement	13	6	20.6	2.1	0.52	0.09	Open graded aggregates
B4	Semi-flexible pavement	13	6	20.6	2.1	0.58	0.10	Open graded aggregates
B5	Dense asphalt max. 20 mm	20	3	17.1	1.2	0.61	0.06	Aggregates with large size.
B6	Dense asphalt max. 13 mm	13	1	10.3	1.0	0.20	0.03	Ordinary type of Japanese public road.
B7	Dense asphalt max. 13 mm	13	5	13.4	1.1	0.40	0.05	Ordinary type of Japanese public road.
B8	Dense asphalt max. 13 mm	13	10	11.8	0.9	0.44	0.06	Test track with reinforced asphalt.
B9	Dense asphalt max. 13 mm	13	1	11.4	1.2	0.16	0.02	Ordinary type of Japanese public road.
B10	Dense asphalt max. 13 mm	13	3	11.6	1.1	0.19	0.02	Rate of small aggregates is relatively higher than ordinary type.
B11	Dense asphalt max. 8 mm	8	2	8.7	0.4	0.17	0.01	Aggregates with small size.
B12	Dense asphalt max. 13 mm	13	1	8.1	0.5	0.14	0.01	Rate of small aggregates is relatively higher than ordinary type.

The TPIN levels were measured with a microphone under the vehicle beside and tire. The individual correlation with TPIN and asperity spacing was reported to be $R^2 = 0.62$ with the standard error of 1.4 dB, while the individual correlation with TPIN and asperity height unevenness was reported to be $R^2 = 0.53$ with the standard error of 1.5 dB. Then multiple regression analysis was employed to correlate TPIN levels with both the parameters. The final equation is given as

$$L_R = 0.25\langle x_A \rangle + 1.55\langle h_d \rangle + 91.8 \tag{192}$$

where L_R is the regressed A-weighted sound pressure level in dBA, $<x_A>$ is the average asperity spacing in mm, and $<h_d>$ is the average asperity height unevenness. The coefficient of determination was $R^2 = 0.83$ with the standard error of 0.9 dB.

It was included that the reduced spacing and height unevenness of pavement asperities will lead to reduced TPIN. In an older study by the same authors, Fujikawa et al. (2004) [198], another pavement parameter mean profile depth (MPD in mm) was also included. The regression equation was given by

$$\begin{aligned} L_R &= 0.34\langle x_A \rangle + 1.80\langle h_d \rangle - 1.15MPD + 93.2 \quad \text{for block pattern tire;} \\ L_R &= 0.33\langle x_A \rangle + 1.07\langle h_d \rangle - 0.22MPD + 91.1 \quad \text{for rib pattern tire.} \end{aligned} \tag{193}$$

The model also analyzed tire tread vibration. Unfortunately, it was only measured on three types of pavements and no relationship equations were given in the study.

5.3.2.7 Reyes and Harvey (Pavement Core, 2011)

Reyes and Harvey (2011) [639] developed a regression model to predict on-board sound intensity (OBSI) noise levels using laboratory pavement cores. The advantage of the method is it is easier to test a pavement core in the lab instead of a full-scale section in the field. The sixteen field pavement cores included those commonly used in California: five open-grated asphalt concrete (OGAC), six open graded rubberized asphalt concrete (RAC-O), three gap graded rubberized asphalt concrete (RAC-G), and two open graded rubberized asphalt concrete with large aggregates (RAC-O F-mixes). The age of the pavements ranged from a few months to six years, and the air void content from 9% to 22%. There were two typical dimensions of cores: 101 mm and 152 mm diameter.

Airflow resistance R_f, air void content, mean profile depth (MPD), root mean square (RMS) and coefficient of uniformity C_u were investigated for their relations with sound intensity levels. Air void content was found to have strong correlation with airflow resistance; root mean square was found to have strong correlation with mean profile depth; coefficient of uniformity was found to have poor correlation with sound intensity levels. As such, specific airflow resistance R_f (in Pa·s/m) and MPD (in m) were selected in the final model, as given below ($R^2 = 0.52$~0.86).

$$SI_f = a_f + b_f \cdot MPD + c_f \cdot \log_{10}\left(R_f\right) \tag{194}$$

where SI_f is the sound intensity level for the frequency band f in dBA referenced to 10^{-12}

watt/m^2, a_f, b_f and c_f are coefficients, which are given in Table 53 (Reyes and Harvey, 2011 [639]).

Table 53: Coefficients for Reyes and Harvey Model (source from Reyes and Harvey, 2011 [639], Table 1; reprinted under fair use provision)

1/3 Octave Band Center Frequency [Hz]	a_f	b_f	c_f
500	91.83	5.45	-1.69
630	90.46	6.36	-1.32
800	93.67	3.38	0.03
1000	90.69	2.59	0.56
1250	83.02	3.04	1.52
1600	79.83	1.90	2.15
2000	82.36	-0.50	1.38
2500	79.75	0.88	0.97
3150	76.16	2.29	1.04
4000	71.09	2.75	1.41
5000	64.86	3.88	1.56
Overall A-weighted Sound Intensity Level	96.95	3.51	0.28

The specific airflow resistance is defined as the division of the pressure difference across a core specimen by the airflow velocity ($R_f = \Delta p/u$, in Pa·s/m). It was measured only in the region of laminar flow (0.2-10 liter/min) where R_f is constant. The range of R_f tested was 51-76075 Pa·s/m. The MPD was obtained using the Model 9200 laser texture scanner developed by AMES Engineering. The author noted that only one core for each section was scanned due to limited funding and time and recommended that at least three cores measured according to ISO 13473-1 (1997) [610]. It is also noted that the laboratory MPD and the measured value in the field has good relation ($R^2 = 0.88$).

It was shown that airflow resistance has positive relation ($R^2 = 0.64 \sim 0.81$) with sound intensity in the range of 1250-2500 Hz (high frequency). MPD has positive relation ($R^2 = 0.3$) with sound intensity in the range of 500-630 Hz (low frequency). However, neither of the two parameters was able to explain the noise at the 800 Hz and 1000 Hz frequency bands ($R^2 \approx 0$) where most spectral content exists and tire contributions might dominate. In addition, neither of the two parameters showed satisfying relations with overall A-weighted sound intensity levels ($R^2 = 0.1$).

5.3.2.8 CNOSSOS (EU, 2012)

The model is the proposed common European Method to predict noise emission for road traffic and was firstly released in 2012 (Kephalopoulos et al., 2012 [839]). The noise emission is

in terms of sound power level, assuming each point source of each vehicle is 0.05 m above the surface. The model presents separate calculations for TPIN and propulsion noise, for five types of vehicles (m = 1 for light vehicle, 2 for medium heavy vehicle, 3 for heavy vehicle, 4 for powered two-wheeler, 5 for other customized vehicles).

For the TPIN noise, the sound power level, $L_{WR,i,m}$, for the vehicle type m, and octave frequency band i (125-4000 Hz), is given by

$$L_{WR,i,m} = A_{R,i,m} + B_{R,i,m} \log_{10}\left(\frac{v}{v_{ref}}\right) + \Delta L_{WR,i,m}(v) \tag{195}$$

where v is the vehicle speed, v_{ref} is reference speed of 70 km/h; A_R and B_R are coefficients for the respective vehicle type m, and octave frequency band i; $\Delta L_{WR,i,m}$ is the total correction accounting for pavement type, studded tires, speed variation and air temperature.

For the propulsion noise, the sound power level, $L_{WR,i,m}$, for the vehicle type m, and octave frequency band i, is given by

$$L_{WP,i,m} = A_{P,i,m} + B_{P,i,m} \log_{10}\left(\frac{v - v_{ref}}{v_{ref}}\right) + \Delta L_{WP,i,m} \tag{196}$$

It was shown that speed has much smaller influence on the propulsion (engine) noise than TPIN for the first three vehicle types. The overall sound power level for the vehicle is the energetic sum of TPIN and propulsion noise

$$L_{W,i,m} = 10\log_{10}\left(10^{\frac{L_{WR,i,m}}{10}} + 10^{\frac{L_{WP,i,m}}{10}}\right) \tag{197}$$

The equivalent sound power level for a steady traffic flow Q (vehicle per hour) with average vehicle speed v_m is given by

$$L_{W,eq,i,m} = L_{W,i,m} + 10\log_{10}\left(\frac{Q}{1000 v_m}\right) \tag{198}$$

5.3.2.9 Syamkumar et al. (Mode-wise, 2013)

Syamkumar et al. (2013) [6] developed statistical equations to predict pass-by TPIN for each combination (mode) of vehicle type and pavement. Six vehicle types were included: heavy commercial vehicle (HCV), bus, light commercial vehicle (LCV), passenger car, auto-rickshaw (AR), and two-wheeler (2W). The pavements include eight asphalt concrete

pavements (AC) and four cement concrete pavements (CC).

The investigated parameters are listed in Table 54.

Table 54: Investigated parameters in Syamkumar Model (Syamkumar et al., 2013 [6])

No.	Parameters	Symbol	Value
1	Vehicle type	m_1	HCV, bus, LCV, car, AR, 2W
2	Pavement type (texture depth)	m_2	AC, CC
3	Loading condition	p_1	Loaded (L), unloaded (UL)
4	Vehicle speed	p_2	10-100 km/h
5	Wind direction	p_3	Towards, away (0 to 180°)
6	Pavement temperature	p_3	20-40 °C
7	Pavement condition	p_5	Wet, dry

The general form of the statistical equations is

$$TPIN_{(mode)} = a_0 + a_1 p_1 + a_2 p_2 + a_3 p_3 + a_4 p_4 + a_5 m_2 \tag{199}$$

where the coefficients for passenger cars on asphalt concrete pavement and cement concrete pavement are in Table 55.

Table 55: Statistical equation coefficients and R^2 for passenger cars in Mode-wise Model (Syamkumar et al., 2013 [6])

	a_0 (Intercept)	a_1 (Load)	a_2 (Speed)	a_3 (Wind)	a_4 (Temperature)	a_5 (MPD)	R^2
$[TPIN_{(Car)}]_{AC}$	79.10	0.0013	0.2817	-0.0059	-0.016	0.1260	0.918
$[TPIN_{(Car)}]_{CC}$	75.43	0.0028	0.4343	-0.02	-0.0015	0.3137	0.911

It was found that TPIN on cement concrete pavements are 2 dB higher than that on asphalt pavements. Wet pavements increase TPIN by 3 dBA for HCV compared to dry pavements. The wind direction has influence on TPIN in the order of 1-2 dBA for HCV.

5.3.2.10 Wayson et al. (FDOT, 2014)

The model (Wayson et al., 2014 [202]) was conducted by researchers at the John A. Volpe National Transportation Systems Center (Cambridge, MA) sponsored by Florida Department of Transportation (FDOT). Various types of pavements at over 45 locations in Florida (especially rigid pavements, dense graded and open graded pavements) were measured and ranked by the OBSI trailer (near field) and a roadside device (far field). The sound levels measured by the two devices have the following relation (i.e., propagation model).

$$SPL_{Wayside} = SIL_{OBSI} - \Delta \tag{200}$$

where $SPL_{Wayside}$ is road side the sound pressure level in dBA, SIL_{OBSI} is the sound intensity level measured by OBSI trailer in dBA, Δ is the correction term and given by

$$\Delta = 32.57 + 0.0349 \cdot FN + 18.094 \cdot MPD - 0.0493 \cdot AG4 \tag{201}$$

where FN is friction number average for ribbed tire, MPD is mean profile depth, $AG4$ is percent aggregate at No. 4 screen (4.74 mm). A residual standard error of 1.0 dBA was reported with $R^2 = 0.73$. For the FDOT OBSI system, the repeatability was an error of 0.26 dB at 95% confidence level.

The pavement aging effect on TPIN was quantified as 0.2 dB/year. Frequency components of TPIN were also investigated in the study. It should be pointed out that the OBSI system was affixed to the wheel casing rather than the wheel hub, so the measurement might not be accurate due to suspension compliance. And unfortunately, the direct relations between pavement parameters and the OBSI or pass-by levels were not reported.

5.3.3 Principal Component Analysis Models

Principal component analysis (PCA) uses an orthogonal transformation to identify a smaller number of uncorrelated variables, called "principal components", from a larger number of possibly correlated variables. Principal component regression (PCR) is a regression analysis technique based on principal component analysis (PCA). The advantage of the PCA models is that least number of variables (principal components) can be used to explain the maximum amount of variance.

5.3.3.1 Ongel et al. (Asphalt Pavement, 2008)

Ongel et al. (2008) [840] combined the predictions for TPIN of different asphalt pavements into one universal statistical equation. OBSI tests following the AASHTO standard (2008) [200] were conducted on 72 pavements, including open-graded, dense-graded, rubberized open-graded and rubberized gap-graded asphalt pavements.

The initial parameters investigated in the study are listed in Table 56.

Table 56: Initial parameters investigated in Ongel Model (Ongel et al., 2008 [840])

Category	Parameter	Symbol	Unit	Description
Pavement Mixture	Mix type	*Type*	[-]	Categorical variable: 1 for open graded mixes and 0 for gap and dense graded
	Age	*Age*	[year]	
	Nominal maximum aggregate size	*NMAS*	[mm]	
	Fineness modulus	*FM*	[-]	A measure of aggregate gradation (larger indicates coarser)
	Coefficient of uniformity	C_u	[-]	$C_u = D_{60}/D_{10}$ where D_{60} is sieve size associated with 60% passing and D_{10} is sieve size associated with 10% passing
	Coefficient of curvature	C_c	[-]	$C_c = D_{30}/D_{10}$ where D_{30} is sieve size associated with 30% passing
	Rubber inclusion	*RI*	[-]	Categorical variable: 1 for rubberized mixes and 0 for non-rubberized
	Air void content	*AV*	[%]	
	Mean profile depth	*MPD*	[μm]	A measure of Macrotexture
	Root mean square of profile deviation	*RMS*	[μm]	A measure of Macrotexture
	International roughness index	*IRI*	[m/km]	
	British pendulum number	*BPN*	[-]	A measure of Macrotexture
	Surface layer thickness	*SLT*	[mm]	
	Well gradation	*WG*	[-]	Categorical variable: 1 for well graded mixes and 0 for poorly graded; If $C_u > 4$ and $1 < C_c < 3$, the mix is well graded, otherwise poorly graded
Pavement Distress Condition	Presence of transverse cracking	*PTC*	[-]	Categorical variable: 1 if the total length of transverse cracks >= 5 m in 150 m section, and 0 otherwise
	Presence of fatigue cracking	*PFC*	[-]	Categorical variable: 1 if the total fatigue cracking >= 5% of the wheelpath area in 150 m section, and 0 otherwise
	Presence of raveling	*PR*	[-]	Categorical variable: 1 if the total raveled area >= 5% of the total area in 150 m section, and 0 otherwise
Environmental	Pavement temperature	*T*	[°C]	Pavement temperature measured during the OBSI measurements
	On-board sound intensity level	*OBSI*	[dBA]	Output parameter, corrected and reported with their equivalent values at 96 km/h

Ten input parameters were selected based on the order of importance to develop the model. The statistics of the ten input parameters and the output parameter (*OBSI*) for all the measurements are shown in Table 57.

Table 57: Statistics of parameters in Ongel Model (Ongel et al., 2008 [840])

	Parameter	Symbol	Unit	Mean	Standard Deviation	Minimum	Maximum
Input 1	Mix type	*Type*	[-]	1.5	0.7	0.7	3.8
Input 2	Age	*Age*	[year]	12.4	5	4.1	21.6
Input 3	Fineness modulus	*FM*	[-]	0.04	0.06	0.000007	0.31
Input 4	Coefficient of uniformity	C_u	[-]	974.6	328.4	405.6	1,807.00
Input 5	Air void content	*AV*	[%]	651.4	196.1	282.3	1,121.60
Input 6	Mean profile depth	*MPD*	[μm]	57	7.8	41	75
Input 7	International roughness index	*IRI*	[m/km]	5	0.5	3.8	5.9
Input 8	Surface layer thickness	*SLT*	[mm]	21.1	14.9	2.9	58
Input 9	Presence of transverse cracking	*PTC*	[-]	3.8	2.4	<0.01	8.7
Input 10	Presence of raveling	*PR*	[-]	43.8	22.1	10.4	112.5
Output	On-board sound intensity level	*OBSI*	[dBA]	37.01	15.1	8.35	56.4

The correlation matrix was generated using Ordinary Least-Squares (OLS) Multiple Regression, as shown in Table 58. Unfortunately, correlations about Input 6 *MPD* were not reported.

Table 58: Correlation matrix for nine input parameters and OBSI output in Ongel Model (source from Ongel et al., 2008 [840], Table 3; reprinted with permission from American Society of Civil Engineers)

	OBSI	*Age*	*Type*	*AV*	*IRI*	*FM*	C_u	*PR*	*PTC*	*SLT*
OBSI	1.000	0.287_a	-0.479_b	-0.417_b	0.364_b	-0.349_b	0.439_b	0.297_a	0.274_a	0.283_a
Age	0.284_a	1.000	−0.069	−0.061	0.477_b	0.010	−0.101	0.206	0.235	−0.129
Type	-0.477_b	−0.069	1.000	0.767_b	−0.139	0.607_b	-0.730_b	0.063	-0.321_b	-0.555_b
AV	-0.416_b	−0.061	0.767_b	1.000	−0.071	0.640_b	-0.763_b	−0.062	−0.238	-0.687_b
IRI	0.384_b	0.477_b	−0.139	−0.071	1.000	0.018	0.113	0.410_b	0.146	0.076
FM	-0.347_b	0.010	0.607_b	0.640_b	0.018	1,000	-0.720_b	0.049	-0.306_a	-0.465_b
C_u	0.446_b	−0.101	-0.730_b	-0.763_b	0.113	-0.720_b	1.000	0.041	0.180	0.508_b
PR	0.300_a	0.206	0.063	−0.062	0.410_b	0.049	0.041	1.000	0.095	0.199
PTC	0.273_a	0.235	-0.321_b	−0.238	0.146	-0.306_a	0.180	0.095	1.000	0.165
SLT	0.281_a	−0.129	-0.555_b	-0.687_b	0.076	-0.465_b	0.508_b	0.199	0.165	1.000

[a]Correlation is significant at the 0.05 level (2-tailed).

[b]Correlation is significant at the 0.01 level (2-tailed).

The final linear regression equation for *OBSI* prediction is

$$\begin{aligned} OBSI = {} & 107.6 + 0.172Age - 1.74Type - 0.10AV - 0.48IRI - 1.25FM - 0.005C_u \\ & +0.004MPD + 1.84PR - 0.09RTC + 0.003SLT \end{aligned} \tag{202}$$

where R^2 = 0.73 and standard error is 0.93 dBA.

In Table 58, it is also seen that many parameters have strong correlations with each other. C_u has significant correlations with *Type*, *AV* and *FM* (absolute value > 0.7). Thus, principal components regression (PCR) was then employed to divide these input parameters into three orthogonal (uncorrelated) groups in the order of importance. The first group is "flow

properties" including *AV*, C_u, *Type*, *FM*, *SLT* (in the order of importance); the second group is "surface roughness" including *PR*, *IRI* and *Age*; the third group is "crack resistance" including *PTC* and *Age*. The statistical equation is

$$OBSI = 100.87 - 1.28 \times FlowProperties + 0.79 \times SurfaceRoughness - 0.43 \times CrackResistance \quad (203)$$

where R^2 = 0.61 and standard error is 1.04 dBA.

In a further study, Ongel and Harvey (2010) [662] investigated the influence of pavement characteristics on the frequency content of tire pavement noise. The effects of pavement parameters on different 1/3 octave band frequencies are shown in Table 59.

Table 59: Effects of Pavement Parameters on Different 1/3 Octave Band Frequencies (Modified from Ongel and Harvey, 2010 [662], Table 3)

Frequency [Hz]	500	630	800	1000	1250	1600	2000	2500	3150	4000	5000
Type	↑	↑	↓	↓	↓	↓	↓	↓	↓	↓	↓
Age					↑	↑				↑	
FM	↑	↑	↓	↓	↓	↓	↓	↓	↓	↓	↓
C_u	↓	↓	↑	↑	↑	↑	↑	↑	↑	↑	↑
AB	↑	↑	↓	↓	↓	↓	↓	↓	↓	↓	↓
MPD	↑	↑				↓	↓	↓	↓	↓	↓
[1]*RMS*	↑	↑				↓	↓	↓	↓	↓	↓
IRI	↑	↑	↑	↑	↑						
SLT	↓	↓		↑	↑	↑	↑	↑	↑	↑	↑
PTC					↑	↑	↑	↑	↑	↑	↑
PR											
[2]*Rubber*			↓								
[3]*NMAS*				↑	↑	↑	↑	↑			
[4]*PFC*					↑	↑	↑				

[1]*RMS* is root mean square of profile deviation in μm.

[2]*Rubber* is pavement material with rubber inclusion (coded as 1 for rubberized mixes and 0 for non-rubberized mixes).

[3]*NMAS* is nominal maximum aggregate size in mm.

[4]*PFC* is presence of fatigue cracking (coded as 1 if the total fatigue cracking 5% of the wheel path area of the 150-m section, and 0 otherwise).

5.3.3.2 Zhang et al. (MTD, 2014)

Zhang et al. (2014) [138,841] was developed to predict the Mean Texture Depth (MTD) of the pavement macro-texture based on the TPIN and vehicle speed. As such, TPIN cannot be explicitly obtained using this model, but it provides sufficient insights into the relationship between TPIN and MTD.

The noise was measured by a microphone underneath the vehicle behind the driver side rear tire (Behind the Tire, BTT method), including TPIN and noise caused by wind and vehicle vibration. The acoustic energy was obtained by integration over the frequency

spectrum (DC to 2 kHz) and then the Principal Component Analysis (PCA) was applied for noise and speed effect reduction (Zhang et al., 2014 [841]; Zhang et al., 2012 [842]), so the combined method is termed as PCA Energy Method. PCA is a successful method to extract features from measurements (Wang et al., 2002 [843]; Hotelling, 1933 [844]; Jolliffe, 2002 [845]). It is a statistical procedure that uses an orthogonal transformation to convert possibly correlated variables into a set of values of linearly uncorrelated variables called principal components.

All the tests (using the same tire) were conducted at National Center for Asphalt Technology (NCAT) in Lee County, Alabama (Zhang et al., 2014 [841]), the same as Hanson Model. Employing Taylor expansion and least-squares analysis (LS), the final equation was given by

$$MTD = 0.2 + 1.55E_n + 0.44V_n + 0.76E_nV_n \tag{204}$$

where MTD is the predicted mean texture depth in mm, E_n and V_n are normalized PCA energy and driving speed (dimensionless) which are given below.

$$E_n = \frac{E - E_{\min}}{E_{\max} - E_{\min}} \tag{205}$$

$$V_n = \frac{V - V_{\min}}{V_{\max} - V_{\min}} \tag{206}$$

where E is PCA energy in Hz·Pa, V is the driving speed in m/s; the subscripts min and max indicate the minimum and the maximum values through all the tests. It was reported that the accuracy of this model is 83.61% with good repeatability with MTD range of 0.2 to 3 mm, which is 10% higher than the Energy Method (40-400 Hz) without PCA. On the other hand, a database is always needed for PCA to do calibration and acquire the limits of the values.

5.3.3.3 Li et al. (Thin Surfacing, 2015)

Li et al. (2015) [613] developed a statistical tire-road noise model accounting for texture and absorption for thin-layer surfacings. Based on different combination of input pavement parameters, three models were developed using principal component regression. The three combinations are displayed in Table 60.

Table 60: Input pavement parameter combination of surface texture and sound absorption (modified from Li et al., 2015 [613], Table 3)

Model	Number of Input Parameters	Surface Texture	Sound Absorption
1	15	TL_{250}, TL_{125}, TL_{63}, TL_{32}, TL_{16}, TL_8, TL_4, TL_2, TL_1	AL_{1000}, AL_{1250}, AL_{1600}, AL_{2000}, AL_{2500}, AL_{3150}
2	7	Mean Profile Depth (MPD)	AL_{1000}, AL_{1250}, AL_{1600}, AL_{2000}, AL_{2500}, AL_{3150}
3	10	TL_{250}, TL_{125}, TL_{63}, TL_{32}, TL_{16}, TL_8, TL_4, TL_2, TL_1	Maximum Absorption Coefficient

TL_x is texture level (dB) at the wavelength of x mm (ref. = 10^{-6} m).

AL_f is sound absorption level at the frequency of f Hz.

The 12 output parameters are overall noise level and 1/3 octave band noise levels from 315 to 3150 Hz. The coefficient of determination (R^2) for the three models are presented in Table 61. In general, the more parameters are included, the more accurate the statistical model is.

Table 61: Coefficient of determination for the three models (Li et al., 2015 [613])

Model	$L_{A,eq}$	L_{315}	L_{400}	L_{500}	L_{630}	L_{800}	L_{1000}	L_{1250}	L_{1600}	L_{2000}	L_{2500}	L_{3150}
1	0.87	0.68	0.76	0.82	0.87	0.90	0.92	0.89	0.82	0.94	0.84	0.90
2	0.66	0.49	0.53	0.66	0.85	0.82	0.72	0.65	0.59	0.71	0.78	0.81
3	0.80	0.70	0.77	0.81	0.87	0.85	0.87	0.80	0.74	0.89	0.93	0.89

5.3.4 Fuzzy Curve Fitting Models

A fuzzy curve fitting model is used to solve a nonlinear complex system by a few simple "If...Then" fuzzy rules (Roychowdhury, 1998 [846]). The increase of such rules gives a better modeling capability, especially with the advancement of computer technology. The advantage is that no specific form of equations is needed to fit the parameters. The fuzzy logic imitates the human learning process, and has a couple of derivative applications, such as artificial neural network (ANN), neuro-fuzzy system, and fuzzy genetic arithmetic (F-GA), which will be discussed in the following. In this sense, the fuzzy curve fitting model can also be called neural computation model.

5.3.4.1 Fry et al. (CPB ANN, 1999)

Fry et al. developed an Artificial Neural Network (ANN) model to correlate vehicle design parameters with vehicle Controlled Pass-By (CPB) noise (Fry et al., 1999 [50]; Fry and Jennings, 2003 [847]).

According to ISO 362 [104,105], the vehicle enters the test track with an initial speed of 50 km/h, then drives through at 100% acceleration. The measurements are conducted in both directions, in 2nd and 3rd gear, while the maximum sound pressure level (Max_{2nd} and Max_{3rd}) is recorded for each test run. The final average drive-by noise level *DBN* is given by

$$DBN = \frac{Max_{2nd} + Max_{3rd}}{2} - 1 \text{ dBA} \tag{207}$$

The input parameters of the ANN model cover seven functional categories: powertrain, intake, exhaust, tire, test conditions, engine bay and vehicle performance. The binary and categorical inputs were encoded to numeric values. 75 were on the short list refined from over 200 parameters by five vehicle noise experts. Unfortunately, the details on these parameters were not published. The only one output of the ANN model is the pass-by noise level.

The suggested number of hidden neurons for an *I-J-K* ANN with *I* inputs, *J* hidden neurons and *K* output neurons is given by (Tarassenko, 1998 [848])

$$J = \sqrt{IK} \tag{208}$$

The number of examples *N* should not be too small in order to capture the trend of the data, but also not too large in order to avoid over-training or over-fitting when the ANN tries to fit the random noise. The rule of thumb is

$$\begin{aligned} W &= (I+1)J + (J+1)K \\ N &= (3 \sim 30)W \end{aligned} \tag{209}$$

where *W* are the number of free variables including weights and biases. As such, the lower limit of number of examples is

$$N_{lower} = 3\sqrt{IK}\left(I + K + \sqrt{\frac{K}{I}} + 1 \right) \tag{210}$$

Usually, *K* is much smaller than *I*, the equation becomes

$$N_{lower} \approx 3I^{1.5}K^{0.5} \tag{211}$$

where it is indicated that *I* is more important than *K*. So at least 2000 test runs were needed, which was barely enough in the beginning (2064 examples) before more data was collected (Fry et al., 1999 [50]). In order to reduce the number of parameters, the ANN was divided into two sub-models, as shown in Figure 114.

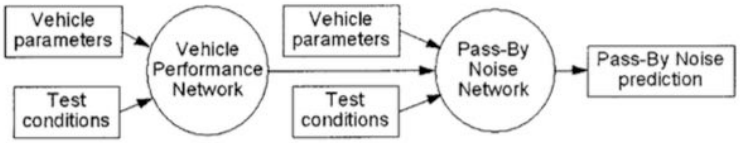

Figure 114: Two-stage ANN Models for pass-by noise (source from Fry and Jennings, 2003 [847], Figure 3; reprinted with permission from Springer)

The vehicle acceleration was firstly used as the output of vehicle performance network (20-5-1) with a mean percentage error (MPE) of ±7% (R^2 = 0.9) (Fry et al., 1999 [50]). Then the output was changed to engine speed at the exit of the test track, based on the fact that the pass-by noise has a strong correlation with the engine speed (9 dBA per 1000 rpm). The error was found to decrease to ±4.8%.

The type of neural network used is multi-layer perceptron (MLP), which is the most widely used. The training algorithm is error back-propagation, or back-propagation. 85% of published neural network applications were created using some variant of back-propagation (Wasserman, 1993, [849]). The corresponding algorithm in MATLAB is RPROP (Resilient Back-Propagation) where the inputs were transformed to zero mean and unit variance to avoid "stuck units" (Tarassenko, 1998 [848]). Both the logsig (logistic sigmoid) and tansig (hyperbolic tangent sigmoid) transfer functions in MATLAB were tried for the hidden neurons. The best network found for vehicle performance network and pass-by noise network is displayed in Table 62.

Table 62: Metrics for two-stage ANN Models for pass-by noise (Fry and Jennings, 2003 [847])

Sub-ANN	Structure	Set for Training and Validation	Set for Test	Accuracy
Vehicle Performance Network	25-15-1	2503 cases from 24 vehicles	997 cases from 13 vehicles	±4.8%
Pass-By Noise Network	58-19-1	4282 cases from 21 vehicles	1424 cases from 7 vehicles	±1.4%

This model provides insight into the vehicle acoustic performance in the early design stage before a prototype has been built, which saves a lot of costs and engineering efforts. The prediction error of the model is within ±1.4% (i.e., ±1.1 dBA for the noise limit of 74 dBA), which is better than the guess from experienced engineer (±3 dBA).

The model also works for diesel and turbo-charged vehicles but is not valid for automatic

transmission since its gear ratio will not be constant during the test. The authors also suggest a technique combining neural networks with Bayesian statistics, called Automatic Relevance Determination (ARD) to refine input selection [850] to potentially obtain better prediction accuracy.

5.3.4.2 Khazanovich and Izevbekhai (Pavement Aging, 2008)

Khazanovich and Izevbekhai (2008) [5] presented statistical equations to predict OBSI levels for different types of pavements using data from 51 test sections. All the tests were conducted using Standard Reference Test Tire (SRTT) (ASTM, 2014 [581]) at 97 km/h. The input parameters were Estimated Single Axle load (*ESAL*), pavement age (*Age*), International Roughness Index (*IRI*) and Surface Rating (*SR*).

The general equations have the following form,

$$I = ESAL^{\alpha} Age^{\beta} IRI^{\mu} SR^{\upsilon} \tag{212}$$

where I is the predicted OBSI sound intensity level, α, β, μ and v are model exponents. For different types of pavements, including asphalt pavements, Astro Turf drag, transversely tined whitetopping and Turf dragged whitetopping, these exponents have different values calculated by the universal Levenberg-Marquardt hybrid algorithm (LMA) of steepest-descent and least-squares non-linear model fitting technique. These minimization problems arise especially in least squares curve fitting. Some of examples are presented in Table 63. However, no global values for all pavements were presented.

Table 63: Exponents for Khazanovich Model (Khazanovich and Izevbekhai, 2008 [5])

Pavement Type	α (*ESAL*)	β (*Age*)	μ (*IRI*)	v (*SR*)
Cracked white topping	-0.0075	2.208	-0.0696	0
Bituminous (asphalt)	0.188	1.245	0.041	-0.025
Transversely tined	-0.00166	1.7678	-.001858	0

It was found that pavement aging increases TPIN on asphalt pavements but increases on rigid concrete pavements. It should be noted that pavement age does not have direct influence on TPIN, but it will affect *IRI* and *SR* due to texture degradation caused by traffic loads and environmental weathering.

In a later study (Izevbekhai, 2012 [851]), Izevbekhai dropped pavement age, *ESAL* and *SR* as the input parameter, but added temperature T, asperity interval measuring texture wavelength

ASP, texture direction relative to the traffic direction *DIR* (categorical variable, 0 or 1), texture depth *TD* and texture spikiness measuring texture amplitude *SP* (categorical variable, 0 or 1). The final equation is

$$I = A + B\left(\frac{293-T}{T}\right) + C\left(\frac{IRI}{IRIT}\right) + D\left[\left(\frac{ASPT}{ASP}\right)(D \times DIR + E)\right] + \left[\left(\frac{TD}{MPD}\right)(F \times DIR + G)\right] + \left[(SP)(J \times DIR + K)\right] \tag{213}$$

where capital letters *A*, *B*, *C*, *D*, *E*, *F*, *G*, *J*, *K* are model constants, *MPD* is the mean profile depth, and *IRIT*, *ASPT* are corresponding values at reference temperature. The errors for the model were found to be within 1.5 dBA for 90% of the field measurements. It was also found that Friction Number (*FN*) and Mean Profile Depth (*MPD*) are not significant parameters for TPIN levels.

5.3.4.3 Li et al. (F-GA, 2009)

Similar to Che et al. Model (ANN), Li et al. (2009) [726,852] used Fuzzy Genetic Arithmetic (F-GA) to statistically correlate tread pattern parameters with noise levels. The input tread pattern parameters include the width and length of tread block, the width and length of groove, the number of pattern strip, the basic number of pattern pitch, the pitch array and the pattern displacement. The output noise levels are the spectral area that excess a noise standard line (curve M) provided by American Test Center (ATC), as given below.

$$\delta = \sum_{i=1}^{k}\left(L_{p,i} - L_{p,i,M}\right) \tag{214}$$

where i is index for each frequency band, $L_{p,i}$ is the sound pressure level corresponding to specific tread pattern input, $L_{p,i,M}$ is the standard sound pressure level in curve M, and δ is the model output. It was claimed that the model successfully optimized the parameters of tread pattern for low noise tires utilizing fitness function iteration. Unfortunately, further details on the optimized parameters and the accuracy of the model were not reported.

It should be noted that both Che et al. Model (ANN) and Li et al. Model (F-GA) assumed tread pattern noise is independent of tread block shape (only size matters). Kumar et al. (2013) [853] utilized Multi-Objective Genetic Arithmetic (MOGA) to optimize tire tread pitch sequence accounting for several performance parameters (noise, handling and wear).

5.3.4.4 Che et al. (ANN, 2012)

Che et al. (2012) [586] utilized Artificial Neural Network (ANN) to correlate tire parameters

with tire noise. ANN is a powerful tool to solve complex and highly nonlinear problems, such as TPIN. Figure 115 shows a schematic representation of a typical neural network.

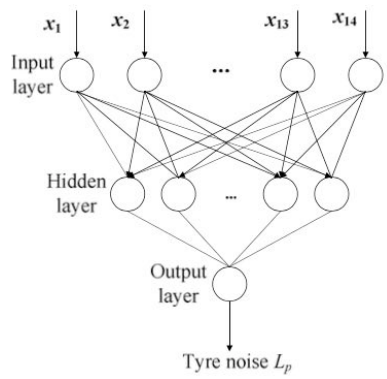

Figure 115: Schematic of a typical artificial neural network (ANN) (source from Che et al., 2012 [586], Figure 2; reprinted with permission from Trans Tech Publications Ltd)

Without getting into a detailed technical description, the ANN consists of multiple layers of neurons. A neuron can be mathematically interpreted as a non-linear transfer function controlled by weights. The ANN receives the input data (tire and pavement parameters) in the "Input layer". In the same way, the layer that outputs the results (noise spectrum in narrowband, 1/1 octave or 1/3 octave) is called "Output layer". In this study, the input and output parameters are shown in Table 64. It is noted that the tests were conducted using Laboratory Drum (DR) method (Yong et al., 2009 [854]), and the surface was considered constant, so there are no inputs of pavement parameters. The ANN statistical equation can be given as

$$L_p(f) = g\left(T_w, T_p, T_R, P_A, P_C, P_N, P_T, P_R, P_L, P_S, P_D, V, L, F\right) \tag{215}$$

where f is the center frequency of corresponding octave band.

Table 64: Input and output parameters of ANN (Che et al., 2012 [586])

	Parameter	Symbol	Description
Input	Tire Structure (Size)	T_w	Tire width
		T_p	Aspect ratio
		T_R	Tire radius
	Tread Pattern	P_A	Area of single-pitch tread pattern block
		P_C	Area of single-pitch tread pattern groove
		P_N	Number of tread blocks per pitch
		P_T	Total number of pattern pitch
		P_R	Arrangement rule of pitch
		P_L	Displacement (offset) between the pattern strips
		P_S	Symmetrical characteristics of tread patterns
		P_D	Groove depth
	Operation	V	Vehicle speed
		L	Tire load
		F	Inflation pressure
Output	Sound Pressure Level	$L_{p,125}$	Sound pressure level at the octave band of 125 Hz
		$L_{p,250}$	Sound pressure level at the octave band of 250 Hz
		$L_{p,500}$	Sound pressure level at the octave band of 500 Hz
		$L_{p,1000}$	Sound pressure level at the octave band of 1000 Hz
		$L_{p,2000}$	Sound pressure level at the octave band of 2000 Hz
		$L_{p,4000}$	Sound pressure level at the octave band of 4000 Hz

The layers between the input layer and output layer are commonly called hidden layers. The simplest neural network is composed of an input and an output layer. The hidden layers usually improve the capacity of the network to solve complex problems. This model had one hidden layer.

The number of neurons in the hidden layers does not follow any special rule and it is chosen by the user. If the number is too small, it will be difficult for the ANN model to capture all the relations. But if the number is too large, the time for training will increase and "over-match" problem might occur. It has the following empirical equation.

$$m = \sqrt{x + l} + \alpha \tag{216}$$

where m is the number of hidden neurons, x is the number of neurons in the input layer, l is the number in output neurons and α is a constant from 1 to 10. The study employed back-propagation (BP) network training based on genetic algorithms (GA) utilizing crossover and mutation operation to determine the number of hidden neurons (6), number of training epochs (6000), and the initial weights (global optimization).

While the network is trained, the bias and the connections (weights) between elements are adjusted. Given a specific input the network produces a specific output. Then, the output is

compared to an expected result or target. This process is repeated, adjusting the weights, until the difference between output and target reaches a desired error tolerance. In this study, the training data obtained from the tests were divided into two parts including training samples (50 groups) and test samples (10 groups). It is reported that the average error was 1.4%.

The main advantages of the ANN over non-linear regression analysis used by current hybrid methods are twofold. Firstly, no knowledge of the functional relationship between the input parameters and the noise spectrum output is needed. Secondly, the amount of data needed for training is less in the ANN than the non-linear regression. The ANN approach can be applied to various research areas.

The other study (Kostial et al., 2013 [216]) correlated the tire radial frequencies (output) with the tire structural parameters (input), such as the nominal width, profile number, rim diameter, load index and speed index. Further input parameters were also included, such as radial static stiffness, circumferential static stiffness, lateral static stiffness, static torsional stiffness. It was reported that the ANN results were qualitatively comparable with FEM simulations with a root mean square error of 4.314 Hz.

Another study (Kongrattanaprasert et al., 2009 [855]; Kongrattanaprasert et al., 2010 [708]) correlated the road surface states (output), such as snowy, slushy, wet, and dry states, with the measured tire noise of passing vehicles (input). An accuracy of approximately 90% was reported. A similar study (Kandpal et al., 2013 [856]) correlated the vehicle categories (output) with the measured noise (input).

For the interest, ANN was also applied for the tire contact optimization to improve the handling and wearing performance (Nakajima, 1999 [857]). The input is the sidewall and tread band contour; the output is the uniformness of contact pressure distribution. El-Gindy et al. (1999 [536], 2001 [858]) developed a tire/pavement contact-stress model based on an artificial neural network for truck tires. The input parameters included were vertical load and inflation pressure. No tire parameters were included, however, ANN models were developed for one radial-ply tire, and one bias-ply tire separately.

5.3.4.5 Yu and Lu (Bayesian, 2013)

Yu and Lu (2013) [859] developed empirical models for four asphalt pavements: dense graded asphalt contcrete (DGAC), open-graded asphalt concrete (OGAC), rubberised open-graded asphalt concrete (RAC-O), and rubberised gap-graded asphalt concrete

(RAC-G). The study presented two types of models: (1) overall model for all the asphalt pavements; (2) individual model for each type of asphalt pavement.

The noise data were collected for a span of four years (296 observations covering 74 sections), so certain observations and circumstances were missing or not considered unavoidably. To address this issue, a multiple imputation (MI) algorithm was used to capture the unobserved heterogeneity due to the absent or ignorance of relevant parameters. A Monte Carlo Markov chain (MCMC) sampling was used to deal with the panel structured data (Lu et al., 2009 [860]; Lu et al., 2010 [861]). Bayesian simulation was adopted to allow potential parameters to be random but in the meantime include all the existing knowledge. The noise level was measured using OBSI method (A-weighted, 500-5000 Hz). The final prediction equation for each pavement type was given by

$$OBSI = \alpha_0 + \alpha_1 \times Age + \alpha_2 \times AirVoid + \alpha_3 \times MPD + \alpha_4 \times AADTC + \alpha_5 \times Pre + \alpha_6 \times Thickness + \varepsilon \quad (217)$$

where *Age* is the number of years since open to traffic, *AirVoid* is the air void content (%), *MPD* is mean profile depth (μm, ASTM E1845 [633]), *AADTC* is average daily traffic on the main lane, *Pre* is the annual total precipitation (mm), *Thickness* is the thickness of surface mix (mm), ε is an error term; α_0 to α_6 are coefficients to be estimated, the results of which are in Table 65. For the overall model, the variable *Thickness* is replaced by *NewThickness* that equals the product of the thickness of the given surface mix and the corresponding probability for this mix to be chosen.

Table 65: Coefficients for Yu and Lu (Bayesian) Model (Yu and Lu, 2013 [859])

Coefficient	DGAC	OGAC	RAC-O	RAC-G	Overall
α_0 (Intercept)	103.6	101.2	102.5	101.1	101.4
α_1 (Age)	0.0137	0.177	0.07	0.187	0.083
α_2 (*AirVoid*)	-0.28	-0.12	-0.25	-0.25	-0.199
α_3 (*MPD*)	2.29×10^{-3}	7.11×10^{-4}	1.58×10^{-3}	2.55×10^{-3}	1.41×10^{-3}
α_4 (*AADTC*)	-3×10^{-5}	6.43×10^{-4}	1.55×10^{-4}	4.88×10^{-4}	1.33×10^{-4}
α_5 (*Pre*)	4.1×10^{-5}	2.17×10^{-4}	1.52×10^{-4}	4.2×10^{-5}	1.69×10^{-4}
α_6 (*Thickness*)	-0.029	-0.034	-0.02	-0.0276	-0.021

It was concluded that TPIN increases with pavement age and mean profile depth (MPD), and decreases with air void content. TPIN levels rank in ascending order as RAC-O < OGAC < RAC-G < DGAC. From Table 65, it was also seen that the ability to resist noise level (small α_1) increase with age ranks as RAC-O > OGAC > RAC-G. The efficiency of air-void content

increase for noise absorption (large absolute value of α_2) is DGAC > RAC-G > RAC-O > OGAC. The efficiency of mix thickness increase for noise reduction (large absolute value of α_6) is RAC-O > OGAC > DGAC > RAC-G.

5.3.5 Summary

The traditional regression models are summarized in Table 66. The regression analysis was most early applied to statistical TPIN modeling. It has been widely used for traffic noise prediction by government transportation agencies. Non-linear regression was dominant before the early 2000's, while linear regression has prevailed thereafter, likely because linear regression has easy forms and needs less data to improve the accuracy. Besides pass-by noise measurement, more advanced and professional noise measurement techniques, such as on-board sound intensity (OBSI), have been frequently used, where the 1/3 octave band noise spectrum was typically the output with large frequency range of 500-5000 Hz. The vehicle speed was usually included in the modeling. Unlike most deterministic models, however, tire load or other tire parameters were not of much interest. Various types of pavement parameters were included, such as pavement type, slope, texture, friction, age, and wetness. Environmental parameters were also of more interest, such as temperature and wind. However, the traditional regression model was unlikely to give insight into noise generation mechanism or separate them.

The principal component analysis models are summarized in Table 67. The input and output parameters of the model are similar to those of the traditional regression model. The principal component regression is more advanced than linear or non-linear regression, and may include more input parameters in one model.

The fuzzy curve fitting models are summarized in Table 68. Fuzzy logic technique, such as artificial neural network, has been widely applied to various engineering problems, including TPIN modeling, since the late 1990's. The input and output parameters are similar to those of the regression models. The tire parameters, however, such as tread pattern, are more commonly included as input parameters.

Table 66: Summary of traditional regression models on TPIN

No.	Author	Model Name	Year	Ref.	Method	Output	Frequency Range [Hz]	Mechanism	Driver Parameter	Tire Parameter	Pavement Parameter	Environment Parameter
1	BMVI	RLS (Germany)	1990	821	Non-linear Regression	Pass-by, L_{eq}	N/A	Traffic	Speed, vehicle type	N/A	Slope	Propagation attenuation
2	CNR	CNR (Italia)	1991	823	Non-linear Regression	Pass-by, L_{eq}	N/A	Traffic	Speed, vehicle type	N/A	Slope	Propagation attenuation
3	FHWA	TNM (US)	1998	825	Non-linear regression	Pass-by, 1/3 octave	500-5000	Vehicle and traffic	Speed, vehicle type, acceleration	N/A	Type	N/A
4	Hanson and James	Dense Graded	2004	108,585	Non-linear Regression	CPX, CPI, OASPL	N/A	TPIN	72 km/h	N/A	FM, voids, age	N/A
5	Rasmussen	Concrete Texture	2009	580	Linear regression, bridging filter	OBSI, 1/3 octave	500-5000 630-1000	Texture impact	Buick Century, 97 km/h	SRTT	Texture, skewness	N/A
6	Fujikawa et al.	Asperity	2009	218	Linear regression	BTT, OASPL, octave	500-4000	TPIN	80 km/h, 3.2 kN, 170 kPa	185/65R15, rib pattern	Asperity spacing, asperity height unevenness, MPD	N/A
7	Reyes and Harvey	Pavement Core	2011	639	Linear regression	OBSI, 1/3 octave, OASIL	500-5000	TPIN	N/A	SRTT	Airflow resistance, MPD	N/A
8	N/A	CNOSSOS (EU)	2012	839	Non-linear Regression	Pass-by, L_w, octave	125-4000	TPIN, vehicle and traffic	Speed, vehicle type, acceleration	Studded	Type, age	Air temperature
9	Syamkumar et al.	Mode-wise	2013	6	Linear regression, sensitivity analysis	CPB, OASPL	N/A	TPIN	Speed, tire load, vehicle type	N/A	Type, wetness	Pavement temperature, wind direction
10	Wayson et al.	FDOT	2014	202	Linear regression	OBSI, OASIL, pass-by, OASPL	500-4000	TPIN	88 km/h 97 km/h	SRTT	FN, MPD, AG4	Wind < 4 km/h

Table 67: Summary of principal component analysis models on TPIN

No.	Author	Model Name	Year	Ref.	Method	Output	Frequency Range [Hz]	Mechanism	Driver Parameter	Tire Parameter	Pavement Parameter	Environment Parameter
1	Ongel et al.	Asphalt Pavement	2008	840	OLS, PCR	OBSI, OASIL	N/A	TPIN	97 km/h	SRTT	Various	Pavement temperature
2	Zhang et al.	MTD	2014	138,841	PCA Energy	BTT, energy	0-2000	TPIN	Speed	Same tire	MTD	N/A
3	Li et al.	Thin Surfacing	2015	613	Principal Component Regression	CPX, 1/3 octave band SPL, OASPL	315-3150	TPIN	80 km/h	N/A	Texture, MPD, absorption	N/A

Table 68: Summary of fuzzy curve fitting models on TPIN

No.	Author	Model Name	Year	Ref.	Method	Output	Frequency Range [Hz]	Mechanism	Driver Parameter	Tire Parameter	Pavement Parameter	Environment Parameter
1	Fry et al.	CPB ANN	1999	50	Resilient BP	CPB, OASPL	N/A	Vehicle	50 km/h (accel.), gear	Material, geometry, slick incl.	ISO 10844	N/A
2	Khazanovich and Izevbekhai	Pavement Aging	2008	5	Levenberg-Marquardt	OBSI, OASIL	N/A	TPIN	97 km/h	SRTT	Type, ESAL, Age, IRI, SR	30 °C
3	Li et al.	F-GA	2009	852	F-GA	Octave band SPL	125-4000	TPIN	N/A	Tread pattern	N/A	N/A
4	Che et al.	ANN	2012	586	GA-BP	DR, octave band SPL	125-4000	TPIN	Speed, tire load, inflation	Size, tread pattern	Standard surface	N/A
5	Yu and Lu	Bayesian	2013	859	Bayesian, MCMC, MI	OBSI, 1/3 octave band, OASIL	500-5000	TPIN	Traffic volume	N/A	Age, voids, MPD, thickness	Precipitation

5.4 Hybrid Models

5.4.1 Introduction

Hybrid model can generally be divided into deterministic sub-models and statistical sub-models. In the deterministic sub-models, physical preprocessing and conditioning of input quantities are conducted to acquire intermediate parameters as inputs to the following statistical sub-models. In most cases, the relations in the statistical sub-models can be significantly improved by including the preprocessing part of data. The purpose of hybrid models is to find a compromise between the level of physical detail and statistical accuracy. During recent years, the hybrid model seems to be more and more popular because it keeps the accuracy of statistical models and meantime gains insight like physical models.

In this section, 19 hybrid models were reviewed, including 9 tire-pavement interface models, 6 mechanism separation models, and 4 noise propagation models. The model name, method, output noise parameter with noise measurement technique, investigated noise generation mechanisms, and investigated input parameters of each model are listed and compared in tables as a summary in Section 5.4.5. The summary tables can be used as a reference for readers to direct to models of interest.

5.4.2 Tire-Pavement Interface Models

These models calculate the excitation characteristics of the interface between the tire and pavement within the contact patch. For example, the pavement texture is converted to what the tire actually sees with envelope technique. The contact force/pressure spectrum is then obtained for further analysis of the tire vibrations. TPIN is finally correlated with the contact force/pressure spectrum (intermediate parameters) using experimental data.

5.4.2.1 Fong (Truck Contact, 1998)

Fong (1998) [540] developed a model to predict near field sound pressure level from computed road surface texture induced contact pressure.

On-road measurements were conducted for 175/70R13 passenger tires (smooth and patterned), as well as 7.00R15 truck tires (radial and cross ply) at a constant speed of 45 km/h using an on-board sound pressure technique (OBSP). The model is one of the few that include

truck tires. The pavements were chipseal surfaces ranging from coarse textured Grade 2 to fine textured Grade 6 (MTD from 0.85 to 2.63 mm). The pavement texture was measured using laser profilometer (3mm sampling distance, 8 μm vertical resolution). Sound pressure was measured around the circumference of the rear right tire at four positions, one of which is close to the center of contact patch. The sound pressure was collected using microphones at 10 kHz with time duration of 104 seconds.

The contact pressure was calculated by assuming that the contact load due to the interaction with the texture asperities was equated to the tire inflation pressure. It was found that the contact pressure increased with the texture levels, as was expected.

Transfer functions were calculated between the output (sound levels) and input (contact pressure). It was found that the transfer functions were independent of the pavement textures, which means the key factor that influence tire noise was actually contact pressure. A good agreement was obtained between the predicted and measured noise levels, generally within 2 dBA across all the frequencies.

5.4.2.2 Domenichini et al. (DGAC Texture, 1999)

The model (Domenichini et al., 1999 [63]) characterized the dense graded asphalt concrete (DGAC) pavement texture and related it to the near field and far field TPIN. The wearing course porosity and thickness of the surface layer were kept constant or ignored in the study. The study was part of TINO research program, the other task of which was to identify the relationship between the mix composition and the pavement texture (D'Andrea, 1999 [862]). Combining the two studies, it will be potential to control TPIN at the pavement design phase, such as the selection of aggregate type/shape/dimensions, aggregate grading curve and the binder type.

11 types of pavements were tested including one porous pavement as a reference and two TINO prototype pavements. The texture measurement was according to ISO 13473-2 (2002) [863] and Italian standard CNR BU 125/88: (1) micro-texture was measured by British Portable Pendulum (low speed friction test); (2) macro-texture was measured by TINO 3D profilometer; (3) mega-texture was measured by TINO 3D profilometer (2-2000 cycle/m or 0.5-500 mm) and "Dipstick" walking profilometer (0.014-3.33 cycle/m, or 0.3-70 m).

Both far field noise tests and near fields tests with four microphone positions were conducted. Two tires were tested (a slick tire and a normal tire) at two speeds (50 km/h and 80

km/h). The correlation between the texture at different spatial frequency (cycle/m) and noise levels at different frequency (Hz) is represented in the form of correlation chromatic plots as shown in Figure 116. The absolute values between 0.75 and 1 indicate good correlations.

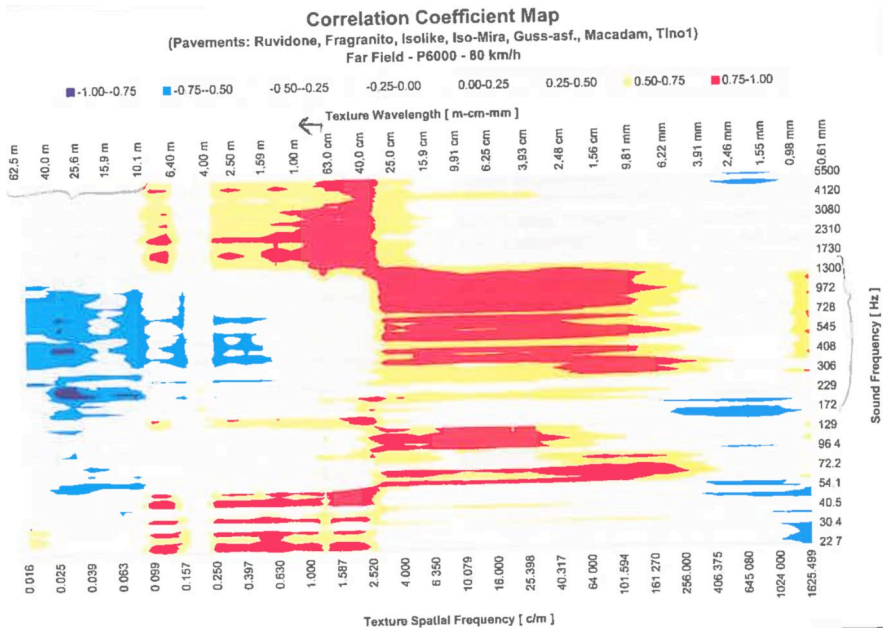

Figure 116: Example of pavement texture - rolling noise correlation chromatic plot (source from Domenichini et al., 1999 [63], Figure 10; reprinted under fair use provision)

The preliminary model was to correlate the near field noise with the Huschek coefficient or Huschek texture index (Huschek, 1996 [611]) ($R^2 = 0.79$). However, the Huschek coefficient didn't account for the pavement unevenness. As a result, a new Texture Index (TI) was proposed and given by

$$TI = 2.5 \cdot PSP + L_{UNE} \tag{218}$$

where *PSP* is the "Peak-Slope Parameter" given by

$$\begin{cases} PSP = \dfrac{L_{PEAK} \cdot i}{100} \\ L_{PEAK} = \dfrac{l_{fPEAK^-} + l_{fPEAK} + l_{fPEAK^+}}{3} \end{cases} \tag{219}$$

L_{PEAK} is the first peak of the texture level above the wavelength of 2 mm (or below the spatial frequency of 500 cycle/m), smoothed over the nearest three spectral lines, as

illustrated in Figure 117. Subscript *fPEAK* is the spatial frequency corresponding to wavelength $\lambda PEAK$ where the peak occurs. Subscripts $fPEAK^-$ and $fPEAK^+$ are the previous and following spatial frequencies respectively. l_{xx} indicates the texture level at the spatial frequency of *xx* cycle/m.

i is the slope of descending portion above *fPEAK* in the macro-texture region and given by

$$i = \frac{L_{PEAK} - L_{500}}{\log_{10}(\lambda PEAK) - \log_{10}(2)} \tag{220}$$

where L_{500} is the texture level at the spatial frequency of 500 cycle/m (wavelength of 2 mm) smoothed over the nearest three spectral lines.

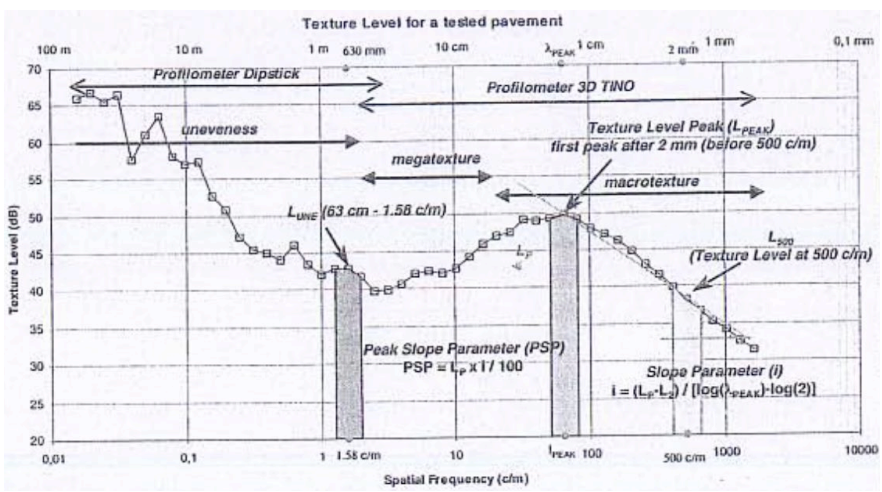

Figure 117: Texture index (TI) illustration for Domenichini et al. Model (source from Domenichini et al., 1999 [63], Figure 14; reprinted under fair use provision)

L_{UNE} is the Unevenness Level and given by

$$L_{UNE} = \frac{l_{1.26} + l_{1.58} + l_{2.00}}{3} \tag{221}$$

As such, the L_{UNE} represents the average texture level centered on 630 mm (500-800 mm).

The final regression equations for the far field sound pressure level at 50 km/h and 80 km/h are

$$\begin{cases} SPL_{50\ \text{km/h}} = 0.47 \cdot TI + 42.94 \\ SPL_{80\ \text{km/h}} = 0.47 \cdot TI + 49.39 \end{cases} \tag{222}$$

where $R^2 = 0.91$.

5.4.2.3 Beckenbauer and Kuijpers (SPERoN, 2001)

Beckenbauer and Kuijpers (2001) [487] developed a statistical and physical model to predict coast-by (CB) noise levels based on pavement parameters. The model is called SPERoN, which is short for Statistical Physical Explanation of Rolling Noise. The noise data were based on the "Sperenberg project" (Influence of the road surface texture on the tyre-road noise) for Federal Highway Research Institute of Germany (BASt), which included coast-by spectra of 840 tire-pavement combinations (21 dense surfaces; 12 normal, 2 slick and 2 grooved passenger car tires) at speed of 50-120 km/h. The coast-by noise was measured 7.5 m away from the center of the vehicle, 1.2 m above the ground.

The model was developed on a stepwise basis, which means one additional input variable was included to expand the model for each step and multivariate regression analysis was employed. The following requirements have to be met for each step: (1) the variables are independent; (2) the addition of new variable has to increase the coefficient of determination R^2; (3) the influence of the variables on the noise spectra must be explainable physically. The final equation of the model includes four input variables ($R^2 = 0.8$): speed, frequency transformed contact pressure spectrum, tire width and shape factor, given as below.

$$L_{pAF,i} = c_{vAF,i} \cdot 10\log_{10}\left(\frac{v}{v_0}\right) + c_{cAF,i} \cdot L_{cF,i} + c_{wAF,i} \cdot w + c_{gAF,i} \cdot L_g \tag{223}$$

where the subscript i is the index for the third octave band; $L_{pAF,i}$ is A-weighted sound pressure level in dB, v is the vehicle speed in km/h, v_0 is the reference vehicle speed (80 km/h), $L_{cF,i}$ is level of the frequency transformed contact pressure in dB, w is the tire width in mm, L_g is the shape level in dB; $c_{vAF,i}$ is regression coefficient for the speed term, $c_{cAF,i}$ is the regression coefficient for the contact pressure term, $c_{wAF,i}$ is regression coefficient for the tire width term, $c_{gAF,i}$ is the regression coefficient for the shape level term.

The model is hybrid, because input parameters $L_{cF,i}$ and L_g are not available at the beginning but deterministically calculated based on other tire-pavement parameters, as shown in Figure 118.

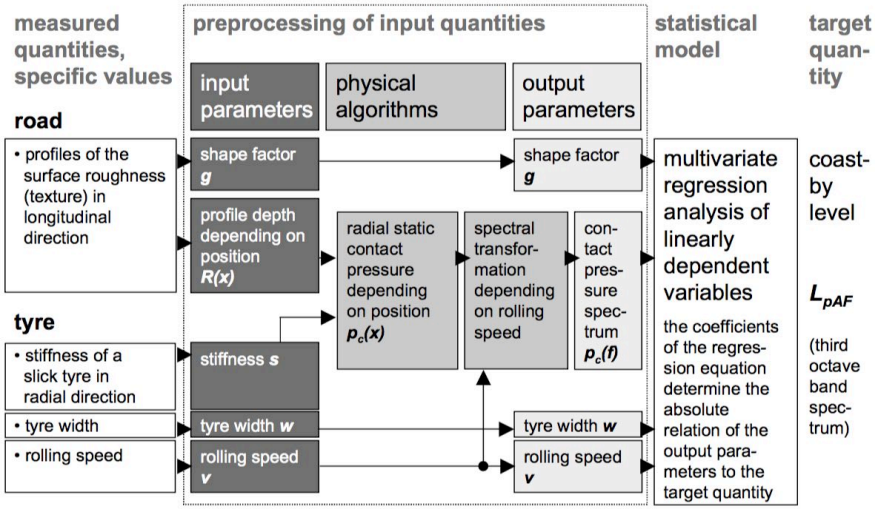

Figure 118: Scheme of SPERoN Model (source from Beckenbauer and Kuijpers, 2001 [487], Figure 1; reprinted under fair use provision)

The shape factor g is derived from the Abbot curve and used to identify convex and concave (or positive and negative) textures. As illustrated in Figure 119(a), a shape factor of 25% in convex shape means if an imaginary horizontal plane is lowered from the top of the surface by $R/2$, it will be in contact with 25% (PCL, percentage contact length) of the texture. The linear scale shape factor g has the following relation with the log scale shape level L_g (dB).

$$L_g = 20\log_{10}\left(\frac{g}{1\%}\right) \tag{224}$$

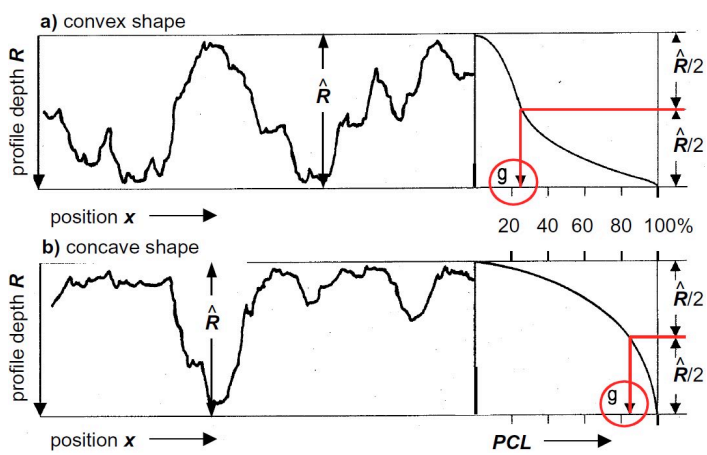

Figure 119: Illustration of shape factor (a. asphalt with surface dressing; b. hot rolled asphalt) (source from Beckenbauer and Kuijpers, 2001 [487], Figure 2; reprinted under fair use provision)

The contact pressure distribution was calculated based on the algorithm Clapp et al. (1988) [864]. A contact patch length of 100 mm was assumed for a stationary tire. The contact pressure $p_c(x)$ as a function of longitudinal position x was derived from the pavement texture profile and the average tire tread radial stiffness s. Assuming the tire rolling speed is v, the spatial domain of contact pressure was transformed to time domain.

$$p_c(t) = p_c\left(\frac{x}{v}\right) \tag{225}$$

Then the frequency domain of the contact pressure $p_c(f)$ was obtained using Fourier transformation of $p_c(t)$. The linear scale $p_c(f)$ has the following relation with the log scale level of contact pressure $L_{cF}(f)$ in dB.

$$L_{cF}(f) = 20\log_{10}\left(\frac{p_c(f)}{p_{c0}}\right) \tag{226}$$

where $p_{c0} = 10^{-6}$ N/m^2. It was concluded that the spectral energy between 800 and 1250 Hz decreases as the speed increases, especially for rough pavement, as shown in Figure 120(b).

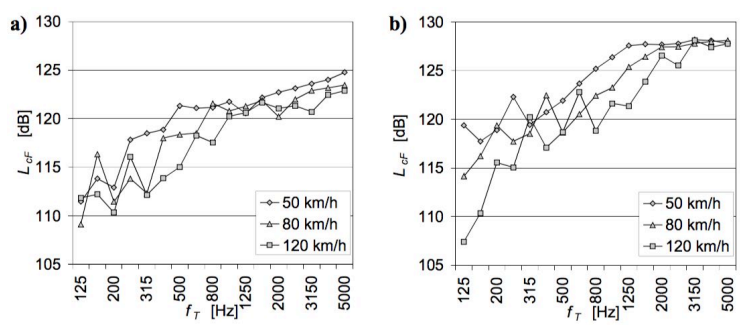

Figure 120: Contact pressure level spectra for different speed (a. stone mastic asphalt 0/8; b. surface dressing 3/5) (source from Beckenbauer and Kuijpers, 2001 [487], Figure 3; reprinted under fair use provision)

The results for coefficient of determination R^2, the regression coefficient for the shape level term c_{gAF}, and the regression coefficient for the speed term c_{vAF} were shown in Figure 121. It can be seen in Figure 121(a) that slick tires have the highest coefficient of determination ($R^2 \approx 0.9$) for most of frequencies, while for the patterned tires, the values are relatively low, especially in the range of 400-800 Hz ($R^2 \approx 0.7$) where tread impact were

assumed to take more effect. It is also concluded that the introduction of shape level L_g improves the reliability (R^2 increases by 0.04) especially at low frequencies. In Figure 121(b), Beckenbauer and Kuijpers (2001) [487] also concluded that the shape level L_g is independent of other input variables such as the level of the frequency transformed contact pressure L_{cF} because different values of L_g do not change the contact pressure regression coefficient c_{cAF}.

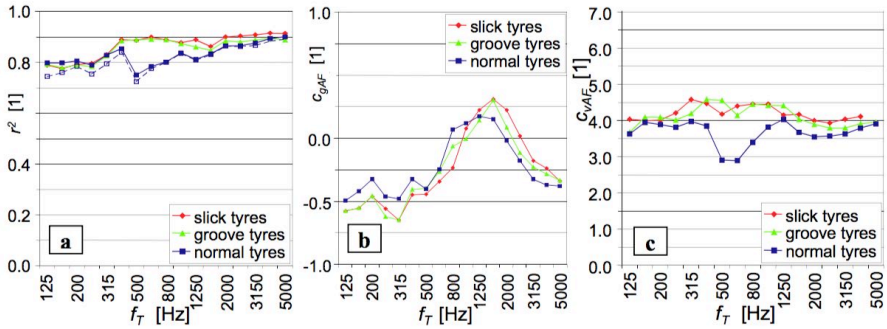

Figure 121: (a) Coefficient of determination R^2, (b) regression coefficient for the shape level c_{gAF} and (c) regression coefficient for the speed term c_{vAF} depending on third-octave canter frequency f_T. Parameter: type of tire. The dashed line in (a) is valid for the statistical model without the variable L_g (shape level) for patterned tires. (Source from Beckenbauer and Kuijpers, 2001 [487], Figure 4; reprinted under fair use provision)

In Figure 121(c), $c_{vAF,i}$ can be considered as speed exponent and indicates the type of noise and corresponding generation mechanism. For slick tires, the speed exponent is above 4, indicating air pumping as the dominant mechanism. For patterned tires, speed exponent is much lower, especially in the range of 400-800 Hz ($c_{vAF} \approx 3$), again indicating tread impact mechanism.

In summary, the first version of SPERoN has the best predictability for slick tires, relatively good for groove tires, but only fair for normally profiled tires. More strictly speaking, the model is only valid on dense pavements with isotropic textures for slick tires.

5.4.2.4 Kuijpers and Blokland (Enhanced SPERoN, 2003)

Kuijpers and Blokland (2003) [865] enhanced the SPERoN model by including the effects of tire tread profiles. The original goal of SPERoN model was to evaluate acoustic performance of pavements, and to develop low-noise pavements rather than low-noise tires. After the incorporation of tread profile parameters, the model became more universal and unified.

In the Enhanced SPERoN model, the contact model is illustrated in Figure 122. The tread

profile was divided into parallel slices across the tire width. Static contact pressure distribution $p_c(x, y)$ for each slice at the lateral position of y was calculated using the corresponding tread profile and pavement texture profile with the same algorithm Clapp et al. (1988) [864]. The texture profile was assumed to be identical for all slices, i.e., 2D texture profile and 3D tread profile. Then the contact pressure in the frequency domain for each slice $p_c(f, y)$ was calculated using Fourier transformation. The input parameter $p_c(f)$ for the later statistical regression model was the average of $p_c(f, y)$ for all slices.

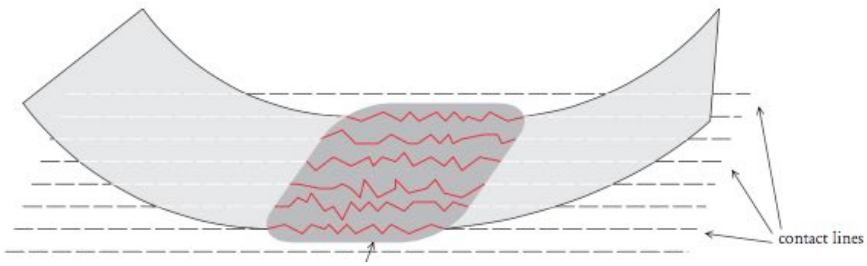

Figure 122: 3D contact model in Enhanced SPERoN Model (source from Kuijpers and Blokland, 2003 [865], Figure 1; reprinted under fair use provision)

It was concluded that the introduction of tread profile parameters reduced the prediction error by about 0.25 dBA between 500 and 1000 Hz. The tests were conducted on a very smooth grinded concrete surface with a specific profiled tire, where tire profile was assumed to have more importance. However, the model prediction ability decreases at other frequencies (125-400 Hz and 1000-1500 Hz).

When it came to all tires with different tread profiles (slick, grooved and normal), the overall prediction ability improves (prediction error decreases by about 0.5 dBA) over the entire frequency range above 400 Hz. As such, it is confident to say, as a unified model for all types of passenger car tires, the Enhanced SPERoN is promising.

The enhanced SPERoN also includes pavement mechanical impedance and tire rubber hardness as input parameters for the statistical regression model. In the same study, the static contact model was compared with the dynamical contact model by Kropp et al. (2001) [866], where the variation of contact stiffness was substituted for tire profile effect. To be more specific, if the contact area becomes smaller due to tread profile changes, the deformation amplitude increases, i.e., the contact stiffness decreases. It was seen that the static contact

model and dynamical contact model gave comparable results, and a speed exponent of 3 in the dominant frequency range was predicted for both models.

However, it should be noted that Kuijpers and Blokland (2003) [865] also concluded that tread profiles do not have influence on the rating of pavement acoustic qualities. As such, one should be careful before using this Enhanced SPERoN model, because tread profile analysis is very complicated and time consuming.

As another enhancement for SPERoN, Blokland and The (2007) [867] included more types of pavements other than dense surfaces. Several further development attempts were performed by Chalmers and Müller-BBM within the German project "Quiet Traffic", the EC 6th framework project ITARI and the DEUFRAKO project P2RN [332]. The information on the new advanced model (Version 3.0) can be found in Table 69. This advanced model includes four TPIN mechanisms, i.e., vibration due to impact (p_{vibr}^2), airflow due to air pumping ($p_{airflow}^2$), cavity due to cavity resonance (p_{cavity}^2) and aerodynamic noise due to air turbulence ($p_{aerodyn}^2$). The mean square value of coast-by sound pressure $p_{coast\text{-}by}^2$ is given by

$$\begin{cases} p_{coast\text{-}by}^2 = p_{vibr}^2 + p_{airflow}^2 + p_{cavity}^2 + p_{aerodyn}^2 \\ p_{vibr}^2 = aF_c^2\Gamma^{\alpha_1}B^{\alpha_2}S^{\alpha_3} \\ p_{airflow}^2 = b\left(F_c^2\Gamma^{-1.5}S^{-2}\right)^{\beta_1} B^{\alpha_2}V^4 \\ p_{cavity}^2 = cG_{pattern}^{\gamma_1} \\ p_{aerodyn}^2 = dV^{\delta_1} \end{cases} \tag{227}$$

where a, b, c, and d are regression coefficients for corresponding 3rd octave band, α_1, α_2, α_3, β_1, γ_1, δ_1 are exponents; F_c is the contact force in N, Γ is the contact air flow resistance in Pa·s/m, B is tire width in m, S is tire tread stiffness in N/m, $G_{pattern}$ is spectral power for the tread pattern variation, V is vehicle speed in m/s.

The most recent version of SPERoN also included parameters of acoustic absorption and mechanical impedance.

5.4.2.5 Klein and Hamet (HyRoNE, 2007)

Very similar to SPERoN, HyRoNE (Hybrid Rolling Noise Estimation) developed by Klein and Hamet (2007) [443] is also a hybrid model to predict pass-by noise levels as operational tools with small computation effort . The work was performed by INRETS (Hamet and Klein, 2004 [868]) and LCPC in the French PREDIT project "Texture&Bruit" and in the DEUFRAKO

project P2RN (Beckenbauer et al., 2008 [332]).

Both the HyRoNE and SPERoN physically analyze the raw texture of the road surface and convert it to relevant roughness parameter that is actually "seen" by the tire. The difference is, the former uses shape factor, the latter uses the method of envelopment before spectral analysis. The envelopment procedure is based on a static contact model between the pavement texture and an elastic half space representing the tire rubber [869], as shown in Figure 123. The tire rubber is characterized its Young's modulus *E*. In the texture profile processing, the long wavelength above 1 m and possible upward peaks are removed.

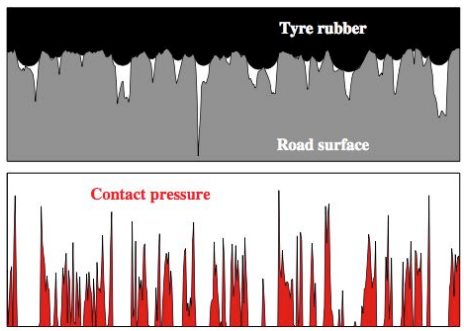

Figure 123: Illustration of envelopment procedure in HyRoNE Model (Beckenbauer et al., 2008 [332], Figure 5; reprinted with permission from Mr. Philippe Herzog on behalf of SFA, France)

Another important difference from SPERoN is HyRoNE also addresses attenuation mechanism (pavement absorption). HyRoNE mainly includes two TPIN mechanisms, tire vibration (100-1250 Hz) and air pumping (1250-5000 Hz), which are clearly separated in the physical and statistical sub-models.

In general, SPERoN is more complicated and universal than HyRoNE. A comparison between the SPERoN and HyRoNE Models is displayed in Table 69 (Beckenbauer et al., 2008 [332]; Klein et al., 2008 [870]).

Table 69: Comparison between SPERoN and HyRoNE Models (Beckenbauer et al., 2008 [332]; Klein et al., 2008 [870])

	SPERoN	HyRoNE
Vehicle and Tire	Passenger car tires (34 types), truck tires (Kuijpers et al., 2007 [871])	One vehicle/tire combination (Renault Scenic 2.0 with Michelin Energy XH1/E3A tires)
Pavement Parameter	Airflow resistance, shape factor	Acoustic absorption, porosity, shape factor and the airflow resistance, porous layer thickness
Texture Profile	Quasi 3D texture (more than six 2D texture profiles of the pavement in parallel, 2 m for each, covering 100 mm width in total, 1 mm resolution)	12 independent profiles (evenly distributed on both sides of the noise measurement point and characterize a 12-m long section, 6 profiles on each wheel track spaced by 1 m)
Texture Analysis	Shape factor	Envelopment
Tire Parameter	Tire type, load, tension, bending stiffness in circumferential and cross direction, tread stiffness (shore hardness) and tread pattern, the radial, uncoupled contact forces, inflation pressure	One specific tire (Michelin Energy XH1/E3A)
Tire Model	Impulse response functions	One specific tire (Michelin Energy XH1/E3A)
Contact Model	Average 3rd octave band spectrum of the contact forces	Envelopment before spectral analysis
Speed	As input parameter, arbitrary between 30-120 km/h	Three nominal speed: 70, 90, 110 km/h
Limitation	Dense pavements*	Isotropic or quasi-isotropic surface
Output	Coast-by, 1/3 octave	Controlled pass-by, 1/3 octave
Accuracy	Maximum 2-dBA error	±2.4 dBA, ±2.0 dBA, ±2.1 dBA at 70, 90, 110 km/h
Computing Time	210 sec (69-120 km/h); 330 sec (50-68 km/h)	25 sec (110 km/h); 45 sec (90 km/h); 65 sec (70 km/h);
Software Application	Windows (Version 3.0), results in xml file	Windows (Version 1.0), results in xls file
Application	Design of existing or artificial surfaces, at laboratory or test track scale	Procurement process and in-situ monitoring at road scale

* The most recent version of SPERoN included acoustic impedance, so it was also applicable to porous pavements.

5.4.2.6 Rustighi et al. (Road Excitation, 2008)

Rustighi et al. (2008) [872–877] developed a three-dimensional elemental model to predict the stochastic tire vibration due to tire/road excitation and the interior and exterior noise.

In this model, it is assumed that a smooth soft tire travelling over a road that is not too rough. The interaction between tire and the ground is modeled as a linear Winkler bedding (Johnson, 1985 [878]). The force **f** on the finite elemental (FE) points within the contact patch, as illustrated in yellow circles in Figure 124, is given by

$$\mathbf{f} = \mathbf{K}(\mathbf{d} - \mathbf{w}) \tag{228}$$

where **d** is the road vertical displacement, **w** is the tire vertical displacement, **K** is the linear contact stiffness matrix. The nodal displacement vector **v** is governed by

$$\left[\mathbf{K}_2 \frac{\partial^2}{\partial \phi^2} + \mathbf{K}_1 \frac{\partial}{\partial \phi} + \mathbf{K}_0 - j\omega\mathbf{G} - \omega^2\mathbf{M}\right]\mathbf{v}(\phi,\omega) = \mathbf{f}(\phi,\omega) \tag{229}$$

where ϕ is the tire circumferential angular coordinate, ω is radian frequency, $\mathbf{K}_2$, $\mathbf{K}_1$, $\mathbf{K}_0$ are elastic force matrices, **M** is the inertial force matrix, **G** is the fluid-structure coupling matrix. In the frequency domain, the road vertical displacement **d** is expressed as excitation spectral density $S_d(f)$ given by

$$S_d(f) = \frac{c}{v}\left(\frac{f}{v}\right)^{-2.5} \tag{230}$$

where f is the excitation frequency in Hz, c is a constant, v is vehicle speed. A two-dimension Gaussian model is used to represent a road surface of which the roughness is homogeneous and isotropic (Robson, 1979 [879]). This approximation is experimentally determined, which is the reason this model falls under the category of hybrid models.

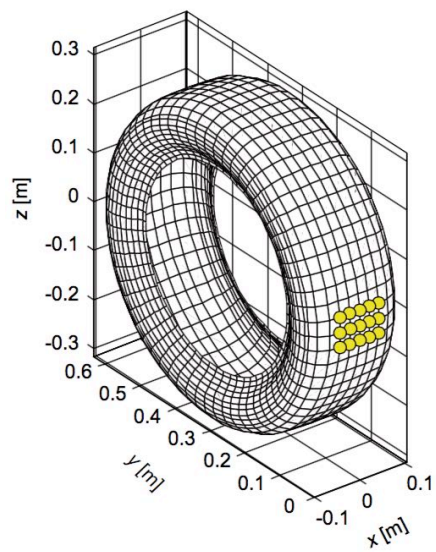

Figure 124: Mesh used for the tire model. The circles indicate the chosen contact points. (Source from Rustighi et al., 2008 [874], Figure 2; reprinted with permission from Elsevier)

The calculated root mean square (rms) velocity of the tire wall and tread surface is shown in Figure 125.

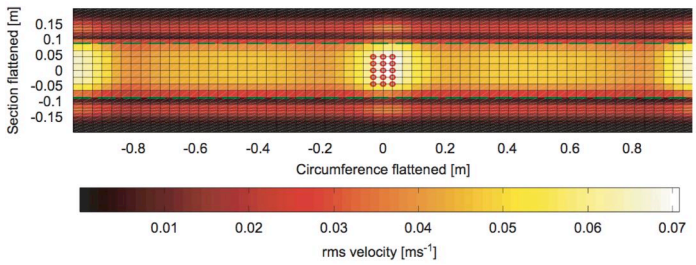

Figure 125: Root mean squared velocity of the tire elements at 80 km/h. Note that distances ±0.1 m in the radial direction correspond to the tread section of the tire and from ±0.1 to ±0.2 m to the sidewalls. (Source from Rustighi et al., 2008 [874], Figure 7; reprinted with permission from Elsevier)

The calculated sound pressure level (SPL) is shown in Figure 126.

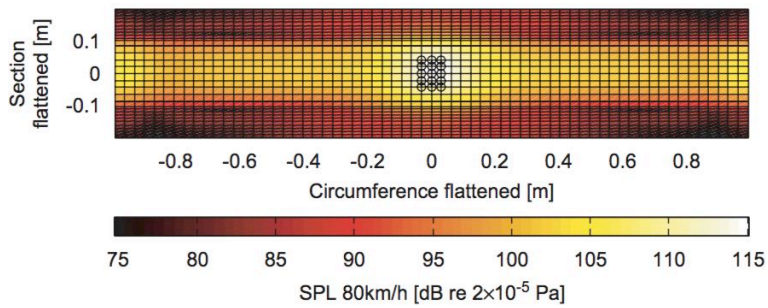

Figure 126: The sound pressure level (SPL) calculated at the surface of the tire elements at 80 km/h (source from Rustighi et al., 2008 [874], Figure 9; reprinted with permission from Elsevier)

The calculated interior sound pressure level at the eight earing points inside the car cavity is shown in Figure 127. The peaks around 60 Hz and 100 Hz may correspond to the first two internal air cavity resonances of the car while the obvious peak at about 230 Hz could be related to the first tire cavity resonance mode.

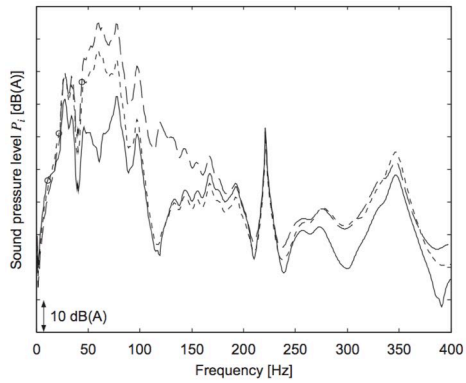

Figure 127: Sound pressure level at the 8 passenger ears at 20 (continuous line), 40 (dotted line) and 80 (dashed line) km/h (source from Rustighi et al., 2008 [874], Figure 13; reprinted with permission from Elsevier)

5.4.2.7 Dubois et al. (Viscoelastic Contact, 2011)

The model [61,880–883] investigated the frictionless viscoelastic contact between a viscoelastic half-space (tire) and a rigid rough multi-indenter surface (pavement) using macro-scale approach (Cesbron et al., 2011 [881]).

The viscoelastic behavior of tire has to be taken into account due to the time-dependent behavior of rubber and large contact area including many road asperities varying in position during rolling. The viscoelastic contact law for the kth asperity was described in terms of convolution integral according to Radok's technique as shown below.

$$P_k(t) = \int_0^t \psi(t-\tau) \frac{d}{d\tau}\left[f_k\left(\delta_k(\tau)\right)\right] d\tau \tag{231}$$

where P_k is the contact force on the summit of the kth asperity, ψ is the relaxation function, f_k the elastic force-displacement law of the kth asperity and δ_k is the local approaching displacement.

Then the TPIN levels were statistically correlated with the contact forces calculated above. The linear regression equation is

$$L_N\left(f_{to}\right) = a_j L_F\left(f_{to}\right) + b_j \tag{232}$$

where L_N is TPIN level, L_F is contact force in the frequency domain, f_{to} is the center frequency of each third-octave band, a_j and b_j are regression parameters. TPIN levels and contact forces are positively correlated in the frequency range 315-1000 Hz ($R^2 = 0.93$, better than the correlation between TPIN levels and pavement texture).

It was found that the viscoelastic contact forces are greater than those using elastic contact

method, and the contact duration is shorter, which fits better with the experiments and gives better prediction for tire noise.

A previous study (Cesbron et al., 2009 [884]) correlated the pavement texture spectrum, contact force spectrum, and the noise level spectrum in 1/3 octave band for a slick tire on six different pavements, as shown in Figure 128.

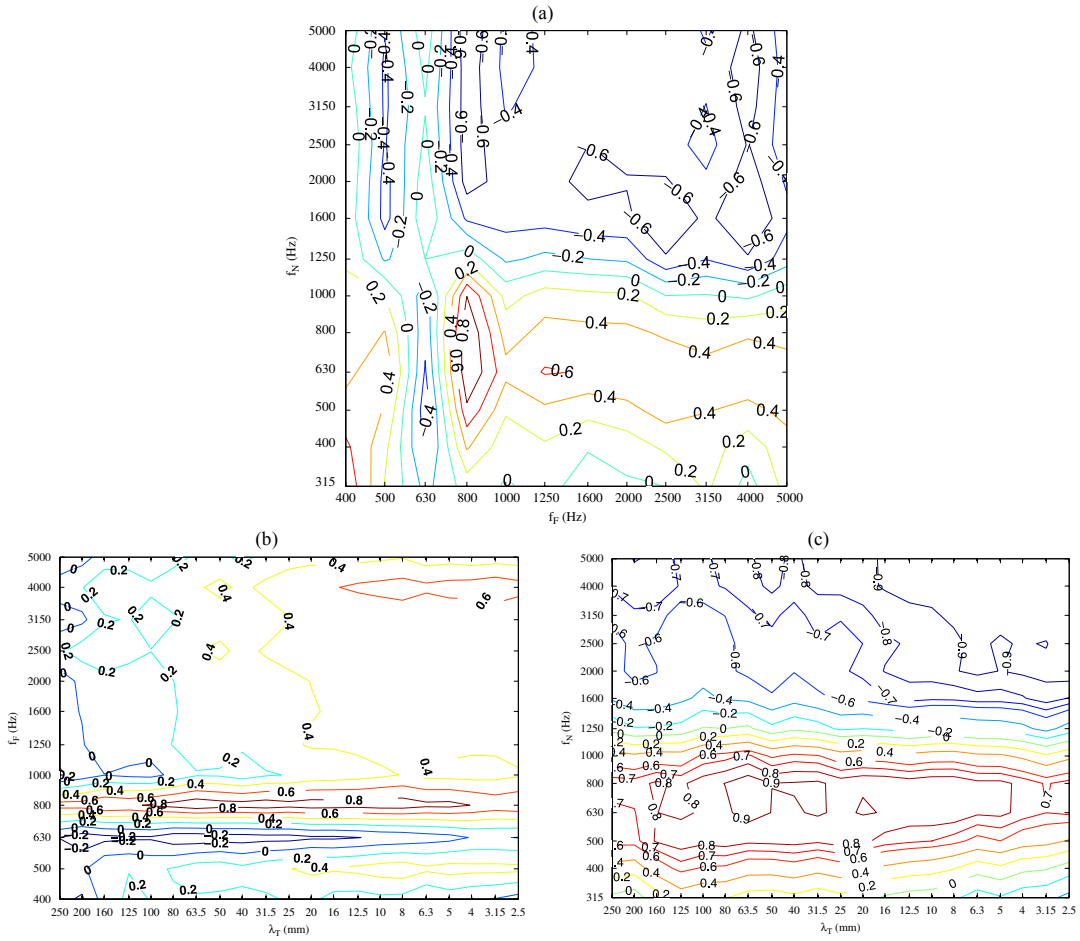

Figure 128: Iso-correlation curves between (a) contact force and noise level; (b) pavement texture and contact force; (c) pavement texture and noise level (source from Cesbron et al., 2009 [884], Figure 17-19; reprinted with permission from Elsevier)

It was found that at 30 km/h the levels of the resultant contact forces around 800 Hz are positively correlated with the texture wavelengths between 4 and 100 mm (macro-texture) and with the noise levels between 500 and 1000 Hz. It was also noted that the contact length

under rolling condition is 20% smaller than that under static condition, which is due to the viscoelasticity effect of the tire rubber.

5.4.2.8 Dubois et al. (Contact Distribution, 2013)

Dubois et al. (2013) [61] improved the Viscoelastic Contact model by utilizing Two-scale Iterative Method (TIM) to obtain the contact pressure distribution. The tire road noise measurements were conducted with close proximity (CPX) method on ten surfaces of the "Reference Test Track" of IFSTTAR (French institute of science and technology for transport, spatial planning, development and networks) in Nantes, France. Two tires were tested: (1) patterned tire (Michelin Energy E3A 195/60R15); (2) slick tire (Michelin Racer Slick 186/57R15).

The speed effect was expressed in the following regression equation.

$$L_N^{m*}\left(f_j\right)=\alpha_j \log_{10}\left(\frac{V}{V_{ref}}\right)+\beta_j \tag{233}$$

where L_N^{m*} is the reprocessed measured noise level at any speed for frequency f_j, V is speed, V_{ref} is reference speed (90 km/h). An example of data set for coefficients α_j, β_j, standard deviation σ_j^m, and correlation coefficient ρ_j^m is in Table 70.

Table 70: Parameters of the linear regression for speed effect on surface DAC 0/10 (source from Dubois et al., 2013 [61], Table 1; reprinted with permission from Elsevier)

f_j [Hz]	315	400	500	630	800	1000
α_j	43.3	39.0	30.2	19.5	18.3	35.0
β_j [dB]	84.6	83.8	84.9	87.0	90.8	93.7
σ_j^m [dB]	±1.57	±1.40	±1.26	±1.24	±1.1	±1.1
ρ_j^m	0.88	0.88	0.84	0.72	0.74	0.9

The 3D pavement texture profiles were used to calculate the contact distribution. This process includes two steps: (1) calculate contact forces at the tips of the asperities (macro-scale) (Dubois et al., 2012 [883]); (2) calculate contact pressure within the tire/road interface (micro-scale). To obtain the spectral contact force, the pressure distribution $p(x, y, t)$ in the time domain is integrated to get the total contact force $F(y, t)$ in the time domain.

$$F(y,t)=\int_{y-\frac{dy}{2}}^{y+\frac{dy}{2}}\int_{-\frac{dx}{2}}^{\frac{dx}{2}} p(\xi,\eta,t)\,d\xi\,d\eta \tag{234}$$

The narrow band contact force spectrum $S_F(f)$ is given as

$$S_F(f) = \frac{1}{\Delta y}\int_{-\frac{\Delta y}{2}}^{\frac{\Delta y}{2}} S_F(y,f)\,dy \tag{235}$$

where Δy is a scaling coefficient. Then the third octave contact force level in dB is

$$L_F^e(f_i) = 20\log_{10}\left(\frac{S_F(f_i)}{F_{ref}}\right) \tag{236}$$

where f_i is center frequency of the third octave band, and F_{ref} is reference force (1×10^{-7} N). The relation between the noise level and contact force is defined as

$$L_N^e(f_i) = a_i L_F^e(f_i) + b_i \tag{237}$$

It was found that the relation is only valid ($R^2 > 0.64$) in low frequencies (315-1250 for slick tire, 315-800 Hz for patterned tire). The coefficients a_i, b_i, standard deviation σ_i^e, and correlation coefficient ρ_i^e are in Table 71 for slick tire and Table 72 for patterned tire.

Table 71: Parameters for the correlation between noise level and contact force for slick tire (error ε = 1.50%) (source from Dubois et al., 2013 [61], Table 2; reprinted with permission from Elsevier)

f_i [Hz]	315	400	500	630	800	1000	1250
a_i	1.59	1.38	1.68	1.73	1.88	2.10	1.86
b_i [dB]	-39.6	-25.2	-50.1	-52.8	-62.8	-80.1	-61.3
σ_i^e [dB]	±1.8	±1.5	±1.8	± 1.3	±1.3	±2.3	±3.5
ρ_i^e	0.94	0.94	0.92	0.97	0.97	0.95	0.83

Table 72: Parameters for the correlation between noise level and contact force for patterned tire (error $\varepsilon = 1.34\%$) (source from Dubois et al., 2013 [61], Table 3; reprinted with permission from Elsevier)

f_i [Hz]	315	400	500	630	800
a_i	1.47	1.51	1.86	1.84	1.38
b_i [dB]	-33.3	-38.1	-65.9	-61.8	-21.5
σ_i^e [dB]	±2.0	±1.6	±1.7	± 1.3	±0.9
ρ_i^e	0.83	0.90	0.90	0.94	0.96

It was also concluded that the estimation for noise levels is better using contact force as input parameter than using pavement texture.

5.4.2.9 Klein and Cesbron (3D Envelopment, 2016)

This model (Klein and Cesbron, 2016 [609]) is an improvement from HyRoNe model (Klein and Hamet, 2007 [443]) where the 2D enveloped texture profiles have been used to calculate the tire-pavement contact without accounting for the lateral/transverse texture inhomogeneities.

It was shown that the 2D model did not work well for smooth pavement such as ISO surface. To address this, in [609], the 3D pavement texture and tread pattern profile were both accounted for, and a new 3D envelopment procedure was developed for the prediction of the tire belt radiation noise.

The input for the 3D envelopment calculation is the 3D combined tire/pavement roughness, obtained by subtracting the tire tread height from the road texture height, as shown in Figure 129.

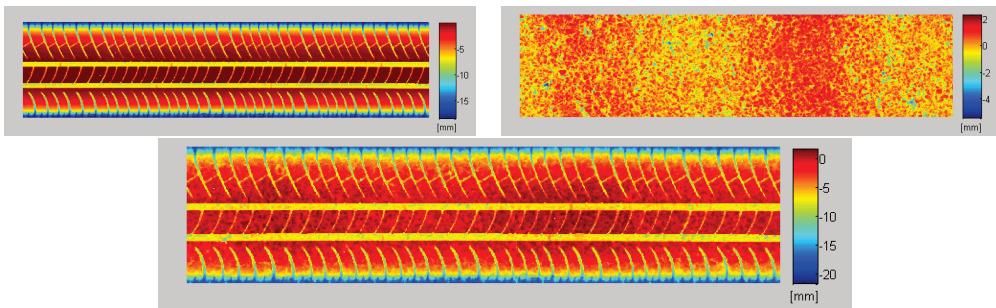

Figure 129: Top left: tire tread pattern; top right: pavement roughness; bottom: combined tire/pavement roughness (longitudinal/lateral spatial resolution = 1 mm, source from Klein and Cesbron, 2016 [609], Figure 10; reprinted under fair use provision)

The tire-pavement contact is modeled as elastic half-space (tire) between a rigid body (pavement). The deflection of the elastic body w is given by the Boussinesq's formula

$$w(x,y)=\iint_C p(u,v)g(x,y;u,v)\,\mathrm{d}u\,\mathrm{d}v$$
$$g(x,y;u,v)=\frac{1-\nu^2}{\pi E}\frac{1}{\sqrt{(x-u)^2+(y-v)^2}} \tag{238}$$

where $p(x,y)$ is the pressure distribution within the contact zone C, E is the Young's modulus of the tread rubber, and ν is the Poisson's ratio. The global equilibrium condition is given by

$$\iint_C p(x,y)\,\mathrm{d}x\,\mathrm{d}y=F \tag{239}$$

where F is the total tire load. The iterative algorithm can be used to solve the contact zone C, the contact pressure p and the half-space surface displacement w. Example of the calculated contact pressure are shown in Figure 130.

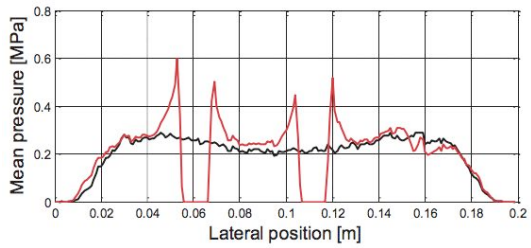

Figure 130: Contact pressure distribution (red curve: patterned E3A tire; black curve: slick tire) (source from Klein and Cesbron, 2016 [609], Figure 13; reprinted under fair use provision)

The surface displacement *w* can be considered as the 3D enveloped combined tire/pavement roughness, which is then spectrally correlated with the tire noise. Good correlations were observed between 250 Hz and 1250 Hz. However, the accuracy of the model in higher frequencies over 1250 Hz where air pumping mechanism is dominant needs to be improved. The error for the 1/3 octave noise level is within 3 dB while the overall noise level within 1 dB. The results for one patterned tire (Michelin Energy E3A 195/60R15) tested on 11 non-absorptive pavements were presented, suggesting that more tires of different tread patterns need to be validated. For the interest, some other studies on the modeling of pavement envelopment can be found in Pinnington, 2012 [617], Pinnington, 2013 [618] and Pinnington, 2016 [885].

5.4.3 Mechanism Separation Models

In these models, an equation form for each noise generation mechanism is assumed based on its physics. Then, the total TPIN is obtained by summing up all the generation mechanisms. Finally, the parameters in the assumed equations are statistically determined via experimental data.

5.4.3.1 Cao et al. (Tire/Road Coupling, 2008)

Cao et al. (2008) [583] studied the coupling noise between tire and road interaction in both time domain and frequency domain. The prediction model for tire tread pattern noise assumed a patterned tire running on a smooth road. Five generation mechanisms were included, which is discussed below.

(1) Air pumping at the leading and trailing edge of the contact patch. The sound pressure

due to this mechanism is given by

$$P_1(t) = g_b \cdot A_b \cdot \sin(\omega_b t + \theta) \cdot |B \cdot \sin \omega_x t| \tag{240}$$

where

$$g_b = \begin{cases} 1 & \sin(\omega_b t + \theta) \geq 0 \\ \xi & \sin(\omega_b t + \theta) < 0 \end{cases}$$

$$\xi \in (0,1)$$

$$B \in \left(\frac{1}{5}A_b, \frac{1}{9}A_b\right)$$

$$\omega_x \in (8\omega_b, 10\omega_b)$$

(2) Air pumping in the tread grooves.

$$P_2(t) = (P_{\max} \cdot \sin\alpha) \cdot g_s \cdot \sin(\omega_s t + \theta) \tag{241}$$

where α is the groove angle, $P_{\max}$ is the maximum sound pressure, and

$$g_s = \begin{cases} 1 & \sin(\omega_s t + \theta) \geq 0 \\ \eta & \sin(\omega_s t + \theta) < 0 \end{cases}$$

$$\eta \in (0,1)$$

(3) Pipe resonance.

$$P_3(t) = \sqrt{d \cdot l} \cdot A \cdot Z(d) \cdot \sin\left\{\left[0.8\omega \pm 0.2R(t)\right] \cdot t\right\} + \frac{\sin \omega t}{|\sin \omega t|} \cdot \frac{\sqrt{d \cdot l} \cdot A \cdot Z(d)}{10} \cdot \sin(10\omega) \tag{242}$$

where d is the groove width, l is the groove length, $Z(d)$ is a function of d, $R(t)$ is random number between -1 and 1.

$$A = \begin{cases} 1, & \sin \omega t \geq 0 \\ \frac{1}{3}, & \sin \omega t < 0 \end{cases} \tag{243}$$

(4) The sound pressure due to cavities and pores in the contact patch was $P_4(t)$.

(5) The sound pressure due to air turbulence was $P_5(t)$.

The prediction model for road noise assumed a smooth tire running on a normal road. Four mechanisms were included.

(6) Smooth tire on a smooth road (base noise).

$$P_6(t)=\left\{\left[0.5+\frac{R_1(t)}{2}\right]\cdot A_1\right\}\cdot\sin\left[\omega_1\left(0.5+\frac{R_2(t)}{2}\right)\cdot t\right] \tag{244}$$

(7) Stick/slip (friction).

$$P_7(t)=\left\{\left[0.5+\frac{R_3(t)}{2}\right]\cdot\frac{A_2}{\xi\cdot k}\right\}\cdot\sin\left[\omega_2\left(0.5+\frac{R_4(t)}{2}\right)\cdot t\right] \tag{245}$$

(8) Road unevenness.

$$P_8(t)=\left\{\left[0.5+\frac{R_5(t)}{2}\right]\cdot\left(A_3\cdot\eta\cdot j\right)\right\}\cdot\sin\left[\omega_3\left(0.5+\frac{R_6(t)}{2}\right)\cdot t\right] \tag{246}$$

(9) Texture impact.

$$P_9(t)=\left\{\left[0.5+\frac{R_7(t)}{2}\right]\cdot\left(A_4\cdot\eta\cdot g\right)\right\}\cdot\sin\left[\omega_4\left(0.5+\frac{R_8(t)}{2}\right)\cdot t\right] \tag{247}$$

where R_1(t) to R_8(t) are random numbers between -1 and 1, A_1 to A_4 are the sound pressure amplitudes, ω_1 to ω_4 are the sound pressure frequencies.

Then total sound pressure in time domain is given by

$$\begin{aligned}P_{TR}(t)&=\zeta_1P_1(t)+\zeta_2P_2(t)+\zeta_3P_3(t)+\zeta_4P_4(t)+\zeta_5P_5(t)+\zeta_6P_6(t)+\zeta_7P_7(t)+\zeta_8P_8(t)+\zeta_9P_9(t)\\&=\begin{bmatrix}\zeta_1 & \cdots & \zeta_9\end{bmatrix}\begin{bmatrix}P_1 & \cdots & P_9\end{bmatrix}^T\end{aligned} \tag{248}$$

where ζ_1 to ζ_9 are best-fit coefficients determined by experiments.

Then total sound pressure in frequency domain $H_{All}(f)$ after accounting for horn effect and pavement absorption is given by

$$H_{All}(f)=\sqrt{1-\alpha(f)}\cdot K(f)\cdot H_{TR}(f) \tag{249}$$

where $\alpha(f)$ is the pavement absorption coefficient, $K(f)$ is horn effect coefficient, and $H_{TR}(f)$ is the Fourier transform of $P_{TR}(t)$.

Unfortunately, no experimental data or the model accuracy was reported.

5.4.3.2 Dare (Mechanism Decomposition, 2012)

Dare (2012) [213] decomposed the on-board sound intensity (OBSI) spectrum into three constituent spectra, representing the contribution from sidewall vibration, treadband vibration, and tangential vibration respectively, illustrated in Figure 131. It is assumed that the shapes of the constituent spectra will not change much, though the magnitudes may

change. The general constituent spectra were derived using SRTT on six different pavements at five speeds (16-42 km/h).

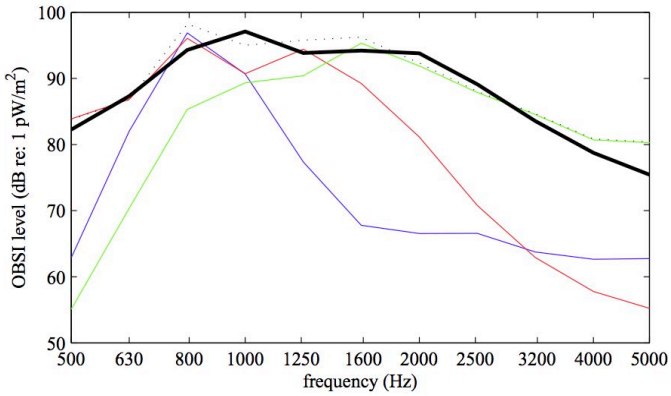

Figure 131: Constituent spectra and predicted total spectrum compared to measured spectrum for cell 1, leading probe. Blue: treadband spectrum. Red: sidewall spectrum. Green: tangential spectrum. Dotted black: predicted total spectrum. Solid black: measured spectrum. (Source from Dare, 2012 [213], Figure 5.10; reprinted with permission from Dr. Tyler Dare of Pennsylvania State University, USA)

For sidewall vibration constituent, the gain function $G_{IV,sidewall}$ between measured sound intensity and vibration levels is given by

$$G_{IV,sidewall}(f) = \frac{I_{sidewall}(f)}{\left|V_{sidewall}(f)\right|^2} \tag{250}$$

where f is frequency, $I_{sidewall}$ is sound intensity for sidewall vibration constituent measured with treadband covered in sound-absorbing insulation, $V_{sidewall}$ is the velocity spectrum measured with the accelerometer mounted to the sidewall.

Similarly, the gain function for treadband vibration is given

$$G_{IV,treadband}(f) = \frac{I_{treadband}(f)}{\left|V_{treadband}(f)\right|^2} \tag{251}$$

where $I_{treadband}$ is measured with sidewall covered with sound-absorbing insulation, and $V_{treadband}$ is measured with the accelerometer mounted to the tread groove.

The tangential vibration results from stick-slip and tangential impact. The tread block was modeled as a dipole source, with two out-of-phase monopole sources at the front and rear edge of the tread block. The sound pressure P generated by a dipole is given by [800]

$$P = \frac{1}{2}\rho_0 c \frac{Q}{\lambda}\left(\frac{1}{r} + \frac{e^{j\omega d}}{r+d}\right) \tag{252}$$

where ρ_0 is air density, c is sound speed, λ is sound wavelength, r is the distance between one monopole source and receiver (2 cm), d is the distance between the two monopole sources (length of tread block). Q is the source strength, given by $Q = whV$ where w is tread block width (2.54 cm), h is tread block height (0.64 cm), and V is tangential velocity of tread block. The gain function is

$$G_{dipole} = \left|\frac{1}{2}\rho_0 c \frac{wh}{\lambda}\left(\frac{1}{r} + \frac{e^{j\omega d}}{r+d}\right)\right| \tag{253}$$

The sound intensity equations for the three constituent spectra at the leading edge are given as

$$\begin{cases} I_{sidewall,lead} = G_{IV,sidewall}\left|V_{sidewall,lead}\right|^2 \\ I_{sidewall,trail} = G_{IV,sidewall}\left|V_{sidewall,trail}\right|^2 \\ I_{tangential,lead} = \left(G_{dipole}\left|V_{tangential,lead}\right|\right)G_{train}G_{horn,close} + \left(G_{dipole}\left|V_{tangential,trail}\right|\right)G_{train}G_{horn,far} \end{cases} \tag{254}$$

where G_{train} is calculated impulse train spectrum due to frequency of tread block impact, $G_{horn,close}$ and $G_{horn,far}$ are measured horn effect gain function for close and far OBSI probe locations.

The sound intensity levels for the three constituent spectra at the leading edge are given as

$$\begin{cases} L_{sidewall,lead} = 10\log_{10}\left(\frac{I_{sidewall,lead}}{I_{ref}}\right) + \Delta_{sidewall,lead} \\ L_{treadband,lead} = 10\log_{10}\left(\frac{I_{treadband,lead}}{I_{ref}}\right) + \Delta_{treadband,lead} \\ L_{tangential,lead} = 10\log_{10}\left(\frac{I_{tangential,lead}}{I_{ref}}\right) + \Delta_{tangential,lead} \end{cases} \tag{255}$$

where I_{ref} is reference sound intensity (1 pW/m^2), Δ is the prediction offset for specific pavement.

The total sound intensity level at the leading edge is

$$L_{total,lead} = 10\log_{10}\left(10^{\frac{L_{sidewall,lead}}{10}} + 10^{\frac{L_{treadband,lead}}{10}} + 2\sqrt{10^{\frac{L_{sidewall,lead}}{10}} \cdot 10^{\frac{L_{treadband,lead}}{10}}}\cos\phi + 10^{\frac{L_{tangential,lead}}{10}}\right) \quad (256)$$

where ϕ is the measured phase difference between sidewall and treadband sources. The average error for one-third octave band between prediction and measurement is 2.3 dB for leading probe and 2.8 dB for trailing probe. The sound levels at the trailing probe are calculated similarly like above.

To predict the total sound intensity for different pavements, statistical model was developed.

$$\begin{cases} I_{treadband} = 10^{\frac{L_{treadband}+\beta_1\xi+\beta_2}{10}} \\ I_{sidewall} = 10^{\frac{L_{sidewall}+\beta_3\xi+\beta_4}{10}} \\ I_{tangential} = 10^{\frac{L_{tangential}+\beta_5\xi+\beta_6}{10}} \end{cases} \quad (257)$$

where β_1 to β_6 are best-fit coefficients and ξ is any pavement parameter such as MPD, texture level at a given wavelength, or absorption. It was found that MPD, texture level at 12.5 mm wavelength, texture level at 3.15 mm wavelength, and skewness are best predictors for this one-parameter OBSI model.

The statistical model can also include two parameters simultaneously, given as

$$\begin{cases} I_{treadband} = 10^{\frac{L_{treadband}+\beta_1\xi_1+\beta_2\xi_2+\beta_3}{10}} \\ I_{sidewall} = 10^{\frac{L_{sidewall}+\beta_4\xi_1+\beta_5\xi_2+\beta_6}{10}} \\ I_{tangential} = 10^{\frac{L_{tangential}+\beta_7\xi_1+\beta_8\xi_2+\beta_9}{10}} \end{cases} \quad (258)$$

It was found that texture level at 12.5 mm wavelength, texture level at 3.15 mm wavelength are the best two predictors within 0.9 dB at the leading probe and 1.1 dB at the trailing probe for the overall sound intensity levels.

It should be pointed that the experimental data did not cover high speed (lower than 42 km/h). Extrapolation with speed exponent was used to account for high speed.

5.4.3.3 Winroth et al. (Air Pumping Separation, 2013)

Winroth et al. (2013) [886] separated the noise component due to tire vibrations and the

component due to air pumping. It was pointed out that the sound generation due to tire vibrations is proportional to the square of vehicle speed while the sound generation due to air pumping is proportional to the fourth power of vehicle speed. Therefore, the sound pressure can be given by

$$p_{rms}^2(f,V) = A_2(f)\cdot V^2 + A_4(f)\cdot V^4 \tag{259}$$

where p_{rms} is the root mean square value of sound pressure, f is frequency, V is vehicle speed, A_2 and A_4 are coefficients as a function of frequency. A_2 and A_4 are statically determined by curve fitting from controlled pass-by (CPB) levels spectra with speed range of 50 to 120 km/h. Several pavements were investigated: mastic asphalt, stone mastic asphalt sealed with synthetic resin, and a sand paper surface. However, only slick tire is considered in this model. It was found that air pumping noise is dominant at over 1000 Hz and at some low frequencies around 400 Hz.

5.4.3.4 Mohamed and Wang (Deterministic SEA, 2016)

Mohamed and Wang (2016) [411] investigated the tire cavity resonance using a combination of deterministic analysis (impedance compact mobility matrix method, ICMM) and statistical energy analysis (SEA). The deterministic part focuses on the cavity pressure response and the compliant wall vibration velocity response in the low frequency, while the statistical part focuses on the high frequency. In the mid frequency, the two methods are combined to identify the characteristics of tire cavity coupling. The authors claimed that the same analysis method could be applied to other similar toroidal shape structural-acoustic systems.

The tire-cavity coupling system is modeled as an annular cylinder where the side and inner wall are assumed as rigid while the outer shell (referred to as tire structure thereafter) as flexible. The vibration energy of tire structure E_1 (large modal density) is statically calculated while the acoustic energy of tire cavity E_2 (small modal density) is deterministically predicted.

$$E_1 = \frac{\Pi_1 + \omega E_2 \dfrac{\eta_1(\omega)}{\eta_2(\omega)}\eta_{12}}{\omega(\eta_1 + \eta_{12})} \tag{260}$$

where Π_1 is the power input to the tire structure, ω is radian frequency, η_1 and η_2 are the damping loss factors of tire structure and tire cavity, η_{12} is the coupling loss factor from tire

structure to tire cavity.

$$E_2 = \frac{1}{V}\iiint_V \frac{1}{2}\int_{\omega_1}^{\omega_2}\left|p_\omega^2(r,\theta,z)\right|^2 \frac{\pi W\left(R_o - R_i\right)^2}{\rho_0 c^2} d\omega\, dV \tag{261}$$

where V is the volume of the cavity, ω_1 and ω_2 are lower and upper limits of the frequency band, p_ω is the time and space-averaged squared pressure of the cavity obtained from experiment, (r, θ, z) is the cylindrical coordinate, W is the tire width, R_o and R_i are the outer and inner radius of the tire cavity, ρ_0 is the air density, c is the sound speed in air.

It can be seen that the coupling in this model is strong coupling where the structure and the fluid influences each other (the equation of E_1 contains E_2).

5.4.3.5 Le Bot et al. (Statistical Vibration, 2017)

This model (Le Bot et al., 2017 [887]) was based on the deterministic model of a prestressed orthotropic plate on visco-elastic foundation (Kropp, 1999 [413]), as illustrated in Figure 132. Modal analysis and statistical analysis were both performed to investigate the tire vibration characteristics at high frequencies.

The plate is of length a and width b, unwrapped in the tire circumferential and transverse direction, respectively.

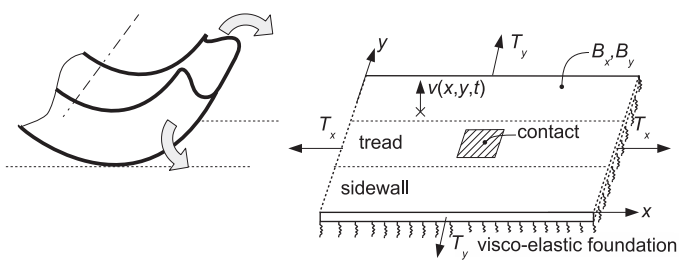

Figure 132: Tyre-road model. Left: the tyre is virtually unwrapped. Right: equivalent prestressed orthotropic plate under visco-elastic foundation. (Source from Le Bot et al., 2017 [887], Figure 1; reprinted with permission from Elsevier)

The governing equation for out-of-plane vibrations is

$$\left[\left(\sqrt{B_x}\frac{\partial^2}{\partial x^2} + \sqrt{B_y}\frac{\partial^2}{\partial y^2}\right)^2 - \left(T_x\frac{\partial^2}{\partial x^2} + T_y\frac{\partial^2}{\partial y^2}\right) + S + c\frac{\partial}{\partial t} + m\frac{\partial^2}{\partial t}\right] v = f(x,y,t) \tag{262}$$

where $v(x, y, t)$ is the displacement field (output response) in direction normal to the plate

and $f(x, y, t)$ is the contact force field (input excitation). In Eq. (262), m is the mass per unit area in kg/m^2, T_x (resp. T_y) is the x-component (resp. y-component) of the tensile force in N/m imposed by the air pressure (always positive), B_x (resp. B_y) is the bending stiffness in the x-direction (resp. the y-direction) in N·m, S is the stiffness per unit area in N/m^3 of the elastic foundation, and c a viscous damping coefficient in N·s/m^3.

The periodic boundary conditions are applied for the x-direction while simply supported boundary conditions are applied for the y-direction. The mode shapes are obtained as

$$\begin{aligned}
&\psi_{ij1}(x,y) = a_{ij}\cos\left(2i\pi\frac{x}{a}\right)\sin\left(j\pi\frac{y}{b}\right); \quad i=0,1,\ldots \quad j=1,2,\ldots \\
&\psi_{ij2}(x,y) = b_{ij}\sin\left(2i\pi\frac{x}{a}\right)\sin\left(j\pi\frac{y}{b}\right); \quad i=1,2,\ldots \quad j=1,2,\ldots \\
&\begin{cases} a_{ij} = \sqrt{2/ab}; & i=0 \\ a_{ij} = b_{ij} = 2/\sqrt{ab}; & i\neq 0 \end{cases}
\end{aligned} \tag{263}$$

The eigenvalues are

$$m\omega_{ij}^2 = \left[\sqrt{B_x}\left(\frac{2i\pi}{a}\right)^2 + \sqrt{B_y}\left(\frac{j\pi}{b}\right)^2\right]^2 + \left[T_x\left(\frac{2i\pi}{a}\right)^2 + T_y\left(\frac{j\pi}{b}\right)^2\right] + S \tag{264}$$

The transfer mobility, i.e., frequency response function between a force applied at $\mathbf{x}_0(x_0, y_0)$ and the vibrational velocity at $\mathbf{x}(x, y)$ is given by

$$\begin{aligned}
&Y(\mathbf{x},\mathbf{x}_0;\omega) = i\omega\sum_{i\geq 0, j\geq 1}\frac{4\varepsilon_i}{ab}\frac{\cos\left(2i\pi\frac{x-x_0}{a}\right)\sin\left(j\pi\frac{y}{b}\right)\sin\left(j\pi\frac{y_0}{b}\right)}{m\left(\omega_{ij}^2 + i\eta_{ij}\omega\omega_{ij} - \omega^2\right)} \\
&\varepsilon_i = \begin{cases} 1/2; & i=0 \\ 1; & i>0 \end{cases}
\end{aligned} \tag{265}$$

The identification of the physical parameters can be performed using a Simplex search method from the point mobility measurement results. The dispersion relationship is

$$
\begin{aligned}
k(\omega) &= \sqrt{\frac{-T+\sqrt{T^2-4B\left(S-m\omega^2\right)}}{2B}} \\
B(\theta) &= \left(\sqrt{B_x}\cos^2\theta+\sqrt{B_y}\sin^2\theta\right)^2 \\
T(\theta) &= T_x\cos^2\theta+T_y\sin^2\theta
\end{aligned}
\tag{266}
$$

where k is the wavenumber, θ is wave propagation angle with respect to x-direction. The cut-on frequency is given by

$$
\omega_{\text{cut-on}} = \sqrt{\frac{S}{m}} \tag{267}
$$

The vibration characteristics are defined by three statistical parameters: modal density $n(\omega)$ indicating the size of the population of resonant modes, modal overlap $M(\omega)$ measuring the overlapping of successive modes, and normalized attenuation factor $m(\omega)$ indicating the number of reflections undergone by a ray during its time life. They are given by

$$
\begin{aligned}
n(\omega) &= \frac{2m}{\pi\Delta\omega}\int_A\int_{\Delta\omega}\mathrm{Re}\left[Y(\mathbf{x},\mathbf{x};\omega)\right]\mathrm{d}\omega\,\mathrm{d}A_{\mathbf{x}} \\
M(\omega) &= \eta(\omega)\omega n(\omega) \\
m(\omega) &= -\ln\left[\frac{1}{2\pi}\int_0^{2\pi}\exp\left(-\frac{\eta\omega}{c_g}l\right)d\theta\right]
\end{aligned}
\tag{268}
$$

where A is plate area ab, $\Delta\omega$ is the bandwidth of interest (e.g., octave band centered at 1 kHz, i.e., [707, 1414] Hz), $Y(\mathbf{x}, \mathbf{x}; \omega)$ is the point mobility at $\mathbf{x}$ and Re denotes the real part; $\eta(\omega)$ is the mean damping loss factor at frequency ω; c_g is group speed defined as $\mathrm{d}\omega/\mathrm{d}k$.

Another statistical parameter characterizing the uniformity of spatial repartition of energy is σ, given by the ratio of spatial standard deviation of local energy and mean energy as below.

$$
\begin{aligned}
\sigma &= \frac{1}{\overline{E}(\omega_0)}\sqrt{\frac{1}{A}\int_A E(\mathbf{x};\omega_0)^2\,\mathrm{d}A_{\mathbf{x}}-\overline{E}(\omega_0)^2} \\
\overline{E}(\omega_0) &= \frac{1}{A}\int_A E(\mathbf{x};\omega_0)\mathrm{d}A_{\mathbf{x}} \\
E(\mathbf{x};\omega_0) &= S_0\int_{\Delta\omega} m\left|Y(\mathbf{x},\mathbf{x}_0;\omega)\right|^2 d\omega
\end{aligned}
\tag{269}
$$

where S_0 is power spectral density of the force f at $\mathbf{x}_0$.

The vibrations in tires can be classified into three regimes based on these statistical

parameters: the modal, diffuse field, and free field regimes, as shown in Figure 133 and Figure 134. For realistic tires, the damping is relatively high and increases with frequency from 0.05 to 0.3. Therefore, as frequency increases, the modal regime directly transitions into the free field regime without reaching the diffuse field regime. It is noted that at low frequencies below 400 Hz, the tire dynamics is dominated by few modes (typically of order of six) whose modal overlap is relatively low. At high frequencies, e.g., 1000 Hz, the dynamics is mainly driven by bending effects where the modal density and modal overlap are so large (e.g., mode count $N = 192$ for the octave at 1 kHz) that the behavior of individual modes is not distinguishable on point mobility. To investigate the non-modal domain, the geometrical acoustics approach is used instead of conventional modal analysis. The energy field may be described in terms of rays that propagate in straight lines with a speed depending on the direction.

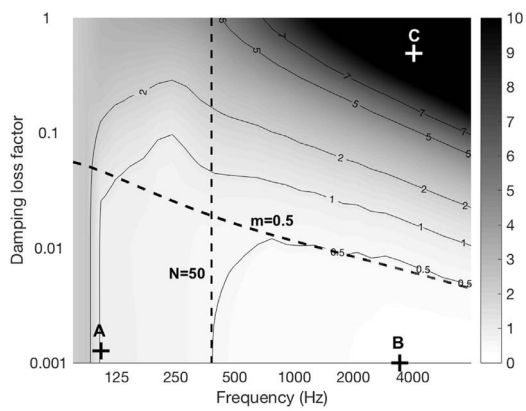

Figure 133: Relative standard deviation of spatial energy repartition in the frequency, damping loss factor plane under a point-excitation. Left side: modal regime with few modes contributing the dynamics. Top right-hand corner (black): free field regime where rays are highly absorbed. Bottom right-hand corner (bright): diffuse field regime. The broken lines are regime boundaries determined by $N(\omega) = n(\omega)\cdot\Delta\omega$ and $m(\omega)$. (Source from Le Bot et al., 2017 [887], Figure 7; reprinted with permission from Elsevier)

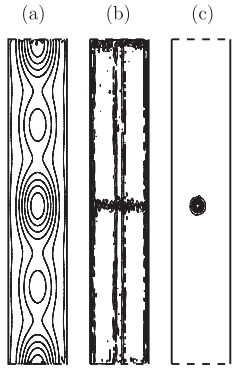

Figure 134: Examples of energy fields corresponding to crosses in Figure 133. (a) Regime of modal field (point A); (b) Regime of diffuse field (point B); (c) Regime of free field (point C). (Source from Le Bot et al., 2017 [887], Figure 8; reprinted with permission from Elsevier)

5.4.3.6 Wang and Duhamel (Network Resonator, 2017)

In this work (Wang and Duhamel, 2017 [888]), the grooves between the tire tread and pavement texture were modeled as acoustic network resonators, as shown in Figure 135. A numerical method for the calculation of resonant frequencies of network resonators was proposed.

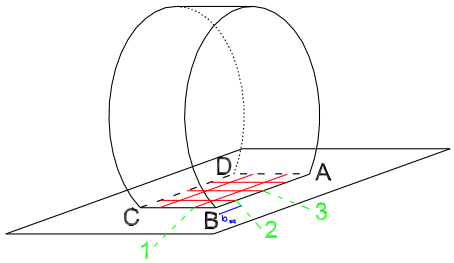

Figure 135: A network (in red) between a round surface and a rigid plane surface (ABCD indicates the contact patch; 1 is a longitudinal pipe while 2 and 3 are transverse pipes; b_{sq} is half the flange width for pipe 2). (Source from Wang and Duhamel, 2017 [888], Figure 2; reprinted with permission from Elsevier)

First, the end corrections for open-ended pipes were calculated. The end correction δ_{sq} of the transverse pipe assuming rectangular flat flanges, as shown in Figure 135, is given by Dalmont's method (Dalmont et al., 2001 [889])

$$\delta_{sq} = \delta_{sq\infty} + \frac{a_{sq}}{b_{sq}}\left(\delta_{sq0} - \delta_{sq\infty}\right) + 0.057\frac{a_{sq}}{b_{sq}}\left[1 - \left(\frac{a_{sq}}{b_{sq}}\right)^5\right]a_{eff}$$
$$\delta_{sq\infty} = 0.811a_{eff}$$
$$\delta_{sq0} = 0.597a_{eff} \tag{270}$$
$$a_{eff} = \frac{2a_{sq}}{\sqrt{\pi}}$$

where $2a_{sq}$ = 0.009 m is the pipe width, $2b_{sq}$ is the flange width. The end correction δ of the longitudinal pipe assuming a cylindrical flange is obtained by boundary element method (BEM) and statistically given by

$$\delta = 0.00808 + 0.22128w - 3.72112w^2 + 19.80897w^3 \tag{271}$$

where $2w$ is the flange width. It is noted that this δ is slightly dependent on frequency, and Eq. (271) gives the mean values from 0-2000 Hz.

Second, the resonant frequencies of the network resonators were solved using finite element software Abaqus where the end corrections were accounted for during physical modeling.

Third, the genetic algorithm (GA) was used to optimize the acoustic network (e.g., pipe positions, junction types) to obtain the targeted resonant frequencies, and validated by experiments of wooden network resonators.

It should be noted that the acoustic resonator in this work was to attenuate the sound pressure level, which is different from the common thought that pipe resonance amplifies the tire noise.

5.4.4 Noise Propagation Models

In these models, the sound power of TPIN is typically statistically acquired. Sound propagation theory is then applied to obtain the sound pressure level (SPL) at a given location.

5.4.4.1 CRTN (UK, 1988)

The model (CRTN, Calculation of Road Traffic Noise) was issued by the UK Department of Transport (DOT) in 1988 [890] and is widely used for traffic noise calculation in United Kingdom, Ireland, Australia, New Zealand and Hong Kong (Leung and Mak, 2008 [891]). A

webpage calculator is also available (NPL, 2005 [892]). Like NMPB 2008, CRTN also includes emission and propagation models. The road was modeled as a line source rather than a set of point sources in NMPB; additional methods to deal with dual source lines, median barriers and corrections for thin surfaces were presented in 2008 (UK Department for Transport, 2008 [893]).

The sound level is in terms of L_{10} (the noise level just exceeded for 10% of the measurement period) for the 18 hours between 06:00 and 24:00 ($L_{A,10,18\text{h}}$) without noise assessment during night between 24:00 and 6:00. The source emission level is

$$L_{10,18\text{h}} = 29.1 + 10\lg(Q) + Correction_{V\&p} + Correction_G + Correction_{TD} \tag{272}$$

where Q is vehicle number for the 18 hours, including all vehicles (light and heavy); $Correction_{V\&p}$ is correction for mean traffic speed V (km/h) and the percentage of heavy vehicles p (%); $Correction_G$ is the correction for the road gradient G (%),$Correction_{TD}$ is the correction for the texture depth (TD) in mm. The equations for the three corrections are

$$Correction_{V\&p} = 33\lg\left(V + 40 + \frac{500}{V}\right) + 10\lg\left(1 + \frac{5p}{V}\right) - 68.8 \tag{273}$$

$$Correction_G = 0.3G \tag{274}$$

$$\begin{cases} Correction_{TD,concrete} = 10\lg(90TD + 30) - 20 \\ Correction_{TD,asphalt} = 10\lg(20TD + 60) - 20 \end{cases} \tag{275}$$

$Correction_{TD}$ is -1 dBA for speed less than 75 km/h.

$L_{A,10,18\text{h}}$ must be converted to L_{den} and L_{night} indicators for noise mapping assessment (Abbott and Nelson, 2002 [894]). However, the noise data at night were not collected in CRTN method. Even though the night noise is available, the correlation between $L_{10,night}$ and $L_{eq,night}$ is not good enough due to the insufficient traffic volume. Another disadvantage of CRTN compared to NMPB 2008 is that it does not consider different traffic flow types, and the fact that speeds for light vehicles and heavy vehicles are generally different.

In different locations, CRTN needs to be recalibrated which is not an easy task. For example, Table 73 shows the several recalibrated CRTN models proposed by local researchers in Hong Kong (Leung and Mak, 2008 [891]). They all have certain errors.

Table 73: Recalibrated CRTN Models Proposed by Local Researchers in Hong Kong (Leung and Mak, 2008 [891])

Reference	Author	Year	Equation
[890]	CRTN	1988	$L_{A,10,18h} = 10\log_{10}(Q) + 33\log_{10}(V + 40 + 500/V) + 10\log_{10}(1 + 5p/V) + 0.3G - 26.6$
[895]	Lam and Tam	1998	$L_{A,10,18h} = 1.0534 \times L_{A,10,18h,CRTN} - 5.3347$
[896]	To et al.	2002	$L_{A,10,18h} = 10.6\log_{10}(Q) + 7.1\log_{10}(pV) - 17\log_{10}(V) + 53$
[897]	Tang et al.	2004	$L_{A,10,18h} = 10\log_{10}(Q) + 42.6\log_{10}(V + 40 + 500/V) + 10\log_{10}(1 + 5p/V) + 0.46G - 49.2$

Based on CRTN results, Abbott and Nelson (2002) [898] correlated L_{eq} and L_{10} using regression. O'Malley et al. (2009) [899] then adapted it to an Irish scenario [36], expressed as

$$L_{den} = 0.86 \times L_{A,10,18h} + 9.86 \text{ dB} \tag{276}$$

Murphy and King (2011) [16] noted that on average it under predicts noise levels by 0.01 dB with an r.m.s. error of 1.6 dB for the case in Dublin, Ireland.

5.4.4.2 NMPB (France, 1996)

NMPB (1996) [900] was described in French standard XPS 31-133 and was recommended by Environmental Noise Directive (END) for traffic noise calculation. The first version of the model is "NMPB-Routes-96 (SETRA-CERTU-LCPCCSTB)" (1996) [901] which only described the sound propagation model while the sound emission model was presented in "Guide du Bruit" (1980) [902]. The revised model NMPB 2008 [903] separates the TPIN and engine noise (Dutilleux, 2013 [904]) and is currently used in France, including both noise emission and noise propagation models (Sétra, 2009 [905]).

In NMPB 2008, each road is modeled as a line source, or several lines for multiple lanes. Each line is then divided into uninform sections; each section is divided into a set of incoherent point sources. For the noise emission model, the sound emission level E in dB for a single vehicle is

$$E = L_W - 10\log V - 50 \tag{277}$$

where L_W is A-weighted sound power per meter in a given octave band in dB, V is vehicle speed. L_W depends on the traffic conditions, as shown in Table 74.

Table 74: Traffic conditions in NMPB 2008 [903]

Conditions	Category
Vehicle Type	Light < 3.5 t; heavy > 3.5 t
Speed	< 20km/h set to 20 km/h; 20-120 km/h
Traffic flow type	Fluid continuous; pulsed continuous; pulsed accelerating; pulsed decelerating
Road slope	Rising > 2% upward; falling > 2% downward; level ≤ 2%

The alternative equation for sound emission level is

$$E = E_0 + a\log_{10}\left(\frac{V}{V_0}\right) \tag{278}$$

where coefficients E_0 and a are determined by the combination of traffic conditions; V_0 is reference speed (20 km/h). The sound power level per meter of lane for each elementary period k is

$$L_{AW/m,k} = E_{lv,k} + 10\lg\left(Q_{lv,k}\right) + E_{hv,k} + 10\lg\left(Q_{hv,k}\right) \tag{279}$$

where Q is the number of vehicles (traffic load); the subscripts lv and hv are light vehicle and heavy vehicle. After considering pavement types, the average sound power level per meter of lane is

$$L_{AW/m,\Psi} = 10\lg\sum_k 10^{\frac{L_{AW/m,k}+\Psi}{10}} \cdot \frac{h_k}{h_p} \tag{280}$$

where Ψ is the correction for pavement type, as shown in Table 75; h_k is the length of the elementary period in hours and h_p is the length of the reference period in hours.

Table 75: Correction for pavement type in NMPB 2008 [903]

Pavement	Noise Level Correction Ψ [dB]
Porous Surface	-1 for 0-60 km/h; -2 for 61-80 km/h; -3 for 81-130 km/h
Smooth Asphalt (Concrete or Mastic)	0
Cement Concrete and Corrugated Asphalt	+2
Paving Stones	+3

The sound power level of an elementary source i in a given octave band j (125-4000 Hz) is

$$L_{AWi} = L_{AW/m,\Psi} + 20 + 10\log_{10}\left(l_i\right) + R_j \tag{281}$$

where l_i is the length of the elementary source line (uniform section), R_j is the spectral correction for each octave band [906] shown in Table 76.

Table 76: Values for Spectral Correction of each Octave Band [906]

j	1	2	3	4	5	6
Octave Band Centre Frequency [Hz]	125	250	500	1000	2000	4000
R_j	-14.5	-10.2	-7.2	-3.9	-6.4	-11.4

For the noise propagation model, geometric divergence, atmospheric absorption (ISO 9613-1, 1993 [907]), ground absorption, diffraction and reflection are taken into consideration, assuming each elementary source is 0.5 m above the ground. Propagation is divided into two distinct types: meteorological conditions favorable to sound propagation with subscript *F*, and neutral (homogeneous) meteorological conditions with subscript *H*. The sound levels for the two conditions are

$$\begin{aligned} L_F &= L_W - A_{div} - A_{atm} - A_{grd,F} - A_{dif,F} \\ L_H &= L_W - A_{div} - A_{atm} - A_{grd,H} - A_{dif,H} \end{aligned} \tag{282}$$

The sound level is often expressed as day-evening-night equivalent level L_{den}, which is appropriate for noise mapping of environment assessment (Murphy and King, 2014 [819,908]).

5.4.4.3 Dai and Lee (Highway, 2010)

Dai and Lee Model (2010) [909–911] is called Highway Prediction Model (HPM) and used to predict highway traffic levels on pavements of asphalt concrete (AC) and asphalt rubber concrete (ARC). The model was developed based on ray acoustics approach that is also applied in ISO 9613 (attenuation of sound during propagation outdoors, with the accuracy up to ±3 dBA within range of 1000 m) (ISO 9613-1, 1993 [907]; ISO 9613-2, 1996 [260]). The advantage of this model is it was presented in the form of Microsoft® Office Excel® 2007 and the users are only required to provide parameter inputs that are very easy to acquire, such as weather conditions, pavement types, pavement porosity and permeability, hourly traffic volume, vehicle nominal speed, and receiver's distance from the road.

Three assumptions were applied to the model: (1) road assumed as an infinite line source; (2) free field condition for the source and receiver; (3) no barrier between the source and receiver. The sound pressure level $L_{ft}(DW)$ at a given distance is

$$L_{ft}(DW) = L_W + D_C - A \tag{283}$$

where the nomenclature is in Table 77, and the total attenuation is given by

$$A = A_{div} + A_{atm} + A_{gr} + A_{bar} + A_{misc} \tag{284}$$

Table 77: Nomenclature for Highway Prediction Model (HPM) (Dai and Lee, 2010 [909])

Symbol	Unit	Description
$L_{ft}(DW)$	[dB]	Sound pressure level at a receiver location for given octave band center frequency f and temperature T
L_W	[dB]	Sound power level
D_C	[dB]	Directivity correction (set to 0 due to free field condition)
A	[dB]	Octave-band attenuation due to multiple effects
A_{div}	[dB]	Attenuation due to geometric divergence
A_{atm}	[dB]	Attenuation due to atmospheric absorption
A_{gr}	[dB]	Attenuation due to ground absorption
A_{bar}	[dB]	Attenuation due to the barrier (set to 0 due to no barrier assumption)
A_{misc}	[dB]	Attenuation due to miscellaneous effects
Q	[m^2]	Noise source directivity index (set to 2 due to hemispherical noise source)
d	[m]	Distance from source to receiver
α	[dB/m]	Atmospheric attenuation coefficient
f	[Hz]	Central frequency for specific octave band
T	[Kelvin]	Ambient atmospheric temperature
T_0	[Kelvin]	Reference air temperature (293.15 K)
f_{rO}	[Hz]	Oxygen relaxation frequency
f_{rN}	[Hz]	Nitrogen relaxation frequency
p_a	[kPa]	Atmospheric pressure
p_r	[kPa]	Reference atmospheric pressure (101.325 kPa)
h	[-]	Molar concentration of water vapor
h_r	[-]	Ambient relative humidity
p_{sat}	[kPa]	Saturation vapor pressure
T_{01}	[Kelvin]	Triple-point isotherm temperature (T_0 + 0.01 K)
A_s	[dB]	Ground attenuation in the source region
A_r	[dB]	Ground attenuation in the receiver region
A_m	[dB]	Ground attenuation in the middle region
α_p	[-]	Ground absorption coefficient
ϕ_p	[-]	Pavement porosity
k_p	[-]	Pavement permeability
A_1, A_2, A_3	[-]	Materials coefficients determined by measurements
A_{tra}	[dB]	Attenuation due to traffic volume
V_{tra}	[vehicles/hour]	Traffic volume
P_{truck}	[%]	Percentage of trucks in the traffic volume

5.4.4.3.1 Attenuation due to geometric divergence

The attenuation due to geometric divergence is calculated by

$$A_{div} = 10\log_{10}\left(\frac{Q}{4\pi d^2}\right) \tag{285}$$

5.4.4.3.2 Attenuation due to atmospheric absorption

The attenuation due to atmospheric absorption is calculated by

$$A_{atm} = \frac{\alpha d}{1000} \tag{286}$$

where the atmospheric attenuation coefficient α depends on weather parameters

(temperature and relative humidity) and is given by

$$\alpha = 8.686 f^2 \left[1.84 \times 10^{-11} \left(\frac{p_a}{p_r} \right)^{-1} \left(\frac{T}{T_0} \right)^{0.5} + \left(\frac{T}{T_0} \right)^{-2.5} \right] \left[0.01275 e^{-\frac{2239.1}{T}} \left(f_{rO} + \frac{f^2}{f_{rO}} \right)^{-1} + 0.1068 e^{-\frac{33352}{T}} \left(f_{rN} + \frac{f^2}{f_{rN}} \right)^{-1} \right] \quad (287)$$

where the oxygen relaxation frequency f_{ro} and nitrogen relaxation frequency f_{rN} are given below.

$$f_{rO} = \left(\frac{p_a}{p_r} \right) \left(\frac{T}{T_0} \right)^{-0.5} \left(24 + 4.04 \times 10^4 h \frac{0.02 + h}{0.391 + h} \right) \quad (288)$$

$$f_{rN} = \left(\frac{p_a}{p_r} \right) \left(\frac{T}{T_0} \right)^{-0.5} \left(9 + 280 h e^{-4.17 \times \left[\left(\frac{T}{T_0} \right)^{-\frac{1}{3}} - 1 \right]} \right) \quad (289)$$

The molar concentration of water vapor in the above equations is given by

$$h = h_r \left(\frac{p_{sat}}{p_r} \right) \left(\frac{p_a}{p_r} \right) \quad (290)$$

where the saturation vapor pressure is calculated using

$$\frac{p_{sat}}{p_r} = 10^{-6.8346 \left(\frac{T}{T_{01}} \right)^{1.261} + 4.6151} \quad (291)$$

5.4.4.3.3 Attenuation due to ground absorption

The attenuation due to ground absorption is given by

$$A_{gr} = A_s + A_m + A_r \quad (292)$$

The specific calculations vary for different central frequency of the octave bands f. However, except 31.5 Hz and 63 Hz, the ground absorption coefficient is important. It is related to pavement parameters and given by

$$\alpha_p = A_1 \ln(\phi_p) + A_2 \ln(k_p) - A_3 \quad (293)$$

5.4.4.3.4 Attenuation due to the barrier

A_{bar} is set to 0 because it is assumed that there are no barriers between that source and receiver.

5.4.4.3.5 Attenuation due to miscellaneous effects

The attenuation due to traffic volume is considered for two pavement types: asphalt concrete (AC) and asphalt rubber concrete (ARC). The equations are

$$A_{tra,AC} = 0.0001V_{tra}^2 - 0.0446V_{tra} - 0.0026P_{truck}^2 + 0.2284P_{truck} + 25.934 \quad (294)$$

$$A_{tra,ARC} = 0.00009V_{tra}^2 - 0.0359V_{tra} - 0.0011P_{truck}^2 + 0.1132P_{truck} + 10.1336 \quad (295)$$

5.4.4.3.6 Results

The model (HPM) was compared with the measured noise using Statistical Pass-by method (SPB), Computer Aided Noise Abatement (CadnaA) simulation software (CadnaA), and Traffic Noise Model (TNM®) LookUp program developed by the United States' Federal Highway Administration (FHWA). The results are shown in Figure 136 (Dai and Lee, 2010 [909]).

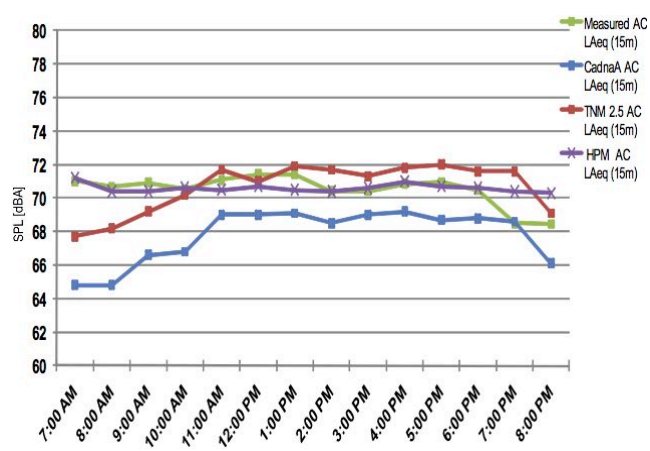

Figure 136: Comparisons between HPM and SPB, CadnaA, and TNM (source from Dai and Lee, 2010 [909], Figure 1; reprinted with permission from Ms. Beth Darchi on behalf of ASME)

Comparing HPM and SPB, larger errors (up to 4 dBA) occur at 7:00 am and 8:00 pm. It is probably due to drastic changes of ambient temperature, leading to atmospheric inversions (Sheadel et al., 2007 [912]). On average, HPM is the most accurate (basically within -1.65 dB to 1 dB) among the three prediction models. The TNM only accounts for dense-graded asphalt concrete (DGAC, a type of AC) and the distance between the source and receiver is 10-300 m. The CadnaA always under-predicts the noise levels, which is possibly because it is based on Road Traffic Noise Pollution Guidelines (RLS-90, published by German Federal Ministry of

Transportation) and not applicable in local areas (Canada).

5.4.4.4 Wei et al. (Air Pumping, 2016)

Wei et al. (2016) [366,913] developed a hybrid numerical-experimental model to predict the air pumping noise at any field point. This model is based on a hand carved tread pattern with two longitudinal grooves and one lateral groove. The groove is meshed into regular triangular or quadrilateral elements, which can be considered as small point acoustic sources. The volume velocity or source strength Q for each element i is given by

$$Q_i(f) = S_i \cdot q(f) \cdot h(\phi) \tag{296}$$

where f indicates frequency domain, S is the surface area of each element, q is the sound source of unit area that is related to the vehicle speed, $h(\phi)$ is a coefficient function of ϕ which is the distance between the element and the contact patch leading edge/trailing edge. The groove volume velocity in the frequency domain is obtained by the summation of all the elements, as written below.

$$Q_n = \sum_i Q_i \tag{297}$$

where n is index of groove sound sources. In this case, there are four sources: two (near the longitudinal grooves) at the leading edge and two at the trailing edge. The sound pressure spectrum P in the frequency domain is obtained as

$$P_m = \sum_n Z_{mn} Q_n \tag{298}$$

where m is index of microphone position in the near field, Z_{mn} is the transfer function between sound pressure P_m and source strength Q_n. The reverse manipulation can give us Q_n if P_m is experimentally measured and Z_{mn} is numerically determined, which is why it is called hybrid model.

5.4.5 Summary

The summary of tire-pavement interface models is shown in Table 78. Since the late 1990's, more efforts were put on the contact force/pressure distribution for TPIN modeling. The pavement texture was also converted to intermediate parameters, such as enveloped profile, that were potentially more correlated with TPIN. For either near field or far field

noise, all the models were able to predict the noise spectrum usually of broad frequency range, not just the overall noise level. Vehicle speed was typically included as an input parameter. However, the contact force/pressure spectrum was generally calculated based on pavement texture while assuming a slick tire tread, which might not be accurate for normal patterned tires.

The summary of mechanism separation models is shown in Table 79. This type of modeling is able to analyze each noise generation mechanism individually and identify each noise source, which has become popular since the late 2000's. Both structure-borne and airborne noise was generally investigated. The output of the models was the noise spectrum in 1/3 octave band or in narrowband. It is seen that pavement texture was more frequently included than tire parameters, such as tread pattern.

The summary of noise propagation models is shown in Table 80. These models were generally used to predict the far-field noise level at a specific distance from the traffic. The input parameters typically included the vehicle speed, vehicle type, and some pavement parameters. The environmental parameters influencing sound propagation were more important than in the other type of models and were usually included.

Table 78: Summary of tire-pavement interface models on TPIN

No.	Author	Model Name	Year	Ref.	Method	Output	Frequency Range [Hz]	Mechanism	Driver Parameter	Tire Parameter	Pavement Parameter	Environment Parameter
1	Fong	Truck Contact	1998	540	Transfer function	OBSP, 1/3 octave band	10-4000	TPIN	45 km/h	Passenger and truck	Texture, contact pressure spectrum	N/A
2	Domenichini et al.	DGAC Texture	1999	63	Cross-correlation, regression	OBSP, pass-by, OASPL	22-5500	TPIN	Speed	Slick & normal	Texture index	N/A
3	Beckenbauer and Kuijpers	SPERoN	2001	487	Multivariate regression analysis	CB, $L_{pA,max}$, 1/3 octave band SPL	125-5000	TPIN	50-120 km/h	Slick, tire width	Shape factor, contact pressure spectrum	N/A
4	Kuijpers and Blokland	Enhanced SPERoN	2003	865	Multivariate regression analysis	CB, $L_{pA,max}$, 1/3 octave band SPL	125-5000	TPIN	50-120 km/h	Tread pattern, tire width, rubber hardness	Shape factor, contact pressure spectrum, mechanical impedance	20 °C
5	Klein and Hamet	HyRoNE	2007	443	Envelopment, regression	CPB, $L_{pA,max}$, 1/3 octave band SPL	100-5000	TPIN	70, 90, 110 km/h	Michelin Energy XH1/E3A	Enveloped texture, absorption, airflow resistance	20 °C
6	Rustighi et al.	Road Excitation	2008	874	FEM, BEM, 2D Gaussian	Vibration, SPL	10-400	Texture impact, radiation, interior	20-100 km/h	Smooth	Texture excitation	N/A
7	Dubois et al.	Viscoelastic Contact	2011	882	Macro-scale, multi-asperity	Near field, 1/3 octave band SPL	315-1000	Texture impact	90 km/h	Slick 186/57R15	Texture, contact force spectrum	N/A
8	Dubois et al.	Contact Distribution	2013	61	Weighted linear regression	CPX, 1/3 octave band	315-1250	Impact	50-110 km/h	Slick and Patterned	Texture, contact force spectrum	N/A
9	Klein and Cesbron	3D Envelopment	2016	609	Envelopment, linear regression	CPX, 1/3 octave band; CB, $L_{p\max}$	250-1250 Hz	Belt vibration	65-110 km/h	Tread pattern	Texture	N/A

Table 79: Summary of mechanism separation models on TPIN

No.	Author	Model Name	Year	Ref.	Method	Output	Frequency Range [Hz]	Mechanism	Driver Parameter	Tire Parameter	Pavement Parameter	Environment Parameter
1	Cao et al.	Tire/Road Coupling	2008	583	N/A	SPL, narrowband	0-5000	Various	N/A	Tread pattern	Texture, absorption	N/A
2	Dare	Mechanism Decomposition	2012	213	Nonlinear least squares	OBSI, 1/3 octave band	500-5000	Sidewall, treadband, tangential vibration	Speed	SRTT	Texture levels, skewness, absorption, friction	N/A
3	Winroth et al.	Air Pumping Separation	2013	886	Curve fitting	CPB, 1/3 octave band SPL	125-4000	Tire vibration, air pumping	50-120 km/h	Slick	Texture	N/A
4	Mohamed and Wang	Deterministic SEA	2016	411	ICMM, SEA	SPL, energy, narrowband	0-500	Cavity resonance	Stationary, shaker	205/65R15	N/A	N/A
5	Le Bot et al.	Statistical Vibration	2017	887	Modal analysis	Mobility	0-4000	Vibration	29 psi	Slick 155/70R13	Point source	N/A
6	Wang and Duhamel	Network Resonator	2017	888	BEM, FEM	Lab, SPL	200-2000	Pipe resonance	Stationary	Tread pattern	Smooth	N/A

Table 80: Summary of noise propagation models on TPIN

No.	Author	Model Name	Year	Ref.	Method	Output	Frequency Range [Hz]	Mechanism	Driver Parameter	Tire Parameter	Pavement Parameter	Environment Parameter
1	DOT	CRTN (UK)	1988	890	Line source	Far field, L_{10}	N/A	Traffic	Speed, vehicle type	N/A	Type, MPD, slope	N/A
2	N/A	NMPB (France)	1996	900	Segmentation of line source	Far field, octave band, power, L_{den}	125-4000	Traffic	Speed, vehicle type, acceleration	N/A	Slope	Atmospheric absorption
3	Dai and Lee	Highway	2010	909	Ray acoustics	Pass-by, octave band SPL	N/A	Traffic	Speed, vehicle type, traffic volume	N/A	Type, porosity, permeability	Temperature, pressure
4	Wei et al.	Air Pumping	2016	366	Transfer function	Drum, SPL, narrowband	0-3500	Air pumping, radiation	461 kg, 180 kPa, 80 km/h	205/55R16, hand cut pattern	ISO 10844	N/A

5.5 Conclusions

In this work, the models on the tire-pavement interaction noise (TPIN) were divided into three categories: deterministic models, statistical models, and hybrid models.

The deterministic TPIN models include conventional physics models, finite element and boundary element models, and computational fluid dynamics models. They generally give insight into the noise generation and propagation mechanisms. The influence of each specific parameter on TPIN can be numerically analyzed. The conventional physics models typically use dynamic laws to calculate the tire vibration modes; the finite element and boundary element models are capable of obtaining the structure-borne tire noise under arbitrary excitations; the computational fluid dynamics models are intended for the airborne noise analysis. However, a large number of tire parameters are unavoidably needed for deterministic modeling, which is usually very difficult in practice. In addition, most of the models were limited to the frequency range of below 500 Hz, and few models went through the experimental validation. Therefore, the accuracy of these models is in question.

The statistical TPIN models include traditional regression models, principal component analysis models, and fuzzy curve fitting models. They generally correlate the noise levels with the influencing parameters using only experimental data without the knowledge of underlying mechanisms. It typically has better accuracy than the deterministic model. The traditional regression, including linear and non-linear regression, is widely used for models with easy form of equations and not too many variables; the principal component analysis can be used to reduce the number of variables; fuzzy logic has the advantage that no specific form of equations is needed for modeling. However, large amounts of data are needed for the statistical modeling, especially when the number of variables is large, which usually requires expensive labor cost. In addition, most of the current models only included variables related to the pavement; few models investigated the influence of tire parameters except for some fuzzy curve fitting models. It was also unlikely or impossible to gain insight into the noise generation mechanisms or separate these mechanisms.

The hybrid TPIN models include tire-pavement interface models, mechanism separation models, and noise propagation models. They combine the advantage of deterministic model

and statistical model. It sheds light on the noise generation mechanism as deterministic model, and meanwhile has good accuracy as statistical model. The tire-pavement interface model gives insight into the interaction and excitation between the tire and pavement; the mechanism separation model investigates the noise source individually; the noise propagation model is capable of predicting the TPIN at arbitrary locations. However, the hybrid model tends to be more complex than deterministic or statistical model. The careful selection of intermediate parameters is often the key to the success of the later statistical correlation procedure.

The deterministic models were dominant before 2000s, especially for conventional physics models. With the development of computing technology, FEM and CFD models thrive thereafter. These attempts have made great contributions to the understanding of TPIN generation mechanisms. Similarly, partly owing to the computing technology and data techniques, the statistical models start to play an important role after 2000s. The application of statistical algorithms to the TPIN modeling proves to be successful, and leads to decent prediction accuracy, which is very encouraging. In the 2010s, the hybrid models become more and more acceptable among researchers. The authors expect that the hybrid modeling approach will be a future direction in this area.

In addition, the on-board noise measurement techniques are more and more accepted in replacement of pass-by noise measurement techniques, because the former are able to obtain noise data of longer duration and with little environmental influence, which is favorable for the data analysis. As the microphone technology advances, narrowband spectrum is more and more frequently used for digital signal processing instead of octave, 1/3 octave band, or 1/12 octave band, owing to which more precise spectral contents can be analyzed and mechanisms identified.

6 Noise Reduction

As traffic noise is expected to be more of a environmental and health concern, the exploration to reduce the noise, especially tire road noise, will be of greater interest (Bückers and Stöckert, 2012 [484]). A lot of attempts have been conducted to reduce tire-pavement interaction noise at the source and to ensure a lasting effect, such as low-noise tires and quite road (Sandberg, 2001 [55]). The pavement seems to have greater potential for noise reduction (10 dB) compared to tire (4 dB) at speed of 60 mph (Mogrovejo et al., 2014 [673]; Saemann et al., 2012 [170]). In the following, the approaches to tire pavement noise reductions are introduced.

6.1 Quiet Tire

For a long time it was assumed that a quiet tire is an unsafe tire in general public. This assumption was based on the belief that quiet tires must be very smooth and consequently have a low skid resistance (Heckl (1986) [13]). As regulations for silent tires and vehicles are introduced internationally (Nijland et al., 2003 [34]), a number of design concepts to reduce tire noise have been presented, as shown in Table 81. Generally, there are two ways to reduce the noise relating to certain modes (Aboutorabi and Kung, 2012 [538]): (1) the mode frequency shifted to where the noise was less likely to be amplified or transferred; (2) more damping introduced into the tire. However, few of these design concepts are commercially viable due to manufacturing complexities and costs, safety and durability.

Table 81: Design concepts for quiet tire (green indicates put into mass production)

Category	Reference	Company/Institution	Modification	Method	Reduction Effect	Illustration
Tread vibration	Iwao and Yamazaki, 1996 [307]	Nissan Motor Co., Ltd. (Japan)	Tire tread	Attaching a rubber ring on the inside surface of the center part of the tread surface	5 dB (800-1600 Hz)	Figure 137
Tread vibration & cavity resonance	Saemann et al., 2011 [914]	Continental Reifen Deutschland GmbH (Germany)	Tire tread and cavity	Application of seal and foam absorber to the inside surface of tread band	7.5 dB (230-240 Hz)	Figure 138
Air pumping, pipe resonance	Zhou, 2013 [604]; Zhou et al., 2014 [915]	Jiangsu University (China)	Tread pattern	Reduction of fluid drag force and noise by using bypass structure and the bionic tread groove	>10 dB (800-1500 Hz)	Figure 139
	Kakumu, 1990 [916]	Sumitomo Rubber Industries (Japan)	Tread pattern	Circumferential length of contact patch is equal to transverse groove pitch multiplied by an integer.	5 dB	Figure 140

Category	Reference	Company/Institution	Modification	Method	Reduction Effect	Illustration
	Cusimano, 1992 [917]	Bridgestone/Firestone, Inc. (USA)	Tread pattern	Strategic placement of grooves such that the amount of groove void across the trailing and/or leading edges of the footprint is substantially uniform about the circumference of the tire	N/A	Figure 141
	Continental AG, 2016 [918]	Continental Reifen Deutschland GmbH (Germany)	Tread pattern	(1) "Harmonic Comfort Chambers" based on the "Helmholtz resonator" positioned on the inner shoulder of the tire pattern (2) "0' dB-Eaters" uniquely shaped in-groove elements designed to split and diffuse noise waves for lower road noise	N/A	Figure 142
Cavity/rim coupling resonance	Fitz and Heck, 2001 [919]	Epilogics Group (USA)	Rim	Lightweight steel rim to shift the modal frequency of the tire rim outside of 200-250 Hz	Ineffective (shift down 1 Hz)	Figure 143
	Sainty et al., 2012 [296]	RMIT University (Australia)	Tire tread	Extrusion of three strips of rubber from the tire into the cavity to shift the modal frequency of the tire cavity	Marginal (shift down 18 Hz)	Figure 144
	Sainty et al., 2012 [296]	RMIT University (Australia)	Rim and cavity	Attaching elastic ring on rim with separator fins which extends into the cavity due to centrifugal forces	Effective (shift up 156 Hz)	Figure 145
Cavity resonance	Molisani et al., 2003 [85,344]	Virginia Tech & Michelin North America, Inc. (USA)	Rim	Incorporation of secondary acoustic cavities to detune and damp out the main tire cavity resonance	15 dB force transmission (230 Hz)	Figure 146
	Kamiyama, 2014 [920]	Honda R&D Co. Ltd. (Japan)	Rim	Assembling separate thin, lightweight plastic resonators in the wheel well	10 dB (190-230 Hz)	Figure 147
	Fernandez, 2006 [921]	KTH University (Sweden)	Rim	Implementation of a Helmholtz resonator attached to the rim	Obvious (205-240 Hz)	Figure 148
	Sainty et al., 2012 [296]	RMIT University (Australia)	Cavity	Introduction of a sound absorption material	14 dB (225 Hz)	Figure 149
	Yukawa et al., 2004 [922]	Sumitomo Rubber Industries (Japan)	Cavity	Gluing layer of foam to the inner liner beneath the tread	Obvious (interior noise)	Figure 150
	Pirelli, 2013 [923]	Pirelli & C. SpA (Italy)	Cavity	Pirelli Noise Cancelling System (PNCS, P ZERO™): polyurethane sponge inserted into the cavity to absorb the vibrations	2~3 dB	Figure 151
	Mohamed and Wang, 2015 [393]	RMIT University (Australia)	Tire	Placing a trim layer onto the inner surface of the tire tread	10 dB (225 Hz)	Figure 152

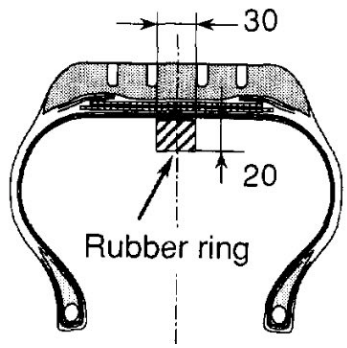

Figure 137: Attaching a rubber ring on the inside surface of the center part of the tread surface (source from Iwao and Yamazaki, 1996 [307], Figure 13; reprinted under fair use provision)

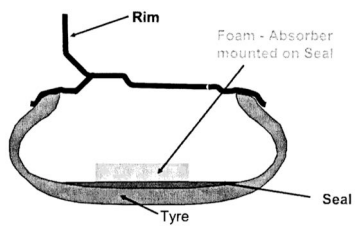

Figure 138: Tire cross section with seal and foam absorber mounted on a rim (source from Saemann et al., 2011 [914], Figure 1; reprinted under fair use provision)

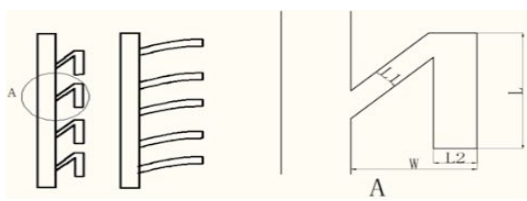

Figure 139: Reduction of fluid drag force and noise by using bypass structure and the bionic tread groove (source from Zhou et al., 2014 [915], Figure 4; reprinted under fair use provision)

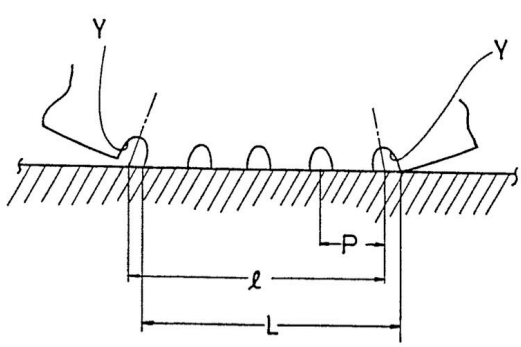

Figure 140: Illustration of low noise transverse groove (L = 4×P) (source from Kakumu, 1990 [916], Figure 2; reprinted under fair use provision)

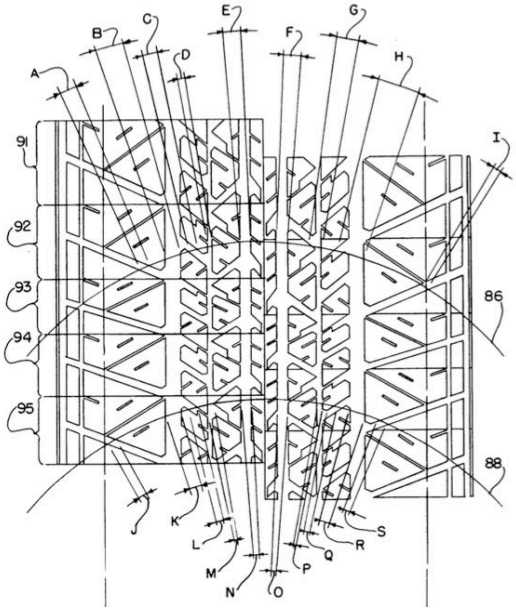

Figure 141: Illustration of low noise tread pattern (The sum of the groove void (A+B+C+D+E+F+G+H+l) along projection 86 is substantially equal to the sum of groove void (J +K+L+M+N+O+P+Q+R+S) along projection 88) (Source from Cusimano, 1992 [917], Figure 1A; reprinted under fair use provision)

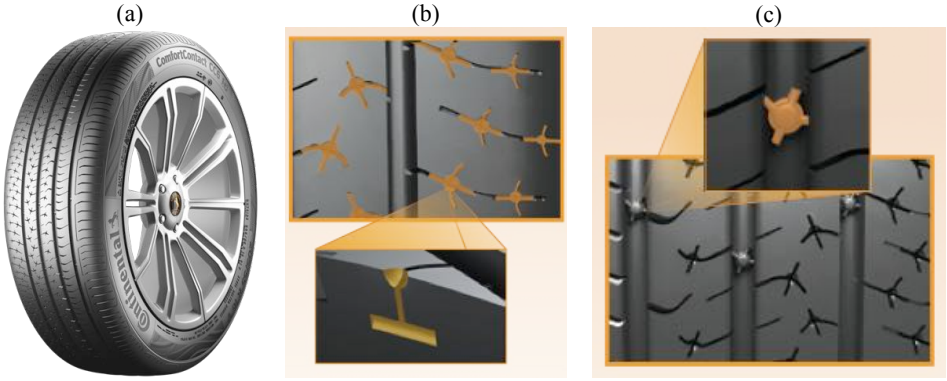

Figure 142: (a) Product image of Continental ComfortContact CC6; (b) harmonic comfort chambers; (c) 0' dB-Eaters (Source from Continental AG, 2016 [918]; reprinted under fair use provision)

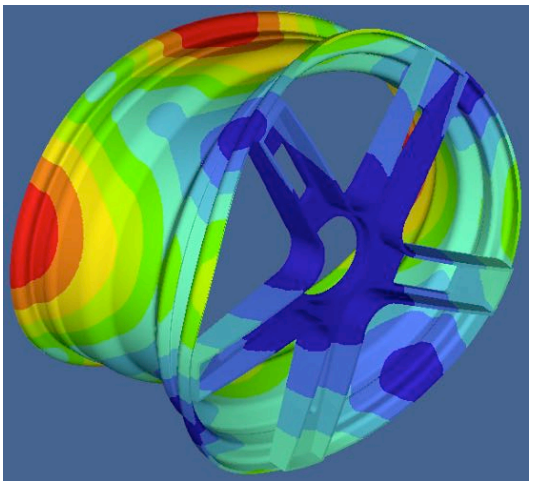

Figure 143: Finite element displacement analysis results for Kühl wheel mode shape at 210 Hz (source from Sainty et al., 2012 [296], Figure 2; reprinted with permission from ASME)

Figure 144: CAD model of a tire with three rubber strips extruded into the cavity (source from Sainty et al., 2012 [296], Figure 6; reprinted with permission from ASME)

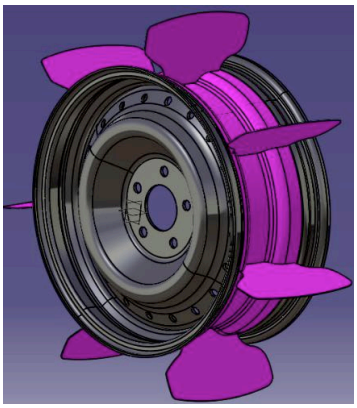

Figure 145: CAD model of proposed elastic ring with the four fins attached (source from Sainty et al., 2012 [296], Figure 10; reprinted with permission from ASME)

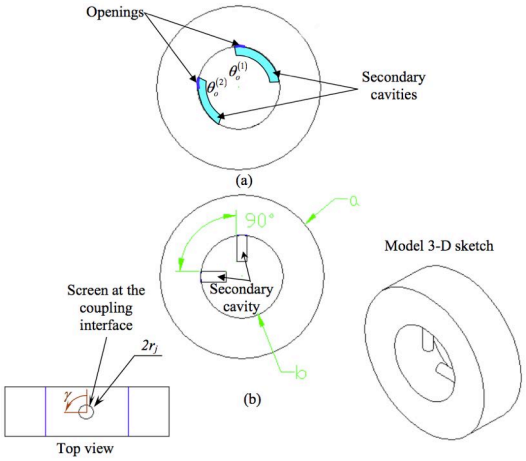

Figure 146: Incorporation of secondary acoustic cavities to detune and damp out the main tire cavity resonance (source from Molisani, 2004 [344], Figure 4.2; reprinted under fair use provision)

Figure 147: Assembling separate thin, lightweight plastic resonators in the wheel well (source from Kamiyama, 2014 [920], Figure 1; reprinted under fair use provision)

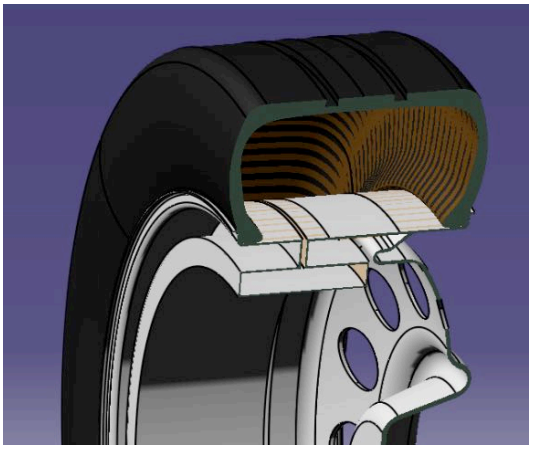

Figure 148: CAD model fitted with Helmholtz resonator (source from Sainty et al., 2012 [296], Figure 4; reprinted with permission from ASME)

Figure 149: Testing tire filled with PU foam prior to the wheel rim and tire assembling (source from Sainty et al., 2012 [296], Figure 7; reprinted with permission from ASME)

Figure 150: TireSilencer with white rigid foam support removed from tire after 1,053 miles (source from Schmidt and Majumdar, 2011 [924], Figure 2; reprinted under fair use provision)

Figure 151: Pirelli Noise Cancelling System (PNCS) (source from Tire Business, 2013 [925] ; reprinted under fair use provision)

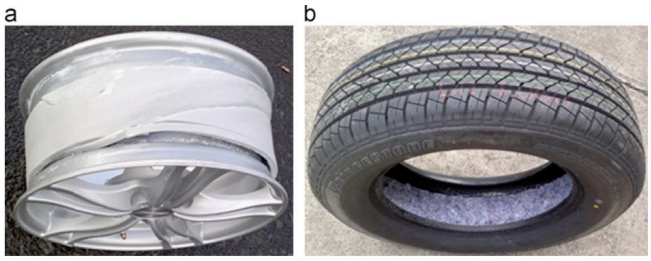

Figure 152: Installation of the trim onto the rim and tire (a. the trim layer on the rim; b. the trim layer onto the tire) (source from Mohamed and Wang, 2015 [393], Figure 7; reprinted with permission from Elsevier)

Tire tread element sequencing has been extensively investigated for reduced noise. Morgan (2002) [926] optimized a three-pitch sequence where the relative length of shortest pitch (S) is 0.8, medium pitch (M) is 1.0, and longest pitch (L) is 1.2. 100 pitch sequences were proposed and the acoustically preferred one is LMSMSLMLMLMLMLMMLMLMLMLMLM.

During tire design process, a lot of parameters have contradictory effects on tire parameters and compromises and optimizations are needed to achieve vehicle performances such as traction, rolling resistance, durability, ride comfort, noise, wear resistance, etc. (Lee et al., 2011 [927]), as shown in Figure 153, Figure 154 and Table 82.

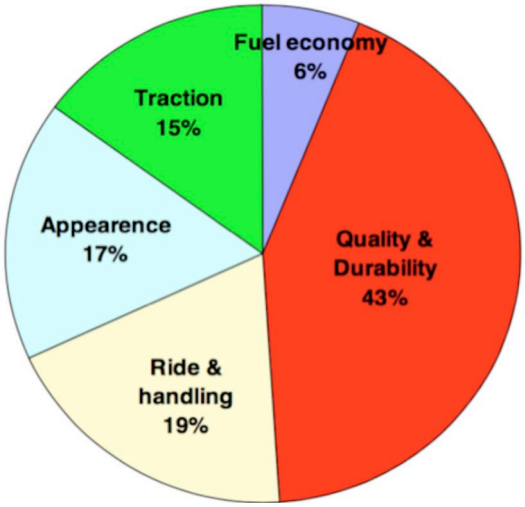

Figure 153: Criteria for the choice of tires by consumers (source from FEHRL, 2001 [28], Figure 49; reprinted under fair use provision)

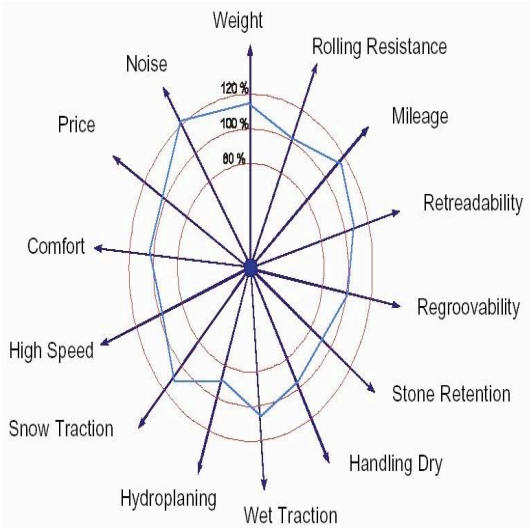

Figure 154: Polar diagram illustrating the property profile of a particular tire (source from FEHRL, 2001 [28], Figure 26, kindly obtained from Dr. Saemann, Continental Tyres; reprinted under fair use provision)

Table 82: Target conflicts in tire development (red indicates bad; green indicates good; yellow indicates ambiguous) (modified from FEHRL, 2001 [28])

Performance	Tread				Construction			
	Compound		Design		Footprint		Sidewall	
	Stiffness	Damping	Increasing Block Size	Increasing Number of Sipes	Round	Squared	Stiff	Soft
Winter (Snow)								
Noise								
Wet Grip								
Handling								
Dry Braking								
Aquaplaning								
Rolling Resistance								
Mileage								
Endurance								
High Speed								
Heat Build-up								
Comfort (NVH)								
Flat Spot								

However, there seems to be no consistent conflict between noise characteristics and friction, rolling resistance, wet braking or aquaplaning speed after examining about 100 modern car tires of similar size (Sandberg et al., 1998 [928]; Sandberg and Ejsmont, 2000 [171]).

On the contrary, reducing noise might meantime also reduces rolling resistance and possibly improve friction characteristics. Low noise tread pattern design includes pattern randomization, ventilating channels, reducing the air/rubber ratio (to 20% from today's common value 30% [28]), increasing the number of circumferential tread elements preferably up to 100 (common is 65), increasing number of sipes, or optimizing tread element pitch sequence (Kim et al., 2012 [462]), most of which are also favorable to hydroplaning performance.

There is also no strong evidence showing tradeoff between low noise emission and high safety either, although there exists common prejudice that low noise tire will sacrifice safety (Sandberg, 2001 [55]). It was also shown that low noise technology could be adapted to run flat tires (FEHRL, 2001 [28]). In general, the tires on the market with high safety show characteristics of high noise, but just statistically ($R^2 = 0.29$) not deterministically (Nelson et al., 1993 [929]; FEHRL, 2001 [28]).

There is no denying that the modifications for noise reduction might influence other tire performances. Saemann et al. (2012) [170] presented that lowering sound level by 3 dB might result in several drawbacks associated with other performance, as listed in Table 83.

Table 83: Modifications to lower tire noise and the drawbacks (Saemann et al., 2012 [170])

Parameter	Modification	Influence
Tread pattern	From 34% void volume to slick	Increase in wet braking by 40 % Increase in aquaplaning in curve by 60 %
Tread material	From summer tread compound to ice tread compound (decrease rubber hardness/stiffness)	Increase in wear by 50 %
Tread material	From normal tread to thicker under tread (decrease contact stiffness)	Increase in rolling resistance by 15 %
Carcass	Increase belt stiffness (such as increasing the number of the plies, adding reinforcement rubber, and using steel ply materials)	Decrease in wear by 20 % Increase in cornering power by 10 %

Major tire companies also produce quiet tires, such as Goodyear Assurance ComforTred, Hankook Optimo H727, Hankook Ventus S1 evo^2 SUV (foam attached on the inside of tire tread), Yokohama "dB-tyre", Michelin Primacy LC, Michelin Defender, Michelin Primacy MXV4, Michelin Energy Saver A/S, and Michelin Primacy 3 ST.

6.2 Quiet Pavement

For the same driving conditions, there can be as much as a 9 dBA difference for a single pavement type and as much as a 14 dBA difference between different types of pavement (Bernhard and Wayson, 2005 [66]). There are some suggestions on noise reduction in terms of pavement characteristics, listed in Table 84.

Table 84: General suggestions on noise reduction in terms of pavement characteristics (Rasmussen, 2010 [831])

Parameter	Suggestion
Texture	Avoid (flatten) texture at intervals > 1 inch or smooth (floated or polished) surfaces to allow for escape channels for air
	Negative texture (grooves, not fins)
	Texture oriented longitudinally; if transverse, should be closely spaced and randomized
Concrete	Strong and durable mortar; mix optimized for placement, finishing, curing
	Siliceous sands for durability and friction (hard, durable, and polish resistant coarse aggregate for diamond grinding; adequate and consistent depth of mortar near the surface for tined and drag textures)
Joints	Narrow, single-cut joints preferred and avoid widened (reservoir) cuts
	Avoid faulted or spalled joints; design or retrofit adequate load transfer
Aggregate	Increase porosity (porous asphalt, over 20%) and depth of the porous layer
	Decrease pavement stiffness (elastic pavement)

A couple of pavements are reported to be quiet pavement or have potential to be, as displayed in Table 85.

Table 85: Quiet pavement technologies (McGhee, 2012 [606]; Mogrovejo et al., 2014 [673])

Category	Technology
Asphalt Concrete	Rubberized Asphalt Concrete (RAC) [909]
	Polymer-Modified Asphalt Concrete (PMAC) or Fiber-Modified Asphalt Concrete (FMAC)
	Porous friction course surfaces with and without rubber
	Open-graded asphalt with small aggregate size and porosity over 20% (reported to be quietest pavement currently in use)
	Poroelastic Road Surface (PERS)
Cement Concrete	Conventional Diamond Grind (CDG)
	Next Generation Concrete Surface (NGCS)
	Surface modification of Portland Cement Concretes (PCC) by introducing 15-20 % porosity: (1) through non-aggregate component of the mixture, resulting in Enhanced Porosity Concrete (EPC); (2) through the use of soft inclusions (cellulose fibers) in the matrix, resulting in Cellulose-Cement Composites (Neithalath, 2004 [930]; Neithalath et al., 2005 [663])

In addition, there are some other novelty pavement designs but might need further

investigation and validation. Hofman and Kooij (2003) [931] demonstrated a three-layer design: the top two layers are assembled as one roll-up layer with a thickness of 30 mm, and the bottom support layer has cavities as Helmholtz resonators. Maennel et al. (2013) [932] presented a similar Helmholtz type porous asphalt, as illustrated in Figure 155. A noise attenuation of 3 dB was found compared to the twin layered porous asphalt and it also had good acoustic durability.

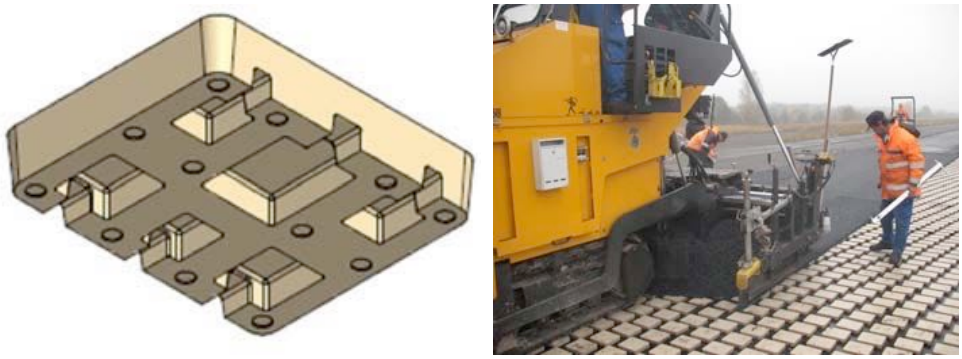

Figure 155: Helmholtz type porous asphalt (left) and laying process (right) (source from Maennel et al. (2013) [932], Figure 7, Figure 8; reprinted with permission from Mr. Manuel Männel of Müller-BBM GmbH, Germany)

For the quiet concrete pavements, Next Generation Concrete Surface (NGCS) might be the most important. NGCS is basically Conventional Diamond Grind (CDG) followed by a flush-grind operation and a longitudinal grooving step (Mogrovejo et al., 2014 [673]). It is a consistent, predictable, and quiet nonporous concrete texture with good lateral stability and hydroplaning resistance.

For the quiet asphalt concrete pavements, Poroelastic Road Surface (PERS) might be the most promising (Nilsson and Zetterling, 1990 [933]). It is a wearing course with a very high porosity (>20%) and high proportion of rubber or epoxy (>20% in weight) either in the shape of granules or elongated fiber-like particles (Sandberg and Goubert, 2011 [313]). It was claimed that it was 10 dBA quieter than conventional pavements. Noise attenuation is likely to occur for almost all noise mechanisms on PERS, such as low texture impact due to aggregate of small maximum size and small stiffness, low air pumping and high absorption due to high void content, low stick/slip and stick/snap motions due to rubber/rubber contact. It is also expected to have good traction and wet skid resistance properties. However, nearly all field

tests so far have failed in in some way or the other, such as bad durability, even though it has been brought up by Nilsson around 40 years ago (Nilsson, 1979 [934]), indicating that further improvements are necessary. For example, PERS increased the tire rolling resistance, which decreased the fuel economy.

6.3 Combination of Tires and Pavements

The contributions on noise reduction from tires and pavements cannot be considered separately. A "quiet tire" on one specific pavement might not be quiet on other type of pavements; similarly, a "quiet pavement" might not work for all the tires.

Fong (1998) [540] reported that the cross ply truck tire (7.00R15) for medium truck was among the noisiest over a relatively coarse chipseal pavement, but was one of the quietest on a smoother chipseal pavement. Blokland and Leeuwen (2010) [712] investigated more than 2000 tire/road combinations and found that the sound reduction due to the combination of silent surfaces and silent tires is smaller then the numeric sum of both, especially for rough pavements where the silencing effects of quiet tires are marginal. Berge and Haukland (2011) [935] indicated that the Bridgestone B-250 has a relatively high type approval level (73 dBA), but is more silent on Norwegian dense (and rough) surfaces than some other tires. The Michelin Energy Saver has been rated as a quiet tire in terms of interior noise but is shown to be rather noisy in the exterior.

However, Berge and Haukland (2011) [935] also demonstrated that some tires seem to perform as low-noise tires independent of the type of pavements.

6.4 Other Considerations

Couche and Fller (1998) [936] applied Active Noise Control (ANC) for cabin noise from power train (40-500 Hz) with advanced speakers. Sun et al. (2012) [937] used Active noise control (ANC) for low-frequency structure-borne vehicle interior from tire road interaction and approved its efficiency. Zafeiropoulos et al. (2015) [938] investigated the active control of structure-borne interior noise based on the separation of front and rear structural noise related dynamics. However, the authors found no literature investigating the active noise control of exterior noise.

As electric and hybrid motor vehicles (E/H vehicles) gained increasing interest, there

might going to be a significant reduction (3-4 dB) of traffic noise emissions (Jabben et al., 2012 [939]). On the other hand, concerns arise that E/H vehicles with quiet pavements might pose a severe threat to the safety of vulnerable road users due to poor vehicle detection ability (Mendonça, 2013 [940]). Some regulations start to focus on limiting the minimum sound of electric vehicles. However, Sandberg (2013) [941] pointed out that it is currently far more justified to work towards reducing the noise emission of the noisiest vehicles than adding noise to the quiet ones.

References

1. Thrasher DB, Miller RF, Bauman RG. Effect of pavement texture on tire/pavement interaction noise. In: *SAE Technical Papers*. 400 Commonwealth Drive, Warrendale, PA 15096-0001, United States; 1976. http://dx.doi.org/10.4271/762011.

2. Miller RF, Thrasher DB. Passby tire/pavement interaction noise measurement problems. In: *SAE Technical Papers*. 400 Commonwealth Drive, Warrendale, PA 15096-0001, United States; 1976. http://dx.doi.org/10.4271/762012.

3. Pottinger MG, Marshall KD, Lawther JM, Thrasher DB. Review Of Tire/Pavement Interaction Induced Noise And Vibration. In: *ASTM Special Technical Publication*. ASTM Special Technical Publication. BFGoodrich Co, Brecksville, OH, USA, BFGoodrich Co, Brecksville, OH, USA; 1986:183-287.

4. Donavan PR. Assessment of tire/pavement interaction noise under vehicle passby test conditions using sound intensity measurement methods. *J Acoust Soc Am*. 1998;103. http://dx.doi.org/10.1121/1.422107.

5. Khazanovich L, Izevbekhai BI. Implication of time-dependent texture degradation on pavement on board sound intensity patterns in MnROAD test cells. In: *Proceedings of the International Noise Conference, Dearborn Michigan July 2008*.; 2008.

6. Syamkumar A, Aditya K, Chowdary V. Development of mode-wise noise prediction models for the noise generated due to tyre-pavement surface interaction. *Adv Mater Res*. 2013;723:50-57. http://dx.doi.org/10.4028/www.scientific.net/AMR.723.50.

7. Sandberg U, Ejsmont JA. *Tyre/road Noise Reference Book*. Kisa, Sweden; Harg, Sweden: INFORMEX; 2002.

8. Sandberg U, Ejsmont JA. The Tire/Road noise computerized bibliography. In: *International Symposium, Euro Noise '95: Software for Noise Control; 1995; Lyon; France*.; 1995:289-294.

9. Sabiniarz P, Kropp W. A waveguide finite element aided analysis of the wave field on a stationary tyre, not in contact with the ground. *J Sound Vib*. 2010;329(15):3041–3064. doi:http://dx.doi.org/10.1016/j.jsv.2010.02.008.

10. Harrison M. Vehicle Refinement: Controlling Noise and Vibration in Road Vehicles. In: MA, USA: Elsevier; 2004.

11. Chen C, Kuan Y, Chen C, Sung M. Using CFD Technique to Investigate the Effect of Tire Roiling-noise with Different Pattern Design. In: *Applied Mechanics and Materials*.Vol 575. Switzerland; 2014:469-472. http://dx.doi.org/10.4028/www.scientific.net/AMM.575.469.

12. Wayson LR. On-Board Sound Intensity (OBSI) Study, Phase 2, Summary. In: *Final Report, FDOT Project No. #BDT06*. United States; 2014:1p-.

13. Heckl M. Tire noise generation. *Wear*. 1986;113:157-170.

14. European Commission. Future Noise Policy. In: *European Commission Green Paper. COM (96) 540 Final, 04 November 1996, Brussels*.; 1996.

15. Remington PJ, Dixon NR, Wittig LE, Kurzweily LG, Menge CW, Stahr JD. Control of wheel/rail noise and vibration. In: *US DOT Report DOT-TSC-UMTA-82-57*.; 1983.

16. Murphy E, King EA. Scenario analysis and noise action planning: Modelling the impact of mitigation measures on population exposure. *Appl Acoust*. 2011;72(8):487–494. http://dx.doi.org/10.1016/j.apacoust.2010.10.006.

17. Kim R. Burden of disease from environmental noise. In: *WHO International Workshop on "Combined Environmental Exposure: Noise, Air Pollutants and Chemicals" Ispra*.; 2007.

18. Pan L, Boulet JAM. Noise exposure level of the drivers of heavy duty diesel trucks. *Noise Control Eng J*. 2014;62(3):132-137. http://dx.doi.org/10.3397/1/376213.

19. Goodwin SE, Shriver WG. Effects of traffic noise on occupancy patterns of forest birds. *Conserv Biol*. 2011;25(2):406-411. doi:10.1111/j.1523-1739.2010.01602.x.

20. Lengagne T. Traffic noise affects communication behaviour in a breeding anuran, Hyla arborea. *Biol Conserv*. 2008;141(8):2023-2031. doi:10.1016/j.biocon.2008.05.017.

21. Bee M a., Swanson EM. Auditory masking of anuran advertisement calls by road traffic noise. *Anim Behav*. 2007;74:1765-1776. doi:10.1016/j.anbehav.2007.03.019.

22. Sandberg U. Noise emissions of road vehicles effect of regulations: Final Report 01-1. *Noise News Int*. 2001;9(3):147-203.

23. European Economic Community. Council Directive 70/157/EEC. In: *6 February 1970 on the Approximation of the Laws of the Member States Relating to the Permissible Sound Level and the Exhaust System of Motor Vehicles. Official Journal NO. L 042, 23/02/1970 P. 0016–0020, and Subsequent Amendments*.; 1970.

24. EC. DIRECTIVE 2002/49/EC OF THE EUROPEAN PARLIAMENT AND OF THE COUNCIL of 25 June 2002 relating to the assessment and management of environmental noise. 2002.

25. EU. REGULATION (EU) No 540/2014 OF THE EUROPEAN PARLIAMENT AND OF THE COUNCIL of 16 April 2014 on the sound level of motor vehicles and of replacement silencing systems, and amending Directive 2007/46/EC and repealing Directive 70/157/EEC. 2014.

26. EU. REGULATION (EU) No 168/2013 OF THE EUROPEAN PARLIAMENT AND OF THE COUNCIL of 15 January 2013 on the approval and market surveillance of two- or three-wheel vehicles and quadricycles. 2013.

27. EC. DIRECTIVE 2001/43/EC OF THE EUROPEAN PARLIAMENT AND OF THE COUNCIL of 27 June 2001 amendingCouncilDirective92/23/EECrelatingtotyresformotorvehiclesandtheirtrailersandto their fitting. 2001.

28. FEHRL (Forum of European National Highway Research Laboratories). Tyre/road noise. In: *FEHRL Final Report SI2.408210*.; 2001.

29. EC. REGULATION (EC) No 661/2009 OF THE EUROPEAN PARLIAMENT AND OF THE COUNCIL of 13 July 2009 concerning type-approval requirements for the general safety of motor vehicles, their trailers and systems, components and separate technical units

intended therefor. In: ; 2009.

30. EC. EGULATION (EC) No 1222/2009 OF THE EUROPEAN PARLIAMENT AND OF THE COUNCIL of 25 November 2009 on the labelling of tyres with respect to fuel efficiency and other essential parameters. In: ; 2009.

31. UNECE. ECE R117/2011 Uniform provisions concerning the approval of tyres with regard to rolling sound emissions and to adhesion on wet surfaces and/or to rolling resistance. 2011.

32. UN/ECE. ECE R51 Concerning the adoption of uniform technical prescriptions for wheeled vehicles, equipment and parts which can be fitted and/or be used on wheeled vehicles and the conditions for reciprocal recognition of approvals granted on the basis of these pr. 2011.

33. European Automobile Manufacturers' Association (ACEA). Vehicle Noise - Setting the right sound levels. 2012.

34. Nijland R, Vos E, Hooghwerff J. The Dutch Noise Innovation Program Road Traffic (IPG). In: *The 32nd International Congress and Exposition on Noise Control Engineering, Inter-Noise 2003*.; 2003.

35. RenMinWang. China Green Tyre Rating Assessment (C-GTRA). 2016. http://auto.people.com.cn/n1/2016/0424/c1005-28300099.html.

36. European Tyre & Rubber Manufacturers' Association (ETRMA). Tyre Labelling. In: *Http://www.etrma.org/tyres/tyre-Labelling*.

37. Federal Highway Administration. Procedures for Abatement of Highway Traffic Noise and Construction Noise. In: *Code 23, Section 772*.; 2010.

38. Ontario Ministry of the Environment (MOE). Noise Assessment Criteria in Land Use Planning. In: *Publication LU-131, Canada, ISBN 0-7778-4919-4*.; 1997.

39. CPCB. The noise pollution (regulation and control) rules. In: *Central Pollution Control Board, Ministry of Environment and Forests, Government of India, New Delhi, India*.; 2000.

40. Kim U, Maunder M, Grant P, Mawdsley D. Developing a Car to Meet New Pass-By Noise Requirements using Simulation and Testing. *SAE Tech Pap 2015-01-2319*. 2015. doi:10.4271/2015-01-2319.Copyright.

41. Mohamed Z, Wang X, Jazar R. A survey of wheel tyre cavity resonance noise. *Int J Veh Noise Vib*. 2013;9(3-4):276-293. http://dx.doi.org/10.1504/IJVNV.2013.055811.

42. Wang G, Shores R, Botts J, Hibbett R. On-Board Sound Intensity Tire-Pavement Noise Study in North Carolina. 2011;(December):210p-.

43. Plotkin KJ, Stusnick E. A Unified Set of Models for Tire/Road Noise Generation. In: *Report: WR-81-26, 63p, Environmental Protection Agency, Arlington, VA. Office of Noise Abatement and Control*. United States; 1981:63p-.

44. Federal Highway Administration. Highway Traffic Noise: Analysis and Abatement Guidance. In: *U.S. Department of Transportation, Federal Highway Administration, Office of Environmental and Planning, Noise and Air Quality Branch, Washington, D.C.*; 2010.

45. Donovan PR, Pierce LM, Lodico DM, Rochat JL, Knauer HS, Donavan PR. Evaluating Pavement Strategies and Barriers for Noise Mitigation. 2013:73p-.

46. Jones W. Highway Noise Control with HMA. *Asphalt*. 2002.

47. Kohler E. OBSI Testing. In: *Presentation at Pavement Evaluation 2010, Roanoke, Virginia*.; 2010.

48. Braun ME, Walsh SJ, Horner JL, Chuter R. Noise source characteristics in the ISO 362 vehicle pass-by noise test: Literature review. *Appl Acoust*. 2013;74(11):1241-1265. doi:10.1016/j.apacoust.2013.04.005.

49. Robert Bosch GmbH. *Automotive Handbook*. 6th ed. SAE; 2004.

50. Fry J, Jennings P, Taylor N, Jackson P. Vehicle drive-by noise prediction: A neural networks approach. In: *SAE Technical Paper Series 1999-01-1740*.; 1999.

51. Biermann J-W. Geräuschverhalten von Kraftfahrzeugen (Noise characteristics of vehicles). In: *Lecture Notes. Aachen: Institute for Vehicles at RWTH Aachen University*.; 2004.

52. Zeller P. *Handbuch Fahrzeugakustik (Handbook Vehicle Acoustic)*. Vieweg+Teubner Verlag; 2009.

53. Alfredson R, Davies P. The radiation of sound from an engine exhaust. *J Sound Vib*. 1970;13:389-408.

54. NZ Transport Agency. *Guide to State Highway Road Surface Noise*.; 2014.

55. Sandberg U. Tyre / road noise – Myths and realities. In: *The 2001 International Congress and Exhibition on Noise Control Engineering*.; 2001.

56. Yang D, Wang Z, Li B, Luo Y, Lian X. Quantitative measurement of pass-by noise radiated by vehicles running at high speeds. *J Sound Vib*. 2011;330(7):1352-1364. http://dx.doi.org/10.1016/j.jsv.2010.10.001.

57. Bravo T, Ibarra D, Cobo P, Ibarra D. Extrapolation of maximum noise levels from near-field measurements to far-field positions. In: *American Society of Mechanical Engineers, Noise Control and Acoustics Division (Publication) NCAD*.Vol 12. New York City, NY, United states; 2012:10337-10348. http://dx.doi.org/10.1115/NCAD2012-0517.

58. Saemann E-U. Holistic approach for rolling sound mitigation. In: *41st International Congress and Exposition on Noise Control Engineering 2012, INTER-NOISE 2012*.Vol 10. New York, NY, United states; 2012:8275-8286.

59. Donavan PR. Investigations of the influence of lower frequency aerodynamic noise on interior cruise and exterior pass-By sound levels. In: *SAE Technical Papers*.Vol 5. 400 Commonwealth Drive, Warrendale, PA 15096-0001, United States; 2012. http://dx.doi.org/10.4271/2012-01-1554.

60. Freeman T, Cerrato G. Vehicle pass-by noise estimations for component-level design. In: *SAE Technical Papers*. Rapids, MI, United states; 2011. http://dx.doi.org/10.4271/2011-01-1608.

61. Dubois G, Cesbron J, Yin HP, Anfosso-Ledee F, Duhamel D. Statistical estimation of low frequency tyre/road noise from numerical contact forces. *Appl Acoust*. 2013;74(9):1085-1093. http://dx.doi.org/10.1016/j.apacoust.2013.03.011.

62. Rasmussen RO, Bernhard RJ, Sandberg U, Mun EP. The Little Book of Quieter Pavements. *Rep No FHWA-IF-08-004*. 2007.

63. Domenichini L, Fracassa A, La Torre F, Loprencipe G, Ranzo A, Scalamandrè A. Relationship between road surface characteristics and noise emission. In: *First International Colloquium on Vehicle Tyre Road Interaction, Rome, Italy, Paper 99.03*.; 1999:1-22.

64. Dechipre H, Hartmann M, Ewert R, Delfs JW. Assessment of Numerical Methods for Computation of Automotive Rain Gutter Wind Noise. In: *16th AIAA/CEAS Aeroacoustics Conference (31st AIAA Aeroacoustics Conference)*.Vol vol.1. Reston, VA, USA; 2010:835-847.

65. Gasparoni S, Czuka M, Kriegisch M, Wehr R, Conter M, Haider M. Controlled-pass-by measurements of electric vehicles within the FOREVER projekt. In: *Proceedings of Forum Acusticum*.Vol 2014-Janua. 30 Mickiewicza Av., Krakow, Poland; 2014:Ecophone; et al.; KFB Poland; Ministry of Science.

66. Bernhard RJ, Wayson RL, Haddock JE, et al. *An Introduction to Tire / Pavement Noise of Asphalt Pavement*.; 2005.

67. Schuhmacher A. Blind Source Separation Applied to Indoor Vehicle Pass-By Measurements. *SAE Int J Passeng Cars - Mech Syst*. 2015;8(3):1034-1041. http://dx.doi.org/10.4271/2015-01-2320.

68. He J, Jin X, Wang W, Jianfeng H, Xiaoxiong J, Wanying W. Analysis of tire tread pattern's impact on interior vibration and noise based on Wavelet Transform. In: *Applied Mechanics and Materials*.Vol 66-68. Nanchang, China; 2011:1755-1761. http://dx.doi.org/10.4028/www.scientific.net/AMM.66-68.1755.

69. Chang J, WanYing W, XiaoXiong J, et al. Study on tire noise transfer path identification. In: *2010 10th International Conference on Signal Processing Proceedings (ICSP 2010)*. 2010 10th International Conference on Signal Processing Proceedings (ICSP 2010). Beijing, China: IEEE; 2010:2629-2632. doi:10.1109/ICOSP.2010.5656122.

70. Jen MU, Lu M-H. Effects of vehicle suspension characteristics on road-induced interior noise. In: *Turkish Acoustical Society - 36th International Congress and Exhibition on Noise Control Engineering, INTER-NOISE 2007 ISTANBUL*.Vol 2. Istanbul, Turkey; 2007:1056-1065.

71. Lim C-S, Han E, Apelian C, Bogema D. A Study on North American Customer Preference to Interior Noise using Sound Balance Analysis. *SAE Int J Passeng Cars - Mech Syst*. 2014;7(1):32-40. http://dx.doi.org/10.4271/2014-01-0023.

72. Aissaoui A, Tupake RS, Bijwe V, et al. Flow-Induced Noise Optimization of SUV HVAC System using a Lattice Boltzmann Method. *SAE Int J Passeng Cars - Mech Syst*. 2015;8(3):1053-1062.

73. Nykänen A. Methods for Product Sound Design. In: *Ph.D. Thesis, Division of Sound and Vibration, Luleå University of Technology, Luleå*.; 2008.

74. Lopez I, Blom REA, Roozen NB, Nijmeijer H. Modelling vibrations on deformed rolling tyres-a modal approach. *J Sound Vib*. 2007;307(3-5):481-494.

doi:10.1016/j.jsv.2007.05.056.

75. Kitahara A, Akashi T, Waki Y, Heguri H, Warning N, Copyright C. Interior noise reduction by tire surface geometry and Helmholtz resonators on tread patterns. In: *40th International Congress and Exposition on Noise Control Engineering 2011, INTER-NOISE 2011*.Vol 1. Osaka, Japan; 2011:608-613.

76. Tsuji H, Maruyama S, Onishi K. Reciprocal Measurements of the Vehicle Transfer Function for Road Noise. *SAE Tech Pap 2015-01-2241*. 2015. doi:10.4271/2015-01-2241.Copyright.

77. Zhao T. Vehicle Interior Noise Identification and Control Based on Transfer Path Analysis. 2008.

78. Saguchi T, Yumii K, Zakelj P. Vehicle interior noise prediction using tire characteristics and vehicle transmissibility. In: *SAE Technical Papers*. Detroit, MI, United states; 2007. http://dx.doi.org/10.4271/2007-01-1533.

79. Kido I, Ueyama S. Coupled vibration analysis of tire and wheel for road noise improvement. In: *SAE Technical Papers*. Traverse City, MI, United states; 2005. http://dx.doi.org/10.4271/2005-01-2525.

80. Geluk T, Van Der Linden P, Vige' D, et al. Noise contribution analysis at suspension interfaces using different force identification techniques. In: *SAE Technical Papers*. Rapids, MI, United states; 2011. http://dx.doi.org/10.4271/2011-01-1600.

81. Bekke DA, Wijnant YH, De Boer A. Experimental review on interior tire-road noise models. In: *Proceedings of ISMA 2010 - International Conference on Noise and Vibration Engineering, Including USD 2010*. Leuven, Belgium; 2010:3953-3960.

82. Sottek R, Philippen B. Separation of airborne and structure-borne tire-road noise based on vehicle interior noise measurements. In: *SAE Technical Papers*. Graz, Austria; 2010. http://dx.doi.org/10.4271/2010-01-1430.

83. Sottek R, Philippen B. Tire-Road Noise Analysis of On-Road Measurements under Dynamic Driving Conditions. In: *SAE Technical Papers*.Vol 5. 400 Commonwealth Drive, Warrendale, PA 15096-0001, United States; 2012. http://dx.doi.org/10.4271/2012-01-1550.

84. Pietrzyk A. Prediction of the dynamic response of a tire. In: *The 2001 International Congress and Exhibition on Noise Control Engineering INTER-NOISE 2001, 27–30 August, The Hague, The Netherlands*.; 2001.

85. Molisani LR, Burdisso RA, Tsihlas D. A coupled tire structure/acoustic cavity model. *Int J Solids Struct*. 2003;40(19):5125-5138. http://dx.doi.org/10.1016/S0020-7683(03)00259-2.

86. Fischer J, Behrendt M, Lieske D, Albers A. Measurement and analysis of the interior noise and the transfer path of acoustic phenomena into the driver cabin of a battery electric vehicle. In: *Inter-Noise 2014*.; 2014.

87. Sung SH, Nefske DJ, Feldmaier DA. A structural-acoustic finite element method for predicting automotive vehicle interior road noise. In: *ASME International Mechanical Engineering Congress and Exposition, Proceedings*.Vol 15. Lake Buena Vista, FL, United states; 2010:527-534. http://dx.doi.org/10.1115/IMECE2009-11065.

88. Sung SH, Nefske DJ. A statistical regression-based energy method for estimating vehicle

interior noise in early vehicle design. In: *SAE Technical Papers*. St. Charles, IL, United states; 2009. http://dx.doi.org/10.4271/2009-01-2201.

89. Gur Y, Pan J, Wagner D. Sound Package Development for Lightweight Vehicle Design using Statistical Energy Analysis (SEA). *SAE Tech Pap 2015-01-2302*. 2015. doi:10.4271/2015-01-2302.Copyright.

90. De Langhe K, Vansant K, Hallez R, Beriot H. Advanced simulation techniques for vehicle acoustic panel loading predictions, including FEM AML and fast multipole BEM (FMBEM). In: *40th International Congress and Exposition on Noise Control Engineering 2011, INTER-NOISE 2011*.Vol 1. Osaka, Japan; 2011:789-802.

91. Lee S-K, Kim B-S, Park D-C. Objective evaluation of the rumbling sound in passenger cars based on an artificial neural network. *Proc Inst Mech Eng - Part D J Automob Eng*. 2005;219(4):457-469. http://dx.doi.org/10.1243/095440705X11112.

92. Peng W, Jin C, Zhou H. An experimental study on the influence of tire noise on the sound quality of car interior noise. In: *39th International Congress on Noise Control Engineering 2010, INTER-NOISE 2010*.Vol 5. Lisbon, Portugal; 2010:3579-3586.

93. Lalor N and P. The prediction of low- and mid-frequency internal road vehicle noise: a literature survey. In: *Proceedings of the Institution of Mechanical Engineers, Part D: Journal of Automobile Engineering, Vol. 221*.; 2007:245–269.

94. Campillo-Davo N, Peral-Orts R, Velasco-Sanchez E, Campello-Vicente H. An experimental procedure to obtain sound power level of tyre/road noise under Coast-By conditions. *Appl Acoust*. 2013;74(5):718-727. http://dx.doi.org/10.1016/j.apacoust.2012.10.007.

95. Siemens Product Lifecycle Management Soft- ware Inc. Standards and regulations in pass-by noise testing. In: *Technical Info, Siemens PLM Software*.; 2014.

96. Zakelj P. Tire tread noise treatment. In: *US Patent US6112167*.; 2000. http://www.google.com/patents/US6112167.

97. He Z, Lu L, Luo L. The energy distribution of tire-road noise and noisy speech based on wavelet packet. In: *Key Eng. Mater. (Switzerland)*.Vol 464. Switzerland; 2011:721-724. http://dx.doi.org/10.4028/www.scientific.net/KEM.464.721.

98. SungWook H, JinHyuk H, KiDuck S, et al. The study of tire pattern noise by using wavelet transform. In: *Applied Mechanics and Materials*.Vol 105-107. Shanghai, China; 2012:267-270. http://dx.doi.org/10.4028/www.scientific.net/AMM.105-107.267.

99. Chen X, Chen L, xia C, Lijun C. Analysis tire tread patterns noise based on Wavelet transform. In: *Advanced Materials Research*.Vol 823. Wuhan, Hubei, China; 2013:180-183. http://dx.doi.org/10.4028/www.scientific.net/AMR.823.180.

100. ISO. Acoustics - Method for measuring the influence of road surfaces on traffic noise - Part 1: The Statistical Pass-By Method. *ISO 11819-1*. 1997.

101. Rasmussen RO, Sohaney RC. Tire/Pavement and Environmental Traffic Noise Research Study. 2012:147p-.

102. ISO. Acoustics -- Method for measuring the influence of road surfaces on traffic noise --

Part 4: SPB method using backing board. *ISO/PAS 11819-4*. 2013.

103. Controlled Pass-By Method. *French Natl Stand NF S S1 119-2*. 1999.

104. ISO. Measurement of noise emitted by accelerating road vehicles -- Engineering method -- Part 1: M and N categories. *ISO 362-1*. 2015.

105. ISO. Measurement of noise emitted by accelerating road vehicles -- Engineering method -- Part 2: L category. *ISO 362-2*. 2009.

106. Copeland TJ, Seth Wilhoit R. Tire noise pass-by testing system meets latest standards. In: *Sound and Vibration*.Vol 46. 27101 East Oviatt Road - P.O. Box 40416, Bay Village, OH 44140, United States; 2012:12-16.

107. ISO. Tyres - Coast-by methods for measurement of tyre-to-road sound emission. *ISO 13325*. 2003.

108. Hanson DI, James RS. Colorado DOT Tire/Pavement Noise Study. In: *Report No. CDOT-DTD-R-2004-5, Colorado Department of Transportation*. United States; 2004.

109. Lodico DM, Rochat JL, Donavan P, Rasmussen RO. Overview and application of the Statistical Isolated Pass-By Method (SIP) for determining the influence of road surfaces on vehicle noise (AASHTO TP-98). In: *41st International Congress and Exposition on Noise Control Engineering 2012, INTER-NOISE 2012*.Vol 3. New York, NY, United states; 2012:2592-2601.

110. AASHTO. Standard Method of Test for Determining the Influence of Road Surfaces on Vehicle Noise Using the Statistical Isolated Pass-By (SIP) Method. *AASHTO TP 98*. 2013.

111. Rasmussen RO. Tire-Pavement Noise Standards - An Update of Tire-Pavement Noise Technical Working Group. In: *Presentation at Pavement Evaluation 2010, Roanoke, Virginia*.; 2010.

112. AASHTO. Standard Method of Test for Measurement of Tire/Pavement Noise Using the On-Board Sound Intensity (OBSI) Method. *AASHTO TP 76*. 2013.

113. AASHTO. Standard Method of Test for Determining the Influence of Road Surfaces on Traffic Noise Using the Continuous Flow Traffic Time-Integrated Method (CTIM). *AASHTO TP 99*. 2013.

114. Rochat JL, Hastings AL, Read DR, Lau M. *FHWA Traffic Noise Model (TNM) Pavement Effects Implementation Study*.; 2012.

115. Rochat JL, Lodico D, Donavan P, Rasmussen RO. Overview and application of the Continuous-Flow Traffic Time-Integrated Method (CTIM) for determining the influence of road surfaces on traffic noise. In: *41st International Congress and Exposition on Noise Control Engineering 2012, INTER-NOISE 2012*.Vol 3. New York, NY, United states; 2012:2602-2611.

116. Illingworth & Rodkin Inc. I-80 Davis OGAC Pavement Noise Study. In: *12 Year Summary Report, California Department of Transportation, Sacramento, CA*.; 2011.

117. Donavan P, Reyff J, Pommerenck A. Quiet Pavement Pilot Program : Progress Report 3. In: *Report FHWA AZ-12-577, Arizona Department of Transportation*.; 2012.

118. DIRECTIVE 2001/43/EC OF THE EUROPEAN PARLIAMENT AND OF THE

COUNCIL of 27 June 2001 amending Council Directive 92/23/EEC relating to tyres for motor vehicles and their trailers and to their fitting. 2001.

119. ISO. Acoustics – Determination of sound power levels of noise sources using sound pressure – Engineering method in an essentially free field over a reflecting plane. *ISO 3744*. 1994.

120. ISO. Acoustics – Noise emitted by machinery and equipment – Rules for the drafting and presentation of a noise test code. *ISO 12001*. 1996.

121. Heijden L van der, Son RJJH van. A note on the neglect of the Doppler effect in the modelling of traffic flow as a line of stationary point sources. *J Sound Vib*. 1982;8(3):442–4.

122. McDaniel R, Shah A, Dare T, Bernhard R. *Hot Mix Asphalt Surface Characteristics Related to Ride , Texture , Friction , Noise and Durability*.; 2014.

123. Dick EB, Izevbekhai BI, Casey T. *Influence of Pavement on Traffic Noise -- Statistical Pass-By Measurements of Traffic on Several Interstate Pavements*.; 2010.

124. ISO. Acoustics -- Measurement of noise emitted by accelerating road vehicles -- Engineering method. *ISO 362*. 1981.

125. ISO. Acoustics -- Measurement of noise emitted by accelerating road vehicles -- Engineering method. *ISO 362/Amd 1*. 1985.

126. Giorjao TC, Yoneda R, Cherman AL, Morais AR. Tire contribution for pass by noise. In: *SAE Technical Papers*. Sao Paulo, Brazil; 2005. http://dx.doi.org/10.4271/2005-01-4165.

127. Ejsmont JA, Sandber U. Tire/Road Noise: Trailer Measurements in Practice. In: *Proc. of INTER-NOISE 85*.; 1985.

128. AASHTO. Standard Method of Test for Determining the Influence of Road Surfaces on Vehicle Noise Using the Statistical Isolated Pass-By (SIP) Method. *AASHTO TP 98*. 2012.

129. AASHTO. Standard Method of Test for Determining the Influence of Road Surfaces on Traffic Noise Using the Continuous Flow Traffic Time-Integrated Method (CTIM). *AASHTO TP 99*. 2012.

130. Siddon T. Noise Generation Mechanisms for Passenger Car Tires. In: *84th Meeting of the ASA*.; 1972.

131. Miller RF, Thrasher DB. Spectral Analyses in Truck Tire Noise Fields. In: *SAE West Coast Meeting, Anaheim, CA, August 1974*. 400 Commonwealth Drive, Warrendale, PA 15096-0001, United States: Society of Automotive Engineers; 1974. http://dx.doi.org/10.4271/740608.

132. Reiter WF, Eberhardt AC, Harper LJ, Atkinson TL. *Truck Noise VII-A Experimental Investigation of Truck Tire Sound Vibration*. Raleigh, NC, United states; 1974.

133. Landers S, Richards G, Bradisse J. Onboard Tire Sound Level Testing Technique. *Highw Tire Noise, Soc Automot Eng*. 1977;(762017).

134. Landers SP. A Vibrational Sound Mechanism of Lug Type Tread Designs. *Highw Tire Noise, Soc Automot Eng*. 1977. http://dx.doi.org/10.4271/762025.

135. Underwood MCP, Nelson P. Lorry Tyre Noise. *Veh Noise Vib*. 1984;(C139/84):50p-.

136. Reiter WF, Eberhardt AC. The Relationship between Truck Tire Vibration and Near and Far Field Sound Levels. *Highw Tire Noise, Soc Automot Eng*. 1977;(762021). http://dx.doi.org/10.4271/762021.

137. Eberhardt AC. *An Experimental and Analytical Investigation of the Vibration Noise Generation Mechanism in Truck Tires*. United States; 1981.

138. Zhang Y, McDaniel JG, Wang ML. Pavement macrotexture estimation using principal component analysis of tire/road noise. In: *Proc. SPIE, Int. Soc. Opt. Eng. (USA)*.Vol 9063. San Diego, CA, United states; 2014:90630K (9 pp.)-pp. http://dx.doi.org/10.1117/12.2045584.

139. Donavan PR, Lodico DM. *Measuring Tire-Pavement Noise at the Source (NCHRP Report 630)*.; 2009.

140. SAE. Sound Level Of Highway Truck Tires. *SAE J 57*. 2014.

141. Sandberg U, Ejsmont JA. Selection of Tyres with Regard to Noise Emissions. In: *Unpublished, VTI, Sweden*.; 1992.

142. Phillips S, Kollamthodi S, Nelson P. Investigations of tyre/road noise – Draft report. In: *Project Report PR/SE/272/2001 S032J/VB, Transport Research Laboratory, Crowthorne, U.K.*; 2001.

143. Osman MM, May DN. Relative Influence of Pavement Texture and Tire Type on Pavement/Tire Noise. In: *Vehicle Noise Regulation and Reduction, SP-456*. 400 Commonwealth Drive, Warrendale, PA 15096-0001, United States; 1980. http://dx.doi.org/10.4271/800282.

144. Ungar E, Bronsdon B. Tire Noise Data Bank. In: *Bolt, Beranek, and Newman, Inc. Report No. 4411, June, 1980, Prepared for the U.S. Environmental Protection Agency, Office of Noise Abatement and Control, EPA Contract No. 68-01-3950.*; 1980.

145. Breyer G. Low-Noise Road Surfaces in Austria. In: *Proceedings of the International Tire/Road Noise Conference 1990, Gothenberg, Sweden*.; 1990.

146. Springborn M. Measurement of Tire/Road Noise and the Influence of the Road Surface. In: *Proceedings of the International Tire/Road Noise Conference 1990, Gothenberg, Sweden*.; 1990.

147. Steven H. Investigations on a Measuring Method for the Tyre/Road Noise of Passenger Cars. In: *Proceedings of the International Tire/Road Noise Conference 1990, Gothenberg, Sweden*.; 1990.

148. Chalupnik JD. Predicting Roadside Noise Levels from Near Field Trailer Measurements. In: *Proceedings of Noise-Con 1996, Seattle, WA*.Vol 1. Bellevue, WA, United states; 1996:61-66.

149. McNerney MT, Landsberger BJ, Turen T, Pandelides A. Comparative Field Measurements of Tire/Pavement Noise of Selected Texas Pavements. In: *Center for Transportation Research, the University of Texas at Austin, Austin, TX, Report No. 7-2957-2*. United States; 2000:56p-.

150. Chuang JSC, Lin H-H, Chen Y-Y, Su T-K. Study of Tire Noise for Vehicle Noise Control. In:

SAE Paper 2005-01-2415, Society of Automotive Engineers Noise and Vibration Conference Proceedings, Traverse City, MI. Traverse City, MI, United states; 2005. http://dx.doi.org/10.4271/2005-01-2415.

151. Ibarra D, Ramirez-Mendoza R, Ibarra S. Characterization of the road surfaces in real time. *Appl Acoust*. 2016;105:93-98. http://dx.doi.org/10.1016/j.apacoust.2015.10.023.

152. ANSI/ASA. American National Standard Method for Determining the Acoustic Impedance of Ground Surfaces. *ANSI/ASA S118*. 2010.

153. Donovan P, Rymer. B. Measurement of Tire Pavement Noise Sound Intensity Methodology. In: *Proceedings of Asphalt Rubber 2003*.; 2003.

154. Biligiri KP. Asphalt mixtures' properties indicative of tire/pavement noise. In: *PhD Dissertation, ARIZONA STATE UNIVERSITY*.; 2008.

155. Donavan P. Sound intensity measurement errors in the presence of large pressure to intensity ratios. In: *SAE Technical Paper 951334*.; 1995.

156. Bloemhof H. Note on the relationship of sound pressure and sound intensity. *Appl Acoust*. 1986;19(3):159–66.

157. Crocker M. *Encyclopedia of Acoustics*. John Wiley & Sons, Inc.; 1997.

158. Fahy F. Sound Intensity. *E FN Spon, London*. 1995.

159. Waser MP, Crocker MJ. Introduction to the Two-Microphone Cross-Spectral Method of Determining Sound Intensity. *Noise Control Eng J*. 1984.

160. Donavan P, Oswald L. Quantification of Noise Mechanisms of Blank, Rib, and Cross-Bar Tread Bias-Ply Truck Tires. In: *General Motors Research Laboratories*.; 1981.

161. Oswald L, Donavan P. Acoustic Intensity Measurements in Low Mach Number Flows of Moderate Turbulence Levels. In: *General Motors Research Laboratories*.; 1980.

162. Donavan P. The Role of Acoustic Tube Resonances in the Radiation of Sound from Circumferentially Ribbed Truck Tires. In: *General Motors Research Laboratories*.; 1981.

163. Oshino Y, Tachibana H. Noise Source Identification on Rolling Tires by Sound Intensity Measurement. In: *Proceedings of the International Tire/Road Noise Conference 1990*.Vol 12. Japan; 1990:87-92. http://dx.doi.org/10.1250/ast.12.87.

164. Bennetts A, Crookes N. Advances in the measurement of road and tyre noise. *Acoust Bull*. 2013;38(4):35-38.

165. Krauss O, Gauterin F. Analysis of tire road noise using a tire cavity sound measurement system. In: *Proceedings - European Conference on Noise Control*. Prague, Czech republic; 2012:911-915.

166. Bschorr O, Wolf A, Mittmann J. Theoretische und experimentelle Untersuchungen zur Abstrahlung von Reifenlärm. In: *Interim Report, Messerschmitt-Bölkow- Blohm GmbH*.; 1981.

167. Bschorr O. Bestimmung des straßenbedingten Verkehrslärms durch Messung des Torusgeräusches. In: *VDI Report Nr. 1632*.; 2001.

168. Wolf A. Bewertung des Reifen-Fahrbahn-Geräusches durch Messung des

Reifeninnengeräusches. In: *Dissertation, University of Stuttgart*.; 1997.

169. Masino J, Daubner B, Frey M, Gauterin F. Development of a tire cavity sound measurement system for the application of field operational tests. In: *2016 Annual IEEE Systems Conference (SysCon). Proceedings*. Piscataway, NJ, USA; 2016:5 pp.-pp. http://dx.doi.org/10.1109/SYSCON.2016.7490624.

170. Saemann E-U, Dimitri G, Kindt P. Tire Requirements for Pavement Surface Characteristics. In: *Presented at 7th Symposium on Pavement Surface Characteristics: SURF 2012 Norfolk, VA*.; 2012:1-33.

171. Sandberg U, Ejsmont JA. Noise emission, friction and rolling resistance of car tires - summary of an experimental study. In: *Proc. of NOISE-CON 2000, Newport Beach, California*.; 2000.

172. ISO. Acoustics -- Measurement of the influence of road surfaces on traffic noise -- Part 2: The close-proximity method. *ISO/DIS 11819-2*. 2014.

173. CROW. CPX trailer comparison round robin test data analysis. In: *Report D12-02*.; 2012.

174. Buytaert A. Differences in rolling noise level between the left and the right tire of a CPX-trailer. In: *Proceedings of Forum Acusticum*.Vol 2014-Janua. 30 Mickiewicza Av., Krakow, Poland; 2014:Ecophone; et al.; KFB Poland; Ministry of Science.

175. GB. Acoustics - Measurement of Noise Inside Motor Vehicles. In: *Chinese Standard, GB/T 18697*.; 2002.

176. AVEC. Full OBSI System Model. In: *Acoustical and Vibrations Engineering Consultants, Blacksburg*.; 2012.

177. GM. Road Tire Noise Evaluation Procedure. *Gen Mot Test Proced GMN7079TP*. 2004.

178. ASTM. New Practice for Measurement of Tire/Pavement Noise Using the On-Board Sound Intensity (OBSI) Method. *ASTM WK26025*. 2009.

179. Donavan PR, Oswald LJ. The Identification and Quantification of Truck Tire Noise Sources under On-Road Operating Conditions. In: *General Motors Research Laboratories*. New York, NY, USA; 1980:253-258.

180. Hamill R. Airborne Tire/Road Noise Test Method Development. In: *Noise & Vibration Laboratory, General Motors Proving Ground*.; 1985.

181. Cantrell D. Airborne Tire Noise Generation – the Effects of Axle Weight, Tire Inflation Pressure, and Suspension Alignment. In: *Noise & Vibration Laboratory, General Motors Proving Ground*.; 1988.

182. Rasmussen G. Pin-Point Noise Sources on Vehicles during Pass-By Using Intensity Technique. In: *Proceedings of the International Tire/Road Noise Conference 1990*.; 1990.

183. Stumpf H. Linking Evaluation of Heavy Truck Tyre Noise Measured by ISO 362 with Scale Factors for Sound Intensity. In: *Proceedings of the International Tire/Road Noise Conference 1990*.; 1990.

184. ANSI. Precision Methods For The Determination Of Sound Power Levels Of Noise Sources In Anechoic And Hemi-Anechoic Rooms. *ANSI S1235*. 2001.

185. Donavan PR. Tire-Pavement Interaction Noise Measurement under Vehicle Operating Conditions of Cruise and Acceleration. In: *Society of Automotive Engineers Noise and Vibration Conference Proceedings*. Traverse City, MI, United states; 1993. http://dx.doi.org/10.4271/931276.

186. Hall H, Bolton S. Cooperative Research Program: Correlation of Tire Intensity and Passby SPL. In: *Ray W. Herrick Laboratories*.; 1994.

187. Bolton JS, Hall HR, Schumacher RF, et al. Correlation of Tire Intensity Levels and Passby Sound Pressure Levels. In: *Society of Automotive Engineers Noise and Vibration Conference Proceedings*. 400 Commonwealth Drive, Warrendale, PA 15096-0001, United States; 1995. doi:10.4271/951355.

188. Donavan PR. An Assessment of the Tire Noise Generation and Sound Propagation Characteristics of an ISO 10844 Road Surface. In: *Society of Automotive Engineers Noise and Vibration Conference Proceedings*. 400 Commonwealth Drive, Warrendale, PA 15096-0001, United States; 1997. http://dx.doi.org/10.4271/971990.

189. Sakamoto I, Tanaka T, Katsura N, Kujikawa Y. Comparison of Sound Intensity Measured Close to Tires Attached to Trailer between On Road and On Roller Bench. In: *Proceedings of Inter-Noise 2003*.; 2003.

190. Sakamoto I, Tanaka T, Katsura N, Fujikawa Y, Kogawa S. Analysis of Tire/Road Noise Radiation Characteristics under Acceleration Conditions by Sound Intensity. In: *Proceedings of Inter-Noise 2004*.; 2004.

191. Donavan PR, Rymer B. Assessment of Highway Pavements for Tire/Road Noise Generation. In: *Society of Automotive Engineers Noise and Vibration Conference Proceedings*. Traverse City, MI, United states; 2003. http://dx.doi.org/10.4271/2003-01-1536.

192. Donavan P, Scofield L. An Evaluation of the Effects of Different Portland Cement Concrete Pavement Texturing on Tire/Pavement Noise. In: *Proceedings of NoiseCon 2003*.; 2003.

193. Donavan P, Rymer B. Quantification of Tire/Pavement Noise: Application of the Sound Intensity Method. In: *Proceedings of Inter-Noise 2004*.; 2004.

194. Donavan P. Further Development of the Sound Intensity Method of Measuring Tire Noise Performance of In-Situ Pavements. In: *California Department of Transportation, Division of Environmental Analysis*.; 2006.

195. SAE. Sound Level Of Highway Truck Tires. *SAE J 57*. 1977.

196. Oshino Y, Tachibana H. Relationships between Road Texture and Tire/Road Noise. In: *Proceedings of Noise-Con 1996, Seattle, WA*.Vol 1. Bellevue, WA, USA; 1996:67-72.

197. Oshino Y, Mikami T, Tachibana H. Study of road surface indices for the assessment of tire/road noise. In: *Proceedings of Inter-Noise 2001, the Haag, the Netherlands*.; 2001.

198. Fujikawa T, Oshino Y, Mikami T, Tachibana H. Examination on Effects of Road Roughness Parameters for Abating Tire/Road Noise. In: *Proceedings of Inter-Noise 2004, Prague, Czech Republic*.; 2004.

199. ISO. Acoustics -- Measurement of the influence of road surfaces on traffic noise -- Part 2:

The close-proximity method. *ISO 11819-2*. 2000.

200. AASHTO. Standard Method of Test for Measurement of Tire/Pavement Noise Using the On-Board Sound Intensity (OBSI) Method. *AASHTO TP 76*. 2008.

201. Khazanovich L, Izevbekhai BI. Trend of pavement on board sound intensity with respect to texture degradation patterns in mnroad test cells. In: *Institute of Noise Control Engineering of the USA - 23rd National Conference on Noise Control Engineering, NOISE-CON 08 and Sound Quality Symposium, SQS 08*.Vol 1. Dearborn, MI, United states; 2008:160-172.

202. Wayson LR, MacDonaldA MJ, Martin A. On-Board Sound Intensity (OBSI) Study: Phase 2. In: *Final Report, FDOT Project No. #BDT06*. United States; 2014:145p-.

203. Wayson RL, MacDonald JM, Berrios M. On-board sound intensity measurements and results in Florida. In: *24th National Conference on Noise Control Engineering 2010, Noise-Con 10, Held Jointly with the 159th Meeting of the Acoustical Society of America*.Vol 1. Baltimore, MD, United states; 2010:573-584.

204. Donavan PR, Lodic D. Applicability of on-board sound intensity (OBSI) method to quantifying the effect of pavement type on tire-pavement noise. In: *Institute of Noise Control Engineering of the USA - 23rd National Conference on Noise Control Engineering, NOISE-CON 08 and Sound Quality Symposium, SQS 08*.Vol 1. Dearborn, MI, United states; 2008:173-184.

205. Rasmussen RO, Sohaney RC, Donavan PR, Rymer BC. Improving wayside noise measurements on roadways and at test tracks using on-board sound intensity. In: *41st International Congress and Exposition on Noise Control Engineering 2012, INTER-NOISE 2012*.Vol 3. New York, NY, United states; 2012:2583-2591.

206. Wang G, Smith G, Shores R. Pavement noise investigation on North Carolina highways: An on-board sound intensity approach. *Can J Civ Eng*. 2012;39(8):878-886. http://dx.doi.org/10.1139/L2012-076.

207. Donavan PR, Lodico DM. Evaluation of on-board sound intensity measurement parameters using a tire noise chassis dynamometer. In: *41st International Congress and Exposition on Noise Control Engineering 2012, INTER-NOISE 2012*.Vol 3. New York, NY, United states; 2012:2555-2569.

208. Trevino M, Dossey T. On-board sound intensity testing of PFC pavements in Texas. In: *Institute of Noise Control Engineering of the USA - 22nd National Conference on Noise Control Engineering, NOISE-CON 2007*.Vol 1. Reno, NV, United states; 2007:423-434.

209. Mogrovejo DE, Flintsch GW, de León Izeppi ED, McGhee KK. Effect of Air Temperature and Vehicle Speed on Tire/Pavement Noise Measured with On-Board Sound Intensity Methodology. In: *The Transportation Research Board (TRB) 92nd Annual Meeting, Washington, D.C., January 13-17, 2013*.; 2013.

210. Carrasco DEM. Effect of Air Temperature , Vehicle Speed , and Pavement Surface Aging on Tire / Pavement Noise Measured with On-Board Sound Intensity Methodology. 2012.

211. Haas E, Hencken J, Bennert T. A statistical evaluation of one-third octave band frequencies measured using the on-board sound intensity method. In: *41st International Congress and Exposition on Noise Control Engineering 2012, INTER-NOISE 2012*.Vol 11. New York, NY,

United states; 2012:9464-9475.

212. Rasmussen RO, Sohaney RC. Measuring and visualizing tire-pavement noise using on-board sound intensity. In: *ASTM Special Technical Publication*.Vol 1555 STP. Tampa, FL, United states; 2012:160-169. http://dx.doi.org/10.1520/STP104444.

213. Dare TP. Generation mechanisms of tire-pavement noise. 2012.

214. Nilsson N-A, Bennerhult O, Soderqvist S. External tire/road noise: its generation and reduction. In: *Inter-Noise 80. Noise Control for the 80's. Proceedings of the 1980 International Conference on Noise Control Engineering*. New York, NY, USA; 1980:245-252.

215. Cvar PA, Bernhard RJ. Tire dynamics. In: *Internal Report 225, Ray W. Herrick Laboratories, West Lafayette, IN*.; 2000.

216. Kostial P, Jancikova Z, Bakosova D, et al. Artificial Neural Networks Application in Modal Analysis of Tires. *Meas Sci Rev*. 2013;13(5):273-278. http://dx.doi.org/10.2478/msr-2013-0040.

217. Reiter WF, Eberhardt AC. Experimental investigation of truck tire noise generated through tire vibration. In: *Proceedings of INTER-NOISE 74, Washington, D.C.*; 1974:467.

218. Fujikawa T, Oshino Y, Mikami T, Tachibana H. Examination of road roughness parameters for abating tire vibration and radiated noise. *Noise Control Eng J*. 2009;57(2):77-83. http://dx.doi.org/10.3397/1.3081450.

219. Burroughs CB, Dugan EL. Measurements of blank tire tread vibration and radiated noise. In: *Proceedings of INTER-NOISE 02, Dearborn, MI*.; 2002:467.

220. Plotkin KJ, Montroll ML, Fuller WR. The generation of tire noise by air pumping and carcass vibration. In: *Proceedings of INTER- NOISE 80, Miami, FL*. New York, NY, USA; 1980:273.

221. Bergmann M. Noise generation by tire vibrations. In: *Proceedings of INTER- NOISE 80, Miami, FL*. New York, NY, USA; 1980:239.

222. Dare T, Bernhard R. Accelerometer Measurements of Tire Tread Vibrations and Implications to Wheel-Slap Noise. *Tire Sci Technol*. 2013;41(2):109-126.

223. Keltie RF. Analytical model of the truck tire vibration sound mechanism. *J Acoust Soc Am*. 1982;71(2):359. http://dx.doi.org/10.1121/1.387460.

224. Dugan EL, Burroughs CB. Measurement of automobile tire tread vibration and radiated noise. In: *Proceedings of Noise-Con 03, Cleveland, OH*.; 2003:168.

225. Rocca G, Kindt P, Middelberg JM, DíAz CG, Peeters B, Auweraer H Van Der. Indoor vibration testing for high-frequency modal characterization of tyres. In: *Proceedings of the ASME 2011 International Design Engineering Technical Conferences & Computers Ana Information in Engineering Conference*.; 2011.

226. Larsson K, Kropp W. A high frequency range tyre model based on two coupled elastic plates. In: *Proceedings of INTER-NOISE 99, Fort Lauderdale, FL*.; 1999:131-136.

227. Kropp W, Larsson K, Wullens F, Andersson P, Becot F-X, Beckenbauer T. The modeling of tyre/road noise - A quasi three-dimensional model. In: *Proceedings of INTER-NOISE 01,*

The Hague, Holland.; 2001:2322.

228. Perisse J, Hamet J-F. A comparison of the 2D ring and 3D orthotropic plate for modelling of radial tire vibration. In: *INTER-NOISE 00, Nice, France,*.; 2000:2497.

229. Fujikawa T, Koike H, Oshino Y, Tachibana H. Generation mechanism of tire/road noise, Part 1: Tire vibration cause by road roughness. In: *Proceedings of INTER-NOISE 99, Fort Lauderdale, FL*.; 1999:319.

230. Ullrich S. Drum-measurements of tyre noise as a function of roadway tempera- ture and circumferential forces. In: *Proceedings of INTER-NOISE 93, Page 659, Leuven, Belgium*.; 1993.

231. JASO. Test procedures for tire noise. In: *Japanese Automobile Standards Organization JASO C606-81*.; 1981.

232. GB. 轮胎噪声测试方法 转鼓法(Tyre noise test - methods of drum). *GB/T32789-2016*. 2016.

233. Sandberg U, Ejsmont JA. Three basic methods for measurement of tire/road noise. In: *Proceedings of INTER-NOISE 84, Page 93, Honolulu, HI*.; 1984.

234. Sandberg U. Review of comparative study of tire:road noise measurements on drums and road. 1983.

235. Ejsmont JA. *Tire/road Noise: Comparison of Road and Laboratory Measurements and Influence of Some Tire Parameters on Generation of Sound*. Linköping, Sweden; 1982.

236. Swieczko-Zurek B, Ejsmont J, Ronowski G, et al. Comparison of road and laboratory measurements of tyre/road noise. In: *INTERNOISE 2014 - 43rd International Congress on Noise Control Engineering: Improving the World Through Noise Control*. Melbourne, VIC, Australia; 2014.

237. ISO. Acoustics - Test surface for road vehicle noise measurement. In: *Technical Report ISO 10844, International Organization for Standardization*.; 1991.

238. Tong G, Wang Q, Yang K, Wang L. Simulation on the radial tire wear noise. In: *Applied Mechanics and Materials*.Vol 488. Xi'an, Shaanxi, China; 2014:1121-1124. http://dx.doi.org/10.4028/www.scientific.net/AMM.488-489.1121.

239. Nilsson N-A. Principles in the control of external tire/road noise. In: *Proceedings of INTER-NOISE 82, Page 123, San Francisco, CA*.; 1982.

240. BASt (Federal Highway Research Institute). Der Prüfstand Fahrzeug/Fahrbahn der BASt (Federal Highway Research Institute's vehicle-pavement interaction test facility). *http://www.bast.de/EN/Automotive_Engineering/Technology/Technology_node.html*.

241. Bernhard RJ, Thornton WD. Preliminary results using the tire/pavement test apparatus. In: *Proceedings of INTER-NOISE 03, Jeju, South Korea*.; 2003.

242. Park S-HS-H, Kim Y-HY-H. Visualization of pass-by noise by means of moving frame acoustic holography. *J Acoust Soc Am*. 2001;110(5):2326-2339. http://dx.doi.org/10.1121/1.1404976.

243. Ruhala RJ, Burroughs CB. Tire/pavement interaction noise source identification using

multi-planar nearfield acoustical holography. In: *SAE Technical Papers*. Traverse City, MI, United states; 1999. http://dx.doi.org/10.4271/1999-01-1733.

244. Ruhala RJ. A study of tire/pavement interaction noise using near-field acoustical holography. In: *PhD Dissertation, Pennsylvania State University*.; 1999.

245. Kwon H-S, Bolton JS, Hallman DL. Nearfield acoustical holography applied to sound radiation from tires. In: *Proceedings - National Conference on Noise Control Engineering*. Ypsilanti, MI, USA; 1998:103-108.

246. Dumbacher S, Blough J, Hallman D, Wang P. Source identification using acoustic array techniques. In: *SAE Technical Papers*. 400 Commonwealth Drive, Warrendale, PA 15096-0001, United States; 1995. http://dx.doi.org/10.4271/951360.

247. Ginn K. Tyre Noise Measurements Using Spatial Transformation of Sound Fields. In: *Proceedings of the International Tire/Road Noise Conference 1990, Gothenberg, Sweden, August, 1990*.; 1990.

248. Hendricx W, Mancosu F. Experimental Determination of the Noise Emitting Parts of a Rotating Tire in the European Research Project TINO. In: *SAE Paper 1999-01-1732, Society of Automotive Engineers Noise and Vibration Conference Proceedings, Traverse City, MI*. Traverse City, MI, United states; 1999. http://dx.doi.org/10.4271/1999-01-1732.

249. Ruhala RJ, Burroughs CB. Application of nearfield acoustical holography to tire/pavement interation noise emissions. In: *SAE Technical Papers*. 400 Commonwealth Drive, Warrendale, PA 15096-0001, United States; 1997. http://dx.doi.org/10.4271/972047.

250. Ruhala RJ, Burroughs CB. Separation of leading edge, trailing edge, and sidewall noise sources from rolling tires. In: *Proceedings - National Conference on Noise Control Engineering*. Ypsilanti, MI, USA; 1998:109-114.

251. Kim B, Lee T. A Study on the Tire Noise. In: *Proceedings of Inter-Noise 2003, Seogwipo, Korea*.; 2003.

252. Ih J-G, Oey A. Effect of patterns on wave propagation and sound radiation over the tire surface. In: *41st International Congress and Exposition on Noise Control Engineering 2012, INTER-NOISE 2012*.Vol 2. New York, NY, United states; 2012:1436-1441.

253. Vercammen S, Bianciardi F, Kindt P, Desmet W, Sas P. Comparison of Two Measurement Methods for Exterior Noise Radiation Characterization of a Loaded Rotating Tyre Stijn Vercammen. *SAE Tech Pap 2015-01-2197*. 2015. doi:10.4271/2015-01-2197.Copyright.

254. Cho DS, Mun S. Determination of the sound power levels emitted by various vehicles using a novel testing method. *Appl Acoust*. 2008;69(3):185-195. doi:10.1016/j.apacoust.2006.08.012.

255. Cho DS, Mun S. Study to analyze the effects of vehicles and pavement surface types on noise. *Appl Acoust*. 2008;69(9):833-843. doi:10.1016/j.apacoust.2007.04.006.

256. Moir J, Stevens WR. Simple sound power measurements. *Appl Acoust*. 1974;7(1):15–22.

257. ISO. Acoustics – determination of sound power levels of noise source – engineering methods for free-field conditions over a reflecting plane. 1981;(3744).

258. Jacobsen F. Sound power determination using the intensity tech- niques in the presence of

diffuse background noise. *J Sound Vib*. 1992;159(2):353–71.

259. Fahy FJ. International standards for the determination of sound power levels of sources using sound intensity measurement: An exposition. *Appl Acoust*. 1997;50(2):97–109.

260. ISO. Acoustics – attenuation of sound during propagation outdoors – part 2: General method of calculation. *ISO 9613-2*. 1996.

261. Fonseca WD, Gerges SNY. Development of a low cost system for pass-by noise beamforming measurements. In: *20th International Congress on Acoustics 2010, ICA 2010 - Incorporating Proceedings of the 2010 Annual Conference of the Australian Acoustical Society*.Vol 3. Sydney, NSW, Australia; 2010:2123-2129.

262. Zavala PAG, Arruda JRDF, Bueno FG, Miranda G, Mothio W, Adas CA. Heavy vehicles pass-by noise beamforming using generalized inverse method and an optimized array. In: *SAE Technical Papers*.Vol 13. Sao Paulo, SP, Brazil; 2013. http://dx.doi.org/10.4271/2013-36-0469.

263. Lustberg RJ. Acoustic beamforming using microphone arrays. 1993.

264. Tanaka T. Identification Methods for Tire/Road Noise during Vehicle Operating Conditions with Acoustic Holography. In: *Proceedings of Inter-Noise 2004, Prague, Czech Republic, August*.; 2004.

265. Maillard J, Jagla J. Auralization of non-stationary traffic noise using sample based synthesis - Comparison with pass-by recordings. In: *41st International Congress and Exposition on Noise Control Engineering 2012, INTER-NOISE 2012*.Vol 1. New York, NY, United states; 2012:608-619.

266. Dutilleux G, Defrance J, Gavreau B, Besnard F. The revision of the French method for road traffic noise prediction. *J Acoust Soc Am*. 2008;123:3150.

267. Dutilleux G, Defrance J, Ecotière D, et al. NMPB-routes-2008: The revision of the french method for road traffic noise prediction. *Acta Acust united with Acust*. 2010;96(3):452-462. doi:10.3813/AAA.918298.

268. Salomons EM, Zhou H, Lohman WJA. Efficient numerical modeling of traffic noise. *J Acoust Soc Am*. 2010;127(2):796-803. doi:10.1121/1.3273890.

269. Maercke D van, Defrance J. Development of an analytical model for outdoor sound propagation within the harmonoise project. In: *Acta Acustica United with Acustica 93*.; 2007:201–212.

270. Can A, Leclercq L, Lelong J, Defrance J. Capturing urban traffic noise dynamics through relevant descriptors. *Appl Acoust*. 2008;69(12):1270-1280. doi:10.1016/j.apacoust.2007.09.006.

271. EU Project "Quiet City Transport" (QCITY), TIP4-CT-2005-516420 (2005-2009). *http://www.qcity.org*.

272. EU Project "CityHush – Acoustically green road vehicles and city areas", SPC8-GA-2009-233655 (2010-2012). *http://www.cityhush.eu*.

273. Kleiner M, Dalenbäck BI, Svensson P. Auralization-an overview. *Journal-Audio Eng Soc*. 1993;41:861–861. http://www.aes.org/e-lib/browse.cfm?elib=6976.

274. Funkhouser T, Tsingos N, Carlbom I, et al. A beam tracing method for interactive architectural acoustics. *J Acoust Soc Am*. 2004;115(2):739-756. doi:10.1121/1.1641020.

275. Funkhouser T, Carlbom I, Elko G, Pingali G, Sondhi M, West J. A beam tracing approach to acoustic modeling for interactive virtual environments. *Proc 25th Annu Conf Comput Graph Interact Tech*. 1998:21-32. doi:10.1145/280814.280818.

276. Laine S, Siltanen S, Lokki T, Savioja L. Accelerated beam tracing algorithm. *Appl Acoust*. 2009;70(1):172-181. doi:10.1016/j.apacoust.2007.11.011.

277. Nilsson ME, Rådsten-Ekman M, Alvarsson J, Lundén P, Forssén J. Perceptual validation of auralized road traffic noise. In: *Proceedings of Inter-Noise 2011. Osaka, Japan: The Institute of Noise Control Engineering of Japan and the Acoustical Society of Japan*.; 2011.

278. Kaczmarek T. Road-vehicle simulation for psychoacoustic studies. In: *ICA 2007, MADRID, Spain*.; 2007.

279. Maillard J, Martin J. A simulation and restitution technique for the perceptive evaluation of road traffic noise. In: *Proc. Paris, France, EURONOISE 2008*.; 2008.

280. Jagla J, Maillard J, Martin N. Sample-based engine noise synthesis using a harmonic synchronous overlap-and-add method. In: *Proc. of IEEE International Conference on Acoustics Speech and Signal Processing*.; 2012:373— 376.

281. Maillard J. Prediction and auralization of construction site noise. *Proc Edinburgh, Scotland, EURONOISE 2009, Oct 26-28*. 2009.

282. Sottek R, Fiebig A, Guidati S, Marla P, Philippen B. Measuring and analyzing road traffic noise. In: *Proceedings - European Conference on Noise Control*. Prague, Czech republic; 2012:1075-1082.

283. Fiebig A, Marla P, Sottek R. Noise of electric and combustion-powered scooters and resulting annoyance. In: *Euronoise 2012, Prague, Czech Republic*.; 2012.

284. Löfdahl M, Johnsson R, Nykänen A. An auralization model for structure-borne tire noise. *Appl Acoust*. 2015;96:61–67.

285. Berckmans D, Kindt P, Sas P, Desmet W. Evaluation of substitution monopole models for tire noise sound synthesis. *Mech Syst Signal Process*. 2010;24(1):240-255. http://dx.doi.org/10.1016/j.ymssp.2009.06.005.

286. Reiter Jr. WF, Eberhardt AC. Truck tire vibration noise. In: *SAE Technical Papers*. 400 Commonwealth Drive, Warrendale, PA 15096-0001, United States; 1974. http://dx.doi.org/10.4271/740609.

287. Donavan PR. The effects of porous pavements on tire/pavement noise source levels and pass-by measurements. In: *Proceedings of Noise-Con 2011, Portland, OR*.; 2011.

288. Sandberg U. Noise emission influence of road surfaces, as measured with the statistical pass-by and close-proximity methods, using different vehicle classes and different tires. In: *Proc. of the Tyre/road Noise Seminar 1997 in Gdansk, Poland*.; 1997.

289. Steven H, Küppers D, van Blokland GJ, van Houten MH, van Loon R. International validation test for the close proximity (CPX) method. In: ; 2000.

290. Konishi S, Fujino T, Usami K, Tomita N, Ozaki T. Drum test method of tire road noise. In:

Conference of the Japanese Soc. of Automotive Engineers (JSAE) in Sapporo, Japan.; 1996.

291. Anfosso-Ledee F. Modelling the local propagation effects of tire-road noise: propagation filter between CPX and CPB measurements. In: *Proceedings of INTER-NOISE 2004, Prague, Czech Republic*.; 2004.

292. Ruhala RJ, Burroughs CB. Localization of tire/pavement noise source regions. *Noise Control Eng J*. 2008;56(5):318-331. http://dx.doi.org/10.3397/1.2984149.

293. Nilsson NA. External Tire/Road Noise from Trailing Contact Edge - The Excitation Process. In: *Report: IFM/TR-6.380.01*. Sweden; 1980:71p-.

294. Conte F, Jean P. CFD modelling of air compression and release in road cavities during tyre/road interaction. In: *EURONOISE 2006 - The 6th European Conference on Noise Control: Advanced Solutions for Noise Control*. Tampere, Finland; 2006.

295. Bernhard RJ, Thornton WD, Baumann J. Effects of Varying the Tire Cap Ply, Sidewall Filler Height and Pavement Surface Texture on Tire/Pavement Noise Generation. In: *SQDH 2003-1, Final Report, Purdue University*. United States; 2003:90-.

296. Sainty S, Tawaf A, Richard JJ, Mohamed Z, Wang X. Analysis of potential solutions to audible tire cavity and rim coupling resonance noise. In: *American Society of Mechanical Engineers, Noise Control and Acoustics Division (Publication) NCAD*.Vol 6. New York City, NY, United states; 2012:4457-4463. http://dx.doi.org/10.1115/NCAD2012-0113.

297. Wang X, Mohamed Z, Ren H, Liang X, Shu H. A study of tyre, cavity and rim coupling resonance induced noise. *Int J Veh Noise Vib*. 2014;10(1-2):25-50. http://dx.doi.org/10.1504/IJVNV.2014.059628.

298. Negrus EM, Teodorescu C. Testing and evaluation of tyre like component part of motor vehicle. In: *ISBN 973-648-027-5, BREN Publisher, Bucharest*.; 2002:102p. https://www.tut.fi/ms/muo/tyreschool/moduulit/moduuli_8/.

299. Yamauchi H, Akiyoshi Y. Theoretical analysis of tire acoustic cavity noise and proposal of improvement technique. *JSAE Rev*. 2002;23(1):89-94. http://dx.doi.org/10.1016/S0389-4304(01)00152-7.

300. Lee TK, Kim BS, Kim GJ. The identification of tyre induced vehicle interior noise. *Appl Acoust (UK)*. 2000;68(1):134-156. http://dx.doi.org/10.1016/j.apacoust.2006.05.020.

301. Essers U, Liedl W, Eberspacher R, Kohler E, Litschel R. Air-Borne, Structure-Borne and Laser-Optical Measurements of Tyre Noise Generating Mechanisms on Dry and Wet Surfaces. :17p-.

302. Larsson K, Kropp W. A high-frequency three-dimensional tyre model based on two coupled elastic layers. *J Sound Vib*. 2002;253(4):889-908. http://dx.doi.org/10.1006/jsvi.2001.4073.

303. Ishihama M, Kagaya T. Modeling high-frequency tire tread vibration as a group of traveling bending waves. In: *American Society of Mechanical Engineers, Noise Control and Acoustics Division (Publication) NCAD*.Vol 8. New York City, NY, United states; 2012:83-91. http://dx.doi.org/10.1115/NCAD2012-0282.

304. Erixon R. Wave propagation in car tyres - A study of the wave types and vibrations of tyre carcass. In: *TRITA-FKT 1998:32, MWL, Royal Inst. of Technology, Stockholm, Sweden*.;

1998.

305. Kropp W. Structure-borne sound on a smooth tyre. *Appl Acoust*. 1989;26(3):181-192. http://dx.doi.org/10.1016/0003-682X(89)90051-0.

306. Lee JJ, Ni AE. Structure-borne tire noise statistical energy analysis model. *Tire Sci Technol*. 1997;25(3):177-186.

307. Iwao K, Yamazaki I. A study on the mechanism of tire/road noise. In: *JSAE Review No. 17*.Vol 17. Amsterdam, Netherlands; 1996:139-144. http://dx.doi.org/10.1016/0389-4304(95)00004-6.

308. Ronneberger D. Reifen Rollgeräusche. In: *Proceedings of DAGA 1985*.; 1985:75.

309. Ronneberger D. Towards quantitative prediction of tire/road noise. In: *Proc. of Workshop on Rolling Noise Generation, Technical University of Berlin, Germany*.; 1989.

310. Descornet G, Sandberg U. Road surface influence on tire/road nose - Part II. In: *Inter-Noise 80. Noise Control for the 80's. Proceedings of the 1980 International Conference on Noise Control Engineering*. New York, NY, USA; 1980:267-272.

311. Saemann E-U, Schmidt H. Schallmessungen bei der Entwicklung von Reifen mit gerigem Vorbeifahrtpegel. *Zeitschrift für Lärmbekämpfung*. 2002;49(2).

312. Doan VQ, Brackin D, Nishihata S, Sauerzapf J. Investigation into the influence of tire construction on coast-by noise. *Tire Sci Technol*. 1995;23(2):96-115.

313. Sandberg U, Goubert L. Poroelastic Road Surface (PERS): A review of 30 years of R & D work. In: *Proc. of Inter-Noise 2011, Osaka, Japan*.; 2011.

314. Kim Y-J, Bolton JS. Modeling tire treadband vibration. In: *Proceedings of INTER-NOISE 01, Hague, Holland*.; 2001:2522.

315. Campanac P, Duhamel D, Nonami K. Modeling of tire vibrations. In: *Proceedings of INTER-NOISE 99, Fort Lauderdale, FL*.; 1999:113.

316. Yum K, Bolton JS. Sound radiation modes of a tire on a reflecting surface. In: *Proceedings of Noise-Con 04, Baltimore, MD*.; 2004:161.

317. Yum K, Hong K, Bolton JS. Experimental relationship between tire structural wave propagation and sound radiation. In: *Institute of Noise Control Engineering of the USA - 35th International Congress and Exposition on Noise Control Engineering, INTER-NOISE 2006*.Vol 1. Honolulu, HI, United states; 2006:450-457.

318. Kuijpers A, Blokland G van. Tyre/road noise models in the last two decades. In: *Proceedings of INTER-NOISE 01, The Hague, Holland*.; 2001:2494.

319. Eberhardt AC. Truck tire vibration sound. In: *Inter-Noise 80. Noise Control for the 80's. Proceedings of the 1980 International Conference on Noise Control Engineering, Miami, FL*. New York, NY, USA; 1980:281-284.

320. Ji L, Bolton JS. Coupling mechanism analysis of structural modes and sound radiations of a tire tread band based on the S-mode technique. *Appl Acoust*. 2015;99:161–170.

321. Sandberg U, Kalman B, Williams AR. The porous tread tire - The quietest pneumatic tire measured so far? In: *International Congress on Noise Control Engineering 2005,*

INTERNOISE 2005.Vol 5. Rio de Janeiro, Brazil; 2005:3996-4005.

322. Sandberg U, Glaeser K-P. Effect of tyre wear on noise emission and rolling resistance. In: *Proceedings of INTER-NOISE 08, Shanghai, China*.; 2008:4066.

323. Larsson K. Modelling of Tangential Contact Forces. In: *Tech Lic Thesis, Report F99-08, Chalmers Univ. of Technology, Gothenburg, Sweden*.; 1999.

324. Hamet J-F, Klein P. Road texture and tire noise. In: *Proceedings of INTER-NOISE 00, Nice, France*.; 2000:2517.

325. Wullens F, Kropp W, Jean P. Quasi-3D versus 3D contact modelling for tyre/road interaction. In: *Proceedings of INTER-NOISE 04, Prague, Czech Republic*.; 2004:3318.

326. Eberhardt AC. Development of a transient response model for tire/pavement interaction. In: *Proceedings of INTER-NOISE 84, Honolulu, HI*.; 1984:77-82.

327. Phillips SM, Morgan PA, Watts GR. Development of methods for understanding tyre/road noise generation and propagation. In: *Proceedings of INTER-NOISE 99, Fort Lauderdale, FL*.; 1999:219.

328. Sandberg U. Road Texture Induced External Tire Noise: Empirical Frequency Response Function for Tires (Vaegtexturinducerat Daeckbuller: Empirisk Oeverfoerings-Funktion foer Bildaeck). In: *VTI Report 174A, Swedish National Road and Transport Research Institute, Linkoping, Sweden*. Sweden; 1979:29p-.

329. Eberhardt AC. An experiment and analytical investigation of the vibration noise generation mechanisms in truck tires. In: *Report No DOT-HS-805-868, U.S. Department of Transportation, Washington, DC, USA*.; 1981.

330. Bergmann M. Geräuschentstehung auf Trockener und Nasser Fahrbahn, Reifengeräusch und Strassenbau (Noise generation on dry and wet pavement, tire noise and road). In: *Mitteilung Nr. 57, Institut Für Strassen- Und Eisenbahn- Und Felsbau and Der E.T.H. Zürich*.; 1984:131.

331. Jennewein M, Bergmann M. Investigations concerning tyre-road noise sources and possibilities of noise control. In: *Vehicle, Noise and Vibration, Institution of Mechancal Engineers, London, 1984 - 1985*.; 1985:235.

332. Beckenbauer T, Klein P, Hamet J-F, Kropp W. Tyre/road noise prediction: A comparison between the SPERoN and HyRoNE models - Part 1. In: *Proceedings of Acoustics08, Paris, France*.; 2008:2933-2938.

333. Liu C, Ning T, Zhang D, Li K. Wavelet denoising method of tire laser spearing speckle interferogram. In: *IEEE International Conference on Automation and Logistics (ICAL)*. Qingdao, China; 2008:388-392. http://dx.doi.org/10.1109/ICAL.2008.4636181.

334. Bremner P, Huff J, Bolton JS. A model study of how tire construction and materials affect vibration-radiated noise. In: *SAE Technical Papers*. 400 Commonwealth Drive, Warrendale, PA 15096-0001, United States; 1997. http://dx.doi.org/10.4271/972049.

335. Walker JC. Noise generated at the tyre-road interface. In: *Ph.D Thesis, University of Aston*.; 1981.

336. Walker JC. Tyre-Road Interaction Studies to Improve Noise and Skid Resistance. In:

Mitteilung Nr. 57, Institut Für Strassen- Und Eisenbahn- Und Felsbau and Der E.T.H. Zürich.; 1984:155.

337. Rochoux D, Biesse F. Tire/road noise, the tire vibration as the main noise source from road texture. In: *39th International Congress on Noise Control Engineering 2010, INTER-NOISE 2010*.Vol 5. Lisbon, Portugal; 2010:3597-3606.

338. Ejsmont JA. Side force influence on tire/road noise. In: *Proceedings of INTROC 90, Gothenburg, Sweden*.; 1990.

339. Wozniak R. Measurement of tyre/road noise in longitudinal slip conditions. In: *Proceedings of Inter-Noise 2001, The Hague, Holland*.; 2001:556.

340. Wozniak R, Taryma S. Investigations in tyre/road noise in longitudinal slip conditions. In: *Proceedings of Inter-Noise 2004, Prague, Czech Republic*.; 2004:2300.

341. Brusarosco M, Cigada A, Manzoni S. Measurement and analysis of tyre and tread block dynamics due to contact phenomena. *Veh Syst Dyn*. 2011;49(6):855-869. doi:10.1080/00423114.2010.497841.

342. Crowther AR, Singh R. Identification and quantification of stick-slip induced brake groan events using experimental and analytical investigations. *Noise Control Eng J*. 2008;56(4):235-255. http://dx.doi.org/10.3397/1.2955772.

343. Timmons FE. An industry viewpoint of tire sound reduction and measurement methodology. In: *SAE Technical Papers*. 400 Commonwealth Drive, Warrendale, PA 15096-0001, United States; 1976. http://dx.doi.org/10.4271/762020.

344. Molisani L. A Coupled Tire Structure-Acoustic Cavity Model. In: *PhD Dissertation, Virginia Tech*.; 2004.

345. Zhang N, Zhang J, Wang Y. Experimental verification of stick-slip motion between two rolling contact surfaces. In: *Advanced Materials Research*.Vol 230-232. Chongqing, China; 2011:1362-1366. http://dx.doi.org/10.4028/www.scientific.net/AMR.230-232.1362.

346. Kroger M, Moldenhauer P. Influences on the vibration frequencies of tire tread blocks. In: *Proceedings of ISMA 2010 - International Conference on Noise and Vibration Engineering, Including USD 2010*. Leuven, Belgium; 2010:4015-4022.

347. Kuijpers A, Blokland G van. Tyre/road noise models in the last two decades: A critical evaluation. In: *Proceedings of Inter-Noise 2001, The Hague, Holland.*; 2001:2494.

348. Nilsson N, Bennerhult O, Soderqvist S. *IFM Research Report 6.371.02*.; 1980.

349. Kroger M, Lindner M, Popp K. Influence of friction on noise and vibrations of tyres. In: *Proceedings of Inter-Noise 2004, Prague, Czech Republic*.; 2004:1457.

350. Taryma S. Tire/road noise measured at the conditions when tire tread becomes “sticky.” In: *11th International Conference “Noise Control 98”, Krynica, Poland*.; 1998.

351. Morizur MF, Deygout F, Naesje K, Fjogstad E, Robertus C. An innovative technique to reduce air polllution on asphalt roads. In: *Proc of 2nd Eurasphalt & Erobitume Congress Barcelona 2000*.; 2000.

352. El-Sebai NA, Watany M, Saad A. Tire/road interface airborne noise characteristics generation. In: *SAE Technical Papers*. Traverse City, MI, United states; 1999.

http://dx.doi.org/10.4271/1999-01-1731.

353. Eisenblaetter J, Walsh SJ, Krylov V V. Air-related mechanisms of noise generation by solid rubber tyres with cavities. *Appl Acoust*. 2010;71(9):854-860. doi:10.1016/j.apacoust.2010.05.002.

354. Hayden RE. Roadside noise from the interaction of a rolling tire with the road surface. In: *Proceedings of the Purdue Noise Control Conference, Purdue University, Indiana, USA*.; 1971.

355. NBS. Truck tire noise - I. Peak A-weighted sound levels due to truck tires. In: *Report No. OST-ONA-71-9, National Bureau of Standards, Building Research Division, Washington, D.C., USA*.; 1970.

356. Leasure WA, Corley DM. Truck noise - I-B. Spectral and directional characteristics of noise generated by truck tires. In: *Report No. NBS-114A, National Bureau of Standards, Department of Commerce, Washington, D.C., USA*.; 1974.

357. Donavan PR, Lodico DM. Tire/pavement noise of test track surfaces designed to replicate California highways. In: *38th International Congress and Exposition on Noise Control Engineering 2009, INTER-NOISE 2009*.Vol 1. Ottawa, ON, Canada; 2009:380-391.

358. Kim S, Jeong W, Park Y, Lee S. Prediction method for tire air-pumping noise using a hybrid technique. *J Acoust Soc Am*. 2006;119(6):3799-3812. http://dx.doi.org/10.1121/1.2200140.

359. Fujikawa T, Koike H, Oshino Y, Tachibana H. Road texture for abating truck tire noise generation. In: *Institute of Noise Control Engineering of the USA - 35th International Congress and Exposition on Noise Control Engineering, INTER-NOISE 2006*.Vol 1. Honolulu, HI, United states; 2006:349-352.

360. Ejsmont JA, Sandberg U, Taryma S. Influence of tread pattern on tire/road noise. In: *Passenger Car Meeting, October 1, 1984 - October 4, 1984*. SAE Technical Papers. Technical University of Gdansk, PolandSwedish Road and Traffic Research Institute, Linkoeping, Sweden: SAE International; 1984:9p-. doi:10.4271/841238.

361. Chiu J-T, Tu F-Y. Application of a pattern recognition technique to the prediction of tire noise. *J Sound Vib*. 2015;350:30–40. http://dx.doi.org/10.1016/j.jsv.2015.04.013.

362. Gagen MJ. Novel acoustic sources from squeezed cavities in car tires. *J Acoust Soc Am*. 1999;106(2):794-801. http://dx.doi.org/10.1121/1.427096.

363. Gagen MJ. Nonlinear acoustic sources in squeezed car tyre cavities. *Noise Vib Worldw*. 2000;31(4):9-19. http://dx.doi.org/10.1260/0957456001497481.

364. Samuels S. Recent Australian Tyre/Road Noise Research. In: *Proc. of the International Tire Noise Conference, STU-Information No. 168-1980, NUTEK, Stockholm*.; 1979:1-25.

365. Plotkin KJ, Montroll ML, Fuller WR. A study to identify advanced methods of reducing tire noise. In: *Wyle Reserach Report WR 80-16, April 1980, Wyle Laboratories, Arlington, Virginia*.; 1980.

366. Wei Y, Feng Q, Wang H, Kaliske M. A hybrid numerical-experimental analysis for tire air-pumping noise with application to pattern optimization. *Noise Control Eng J*. 2016;64(1):56-63.

367. Hamet J-F, Deffayet C, Pallas M-A. Air-pumping phenomena in road cavities. In: *Proc. of the International Tire Noise Conference 1990, STU-Information No. 794-1990, NUTEK, Stockholm*.; 1990.

368. Fahy F, Elliott S. Acoustic intensity measurements of transient noise sources. *Noise Contr Eng*. 1981;17(3):120-125.

369. Gautam P, Chandy. AJ. "Understanding Tire Acoustics Through Computational Fluid Dynamics (CFD) of Grooves With Deforming Walls." . In: *ASME 2015 Noise Control and Acoustics Division Conference at InterNoise 2015. American Society of Mechanical Engineers, 2015*.; 2015.

370. Chanaud RC. Experiment study of aerodynamic sound from a rotating disc. *J Acoust Soc Am*. 1969;45(2).

371. Heckl M. Tire noise generating mechanisms - state-of-the-art report. In: *Proc. of International Tire Noise Conference, Stockholm Sweden*.; 1979:41-55.

372. Donavan PR. Contributors to Lower Frequency Pass-by Noise Levels under Cruise Conditions. In: *SAE Technical Papers*.Vol 4. 400 Commonwealth Drive, Warrendale, PA 15096-0001, United States; 2011:1132-1141. http://dx.doi.org/10.4271/2011-01-1613.

373. Leasure WA, Bender EK. Tire-Road Interaction Noise. In: *Proceedings of INTER-NOISE 73, Copenhagen, Denmark*. United States; 1973:421.

374. Wilken ID, Oswald LJ, Hickling R, J. OL, Hickling R. Research on Individual Noise Source Mechanisms of Truck tires: Aeroacoustic Sources. In: *SAE Highway Tire Noise Symposium Proceedings P-70, Paper 762022, Detroit, Ml, Nov. 1976*. 400 Commonwealth Drive, Warrendale, PA 15096-0001, United States; 1976:155-165. http://dx.doi.org/10.4271/762022.

375. Ronneberger D, Flötke H, Helmsen F, K. Schaaf. Untersuchung der Schallab- strahlung von rollenden luftumstromten Reifen (Investigation of the sound radiation of rolling air flow around tires). In: *Interner Bericht Des Dritten Physikalischen Instituts Der Universität Göttingen*.; 1982.

376. Gent AN, Walter JD. The Pneumatic Tire. *Rubber World*. 2006;(February):707.

377. Kropp W, Larsson K, Barrelet S. The influence of belt and tread band stiffness on the tyre noise generation mechanisms. In: *Proc. of the International Congress on Acoustics (ICA) 1998, Seattle, WA, USA*.; 1998.

378. Richards MG. Cross lug tire noise mechanisms. In: *SAE Technical Papers*. 400 Commonwealth Drive, Warrendale, PA 15096-0001, United States; 1976. http://dx.doi.org/10.4271/762024.

379. Richards MG. Automotive tire noise: a comprehensive study. *Sound Vib*. 1974;8(5):42-47.

380. Bolton JS, Song HJ, Kim YK, Kang YJ. Wave number decomposition approach to the analysis of tire vibration. In: *Proceedings - National Conference on Noise Control Engineering*. Ypsilanti, MI, USA; 1998:97-102.

381. Rhyne TB, Cron SM. Development of a non-pneumatic wheel. *Tire Sci Technol*. 2006;34(3):150-169.

382. Bschorr O. Reduction of tire noise. In: *Proc. of INTER-NOISE 85, Munich, Germany*.; 1985:271-274.

383. Tanaka Y, Horikawa S, Murata S. An evaluation method for measuring SPL and mode shape of tire cavity resonance by using multi-microphone system. *Appl Acoust*. 2016;105:171-178. http://dx.doi.org/10.1016/j.apacoust.2015.12.009.

384. Sakata T, Morimura H, Ide H. Effects of tire cavity resonance on vehicle road noise. *Tire Sci Technol*. 1990;18(2):68–79.

385. Thompson JK. Plane wave resonance in the tire air cavity as a vehicle interior noise source. *Tire Sci Technol*. 1995;23(1):2-10.

386. Walker C, Cortés L. Tire tread pattern excited noise - interference between noise from contact patch ends. In: *Proc of Workshop on Rolling Noise Generation, Technical University of Berlin, Germany*.; 1989.

387. Richards TL. Finite element analysis of structural-acoustic coupling in tyres. *J Sound Vib*. 1991;149(2):235-243. http://dx.doi.org/10.1016/0022-460X(91)90633-U.

388. Gunda R, Gau S, Dohrmann C. Analytical model of tire cavity resonance and coupled tire/cavity modal model. *Tire Sci Technol*. 2000;28(1):33-49.

389. Gu P, Ni A, Park J, Schaffer D. Study of tire acoustic cavity resonance. In: *Ford Global Noise and Vibration Conference*.; 2002.

390. Kim BS, Kim GJ, Lee TK. The identification of sound generating mechanisms of tyres. *Appl Acoust*. 2007;68(1):114-133. doi:10.1016/j.apacoust.2006.05.019.

391. Gu P, Feng ZC, Chen Y, et al. Modeling and experimental investigation of tire cavity noise generation mechanisms for a rolling tire. In: *SAE Technical Papers*.Vol 2. St. Charles, IL, United states; 2009:1414-1423. http://dx.doi.org/10.4271/2009-01-2104.

392. Hayashi T. Experimental analysis of acoustic coupling vibration of wheel and suspension vibration on tire cavity resonance. In: *SAE Technical Papers*. St. Charles, IL, United states; 2007. http://dx.doi.org/10.4271/2007-01-2345.

393. Mohamed Z, Wang X. A study of tyre cavity resonance and noise reduction using inner trim. *Mech Syst Signal Process*. 2015;50-51:498-509. http://dx.doi.org/10.1016/j.ymssp.2014.05.044.

394. Nakajima Y, Inoue Y, Ogawa H. Application of the boundary element method and modal analysis to tire acoustics problems. *Tire Sci Technol*. 1993;21(2):66-90.

395. Scavuzzo RW, Charek LT, Sandy PM, Shteinhauz GD. Influence of wheel resonance on tire acoustic cavity noise. In: *SAE Technical Papers*. Detroit, MI, United states; 1994. http://dx.doi.org/10.4271/940533.

396. Ni E-J, Snyder DS, Walton GF, et al. Radiated noise from tire/wheel vibration. *Tire Sci Technol*. 1997;25(1):29-42.

397. Mioduszewski P. Wplyw opon na halas w kabinie samochodu osobowego. In: *PhD Dissertation, Technical University of Gdansk, Poland*.; 1999.

398. Haverkamp M. Investigation of the wheel cavity resonance by analysis of the transmission of vibrational energy. *VDI Berichte*. 1999;1494:107–116.

399. Haverkamp M. Solving vehicle noise problems by analysis of the transmitted sound energy. In: *Proceedings of the 25th International Conference on Noise and Vibration Engineering, ISMA*. Leuven, Belgium; 2000:1361-1368.

400. Periyathamby H. Helmholtz resonator for reducing tire cavity resonance and in-vehicle noise. In: *Can. Acoust. (Canada)*.Vol 32. Canada; 2004:27-31.

401. Fernandez ET. The Influence of Tyre Air Cavities on Vehicle Acoustics. In: *PhD Thesis, KTH University, Stockholm, Sweden*.; 2006.

402. Douville H, Masson P, Berry A. On-resonance transmissibility methodology for quantifying the structure-borne road noise of an automotive suspension assembly. *Appl Acoust*. 2006;67(4):358-382. doi:10.1016/j.apacoust.2005.07.002.

403. Gu P, Chen Y, Z L, Kim H, Bi S, Schandevel B. Development of Vehicle and Systems Design Specifications for Mitigating Tire Cavity Noise. In: *Ford Global Noise and Vibration Conference, June 11- 12*.; 2008.

404. Waisanen AS, Blough JR. Road noise TPA simplification for improving vehicle sensitivity to tire cavity resonance using helium gas. In: *SAE Technical Papers*. St. Charles, IL, United states; 2009. http://dx.doi.org/10.4271/2009-01-2092.

405. Kindt P, Berckmans D, De Coninck F, Sas P, Desmet W. Experimental analysis of the structure-borne tyre/road noise due to road discontinuities. *Mech Syst Signal Process*. 2009;23:2557–2574.

406. Behzad M, Hodaei M, Alimohammadi I. Experimental and numerical investigation of the effect of a speed bump on car noise emission level. *Appl Acoust*. 2007;68(11-12):1346-1356. doi:10.1016/j.apacoust.2006.07.003.

407. Bekke DA, Wijnant YH, de Boer A. Experimental review on interior tire-road noise models. In: *2010 International Conference on Noise and Vibration Engineering, 20–22 September, Leuven, Belgium*.; 2010.

408. Jessop AM, Bolton JS. Tire surface vibration and sound radiation resulting from the tire cavity mode. In: *Tire Science and Technology*.Vol 39. P.O. Box 1502, Akron, OH 44309-1502, United States; 2011:245-255. http://dx.doi.org/10.2346/1.3670037.

409. Choi WH. Influence of the Cavity Mode on Tire Surface Vibration. In: *MSc Thesis, Purdue University, USA*.; 2011.

410. Bharadwaja BVSS, Siva PN. A Numerical Study on the Influencing Parameters of Tire-acoustic Cavity. In: *Applied Mechanics and Materials*.Vol 459. Singapore; 2013:390-395. http://dx.doi.org/10.4028/www.scientific.net/AMM.459.390.

411. Mohamed Z, Wang X. A deterministic and statistical energy analysis of tyre cavity resonance noise. *Mech Syst Signal Process*. 2016;70-71:947-957. http://dx.doi.org/10.1016/j.ymssp.2015.09.012.

412. Waki Y, Kozuki K, Heguri H. Estimation of noise radiating parts of a tire using the wave finite element method. In: *40th International Congress and Exposition on Noise Control Engineering 2011, INTER-NOISE 2011*.Vol 1. Osaka, Japan; 2011:577-584.

413. Kropp W. A Mathematical model of tyre noise generation. *Heavy Veh Syst*.

1999;6(1-4):310-329. doi:http://dx.doi.org/10.1504/IJHVS.1999.054504.

414. Nelson P, Phillips S. Quieter Road Surfaces. In: *Transportation Research Laboratory, Wokingham, UK, TRL Annual Review*.; 1997.

415. Morgan P, Nelson P, Steven H. Integrated Assessment of Noise Reduction Measures in the Road Transport Sector. In: *Transportation Research Laboratory, Wokingham, UK, TRL Project Report PR SE/652/03*.; 2003.

416. Keulen W, Duskov M. Inventory Study of Basic Knowledge on Tire/Road Noise. In: *Road and Hydraulic Engineering Division of Rijkswaterstaat, Delft, the Netherlands.*; 2005.

417. Eberhardt AC. Investigations of the truck tire vibration sound mechanisms. In: *Paper Presented at the International Tire Noise Conference, Stockholm*.; 1979.

418. Bruneau M. *Fundamentals of Acoustics*.; 2010. doi:10.1002/9780470612439.

419. Fabrizi C. Computational Aeroacoustic Analysis of a Rolling Tire. *Tire Sci Technol*. 2016;44(4):262-279. doi:10.2346/tire.16.440403.

420. Lassiter LW, Hubbard HH. Experimental studies of noise from subsonic jets in still air. *Natl Advis Comm Aeronaut -- Tech Notes*. 1952:35-.

421. Fitzpatrick HM, Lee R. Measurements of noise radiated by subsonic air jets. *United States Navy Dep -- David W Taylor Model Basin -- Rep*. 1952;(835):27-.

422. Donavan PR. Examination of tire/road noise at frequencies above 630 hertz. In: *Proceedings of Inter-Noise 2002, Dearborn, MI*.; 2002:241.

423. Oswald LJ, Arambages A. The noise mechanisms of cross groove tire tread pattern elements. In: *BT - Surface Vehicle Noise and Vibration Conference Proceedings.* Proceedings - Society of Automotive Engineers. GM Research Lab, Engineering, Mechanics Dep, Warren, MI, USA, GM Research Lab, Engineering Mechanics Dep, Warren, MI, USA: SAE; 1985.

424. Koike H, Fujikawa T, Oshino Y, Tachibana H. Generation Mechanism Of Tire/Road Noise Part 2 Pipe Resonance In Tread Groove Of Tire. In: *Inter-Noise 99*.; 1999.

425. ISO. Acoustics -- Specification of test tracks for measuring noise emitted by road vehicles and their tyres. *ISO 10844*. 2014.

426. Favre B. Some results concerning current research on tire noise in France. In: *Proceedings of the International Tire Noise Conference 1979, Stockholm, Sweden*.; 1979.

427. Donavan PR. Quantification of noise mechanisms for a straight-ribbed, HCR bias-ply truck tire. In: *Report No. EM-547, General Motors Research Laboratories, Warren, MI*.; 1982.

428. Fujiwara S, Yumii K, Saguchi T, Kato K. Reduction of tire groove noise using slot resonators. *Tire Sci Technol*. 2009;37(3):207-223. http://dx.doi.org/10.2346/1.3138766.

429. Nilsson N-A. Air resonant and vibrational radiation - possible mechanisms for noise from cross-bar tires. In: *Proc. International Tire Noise Conference, Stockholm, Sweden*.; 1979:93-109.

430. Nilsson NA, Soederqvist S, Bennerhult O. Air-Resonant Radiation - A Possible Mechanism for High Frequency Noise from Cross-Bar Tires. In: *Technical Report 6.084.02, IFM*

Akustikbyran AB, Stockholm, Sweden. Sweden; 1979:86p-.

431. Schaaf K, Ronneberger D. Noise radiation from rolling tires - sound amplification by the "horn-effect." In: *Proceedings of Inter-Noise 1982, San Francisco, CA*.; 1982:131.

432. Graf RAG, Kuo C-Y, Dowling AP. Horn amplification at a tire/road interface - Part I: experiment and computation. In: *Proc. of Inter-Noise 1999, Fort Lauderdale, Florida, USA*.; 1999.

433. Kropp W, Becot FX, Barrelet S. On the sound radiation fruom tires. *Acta Acust*. 2000;86:769-779.

434. Graf RAG, Kuo C-Y, Dowling AP, Graham WR. On the horn effect of a tyre/road interface, Part I: Experiment and computation. *J Sound Vib*. 2002;256(3):417-431. http://dx.doi.org/10.1006/jsvi.2001.4238.

435. Schutte JH, Wijnant YH, De Boer AD. The influence of the horn effect in tyre/road noise. *Acta Acust united with Acust*. 2015;101(4):690-700.

436. Iwai S, Miura Y, Koike H, Levy G. Influence of porous asphalt pavement characteristics on the horn amplification of tire/road contact noise. In: Vol 1. Yokohama, Japan; 1994:431.

437. Lui WK, Li KM. A theoretical study for the propagation of rolling noise over a porous road pavement. *J Acoust Soc Am*. 2004;116(1):313-322. http://dx.doi.org/10.1121/1.1751153.

438. Mioduszewski P, Ejsmont JA. Directivity of tire/road noise emission for selected tires and pavements. *Noise Control Eng J*. 2009;57(2):129-138. http://dx.doi.org/10.3397/1.3102007.

439. Mioduszewski P, Ejsmont JA. Tire noise emission directivity for various tires and pavements. In: *Institute of Noise Control Engineering of the USA - 35th International Congress and Exposition on Noise Control Engineering, INTER-NOISE 2006*.Vol 1. Honolulu, HI, United states; 2006:392-401.

440. Graham WR. Influence of tire geometry on the horn effect. In: *41st International Congress and Exposition on Noise Control Engineering 2012, INTER-NOISE 2012*.Vol 8. New York, NY, United states; 2012:6995-7008.

441. Sakamoto I, Tanaka T, Murakami T, Ogata S. Tire noise reduction by using sound absorbing material. In: *Proceedings of INTER- NOISE 99, Fort Lauderdale, FL*.; 1999:137.

442. Anfosso-Lédée F. Modeling the local propagation effects of tire-road noise: Propagation filter between CPX and CPB measurements. In: *Proceedings of INTER-NOISE 04, Prague, Czech Republic*.; 2004:2543.

443. Klein P, Hamet J-F. Tyre/road noise prediction with the HyRoNE model. In: *Proceedings of INTER-NOISE 07, Istanbul, Turkey*.; 2007:191.

444. Yoshihisa K, Okada Y, Yokota T, Iwase T. Experimental study on the effects of wind and the ground on horizontal propagation of sound. In: *Proceedings of INTER-NOISE 06, Honolulu, HI*.; 2006:5540.

445. Sandberg U. Semi-generic temperature corrections for tyre/road noise. In: *Proceedings of INTER-NOISE 04, Prague, Czech Republic*.; 2004:3302.

446. Rochat JL. Investigation of Temperature Correction for Tire/Pavement Noise

Measurements. :70p-.

447. Sandberg U. Low Noise Road Surfaces - A State-of-the-Art Review. *J Acoust Soc Japan*. 1999;20(1):1-17.

448. Taherzadeh S, Attenborough K. Deduction of ground impedance from measurements of excess attenuation spectra. *J Acoust Soc Am*. 1999;105(3):2039.

449. Bérengier MC, Stinson MR, Daigle GA, Hamet JF. Porous road pavements: Acoustical characterization and propagation effects. *J Acoust Soc Am*. 1997;101(1):155.

450. Nilsson N-A. TIRE/ROAD NOISE AT LOW FREQUENCIES: PLANE-WAVE RADIATION. BT - Proceedings - 1986 International Conference on Noise Control Engineering, Progress in Noise Control: Inter-Noise 86. In: Vol 1. VIAK AB, Vallingby, Swed, VIAK AB, Vallingby, Swed: Noise Control Foundation; 1986:223-931784131.

451. Maderuelo-Sanz R, Nadal-Gisbert A V, Crespo-Amoros JE, Parres-Garcia F. A novel sound absorber with recycled fibers coming from end of life tires (ELTs). *Appl Acoust (UK)*. 2012;73(4):402-408. http://dx.doi.org/10.1016/j.apacoust.2011.12.001.

452. Venslovas A, Aleksandraviciute D, Idzelis RL. Experimental investigation of scrap-tire crumb rubber application in noise-suppression structures. *Balt J Road Bridg Eng*. 2011;6(2):102-106. http://dx.doi.org/10.3846/bjrbe.2011.14.

453. Misik L, Radvanska A. Absorption properties of the noise barriers made of scrap tires. In: *Annals of DAAAM and Proceedings of the International DAAAM Symposium*. Trnava, Slovakia; 2008:885-886.

454. Hidaka Y, Tachibana H. Measurement of sound power radiation from elevated road structures by sound intensity method. In: *Proc. of Inter-Noise 92, Toronto, Canada*.; 1992:841-844.

455. Michishita K, Sakagami K, Morimoto M, Svensson UP. Sound radiation from an unbaffled elastic plate strip of infinite length. *Appl Acoust*. 2000;61:45-63.

456. Goromaru H, Komori T, Sava N. Study on control of bridge vibration and radiated noise. In: *Proc. of 7th International Congress on Sound and Vibration, Garmish-Partenkirchen, Germany*.; 2000.

457. van Haaren R. Validation of noise radiation of concrete railway bridges. In: *Proc. of Inter-Noise 1999, Fort Lauderdale, Florida, USA*.; 1999:1811-1816.

458. Archibald FR. An elementary analysis of a vehicle tire tread noise source. *J Sound Vib*. 1974;34(2):285-286. http://dx.doi.org/10.1016/S0022-460X(74)80311-1.

459. Kuemmel DA, Jaeckel JR, Satanovsky A, Shober SF, Schmiedlin RB. Impacts Related to Pavement Texture Selection. In: *WI/SPR-06-96 MU-CHTE-97-01 Final Report*. United States; 1997.

460. Andersson P. Modelling interfacial details in tyre/road contact - Adhesion forces and non-linear contact stiffness. *Doktorsavhandlingar vid Chalmers Tek Hogsk*. 2005;(2334):1-136.

461. Wullens F. Modelling of the local deformation at the tyre/road contact for the description of air pumping. *Acta Acust united with Acust*. 2003;89(SUPP.):S84-S84.

462. Kim E-Y, Hwang S-W, Lee S-K. Image-based approach to optimize the tyre pitch sequence for a reduction in the air-pumping noise based on a genetic algorithm. *Proc Inst Mech Eng Part D J Automob Eng*. 2012;226(9):1171-1184. http://dx.doi.org/10.1177/0954407012439950.

463. Kohli M, Moorthy SN, Rao MV, Raghavendran P. Experimental determination of acoustic cavity resonances of vehicle sub-systems. In: *SAE Technical Papers*.Vol 1. Detroit, MI, United states; 2014. http://dx.doi.org/10.4271/2014-01-0015.

464. Pope J, Reynolds WC. Tire noise generation: The roles of tire and road. In: *SAE Technical Papers*. 400 Commonwealth Drive, Warrendale, PA 15096-0001, United States; 1976. http://dx.doi.org/10.4271/762023.

465. Swieczko-Zurek B. Biological hazards in low noise, poroelastic road surfaces. In: *20th International Congress on Sound and Vibration 2013, ICSV 2013*.Vol 4. Bangkok, Thailand; 2013:2813-2818.

466. Sandberg U, Kropp W, Larsson K. The Multi-Coincidence Peak around 1000 Hz in Tyre / Road Noise Spectra. In: *Euronoise Naples 2003*.Vol 89.; 2003:1-8.

467. Nilsson N-A. Possible method of reducing external tire noise. In: *Proceedings of the International Tire Noise Conference 1979, Stockholm, Sweden*.; 1979.

468. Li KM, Lui WK. A study of the horn effect above a porous road pavement. In: *8th International Congress on Acoustics*. Japan; :4 pp.-pp.

469. Kuo C-Y, Graf RAG, Dowling AP, Graham WR. On the horn effect of a tyre/road interface, Part II: Asymptotic theories. *J Sound Vib*. 2002;256(3):433-445. http://dx.doi.org/10.1006/jsvi.2001.4217.

470. Peeters B, Ammerlaan I, Kuijpers A, Van Blokland G. Reduction of the horn effect for car and truck tyres by sound absorbing road surfaces. In: *39th International Congress on Noise Control Engineering 2010, INTER-NOISE 2010*.Vol 5. Lisbon, Portugal; 2010:3569-3578.

471. Virmalwar AD, Athavale SM, Sajanpawar PR. Application Of Fem And Experimental Techniques For Simulation Of Tyre/Road Air Pumping Noise, Horn Effect And Vibration Of Tyre Sidewalls. In: *Inter-Noise 99*.; 1999.

472. Dare T, Woldemariam W, McDaniel R, Olek J, Bernhard R. Comparing tests for near-grazing-incidence noise reduction and sound absorption tests for hot-mix asphalt. *Transp Res Rec*. 2012;(2270):1-8. http://dx.doi.org/10.3141/2270-01.

473. Seybert AF, Han J. Measurement of pavement absorption using ISO 13472-2. In: *Proceedings - European Conference on Noise Control*. Paris, France; 2008:4907-4911.

474. Guo J, Zhang R, Wang R. Experimental research on sound absorption performance of low-noise pavement. In: *Advanced Materials Research*.Vol 374-377. Xi'an, China; 2012:1400-1404. http://dx.doi.org/10.4028/www.scientific.net/AMR.374-377.1400.

475. Rochat JL, Donavan P, Seybert A, Dare T. Pavement sound absorption measurements in the U.S. In: *41st International Congress and Exposition on Noise Control Engineering 2012, INTER-NOISE 2012*.Vol 3. New York, NY, United states; 2012:2612-2626.

476. Sandberg U. ROAD TRAFFIC NOISE - THE INFLUENCE OF THE ROAD SURFACE

AND ITS CHARACTERIZATION. *Appl Acoust*. 1987;21(2):97-118. http://dx.doi.org/10.1016/0003-682X(87)90004-1.

477. Anfosso F, Houari A, Tahar M Ben. On a possible influence of road stiffness on tire/road noise generation. *Acta Acust united with Acust*. 2003;89(SUPP.):S81-S82.

478. Crocker MJ, Hanson D, Li Z, Karjatkar R, Vissamraju KS. Measurement of acoustical and mechanical properties of porous road surfaces and tire and road noise. In: *Transportation Research Record*.; 2004:16-22.

479. Sandberg U, Kropp W, Larsson K. The multi-coincidence peak around 1kHz in tyre/road noise spectra. *Acta Acust united with Acust*. 2003;89(SUPP.):S84-S84.

480. IEC. Electroacoustics – Sound Level Meters. *IEC 61672*. 2003.

481. Bernhard RJ. Tire Noise Fundamentals. In: *Presented at Universidade Estadual de Campinas, 2005 August 12*.; 2005.

482. Jonza JM, Herdtle T, Kalish J, Gerdes R, Yoo T, Eichhorn G. Acoustically Absorbing Lightweight Thermoplastic Honeycomb Panels. *SAE Int J Veh Dyn, Stab, NVH*. 2017;1:445-454.

483. Sorenson S, Jorro S. Effect of exterior absorption on heavy vehicle tire/surface noise at highway speeds. In: *41st International Congress and Exposition on Noise Control Engineering 2012, INTER-NOISE 2012*.Vol 2. New York, NY, United states; 2012:889-900.

484. Buckers C, Stockert U. Quiet Road Traffic 3 - An interdisciplinary approach to reduce the noise emission at the source. In: *Proceedings - European Conference on Noise Control*. Prague, Czech republic; 2012:984-991.

485. Biermann J-W, Viehofer J. Development of cars specified for tire-road noise measurement. In: *41st International Congress and Exposition on Noise Control Engineering 2012, INTER-NOISE 2012*.Vol 11. New York, NY, United states; 2012:9230-9241.

486. Kim H. A Study of Wheel Guards for Reduction of High Frequency Road-Noise. *SAE Int J Passeng Cars - Mech Syst*. 2015;8(1):46-51. http://dx.doi.org/10.4271/2015-01-1309.

487. Beckenbauer T, Kuijpers A. Prediction of pass-by levels depending on road surface parameters by means of a hybrid model. In: *Proceedings of Inter-Noise 2001, The Hague, Holland*.; 2001:2528-2533.

488. Anderson DG, Landers SP. On-board passenger tire sound generation study road versus lab wheel. In: *SAE Technical Papers*. 400 Commonwealth Drive, Warrendale, PA 15096-0001, United States; 1976. http://dx.doi.org/10.4271/762016.

489. Nilsson N-A. On generating mechanisms for external tire noise. In: *SAE Technical Papers*. 400 Commonwealth Drive, Warrendale, PA 15096-0001, United States; 1976. http://dx.doi.org/10.4271/762026.

490. Anonymous. Truck Tire Noise. In: *Rubber Manufacturers Association (RMA), Washington, D.C., USA*.; 1971.

491. Corcoran DA. Effects of operating parameters on truck tire sounds. In: *SAE SP-373, SAE Special Publication, Paper 720925*.; 1972.

492. Walker JC, Williams AR. The improvement of noise and traction due to road/tire interaction.

In: *Proceedings of International Tire Noise Conference 1979, Stockholm, Sweden*.; 1979.

493. Tetlow D. Truck tire noise - an initial survey of tire noise variables. In: *General Motors Proving Ground Report*.; 1968.

494. Hamet J-F. Measurement of power and directivity of tire/road surface noise. In: *Proc. of INTER-NOISE 88, Avignon, France*.; 1988.

495. Köhler E, Liedl W. Grenzen der Beeinflussungdes Reifenabrollgerausches bei nasser Fahrbahn. In: *Entwicklungslinien in Kraftfahrzeu-Technik Und Strassenverkehr, Forschungsbilanz 1981, Verlag TUV Rheinland, Germany*.; 1981.

496. Steven H, Pauls H. Entwicklung eines Messverfahrens für das Reifen-Fahrbahn-Geräusch. In: *Report from FIGE, Herzogenrath, Germany*.; 1990.

497. Ivannikov A, Haberkorn U, Langenberg H. Einflussgrössen auf Riefen/Fahrbahn-Geräusche eines LKW bei unterschiedlichen Fahrbedingunen. In: *FAT Schriftenreihe Nr. 158, Forschungsvereinigung Automobiltechnik E.v. (FAT), Germany (ISSN 0933-050 X)*.; 1998.

498. Ho K-Y, Hung W-T, Ng C-F, Lam Y-K, Leung R, Kam E. The effects of road surface and tyre deterioration on tyre/road noise emission. *Appl Acoust*. 2013;74(7):921-925. http://dx.doi.org/10.1016/j.apacoust.2013.01.010.

499. Lopez Arteaga I. Green's functions for a loaded rolling tyre. *Int J Solids Struct*. 2011;48(25-26):3462-3470. doi:10.1016/j.ijsolstr.2011.09.006.

500. Kim YJ, Bolton JS. Effects of rotation on the dynamics of a circular cylindrical shell with application to tire vibration. *J Sound Vib*. 2004;275(3-5):605-621. doi:10.1016/j.jsv.2003.06.003.

501. Huang SC, Soedel W. Effects of coriolis acceleration on the free and forced in-plane vibrations of rotating rings on elastic foundation. *J Sound Vib*. 1987;115(2):253-274. doi:10.1016/0022-460X(87)90471-8.

502. Huang SC, Soedel W. Effects of Coriolis acceleration on the forced vibration of rotating cylindrical shells. *J Appl Mech*. 1988;55:231-233.

503. Ulrich S. Rollgeräuschmessungen der Bundesanstalt für Strassenwesen an Strassen mit unterschiedlichen Decken und an einem Innentrommelprüfstand (Rolling noise measurements of the Federal Highway Research Institute on roads with different ceilings and an indoor drum. In: *Mitteilung Nr. 57, Institut Für Strassen- Und Eisenbahn- Und Felsbau and Der E.T.H. Zürich*.; 1984:207.

504. Moore DB. The Revised ISO 362 Standard for Vehicle Exterior Noise Measurement. *Sound Vib*. 2006;(October):19-23. doi:10.4271/2005-01-2417.

505. Yamazaki S, Fujikawa T, Hosegawa A, Ogasawara S. Indoor test procedure for evaluation of tire treadwear and influence of suspension alignment. *Tire Sci Technol*. 1989;17(4).

506. Ejsmont JA. Tire/road noise and rolling resistance - is there a trade-off? In: *Proc. of International Tire/Road Noise Conference 1990, Gothenburg, Sweden*.; 1990:439-452.

507. Senda T, Nakai M, Yokoi M, Chiba Y. Tire squeal. *Bull Jpn Soc Mech Eng*. 1984;27(231):2016-2023. http://dx.doi.org/10.1299/jsme1958.27.2016.

508. Trivisonno NM, Beatty JR, Miller RF. Origin of tire squeal -- 2. *Rubber Chem Technol*. 1968;41(4):953-976.

509. Taryma JAES. Halas Opon Samochodow Osobowych Poruszajacych Sie Posuchych Nawierzchniach asfaltowych I Betonowych. In: *Ph.D Thesis, Technical University of Gdansk, Poland. (In Polish)*.; 1982.

510. Leasure Jr. WA, Bender EK. Tire-road interaction noise. *J Acoust Soc Am*. 1975;58(1):39-50. doi:10.1121/1.380662.

511. Leasure WA, Corley DM, Flynn DR, Forrer JS. Truck noise - I. peak A-weighted sound levels due to truck tires. In: *Report No. OST/TST-72-1, National Bureau of Standards, Building Research Division, Washington, D.C., USA*.; 1972.

512. Kilmer RD. Test Procedures for Future Tire Noise Regulations. In: *Proceedings P-70, SAE Highway Tire Noise Symposium, San Francisco, Soc. of Automotive Engineers, Warrendale, PA, USA*. United States; 1976:6p-.

513. Kilmer RD, Cadoff MA, Mathews DE, Shoemaker CO. Effects of Load, Inflation Pressure and Tire Deflection on Truck Tire Noise Levels. In: *DOT-HS-803 874, US Department of Transportation, Washington, D.C.* United States; 1979:49p-.

514. Underwood MCP. THe origins of tire noise. In: *University of Southampton, Inst. of Sound and Vibration Research, Southampton, United Kingdom*.; 1980.

515. Nelson PM, Underwood MCP, Nelson PM. Lorry Tire Noise. *Veh Noise Vib*. 1984;(C139/84):50p-.

516. Walker JC. Noise Generated at the Tire-Road Interface. In: *PhD Dissertation TD 1292, Dunlop Ltd., Birmingham, United Kingdom*.; 1981.

517. Köllman A. Ermittlung des Standes der Technik hinsichtlich der Geräuschemission von PKW-Reifen. In: *Research Report 105 05 144, FIGE GmbH, Herzogenrath, Germany*.; 1993.

518. Wolf A, Schuh B-M, Krauss O. Erfassung des Wissenstandes über Reifen/Fahrbahngeräusche beim Nutzfahrzeug. In: *FAT Schriftenreihe Nr. 97, Forschungsvereinigung Automobiltechnik E.v. (FAT), Frankfurt, Germany*.; 1992.

519. von Meier A, van Bloklan GJ, Descornet G. The influence of texture and sound absorption on the noise of porous road surfaces. In: *Proc. of the Second International Symposium of Road Surface Characteristics, 23-26 Jun 1992, Technical University of Berlin, Berlin, Germany*.; 1992.

520. Tong G, Wang Q, Yang K, Wang XC. An experiment investigation to the radial tire noise. In: *Advanced Materials Research*.Vol 694 697. Switzerland; 2013:400-404. http://dx.doi.org/10.4028/www.scientific.net/AMR.694-697.361.

521. Beniguel JF, Le Pen D. Tire-alone criterion for structure borne road noise performance. In: *International Conference on Noise and Vibration Engineering 2012, ISMA 2012, Including USD 2012: International Conference on Uncertainty in Structure Dynamics*.Vol 2. Leuven, Belgium; 2012:1527-1539.

522. Tong G, Jin X, Tian W, Yang K. Simulation on factors affecting radial tire noise. *J Converg*

Inf Technol (South Korea). 2013;8(8):209-216. http://dx.doi.org/10.4156/jcit.vol8.issue8.26.

523. Muthukrishnan M. Effects of material properties on tire noise. In: *SAE Technical Papers*. Detroit, MI, United states; 1990. http://dx.doi.org/10.4271/900762.

524. Anonymous. Foreign Research in TIre Noise. In: *Office of Noise Abatement and Control, U.S., Environmental Protection Agency*.; 1980.

525. Kindt P, De Coninck F, Sas P, Desmet W. Analysis of tire/road noise caused by road impact excitations. In: *SAE Technical Papers*. St. Charles, IL, United states; 2007. http://dx.doi.org/10.4271/2007-01-2248.

526. Kindt P, De Coninck F, Sas P, Desmet W. Experimental modal analysis of radial tires under different boundary conditions. In: *13th International Congress on Sound and Vibration 2006, ICSV 2006*.Vol 6. Vienna, Austria; 2006:5111-5118.

527. Wozniak R, Taryma S, Mioduszewski P. Tire camber angle influence on tire-pavement noise. *Noise Control Eng J*. 2015;63(3):216-224.

528. Reinink HF, de Graaff DF, Peeters AAA, Peeters HM. Tyre/road noise measurements of truck tyres. In: *Report No. M+P.DWW.03.7.1 (5 February 2005), M+P Raadgevende Ingenieurs Bv, P.O. Box 2094, NL-5260 CB Vught, The Netherlands*.; 2005.

529. Takahashi M, Iimura K, Hidaka Y, Tachibana H. Sound power levels of road vehicles measured using a reverberant tunnel - statistical analysis. In: *Proceedings of INTER-NOISE 95, Newport Beach, California, USA*.; 1995:207-210.

530. Mioduszewski P. Vehicle noise simulation - computer program. In: *Proc. of EURO/NOISE '95 Symposium, Lyon, France*.; 1995.

531. Chang L. Numerical method of evaluating noise from vibrating tyre. In: *Applied Mechanics and Materials*.Vol 105-107. Shanghai, China; 2012:719-722. http://dx.doi.org/10.4028/www.scientific.net/AMM.105-107.719.

532. VTI. Effects of winter tyres – state of the art IN SWEDISH. In: *VTI Rapport 543*.; 2006.

533. Tanizaki T, Ueda K, Murabe T, Nomura H, Kamakura T. Discrimination between summer and winter tires using tire/road noises emitted by running vehicles. *IEEJ Trans Ind Appl*. 2013;133(5):558-565. http://dx.doi.org/10.1541/ieejias.133.558.

534. Bekke D, Wijnant Y, Weegerink T, De Boer A. Tire-road noise: An experimental study of tire and road design parameters. In: *42nd International Congress and Exposition on Noise Control Engineering 2013, INTER-NOISE 2013: Noise Control for Quality of Life*.Vol 1. Innsbruck, Austria; 2013:173-180.

535. Seamenn EU. Development of low noise tyres in EU project SILENCE. In: *Proceedings of Paris Acoustics*.; 2008.

536. El-Gindy M, Lewis HL, Lewis AS. Development of a tire/pavement contact-stress model based on an artificial neural network. *Am Soc Mech Eng Des Eng Div*. 1999;101:25-34.

537. Moore DF. *The Friction of Pneumatic Tires*. Amsterdam, Elsevier; 1975.

538. Aboutorabi HMR, Kung L. Application of Coupled Structural Acoustic Analysis and Sensitivity Calculations to a Tire Noise Problem. *Tire Sci Technol*. 2012;40(1):25-41.

http://dx.doi.org/10.2346/1.3684489.

539. Staadt RL. Truck noise control. *SAE Publ SP-386, Soc Automot Eng*. 1974.

540. Fong S. Tyre noise predictions from computed road surface texture induced contact pressure. In: *Proceedings of INTER-NOISE 98 Christchurch, New Zealand*.; 1998:137-140.

541. Pei X, Wang G, Zhou H, Zhao F, Yang J. Influence of tread structure design parameters on tire vibration noise. In: *Proceedings of SAE-China Congress 2015: Selected Papers Volume 364 of the Series Lecture Notes in Electrical Engineering*.; 2015:325-338.

542. Kumar A, Tandon A, Paul S, et al. Influence of Tyre's Dimensional Characteristics on Tyre-Pavement Noise Emission. *Phys Rev Res Int*. 2011;1(4):124-137.

543. Sandberg U, Ejsmont J. Tire/road noise - a subject of international concern. In: *Proceedings of INTER-NOISE 88, Page 1309, Avignon, France*.; 1988.

544. Yang JS, Fwa TF, Ong GP, Chew CH. Finite-element analysis of effect of wide-base tire on tire-pavement noise. *Adv Mater Res*. 2013;723:105-112. doi:10.4028/www.scientific.net/AMR.723.105.

545. Storeheier SA, Sandberg U. Vehicle Related Parameters Affecting Tyre/Road Noise. In: *Proceedings of the International Tire/Road Noise Conference 8-10 August 1990 Gothenburg, STU-Information No. 794-1990, NUTEK, Stockholm*.; 1990.

546. Landau LD, Lifshitz EM. *Theory of Elasticity*. Vol. 7 (3rd ed.). Butterworth-Heinemann; 1986.

547. O'Boy DJ, Dowling AP. Tyre/road interaction noise-Numerical noise prediction of a patterned tyre on a rough road surface. *J Sound Vib*. 2009;323(1-2):270-291. doi:10.1016/j.jsv.2008.12.024.

548. Watanabe T, Tomita N, Kishinami S, Yamaguchi H, Konishi S, Kawana A. Noise generation mechanism of cross-bar tyres and countermeasures against it. *Int J Veh Des*. 1988;9(6):641-653.

549. Doan VQ. Influence of tire construction and tire mold profile on coast-by noise. In: *Tire Technology International 1996, The Annual Review of Tire Materials and Tire Manufacturing Technology*.; 1996.

550. Sandberg U, Ejsmont JA. Influence of tyre rubber hardness on tyre/road noise emission. In: *Turkish Acoustical Society - 36th International Congress and Exhibition on Noise Control Engineering, INTER-NOISE 2007 ISTANBUL*.Vol 1. Istanbul, Turkey; 2007:394-403.

551. ISO. Plastics and ebonite -- Determination of indentation hardness by means of a durometer (Shore hardness. *ISO 868*. 2003.

552. ASTM. Standard Test Method for Rubber Property - Durometer Hardness. *ASTM D2240 - 05(2010)*. 2005.

553. Oddershede J, Kragh J. Changes in noise levels from Standard Reference Test Tyres due to increasing tyre tread hardness. In: *Proceedings of Forum Acusticum, v 2014-January, 2014, Forum Acusticum, FA 2014*.; 2014.

554. Wullens F, Kropp W. Influence of the local stiffness of the rubber layer of the tire on the generation of tire/road noise. In: *Proc. of ICA 2001, Rome, Italy*.; 2001.

555. Wullens F. Towards an optimisation of tire/road parameters for noise reduction. In: *Lic Thesis, Report F 02-01, Dept. of Applied Acoustics, Chalmers Univ. of Technology, Gothenburg, Sweden*.; 2002.

556. E.U. Saemann. Contribution of the tyre to further lowering tyre/road noise. In: *Proceedings of ParisAcoustics'08*.; 2008.

557. Swieczko-Zurek B, Ejsmont J, Mioduszewski P, Ronowski G, Taryma S. The effect of tire aging on acoustic performance of CPX reference tires. In: *INTER-NOISE 2015 - 44th International Congress and Exposition on Noise Control Engineering*. San Francisco, CA, United states; 2015.

558. Buhlmann E, Schulze S, Ziegler T. Ageing of the new CPX reference tyres during a measurement season. In: *42nd International Congress and Exposition on Noise Control Engineering 2013, INTER-NOISE 2013: Noise Control for Quality of Life*.Vol 1. Innsbruck, Austria; 2013:369-376.

559. Schubert S, Mannel M, Ertsey M, Hoever C. Influence of the tyre impedance on CPX level used to evaluate tyre/road noise. In: *Proceedings of the INTER-NOISE 2016 - 45th International Congress and Exposition on Noise Control Engineering: Towards a Quieter Future*. Hamburg, Germany; 2016:4945-4954.

560. Langwieder et al. Die Ergebnisse des ReifenCheck 2001 und deren Bedeutung für die Verkehrs- sicherheit (in German). In: *VDI-Berichte Nr. 1632, 2001, VDI, Germany*.; 2001.

561. Gothié M. Information presented at the meeting of PIARC/C1 in Copenhagen, Denmark, September 2001. In: *Presentation by by Mr Gothié of LCPC in Lyon, France*.; 2001.

562. Gothié M. Presentation at the meeting of PIARC/C1 in Rome, Italy, October 2005. In: *Presentation by Mr Gothié of LCPC in Lyon, France*.; 2005.

563. ETRTO. ETRTO recommendations 2002. In: *The European Tire and Rim Technical Organization (ETRTO), Brussels*.; 2002.

564. Thiriez K, Subramanian R. Tire pressure special study: tread depth analysis. In: *DOT HS 809 359, National Center for Statistics and Analysis*.; 2001.

565. Walker JC, Major DJ. Noise generated at the tire-road interface. In: *Annual Conference Stress Analysis Group of Institute of Physics, University of Aston in Birmingham, England*.; 1974.

566. Walker JC. Noise from the tire-road interface with heavy commercial vehicles. *Transp Eng*. 1975.

567. Flanagan W. Recent studies give unified picture of tire noise. *Automot Eng*. 1972.

568. Hillquist RK, Carpenter PC. A basic study of automobile tire noise. In: *GM Engineering Publication 5269, General Motors, Milford, Michigan*.; 1973.

569. Tetlow D. Truck Tire Noise. *Sound Vib*. 1971.

570. Archard JF. Contact and Rubbing of Flat Surfaces. *J Appl Phys*. 1953;24(8):981-988.

571. Sandberg U. Survey of noise emission from truck tires. In: *Proc. of Inter-Noise 91, Sydney, Australia*.; 1991.

572. Johnsson R, Nykänen A. Stud Noise Auralization. *Int J Passeng Cars - Mech Syst*. 2013;6(3). http://dx.doi.org/10.4271/2013-01-9122.

573. Ejsmont J, Ronowski G, Taryma S, Mioduszewski P, Sobieszczyk S, Swieczko-Zurek B. Relations between tire/road noise and tire rolling resistance on different road pavements. In: *41st International Congress and Exposition on Noise Control Engineering 2012, INTER-NOISE 2012*.Vol 11. New York, NY, United states; 2012:9476-9485.

574. Stenschke R, Vietzke P. Noise and use characteristics of modern car tyres (State of the art). In: *7th International Congress on Sound and Vibration, 4-7 July 2000, Garmisch-Partenkirchen, Germany*.; 2000.

575. Hoever C, Kropp W. A simulation-based parameter study of car tyre rolling losses and sound generation. In: *Proceedings - European Conference on Noise Control*. Prague, Czech republic; 2012:926-931.

576. ISO. Passenger car, truck, bus and motorcycle tyres -- Methods of measuring rolling resistance. *ISO 18164*. 2005.

577. ISO. Passenger car tyres -- Methods of measuring rolling resistance. *ISO 8767*. 1992.

578. ISO. Truck and bus tyres -- Methods of measuring rolling resistance. *ISO 9948*. 1992.

579. ISO. Motorcycle tyres -- Method of measuring rolling resistance. *ISO 13327*. 1998.

580. Rasmussen R. Measuring and modeling tire-pavement noise on various concrete pavement textures. *Noise Control Eng J*. 2009;57(2):139-147. http://dx.doi.org/10.3397/1.3081451.

581. ASTM. Standard Specification for P225/60R16 97S Radial Standard Reference Test Tire. *ASTM F2493*. 2014.

582. Donavan PR, Lodico D. Parameters affecting the noise performance of ASTM standard reference test tires. In: *SAE Technical Papers*.Vol 4. 400 Commonwealth Drive, Warrendale, PA 15096-0001, United States; 2013. http://dx.doi.org/10.4271/2013-01-1910.

583. Cao P, Yan X, Xiao W, Chen L. A prediction model to coupling noise of tire tread patterns and road texture. In: *Proceedings of the 8th International Conference of Chinese Logistics and Transportation Professionals - Logistics: The Emerging Frontiers of Transportation and Development in China*. Chengdu, China: American Society of Civil Engineers; 2008:2332-2338. doi:10.1061/40996(330)344.

584. Alt N, Wolff K, Eisele G, Pichot F. Fahrzeug Außen Geräuschsimulation (Vehicle exterior noise simulation). *Automob Zeitschrift*. 2006;108:832-836.

585. Hanson DI, James C RS, NeSmith C. Tire/Pavement Noise Study. In: *NCAT Report 04-02*. United States; 2004:49p-.

586. Che Y, Xiao W, Chen L, et al. GA-BP Neural Network Based Tire Noise Prediction. *Adv Mater Res*. 2012;443-444:65-70. http://dx.doi.org/10.4028/www.scientific.net/AMR.443-444.65.

587. Ge J, Fan J, Gu Q, Qian R, Youming L. Design method and application of low noise tire. In: *Symposium of International Rubber Conference 2004*.; 2004.

588. Saemann E-U. Reducing tire/road rolling noise. In: *PowerPoint Presentation by Dr Saemann of NVH Engineering, Continental Tyres, Hanover, Germany, at Conference*

Intelligent Tire Technology, November 29-30, 2005, Steigenberger Airport Hotel, Frankfurt, Germany.; 2005.

589. Xie K-J. Method of developing tread pattern. In: *US Patent US6514366 B1*.; 2003. http://www.google.com/patents/US6514366.

590. Oswald LJ. IDENTIFYING THE NOISE MECHANISMS OF A SINGLE ELEMENT OF A TIRE TREAD PATTERN. BT - Proceedings - NOISE-CON 81, 1981 National Conference on Noise Control Engineering: Applied Noise Control Technology. In: Proceedings - National Conference on Noise Control Engineering. Raleigh, NC, USA: Noise Control Found; 1981:53-931784042.

591. Liljegren K. Visual and acoustic tyre tread design. In: *Master's Thesis, Chalmers University of Technology*.; 2008.

592. Williams TA. Tire tread pattern noise reduction through the application of pitch sequencing. In: *SAE Technical Papers*. 400 Commonwealth Drive, Warrendale, PA 15096-0001, United States; 1995. http://dx.doi.org/10.4271/951352.

593. Bandel P, Bergomi R, Monguzzi C. Low noise sequence of tread elements for vehicle tires and related generation method. In: *US Patent US5371685*.; 1994. http://www.google.com/patents/US5371685.

594. ISO. Acoustics -- Description, measurement and assessment of environmental noise -- Part 2: Determination of environmental noise levels. *ISO 1996-2*. 2007.

595. Ewart ES. Pneumatic Tire. In: *US Patent US2006197*. U.S.; 1935.

596. Varterasian JH. Quieting noise mathematically its application to snow tires. In: *BT - Mid-Year Meeting, May 19, 1969 - May 23, 1969*. SAE Technical Papers. Research Labs., General Motors Corp: SAE International; 1969. doi:10.4271/690520.

597. Buddenhagen FE. Tire casing with noiseless tread. In: *US Patent US2612928*.; 1952. https://www.google.com/patents/US2612928.

598. Landers SP. Spreading noise generated by load supporting elements. In: *US Patent US4327792*.; 1982. https://www.google.com/patents/US4327792.

599. Williams TA. Tire pitch sequencing for reduced tire tread noise. In: *US Patent US5314551*.; 1994. https://www.google.com/patents/US5314551.

600. Michelin. Michelin Primacy 3 ST Tyres - Lasts Longer & Maximum Safety on wet roads. 2016. http://www.michelin.in/IN/en/tyres/products/primacy-3-st.html.

601. Dong Y, Tan Y, Liu H, Yang L. Noise performance of drainage asphalt pavement. *Int J Pavement Res Technol*. 2010;2(6):280-283.

602. Oshino Y, Mikami T, Ohnishi H, Tachibana H. Investigation into road vehicle noise reduction by drainage asphalt pavement. *J Acoust Soc Jpn*. 1999;20(1):75-84. http://dx.doi.org/10.1250/ast.20.75.

603. Wang G-L, Zhou H-C, Yang J, et al. Influence of Bionic Non-smooth Surface on Water Flow in Antiskid Tire Tread Pattern. *J Donghua Univ (English Ed*. 2013;30(4):336-342.

604. Zhou H. Investigate into Influence of Tire tread Pattern on Noise and Hydroplaning and Synchronously Improving Methods. In: *PhD Dissertation, Jiangsu University, China*.;

2013:1-178.

605. Donavan PR. Comparative measurements of tire/pavement noise in Europe and the United States. In: *Noise News International 13.2*. United States; 2005:46-53.

606. Mcghee K. Virginia Quiet Pavement Study. In: *Presented at SURF 2012 Norfolk, VA*.; 2012.

607. Sandberg U, Ejsmont JA, Gustavsson E. Tire/Road Noise on Rubberized Asphalt and Cement Concrete Surfaces in Sweden. 1990:60p-.

608. Li M, Molenaar A, Ven M van de, Huurman R, Keulen W van. New Approach for Modelling Tyre/Road Noise. In: *Inter-Noise 2009*.; 2009.

609. Klein P, Cesbron J. A 3D envelopment procedure for tyre belt radiated noise level prediction. In: *Proceedings of the INTER-NOISE 2016 - 45th International Congress and Exposition on Noise Control Engineering: Towards a Quieter Future*. Hamburg, Germany; 2016:2230-2241.

610. ISO. Characterization of pavement texture by use of surface profiles -- Part 1: Determination of Mean Profile Depth. *ISO 13473-1*. 1997.

611. Huschek S. Characterization of pavement surface texture and its influence on tire/road noise. In: *Proceedings of the Third International Symposium on Pavement Surface Characteristics: Christchurch, New Zealand 3-4 September 1996*.; 1996.

612. Wayson RL. NCHRP Synthesis 268 - Relationship between pavement surface texture and highway traffic noise. In: *Transportation Research Board, National Academy Press, Washington D.C, USA*. United States; 1998:94p-.

613. Li M, Keulen W van, Ceylan H, Tang G, Ven M van de, Molenaar. A. Influence of Road Surface Characteristics on Tire-Road Noise for Thin-Layer Surfacings. *J Transp Eng*. 2015;141(11). http://dx.doi.org/10.1061/(ASCE)TE.1943-5436.0000790.

614. Biermann J, von Estorff O, Petersen S, Schmidt H. Computational model to investigate the sound radiation from rolling tires. In: *Tire Science and Technology*.Vol 35. P.O. Box 1502, Akron, OH 44309-1502, United States; 2007:209-225. http://dx.doi.org/10.2346/1.2768608.

615. Hamet J-F, Klein P. Road texture and tire noise. In: *Proceedings of Inter-Noise 2000, Nice, France*.; 2000:178-183.

616. Hanson DI, Waller B. Evaluation Of The Noise Characteristics Of Minnesota Pavements. In: *Minnesota Department of Transportation*.; 2005.

617. Pinnington RJ. A particle-envelope surface model for road–tyre interaction. *Int J Solids Struct*. 2012;49(3-4):546-555. doi:10.1016/j.ijsolstr.2011.10.022.

618. Pinnington RJ. Tyre-road contact using a particle-envelope surface model. *J Sound Vib*. 2013;332(26):7055-7075. http://dx.doi.org/10.1016/j.jsv.2013.08.018.

619. He D-C, Wang L. Texture features based on texture spectrum. *Pattern Recognit*. 1991;24(5):391-399. doi:10.1016/0031-3203(91)90052-7.

620. Lee YG, Lee JH, Hsueh YC. Texture classification using fuzzy uncertainty texture spectrum. *Neurocomputing*. 1998;20(1-3):115-122. doi:10.1016/S0925-2312(97)00095-7.

621. Wang L, He D-C. Texture classification using texture spectrum. *Pattern Recognit*. 1990;23(8):905-910. doi:10.1016/0031-3203(90)90135-8.

622. ISO. Characterization of pavement texture by use of surface profiles -- Part 4: Spectral analysis of surface profiles. *ISO/TS 13473-4*. 2008.

623. ISO. Characterization of pavement texture by use of surface profiles -- Part 3: Specification and classification of profilometers. *ISO 13473-3*. 2002.

624. ASTM. Standard Test Method for Measuring Pavement Macrotexture Properties Using the Circular Track Meter. *ASTM E2157, ASTM, West Conshohocken, PA*. 2009.

625. Hamet J-F, Klein P. Use of a rolling model for the study of correlation between road texture and tire noise. In: *The 2001 International Congress and Exhibition on Noise Control Engineering, The Hague, The Netherlands*.; 2001.

626. Dare T, Bernhard R. Predicting tire-pavement noise on longitudinally ground pavements using a nonlinear model. In: *38th International Congress and Exposition on Noise Control Engineering 2009, INTER-NOISE 2009*.Vol 1. Ottawa, ON, Canada; 2009:405-415.

627. Sandberg U, Ejsmont JA. Texturing of cement concrete pavements to reduce traffic noise. *Noise Control Eng J*. 1998;46(6):231.

628. Rasmussen R, Karamihas S, Mun E, Chang G. Relating pavement texture to tire-pavement noise. In: *Institute of Noise Control Engineering of the USA - 35th International Congress and Exposition on Noise Control Engineering, INTER-NOISE 2006*.Vol 1. Honolulu, HI, United states; 2006:422-431.

629. FHWA. Technical Advisory T 5040.36 – Surface Texture for Asphalt and Concrete Pavements. In: *FHWA, Washington, DC*.; 2005.

630. Henry JJ. Evaluation of pavement friction characteristics. In: *Vol. 291, Transportation Research Board*.; 2000.

631. Flintsch GW, de Leon E, McGhee K, Al-Qadi I. Pavement Surface Macrotexture Measurement and Application. In: *Transportation Research Record: Journal of the Transportation Research Board 1860.1*.; 2003:168-177.

632. ASTM. Standard Test Method for Measuring Pavement Macrotexture Depth Using a Volumetric Technique. *ASTM E965*. 2006.

633. ASTM. Standard Practice for Calculating Pavement Macrotexture Mean Profile Depth. *ASTM E1845*. 2009.

634. ISO. Characterization of pavement texture by use of surface profiles -- Part 5: Determination of megatexture. *ISO 13473-5*. 2009.

635. ISO. Mechanical vibration -- Road surface profiles -- Reporting of measured data. *ISO 8608*. 1995.

636. Barbosa RS. Vehicle dynamic response due to pavement roughness. *J Brazilian Soc Mech Sci Eng*. 2011;33(3):302-307. http://dx.doi.org/10.1590/S1678-58782011000300005.

637. Stroup-Gardiner M, Brown ER. Segregation in hot-mix asphalt pavements. In: *Report No. 441, Transportation Research Board*.; 2000.

638. Saykin VV. Pavement macrotexture monitoring through sound generated by the tire-pavement interaction. In: *Northeastern University, Master's Thesis*.; 2011.

639. Reyes CH, Harvey J. A method for predicting sound intensity noise levels using laboratory pavement cores. In: *Proceedings of Noise-Con 2011, Portland, OR*.; 2011:522-534.

640. ASTM. Standard Practice for Computing International Roughness Index of Roads from Longitudinal Profile Measurements. *ASTM E1926*. 2008.

641. ASTM. Standard Test Method for Measuring Road Roughness by Static Level Method. *ASTM E1364*. 2012.

642. Sayers MW, Gillespie TD, Paterson WD. Guidelines for the Conduct and Calibration of Road Roughness Measurements. In: *World Bank Technical Paper No. 46, The World Bank, Washington DC*.; 1986.

643. ASME. Surface Texture (Surface Roughness, Waviness, and Lay). *ASME B461*. 2009.

644. Rasmussen RO, Garber SI, Fick GJ, Ferragut TR, Wiegand PD. *How to Reduce Tire-Pavement Noise- Interim Better Practices*.; 2008.

645. Kane A. Concrete pavement joints. In: *FHWA Technical Advisory T 5040.30, Federal Highway Administration, Washington, D.C.*; 1990.

646. Donavan P. Influence of PCC Surface Texture and Joint Slap on Tire/Pavement Noise Generation. In: *Proceedings of Noise-Con 2004, Baltimore*.; 2004:251-262.

647. Meiarashi S, Gagarin N, Coppage T. Effect of transverse tines/grooves spacing on tire/pavement noise from aspect of annoyance caused by wailing. In: *Proc. of Inter-Noise 98, Christchurch, New Zealand*.; 1998:203-208.

648. Dare T, Bernhard R, Thornton W. Effects of contraction joint width, fill condition, faulting and beveling on wheel-slap noise. *Noise Control Eng J*. 2011;59(3):228-233. http://dx.doi.org/10.3397/1.3562544.

649. Dare T, Bernhard R. Noise generation in contraction joints in Portland cement concrete. In: *24th National Conference on Noise Control Engineering 2010, Noise-Con 10, Held Jointly with the 159th Meeting of the Acoustical Society of America*.Vol 1. Baltimore, MD, United states; 2010:561-572.

650. Marriner D, Wakefield C. Modular expansion joint noise in B.C. In: *40th International Congress and Exposition on Noise Control Engineering 2011, INTER-NOISE 2011*.Vol 1. Osaka, Japan; 2011:763-768.

651. Sexton T. Controlling expansion joint noise on the Tacoma narrows bridge in Washington State, USA. In: *40th International Congress and Exposition on Noise Control Engineering 2011, INTER-NOISE 2011*.Vol 1. Osaka, Japan; 2011:734-739.

652. Glaeser K-P, Schwalbe G, Zoller M. Mitigation the noise emissions of vehicles travelling over bridge expansion joints. In: *40th International Congress and Exposition on Noise Control Engineering 2011, INTER-NOISE 2011*.Vol 1. Osaka, Japan; 2011:753-762.

653. Wakefield CW, Marriner DE. Analysis and control of bridge expansion joint croaking noise. In: *Canadian Acoustics - Acoustique Canadienne*.Vol 39. P.O. Box 74068, Ottawa, K1M 2HG, Canada; 2011:138-139.

654. Tournour MA, Cuschieri JM. Contribution to the overall noise level of the vibration of an open grid bridge deck. In: *Proceedings - National Conference on Noise Control Engineering*. Fort Lauderdale, FL, USA; 1994:105-110.

655. Cuschieri JM, Gregory S, Tournour M. Open grid bridge noise from grid and tire vibrations. *J Sound Vib*. 1996;190(3):317-343. http://dx.doi.org/10.1006/jsvi.1996.0067.

656. Tournour MA, Cuschieri JM. The contribution to the overall noise level of the vibration of an open grid bridge deck. In: *NOISE-CON 94 Proceedings. 1994 National Conference on Noise Control Engineering. Progress in Noise Control for Industry*. New York, NY, USA; 1994:105-110.

657. Payne AR, Scott JR. *Engineering Design with Rubber*. Interscience Publishers Inc.; 1960.

658. Donavan PR. Effect of porous pavement on wayside traffic noise levels. *Transp Res Rec*. 2014;2403:28-36.

659. ASTM. Standard Test Method for Effective Porosity and Effective Air Voids of Compacted Bituminous Paving Mixture Samples. *ASTM D7063/D7063M*. 2011.

660. AASHTO. Theoretical Maximum Specific Gravity and Density of Hot Mix Asphalt (HMA). *AASHTO T 209*. 2011.

661. AASHTO. Bulk Specific Gravity and Density of Compacted Hot Mix Asphalt (HMA) Using Automatic Vacuum Sealing Method. *AASHTO T 331*. 2010.

662. Ongel A, Harvey J. Pavement characteristics affecting the frequency content of tire/pavement noise. *Noise Control Eng J*. 2010;58(6):563-571. doi:10.3397/1.3514588.

663. Neithalath N, Weiss J, Olek J. *Reducing the Noise Generated in Concrete Pavements through Modification of the Surface Characteristics*.; 2005.

664. Roo F De, Gerretsen E. TRIAS - tyre road interaction acoustic simulation model. In: *InterNoise 2000, The 29th International Congress and Exhibition on Noise Control Engineering 27-30 August 2000, Nice, FRANCE, Volume 4*.; 2000:2488-2496.

665. Olek J, Weiss WJ, Neithalath N, Marolf A, Sell E, Thornton WD. Development of Quiet and Durable Porous Portland Cement Concrete Paving Materials. In: *Department of Transportation, Washington, DC. University Transportation Centers Program. Report: SQDH-2003-5*. United States; 2003:181-.

666. ISO. Acoustics -- Determination of sound absorption coefficient and impedance in impedance tubes -- Part 1: Method using standing wave ratio. *ISO 10534-1*. 1996.

667. ISO. Acoustics -- Determination of sound absorption coefficient and impedance in impedance tubes -- Part 2: Transfer-function method. *ISO 10534-2*. 1998.

668. ASTM. Standard Test Method for Impedance and Absorption of Acoustical Materials Using a Tube, Two Microphones and a Digital Frequency Analysis System. *ASTM E1050*. 2012.

669. ISO. Acoustics -- Measurement of sound absorption properties of road surfaces in situ -- Part 1: Extended surface method. *ISO 13472-1*. 2002.

670. ISO. Acoustics -- Measurement of sound absorption properties of road surfaces in situ -- Part 2: Spot method for reflective surfaces. *ISO 13472-2*. 2010.

671. ISO. Acoustics -- Materials for acoustical applications -- Determination of airflow resistance. *ISO 9053*. 1991.

672. Ren R, Gao C. Improved porous noise reducing asphalt mixture design method. *Int J Pavement Res Technol*. 2009;2(6):275-279.

673. Mogrovejo DE, Flintsch GW, De Leon Izeppi ED, McGhee KK, Burdisso RA. Short-term effect of pavement surface aging on tire-pavement noise measured with onboard sound intensity methodology. *Transp Res Rec*. 2014;(2403):17-27. http://dx.doi.org/10.3141/2403-03.

674. Berge T, Storeheier SA. Low noise pavements in a Nordic climate. Results from a four year project in Norway. In: *Proceedings of Inter-Noise 2009, Ottawa, Canada,.*; 2009:1936.

675. Li M, Molenaar AAA, van de Ven MFC, van Keulen W. Mechanical impedance measurement on thin layer surface with impedance hammer device. *J Test Eval*. 2012;40(5):6 pp. http://dx.doi.org/10.1520/JTE20120089.

676. Sandberg U, Goubert L. PERSUADE - A European project for exceptional noise reduction by means of poroelastic road surfaces. In: *40th International Congress and Exposition on Noise Control Engineering 2011, INTER-NOISE 2011*.Vol 1. Osaka, Japan; 2011:673-683.

677. Storeheier SA. Preliminary Investigation on a Poroelastic Material Used as a Low Noise Road Surface. In: *SINTEF Foundation Ofscient and Industrial Research*. Norway; 1987:41p-.

678. Nilsson N-A, Sylwan O. New vibro-acoustical measurement tools for characterization of poroelastic road surfaces with respect to tire/road noise. In: *Proceedings of the Tenth International Congress on Sound and Vibration*. Stockholm, Sweden; 2003:4343-4350.

679. Bilawchuk S. Tire noise assessment of asphalt rubber crumb pavement. *Can Acoust*. 2005;33(1):37-41.

680. Ponniah J, Tabib S, Lane B, Raymond C. Evaluation of the effectiveness of different mix types to reduce noise level at the tire/pavement interface. In: *TAC/ATC 2010 - 2010 Annual Conference and Exhibition of the Transportation Association of Canada: Adjusting to New Realities*. Halifax, NS, Canada; 2010.

681. Beckenbauer T. Akustische Eigenschaften von Fahrbahnoberflaechen. *Strasse+Autobahn*. 2001;54(10):553-561.

682. Stenschke R. Activities of the German Federal Environmental Agency to reduce tire/road noise. In: *Proc. of International Tire/Road Noise Conference 1990, Gothenburg, Sweden.*; 1990.

683. Liao G, Heitzman M, West R, Wang S, Ai C. Temperature Effects on the Correlations between Tire-Pavement Noises and Pavement Surface Characteristics. *New Front Road Airpt Eng*. 2015:219-232.

684. AASHTO. Standard Method of Test for Determining Dynamic Modulus of Hot-Mix Asphalt Concrete Mixtures. *AASHTO T 342*. 2011.

685. Rao C, Quintus HL Von. Determination of In Place Elastic Layer Modulus – Selection and Demonstration of Backcalculation Methodology and Practice: Phase I Interim Report, Long

Term Pavement Performance Program. In: *Federal Highway Administration, Washington, DC*.; 2012.

686. ASTM. Standard Test Method for Measuring the P-Wave Speed and the Thickness of Concrete Plates Using the Impact-Echo Method. *ASTM C1383*. 2010.

687. Biligiri KP. Effect of pavement materials' damping properties on tyre/road noise characteristics. *Constr Build Mater*. 2013;49:223-232. http://dx.doi.org/10.1016/j.conbuildmat.2013.08.016.

688. ASTM. Standard Test Method for Skid Resistance of Paved Surfaces Using a Full-Scale Tire. *ASTM E274 / E274M*. 2011.

689. ASTM. Standard Specification for Standard Rib Tire for Pavement Skid-Resistance Tests. *ASTM E501*. 2008.

690. ASTM. Standard Specification for Standard Smooth Tire for Pavement Skid-Resistance Tests. *ASTM E524*. 2008.

691. ASTM. Standard Test Method for Measuring Paved Surface Frictional Properties Using the Dynamic Friction Tester. *ASTM E1911*. 2009.

692. ASTM. Standard Practice for Calculating International Friction Index of a Pavement Surface. *ASTM E1960*. 2011.

693. ASTM. Standard Test Method for Measuring Surface Frictional Properties Using the British Pendulum Tester. *ASTM E303*. 2013.

694. Khaki AM, Forouhid AE, Zare M. Comparison of the noise level and the skid resistance of asphalt pavement mixtures on road surface. *J Meas Eng*. 2015;3(3):71-76.

695. McDaniel RS, Kowalski KJ, Shah A, Olek J, Bernhard RJ. Long-Term Performance of a Porous Friction Course. In: *FHWA/IN/JTRP-2009/22, Joint Transportation Research Program, Indiana Department of Transportation and Purdue University, West Lafayette, IN*.; 2010.

696. Kowalski KJ, McDaniel RS, Olek J. Identification of Laboratory Technique to Optimize Superpave HMA Surface Friction Characteristics. In: *FHWA/IN/JTRP-2010/06, Joint Transportation Research Program, Indiana Department of Transportation and Purdue University, West Lafayette, IN*.; 2010.

697. Paje SE, Bueno M, Teran F, Vinuela U. Monitoring road surfaces by close proximity noise of the tire/road interaction. *J Acoust Soc Am*. 2007;122(5):2636-2641. http://dx.doi.org/10.1121/1.2766777.

698. Ng WK, Ng PS, Hung WT. Measurement of tyre/road surface noise with close-proximity method in Hong Kong. In: *Proceedings of INTER-NOISE 09, Ottawa, Canada*.; 2009:1178.

699. Dare T, Wulf T, Thornton W, Bernhard RJ. Acousti- cal e↵ects of grinding and grooving on Portland cement concrete pavements. In: *Technical Report, The Institute for Safe, Quiet and Durable Highways*.; 2009.

700. Bendsten H, Kohler E, Lu Q. Acoustic Aging of Asphalt Pavements - A California Danish Comparison. In: *Road Directate, Danish Road Institute, Report 171*.; 2009.

701. Anderson KW, Uhlmeyer JS, Sexton T, Russell M, Weston J. Evaluation of Long-Term Pavement Performance and Noise Characteristics of the Next Generation Concrete Surface: Final Report. In: *Washington (State). Dept. of Transportation, WA-RD 767.2*. United States; 2014:52p-.

702. Hencken J, Haas E, Bennert T. Using Tire/Pavement Interface Noise Results to Define Statistically Similar Bituminous Pavements in Massachusetts. In: *Presented at 7th Symposium on Pavement Surface Characteristics: SURF 2012 Norfolk, VA*.; 2012.

703. Kay RK. Pavement Surface Condition Rating Manual. In: *Washington State Department of Transportation Report*.; 1992.

704. MNDOT. MnDOT Distress Identification Manual. In: *Report, Minnesota Department of Transportation, Office of Materials and Road Research*.; 2003.

705. Miller JS, Bellinger. WY. Distress identification manual for the long-term pavement performance program. In: *FHWA Report No. FHWA-RD-03-031*.; 2003.

706. Boullosa RR, Lopez AP. Tra. *Noise Control Eng J*. 1987;29(2):54.

707. Descornet G. Vehicle noise emission on wet road surfaces. In: *Proceedings of INTER-NOISE 00, Nice, France*.; 2000:4968.

708. Kongrattanaprasert W, Nomura H, Kamamura T, Ueda K. Automatic detection of road surface states from tire noise using neural network analysis. In: *20th International Congress on Acoustics 2010, ICA 2010 - Incorporating Proceedings of the 2010 Annual Conference of the Australian Acoustical Society*.Vol 4. Sydney, NSW, Australia; 2010:2965-2968.

709. Kocak S, M. E. Kutay. Relationship between Material Characteristics of Asphalt Mixtures and Highway Noise. In: *Paper No. 12-4309, TRB 91st Annual Meeting Compendium of Papers, TRB, National Research Council*.; 2012.

710. Sohaney R, Rasmussen R, Seybert A, Donavan P. New ISO test track specification for measuring tire and vehicle noise. In: *Sound and Vibration*.Vol 46. 27101 East Oviatt Road - P.O. Box 40416, Bay Village, OH 44140, United States; 2012:9-14.

711. Moore D. Revised ISO 10844 Test Surface: Technical Principles. *SAE Int J Passeng Cars - Mech Syst*. 2011;4(2):1126-1131. doi:10.4271/2011-01-1607.

712. Van Blokland G, Van Leeuwen M. Efficiency of the combined application of silent tyres and silent road surfaces. In: *39th International Congress on Noise Control Engineering 2010, INTER-NOISE 2010*.Vol 5. Lisbon, Portugal; 2010:3469-3478.

713. Kuijpers AHWM. Further analysis of the Sperenberg data - Towards a better understanding of the processes influencing tire/road noise. In: *Report No. M+P.MVM.99.3.1 Rev. 1, Hertogenbosch, the Netherlands*.; 2001.

714. Konishi S, Fujino T, Tomita N, Sakamoto M. Temperature effect on tire/road noise. In: *Proceedings - International Conference on Noise Control Engineering*.Vol 1. Newport Beach, CA, United states; 1995:147.

715. Anfosso-LédéE F, Pichaud Y. Temperature effect on tyre-road noise. *Appl Acoust*. 2007;68(1):1-16. doi:10.1016/j.apacoust.2006.06.001.

716. EEC. Tyre Noise: legal requirements. *EC Dir*. 2001.

717. Jabben J. Temperature effects on road traffic noise measurements. In: *40th International Congress and Exposition on Noise Control Engineering 2011, INTER-NOISE 2011*.Vol 1. Osaka, Japan; 2011:552-556.

718. Bae A, Stoffels SM, Lee SW. Observed Effects of Subgrade Moisture on Longitudinal Profile. In: *Paper No. 06-2312, TRB 85th Annual Meeting Compendium of Papers CD-ROM, TRB, National Research Council, Washington, DC*.; 2006.

719. Oldenettel H, Koster HJ. Test procedure for the quantification of rolling tire belt vibrations. In: *Vehicle System Dynamics*.Vol 27. Berlin, Ger; 1997.

720. Hung W-T, Lam Y-K, Ng C-F, Leung RC-K. The impacts of tyre hardness and tread depth on tyre/road noise. In: *20th International Congress on Sound and Vibration 2013, ICSV 2013*.Vol 4. Bangkok, Thailand; 2013:2846-2852.

721. Thrasher DB. Effect of tread wear on tire/pavement interaction noise. In: *Inter-Noise 80. Noise Control for the 80's. Proceedings of the 1980 International Conference on Noise Control Engineering*. New York, NY, USA; :277-280.

722. Spelman RH. Truck tires - Effects of design and construction on wear and noise. In: *SAE Technical Papers*. 400 Commonwealth Drive, Warrendale, PA 15096-0001, United States; 1963. http://dx.doi.org/10.4271/630515.

723. Raabe RC, Burche I. Retreaded truck tire noise tests. In: *BT - Truck Meeting, November 4, 1974 - November 7, 1974*. SAE Technical Papers. Bandag, Inc.: SAE International; 1974. doi:10.4271/741132.

724. Hasebe M. Experimental study of the noise generated by a passenger automobile equipped with studded and regular snow tyres. *Appl Acoust*. 1984;17(4):247-254. http://dx.doi.org/10.1016/0003-682X(84)90008-2.

725. AASHTO. Effects of Studded Tires. In: *TRB/NCHRP/SYN-32, Transportation Research Board, Washington, D.C.; Federal Highway Administration, Washington, D.C.;American Association of State Highway and Transportation Officials, Washington, D.C.* United States; 1975:58p-.

726. Liu Y, Li T, Liu Y, Su Y. Optimize the Structure Parameters of Tread Pattern Based on the Fuzzy Genetic Arithmetic. In: *2010 International Conference on Measuring Technology and Mechatronics Automation (ICMTMA 2010)*.Vol 2. Piscataway, NJ, USA; 2010:860-863. http://dx.doi.org/10.1109/ICMTMA.2010.122.

727. Sandberg U, Mioduszewski P. Gaining extra noise reduction and lower rolling resistance by grinding a porous asphalt pavement. In: *41st International Congress and Exposition on Noise Control Engineering 2012, INTER-NOISE 2012*.Vol 8. New York, NY, United states; 2012:6958-6969.

728. Van Blokland G-J, Von Meier A. Reducing tyre/road noise with porous road surfaces and the effect of tyre choice. In: *SAE Technical Papers*. Traverse City, MI, United states; 1993. http://dx.doi.org/10.4271/931279.

729. Sachakamol P, Dai L. Impact of porous pavement characteristics on tire/pavement noise emission from ARC roads. In: *17th International Congress on Sound and Vibration 2010, ICSV 2010*.Vol 4. Cairo, Egypt; 2010:2464-2473.

730. Hubelt J, Bartolomaeus W, Wellner F. On the correlation between motor vehicle noise levels and in situ measurement data of airflow resistance, water permeability and sound absorption coefficient of open porous asphalts. In: *Institute of Noise Control Engineering of the USA - 35th International Congress and Exposition on Noise Control Engineering, INTER-NOISE 2006*.Vol 2. Honolulu, HI, United states; 2006:1119-1123.

731. Altreuther B, Beckenbauer T. Dynamic measurement of air flow resistance. In: *EURONOISE 2006 - The 6th European Conference on Noise Control: Advanced Solutions for Noise Control*. Tampere, Finland; 2006:6P-6P.

732. Crocker MJ. *Handbook of Noise and Vibration Control*. John Wiley and Sons Inc., USA; 2007.

733. Brinkmeier M, Nackenhorst U, Petersen S, von Estorff O. A finite element approach for the simulation of tire rolling noise. *J Sound Vib*. 2008;309(1-2):20-39. doi:10.1016/j.jsv.2006.11.040.

734. Lou Z. An experimental and numerical study of tire/pavement noise on Asphalt Rubber Concrete pavement. 2007.

735. Wang G, Zhou H, Mao Z, Gao L. Boundary element analysis of rolling tire noise. In: *Proceedings 2011 International Conference on Transportation, Mechanical, and Electrical Engineering, TMEE 2011*. Changchun, China; 2011:1970-1973. http://dx.doi.org/10.1109/TMEE.2011.6199601.

736. Kropp W. Ein Modell zur Beschreibung des Rollgeräusches eines unprofiliertenGürtelreifens auf rauher Straβenoberfläche. In: *Thesis, Fortschritt-Berichte Reihe 11, Nr 166, VDI Verlag, Düsseldorf*.; 1992.

737. Andersson P, Larsson K, Kropp W. A method for experimental collection of global material data for tyres. In: *Conference Nordic Vibration Research 2001, Stockholm, Sweden*.; 2001.

738. Andersson P, Larsson K. Validation of a high frequency three-dimensional tyre model. *Acta Acust united with Acust*. 2005;91(1):121-131.

739. Bohm F. Zur Statik und Dynamik Des Gurtelreifens. *ATZ*. 1967;69:225-261.

740. Plotkin KJ, Montroll ML, Fuller WR. A study to indentify advanced methods of reducing tire noise. In: *Wyle Reserach Report WR 80-16, for the U.S. Environmental Protection Agency*.; 1980.

741. Nilsson NA. Generation mechanism of external tire noise. In: *IFM Akustikbyran Report No. TR3.709.14*.; 1976.

742. Morse PM. Theoretical Acoustics. *Am J Phys*. 1970;38(5):666. doi:10.1119/1.1976432.

743. Kung LE, Soedel W, Yang TY, Charek LT. Natural Frequencies and Mode Shapes of an Automotive Tire with Interpretation and Classification Using 3-D Computer Graphics. *J Sound Vib*. 1985;102(3):329-346.

744. Kung LE, Soedel W, Yang TY. Free Vibration of a Pneumatic Tire-Wheel Unit Using a Ring on an Elastic Foundation and a Finite Element Model. *J Sound Vib*. 1986;107(2):181-194. http://dx.doi.org/10.1016/0022-460X(86)90231-2.

745. Kung LE, Soedel W, Yang TY. On the dynamic response at the wheel axle of a pneumatic

tire. *J Sound Vib*. 1986;107(2):195-213. http://dx.doi.org/10.1016/0022-460X(86)90232-4.

746. Huang SC, Soedel W. Response of rotating rings to harmonic and periodic loading and comparison with the inverted problem. *J Sound Vib*. 1987;118(2):255-270.

747. Huang SC, Su CK. In-plane dynamics of tires on the road based on an experimentally verified ring model. *Veh Syst Dyn*. 1992;21:247-267.

748. Wheeler RL, Dorfi HR, Keum BB. Vibration modes of radial tires: Measurement, prediction, and categorization under different boundary and operating conditions. In: *SAE Technical Paper 2005-01-2523*. Traverse City, MI, United states; 2005. http://dx.doi.org/10.4271/2005-01-2523.

749. Böhm F. Mechanik des Gürtelreifens. *Ing-Arch*. 1966;35:82.

750. Boehm F. Mechanik des Gürtelreifens (Mechanics of the radial tire). *Ing-Arch*. 1966;35:82.

751. Ronneberger D. Experimentelle und Theoretische Untersuchungen Spezieller Mechanismen der Rollgeräuschentstehung und -abstrahlung (Experimental and theoretical studies specifically mechanisms of rolling noise generation and radiation). In: *Mitteilung Nr. 57, Institut Für Strassen- Und Eisenbahn- Und Felsbau and Der E.T.H. Zürich*.; 1984:79.

752. Mikulas M, McElman. On free vibrations of eccentrically stiffened cylindrical shells flat plates. In: *NASA TN D-3010*.; 1965.

753. Rennison DC. Interior noise control prediction study for high-speed propeller driven aircraft. In: *NASA Contractor Report, CR159200*.; 1979.

754. Saigal S, Yang TY. Free vibrations of a tire as a toroidal membrane. *J Sound Vib*. 1986;107(1):71–82.

755. Bolton JS, Kim Y-J. Wave-number domain representation of tire vibration. In: *The 29th International Congress and Exhibition on Noise Control Engineering 27-30 August 2000, Nice, FRANCE*.; 2000.

756. Cremer L. Die Synthese des Schallfeldes eines beliebigen festen Körpers in Luft mit beliebiger Schnelleverteilung aus Kugelschallfeldern. *Acustica*. 1984;55:44.

757. Heckl M. Bemerkungen zur Berechnung der Schallabstrahlung nach der Methode der Kugelfeldsynthese. *Acustica*. 1989;68:251.

758. Übler MF. Calculation of tyre motions with the folded plate model and comparison with measurements. In: *Poster Presented at the Transport Noise Conference, St. Petersburg, Russia*.; 1994.

759. Kim Y-J, Bolton JS. Effect of Rotation on the Vibration Characteristics of Tires. In: *InterNoise 2002, The 2002 International Congress and Exposition on Noise Control Engineering Dearborn, MI, USA*.; 2002.

760. Matsubara M, Tsujiuchi N, Koizumi T, Ito A, Bito K. Natural Frequency Analysis of Tire Vibration Using a Thin Cylindrical Shell Model. *SAE Tech Pap 2015-01-2198*. 2015. doi:10.4271/2015-01-2198.Copyright.

761. Feng ZC, Gu P. Modeling and experimental verification of vibration and noise caused by the cavity modes of a rolling tire under static loading. In: *SAE Technical Papers*. Rapids, MI,

United states; 2011. http://dx.doi.org/10.4271/2011-01-1581.

762. O'Boy DJ, Dowling AP. Tyre/road interaction noise-A 3D viscoelastic multilayer model of a tyre belt. *J Sound Vib*. 2009;322(4-5):829-850. doi:10.1016/j.jsv.2008.09.021.

763. Graff KF. *Wave Motion in Elastic Solids*.; 1991.

764. Hamet J-F. Tire/road noise: Time domain Green's function for the orthotropic plate model. *Acta Acust united with Acust*. 2001;87(4):470-474.

765. Meftah R, Duhamel D, Cesbron J, Yin H. A fast method for computing convolutions with structural Greens functions: Application to tyre dynamic contact problems. *Eur J Comput Mech*. 2013;22(5-6):284-303. doi:10.1080/17797179.2013.849483.

766. Meftah R, Duhamel D. A fast method for computing convolutions with structural green's function : Application to tire/road contact problems. In: *ECCOMAS Thematic Conference - COMPDYN 2011: 3rd International Conference on Computational Methods in Structural Dynamics and Earthquake Engineering: An IACM Special Interest Conference, Programme*. Corfu, Greece; 2011.

767. Bolton JS, Cao R. Effect of Rotation on the Natural Frequencies of Coupled Tire Structural-Acoustical Mode. In: *Publications of the Ray W. Herrick Laboratories. Paper 94.*; 2013. http://docs.lib.purdue.edu/herrick/94.

768. Cao R, Sakamoto N, Bolton JS. Improved model for coupled structural-acoustic modes of tires. *J Acoust Soc Am*. 2014;136(4):2141 (1 pp.)-pp. http://dx.doi.org/10.1121/1.4899725.

769. Cao R, Bolton JS. Improved Model for Coupled Structural-Acoustic Modes of Tires. *SAE Int J Passeng Cars - Mech Syst*. 2015;8(3):845-854. http://dx.doi.org/10.4271/2015-01-2199.

770. Cao R, Bolton JS. Improved Model for Coupled Structural-Acoustic Modes of Tires. In: *Publications of the Ray W. Herrick Laboratories. Paper 114.*; 2015.

771. Bolton JS, Cao R. Point Excitation of a Coupled Structural-Acoustical Tire Model with Experimental Verification. In: *Publications of the Ray W. Herrick Laboratories. Paper 111.*; 2015.

772. Diaz CG, Kindt P, Middelberg J, et al. Dynamic behaviour of a rolling tyre: Experimental and numerical analyses. *J Sound Vib*. 2016;364:147-164. doi:10.1016/j.jsv.2015.11.025.

773. Wright C, Koopmann GH. A Technique to Predict the Acoustic Radiation Characteristics of an Automobile Tire. *Tire Sci Technol*. 1986;14(2):102-115. doi:10.2346/1.2148767.

774. Richards TL. Finite element analysis of cord-rubber structures in cylindrical coordinates. In: *Firestone Tire and Rubber Co., Internal Report*.; 1987.

775. Berge T, Storeheier SA. Tyre/road noise and road texture - A comparison study of modelling and measurements results. In: *International Congress on Noise Control Engineering 2005, INTERNOISE 2005*.Vol 5. Rio de Janeiro, Brazil; 2005:4016-4022.

776. Roo F de, Gerretsen E, Hoffmans WGJ, Doelman NJ. Dutch tyre-road noise emission model - adjustments and validation. In: *Proceedings Inter-Noise '99, Fort Lauderdale, Florida, USA*.; 1999:243-248.

777. Gerretsen E, Salomons E, Roo F de. State of the art in tyre-road noise modelling. In:

Proceedings of Inter-Noise 1997, Budapest, Hungary,.; 1997.

778. Roo F de, Gerretsen E, Mulder EH. Predictive performance of the tyre- road noise model TRIAS. In: *Proceedings of Inter-Noise 2001, The Hague, Holland*.; 2001.

779. Eerden FJM van der, Gerretsen E, Roo F de, Mulder EH, Schoen ED. A parameter study with the tyre-road noise simulation tool TRIAS. In: *Proceedings of Inter-Noise 2002, Dearborn, MI*.; 2002.

780. Doelman NJ, Mulder EH, Eerden FJM van der, Roo F de. 3-D characterisation of road surface textures in TRIAS. In: *Proceedings of Inter-Noise 2004, Prague, Czech Republic*.; 2004.

781. Nilsson C-M. Waveguide finite elements applied on a car tyre. In: *Doctoral Thesis, Department of Aeronautical and Vehicle Engineering, Royal Institute of Technology*.; 2004.

782. Fraggstedt M. Power dissipation in car tyres. In: *Licentiate Thesis, Department of Aeronautical and Vehicle Engineering, Royal Institute of Technology*.; 2006.

783. Hoever C, Tsotras A, Saemann E-U, Kropp W. A comparison between finite element and waveguide finite element methods for the simulation of tire/road interaction. In: *42nd International Congress and Exposition on Noise Control Engineering 2013, INTER-NOISE 2013: Noise Control for Quality of Life*.Vol 1. Innsbruck, Austria; 2013:127-136.

784. Brinkmeier M, Nackenhorst U. An approach for large-scale gyroscopic eigenvalue problems with application to high-frequency response of rolling tires. *Comput Mech*. 2008;41(4):503-515. http://dx.doi.org/10.1007/s00466-007-0206-6.

785. Brinkmeier M, Nackenhorst U, Volk H. A finite element approach to the transient dynamics of rolling tires with emphasis on rolling noise simulation. In: *Tire Science and Technology*.Vol 35. P.O. Box 1502, Akron, OH 44309-1502, United States; 2007:165-182. http://dx.doi.org/10.2346/1.2768975.

786. Brinkmeier M, Nackenhorst U. Computational investigations on the dynamics of tires rolling on rough roads. In: *Tire Science and Technology*.Vol 37. P.O. Box 1502, Akron, OH 44309-1502, United States; 2009:47-59. http://dx.doi.org/10.2346/1.3078488.

787. Brinkmeier M, Nackenhorst U, Biermann J, Von Estorff O. Prediction of tire/road noise - Modelling and validation. In: *Turkish Acoustical Society - 36th International Congress and Exhibition on Noise Control Engineering, INTER-NOISE 2007 ISTANBUL*.Vol 1. Istanbul, Turkey; 2007:246-255.

788. Brinkmeier M, Nackenhorst U, Biermann J, Von Estorff O, Petersen S. Simulation and analysis of tire road noise using a finite element approach. In: *EURONOISE 2006 - The 6th European Conference on Noise Control: Advanced Solutions for Noise Control*. Tampere, Finland; 2006:6P-6P.

789. Waki Y, Mace BR, Brennan MJ. Free and forced vibrations of a tyre using a wave/finite element approach. *J Sound Vib*. 2009;323:737-756.

790. Ahmad ZA Bin, Perez JMV, Willberg C, Gabbert U. Lamb wave propagation using wave finite element method. *Proc Appl Math Mech PAMM*. 2009;9(1):509-510. doi:10.1002/pamm.200910227.

791. Díaz CG, Vercammen S, Middelberg J, P. Kindt CT, Leyssens J. Numerical prediction of the dynamic behaviour of rolling tyres. In: *PROCEEDINGS OF ISMA 2012*.; 2012:1541-1551.

792. Kido I, Ueyama S, Hashioka M, Yamamoto S, Tsuchiyama M, Yamaoka H. Tire and Road Input Modeling for Low-Frequency Road Noise Prediction. In: *SAE Technical Papers*.Vol 4. 400 Commonwealth Drive, Warrendale, PA 15096-0001, United States; 2011:1277-1282. http://dx.doi.org/10.4271/2011-01-1690.

793. Wagner C, Huttl T, Sagaut P. *Large-Eddy Simulation For Acoustics*.; 2007. doi:10.1017/CBO9780511546143.

794. PIARC. Specification for a Standard Test Tire for Friction Coefficient Measurement of a Pavement Surface: Smooth Test Tire. *World Road Assoc*. 2004.

795. Tong G, Jin X. Study on the Simulation of Radial Tire Vibration Noise. In: *Applied Mechanics and Materials*.Vol 273. Chongqing, China; 2013:203-207. http://dx.doi.org/10.4028/www.scientific.net/AMM.273.203.

796. Vlahopoulos N, Zhang G, Brophy W, Ramaswami M. Vehicle airborne noise analysis using the energy finite element method. In: *SAE Technical Papers*.Vol 4. Grand Rapids, MI, United states; 2013. http://dx.doi.org/10.4271/2013-01-1998.

797. Blevins RD. *Formulas for Natural Frequency and Mode Shapes*. Krieger Pub Co, Florida; 1995.

798. Wei Y, Feng X, Fuqiang Z, Xiang D. Simulation of rolling noise based on the mixed Lagrangian-Eulerian method. *Tire Sci Technol*. 2016;44(1):36-50. http://dx.doi.org/10.2346/tire.16.440103.

799. Banz L, Gimperlein H, Nezhi Z, Stephan EP. Time domain BEM for sound radiation of tires. *Comput Mech*. 2016;58(1):45–57. http://dx.doi.org/10.1007/s00466-016-1281-3.

800. Kinsler LE, Frey AR, Coppens AB, Sanders J V. Fundamentals of acoustics. *4th Ed ISBN 0-471-84789-5 Wiley-VCH*. 1999:560. doi:10.1002/9780470612439.

801. Gautam P, Chandy AJ. Numerical investigation of the air pumping noise generation mechanism in tire grooves. *J Vib Acoust Trans ASME, Pap No VIB-15-1493*. 2016;138(5):51002-051002-051008. http://dx.doi.org/10.1115/1.4033342.

802. Gautam P, Chandy AJ. A Three-Dimensional Numerical Investigation of Air Pumping Noise Generation in Tires. *J Vib Acoust Trans ASME*. 2016;138(6). http://dx.doi.org/10.1115/1.4034100.

803. Takami K, Furukawa T. Study of Tire Noise Characteristics With High-Resolution Synchronous Images. In: *EURONOISE, Maastricht, The Netherlands, May 31–June 3*.; 2015:2113–2118.

804. Takami K, Furukawa T. High-resolution deformation measurement system for fast rotating tires. In: *Proceedings of the ASME Design Engineering Technical Conference*.Vol 8. Boston, MA, United states; 2015:6 pp. doi:10.1115/DETC2015-47495.

805. Lighthill MJ. On sound generated aerodynamically. I. General theory. *Proc R Soc London, Ser A (Mathematical Phys Sci*. 1952;211:565-587.

806. Lighthill MJ. On sound generated aerodynamically. II. Turbulence as a source of sound.

Proc R Soc London, Ser A (Mathematical Phys Sci. 1954;222:1-32.

807. Rasmussen R, Ferragut T, Mun E, Wiegand P. A comprehensive field study on concrete pavement solutions for reducing tire-pavement noise. In: *Institute of Noise Control Engineering of the USA - 35th International Congress and Exposition on Noise Control Engineering, INTER-NOISE 2006*.Vol 1. Honolulu, HI, United states; 2006:412-421.

808. Fujikawa T, Oshino Y, Tachibana H. Effect of road roughness on tire/road noise - Approach by frequency analysis. In: *Turkish Acoustical Society - 36th International Congress and Exhibition on Noise Control Engineering, INTER-NOISE 2007 ISTANBUL*.Vol 5. Istanbul, Turkey; 2007:3130-3134.

809. Storeheier SA. Investigation on road surface texture levels in tyre/road noise mitigation. In: *Proceedings of INTER-NOISE 04, Page 3403, Prague, Czech Republic*.; 2004.

810. Quartieri J, Mastorakis NE, Iannone G, et al. A Review of Traffic Noise Predictive Models. In: *Proceedings of the 5th WSEAS Int. Conf. on "Applied and Theoretical Mechanics"(MECHANICS'09), Puerto De La Cruz, Canary Islands, Spain*.; 2009:72-80.

811. Anon. Handbook of acoustic. In: *Noise Control WADC Technical Report, 52-204. Wright Air Development Center*.; 1952.

812. Nickson A. Can community reaction to increased traffic noise be forecast? In: *Proc. Fifth International Congress on Acoustics*.; 1965.

813. Johnson D, Saunders E. The evaluation of noise from freely flowing road traffic. *J Sound Vib*. 1968;7(2):287-309.

814. Griffiths I, Langdon F. Subjective Response to road traffic noise. *J Sound Vib*. 1968;8:16-32.

815. Galloway W. Urban highway noise: measurement, simulation and mixed reactions. In: *NCHRP Report, 78*.; 1969.

816. Burgess MA. Noise prediction for Urban Traffic Conditions. Related to Measurement in Sydney Metropolitan Area. *Appl Acoust*. 1977;10:1-7.

817. Centre Scientifique et Technique du Batiment. Etude théorique et expérimentale de la propagation acoustique. In: *Revue d'Acoustique n.70*.; 1991.

818. Fagotti C, Poggi A. Traffic Noise Abatement Strategies. The Analysis of Real Case not Really Effective. In: *Proc. of 18th International Congress for Noise Abatement, Pp. , Bologna, Italy*.; 1995:223-233.

819. Murphy E, King EA. *Environmental Noise Pollution, 1st Edition: Noise Mapping, Public Health, and Policy*. Elsevier; 2014.

820. Der Bundesminister für Verkehr. Richtlinien fur den Larmschutz an Strassen. In: *RLS81*.; 1981.

821. RLS. Richtlinien für den Lärmschutz an Strassen. In: *BM Für Verkehr, Bonn*.; 1990.

822. Canelli GB, Gluck K, Santoboni SA. A mathematical model for evaluation and prediction of mean energy level of traffic noise in Italian towns. *Acustica*. 53(31):1983.

823. Cocchi A, Farina A, Lopes G. Modelli matematici per la previsione del rumore stradale:

verifica ed affinazione del modello CNR in base a rilievi sperimentali nella città di Bologna. In: *Acta of 19° Convegno Nazionale AIA*.; 1991.

824. Federal Highway Authority. Code of Federal Regulations, Title 23 – Highways Part, Section 772.9 – Traffic noise prediction. *US Dep Transp*. 2012.

825. Federal Highway Authority. FHWA Traffic Noise Model Users Guide. In: *US Department of Transportation, Report N. FHWA-PD-96-009 and DOT-VNTSC-FHWA-98-1*.; 1998.

826. Fleming G, Rapoza A, Lee C. Development of national reference energy mean emis- sion levels for the FHWA Traffic Noise Model. In: *Report No FHWA-PD-96-008 and DOT-VNTSC-96-2 John A. Volpe National Transportation Systems Center*.; 1995.

827. FHWA. FHWA Traffic Noise Model Version 3.0. In: *http://www.fhwa.dot.gov/environment/noise/traffic_noise_model/tnm_v30/*.; 2013.

828. Rochat JL, Hastings AL, Read DR, Lau M. FHWA Traffic Noise Model (TNM) Pavement Effects Implementation Study : Progress Report 1. In: *Report #: FHWA-HEP-12-034*.; 2012.

829. TXDOT. Fineness Modulus of Fine Aggregate. In: *TxDOT Designation: Tex-402-A*.; 1999.

830. ASTM. Method of Calculation of the Fineness Modulus of Aggregate. *CRD-C 104*. 1980. http://gsl.erdc.usace.army.mil/SL/MTC/handbook/crd_c104.pdf.

831. Rasmussen RO. Quieter Concrete Pavements - An Update of Pooled Fund TPF-5 (139). In: *Presented at Pavement Evaluation 2010, Roanoke, Virginia*.Vol 5.; 2010.

832. ISO. Geometrical Product Specifications (GPS) -- Surface texture: Profile method; Surfaces having stratified functional properties -- Part 2: Height characterization using the linear material ratio curve. *ISO 13565-2*. 1996.

833. Fujikawa T, Oshino Y, Mikami T, Tachibana H. Examination on effects of road roughness parameters for abating tire/road noise. In: *Proceedings of Inter-Noise 2004, Prague, Czech Republic*.; 2004:1122.

834. Fujikawa T, Oshino A, Tachibana H. Effect of road roughness on tire/road noise - Approach by frequency analysis. In: *Proceedings of Inter-Noise 2007, Istanbul, Turkey*.; 2007:708.

835. Fujikawa T, Koike H, Oshino Y. Relation between Road Roughness Parameters and Tyre Vibration Noise - Examination Using a Simple Tyre Model. In: *Proceedings of Inter-Noise 2003, Seogwipo, Korea*.; 2003.

836. Fujikawa T, Oshino Y, Hideki Tachibana. Development of Method to Predict Tire/Road Noise Reduction by Road-Surface Improvements. In: *Proceedings of Inter-Noise 2008, Shanghai, China*.; 2008.

837. Fujikawa T, Oshino Y, Tachibana H. Application of road-profile enveloping procedure to height-unevenness method for prediction tire/road noise. In: *Proceedings of Inter-Noise 2010, Lisbon, Portugal*.; 2010.

838. Fujikawa T, Tachibana H. Prediction of tire/road noise reduction by road-surface improvements. In: *Proceedings of Inter-Noise 2009, Ottawa, Canada*.; 2009.

839. Kephalopoulos S, Paviotti M, Anfosso-Ledee F. Common Noise Assessment Methods in Europe (CNOSSOS-EU). In: *European Commission Joint Research Centre, Luxembourg*

Publications Office of the European Union.; 2012.

840. Ongel A, Kohler E, Harvey J. Principal components regression of onboard sound intensity levels. *J Transp Eng*. 2008;134(11):459-466. http://dx.doi.org/10.1061/(ASCE)0733-947X(2008)134:11(459).

841. Zhang Y, McDaniel JG, Wang ML. Estimation of Pavement Macrotexture by Principal Component Analysis of Acoustic Measurements. *J Transp Eng*. 2014;140(2):04013004 (11 pp.)-pp. http://dx.doi.org/10.1061/(ASCE)TE.1943-5436.0000617.

842. Zhang Y, Ma X, McDaniel JG, Wang ML. Statistical Analysis of Acoustic Measurements for Assessing Pavement Surface Condition. In: *Proc. of SPIE Smart Structures and Materials+ Nondestructive Evaluation and Health Monitoring (Pp. 83471F-83471F). International Society for Optics and Photonics, Bellingham, WA*.; 2012.

843. Wang HQ, Song ZH, Wang H. Statistical Process Monitoring Using Improved PCA with Optimized Sensor Locations. *J Process Contr*. 2002;12(6):735-744.

844. Hotelling H. Analysis of a Complex of Statistical Variables into Principal Components. *J Educ Psychol*. 1933;24(6):417–441–520.

845. Jolliffe IT. *Principal Component Analysis*. 2nd Ed. Springer-Verlag, New York; 2002.

846. Roychowdhury S. Fuzzy curve fitting using least square principles. In: *Proceedings of the IEEE International Conference on Systems, Man and Cybernetics*.Vol 4. San Diego, CA, USA; 1998:4023-4027.

847. Fry J, Jennings P. Using Multi-Layer Perceptrons to Predict Vehicle Pass-By Noise. *Neural Comput Appl*. 2003;11(3):161–7. doi:10.1007/s00521-003-0354-3.

848. Tarassenko L. *Guide to Neural Computing Applications*. Butterworth-Heinemann; 1998. doi:10.1016/B978-034070589-6/50009-9.

849. Wasserman PD. *Advanced Methods in Neural Computing*. Van Nostrand Reinhold, New York; 1993.

850. Neal RN. *Bayesian Learning for Neural Networks*. Springer-Verlag; 1996.

851. Izevbekhai BI. Tire pavement interaction noise of concrete pavements. In: *PhD Dissertation, University of Minnesota*.; 2012.

852. Li X-H, Liu J, Liu D-Q, Sun K-M. Application of tread patterns noise-reduction based on self-adaptive fuzzy genetic algorithm. *Comput Eng Appl*. 2009;45(22).

853. Kumar U, Prakash J, Unnikrishnan G, Thomas T. Tire Pitch Sequence Optimization using HyperStudy. In: *Altair Technology Conference, India*.; 2013.

854. Yong C, Wangxin X, Lijun C. Laboratory test and spectrum analysis method of tire noise. In: *2009 International Conference on Measuring Technology and Mechatronics Automation (ICMTMA), IEEE Press, Apr. 2009*.Vol 1. Zhangjiajie, Hunan, China; 2009:487-490. http://dx.doi.org/10.1109/ICMTMA.2009.483.

855. Kongrattanaprasert W, Nomura H, Kamakura T, Ueda K. Application of neural network analysis to automatic detection of road surface conditions utilizing tire noise from vehicles. In: *2009 ICROS-SICE International Joint Conference. ICCAS-SICE 2009*. Fukuoka, Japan; 2009:2354-2358.

856. Kandpal M, Kakar VK, Verma G. Classification of ground vehicles using acoustic signal processing and neural network classifier. In: *2013 International Conference on Signal Processing and Communication, ICSC 2013*. Noida, India; 2013:512-518. http://dx.doi.org/10.1109/ICSPCom.2013.6719846.

857. Nakajima Y, Kadowaki H, Kamegawa T, Ueno K. Application of a Neural Network for the Optimization of Tire Design. *Tire Sci Technol*. 1999;27(2):62-83. doi:10.2346/1.2135978.

858. El-Gindy M, Lewis H. Development of a Tire/Pavement Contact-Stress Model Based on Artificial Neural Networks. In: *Final Report No. FHWA-RD-99-041*.; 2001.

859. Yu B, Lu Q. Bayesian model for tyre/asphalt pavement noise. *Proc Inst Civ Eng - Transp*. 2013;166(4):241-252.

860. Lu Q, Kohler E, Harvey J, Ongel A. Investigation of Noise and Durability Performance Trends for Asphaltic Pavement Surface Types: Three-year Reports. In: *University of California, Davis, CA, USA, Report No. UCPRC-RR- 2009–01*.; 2009.

861. Lu Q, Kohler E, Harvey J. Field investigation of acoustic performance of various asphalt surface mixes. In: *ICCTP 2010: Integrated Transportation Systems: Green, Intelligent, Reliable - Proceedings of the 10th International Conference of Chinese Transportation Professionals*.Vol 382. Beijing, China; 2010:3937-3947. http://dx.doi.org/10.1061/41127(382)425.

862. D'Andrea A. TINO prototype of a low noise asphalt. In: *First International Colloquium on Vehicle Tyre Road Interaction- The Noise Emission, Rome, Italy*.; 1999.

863. ISO. Characterization of pavement texture by use of surface profiles -- Part 2: Terminology and basic requirements related to pavement texture profile analysis. *ISO 13473-2*. 2002.

864. Clapp TG, Eberhardt AC, Kelley CT. Development and validation of a mehod for approximating road surface texture-induced contact pressure in tire-pavement interaction. *Tire Sci Technol*. 1988;16(1):2-17.

865. Kuijpers A, Blokland G van. Tyre/road noise modeling: The road from a tyre's point-of-view. In: *Proceedings of Inter-Noise 2003, The 32nd International Congress and Exposition on Noise Control Engineering Jeju International Convention Center, Seogwipo, Korea, August 25-28, 2003*.; 2003:249.

866. Kropp W, Larsson K, Wullens F, Andersson P, Bécot F-X, Thomas Beckenbauer. The Modelling of Tyre/Road Noise — A Quasi Three-Dimensional Model. In: *InterNoise2001, The Hague, The Netherlands*.; 2001:657.

867. Blokland G van, The P. Test sections for development of a hybrid tyre/road interaction noise model. In: *Proceedings of Inter-Noise 2007, Istanbul, Turkey*.; 2007.

868. Hamet JF, P. Klein. Evaluation of tire road noise from road texture profiles using INRETS rolling tire model: Evaluation from a profile measured by the LCPC. In: *Rapport de Recherche*.; 2004:18p.

869. Klein P, Hamet JF, Anfosso-Lédée F. An envelopment procedure for tyre/road contact. In: *Proceedings of the 5th Symposium on Pavement Surface Characteristics, SURF, Toronto, Canada, 2004*.; 2004.

870. Klein P, Beckenbauer T, Hamet J-F, Kropp W. Tyre/road noise prediction: A comparison between the SPERoN and HyRoNE models - Part 2. In: *Proceedings of Acoustics08, Paris, France*.; 2008.

871. Kuijpers A, Peeters B, Kropp W, Beckenbauer T. Acoustic Optimization Tool – modeling refinements in the SPERoN framework. In: *Technical Report M+P.DWW.06.04.7, M+P, Vught*.; 2007.

872. Rustighi E, Elliott SJ, Finnveden S, Gulyas K, Mocsai T, Danti M. Linear stochastic evaluation of tyre vibration due to tyre/road excitation. In: *EURONOISE 2006 - The 6th European Conference on Noise Control: Advanced Solutions for Noise Control*. Tampere, Finland; 2006:6P-6P.

873. Rustighi E, Elliott SJ. Shape of a spectral excitation matrix for a linear road/tyre interaction numerical analysis. In: *Turkish Acoustical Society - 36th International Congress and Exhibition on Noise Control Engineering, INTER-NOISE 2007 ISTANBUL*.Vol 1. Istanbul, Turkey; 2007:424-433.

874. Rustighi E, Elliott SJ, Finnveden S, Guly K, Mocsai T, Danti M. Linear stochastic evaluation of tyre vibration due to tyre/road excitation. *J Sound Vib*. 2008;310(4-5):1112-1127. http://dx.doi.org/10.1016/j.jsv.2007.08.032.

875. Rustighi E, Elliot SJ, Finnveden S, Danti KGM. Linear stochastic evaluation of tyre vibration due to tyre/road excitation. *Acta Acust United With Acust*. 2008;92(suppl1):74-75.

876. Rustighi E, Sek MA, Elliott SJ. Stochastic analysis of the non-linear road/tyre excitation. In: *EURONOISE 2006 - The 6th European Conference on Noise Control: Advanced Solutions for Noise Control*. Tampere, Finland; 2006:6P-6P.

877. Rustighi E, Elliott SJ. A model of tyre vibration with stochastic excitation. In: *12th International Congress on Sound and Vibration 2005, ICSV 2005*.Vol 4. Lisbon, Portugal; 2005:3147-3154.

878. Johnson KL. Contact Mechanics. *J Am Chem Soc*. 1985;37:1-17. doi:10.1115/1.3261297.

879. Robson JD. Road surface description and vehicle response. *Int J Veh Des*. 1979;1(1):25-35.

880. Yin H-P, Dubois G, Cesbron J, Anfosso-Ledee F, Bui Q-H, Duhamel D. A numerical macro-scale approach for the tire/road viscoelastic contact for the noise prediction. In: *41st International Congress and Exposition on Noise Control Engineering 2012, INTER-NOISE 2012*.Vol 8. New York, NY, United states; 2012:6979-6987.

881. Cesbron GDJ, Yin HP, Anfosso-Lédée F. Macro-Scale Approach for Rough Frictionless multi-Indentation on a Viscoelastic Half-Space. *Wear*. 2011;272.

882. Dubois G, Cesbron J, Anfosso-Lédée F, Yin HP. A Multi-Asperity Tyre/Road Contact Model for Rolling Noise Prediction. In: *Forum Acusticum 2011*.; 2011.

883. Dubois G, Cesbron J, Yin HP, Anfosso-Lédée F. Numerical Evaluation of Tyre/Road Contact Pressures Using a Multi-Asperity Approach. *I J Mech Sci*. 2012;54.

884. Cesbron J, Anfosso-Ledee F, Duhamel D, Ping Yin H, Le Houedec D. Experimental study of tyre/road contact forces in rolling conditions for noise prediction. *J Sound Vib*. 2009;320(1-2):125-144. http://dx.doi.org/10.1016/j.jsv.2008.07.018.

885. Pinnington RJ. Tyre contact forces on a particulate road surface. In: *Proceedings of the INTER-NOISE 2016 - 45th International Congress and Exposition on Noise Control Engineering: Towards a Quieter Future*. Hamburg, Germany; 2016:2207-2218.

886. Winroth J, Hoever C, Kropp W, Beckenbauer T. The contribution of air-pumping to tyre/road noise. In: *Proceedings of AIA-DAGA 2013*.; 2013:1594-1597.

887. Le Bot A, Bazari Z, Klein P, Lelong J. Statistical analysis of vibration in tyres. *J Sound Vib*. 2017;392:187-199. http://dx.doi.org/10.1016/j.jsv.2016.12.030.

888. Wang B, Duhamel D. On the design and optimization of acoustic network resonators for tire/road noise reduction. *Appl Acoust*. 2017;120:75-84. http://dx.doi.org/10.1016/j.apacoust.2017.01.017.

889. Dalmont J-P, Nederveen CJ, Joly N. Radiation impedance of tubes with different flanges: numerical and experimental investigations. *J Sound Vib*. 2001;244(3):505-534. doi:10.1006/jsvi.2000.3487.

890. Department for Transport. Calculation of Road Traffic Noise. In: *Department for Transport Welsh Office, ISBN 0 11 550847 3*.; 1988.

891. Leung BKH, Mak CM. Is the CRTN method reliable and accurate for Traffic Noise prediction in Hong Kong? *HKIE Trans Hong Kong Inst Eng*. 2008;15(2):17-23.

892. National Physical Laboratory (NPL). Technical Guides - Calculation of Road Traffic Noise 1988. In: *Http://resource.npl.co.uk/acoustics/techguides/crtn/*.; 2005.

893. Department for Transport (UK). Design Manual for Roads and Bridges. In: *Department for Transport, Highways Agency, UK*.; 2008.

894. Abbott P, Nelson P. Converting the UK traffic noise index LA10,18h to EU noise indices for the purposes of noise mapping. In: *TRL Limited, Project Report PR/SE/451/02*.; 2002.

895. Lam HK, Tam ML. Reliability analysis of traffic noise estimates in Hong Kong. *Transpn Res D, Hong Kong*. 1998;3(4):239-248.

896. To WM, Ip CW, Lam CK, Yau TH. A multiple regression model for urban traffic noise in Hong Kong. *J Acoust Soc Am*. 2002;112(2):551-556.

897. Tang SK, K.K.. T. Estimating traffic noise for inclined roads with freely flowing traffic. *Appl Acoust Hong Kong*. 2004;65:171-181.

898. Abbott PG NP. Converting the UK traffic noise index LA10, 18 h to EU noise indices for the purposes of noise mapping. *UK, TRL Ltd*. 2002.

899. O'Malley V, King E, Kenny L DC. Assessing methodologies for calculating road traffic noise levels in Ireland – converting CRTN indicators to the EU indicators (Lden, Lnight). *Appl Acoust*. 2009;70:284–96.

900. Bruit des infrastructures de transports terrestres. *French Stand XPS 31-133*. 2001.

901. Arrêté du 5 mai 1995 relatif au bruit des infrastructures routières. *J Off du 10 mai 1995, Artic 6*. 1996.

902. Guide du bruit des transports terrestres, fascicule prévision des niveaux sonores. *CETUR*. 1980.

903. Service d'e´tudessur les transports, les routes etleursame´nagements (SETRA). In: *Road Traf- Fic Noise Prediction 1 – Calculating Sound Emissions from Road Traffic. Ministe`re de L'e´co- Logie, de L'e´nergie et Du de´veloppement Durable (France)*.; 2009.

904. Dutilleux D. Road traffic noise. In: Noise Mapping in the EU: Models and Procedures. *CRC Press Taylor Fr Group, Boca Raton, FL*. 2013:77.

905. Sétra. Road noise prediction - Part 2: Noise propagation computation method including meteorological effects (NMPB2008). 2009:1-136.

906. Road traffic noise reducing devices. Test method for determining the acoustic performance. Normalized traffic noise spectrum. *BS EN 1793-3*. 1998.

907. ISO. Acoustics -- Attenuation of sound during propagation outdoors -- Part 1: Calculation of the absorption of sound by the atmosphere. *ISO 9613-1*. 1993.

908. Murphy E, King EA. *Environmental Noise Pollution*.; 2014. doi:10.1016/B978-0-12-411595-8.00004-5.

909. Dai L, Lee HS. Ray acoustics approach to quantitative prediction of highway traffic noise. In: *ASME International Mechanical Engineering Congress and Exposition, Proceedings (IMECE)*.Vol 8. Vancouver, BC, Canada; 2010:223-228. http://dx.doi.org/10.1115/IMECE2010-37043.

910. Dai L, Lee H. Prediction of the effects of pavement permeability on the traffic noise generated by tire and road surface interactions. In: *ASME International Mechanical Engineering Congress and Exposition, Proceedings*.Vol 11. Boston, MA, United states; 2009:909-914. http://dx.doi.org/10.1115/IMECE2008-66560.

911. Sachakamol P, Dai L. Noise prediction model development for the traffic noise on asphalt rubber roads. In: *American Society of Mechanical Engineers, Design Engineering Division (Publication) DE*. Chicago, IL, United states; 2006. http://dx.doi.org/10.1115/IMECE2006-13327.

912. Sheadel D, Ma Y, Cao J. Meteorological Effects on Sound Propagation. In: *Spring Noise Conference on Environmental and Occupational Noise, Banff*.; 2007.

913. Wei Y-T, Feng Q-Z. PCR tire air-pumping noise prediction and optimization method. *Zhongguo Gonglu Xuebao/China J Highw Transp*. 2016;29(2):130-135.

914. Saemann E-U, Dahlke M, Nolte B. Improving noise performance with sealed tyre and cavity absorber technology. In: *40th International Congress and Exposition on Noise Control Engineering 2011, INTER-NOISE 2011*.Vol 1. Osaka, Japan; 2011:593-599.

915. Zhou H, Wang G, Yang J, Ying S. Simulation and Analysis of the bypass Influences on Tire Noise. *Res J Appl Sci Eng Technol*. 2014;7(3):576-580.

916. Kakumu K. Low noise tyre. In: *European Patent EP0402021 A2*.; 1990.

917. Cusimano FJI. Low noise pneumatic tire tread and method for producing same. In: *European Patent EP0513676 A1*. Google Patents; 1992:1-14. http://www.google.co.ug/patents/EP0513676A1?cl=en.

918. Continental AG. ComfortContact CC6. 2016. http://www.continental-tyres.com.my/car/tires/car/summer-plt/comfortcontactcc6.

Accessed December 16, 2016.

919. Fitz F, Heck T. Development of Tooling for a Light Weight Steel Kühl Wheel. In: *SAE Technical Paper 2001-01-0750*.; 2001.

920. Kamiyama Y. Development of a new on-wheel resonator for tire cavity noise. In: *SAE Technical Papers*.Vol 1. Detroit, MI, United states; 2014. http://dx.doi.org/10.4271/2014-01-0022.

921. Fernandez ET. The Influence of T yre Air Cavities on Vehicle Acoustics. In: *PhD Thesis, KTH University, Stockholm, Sweden*.; 2006.

922. Yukawa N, Nishikawa M, Nakajima T, Aoki C, Sugihara H. Tire noise reducing system. In: *U.S. Patent 6,726,289 B2 (Assigned to Sumitomo), Granted April 27, 2004*.; 2004.

923. Pirelli. Pirelli noise cancelling system. 2013. https://www.pirelli.com/tires/en-us/car-light-truck/original-equipment-tires/noise-cancelling-system.

924. Schmidt KC, Majumdar RN. Tech Service: Silencing tire noise. *Rubber World*. 2011;244(6):18-19+50.

925. Tire Business. Pirelli absorbs tire noise with PU sponge. 2013. http://www.tirebusiness.com/article/20130717/NEWS/130719921/pirelli-absorbs-tire-noise-with-pu-sponge.

926. Morgan CD. Tire tread pitch sequencing for reduced noise. In: *US Patent US6363984*.; 2002.

927. Lee DW, Kim JK, Kim SR, Lee K-H. Shape design of a tire contour based on approximation model. *J Mech Sci Technol*. 2011;25(1):149-155. http://dx.doi.org/10.1007/s12206-010-1108-7.

928. Sandberg U, Ejsmont JA, Mioduszewski P, Taryma S. Relation between noise emission, friction and rolling resistance of car tires - a pilot study. In: *Proc. of Inter-Noise 98, 16-18 Nov. 1998, Christchurch, New Zealand*.; 1998.

929. Nelson PM, Harris GJ, Robinson BJ. An examination of the relationship between tyre noise and safety performance. In: *Project Report PR047/93, Transport Research Laboratory. Crowthorne, England. Also: ERGA-Noise Document No. 39*.; 1993.

930. Neithalath N. Development and Characterization of Acoustically Efficient Cementitious Materials. In: *PhD Dissertation, Purdue University*.; 2004.

931. Hofman R, Kooij J van der. Results from the Dutch Noise Innovation Program Road traffic (IPG) and Roads to the Future Program (WnT) Authors. In: *The 32nd International Congress and Exposition on Noise Control Engineering, Inter-Noise 2003*.; 2003.

932. Maennel M, Forssen J, Van Der Aa B. Improving the acoustic performance of low noise road surfaces using resonators. In: *Proceedings of Meetings on Acoustics*.Vol 19. Montreal, QC, Canada; 2013. http://dx.doi.org/10.1121/1.4800464.

933. Nilsson N-A. Noise reduction mechanisms for poroelastic road surfaces. In: *Proc. of International Tire/Road Noise Conference 1990, Gothenburg, Sweden*.; 1990:47-66.

934. Nilsson N-A. Possible Method of Reducing External Tyre Noise. In: *Proc. of the Interna-*

Tional Tire Noise Conference 1979, Stockholm, Sweden.; 1979.

935. Berge T, Haukland F. Low-noise tyres-in-use - Do they exist? In: *40th International Congress and Exposition on Noise Control Engineering 2011, INTER-NOISE 2011*.Vol 1. Osaka, Japan; 2011:518-529.

936. Couche JC, Fuller CR. Active control of automobile cabin noise with advanced speakers. In: *Presentation at 136th Acoustical Society of America Meeting, Norfolk, VA*.; 1998.

937. Sun G, Li M, Lim TC. Modified filtered-x LMS algorithm for active control of vehicle road impact noise. In: *41st International Congress and Exposition on Noise Control Engineering 2012, INTER-NOISE 2012*.Vol 1. New York, NY, United states; 2012:58-69.

938. Zafeiropoulos N, Moorhouse A, Mackay A, Ballatore M. Active Control of Structure-Borne Road Noise Based on the Separation of Front and Rear Structural Road Noise Related Dynamics. *SAE Int J Passeng Cars - Mech Syst*. 2015;8(3). http://dx.doi.org/10.4271/2015-01-2222.

939. Jabben J, Verheijen E, Potma C. Noise reduction by electric vehicles in the Netherlands. In: *41st International Congress and Exposition on Noise Control Engineering 2012, INTER-NOISE 2012*.Vol 3. New York, NY, United states; 2012:2505-2512.

940. Mendonca C, Freitas E, Ferreira JP, Raimundo ID, Santos JA. Noise abatement and traffic safety: The trade-off of quieter engines and pavements on vehicle detection. *Accid Anal Prev*. 2013;51:11-17. http://dx.doi.org/10.1016/j.aap.2012.10.018.

941. Sandberg U. What is the biggest threat to health and safety- Quiet or noisy vehicles. *J Acoust Soc Am*. 2013;134.